This document downloaded from
vulcanhammer.net vulcanhammer.info
Chet Aero Marine

Don't forget to visit our companion site
http://www.vulcanhammer.org

Use subject to the terms and conditions of the respective websites.

U.S. Department of Transportation

Publication No. FHWA NHI-16-072
**April** 20**17**

## NHI Course No. 132031

## Geotechnical Engineering Circular No.5

# Geotechnical Site Characterization

NATIONAL HIGHWAY INSTITUTE
*Training Solutions for Transportation Excellence*

## NOTICE

The contents of this report reflect the views of the authors, who are responsible for the facts and accuracy of the data presented herein. The contents do not necessarily reflect policy of the Department of Transportation. This report does not constitute a standard, specification, or regulation. The United States Government does not endorse products or manufacturers. Trade or manufacturer's names appear herein only because they are considered essential to the object of this document.

**Technical Report Documentation Page**

| 1. Report No. | 2. Government Accession No. | 3. Recipient's Catalog No. |
|---|---|---|
| FHWA NHI-16-072 | | |

| 4. Title and Subtitle | 5. Report Date |
|---|---|
| GEOTECHNICAL SITE CHARACTERIZATION<br>GEOTECHNICAL ENGINEERING CIRCULAR NO.5 | November 2016<br>6. Performing Organization Code |

| 7. Principal Investigator(s): See Acknowledgements for Authors and Contributors | 8. Performing Organization Report No. |
|---|---|
| J. Erik Loehr, Ph.D.[1], P.E., Alan Lutenegger[2], Ph.D., P.E., Brent Rosenblad, Ph.D., P.E., [1], and Andrew Boeckmann, P.E.[1] | |

| 9. Performing Organization Name and Address | 10. Work Unit No. (TRAIS) |
|---|---|
| Parsons Brinckerhoff, Inc.<br>One Penn Plaza, New York, NY 10119<br><br>[1] University of Missouri, Columbia, MO 65211<br>[2] University of Massachusetts, Amherst, MA 01003 | 11. Contract or Grant No.<br>DTFH61-11-D-00047-T004 |

| 12. Sponsoring Agency Name and Address | 13. Type of Report and Period Covered |
|---|---|
| National Highway Institute<br>U.S. Department of Transportation<br>Federal Highway Administration, Washington, D.C. 20590 | 14. Sponsoring Agency Code |

15. Supplementary Notes

*FHWA COR: Heather Shelsta*
*FHWA Task Manager: Silas Nichols, P.E.*
*FHWA Technical Reviewers: Silas Nichols, P.E. and Benjamin Rivers, PE*
*Contractor Project Manager: C. Jeremy Hung, PE*

16. Abstract

Characterization of subsurface conditions is one of the most challenging yet important activities required for successful planning, design, construction, and operation of transportation infrastructure. This manual is intended to provide a technical resource for geotechnical and highway engineers responsible for planning and performing subsurface investigations so that project subsurface conditions can be characterized effectively and risks attributed to ground conditions can be identified and addressed. The manual is organized to reflect the strong emphasis on interpretation of geotechnical parameters for design and construction. It describes important considerations for planning and scoping of geotechnical investigations; means and methods for classification of soil and rock based on index property measurements; identifying and characterizing potentially problematic soil and rock types for design and construction; guidance for interpretation of soil and rock properties from field and laboratory measurements; interpretation of geotechnical design parameters from collections of individual measurements; identification and characterization of geotechnical hazards; and lastly, guidance for documenting and reporting results from geotechnical investigations.

| 17. Key Words | 18. Distribution Statement |
|---|---|
| Site characterization, subsurface investigation, geotechnical parameters, soil and rock classification, problematic soils, consolidation, shear strength, stress-strain and stiffness, groundwater, geotechnical report. | No restrictions. |

| 19. Security Classif. (of this report) | 20. Security Classif. (of this page) | 21. No. of Pages | 22. Price |
|---|---|---|---|
| UNCLASSIFIED | UNCLASSIFIED | | |

A copy of the SI (Modern Metric) Conversion Factors table may be found at:
http://www.fhwa.dot.gov/publications/convtabl.cfm

## CONVERSION FACTORS

| Approximate Conversions to SI Units | | | Approximate Conversions from SI Units | | |
|---|---|---|---|---|---|
| When you know | Multiply by | To find | When you know | Multiply by | To find |
| (a) Length | | | | | |
| inch | 25.4 | millimeter | millimeter | 0.039 | inch |
| foot | 0.305 | meter | meter | 3.28 | foot |
| yard | 0.914 | meter | meter | 1.09 | yard |
| mile | 1.61 | kilometer | kilometer | 0.621 | mile |
| (b) Area | | | | | |
| square inches | 645.2 | square millimeters | square millimeters | 0.0016 | square inches |
| square feet | 0.093 | square meters | square meters | 10.764 | square feet |
| acres | 0.405 | hectares | hectares | 2.47 | acres |
| square miles | 2.59 | square kilometers | square kilometers | 0.386 | square miles |
| (c) Volume | | | | | |
| fluid ounces | 29.57 | milliliters | milliliters | 0.034 | fluid ounces |
| gallons | 3.785 | liters | liters | 0.264 | gallons |
| cubic feet | 0.028 | cubic meters | cubic meters | 35.32 | cubic feet |
| cubic yards | 0.765 | cubic meters | cubic meters | 1.308 | cubic yards |
| (d) Mass | | | | | |
| ounces | 28.35 | grams | grams | 0.035 | ounces |
| pounds | 0.454 | kilograms | kilograms | 2.205 | pounds |
| short tons (2000 lb) | 0.907 | megagrams (tonne) | megagrams (tonne) | 1.102 | short tons (2000 lb) |
| (e) Force | | | | | |
| pound | 4.448 | Newton | Newton | 0.2248 | pound |
| (f) Pressure, Stress, Modulus of Elasticity | | | | | |
| pounds per square foot | 47.88 | Pascals | Pascals | 0.021 | pounds per square foot |
| pounds per square inch | 6.895 | kiloPascals | kiloPascals | 0.145 | pounds per square inch |
| (g) Density | | | | | |
| pounds per cubic foot | 16.019 | kilograms per cubic meter | kilograms per cubic meter | 0.0624 | pounds per cubic feet |
| (h) Temperature | | | | | |
| Fahrenheit temperature($^{o}$F) | 5/9($^{o}$F- 32) | Celsius temperature($^{o}$C) | Celsius temperature($^{o}$C) | 9/5($^{o}$C)+ 32 | Fahrenheit temperature($^{o}$F) |

Notes: 1) The primary metric (SI) units used in civil engineering are meter (m), kilogram (kg), second(s), newton (N) and pascal ($Pa=N/m^2$).
2) In a "soft" conversion, an English measurement is mathematically converted to its exact metric equivalent.
3) In a "hard" conversion, a new rounded metric number is created that is convenient to work with and remember.

## PREFACE

This publication, titled “GEC5 – Geotechnical Site Characterization” is the fifth in the series of geotechnical engineering guidelines called "Geotechnical Engineering Circulars (GECs)" published by Federal Highway Administration (FHWA) covering geotechnical engineering design and construction. The document replaces the 2002 version of GEC No.5 “Evaluation of Soil and Rock Properties” (FHWA-IF-02-034) developed by GeoSyntec Consultants and authored by P.J. Sabatini, R.C. Bachus, P.W. Mayne, J.A. Schneider, and T.E. Zettler. The objective of GEC-5 is to improve site characterization practices among transportation agencies, private consultants, and contractors involved in the planning, design, construction, and operation of transportation features. It is intended to be a comprehensive and practical reference to guide planning and execution of geotechnical investigations, interpretation of the acquired measurements to develop reliable geotechnical design parameters, and identifying and characterizing geotechnical hazards. This publication is also intended to serve as the reference manual for future NHI training products addressing site characterization.

The current GEC5 is considerably different from the previous version it replaces. Most notably, the current manual does not provide explicit guidance for the type and number of tests required for specific design parameters. Rather, the manual recommends characterizing important design parameters to achieve a specific level of reliability and describes methods for quantifying reliability based on available measurements. This position was adopted because the reliability of geotechnical design parameters depends on many factors and it is not possible to reduce these effects to simple rules while still consistently achieving a target reliability at reasonable cost. While the guidance provided may initially seem ambiguous and unfamiliar, readers will find that they will quickly develop judgment regarding appropriate quantities of measurements with consistent application of guidance provided in Chapters 3 and 11. Readers unfamiliar with methods for characterizing uncertainty are strongly recommended to read these chapters carefully, along with the examples provided in Appendix 2. Readers will also find that these methods can be used to assess the value of different site characterization practices, to place site characterization activities into context that is meaningful to both technical and non-technical professionals, and to facilitate effective decision making for geotechnical investigations in light of the risks and costs involved.

Additional notable changes to the manual include:

- Changes to address load and resistance factor design (LRFD) and more explicit awareness of risk and reliability for planning, design, construction, and operation of transportation features;

- Explicit consideration of “direct” and “indirect” measurements of geotechnical properties;
- Updates to address numerous technological advancements to site characterization practice, including expanded use of remote sensing, data management systems, new and improved testing devices and methods, geophysical methods, and in situ tests, among others;
- Expanded and updated coverage of methods for interpreting measurements from individual field and laboratory tests;
- Updates to reflect changes to project delivery, most notably the expanded use of design-build and other alternative project delivery mechanisms;
- Addition of content on problematic soils including permafrost, pyritic/acid rock, high sulfate soils, corrosive soils, dispersive soils, and liquefiable soils;
- Updates to reflect use of the Geological Strength Index approach for design in rock masses;
- Expanded content on investigation of groundwater conditions; and
- Specific content for identification and characterization of geotechnical hazards.

The GEC5 is not intended to provide prescriptive procedures, nor to dictate methods for collection of field or laboratory measurements. Guidance for performing specific tests and executing investigations for site characterization is available from numerous other sources, including state, federal, and international standards and procedures, as well as the AASHTO *Manual on Subsurface Investigations* that is currently being revised and updated to reflect changes to practice since it was last published in 1988. This publication is intended for use in conjunction with these sources. Where appropriate, standard methods for executing site characterization investigations are cited throughout the manual.

**ACKNOWLEDGEMENTS**

The authors would like to acknowledge the contributions of numerous individuals and groups who helped with preparation of this document. The authors appreciate the reviews and recommendations provided by members of the Technical Working Group for this update:

- Tom Badger, Formerly of Washington State DOT
- Carl Benson, Virginia DOT
- Brian Collins, FHWA Federal Lands
- Derrick Dasenbrock, Minnesota DOT
- David Horhota, Florida DOT
- Cyrus Parker, North Carolina DOT

Additional technical review was also provided by Ray Castelli and Taehong Kim from Parsons Brinckerhoff, as well as by anonymous industry reviewers affiliated with several TRB committees and the Subsurface Characterization Committee of the Deep Foundations Institute. In addition, the Principal Investigators wish to extend their gratitude for the support provided by a number of professionals at Parsons Brinckerhoff, including Damian Okon, Kirsten Vaughn and Steve Dorneles. Assistance from Grace Jao of No Boundaries is also greatly appreciated.

THIS PAGE IS LEFT INTENTIONALLY BLANK

# TABLE OF CONTENTS

List of Figures……..……...….xv

List of Tables……...……xxxiii

Chapter 1 Introduction ..... 1-1

1.1 Role and Value of Site Characterization ..... 1-1
1.2 Challenges for Effective Site Characterization ..... 1-2
1.3 Purpose of Circular ..... 1-3
1.4 Organization of Circular ..... 1-4

Chapter 2 Objectives, Uses, and Products of Site Characterization Investigations ..... 2-1

2.1 General Objectives for Site Characterization ..... 2-1
2.2 Classes of Site Characterization investigations ..... 2-3

2.2.1 Desk Studies ..... 2-3
2.2.2 Preliminary Investigations ..... 2-4
2.2.3 Design Investigations ..... 2-4
2.2.4 Borrow Site Investigations ..... 2-5
2.2.5 Investigations for Performance Monitoring and Condition Assessment ..... 2-6
2.2.6 Forensic Investigations ..... 2-7
2.2.7 Investigations for Design-Build Projects ..... 2-7

2.3 Geotechnical Reporting Documents ..... 2-8

2.3.1 Field Investigation Logs ..... 2-8
2.3.2 Geotechnical Data Reports ..... 2-8
2.3.3 Geotechnical Design Reports ..... 2-9
2.3.4 Geotechnical Baseline Reports ..... 2-9

2.4 Benefits of Site Characterization ..... 2-10

Chapter 3 Planning and Scoping For Site Characterization Activities ..... 3-1

3.1 Information Requirements for Design and Construction ..... 3-1
3.2 Collection and Interpretation of Existing Information ..... 3-3

3.2.1 Desk Study ..... 3-4

3.2.2 Open Source and Commercial Remote Sensing Data ..... 3-8
3.2.3 Historical Data ..... 3-9

3.3 Site Reconnaissance ..... 3-10
3.4 Influence of Number of Measurements ..... 3-11

3.4.1 General Perspectives on Reliability of Geotechnical Design Parameters ..... 3-11
3.4.2 Statistical "Sampling" for Geotechnical Site Characterization ..... 3-13
3.4.3 Influence of Number of Measurements on Estimates for Geotechnical Design Parameters ..... 3-15
3.4.4 Influence of Number of Measurements on Estimates of Variability and Uncertainty ..... 3-19
3.4.5 Influence of Number of Measurements for Geotechnical Design ..... 3-20
3.4.6 Application of Judgment for Establishing Appropriate Number of Measurements ..... 3-24

3.5 Influence of Type of Measurements ..... 3-25
3.6 Influence of Boring, Sampling and Testing Methods ..... 3-29
3.7 Considerations for Time Varying Conditions ..... 3-31
3.8 Selection from Among Alternative Methods of Investigation ..... 3-32
3.9 Considerations for Different Levels of Site Characterization ..... 3-33
3.10 Development of Scope for Field Investigations ..... 3-34

3.10.1 Developing Preliminary Scopes ..... 3-35
3.10.2 Refining Preliminary Scope ..... 3-38

3.11 Development of Scope for Laboratory and Field Testing ..... 3-40
3.12 Special Considerations for Alternative Contracting Methods ..... 3-42
3.13 Communication and Execution of Site Characterization Activities ..... 3-43

Chapter 4 Identification and Classification of Soil and Rock ..... 4-1

4.1 Objectives for Identification and Classification of Soil and Rock ..... 4-1
4.2 Boring and Sampling Requirements for Index Testing ..... 4-1
4.3 Fundamental Concepts for Identification and Classification ..... 4-2
4.4 Grain-Size Distribution ..... 4-3

4.4.1 Coarse-Grained Soils ..... 4-3
4.4.2 Fine-Grained Soils ..... 4-5

4.5 Grain Shape – Coarse-Grained Soils....4-6
4.6 Water Content....4-6
4.7 Unit Weight and Specific Gravity....4-7
4.8 Atterberg Limits....4-9
4.8.1 Determining the Liquid Limit....4-11
4.8.2 Determining the Plastic Limit....4-13
4.8.3 Determining the Shrinkage Limit....4-13
4.8.4 Derived Indices from Atterberg Limits....4-14
4.9 Activity....4-14
4.10 Soil Composition....4-15
4.10.1 X-Ray Diffraction....4-15
4.10.2 Specific Surface Area....4-16
4.10.3 Cation Exchange Capacity....4-17
4.10.4 Carbonate Content....4-18
4.10.5 Organic Content....4-19
4.11 Electro-Chemical Classification Tests....4-19
4.12 Rock Hardness....4-19
4.13 Rock Abrasion....4-20
4.14 Rock Durability....4-20
4.15 Rock Core Measurements....4-21
4.15.1 Rock Core Recovery....4-21
4.15.2 Rock Quality Designation ($RQD$)....4-22
4.15.3 Rock Fracture Frequency (FF)....4-22
4.16 Classification of Soil Using Laboratory Test Measurements....4-23
4.16.1 Unified Soil Classification System (USCS)....4-24
4.16.2 AASHTO System....4-26
4.16.3 Comparison Between USCS and AASHTO Soil Classification Systems....4-28
4.17 Soil Identification Using In Situ Test Measurements....4-28
4.17.1 Identification from CPT and CPTU Measurements....4-30
4.17.2 Identification from Normalized CPT and CPTU Measurements....4-32

4.17.3 Identification from Soil Behavior Type Index ..... 4-33
4.17.4 Additional Characterization Using CPT and CPTU Tests ..... 4-35
4.17.5 Identifying Cemented or Unusual Soils from Seismic Cone Penetrometer (SCPT) and Seismic Piezocone (SCPTU) ..... 4-35
4.17.6 Soil Identification from Dilatometer (DMT) ..... 4-35

4.18 Classification of Intact Rock ..... 4-37

4.18.1 Rock Type ..... 4-37
4.18.2 Grain Size ..... 4-38
4.18.3 Weathering State ..... 4-38
4.18.4 Relative Rock Strength ..... 4-41
4.18.5 Rock Color ..... 4-42

4.19 Characterization of soil and Rock Using Drilling Parameters ..... 4-43

Chapter 5 Identification and Characterization of Problematic Soil And Rock ..... 5-1

5.1 Problematic Soil and Rock Types ..... 5-1
5.2 Collapsible Soils ..... 5-4

5.2.1 Occurrence of Collapsible Soils ..... 5-5
5.2.2 Indirect Identification of Collapsible Soils ..... 5-6
5.2.3 Direct Characterization of Collapsible Soils ..... 5-7
5.2.4 Challenges for Subsurface Exploration in Collapsible Soils ..... 5-10

5.3 Expansive/Shrinking Soils ..... 5-11

5.3.1 Occurrence of Expansive Soils ..... 5-12
5.3.2 Identification and Characterization of Expansive Soils Using Indirect Methods ..... 5-13
5.3.3 Characterization of Swell Potential Using Direct Methods ..... 5-17
5.3.4 Swell “Sensitivity” ..... 5-19
5.3.5 Characterization of Shrinkage ..... 5-20
5.3.6 Linear Shrinkage Test ..... 5-21
5.3.7 Shrink Test ..... 5-22

5.4 Organic Soils ..... 5-22

5.4.1 Occurrence of Organic Soils ..... 5-23

5.4.2 Identification of Organic Soils ..... 5-23
5.4.3 Challenges for Subsurface Exploration of Organic Soils and Peat ..... 5-24
5.4.4 Shear Strength of Organic Soils and Peats ..... 5-24
5.4.5 Compressibility of Organic Soils and Peats ..... 5-25

5.5 Dispersive Soils ..... 5-27

5.5.1 Identification of Dispersive Soils Using Indirect Measurements ..... 5-28
5.5.2 Identification of Dispersive Soils Using Direct Measurements ..... 5-28

5.6 Liquefiable Soils ..... 5-30

5.6.1 Occurrence of Liquefiable Soils ..... 5-31
5.6.2 Identification of Liquefiable Soils ..... 5-31

5.7 Colluvium and Talus ..... 5-34

5.7.1 Identification of Colluvium and Talus ..... 5-34
5.7.2 Challenges for Subsurface Exploration and Testing in Colluvium ..... 5-34
5.7.3 Challenges for Subsurface Exploration and Testing in Talus ..... 5-35
5.7.4 Compressibility of Colluvium and Talus ..... 5-36
5.7.5 Shear Strength of Colluvium and Talus ..... 5-36

5.8 Degradable Rock ..... 5-37

5.8.1 Identification of Degradable Materials ..... 5-37
5.8.2 Classification of Shale and Degradable Rock ..... 5-39

5.9 Corrosive Soils ..... 5-40

5.9.1 Occurrence of Corrosive Soils ..... 5-40
5.9.2 Identification of Corrosive Soils ..... 5-41
5.9.3 Classification of Corrosive Soils ..... 5-43

5.10 Cemented Sands ..... 5-43

5.10.1 Identification of Cemented Sands ..... 5-44
5.10.2 Challenges for Subsurface Exploration and Testing in Cemented Sands ..... 5-45
5.10.3 Interpretation of Laboratory and Field Testing Results in Cemented Sands ..... 5-46

5.11 Sensitive “Quick” Clays....5-47

5.11.1 Occurrence of “Quick” Clays....5-47
5.11.2 Identification of “Quick” Clays....5-47
5.11.3 Challenges for Subsurface Exploration and Testing in Sensitive Clays....5-48

5.12 High Sulfate Soils....5-49

5.12.1 Occurrence of High Sulfate Soils....5-50
5.12.2 Identification of High Sulfate Soils....5-50

5.13 Pyritic/Acid Rock....5-51
5.14 Unsaturated Soils....5-51
5.15 Permafrost....5-54

5.15.1 Occurrence of Permafrost....5-54
5.15.2 Identification of Permafrost....5-54
5.15.3 Challenges with Subsurface Investigation and Testing for Permafrost....5-55

Chapter 6 Measurement and Interpretation of Consolidation Properties of Soil....6-1

6.1 Fundamental Consolidation Concepts....6-1
6.2 Boring and Sampling Requirements for Laboratory Consolidation Tests....6-5
6.3 Selection of Samples for Laboratory Consolidation Testing....6-5
6.4 Effects of Sampling Disturbance....6-6
6.5 Types of Laboratory Consolidation Tests....6-9

6.5.1 Incremental Load Consolidation Test....6-10
6.5.2 Constant Rate of Strain Consolidation Test....6-12

6.6 Evaluation of Preconsolidation Stress from Laboratory Consolidation Tests....6-13

6.6.1 Interpretation of Preconsolidation Stress Using Casagrande Method....6-13
6.6.2 Interpretation of Preconsolidation Stress Using Strain Energy Method....6-14
6.6.3 Influence of Strain Rate and Temperature....6-16

6.7 Evaluation of Compression and Recompression Indices from Laboratory Consolidation Tests....6-16
6.8 Tangent Modulus Method for Interpreting Consolidation Test Results....6-18
6.9 Adjustment of laboratory consolidation tests to obtain Field Consolidation Curve....6-20

6.10 Evaluation of Coefficient of Consolidation from Laboratory Consolidation Tests ..... 6-22

6.10.1 Casagrande's Log Time Method ..... 6-23
6.10.2 Taylor's Square Root of Time Method ..... 6-23

6.11 Evaluation of Coefficient of Secondary Compression From laboratory Consolidation Tests ..... 6-26
6.12 Evaluation of Preconsolidation Stress from In Situ Tests ..... 6-27

6.12.1 CPT/CPTU ..... 6-28
6.12.2 DMT ..... 6-30
6.12.3 Field Vane Shear Test (FVT) ..... 6-31
6.12.4 Pressuremeter Test (PMT) ..... 6-32
6.12.5 Standard Penetration Test (SPT) ..... 6-35

6.13 Evaluation of Coefficient of Lateral Consolidation from In Situ Tests ..... 6-35

6.13.1 CPTU Dissipation Tests ..... 6-36
6.13.2 DMT Dissipation Tests ..... 6-39

6.14 Estimation of Consolidation Parameters from Index Properties ..... 6-42

6.14.1 Compression Index and Recompression Index ..... 6-43
6.14.2 Coefficient of Consolidation ..... 6-45
6.14.3 Coefficient of Secondary Compression ..... 6-46
6.14.4 Stress History ..... 6-47

Chapter 7 Measurement and Interpretation of Shear Strength Properties of Soil ..... 7-1

7.1 Uses for Shear Strength Properties in Design and Construction ..... 7-1
7.2 Fundamental Concepts of Soil Shear Strength ..... 7-1

7.2.1 Shear Strength Envelopes ..... 7-2
7.2.2 Defining Failure ..... 7-5
7.2.3 Measures of Shear Strength ..... 7-7
7.2.4 Drainage and Excess Pore Water Pressures ..... 7-8
7.2.5 Influence of Stress Path ..... 7-9
7.2.6 Undrained Shear Strength and Total Stress Strength Envelopes ..... 7-12
7.2.7 Normalized Soil Behavior ..... 7-16
7.2.8 Influence of Anisotropy ..... 7-17

7.2.9 Influence of Strain Rate ..... 7-18
7.2.10 Influence of Cyclic Loading ..... 7-20

7.3 Boring and Sampling Requirements for Laboratory Strength Tests ..... 7-20
7.4 Evaluation of Undrained Shear Strength ..... 7-21

7.4.1 Unconsolidated-Undrained Triaxial Tests ..... 7-21
7.4.2 Unconfined Compression Tests ..... 7-24
7.4.3 Consolidated-Undrained Triaxial Tests ..... 7-25
7.4.4 Direct Simple Shear Tests ..... 7-26
7.4.5 Effects of Sample Disturbance ..... 7-27
7.4.6 SHANSEP Procedure ..... 7-29
7.4.7 Selection of Specimens for Measurement of Undrained Shear Strength ..... 7-32
7.4.8 Estimation of Undrained Shear Strength from Indirect Measurements ..... 7-32
7.4.9 Selection of Testing Method(s) for Undrained Shear Strength ..... 7-42

7.5 Evaluation of Total Stress Strength Parameters for Unsaturated Soils ..... 7-46
7.6 Evaluation of Effective Stress Strength Parameters ..... 7-48

7.6.1 Consolidated-Undrained Triaxial Tests with Pore Pressure Measurements ..... 7-48
7.6.2 Consolidated-Drained Triaxial Tests ..... 7-49
7.6.3 Direct Shear Tests ..... 7-50
7.6.4 Effects of Sample Disturbance ..... 7-50
7.6.5 Selection of Samples for Measurement of Effective Stress Strength Parameters ..... 7-51
7.6.6 Selection of Laboratory Testing Method ..... 7-52
7.6.7 Measurement of Effective Stress Strength Parameters Using Borehole Shear Test ..... 7-53
7.6.8 Estimation of Effective Stress Strength Parameters from Indirect Measurements ..... 7-53
7.6.9 Estimation of Effective Stress Strength Parameters from Empirical Correlations ..... 7-57

7.7 Evaluation of Residual and Fully-Softened Shear Strength Parameters ..... 7-59

7.7.1 Direct-Residual Shear Test ..... 7-60
7.7.2 Ring Shear Test ..... 7-61
7.7.3 Selection of Samples for Residual Shear Strength Measurement ..... 7-61
7.7.4 Estimation of Residual and Fully Softened Shear Strength Parameters from Empirical Correlations ..... 7-62

7.8 Evaluation of Shear Strength Parameters for Compacted Soils ..... 7-64

Chapter 8 Measurement and Interpretation of Stress-Strain and Stiffness Properties ..... 8-1

8.1 Uses for Stress-Strain and Stiffness Properties ..... 8-1
8.2 General Stress-Strain Response of Soil ..... 8-3
8.3 Boring and Sampling Requirements for Measurement of Stress-Strain and Stiffness Properties 8-6
8.4 Evaluation of Small-Strain Modulus from Stress-Wave Velocity Measurements ..... 8-6

8.4.1 Intrusive Field Methods for Stress-Wave Measurements ..... 8-7
8.4.2 Non-Intrusive Field Methods for Stress-wave Measurements ..... 8-10

8.5 Laboratory Measurement of Small-Strain Modulus ..... 8-13

8.5.1 Bender Elements ..... 8-14
8.5.2 Resonance Testing ..... 8-14
8.5.3 Direct Measurement from Stress-Strain Curve ..... 8-15
8.5.4 Effects of Sample Disturbance ..... 8-15

8.6 Estimation of Small-Strain Modulus from Indirect Methods ..... 8-15

8.6.1 Estimation of Small-Strain Shear Modulus from Soil Index Properties ..... 8-15
8.6.2 Estimation of Small-Strain Shear Modulus from Indirect In situ Measurements ..... 8-18

8.7 Evaluation of Modulus Degradation Curves from Laboratory Measurements ..... 8-22
8.8 Estimation of Modulus Degradation from Empirical Relationships ..... 8-23
8.9 Modulus Values at Intermediate Strain Levels for Settlement Analysis ..... 8-24

8.9.1 Simple Estimates for Equivalent Modulus ..... 8-25
8.9.2 Equivalent Modulus Using Modulus Degradation ..... 8-25
8.9.3 Pressuremeter Modulus ..... 8-27
8.9.4 Dilatometer Modulus ..... 8-28

8.10 Other Soil Stiffness Properties ..... 8-29

8.10.1 Coefficient of Subgrade Reaction ..... 8-29
8.10.2 $p$-$y$ Curves ..... 8-30

Chapter 9 Measurement and Interpretation of Rock Properties ..... 9-1

9.1 Uses for Rock Properties in Design and Construction ..... 9-1
9.2 Fundamental Concepts in Rock Behavior ..... 9-2
9.3 Boring and Sampling Requirements for Characterization of Intact Rock and Rock Masses ..... 9-6
9.4 Measurement and Interpretation of Intact Rock Properties ..... 9-7

9.4.1 Uniaxial Compressive Strength ..... 9-7
9.4.2 Shear Strength of Intact Rock ..... 9-9
9.4.3 Tensile Strength of Intact Rock ..... 9-11
9.4.4 Intact Rock Modulus ..... 9-12
9.4.5 Evaluation of Intact Rock Properties from Indirect Measurements ..... 9-15
9.4.6 Selection of Specimens for Measurement of Intact Rock Properties ..... 9-23
9.4.7 Special Considerations for Degradable Rock ..... 9-23

9.5 Characterization of Discontinuities in Rock ..... 9-24

9.5.1 Representation of Discontinuity Orientation ..... 9-24
9.5.2 Characterization of Discontinuities from Borehole and Rock Core Measurements ..... 9-25
9.5.3 Characterization of Discontinuities from Mapping of Rock Exposures ..... 9-27
9.5.4 Shear Strength of Rock Discontinuities ..... 9-29
9.5.5 Surface Roughness ..... 9-30
9.5.6 Discontinuity Infilling ..... 9-32

9.6 Rock Mass Classification ..... 9-32

9.6.1 Alternative Rock Mass Classification Systems ..... 9-33
9.6.2 Rock Mass Rating ($RMR$) Classification System ..... 9-33
9.6.3 Geological Strength Index ($GSI$) Classification System ..... 9-34

9.7 Evaluation of Rock Mass Modulus ..... 9-37

9.7.1 Evaluation of Rock Mass Modulus from in situ Test Measurements ..... 9-38
9.7.2 Estimation of Rock Mass Modulus from $RQD$ ..... 9-46
9.7.3 Estimation of Rock Mass Modulus from Rock Mass Rating ..... 9-47
9.7.4 Estimation of Rock Mass Modulus from Geological Strength Index ..... 9-48

9.8 Evaluation of Shear Strength of Rock Masses ..... 9-50

Chapter 10 Measurement and Interpretation of Groundwater Conditions and Hydraulic Properties of Soil and Rock ..... 10-1

10.1 Uses for Hydraulic Properties and Groundwater Conditions for Design and Construction ..... 10-1
10.2 Fundamental Concepts of Seepage through Soil and Rock ..... 10-2

10.2.1 Temporal Changes in Pore Water Pressures and Water Levels ..... 10-3
10.2.2 Water Flow and Hydraulic Conductivity ..... 10-4
10.2.3 Fundamental Means for Measurement of Hydraulic Conductivity ..... 10-5

10.3 Boring and Sampling Requirements ..... 10-7
10.4 Evaluation of Groundwater Conditions from Observations During Drilling ..... 10-8
10.5 Investigation of Groundwater Conditions Using Monitoring Wells ..... 10-8
10.6 Investigation of Groundwater Conditions Using Piezometers ..... 10-10

10.6.1 Standpipe Piezometers ..... 10-12
10.6.2 Twin-tube Hydraulic Piezometers ..... 10-15
10.6.3 Pneumatic Piezometers ..... 10-16
10.6.4 Strain Gage Piezometers ..... 10-17
10.6.5 Installation of Piezometer Elements ..... 10-17

10.7 Evaluation of Groundwater Conditions Using In situ Test Measurements ..... 10-19
10.8 Evaluation of Groundwater Conditions Using Geophysical Measurements ..... 10-22

10.8.1 Location of Groundwater Surface ..... 10-22
10.8.2 Investigation of Groundwater Flow ..... 10-23

10.9 Methods for Evaluating Hydraulic Conductivity of Soil and Rock ..... 10-24
10.10 Factors Affecting Hydraulic Conductivity from Laboratory Tests ..... 10-25

10.10.1 Size of Test Specimens ..... 10-25
10.10.2 Stress Level ..... 10-26
10.10.3 Sample Disturbance ..... 10-26
10.10.4 Hydraulic Gradient ..... 10-26
10.10.5 Permeant ..... 10-27
10.10.6 Temperature ..... 10-27
10.10.7 Anisotropy of Hydraulic Conductivity ..... 10-27

10.11 Evaluation of Hydraulic Conductivity Using Laboratory Tests ..... 10-29

10.11.1 One-dimensional Consolidation Tests ..... 10-30
10.11.2 Thin-Wall Shelby Tube Permeameters ..... 10-31
10.11.3 Compaction Mold Permeameters ..... 10-32
10.11.4 Double-Ring Compaction Mold Permeameters ..... 10-33
10.11.5 Oversized Rigid-Wall Permeameter ..... 10-34
10.11.6 Variable Vertical Stress Rigid-Wall Permeameter ..... 10-34
10.11.7 Flexible-Wall Permeameters ..... 10-34

10.12 Evaluation of Hydraulic Conductivity from Borehole Measurements ..... 10-35

10.12.1 Auger Hole Method ..... 10-36
10.12.2 Open End Pumping Tests ..... 10-37
10.12.3 Slug/Bail Tests in Standpipe Piezometers ..... 10-38
10.12.4 Packer Pumping Tests ..... 10-40
10.12.5 Guelph Permeameter ..... 10-41
10.12.6 Boutwell Two-Stage Permeameter ..... 10-43
10.12.7 Self-Boring (Reaming) Permeameter ..... 10-45
10.12.8 Field Pumping Tests ..... 10-46

10.13 Evaluation of Hydraulic conductivity Using Infiltrometer Methods ..... 10-47

10.13.1 Open Single-Ring Infiltrometer ..... 10-48
10.13.2 Sealed Single-Ring Infiltrometer ..... 10-49
10.13.3 Open Double-Ring Infiltrometer ..... 10-50
10.13.4 Sealed Double-Ring Infiltrometer ..... 10-50
10.13.5 Air Entry Permeameter ..... 10-51

10.14 Evaluation of Hydraulic Conductivity Using In situ Field tests ..... 10-52

10.14.1 Driven/Pushed Porous Probe ..... 10-53
10.14.2 Piezocone (CPTU) Dissipation Tests ..... 10-53
10.14.3 Flat Dilatometer ..... 10-55
10.14.4 BAT Probe ..... 10-55

10.15 Estimation of Hydraulic Conductivity from Correlations ..... 10-56

10.15.1 Estimating Hydraulic Conductivity for Granular Soils ..... 10-57
10.15.2 Estimating Hydraulic Conductivity for Fine-Grained Soils ..... 10-59

Chapter 11 Development of Design Models and Selection of Design Parameters ..... 11-1

11.1 Objectives for Interpretation of Design Parameters ..... 11-1
11.2 Process for Interpretation of Design Parameters ..... 11-4
11.3 Interpretation of Subsurface Stratigraphy ..... 11-6
11.4 Interpretation of Design Parameters From Available measurements ..... 11-8

11.4.1 Selection of Design Parameters from Direct Measurements ..... 11-9
11.4.2 Estimation of Design Parameters from Indirect Measurements ..... 11-14
11.4.3 Use of Historical Data for Establishing Design Parameters ..... 11-16

11.5 Calculation of Variability and Uncertainty for Design Parameters ..... 11-17

11.5.1 Calculation of Variability and Uncertainty for Direct Measurements ..... 11-18
11.5.2 Calculation of Variability and Uncertainty for Indirect Measurements ..... 11-25
11.5.3 Calculation of Variability & Uncertainty for Combined Direct & Indirect Measurements ..... 11-29

11.6 Identifying Outliers and Resolving Inconsistencies ..... 11-32
11.7 Use of Observational Method ..... 11-34
11.8 Interpretation of In situ Stress State for Design ..... 11-34

11.8.1 Total Vertical Stress ..... 11-35
11.8.2 Pore Water Pressure ..... 11-36
11.8.3 Vertical Effective Stress ..... 11-37
11.8.4 Preconsolidation Stress and Overconsolidation Ratio ($OCR$) ..... 11-37
11.8.5 Horizontal Stresses ..... 11-39

11.9 Interpretation of Undrained Shear Strength for Design ..... 11-42

11.9.1 Interpretation of $su$ from UU Triaxial Tests and Unconfined Compression Tests ..... 11-43
11.9.2 Interpretation of $su$ from Consolidated-Undrained Tests ..... 11-44
11.9.3 Interpretation of Undrained Shear Strength from Indirect Laboratory and Field Tests ..... 11-47

11.10 Interpretation of Total Stress Strength Parameters for Design in Unsaturated Soils ..... 11-47
11.11 Interpretation of Effective Stress Strength Parameters for Design ..... 11-48
11.11.1 Interpretation of Effective Stress Strength Parameters from Laboratory Tests ..... 11-49
11.11.2 Interpretation of Effective Stress Friction Angle from In Situ Tests ..... 11-51
11.12 Interpretation of Consolidation Parameters for Design ..... 11-52
11.12.1 Compressibility Parameters ..... 11-52
11.12.2 Coefficient of Consolidation ..... 11-52
11.12.3 Coefficient of Secondary Compression ..... 11-53
11.13 Evaluation of Groundwater Conditions for Design ..... 11-53
Chapter 12 Identification and Characterization of Geotechnical Hazards ..... 12-1
12.1 Objectives for Identification and Characterization of Geotechnical Hazards ..... 12-1
12.2 Karst Hazards ..... 12-1
12.2.1 Implications of Karst Hazard for Transportation Projects ..... 12-2
12.2.2 Identification and Characterization of Karst Hazards ..... 12-5
12.3 Underground Mine Hazards ..... 12-13
12.3.1 Implications of Underground Mine Hazards for Transportation Projects ..... 12-14
12.3.2 Identification and Characterization of Underground Mine Hazards ..... 12-14
12.4 Seismic Hazards ..... 12-16
12.4.1 Implications of Seismic Hazards for Transportation Projects ..... 12-17
12.4.2 Identification and Characterization of Geotechnical Seismic Hazards ..... 12-19
12.5 Groundwater Hazards ..... 12-24
12.5.1 Implications of Groundwater Hazards for Transportation Projects ..... 12-25
12.5.2 Identification and Characterization of Groundwater Hazards ..... 12-26
12.6 Landslide and Rockfall Hazards ..... 12-27
12.6.1 Implications of Landslide and Rockfall Hazards for Transportation Projects ..... 12-27
12.6.2 Identification and Characterization of Landslide and Rockfall Hazards ..... 12-28

12.7 Landfill and Geoenvironmental Hazards ..... 12-32

12.7.1 Implications of Landfill and Geoenvironmental Hazards for Transportation Projects ..12-32
12.7.2 Identification and Characterization of Landfill and Geoenvironmental Hazards ..... 12-33

Chapter 13 Documentation, Reporting, and Communication for Site Characterization ..... 13-1

13.1 Objectives for Documentation and Reporting of Site Characterization ..... 13-1
13.2 Documentation and Reporting of Laboratory and Field Test Measurements ..... 13-1
13.3 Documentation and Reporting for Design Parameters ..... 13-3
13.4 Geotechnical Baseline Reports ..... 13-5
13.5 General Forms of Documentation for Site Characterization ..... 13-6

13.5.1 Site Plans ..... 13-6
13.5.2 Final Field Investigation Logs ..... 13-7
13.5.3 Laboratory Test Reports ..... 13-11
13.5.4 Design Profiles and Design Cross-sections ..... 13-11
13.5.5 Observations from Field Instrumentation ..... 13-16

13.6 Geotechnical Data Management Systems ..... 13-1

Chapter 14 References ..... 14-1

# LIST OF APPENDICES

Appendix 1 – ASTM/AASHTO Standards Referenced ..... A-1
Appendix 2 – Examples ..... A-2
Appendix 3 – Statistics of Geotechnical Site Characterization ..... A-3

THIS PAGE IS LEFT INTENTIONALLY BLANK

# LIST OF FIGURES

FIGURE 3-1 CORROSION-RISK RATINGS FROM THE NRCS WEB SOIL SURVEY INTERACTIVE TOOL (NRCS, 2016). ....3-6
FIGURE 3-2 USGS TOPOGRAPHIC MAP (NRCS, 2016). ....3-6
FIGURE 3-3 AREAS OF KNOWN DAMAGE FROM 1993 MIDWEST FLOODS (COURTESY COMMUNITY COMMONS). ....3-7
FIGURE 3-4 KARSTIC CONDITIONS AND LOCATIONS OF KNOWN SINKHOLES (COURTESY COMMUNITY COMMONS). ....3-7
FIGURE 3-5 AERIAL PHOTOGRAPH (LEFT) AND ASSOCIATED "BARE-EARTH" LIDAR IMAGE (RIGHT) OF VEGETATED AREA (FROM ANDERSON, 2013). ....3-9
FIGURE 3-6 ALTERNATIVE SAMPLES OF SIZE $n$=4 FROM POPULATION OF SIMULATED *Su* MEASUREMENTS: (A) POPULATION, (B) SUBSAMPLE ONE, (C) SUBSAMPLE TWO, AND (D) SUBSAMPLE THREE. ....3-14
FIGURE 3-7 ALTERNATIVE SAMPLES OF SIZE $n$=20 FROM POPULATION OF SIMULATED *Su* MEASUREMENTS: (A) POPULATION, (B) SUBSAMPLE ONE, (C) SUBSAMPLE TWO, AND (D) SUBSAMPLE THREE. .... 3-14
FIGURE 3-8 HISTOGRAMS OF MEAN *Su* FROM SUBSAMPLES OF SIZE: (A) $n$=5, AND (B) $n$=20. ....3-16
FIGURE 3-9 INTERPRETED MEAN $su$ FROM SUBSAMPLES OF DIFFERENT SIZES: (A) RELATIVELY UNIFORM SITE, AND (B) HIGHLY VARIABLE SITE (ADAPTED FROM LOEHR, ET AL., 2015)....3-17
FIGURE 3-10 SIMULATED POPULATIONS OF *Su* MEASUREMENTS FOR: (A) RELATIVELY UNIFORM SITE AND (B) HIGHLY VARIABLE SITE....3-18
FIGURE 3-11 RANGES OF *COVμsu* TERMINED FROM SUBSAMPLES OF DIFFERENT SIZES FOR: (A) RELATIVELY UNIFORM SITE AND (B) HIGHLY VARIABLE SITE (ADAPTED FROM LOEHR, ET AL., 2015). ....3-20
FIGURE 3-12 PERCENTAGES OF SPREAD FOOTINGS THAT PRACTICALLY ACHIEVE TARGET PROBABILITY OF FAILURE WHEN DESIGNED USING AASHTO LRFD PROVISIONS FOR A RELATIVELY UNIFORM SITE: (A) "SATISFACTORY" CASES, AND (B) "UNDER-RELIABLE" AND "OVER-RELIABLE" CASES (ADAPTED FROM LOEHR, ET AL., 2015). ....3-22
FIGURE 3-13 PERCENTAGES OF SPREAD FOOTINGS THAT PRACTICALLY ACHIEVE TARGET PROBABILITY OF FAILURE WHEN DESIGNED USING AASHTO LRFD PROVISIONS FOR A VARIABLE SITE: (A) "SATISFACTORY" CASES, AND (B) "UNDER-RELIABLE" AND "OVER-RELIABLE" CASES, (ADAPTED FROM LOEHR, ET AL., 2015). ....3-22

FIGURE 3-14 PERCENTAGES OF SPREAD FOOTINGS THAT PRACTICALLY ACHIEVE TARGET PROBABILITY OF FAILURE WHEN DESIGNED USING MODOT LRFD PROVISIONS FOR A UNIFORM SITE: (A) "SATISFACTORY" CASES, AND (B) "UNDER-RELIABLE" AND "OVER-RELIABLE" CASES (ADAPTED FROM LOEHR, ET AL., 2015). ....3-23
FIGURE 3-15 EMPIRICAL TRANSFORMATION BETWEEN *Is* AND $q_u$ (DENOTED AS $UCS$) FROM RUSNAK AND MARK (2000). ....3-27
FIGURE 4-1 GRAIN-SIZE DISTRIBUTION CURVES FOR TWO COARSE-GRAINED SOILS. ....4-4
FIGURE 4-2 PARTICLE SHAPES FOR COARSE-GRAINED SOILS (FROM MITCHELL AND SOGA, 2005). ....4-6
FIGURE 4-3 CONCEPTUAL MODEL OF ATTERBERG LIMITS (FROM CODUTO, 2001). ....4-10
FIGURE 4-4 IDEALIZED RELATION BETWEEN VOLUME AND WATER CONTENT OF SOIL INCLUDING ATTERBERG LIMITS. ....4-10
FIGURE 4-5 EQUIPMENT USED FOR DETERMINING LIQUID LIMIT BY CASAGRANDE CUP METHOD....4-11
FIGURE 4-6 FALL CONE EQUIPMENT USED FOR DETERMINING LIQUID LIMIT. ....4-12
FIGURE 4-7 DETERMINATION OF LIQUID LIMIT FROM FALL CONE TEST ACCORDING TO BRITISH STANDARD BS1377 (ADAPTED FROM AZADI AND MONFARED, 2012). ....4-12
FIGURE 4-8 MINERALOGICAL CHARACTERIZATION OF A NATURAL CLAY: (A) NATURAL WATER CONTENT AND ATTERBERG LIMITS, (B) RELATIVE ABUNDANCE OF MINERALS FROM BULK SAMPLE, AND (C) RELATIVE ABUNDANCE OF MINERALS FROM CLAY-SIZE FRACTION. ....4-16
FIGURE 4-9 GENERAL SEQUENCE FOR SITE CHARACTERIZATION. ....4-23
FIGURE 4-10 SUMMARY OF MAJOR SOIL TYPES IDENTIFIED BY USCS (FROM HOLTZ ET, AL., 2011). ....4-24
FIGURE 4-11 CASAGRANDE PLASTICITY CHART FOR CLASSIFICATION OF FINE-GRAINED SOILS (FROM ASTM D2487, 2011). ....4-25
FIGURE 4-12 AASHTO SOIL CLASSIFICATIONS FOR FINE-GRAINED SOILS (FROM ASTM D3282, 2015). ....4-27
FIGURE 4-13 SUBSURFACE PROFILE DERIVED FROM CPT MEASUREMENTS (FROM MAYNE, 2007) ....4-29
FIGURE 4-14 SOIL BEHAVIOR TYPE ($SBT$) CHARTS FOR CPT MEASUREMENTS: (A) ORIGINAL CHART FROM ROBERTSON ET AL. (1986), AND (B) UPDATED CHART FROM ROBERTSON (2010). ....4-31
FIGURE 4-15 SOIL BEHAVIOR TYPE ($SBT$) CHART FOR CPTU MEASUREMENTS (FROM ROBERTSON ET AL., 1986). ....4-32
FIGURE 4-16 SOIL BEHAVIOR TYPE ($SBTn$) CHART FOR NORMALIZED CPT AND CPTU MEASUREMENTS (FROM ROBERTSON, 1990). ....4-33
FIGURE 4-17 SOIL BEHAVIOR TYPE CHART FROM ROBERTSON (2010) WITH CONTOURS OF (FROM ROBERTSON, 2010). ....4-34

FIGURE 4-18 USE OF SCPT TO DISTINGUISH CEMENTED FROM UNCEMENTED SOILS (FROM MAYNE ET AL., 2009). ....4-36
FIGURE 4-19 APPROXIMATE RELATIONSHIP BETWEEN CPT $Ic - RW$ AND DMT $ID$ (FROM ROBERTSON, 2009). ....4-37
FIGURE 4-20 INSTRUMENTED DRILL RIG TO MEASURE DRILLING PARAMETERS. ....4-43
FIGURE 4-21 TYPICAL FINAL LOGS OF DRILLING PARAMETERS. ....4-44
FIGURE 5-1 GIBBS AND BARA (1967) CRITERION FOR COLLAPSIBLE SOILS (CASE I-COLLAPSE; CASE III- EXPANSION). ....5-7
FIGURE 5-2 RESULTS FROM SINGLE-OEDOMETER COLLAPSE TEST FOR SOUTHEAST IOWA LOESS. ....5-9
FIGURE 5-3 RESULTS OF DOUBLE OEDOMETER COLLAPSE TEST FOR UNDISTURBED NEBRASKA LOESS. .5-9
FIGURE 5-4 DISTRIBUTION OF EXPANSIVE SOILS IN THE U.S. (OLIVE ET AL., 1989; FROM GEOLOGY.COM). ....5-12
FIGURE 5-5 COMMON CRACKING PATTERN IN LIGHTLY LOADED STRUCTURES ON EXPANSIVE SOILS. ..5-13
FIGURE 5-6 CHARACTERIZATION OF SWELL POTENTIAL FROM CLAY-SIZE FRACTION AND ACTIVITY (AFTER SEED, ET AL., 1962). ....5-14
FIGURE 5-7 CHARACTERIZATION OF SWELL POTENTIAL FROM CLAY-SIZE FRACTION AND PLASTICITY INDEX (AFTER VAN DER MERE, 1964). ....5-15
FIGURE 5-8 CHARACTERIZATION OF SWELLING SEVERITY FROM HOLTZ AND GIBBS (1956). ....5-16
FIGURE 5-9 FINAL VOLUME FROM FREE SWELL TEST FOR KAOLINITE (LEFT) AND MONTMORILLONITE (RIGHT). ....5-17
FIGURE 5-10 EXAMPLE MEASUREMENTS FROM ONE-DIMENSIONAL SWELL TEST ON HIGHLY PLASTIC CLAY. ....5-18
FIGURE 5-11 RELOADING TEST ON SPECIMEN FROM FIGURE 5-10 TO DETERMINE SWELL PRESSURE. ...5-19
FIGURE 5-12 COMPARISON OF SWELL BEHAVIOR BETWEEN UNDISTURBED AND REMOLDED SOIL. ....5-20
FIGURE 5-13 IDEALIZED SHRINKAGE CURVE FOR AN INITIALLY SATURATED SOIL. ....5-21
FIGURE 5-14 MEASURED SHRINKAGE CURVES USING SHRINKAGE LIMIT DISH AND LINEAR SHRINKAGE MOLD (FROM CERATO AND LUTENEGGER, 2006). ....5-22
FIGURE 5-15 ONE-DIMENSIONAL CONSOLIDATION TEST MEASUREMENTS FOR PEAT FROM PITTSFIELD, MA. ....5-26
FIGURE 5-16 VALUES OF NATURAL WATER CONTENT AND COMPRESSION INDEX FOR PEATS, CLAYS, AND SILTS (FROM MESRI, ET AL., 1997). ....5-26
FIGURE 5-17 IDENTIFICATION OF DISPERSIVE SOILS FROM $TDS$ AND $ESP$ (FROM SHERARD, ET AL., 1976B). ....5-29

FIGURE 5-18 SCHEMATIC OF PINHOLE TEST FOR CHARACTERIZING DISPERSIVE SOIL (FROM ASTM D4647, 2013).....5-30
FIGURE 5-19 LIQUEFACTION POTENTIAL CHARTS FOR SPT MEASUREMENTS (FROM YOUD, ET AL., 2001).....5-32
FIGURE 5-20 LIQUEFACTION POTENTIAL CHARTS FOR CPT MEASUREMENTS (FROM YOUD, ET AL., 2001).....5-33
FIGURE 5-21 LIQUEFACTION POTENTIAL CHART FOR SHEAR WAVE VELOCITY MEASUREMENTS (FROM ANDRUS AND STOKOE, 2000).....5-33
FIGURE 5-22 MAP OF LARGE-SCALE OCCURRENCES OF WEAK ROCK IN THE U.S. (FROM SANTI, 2006). .....5-38
FIGURE 5-23 FRANKLIN'S SHALE RATING SYSTEM (FROM WALKINSHAW AND SANTI, 1996).....5-39
FIGURE 5-24 TYPICAL STRESS-STRAIN-VOLUME CHANGE RESPONSE FOR CEMENTED SANDS: (A) STRESS-STRAIN RESPONSE, AND (B) PEAK STRESS FAILURE ENVELOPES (FROM CLOUGH, ET AL., 1981). .....5-45
FIGURE 5-25 SENSITIVITY OF MARINE CLAYS AS RELATED TO LIQUIDITY INDEX (FROM HOLTZ AND KOVACS, 1981).....5-48
FIGURE 5-26 TYPICAL SOIL PROFILES IN PERMAFROST: CONTINUOUS PERMAFROST (LEFT) AND DISCONTINUOUS PERMAFROST (RIGHT) (FROM BROWN, 1970).....5-55
FIGURE 6-1 IDEALIZED CONSOLIDATION TEST PLOTTED IN TERMS OF VOID RATIO. .....6-2
FIGURE 6-2 COMMON ALTERNATIVE PRESENTATIONS FOR CONSOLIDATION TESTS: (A) LOG OF EFFECTIVE VERTICAL STRESS VS. VERTICAL STRAIN, AND (B) NATURAL LOG OF EFFECTIVE VERTICAL STRESS VS. SPECIFIC VOLUME. .....6-4
FIGURE 6-3 INTERPRETATION OF PRECONSOLIDATION STRESS FROM ONE-DIMENSIONAL CONSOLIDATION TESTS.....6-7
FIGURE 6-4 INFLUENCE OF SAMPLING METHOD ON CONSOLIDATION TEST RESULTS (BOZOZUK, 1970). .6-8
FIGURE 6-5 COMPARISON OF CONSOLIDATION TESTS FOR SPECIMENS ACQUIRED FROM BLOCK SAMPLES, FIXED PISTON SAMPLES FOR BORINGS ADVANCED USING DRILLING MUD, AND FREE PISTON SAMPLES FOR BORINGS ADVANCED WITHOUT DRILLING MUD (FROM LANDON, ET AL., 2007). .....6-9
FIGURE 6-6 RESULTS FROM CONSOLIDATION TESTS FOR SAMPLES OF STIFF GLACIAL TILL OF VARYING QUALITY (FROM HOLTZ AND KOVACS, 1981; AFTER SODERMAN AND KIM, 1970). .....6-10
FIGURE 6-7 SCHEMATIC OF INCREMENTAL LOAD OEDOMETER CELL (FROM GERMAINE AND GERMAINE, 2009). .....6-11
FIGURE 6-8 MEASURED RESPONSE FROM AN INCREMENTAL LOAD CONSOLIDATION TEST. .....6-11
FIGURE 6-9 SCHEMATIC OF CRS OEDOMETER CELL (ASTM D4186, 2012). .....6-12
FIGURE 6-10 MEASURED RESPONSE FROM A CRS CONSOLIDATION TEST. .....6-13

FIGURE 6-11 ILLUSTRATION OF CASAGRANDE METHOD FOR INTERPRETING PRECONSOLIDATION STRESS. ....6-14
FIGURE 6-12 ILLUSTRATION OF STRAIN-ENERGY METHOD FOR INTERPRETING PRECONSOLIDATION STRESS. ....6-15
FIGURE 6-13 INFLUENCE OF STRAIN RATE ON INTERPRETED PRECONSOLIDATION STRESS FOR SEVERAL CLAYS (SOGA AND MITCHELL, 1996). ....6-17
FIGURE 6-14 VARIATION IN PRECONSOLIDATION STRESS WITH TEMPERATURE FOR SEVERAL CLAYS (FROM LEROUEIL AND MARQUES, 1996). ....6-17
FIGURE 6-15 CONSOLIDATION TEST MEASUREMENTS PLOTTED AS STRESS VERSUS STRAIN USING: (A) LOGARITHMIC SCALE, AND (B) ARITHMETIC SCALE (ADAPTED FROM KARLSRUD AND HERNANDEZ-MARTINEZ, 2013) ....6-18
FIGURE 6-16 TANGENT MODULUS VS. EFFECTIVE STRESS SHOWING ESTIMATE FOR PRECONSOLIDATION STRESS (ADAPTED FROM KARLSRUD AND HERNANDEZ-MARTINEZ, 2013). ....6-19
FIGURE 6-17 SCHMERTMANN (1955) METHOD TO OBTAIN FIELD CONSOLIDATION CURVE FOR NORMALLY CONSOLIDATED SOILS (FROM HOLTZ ET AL., 2011). ....6-21
FIGURE 6-18 SCHMERTMANN (1955) METHOD TO OBTAIN FIELD CONSOLIDATION CURVE FOR OVERCONSOLIDATED SOILS (FROM HOLTZ ET AL., 2011) ....6-22
FIGURE 6-19 CASAGRANDE'S LOG TIME METHOD FOR DETERMINING THE COEFFICIENT OF CONSOLIDATION. ....6-24
FIGURE 6-20 TAYLOR'S SQUARE ROOT OF TIME METHOD FOR DETERMINING THE COEFFICIENT OF CONSOLIDATION. ....6-24
FIGURE 6-21 COEFFICIENTS OF CONSOLIDATION DETERMINED USING THE LOG TIME AND SQUARE ROOT TIME METHODS FOR DIFFERENT APPLIED EFFECTIVE STRESS. ....6-25
FIGURE 6-22 EVALUATION OF $C\alpha$ FROM TIME-DEFORMATION RESPONSE FOR IL CONSOLIDATION TEST INCREMENT. ....6-27
FIGURE 6-23 TRANSFORMATION FROM CORRECTED NET CONE TIP RESISTANCE TO PRECONSOLIDATION STRESS, OR "YIELD STRESS" (FROM MAYNE, 2014) ....6-29
FIGURE 6-24 TRANSFORMATIONS FROM MEASURED CPTU PORE PRESSURE TO PRECONSOLIDATION STRESS FOR CLAYS: (A) TYPE 1 PIEZOCONES, AND (B) TYPE 2 PIEZOCONES (FROM MAYNE, 2007). ....6-30
FIGURE 6-25 TRANSFORMATION FROM DMT $p_o$ TO PRECONSOLIDATION STRESS (FROM MAYNE, 1995). ....6-32
FIGURE 6-26 TRANSFORMATION FROM FIELD VANE SHEAR STRENGTH TO PRECONSOLIDATION STRESS (FROM MAYNE AND MITCHELL, 1988). ....6-33

FIGURE 6-27 RELATIONSHIP BETWEEN $\alpha_{FV}$ AND PLASTICITY INDEX (FROM MAYNE AND MITCHELL, 1988). ..... 6-33
FIGURE 6-28 TRANSFORMATION FROM SELF-BORING PMT $p_L$ TO PRECONSOLIDATION STRESS (FROM KULHAWY AND MAYNE, 1990). ..... 6-34
FIGURE 6-29 TRANSFORMATION FROM PMT UNDRAINED SHEAR STRENGTH AND RIGIDITY INDEX TO PRECONSOLIDATION STRESS (FROM KULHAWY AND MAYNE, 1990). ..... 6-34
FIGURE 6-30 TRANSFORMATION FROM SPT $N_{60}$ TO $\sigma'_p$ (FROM MAYNE, 1995). ..... 6-35
FIGURE 6-31 PORE PRESSURE DISSIPATION MEASUREMENTS FROM CPTU IN SOFT, CLAYEY SILT. ..... 6-36
FIGURE 6-32 NORMALIZED PORE PRESSURE DISSIPATION FOR MEASUREMENTS IN FIGURE 6-31. ..... 6-38
FIGURE 6-33 RELATION BETWEEN RIGIDITY INDEX AND *OCR* (FROM MAYNE, 2007) ..... 6-39
FIGURE 6-34 ROBERTSON ET AL. (1992) CHART FOR DETERMINING $c_h$ FROM $t_{50}$ (FROM SCHNAID, 2009) ..... 6-39
FIGURE 6-35 MEASUREMENTS FROM DMTA AND DMTC DISSIPATION TESTS IN CLAY FOR TWO DIFFERENT DEPTHS. ..... 6-40
FIGURE 6-36 CORRELATION BETWEEN PLASTICITY INDEX AND RECOMPRESSION AND COMPRESSION PARAMETERS (FROM KULHAWY AND MAYNE, 1990). ..... 6-44
FIGURE 6-37 CORRELATION OF COEFFICIENT OF CONSOLIDATION TO LIQUID LIMIT (NAVFAC, 1986). ..... 6-46
FIGURE 6-38 TYPICAL RELATIONSHIP BETWEEN $C_{\alpha\varepsilon}$ AND $C_c$ FOR TWO CLAYS (FROM MESRI, ET AL., 1995). ..... 6-47
FIGURE 6-39 GENERALIZED RELATIONSHIP BETWEEN PRECONSOLIDATION STRESS AND LIQUIDITY INDEX (NAVFAC, 1986). ..... 6-48
FIGURE 7-1 MOHR-COULOMB DIAGRAM SHOWING MOHR'S CIRCLES REPRESENTING FAILURE AND STABLE STATE OF STRESS ..... 7-2
FIGURE 7-2 MOHR-COULOMB DIAGRAM SHOWING STATES OF STRESS AT FAILURE FOR TESTS PERFORMED AT DIFFERENT EFFECTIVE CONFINING STRESS. ..... 7-3
FIGURE 7-3 MODIFIED MOHR-COULOMB DIAGRAM SHOWING STATE OF STRESS AT FAILURE AND STABLE STATE OF STRESS. ..... 7-4
FIGURE 7-4 MODIFIED MOHR-COULOMB DIAGRAM SHOWING SAME STATES OF STRESS AS SHOWN IN FIGURE 7-2 ..... 7-5
FIGURE 7-5 STRESS-STRAIN RESPONSE FOR KAOLINITE SPECIMENS SHOWING TWO ALTERNATIVE FAILURE CRITERIA: (A) NORMALLY CONSOLIDATED CONDITION AND (B) OVERCONSOLIDATED CONDITION. ..... 7-6

FIGURE 7-6 DRAINED STRESS-STRAIN BEHAVIOR SHOWING STRAIN SOFTENING RESPONSE TYPICAL OF STIFF, HEAVILY OVERCONSOLIDATED CLAYS. ..... 7-7
FIGURE 7-7 MOHR'S CIRCLE AT FAILURE SHOWING ALTERNATIVE VALUES OF SHEAR STRESS USED TO DEFINE SHEAR STRENGTH. ..... 7-8
FIGURE 7-8 MODIFIED MOHR-COULOMB DIAGRAM SHOWING DRAINED STRESS PATHS AND DRAINED SHEAR STRENGTHS FOR TRIAXIAL EXTENSION, DIRECT SIMPLE SHEAR, AND TRIAXIAL COMPRESSION TESTS. ..... 7-10
FIGURE 7-9 MODIFIED MOHR-COULOMB DIAGRAMS SHOWING UNDRAINED STRESS PATHS AND SHEAR STRENGTHS FOR TRIAXIAL EXTENSION, DIRECT SIMPLE SHEAR, AND TRIAXIAL COMPRESSION TESTS: (A) NORMALLY CONSOLIDATED CONDITION AND (B) OVERCONSOLIDATED CONDITION. ..... 7-11
FIGURE 7-10 SHEARING MODES ALONG DIFFERENT PORTIONS OF A POTENTIAL SLIDING SURFACE FOR AN EMBANKMENT ON A SOFT FOUNDATION. ..... 7-13
FIGURE 7-11 TOTAL STRESS STRENGTH ENVELOPES FOR UNSATURATED SOILS: (A) MOHR-COULOMB DIAGRAM AND (B) MODIFIED MOHR-COULOMB DIAGRAM. ..... 7-14
FIGURE 7-12 TOTAL STRESS STRENGTH ENVELOPES FOR SATURATED SOILS ($\phi = 0$): (A) MOHR-COULOMB DIAGRAM AND (B) MODIFIED MOHR-COULOMB DIAGRAM. ..... 7-15
FIGURE 7-13 STRESS-STRAIN RESPONSE FOR NORMALLY CONSOLIDATED KAOLINITE: (A) MEASURED RESPONSE, AND (B) NORMALIZED RESPONSE. ..... 7-16
FIGURE 7-14 MEASURED $s_u/\sigma'_{vc}$ FOR KAOLINITE SPECIMENS AT DIFFERENT $OCR$. ..... 7-17
FIGURE 7-15 STRESS-INDUCED ANISOTROPY FOR UNDRAINED SHEAR STRENGTH OF NORMALLY CONSOLIDATED CLAYS (LADD, 1991). ..... 7-18
FIGURE 7-16 MEASURED INHERENT ANISOTROPY FOR SEVERAL STIFF CLAYS AND SHALES (DUNCAN, ET AL., 2014). ..... 7-19
FIGURE 7-17 INFLUENCE OF STRAIN RATE ON LABORATORY $S_u$ FROM DIFFERENT TEST METHODS (KULHAWY AND MAYNE, 1990). ..... 7-19
FIGURE 7-18 REDUCTION OF UNDRAINED SHEAR STRENGTH FOR SILTY CLAY WITH NUMBER OF LOADING CYCLES (SEED AND WILSON, 1967) ..... 7-20
FIGURE 7-19 STRESS-STRAIN RESPONSE FOR UU TRIAXIAL COMPRESSION TEST ON SATURATED KAOLINITE. ..... 7-22
FIGURE 7-20 STRESS-STRAIN RESPONSE FOR UU TRIAXIAL COMPRESSION TESTS ON IDENTICAL SPECIMENS OF SATURATED KAOLINITE. ..... 7-23
FIGURE 7-21 INTERPRETATION OF FAILURE ENVELOPE FROM TESTS ON FIVE IDENTICAL SPECIMENS OF SATURATED KAOLINITE: (A) MOHR-COULOMB DIAGRAM AND (B) MODIFIED MOHR-COULOMB DIAGRAM. ..... 7-23

FIGURE 7-22 SUCCESSIVE STATES OF STRESS FOR UNCONFINED COMPRESSION TEST ..... 7-24
FIGURE 7-23 STRESS PATHS FROM *CU* TRIAXIAL COMPRESSION TESTS. ..... 7-26
FIGURE 7-24 COMPARISON OF $s_u/(\sigma'_{vc})$ RELATIONSHIP FOR CIUC AND DSS TESTS FOR SILTY CLAY. ..... 7-27
FIGURE 7-25 NORMALIZED STRESS-STRAIN RESPONSE FOR NORMALLY CONSOLIDATED SPECIMENS WITH VARYING LEVELS OF DISTURBANCE (FROM SANTAGATA AND GERMAINE, 2002). ..... 7-28
FIGURE 7-26 CONSOLIDATION FOR SHANSEP METHOD TO ACHIEVE A KNOWN (ADAPTED FROM LADD AND FOOTT, 1974). ..... 7-30
FIGURE 7-27 EVALUATION OF WHETHER SOIL IS "NORMALIZABLE". ..... 7-31
FIGURE 7-28 EMPIRICALLY DERIVED CORRECTION FOR FIELD VANE SHEAR TEST (FVT, OR VST). ..... 7-33
FIGURE 7-29 COMPARISON OF $S_u$ DERIVED FROM DIFFERENT IN SITU TEST MEASUREMENTS USING "GENERAL" TRANSFORMATIONS (AFTER FINNO AND CHUNG, 1992). ..... 7-34
FIGURE 7-30 CORRECTION FACTOR FOR FVT MEASUREMENTS FROM ASTM D2573 (AFTER CHANDLER, 1988). ..... 7-35
FIGURE 7-31 INTERPRETATION OF $S_u$ FROM PRESSUREMETER TEST (FROM SOLEIMANBEIGI, 2013)..... 7-36
FIGURE 7-32 EMPIRICAL MEASUREMENTS RELATING $S_u$ TO DMT HORIZONTAL STRESS INDEX, (FROM SCHNAID, 2009)..... 7-38
FIGURE 7-33 NORMALIZED UNDRAINED SHEAR STRENGTH FROM DSS TESTS FOR SEVERAL DIFFERENT CLAYS (FROM HOLTZ AND KOVACS, 1981, AFTER LADD, ET AL., 1977)..... 7-40
FIGURE 7-34 COMPARISON OF $S_u$ INTERPRETATIONS FROM: (A) SHANSEP USING CIUC TRIAXIAL, (B) UU- TRIAXIAL COMPRESSION, (C) UNCONFINED COMPRESSION, AND (D) TORVANE TESTS. ..... 7-43
FIGURE 7-35 COMPARISON OF RELATIVE $S_u$ VALUES DETERMINED FROM DIFFERENT TESTING METHODS: (A) UNCORRECTED VALUES AND (B) VALUES CORRECTED FOR STRAIN RATE AND SECONDARY COMPRESSION. ..... 7-43
FIGURE 7-36 INTERPRETATION OF TOTAL STRESS STRENGTH ENVELOPE FROM UU TRIAXIAL COMPRESSION TESTS ON UNSATURATED COMPACTED CLAYEY SILT..... 7-47
FIGURE 7-37 INTERPRETATION OF *CU* TRIAXIAL COMPRESSION TESTS TO ESTABLISH EFFECTIVE STRESS SHEAR STRENGTH PARAMETERS. ..... 7-49
FIGURE 7-38 ILLUSTRATION OF INTERPRETATION OF DIRECT SHEAR TEST. ..... 7-51
FIGURE 7-39 EFFECTIVE STRESS STRENGTH ENVELOPES DETERMINED FROM DIRECT SHEAR AND TRIAXIAL TESTS. ..... 7-52
FIGURE 7-40 FAILURE ENVELOPES FROM BOREHOLE SHEAR TESTS (FROM LUTENEGGER AND POWELL, 2008). ..... 7-54
FIGURE 7-41 CHART RELATING $\phi'$ TO SPT $N_{60}$-VALUE AND $\sigma'_{vo}$ (AFTER SCHMERTMANN, 1975). ..... 7-55

FIGURE 7-42 RELATION FOR $\phi'$ FROM CPT $q_t$ AND $\sigma'_{vo}$ (AFTER ROBERTSON AND CAMPANELLA, 1983). ..... 7-56
FIGURE 7-43 RELATION BETWEEN $\phi'$, $Dr$, AND $\sigma'_v$ FOR SANDS (FROM ANDERSEN AND SCHJETNE, 2013). ..... 7-58
FIGURE 7-44 EFFECTIVE STRESS FRICTION ANGLES FOR ROCK FILL AND GRAVELS (FROM DUNCAN, ET AL., 2014). ..... 7-58
FIGURE 7-45 ESTIMATES OF $\phi'$ BASED ON PLASTICITY INDEX, (ADAPTED FROM TERZAGHI, ET AL., 1996) ..... 7-59
FIGURE 7-46 SHEAR STRESS VERSUS CUMULATIVE DISPLACEMENT FROM DIRECT-RESIDUAL SHEAR TEST ..... 7-60
FIGURE 7-47 COMPARISON OF PEAK AND RESIDUAL STRENGTH ENVELOPES FROM DIRECT-RESIDUAL SHEAR TEST ..... 7-61
FIGURE 7-48 EMPIRICAL ESTIMATES FOR DRAINED RESIDUAL FRICTION ANGLE FROM LIQUID LIMIT AND CLAY SIZE FRACTION (FROM STARK AND HUSSAIN, 2013) ..... 7-62
FIGURE 7-49 ESTIMATED DRAINED, FULLY SOFTENED FRICTION ANGLE FROM *LL* AND *CF* (FROM STARK AND HUSSAIN, 2013) ..... 7-63
FIGURE 7-50 PROCTOR CURVE FOR COMPACTED SILTY CLAY SHOWING REGION OF COMPACTION SPECIFICATION AND COMPACTION CONDITIONS FOR "WET" AND "DRY" SPECIMENS USED FOR SOIL STRENGTH TESTING. ..... 7-65
FIGURE 7-51 TOTAL STRESS SHEAR STRENGTH ENVELOPES DETERMINED FROM UU TRIAXIAL COMPRESSION TESTS FOR SILTY CLAY SPECIMENS COMPACTED "WET" AND "DRY" ..... 7-65
FIGURE 7-52 EFFECTIVE STRESS STRENGTH ENVELOPES DETERMINED FROM CU TYPE TRIAXIAL COMPRESSION TESTS FOR SPECIMENS COMPACTED "WET" AND "DRY" OF STANDARD PROCTOR OPTIMUM MOISTURE CONTENT. ..... 7-66
FIGURE 8-1 NONLINEAR STIFFNESS OF SOIL IN SHEAR: (A) GENERAL STRESS-STRAIN RESPONSE, AND (B) SECANT SHEAR MODULUS AT DIFFERENT STRAIN LEVELS. ..... 8-3
FIGURE 8-2 VARIATION OF SHEAR MODULUS WITH SHEARING STRAIN. ..... 8-4
FIGURE 8-3 VARIATION IN SMALL-STRAIN MODULUS MEASURED IN THE LAB AND FIELD (STOKOE AND SANTAMARINA, 2000). ..... 8-5
FIGURE 8-4 COMMON INTRUSIVE METHODS TO MEASURE SMALL-STRAIN VELOCITY: (A) CROSSHOLE, (B) DOWNHOLE, (C) SEISMIC CPT, AND (D) SUSPENSION LOGGING (STOKOE AND SANTAMARINA, 2000) ..... 8-8
FIGURE 8-5 DATA COLLECTION METHODS FOR REFLECTION SURVEYS: (A) NORMAL MOVEOUT (B) COMMON OFFSET AND (C) COMMON DEPTH POINT (STOKOE AND SANTAMARINA, 2000). ..... 8-11

FIGURE 8-6 GENERAL TESTING ARRANGEMENT FOR REFRACTION SURVEYS SHOWING ARRIVAL OF CRITICALLY REFRACTED WAVES (STOKOE AND SANTAMARINA, 2000).....8-12
FIGURE 8-7 DATA COLLECTION ARRANGEMENT FOR SASW SURFACE WAVE METHOD (STOKOE AND SANTAMARINA, 2000). .....8-13
FIGURE 8-8 SHEAR MODULUS FOR UNDISTURBED AND DISTURBED DENSE SAND (FROM ISHIHARA, 1996).....8-16
FIGURE 8-9 SHEAR WAVE VELOCITY VERSUS $N$-VALUE RELATIONSHIP FROM OHTA AND GOTO (1978). .....8-19
FIGURE 8-10 ARITHMETIC PLOT OF $V_S$ VERSUS $N$-VALUE (FROM SYKORA AND STOKOE, 1983). .....8-20
FIGURE 8-11 MEASUREMENTS USED TO DEVELOP TRANSFORMATIONS BETWEEN CONE TIP RESISTANCE AND: (A) $G_{MAX}$ (MAYNE AND RIX, 1993), AND (B) $V_S$ (MAYNE AND RIX, 1995).....8-21
FIGURE 8-12 RATIO OF $G_{MAX}/E_D$ AS A FUNCTION OF: (A) $K_D$, AND (B) $I_D$ (MARCHETTI, ET AL., 2008).....8-22
FIGURE 8-13 MODULUS REDUCTION CURVES FOR FINE-GRAINED SOILS OF DIFFERENT PLASTICITY (VUCETIC AND DOBRY, 1991). .....8-24
FIGURE 8-14 MODULUS VARIATION WITH STRAIN COMPARED WITH STRAIN RANGE OF COMMON FIELD TESTS. .....8-25
FIGURE 8-15 RECOMMENDED MODULUS DEGRADATION RATIO FOR INTACT CLAYS AND UNCEMENTED SANDS. .....8-27
FIGURE 8-16 TYPICAL MEASUREMENTS FROM A PRE-BORED PRESSUREMETER TEST. .....8-28
FIGURE 8-17 EXAMPLE $p$-$y$ CURVE (REESE ET AL., 2006). .....8-31
FIGURE 9-1 TYPICAL STRENGTH ENVELOPE FOR INTACT ROCK. .....9-2
FIGURE 9-2 SCHEMATIC ILLUSTRATION OF ROCK MASS SHOWING RELEVANT CHARACTERISTICS THAT AFFECT MECHANICAL BEHAVIOR (WYLLIE, 1999). .....9-4
FIGURE 9-3 EXAMPLE RESULT FROM UNIAXIAL COMPRESSION TEST. .....9-8
FIGURE 9-4 CONSTRUCTION OF MOHR-COULOMB FAILURE ENVELOPE FROM MEASUREMENTS OF TRIAXIAL TESTS ON INTACT ROCK (FROM ASTM D7012, 2014). .....9-10
FIGURE 9-5 RESULTS FROM DIRECT SHEAR TESTS PERFORMED ON INTACT ROCK (FROM ASTM D5607, 2008).....9-10
FIGURE 9-6 COMPARISON OF $q_t$ AND $q_u$ FOR INTACT ROCK SPECIMENS (FROM PERRAS AND DIEDERICHS, 2014). .....9-11
FIGURE 9-7 AXIAL STRESS VERSUS AXIAL STRAIN RESPONSE FROM UNIAXIAL COMPRESSION TEST ON INTACT ROCK. .....9-13

FIGURE 9-8: DIFFERENT METHODS FOR ESTABLISHING YOUNG'S MODULUS FROM UNIAXIAL COMPRESSION TESTS (FROM ASTM D7012, 2014).....9-13
FIGURE 9-9 UNIAXIAL COMPRESSION TEST RESULTS SHOWING $\sigma_a$ VERSUS $\varepsilon_a$ AND $\varepsilon_l$ TO ILLUSTRATE METHOD FOR CALCULATING POISSON'S RATIO (FROM ASTM D7012, 2014). .....9-14
FIGURE 9-10 POINT LOAD STRENGTH INDEX TEST ON SEGMENT OF ROCK CORE. .....9-15
FIGURE 9-11 RELATIONSHIP BETWEEN $I_{s(50)}$ AND $q_u$ FOR SEVERAL ROCK TYPES (AFTER OSOULI, ET AL., 2014). .....9-18
FIGURE 9-12 APPARATUS FOR SCHMIDT HAMMER TEST (PHOTO COURTESY CONTROLS GROUP). .....9-18
FIGURE 9-13 EMPIRICAL TRANSFORMATION FROM SCHMIDT HAMMER REBOUND ($R$) TO (ADAPTED FROM TANDON AND GUPTA, 2015). .....9-19
FIGURE 9-14 RELATIONSHIP BETWEEN STATIC AND DYNAMICS MEASUREMENTS OF CONSTRAINED MODULUS UNDER UNIAXIAL COMPRESSIVE STRESS UP TO 5000 PSI (FROM DEERE AND MILLER, 1966). .....9-21
FIGURE 9-15 EMPIRICAL MEASUREMENTS OF SONIC VELOCITY ($V_p$) AND $q_u$ (FROM TANDON AND GUPTA, 2015). .....9-22
FIGURE 9-16 SPLIT TENSION TEST ON A CYLINDRICAL CONCRETE SPECIMEN (FROM ASTM C496, 2011) .....9-22
FIGURE 9-17 DIP AND DIP DIRECTION FOR A PLANAR FEATURE (HTTP://STRUCTURALGEOLOGY.ORG) ..9-25
FIGURE 9-18 STEREO NET DEVELOPED FROM ACOUSTIC TELEVIEWER MEASUREMENTS (COURTESY OF DAN BROWN AND ASSOCIATES). .....9-26
FIGURE 9-19 DOWNHOLE TELEVIEWER MEASUREMENTS (COURTESY OF DAN BROWN AND ASSOCIATES). .....9-28
FIGURE 9-20 COMPARISON OF DISCONTINUITY ORIENTATION FOR EXPOSED ROCK FACE FROM CONVENTIONAL MAPPING AND AUTOMATED LIDAR MAPPING (FROM KEMENY AND TURNER, 2008). .....9-29
FIGURE 9-21 STANDARD PROFILES FOR DISCONTINUITY ROUGHNESS AND THE JOINT ROUGHNESS COEFFICIENT (AFTER BARTON AND CHOUBEY, 1977). .....9-31
FIGURE 9-22 CARPENTERS "COMB" FOR MEASURING DISCONTINUITY ROUGHNESS (COURTESY OF CONTROLS GROUP). .....9-32
FIGURE 9-23 QUALITATIVE CHART FOR ESTIMATION OF GEOLOGICAL STRENGTH INDEX (GSI) IN ROCK (FROM MARINOS ET AL., 2005). .....9-36
FIGURE 9-24 QUANTITATIVE VERSION OF THE GEOLOGIC STRENGTH INDEX (GSI) CHART (FROM HOEK ET AL., 2013). .....9-39

FIGURE 9-25 QUALITATIVE METHOD FOR ESTABLISHING GSI FOR HETEROGENEOUS ROCK MASSES (FROM MARINOS ET AL., 2005). 9-40
FIGURE 9-26 TYPICAL PRESSURE-DILATION GRAPH FOR BOREHOLE DILATOMETER (AFTER ISRM, 1987). 9-41
FIGURE 9-27 PRESSURE-DISPLACEMENT PLOT FOR BOREHOLE JACK. 9-42
FIGURE 9-28: RELATIONSHIP BETWEEN $E_{true}$ AND $E_{calc}$ (AFTER ASTM D4971). 9-43
FIGURE 9-29 EXAMPLE PLATE LOAD TEST RESULT (FROM COATES AND GYENGE, 1966). 9-44
FIGURE 9-30 RELATIONSHIP BETWEEN *RQD* AND VELOCITY INDEX (FROM COON AND MERRITT, 1970). 9-45
FIGURE 9-31 RIPPABILITY CHART FOR CATERPILLAR D10R RIPPER (CATERPILLAR, 2015). 9-46
FIGURE 9-32 RELATION BETWEEN $E_m$ AND *RMR* (AFTER BIENIAWSKI, 1978; SERAFIM AND PEREIRA, 1983). 9-48
FIGURE 9-33 SIMPLIFIED HOEK AND DIEDERICHS (2006) RELATION FOR ESTIMATING $EM$ FROM $GSI$. . 9-49
FIGURE 9-34 RIGOROUS HOEK AND DIEDERICHS (2006) RELATION FOR ESTIMATING $EM$ FROM $GSI$. . . 9-49
FIGURE 9-35 SHEAR STRENGTH ENVELOPE DEFINED BY HOEK-BROWN FAILURE CRITERION (HOEK, 1983). 9-51
FIGURE 9-36 COMPARISON OF HOEK-BROWN FAILURE CRITERION WITH APPROXIMATE MOHR-COULOMB ENVELOPE (FROM HOEK, ET AL., 2002) 9-54
FIGURE 10-1 GROUNDWATER LEVEL FLUCTUATIONS AT AN ALLUVIAL SITE. 10-3
FIGURE 10-2 MEASURED VALUES OF TOTAL HEAD WITH DEPTH FROM DATA IN FIGURE 10-1. 10-4
FIGURE 10-3 DIAGRAM ILLUSTRATING DARCY'S LAW (FROM DAS, 1985A). 10-5
FIGURE 10-4 CONCEPTUAL PERMEABILITY TESTS: (A) CONSTANT HEAD SETUP, AND (B) FALLING HEAD SETUP (FROM SEVEE, 2006). 10-6
FIGURE 10-5 TYPICAL MONITORING WELL (FROM NIELSEN AND SCHALLA, 2006). 10-9
FIGURE 10-6 STANDPIPE PIEZOMETER INSTALLED IN A BOREHOLE (FROM DUNNICLIFF, 1993). 10-12
FIGURE 10-7 PUSHED/DRIVEN OPEN STANDPIPE PIEZOMETER (FROM DUNNICLIFF, 1993). 10-14
FIGURE 10-8 TWIN-TUBE HYDRAULIC PIEZOMETER (FROM DUNNICLIFF, 1993). 10-15
FIGURE 10-9 TYPICAL PNEUMATIC PIEZOMETER (FROM DUNNICLIFF, 1993). 10-16
FIGURE 10-10 ELECTRICAL RESISTANCE GAGE PIEZOMETER (FROM DUNNICLIFF, 1993). 10-18
FIGURE 10-11 VIBRATING WIRE PIEZOMETER (FROM DUNNICLIFF, 1993). 10-18
FIGURE 10-12 PUSH-IN PNEUMATIC PIEZOMETER (FROM DUNNICLIFF, 1993). 10-19
FIGURE 10-13 ALTERNATIVE METHODS FOR DETERMINING VARIATION OF PORE WATER PRESSURES WITH DEPTH USING PIEZOMETERS (FROM DALTON, ET AL., 1991). 10-20

FIGURE 10-14 EXAMPLE CPTU MEASUREMENTS SHOWING LOCATION OF GROUNDWATER LEVEL IN CLEAN SAND. ..... 10-20
FIGURE 10-15 EXAMPLE CPTU MEASUREMENTS IN CLAYEY SOIL WITH SAND LENSES (FROM MAYNE, 2007). ..... 10-21
FIGURE 10-16 ILLUSTRATION OF TIME-DOMAIN ELECTROMAGNETIC METHOD (FROM WIGHTMAN, ET AL., 2004). ..... 10-23
FIGURE 10-17 SELF-POTENTIAL ANOMALIES FROM FLOWING WATER (WIGHTMAN, ET AL., 2004) ..... 10-24
FIGURE 10-18 TRIMMING ORIENTED SPECIMENS TO DETERMINE HYDRAULIC CONDUCTIVITY ANISOTROPY (FROM CHAPUIS AND GILL, 1989). ..... 10-28
FIGURE 10-19 RELATIONSHIP BETWEEN HYDRAULIC CONDUCTIVITY ANISOTROPY RATIO AND DENSITY INDEX (FROM CHAPUIS AND GILL, 1989). ..... 10-29
FIGURE 10-20 ONE-DIMENSIONAL CONSOLIDATION CELL USED FOR DIRECT MEASUREMENT OF HYDRAULIC CONDUCTIVITY (FROM DANIEL, 1994). ..... 10-31
FIGURE 10-21 DIRECT MEASUREMENT OF HYDRAULIC CONDUCTIVITY IN SHELBY TUBE (FROM DANIEL, 1994). ..... 10-32
FIGURE 10-22 DIRECT MEASUREMENT OF HYDRAULIC CONDUCTIVITY IN COMPACTION MOLD (FROM DANIEL, 1994). ..... 10-33
FIGURE 10-23 SCHEMATIC OF A FLEXIBLE-WALL PERMEAMETER (FROM DANIEL, 1994). ..... 10-35
FIGURE 10-24 SHAPE FACTOR FOR AUGER HOLE SEEPAGE TESTS (FROM SPANGLER AND HANDY, 1973). ..... 10-38
FIGURE 10-25 SCHEMATIC DIAGRAM OF OPEN END PUMPING TEST (FROM SPANGLER AND HANDY, 1973). ..... 10-39
FIGURE 10-26 TYPICAL RESULTS FROM A SLUG TEST IN CLAY (FROM LUTENEGGER AND DEGROOT, 1992). ..... 10-40
FIGURE 10-27 SCHEMATIC OF A BOREHOLE PACKER TEST (SEVEE, 2006). ..... 10-41
FIGURE 10-28 SCHEMATIC OF A GUELPH PERMEAMETER (FROM REYNOLDS AND ELRICK, 1986). ..... 10-42
FIGURE 10-29 VALUES OF CONSTANT $C$ FOR GUELPH PERMEAMETER (FROM DANIEL, 1989). ..... 10-43
FIGURE 10-30 SCHEMATIC OF BOUTWELL PERMEAMETER: (A) STAGE I AND (B) STAGE II (FROM DANIEL, 1989). ..... 10-44
FIGURE 10-31 SCHEMATIC OF A SELF-BORING PERMEAMETER (FROM CHANDLER, ET AL., 1990). ..... 10-45
FIGURE 10-32 SCHEMATIC OF OPEN SINGLE-RING INFILTROMETER (FROM TRAUTWEIN AND BOUTWELL, 1994) ..... 10-49
FIGURE 10-33 SCHEMATIC OF SEALED SINGLE-RING INFILTROMETER (FROM TRAUTWEIN AND BOUTWELL, 1994) ..... 10-50

FIGURE 10-34 SCHEMATIC OF SEALED DOUBLE-RING INFILTROMETER (FROM TRAUTWEIN AND BOUTWELL, 1994).....10-51
FIGURE 10-35 SCHEMATIC OF AIR ENTRY PERMEAMETER (FROM TRAUTWEIN AND BOUTWELL, 1994).....10-52
FIGURE 10-36 SCHEMATIC OF DOUBLE-RING AIR ENTRY PERMEAMETER (FROM TRAUTWEIN AND BOUTWELL, 1994).....10-52
FIGURE 10-37 EMPIRICAL RELATIONSHIP BETWEEN $K_h$ AND CPTU $t_{50}$ (FROM MAYNE, 2007). .....10-55
FIGURE 10-38 BAT SYSTEM FOR DETERMINING HYDRAULIC CONDUCTIVITY (FROM TRAUTWEIN AND BOUTWELL, 1994).....10-56
FIGURE 10-39 HYDRAULIC CONDUCTIVITY FOR SANDS AS A FUNCTION OF POROSITY (FROM SEVEE, 2006).....10-57
FIGURE 10-40 HYDRAULIC CONDUCTIVITY OF A CLAY AS A FUNCTION OF VOID RATIO (LEROUEIL, ET AL., 1983). .....10-60
FIGURE 10-41 RELATIONSHIP BETWEEN $k$ AND $e$ FOR FIVE DIFFERENT CLAYS (FROM TERZAGHI, ET AL., 1996).....10-60
FIGURE 11-1 DESIGN CROSS-SECTION ILLUSTRATING CONCEPTUAL STRATIGRAPHY ADOPTED FOR DESIGN.....11-2
FIGURE 11-2 DESIGN PROFILE SHOWING CONSTANT OR LINEARLY VARYING $q_u$ INTERPRETED FOR INDIVIDUAL STRATA (ADAPTED FROM LOEHR, ET AL., 2011). .....11-2
FIGURE 11-3 ALTERNATIVE INTERPRETATIONS OF $C_c$ MEASUREMENTS. .....11-4
FIGURE 11-4 DIRECT MEASUREMENTS OF $q_u$ FROM UNIAXIAL ($UCS$) AND CONFINED COMPRESSION TESTS ($CCS$) FROM FOUR BORINGS PLOTTED USING DIFFERENT SYMBOLS: (A) FULL SCALE AND (B) EXPANDED SCALE.....11-9
FIGURE 11-5 INTERPRETATION OF STRATIGRAPHY AND $q_u$ FROM DIRECT MEASUREMENTS: (A) FULL SCALE AND (B) EXPANDED SCALE. .....11-12
FIGURE 11-6 ALTERNATIVE APPROACHES FOR INTERPRETING INDIRECT MEASUREMENTS: (A) INTERPRETATION OF $I_s$ PRIOR TO TRANSFORMATION AND (B) TRANSFORMATION OF $I_s$ PRIOR TO INTERPRETATION.....11-16
FIGURE 11-7 COMPARISON OF SPT $N$-VALUES MEASURED AT SIMILAR LOCATION IN 1978 AND 1999. .....11-18
FIGURE 11-8 MEASURED VALUES OF $q_u$ SHOWING THREE MEASURES OF VARIABILITY AND UNCERTAINTY.....11-21
FIGURE 11-9 MEASURED VALUES OF $q_u$ SHOWING VARIABILITY AND UNCERTAINTY FOR FEWER MEASUREMENTS. .....11-21

FIGURE 11-10 INTERPRETATION OF $s_u$ ASSUMING LINEAR VARIATION DEPTH. ..... 11-24
FIGURE 11-11 INTERPRETATION OF $s_u$ PRESUMING MEASUREMENTS ARE LOGNORMALLY DISTRIBUTED. ..... 11-25
FIGURE 11-12 TRANSFORMATION FROM $I_s$ TO $q_u$ USING SITE SPECIFIC MEASUREMENTS FROM FIGURES 11-5 AND 11-6. ..... 11-28
FIGURE 11-13 INTERPRETATION OF $I_s$ MEASUREMENTS AND ASSOCIATED MEASURES OF VARIABILITY AND UNCERTAINTY. ..... 11-28
FIGURE 11-14 MEASURES OF VARIABILITY AND UNCERTAINTY FOR $q_u$ WHEN ESTABLISHED FROM MEASUREMENTS. ..... 11-29
FIGURE 11-15 INTERPRETATION OF $q_u$ ESTABLISHED FROM COMBINED DIRECT AND INDIRECT MEASUREMENTS. ..... 11-32
FIGURE 11-16 GENERALIZED PROFILE, MOISTURE CONTENT, TOTAL UNIT WEIGHT, AND IN SITU STRESS PROFILE. ..... 11-36
FIGURE 11-17 TYPICAL PROFILES OF $\sigma'_p$ AND OCR FOR: (A) SOFT CLAY SITE, (B) STIFF CLAY SITE. ..... 11-39
FIGURE 11-18 IN SITU HORIZONTAL STRESS FROM LABORATORY AND IN SITU TESTS (FROM BENOIT AND LUTENEGGER, 1992). ..... 11-41
FIGURE 11-19 MEASURED VALUES OF $K_o$ : (A) AS FUNCTION OF $\phi'$ FOR NORMALLY CONSOLIDATED SOILS, AND (B) AS FUNCTION OF $OCR$ (FROM KULHAWY AND MAYNE, 1990). ..... 11-41
FIGURE 11-20 UNDRAINED STRENGTH MEASUREMENTS FROM: (A) SOFT CLAY SITE AND (B) STIFF CLAY SITE. ..... 11-43
FIGURE 11-21 INTERPRETATION OF $s_u$ FROM CIUC TESTS: (A) $\sigma'_p$, AND (B) $s_u$. ..... 11-46
FIGURE 11-22 $s_u/\sigma'_{vc}$ VERSUS $OCR$ RELATION USED TO ESTABLISH $s_u$ SHOWN IN FIGURE 11-21. ..... 11-46
FIGURE 11-23 MOHR-COULOMB DIAGRAM SHOWING LINEAR APPROXIMATION OF CURVED FAILURE ENVELOPE. ..... 11-48
FIGURE 11-24 EFFECTIVE STRESS FAILURE ENVELOPE FROM CU TYPE TRIAXIAL COMPRESSION TESTS. ..... 11-50
FIGURE 11-25 EFFECTIVE STRESS FAILURE ENVELOPE INTERPRETED USING WEIGHTED LEAST SQUARES REGRESSION. ..... 11-51
FIGURE 11-26 INTERPRETATION OF CONSOLIDATION PARAMETERS (MODIFIED AFTER DING, ET AL., 2014). ..... 11-53
FIGURE 12-1 SURFACE EXPRESSIONS OF KARST: (A) SINKHOLE IN TENNESSEE AND (B) PINNACLED BEDROCK (PHOTOS COURTESY OF BEN RIVERS). ..... 12-2
FIGURE 12-2 FEATURES OF EXTREME KARST LANDSCAPE (WALTHAM AND FOOKES, 2003). ..... 12-3

FIGURE 12-3 MAP OF KARST AND POTENTIAL KARST AREAS IN SOLUBLE ROCKS IN THE CONTIGUOUS UNITED STATES (USGS, 2014).....12-3
FIGURE 12-4 COMMONLY ENCOUNTERED PROBLEMS IN PINNACLED LIMESTONE (BROWN, 1990).....12-4
FIGURE 12-5 COMPARISON OF AERIAL PHOTOGRAPH AND LIDAR IMAGERY SHOWING DETECTION OF SMALL SURFACE DEPRESSIONS (BLACK ARROWS) USING LIDAR IMAGERY (ILLINOIS STATE GEOLOGICAL SURVEY, 2016).....12-6
FIGURE 12-6 STRESS DISTRIBUTION BENEATH A SQUARE FOUNDATION.....12-7
FIGURE 12-7 GPR FOR DETECTING SUBSURFACE VOIDS (WIGHTMAN, ET AL., 2004). .....12-9
FIGURE 12-8 IDEALIZED GRAVITY MEASUREMENTS OVER A SUBSURFACE VOID (WIGHTMAN, ET AL., 2004). .....12-9
FIGURE 12-9 SEISMIC REFLECTION MEASUREMENTS FOR DETECTING SUBSURFACE VOIDS (WIGHTMAN, ET AL., 2004). .....12-10
FIGURE 12-10 SEISMIC REFRACTION MEASUREMENTS FOR DETECTING SUBSURFACE VOIDS (WIGHTMAN, ET AL., 2004). .....12-11
FIGURE 12-11 EXAMPLE RESISTIVITY IMAGE SHOWING LOW VALUES INDICATIVE OF VOIDS OR HIGHLY FRACTURED ROCKS (WIGHTMAN, ET AL., 2004) .....12-11
FIGURE 12-12 TIME-DOMAIN ELECTROMAGNETIC MEASUREMENTS (WIGHTMAN, ET AL., 2004).....12-12
FIGURE 12-13 CHANGES IN SURFACE WAVE MOTIONS DUE TO SUBSURFACE VOIDS (WIGHTMAN, ET AL., 2004) .....12-13
FIGURE 12-14 SUBSURFACE CROSS-HOLE SEISMIC TOMOGRAPHY METHOD (WIGHTMAN, ET AL., 2004) .....12-13
FIGURE 12-15 SURFACE EFFECTS FROM SUBSURFACE MINES IN OHIO: (A) I-470 AND (B) I-70 (LEFCHIK, ET AL., 2003). .....12-14
FIGURE 12-16 SURFACE WATER COLLECTED IN SUBSIDENCE FEATURE IN MISSOURI (LEFCHIK, ET AL., 2003). .....12-16
FIGURE 12-17 USE OF GPR TO CHECK FOR VOIDS BENEATH A PAVEMENT DURING WORK TO REPAIR A MINE (LEFCHIK, ET AL., 2003).....12-16
FIGURE 12-18 USGS 2008 SEISMIC HAZARD MAP FOR SEISMIC DESIGN COEFFICIENT AT ONE SECOND PERIOD FOR 7 PERCENT *PE* IN 75 YEARS AND COMPETENT (B/C BOUNDARY) SOIL (MARSH, ET AL., 2014). .....12-17
FIGURE 12-19 ROUTE 17 LANDSLIDE FROM LOMA PRIETA EARTHQUAKE (FROM KAVAZANJIAN, ET AL., 2011).....12-18
FIGURE 12-20 DISRUPTED FILL AND PAVEMENT DUE TO LIQUEFACTION IN RIO ESTRELLA, COSTA RICA DURING 1991 EARTHQUAKE (KAVAZANJIAN, ET AL., 2011). .....12-18

FIGURE 12-21 COLLAPSE OF OVERPASS ON HIGHWAY IN KOCAELI, TURKEY EARTHQUAKE (FROM ERDIK, 2001). ..... 12-19
FIGURE 12-22 SETTINGS THAT PRODUCE ARTESIAN CONDITIONS (EARTH SCIENCE AUSTRALIA, 2017) ..... 12-25
FIGURE 12-23 MODES OF ROCK SLOPE FAILURE LEADING TO ROCKFALL EVENTS (TURNER AND SCHUSTER, 2012). ..... 12-28
FIGURE 12-24 LANDSLIDE EVENT AFFECTING HIGHWAY 3 IN TAIWAN (PETLEY, 2010) ..... 12-29
FIGURE 12-25 ROCKFALL EVENT IN GLENWOOD CANYON, CO AFFECTING I-70 IN 2010 (CDOT, 2017). ..... 12-29
FIGURE 13-1 SITE PLAN SHOWING LOCATIONS OF BORINGS AND IN SITU TEST SOUNDINGS (MNDOT, 2013). ..... 13-7
FIGURE 13-2 EXAMPLE BORING LOG FROM CALIFORNIA DEPARTMENT OF TRANSPORTATION (CALTRANS, 2010). ..... 13-8
FIGURE 13-3 EXAMPLE BORING LOG FROM MINNESOTA DEPARTMENT OF TRANSPORTATION (MNDOT, 2013). ..... 13-9
FIGURE 13-4 EXAMPLE CPTU LOG FROM CALIFORNIA DEPARTMENT OF TRANSPORTATION (CALTRANS, 2010). ..... 13-10
FIGURE 13-5 EXAMPLE LABORATORY TEST REPORT FOR *UU* TRIAXIAL COMPRESSION TESTS. ..... 13-12
FIGURE 13-6 EXAMPLE SUMMARY TABLE FOR ONE-DIMENSIONAL CONSOLIDATION TESTS. ..... 13-13
FIGURE 13-7 EXAMPLE SUMMARY TABLE FOR *UU* TRIAXIAL COMPRESSION TESTS. ..... 13-13
FIGURE 13-8 EXAMPLE SUMMARY TABLE FOR *CU* TRIAXIAL COMPRESSION TESTS PERFORMED FOLLOWING SHANSEP PROCEDURE. ..... 13-14
FIGURE 13-9 DESIGN PROFILE SHOWING MEASUREMENTS WITH INTERPRETATION FOR EACH STRATUM. ..... 13-15
FIGURE 13-10 DESIGN CROSS-SECTION SHOWING INTERPRETATION OF STRATIGRAPHY. ..... 13-15
FIGURE 13-11 OBSERVATIONS FROM PIEZOMETERS AND NEARBY WATERWAY. ..... 13-16

THIS PAGE IS LEFT INTENTIONALLY BLANK

# LIST OF TABLES

TABLE 3–1 USEFUL MAPS AND DATA SOURCES FOR EXISTING INFORMATION. ..... 3-5
TABLE 3–2 GUIDELINES FOR MINIMUM NUMBER, LOCATION, AND DEPTH OF EXPLORATION POINTS (ADAPTED FROM AASHTO, 2014). ..... 3-36
TABLE 4-1 SOIL CHARACTERISTICS AFFECTING BEHAVIOR OF COARSE- AND FINE-GRAINED SOILS. ..... 4-2
TABLE 4-2 DESCRIPTIVE TERMS FOR SOIL PARTICLE SIZE RANGES. ..... 4-3
TABLE 4-3 USCS CRITERIA FOR WELL-GRADED COARSE-GRAINED SOILS. ..... 4-5
TABLE 4-4 GRAIN-SIZE CHARACTERISTICS FOR THE TWO SANDS IN FIGURE 4-1. ..... 4-5
TABLE 4-5 TYPICAL VALUES OF SPECIFIC GRAVITY FOR SEVERAL NATURAL SOILS. ..... 4-9
TABLE 4-6 TYPICAL VALUES OF ACTIVITY FOR SEVERAL DIFFERENT SOILS. ..... 4-15
TABLE 4-7 TYPICAL VALUES OF *SSA* AND *CEC* FOR SEVERAL CLAY MINERALS AND FINE-GRAINED SOILS. ..... 4-17
TABLE 4-8 TYPICAL RANGES OF TOTAL CARBONATE CONTENT FOR DIFFERENT SOILS. ..... 4-18
TABLE 4-9 CLASSIFICATION OF ORGANIC CONTENT PROPOSED BY HUANG ET AL. (2009). ..... 4-19
TABLE 4-10 DESCRIPTIONS FOR FIELD EVALUATION OF ROCK HARDNESS. ..... 4-20
TABLE 4-11 JAR SLAKE INDEX DESCRIPTIONS. ..... 4-21
TABLE 4-12 ROCK QUALITY BASED ON *RQD* (FROM DEERE AND DEERE, 1988). ..... 4-22
TABLE 4-13 AASHTO SOIL CLASSIFICATION SYSTEM (FROM ASTM D3282, 2015) ..... 4-27
TABLE 4-14 APPROXIMATE COMPARISON BETWEEN USCS AND AASHTO SOIL CLASSIFICATIONS (HANDY AND SPANGLER, 2007). ..... 4-28
TABLE 4-15 SOIL BEHAVIORAL TYPE DESIGNATIONS FOR ORIGINAL CHART BY ROBERTSON ET AL. (1986). ..... 4-31
TABLE 4-16 SOIL BEHAVIORAL TYPE DESIGNATIONS FOR UPDATED ROBERTSON (2010) CHART (AFTER MAYNE ET AL., 2009). ..... 4-32
TABLE 4-17 FINES CONTENT FROM CPT INDEX $I_{c\text{-}JB}$ (AFTER MAYNE ET AL., 2009). ..... 4-35
TABLE 4-18 SOIL IDENTIFICATION USING DMT MATERIAL INDEX, $I_D$ (FROM MARCHETTI, 1975). ..... 4-36
TABLE 4-19 ROCK TYPE CLASSIFICATION (FROM NRCS, 2012). ..... 4-39
TABLE 4-20 CHARACTERISTICS OF COMMON IGNEOUS ROCK. ..... 4-40
TABLE 4-21 CHARACTERISTICS OF COMMON SEDIMENTARY ROCKS. ..... 4-40
TABLE 4-22 CHARACTERISTICS OF COMMON METAMORPHIC ROCKS. ..... 4-40
TABLE 4-23 CRITERIA FOR DEFINING ROCK GRAIN SIZE. ..... 4-41
TABLE 4-24 DESCRIPTIVE TERMS FOR WEATHERING STATE OF ROCK. ..... 4-41
TABLE 4-25 CRITERIA AND DESCRIPTIONS FOR RELATIVE ROCK STRENGTH. ..... 4-42

TABLE 4-26 ROCK COLOR DESCRIPTORS (AFTER GEOLOGICAL SOCIETY OF LONDON, 1977). ....4-42
TABLE 4-27 IMPORTANT DRILLING PARAMETERS (FROM GUI ET AL., 2002). ....4-44
TABLE 5-1 CHARACTERISTICS OF PROBLEMATIC SOIL AND ROCK. ....5-2
TABLE 5-1 (CONT'D) CHARACTERISTICS OF PROBLEMATIC SOIL AND ROCK. ....5-3
TABLE 5-2 SUMMARY OF CRITERIA FOR IDENTIFYING COLLAPSIBLE SOILS. ....5-6
TABLE 5-3 ALTERNATIVE CRITERIA FOR DEFINING SEVERITY OF COLLAPSE. ....5-10
TABLE 5-4 CHARACTERIZATION OF SWELL SEVERITY FROM DAKSHANAMURTHY AND RAMAN (1973). ....5-14
TABLE 5-5 CHARACTERIZATION OF SWELL SEVERITY FROM RAMAN (1967). ....5-15
TABLE 5-6 CHARACTERIZATION OF SWELL SEVERITY FROM ALTEMEYER (1955). ....5-15
TABLE 5-7 SEVERITY OF SWELLING BASED ON THE FREE SWELL INDEX, (HOLTZ AND GIBBS, 1956). ....5-16
TABLE 5-8 DESCRIPTIONS FOR DIFFERENT LEVELS OF SWELL POTENTIAL (FROM PECK ET AL., 1974). ....5-18
TABLE 5-9 ORGANIC SOIL AND PEAT CLASSIFICATION FROM LANDVA, ET AL. (1983). ....5-24
TABLE 5-10 VALUES OF RATIO $C\alpha/Cc$ FOR SEVERAL ORGANIC SOILS (FROM MESRI AND GODLEWSKI, 1977). ....5-27
TABLE 5-11 CRITERIA FOR CLASSIFYING DISPERSIVE SOILS FROM PINHOLE TEST (FROM ASTM D4647, 2013). ....5-30
TABLE 5-12 SUITABILITY OF SHALE MATERIALS FOR ROCK FILL (AFTER STROHM, ET AL., 1978). ....5-40
TABLE 5-13 SOIL TYPES WITH HIGH CORROSION POTENTIAL (ADAPTED FROM ELIAS, ET AL., 2009). ....5-41
TABLE 5-14 DEGREE OF SOIL CORROSIVITY BASED ON RESISTIVITY (FROM ROBERGE, 2000). ....5-42
TABLE 5-15 NUMERICAL CORROSIVITY SCORING (FROM EARTH CONTACT PRODUCTS). ....5-43
TABLE 5-16 SOIL CORROSION POTENTIAL BASED ON CORROSIVITY SCORE (FROM EARTH CONTACT PRODUCTS). ....5-43
TABLE 5-17 CLASSIFICATION OF CLAY SENSITIVITY (FROM SKEMPTON AND NORTHEY, 1952). ....5-49
TABLE 5-18 RISK FOR LIME STABILIZATION OF SULFATE-BEARING CLAYS (FROM LITTLE AND NAIR, 2009). ....5-50
TABLE 5-19 SEVERITY OF SULFATE ENVIRONMENT FOR CONCRETE CORROSION (AFTER ACI, 2008). ....5-51
TABLE 6-1 CHARACTERIZATION OF SAMPLE QUALITY FROM VOLUMETRIC STRAIN TO REACH THE IN SITU VERTICAL EFFECTIVE STRESS (FROM TERZAGHI, ET AL., 1996). ....6-7
TABLE 6-2 CHARACTERIZATION OF SAMPLE QUALITY FROM $\Delta e/e_0$ TO REACH THE IN SITU VERTICAL EFFECTIVE STRESS (FROM LUNNE, ET AL., 1997). ....6-7

TABLE 6-3 SOIL TERMINOLOGY APPLIED TO STRESS HISTORY.....6-16
TABLE 6-4 ALTERNATIVE METHODS FOR DETERMINING THE COEFFICIENT OF CONSOLIDATION, $cv$. ....6-23
TABLE 6-5 SUMMARY OF IN SITU TEST METHODS FOR DETERMINING PRECONSOLIDATION STRESS.....6-28
TABLE 6-6 SUMMARY OF EMPIRICAL TRANSFORMATIONS BETWEEN PRECONSOLIDATION STRESS AND DMT $KD$.....6-31
TABLE 6-7 MODIFIED TIME FACTORS, $T^*$, FOR ANALYSIS OF CPTU DISSIPATION TESTS (AFTER TEH AND HOULSBY, 1991).....6-37
TABLE 6-8 RATING OF CONSOLIDATION SPEED BASED ON $T_{flex}$ (MARCHETTI AND TOTANI, 1989).....6-40
TABLE 6-9 REPORTED CORRELATIONS BETWEEN COMPRESSION INDEX, $Cc$, AND LIQUID LIMIT, $LL$.....6-43
TABLE 6-10 REPORTED CORRELATIONS BETWEEN COMPRESSION INDEX, $Cc$, AND NATURAL WATER CONTENT, $\omega n$.....6-44
TABLE 6-11 REPORTED CORRELATIONS BETWEEN COMPRESSION INDEX, $Cc$, AND INITIAL VOID RATIO, $eo$.....6-44
TABLE 6-12 REPORTED CORRELATIONS BETWEEN COMPRESSION INDEX, $Cc$, INITIAL VOID RATIO, $eo$, AND LIQUID LIMIT, $LL$.....6-45
TABLE 6-13 REPORTED CORRELATIONS BETWEEN COMPRESSION INDEX, $Cc$, NATURAL WATER CONTENT, $\omega n$, AND LIQUID LIMIT, $LL$.....6-45
TABLE 6-14 REPORTED CORRELATIONS BETWEEN COMPRESSION INDEX, $Cc$, INITIAL VOID RATIO, $eo$, AND NATURAL WATER CONTENT, $\omega n$.....6-45
TABLE 6-15 REPORTED CORRELATIONS BETWEEN COMPRESSION INDEX, $Cc$, AND PLASTICITY INDEX, $PI$.....6-45
TABLE 6-16 REPORTED CORRELATIONS BETWEEN COMPRESSION INDEX, $Cc$, INITIAL VOID RATIO, $eo$, LIQUID LIMIT, $LL$, AND NATURAL WATER CONTENT, $wn$.....6-45
TABLE 6-17 VALUES OF $C\alpha Cc$ FOR SEVERAL INORGANIC CLAYS AND SILTS (FROM MESSI AND GODLEWSKI, 1977).....6-47
TABLE 7-1 COMMON MODIFIED MOHR-COULOMB DIAGRAMS.....7-5
TABLE 7-2 EFFECT OF SAMPLE DISTURBANCE ON EFFECTIVE STRESS AND FOR DIFFERENT SOIL TYPES (AFTER VAUGHAN, ET AL., 1993).....7-29
TABLE 7-3 ESTIMATES FOR NORMALIZED UNDRAINED STRENGTH PARAMETERS, AND (ADAPTED FROM LADD AND DEGROOT, 2003).....7-40
TABLE 7-4 ESTIMATES FOR NORMALIZED UNDRAINED STRENGTH PARAMETERS, $S$ AND (ADAPTED FROM LADD AND DEGROOT, 2003).....7-44

TABLE 7-5 RELATIONSHIP AMONG RELATIVE DENSITY, SPT $N$-VALUE, AND FOR COARSE-GRAINED SOILS (AFTER MEYERHOF, 1956) ..... 7-54
TABLE 7-6 PARAMETER VALUES FOR USE WITH EQUATION 7.26 (DUNCAN, ET AL., 2014). ..... 7-59
TABLE 7-7 ESTIMATED FOR EFFECTIVE STRESS STRENGTH PARAMETERS FOR COMPACTED SOILS (ADAPTED FROM U.S. BUREAU OF RECLAMATION, 1973). ..... 7-67
TABLE 8–1 COMMON DEFORMATION PROPERTIES USED FOR GEOTECHNICAL APPLICATIONS. ..... 8-2
TABLE 8–2 VALUES OF $A$, $F(e)$ AND $R$ FOR COARSE-GRAINED SOILS (MODIFIED FROM KOKUSHO, 1987). ..... 8-17
TABLE 8–3 $K_{2,max}$ VALUES FOR SAND (ESTIMATED FROM SEED AND IDRISS, 1970). ..... 8-17
TABLE 8–4 VALUES OF $k$ AS A FUNCTION OF $PI$ (HARDIN, 1978). ..... 8-18
TABLE 8–5 TRANSFORMATIONS BETWEEN $Vs$ AND $N_{60}$ FOR ALL SOIL TYPES (MODIFIED FROM WAIR, ET AL., 2012). ..... 8-20
TABLE 8–6 TRANSFORMATIONS BETWEEN $G_{max}$ AND SPT $N_{60}$ VALUES. ..... 8-21
TABLE 8–7 TRANSFORMATIONS BETWEEN $G_{max}$ AND CPT TIP RESISTANCE. ..... 8-21
TABLE 8–8 TRANSFORMATIONS BETWEEN $V_S$ AND CPT TIP AND SLEEVE RESISTANCE. ..... 8-21
TABLE 8–9 TRANSFORMATIONS BETWEEN $E_D$ AND $G_{max}$ FOR SAND. ..... 8-22
TABLE 8–10 TYPICAL VALUES FOR $E_S$ AND $\nu$ FOR DIFFERENT SOIL TYPES (MODIFIED FROM AASHTO, 2012). ..... 8-26
TABLE 8–11 TRANSFORMATIONS BETWEEN $E_s$ AND SPT $(N_1)_{60}$ (MODIFIED FROM AASHTO, 2012). ..... 8-26
TABLE 8–12 TYPICAL SUBGRADE REACTION VALUES FOR 0.3 M BY 0.3 M SQUARE LOADING (DAS, 2011). ..... 8-30
TABLE 8–13 COMMON $p$-$y$ MODELS FOR DIFFERENT SOIL OR ROCK CONDITIONS (FHWA, 2006). ..... 8-31
TABLE 9-1 REPRESENTATIVE STRENGTHS FOR DIFFERENT TYPES OF INTACT ROCK (AFTER GOODMAN, 1989). ..... 9-5
TABLE 9-2 SUMMARY OF RELATIONS PROPOSED TO TRANSFORM $I_{s(50)}$ TO $q_u$ (AFTER SINGH, ET AL., 2012) ..... 9-17
TABLE 9-3 SELECTED RELATIONS FOR TRANSFORMING REBOUND HAMMER $R$ TO $qu$. ..... 9-19
TABLE 9-4 SELECTED RELATIONS TO TRANSFORM REBOUND HAMMER $R$ TO $E50$. ..... 9-20
TABLE 9-5 ROCK MASS RATING ($RMR$) SYSTEM OF ROCK MASS CLASSIFICATION (FROM ASTM D5878, 2008). ..... 9-35
TABLE 9-6 $RMR$ SYSTEM PARAMETER $R_6$ (FROM ASTM D5878, 2008). ..... 9-35

TABLE 9-7 DEFINITION OF $JCond_{89}$ OR ESTIMATING *GSI* (BIENIAWSKI, 1989; HOEK ET AL., 2013)...9-37
TABLE 9-8 GUIDELINES FOR CLASSIFYING DISCONTINUITY CONDITION (BIENIAWSKI, 1989; HOEK ET AL., 2013) ....9-38
TABLE 9-9 RATIO OF ROCK MASS MODULUS TO INTACT ROCK MODULUS (O'NEILL, ET AL., 1996).....9-47
TABLE 9-10 VALUES OF MATERIAL CONSTANT, $m_2$ (FROM MARINOS AND HOEK, 2001).....9-52
TABLE 10-1 RECOMMENDED FILTER CHARACTERISTICS FOR COMMON SCREEN SLOT SIZES (ASTM D5092, 2010).....10-10
TABLE 10-2 INSTRUMENTS FOR MEASURING GROUNDWATER PRESSURE (MODIFIED FROM DUNNICLIFF, 1993).....10-11
TABLE 10-3 SUMMARY OF METHODS FOR DETERMINING HYDRAULIC CONDUCTIVITY.....10-25
TABLE 10-4 REPORTED HYDRAULIC CONDUCTIVITY ANISOTROPY. .....10-29
TABLE 10-5 SUMMARY OF LABORATORY METHODS FOR DETERMINING HYDRAULIC CONDUCTIVITY. .....10-30
TABLE 10-6 SUMMARY OF ADVANTAGES AND DISADVANTAGES OF RIGID- AND FLEXIBLE-WALL PERMEAMETERS (MODIFIED FROM DANIEL, 1994). .....10-36
TABLE 10-7 BOREHOLE METHODS FOR DETERMINING IN SITU HYDRAULIC CONDUCTIVITY. .....10-37
TABLE 10-8 INFILTROMETER METHODS FOR DETERMINING HYDRAULIC CONDUCTIVITY OF COMPACTED CLAY LINERS AND COVERS. .....10-47
TABLE 10-9 ADVANTAGES AND DISADVANTAGES OF DIFFERENT INFILTROMETERS (MODIFIED FROM DANIEL, 1989). .....10-48
TABLE 10-10 DIRECT PUSH METHODS FOR DETERMINING IN SITU HYDRAULIC CONDUCTIVITY. .....10-53
TABLE 10-11 SUMMARY OF $u$ VALUES FOR ESTIMATING CONSTRAINED MODULUS FROM $qc$. .....10-54
TABLE 11–1 MEASURES OF VARIABILITY AND UNCERTAINTY FOR $q_u$ FROM FIGURES 11-8 AND 11-9. .....11-22
TABLE 11–2 COEFFICIENTS OF VARIATION FOR DIRECT MEASUREMENTS OF FROM FIGURES 11-8 AND 11-9. .....11-23
TABLE 11–3 CALCULATION OF VARIABILITY AND UNCERTAINTY IN $q_u$ FROM $I_s$. .....11-29
TABLE 11–4 SUMMARY OF VARIABILITY AND UNCERTAINTY IN $q_u$ FROM DIRECT MEASUREMENTS, INDIRECT MEASUREMENTS, AND COMBINED DIRECT AND INDIRECT MEASUREMENTS. .....11-31

TABLE 12-1 APPLICABILITY OF GEOPHYSICAL METHODS FOR IDENTIFYING VOIDS AND SINKHOLES (ASTM D6429, 2011) ..... 12-8
TABLE 12-2 APPLICABILITY OF GEOPHYSICAL METHODS FOR IDENTIFYING DEPTH TO BEDROCK (AFTER ASTM D6429, 2011) ..... 12-8
TABLE 12-3 SITE CLASS DEFINITIONS (AASHTO, 2012). ..... 12-20
TABLE 12-4 VALUES FOR SITE FACTOR ($Fpga$) AT ZERO PERIOD ON ACCELERATION SPECTRUM (AASHTO, 2012). ..... 12-21
TABLE 12-5 LIQUEFACTION SUSCEPTIBILITY OF SEDIMENTARY DEPOSITS DURING STRONG GROUND MOTION (YOUD AND PERKINS, 1978). ..... 12-22

# CHAPTER 1
# INTRODUCTION

## 1.1 ROLE AND VALUE OF SITE CHARACTERIZATION

Characterization of subsurface conditions is one of the most challenging yet important activities required for successful planning, design, construction, and operation of transportation infrastructure. The broad purpose of site characterization is to inform geotechnical specialists, planners, designers, constructors, and other professionals about ground conditions so that these decision makers can effectively identify and address risks attributed to ground conditions. In this manual, the term "risk" will be used to represent a potential for loss, generally expressed in terms of financial costs. The term will generally be used qualitatively, but risk can also be expressed quantitatively as the product of some potential cost and the likelihood of that cost being incurred. In this context, the costs involved broadly include costs incurred to resolve construction or performance problems that may arise from failure to effectively characterize ground conditions. Costs may also often include indirect costs associated with reduced mobility or public safety. The likelihood of these potential costs depends on the reliability of measures taken to characterize ground conditions, which in turn depends on the reliability of available information regarding ground conditions. Risks attributed to ground conditions commonly represent the greatest risks present for many infrastructure projects (Ground Board, 1991). Many, if not most of these risks are directly or indirectly affected by the quantity and quality of subsurface investigations (Hoek and Palmeiri, 1998; Clayton, 2001).

Improved site characterization will generally reduce risks associated with design, construction, and operation of transportation infrastructure. Improved site characterization directly reduces the likelihood of encountering unforeseen ground conditions during construction, which often lead to claims, change orders, and cost overruns during construction, and may lead to unacceptable performance following construction. Improved site characterization also increases the reliability of estimates of important soil and rock properties and design parameters (Loehr, et al., 2015), which in turn can reduce the likelihood of unacceptable performance and/or allow designers to achieve some target reliability for less cost. Improved site characterization reduces the likelihood of failing to identify relevant geotechnical hazards that may negatively affect the construction or performance of a structure and lead to increased costs. Improved site characterization also often reduces construction risk, which inevitably leads to lower costs for dealing with ground conditions during construction and lower bid costs.

Despite these considerable benefits, it is important to recognize that improved site characterization generally comes at some cost. Thus, there are consequences associated with conducting more extensive investigations. The value of investigations performed for site characterization is derived from the fact that costs for the investigations are often substantially less than costs associated with constructing features to accommodate uncertain and ambiguous ground conditions and potential costs that may be incurred if construction or performance problems are encountered. The fundamental value proposition for site characterization is established from comparison of costs required to complete some scope of investigations with cost savings that can be realized by having the information collected from the investigations. The fundamental value question is, "Will the site investigations permit features to be designed, constructed, operated and/or maintained for less cost than would be required if the information derived from the investigations was not available?" Furthermore, will the cost savings produced by having the information exceed the costs for the investigation itself? If the financial benefits derived from site characterization exceed the cumulative costs of investigations performed, the investigations produce value and are therefore justified. While this value proposition is relatively simple and straightforward, it is complicated by numerous challenges associated with site characterization.

## 1.2 CHALLENGES FOR EFFECTIVE SITE CHARACTERIZATION

There are numerous challenges to effective site characterization, especially when considered in light of the fundamental value proposition. Several of these challenges include:

1. The volume of material to be characterized is generally very large in comparison to the volume of material that can be sampled and/or tested, even for the most extensive investigations.
2. The materials to be characterized are inherently heterogeneous with characteristics that can vary substantially in both space and time.
3. The mechanical behavior of soil and rock is relatively complex and affected by many factors that can be difficult to understand and accurately replicate in laboratory and/or field tests.
4. A large number of different measurements can be made to evaluate different ground characteristics, each with different advantages and disadvantages, but the relative value of different types of measurements for specific conditions is generally not quantitatively established and often not widely recognized.
5. Site characterization is commonly performed in the early stages of projects, sometimes before locations and important details about specific structures are established, before anticipated loading conditions are completely defined, and/or before all potentially important limit states are identified.

6. The mechanical behavior of soil and rock is influenced by groundwater conditions, which inevitably vary over time and are often difficult to predict.
7. Practical issues like site access constraints, regulatory requirements, and complex budgeting issues may restrict the type, quantity, and/or location of measurements that can be made.

These challenges, and others, lead to the condition that some level of uncertainty about ground conditions is inevitable, regardless of the scope of investigations performed. Perfect site characterization is simply not possible; thus, the objective for site characterization should be to characterize the site to some acceptable level commensurate with comparison of costs for investigation and costs and risks associated with design, construction, and operation of the features being considered. Because risk is necessarily dependent on uncertainty, site characterization should also include characterization of the reliability or uncertainty of the information obtained in addition to establishing appropriate characteristics and parameters required for design and construction.

An additional challenge for site characterization is that there are risks that apply to the site characterization process itself. It is possible to perform investigations that are entirely appropriate and consistent with the value proposition discussed here, yet occasionally still fail to identify important features or fail to accurately capture important behavioral characteristics of the soil/rock encountered. Similarly, hindsight may sometimes reveal that the scope of a specific investigation was insufficient or excessive, despite judicious decisions considering the expected value of the investigation. Unfortunately, sometimes doing the "right thing" does not lead to the desired outcome for specific projects. However, consistent consideration of the value proposition will lead to reduced risks and improved use of funds when considered over a large collection of individual projects that make up an agency's portfolio of projects. Despite all of these challenges and despite the risks present, the objective of site characterization should be to characterize the ground to a level of reliability suggested by the value proposition described in the previous section.

## 1.3 PURPOSE OF CIRCULAR

The objective of Geotechnical Engineering Circular (GEC) No. 5 is to improve site characterization practices among government agencies, private consultants, and contractors involved in the planning, design, construction, and operation of transportation features. The manual is intended to serve as a comprehensive and practical reference to guide planning and execution of geotechnical investigations and interpretation of the acquired data to develop reliable geotechnical design parameters. The manual is not intended to provide prescriptive procedures, nor to dictate methods for collection of field or laboratory

measurements. Rather, the manual is intended to provide guidance to address the fundamental problems of identifying and characterizing geotechnical hazards, interpreting soil and rock properties from field and laboratory measurements, and, perhaps most importantly, establishing reliable values for geotechnical design parameters from collective interpretation of field and laboratory measurements. The manual addresses recent changes to design practice, specifically addressing load and resistance factor design (LRFD) and more explicit awareness of risk and reliability for planning, design, construction, and operation of transportation features. The manual also provides methods to quantify the variability and uncertainty present in geotechnical design parameters. Finally, the manual provides methods that can be used to assess the value of different site characterization practices, to place site characterization activities into context that is meaningful to both technical and non-technical professionals, and to facilitate effective decision making for geotechnical investigations in light of the risks and costs involved.

The manual is intended for use by designers and users of site characterization products, geotechnical specialists charged with specifying and directing field and laboratory investigations, and especially those that develop appropriate values for specific geotechnical design parameters. These professionals commonly include geotechnical engineers, engineering geologists, geologists, civil engineers, structural engineers, construction engineers, and construction managers.

## 1.4 ORGANIZATION OF CIRCULAR

The manual is organized to reflect the strong emphasis on interpretation of geotechnical parameters for design and, to a lesser extent, on identification and characterization of geotechnical hazards. Chapter 2 provides content describing the objectives, products, and uses for geotechnical investigations to convey the fundamental motivations for performing effective site characterization. Chapter 3 describes important considerations for planning and scoping of geotechnical investigations. The chapter includes discussions about the relative value of different types of measurements, rational use of remote sensing and geophysical measurements, and guidance for development of appropriate scopes for geotechnical investigations.

Chapter 4 describes means and methods for classification of soil and rock based on relatively simple index property measurements. The important topic of identifying and characterizing potentially problematic soil and rock types for design and construction is addressed in Chapter 5. Common problematic soil and rock types are identified and potential consequences associated with those soil and rock types are described. Guidance for effective identification of problem soil/rock types, commonly

using simple index property measurements, is then provided and special issues and requirements for investigation and use of the specific problematic soil and rock types are described.

Chapters 6 through 10 provide guidance for interpreting soil and rock properties from field and laboratory measurements. The focus of these chapters is on interpretation of properties from individual test measurements, in contrast to interpretation of design parameters from collections of individual measurements. Several alternative definitions for "property" and "parameter" are often adopted. Throughout this manual, the term "property" is used to refer to a specific characteristic of soil or rock, something that can generally be directly measured in a test. Properties can include characteristics such as mineralogy, water content, and Atterberg limits that are seldom used directly for design and analysis, as well as properties such as unit weight, shear strength, and compressibility that are frequently used for design and analysis. In contrast, the term "parameter" is used to represent a specific term or variable in some model or design and analysis method. More specifically, the term "design parameter" is used to refer to a required input for a specific design method. The potential for confusion is clear because many soil properties are also common design parameters. The difference in such cases is that the property generally represents a characteristic of the soil at a given location in time and space whereas a design parameter may represent some interpretation of soil properties over some area or volume of soil for design, or interpretation of model parameters over some range of conditions (e.g., Mohr-Coulomb shear strength parameters). For example, undrained shear strength is a common design parameter required for many evaluations of strength limit states. However, a specific soil sample also has some specific undrained shear strength as determined by a specific test method. Thus, some soil and rock properties can serve as design parameters, but not all design parameters are necessarily properties.

Each of Chapters 6 through 10 addresses specific soil or rock properties that are commonly used for geotechnical design: Chapter 6 addresses consolidation properties; Chapter 7 addresses strength properties for soil; Chapter 8 addresses stress-strain response and stiffness properties; Chapter 9 addresses rock properties; and Chapter 10 address hydraulic properties and groundwater conditions. Within each of these chapters, guidance for interpreting properties from different test measurements is provided along with recommendations regarding the appropriateness of different test methods for different applications.

Chapter 11 describes the culmination of site characterization activities – interpretation of geotechnical design parameters from collections of individual measurements. The chapter includes discussion of objectives for interpretation and a recommended process for developing rational, reliable, and defensible "models" for design. The importance of integrating judgment is addressed along with use of the observational method to achieve reliable design, construction, and performance for transportation

features. The chapter provides guidance and recommendations for interpreting stratigraphy, as well as guidance for interpreting specific geotechnical design parameters for different applications and conditions. Importantly, the chapter also provides guidance to promote appropriate use of both "direct" and "indirect" measurements of geotechnical properties, as well as guidance regarding use of historical measurements that may be available. Finally, the chapter describes explicit methods for calculating the variability and uncertainty of specific geotechnical design parameters based on the quantity and type(s) of measurement that are available.

Identification and characterization of geotechnical hazards are addressed in Chapter 12. Effective and practical means to identify and characterize hazards including karstic conditions, underground mines, seismic hazards, groundwater hazards, landslide-prone conditions, and landfills are described.

Finally, Chapter 13 provides guidance for documenting and reporting results from geotechnical investigations. The chapter includes specific recommendations for documenting different aspects of the site characterization process, including different types of boring logs and different types of geotechnical reports. Three appendices are also included to provide important supplementary information to assist professionals in applying the guidance provided in this manual. Appendix 1 includes a summary of AASHTO and ASTM standards that are referenced throughout the manual. Appendix 2 includes three site characterization examples to illustrate application of the guidance provided. Appendix 3 provides documentation of methods for quantifying variability and uncertainty for geotechnical design parameters.

# CHAPTER 2
# OBJECTIVES, USES, AND PRODUCTS OF SITE CHARACTERIZATION INVESTIGATIONS

In the context of site characterization, the word "investigation" is used to represent a systematic study conducted to identify the ground conditions present at a site and to accurately characterize the behavior of the soil and/or rock. Investigations performed for site characterization may include subsurface investigations that involve boring, probing, excavation, or other testing below the ground surface; geophysical investigations that may or may not require access to the soil and/or rock below the ground surface; laboratory investigations that generally involve testing of soil and/or rock specimens acquired from the site; and examination of maps, imagery, and other information that often do not require access to the specific site. Prior to planning and executing specific investigations for site characterization, it is important to fully understand the objectives and anticipated products of the investigations. Planning and execution of investigations for site characterization will also be improved with knowledge of the anticipated or potential uses for such products. In this chapter, common objectives for site characterization are presented and discussed. Different classes or phases of investigations are described along with common products resulting from the different investigations to provide readers with knowledge of the end products of site characterization.

## 2.1 GENERAL OBJECTIVES FOR SITE CHARACTERIZATION

Specific investigations for site characterization are conducted for a broad range of reasons. The products of these investigations are also used for different purposes by different personnel. Such broad motivation and use contributes to the value and importance of site characterization since it directly contributes to and affects projects during planning, design, construction, and operation. While products from the investigations are used for many purposes, specific investigations are generally performed with specific objectives in mind. The specific objectives being addressed can affect the quantity, scope, and type of investigations that should be performed, and the resulting value of the products developed from the investigations.

Investigations performed for site characterization are generally intended to address one or more of the following objectives:

1. Stratigraphy – identify and qualitatively characterize the types of soil and/or rock present at a site, including definition of discrete strata and development of cross-sections (profiles) that describe how stratigraphy varies across a site.

2. Groundwater Conditions – characterize groundwater conditions at a site and identify potential impacts that such conditions may have for design, construction, and operation.
3. Design Parameters – develop reliable estimates for relevant design parameters needed for design.
4. Constructability – characterize ground conditions that may affect construction methods and schedule, and identify risks that may impact project delivery.
5. Hazard Identification – identify geotechnical hazards that are present and characterize those hazards that may impose risks to design, construction, operation, and/or performance.
6. Suitability – characterize the suitability of soil and/or rock encountered for specific uses (e.g., use as engineered fill or aggregate source).
7. Condition Assessment and Performance Monitoring – assess current ground conditions to inform condition assessment for transportation features.
8. Location and Alignment – qualitatively characterize ground conditions to inform location and alignment decisions for infrastructure projects (e.g., identifying conditions that may necessitate substantial remediation or motivate re-alignment of a corridor).

Throughout this manual, the term "hazard" is used to reflect a condition or feature that has the potential to negatively impact construction or operation of transportation infrastructure; this is contrasted with use of the term "risk", which represents potential for experiencing loss. Risk is a measure that combines the likelihood of a hazard impacting a project with the potential consequences (i.e., costs) that will be incurred if the hazard does impact the project. Presence of a hazard may, or may not, pose a substantial risk to a specific project, but identification and characterization of hazards are critical to identifying and quantifying risks.

The suitability of different types of investigations, and of specific site characterization methods, is intimately tied to the objectives of the investigation. Some field and laboratory tests that may be suitable for hazard identification or location and alignment studies may be poorly suited for characterizing geotechnical design parameters. Conversely, field and laboratory tests that are well-suited for characterizing geotechnical design parameters may be poor choices for profiling or constructability evaluations. In many cases, specific field and laboratory techniques can be used to address several or even all of the objectives listed above. The suitability of specific techniques for addressing the disparate objectives listed above is addressed in subsequent chapters.

While different types of investigations are often performed to achieve one or more of the specific objectives listed above, it is important to recognize that site characterization products may serve different purposes for agency or contractor personnel serving in different roles. For example, geotechnical

designers will often use information from boring logs to characterize subsurface stratigraphy for development of rational, yet simplified design models that include characterization of specific design parameters. Such use is often quantitative and relatively refined. Project planning personnel might use the same boring logs in a completely different manner for relatively simple and qualitative interpretation of a site to develop preliminary cost estimates for a project. Prospective bidders may use the same boring logs to facilitate identification of appropriate construction techniques and potential construction risks. In some cases, boring logs may also become a part of legal or contractual documents that may influence bid prices and payment quantities for a project. Unfortunately, it is often difficult to identify individual practices that will produce results that simultaneously address the objectives for all potential end-users. Nevertheless, it is helpful to identify relevant objectives for all involved parties, so that the value of geotechnical investigations can be enhanced.

## 2.2 CLASSES OF SITE CHARACTERIZATION INVESTIGATIONS

Because objectives for specific site characterization investigations can vary and sometimes be competing, different classes or phases of investigations are generally conducted to provide a systematic approach to site characterization. While the terminology used by different organizations to refer to different classes or phases of investigations varies, specific activities for different classes of investigations often share common characteristics and objectives as described in the following sections.

### 2.2.1 Desk Studies

A critical first step for practically all site characterization programs is a study to gather and evaluate available information about conditions that may be present at a site. These activities are often referred to as "desk studies" because they are often completed prior to conducting field or laboratory activities. Common sources of information for desk studies include:

- historical records from prior site investigations at or near a project site;
- performance records from nearby structures or facilities, potentially even including review of articles from the popular press;
- geologic reports and publications;
- various maps that commonly include geologic maps, soil survey maps, topographic maps, utility maps, insurance maps, etc.;
- aerial photographs, satellite imagery, and other remote-sensing products;
- consultation with professional colleagues with experience at or near a project site; and

- review of pertinent laws, policies, and regulations that may govern a particular site (e.g., U.S. Army Corps of Engineers rules, railroad regulations, water quality regulations, local government regulations, etc.).

These sources of information contribute to characterization of a site and development of practical, yet effective geotechnical site characterization programs. Desk studies inform planning and scoping of investigations for site characterization and help ensure that field crews are suitably equipped and prepared for the conditions that are likely to be encountered. Desk studies also contribute significantly to location and alignment decisions prior to conducting field or laboratory investigations, and often contribute to early identification of geotechnical hazards that may introduce risks and warrant further investigation. Additional discussion of specific sources and uses of preliminary information is provided in Section 3.2.

### 2.2.2 Preliminary Investigations

Preliminary investigations are usually performed in the early stages of project development to support project planning, to provide somewhat simple and often qualitative information for preliminary design, and to provide information to support planning for more rigorous investigations. Preliminary investigations also often contribute to early identification and characterization of potential risks that may be imposed by geotechnical hazards.

For roadway projects, preliminary investigations often include relatively sparse subsurface investigations that may include shallow borings, test pits, and/or in situ test soundings located at relatively large spacing along the anticipated project alignment. Preliminary investigations often include collection of bulk or disturbed samples that are used for simple "index property" tests that support initial characterization of the soil/rock present. Preliminary investigations seldom include collection of higher quality samples that are appropriate for "performance" tests to measure strength and stress-strain properties for soil and rock. Geophysical measurements, particularly "scanning" methods that provide measurements over relatively large areas (e.g., seismic reflection/refraction, MASW, electrical resistivity), can be effectively used for preliminary investigations to help interpret conditions between relatively sparse borings or soundings.

### 2.2.3 Design Investigations

Design investigations are typically performed after the project alignment and grade have been set and after locations for retaining walls, bridge piers, bridge abutments, and cut/fill slopes have been established. Compared to preliminary investigations, design investigations are more rigorous and "targeted" investigations that usually involve more advanced, and more costly field and laboratory

techniques. The principle objectives for design investigations are to: (1) confirm or refine preliminary interpretations of site stratigraphy, and (2) establish reliable values for relevant design parameters. Design investigations may also include specific tests to better characterize geotechnical hazards and to specifically address constructability issues. For large projects, several phases of design investigations may be performed, either to address different design and construction issues, or to sequentially refine interpretations as more information is acquired and as specific details of a project are established. Conversely, for small projects, preliminary investigations and design investigations may be combined into a single investigation, although this practice introduces some risk into the site characterization process. Much of the content of this manual is directed towards practices to produce effective and reliable design investigations.

As described in more detail in Chapter 3, design investigations often involve use of more advanced boring, sampling, and testing techniques that are intended to produce accurate and reliable estimates for design parameters. Design investigations often include specialized boring techniques, relatively advanced laboratory testing, and in situ field tests that are intended to produce estimates of engineering properties for design. Design investigations may include use of various geophysical techniques, either to refine interpretations of stratigraphy, to help establish geotechnical design parameters, or to better characterize geotechnical hazards that may be present.

In addition to routine design investigations, "special" investigations are sometimes performed to investigate specific geotechnical challenges for a project. Such investigations often include field and/or laboratory tests that are not commonly performed for routine design investigations and often include greater quantities of tests than would be performed for routine projects. Examples of special investigations include investigations for design and construction of significant embankments on soft foundations, investigations for design of foundations for particularly large or challenging bridges, and more refined investigation of specific geotechnical hazards (e.g., karst, underground mines, seismic hazards, or problematic geomaterials, etc.).

### 2.2.4 Borrow Site Investigations

For projects that require substantial quantities of off-site "borrow" materials for construction, borrow site investigations may be performed to evaluate the suitability of potential borrow sources. Borrow site investigations generally focus on characterizing stratigraphy and general soil and/or rock type, as opposed to characterizing in situ soil properties, since the soil properties will change as a result of excavation, transport, and placement of the borrow soil or rock. Borrow site investigations are therefore commonly

conducted using relatively rapid, but cost effective boring techniques, disturbed sampling, and inexpensive "index" property tests. Borrow site investigations may also include test pits and other destructive means to characterize stratigraphy and to obtain relatively large quantities of disturbed samples for further laboratory characterization. As borrow sources are refined, and the suitability of a particular source is confirmed, borrow site investigations may include more extensive laboratory testing on compacted specimens of the borrow material to further characterize relevant engineering properties for design.

For projects that involve large quantities of soil/rock that is unsuitable for use as embankment fill, similar investigations may also be performed to identify suitable locations for "wasting" undesirable materials. Such investigations are primarily focused on ensuring that wasting of soil or rock will not adversely impact the project, adjacent landowners, or the environment (e.g. disposal of pyritic rock).

### 2.2.5 Investigations for Performance Monitoring and Condition Assessment

Site characterization investigations are also occasionally performed during, or following construction to characterize the performance of specific features (e.g., a wall, bridge, embankment, etc.), or to support condition assessment for such features. The primary focus of such investigations is to collect measurements that reliably reflect the performance of specific features or provide information that facilitates condition assessment. Such measurements are commonly different than those used for other classes of investigations, and often involve installation of instrumentation to measure stress, deformation, pore water pressure, and/or load. While such investigations have been used for many years, the subjects of performance monitoring and condition assessment are currently undergoing substantial changes with the broadening application of asset management principles throughout the transportation industry. It is therefore likely that current practices for site characterization to support performance monitoring and condition assessment may undergo substantial changes in coming years, in terms of specific methods employed, in terms of the frequency of use, and in terms of importance for the broader transportation community.

Performance monitoring and condition assessment may be performed during construction to help guide construction (e.g., installation of settlement plates and piezometers beneath embankments constructed on soft soils), or many years following construction if problematic performance is observed (e.g., installation of inclinometers to evaluate excessive slope or foundation movements, etc.). Since performance monitoring and condition assessment are conducted to observe and document performance or condition rather than to specifically characterize sites, such investigations are not specifically addressed further in

this manual. However, the practices and techniques described in this manual are likely to apply and contribute to such investigations.

### 2.2.6 Forensic Investigations

An additional type of investigation performed by or for transportation agencies is forensic investigations. Forensic investigations are in some ways similar to design investigations in that they often involve use of relatively advanced boring, sampling, and testing techniques. However, forensic investigations are primarily focused on identifying the cause(s) of problems that have already occurred, and thus tend to be more directed and focused on specific locations than common design investigations. For example, it is relatively common to perform forensic investigations following slope failure or rockfall events. Such investigations commonly involve attempts to identify the location of the observed sliding surface, characterize groundwater conditions that may have existed when the slide occurred, and identify whether movements are continuing. In many cases, forensic investigations will also include additional measurements that may be needed to establish appropriate design parameters for remedial design. Such investigations are often performed with some degree of emergency and may involve use of equipment and techniques that extend beyond those commonly used for more routine investigations.

### 2.2.7 Investigations for Design-Build Projects

Site characterization for projects procured under design-build contracts or other similar procurement mechanisms necessarily differ from those performed for traditional design-bid-build projects. For design-build projects, the project owner should generally provide site characterization information that is sufficient to allow prospective bidders to confidently develop designs and estimate costs during the bid period, and to reduce risks for changed site condition claims after contract award. The site characterization data furnished by the owner should be sufficient to generally characterize stratigraphy, soil and rock properties, and groundwater conditions. However, since the specific facility arrangement and loading requirements are not known in advance of contract award, it is not possible for the owner to provide all information needed for final design. As such, the selected design-build organization is responsible for conducting additional investigations necessary to finalize the specific design, generally following contract award. For most design-build projects, the site investigations conducted by the owner should be more extensive than routine preliminary investigations performed for conventional design-bid-build projects described in Section 2.2.2. However, these investigations seldom achieve the rigor of final design investigations described in Section 2.2.3 and must generally be supplemented by additional investigations performed by the design-build organization after contract award.

## 2.3 GEOTECHNICAL REPORTING DOCUMENTS

A number of different documents are generated from investigations for site characterization. The most common of these include field investigation logs, geotechnical data reports, and geotechnical design reports. The following sections provide general descriptions of different geotechnical reporting documents for the purpose of understanding common products that result from site characterization. More detailed description of the different reporting documents, including recommendations for specific content, is provided in Chapter 13.

### 2.3.1 Field Investigation Logs

The most common products from investigations for site characterization are field investigation logs that may include boring logs, test pit logs, in situ testing (e.g., CPT, DMT, VST, etc.) logs, groundwater monitoring logs, and geophysical survey reports. While the specific form and content of field investigation logs vary substantially for different types of investigations, and from agency to agency, the logs generally include some representation of stratigraphy determined from the investigation, engineering descriptions of the soil and rock materials encountered, documentation of groundwater level observations, as well as test measurements from laboratory or field tests. Field investigation logs should also preferably include important field observations that may impact decision making such as difficult drilling, loss of drilling fluid, "rod drops" that may indicate karst, and borehole stability problems that may indicate flowing sands.

### 2.3.2 Geotechnical Data Reports

Products from geotechnical investigations commonly include some form of "geotechnical data report", which generally includes a description of the investigations performed, field investigation logs, and results of laboratory and field test measurements. As is true for field investigation logs, the content of geotechnical data reports varies substantially with the type of investigation(s) that is (are) performed and with the requirements for the specific project. Geotechnical data reports produced from preliminary investigations are commonly brief and include only measurements from relatively simple index property tests that facilitate identification and classification of soil and/or rock and potential geotechnical hazards. Conversely, geotechnical data reports from design investigations or special investigations may be rather lengthy and include results from large numbers of lab and/or field measurements of both index properties and "performance" properties. Geotechnical data reports may also be produced for geophysical investigations (e.g., seismic velocity or electrical resistivity) or other highly specialized investigations. In some cases, geotechnical data reports may also include relevant existing data collected from desk studies.

An important characteristic of all geotechnical data reports is that they include only factual data; geotechnical data reports should not include interpretations derived from reported measurements or recommendations for design and construction. Because only factual information is provided, geotechnical data reports are sometimes included as part of project plans and bid documents, and are an essential part of design-build contracts. As such, geotechnical data reports may become legally binding and may often influence potential claims and change orders, and overall project costs.

### 2.3.3 Geotechnical Design Reports

In contrast with geotechnical data reports, "geotechnical design reports" generally include much more than just factual data. Geotechnical design reports usually include relatively detailed descriptions of a characterized site along with additional content such as descriptions of analysis and design methods, results from design analyses, interpretation of analysis results, and recommendations for design and construction. Geotechnical design reports often include descriptions of the soil and/or rock encountered, interpretations of stratigraphy, descriptions of observed and anticipated groundwater conditions, descriptions of geotechnical hazards and potential risks that may be introduced by those hazards, and interpretations of relevant geotechnical design parameters. Geotechnical design reports also often include much of the factual information that is included in geotechnical data reports to support the interpretations provided. Alternatively, geotechnical design reports may reference one or more geotechnical data reports. Because geotechnical design reports often include rather complete and comprehensive interpretations of ground conditions, and because they often include much or most of the factual information collected, geotechnical design reports can be considered as the "complete" characterization of a site and the ultimate end product of site characterization activities. However, because geotechnical design reports often include subjective interpretations about ground conditions based on available information, the reports are rarely, if ever, included as part of project plans and bid documents. Nevertheless, geotechnical design reports document design assumptions, parameters and procedures, and design and construction considerations, and may have different legal ramifications depending upon the project location and prevailing law.

### 2.3.4 Geotechnical Baseline Reports

In special cases such as design-build projects, the products of site characterization investigations may be used to develop a "geotechnical baseline report", or GBR (ASCE, 2007). GBR are a special type of site characterization product that is intended to establish a contractually binding interpretation of ground conditions for a specific project. The general content of a GBR is often similar to the site characterization

content from geotechnical design reports in the sense that they include complete interpretations of ground conditions. The principal difference is that a GBR establishes a "baseline" for ground conditions that is accepted by all parties for contractual purposes prior to execution of construction. GBR, and the interpretations included therein, are therefore contractually binding and serve as the basis for claims and change orders associated with ground conditions. Additional discussion of GBR is provided in Chapter 13.

## 2.4 BENEFITS OF SITE CHARACTERIZATION

As described in Chapter 1, the fundamental value of site characterization is derived from benefits that arise during planning, design, construction, and operation of transportation infrastructure. These benefits include direct financial benefits as well as improved public safety and mobility that are more difficult to express in financial terms. If the financial benefits produced from site characterization exceed the cumulative costs for those investigations, the investigations contribute value to the project and the funding agency. While financial benefits from effective site characterization arise for many reasons, the most common sources include:

1. More reliable estimates for geotechnical design parameters allow designers to design more efficient and cost-effective transportation features because the reliability of the design necessarily depends on the reliability of the design parameters used. In contrast, designers must design more conservatively to produce acceptable reliability when design parameters are less reliably established, or when parameter values are ambiguous; costs for constructing such designs are often substantially greater than is required with more reliable information.
2. Early identification of geotechnical hazards allow project risks to be identified early in the project cycle, when it is often easier and less costly to address the risk. For example, early identification of problematic soil or rock may permit roadways or structures to be relocated to avoid the hazard entirely or permit foundations for bridges or other structures to be selected to alleviate risks to the structures. If risks attributed to geotechnical hazards are not identified until later in the design process or, even worse, during or after construction, costs for redesigning later in the design process, or remediating the hazard during or after construction, are inevitably far greater than if the risks had been identified earlier.
3. Accurate characterization of stratigraphy, groundwater conditions, and the types of soil and/or rock present can substantially influence project costs, both directly and indirectly. The accuracy of information like excavation and fill quantities and driven pile quantities are directly related to the accuracy of stratigraphic characterization. Incomplete or ambiguous characterization of

stratigraphy increases the likelihood for claims, change orders, and cost overruns due to unanticipated ground conditions, which increase costs over those that would be incurred if ground conditions were better established (Boeckmann and Loehr, 2016). Even if incomplete characterization does not lead to claims, change orders, or cost overruns, increased uncertainty about ground conditions leads to greater risks for contractors, which in turn leads to greater bid costs. Conversely, effective site characterization increases confidence about ground conditions, which in turn reduces the likelihood of claims, change orders, and cost overruns, and reduces risks associated with ground conditions, both of which can produce substantial cost savings for agencies and projects.

Each of these sources can be substantial when considered individually and the combined benefits from all sources can dramatically affect both project level and agency level budgets. Additional consideration of the financial benefits of site characterization, including consideration of such benefits during scoping for site characterization investigations is provided in Chapter 3 and subsequent chapters.

THIS PAGE IS LEFT INTENTIONALLY BLANK

# CHAPTER 3
# PLANNING AND SCOPING FOR SITE CHARACTERIZATION ACTIVITIES

Planning and scoping for site characterization activities is challenging due to the numerous requirements and constraints for characterization and the wide variety of available techniques and approaches. Planning and scoping are further complicated because the reliability of the acquired information, and more specifically the reliability of estimates for design parameters, is dependent on both the quantity and quality of measurements that are made. Thus, many possible alternative scopes can be developed, with a wide range of resulting reliabilities for the acquired information. This chapter addresses these challenges by describing common information requirements for design and construction, and sources of preliminary information that can inform effective planning and scoping for site investigations. The chapter also describes how the quantity and type of laboratory and field measurements influence the reliability of interpreted design parameters, as well as several other important considerations for planning and scoping of site characterization activities.

## 3.1 INFORMATION REQUIREMENTS FOR DESIGN AND CONSTRUCTION

There are three broad requirements for most site characterization programs:

1. Characterize the stratigraphy and general characteristics of soil and rock units, including how these characteristics vary across the site;
2. Establish appropriate and reliable values for required design parameters and characterize groundwater conditions for design; and
3. Identify and characterize hazards that may impact design, construction, and performance.

The first and third requirements are generally similar for most projects, although specific measurements may vary from one site to the next based on site characteristics. For example, greater numbers of borings or in situ test soundings are appropriate for defining stratigraphy at sites with highly variable stratigraphy than at sites with more consistent stratigraphy. Similarly, the types of borings or measurements made to identify hazards may vary substantially depending on the geologic setting and the potential for encountering specific hazards. In contrast, the second requirement can vary substantially from project to project depending on the specific features being designed and constructed, the magnitude of potential consequences associated with unacceptable performance, as well as specific site characteristics. Specific requirements for establishing design parameters depend on the ground conditions present (which may be largely unknown at the beginning of investigations), the planned structure and anticipated loads, and the

potential for extreme events of various types (e.g., wind, wave, traffic or barge impacts, seismic loading, etc.), among other factors. Because requirements for establishing design parameters vary substantially, the majority of this chapter and, in fact, the entire manual focuses on determining appropriate values for geotechnical design parameters. This emphasis should not be taken to imply that stratigraphy and hazard identification are not important, but rather that these requirements are often more straightforward and consistent for most projects.

A broad collection of design parameters may be required and used for geotechnical design. Common design parameters for soil and rock include some measure(s) of strength, compressibility or stiffness, in situ stress, and stress history, as well as the location of the water table, seepage parameters, and/or some representation of pore water pressures. Use of design parameters derived from in situ tests is also quite common as a surrogate for more fundamental soil and rock properties. The specific parameters required for a project depend on a number of factors that include:

- Soil or rock type
- Type of geotechnical feature being designed
- Specific limit states or design conditions being evaluated
- Agency performance requirements, design practices, and policies (i.e., design methods)
- Agency or site investigation contractor equipment and capabilities

It is also common that specific features may be designed using one of several alternative methods that require design parameters derived from different types of measurements. For example, driven piles may be designed using so-called "rational" methods that require fundamental measures of soil or rock strength as inputs. Alternatively, driven piles may be designed using methods that require parameters obtained from in situ test measurements such as standard penetration tests (SPT) or cone penetration tests (CPT). Specific requirements for site characterization therefore depend on the design methods that will be used. As such, it is important to maintain awareness of agency practices and communicate with those that use the products of site characterization to ensure that appropriate types of measurements are obtained.

Because of the wide range of alternative methods that may be used for site characterization, and because of the additional challenges described, appropriate scopes for site investigations should be developed considering the following activities:

1. Communicating with project managers, designers, and/or owners to develop a thorough understanding of the broader project, including special constraints, anticipated schedule, anticipated method of procurement, etc.;

2. Assessing soil and/or rock types that are anticipated to exist at the site;
3. Identifying appropriate design conditions and limit states, along with associated design and analysis methods that will be used for design;
4. Identifying design parameters that are required for the identified design and analysis methods;
5. Identifying constructability issues that may exist and establishing measurements needed to inform constructability decisions;
6. Identifying appropriate site characterization methods for establishing the identified design parameters, with consideration for agency and site investigation contractor capabilities;
7. Evaluating the relative merits of alternative types of measurements for the respective design parameters;
8. Estimating the number of measurements required to establish values for the identified design parameters with an appropriate level of reliability;
9. Developing a scope and plan for investigations that will produce the appropriate number and type(s) of measurements, with appropriate consideration for cost and schedule; and
10. Communicating the scope and plan for site characterization to those that will execute the investigations (which may range from relatively straightforward internal communications to more complex legal and procurement documents for contracting site characterization investigations).

Most of these activities require deliberate coordination and communication among designers and users of geotechnical reports. The activities are often best completed by geotechnical design engineers in consultation with geologists, structural design engineers, construction engineers, project managers, and field crews. The remainder of this chapter addresses these activities in more detail.

## 3.2 COLLECTION AND INTERPRETATION OF EXISTING INFORMATION

Collection and interpretation of existing information is one of the most effective ways to improve planning and scoping for site characterization, which in turn improves the effectiveness of site characterization programs. Existing information informs those that plan and execute site characterization programs about ground conditions that can be anticipated so that appropriate means and methods for investigation can be selected. Existing information also often serves as the initial basis for identifying potential hazards, which in turn may dictate the type and scope of investigations that should be performed, and influence planning and decision making for the broader transportation project.

Capabilities and tools for collecting and evaluating existing information have improved dramatically over the past decade. Site characterization specialists and designers now have convenient, and often near

instantaneous access to a variety of maps, images, reports, and other information that previously required substantial effort to simply acquire and collect. Information that formerly was often stored and cataloged by organizations in hard copy form, at substantial expense, is now readily available electronically, often for little or no cost. Tools like Google® Earth™, Google® Maps™, geographic information systems (GIS), and other online services have become indispensable tools for site characterization and design.

### 3.2.1 Desk Study

Preliminary information about sites can be derived from a number of sources, many of which are publicly available. Table 3–1 provides a summary of many such sources, along with indications of how such data can be used for site characterization.

Soil survey maps and data developed by the National Resource Conservation Service (NRCS) and associated state agencies are extremely valuable sources of information for characterizing shallow (< 5 feet) soils. The NRCS Soil Survey Geographic Database (SSURGO) is particularly useful in that it often provides quantitative soil classification data such as USCS (Unified Soil Classification System) and AASHTO soil classification, moisture characteristics, Atterberg limits, hydrologic classification, grain-size distribution, and some chemical properties. The provided data also often includes various ratings for different uses that include engineering and construction. Much of the information is available through user-friendly and convenient online tools such as the NRCS "Web Soil Survey" that allows one to overlay soil characteristics upon aerial photographs or topographic maps (http://websoilsurvey.nrcs.usda.gov/). Figure 3-1 shows an example of ratings provided for "corrosion risk".

Another useful source of existing information is maps produced by the United States Geological Survey (USGS) and associated state agencies. Useful maps include USGS topographic maps as well as a suite of geologic maps that identify bedrock geology, quaternary (recent) geology, and geologic faults, among others. Many states also have agencies that produce maps indicating locations of mines and sinkholes, bedrock depth, bedrock type, surficial geology, and various hydrologic characteristics. All of these sources can be extremely useful for preliminary evaluation of sites. The USGS National Geologic Map Database (http://ngmdb.usgs.gov/) is a convenient source for identifying and acquiring geologic maps.

Some state agencies and other organizations also provide useful online tools and data sets, including demographic data and geographic data from past events. Figure 3-2 through 3-4 show examples of such maps for the same region. Figure 3-2 shows a conventional USGS topographic map. Figure 3-3 shows a map of flood damage during the 1993 Midwest Floods overlaying the USGS map. Figure 3-4 shows the same area, but with karst hazard areas shaded and locations of known sinkholes identified, in this case

overlaying a photographic image. Many of the available mapping tools also provide the capability to simultaneously plot several data sets, which can be useful when multiple hazards or characteristics are pertinent to specific evaluations.

**Table 3–1 Useful maps and data sources for existing information.**

| Map/Data Source | Use | Source(s) |
|---|---|---|
| USGS Topographic Maps | • Topography<br>• Crude recent and historical land use | USGS |
| Aerial Photographs | • Historical and recent land use & vegetation<br>• Structure, roadway, stream locations, etc.<br>• Identification of potential hazards | Google® Earth™, Google® Maps™, NAIP , Other public and commercial sources |
| Physiographic Landforms | • General soil/rock type | USGS, state agencies |
| Surficial geology | • General soil/rock type at surface | USGS, state agencies |
| Bedrock geology | • General rock type, age at depth | USGS, state agencies |
| Bedrock Depth Contours | • Crude bedrock depths | State agencies |
| Soil Survey Maps and Data | • Map scale characterization of general soil types and characteristics<br>• Quantitative classification data<br>• Identification of problematic soils | NRCS, state agencies |
| Fault Maps | • Identification of potential hazards | USGS, state agencies |
| Flood inundation maps | • Identification of potential flooding and related hazards (e.g., scour) | FEMA, USGS, USACE, state agencies |
| Stream gage records | • Identification of potential flooding and related hazards (e.g., scour) | USGS National Water Information System |
| Climatic data | • Historical climate records for temperature, precipitation, and stream gage records | NOAA National Centers for Environmental Information |
| Mine location/type | • Aggregate source<br>• Rock type<br>• Potential underground mine hazard | Federal and state agencies |
| Sinkhole/karst maps | • Identify karst hazard | Federal and state agencies |
| Natural Hazards Information | • Identification of potential hazards | Federal and state agencies, http://www.usgs.gov/hazards/ |
| Landfill/Superfund Sites Maps | • Identification of potential hazards | Federal and state agencies |
| Impaired Streams and Waterways Maps | • Identification of potential hazards or special environmental requirements | Federal and state agencies |
| Hydrologic maps | • Identification of springs and other groundwater hazards | Federal and state agencies |
| Utility maps | • Selecting investigation locations | Public and private sources |
| Well maps and well logs | • Indications of groundwater conditions | State agencies |
| Sanborn Fire Insurance Maps | • Historical land use<br>• Identification of potential environmental hazards | Library of Congress, state & university libraries, http://www.loc.gov/collections/sanborn-maps/ |

While current maps are often useful for preliminary study of site conditions, historical maps may also provide important and useful information regarding past use of specific sites. For example, historical USGS topographic maps and Sanborn Fire Insurance maps may show past industrial activity that might

indicate potential contamination, locations of abandoned foundations, and locations of substantial excavations or fills that might impact the stress history of the site (which, in turn, could influence the strength and/or compressibility of soil at the site). Historical maps may also show evidence of natural or man-made hazards such as sinkholes or underground mines, etc.

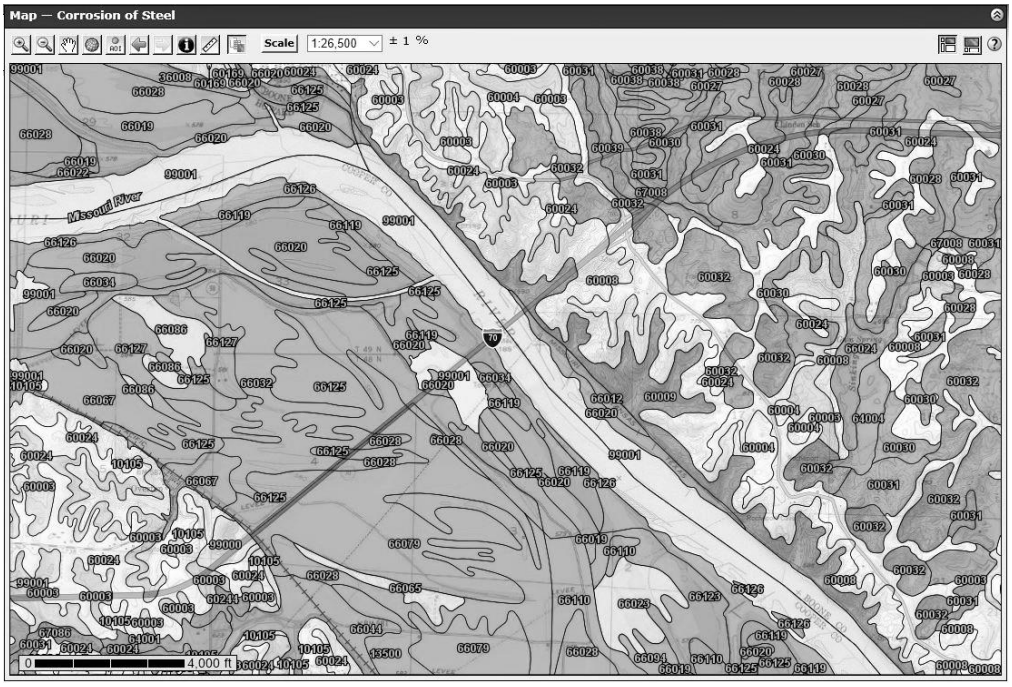


**Figure 3-1 Corrosion-risk ratings from the NRCS Web Soil Survey interactive tool (NRCS, 2016).**

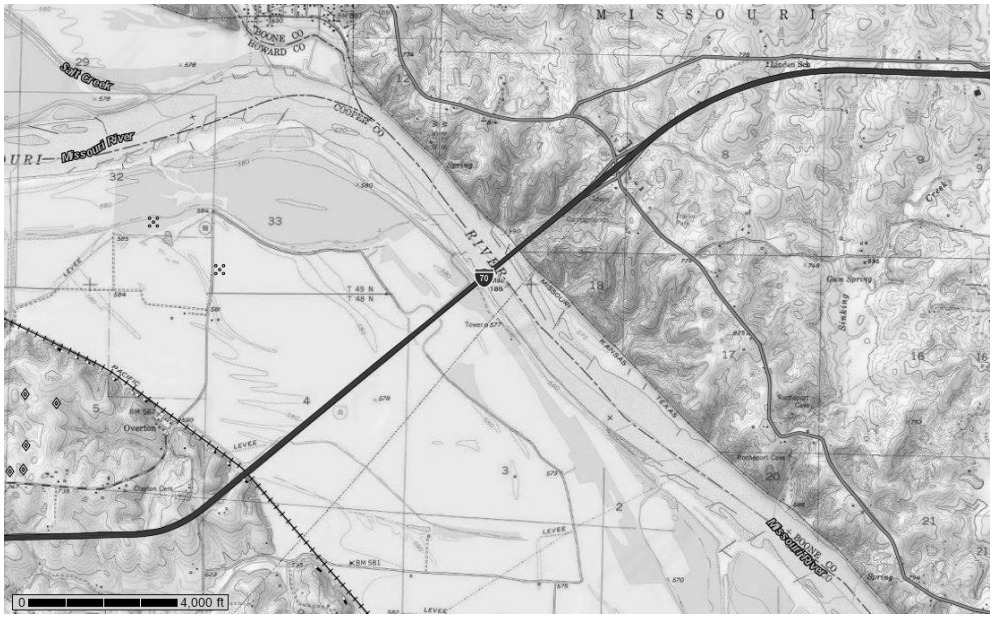


**Figure 3-2 USGS topographic map (NRCS, 2016).**

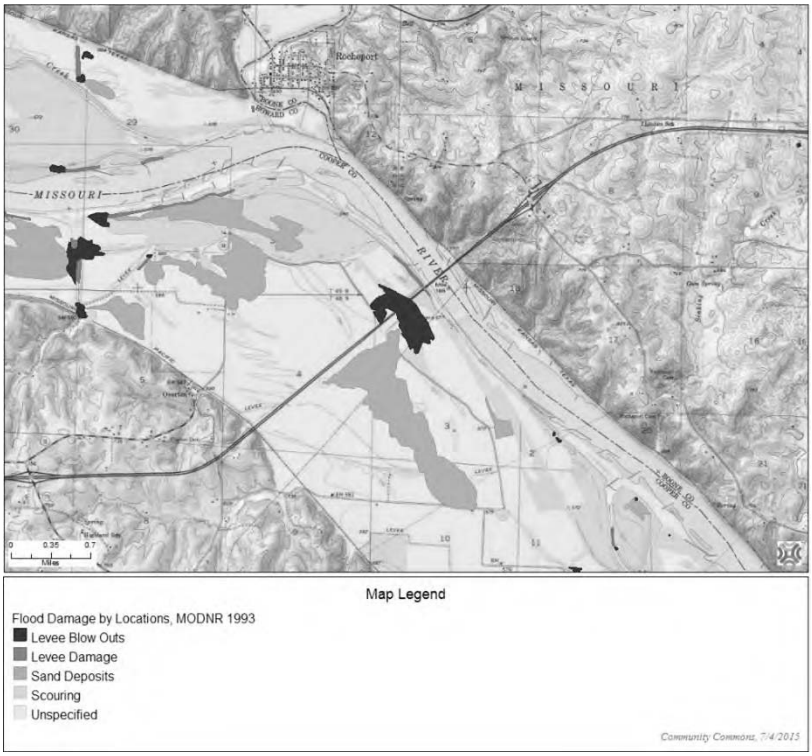


**Figure 3-3 Areas of known damage from 1993 Midwest Floods (courtesy Community Commons).**

**Figure 3-4 Karstic conditions and locations of known sinkholes (courtesy Community Commons).**

The primary limitation of using maps and mapping information is that most maps have inadequate spatial resolution for geotechnical site characterization. Mapped measurements and ratings may also not be completely appropriate or applicable for engineering design. Most sources represent relatively rudimentary estimates for design and construction and, thus, offer little potential to replace some components of site investigations. Nevertheless, the data are highly valuable for preliminary evaluation of site conditions and identification of potential hazards, which is beneficial for planning and scoping of site investigations to ensure that appropriate equipment and techniques are used.

Additional information can sometimes be obtained from technical and popular literature sources. Technical manuscripts describing the performance of features at similar sites can be particularly helpful, especially if describing performance of features similar to those being planned, since they often provide details regarding design, construction, and performance. However, even articles from the popular press may provide useful information regarding potential problems or hazards that may be encountered or accounts of historical performance of various infrastructure features.

### 3.2.2 Open Source and Commercial Remote Sensing Data

The availability of open-source and commercial remote sensing products has increased dramatically in recent years. Such imagery was largely unavailable, or at least difficult to acquire, only a short time ago but provides numerous benefits for planning, scoping, and execution of site investigations. Recent and historical air photos can provide valuable information on current and past conditions and uses for different sites. Air photos often provide indications of potential hazards at a site (e.g., past industrial use of a site, old landslides), or indications of potential variability (e.g., indications of a meandering stream may suggest a highly variable alluvial soils, etc.). Visual observation of past excavations may also suggest potential changes in in situ stress or presence of random fill. Open-source air photos, with generally high quality, are readily available through a variety of sources that include Google® Earth™ and Google® Maps™. Even higher resolution imagery can be obtained from some commercial and government sources.

One particularly useful form of imagery for preliminary investigation is so-called "bare-earth" imagery from airborne lidar (Light Detection and Ranging) measurements (Anderson, 2013). As shown in Figure 3-5, such imagery can provide excellent indications of historical landslides, sinkholes, or other ground deformations, even in areas where such features are hidden by vegetation in photographic imagery.

Radar imagery can also provide useful information, particularly regarding terrain attributes (e.g., slope, elevation, aspect, etc.). Interferometric radar processing (e.g., InSAR) can also provide indications of

larger scale surface deformation. For example, interferometric radar processing has been used to identify and characterize subsidence associated with groundwater withdrawal or underground construction (Rosenblad, et al., 2013). Hyperspectral imagery may also provide indications of vegetation, land use, moisture content, and potentially even soil or rock type at specific sites (Chabrillat, et al, 2002). Such imagery has been more commonly used for agricultural, ecological, and land-use applications, but has some potential for application to geotechnical investigations when large-scale characterization is desired. Mulder, et al. (2011) provides a comprehensive summary of the advantages and limitations of many remote sensing techniques.

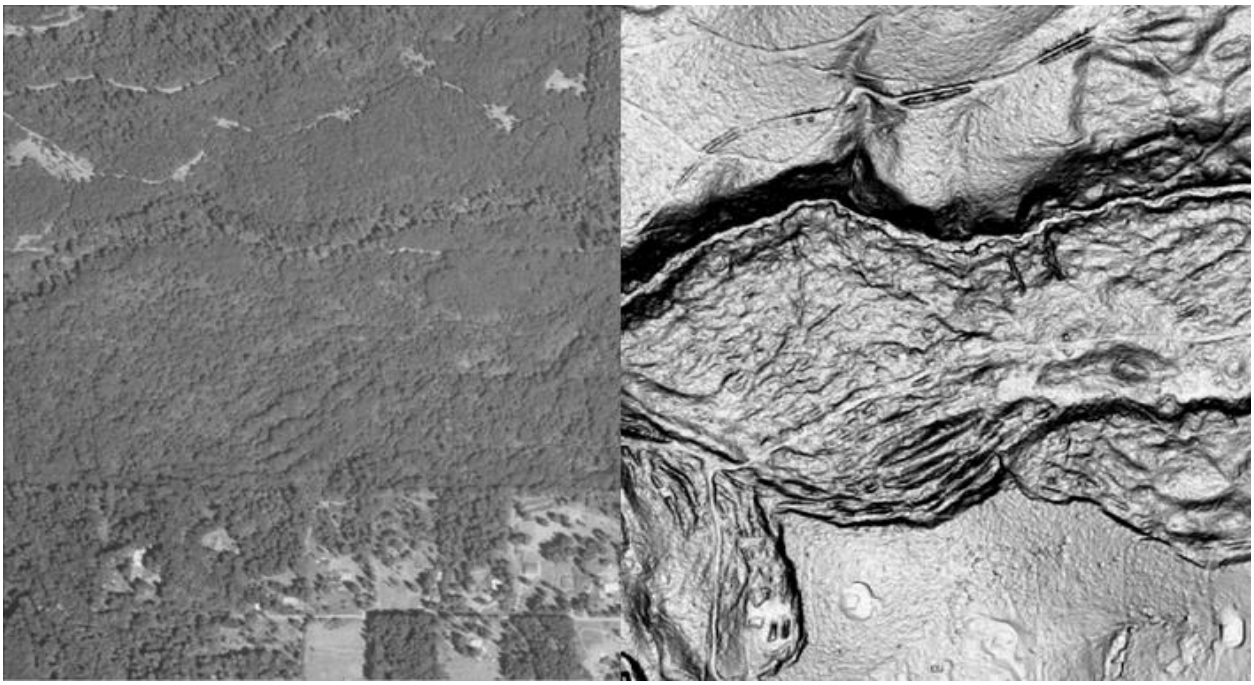

**Figure 3-5 Aerial photograph (left) and associated "bare-earth" lidar image (right) of vegetated area (from Anderson, 2013).**

### 3.2.3 Historical Data

Agencies and companies generally maintain records of geotechnical investigations performed for prior projects that can be helpful for new projects and influence the required scope for site characterization activities. While many projects are located at sites that lack significant historical data from previous investigations, projects such as roadway widenings and bridges replacements often have historical data from previous site investigations. Historical performance data may also be available for some projects.

While historical data represent important information that should be reviewed and evaluated when it is available, its use for establishing values for design parameters must be carefully considered because

historical measurements may or may not reflect current practices or conditions. Some soil and/or rock properties are unlikely to change substantially over time while others may change over relatively short periods of time. For example, many index properties and basic characteristics of soil and rock, such as grain-size distribution and Atterberg limits, are likely to remain practically consistent over long periods in the absence of unique external factors. However, properties like water content, strength, and compressibility may change dramatically over relatively short periods of time. Physio-chemical changes in soil and rock are also known to occur under some conditions so these issues must be carefully considered when using historical data for site characterization and design. The quality of historical data may also not be consistent with current standards of practice and, thus, may not be appropriate for direct use. Finally, while boring logs may be available from old projects, laboratory test data is often more difficult to locate.

Despite the potential for changes in some soil and/or rock properties, historical data can provide an efficient and effective basis for preliminary interpretation of a site. Additionally, when historical data are extensive and appropriate for the intended use, the objectives and scope for site investigations can change to one of confirming preliminary interpretations using more limited laboratory and field testing programs than may be required for sites where historical information is not available.

In recent years, the products of geotechnical investigations are increasingly being stored in various geotechnical data management systems. Geotechnical data management systems are computer databases developed to facilitate effective use of, and access to, historical geotechnical data and information that can meaningfully inform investigations for future projects. The specific form and content for geotechnical data management systems varies from agency to agency, with some agencies using relatively mature and well-established systems and other agencies using relatively simple systems. Some agencies make the systems, data, and information available for public use while other agencies restrict access. Many current systems are proprietary commercial systems, although some agencies have developed "in-house" systems. While geotechnical data management systems are currently evolving, several national and international efforts to develop data transfer standards for geotechnical data are underway to facilitate exchange of geotechnical data among different computer systems, software, and applications. Additional description of geotechnical data managements systems is included in Chapter 13.

## 3.3 SITE RECONNAISSANCE

Despite recent advances that provide convenient access to information about site characteristics from an individual's desktop, there remains no substitute for on-site reconnaissance visits. Site reconnaissance

provides an individual with a first-hand account of actual conditions at a site and can often reveal conditions that can be overlooked without an on-site evaluation. For example, a site visit might reveal the presence of localized groundwater "seeps", or provide indications of other hazards and conditions that may not be identified without site reconnaissance. Site reconnaissance offers the chance to confirm and explore notable issues or concerns identified from the desk study (e.g., investigate potential hazards). Site reconnaissance visits are also important for planning and execution of on-site investigations. Special attention should be paid to conditions that might impact access for equipment (e.g., soft surficial soils, gates, uneven topography, distressed vegetation, flags, need for land clearing, power lines, evidence of underground utilities, etc.) and resources needed to conduct subsurface investigations (e.g., benchmarks, water supply, etc.). In many cases, the likelihood of encountering problems at a site during field investigations can be dramatically reduced with effective site reconnaissance.

## 3.4 INFLUENCE OF NUMBER OF MEASUREMENTS

Both the cost effectiveness and reliability of designs for geotechnical features are directly influenced by the reliability of geotechnical design parameters. The reliability of geotechnical design parameters, in turn, directly depends on both the quantity and quality of measurements used to establish values for the parameters. In this section, the influence of the quantity of measurements used for estimating values for design parameters is described. General perspectives on the site characterization "problem" are first presented, followed by description of how the number of measurements affects estimates for a nominal or mean value for geotechnical design parameters. Finally, the issues of how the number of measurements affects the reliability of estimates for geotechnical design parameters, and how the number of available measurements affects the reliability of designs are addressed. The influence of the type or quality of measurements is subsequently described in Section 3.5.

### 3.4.1 General Perspectives on Reliability of Geotechnical Design Parameters

It is widely recognized that confidence in geotechnical design parameters improves with increasing numbers of measurements. Design parameters interpreted from small numbers of measurements will have great uncertainty and may be completely inappropriate regardless of the methods used for testing and interpretation (Christian, 2004). Fortunately, this uncertainty can be reduced by acquiring greater numbers of measurements. Soil and/or rock properties can theoretically be characterized to any desired level of uncertainty if sufficient numbers of measurements are available (Baecher, 1982; Baecher, 1983; Christian, 2004; Mitchell, 2009). These issues have long been qualitatively recognized by geotechnical engineers, and addressed through application of judgment when selecting values for design parameters.

While it is widely recognized that having greater numbers of measurements will reduce uncertainty in geotechnical design parameters, the quantitative influence of having more measurements is seldom explicitly evaluated or fully recognized. While engineering judgment is absolutely necessary for interpretation of geotechnical design parameters, heavy reliance on qualitative judgment introduces the potential for inconsistent and perhaps inappropriate interpretation of geotechnical design parameters, inappropriate scoping for site investigations, as well as inconsistent reliability for designed geotechnical features. However, the transition to load and resistance factor design (LRFD), and the desire to achieve target levels of reliability for specific transportation features and limit states, has led to increased recognition for how site characterization activities influence the reliability of transportation features. Such knowledge and motivation does not replace or diminish the need for sound engineering judgment, but it can better inform such judgment and lead to improved consistency among different designers and more consistent achievement of target reliabilities for geotechnical features. Consistent achievement of target reliabilities, in turn, leads to more cost effective designs that balance considerations of costs for construction with risks introduced by incomplete knowledge of site conditions.

It is important to distinguish between "variability" and "uncertainty" in the context of site characterization. Throughout this manual, the term "variability" is used to represent the consistency of actual properties, or measurements of a property, within a particular site or stratum. In contrast, the term "uncertainty" is used to represent the level of confidence one has in estimates of a specific property or design parameter. Uncertainty therefore represents the level of knowledge about a specific condition or property, whereas variability represents how significantly a specific condition or property varies over some volume of material. It is possible for a specific parameter to have little variability (e.g., for a very consistent site) but substantial uncertainty (e.g., estimated from few measurements). It is also possible for the same parameter to have substantial variability and little uncertainty depending on the characteristics of the specific site and the quality and quantity of measurements available for estimating the parameter. Variability of a soil or rock property is generally site specific and, often, little can be done to reduce variability at a specific site. In contrast, the uncertainty associated with a specific property or design parameter can often be dramatically reduced by making additional measurements. Variability is often best addressed through design decisions (e.g., selection of foundation types to address the variability, ground improvement, or sizing a specific foundation type to account for the variability). However, uncertainty is often best addressed through effective site characterization, and much of uncertainty is governed by the scope of site investigations as described subsequently in this chapter.

### 3.4.2 Statistical "Sampling" for Geotechnical Site Characterization

When interpreting geotechnical design parameters, it is important to recognize that available measurements for some soil or rock property are simply "samples" from a larger population of measurements that could be obtained in the absence of constraints of time and money. In the context intended here, "samples" is used according to the statistical definition to represent some arbitrary collection of measurements from a large population of measurements that could be made. From this perspective, available measurements should therefore be considered to be estimates of a property taken from some large population of possible values that represent actual in situ conditions rather than a deterministic measurement of actual conditions. Figure 3-6 and 3-7 illustrate this concept using a simulated population of 7800 measurements of undrained shear strength, $s_u$, for a single stratigraphic layer. The overall population of $s_u$ measurements is shown in Figure 3-6a and 3-7a. This population of measurements represents the actual undrained shear strength for the stratum. Figures 3-6b through 3-6d and 3-7b through 3-7d show arbitrary collections, or statistical "subsamples", of these measurements that might be obtained from different site investigations. Figure 3-6 shows measurements obtained by taking subsamples of four measurements (i.e., $n$=4) to represent what might occur when relatively few measurements are used to characterize $s_u$ for the layer. Figure 3-7 shows measurements obtained considering subsamples of twenty measurements (i.e., $n$=20) to reflect what might occur when substantially greater numbers of measurements are used.

As shown in Figure 3-6, measurements obtained for each of the three "subsamples" of size $n$=4 are substantially different. Measurements shown for the first subsample in Figure 3-6b are relatively consistent, but generally fall among the lower measurements observed for the entire population. Measurements shown for the second subsample in Figure 3-6c are more scattered, with two measurements reflecting some of the greater values of $s_u$ from the population and two measurements reflecting values near the mean trend of the population. Measurements from the third subsample in Figure 3-6d reflect an intermediate condition with slightly less scatter, but with one measurement substantially exceeding the other three. The solid lines in Figure 3-6 indicate interpretations developed considering only the available measurements for each subsample while the dotted lines indicate the interpretation derived from the entire population. It is clear that the three interpretations of $s_u$ derived from the three different subsamples are both substantially different from one another and substantially different from the "true" value of $s_u$ established from the entire population of measurements. The differences in the interpretations are great enough to have a meaningful impact on designs derived from the different interpretations.

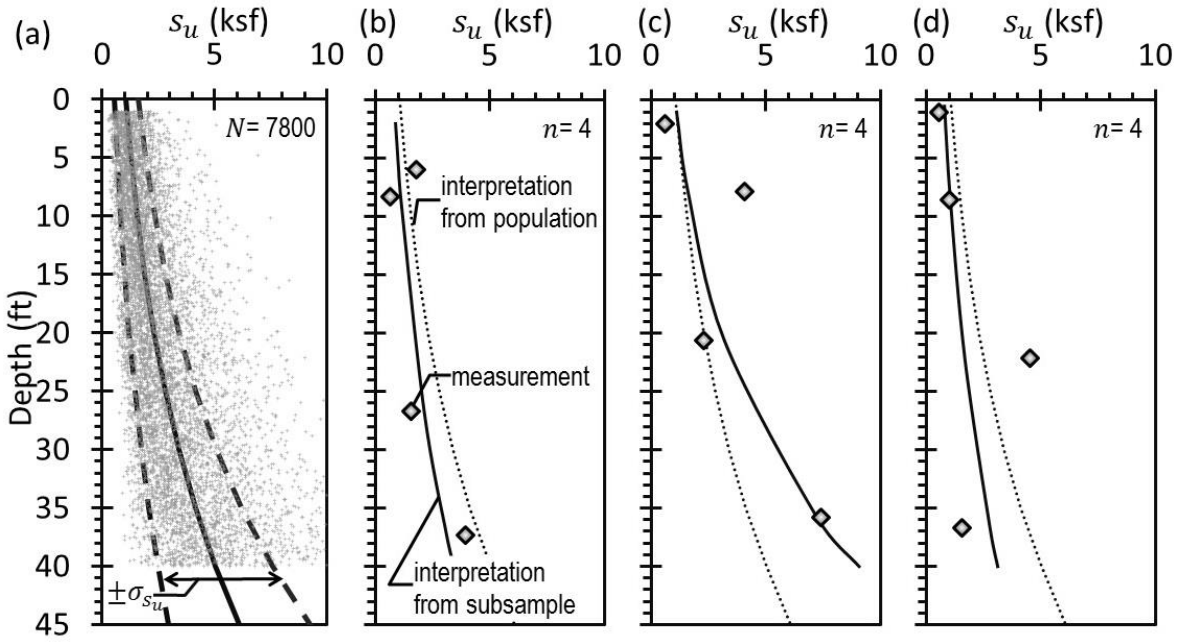


**Figure 3-6 Alternative samples of size $n$=4 from population of simulated $s_u$ measurements: (a) population, (b) subsample one, (c) subsample two, and (d) subsample three.**

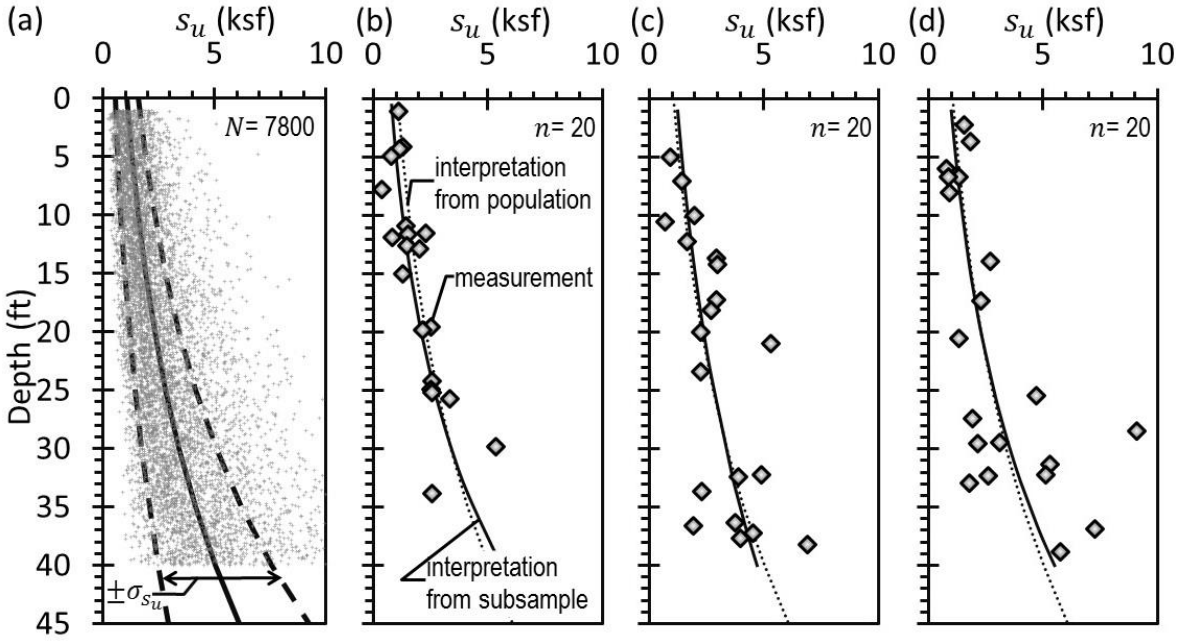


**Figure 3-7 Alternative samples of size $n$=20 from population of simulated $s_u$ measurements: (a) population, (b) subsample one, (c) subsample two, and (d) subsample three.**

Measurements plotted for subsamples with size $n$=20 in Figure 3-7 again reveal different collections of measurements for each subsample. However, with twenty measurements in each subsample, interpretations derived exclusively from the available measurements in each subsample are both more

consistent with each other and more consistent with the "true" value of $s_u$ established from the entire population of measurements. As a practical matter, any of the three interpretations shown in Figure 3-7 are acceptable representations of actual conditions that are likely to produce similar designs. The same cannot be said of the three interpretations derived from fewer measurements shown in Figure 3-6. Designs based on the interpretation shown in Figure 3-6c would likely lead to a condition where a feature would not achieve the desired margin of safety or established target reliability, which increases the likelihood of having performance problems and incurring future costs for repair and rehabilitation. Use of the interpretations established in Figure 3-6b and 3-6d would likely be conservative, which is more desirable than being unconservative but would lead to certain additional costs for construction that are greater than necessary.

It is important to recognize that the population of measurements, i.e., the "true" properties, is generally unknown. Although one can select specific locations for sampling and/or testing, one does not generally know in advance whether specific measurements will be representative of the mean value of a property, or the lower or upper ranges of a property. Furthermore, for a given collection of measurements, one cannot determine whether the measurements obtained or the interpretations derived from the measurements are truly representative of the entire population. One can only control the quantity and quality of measurements that are made. Fortunately, there are statistical measures that can be used to characterize the likelihood of having a representative collection of measurements, and such measures can be used to guide scoping of site characterization activities. Additional descriptions of these statistical measures are provided in Chapter 11.

### 3.4.3 Influence of Number of Measurements on Estimates for Geotechnical Design Parameters

The examples presented in the previous section represent a small number of potential outcomes from different site investigations for the stratum considered. The influence of considering different numbers of measurements can be further demonstrated by performing large numbers of simulations similar to those presented in the previous section for different numbers of measurements (i.e., for different $n$). Figure 3-8 shows histograms of the interpreted mean undrained shear strength at a specific depth ($z$=7 feet) for 10,000 different simulated site investigations using the populations shown in Figure 3-6 and 3-7. The histograms were established by repeatedly selecting random subsamples of a given size ($n$) from the entire population of measurements and developing interpretations of $s_u$ based on the subsampled measurements alone. Figure 3-8a shows the histogram of the interpreted mean $s_u$ for subsamples with $n = 5$ while Figure 3-8b shows the histogram determined for subsamples with $n = 20$.

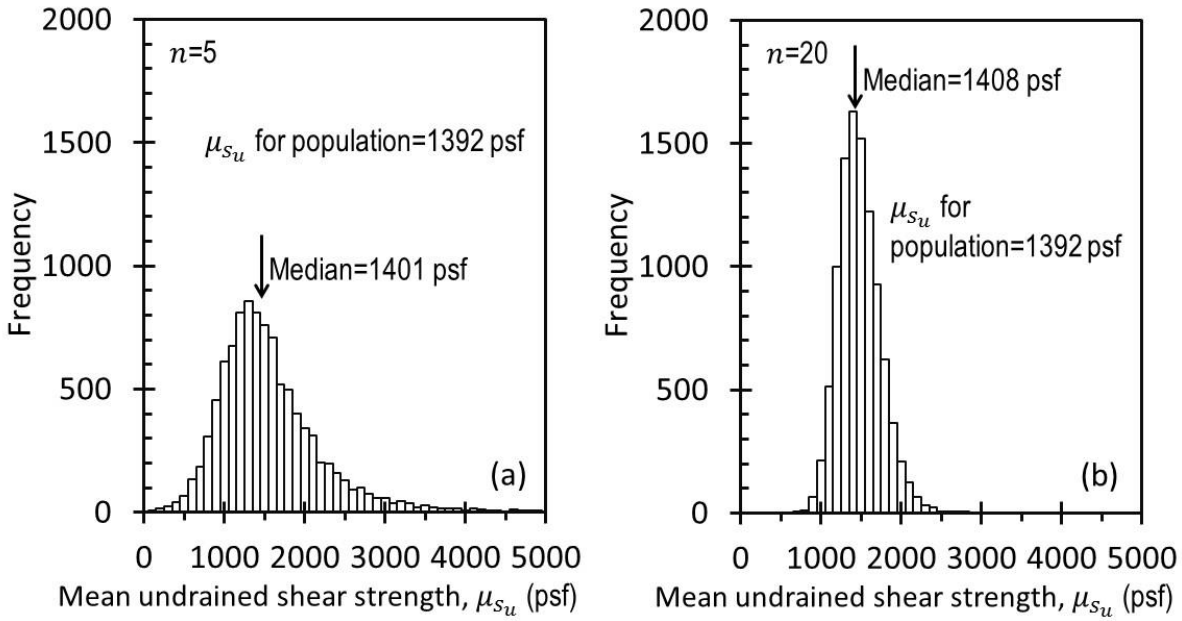


**Figure 3-8 Histograms of mean $s_u$ from subsamples of size: (a) $n$=5, and (b) $n$=20.**

For both $n = 5$ and $n = 20$, the histograms in Figure 3-8 indicate that the most likely result of a single investigation is to produce a mean value that is similar to the true mean value of $s_u$. However, there is some likelihood of substantially over- or under-estimating the true mean value from the population. Comparison of the histograms indicates that there is substantially greater likelihood for accurately estimating the true mean value from an arbitrary collection of measurements when twenty measurements are considered. Conversely, there is substantially greater likelihood of estimating a significantly erroneous mean value when five measurements are used to estimate the mean. Furthermore, the histograms indicate that the range of potential estimates for the mean value, and thus the magnitude of potential errors, are substantially greater when five measurements are considered. For the case shown, the mean value established from the entire population of measurements is 1392 psf. The practical range of estimates established (using the 5$^{th}$ and 95$^{th}$ percentiles) considering five measurements extends from a low of 715 psf to a high of 2840 psf. Thus, for this site, there is a small chance of underestimating the true mean value by 50 percent or overestimating the mean value by a factor of two when five measurements are used to interpret the mean value. When considering twenty measurements, estimates established for the mean value range from 1050 psf to 1890 psf, which suggest that there is a small chance of underestimating the mean value by 25 percent or overestimating the mean value by 35 percent of the true mean value. Thus, using greater numbers of measurements not only increases the likelihood of obtaining an accurate estimate for the mean value but also decreases the magnitude of potential errors in estimating the mean value.

The variability of a site also affects the influence of the number of measurements. Figure 3-9 shows results of simulated site investigations performed for two sites: one site having little variability in undrained shear strength measurements and the other having great variability. Figure 3-10 shows the populations of measurements used for the respective sites. The results shown in Figure 3-9 represent simulations performed for $n$ ranging from 3 to 50 for each of the two sites. The solid symbols in the figure indicate the median value from 10,000 different simulations for each $n$, while the vertical bars represent a "practical range" of mean values established considering the 5th and 95th percentile estimates of the mean value.

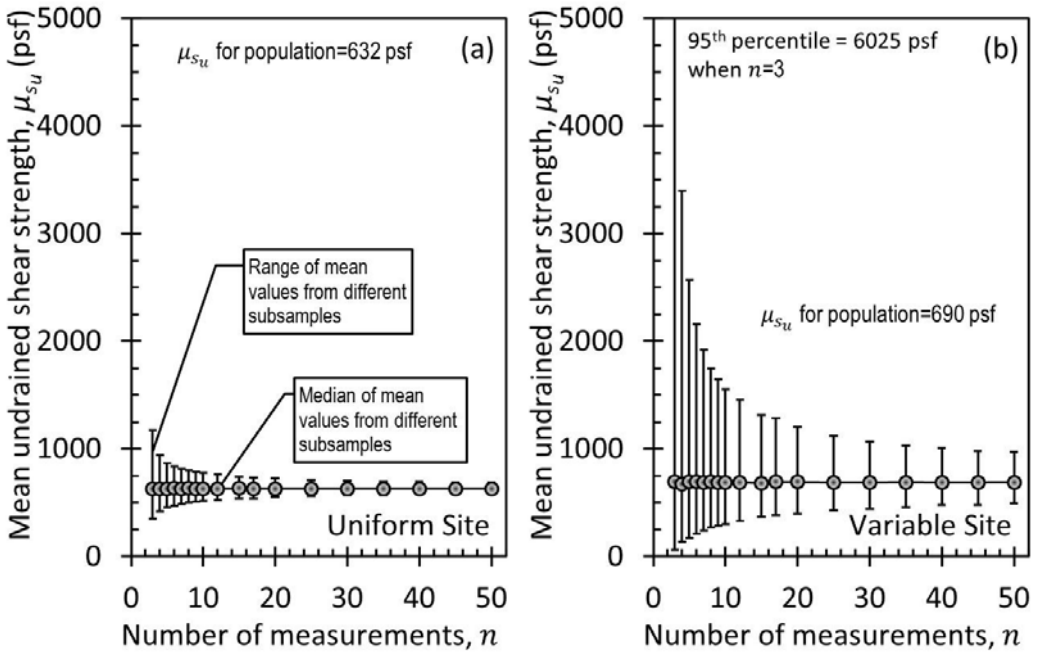


**Figure 3-9 Interpreted mean $s_u$ from subsamples of different sizes: (a) relatively uniform site, and (b) highly variable site (adapted from Loehr, et al., 2015).**

Figure 3-9 shows that the median value of the interpreted $s_u$ from all simulated site investigations is similar to the actual mean value from the entire population for both the uniform and variable sites, regardless of the number of measurements considered. This is consistent with the histograms shown in Figure 3-8, and suggests that there is substantial likelihood for obtaining a representative statistical sample that produces an $s_u$ estimate similar to the true value regardless of the site and number of measurements. However, the ranges of estimated $s_u$ values from different site investigations vary substantially with the variability of the site and with the number of available measurements. For the uniform site, estimated $s_u$ values range from 350 psf (55 percent of the true mean) to 1175 psf (190 percent of the true mean) when considering only three measurements. For the uniform site, nine

measurements are required to reduce the range of estimates to fall within 25 percent of the actual mean value and forty measurements are necessary to reduce the potential range to fall within 10 percent of the actual mean value. In contrast, estimated $s_u$ values for the variable site range from 63 psf (1 percent of the true mean) to 6000 psf (875 percent of the true mean) when considering only three measurements, and greater than fifty measurements are needed just to reduce the range of estimates to fall within 25 percent of the actual mean value.

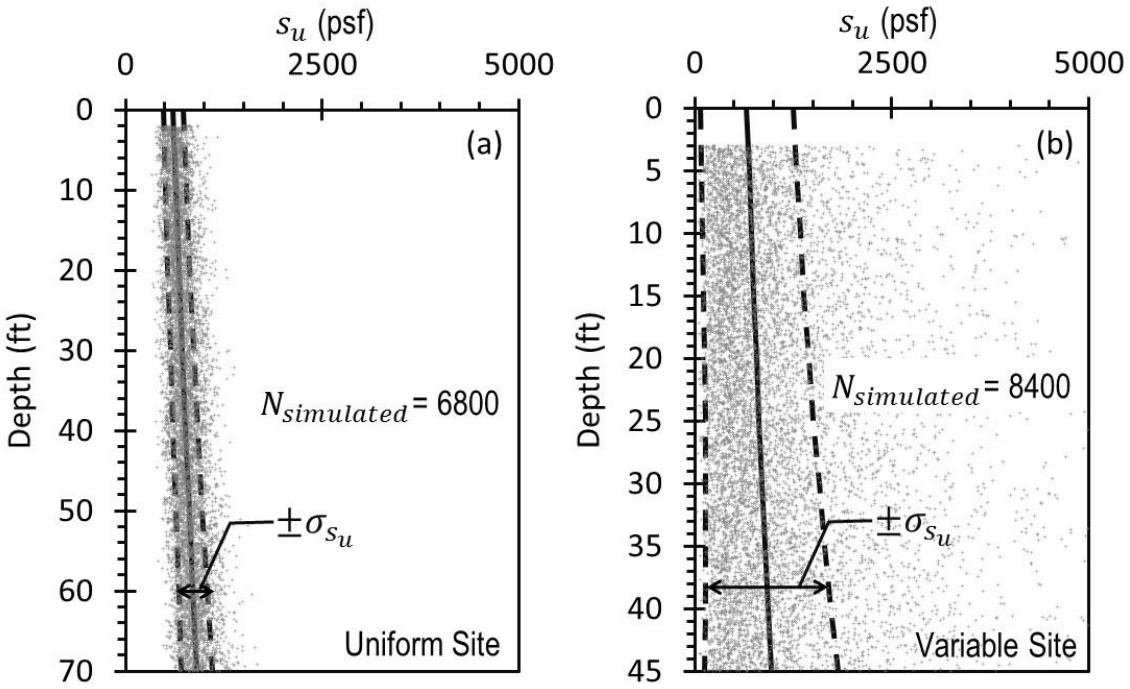


**Figure 3-10 Simulated populations of $s_u$ measurements for: (a) relatively uniform site and (b) highly variable site.**

Fortunately, Figure 3-9 also shows that the practical range of estimated $s_u$ values obtained from the different simulated investigations decreases rapidly with additional measurements for both the uniform and highly variable sites. This is especially true when relatively small numbers of measurements (e.g., $n < 10$) are available, which suggests that a few additional measurements have a dramatic effect on reliability when small numbers of measurements are available. A few additional measurements also improve reliability when larger numbers of measurements are available, but the magnitude of improvement is diminished.

One caveat for the results presented in this section is that "interpretation" was performed automatically using regression techniques, without the benefit of engineering judgment that should be invoked in developing interpretations for $s_u$. It is therefore likely that the ranges shown for estimates of $s_u$ are

greater than would be produced if the different site investigations were interpreted with sound judgment. It is also likely that application of sound judgment might introduce some bias into interpretations of $s_u$, since many engineers will give greater consideration to lesser measurements than to greater measurements, especially when there is substantial scatter in the measurements. Nevertheless, the results presented demonstrate the strong influence of the number of available measurements, and that greater numbers of measurements will dramatically reduce the magnitude of potential errors in estimates for geotechnical design parameter values. The results presented are also predicated on the population being composed of measurements from a single soil or rock stratum rather than a combination of measurements from different materials.

### 3.4.4 Influence of Number of Measurements on Estimates of Variability and Uncertainty

In addition to affecting estimates of the mean value for a design parameter, the number of available measurements also influences the accuracy of estimates for variability and uncertainty (Baecher and Christian, 2003; Loehr, et al., 2015). While estimates for variability and uncertainty are seldom required for many current geotechnical design methods, they are required for design of some geotechnical features according to current AASHTO LRFD Bridge Design Specifications (AASHTO, 2014). In addition, some agencies and organizations have adopted methods that require estimates of uncertainty for selection of resistance factors for design of some geotechnical features (e.g., MoDOT, 2015; EPRI, 2012) as described in more detail in Section 3.4.5.

Figure 3-11 shows ranges for estimates of uncertainty computed from the same simulated site investigations used to produce Figure 3-9. The measure plotted in Figure 3-11 is the coefficient of variation of the mean value of undrained shear strength, $COV_{\mu_{s_u}}$, which represents the uncertainty in the estimated value of $s_u$ based on available measurements (i.e., the confidence in the estimated value). As described in more detail in Chapter 11, this measure is generally the appropriate measure to consider for design, and is often denoted as $COV_{model}$ and referred to as model uncertainty.

Figure 3-11 clearly shows that both the range and median value of $COV_{\mu_{s_u}}$ decrease with increasing numbers of measurements, which reflects increasing confidence in the estimated $s_u$ value with increasing numbers of measurements. The range and median values of $COV_{\mu_{s_u}}$ are generally smaller for measurements from the uniform site than for the variable site for similar values of $n$, which indicates that greater numbers of measurements are required to achieve a given reliability for soil/rock properties at sites with greater variability. Figure 3-11 also shows that the range of estimated $COV_{\mu_{s_u}}$ values is extremely large when the number of available measurements is small, suggesting that there is high

likelihood that uncertainty in the estimated value of $s_u$ may be substantially underestimated or overestimated when small numbers of measurements are available. It is also notable that both the median and the range of estimated values for $COV_{\mu_{s_u}}$ asymptotically approach zero as the number of measurements becomes large, which reflects the fact that uncertainty in estimated values of design parameters can be practically eliminated if sufficient numbers of measurements are made.

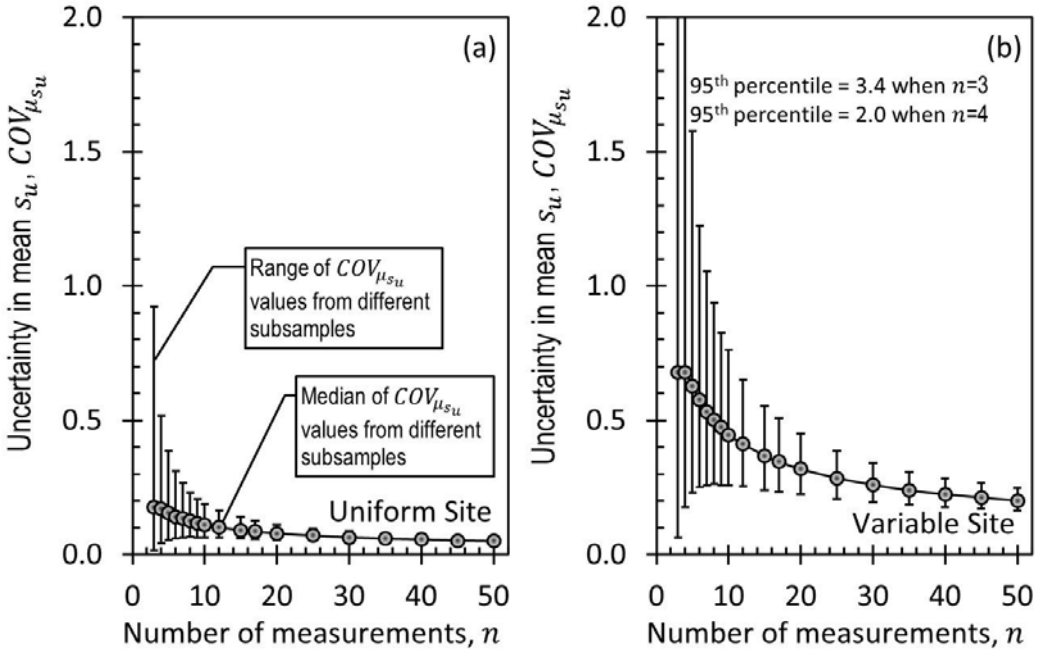


**Figure 3-11 Ranges of $COV_{\mu_{s_u}}$ determined from subsamples of different sizes for: (a) relatively uniform site and (b) highly variable site (adapted from Loehr, et al., 2015).**

### 3.4.5 Influence of Number of Measurements for Geotechnical Design

While establishing reliable values for geotechnical design parameters is an important objective for geotechnical site characterization, the ultimate objective for design is to produce features that achieve some target reliability (or probability of failure). It is therefore useful to consider how the reliability of geotechnical design parameters, and more specifically the number of available measurements, influences the reliability of geotechnical features. Loehr et al. (2015) evaluated the influence of the number of $s_u$ measurements for geotechnical design of shallow foundations using simulated site investigations similar to those described in the preceding sections. For these analyses, spread footings were repeatedly designed (sized) using estimates of $s_u$ established from randomly selected subsamples of measurements taken from the large populations of measurements shown in Figure 3-10. Probabilities of failure for these spread footings were subsequently determined considering the "true" soil properties established from the entire

population of measurements. The resulting probabilities of failure were then compared to established target probabilities of failure to characterize how the number of available measurements affects the likelihood that the designed footings achieve the target reliability.

Figure 3-12 and 3-13 show the percentage of cases where designs performed according to the AASHTO LRFD Bridge Design Specifications (AASHTO, 2014) using $s_u$ established from the simulated site investigations were deemed to be "satisfactory", "over-reliable", and "under-reliable". Here, "satisfactory" is used to represent cases where the site characterization was just sufficient for designs to practically achieve the target reliability. "Over-reliable" is used to represent cases where the site characterization led to foundation designs with reliability that is substantially greater than the target reliability. "Under-reliable" is used to represent cases were the site characterization was insufficient for designs to achieve the target reliability. Satisfactory cases were identified as cases with computed probabilities of failure, $p_f$, between 0.5 and 1.5 times the target probability of failure, $p_T$ (i.e., $0.5 \cdot p_T \leq p_f \leq 1.5 \cdot p_T$). Over-reliable cases were identified as those with computed probabilities of failure less than 0.5 times the target probability of failure (i.e., $p_f < 0.5 \cdot p_T$). Under-reliable cases were identified as those with computed probabilities of failure greater than 1.5 times the target probability of failure (i.e., $p_f > 1.5 \cdot p_T$). The probability of failure thresholds used for these criteria were established based on consideration of "perfect" site characterization; with no uncertainty in $s_u$, simulated designs produce computed probabilities of failure between 0.5 and 1.5 times the target probability of failure due to uncertainty in the design method. Results shown in Figure 3-12 reflect designs performed using the population of $s_u$ measurements for the "uniform" site shown in Figure 3-10a while results in Figure 3-13 reflect designs derived from the population of measurements for the highly "variable" site shown in Figure 3-10b.

Figure 3-12 shows that, for uniform sites, the vast majority of cases are observed to be either satisfactory or over-reliable regardless of the number of measurements used to interpret $s_u$. This means that most site characterizations for "uniform" sites are sufficient to produce designs that practically achieve or exceed the target reliability from the AASHTO code, even when as few as three measurements are used to establish values for design parameters. In contrast, substantial percentages of under-reliable cases are observed for the highly "variable" site when few $s_u$ measurements are used for characterization, as shown in Figure 3-13. With few measurements, nearly 50 percent of the cases were insufficient to produce designs that achieve the target reliability. For the specific population of measurements considered, fourteen measurements are needed to reduce the likelihood of insufficiently characterizing $s_u$ to less than 10 percent, and twenty measurements are needed to reduce the likelihood to less than 5 percent.

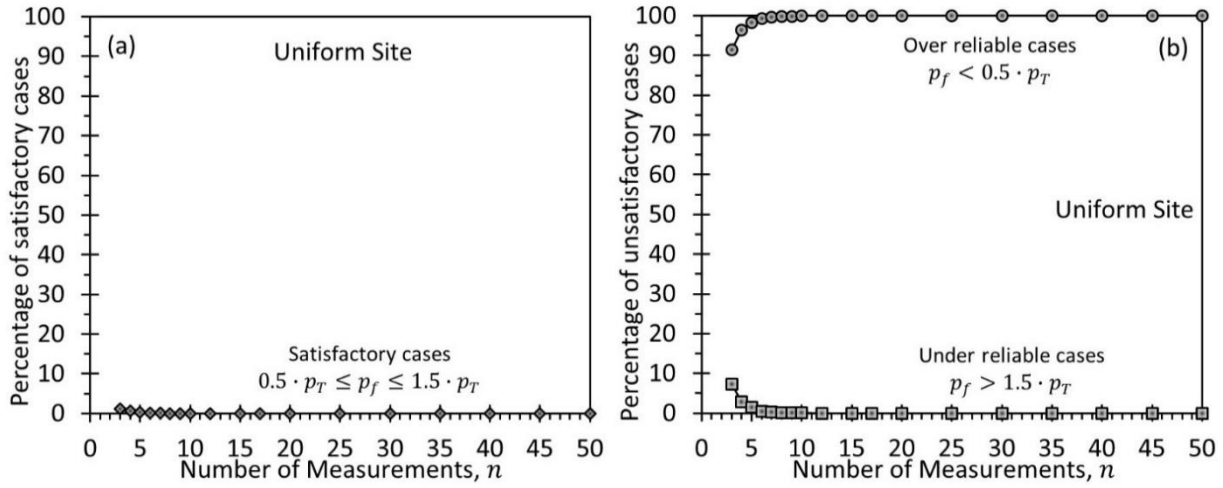


**Figure 3-12 Percentages of spread footings that practically achieve target probability of failure when designed using AASHTO LRFD provisions for a relatively uniform site: (a) "satisfactory" cases, and (b) "under-reliable" and "over-reliable" cases (adapted from Loehr, et al., 2015).**

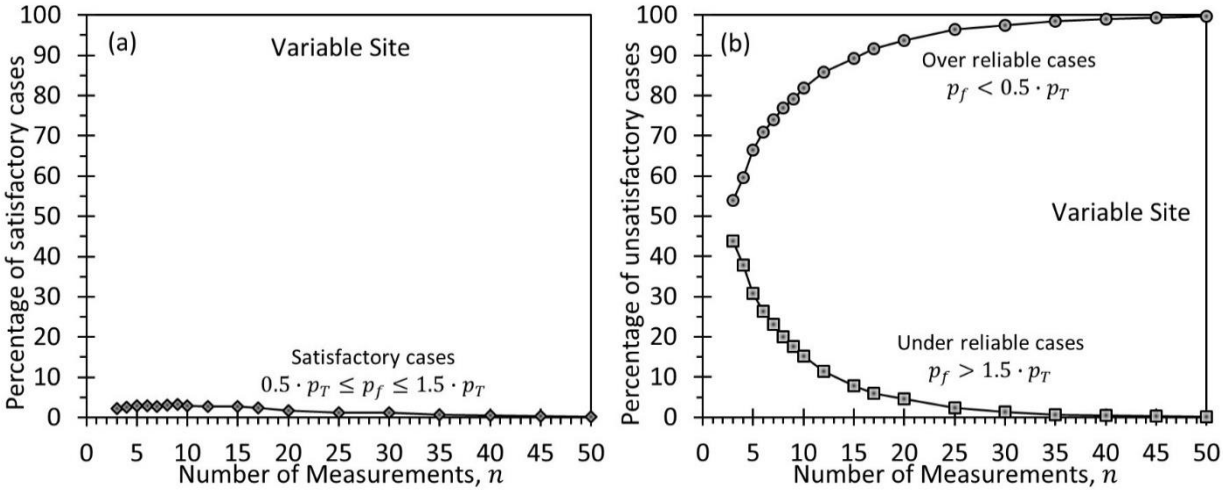


**Figure 3-13 Percentages of spread footings that practically achieve target probability of failure when designed using AASHTO LRFD provisions for a variable site: (a) "satisfactory" cases, and (b) "under-reliable" and "over-reliable" cases, (adapted from Loehr, et al., 2015).**

In practice, one cannot definitely direct or determine whether a design based on a specific collection of measurements will achieve the target probability of failure because the specific measurements collected from the broader population of measurements is a random occurrence beyond the control of those performing the site investigation. Fortunately, however, the likelihood of not achieving the target probability of failure decreases as greater numbers of measurements are considered for design and the number of measurements can be controlled by those conducting site investigations. Comparison of Figure 3-12 (uniform site) and 3-13 (highly variable site) suggests that the number of measurements

required to achieve some acceptable likelihood for sufficient characterization is strongly dependent upon the variability of a given site. The two sites presented are generally representative of the extremes of site variability; thus, most other sites will fall between the two extremes presented.

Figure 3-12 and 3-13 both show that the percentage of cases identified as "satisfactory" is quite small, for all values of $n$ and for both the uniform and variable sites. Interestingly, some agencies such as the Missouri Department of Transportation (MoDOT) and the Electrical Power Research Institute (EPRI) have adopted design provisions that specify resistance factors as a function of uncertainty in geotechnical design parameters (e.g., Phoon, et al., 1995; Phoon, et al., 2000; Loehr, et al., 2011a, b, c; Loehr, et al., 2013b). Adoption of such resistance factors for design changes how the number of measurements affects the likelihood of producing satisfactory, under-reliable, and over-reliable designs (Loehr, et al., 2015). Figure 3-14 illustrates this point by showing percentages of satisfactory, under-reliable, and over-reliable characterizations determined using simulated site investigations for the uniform site considered previously along with resistance factors adopted in current MoDOT design provisions (MoDOT, 2015). As shown in the figure, the percentage of satisfactory cases that practically achieve the target reliability increases with increasing numbers of measurements. The percentage of over-reliable cases simultaneously decreases in a complementary manner while the percentage of under-reliable cases remains practically constant. This contrasts with results presented in Figure 3-12 and 3-13, which indicate consistently small percentages of satisfactory cases, decreasing percentages of under-reliable cases, and increasing percentages of over-reliable cases with increasing numbers of measurements.

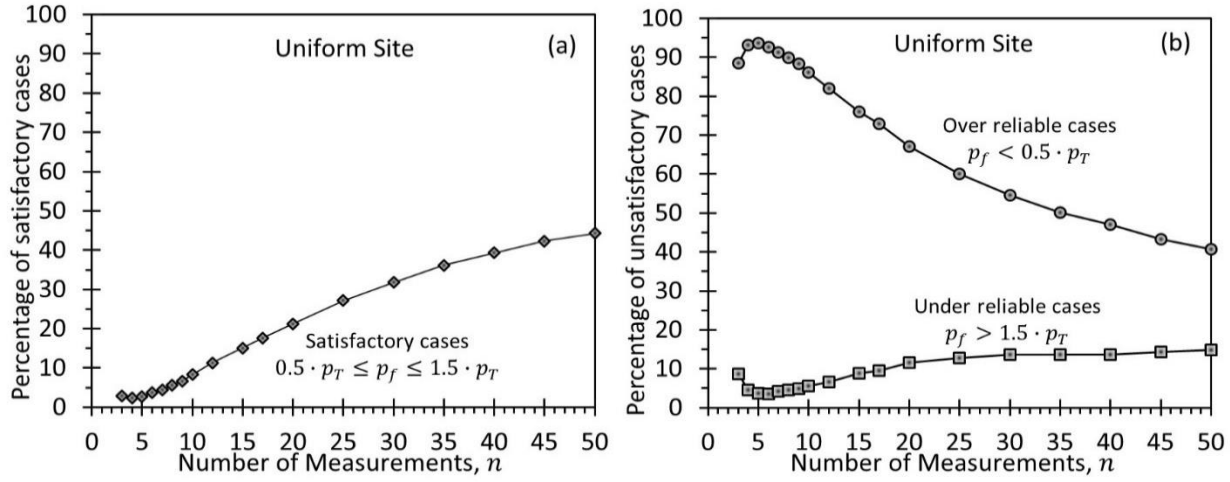


**Figure 3-14 Percentages of spread footings that practically achieve target probability of failure when designed using MoDOT LRFD provisions for a uniform site: (a) "satisfactory" cases, and (b) "under-reliable" and "over-reliable" cases (adapted from Loehr, et al., 2015).**

Use of design provisions that adopt variable resistance factors to account for uncertainty in design parameters leads to different motivations for considering greater number of measurements for design. As shown in Figure 3-14, the likelihood of an under-reliable characterization is controlled by the specified resistance factors (which are calibrated considering different levels of uncertainty for relevant design parameters), regardless of the number of measurements used and regardless of the uncertainty in the established design parameters. As such, the motivation for considering additional measurements changes from trying to limit the potential for producing under-reliable designs to one of trying to maximize the likelihood of producing "satisfactory" designs. This alternative approach therefore motivates performing site characterization that will maximize design efficiency while still limiting the likelihood of under-reliable design. The approach also tends to simplify decision making when establishing scopes for site characterization because decisions can be based on a direct comparison of costs required for obtaining additional measurements with cost savings that may be realized with additional measurements and greater resistance factors. While such comparisons necessarily require judgment about the magnitude of savings for construction, the comparisons are more direct and more consistent with the fundamental value proposition for site characterization described in Chapter 2. In contrast, scoping for site characterization when adopting constant resistance factors is driven by concern for limiting the likelihood of under-reliable design, which is more difficult to quantify in terms of costs.

The influence of the number of available measurements is also dependent on the specific application and design method being considered, and specifically the reliability of the design method used. As such, the quantitative influence of the number of measurements presented in this section may not accurately represent the quantitative influence of relevant design parameters for other design methods or other types of features. Nevertheless, the general influence demonstrated and described in this section is qualitatively applicable to other design methods and applications. Additional research is needed to develop more quantitative guidance regarding how the number of measurements affects the reliability of designed features for other methods and applications.

### 3.4.6 Application of Judgment for Establishing Appropriate Number of Measurements

Preceding sections of this chapter have demonstrated that there is substantial likelihood that estimates for a geotechnical design parameter may be substantially greater than or less than the actual or appropriate value of the parameter when small numbers of measurements are used to establish the estimates. The potential for such errors arises directly from statistical sampling considerations rather than from human error or problems with sampling and measurement (although those can obviously introduce error as well). The likelihood of such errors cannot, therefore, be controlled by selective or directed sampling because

characteristics of the population are not known in advance. Thus, the primary means for control of such errors is through collection and use of sufficient numbers of measurements.

Unfortunately, the content presented in Section 3.4.5 also shows that the number of measurements required to limit the likelihood for producing under-reliable designs using current AASHTO design methods is strongly dependent on the variability of a specific site. Since the variability of properties is seldom known prior to developing scopes for site characterization programs, considerable judgment is necessary to develop appropriate scopes for geotechnical site characterization. There simply is no single number of measurements that is universally appropriate for all sites; rather, the appropriate number of measurements depends on the variability of a site, the type of geotechnical feature being designed, as well as the specific design methods adopted. Judgment regarding scoping decisions can certainly be informed by understanding of geologic processes that formed the deposits, by experience in similar conditions, by historical or preliminary measurements at a site, or through "phasing" of investigations such that results from initial phases of an investigation can be used to refined estimates for the required number of measurements for subsequent investigations. Alternatively, one can also make preliminary assumptions regarding the variability of a given site to develop a scope for investigations, and then evaluate whether those assumptions are reasonable based on the measurements obtained. If the assumptions are found to be unreasonable, additional investigations can be conducted to collect the additional measurements needed for the site conditions and design applications present.

## 3.5 INFLUENCE OF TYPE OF MEASUREMENTS

In addition to being affected by the number of measurements, the reliability of design parameters established from site characterization activities is also often affected by the type and quality of measurements used. It is often the case that specific geotechnical properties can be measured or estimated in several different ways. For example, $s_u$ for saturated, fine-grained soils can be measured using several forms of laboratory tests, such as triaxial tests, unconfined compression tests, pocket penetrometer tests, torvane tests, and lab vane shear tests, among others. Undrained shear strength can also be estimated from various in situ test measurements including SPT, CPT, and field vane shear tests (FVT). However, it also is fundamentally true that all such measures are not equivalent measures of the true undrained shear strength and are not equally reliable. While the concepts presented in the previous section apply to all types of measurements, quantitative application of the methods for developing design parameters is predicated on the assumption that the measurements are direct and unbiased measures of the relevant design parameter. While this assumption practically holds for some types of measurements collected for geotechnical site characterization, it is not true of all measurements.

It is common in geotechnical engineering practice to estimate values for design parameters from both "direct" and "indirect", or "surrogate" measurements. Throughout this manual, the term "direct measurement" will be used to refer to measurements that do not require an explicit transformation or manipulation to produce estimates of the fundamental design parameter. Direct measurements are often measures of fundamental soil or rock properties, but this is not always the case as explained subsequently in this section. Examples of common direct measurements include:

- use of uniaxial compression tests to establish the uniaxial compressive strength, $q_u$ for rock;
- use of unconfined compression tests or triaxial compression tests to establish $s_u$ for soils;
- use of direct shear tests or triaxial compression tests to establish effective stress shear strength parameters, $c'$ and $\phi'$, for soils; and
- use of one-dimensional consolidation tests to establish the compression index, $C_c$, recompression index, $C_r$, and preconsolidation stress, $\sigma_p'$, for soils.

These direct measurements, and others, are subject to variability introduced due to variability in the soil or rock specimens acquired for testing and due to variability and uncertainty in the measurement techniques themselves. As such, the variability and uncertainty in design parameters established from direct measurements is controlled by these same sources of variability and uncertainty.

In contrast, the term "indirect measurement", or "surrogate measurement" will be used to refer to measurements that require some manipulation or transformation to produce an estimate of the actual design parameter. Common indirect measurements include, among many others:

- use of CPT tip resistance, $q_c$ or $q_t$, to estimate $s_u$ or $\phi'$ for soils;
- use of SPT $N$-values to estimate $s_u$ or $\phi'$ for soils;
- use of point load strength index, $I_s$, to estimate $q_u$ for rock;
- use of pocket penetrometer or torvane tests to estimate $s_u$ or $q_u$ for soils;
- use of Atterberg limits to estimate peak or residual values of $\phi'$ for soils;
- use of Atterberg limits to estimate compressibility for soils; and
- use of borehole permeability tests to estimate the hydraulic conductivity, $k$, for soil or rock.

Manipulations required to "transform" indirect measurements to estimates for design parameters often involve relations derived from empirical measurements, from theoretical considerations, or from combined theoretical and empirical considerations. Many transformations, such as the one shown in Figure 3-15, are derived exclusively from empirical measurements and can appropriately be termed

"correlations". However, the term "transformation" is used throughout this manual to reflect the fact that indirect measurements do not always rely on empirical correlations to produce estimates for design parameters.

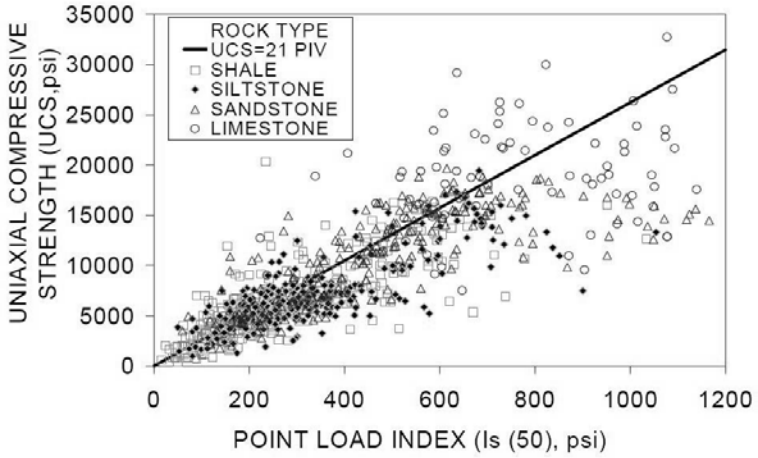


**Figure 3-15 Empirical transformation between $I_s$ and $q_u$ (denoted as $UCS$) from Rusnak and Mark (2000).**

Like direct measurements, indirect measurements are subject to variability and uncertainty due to variability and uncertainty in the measurements themselves and variability in the soil or rock being tested. However, the variability and uncertainty for design parameters established from indirect measurements is also influenced by uncertainty in the relation used to transform the indirect measurements into estimates for design parameters, as shown in Figure 3-15. Thus, indirect measurements are subject to an additional source of uncertainty that is not present with direct measurements.

Estimates for geotechnical design parameters from indirect measurements are often less reliable than estimates from direct measurements because indirect measurements are subject to additional uncertainty associated with the required transformation. However, there are instances when indirect measurements can be used to produce more reliable estimates for design parameters than can be obtained using direct measurements. Such instances generally occur when large numbers of indirect measurements can be acquired cost effectively and when the indirect measurements are reliably related to the design parameter of interest. Such instances also sometimes occur when acquiring reliable direct measurements is challenging, such as occurs when considering rocky soils that are notoriously difficult to sample. This issue was described by Peck (1967) as follows:

> *"Because of the prevalence of heterogeneity, there appear to be serious shortcomings to design methods based on the results of elaborate tests on a few selected samples.*

*Even if the foundation engineer possessed enough reliable information to duplicate in a sample all the successive states of stress that might be experienced at a point in the subsoil—a situation rarely likely to be realized—the variability of the subsoil would introduce the greatest of uncertainties when the results were extrapolated from the few samples that could be so tested to the subsoil as a whole. More often than not, the benefits of the superior replication of the stress history would be smaller than those derived from the application of cruder tests and procedures with respect to a more representative conception of the soil conditions."*

It is important to recognize that even "perfect" direct tests on completely unrepresentative samples will be less relevant and less reliable than "imperfect" indirect measurements on representative samples. A common example of this issue is use of SPT and CPT measurements in clean, coarse-grained soils where acquisition of representative samples for direct measurements is difficult if not impossible. In such cases, indirect measurements may be superior to direct measurements.

It is also true that measurements that would generally be considered to be direct measurements can be subject to systematic source(s) of bias that can effectively render them to be indirect measures. For example, measurements of $s_u$ using unconsolidated-undrained type triaxial compression tests are generally considered to be direct measurements. However, such measurements are also known to be influenced by sample disturbance, differences in loading rate between laboratory tests and field loading, and potential differences in stress paths between the loading applied in the laboratory and that anticipated in the field. Each of these phenomena introduce some bias into the direct measurements, and corrections to account for each phenomenon should strictly be applied before establishing appropriate values for geotechnical design parameters and quantifying the uncertainty present in those parameters. However, the corrections themselves are not known with certainty; thus, the corrections represent a form of uncertain transformations that are similar to those required for indirect measurements.

Finally, it is also possible to estimate values for design parameters by simultaneously considering both direct and indirect measurements. Combined consideration of direct and indirect measurements may substantially reduce the uncertainty for estimated design parameters compared to consideration of direct or indirect measurements alone (Loehr, et al., 2013a). While methods for quantifying uncertainty in design parameters established from multiple types of measurements are more complex than methods for quantifying uncertainty for a single type of measurement, the potential advantages often justify the increased complexity. In this context, a single indirect measurement may not fully "count" as a single measurement in the sense considered in Section 3.4 and it may take several, or even many indirect

measurements to be functionally equivalent to a single direct measurement. Nevertheless, the potential to combine both direct and indirect measurements can produce meaningful reductions in uncertainty for some design parameters. Whether direct measurements, indirect measurements, or some combination of direct and indirect measurements will produce the least uncertainty for a specific case depends predominantly on the number of direct and indirect measurements, and the reliability of the transformation between the indirect measurement and the design parameter of interest. The methods and procedures described in this manual provide a sound basis upon which to judge the relative benefits of direct and indirect tests, both on a site or project specific basis, as well as more generally.

Preceding discussions in this section presume that the design parameters of interest are fundamental soil properties. However, there are instances when requirements may be practice and/or design method dependent. For example, driven pile design can be conducted using a variety of approaches ranging from so-called "rational" methods that require knowledge of soil/rock strength properties, to largely empirical methods that require specific in situ test measurements (e.g., SPT or CPT measurements). In such cases, measurements that might normally be considered as indirect measurements when used to establish fundamental soil/rock properties should be considered as "direct" measurements since they serve as direct inputs to a design method and do not require any transformation. In such cases, the transformation is implicit to the design methods; thus, uncertainty associated with the transformation is considered as part of uncertainty in the design method and should not be considered as part of the design input parameter.

Many transformation equations are presented for individual soil and rock properties in subsequent chapters. Methods for quantifying uncertainty for design parameters from both direct and indirect measurements are described in Chapter 11. Additional guidance for the requisite computations is provided in Appendix 3.

## 3.6 INFLUENCE OF BORING, SAMPLING AND TESTING METHODS

Considerations presented in Sections 3.4 and 3.5 are based on the presumption that measurements for a specific property are unbiased, meaning that the measurements are void of any systematic bias between the actual property in the field and estimates of a property or design parameter. Unfortunately, some practices for drilling, sampling, and testing can introduce substantial bias into some laboratory and field measurements. Perhaps the most commonly cited source of bias for geotechnical measurements is so-called "sample disturbance", which can affect measured values for a number of different soil and rock properties. Additional bias can be introduced by loading rate effects and loading method (i.e., stress path), among other sources. Additional discussion about specific effects attributed to sample disturbance

and other sources for specific measurements is provided in subsequent chapters. Additionally readers are referred to excellent references that are available on the subject (e.g., Hvorslev, 1949; Santagata and Germaine, 2002). However, it is important that these effects be considered during scoping of investigations for site characterization to ensure that results of the investigations are appropriate for the intended use.

The term "sample disturbance" is most often associated with specific methods and devices for acquiring soil samples. However, the fact is that disturbance can be caused by poor drilling techniques prior to a sampler being put into the ground, poor handling and transportation following acquisition of samples, poor sealing of samples, and poor practices in the laboratory as part of specimen preparation for testing. It is also true that some degree of sample disturbance is inevitable as a result of stress relief induced by removing samples from the ground (where they are under stress) and bringing them into the laboratory (where the stress is inevitably relieved and reapplied differently). Such considerations motivate use of in situ tests, since such tests are performed in the ground, which eliminates some sources of disturbance. However, even in situ tests can be biased by poor boring and testing techniques. For example, SPT measurements made in coarse-grained soils at the bottom of a borehole can be biased downward if inward flow of groundwater loosens soil near the base of the borehole, or biased upward if large particles plug the sampler. Care is therefore required for all types of testing.

While it is generally desirable to minimize disturbance to the extent possible, there are some instances where doing so must be carefully considered. Many commonly used design methods are empirically established, usually based on a "typical" standard of care for drilling, sampling, and testing. Because the methods are empirical, the design methods inherently account for "typical" bias in measurements that produce inputs for the methods. With such methods, elimination of one or more sources for typical bias can actually introduce an unintended, and generally unquantified, bias into design since the measurements will not be consistent with the intended use. Similarly, even design methods that are theoretically based often rely on compensating sources of bias (Ladd and Foott, 1974; Ladd, 1991), which mandates careful consideration about eliminating one source of bias without considering others. Combined, these issues demonstrate the importance of considering the expected use for specific measurements and ensuring that the acquired measurements will be consistent with the intended use.

Finally, it is also true that some soil and rock properties are not strongly affected by drilling and sampling techniques. In particular, most index properties for soil and rock are insensitive to the quality of samples. Drilling and sampling techniques can therefore be selected more liberally when the primary purpose for specific borings is classification.

## 3.7 CONSIDERATIONS FOR TIME VARYING CONDITIONS

It is important to consider that ground conditions can vary with time when developing and executing site characterization programs. The predominant mechanism causing changes in soil properties with time is changing groundwater conditions, which commonly fluctuate over relatively short time periods because of changes in precipitation and surface water runoff, tidal fluctuations, and/or nearby pumping, irrigation, or drainage activities. Rising and falling groundwater levels produce changes in effective stress, which in turn produce changes in soil properties that depend on the magnitude of effective stress in the ground. Conditions may also vary with time in cases where soil continues to consolidate under previously applied loads or where prior development produces permanent changes to groundwater conditions.

Soil properties that are most susceptible to changes in effective stress include undrained shear strength, total stress strength parameters, and overconsolidation ratio. Preconsolidation stress may also be influenced by changes in effective stress, but only if the changes lead to effective stresses that are greater than have been experienced in the past. Many other soil properties, especially those that describe how soil responds to changes in effective stress, are practically time invariant and vary only marginally due to changes in effective stress. Properties falling into this category include many index properties, effective stress strength parameters, as well as many stiffness and compressibility parameters. While many properties of intact rock also strictly depend on the magnitude of effective stress, they can often be considered to be independent of small changes in effective stress as a practical approximation.

In addition to changes in properties that result from changing pore water pressures, properties for some types of soil and rock may change due to physical or chemical alteration. Such changes generally occur over longer periods than is usually observed from changes in groundwater levels, but still short enough to be relevant for design of transportation features. Such changes may arise because of physicochemical changes to the soil or rock, due to stress relief induced by excavation, or other unusual phenomena. Many shale formations, for example, are known to lose significant strength when subjected to stress relief and/or exposure to the atmosphere.

In the context of developing scopes for site characterization, the potential for changes in soil or rock properties must be considered from two different perspectives. First, it is generally important that acquired samples be carefully protected to minimize potential changes to soil/rock characteristics and to complete laboratory testing as promptly as practical following sampling. Second, it is important to consider the potential for changes in properties that may occur from the time of sampling to the time of construction. Changes in soil properties between sampling and construction can be either conservative or

unconservative, often depending on how effective stresses change in the field. If sampling is conducted during a time when effective stresses are relatively high (e.g., during a dry summer) but construction occurs during a time when effective stresses are lower (e.g., during a wet spring), there is potential for the measured magnitude of some properties to be unrepresentative of actual conditions that exist during construction. Such changes may also influence many in situ test measurements.

Unfortunately, changes in ground conditions over time can be difficult to address in the context of design and construction. However, since many of the changes can be attributed to rising and falling groundwater conditions, the changes can often be reasonably addressed by monitoring groundwater conditions over time as described in more detail in Chapter 10. Changing conditions can also sometimes be addressed during design (e.g., using deep foundations) or in construction specifications (e.g., by specifying overexcavation of poor soils).

## 3.8 SELECTION FROM AMONG ALTERNATIVE METHODS OF INVESTIGATION

A great challenge for site characterization is that there are many alternative means for conducting investigations, and seldom, if ever, is a single method or set of methods clearly more advantageous than others. As a result, individuals often develop preferences based on past experience and success (or lack thereof) and may become partial to specific methods. Such practices are entirely appropriate; however, it is important for those planning site investigations to maintain some degree of objectivity so that the most appropriate methods are selected based on the identified information needs, anticipated ground conditions, and expected uses for site characterization data.

Unfortunately, there simply is no recipe that will lead to identification of clearly preferable methods for site characterization for every project. The question that often lacks a clear and definitive answer is whether it is preferable to perform a greater number of relatively simple measurements or a lesser number of more refined measurements to establish values for a specific design parameter. There are certainly instances where some methods are clearly preferable over others, and instances where some approaches are completely inappropriate. However, in many cases there are multiple approaches that can be considered appropriate, which leaves selection of methods for site characterization to rely on the judgment of those planning the investigations and applicable standards of practice. In this regard, it is important and useful to quantitatively evaluate the reliability of relevant design parameters during and following completion of the investigations using methods described in Chapter 11 and Appendix 3. Such quantitative evaluations provide an objective assessment of the effectiveness of the investigations performed, which can be used to modify and improve investigations in progress and serve as valuable

feedback to those developing scopes for site characterization after investigations are completed. Both will lead to improved judgment over time.

While it is desirable to establish some "optimum" scope for site investigations that will allow potential problem conditions to be accurately identified and allow design parameters to be established to some desired level of reliability, achieving this objective is not practical for every individual project. Geotechnical engineers should therefore seek to establish scopes for investigations that practically balance costs for the investigations with the value that the investigations contribute to a project, with due consideration of the complexities of producing reliable estimates for geotechnical design parameters that are described in this chapter, and throughout this manual. Hindsight will often lead to conclusions that the scope for a specific characterization was greater than or less than truly needed given the results of the investigation. Such conclusions should be expected. The important thing is that site characterization planners use "post mortem" evaluation to develop judgment that can be applied to planning for future site characterization programs. It is also important that geotechnical engineers be engaged during execution of site characterization activities so that investigations can be adapted to respond to unanticipated conditions if needed.

## 3.9 CONSIDERATIONS FOR DIFFERENT LEVELS OF SITE CHARACTERIZATION

Historically, it has been common practice to consider different levels of site characterization depending on the significance of features being considered and, more specifically, the potential consequences of unacceptable performance. For example, the scope of site investigations for ancillary structures such as rest areas and toll plazas might be limited to a few borings and relatively few tests. The scope for more typical projects such as routine bridges might be considered "typical", with one or more borings at each bridge bent and more extensive laboratory or field testing to more reliably establish values for important design parameters. Finally, the scope of investigations for "signature" projects such as major river crossings and highway interchanges are frequently extensive, with relatively large numbers of borings, and significant numbers of laboratory and field tests. The scope of investigations for signature projects may also include "special" or "advanced" testing that is not commonly used for more routine projects with the objective of more reliably establishing values for important design parameters.

Such practice is rational, and prudent from the perspective that features with lesser consequences can be designed to lesser reliability without imposing inappropriate risk to the transportation system. Recall that risk can be quantified as the product of the probability of an undesirable event (often termed the probability of "failure") and the consequences associated with that undesirable event, or:

$$R = p_f \times C = (1 - r) \times C \quad (3.1)$$

where $R$ is quantitative risk, $p_f$ is the probability of an undesirable event, $C$ represents the consequences associated with the undesirable event (generally expressed in financial terms), and $r$ is reliability. Thus, when consequences are low, it is possible to accept a greater probability of failure, or a lesser reliability, without increasing risk to the transportation system. However, it is also important to recognize that such practices do produce lesser reliability. Or, stated more precisely, such practices increase the likelihood that the target reliability associated with LRFD methods will not be achieved, as demonstrated in Section 3.4. This should not be taken to imply that the practice should be eliminated. However, consideration of lesser scopes for site characterization produces what is, in effect, a policy decision to accept lesser reliability. Such decisions should be made with careful consideration. Governing codes like the AASHTO LRFD Bridge Design Specifications often dictate minimum requirements for site characterization for different facilities and features, and these requirements typically reflect the importance of the feature being addressed and the consequences of poor performance.

It is also important to emphasize again that site variability also plays an important role in determining the reliability of design parameters, and in turn the reliability of the designed features, as demonstrated in Section 3.4. The fact is that greater numbers of measurements are required to achieve a given reliability for more variable formations than for more uniform formations. Thus, while it may be appropriate to adopt lesser scopes for site characterization for features with lesser consequences, this does not necessarily imply that site characterization for all features with lesser consequences should have lesser scopes than characterization for features with greater consequences. Both the consequences and site characteristics must be considered.

## 3.10 DEVELOPMENT OF SCOPE FOR FIELD INVESTIGATIONS

Field investigations for site characterization generally involve completion of test borings and in situ test soundings, and collection of soil and/or rock samples for laboratory testing. Field investigations may also include various types of geophysical measurements that are sometimes performed in conjunction with drilling, sampling, and in situ testing, but may also be performed independent of such activities. Field investigations may also include geologic mapping of rock outcrops, when relevant to the feature being designed and constructed. Finally, field investigations should also include activities to characterize groundwater conditions.

The scope of field investigations for a specific project should be developed to satisfy all three of the broad requirements for site characterization presented in Section 3.1. These requirements generally include:

(1) characterizing stratigraphy, (2) establishing appropriate and reliable values for relevant design parameters, and (3) identifying and characterizing potential hazards. The scope should also be developed considering the anticipated value and cost of specific activities and, similarly, the potential consequences and risks that may be present if specific site characterization activities are not performed. In developing scopes for field and laboratory investigations, geotechnical engineers should consider these requirements and seek to balance the cost of investigations with costs that would be required for designing and constructing the anticipated features to mitigate risk in the absence of the proposed information. The scope should also satisfy minimum requirements for applicable codes and standards.

### 3.10.1 Developing Preliminary Scopes

In developing a scope for field investigations, it is often useful to first develop a preliminary estimate for the number and general location of "exploration points" (i.e., borings and/or in situ test soundings) based on consideration of the need to characterize stratigraphy. This preliminary plan should then be adapted based on consideration of potential hazards and based on testing requirements for establishing reliable values for relevant design parameters. Recommended minimum requirements for the number and spacing of exploration points provided in Table 3–2 are often a good place to start since these requirements have been adapted over time to be generally acceptable for characterizing stratigraphy at most sites. These requirements suggest at least one exploration point for every 100 feet of substructure for bridge foundations and abutments and one exploration point for every 100 to 200 feet of alignment for retaining walls. Exploration point spacing for other significant features such as notable cuts and fills should be generally similar to those for retaining structures, while exploration point spacing for general corridor sections can be substantially greater. Preliminary exploration point spacing for other specific features (e.g., sign and tower foundations, ancillary structures) should also generally be consistent with spacing requirements for bridge foundations and abutments.

Given an initial estimate for exploration point spacing, the spacing and locations should be adapted based on the anticipated stratigraphic variability at the specific site. Much closer exploration point spacing should be adopted at sites where stratigraphy is suspected to be more variable. Decisions about exploration point spacing can be greatly facilitated by historical borings and other preliminary information described in Section 3.2, as well as from many surface geophysical methods. For example, seismic, resistivity, and electromagnetic methods can often be used to efficiently characterize general stratigraphy (including depth to rock), which can provide valuable information regarding the anticipated variability of stratigraphy. Use of such techniques can serve as the basis for increasing exploration point spacing at some sites, for motivating and justifying considerably tighter exploration point spacing at

others, or for locating specific borings to investigate local anomalous conditions revealed by the geophysical measurements.

**Table 3–2 Guidelines for minimum number, location, and depth of exploration points (adapted from AASHTO, 2014).**

| Application | Minimum Number and Location of Exploration Points | Minimum Depth of Exploration |
|---|---|---|
| Retaining Walls | • Minimum of one exploration point<br>• Exploration points every 100-200 ft.<br>• Additional exploration points behind walls for anchored structures | • Depth below bottom of wall where stress increase becomes less than 10 percent of existing effective overburden stress<br>• Depth should extend below any soft, compressible soils into competent bearing material |
| Shallow Foundations | • Minimum of one exploration point per substructure<br>• For substructures with plan dimensions greater than 100 ft, a minimum of two exploration points<br>• Additional exploration points for erratic subsurface conditions | • Depth below footing elevation where stress increase is less than 10 percent of existing overburden stress<br>• Depth should extend below any soft, compressible soils into competent bearing material<br>• Minimum of 10-ft penetration into competent rock if encountered prior to meeting other depth criteria<br>• In formations with highly variable rock and/or boulders, great than 10-ft penetration into rock may be required |
| Deep Foundations | • Minimum of one exploration point per embankment<br>• For substructures with plan dimensions greater than 100 ft, a minimum of two exploration points<br>• Additional exploration points for erratic subsurface conditions | • Depth below anticipated tip of foundation that is the greater of 20 ft or two times the maximum foundation group dimension<br>• Depth should extend below any soft, compressible soils to reach competent materials<br>• Minimum of 10-ft penetration into competent rock for piles bearing on rock<br>• Minimum penetration into competent rock should be 10 ft for piles tipped on rock and greater of 10 ft, three times the shaft diameter for individual drilled shafts, or two times the maximum group dimension below the anticipated tip elevation for drilled shafts |
| Embankment Foundations | • Minimum of one exploration point per embankment<br>• Minimum of one exploration point at each bridge abutment location<br>• Minimum of one exploration point per 300 ft of embankment, locations staggered in transverse direction<br>• Minimum of three exploration points in transverse direction<br>• Additional exploration points for erratic subsurface conditions | • Minimum depth is greater of:<br>o depth where induces vertical stress is less than 10 percent of applied stress at base of embankment, or<br>o depth equal to twice embankment height below base of embankment<br>unless competent hard stratum is encountered at shallower depth |
| Excavated Slopes | • Minimum of one exploration point per 300 ft of slope length<br>• Minimum of three exploration points in transverse direction<br>• Additional exploration points for erratic subsurface conditions | • Minimum depth is depth equal to the maximum slope height below the minimum excavation elevation unless competent hard stratum encountered at shallower depth<br>• Exploration depth should extend below potential soft or weak strata that might impact stability |

When selecting preliminary locations for exploration points, it is important to remember that stratigraphy is inevitably three-dimensional so exploration points should be located to facilitate evaluation of how stratigraphy varies along the feature alignment and in a direction perpendicular to that alignment. In particular, one should avoid locating all exploration points along a single line, but instead should stagger locations so that some borings are located along the centerline of the feature, while others are located towards the "front" or "back" of the feature. Exploration point locations must also be selected with consideration for traffic control, utility conflicts, existing structures, and equipment access. If different methods of exploration are planned, such as traditional borings and in situ test soundings, it is also preferable to stagger or alternate locations for different types of exploration so that interpretations derived from the different explorations can be evaluated collectively. At a few locations, both borings and in situ test soundings should be performed in close proximity to facilitate development of site specific transformations among the boring, laboratory test measurements, and in situ test measurements. Several types of "scanning" geophysical methods can also be used to help interpret conditions between exploration points and to interpret how stratigraphy may vary beyond the specific locations of borings or in situ test soundings.

Depths for borings and in situ test soundings should generally extend below the volume of material that will be influenced by construction of the transportation features being considered. For foundation design, this generally means that borings should extend to depths that are two to three times the nominal plan dimensions of the foundation below the anticipated foundation depth. For earth slopes and retaining structures, borings and soundings should generally extend to depths below where the influence of the slope or retaining structure will become negligible. Such considerations generally require that borings and soundings extend through poor quality materials, and may require penetration for some distance into rock.

### 3.10.2 Refining Preliminary Scope

Once an initial field exploration plan is established based on stratigraphy, the plan should be evaluated with respect to appropriateness for characterization of relevant design parameters and for identification and characterization of potential hazards. In some cases, the preliminary plan for field investigations may prove to be sufficient to achieve all three investigation objectives. However, in other cases, additional exploration points may be needed to facilitate better identification and characterization of geotechnical hazards, or to facilitate acquisition of sufficient numbers of samples or in situ test measurements for reliable characterization of relevant design parameters. For example, additional exploration points may be appropriate for sites with suspected karst or underground mines in order to increase the likelihood of

identifying such hazards or to allow for more precise characterization of the location and extent of karst or mine features. Alternatively, at sites with relatively consistent stratigraphy, but relatively variable properties, additional borings or in situ test soundings may be required to acquire sufficient numbers of measurements to reduce uncertainty in estimates for important design parameters. Additional discussion about selecting appropriate numbers of samples and in situ test measurements is provided in Section 3.11.

In addition to specifying the number, location, and depth of all borings and in situ test soundings, specifications for field work should include clear instructions for the method of drilling, method(s) for support of the borehole, and methods for acquiring samples and conducting in situ tests. As described previously, the method of drilling and sampling can introduce potential bias into some laboratory and field measurements; methods for drilling and sampling should therefore be carefully selected based on the anticipated ground conditions and use of the acquired information. State-of-the-practice drilling and sampling techniques should generally be used to acquire samples for laboratory performance tests (i.e., tests that can often be considered "direct" measurements) and for borings where in situ tests will be conducted. In many cases, it may even be necessary to transition from one boring and/or sampling method to another as boreholes penetrate through strata with different characteristics. Drilling and sampling techniques should be selected in consultation with drilling personnel with due consideration to the ground conditions that will be encountered since there is no single "best" method for boring and sampling in all materials. It is also important to maintain close communication among drilling crews, on-site engineering staff or inspectors, and designers as investigations progress so that drilling and testing methods can be adapted to suit the conditions encountered.

Another important consideration for establishing the scope for field investigations is to establish appropriate intervals for acquiring samples and/or in situ test measurements. Appropriate sampling intervals should be developed considering stratigraphy, as well as the need to acquire sufficient numbers of samples and/or test measurements for reliable characterization of design parameters. Sampling and/or testing intervals should also be established considering the intended use of the acquired information and the importance of small stratigraphic features. For example, the presence of a thin, weak clay seam may have little impact on the performance of deep foundations that extend through the seam since performance is predominantly governed by the average strength of the soil/rock along the entire length of the deep foundation. Conversely, the same thin, weak seam may completely dominate performance of a slope or retaining structure, and could be the difference between stability and instability in some cases (e.g., Hendron and Patton, 1985). Thus, sporadic sampling/testing along the depth of a boring/sounding may be perfectly adequate if intended for design of deep foundations, but completely inadequate if intended for design of earth slopes or retaining structures. Since it is common for ground conditions

encountered in the field to differ from those anticipated, field investigations should be observed and directed by an on-site engineer or geologist that is familiar with project requirements so that changes to planned boring, sampling, and testing can be made as the investigation progresses.

As a general rule, sampling and testing should be distributed throughout the boring/sounding depths and locations in an approximately uniform manner to ensure that acquired samples and measurements capture the condition and behavior of the entire volume of material that will be influenced by construction. However, there are some exceptions to this guidance and some qualification is necessary. One exception is cases where conditions and properties within some stratigraphic units may not significantly affect design or construction of specific features. Another exception is cases where particular stratigraphic units tend to dominate performance of a transportation feature. In such cases, sampling and testing locations should generally be distributed uniformly throughout all boring depths and locations, but additional sampling and testing should be specified to better characterize the units that dominate performance. Finally, consideration should also be given to the fact that sufficient numbers of measurements need to be acquired from each significant stratigraphic unit (which represents a distinct population). This requirement may motivate use of relatively small sampling intervals in stratigraphic units of limited thickness and/or greater sampling intervals in units of substantial thickness simply based on the need to acquire sufficient numbers of samples for laboratory testing.

A significant challenge with implementing the recommendations provided in this section is that much of the information needed to make effective scoping decisions may be unavailable, or poorly established when the scope of site investigations is initially developed. Fortunately, scoping can be improved by diligent evaluation of existing information as described in Section 3.2. The effectiveness of investigations can also be improved, and frequently made more efficient, by having a well-qualified engineer or geologist on site during investigations and by planning to execute field investigations in phases. In a phased approach, preliminary borings, soundings, or geophysical measurements are conducted at widely spaced locations to facilitate development of a preliminary interpretation of stratigraphy. Initial investigations may often include relatively simple laboratory or field measurements to facilitate general characterization of the soil and/or rock types present, as well as for preliminary evaluation of potential hazards. Preliminary interpretations of stratigraphy can be developed from these investigations, and subsequently used to scope more informed and directed investigations that target important hazards and design parameters, while also refining interpretations of stratigraphy. Phasing of investigations can also be coordinated with various phases of design, thereby allowing investigations to target locations of specific features as they are established. Phased investigations may not be appropriate for smaller projects, in which case it is often necessary to develop conservative scopes for investigations to ensure

that the acquired information will be sufficient for design and construction, or to adapt the scope on-site as investigations are completed. In all cases, field investigations should be inspected by qualified geotechnical engineers, geologists, or technicians, and close communication should be maintained with the responsible geotechnical engineer to verify that necessary information and samples are obtained. Such communication will enable the engineer to authorize or direct appropriate changes to the scope of investigations so that the objectives of the investigation can be achieved.

Finally, it is also important to consider characterization of groundwater conditions when developing scopes for field investigations. As described in Section 3.7 and subsequent chapters, groundwater conditions can have significant influence on measurements of many soil properties, and groundwater conditions are known to vary substantially over time. It is therefore critical that the scope of field investigations include specific activities and methods to accurately characterize groundwater conditions during field investigations, as well as over longer time periods. Failure to accurately characterize groundwater conditions and hydraulic properties for soil and rock, and failure to identify potential hazards that arise from groundwater conditions (e.g., artesian conditions or high flow rates), can impact both design and construction, and often result in substantial impacts to overall project costs (Clayton, 2001; Boeckmann and Loehr, 2016).

## 3.11 DEVELOPMENT OF SCOPE FOR LABORATORY AND FIELD TESTING

Appropriate scopes for laboratory and field testing are largely driven by the design parameters that must be established and the type and quantity of measurements needed to reliably establish values for relevant design parameters. As described in Section 3.1, the specific design parameters needed depend on the specific features being considered as well as specific agency design practices. Once appropriate design parameters are identified, scoping for laboratory and field testing primarily becomes one of selecting the types of measurements that are most appropriate for establishing specific design parameters and selecting the quantity of measurements needed to produce reliable estimates for the parameters.

The content provided in Sections 3.4 through 3.6 of this chapter and calculations described in Chapter 11 provide a general framework for objective assessment of different types of measurements that can be used to develop appropriate scopes for laboratory and field testing. Results presented in Section 3.4.5, and in Loehr et al. (2015), suggest that under-reliable designs are unlikely to result when design parameters are established to have model uncertainty, as defined by $COV_{model}$ and computed as described in Chapter 11, less than approximately 0.3. Scopes for laboratory and field testing should therefore include sufficient measurements to produce $COV_{model} \leq 0.3$ for soil and rock strata and design parameters that are

important for design. It is likely that threshold values other than 0.3 may be appropriate for other design parameters and other design methods. The threshold value of 0.3 should therefore be considered as an interim requirement adopted until additional study can be undertaken for other design parameters and design methods. Specific methods required for quantifying model uncertainty are described in Chapter 11, and in Appendix 3.

Unfortunately, the specific number of tests required to achieve $COV_{model} \leq 0.3$ depends on the variability of the specific stratum, the reliability of test measurements, and the reliability of transformations when indirect measurements are used. Considerable judgment is therefore still required to determine an appropriate quantity of tests. Results presented previously in this chapter suggest that approximately twenty direct measurements may be required to produce $COV_{model} \leq 0.3$ for highly variable strata. Fewer direct measurements will be necessary to achieve this threshold for less variable strata, potentially dropping to fewer than five measurements for strata with little variability. Greater numbers of indirect measurements will generally be necessary to achieve the threshold, since indirect measurements are subject to additional uncertainty arising from transformation of the actual measurements to estimates for the design parameter of interest. For indirect measurements that are quite reliable, similar numbers of indirect measurements as direct measurements may be sufficient to achieve the model uncertainty threshold; for less reliable indirect measurements, many more indirect measurements will be required to produce $COV_{model} \leq 0.3$. In some cases, transformations for indirect measurements may be so unreliable that indirect measurements alone cannot produce estimates for design parameters with sufficient reliability. In such cases, alternative measurements, or some combination of direct and indirect measurements, should be used. While the recommended test quantities suggested here are approximate, it is likely that improved guidance for test quantities can be established from additional research and experience.

It is important to emphasize that the number of measurements discussed here applies to all individual strata that are important for design. Thus, one might require as many as twenty direct measurements in each stratum if all strata are highly variable and all strata are relevant for design. However, it is neither necessary, nor desirable, for all such measurements to come from a single boring or in situ test sounding since a better representation of variability within a single stratigraphic layer will be acquired from measurements from several different borings or in situ test soundings as long as the measurements are representative of the same basic material. It is also relatively common that design is dominated by characteristics of a small number of "important" strata and it is perfectly reasonable to acquire fewer measurements in strata that are not important for design. The numbers of tests discussed here also presumes that acquired samples will have quality that is sufficient for the designated tests. Since it is

relatively common for some samples to be of poorer quality, it is usually wise to collect more samples from the field than are needed for testing.

In addition to laboratory and field tests performed to establish relevant design parameters, it is also important to complete sufficient numbers of "index" property tests to allow for characterization of the soil and/or rock types present at a site and to correctly identify individual populations. Such classifications are often crucial for stratigraphic interpretation, for identification of problematic soil and rock, and for comparison and collective interpretation of laboratory and field "performance" tests as described in more detail in Chapter 11. Such measurements allow designers to compare general characteristics of different samples as part of evaluating whether different measurements for design parameters can be considered collectively. Index property tests are generally quick and inexpensive to perform, and can often be performed on poorer quality samples and, thus, should be assigned rather liberally.

## 3.12 SPECIAL CONSIDERATIONS FOR ALTERNATIVE CONTRACTING METHODS

Fundamentally, the concepts and recommendations presented in this chapter, and throughout this manual, apply equally to all methods of project delivery. If properly executed, design-build and other similar contracts will produce site characterizations that fully achieve the objectives described earlier in this chapter and fulfill the value proposition for site characterization described in Chapter 2. However, use of alternative contracting methods can introduce challenges to conventional processes for site characterization and the potential for perverse incentives in some cases. In a study of cost increases associated with site characterization, Clayton (2001) concluded that increasing use of innovative contracting methods like design-build may increase problems with cost overruns unless changes are made to site characterization practices. Deliberate attention to site characterization is therefore required for proper execution of design-build and other similar contracts.

While site characterization practices for design-build projects vary substantially from one agency to another, all projects include a site characterization program that is completed prior to competing the contract to provide bidders with information regarding ground conditions at the site. Pre-award site investigations are necessarily more limited in scope than what is normally performed for projects of similar size and scope because specific details like foundations locations are not know prior to contract award. Pre-bid site investigations should therefore be developed to provide prospective bidders with sufficient information to prepare bids and to reduce the risk of differing site condition claims after contract award. Pre-bid investigations should also seek to characterize ground conditions with sufficient detail and reliability so as not to impose undue risks to the design-build contractors, which will usually

increase bid prices. Additional site characterization is generally completed by the design-build contractor following contract award and should be contractually required as part of design-build contracts. Such requirements should include provisions that mandate site characterization activities that satisfy minimum levels of investigation for projects of similar size, and may include additional project specific requirements. Contract provisions should also require that appropriate approvals be obtained from the owner agency to ensure that the completed site characterization following award is sufficient to produce acceptable reliability for the completed structures.

## 3.13 COMMUNICATION AND EXECUTION OF SITE CHARACTERIZATION ACTIVITIES

The final step in planning and scoping for site characterization is to clearly document and communicate the established plan so that those charged with executing the investigations can fulfill the intended purpose. Practices for communicating and executing site characterization activities vary substantially among different agencies and private organizations (e.g., design consultants, design-build contractors) based on the equipment and personnel that are available, as well as based on workload and project requirements. In some states, geotechnical investigations and site characterization are conducted almost exclusively using agency personnel and equipment. For other agencies, geotechnical investigations are almost exclusively performed by agency contractors. Most agencies use some combination of agency personnel and contractors to varying degrees. For example, some agencies may perform the majority of investigations "in-house", but use contractors for performing specialized field or laboratory tests, or to balance workloads during periods where agency resources are insufficient to keep up with workload demands. For some agencies, preliminary investigations are performed by "local" or "district" crews, whereas for others preliminary investigations may be performed using "statewide" crews and equipment. Some agencies will contract out all or part of preliminary investigations, especially if the investigations involve use of specialized techniques (e.g., geophysics). For many large projects, site characterization may be included within contracts for design or construction and overseen by consultants.

Regardless of specific agency practices, it is critical that planned investigations be communicated in a clear and detailed manner, and that individuals responsible for geotechnical design be directly involved during execution of investigations. When investigations and design are both performed by agency personnel, communications may be relatively brief and draw heavily on historical practice or documented agency standards. In contrast, communications for investigations performed by site investigation contractors may be quite lengthy and form the basis for contractual documents. Individual agencies generally adopt different processes for execution of geotechnical investigations and it is important to understand these processes so that one can conform to the processes where appropriate, or depart from

typical processes when such departures will lead to measurable benefits for design, construction, and operation of transportation infrastructure.

Regardless of whether investigations will be performed in-house or contracted, communications regarding the scope of investigations should include detailed instructions regarding all aspects of the investigations. Such details should include documentation of the following items:

1. Planned locations for all borings, soundings, and other exploration points, including requirements for documenting the actual location of investigations and allowable deviations from planned locations;
2. Requirements for drilling, sampling and testing methods, including required equipment, as well as requirements or allowances for modifying these methods based on observations from the field;
3. Plans and requirements for site access, utility clearances, maintenance of traffic, and environmental controls;
4. Requirements for sampling and testing intervals, or requirements for sampling and testing depths, along with instructions for protocols if problems are encountered with sampling and/or testing;
5. Requirements for documenting field activities in the form of field boring logs and other records;
6. Requirements for sample care and storage during field work, transportation, delivery, and in the laboratory;
7. Requirements for completion or closure of borings (e.g., grout holes, install monitoring well, etc.);
8. Requirements for monitoring groundwater conditions and installation of instrumentation as part of investigations;
9. Requirements for laboratory testing, including proposed methods for selecting samples to be tested; and
10. Requirements for routinely communicating with the geotechnical design engineer during the course of investigations.

Adaptations to planned investigations are commonly required, even with the best effort of site characterization planners, because conditions in the field may be different than expected, because of equipment problems, or other unforeseen events and occurrences. As such, it is also important to maintain communication with designers and users throughout execution of the planned investigations so that the activities can achieve the desired objectives.

# CHAPTER 4
# IDENTIFICATION AND CLASSIFICATION OF SOIL AND ROCK

Measurements from relatively simple laboratory and field "index" tests are commonly collected for all projects because they provide an inexpensive way to identify and formally classify soil and rock encountered at a site. Common index tests for soils include water content, unit weight, Atterberg limits, particle-size distribution, and specific gravity. Hardness, unit weight, abrasivity, and durability are often measured for intact rock as are several measurements performed on rock core. In this chapter, common measures of soil and rock characteristics obtained from laboratory and field index tests are described along with practical uses for such measures in the context of geotechnical design. Methods for classification of soil and intact rock, and identification of soil type from in situ tests are also presented.

## 4.1 OBJECTIVES FOR IDENTIFICATION AND CLASSIFICATION OF SOIL AND ROCK

Formal soil and rock classifications derived from laboratory and field index property measurements are commonly used for several purposes. Index properties are often effectively used as an indication of anticipated engineering behavior and to assess general characteristics of soil and rock. For example, high plasticity clay is often identified based on measurements of Atterberg limits and, as a first approximation, may indicate significant potential for low strength, low hydraulic conductivity, and high swell potential. If such behavior may substantially impact a project, the behavior should be confirmed using more rigorous "performance" tests described in subsequent chapters of this manual. However, identification of potential issues based on relatively simple tests provides significant benefit for geotechnical design.

Soil and rock classification is also used to help select samples for engineering property testing and to assess general variability and consistency among samples collected from a given site. In this context, the presumption is that soil and rock samples with similar classification are expected to behave similarly, again as a first approximation. Thus, index property measurements and classifications can be used to establish whether samples collected from one boring are likely to be similar to samples collected from another and whether the samples can be considered to be from a single stratigraphic unit. In essence, index properties and classifications can be considered as "screening" tests that will often motivate additional investigations or measurements and facilitate grouping of different samples for design.

## 4.2 BORING AND SAMPLING REQUIREMENTS FOR INDEX TESTING

Most index property measurements are insensitive to sample quality, so special boring and sampling procedures or equipment are seldom required. Samples for specific tests may require some care, but

generally these requirements are easily satisfied. For example, it is important to prevent wetting or drying of samples acquired for measuring water content. Similarly, samples acquired for measuring unit weight should be relatively undisturbed. Measurements for rock core also require care during coring and handling to prevent artificially breaking the rock core, which can bias index property measurements for rock. However, most index property tests can be performed on "bulk" or disturbed samples.

## 4.3 FUNDAMENTAL CONCEPTS FOR IDENTIFICATION AND CLASSIFICATION

The objective of identification and classification is to group soil or rock types that are expected to behave similarly. In this regard, it is important to distinguish between "coarse-grained" soils and "fine-grained" soils because their engineering behavior is different and controlled by different factors. Table 4-1 summarizes the most important compositional and "state" variables that influence the mechanical behavior of coarse-grained and fine-grained soils.

**Table 4-1 Soil characteristics affecting behavior of coarse- and fine-grained soils.**

| Coarse-Grained Soils | | Fine-Grained Soils | |
|---|---|---|---|
| **Parameter Type** | **Parameter** | **Parameter Type** | **Parameter** |
| Composition | Mean Grain Size<br>Grain-Size Distribution<br>Grain Mineralogy<br>Grain Shape/Angularity<br>Other Constituents (Carbonates, etc.) | Composition | Clay Size Fraction<br>Clay Mineralogy<br>Specific Surface Area<br>Cation Exchange<br>Other Constituents (Carbonates, etc.) |
| State | Void Ratio/Relative Density<br>Confining Stress<br>Stress History | State | Water Content<br>Void Ratio<br>Confining Stress<br>Stress History |

Coarse-grained soils, such as sands and gravels, are assemblages of individual particles with collective behavior that depends on confinement, stress conditions, cementation, and particle packing. Since coarse-grained soils behave as particulate materials, characteristics of the individual particles and the collection of particles strongly influence mechanical behavior. The most important of these characteristics include mean grain size, grain-size distribution, grain shape, and grain hardness. Stress history also influences the behavior of course-grained soils, although not to the degree observed for fine-grained soils.

In contrast, fine-grained soils are predominantly composed of small particles with large surface area. Silt particles are similar to sand particles, but much smaller. Silt particles are electrochemically neutral and are sometimes referred to as "surface dead" as they have no inherent attraction for other soil particles. Conversely, clay particles are often "platy" in shape with unbalanced electrical charges that produce an

affinity for water and other soil particles. The proportion and type of clay minerals in a soil influence the particle surface area, surface charge, and cation exchange capacity. These compositional factors influence microscopic surface phenomena that, in turn, strongly influence mechanical behavior. Confining stress and stress history also strongly influence the mechanical behavior of fine-grained soils. Individual particles of coarse-grained soils can generally be seen with the naked eye, or perhaps a magnifying lens, whereas individual particles of fine-grained soils can only be seen with a microscope.

## 4.4 GRAIN-SIZE DISTRIBUTION

Grain-size distribution refers to the proportion (by dry mass) of soil particles of different sizes within a soil sample. Grain-size distribution is commonly measured using mechanical sieves and/or hydrometer tests and is used to distinguish between fine- and coarse-grained soils, as well as to further classify coarse-grained soils. Table 4-2 summarizes common criteria for characterizing different particle sizes along with descriptive terms used to refer to particles of different sizes.

**Table 4-2 Descriptive terms for soil particle size ranges.**

| Soil | Particle Size Ranges | Descriptive Term |
|---|---|---|
| Coarse-Grained | >12 in. (305 mm) | Boulders |
| | 3 in. – 12 in. (75 mm – 305 mm) | Cobbles |
| | ¾ in. – 3 in. (19 mm – 75 mm) | Coarse Gravel |
| | No. 4 Sieve – ¾ in. (4.75 mm – 19 mm) | Fine Gravel |
| | No. 10 – No 4 Sieve (2.00 mm – 4.75 mm) | Coarse Sand |
| | No. 40 – No. 10 Sieve ( 0.0425 mm – 2.00 mm) | Medium Sand |
| | No. 200 – No. 40 Sieve (0.075 mm – 0.0425 mm) | Fine Sand |
| Fine-Grained | 0.075 mm – 0.002 mm | Silt |
| | < 0.002 mm | Clay |

The distinction between coarse-grained soils and fine-grained soils is generally based on the proportion of soil retained on a No. 200 sieve, which has an opening size of 0.074 mm. For the Unified Soil Classification System (USCS) described in Section 4.16.1, soils having greater than 50 percent of particles (by mass) retained on the No. 200 sieve are considered to be coarse-grained. Soils where greater than 50 percent of particles by mass are finer than, or pass through, the No. 200 sieve are considered to be fine-grained. For the AASHTO Soil Classification System described in Section 4.16.2, coarse-grained soils are those with less than 35 percent of the soil particles passing the #200 sieve.

### 4.4.1 Coarse-Grained Soils

The traditional technique for determining the grain-size composition of coarse-grained soils is by mechanical sieve analysis (AASHTO T88, ASTM D422, and ASTM D6913). Results from mechanical sieve analyses are expressed collectively using a grain-size distribution curve similar to that shown in

Figure 4-1. The curves shown represent the cumulative percentage of soil particles (by dry mass) of different sizes. Curves plotting to the right of others in the diagram represent soils with more coarse grains while curves plotting to the left indicate soils with greater percentages of fine-grained particles.

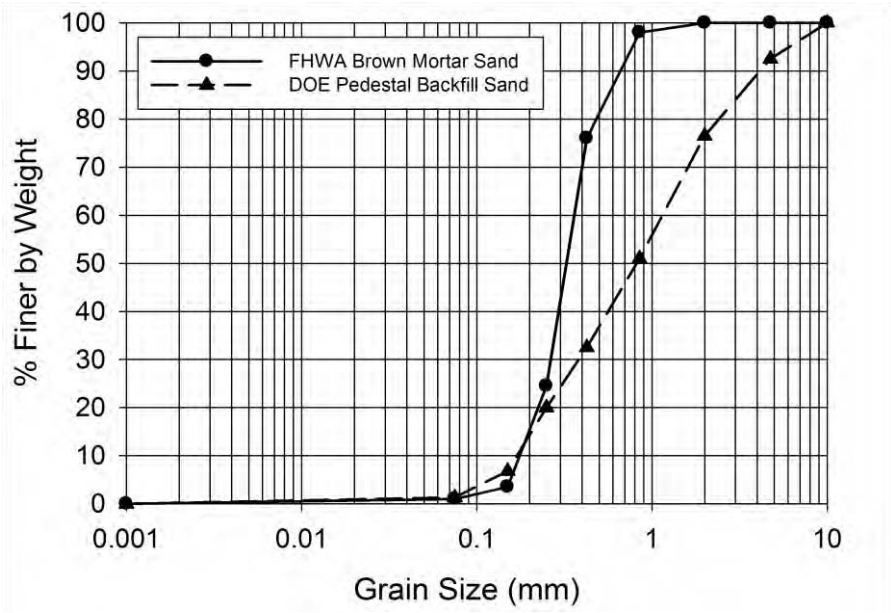


**Figure 4-1 Grain-size distribution curves for two coarse-grained soils.**

Grain-size distribution curves can be used to establish several important quantitative measures that describe the shape and position of grain-size distribution curves and provide useful means for comparing different coarse-grained soils. The mean particle size, $D_{50}$, defined as the particle size (diameter) for which 50 percent of the soil particles are finer, serves as a measure of the relative position of different grain-size distribution curves. The "coefficient of uniformity", $C_U$, and "coefficient of curvature", $C_C$, are quantitative measures of the dispersion of particle sizes. The coefficient of uniformity is defined as

$$C_U = \frac{D_{60}}{D_{10}} \tag{4.1}$$

where $D_{60}$ is the grain size for which 60 percent of the soil particles are finer and $D_{10}$ is the grain size for which 10 percent of the soil particles are finer. The coefficient of curvature, $C_C$, is defined as

$$C_C = \frac{(D_{30})^2}{(D_{10} \cdot D_{60})} \tag{4.2}$$

where $D_{30}$ is the grain size for which 30 percent of the soil particles are finer. Finally, the "percent fines" is often measured and reported as the percentage of the soil particles that pass through the No. 200 sieve, which includes the silt and clay fractions.

The coefficient of uniformity is used to help classify coarse-grained soils. The term "well-graded" is used to describe soils composed of a wide range of particle sizes while the term "poorly graded" is used to indicate that most of the particles fall within a narrow range. Table 4-3 gives criteria for identifying well-graded sands and gravels from results of sieve analyses for the USCS. Coarse-grained soils not meeting both of the criteria shown are considered poorly graded. Table 4-4 summarizes values for the mean particle size, coefficient of uniformity, coefficient of curvature, percent fines, and descriptive gradation for the two particle size distributions in Figure 4-1.

**Table 4-3 USCS criteria for well-graded coarse-grained soils.**

| Soil | Grading | $C_U$ | $C_C$ |
|---|---|---|---|
| Sand | Well-Graded | $C_U \geq 6$ | $1 \leq C_C \leq 3$ |
| Gravel | Well-Graded | $C_U \geq 4$ | $1 \leq C_C \leq 3$ |

**Table 4-4 Grain-size characteristics for the two sands in Figure 4-1.**

| Soil | $D_{50}$ (mm) | $C_U$ | $C_C$ | Fines (%) | Gradation |
|---|---|---|---|---|---|
| FHWA Sand | 0.31 | 2.06 | 1.14 | 2.5 | Poorly graded |
| DOE Sand | 0.85 | 6.47 | 0.86 | 2.7 | Poorly graded |

Grain-size distribution can have a profound influence on the mechanical behavior of coarse-grained soils. Well-graded soils are generally easier to compact and have higher strength and lower compressibility compared to poorly graded soils. The wide range of particle sizes in a well-graded soil allows for tighter packing as the smaller grains fit into the void space between larger grains.

### 4.4.2 Fine-Grained Soils

For most fine-grained soils, sieve analyses do not provide sufficient data to describe composition since the soils consist of smaller particles that cannot be separated by sieves. Grain-size distributions for fine-grained soils are therefore generally determined using the hydrometer test (AASHTO T88; ASTM D422). The hydrometer test determines the proportion of silt- and clay-size particles using a sedimentation procedure and can be used to separate the fine-grained particle fraction into various sizes. It is sometimes useful to define not only the total silt content (percent between 0.075 mm and 0.002 mm) and clay content (percent < 0.002 mm) but also the coarse silt content (percent between 0.075 mm and 0.020 mm), fine silt content (percent between 0.020 mm and 0.002 mm), and fine clay content (percent < 0.001 mm, sometimes referred to as "colloids"). ASTM D422, which documents standard procedures for hydrometer

tests, was formally withdrawn in January of 2016; however, the procedures are still useful for characterizing the grain-size distribution of fine-grained soils.

## 4.5 GRAIN SHAPE – COARSE-GRAINED SOILS

The shape of soil particles can exert a strong influence on the mechanical behavior of coarse-grained soils. While the shapes of individual particles can be highly variable, it is useful to characterize particle shape as being rounded, angular, or an intermediate shape. Figure 4-2 shows a comparison of different particle shape descriptions with illustrations showing the intended use. Generally, collections of angular soil particles produce more interlocking of particles that tends to create higher shear strength compared to rounded particles with the same degree of packing. Grain shape is not relevant for classification of fine-grained soils since individual particles cannot be distinguished with the naked eye.

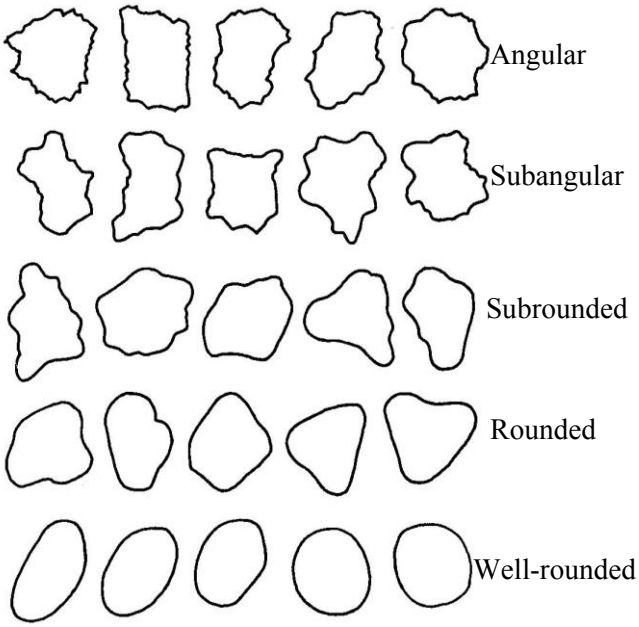


**Figure 4-2 Particle shapes for coarse-grained soils (from Mitchell and Soga, 2005).**

## 4.6 WATER CONTENT

The water content of soils is an important index property that is used to help interpret soil unit weight, relative consistency, and stress history, as well as to interpret groundwater levels. Water content, $w$, is generally expressed as a percentage and defined as

$$w = \frac{m_w}{m_s} = \frac{mass\ of\ water}{mass\ of\ soil\ solids} \cdot 100\% \tag{4.3}$$

Natural water contents, $w_n$, for sands typically range from 0 to 20 percent whereas natural water contents for inorganic and insensitive silts and clays generally range from 10 to 40 percent. However, it is possible to have more water than solids so that water contents can exceed 100 percent depending upon mineralogy, formation environment, and structure. Soft and highly compressible clays, as well as sensitive, quick, or organic clays, can exhibit water contents of 40 to 300 percent, or more.

Water content is relatively simple to measure using several different methods that include: (1) a drying oven (AASHTO T265; ASTM D2216); (2) a microwave oven (ASTM D4643); (3) a field stove or blowtorch (ASTM D4959); (4) calcium carbide gas pressure tester (AASHTO T217; ASTM D4944); and (5) nuclear methods (AASHTO T310; ASTM D3017 and ASTM D6031). Use of a drying oven (AASHTO T265; ASTM D2216) is universally considered to produce the most accurate measurement of water content for soil and rock. While the microwave and field stove (or blowtorch) methods provide for rapid evaluation of water content, potential errors inherent with these methods require confirmation using AASHTO T265. Similarly, nuclear methods may indicate potentially erroneous water contents for micaceous soils so results from nuclear methods should be "calibrated" or confirmed using the drying oven (AASHTO T265; ASTM D2216).

Sampling, handling, and storage may alter the in situ water content of collected samples and, therefore, produce errors even when water content is measured by oven drying. Because the top end of samplers may contain water or collapse material from the borehole, water contents should not be measured using material taken from near the top of samplers. Drying of samples and water loss may also occur if samples are not properly sealed. Water may also migrate within a specimen and lead to altered water content values if samples are stored for significant periods prior to testing. As such, samples for water content measurements should be carefully sealed and measurements should be performed as soon as practical following sampling.

## 4.7 UNIT WEIGHT AND SPECIFIC GRAVITY

The moist (total) mass density, $\rho_t$, of a soil or rock sample is given by

$$\rho_t = \frac{m_t}{V_t} \tag{4.4}$$

where $m_t$ is the total mass of the sample and $V_t$ is the total volume of the sample. Dry mass density, $\rho_d$, is similarly given by

$$\rho_d = \frac{m_s}{V_t} \tag{4.5}$$

where $m_s$ is the dry mass of the sample. The moist (total) unit weight, $\gamma_t$, and dry unit weight, $\gamma_d$, are similarly given by

$$\gamma_t = \frac{W_t}{V_t} \tag{4.6}$$

$$\gamma_d = \frac{W_s}{V_t} \tag{4.7}$$

where $W_t$ and $W_s$ are respectively the total and dry weight of the sample. The total and dry mass density and the total and dry unit weight are respectively related by the natural water content, $w_n$, as

$$\rho_d = \frac{\rho_t}{1+w_n} \tag{4.8}$$

$$\gamma_d = \frac{\gamma_t}{1+w_n} \tag{4.9}$$

The terms density and unit weight are often used incorrectly and interchangeably. The correct usage is that density implies mass measurements while unit weight implies weight measurements. When the usage is independent of the specific definition, these terms will be referred to as "density (unit weight)".

Field measurements of soil mass density (unit weight) are generally restricted to shallow surface samples, usually when placing compacted fills, and can be accomplished using drive tubes (ASTM D2937), the sand cone method (AASHTO T191; ASTM D1556), the rubber balloon method (ASTM D2167), or nuclear gauges (AASHTO T310; ASTM D6938). To measure the in-place unit weight or mass density at depth, these quantities can be measured in the laboratory on high quality, thin-walled tube samples taken from appropriate locations in the field. Unit weights determined from highly disturbed samples of coarse-grained soils (e.g., from thick-walled samplers) should be considered as approximate due to changes in water content and sample volume during sampling, handling, transportation, and laboratory preparation of samples. In-place unit weights can also be measured at depth using relatively expensive gamma ray techniques (ASTM D5195).

The specific gravity, $G_s$, of soil or rock solids is a measure of the density of the solid mineral particles referenced to the density of water. Specific gravity is computed as

$$G_s = \frac{m_s}{V_s \cdot \gamma_w} \tag{4.10}$$

where $m_s$ is the mass of soil or rock solids, $V_s$ is the volume of soil or rock solids, and $\gamma_w$ is the unit weight of water. Specific gravity can be measured according to AASHTO T100, ASTM D854, or ASTM D5550. However, since the specific gravity of most common soil and rock materials is confined to a relatively narrow range, and since these tests are relatively time consuming and difficult to conduct, it is quite common to simply estimate values for specific gravity unless unusual materials are encountered or suspected. As shown in Table 4-5, typical values of specific gravity for most soils lie within the narrow range of $G_s = 2.7 \pm 0.1$. Exceptions to typical values occur for soil with appreciable organics (e.g., peat), ores and mine tailings, and soil or rock with high calcium carbonate content.

**Table 4-5 Typical values of specific gravity for several natural soils.**

| Soil | Specific Gravity, $G_s$ |
|---|---|
| Kaolinite | 2.61 |
| Omaha Lake Clay | 2.65 |
| Boston Blue Clay | 2.71 |
| Platte River Sand | 2.65 |
| Iowa Loess | 2.70 |

## 4.8 ATTERBERG LIMITS

Atterberg limits are used to describe phase changes that fine-grained soils pass through at different water contents as illustrated in Figure 4-3. At very high water content, a disturbed mixture of soil and water behaves as a viscous liquid. As the water content is reduced, the mixture takes on characteristics of a semi-solid and, finally, at a sufficiently low water content, the mixture behaves as a solid. The water contents where these changes in behavior occur are called Atterberg limits, after the Swedish soil scientist A. Atterberg. The "liquid limit", $LL$ or $w_L$, is the water content where disturbed soil transitions from liquid to plastic behavior. The "plastic limit", $PL$ or $w_P$, is the water content at the transition between the plastic and semisolid states of a soil. Finally, the "shrinkage limit", $SL$, is the water content corresponding to the transition between the semisolid and solid states of the soil.

Figure 4-4 illustrates the change in volume associated with changes in water content at the various Atterberg limits. Conceptually, the volume decreases linearly from the liquid limit through the plastic limit to the shrinkage limit as the water content decreases. At the shrinkage limit, the volume of the soil becomes constant and further drying produces no further reduction in volume.

Tests for determining the liquid and plastic limits are well established and standardized by both ASTM (D4318) and AASHTO (T89 and T90). The tests are true index tests in that they derive value purely from the fact that they are standardized. Nevertheless, the limits have considerable value for geotechnical engineering practice because soils exhibit different characteristics depending on both the absolute values

of the liquid, plastic, and shrinkage limits and on relative differences between the limits. As a general rule, soils producing similar values of Atterberg limits share common characteristics and often have similar strength, permeability, compressibility, and shrink/swell potential properties. Atterberg limits provide a relative indication of the ability for a silt or clay to retain water without changing state from a semi-solid to a viscous liquid. Atterberg limits can also provide an indication of the relative stiffness of soil by comparing the natural water content to the liquid and plastic limits; soils with water contents near the liquid limit can be expected to be soft while soils with water contents near the plastic limit can be expected to be much stiffer. Finally, Atterberg limits serve as the primary basis for classification of fine-grained soils, as described in Section 4.16.

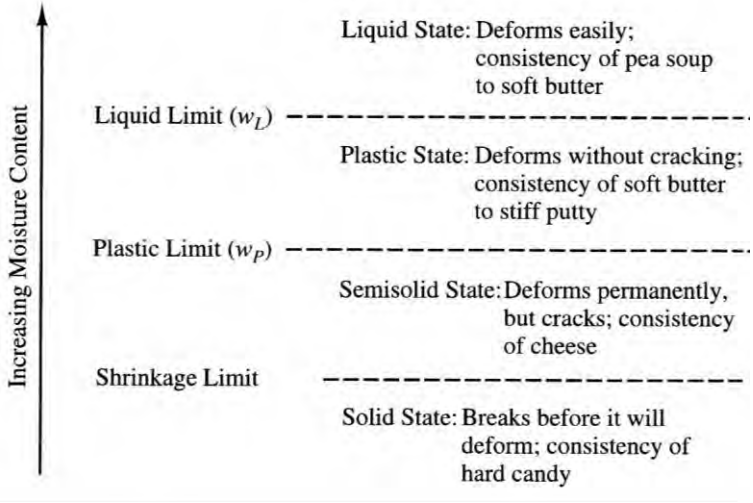


**Figure 4-3 Conceptual model of Atterberg limits (from Coduto, 2001).**

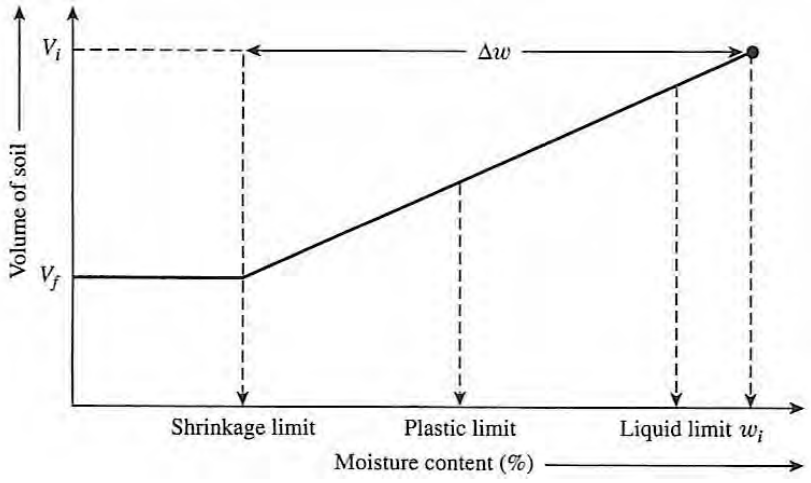


**Figure 4-4 Idealized relation between volume and water content of soil including Atterberg limits.**

### 4.8.1 Liquid Limit

In the U.S., the liquid limit is most often determined using the Casagrande cup device following AASHTO T89 or ASTM D4318. In this method, the liquid limit is defined as the water content at which a standard groove cut in a remolded sample will close over a distance of ½ inch at 25 blows of the liquid limit device. Figure 4-5 shows the Casagrande cup equipment used to obtain the liquid limit.

**Figure 4-5 Equipment used for determining liquid limit by Casagrande cup method.**

In recent years, engineers around the world have argued that using the Casagrande cup for determining the liquid limit can give variable results because the procedure is dependent on the experience of the operator. An alternative test method that has gained popularity in many countries is the fall cone test shown in Figure 4-6. In the fall cone test, the soil is mixed with water to form a soil-water paste as is done with the Casagrande method. The soil-water paste is placed in a small cup and the device's stainless steel cone is brought down so that the tip just touches the top of the paste. The cone is then released and allowed to penetrate into the soil. The penetration is measured after 5 seconds and plotted versus the water content of the paste to determine the liquid limit.

At present, the fall cone test has not been standardized by either AASHTO or ASTM, although it has become an International Organization for Standardization (ISO) Reference Test Method (ISO/TS 17892-12) and there is current action to ballot the fall cone procedure through ASTM Subcommittee D18. A useful standard to follow prior to formal adoption by AASHTO or ASTM is the British Standard BS1377 "Liquid Limit – Cone Penetrometer Method". This method requires use of a cone with an apex angle of 30 degrees and a mass of 80 gm. As is done with the Casagrande cup, several determinations of penetration are made for different water contents and a graph of water content versus penetration is

prepared as shown in Figure 4-7. The water content corresponding to a penetration of 20 mm is taken to be the liquid limit. Other procedures vary in terms of the mass and geometry of the cone, and the penetration that corresponds to the liquid limit, but are otherwise similar to the British standard. Many investigations have shown that values of liquid limit determined using the fall cone and Casagrande cup are practically identical for soils with liquid limits less than about 120 (e.g., Ozer, 2009; Budhu, 1985; Matteo, 2012).

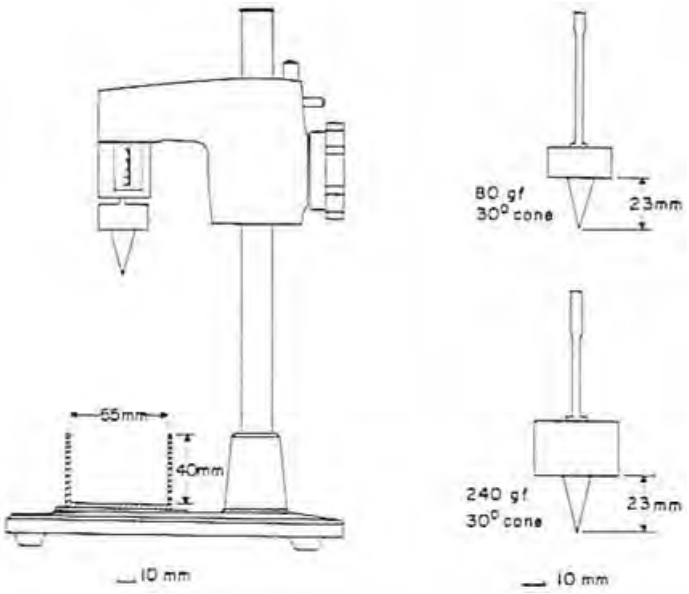


**Figure 4-6 Fall Cone equipment used for determining liquid limit.**

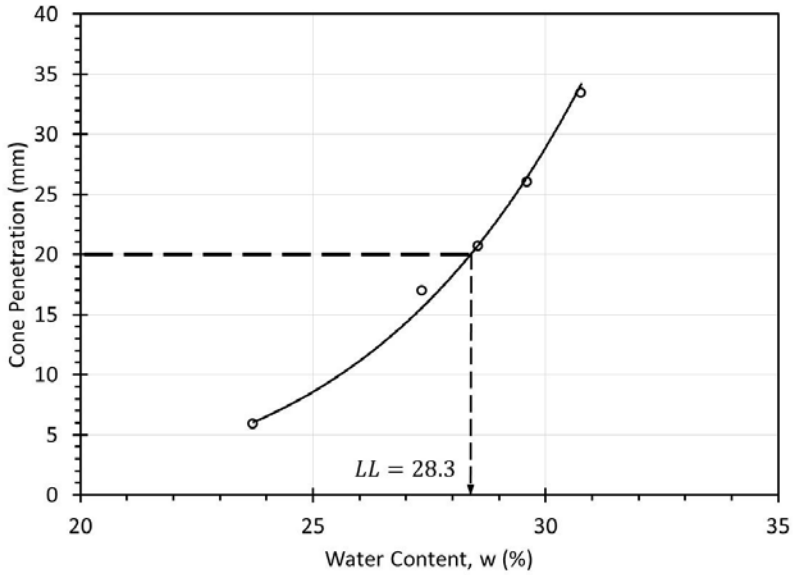


**Figure 4-7 Determination of liquid limit from Fall Cone test according to British Standard BS1377 (adapted from Azadi and Monfared, 2012).**

### 4.8.2 Plastic Limit

The plastic limit is most often determined using the thread method described in AASHTO T90 and ASTM D4318. The method consists of mixing a small amount of soil with water and rolling the soil into a thread on a clean glass plate. The plastic limit is defined as the water content at which a thread of soil just crumbles when it is carefully rolled out to a diameter of 1/8 inch (3.2 mm). If the thread crumbles before reaching 1/8 inch diameter, the water content is less than the plastic limit and additional water is needed to achieve the plastic limit. If the thread still maintains its shape when reaching a diameter of 1/8 inch, the water content is greater than the plastic limit and the soil must be dried to reach the plastic limit.

While the thread test for plastic limit is somewhat arbitrary, it has proven to be consistent and effective over the past 50 years. Because many engineers feel that the thread test is subject to the experience and skill of the operator, some have suggested the plastic limit be redefined as the water content at which there is a 100-fold increase in undrained shear strength over that measured with the fall cone at the liquid limit (i.e., about 160 kPa). However, in order to actually determine this value with a fall cone, the mass of the cone needs to be increased and the penetration depth reduced.

### 4.8.3 Shrinkage Limit

The shrinkage limit is defined as the water content at which further reduction in water content will not result in a decrease in the volume of the soil. The shrinkage limit is generally measured following ASTM D4943, which involves preparation of a wet soil "pat" of known volume with a known water content that is approximately equal to the liquid limit. The soil pat is then dried through a combination of air and oven drying and the volume of the dry soil pat is determined by coating the pat in wax and submerging it in water. The shrinkage limit is then calculated as

$$SL = w - \left[\frac{(V - V_d)\rho_w}{m_s}\right] \cdot 100\% \tag{4.11}$$

where $w$ is the water content of the wet soil pat, $V$ is the initial volume of the soil pat, $V_d$ is the volume of the dry soil pat, $m_s$ is the mass of the dry soil pat, and $\rho_w$ is the mass density of water (1.00 g/cm$^3$). Since the shrinkage limit is not required for classification of fine-grained soils, it is measured less frequently than the liquid and plastic limits, generally when volume changes for highly expansive clays are of interest. It is equally important in fine-grained soils where the natural water content is near or below the plastic limit.

### 4.8.4 Derived Indices from Atterberg Limits

Several important indices are commonly established from measured Atterberg limits and used to describe the nature of fine-grained soils. The "plasticity index", $PI$, and "liquidity index", $LI$, are the most common of these indices, and are respectively computed as

$$PI = LL - PL \tag{4.12}$$

$$LI = \frac{w_n - PL}{LL - PL} = \frac{w_n - PL}{PI} \tag{4.13}$$

where $w_n$ is the in situ water content for the soil. The plasticity index is commonly used to classify soils using the Casagrande Plasticity Chart as described in Section 4.16. The liquidity index is used as an indicator of the magnitude of the natural water content relative to the liquid and plastic limits. The liquidity index is equal to unity when the natural water content is equal to the liquid limit, whereas the liquidity index is equal to zero when the natural water content is equal to the plastic limit. Soils with *LI* less than or equal to zero are likely to be heavily overconsolidated or highly expansive. Soils with *LI* greater than approximately 0.7 are likely to be relatively soft and compressible. Soils with *LI* greater than unity are often sensitive.

Additional indices are also sometimes computed, although much less frequently. These include the "shrinkage index", $SI$, which is computed as

$$SI = LL - SL \tag{4.14}$$

and the "consistency index", which is computed as

$$CI = \frac{LL - w_n}{LL - PL} = \frac{LL - w_n}{PI} \tag{4.15}$$

The shrinkage index is used as an indicator of potential volume change with wetting and drying, while the consistency index is used in a manner similar to the liquidity index.

## 4.9 ACTIVITY

Skempton (1953) proposed a useful parameter that combines the Atterberg limits and the clay-size fraction ($CF$) of the soil. The "activity", $A$, is defined as:

$$A = \frac{PI}{CF} \tag{4.16}$$

where $CF$ is the percentage of particle sizes (by dry mass) that are smaller than 0.002 mm. Activity provides a general indication of the clay mineralogy of fine-grained soils and can be a useful means for estimating the presence of expansive clays at a site (discussed further in Chapter 5). Activity values range from about 0.4 for kaolinite to about 8.0 for montmorillonite. Most natural soils have values ranging from about 0.4 to 2.5. Typical values of activity for several different clay minerals are given in Table 4-6.

**Table 4-6 Typical values of activity for several different soils.**

| Soil | PI | Clay Fraction (% < 0.002 mm) | Activity |
|---|---|---|---|
| Peerless Clay (Kaolin) | 28 | 76.0 | 0.37 |
| Theile Clay | 27 | 36.2 | 0.75 |
| Texas Calcium Montmorillonite | 98 | 73.3 | 1.34 |
| Wyoming Bentonite (Sodium Montmorillonite) | 484 | 60.4 | 8.01 |

## 4.10 SOIL COMPOSITION

The mineralogy of soils generally controls the size, shape, and properties of individual soil particles, and by extension, the physical properties of soils (Mitchell and Soga, 2005). Coarse-grained soil particles and most silt-size particles are usually composed of practically inert minerals such that the mechanical behavior is dominated by physical interaction among the particles. However, the mineralogy of clay-size particles strongly influences interparticle interaction and the mechanical response of many soils. Index properties like Atterberg limits are commonly used to provide some indication of the composition of fine-grained soils based on physical behavior. However, there are times when more explicit identification of mineralogy can meaningfully inform judgment about likely behavior and potential problem conditions. Several different tests are commonly used for this purpose including X-ray diffraction tests and tests for specific surface area, cation exchange capacity, carbonate content, and organic content. The content of the following sections provides a brief summary of the most common methods used for characterizing the composition of soils, with particular focus on characterization of fine-grained soils. Mitchell and Soga (2005) provide more comprehensive coverage of soil mineralogy, the relation between mineralogy and physical properties, and available methods for evaluation of mineralogy.

### 4.10.1 X-Ray Diffraction

X-ray diffraction (XRD) is the most useful means for identifying the mineralogical composition of fine-grained soils. As the name implies, the technique consists of measuring the diffraction of X-rays that are

passed through soil particles to determine the spacing of interatomic planes using Bragg's law. Since the spacing of interatomic planes is unique for different minerals, the technique can be used to identify the minerals present in a given soil. Semi-quantitative determinations of the relative abundance of different minerals can also be derived from the relative size of "peaks" in the diffraction measurements.

XRD can be performed on "bulk powders" that include all components of a given soil to determine the relative abundance of clay and non-clay minerals. However, XRD is more commonly performed using only the clay-size fraction of a soil to identify the presence and relative abundance of different clay minerals (e.g., kaolinite, smectite, illite, and chlorite). Figure 4-8 shows results from XRD tests on a clayey soil of high plasticity, along with measured values for Atterberg limits. For this soil, the predominant clay mineral is smectite (montmorillinite), a highly expansive clay mineral. Changes in Atterberg limits with depth are seen to correspond to changes in the relative abundance of clay minerals and quartz with depth.

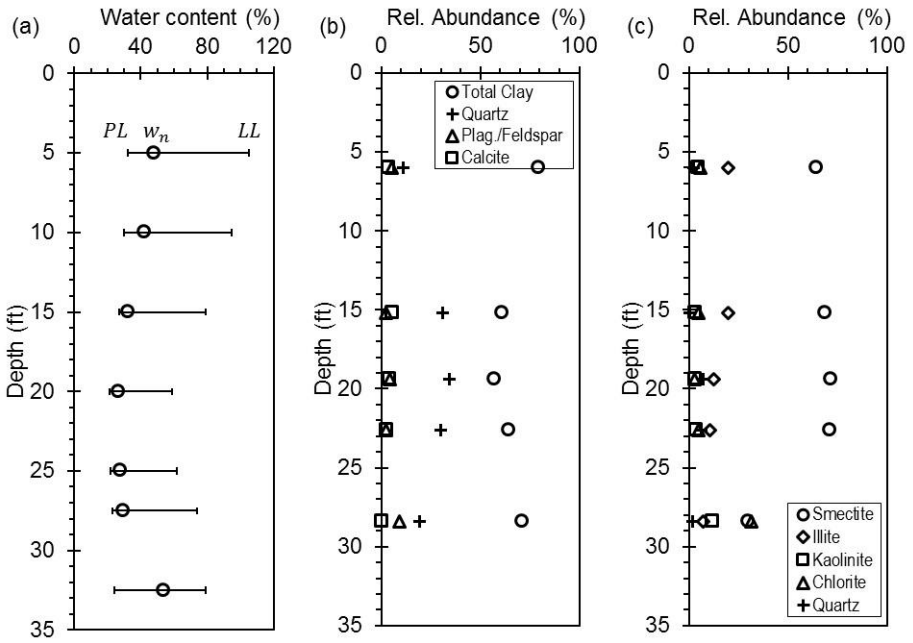


**Figure 4-8 Mineralogical characterization of a natural clay: (a) natural water content and Atterberg limits, (b) relative abundance of minerals from bulk sample, and (c) relative abundance of minerals from clay-size fraction.**

### 4.10.2 Specific Surface Area

The term "specific surface area", *SSA*, refers to the surface area of soil particles per unit mass of soil, usually expressed in $m^2/g$. The most common method for measuring *SSA* is the ethylene glycol monoethyl ether (EGME) method (Carter, et al., 1965; Cerato and Lutenegger, 2002), which takes about

16 to 24 hours to complete. Values of $SSA$ for different clay minerals fall into largely distinct ranges so measurement of $SSA$ for natural clays can be helpful for qualitatively judging the predominate mineral(s) present. Specific surface area is also strongly correlated with specific soil behavior and basic engineering properties for clays; SSA is correlated with the liquid limit (e.g., Farrar and Coleman, 1967; Kuzukami et al., 1971; Warkentin, 1972; Ohtsubo et al., 1983; Locat et al., 1984; Smith et al., 1985; Morin and Dawe, 1986; Churchman and Burke, 1991), swelling potential (e.g., Dos Santos and Castro, 1965; Low, 1980; Morgenstern and Balasubramanian, 1980; Ross, 1978; Dasog et al., 1988), and frost heave (e.g., Anderson and Tice, 1972; Rieke et al., 1983; Nixon, 1991). Soils with large specific surface area are generally expected to have high liquid limits, high swell potential, and the potential for relatively low strength or strength parameters. Table 4-7 shows typical values of $SSA$ for several clay minerals and fine-grained soils.

**Table 4-7 Typical values of $SSA$ and $CEC$ for several clay minerals and fine-grained soils.**

| Soil | Specific Surface Area, $SSA$ ($m^2$/gm) | Cation Exchange Capacity, $CEC$ (meq./100 gm) |
|---|---|---|
| Peerless Clay (Kaolinite) | 23 | 1 |
| Theile Kaolin | 38 | 2 |
| Texas Calcium Montmorillonite | 534 | 84 |
| Wyoming Bentonite | 637 | 76 |
| Boston Blue Clay | 85 | 15 |
| Leda Clay | 42 | 18 |
| Houston Clay | 153 | 29 |
| Nebraska Lake Clay | 217 | 39 |
| Salt Lake City Clay | 48 | 20 |
| Omaha Loess | 136 | 17 |
| San Francisco Bay Mud | 135 | 22 |
| Buckshot Clay | 245 | 30 |

### 4.10.3 Cation Exchange Capacity

Clay particles are often negatively charged as a result of isomorphous substitution and imperfections in the crystal lattice that lead to unsatisfied valence charges at the edges of the crystals. This charge deficiency means that clay particles attract other cations in order to become electrically neutral. Different clay minerals have different charge deficiencies and therefore different potential to attract cations. The cation exchange capacity, $CEC$, is a measure of this charge deficiency, generally expressed in units of milliequivalents per 100 grams of dry soil, that can be determined following ASTM D7503. Typical values of $CEC$ for several fine-grained soils are given in Table 4-7. Like $SSA$, $CEC$ can be used to

provide a general indication of the clay minerals present and as an indication of potential for swelling and low shear strength.

### 4.10.4 Carbonate Content

Carbonate minerals (calcium carbonate and calcium-magnesium carbonate) may be present in many geologic deposits and can act as cementing agents to hold individual particles or clusters of particles together, influencing soil behavior. The presence of carbonates in varying degree can alter the plasticity of fine-grained soils and influence the apparent preconsolidation stress (Boone and Lutenegger, 1997). Soils with high carbonate content often have high strength and stiffness, but the carbonate cementation may serve as a source of soil sensitivity (Mitchell and Soga, 2005) if the soil is disturbed during site characterization or construction. The actual amount and type of carbonate present in a given soil depends on the geologic origin and the degree of alteration (e.g., leaching, precipitation, etc.) that has occurred. Table 4-8 provides typical ranges of carbonate content for several different geologic deposits.

**Table 4-8 Typical ranges of total carbonate content for different soils.**

| Location | Geology | Range of Total Carbonates (%) |
|---|---|---|
| Boston, Massachusetts | Boston Blue Clay | 2.8 – 16.1 |
| Massena, New York | Leda Clay | 10.4 – 21.0 |
| Amherst, Massachusetts | Connecticut Valley Varved Clay | 2.0 - 6.6 |
| Albany, New York | Glacial Lake Clay | 14.4 – 27.1 |
| Evanston, Illinois | Chicago Clay | 22.2 – 31.8 |
| Clinton County, Iowa | Loess | 2.9-21.8 |
| Ames, Iowa | Glacial Till | 5.5 – 16.5 |
| Centralia, Missouri | Glacial Clay and Till | 2.1 – 8.8 |
| Houston, Texas | Beaumont & Montgomery Clay | 2.1 – 25.2 |
| Salt Lake City, Utah | Lacustrine Clay | 13.6 – 34.4 |
| Treasure Island, California | San Francisco Bay Mud | 2.8 – 4.3 |

In the field, the presence of carbonates can be easily detected by applying a few drops of dilute hydrochloric acid to a soil sample and observing the speed and vigor of the reaction. The reaction depends on the water content of the soil and the presence of other minerals. However, such observations are useful and should be recorded on field boring logs and included in soil descriptions. Quantitative determination of the amount of carbonates is typically performed using a laboratory gasometric technique in which dry soil is subjected to digestion by dilute hydrochloric acid in a closed vessel (ASTM D4373; Dreimanis, 1968). Other potential methods include differential thermal analysis, XRD, and chemical analyses.

### 4.10.5 Organic Content

Soils with substantial organic content have the ability to retain water, resulting in high water content, high primary and secondary compressibility, and potentially high corrosion potential. Organic soils may or may not be relatively weak depending on the nature of the organic material. Highly organic fibrous peats can exhibit surprising strength despite having high compressibility.

Organic soils are commonly identified by a characteristic odor, dark gray to black color, and potential presence of organic fibers. However, visual assessments of organic materials are subjective and may be misleading. More definitive and quantifiable means are sometimes needed to objectively characterize the presence and proportion of organic material. Organic content is most commonly evaluated according to AASHTO T267 or ASTM D2974, which involves heating an oven-dried sample to temperatures of 440°C to burn off organic matter so that the relative proportion of organic matter can be determined. Huang et al. (2009) notes that this test can sometimes lead to overestimation of the true organic content for some soils and describes several alternative direct and indirect means for characterizing the organic content of soils. Huang et al. (2009) also propose the criteria shown in Table 4-9 for characterizing organic soils.

**Table 4-9 Classification of organic content proposed by Huang, et al. (2009).**

| Organic Content (%) | Soil Designation |
|---|---|
| 0 to 3% | Mineral soil |
| 3 to 15% | Mineral soil with organic matter |
| 15 to 30% | Organic soil |
| > 30% | Highly organic soil (Peat) |

## 4.11 ELECTRO-CHEMICAL CLASSIFICATION TESTS

Electro-chemical classification tests provide quantitative information regarding the aggressiveness of soil conditions and the potential for deterioration of buried materials. Common electro-chemical tests include (1) pH; (2) resistivity; (3) sulfate ion content; and (4) chloride ion content. Results from these tests are helpful for identifying potentially corrosive soils based on criteria described in Chapter 5. Identification of such soils is important for design applications that include buried metallic elements.

## 4.12 ROCK HARDNESS

Rock hardness is useful for separating rock types and differentiating weak zones within a rock mass. Since hardness is a behavior rather than an absolute material property, quantitative measures of rock hardness depend on the type of test performed. Historically, rock hardness has been determined from indentation tests, rebound tests, or scratch tests. Rebound tests such as the Schmidt rebound hammer test

(ASTM D5873) and scratch tests are simple, portable, and more common. Indentation tests are less common. Alternatively, the guidelines given in Table 4-10 may be used in the field.

**Table 4-10 Descriptions for field evaluation of rock hardness.**

| Hardness Description | Characteristics |
|---|---|
| Soft | Very weak plastic material. |
| Friable | Easily crumbled by hand, pulverized or reduced to powder sand is too soft to be cut by a pocket knife. |
| Low Hardness | Can be gouged deeply or carved with a pocket knife. |
| Moderately Hard | Can be readily scratched by a pocket knife; scratch leaves a heavy trace of dust and scratch is readily visible after the powder has been blown away. |
| Hard | Can be scratched by a pocket knife with difficulty; scratch produces little powder and is only faintly visible; traced of knife's steel may be visible. |
| Very Hard | Cannot be scratched with a pocket knife; leaves knife steel marks on surface. |

## 4.13 ROCK ABRASION

Abrasion is a measure of the resistance of rock to wear when in contact with metal or between rocks. Abrasion resistance is often important for constructability as it can significantly affect selection and costs for tooling and equipment for tunneling and other underground construction. However, there is no universally adopted test method for directly evaluating abrasivity (Gharahbagh, et al., 2011). Many of the same characteristics that affect hardness, such as rock type, degree of weathering, mineral constituents, and bond strength between individual mineral grains, also affect resistance to abrasion. The Los Angeles Abrasion Test (ASTM C131 and C535) provides a measure of attrition between rock pieces and steel spheres that reflects the physical breakdown of rock. While this test is an appropriate measure of aggregate durability, it is not a direct measure of abrasivity for geotechnical construction and tooling.

## 4.14 ROCK DURABILITY

An abundant group of sedimentary rocks, especially those with high clay content, may be prone to weakening or disintegration when exposed to short-term weathering processes, such as wetting or drying. The slake durability test (ASTM D4644) is a standardized index test performed using a special apparatus that tumbles rock pieces within mesh drums while partially submerged in water. The result of the test is reported as the slake durability index, $I_d(2)$, that reflects the proportion of material lost through the mesh drums during the test. $I_d(2)$ provides a quantitative indication of the tendency for the rock to degrade.

Several variations to the standardized procedure in ASTM D4644 are sometimes adopted to evaluate durability for specific applications. For example, Keaton et al. (2012) recommend using a modified slake durability test proposed by Dickenson and Baillie (1999) wherein the oven-drying step of the standardized

test is excluded for evaluation of scour susceptibility. Similarly, Likos et al. (2005) describe slake durability tests wherein the drums are partially submerged in polymer slurry instead of water to evaluate degradation of shales for drilled shaft applications. Several additional modifications or alternatives to the standard slake durability test have also been proposed (e.g., Santi, 1998; Bryson et al., 2012).

A commonly used alternative to the slake durability test is the so-called "jar slake" test (Santi, 1998). The test basically consists of immersing an oven-dried sample of rock in distilled water and observing the condition of the sample over a 24 hour period. A numerical jar slake index, $I_j$, is then assigned based on the observed degradation of the sample as provided in Table 4-11. The jar slake test is largely qualitative, but has been adopted by many state transportation agencies for simple identification of degradable rock.

**Table 4-11 Jar slake index descriptions.**

| Jar Slake Index, $I_J$ | General behavior during test |
|---|---|
| 1 | Degrades rapidly into a pile of flakes or mud |
| 2 | Breaks readily and/or forms many chips |
| 3 | Breaks slowly and/or forms few chips |
| 4 | Breaks rapidly and/or develops several fractures |
| 5 | Breaks slowly and/or develops few fractures |
| 6 | Very little or no change |

## 4.15 ROCK CORE MEASUREMENTS

As described in more detail in Chapter 9, discontinuities in rock can have significant influence on the behavior of rock masses. Several different measurements are commonly collected for rock core as part of site characterization, including rock core recovery, rock quality designation, and rock fracture frequency. These measurements provide means to qualitatively assess the condition of a rock mass, as well as a basis for more quantitative classification of rock mass conditions as described in Chapter 9.

### 4.15.1 Rock Core Recovery

One measure of the quality of a segment of rock core is core recovery, $CR$. $CR$ is defined as the ratio of the cumulative length of core recovered in a core run to the length of the core run, usually expressed as a percentage:

$$CR = \frac{total\ length\ of\ core\ recovered}{total\ length\ of\ core\ run} \times 100\% \tag{4.17}$$

Core recovery can be an indication of the quality of the rock to withstand the coring process and flushing by drilling fluid, and an indication of rock weathering and decomposition.

### 4.15.2 Rock Quality Designation ($RQD$)

Rock quality designation, $RQD$, is a modified core recovery parameter that was developed to serve as a simple measure of rock mass quality (Deere and Deere, 1988). $RQD$ is computed according to ASTM 6032 as the ratio of the summed length of all "sound" pieces of intact rock core greater than 4 in. (100 mm) in length to the total length of the core run (Deere, et al., 1967):

$$RQD = \frac{\sum length\ of\ sound\ pieces > 4\ inches}{Total\ length\ of\ core\ run} \times 100\% \tag{4.18}$$

$RQD$ is preferably established from NX-size (2.16-in diameter) core, although larger and smaller core sizes can be used as long as appropriate drilling techniques are used to prevent excessive breakage or poor core recovery. Mechanical breaks caused by drilling or handling of the core should not be included in the calculation for $RQD$. Table 4-12 gives suggested terms to describe rock mass quality based on $RQD$.

**Table 4-12 Rock quality based on $RQD$ (from Deere and Deere, 1988).**

| $RQD$ | Rock Mass Quality |
|---|---|
| 0 – 25 | Very Poor |
| 25 – 50 | Poor |
| 50 – 75 | Fair |
| 75 – 90 | Good |
| 90-100 | Excellent |

When reporting $RQD$, the number of core pieces making up the summed length of core greater than 4 inches should also be noted on the log. The reason for this is that the same $RQD$ would be obtained from a core run of say 5 feet with 4 pieces each having a length of 1.25 feet as compared to a core composed of a single piece with a length of 5 feet.

### 4.15.3 Rock Fracture Frequency (FF)

A third measure of rock mass quality from rock core is the "fracture frequency", $FF$. Fracture frequency is defined as the number of natural fractures per unit length of core recovered:

$$FF = \frac{number\ of\ natural\ fractures}{total\ length\ of\ core\ recovered} \tag{4.19}$$

The fracture frequency can be determined for the entire length of a core run, or for a smaller segment of core. As is the case with $RQD$, artificial fractures created during drilling or core handling should be neglected when calculating fracture frequency.

## 4.16 CLASSIFICATION OF SOIL USING LABORATORY TEST MEASUREMENTS

Figure 4-9 shows a flow chart illustrating major tasks for site characterization. Initial identification and descriptions of soils are produced in the field based on observations made during drilling, usually based on ASTM D2488 or similar alternative standards. These descriptions are an important step in the site characterization process because they meaningfully inform subsequent testing and interpretation, and because they document physical characteristics that may not be captured during subsequent laboratory tests. However, field descriptions are largely qualitative, and somewhat subjective, and should be modified based on formal soil classification derived from quantitative measurements from standardized laboratory index tests. The basic premise of soil classification is that soils with similar classification can be expected to exhibit similar response to changes in load and environmental conditions. Soil classification provides for objective grouping of soils that are expected to have similar engineering behavior and allows engineers to make use of previous experience with similar soils. The two most common soil classification systems used throughout the world are the Unified Soil Classification System (USCS) prescribed in ASTM D2487 and the AASHTO soil classification system prescribed in AASHTO M145 and ASTM D3282.

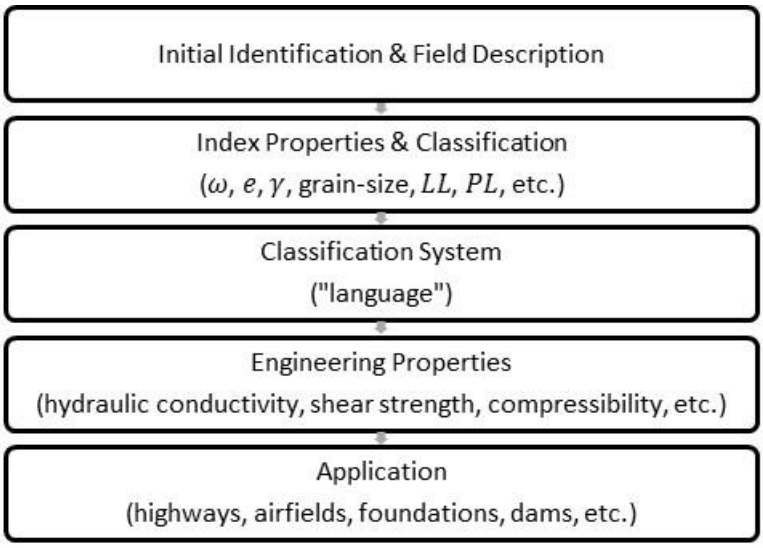


**Figure 4-9 General sequence for site characterization.**

### 4.16.1 Unified Soil Classification System (USCS)

The USCS classifies soils into fifteen primary soil types, designated using two-letter symbols, plus the potential for several additional combined designations as shown in Figure 4-10. Inorganic soils are first characterized as being coarse-grained or fine-grained based on the percentage of the soil (by dry mass)

passing the #200 sieve. Soils with less than 50 percent passing the #200 sieve are considered to be coarse-grained soils that are given the primary designation of "G" for gravel or "S" for sand based on additional particle-size criteria. Soils with greater than 50 percent passing the #200 sieve are considered to be fine-grained soils that are given the primary designation of "M" for silts or "C" for clay based on additional criteria derived from Atterberg limits. Organic soils are given the primary designation "O", or in the case of highly organic soils, the designation "Pt".

| Criteria for Assigning Group Symbols and Group Names Using Laboratory Tests[a] | | | | Soil Classification | |
|---|---|---|---|---|---|
| | | | | Group Symbol | Group Name[b] |
| (1) | (2) | (3) | (4) | (5) | (6) |
| COARSE-GRAINED SOILS<br>More than 50% retained on No. 200 sieve | GRAVELS<br>More than 50% of coarse fraction retained on No. 4 sieve | CLEAN GRAVELS<br>Less than 5% fines[c] | $C_u \geq 4$ and $1 > C_c < 3^e$ | GW | Well-graded gravel[f] |
| | | | $C_u < 4$ and/or $1 > C_c < 3^e$ | GP | Poorly graded gravel[f] |
| | | GRAVELS WITH FINES<br>More than 12% fines[c] | Fines classify as ML or MH | GM | Silty gravel[f,g,h] |
| | | | Fines classify as CL or CH | GC | Clayey gravel[f,g,h] |
| | SANDS<br>50% or more of coarse fraction passes No. 4 sieve | CLEAN SANDS<br>Less than 5% fines[d] | $C_u > 6$ and $1 < C_c < 3^e$ | SW | Well-graded sand[i] |
| | | | $C_u < 6$ and/or $1 > C_c > 3^e$ | SP | Poorly graded sand[i] |
| | | SANDS WITH FINES<br>More than 12% fines[d] | Fines classify as ML or MH | SM | Silty sand[g,h,i] |
| | | | Fines classify as CL or CH | SC | Clayey sand[g,h,i] |
| FINE-GRAINED SOILS<br>50% or more passes No. 200 sieve | SILTS AND CLAYS<br>Liquid limit less than 50 | Inorganic | PI > 7 and plots on or above "A"-line[j] | CL | Lean clay[k,l,m] |
| | | | PI < 4 and plots below "A"-line[j] | ML | Silt[k,l,m] |
| | | Organic | $\frac{LL_{oven\text{-}dried}}{LL_{natural}} < 0.75$ | OL | Organic clay[k,l,m,n]<br>Organic silt[k,l,m,o] |
| | SILTS AND CLAYS<br>Liquid limit 50 or more | Inorganic | PI plots on or above "A"-line | CH | Fat clay[k,l,m] |
| | | | PI plots below "A"-line | MH | Elastic silt[k,l,m] |
| | | Organic | $\frac{LL_{oven\text{-}dried}}{LL_{natural}} < 0.75$ | OH | Organic clay[k,l,m,p]<br>Organic silt[k,l,m,q] |
| Highly organic soils | | Primarily organic matter, dark in color, having organic odor | | Pt | Peat |

**Figure 4-10 Summary of major soil types identified by USCS (from Holtz, et al., 2011).**

For fine-grained soils, the second symbol is determined based on plasticity with the designation "L" being used to indicate low plasticity and the designation "H" being used to indicate high plasticity. This provides for four principle subgroups of fine-grained soils:

- ML – Low Plasticity Silt
- MH – High Plasticity Silt
- CL – Low Plasticity Clay
- CH – High Plasticity Clay

The secondary designation for a particular fine-grained soil is determined from the liquid limit and plasticity index for the soil and the Casagrande Plasticity Chart shown in Figure 4-11. Low and high plasticity soils are distinguished based on the liquid limit. Clays and silts are identified based on whether the liquid limit and plasticity index plot above or below the "A-line" defined by

$$PI = 0.73(LL - 20) \tag{4.20}$$

The "U-line" defined by

$$PI = 0.9(LL - 8) \tag{4.21}$$

is generally considered to be the upper limit for natural soils. Thus, test results plotting above this line should be carefully scrutinized and probably repeated.

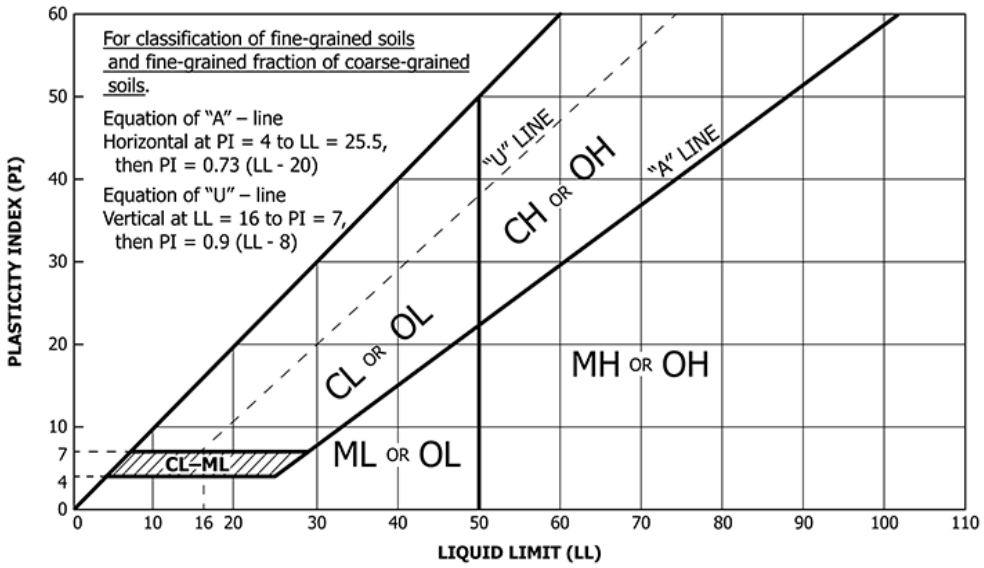


**Figure 4-11 Casagrande Plasticity Chart for classification of fine-grained soils (from ASTM D2487, 2011).**

For coarse-grained soils, the second symbol (letter) is used to represent the gradation of the soil based on criteria provided in Table 4-3. The symbol "W" is used to indicate the soil is well-graded while the symbol "P" is used to indicate the soil is poorly graded. Combining the primary and secondary symbols provides four principle subgroups for coarse-grained soils:

- GP – Poorly Graded Gravel
- GW – Well-Graded Gravel
- SP – Poorly Graded Sand
- SW – Well-Graded Sand

Additional secondary designations are used for coarse-grained soils containing appreciable amounts of fines, based on the plasticity of the fine-grained fraction of the sample. These include silty and clayey gravel (GM and GC) and silty and clayey sand (SM and SC). Finally, it is also possible to have coarse-grained soils with substantial fine-grained fractions that are given combined classifications (e.g., GW-GC, SP-SM, etc.).

Organic soils are often classified by repeating the liquid limit test for an identical specimen that has been oven-dried (i.e., dry preparation method). If the liquid limit for the oven-dried sample is less than 75 percent of the liquid limit from a specimen that was not oven dried, the soil is considered to be "organic" and is given the primary designation "O". In such cases, the secondary symbol is again determined from the Casagrande Plasticity Chart in Figure 4-11. Dark-brown to black soils composed of fibrous organic matter with an organic odor should be classified as peat and given the symbol "Pt".

### 4.16.2 AASHTO System

The AASHTO soil classification system makes use of similar laboratory characterization tests but groups soils differently based on their expected suitability for highway applications, primarily in terms of suitability as pavement subgrade. As summarized in Table 4-13, the AASHTO system uses eight primary soil groups, designated as A-1 through A-8, with several additional subgroups. A-1 through A-3 soils are considered coarse-grained soils with less than 35 percent fine-grained particles that serve as excellent to good subgrade soils. A-1 soils include well-graded gravel, coarse sand, and stone with no soil binder. A-2 soils are silty or clayey sands and gravels. A-3 soils are fine sands without silty or clayey fine-grained particles or with a small amount of nonplastic silt.

AASHTO group A-4 through A-7 soils are all fine-grained soils with greater than 35 percent fine-grained particles. The distinctions among these AASHTO soil groups are based on Atterberg limits as shown in Figure 4-12. A-4 soils include nonplastic or moderately plastic silty soils while A-5 soils are similar but with higher liquid limits. Groups A-6 and A-7 are clayey soils with low and high plasticity, respectively. A-8 soils include highly organic soils (peat and muck).

**Table 4-13 AASHTO soil classification system (from ASTM D3282, 2015).**

| General Classification | Granular Materials 35 % or Less Passing 75 µm (No. 200) | | | | | | | Silt-Clay Materials More Than 35 % Passing 75 µm (No. 200) | | | |
|---|---|---|---|---|---|---|---|---|---|---|---|
| Group Classification | A-1 | | A-3 | A-2 | | | | A-4 | A-5 | A-6 | A-7 |
| | A-1-a | A-1-b | | A-2-4 | A-2-5 | A-2-6 | A-2-7 | | | | A-7-5, A-7-6 |
| Sieve analysis, % passing: | | | | | | | | | | | |
| 2.00 mm (No. 10) | 50 max | ... | ... | ... | ... | ... | ... | ... | ... | ... | ... |
| 425 µm (No. 40) | 30 max | 50 max | 51 min | ... | ... | ... | ... | ... | ... | ... | ... |
| 75 µm (No. 200) | 15 max | 25 max | 10 max | 35 max | 35 max | 35 max | 35 max | 36 min | 36 min | 36 min | 36 min |
| Characteristics of fraction passing 425 µm (No. 40): | | | | | | | | | | | |
| Liquid Limit | ... | | ... | 40 max | 41 min | 40 max | 41 min | 40 max | 41 min | 40 max | 41 min |
| Plasticity Index | 6 max | | N.P. | 10 max | 10 max | 11 min | 11 min | 10 max | 10 max | 11 min | 11 min[A] |
| Usual types of significant constituent materials | Stone Fragments, Gravel and Sand | | Fine Sand | Silty or Clayey Gravel and Sand | | | | Silty Soils | | Clayey Soils | |
| General rating as subgrade | Excellent to Good | | | | | | | Fair to Poor | | | |

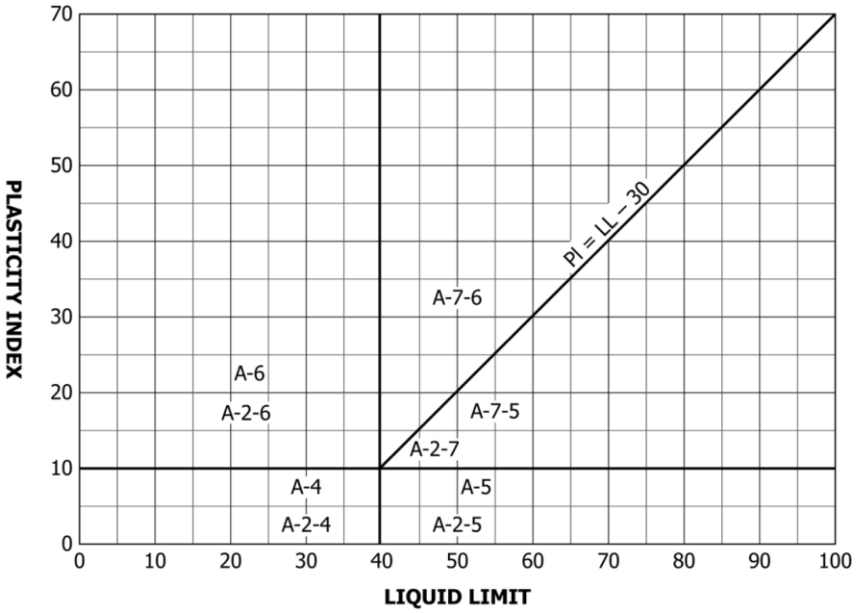


**Figure 4-12 AASHTO soil classifications for fine-grained soils (from ASTM D3282, 2015).**

The AASHTO system also provides an option to further classify soils using the "Group Index", which is calculated using grain-size characteristics and Atterberg limits as:

$$Group\ Index = (F - 35)[0.2 + 0.005(LL - 40)] + [0.01(F - 15)(PI - 10)] \quad (4.22)$$

where $F$ is the percent passing the #200 sieve, $LL$ is liquid limit, and $PI$ is plasticity index.

### 4.16.3 Comparison Between USCS and AASHTO Soil Classification Systems

There is no direct comparison between the USCS and AASHTO soil classification systems that works exactly on all soils; however, since the two systems are based on the same laboratory measurements, the

classifications generally overlap for most cases. Handy and Spangler (2007) provides a reasonable comparison shown in Table 4-14.

**Table 4-14 Approximate comparison between USCS and AASHTO soil classifications (Handy and Spangler, 2007).**

| AASHTO System | USCS |
|---|---|
| A-1-a | GW |
| A-1-b | SW |
| A-2 | SM or SC |
| A-3 | SP |
| A-4 | ML |
| A-5 | MH |
| A-6 | CL |
| A-7-5 | Most MH |
| A-7-6 | CH |
| A-8 | Pt |

## 4.17 SOIL IDENTIFICATION USING IN SITU TEST MEASUREMENTS

Measurements from in situ tests may also be used to identify soil type as an alternative, or supplement to the more formal soil classification using the USCS or AASHTO classification systems. Cone penetrometer (CPT), piezocone (CPTU), and dilatometer (DMT) tests are especially suited to efficiently evaluating soil type and stratigraphic changes, as illustrated in Figure 4-13. It is important to note, however, that identification of soil type from in situ tests is not the same as formal classification because in situ tests are measures of the mechanical response of soils rather than the specific classification criteria established for the USCS or AASHTO systems (Robertson, 2010). As such, soil types identified from in situ tests are referred to as "soil behavior type", $SBT$, to distinguish the types from formal classifications. Both classification and $SBT$ identification can meaningfully contribute to site characterization since the ultimate objective from an engineering perspective is to understand material properties and mechanical behavior. However, they are not the same.

Cone penetration tests (CPT) are performed by advancing a specially shaped steel cone into the ground at a constant rate and measuring the cone tip resistance, $q_c$, and "sleeve friction", $f_s$, as the cone is advanced through the ground (ASTM D5778). Piezocone tests (CPTU) additionally include measurements of pore water pressure on the cone face (denoted as $u_1$), just above the cone (denoted as $u_2$), and/or behind the friction sleeve (denoted as $u_3$) depending on the specific device used. When pore water pressures are measured just above the cone, the pore water pressure can influence the measured tip resistance; in such cases, a corrected tip resistance, $q_t$, is computed as

$$q_t = q_c + u_2(1 - a) \tag{4.23}$$

where $a$ is a net area ratio (between the load cell and the projected area of the cone) determined through calibration. A corrected sleeve friction, $f_t$, can also be computed if both $u_2$ and $u_3$ are measured. However, this correction is generally small and often not applied since $u_3$ measurements are relatively uncommon.

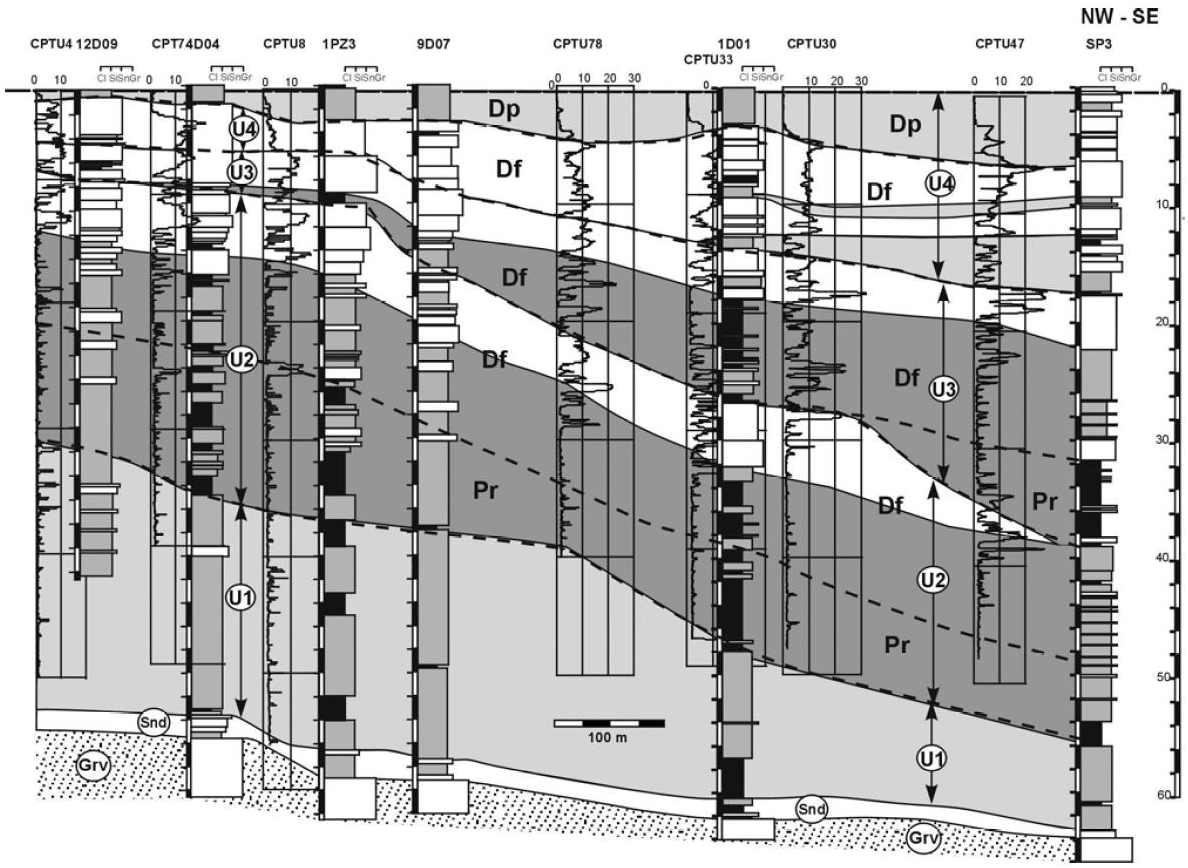


**Figure 4-13 Subsurface profile derived from CPT measurements (from Mayne, 2007)**

The dilatometer test (DMT) is performed by advancing the device to some depth of interest and then pressurizing the membrane to measure the "lift-off" pressure required to move the membrane (the "A" pressure) and the pressure required to displace the membrane 1.1 mm (the "B" pressure). These pressures are then corrected using calibration factors to establish $p_o$ and $p_1$ readings. In some cases, a third reading representing the closing pressure (the "C" pressure) may also be made.

### 4.17.1 *SBT* Identification from CPT and CPTU Measurements

$SBT$ identification from CPT measurements is generally based on the measured or corrected tip resistance ($q_c$ or $q_t$) and the "friction ratio", $R_f$ (sometimes denoted $FR$). $R_f$ is computed as

$$R_f = FR = \left(\frac{f_s}{q_c}\right) \times 100\% \tag{4.24}$$

$R_f$ is sometimes also computed using the corrected tip resistance $q_t$. The difference between $q_c$ and $q_t$ is usually small except in soft, fine-grained soils that generate substantial penetration-induced pore water pressures. Robertson (2010) and Tumay and Hatipkarasulu (2011) both report little impact from use of corrected and uncorrected tip resistance values for identification of soil behavioral type.

Begemann (1965) suggested values of $R_f$ less than about 2.5 percent indicate sand, greater than 3.5 percent indicate clays, and between 2 and 4 percent indicate mixed composition soils. Subsequently, several alternative charts have been proposed for identifying soil type from the friction ratio and cone tip resistance (e.g., Douglas and Olsen, 1981; Douglas, 1984; Robertson, et al., 1986). Figure 4-14 shows the most commonly used of these charts by Robertson et al. (1986), along with an update of this chart from Robertson (2010). The original Robertson et al. (1986) chart establishes twelve different $SBT$ designations that are summarized in Table 4-15. The updated chart reduces the number of designations to nine to be consistent with alternative charts that use normalized CPT measures described in Section 4.17.2 (Robertson, 2010). Table 4-16 shows $SBT$ designations for the updated chart in Figure 4-14b.

Several additional soil identification charts have been proposed for use with CPTU measurements (e.g., Jones and Rust, 1982; Senneset and Janbu, 1985; Campanella and Robertson, 1988). Figure 4-15 shows the most commonly used of these charts from Robertson et al. (1986) that considers the normalized pore water pressure parameter, $B_q$, computed as

$$B_q = \frac{(u_2 - u_0)}{(q_t - \sigma_{vo})} \tag{4.25}$$

where $u_2$ is the pore pressure measured just above the shoulder of the cone, $u_0$ is the estimated in situ pore water pressure, $q_t$ is the corrected cone tip resistance, and $\sigma_{vo}$ is the total vertical overburden stress at the test depth. Figure 4-15 is particularly useful for identification of soft, saturated fine-grained soils that generate substantial excess pore water pressures during testing (Robertson and Cabal, 2015).

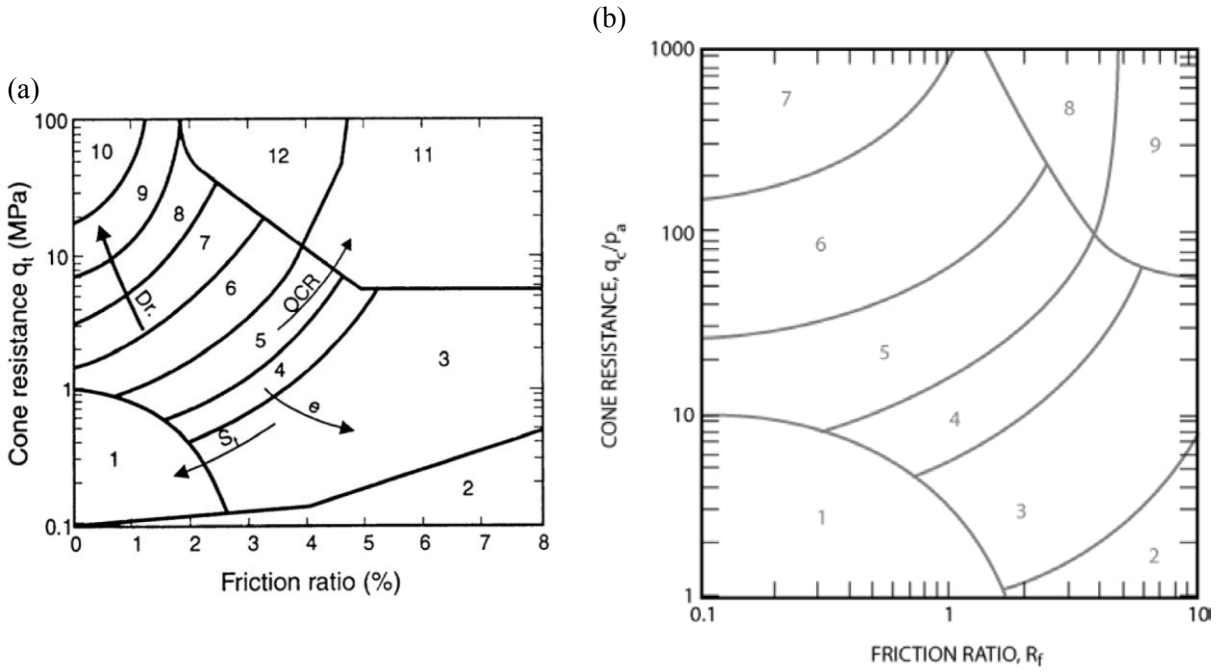


**Figure 4-14 Soil behavior type (*SBT*) charts for CPT measurements: (a) original chart from Robertson, et al. (1986), and (b) updated chart from Robertson (2010).**

**Table 4-15 Soil behavioral type designations for original chart by Robertson, et al. (1986).**

| ***SBT* Zone** | **Soil Behavior Type** |
|---|---|
| 1 | Sensitive fine-grained |
| 2 | Organic material |
| 3 | Clay |
| 4 | Silty clay to clay |
| 5 | Clayey silt to silty clay |
| 6 | Sandy silt to clayey silt |
| 7 | Silty sand to sandy silt |
| 8 | Sand to silty sand |
| 9 | Sand |
| 10 | Gravelly sand to sand |
| 11 | Very stiff fine-grained (overconsolidated or cemented) |
| 12 | Sand to clayey sand (overconsolidated or cemented) |

**Table 4-16 Soil behavioral type designations for updated Robertson (2010) chart (after Mayne, et al., 2009).**

| $SBT_n$ Zone | Soil Behavior Type | $I_{c-RW}$[1] | $I_{c-JB}$[2] |
|---|---|---|---|
| 1 | Sensitive fine-grained | N/A | N/A |
| 2 | Clay – organic soil | $I_{c-RW} > 3.60$ | $I_c > 3.22$ |
| 3 | Clays: clay to silty clay | $2.95 < I_{c-RW} < 3.60$ | $2.76 < I_c < 3.22$ |
| 4 | Silt mixtures: clayey silt & silty clay | $2.60 < I_{c-RW} < 2.95$ | $2.40 < I_c < 2.76$ |
| 5 | Sand mixtures: silty sand to sandy silt | $2.05 < I_{c-RW} < 2.60$ | $1.80 < I_c < 2.40$ |
| 6 | Sands: clean sands to silty sands | $1.31 < I_{c-RW} < 2.05$ | $1.25 < I_c < 1.80$ |
| 7 | Dense sand to gravelly sand | $I_{c-RW} < 1.31$ | $I_c < 1.25$ |
| 8 | Stiff sand to clayey sand (overconsolidated or cemented) | N/A | N/A |
| 9 | Stiff fine-grained (overconsolidated or cemented) | N/A | N/A |

[1] from Robertson and Wride (1998)
[2] from Jefferies and Been (2006)

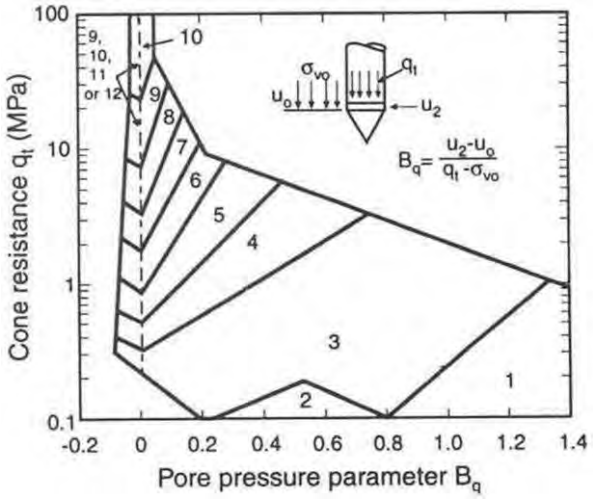


**Figure 4-15 Soil behavior type (*SBT*) chart for CPTU measurements (from Robertson and Cabal, 2015).**

### 4.17.2 *SBT* Identification from Normalized CPT and CPTU Measurements

Measured tip and sleeve resistance values generally increase with depth due to the confining stress at the testing depth, regardless of soil type. It is therefore desirable to normalize CPT and CPTU measurements by the overburden stress for identification of soil behavioral type in order to remove the influence of overburden stress. Normalized values of the tip resistance ($Q_t$) and sleeve resistance ($F_r$) are computed as

$$Q_t = \frac{(q_t - \sigma_{vo})}{\sigma'_{vo}} \tag{4.26}$$

$$F_r = \frac{f_s}{(q_t - \sigma_{vo})} \times 100\% \quad (4.27)$$

where $\sigma'_{vo}$ is the estimated in situ effective vertical stress at the testing depth. When this is done, the soil behavior type is often indicated as $SBT_n$ to signify that the behavioral type was established from normalized measurements. Figure 4-16 shows charts from Robertson (1990) for establishing $SBT_n$ from normalized measurements determined using Equations 4.26 and 4.27. Soil behavioral types associated with this chart are provided in Table 4-16.

Soil behavioral types produced using normalized measurements are generally more reliable than those established from non-normalized measurements (Robertson, 2010). However, use of normalized measurements requires knowledge of soil unit weight and in situ pore water pressures that are not generally available during testing. As such, use of non-normalized measurements has the distinct advantage of providing immediate identification of $SBT$. Differences between normalized and non-normalized soil behavioral types are relatively small for depths between 20 and 60 feet, but can be substantial at shallower and deeper depths.

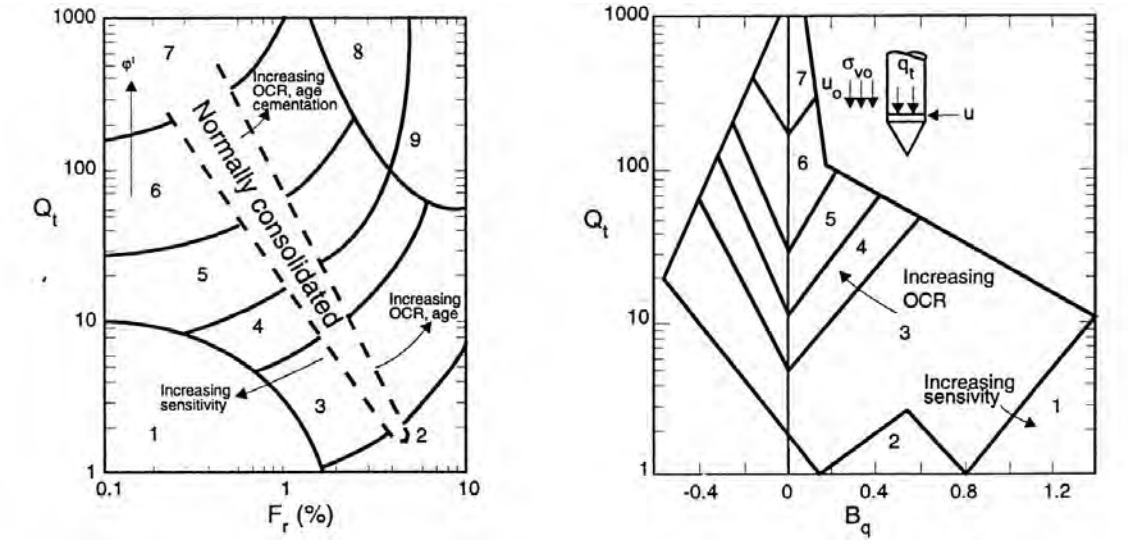


**Figure 4-16 Soil behavior type ($SBT_n$) chart for normalized CPT and CPTU measurements (from Robertson and Cabal, 2015).**

### 4.17.3 *SBT* Identification from Soil Behavior Type Index

As an alternative to using the charts provided in Figure 4-14 and 4-16, soil behavioral types can also be established using one of several different soil behavioral type indices, generally denoted as $I_c$. These indices combine normalized tip and sleeve resistance, and potentially the normalized pore water pressure

($B_q$), to establish a parameter that can be related to soil behavior type. For CPT measurements without pore water pressure measurements, Robertson and Wride (1998) defined the following soil behavior type index:

$$I_{c-RW} = \sqrt{\{3.47 - \log(Q_t)\}^2 + \{1.22 + \log(F_r)\}^2} \tag{4.28}$$

where the notation $I_{c-RW}$ is used to distinguish this soil behavior type index from alternative definitions by others. For CPTU measurements, the soil behavior type recommended by Jefferies and Been (2006) is:

$$I_{c-JB} = \sqrt{\left[3 - \log\left(Q_t \cdot \left(1 - B_q\right) + 1\right)\right]^2 + [1.5 + 1.3\log(F_r)]^2} \tag{4.29}$$

Suggested ranges for $I_{c-RW}$ and $I_{c-JB}$ for different soil behavioral types are provided in Table 4-16. Figure 4-17 shows the updated chart from Robertson (2010) with contours of $I_{c-RW}$ from Equation 4.28 to illustrate the comparison between using soil behavior type indices and the soil behavior type charts. The primary advantage of using soil behavior type indices is that they are more easily implemented in spreadsheet calculations.

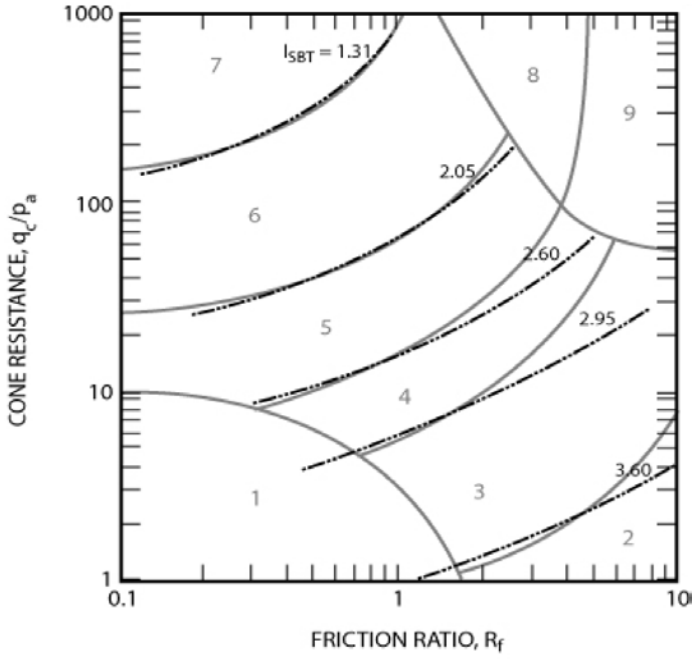


**Figure 4-17 Soil behavior type chart from Robertson (2010) with contours of $I_{c-RW}$ (from Robertson, 2010)**

### 4.17.4 Additional Characterization Using CPT and CPTU Tests

CPT and CPTU measurements can also be used to infer additional soil characteristics. Some investigations (e.g., Muromachi, 1981; Zervogiannis and Kalteziotis, 1988) have shown that the friction ratio, $R_f$, can be correlated to mean grain size, $D_{50}$. There is also some evidence that the friction ratio is related to the fines content in some deposits (e.g., Suzuki et al., 1995). However, other studies have shown large scatter and an apparent lack of correlation between friction ratio and fines content (e.g., Arango, 1997). The percent fines can also be estimated using $I_{c-JB}$ as shown in Table 4-17.

**Table 4-17 Fines content from CPT index $I_{c-JB}$ (after Mayne, et al., 2009).**

| $I_{c-JB}$ | % Fines |
|---|---|
| $I_{c-JB} < 1.26$ | 0 |
| $1.26 < I_{c-JB} < 3.50$ | $\%\ \text{fines} = 1.75{I_{c-JB}}^{3.25} - 3.7$ |
| $I_{c-JB} > 3.50$ | 100 |

### 4.17.5 Identifying Cemented or Unusual Soils from Seismic Cone Penetrometer (SCPT) and Seismic Piezocone (SCPTU)

The SCPT can be useful for identifying unusual soil conditions, such as cemented sands or fissured clays, by combining the interpreted maximum shear modulus, $G_{max}$ or $G_o$, obtained from shear wave velocity measurements with the normalized cone tip resistance. Schnaid (2009) suggests guidelines for expected behavior, separating cemented soils from uncemented soils, as shown in Figure 4-18. Uncemented soils generally exhibit a lower bound value of $B_x$ equal to 110 and an upper bound of $B_x$ equal to 280, while cemented soils generally give values of $B_x$ between 280 and 800. More recently, Schneider and Moss (2011) have suggested use of the term $K_G$ in place of $B_x$ and have indicated that aged, cemented and calcareous sands generally have values of $K_G$ between about 330 and 1100, while Holocene (recent) sands tend to have values of $K_G$ of around 110 to 330.

### 4.17.6 Soil Identification from Dilatometer (DMT)

Marchetti (1975) proposed a simple system based on the DMT Material Index, $I_D$, be used to establish the soil type as shown in Table 4-18. The value of $I_D$ is computed as:

$$I_D = \frac{(p_1 - p_o)}{(p_o - u_o)} \tag{4.30}$$

where $p_o$ is the corrected DMT lift-off pressure, $p_1$ is the corrected 1.1-mm expansion pressure, and $u_o$ is the in situ pore water pressure. $I_D$ is a measure of the relative change in pressure from $p_o$ to $p_1$,

normalized with respect to $p_o$, accounting for the in situ pore water pressure, $u_o$. As $I_D$ increases, the soil type changes from very soft cohesive soil to very stiff granular soil, with several intergrades. Marchetti et al. (2001) suggests that finer detail for identifying mixed soil composition might be possible using the DMT.

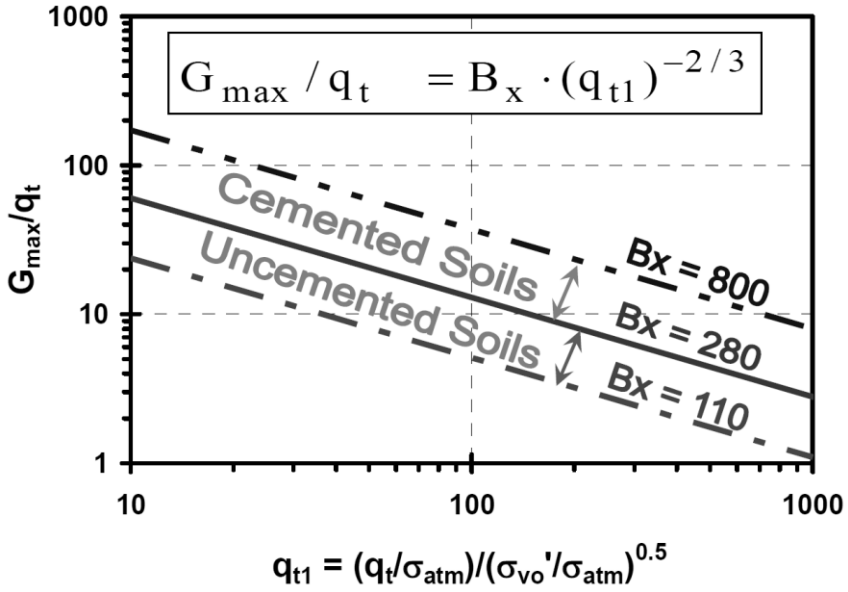


**Figure 4-18 Use of SCPT to distinguish cemented soils (from Mayne, et al., 2009).**

**Table 4-18 Soil identification using DMT Material Index, $I_D$ (from Marchetti, 1975).**

| Soil Type | DMT $I_D$ |
|---|---|
| Peat or Sensitive Clay | < 0.10 |
| Clay | 0.10 |
| Silt Clay | 0.35 |
| Clayey Silt | 0.60 |
| Silt | 0.90 |
| Sandy Silt | 1.2 |
| Silty Sand | 1.8 |
| Sand | 3.3 |

Robertson (2009) identified an approximate relationship between the CPT soil behavioral type index ($I_{c-RW}$) and the DMT Material Index, $I_D$. The relation is shown in Figure 4-19 and can be expressed as:

$$I_D = 10^{(1.67-0.67 \cdot I_{c-RW})} \tag{4.31}$$

or, equivalently as

$$I_{c-RW} = 2.5 - 1.5 \log(I_D) \tag{4.32}$$

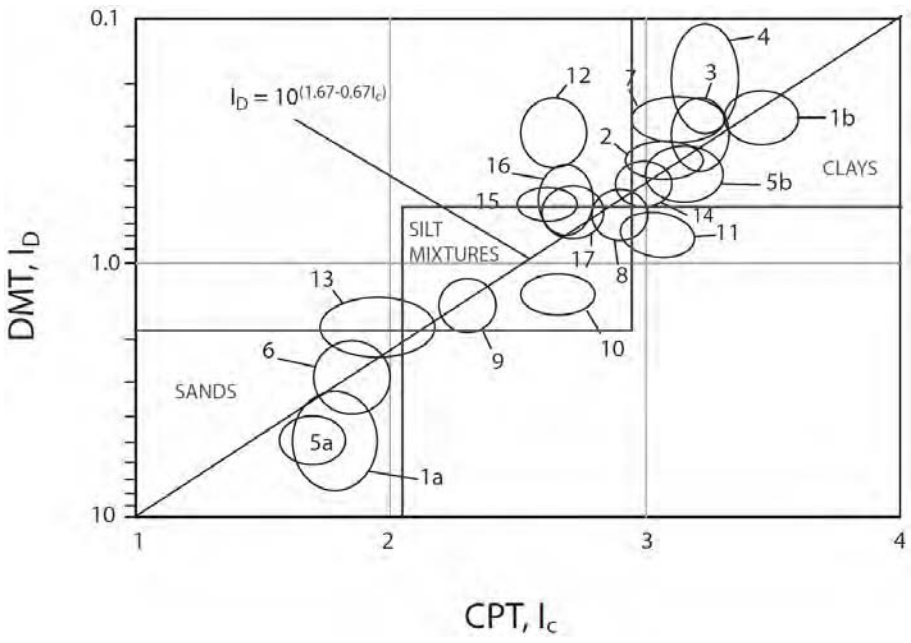


**Figure 4-19 Approximate relationship between CPT $I_{c-RW}$ and DMT $I_D$ (from Robertson, 2009).**

## 4.18 CLASSIFICATION OF INTACT ROCK

The performance of "rock masses" is controlled by characteristics of the intact rock as well as characteristics of discontinuities in the rock mass. As a result, rock is often classified at two different levels. Intact rock is generally classified based on qualitative observations and simple measurements as described in the following sections. Rock masses are further classified using one of several rock mass classification systems developed to facilitate practical design. Classification of intact rock is describe here because it is generally used in a manner similar to soil classification systems to distinguish rock types that are likely to have similar mechanical behavior. Unlike soil classification, however, classification of intact rock is not reduced to a small number of explicit designations, but rather is generally left in the form of qualitative descriptions. Rock mass classification systems are described in Chapter 9.

### 4.18.1 Rock Type

The primary basis for classification of intact rock is rock type. While rock type can be established through rather intensive petrographic testing and analysis, standard practice generally relies on establishing rock type based on physical characteristics that influence engineering behavior. Rock type is generally established by first identifying whether the intact rock is igneous, sedimentary, or metamorphic in origin. The specific rock type is then subsequently established from consideration of additional

characteristics such as mineralogy and texture. Igneous rock is formed by solidification of molten or partially molten material and is characterized based on mineralogical composition (generally distinguished by color), texture, and method of placement (intrusive or extrusive). Sedimentary rock is formed from deposition and lithification of sediments, from chemical precipitation from solutions, or from the secretion of organisms. Sedimentary rock is characterized based on whether it is derived from clastic sediments or chemical precipitates/organisms. Metamorphic rock is formed from pre-existing rock when the rock is changed ("metamorphosed") in response to changes in temperature and/or pressure. Metamorphic rock is characterized based on whether it is foliated or non-foliated (i.e., "massive"). Table 4-19 provides a concise summary to assist with establishing rock type. Table 4-20 through 4-22 respectively provide additional characteristics of common igneous, sedimentary, and metamorphic rock types to facilitate identification of rock type.

Beyond rock type, intact rock is additionally classified according to grain size or texture, degree of weathering, relative strength or hardness, and even color. Color and grain size are often key characteristics that facilitate identification of rock type. Relative strength, hardness, and weathering provide additional characterization of the quality of the intact rock.

### 4.18.2 Grain Size

Grain size refers to the sizes of individual particles or mineral crystals that comprise the intact rock. Unlike soils, where grain size is generally characterized based on sieve or hydrometer tests, the grain size for intact rock is generally characterized from visual observation. Unfortunately, there is no universally established grain-size criteria for rock and several alternative criteria are commonly used by different agencies. Table 4-23 provides one commonly used criteria for U.S. practice.

### 4.18.3 Weathering State

Weathering refers to the mechanical and/or chemical breakdown of rock over time through exposure to rain, groundwater, temperature changes, etc. As a general rule, weathering degrades the strength, stiffness, and general quality of intact rock and is therefore an important component of classification for engineering purposes. The degree of weathering should be classified according to weathering grades established by the International Society of Rock Mechanics (ISRM) provided in Table 4-24.

**Table 4-19 Rock type classification (from NRCS, 2012).**

| Genetic group | | | Detrital sedimentary | | | | Chemical organic | Metamorphic | | Pyroclastic | Igeneous | | | |
|---|---|---|---|---|---|---|---|---|---|---|---|---|---|---|
| Usual structure | | | Bedded | | | | Bedded | Foliated | Massive | Bedded | Massive | | | |
| Composition | | | Grains of rock, quartz, feldspar, and clay minerals | | | At least 50% of grains are of carbonate | Salts, carbonates, silica, carbonaceous | Quartz, feldspars, micas, dark minerals | Quartz, feldspars, micas, dark minerals, carbonates | At least 50% of grains are of igneous rock | Quartz, feldspars, micas, dark minerals | | Feldspar; dark minerals | Dark minerals |
| | | | | | | | | | | | Acid | Intermediate | Basic | Ultrabasic |
| Very coarse-grained | Predominant grain size, mm (sieve no.) 75 (3") | Rudaceous | Grains are of rock fragments | | | | CLINKER (31) | TECTONIC BRECCIA (41) | | Rounded grains: AGGLOMERATE (61) | PEGMATITE (71) | | | PYROXENITE (01) |
| Coarse-grained | | | Rounded grains: CONGOMERATE (11) Angular grains: BRECCIA (12) | | | CALCIRUDITE (23) | SALINE ROCKS Halite (32) Anhydrite (33) Gypsum (34) | MIGMATITE (42) | METACONGLOMERATE (51) | Angular grains: VOLCANIC BRECCIA (62) | GRANITE (72) | DIORITE (81) GRANODIORITE (82) | GABBRO (91) | |
| Medium-grained | 4.75 (4) | Arenaceous | Grains are mainly mineral fragments | | | CALCARENITE (27) | CALCAREOUS ROCKS | GNEISS (43) | MARBLE (52) GRANULITE (53) | TUFF (63) | SYENITE (73) | ANORTHOSITE (83) | DIABASE (92) | PERIDOTITE (02) |
| Fine-grained | 0.074 (200) | | SANDSTONE (13) ARKOSE (14) GRAYWACKE (Argillaceous ss) (15) | | | | | SCHIST (44) | QUARTZITE (54) | | APLITE (74) | MONZONITE (84) | | DUNITE (03) |
| Very fine-grained | 0.005 | Argillaceous or Lutaceous | MUDSTONE (16) SHALE: fissile mudstone (17) | SILTSTONE>50% fine-grained particles (18) CLAYSTONE>50% very fine grained particles (19) | MARLSTONE (22) | LIMESTONE (undifferentiated (21) CALCISILTITE (25) CHALK (26) CALCILUTITE (27) | LIMESTONE (35) DOLOMITE (36) | Amphibolite (45) PHYLLITE (46) Mylonite (47) SLATE (48) | HORNFELS (55) | Fine-grained TUFF (64) Very fine-grained TUFF (65) | RHYOLITE or FELSITE (75) | Dacite (85) ANDESITE (86) | BASALT (93) | NEPHELINE-BASALT (04) |
| Glassy amorphous | | | | | | | SILICEOUS ROCKS Chert (37) Flint (38) CARBONACEOUS ROCKS LIGNITE/COAL (39) | Ultramylonite (49) | | Welded TUFF (66) PUMICE (67) | VOLCANIC GLASSES OBSIDIAN (76) | PITCHSTONE (87) | TACHYLYTE (87) | |

**Table 4-20 Characteristics of common igneous rock.**

| Intrusive | Extrusive | Primary Minerals | Common Secondary Minerals |
|---|---|---|---|
| Granite | Rhyolite | Quartz, K-Feldspar | Plagioclase, Mica, Amphibole, Pyroxene |
| Quartz Diorite | Dacite | Quartz, Plagioclase | Hornblende, Pyroxene, Mica |
| Diorite | Andesite | Plagioclase | Mica, Amphibole, Pyroxene |
| Gabbro | Basalt | Plagioclase, Pyroxene | Amphibole Olivine |

**Table 4-21 Characteristics of common sedimentary rocks.**

| Clastic | | Non-Clastic | | |
|---|---|---|---|---|
| **Rock Type** | **Original Sediment** | **Rock Type** | **Primary Mineral** | **HCl Reaction** |
| Conglomerate | Sand, gravel, cobbles | Limestone | Calcite | Strong |
| Sandstone | Sand | Dolomite | Dolomite | Weak |
| Siltstone | Silt | Chert | Quartz | None |
| Claystone | Clay | | | |
| Shale | Laminated clay & silt | | | |

**Table 4-22 Characteristics of common metamorphic rocks.**

| Foliation | Rock Type | Texture | Formed From | Primary Minerals |
|---|---|---|---|---|
| Foliated | Slate | Platy, fine-grained | Shale, Claystone | Quartz, Mica |
| | Phyllite | Platy, fine-grained with silky sheen | Shale, Claystone, Fine-grained Pyroclastic | Quartz, Mica |
| | Schist | Medium grained with irregular layers | Sedimentary & Igneous Rocks | Mica, Quartz, Feldspar, Amphibole |
| | Gneiss | Layered, medium to coarse grained | Sedimentary & Igneous Rocks | Mica, Quartz, Feldspar, Amphibole |
| Non-Foliated | Greenstone | Crystalline | Intermediate Volcanics & Mafic Igneous | Mica, Hornblende, Epidote |
| | Marble | Crystalline | Limestone & Dolomite | Calcite & Dolomite |
| | Quartzite | Crystalline | Sandstone & Chert | Quartz |
| | Amphibole | Crystalline | Mafic Igneous & Calcium-Iron Bearing Sediments | Hornblende & Plagioclase |

**Table 4-23 Criteria for defining rock grain size.**

| Grain Size | Description | Criteria |
|---|---|---|
| < 0.003 in. (< 0.075 mm) | Very Fine-Grained | Cannot be distinguished by unaided eye. Few to no mineral grains are visible with a hand lens |
| 0.003 – 0.02 in. (0.075 – 0.425 mm) | Fine-Grained | Few crystal boundaries are visible; grains can be distinguished with difficulty by the unaided eye but can be somewhat distinguished by hand lens |
| 0.02 – 0.8 in. (0.425 – 2 mm) | Medium-Grained | Most crystal boundaries are visible; grains distinguishable by eye and with hand lens |
| 0.8 – 2 in. (2 – 4.75 mm) | Coarse-Grained | Crystal boundaries are visible; grains distinguishable with naked eye |
| 2 in. (> 4.75 mm) | Very Coarse-Grained | Crystal boundaries are clearly visible; grains are distinguishable with the naked eye |

**Table 4-24 Descriptive terms for weathering state of rock.**

| Term | Description | Weathering Grade |
|---|---|---|
| Fresh (F) | No visible sign of rock material weathering; slight discoloration on major discontinuity surfaces is possible. | I |
| Slightly Weathered (WS) | Discoloration indicates weathering of rock material and discontinuity surfaces. All rock material may be discolored by weathering and the external surface may be somewhat weaker than in its fresh condition. | II |
| Moderately Weathered (WM) | Less than half of the rock material is decomposed and/or disintegrated to a soil. Fresh or discolored rock is present either as a discontinuous framework or as corestones. A minimum 2 in. diameter sample cannot be broken readily by hand across the rock fabric. | III |
| Highly Weathered (WH) | More than half of the rock is decomposed and/or disintegrated to soil. Fresh or discolored rock is present either as a discontinuous framework or as corestones. A minimum 2 in. diameter sample can be broken readily by hand across the rock fabric. | IV |
| Completely Weathered (WC) | All rock material is decomposed and/or disintegrated to soil. The original mass structure is largely still intact. Material can by granulated by hand. | V |
| Residual Soil (RS) | All rock material is converted to soil. Material can be easily broken apart by hand. | VI |

### 4.18.4 Relative Rock Strength

Rock strength is controlled by a number of factors including degree of cementation, mineral type, weathering, etc. Relative rock strength may be estimated by simple field tests, which can be refined or verified by additional lab testing. ISRM has established a grading system for relative strength provided in Table 4-25. Rock strength grades can be determined using the qualitative methods provided. Schmidt Hammer and Point Load Index tests described in Chapter 9 can also be effectively used to qualitatively evaluate intact rock strength for purposes of classification.

**Table 4-25 Criteria and descriptions for relative rock strength.**

| Grade | Description | Field Identification | Approximate Compressive Strength (psi) |
|---|---|---|---|
| R0 | Extremely Weak Rock | Specimen can be indented by thumbnail. | 35-150 |
| R1 | Very Weak Rock | Specimen crumbles under sharp blow with point of geological hammer and can be peeled with a pocket knife. | 150-725 |
| R2 | Weak Rock | Shallow cuts or scrapes can be made in a specimen with a pocket knife. A firm blow with a geological hammer creates shallow indents. | 725-3500 |
| R3 | Medium Strong Rock | Specimen cannot be scraped or cut with a pocket knife. Specimen can be fractured with a single firm blow with a geological hammer point. | 3500-7250 |
| R4 | Strong Rock | Specimen requires more than one firm blow of the point of a geological hammer to fracture. | 7250-14,500 |
| R5 | Very Strong Rock | Specimen requires many firm blows from the hammer end of a geological hammer to fracture. | 14,500-36,250 |
| R6 | Extremely Strong Rock | Specimen can only be chipped with firm blows from the hammer end of a geological hammer. | >36,250 |

### 4.18.5 Rock Color

Color is not an engineering property but it can be used to help distinguish among rock units, or to identify alteration or weathering of rock. Rock color is also somewhat subjective but should be based on a consistent system, such as the 1977 Rock Color Chart from the Geologic Society of London provided in Table 4-26. In this system, three descriptors are used to create a color description. Only those descriptors needed to create a reasonable color are used (e.g., *Light Greyish Green; Dark Brown*).

**Table 4-26 Rock color descriptors (after Geological Society of London, 1977).**

| 1st Descriptor | 2nd Descriptor | 3rd Descriptor |
|---|---|---|
| Light | Yellowish | White |
| Dark | Buff | Yellow |
| | Orangish | Buff |
| | Brownish | Orange |
| | Pinkish | Brown |
| | Reddish | Pink |
| | Bluish | Red |
| | Purplish | Blue |
| | Orange | Green |
| | Olive | Purple |
| | Greenish | Olive |
| | Greyish | Grey |
| | | Black |

## 4.19 CHARACTERIZATION OF SOIL AND ROCK USING DRILLING PARAMETERS

A growing global trend for geotechnical site characterization is the automated recording of drilling parameters during drilling. While this technology is far from standard practice, it is likely to make important contributions to site characterization in the near future. In many ways, the technology is similar to technology currently being used to monitor installation of auger cast piles (ACIP) and auger cast displacement piles (ACIPD). Figure 4-20 shows a typical arrangement for measuring drilling parameters on a conventional track-mounted drill rig.

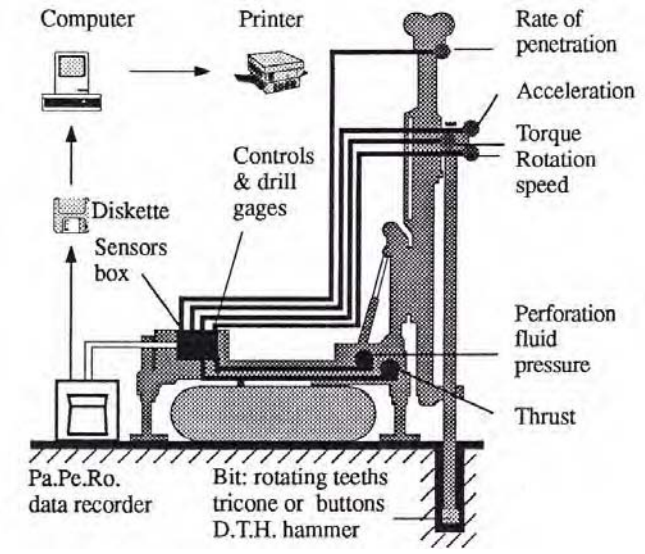


**Figure 4-20 Instrumented drill rig to measure drilling parameters.**

Drilling parameters may be recorded with both destructive drilling, such as mud rotary drilling, and rock coring. The measured parameters depend on the drilling method and specific tooling used but typically include instrumentation for downward thrust (or "crowd"), penetration distance, time, drilling fluid pressure and torque, as noted in Table 4-27 These parameters may be combined to produce other parameters such as penetration rate and energy to help characterize changes in subsurface conditions.

Several examples have been reported where drilling parameters have been used to evaluate the uniformity of rock and to determine the transition from soil to weathered rock to unweathered rock or boundaries between different rock units. Figure 4-21 shows a typical final log of drilling parameters. In some cases, attempts have also been made to correlate drilling parameters to rock properties, such as uniaxial compressive strength.

**Table 4-27 Important drilling parameters (from Gui, et al., 2002).**

| Parameter | Method | Tolerance | Note |
|---|---|---|---|
| Fluid pressure | Transducer (0-35 bars) | ±3 % | The pump normally provides a relatively constant hydraulic flow into the borehole. Ideally, pressure would be measured at the bit, but because of the impracticality of placing a transducer near the nozzle, the pressure is measured adjacent to the pump at the ground surface |
| Torque | Transducer (0-250 bars) | ±3 % | Torque is measured and applied to the drilling rod, and transmitted to the drilling bit, while aiming to keep a constant rotation speed. |
| Thrust on bit | Transducer (0-250 bars) | ±3 % | This is the main parameter that affects the drilling speed because for a given soil formation, the drilling speed is roughly proportional to the down-thrust. Hence, to obtain information directly from the drilling speed, it is recommended that the down-thrust is kept as constant as possible during the drilling process. |
| Hold-back | Transducer (0-35 bars) | ±3 % | Holdback pressure is necessary to prevent the drilling rod from penetrating too fast, especially into very soft ground, and to prevent the equipment falling into a hold when a cavity is encountered. In order to derive the effective net weight on the bit (W'), the holdback pressure has to be subtracted from the down-thrust, taking into consideration the self-weight of the rods. |
| Time | Internal clock (sec/5 mm) | 122 μsec | This is the time required to drill 5 mm of soil. A movement transmitter sensor measures the distance of 5 mm. This is important because the recorder is configured to record drilling data at 5 mm intervals. |
| Drilling speed | 1/Time | < 3 % | It is the reciprocal of time and because of this reciprocation, it can be used as a "magnifying glass" when the time is very large. It is closely related to the "hardness" of the strata being drilled when the down-thrust is kept reasonably constant. |
| Rotation speed | Electro-magnetic proximity sensor | ±3 % | It is normally chosen to suit the drilling conditions, taking into account the type of drilling rig, and the wear and tear of the bit. A reasonably constant value of rotation speed should be used throughout the drilling process in order to obtain more consistent information from the drilling speed and torque measurement. |

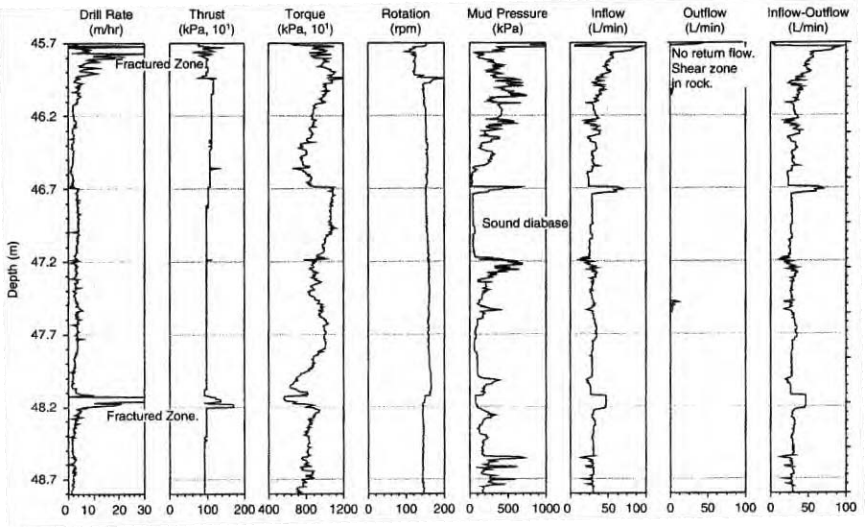


**Figure 4-21 Typical final logs of drilling parameters.**

# CHAPTER 5
# IDENTIFICATION AND CHARACTERIZATION OF PROBLEMATIC SOIL AND ROCK

Problematic soil and rock are commonly encountered at many project sites. The presence of problematic soil or rock can increase project costs if these materials must be removed and replaced with more suitable materials or if special construction methods are needed to mitigate problems. Undetected occurrence of problematic soil or rock can also lead to unexpected consequences during or following construction, which can require costly remediation and repair. It is therefore important to recognize when problematic soil and rock may be present at a site and understand methods for identifying these materials. The most common types of problematic soil and rock are covered in this chapter, with each type of soil/rock being covered in a separate section. Within each section, potential problems and consequences associated with the soil/rock type are described along with general information regarding the occurrence of the soil/rock type. Methods for identification of the respective problem materials are also provided along with discussion of challenges for site characterization. Additional hazards related to geotechnical conditions, rather than specific materials, are addressed in Chapter 12.

## 5.1 PROBLEMATIC SOIL AND ROCK TYPES

A number of natural geologic conditions produce problematic soil deposits and rock formations. The most common forms of problematic soil/rock include:

1. Collapsible Soils
2. Expansive/Shrinking Soils
3. Organic Soils and Peat
4. Dispersive Soils
5. Liquefiable Soils
6. Colluvium and Talus
7. Degradable Rock
8. Corrosive Soils
9. Cemented Sands
10. Sensitive Clays
11. High Sulfate Soils
12. Pyritic/Acid Rock
13. Unsaturated Soils
14. Permafrost

Each of these types of deposits have unique characteristics and unique challenges for site characterization as summarized in Table 5-1.

**Table 5-1 Characteristics of problematic soil and rock.**

| Problematic Soil | General Description | Common Engineering Characteristics | Common Characterization Challenges |
|---|---|---|---|
| Collapsible Soils | fine sand and silt with loose structure and weak inter-particle bonds | • potential for irrecoverable collapse upon inundation<br>• highly erodible<br>• low moisture content & unit weight | • assessing soil response at design moisture contents<br>• sensitive structure may collapse during sampling |
| Expansive/ Shrinking Soils | soils with large proportions of expansive clay minerals | • large volume changes with wetting/drying<br>• often stiff and fissured<br>• substantial undrained strength<br>• low frictional strength | • establishing zone of seasonal moisture change<br>• establishing volume change characteristics |
| Organic Soils and Peat | soils with high organic content, often found in low topographic areas with high water table | • soft & highly compressible<br>• high secondary compression<br>• potentially corrosive<br>• high moisture content<br>• may have fibrous texture | • soft, fibrous soil difficult to sample<br>• in situ tests may over-estimate strength due to fibrous nature of material |
| Dispersive Soils | highly erodible clays that often appear as "normal" clay | • low to medium plasticity<br>• susceptible to severe erosion and piping | • difficult to identify from visual inspection or common index tests |
| Liquefiable Soils | loose, saturated coarse-grained soils subject to strength loss during seismic events | • loose, coarse-grained soils below water table without appreciable fines<br>• low SPT blow counts | • difficult to obtain undisturbed samples |
| Colluvium and Talus | mixed fine-grained (colluvium) or coarse-grained materials (talus) that accumulate on slopes | • colluvium will often contain thin lenses of weak material<br>• talus slopes often near angle of repose (i.e., FOS=1) | • mixed materials difficult to sample<br>• identifying thin layers that influence performance<br>• localized "perched" water |
| Degradable Rock | poorly indurated rock that degrades to the parent soil material when exposed | • exposed material will degrade<br>• undesirable material for aggregate and fill<br>• often anisotropic with low frictional strength | • in situ material may be difficult to sample<br>• rapid degradation of materials after sampling |
| Corrosive Soils | soil that produce high rates of corrosion of buried steel elements | • engineering characteristics vary | • Special tests required to evaluate corrosion potential |

(cont'd)

**Table 5-1 (cont'd) Characteristics of problematic soil and rock.**

| Problematic Soil | General Description | Common Engineering Characteristics | Common Characterization Challenges |
|---|---|---|---|
| Cemented Sands | sandy soils with salt or calcareous bonding at grain-to-grain contacts | • often strong, but brittle and potentially sensitive<br>• high penetration resistance for in situ tests<br>• potential for collapse if binder is soluble | • difficult to obtain undisturbed samples<br>• rock coring techniques may be required<br>• drilling fluid may degrade cementation |
| Sensitive Clays | marine deposits with metastable structure and potential for dramatic strength loss | • disturbance produces dramatic strength loss to almost liquid | • undisturbed sampling difficult<br>• extreme care required for sampling & testing |
| High Sulfate Soils | sulfate-rich soils may swell when mixed with calcium from lime or cement | • engineering characteristics vary | • difficult to identify from visual inspection or common index tests |
| Pyritic/Acid Rock | rock materials that are capable of producing acidic runoff | • engineering characteristics vary | • requires devoted and somewhat unique sampling and testing |
| Unsaturated Soils | Common soil condition above water table with in situ strengths that may be greater than appropriate for design | • stronger and stiffer than similar saturated soils<br>• in situ effective stress difficult to predict<br>• shallow fine-grained soils may be cracked and fissured | • some lab and field measures of strength may not represent appropriate design condition |
| Permafrost | Permanently frozen ground with potential for weakening and settlement if thawed | • stiffer, stronger, and less permeable than similar unfrozen soils<br>• creep behavior more important than conventional mechanical properties | • rotary coring generally required to obtain samples<br>• in situ tests and geophysics often required<br>• creep response properties needed |

Both indirect and direct methods can be used to identify problematic soil and rock. Indirect methods typically rely on common index properties such as Atterberg limits, grain-size distribution, composition tests, or even visual observations to provide an indication of problematic soil or rock. Direct methods usually involve special laboratory or field tests to identify and characterize the suspected problematic behavior. For example, the presence of swelling soils can often be indirectly identified using measured Atterberg limits. However, swelling soils can also be characterized by wetting the soil in the laboratory under carefully controlled conditions to directly measure the magnitude of swelling. While direct measurements are often more expensive and time consuming, it is important to recognize that indirect

methods are generally approximate indicators of potential problems whereas direct measurements are more reliable and quantitative. Thus, while indirect measures can and should be used as screening tests for potential problems, indications from indirect methods should generally be confirmed and more carefully characterized using direct measurements.

Identification and characterization of problematic soil and rock is key to development and implementation of appropriate mitigation methods. Identification generally results from several considerations that include:

1. Understanding of the geologic setting at the site;
2. Knowledge of previously reported cases of problems with local soil or rock;
3. Deliberate observation and investigation of site conditions; and
4. Understanding of the project plans and requirements.

Since most problematic soil and rock types result from geologic processes, evaluation and understanding of site and regional geology is critical to identifying the potential occurrence of problematic materials. Once the potential for problematic soil or rock is identified, it is generally necessary to undertake additional investigations to effectively characterize the significance of potential problems and to develop effective mitigation measures.

## 5.2 COLLAPSIBLE SOILS

Collapsible soils are sometimes referred to as "meta-stable" soils that have the potential to undergo rapid and dramatic deformation when inundated with water under constant applied load. Collapsible soils usually have some type of bonding between individual soil particles or groups of particles that prevents the particles from rearranging into a denser arrangement. Sources of inter-particle bonding may include: clay particles that are joined to, and shared by, larger silt or sand particles; calcium or calcium/magnesium carbonate precipitates; oxides of iron, magnesium or manganese; and/or negative pore water pressure (matric suction). Inter-particle bonding is often complex and may include one or more of these cementing agents acting with variable strength to keep the soil matrix in a metastable state. Some bonding agents are water soluble or water sensitive, while others may be less sensitive or even insensitive to wetting. Bonding agents may also be sensitive to disturbance, with undisturbed specimens producing less collapse than disturbed specimens compacted to the same initial water content and dry density (Lutenegger, 2012).

Strictly speaking, collapse is a soil behavior rather than a soil property. Collapsible soils often have low dry density (usually less than 90 pcf) and low natural water content. Many collapsible soils have little to

no plasticity and often classify as ML or CL according to the USCS. Some collapsible soils may be very stiff but can become soft when water becomes available, even if the water does not saturate the soil. In most cases, soils that have been previously saturated from periodic flooding or high groundwater levels will not be collapsible, although they may be highly compressible.

Collapse behavior is counter to soil mechanics principles that suggest that soil will expand when subjected to reductions in effective stress. Four conditions are necessary for collapse to occur (Dudley, 1970; Barden, et al., 1973; Lawton, et al., 1989; Mitchell and Soga, 2005):

1. An open, partially unstable, partially saturated fabric;
2. Sufficient total stress to make the soil structure metastable;
3. Presence of a bonding agent or sufficient soil suction to stabilize the soil in the metastable condition; and
4. Addition of water, which reduces soil suction, or softens or destroys the bonding agent, thereby causing shear failures at the inter-aggregate or inter-particle contacts.

The magnitude of collapse depends on soil composition, the nature of cementation, initial dry density, initial water content, degree of compression up to collapse stress, and the stress level at which collapse is initiated. For any given set of conditions, the magnitude of collapse generally decreases with increasing pre-collapse water content, increasing pre-collapse dry density, and decreasing overburden pressure. For any soil, there are combinations of initial dry density, water content, and overburden pressure for which no volume change will occur when the soil is inundated and there appears to be a critical initial water content above which no collapse will occur. Finally, there is a critical initial degree of saturation above which negligible collapse will occur regardless of the magnitude of the pre-wetting overburden pressure (Lawton, et al., 1989).

### 5.2.1 Occurrence of Collapsible Soils

Collapsible soil deposits exist throughout the world, with varying degrees of collapse severity. Documented occurrences of collapsible soils are present in a wide range of geologic deposits, including both transported and residual soils (e.g., Knight, 1963; Dudley, 1970; Clemence and Finbarr, 1981; Rogers, et al., 1994; Rogers, 1995). Natural collapsible deposits primarily include loess (windblown or eolian silt), windblown desert sands, alluvial flow deposits (alluvial fans and mudflows) in arid and semi-arid regions, colluvial deposits (slopewash), and decomposed/weathered rock (residual and tropical lateritic soils). Some compacted soils may also show tendency for collapse if the soil is loaded and subsequently becomes saturated. Collapse tends to be more problematic for soils compacted dry of the

optimum water content but can also occur for soils compacted wet of optimum (Lim and Miller, 2004). Collapsible compacted soils can include fine-grained (CL, CH, ML) to mixed coarse- and fine-grained (SM, SC) soils (Lawton, et al., 1989; Lawton, et al., 1992; Alwail, et al., 1994; Jotisankasa, et al., 2007).

### 5.2.2 Indirect Identification of Collapsible Soils

Preliminary information regarding the potential for encountering collapsible soils can sometimes be derived from soil surveys and geologic maps. Site specific identification of collapsible soils from indirect measurements is more challenging. Criteria for identifying collapsible soils based on values of initial dry density, liquid limit, void ratio, and other index properties have been proposed, several of which are summarized in Table 5-2. Figure 5-1 shows an additional criterion to identify collapsible soils based on measurements of dry unit weight and liquid limit (Gibbs and Bara, 1962; Gibbs and Bara, 1967). Soils with dry unit weight and liquid limit plotting above the line shown are considered susceptible to collapse when wetted, while soils plotting below the line are likely to expand when wetted. Mock and Pawlak (1983) propose another alternative method for identifying collapsible soils that relies on dry density and fines content.

**Table 5-2 Summary of criteria for identifying collapsible soils.**

| Reference | Method | Parameter Range | Description |
|---|---|---|---|
| Denisov (1951) | Coeff. of Subsidence $K = \frac{e_L}{e_o}$ | $0.5 \le K \le 0.75$<br>$K = 1.0$<br>$1.5 \le K \le 2.0$ | highly collapsible soil<br>non-collapsible loams<br>non-collapsible soils |
| Gibbs (1961) | Collapse Ratio $R = \frac{w_{sat}}{LL}$ | $R > 1.0$ | soil subject to collapse |
| Kassif and Henkin (1967) | Product $w_o \cdot \rho_d$ | $w_o \cdot \rho_d > 15$ | minimal collapse |
| Feda (1964) | $K_1 = \frac{w_o}{S_o} - \frac{PL}{PI}$ | $S_o < 100\%$ and $K_1 > 0.85$ | "subsident soils" |

$e_L$=void ratio at $LL$
$e_o$=in situ void ratio
$w_o$=in situ moisture content
$S_o$=initial degree of saturation
$PL$=plastic limit
$PI$=plasticity index
$LL$=liquid limit
$w_{sat}$=saturated moisture content
$\rho_d$=dry density (gm/cm$^3$)

None of these criteria are direct indicators of actual collapse behavior, nor do they quantify the amount of collapse that can occur under a given vertical stress. In many cases, these "indicators" may give false indications of collapse potential because the criteria do not account for natural soil structure, cementation, or other factors that influence collapse. As with other types of empirical methods, specific collapse criteria are often strictly appropriate only for the specific geologic deposits and/or specific geographic

areas for which they were developed. Despite these limitations, the methods can serve as effective screening tools for identifying when direct laboratory tests are needed to characterize site specific behavior.

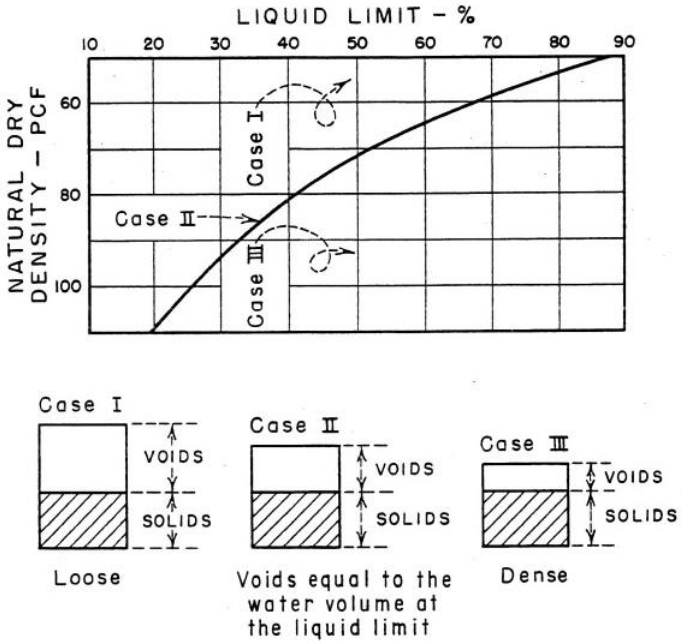


**Figure 5-1 Gibbs and Bara (1967) criterion for collapsible soils (Case I-collapse; Case III-expansion).**

### 5.2.3 Direct Characterization of Collapsible Soils

If collapsible soils are suspected, undisturbed samples of the suspect soil(s) should be acquired for direct evaluation of collapse potential and quantification of the magnitude of collapse that may occur when wetted under an appropriate vertical stress. The most accepted laboratory method for such evaluations was suggested by Lutenegger and Saber (1988) and is documented in ASTM D5333. In this test, a trimmed specimen of soil is placed in a conventional one-dimensional consolidation apparatus and loaded to some prescribed vertical stress. The specimen is then inundated with water and the change in height of the specimen is recorded with time to observe the magnitude of collapse displacements. The "collapse potential", $CP$, is computed as

$$CP = \frac{\Delta e_c}{1+e_o} \times 100\% \tag{5.1}$$

where $\Delta e_c$ is the change in void ratio upon wetting, and $e_o$ is the initial or "natural" void ratio. Alternatively, collapse potential can be calculated from the measured compression of the specimen as

$$CP = \frac{\Delta H}{H_o} \times 100\% \quad (5.2)$$

where $\Delta H$ is the change in height of the specimen when inundated with water at the prescribed vertical stress and $H_o$ is the initial specimen height. Use of Equation 5.2 eliminates the need to determine (or estimate) the specific gravity of soil solids in order to calculate the void ratio and is more convenient for expressing behavior in terms of soil strains. ASTM D5333 is sometimes referred to as the "single oedometer" collapse test because it involves testing a single soil sample. ASTM D5333 was officially withdrawn in July of 2012, but the method nevertheless remains a practical and reliable means for quantifying collapse potential. An alternative, but conceptually similar procedure is also described in AASHTO T258 or ASTM D4546.

Figure 5-2 shows results from a single oedometer collapse test performed on a sample of loess from southeastern Iowa. The observed response includes three distinct stages. The initial stage of the test is the response-to-loading or compression stage observed while loading the sample to a vertical total stress of 2 ksf, prior to inundation of the specimen. The initial compression stage is followed by the response-to-wetting, or collapse, stage of the test wherein the specimen is inundated with water and the resulting displacement of the specimen is observed. Figure 5-2 shows a large decrease in specimen height as a result of water being added to the specimen at a vertical stress of 2 ksf. Following collapse, additional vertical stress applied to the specimen results in consolidation (as pore water is squeezed out of the now saturated soil) during the third test stage. The third stage of the test is sometimes omitted. Collapse potential depends on the applied vertical stress level when the sample is inundated. Tests should therefore be performed at stress levels that are anticipated in the field.

An alternative to the single-oedometer test is the so-called "double-oedometer" test wherein duplicate specimens are tested in one-dimensional compression. One specimen is loaded at the natural water content, without inundation, while another identical specimen is saturated prior to loading over the same range of vertical stress. Results from a typical set of double-oedometer tests performed on samples of loess from eastern Nebraska are shown in Figure 5-3. For the double-oedometer test, the collapse strain is taken as the difference in measured strains from the two specimens at the same stress. The advantage of the double-oedometer test compared to the single-oedometer test is that collapse potential is established for different stress levels. However, the saturated specimen in the double-oedometer test is never really subjected to the process of wetting under an applied load, which may produce different collapse response than is measured in the single-oedometer collapse test.

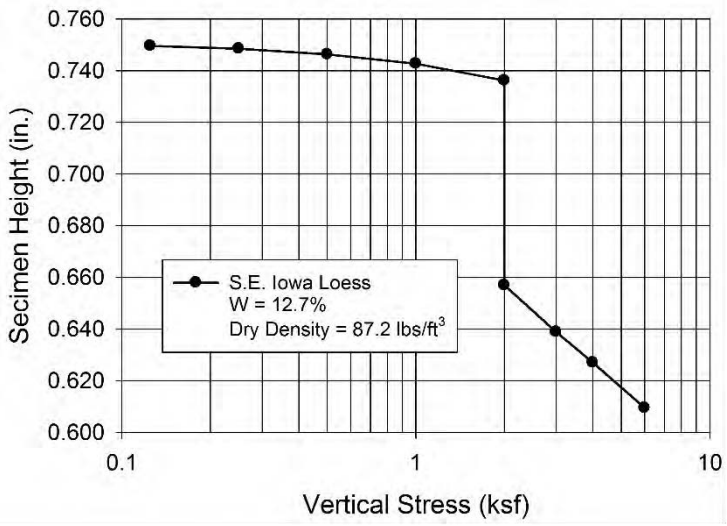


**Figure 5-2 Results from single-oedometer collapse test for southeast Iowa loess.**

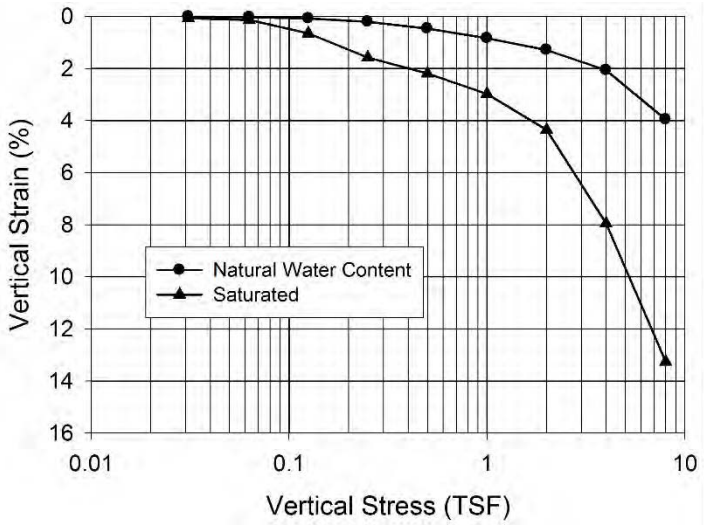


**Figure 5-3 Results of double oedometer collapse test for undisturbed Nebraska loess.**

The collapse potential, $CP$, is a quantitative measure of the likely magnitude of collapse deformations under a given stress. However, it can also be used to establish qualitative descriptions of collapse severity using one of several ratings summarized in Table 5-3. Note that the different ratings are based on values of $CP$ established at different stress levels, and sometimes using slightly different definitions for $CP$.

**Table 5-3 Alternative criteria for defining severity of collapse.**

| Reference | Collapse Potential, $CP$ | Severity of Collapse |
|---|---|---|
| Mock and Pawlak (1983) (Collapse Stress = 0.5 tsf) | 0% to 1% | No Problem |
| | 1% to 3% | Low |
| | 3% to 5% | Moderate |
| | > 5% | High |
| Jennings and Knight (1975) (adopted by NAVFAC DM-7) (Collapse Stress = 2 tsf) | 0% to 1% | No Problem |
| | 1% to 5% | Moderate Trouble |
| | 5% to 10% | Trouble |
| | 10% to 20% | Severe Trouble |
| | > 20% | Very Severe Trouble |
| Lutenegger and Saber (1988)[1] (Collapse Stress = 3 tsf) | 2.0% | Slight |
| | 6.0% | Moderate |
| | 10.0% | Severe |
| ASTM D5333-03 (Collapse Stress = 2 tsf) | 0 | None |
| | 0.1% to 2.0% | Slight |
| | 2.1% to 6.0% | Moderate |
| | 6.1% to 10.0% | Moderately Severe |
| | > 10% | Severe |

[1] $CP = \Delta e/(1 + e_1)$ where $\Delta e$ is change in void ratio from wetting and $e_1$ is void ratio at beginning of wetting

Field tests can also be used to quantify the magnitude of expected collapse deformation under specific project conditions (e.g., stresses, water changes, etc.). A "response-to-wetting" test is set up using a loading platform such as a plate or small concrete footing placed directly on the soil. The test may be performed at the ground surface or in a shallow excavation as needed. After applying load, the soil is wetted by adding water at the surface or in surrounding boreholes and the vertical settlement of the loaded area is measured. The obvious advantage of conducting field tests is that the measurements are more representative of actual loading conditions in the field.

### 5.2.4 Challenges for Subsurface Exploration in Collapsible Soils

Typical drilling and disturbed sampling procedures can be used to obtain samples of collapsible soil for laboratory index tests like sieve analysis, hydrometer, soil classification, and Atterberg limits testing. However, samples for direct measurement of collapse potential should be acquired using procedures that minimize disturbance because collapse potential is sensitive to changes in void ratio as well as disturbance of inter-particle bonding. For samples collected from shallow depths, block samples from trenches or test pits can provide high quality samples for testing. At greater depths, borehole sampling is necessary. Samples with limited disturbance can often be obtained using conventional thin-walled samplers as long as the soil is not so stiff as to prevent penetration of the sampler by pushing. In stiffer soils, Pitcher or Denison samplers may be used to acquire samples with limited disturbance. Since collapsible soils are moisture sensitive, it is preferable to advance borings using dry drilling methods if

possible. Fortunately, collapsible soils are generally located at limited depths and above the water table where hollow-stem drilling and thin-walled tube sampling can be effectively used.

Another challenge lies in characterization of in situ water contents (or the related degree of saturation) and anticipated changes in water content that are likely to be experienced prior to potential wetting. Such characterization generally requires careful monitoring of the depth to groundwater and careful measurement of water contents, preferably over some period of time.

In situ tests should generally be avoided in collapsible soils because the measurements reflect current conditions rather than conditions that will be present at the time of wetting. Additionally, the behavior of collapsible soils is rather unusual, and in some ways contrary to fundamental soil mechanics principles. As a result, common empirical methods to transform in situ test measurements to common engineering design parameters may not be appropriate for collapsible soils.

## 5.3 EXPANSIVE/SHRINKING SOILS

Expansive soils are clayey soils that undergo large volume changes in response to changes in water content. Unlike collapsible soils, expansive soils tend to increase in volume, or swell, as the water content increases and decrease in volume, or shrink, as the water content decreases. The magnitude of volume changes is primarily controlled by the proportion of expansive clay minerals in the soil and the magnitude of water content changes. Clayey soils that predominantly contain kaolinite tend to produce less volume change than soils containing large proportions of montmorillonite (smectite). For a given soil, the magnitude of volume change increases as the initial water content decreases and as the initial dry density increases. Soil structure and environmental conditions also have a secondary influence on the magnitude of swelling, and there is considerable evidence that disturbed or remolded soils will swell more than undisturbed soils at the same initial water content and dry density (Schmertmann, 1969; Lutenegger, 2008). Compacted soils containing expansive clay minerals will also swell when wetted.

While expansive soils can be found at great depth, most problematic volume changes are restricted to shallower depths affected by seasonal water content changes. The depths over which volume changes are most likely to occur is referred to as the “active zone”, which can be evaluated from measured water contents for samples taken during wet and dry seasons. The depth at which water contents practically cease to change seasonally is often referred to as the “depth of seasonal moisture change” and generally defines the lower limit of the active zone. The active zone is an important consideration for foundation design because it is desirable to extend foundations beneath this zone when expansive soils are encountered. Additionally, it is important to recognize that side resistance for deep foundations may be

compromised in the active zone. Expansive soils are also often detrimental to the performance of pavements and lightly loaded structures on shallow foundations.

### 5.3.1 Occurrence of Expansive Soils

As shown in Figure 5-4, expansive soils are found throughout the continental U.S.; however, damage caused by expansive clays is most prevalent in California, Wyoming, Colorado, and Texas where there are extensive deposits of expansive clay combined with a semi-arid climate. Most expansive soils are highly plastic, stiff, and overconsolidated with low natural water content and high natural dry unit weight. In situ water contents are often close to or below the plastic limit, which produces liquidity index values that are close to zero and may be negative in some cases. Many natural expansive soils are also fissured because of repeated wetting and drying.

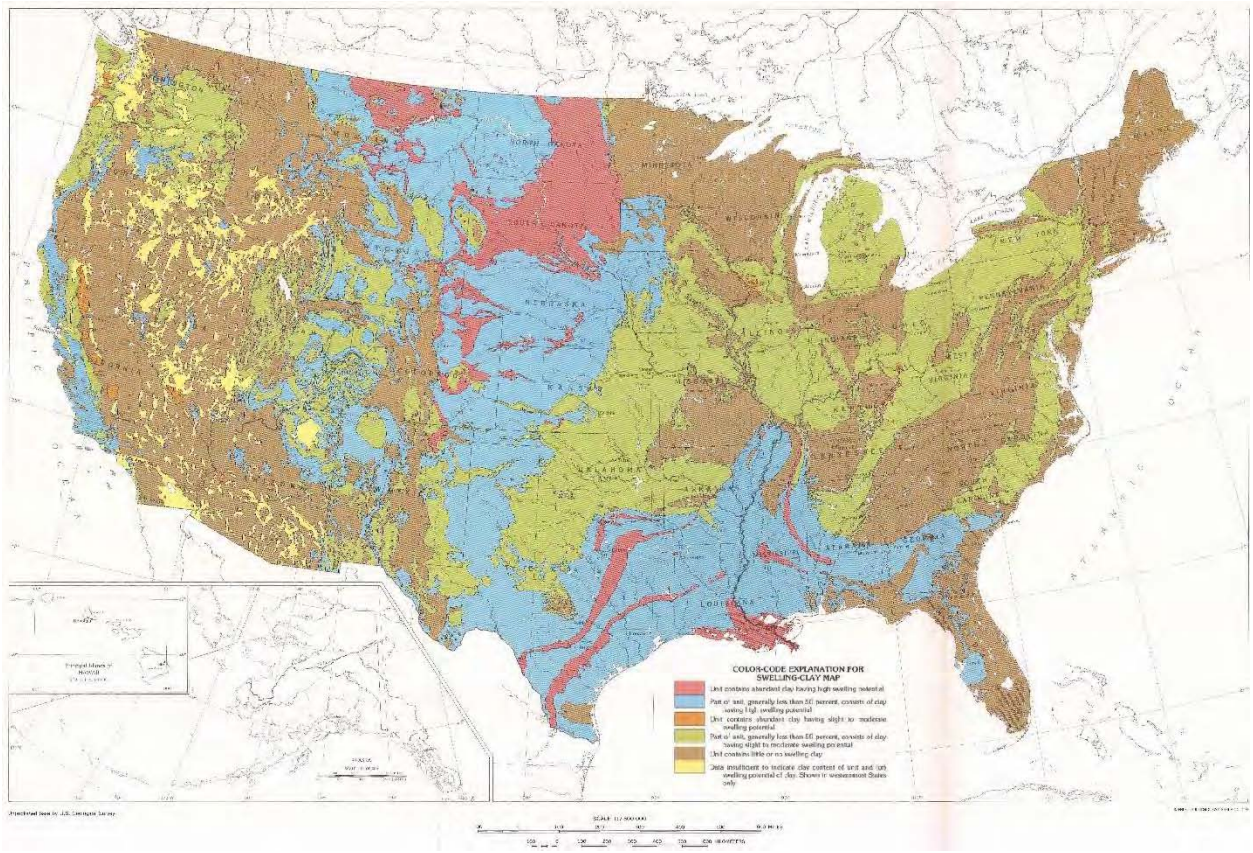


**Figure 5-4 Distribution of expansive soils in the U.S. (from Olive, et al., 1989).**

### 5.3.2 Identification and Characterization of Expansive Soils Using Indirect Methods

Initial indications of the presence of expansive soils can and should be acquired during desk studies and site visits. Indications of the potential for encountering expansive soils can often be derived from local or

regional soil surveys and geologic maps as described in Chapter 2. Observations during site visits can also meaningfully inform identification of expansive soils. The presence of large surface desiccation cracks and/or fissures, or characteristic damage to nearby structures as shown in Figure 5-5, should be noted and carefully assessed during site visits because they provide strong indication of expansive soils.

**Figure 5-5 Common cracking pattern in lightly loaded structures on expansive soils.**

Expansive soils are often identified from results of index property measurements, most of which can be performed on highly disturbed or bulk soil samples. Since the severity of swelling is closely related to the proportion of expansive clay minerals within a soil, available criteria for identifying expansive clays generally rely on index properties that are related to soil mineralogy and clay-size fraction. For example, soils having a liquid limit greater than 50, activity greater than 0.8, or plasticity index greater than 15 are likely to have significant swell potential. Similarly, soils with specific surface area greater than about 200 $m^2/g$, cation exchange capacity greater than about 25 meq/100 g, or prevalent proportions of smectite clay minerals are likely to have significant swell potential. Such indications of expansive clays should only be considered as "screening" tools to help identify possible problems and the need for more careful evaluation using direct measurements described in Section 5.3.3.

Several classification methods have also been proposed to characterize the severity of swell potential. No standard classification currently exists and it is common for different classifications to be used in different geographic regions. Most of the methods rely on commonly measured index properties. For example, Dakshanamurthy and Raman (1973) suggest a method for characterizing swell potential for expansive

soils based on the liquid limit, as summarized in Table 5-4. Figure 5-6 shows a classification by Seed et al. (1962) based on soil activity and clay size fraction. Van der Merwe (1964) similarly developed a classification based on clay-size fraction and plasticity index that is provided in Figure 5-7.

**Table 5-4 Characterization of swell severity from Dakshanamurthy and Raman (1973).**

| *LL* (%) | Swell Severity |
|---|---|
| 0 to 20 | Non-Swelling |
| 20 to 35 | Low Swelling |
| 35 to 50 | Medium Swelling |
| 50 to 70 | High Swelling |
| 70 to 90 | Very High Swelling |
| > 90 | Extra High Swelling |

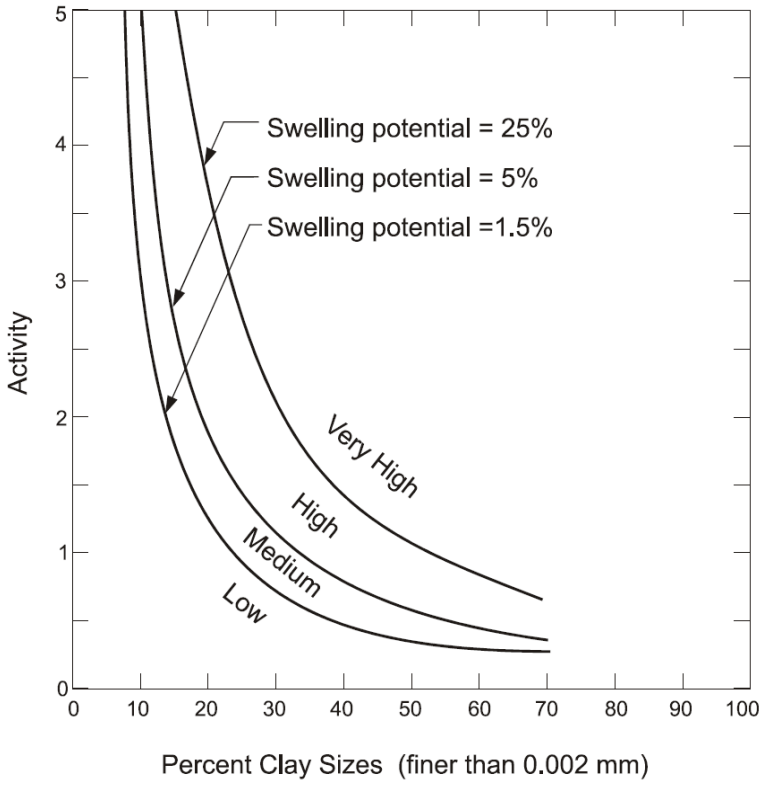


**Figure 5-6 Characterization of swell potential from clay-size fraction and activity (after Seed, et al., 1962).**

Several addition classifications have been proposed that rely on index properties that are less routinely measured such as the shrinkage limit, shrinkage index, or linear shrinkage. Holtz and Gibbs (1956) proposed a method for characterizing swell severity based on the plasticity index, shrinkage limit, and fine clay-size fraction (< 0.001 mm) as shown in Figure 5-8. Raman (1967) characterized the degree of swell potential based on the plasticity index and shrinkage index ($SI = LL - SL$) as shown in Table 5-5.

Table 5-6 shows a characterization proposed by Altmeyer (1955) based on the shrinkage limit and linear shrinkage, which is described in Section 5.3.6.

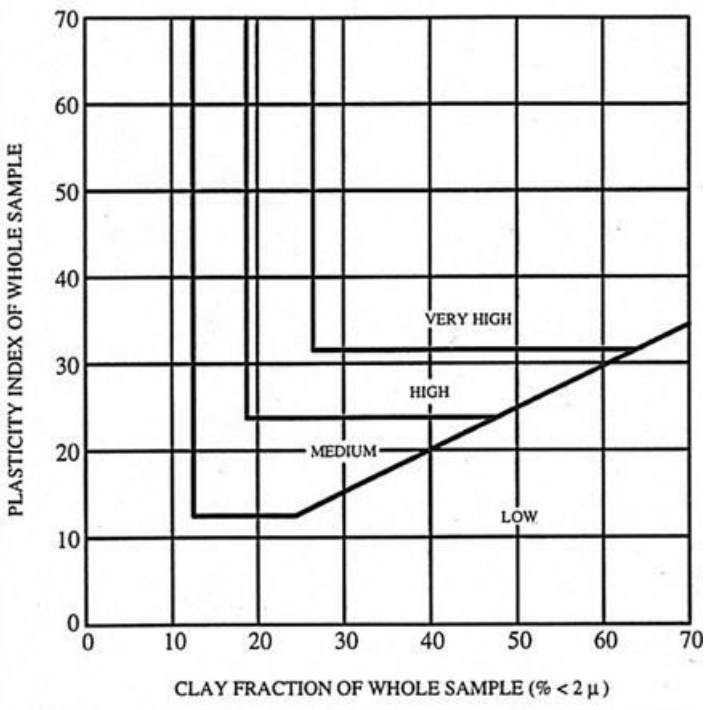


**Figure 5-7 Characterization of swell potential from clay-size fraction and plasticity index (after Van der Mere, 1964).**

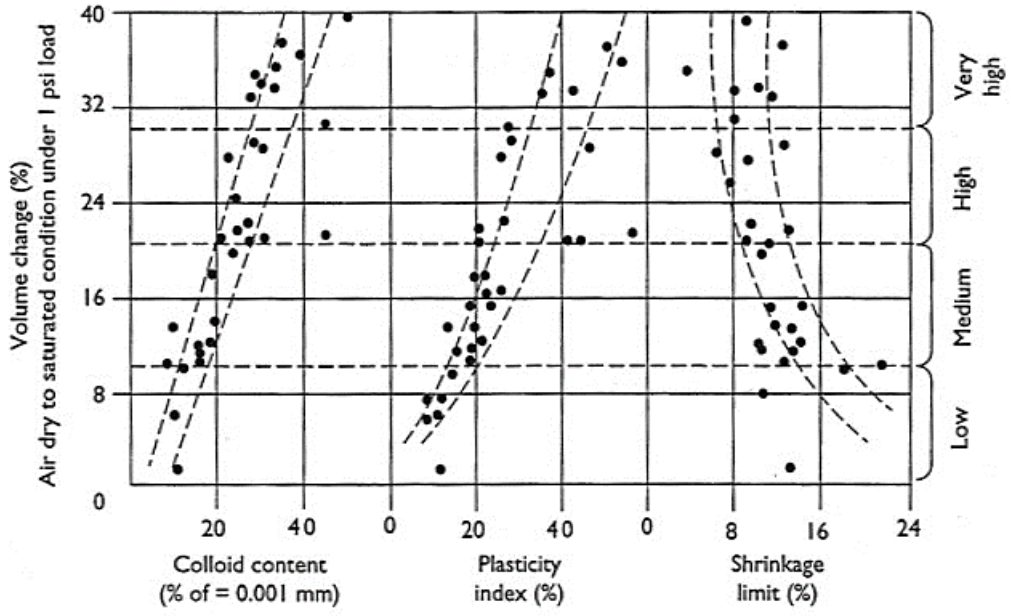


**Figure 5-8 Characterization of swelling severity from Holtz and Gibbs (1956).**

**Table 5-5 Characterization of swell severity from Raman (1967).**

| Plasticity Index (%) | Shrinkage Index (%) | Swell Severity |
|---|---|---|
| < 12 | < 15 | Low |
| 12 to 23 | 15 to 30 | Medium |
| 23 to 32 | 30 to 40 | High |
| > 32 | > 40 | Very High |

**Table 5-6 Characterization of swell severity from Altmeyer (1955).**

| Shrinkage Limit (%) | Linear Shrinkage (%) | Swell Severity |
|---|---|---|
| > 12 | < 5 | Non-Critical |
| 10 to 12 | 5 to 8 | Marginal |
| < 10 | > 8 | Critical |

Holtz and Gibbs (1956) also suggested that swell potential can be simply evaluated from results of "free swell tests". The free swell test is an inexpensive and simple test that can be used to quickly evaluate the swelling potential of a soil. In this test, 10 grams of oven dry soil passing the No. 40 sieve is prepared and the initial (dry) volume of the sample is determined using a 25 ml graduated cylinder. The soil is then slowly added to a 100 ml graduated cylinder filled with distilled water. The volume of soil after 24 hours is then measured in the graduated cylinder and used to calculate the "free swell index", $FSI$, as

$$FSI = \frac{V_f - V_o}{V_o} \times 100\% \tag{5.3}$$

where $V_o$ is the initial (dry) volume of soil and $V_f$ is the final swelled volume of the soil. Figure 5-9 shows the final swelled volume for two different clays: an expansive montmorillonitic clay and a non-expansive kaolinitic clay. The swelled volume of the montmorillonite clay is about three times that of the kaolinite. Table 5-7 provides suggested guidelines for swelling severity as a function of $FSI$.

**Table 5-7 Severity of swelling based on the free swell index, *FSI* (Holtz and Gibbs, 1956).**

| *FSI* (%) | Swelling Severity |
|---|---|
| < 50 | Low |
| 50 to 100 | Medium |
| 100 to 140 | High |
| > 140 | Very High |

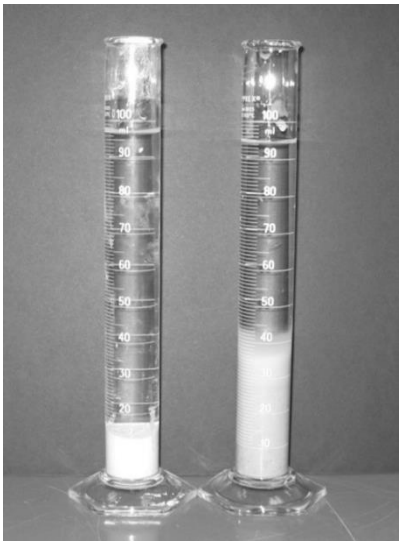

**Figure 5-9 Final volume from free swell test for kaolinite (left) and montmorillonite (right).**

### 5.3.3 Characterization of Swell Potential Using Direct Methods

When indirect measurements suggest that expansive soils are present and when large volume changes have the potential to impact construction or performance, the swelling behavior of potentially expansive soils should be more carefully evaluated using direct measurements. The best and most direct method for measuring swelling behavior is to perform one-dimensional swell tests (AASHTO T258; ASTM D4546) on representative undisturbed or compacted samples. In this test, a specimen at the natural water content is carefully trimmed and placed in a conventional oedometer. The specimen is loaded with a nominal "seating" load or, alternatively, loaded to a stress level representing anticipated stress levels in the field (often the existing overburden stress or the overburden stress plus anticipated foundation stress). Water is then added to the cell and the amount of swell is recorded over time.

Swell test measurements are commonly presented in terms of the swell strain or swell potential, $SP$, computed as

$$SP = \frac{\Delta H}{H_o} \times 100\% \tag{5.4}$$

where $\Delta H$ is the change in specimen height and $H_o$ is the original specimen height. Swelling behavior is generally time dependent as water is adsorbed by the clay minerals. Measurements from a one-dimensional swell test for a high plasticity, expansive clay from Mt. Union, Iowa are plotted versus time in Figure 5-10. Note that swelling occurs rapidly at first but actually takes several days to complete. For some soils, several weeks may be required to reach equilibrium. Table 5-8 provides terminology from

Peck et al. (1974) to describe the severity of volume changes associated with different swell potential. The swell potential for the measurements shown in Figure 5-10 is on the order of 8.6 percent, which would be considered "high" based on the criteria shown.

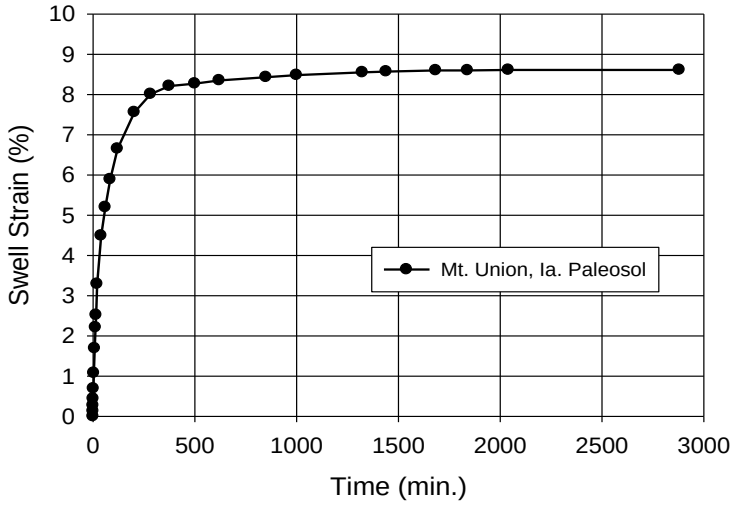


**Figure 5-10 Example measurements from one-dimensional swell test on highly plastic clay.**

**Table 5-8 Descriptions for different levels of swell potential (from Peck, et al., 1974).**

| Swell Potential (%) | Description of Volume Change |
|---|---|
| $SP < 1.5\%$ | Low |
| $1.5\% < SP < 5\%$ | Medium |
| $5\% < SP < 25\%$ | High |
| $SP > 25\%$ | Very high |

Swell potential is influenced by the vertical stress applied to the specimen. The maximum swell potential is experienced when the applied vertical stress is zero. The magnitude of the swell potential decreases with increasing vertical stress up to some value of vertical stress that prevents swelling, termed the "swell pressure". Figure 5-11 shows measurements of swell strain taken for increasing applied vertical stress following completion of the test shown in Figure 5-10. The vertical stress required to bring the specimen height back to its original value is 7 ksf. While this vertical stress is not technically the swell pressure, since the soil was allowed to strain during the initial test, it is a reasonable estimate. Swell pressures of 7 ksf are certainly large enough to lift lightly or moderately loaded structures. Swell pressures for some soils can exceed 40 ksf or more (Peck et al., 1974).

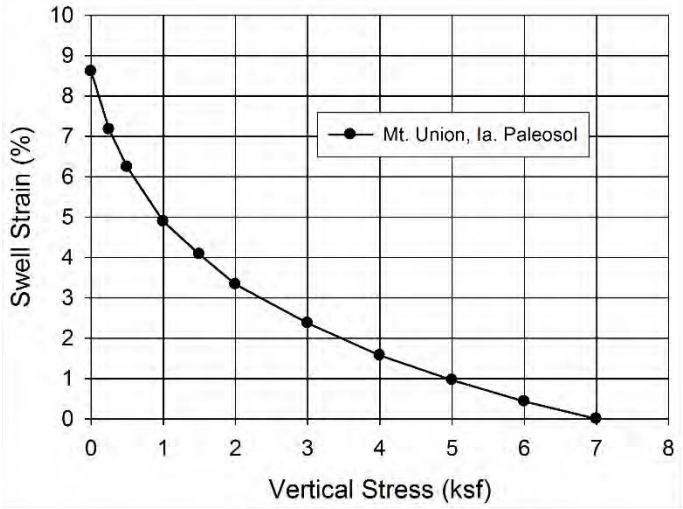


**Figure 5-11 Reloading test on specimen from Figure 5-10 to determine swell pressure.**

Use of one-dimensional swell tests for evaluating the in situ swell potential of natural and compacted clay soils has some limitations including:

1. Lateral swell and lateral confining pressure are not simulated in the laboratory. The calculated magnitude of swell in the vertical direction may not be a reliable estimate of soil expansion for structures that are not confined laterally (e.g., bridge abutments).
2. The rate of swell calculated in the laboratory will not likely be indicative of rates of swell experienced in the field since laboratory tests cannot simulate the availability of water in the field.

Long-term swell (or "secondary swell") may also be significant for some soils and should be added to primary swell, especially if the design is anticipated to have long-term access to water.

### 5.3.4 Swell "Sensitivity"

If a natural soil is disturbed, for example by remolding or compaction, the shrink and swell behavior can be altered, typically becoming more problematic. This is largely the result of destroying natural bonds in the soil that may inhibit swelling. The term "swell sensitivity" was suggested by Schmertmann (1969) to describe the increase in swelling observed for a remolded soil compared to swelling of the undisturbed soil at the same initial water content and density. Swell sensitivity is calculated from results of one-dimensional swell tests conducted under zero applied stress (often referred to as "free swell tests", but different from the test described in Section 5.3.2) as

$$SS_{FS} = \frac{SP_{remolded}}{SP_{undisturbed}} \tag{5.5}$$

where $SP_{undisturbed}$ is the swell potential for an undisturbed specimen and $SP_{remolded}$ is the swell potential for a remolded specimen at the same initial water content and dry density. $SS_{FS}$ is a numerical comparison of the swelling magnitude for the two samples. Schmertmann (1969) and Lutenegger (2008) show that many clays exhibit swell sensitivity on the order of 2 to 4, meaning that a remolded soil will swell about 2 to 4 times as much as the same soil in the undisturbed state. Figure 5-12 shows a comparison of free swell tests performed on undisturbed and remolded specimens of the same soil at similar initial water content and dry unit weight. For this test, $SS_{FS}$ is approximately equal to 3.3.

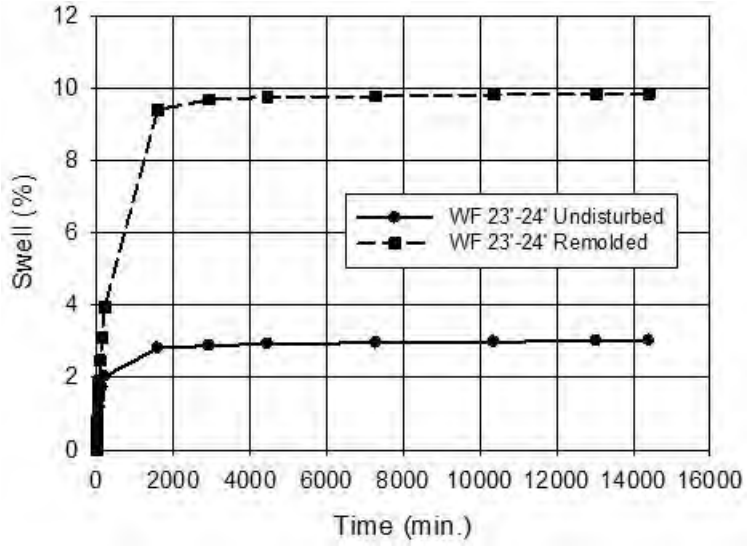


**Figure 5-12 Comparison of swell behavior between undisturbed and remolded soil.**

### 5.3.5 Characterization of Shrinkage

Damage caused by soil shrinkage can be just as severe as that caused by swelling. Most fine-grained soils that swell with the addition of water will also shrink when there is a reduction in water content. Figure 5-13 shows the idealized change in soil volume as the water content of a saturated soil is reduced from the liquid limit to a water content of zero. The slope of the curve is a straight line at water contents above the plastic limit. However, as the water content decreases and approaches the shrinkage limit, the soil becomes unsaturated and the shape of the drying curve deviates from the straight line and eventually becomes flat. The shrinkage limit has traditionally been defined as the point of intersection between the two straight line parts of the curve, as shown by Point E in Figure 5-13. However, many soils continue the shrink slightly at water contents below this interpretation of shrinkage limit as high soil suction develops in the now unsaturated soil. The true shrinkage limit is actually the point of tangency between the curved and straight line portions of the curve, denoted as Point C in Figure 5-13.

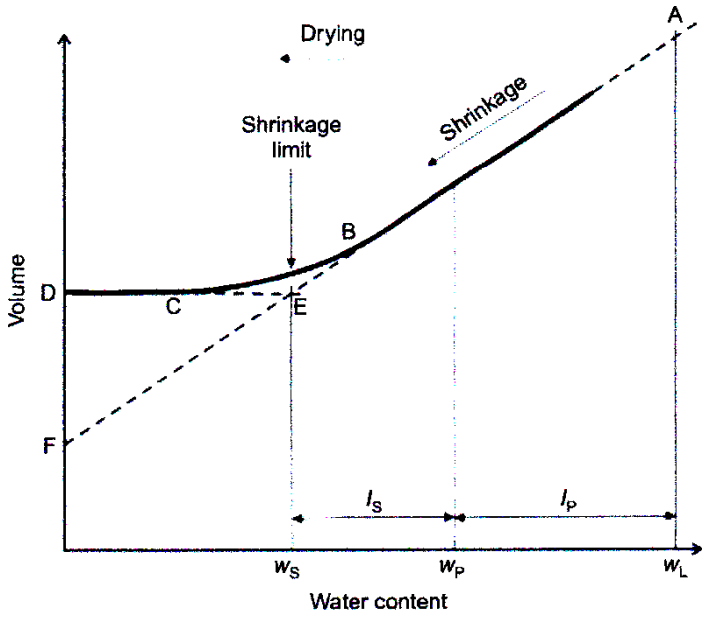


**Figure 5-13 Idealized shrinkage curve for an initially saturated soil.**

The shrinkage limit determined from the traditional shrinkage limit test (the withdrawn ASTM D427, or ASTM D4943) is a single-point measurement in which the shrinkage limit is calculated according to Equation 4.11. However, this value may not represent the true shrinkage limit (Cerato and Lutenegger, 2006). Figure 5-14 shows two shrinkage curves: one measured using the round metal dish commonly used for shrinkage limit tests and one measured using the linear shrinkage test described in Section 5.3.6. For this soil, the measured/calculated shrinkage limit from ASTM D427 was determined to be 11.2 percent, while the true shrinkage limit determined from both shrinkage curves is approximately 18 percent. Thus, in cases where accurate determination of the shrinkage limit is required, the shrinkage limit should be determined by measuring the entire shrinkage curve rather than ASTM 4943.

### 5.3.6 Linear Shrinkage Test

The magnitude of shrinkage can also be quantified using the linear shrinkage test (e.g., Heidema, 1957). In this test, a sample of soil is first mixed to an initial water content slightly above the liquid limit. The mixture is then placed in a lubricated brass fixture that has the shape of a semicircular trough and allowed to slowly dry, first in air and then in an oven. The linear shrinkage, $LS$, is calculated from the measured initial and final lengths of the specimen as

$$LS = \frac{L_o - L_f}{L_o} \times 100\% = \left(1 - \frac{L_f}{L_o}\right) \times 100\% \tag{5.6}$$

where $L_o$ is the initial specimen length and $L_f$ is the final (oven dry) specimen length.

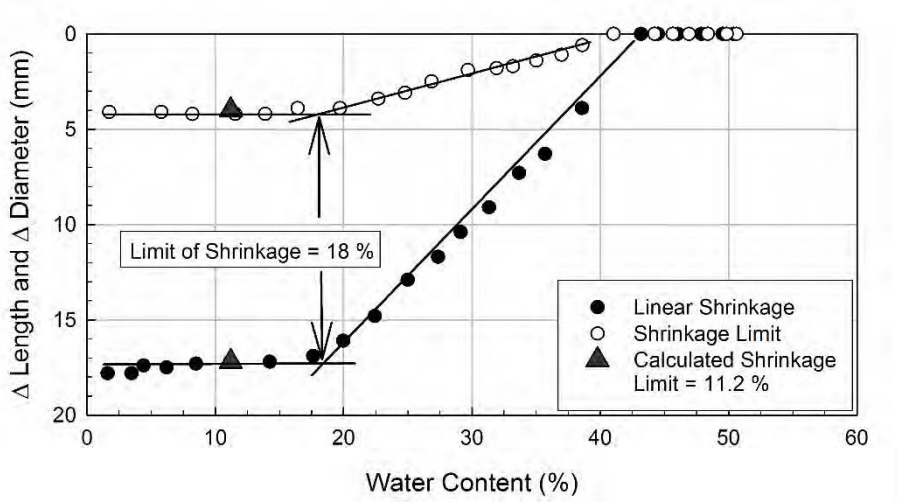


**Figure 5-14 Measured shrinkage curves using shrinkage limit dish and linear shrinkage mold (from Cerato and Lutenegger, 2006).**

### 5.3.7 Shrink Test

Both the shrinkage limit and linear shrinkage tests are conducted on remolded soil-water mixtures, usually prepared to an initial water content close to or slightly above the liquid limit. While both tests are useful index tests to quantify soil shrinkage, neither can be directly used to predict actual shrinkage that a natural soil with inherent structure and natural water content will undergo. An alternative test, referred to as the "shrink test" (Briaud et al., 2003) can be used to directly estimate shrinkage of natural soils. The shrink test is performed by carefully trimming an undisturbed specimen into a cylindrical disk with a diameter of 3 in. and a height of 0.75 to 1.0 in. The specimen is allowed to dry slowly for several days while the dimensions and mass are periodically measured (about every 3 to 4 hours). When the mass stops changing significantly, the specimen is placed in the oven and dried for 24 hours after which the final, oven dry dimensions and mass are obtained. Measurements from a shrink tests are used to create a drying curve of volume change versus water content, similar to the shrinkage curve from the linear shrinkage test (e.g., Figure 5-14).

## 5.4 ORGANIC SOILS

Organic soils and peats present similar engineering challenges to soft silts and clays, including low undrained shear strength and high compressibility. In addition, organic silts and clays undergo significant secondary compression (or creep deformations) long after primary consolidation is complete. Almost all organic soils are a "red flag" to geotechnical engineers who associate organic soils with poor load bearing capacity, long-term chronic settlement, and high corrosion potential. Several cases have been described in which organic soils underlying structures have led to failures (e.g., Gould, et al., 2002). Deposits of

peat are especially problematic and are usually avoided or removed prior to construction and replaced with suitable engineered fill. In general, organic soils are not considered suitable bearing material for most structures, even lightly loaded ones, so identification and characterization of organic soils is important for geotechnical design and construction. In this section, identification and classification of organic soils and peats are discussed along with information on evaluating shear strength and compression properties for these materials.

### 5.4.1 Occurrence of Organic Soils

Most highly organic soils occur in low topographic positions or depressions that hold water. The water table is usually very high, which accounts for the presence of the organic materials. In oxidizing environments above the water table, organic materials have generally decayed and are no longer present. Peats and organic fine-grained soils are sometimes associated with specific regions or geologic settings, such as previously glaciated regions of the upper Midwest and Canada, and alluvial, lacustrine, and some marine deposits around the world. A special type of organic soil, Muskeg, is a peat material often found in arctic or northern climates that can reach depths of 100 feet depending on the underlying topography.

### 5.4.2 Identification of Organic Soils

Highly organic soils, such as peats, are often visually identified from their dark brown to black color, organic odor, and the presence of decaying plant matter. Organic soils often have low unit weight, high water content, and may have a fibrous texture. When exposed to air, organic soils oxidize quickly, often turning from black to brown in just a few minutes. Cone penetration tests (CPT) can sometimes be used to identify subsurface layers of highly organic materials based on low cone tip resistance and relatively high friction ratios. Classification charts for piezocone (CPTU) and dilatometer (DMT) measurements have also been developed to aid in identifying organic materials and peat. However, indications of organic materials from in situ tests should be confirmed using collected samples and laboratory measurements since clayey soils and organic soils may produce similar in situ test response.

In the laboratory, the proportion of organic material can be determined following procedures in AASHTO T267 or ASTM D2974. Landva et al. (1983) developed a system for classifying organic soils and peats based on the "ash content" ($A_c$) determined from ASTM D2974, in situ water content, specific gravity, and fiber content as summarized in Table 5-9. In this system, organic soils are classified as peats (Pt), peaty organic soils (PtO), organic soils (O), or silts and clays with organic content (MO and CO, respectively). Measurements of liquid limit from oven-dried and non-oven-dried soils can also be used as a qualitative indication of organic content as described in Section 4.16.1.

**Table 5-9 Organic soil and peat classification from Landva, et al. (1983).**

| Classification | Ash Content ($A_c$) | Moisture Content ($\omega_n$) | Specific Gravity ($G_s$) | Fiber Content |
|---|---|---|---|---|
| Pt | < 20% | > 500% | < 1.7 | > 50% |
| PtO | 20 to 40% | 150 to 800% | 1.6 to 1.9 | < 50% |
| O | 40 to 95% | 100 to 500% | > 1.7 | Insignificant |
| MO, CO | 95 to 99% | < 100% | > 2.4 | None |

### 5.4.3 Challenges for Subsurface Exploration of Organic Soils and Peat

Organic soils and non-fibrous (amorphous) peats are often weak and compressible due to high water content and large void ratio. As a result, it can be difficult to obtain undisturbed samples of organic soils for measuring engineering properties like strength, compressibility, and hydraulic conductivity in the laboratory. Thin walled, fixed piston samplers are generally most suitable for undisturbed sampling of organic soils. Undisturbed sampling in fibrous peats, however, is extremely difficult due to the likely compression of the peat fibers during sampler advancement. Where undisturbed sampling with piston samplers is attempted, it is critical that the sampler have a sharp edge. When possible, fibrous peats should be sampled using block-sampling techniques. Disturbed sampling techniques such as auger cuttings can be used to acquire samples for visual assessment and identification of organic soils.

Engineering properties of peats and organic soils often vary significantly, both spatially and with depth. Samples obtained within a few feet of each other may exhibit vastly different behaviors during loading. As such, subsurface investigations that encounter organic soils and peats should generally involve more extensive sampling and testing compared to sites composed of inorganic soils.

### 5.4.4 Shear Strength of Organic Soils and Peats

Like all soils, the shear strength of organic soils is directly related to the effective stress in the ground and the stress history of the deposit. Undrained shear strengths for organic soils are commonly low since organic soils generally have low unit weight, are saturated, and have no significant stress history. Where good quality undisturbed samples can be obtained, laboratory triaxial strength tests should be performed to measure undrained shear strength for design. CPT and CPTU measurements can often be effectively used to supplement direct measurements of undrained shear strength. However, common CPT and CPTU transformations are unlikely to produce reliable estimates for undrained shear strength and should be avoided except for preliminary estimation. When using CPT or CPTU measurements to establish strength parameters for design, site specific transformations should be developed from site specific CPT or CPTU measurements and laboratory measurements of shear strength.

Field vane shear tests (VST) can also be effectively used to evaluate undrained shear strengths in non-fibrous organic soils. In using the field vane shear test in organic soils, it should be noted that the time to failure in the test will have an impact on the measured vane shear strength. Some organic soils may also possess enough fibrous matter to act as localized reinforcement and lead to vane shear strengths that are greater than is truly appropriate. The vane shear test is, therefore, inappropriate for use in fibrous organic soils and peats.

Drained shear strength parameters are often more easily measured because they are less sensitive to sample disturbance. Most fibrous peats tend to be almost entirely frictional (i.e., have low cohesion intercepts) with larger friction angles than might be surmised because peat fibers tend to act as tensile reinforcement. However, the shearing resistance may also be anisotropic because peat fibers are often oriented horizontally. Peat samples may sometimes require greater than 20 percent axial strain to mobilize the peak shear strength of the material, something that must be considered when establishing appropriate values for design parameters.

### 5.4.5 Compressibility of Organic Soils and Peats

Organic soils and peats are notorious for being highly compressible. Considerable effort and attention is therefore warranted when characterizing the compressibility of organic soils and peats if shallow foundations or embankments will be constructed over organic soil or peat layers. Figure 5-15 shows results from a one-dimensional consolidation test conducted on a specimen of peat with an initial water content of 341 percent and an initial dry unit weight of 12.4 lbs/ft$^3$. The high compressibility of the peat is clearly indicated by the large vertical strains. Because many organic soils and peats have relatively high hydraulic conductivity, primary (consolidation) settlements generally occur over a relatively short time (often within a few days or months). The majority of post-construction settlements therefore often result from long-term, secondary compression, which requires that coefficients of secondary compression be established in addition to compression and recompression indices.

Because of high in situ void ratios, organic soils and peats have high compressibility, with $C_c$ values often exceeding 1.0. The compressibility of organic soils is often related to the initial water content, as shown in Figure 5-16, which in turn is related to the organic content. While figures like Figure 5-16 can be used to estimate values for $C_c$ based on in situ water content, it is important to recognize that the figure is plotted using logarithmic scales and that there is considerable scatter in estimates derived from water content alone (potentially varying by a factor of 5). In general, compression indices should therefore be determined from actual measurements when settlement estimates are important for design of highway

structures and embankments. Methods for interpretation of compression indices from one-dimensional consolidation tests are described in Chapter 6.

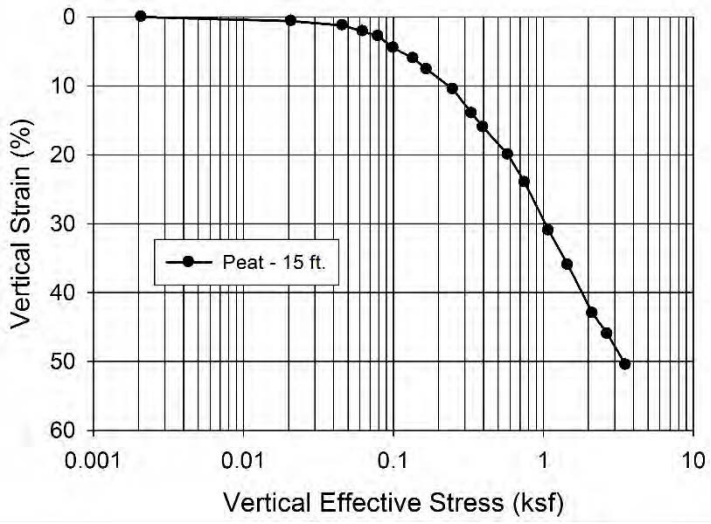


**Figure 5-15 One-dimensional consolidation test measurements for peat from Pittsfield, MA.**

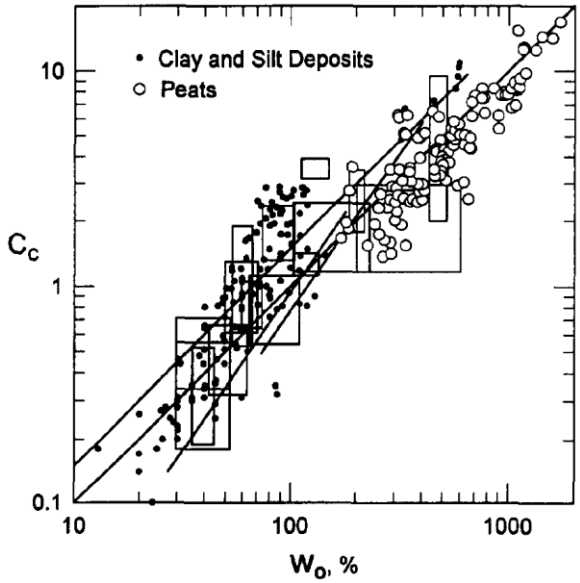


**Figure 5-16 Values of natural water content and compression index for peats, clays, and silts (from Mesri, et al., 1997).**

Values for the coefficient of secondary compression, $C_\alpha$, should similarly be determined from one-dimensional consolidation tests on undisturbed specimens acquired for the specific site and material being evaluated, as described in Chapter 6. In peaty soils, it is sometimes difficult to identify the end of primary consolidation because the transition from primary to secondary compression is not easily identified using standard interpretation methods. Additionally, the anticipated magnitude of imposed stresses should be

assessed so that appropriate values for secondary compression can be established for design. Like many soils, values of $C_\alpha$ for organic soils and peats will often increase at stress levels that just exceed the preconsolidation stress, $\sigma_p'$, and decrease at stress levels that are significantly greater than $\sigma_p'$. Consolidation tests should therefore be performed for loads that are sufficient to capture this response, and values for $C_\alpha$ should be established for stresses that are consistent with anticipated field loading.

Estimates for $C_\alpha$ can also be derived from values of the compression index, $C_c$ and the ratio $C_\alpha/C_c$ (Mesri and Godlewski, 1977; Mesri and Castro, 1987). Values for $C_\alpha/C_c$ are often in the range of 0.05±0.01 for organic clays and silts and 0.075±0.01 for peats. Table 5-10 provides values of $C_\alpha/C_c$ for several different organic soils and peats.

**Table 5-10 Values of ratio $C_\alpha/C_c$ for several organic soils (from Mesri and Godlewski, 1977).**

| Soil Type | Soil Description | $c_\alpha/c_c$ |
|---|---|---|
| Organic clays and silts | Norfolk organic silt | 0.05 |
| | Calcareous organic silt | 0.035 to 0.06 |
| | Postglacial organic clay | 0.05 to 0.07 |
| | Organic clays and silts | 0.04 to 0.06 |
| | New Haven organic clay silt | 0.04 to 0.075 |
| Peats | Amorphous and fibrous peat | 0.035 to 0.083 |
| | Canadian muskeg | 0.09 to 0.10 |
| | Peat | 0.075 to 0.085 |
| | Peat | 0.05 to 0.08 |
| | Fibrous peat | 0.06 to 0.085 |

## 5.5 DISPERSIVE SOILS

Dispersive soils often appear like normal clays, but are highly susceptible to erosion and piping. Dispersion occurs in soils when the repulsive forces between clay particles exceed the attractive forces (Bell and Maud, 1994). This brings about deflocculation so that particles repel each other when exposed to relatively pure water. This is actually the basis for adding a "dispersing agent" to soil suspensions when conducting hydrometer tests. The "dispersing agent" changes the chemistry of the fluid and produces deflocculation so that soil particles act individually. Dispersive soils can represent significant hazards to transportation infrastructure, mostly related to consequences associated with surface or subsurface erosion (i.e., piping).

### 5.5.1 Identification of Dispersive Soils Using Indirect Measurements

Dispersive soils cannot be differentiated from normal soils using conventional laboratory index tests. However, indications of dispersive soils can be derived from results of chemical tests. The presence and

quantity of exchangeable sodium ions in soils is the main chemical attribute contributing to dispersive behavior. The amount of exchangeable sodium can be quantified by the exchangeable sodium percentage, $ESP$, computed as

$$ESP = \frac{ES}{CEC} \times 100\% \tag{5.7}$$

where $ES$ is the quantity of exchangeable sodium and $CEC$ is the cation exchange capacity, both measured in units of meq/100 g. $ESP$ is an index representing the proportion of exchangeable sodium relative to all exchangeable cations. $ESP$ alone is not a perfect predictor for dispersive soils, but values of $ESP$ greater than approximately 10 suggest that a soil is potentially dispersive. Sherard et al. (1976b) proposed that the total dissolved salts ($TDS$) in a soil could be used with $ESP$ to identify dispersive soils, as shown in Figure 5-17. Soils plotting within Zone A of the figure are considered to be dispersive while soils plotting within Zone B are considered to be non-dispersive. Soils plotting in Zone C are considered to be potentially dispersive. Gerber and Von Maltitz Harmse (1987) propose an alternative chart based on similar measures.

### 5.5.2 Identification of Dispersive Soils Using Direct Measurements

Dispersive soils can also be identified using the "double hydrometer test" and the "pinhole dispersion test". The double hydrometer test was developed in the 1940s by the U.S. Soil Conservation Service (Sherard, et al., 1976b). In the test, a standard hydrometer test is performed using a dispersing agent with agitation. A second hydrometer test is then performed on an identical soil sample but without using a dispersing agent and with no agitation. The percentage of soil finer than 0.005 mm is determined from both tests and the "percent dispersion" is calculated as

$$\%\, Dispersion = \frac{A}{B} \times 100\% \tag{5.8}$$

where $A$ is the particle-size fraction smaller than 0.005 mm from the hydrometer test performed without a dispersing agent, and $B$ is the particle-size fraction smaller than 0.005 mm from the hydrometer test performed with a dispersing agent. If the soil "dispersed" in plain water produces similar results as the test performed with the dispersing agent and agitation, the soil itself is considered highly dispersive. Decker and Dunnigan (1977) found that about 85 percent of soils producing dispersion of greater than 30 percent according to Equation 5.8, and 95 percent of soils producing dispersion greater than 60 percent, are subject to dispersive erosion. The double-hydrometer test has been standardized by ASTM as test method D4221 and is attractive because it is simple to perform and requires no special test equipment.

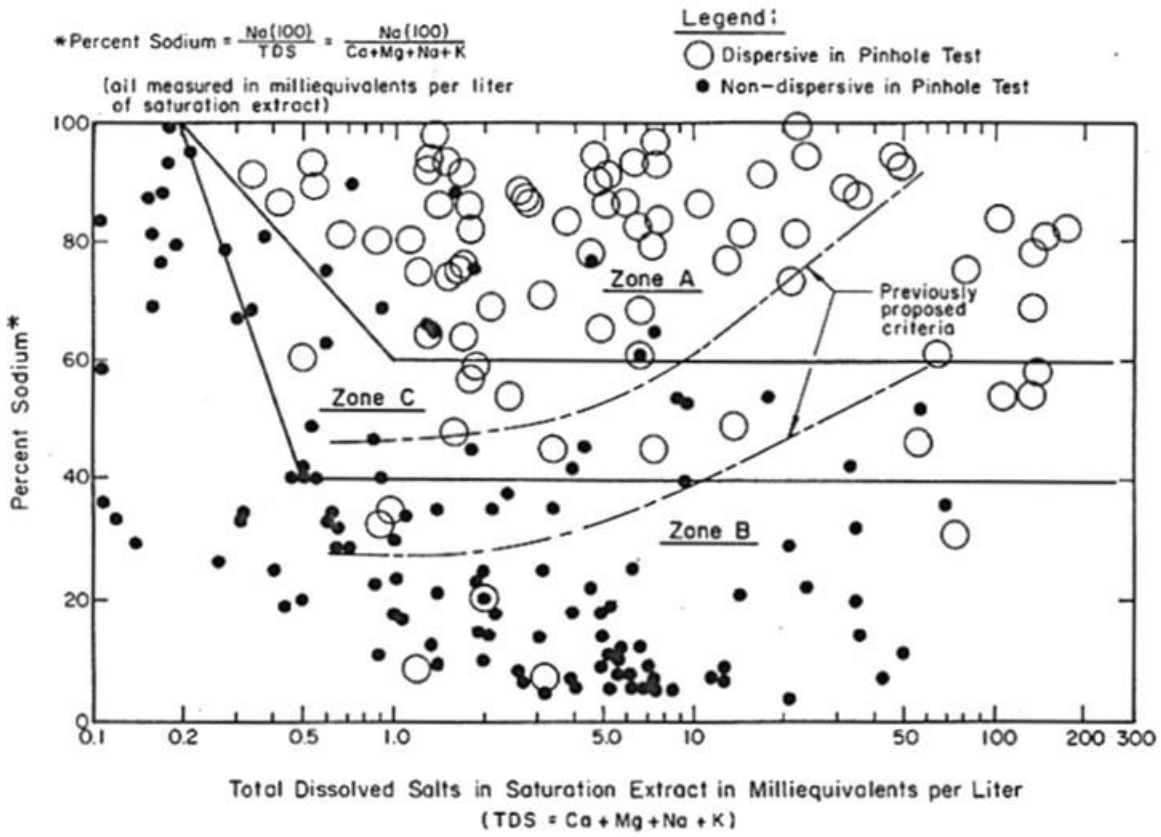


**Figure 5-17 Identification of dispersive soils from *TDS* and *ESP* (from Sherard, et al., 1976b).**

The pinhole dispersion test (ASTM D4647) was developed to aid in identifying and classifying compacted soil specimens (Sherard et al., 1976a). In this test, distilled water is allowed to flow under a small gradient through a 1.0 mm diameter hole in a compacted soil sample, as shown in Figure 5-18. The condition of the water exiting the specimen, the hole size, and the flow rate are monitored and used to distinguish between dispersive and non-dispersive soils, and to classify the soil. The outflow for highly dispersive soils will be dark and the hole through the specimen will quickly enlarge. The outflow for moderately dispersive soils will be cloudy, but the hole size and flow rate will generally remain stable. The outflow for non-dispersive soils will be clear. The pinhole test can also be performed on intact soil specimens, although some investigations have observed problems with the test for highly sensitive clays (Dascal, et al., 1977).

Table 5-11 shows criteria used to classify soils based on results of the pinhole test. Soils classifying as D1 or D2 are considered to be dispersive. Soils classifying as ND3 or ND4 are considered moderately or slightly dispersive. Finally, soils classifying as ND1 or ND2 are considered to be non-dispersive.

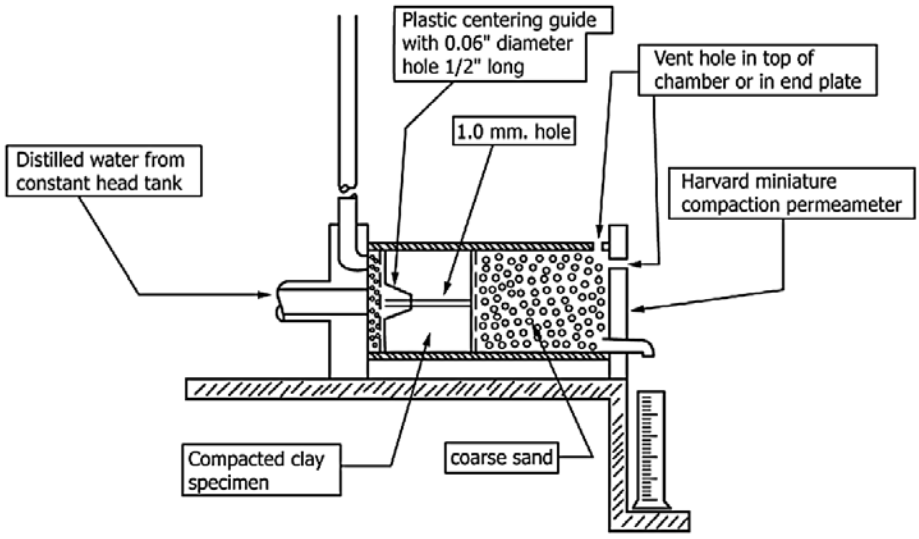


**Figure 5-18 Schematic of pinhole test for characterizing dispersive soil (from ASTM D4647, 2013).**

**Table 5-11 Criteria for classifying dispersive soils from pinhole test (from ASTM D4647, 2013).**

| Dispersive Classification[B] | Head, mm | Test time for given head, min. | Final flow rate through specimen, mL/s | Cloudiness of flow at end of test | | Hole size after test, mm |
|---|---|---|---|---|---|---|
| | | | | from side | from top | |
| D1 | 50 | 5 | 1.0–1.4 | dark | very dark | ≥2.0 |
| D2 | 50 | 10 | 1.0–1.4 | moderately dark | dark | >1.5 |
| ND4 | 50 | 10 | 0.8–1.0 | slightly dark | moderately dark | ≤1.5 |
| ND3 | 180 | 5 | 1.4–2.7 | barely visible | slightly dark | ≥1.5 |
| | 380 | 5 | 1.8–3.2 | | | |
| ND2 | 1020 | 5 | >3.0 | clear | barely | <1.5 |
| ND1 | 1020 | 5 | ≤3.0 | perfectly clear | perfectly clear | 1.0 |
| | | | Method B | | | |
| D | 50 | 10 | ... | slightly dark to dark | very dark to moderately dark | ≥1.5 |
| SD | 180–380 | 5 | ... | barely visible | slightly dark | ≥1.5 |
| ND | 380 | 5 | ... | clear | barely visible to clear | <1.5 |

## 5.6 LIQUEFIABLE SOILS

Liquefiable soils pose significant hazard to transportation infrastructure during seismic events. Liquefaction occurs when pore water pressure generated due to seismic shaking reduces the effective stress in the ground to the extent that soil begins to behave like a liquid. Liquefaction reduces the strength and stiffness of soil, which in turn commonly produces slope failures and lateral spreads, reduced bearing resistance for foundations, and vertical ground settlement that negatively impact many types of transportation infrastructure.

### 5.6.1 Occurrence of Liquefiable Soils

Potentially liquefiable soils exist in virtually all geographic regions. The potential for liquefaction strongly depends on characteristics of seismic shaking that are beyond the scope of this manual. However, the occurrence of liquefaction also strongly depends on ground characteristics that must be

characterized as part of site characterization. Liquefiable soils generally occur as saturated, loose, coarse-grained soils that include sands, gravels, silty sand, silty gravel, and gravelly sands. Key conditions for liquefaction to occur include:

1. The soil is saturated (i.e., below the water table);
2. The soil is predominantly coarse-grained (typically less than about 20 percent fines);
3. The soil is loose (relative density less than about 40 percent); and
4. The ground motion is sufficiently strong.

Liquefaction may also occur in some fine-grained soils, particularly silts with little or no plasticity (e.g., Lutenegger and Hallberg, 1988; Guo and Prakash, 1999; Boulanger and Idriss, 2006).

### 5.6.2 Identification of Liquefiable Soils

Site characterization measurements required for evaluation of liquefaction potential generally include characterization of grain-size distribution, characterization of groundwater conditions, and some measure of relative density. Since liquefaction is most common in clean, coarse-grained soils that are difficult to sample, most evaluations of liquefaction rely on in situ tests that produce measurements related to relative density. Liquefaction potential is generally evaluated using charts like those shown in Figure 5-19 through 5-21, which show the cyclic stress ratio, $CSR$, or cyclic resistance ratio, $CRR$, versus a corrected in situ test measurement. $CSR$ and $CRR$ are measures of the magnitude of seismic shaking whereas the in situ test measurements are indirect measures of density, which is strongly related to liquefaction potential. The curves on the diagrams represent empirical boundaries between conditions that are likely to produce liquefaction and conditions where liquefaction is unlikely to occur (Kramer, 1996).

The most commonly used method for evaluation of liquefaction potential relies on corrected Standard Penetration Test (SPT) $N$-values, measurements of the fine-grained particle fraction, and the chart shown in Figure 5-19. To use this method, measured SPT $N$-values must be corrected for both overburden pressure and hammer energy using the following formula (Kramer, 1996):

$$(N_1)_{60} = N \cdot C_N \frac{E_m}{0.60 E_{ff}} \tag{5.9}$$

where $N$ is the measured SPT blow count, $C_N$ is an overburden correction factor, $E_m$ is the actual hammer energy, and $E_{ff}$ is the theoretical free-fall hammer energy. The value for $C_N$ is generally computed as

$$C_N = \sqrt{\frac{p_a}{\sigma'_{vo}}} \tag{5.10}$$

where $\sigma'_{vo}$ is the effective overburden stress at the depth of the SPT measurement and $p_a$ is atmospheric pressure in the same units (Liao and Whitman, 1986; Youd, et al., 2001).

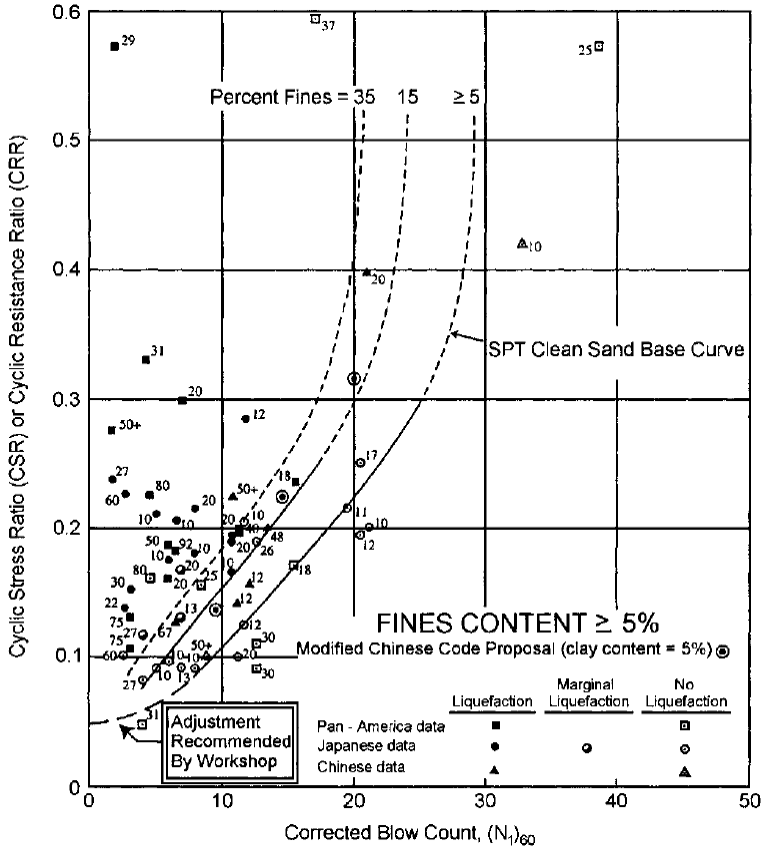


**Figure 5-19 Liquefaction potential charts for SPT measurements (from Youd, et al., 2001).**

Liquefaction potential can be similarly evaluated using corrected CPT tip resistance and the chart from Robertson and Wride (1998) shown in Figure 5-20. Measured values for the cone tip resistance, $q_c$, must also be corrected for overburden stress using the following equation (Youd, et al., 2001):

$$q_{c1N} = C_Q \left(\frac{q_c}{p_a}\right) \tag{5.11}$$

where $C_Q$ is a normalization factor for overburden stress, computed as

$$C_Q = \left(\frac{p_a}{\sigma'_{vo}}\right)^n \tag{5.12}$$

and $n$ is an exponent that varies from 0.5 to 1.0 depending on grain-size characteristics of the soil as described in Youd, et al. (2001).

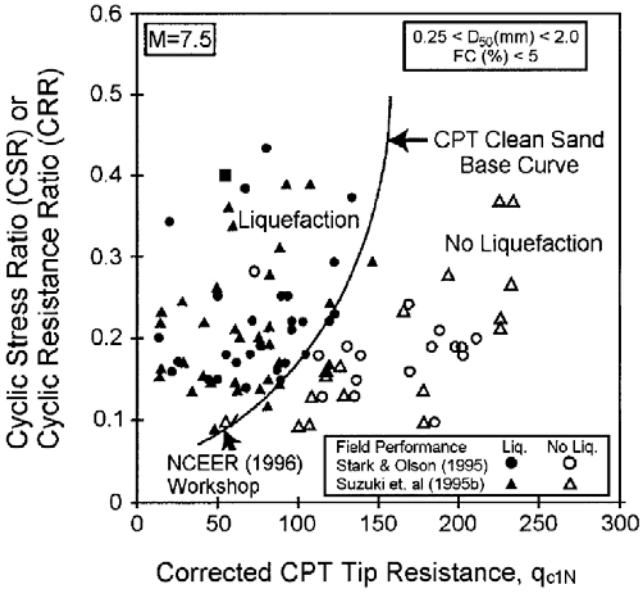


**Figure 5-20 Liquefaction potential charts for CPT measurements (from Youd, et al., 2001).**

Finally, liquefaction potential can also be evaluated using corrected shear wave velocities with the chart proposed by Andrus and Stokoe (2000) and shown in Figure 5-21. For this chart, the measured shear wave velocity, $V_s$, should be corrected for overburden stress as

$$V_{S1} = V_s \left(\frac{p_a}{\sigma'_{vo}}\right)^{0.25} \tag{5.13}$$

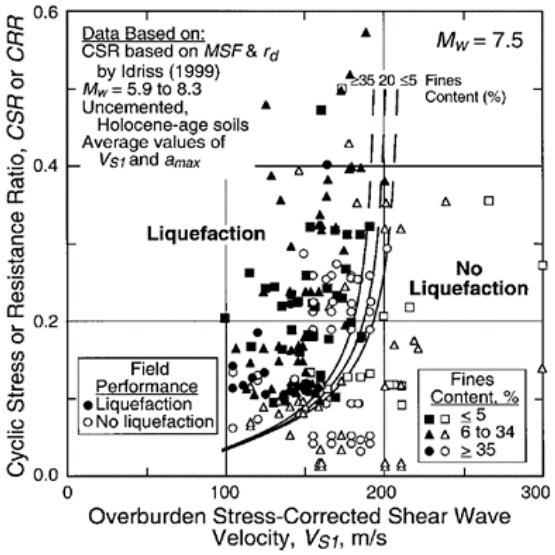


**Figure 5-21 Liquefaction potential chart for shear wave velocity measurements (from Andrus and Stokoe, 2000).**

Criteria for assessment of liquefaction potential in fine-grained soils are a subject of some debate. Many designers have adopted the criterion that soils with plasticity index greater than 7 will not be subject to liquefaction (Boulanger and Idriss, 2006). Others adopt criteria by Bray and Sancio (2006) that soils with plasticity index less than 12 and a natural water content to liquid limit ratio ($\omega_n/LL$) greater than 0.85

may be susceptible to liquefaction. Soils judged to be susceptible to liquefaction according to these criteria are evaluated based on the charts provided in Figure 5-19 to 5-21.

## 5.7 COLLUVIUM AND TALUS

Colluvium (colluvial soil) and talus are often relatively loose deposits found near the base of slopes and accumulated in valleys, swales, or other low-lying topographic features. Colluvial soils generally result from in-place weathering of the parent rock and subsequent migration downslope by gravity through creep and/or fluvial transport. Accumulations of colluvium and talus on and at the base of natural slopes are often associated with slope stability problems. Because these materials typically form by migration and sliding along the slope, they are often only marginally stable in their natural state. Therefore, cut slopes made in these deposits tend to disrupt the natural equilibrium, which generally necessitates careful monitoring, maintenance, or remediation.

### 5.7.1 Identification of Colluvium and Talus

Colluvium and talus are most prevalent in hilly or mountainous terrain. Characteristics of the parent bedrock and the climate in which the weathering and migration take place determine the characteristics of colluvium and talus deposits. Colluvium commonly consists of rock fragments in a heterogeneous clayey to sandy matrix whereas talus generally consists of mechanically weathered to unweathered fragments of the parent rock. Talus slopes are commonly characterized as well-graded boulders to sand- or silt-sized particles, and may contain large voids. In general, colluvium occurs in temperate and humid environments while talus predominantly occurs in arid and semi-arid regions.

### 5.7.2 Challenges for Subsurface Exploration and Testing in Colluvium

Typical drilling and sampling techniques can be utilized in colluvium to obtain samples for laboratory testing, provided the colluvium consists primarily of fine-grained particles. In some cases, colluvium exists as massive deposits upwards of 20 feet or more in thickness. In other cases, colluvium may occur as relatively thin (e.g., a few feet thick or less) lenses of weathered material. In cases where colluvial material occurs as thin lenses within a soil profile, it is easy to drill through the material without realizing its presence. Drilling and sampling in colluvial soils with large rock fragments can be difficult and may require changes to drilling and sampling methods within a single boring. In addition to the above concerns, potential access problems due to relatively steep slopes and marginal stability typically make drilling and sampling in colluvium relatively difficult, and sometimes costly.

Test pits and trenches represent economical alternative exploration methods for colluvium. Test pits and trenches allow for visual observation of subsurface conditions in these materials, which is helpful when colluvium is present in thin lenses. Test pits and trenches are typically backhoe-excavated; however, shallow hand-excavated test pits can sometimes provide subsurface information in inaccessible areas. Undisturbed block samples of colluvium can also be cut from the base or sidewalls of test pits and trenches. In cases where rock fragments do not preclude sampling, colluvium may be sampled by manually advancing (i.e., pushing or driving) sampling tubes from the sidewalls of test pits. Test pits and trenches are also used to evaluate the depth to bedrock and groundwater conditions.

Inclinometers and piezometers are sometimes used as another means to characterize the performance of colluvial deposits. Inclinometers socketed into underlying bedrock are used to assess whether colluvium is actively creeping down slope. Measured displacements provide an indication of the relative stability of the colluvial soil slope. Piezometers installed at various depths within the colluvium, especially at the colluvium-bedrock interface, provide vital information regarding groundwater conditions within the colluvium. It is common that the colluvium/rock interface serves as a shallow aquitard that allows water to accumulate in the colluvium. This water can foster further degradation of the parent rock (particularly if the underlying rock is poorly indurated shale and/or mudstone) and may cause seepage to occur along the interface, both of which reduce stability of the colluvium veneer along the slope.

### 5.7.3 Challenges for Subsurface Exploration and Testing in Talus

Because materials in talus slopes include particles that range from silt- and sand-size to boulders, site exploration is often extremely difficult. Although individual samples of talus fragments may be recovered, they are often of little use because the samples are indicative of the matrix component of the talus, and not the mass itself. Thus, characterizing the global behavior or global properties is extremely difficult when using conventional drilling and sampling equipment. Similarly, any in situ tests requiring penetration are not useful because the penetration will likely meet refusal on large rock/boulders.

The occurrence of talus is generally best identified using desk study materials, including maps and aerial photographs, and on-site reconnaissance. Subsurface characterization is probably best performed using non-intrusive geophysical methods likes those described in Section 8.4.2. In most cases, foundation support will be achieved in competent rock below the talus material, provided the talus slope is stable and will not cause lateral displacement or loading of the foundation. For this reason, geophysical techniques that can identify the depth to competent rock are often particularly useful.

### 5.7.4 Compressibility of Colluvium and Talus

The compressibility of colluvial soils can generally be assessed in the laboratory using standard oedometer tests, provided representative undisturbed samples can be obtained. Additionally, settlements for these materials can be calculated based on results of geophysical tests and elastic theory. The shear wave velocity obtained from geophysical testing provides a reliable means for evaluating the small-strain shear modulus of soil, as described in more detail in Chapter 8.

Talus often exists in situ as a loose mixture of granular material and boulders that may experience settlements during construction. Compression properties are difficult to assess due to the "scale" of the materials (i.e., large boulders to fine-grained soils) and the heterogeneity of the material (i.e., large particles with large void spaces). The void spaces create the potential for large concrete over pours and/or lost grout in the construction of drilled shafts and anchors unless casing is used through the talus. Therefore, the assumed side resistance for design may not be realized. Because of this and the compression potential of the material, foundation systems are generally not designed to derive resistance from talus materials but, instead, are founded in competent material below the talus.

### 5.7.5 Shear Strength of Colluvium and Talus

Shear strength of colluvium can be assessed from laboratory tests on undisturbed samples. In some cases, the colluvium itself may be relatively strong but the interface between the colluvial soil and underlying rock may be much weaker because of accumulated water at the colluvium/rock interface. The shear strength of the material at the colluvium/rock interface can be evaluated by performing laboratory direct shear tests on remolded samples of the material at the expected in situ water content. In the test, residual conditions should be evaluated, especially if there is potential that the material has previously displaced because of sliding or creep.

An alternative method to evaluate the strength of both colluvium and talus is to back-calculate a failed or failing slope in close proximity to the project location. Unless governed by the shear strength of underlying material, many talus slopes can be assumed to be at the angle of repose with a factor of safety for slope stability of near 1.0. Back analyses involve performing stability analyses where values of the cohesion intercept and friction angle are varied to achieve a factor of safety of 1.0. For talus materials, back analysis is often the only method available for evaluating shear strength because of sampling difficulties. This method for determining shear strengths is necessarily non-unique, and is generally more reliable when thorough assessment of slope geometry, stratigraphy, and groundwater conditions are made to reduce uncertainties introduced by parameters other than shear strength.

## 5.8 DEGRADABLE ROCK

Some rock types are prone to degradation when exposed to the atmosphere and/or subjected to stress relief, cyclic wet/dry and freeze/thaw effects, or other weathering processes. In many cases, susceptible materials will exhibit rock-like characteristics when initially exposed, but degrade with time. Degradation can sometimes occur quickly (e.g., within minutes), or may occur more gradually over a period of years. Poorly indurated shales, claystones, siltstones, mudstones, and other similar sedimentary rock types are particularly susceptible to degradation from these processes, but other rock types such as poorly cemented metamorphic rock can also be degradable. Degradation can take many forms, but often includes softening, slaking, and potentially complete disintegration into soil-like materials.

Degradation of rock can produce slope instability that ranges from surficial sloughing to catastrophic slope failures. Differential weathering of alternating beds of durable and degradable rock can produce rockfall hazards because of "hanging" ledges of durable rock. Degradation can also reduce the capacity of shallow and deep foundations if materials degrade during, or potentially after construction. Some degradable materials are subject to scour (Keaton, et al., 2012), which can impact foundation and structure stability. Finally, use of degradable rock as fill for transportation projects can lead to substantial problems during construction, and over the life of the constructed feature, if the materials are not appropriately characterized and used. In some cases, use of degradable materials is possible with appropriate placement and treatment. In other cases, degradable materials should be "wasted" to avoid construction and performance problems.

### 5.8.1 Identification of Degradable Materials

Identification is the first step for effective management of degradable materials. Recognition of potentially degradable materials should begin with the desk study, where various maps and historical records should be reviewed for indications of potentially degradable materials at a specific site. Figure 5-22 shows a large-scale map of weak rock for the continental U.S. that provides some indication of the potential presence of degradable materials. While "weak" does not necessarily imply "degradable", nor does "strong" or "hard" imply "non-degradable", there is certainly correlation between strength and/or hardness and durability, at least as a first approximation. Similar maps, preferably with smaller scale, should therefore be consulted for indications of degradable rock in addition to review of historical project records and other sources.

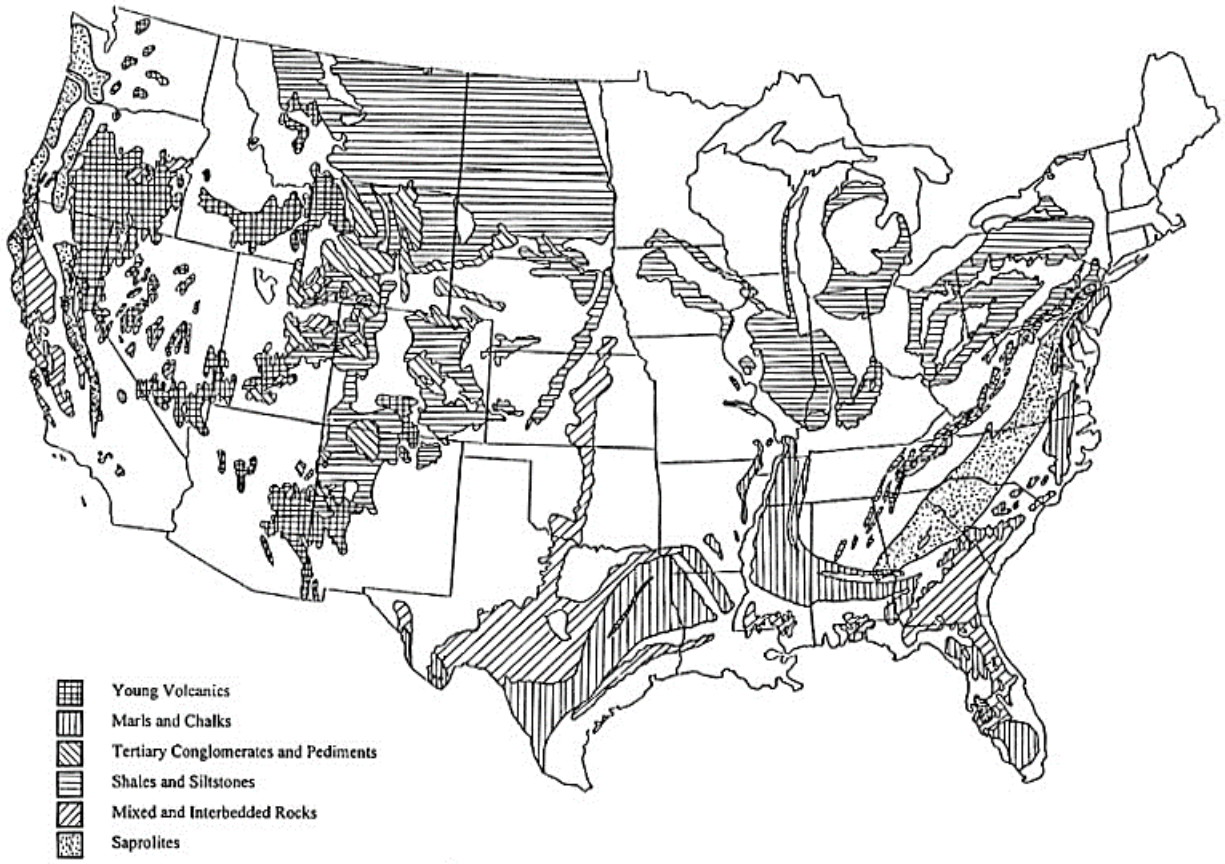


**Figure 5-22 Map of large-scale occurrences of weak rock in the U.S. (from Santi, 2006).**

Indications of degradability can also often be derived from site visits and observations during field investigations. The condition of nearby exposures should be inspected for signs of degradable rock. Signs of degradation of rock core (e.g., slaking, popping, cracking) following extraction should also be carefully noted in borings logs, with clear descriptions of the degradation and the time required for degradation to occur. Sloughing of borehole walls is another indication of potential degradation that should be noted in field boring logs.

Once specific formations are identified as being potentially degradable, tests should be performed on collected samples to quantify the level of degradability. The most common tests for this purpose are the slake durability and jar slake tests described in Section 4.14. Measurements of rock strength and hardness can also sometimes be used, although such measurements provide only indirect assessment of degradability. Soil and rock composition, as measured from XRD tests may also contribute to identification of degradability in some cases. Santi (2006) describes several approaches for identifying weak rock from field observations and measurements, including use of point load strength index tests.

### 5.8.2 Classification of Shale and Degradable Rock

Once degradable materials are identified, it is important to further characterize the anticipated competency of the materials over the service life of a specific project. Common rock mass classification systems described in Chapter 9 are poorly suited to evaluation of weak and degradable rock. However, several alternative classification systems and criteria that are specific to weak and degradable rock have been developed, especially for shales and other similar rock types. For example, Strohm et al. (1978) developed the criteria shown in Table 5-12 to classify the suitability of shale materials for use as rock fill based on measurements of the slake durability index, $I_{D(2)}$, or jar slake index, $I_J$. Franklin (1981) developed a shale rating system that produces a rating, $R$, based on the slake durability index and the plasticity index (for more degradable shales) or point load strength index (for less degradable shales), as shown in Figure 5-23. $R$ ratings determined from Figure 5-23 can be used for classification, and also to establish appropriate design and construction criteria for parameters like lift thickness, slope angle, slope height, and bearing capacity (Maerz, et al., 2010).

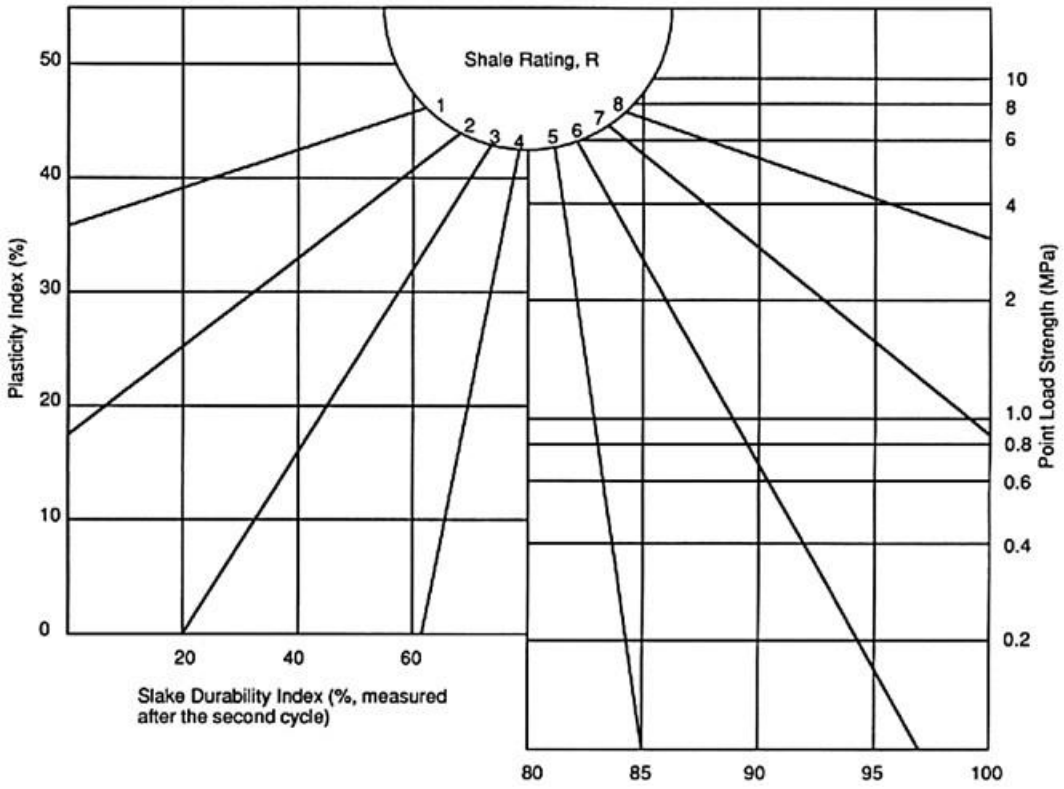


**Figure 5-23 Franklin's shale rating system (from Walkinshaw and Santi, 1996).**

**Table 5-12 Suitability of shale materials for rock fill (after Strohm, et al., 1978).**

| Slake Durability Index, $I_{D(2)}$ | Jar Slake Index, $I_J$ | Suitability of Material for Rockfill |
|---|---|---|
| > 90 | = 6 | Durable rockfill materials, if minus gravel-size fraction less than 20 to 30 percent |
| 60 to 90 | 3 to 5 | Hard, non-durable intermediate material |
| < 60 | < 2 | Soft, non-durable materials treated as soil |

## 5.9 CORROSIVE SOILS

Corrosion is caused by electrochemical interaction between a buried metal and the surrounding soil. Metallic surfaces have areas with differences in electrical potential that establish anode and cathode sites that interact with the surrounding soil and pore fluid. At the anode, iron molecules pass into solution, releasing electrons that travel to the cathode and react with oxygen and water to form hydroxyls. Metal is consumed at the anode as electrons are lost and combine with hydroxyls to form ferrous hydroxide and ferric hydroxide (i.e., rust). Corrosive soils promote this reaction that produces long-term deterioration of buried steel components such as steel foundation piles, sheet piles, soil anchors, MSE wall reinforcement, and buried pipes. Proper identification and evaluation of corrosive soils is therefore important for projects with buried steel elements. Characterization of corrosion potential and corrosion rates is also likely to become more routine with the emergence of geotechnical asset management and performance management.

### 5.9.1 Occurrence of Corrosive Soils

Soils with high corrosion potential are found throughout the world, although specific characteristics of corrosive soils vary regionally. Table 5-13 summarizes several corrosive soil types, along with locations where each soil type is commonly found and general characteristics of each soil type. Corrosive soils commonly include naturally acidic or alkaline soils and organic soils, such as peat or marshy deposits. Industrial fills and soils contaminated from industrial wastes may also be highly corrosive.

The availability of moisture and oxygen is an important factor in the corrosion process. Fluctuations in the groundwater table provide conditions for both moisture and oxygen to be present in the soil. Greater corrosion rates are generally observed above the water table, in the zone of groundwater fluctuation, where both moisture and oxygen are present (Decker, et al., 2008). Below the groundwater table, sites with low hydraulic gradients tend to show less corrosion since there is less free oxygen than in soils with significant hydraulic flow.

**Table 5-13 Soil types with high corrosion potential (adapted from Elias, et al., 2009).**

| Soil Type | Prevalence | Characteristics |
|---|---|---|
| Acid-Sulfate soils | Appalachian Regions | • Pyritic<br>• $pH < 4.5$<br>• High sulfate and chloride content |
| Sodic Soils | Western States | • $pH > 9$<br>• High salt content |
| Calcareous Soils | FL, TX, NM and Western States | • High carbonate content<br>• Alkaline, but $pH < 8.5$<br>• Mildly corrosive |
| Organic Soils | FL (Everglades), GA, NC, MI, WI, MN | • Organic content > 1%<br>• Microbial induced corrosion |
| Industrial Fills (e.g., slag, cinders, fly ash, mine tailings) | Nation wide | • May be acidic or alkaline<br>• May have high sulfate and chloride content |

### 5.9.2 Identification of Corrosive Soils

Direct measurement of corrosion potential for buried elements is simply not practical. However, indications of high corrosion potential can be identified using several indirect measurements. Corrosion rates for buried steel are related to several interrelated factors that include: (1) soil type; (2) soil moisture, (3) oxygen content; (4) soil resistivity; (5) soil $pH$; (6) soluble salts content (e.g., sulfate, sulfide, and chloride); (7) redox potential, (8) soil cation exchange capacity; and (9) microbial activity. While any of these factors can theoretically provide an indirect indication of corrosion potential, measurements of soil resistivity, $pH$, and soluble salts are most commonly used for identifying corrosive soils. Corrosion is generally more severe in moist soils with low resistivity, extreme $pH$, and high salt concentrations.

***Electrical Resistivity***

Electrical resistivity is generally considered to provide the most accurate indication of corrosion potential for buried steel elements (Elias, et al., 2009). Electrical resistivity can be measured in the laboratory using a two-electrode array according to AASHTO T288 or ASTM G187. Electrical resistivity can also be measured in the field or laboratory using a four-electrode Wenner array according to ASTM G57. The measured resistivity is generally dependent on the prevalence of soluble salts in the soil as well as the water content. ASTM G187 dictates that the soil be saturated during specimen preparation while AASHTO T288 dictates that resistivity be measured for soils at different water contents and that the minimum resistivity be reported. Field measurements of resistivity should be interpreted considering the in situ water content, recognizing that resistivity will generally decrease with increasing water content. The *AASHTO LRFD Bridge Design Specifications* (AASHTO, 2014) stipulate that significant corrosion

may occur when the measured resistivity is less than 2000 Ω-cm. The degree of corrosion potential can be further categorized according to Table 5-14 (Roberge, 2000).

**Table 5-14 Degree of soil corrosivity based on resistivity (from Roberge, 2000).**

| Soil Resistivity (Ω-cm) | Corrosivity Rating |
|---|---|
| > 20,000 | Noncorrosive |
| 10,000 to 20,000 | Mildly Corrosive |
| 5,000 to 10,000 | Moderately Corrosive |
| 3000 to 5000 | Corrosive |
| 1,000 to 3,000 | Highly Corrosive |
| < 1000 | Extremely Corrosive |

***pH***

The measure of acidity or alkalinity of soils in a solution of distilled/deionized water is given as $pH$, which is a measure of the hydrogen ion concentration. For corrosion testing, $pH$ can be measured according to AASHTO T289 or ASTM G51. The tests are simple to perform and are generally used to supplement resistivity measurements for evaluation of corrosion potential. Soils with $pH$ less than 4 (extremely acidic) or greater than 10 (extremely alkaline) are generally considered to have significant potential for high corrosion rates (Elias, et al., 2009). The *AASHTO LRFD Bridge Design Specifications* stipulate that corrosive conditions may exist for soils with $pH$ less than 5.5.

***Soluble Salts***

The concentration of soluble salts in a soil, most notably chlorides and sulfates, is directly proportional to electrical conductivity and corrosivity. The concentration of chlorides can be measured using AASHTO T291 while the quantity of sulfates can be measured according to AASHTO T290. Alternatively, the concentration of chlorides and sulfates can both be measured according to ASTM D4327, as recommended by Elias et al. (2009). Concentrations of chlorides or sulfates greater than 500 ppm are considered to be indicative of significant corrosion potential (AASHTO, 2014).

***Organic Content***

Organic soils are also generally corrosive, although through different means than mineral soils. As described in Section 5.4.2, the organic content of soils can be determined following procedures in AASHTO T267 or ASTM D2974. Soils with high organic content have the potential to produce "pitting" corrosion in buried metallic elements.

### 5.9.3 Classification of Corrosive Soils

Several classification systems are available to rate corrosion potential. The American Water Works Association (AWWA) developed a rating system that relates corrosivity to soil conditions for cast iron pipes. The system is somewhat complicated but includes a number of factors known to influence corrosivity. Another system has been developed by the American Iron and Steel Institute (AISI) for galvanized pipe using soil $pH$ and resistivity. Some manufacturers of steel piles have developed corrosion rating systems using a similar approach. For example, Earth Contact Products, LLC has suggested a numerical corrosivity score as shown in Table 5-15. In this system, points established based on resistivity, $pH$, and soil water content are summed to produce a numerical corrosivity score for a particular site/depth, which can be used to establish corrosion severity as shown in Table 5-16.

**Table 5-15 Typical Numerical Corrosivity Scoring System.**

| Soil Parameter | Value | Score |
|---|---|---|
| Resistivity (Ω-cm) | < 500 | 10 |
| | 500 to 999 | 8 |
| | 1,000 to 1,999 | 5 |
| | 2,000 to 4,999 | 2 |
| | 5,000 to 10,000 | 1 |
| | > 10,000 | 0 |
| $pH$ | 2 to 4.5 | 6 |
| | 5 to 6 | 0 |
| | 7 to 9 | 6 |
| | 10.5 to 12 | 2 |
| Moisture | Tidal or Salt Water | 5 |
| | Poor Drainage - Always Wet | 2 |
| | Fair Drainage - Moist | 1 |
| | Good Drainage – Usually Dry | 0 |

**Table 5-16 Soil Corrosion Potential Based on Corrosivity Score (Typical).**

| Total Corrosivity Score | Soil Corrosion Potential |
|---|---|
| 0 to 2 | Unlikely |
| 3 to 4 | Slight |
| 5 to 6 | Mild |
| 7 to 8 | Moderate |
| 9 to 13 | Aggressive |
| 14 to 20 | Severe |

## 5.10 CEMENTED SANDS

Cemented sands are naturally occurring granular materials that have a cementing agent either in the void space between individual grains or at points of grain-to-grain contact. Cemented sands are usually

"stronger" than similar uncemented sands. However, this increased strength comes with several potential problems:

1. the cementing agent may be so weak that it is destroyed during sampling, thus resulting in poor characterization of the in situ deposit;
2. the cementation may be damaged and/or compromised during construction, thus resulting in different material behavior than was present during site characterization;
3. the cementing agent may be soluble or extremely weak, such that the increased strength due to cementation cannot be relied upon for long-term design conditions; and
4. cemented sand exhibits a brittle load-deformation response that must be recognized for design.

Weakly cemented sands can form due to grain-to-grain point-contact welding as a result of aging, or from clay-silt binder that often accompanies wind-blown dune deposits. At the other extreme, some cemented sands formed when carbonate bonds precipitate at grain contacts can be quite strong and potentially even characterized as weak sandstone. Regardless of origin, cementation often results in relatively strong and stiff, but brittle, load-deformation behavior as illustrated in Figure 5-24. Cementation also generally results in the sand exhibiting "true cohesion" (i.e., a component of shear strength that is independent of confining pressure). Such behavior must be carefully assessed when evaluating parameters for design.

### 5.10.1 Identification of Cemented Sands

Cemented sands are most commonly identified based on brittle load-deformation behavior and prior experience in an area. It is also possible to correctly identify cemented sands through careful observation during field reconnaissance, drilling, and sampling. Observation of substantial vertical to near vertical slopes in exposed excavations or natural cuts provides strong indication of cementation. Cemented soils can sometimes be identified by carefully observing recovered cuttings looking for small pieces of cemented materials that are returned within the matrix of uncemented sands. In some cases, cemented sands may also be identified through the presence of cementing agents (e.g., carbonates) within a soil or rock as described in Chapter 4. However, measurements for identifying cementing agents (e.g., XRD, carbonate content, etc.) are not routinely performed without some initial indication of cementation. Identification of cementing agents is further complicated because several different types of cementation are common.

"Anomalous" behavior during drilling and sampling, such as uncharacteristically high blow counts during sampling or poor core recovery despite relatively uniform drilling resistance, also provides possible indications of cementation. Unfortunately, there are other reasons for high blow counts and poor

recovery, so such observations alone cannot be taken as reliable indicators of cemented sands. Additional indications can be derived from measurement of unit weight on recovered samples to evaluate whether the soil is as dense as the high blow counts would indicate. It is also often helpful to immerse a sample in water or to simply add water to a piece of the intact sample to assess whether the cementing agent is soluble or if the material softens when inundated with water. In the end, identification of cemented sands often requires consideration of multiple observations and sound judgment.

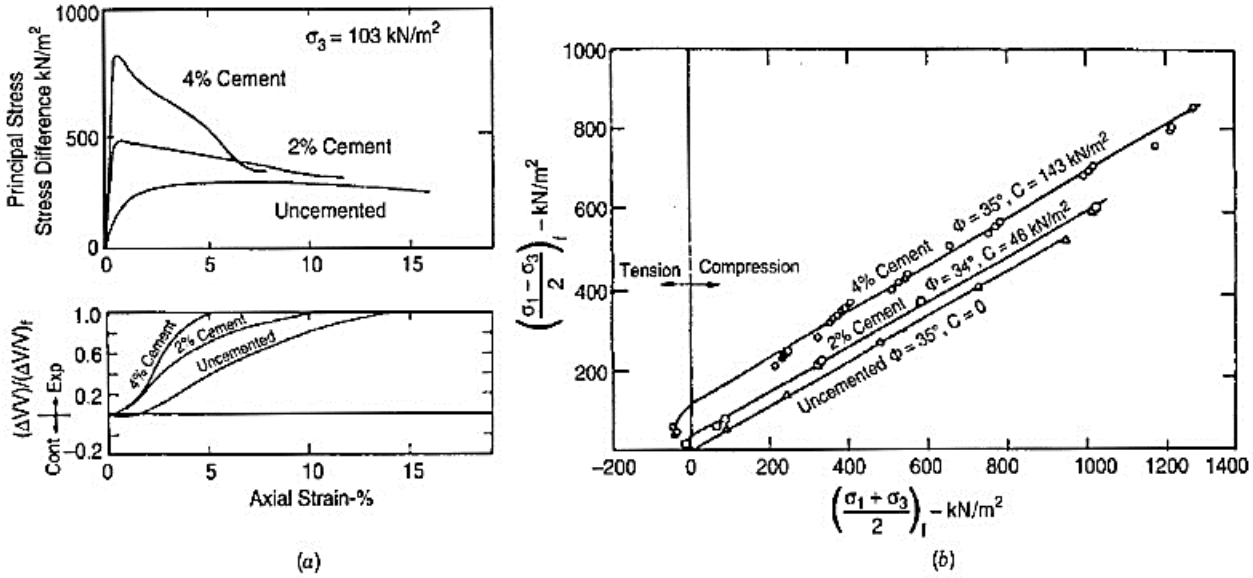


**Figure 5-24 Typical stress-strain-volume change response for cemented sands: (a) stress-strain response, and (b) peak stress failure envelopes (from Clough, et al., 1981).**

### 5.10.2 Challenges for Subsurface Exploration and Testing in Cemented Sands

Cemented sands are often difficult to sample. The strength of cemented sand is often sufficient to preclude sampling using thin-walled Shelby tubes. Block sampling is often an effective technique for acquiring undisturbed samples of cemented sands from shallow depths. "Over coring" samplers, such as Pitcher or Denison samplers, can also be used to acquire representative samples from deeper deposits in some cases. Cemented sands may also be characterized and investigated as soft rock; however, conventional coring techniques may produce poor sample recovery due to disturbance induced during drilling and the effects of drilling fluids. If the soil is weakly cemented, the cemented structure may not be recognized when conventional soil sampling techniques are used. SPT blow counts may appear to be uncharacteristically high, but the recovered materials may appear to be uncemented because relatively weak cementing materials can be easily disturbed during drilling and sampling. In such cases, the driving/pushing resistance can be mistakenly interpreted as being characteristic of dense uncemented

sands. Such mischaracterization is often conservative at low working stress levels, but may be unconservative at higher working stresses since dense, uncemented sand may actually be stronger than loose cemented sand at high confining stresses.

For laboratory testing, extreme care is necessary when extruding and handling cemented soils. Relatively weak and brittle cementation can often yield to even gentle fingertip pressure during handling and trimming. If possible, recovered cemented materials should not be trimmed, but rather tested at the as-recovered diameter. For recovered block samples, the material should be carefully "shaved" in the laboratory to obtain specimens suitable for testing.

### 5.10.3 Interpretation of Laboratory and Field Testing Results in Cemented Sands

Laboratory triaxial or direct shear testing should be performed if specific strength and/or stiffness properties are needed. Because of the sensitive and brittle nature of the cementing materials, these tests must be carefully conducted and interpreted. In situ testing using a pressuremeter can often be effectively used to provide quantitative strength and stiffness measurements. Other in situ testing techniques, specifically the SPT and dilatometer tests, provide useful qualitative results, but must be calibrated to specific site conditions to provide quantitative estimates for cemented soil properties.

The load versus deformation response of cemented sands must also be interpreted with recognition of the likely brittle nature of the soil. At low confining pressures, the response due to cementation will dominate the measured strength and stiffness because the frictional component of resistance is relatively small. This results in an initial stiff response due to the cementation, followed by strain softening after rupture of the cementing bonds as illustrated in Figure 5-24a. As the confining pressure increases, differences between peak and post-peak strengths will generally decrease. At high confining pressures, it is possible that application of the confining pressure will result is disruption of cementing bonds, resulting in a load-deformation response that is consistent with that of an uncemented sand. The range of confining pressures used for testing must therefore be carefully selected to match anticipated service conditions. Additionally, because the cementing bonds can be disrupted at low strains, the anticipated strains under anticipated working stresses should be assessed to judge whether the peak or the large-displacement strengths are appropriate for design. As an example, large-displacement piles driven into calcium carbonate sands will likely exhibit resistance that is significantly less than that predicted using measured peak shear strengths derived from undisturbed samples (e.g., Murff, 1987).

## 5.11 SENSITIVE "QUICK" CLAYS

Sensitive clays are highly structured clay soils that experience dramatic strength loss when disturbed or remolded. Sensitivity, $S_t$, for a soil is defined as

$$S_t = \frac{s_{u-undisturbed}}{s_{u-remolded}} \tag{5.14}$$

where $s_{u-undisturbed}$ is the undrained shear strength in the undisturbed state and $s_{u-remolded}$ is the undrained shear strength of the same soil at the same water content in a completely remolded state. Practically all clayey soils exhibit some degree of sensitivity; however, a few clay soils exhibit extreme sensitivity, with the soil essentially turning into a viscous liquid when remolded. Clays with extreme sensitivity are often called "quick" clays and are associated with notorious failures that include the 1978 landslide in Rissa, Norway and the 1964 landslide in Anchorage, Alaska. In extreme cases, quick clays may have sensitivities that exceed 500, meaning that there is a 500-fold decrease in undrained shear strength upon remolding.

Quick clays have a fragile and open soil structure, referred to as a "metastable" structure. The metastable structure is formed when clays are initially deposited in a marine environment, but subsequently leached with fresh water when the deposits are uplifted (often due to retreating glaciers). Quick clays generally have high void ratios and high water contents, often substantially greater than the liquid limit with *LI* up to 2 or 3.

### 5.11.1 Occurrence of "Quick" Clays

Fortunately, the natural occurrence of quick clays is rare, and generally restricted to formerly glaciated regions that have been subjected to isostatic uplift due to retreating ice sheets. In North America, quick clays are generally restricted to the region along the St. Lawrence Seaway in the northeast and portions of Alaska. Other highly sensitive soils are found in other areas of the U.S., but such soils often have sensitivities that are substantially less than required to be considered as quick clays.

### 5.11.2 Identification of "Quick" Clays

Highly sensitive clays are often easily identified. The liquidity index is a commonly used, simple, and generally reliable indicator of sensitivity. As illustrated in Figure 5-25, values of liquidity index greater than 1.0 suggest that sensitivity is likely to be greater than 5. Sensitivity generally increases with increasing liquidity index, with highly sensitive or quick clays often having liquidity index values greater than 1.5 or 2. Sensitivity can also be established directly by measuring undrained shear strength for

undisturbed and remolded specimens at the same water content. Laboratory measurements of sensitivity will tend to underestimate the actual sensitivity because some disturbance of samples is unavoidable. More accurate measurements of sensitivity can often be acquired using field vane shear tests (VST) wherein the remolded shear strength is measured by rotating the vane to induce large shear displacements that are representative of remolded conditions. Sensitivity may also be similarly evaluated from undisturbed samples in the laboratory using a miniature lab vane or from fall cone tests on undisturbed and remolded samples at the same water content. Several different classifications for sensitivity have been proposed. One such classification by Skempton and Northey (1952) is provided in Table 5-17.

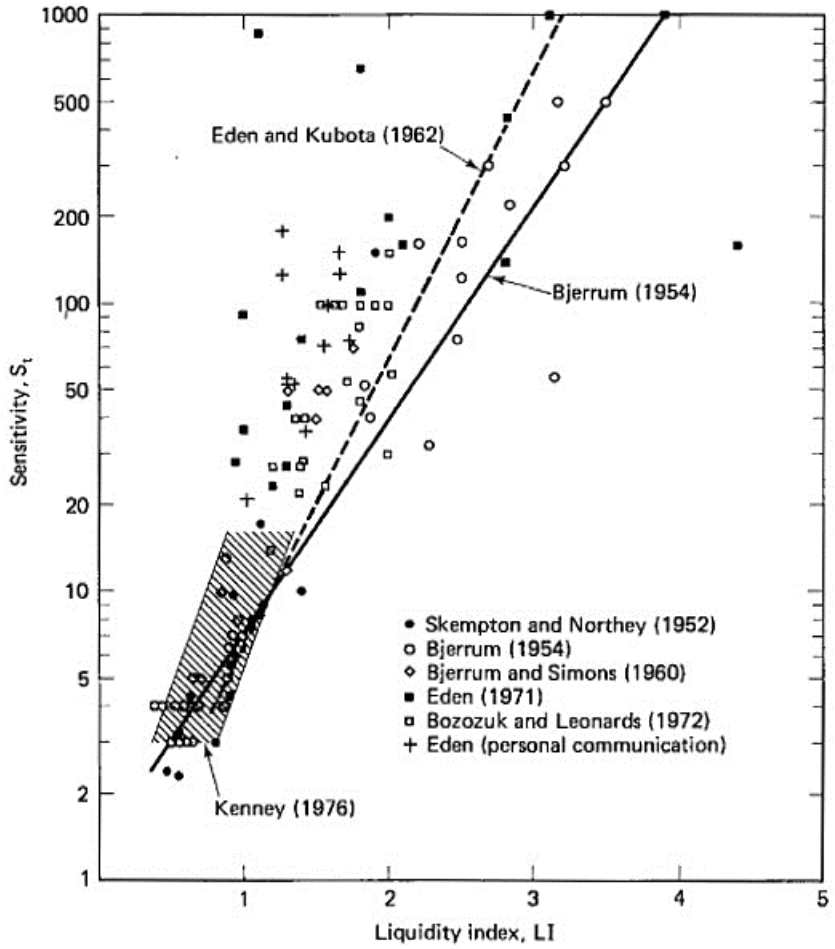


**Figure 5-25 Sensitivity of marine clays as related to liquidity index (from Holtz and Kovacs, 1981).**

### 5.11.3 Challenges for Subsurface Exploration and Testing in Sensitive Clays

Sampling and laboratory testing of sensitive clays is extremely difficult, primarily because disturbance from conventional sampling and testing techniques may be sufficient to disrupt the in situ soil structure. Conventional thin-walled tube samplers that are deployed rapidly may be appropriate for moderately

sensitive materials. For more highly sensitive soils, thin-walled samplers with diameters greater than conventional 3-inch diameter Shelby tubes will provide better recovery and produce less disturbance. Regardless of sample size, rapid sampler deployment has been shown to effectively reduce disturbance induced by friction along the walls of the sampler. In extremely sensitive soils, special samplers that rely on foil liners to encapsulate samples should be used. This equipment is specialized, but can be found in regions where extremely sensitive clays are encountered. Hand-carved block samples are also an excellent alternative for acquiring samples with little disturbance from shallow depths.

**Table 5-17 Classification of clay sensitivity (from Skempton and Northey, 1952).**

| Sensitivity | Classification |
|---|---|
| $S_t < 1.0$ | Insensitive Clays |
| $S_t = 1$ to 2 | Clays of Low Sensitivity |
| $S_t = 2$ to 4 | Clays of Medium Sensitivity |
| $S_t = 4$ to 8 | Sensitive Clays |
| $S_t = 8$ to 16 | Extra-Sensitive Clays |
| $S_t > 16$ | Quick-Clays |

Field vane shear tests are an excellent alternative or compliment to laboratory testing on undisturbed specimens. Field vane equipment can be extremely portable and easy to deploy over soft, sensitive materials. For very soft soils, the size of the vane and methods for deployment can be modified to match the strength of the soil based on local experience.

The metastable structure of highly sensitive soils also poses challenges for laboratory testing. Extreme care is required for sample transportation, handling, and specimen preparation. It is generally preferable to extrude samples directly onto the testing pedestal and to provide confinement using thin membranes. Care must also be taken to ensure that the structure is not substantially altered as a result of testing procedures. For example, consolidation of specimens to large effective confining stresses prior to shearing may compromise the in situ structure and produce measurements of shear strength that are not representative of in situ conditions. Such considerations generally preclude use of the SHANSEP technique (Ladd and Foott, 1974) for reducing effects of sample disturbance and normalized soil properties that are described in Chapter 7. As a general practice, highly sensitive soils should not be consolidated to effective stresses that exceed the in situ effective stresses to avoid the potential for destructuring the soil.

## 5.12 HIGH SULFATE SOILS

Fine-grained soils containing large concentrations of sulfates such as calcium sulfate (gypsum, $CaSO_4\ 2H_2O$) or sodium sulfate ($Na_2SO_4$) pose two potential hazards for transportation infrastructure.

"Sulfate-induced heave" may occur when lime, fly-ash, or cement are used to modify and stabilize sulfate-rich soils, causing distress to lightly loaded structures such as highway pavements and slabs (Hunter, 1988). Calcium from the lime or cement can react with the natural sulfate to produce expansive minerals such as ettringite and thaumasite, both of which increase in volume during formation and produce heave. Sulfate-rich soils may also be corrosive to Portland cement paste, which can lead to cracking and strength degradation for concrete foundations.

### 5.12.1 Occurrence of High Sulfate Soils

Fine-grained, sulfate-rich soils occur throughout the world but are most prevalent in arid and semi-arid regions. In the U.S., sulfate soils have been documented in Texas, Colorado, Kansas, Georgia, Nevada, Louisiana, California, and New Mexico (Puppala, et al., 2003). Sulfates are seldom uniformly distributed throughout a soil profile, but rather are present in concentrated seams or pockets, often near the ground surface. Groundwater flow tends to leach sulfates from soil so sulfates tend to be present in areas with little groundwater flow, often in low-lying areas.

### 5.12.2 Identification of High Sulfate Soils

The potential presence of sulfate-rich soils can often be identified during desk studies, especially through investigation of soil surveys. If sulfate-rich soils are suspected, sulfate content should be measured according to AASHTO T290, ASTM C1580, or ASTM D4327. Specific threshold levels that can produce swell issues depend on other aspects of soil composition and vary considerably, but typically are in the range of 300 to 25,000 ppm (Little and Nair, 2009; Talluri, et al., 2013). However, field evidence suggests that heave is not significant if the sulfate concentration is less than about 2,000 ppm (Petry and Little, 1992; Harris, et al., 2004). Table 5-18 summarizes risk associated with lime stabilization for different sulfate concentrations.

**Table 5-18 Risk for lime stabilization of sulfate-bearing clays (from Little and Nair, 2009).**

| Risk Involved | Soluble Sulfate Concentrations (ppm) | Soluble Sulfate Concentrations (% dry weight) |
|---|---|---|
| Low Risk | < 3,000 ppm | < 0.3% |
| Moderate Risk | 3,000 to 5,000 ppm | 0.3% to 0.5% |
| Moderate to High Risk | 5,000 to 8,000 ppm | 0.5% to 0.8% |
| High to Unacceptable Risk | > 8,000 ppm | > 0.8% |
| Unacceptable Risk | > 10,000 ppm | > 1.0% |

The severity of concrete corrosion is also related to the concentration of water-soluble sulfates. The American Concrete Institute (ACI) identifies several different "exposure classes" for concrete in contact

with soil (or water) containing deleterious amounts of water-soluble sulfates, as summarized in Table 5-19. These classes are used to establish criteria for mix-design of concrete related to the type and quantity of different cementitious materials.

**Table 5-19 Severity of sulfate environment for concrete corrosion (after ACI, 2008).**

| Severity of Environment | Concentration of Water-soluble Sulfates in Soil (% by weight) | Concentration of Water-soluble Sulfates in Water (ppm) |
|---|---|---|
| Class S0 – Not applicable | < 0.10 | < 150 |
| Class S1 – Moderate | 0.10 to 0.20 | 150 to 1,500 |
| Class S2 – Severe | 0.20 to 2.00 | 1,500 to 10,000 |
| Class S3 – Very Severe | > 2.00 | > 10,000 |

## 5.13 PYRITIC/ACID ROCK

Some soil and rock formations, especially shales and carbonaceous sedimentary rock, have sufficient pyrite to pose hazards to transportation infrastructure and the environment. Pyrite can be oxidized with the help of autotrophic bacteria, which can mix with calcium in groundwater and react to form gypsum crystals ($CaSO_4\ 2H_2O$) and sulfuric acid. Calcite ($CaCO_3$) may also contribute by reaction with the sulfuric acid to produce gypsum. The formation of gypsum crystals causes the rock to expand, which can cause severe distress in underground structures if present in sufficient quantities (Quigley et al., 1973; Penner, et al., 1972; Lutenegger et al., 1979). Acid runoff from pyritic soil or rock is also an environmental problem and can accelerate corrosion of concrete and metals.

The presence of pyrite is most commonly identified from inspection of sampled soil or rock. Pyrite generally occurs as small, distributed, crystalline grains that often have cubic shape, brassy-yellow color, and a metallic luster, and is often mistaken for gold (i.e., “fool’s gold”). When tarnished, pyrite may appear gray in color. Weathering of pyrite will also produce iron staining on open exposures. Explanations for geologic maps may also mention the presence of pyrite if present in significant quantities. Lack of vegetation, or stunted/dead vegetation in drainage areas may also indicate presence of pyritic rock, although such indications can be the result of other factors.

If pyrite is present, laboratory testing of recovered core may include compositional analyses to estimate the volume fraction of pyrite, either from visual inspection of rock fragments or from analysis of thin-sections. Additionally, chemical tests may be performed to characterize the potential to produce acid.

## 5.14 UNSATURATED SOILS

Unsaturated soils seldom represent hazards to transportation infrastructure strictly because they are unsaturated. Unsaturated soils are, therefore, not "problematic soils" in the sense this term is used for other soil types described in this chapter. However, the fact that many soils are at least occasionally unsaturated complicates the process of measuring soil properties and interpreting those measurements for design. It is important to consider these complications as part of site characterization so that appropriate judgment can be applied to interpretation of design parameters for soil and rock.

As a general rule, unsaturated soils often exhibit better performance than similar saturated soils: unsaturated soils are generally stronger, stiffer, and less permeable than similar saturated soils. Much of the improved performance observed for unsaturated soils is a result of matric suction (i.e., negative pore water pressure) that, in effect, increases the effective confining stress over what would exist if the soil were saturated. Unfortunately, the magnitude of matric suction is inevitably transient (also true for positive pore water pressures) and somewhat difficult to predict as a matter of routine practice. Furthermore, in the context of design, it is crucial to consider the most critical conditions that are likely to be encountered over the life of a specific feature. In the vast majority of cases, the most critical condition is associated with saturated soil conditions. With a few notable exceptions, common geotechnical design practice therefore appropriately relies on design parameters and pore water pressures that are established considering saturated conditions, despite the fact that conditions may be unsaturated when site characterization is performed.

The primary complication introduced for unsaturated soils is that the actual in situ properties that exist at a given time are governed by the magnitude of matric suction and the mechanics of unsaturated soils rather than the mechanics of saturated soils that are generally adopted for design. While saturated and unsaturated soil mechanics are largely compatible, they may predict different strength, compressibility, and hydraulic conductivity for specific conditions. Detailed description of unsaturated soil mechanics is beyond the scope of this manual. However, interested readers can consult one of several excellent texts on the subject (e.g., Lu and Likos, 2004; Fredlund, et al., 2012; Briaud, 2013) for further study.

When designing for fully drained conditions (e.g., for long-term stability analyses, settlement analyses, etc.), analyses are commonly performed using parameters established in terms of effective stresses (e.g., effective stress strength parameters, compressibility parameters) and pore water pressures established considering saturated, steady-state seepage. This approach is generally straightforward and usually consistent with the worst-case conditions that may be experienced over the life of a feature. Effective

stress parameters are almost universally established from tests performed for saturated soil specimens, which is appropriate for the analyses performed. If the worst-case conditions experienced are actually unsaturated, this design approach will be conservative since the effective stress strength parameters are still likely to be practically appropriate and since the pore water pressures considered for design will be greater than actually observed.

However, the situation is more complex when designing for short-term, undrained conditions that are generally analyzed in terms of total stresses. Design parameters for total stress analyses are established without explicit regard for the pore water pressure (positive or negative) that exists when measuring soil properties. However, the actual magnitude of the measured property is inevitably linked to the actual effective stress that exists at the time of testing. Thus, for example, measurements of undrained shear strength (or total stress strength parameters) are inherently linked to the magnitude of the effective stress that exists at the time of sampling (or, strictly speaking, at the time of testing, although the two are at least qualitative related). Measurements of "undrained" shear strength made for samples acquired during dry summer months, when soils are more likely to be unsaturated and pore water pressures are more likely to be negative, will tend to be greater than the undrained shear strength that will actually exist following an extended wet period. Conversely, measurements of undrained shear strength made for samples acquired following an extended wet period, when effective stresses are likely to be relatively low, will tend to be less than the undrained shear strength that will actually exist during dry summer months. Thus, measurements made in terms of total stresses are only representative of actual conditions to the extent that current in situ conditions are consistent with those present during sampling/testing. Similar arguments hold true for in situ test measurements; in situ measurements are generally only consistent with actual conditions to the extent that actual conditions are similar to those present during testing. Thus, it is possible for design for short-term conditions to be conservative or unconservative depending on how actual conditions compare to those present during sampling/testing.

An additional complication with unsaturated soils is that actual performance of a feature will be dictated by conditions that exist in the field (whether saturated or unsaturated), rather than the "design" conditions that may be appropriately presumed for design. Given that design conditions are, and should be, selected to represent the likely worst-case conditions that may be encountered, there is often a high likelihood that actual performance in the field may be better than predicted during design. This is entirely appropriate, and desirable, for engineering work. However, it is important to recognize that actual conditions must be considered when trying to match predictions with observations, such as is commonly done for back-analysis of failures, when developing empirical design methods, or when developing empirical relations between in situ test measurements and measured soil properties.

## 5.15 PERMAFROST

Permafrost is permanently frozen ground, generally defined as being continuously frozen for a period of at least two years. The concentration of ice within permafrost is often highly variable and, in some cases, massive bodies of relatively pure ice may exist with the permafrost. Frozen soils generally have greater strength, greater stiffness, and lower hydraulic conductivity than similar unfrozen soils. However, frozen soils are also susceptible to long-term creep deformations, particularly when the soil pores are filled with ice.

Permafrost is usually overlain by an "active layer" where the soil is subjected to repeated freezing and thawing that is often accompanied by substantial volume changes. Freezing soil can produce growth of "ice lenses", concentrated locations of pure ice that grow in the direction of heat loss (usually upward) if water sources are present (e.g., from capillary action, infiltration, or seepage), and produce frost heave. In contrast, thawing soil loses volume due to the phase change from solid to liquid while simultaneously producing "thaw weakening" as the ice melts. If the soil thaws faster than drainage can occur, pore water pressures will also increase, which further softens and weakens the soil. The repeated expansion and contraction within the active zone is somewhat similar to that observed for expansive soils with changes in water content, both of which can produce significant damage to overlying structures and pavements. However, expansion and contraction from freezing and thawing is often more localized and variable such that hummocky landscapes are often produced. Permafrost is also practically impermeable, which often causes water to collect and move within the active layer thereby worsening freeze-thaw problems.

### 5.15.1 Occurrence of Permafrost

The presence and character of permafrost at a particular location is controlled by the thermal regime within the ground. In the U.S., permafrost is predominantly located across much of Alaska, although it also exists at high elevations in the mountain west from Washington to Arizona. Permafrost at higher latitudes and higher elevations is generally continuous and may be hundreds of feet thick whereas permafrost at lower latitudes and/or elevations is generally discontinuous and much thinner, as shown in Figure 5-26. The thickness of the active layer is also generally greater at lower latitudes and elevations.

### 5.15.2 Identification of Permafrost

Permafrost can usually be identified using common site characterization methods. Initial indications of permafrost can often be established from observation of unique geomorphic features that may be visible in aerial photographs and during site visits. Specific geomorphic features that are indicative of permafrost

include polygonal ground, stone nets, solifluction sheets, thaw lakes, beaded drainage, ice wedges and pingos. Permafrost can also be identified and characterized using geophysical measurements such as seismic refraction, galvanic resistivity, and airborne electromagnetic resistivity surveys. Traditional borings can also often be used to identify and characterize permafrost when drilling resistance in the permafrost is different than that of surrounding soil/rock. If the drilling resistance of surrounding ground is similar to that for frozen ground, temperature measurements may be made on recovered samples to identify whether the ground is frozen.

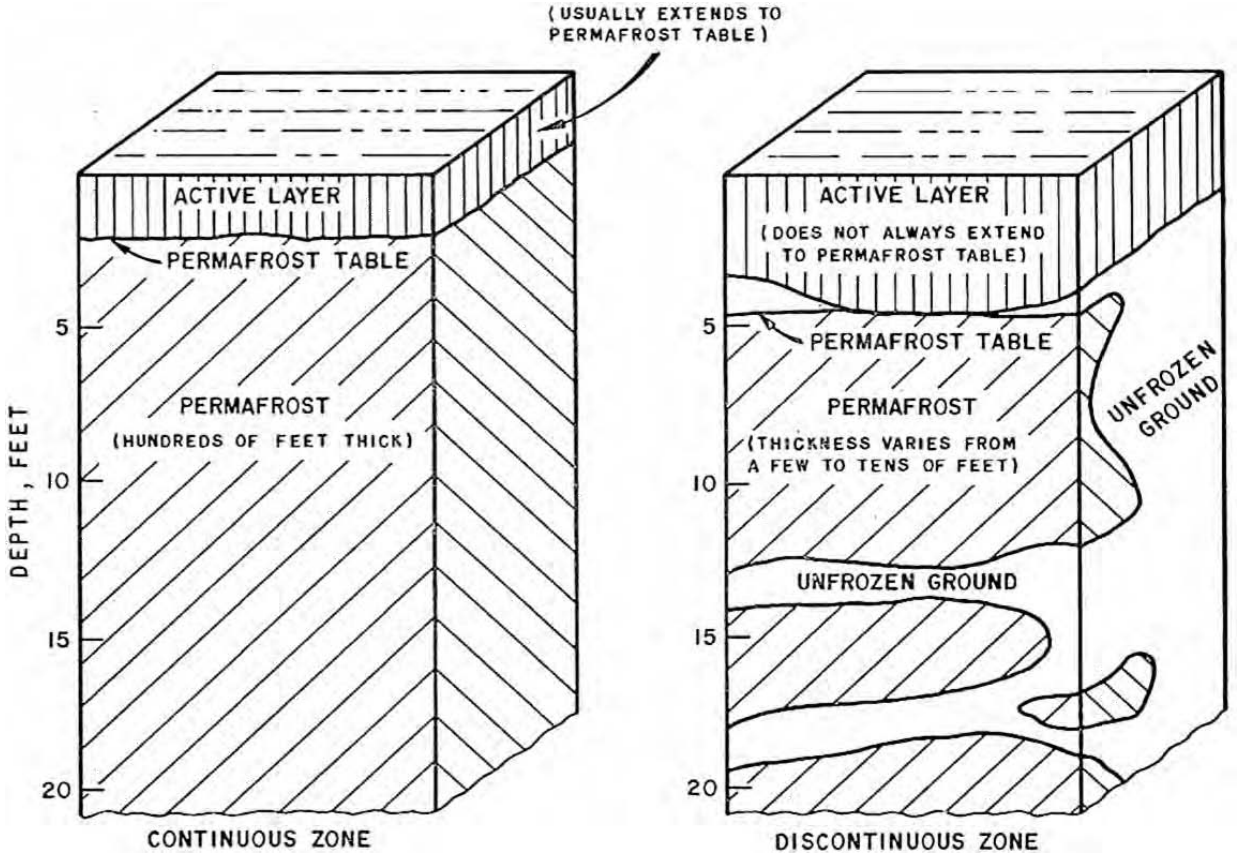


**Figure 5-26 Typical soil profiles in permafrost: continuous permafrost (left) and discontinuous permafrost (right) (from Brown, 1970).**

### 5.15.3 Challenges with Subsurface Investigation and Testing for Permafrost

Subsurface investigations in permafrost are subject to several complications compared to more traditional investigations, most notably dealing with the temperature sensitivity of acquire samples. Permafrost is generally resistant to conventional sample disturbance because of its inherent strength and stiffness. However, thawing of frozen soils, or freezing of unfrozen soils, can severely disturb samples and render them unrepresentative of in situ conditions. Extreme care must therefore be taken to maintain the in situ

condition of acquired samples, whether they be frozen or unfrozen. The strength and stiffness of permafrost is usually sufficient to necessitate coring for collection of samples, which can sometimes thaw portions of acquired core. Relatively large core barrels should therefore be used so that thawed material can be removed prior to testing. Block samples can also be effectively acquired from relatively shallow depths. Pressuremeter tests (PMT) and mechanical cone penetration tests (Schmertmann, 1970a) are sometimes performed in permafrost to avoid challenges associate with sample care or to complement laboratory measurements on collected samples.

Permafrost will often vary substantially in both space and time so it is common to require relatively dense placement of borings in order to characterize localized pockets of ice or unfrozen soils. Variations in the thermal regime with time are commonly needed to characterize seasonal changes in permafrost conditions. Variations in the thermal regime are generally best measured over time using thermocouples or thermistors installed in boreholes at regular depth intervals in a manner similar to what might be used to monitor groundwater conditions using piezometers.

# CHAPTER 6
# MEASUREMENT AND INTERPRETATION OF CONSOLIDATION PROPERTIES OF SOIL

Consolidation properties of fine-grained soils are necessary for estimating the magnitude and time rate of consolidation settlement for shallow foundations, embankments, and retaining walls. Results from consolidation tests are also used to estimate secondary compression and evaluate stress history, which can be used to establish strength characteristics of the same soils. Consolidation properties are traditionally determined in the laboratory using one-dimensional consolidation (oedometer) tests. Interpretation of laboratory-measured properties describing primary consolidation, secondary compression, time rate of consolidation, and stress history for fine-grained soils is presented in this chapter. Methods for estimating preconsolidation stress from various in situ test methods and evaluating the horizontal coefficient of consolidation from in situ pore pressure dissipation tests are also described. Finally, methods for developing preliminary estimates of consolidation properties from empirical correlations are presented.

## 6.1 FUNDAMENTAL CONSOLIDATION CONCEPTS

Consolidation refers to the time dependent decrease in volume of a soil due to an increase in effective stress that results from time dependent dissipation of pore water pressures within the soil. When a soil is loaded, the stresses are initially transmitted to the pore fluid in the soil mass, resulting in "excess" pore pressures that exceed those that existed just prior to loading. As the excess pore pressures dissipate with time, the load is gradually transferred to the soil skeleton, which produces changes in effective stress and a proportionate decrease in volume and water content that produces settlement.

General consolidation characteristics of soils usually dictate whether settlement problems should be anticipated for a particular transportation feature. Gravels, sands, and non-plastic silts consolidate rapidly under load and are often relatively stiff compared to other soil types. These soils seldom present settlement problems unless close tolerances are required or the soil is very loose or heavily loaded. In contrast, plastic silts, clays, and mixtures of clay with other soils consolidate more slowly and may pose settlement problems depending on the stiffness of the soil and the magnitude of loading. Soft silts and clays are especially compressible and often require considerable effort and attention during site characterization, design, and construction to avoid serviceability problems from excessive settlements. Settlement in clayey soils often continues long after construction is complete. Finally, organic soils are usually highly compressible and biodegradable. Consolidation settlement in some organic soils may occur quickly, but secondary compression can result in large settlements that occur for many years.

Laboratory consolidation tests that generally mimic loading applied from earth fills and shallow foundations are commonly conducted on settlement-prone soils. Results from such tests are traditionally presented as a graph of void ratio, $e$, versus the logarithm (base-10) of the vertical effective stress, $\sigma_v'$. Results from an idealized consolidation test are illustrated in Figure 6-1. Initially, the soil undergoes "recompression" at low effective stresses, which represents the elastic response of the soil wherein a small amount of recoverable strain occurs for a given increment of effective stress. The elastic response theoretically continues up to the preconsolidation stress, $\sigma_p'$, after which the soil undergoes much larger deformation for a given increment of effective stress. The response for effective stresses that exceed the preconsolidation stress is traditionally called "virgin" compression and represents plastic (i.e., irrecoverable) deformation. Rebound or swelling response occurs when the soil is unloaded. Rebound response generally occurs along a curve that is essentially parallel to the recompression curve, although some hysteresis is usually observed for unload-reload cycles for actual soils as shown in Figure 6-1.

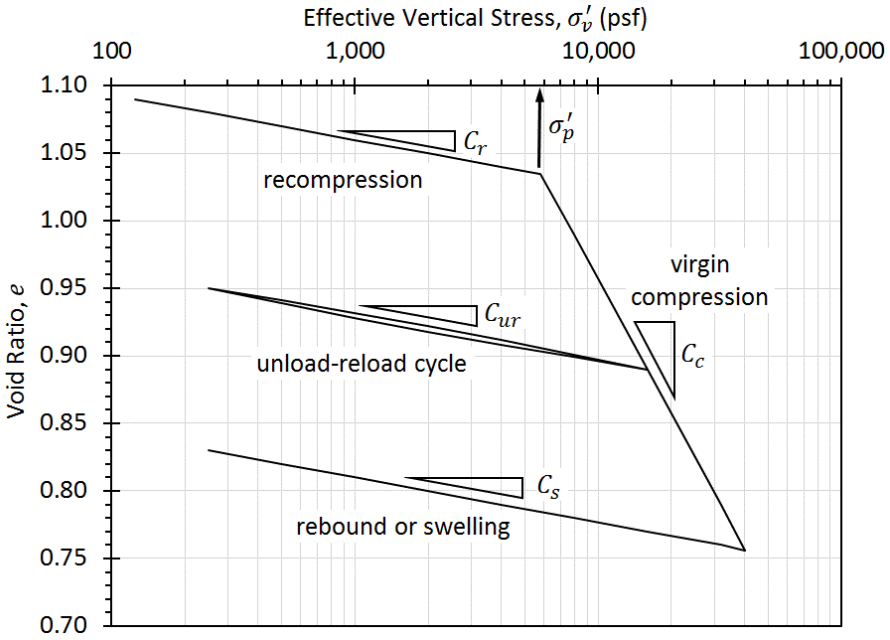


**Figure 6-1 Idealized consolidation test plotted in terms of void ratio.**

The preconsolidation stress, $\sigma_p'$, is technically a yield stress in one-dimensional compression that separates elastic response from plastic response. The preconsolidation stress generally represents the maximum effective stress that the soil has experienced and, thus, is a measure of the stress history for the soil. Soils that are currently subjected to effective stresses that are less than $\sigma_p'$ are said to be "overconsolidated". Soils currently subjected to effective stresses that are greater than or equal to any previously experienced are considered to be "normally consolidated". Loading along the virgin

compression curve causes $\sigma_p'$ to increase according to the magnitude of the effective stress, in what is technically plastic hardening.

The response observed in one-dimensional consolidation tests is generally characterized using compressibility parameters established from plots similar to Figure 6-1. The recompression index, $C_r$, represents the slope of the response in the recompression range of loading while the compression index, $C_c$, represents the slope of the response in the virgin compression range. The preconsolidation stress, $\sigma_p'$, characterizes the boundary between the two loading ranges. The slope of the response during unloading or swelling is often denoted as $C_s$ while the response during an unload-reload cycle is often denoted as $C_{ur}$. As a practical matter, values for $C_r$, $C_s$, and $C_{ur}$ are practically identical and often used interchangeably. Each of the compression indices represent the change in void ratio per log cycle of change in effective stress (i.e., $C = \Delta e / \Delta \log \sigma_v'$).

Consolidation test results are also sometimes plotted using alternative diagrams that are conceptually similar to the $e$ versus log $\sigma_v'$ diagram. Two common alternatives, shown in Figure 6-2, are to plot the vertical strain, $\varepsilon_v = \Delta e/(1 + e_o)$ versus the base-10 logarithm of effective vertical stress, or to plot the specific volume, $v = 1 + e$, versus the natural logarithm (base-$e$) of the effective vertical stress. As shown in Figure 6-2, the compressibility established for the recompression range from graphs of effective vertical stress versus strain is referred to as the modified recompression index or recompression ratio, $C_{r\varepsilon}$. Similarly, the compressibility for the virgin compression range is termed the modified compression index or compression ratio, $C_{c\varepsilon}$. For graphs of specific volume versus the natural log of effective stress, the compressibilities are respectively denoted as $\kappa$ and $\lambda$ for the recompression and virgin compression ranges. The choice of the specific diagram is usually a matter of personal preference, but numeric values established from the different diagrams cannot be used interchangeably. Compressibility values established from the different diagrams are interrelated, however, according to the following equations:

$$C_c = C_{c\varepsilon}(1 + e_o) \tag{6.1}$$

$$C_r = C_{r\varepsilon}(1 + e_o) \tag{6.2}$$

$$C_c = \lambda \cdot \ln(10) \cong 2.3\lambda \tag{6.3}$$

$$C_s \cong \kappa \cdot \ln(10) \cong 2.3\kappa \tag{6.4}$$

where $e_o$ is the initial void ratio. The approximation in the relation between $C_s$ and $\kappa$ is attributed to theoretical considerations (Wood, 1990).

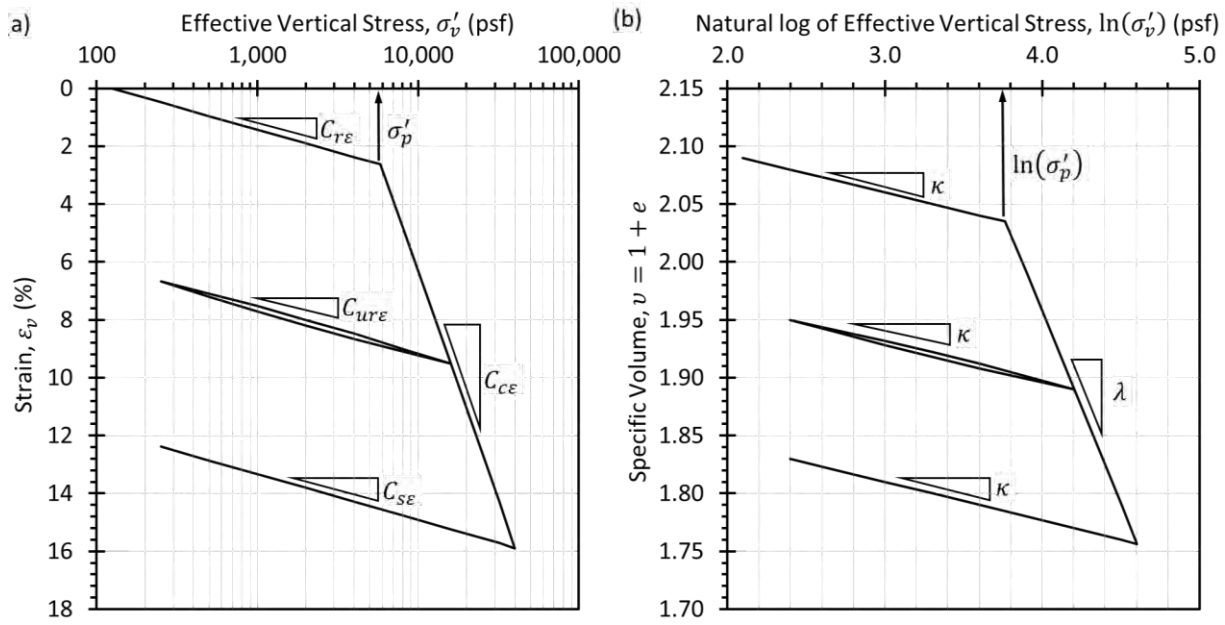


**Figure 6-2 Common alternative presentations for consolidation tests: (a) log of effective vertical stress vs. vertical strain, and (b) natural log of effective vertical stress vs. specific volume.**

The degree of overconsolidation is commonly expressed using the overconsolidation ratio, $OCR$, defined as

$$OCR = \frac{\sigma_p'}{\sigma_{vo}'} \tag{6.5}$$

where $\sigma_{vo}'$ is the current in situ vertical effective stress. In some cases, the degree of overconsolidation may also be expressed using the overconsolidation difference, $OCD$, defined as

$$OCD = \sigma_p' - \sigma_{vo}' \tag{6.6}$$

$OCD$ appears to have been first suggested by Olsen et al. (1986) and is a measure of the additional effective stress that may be applied to a soil before virgin compression occurs. Other important parameters obtained from consolidation tests include the constrained modulus, $M = \Delta\sigma_v/\Delta\varepsilon_v$, and time-dependent consolidation parameters including the coefficient of consolidation, $c_v$, and the coefficient of secondary compression, $C_\alpha$.

## 6.2 BORING AND SAMPLING REQUIREMENTS FOR LABORATORY CONSOLIDATION TESTS

As described subsequently in Section 6.4, laboratory measurements of consolidation properties for many soils are sensitive to the degree of sample disturbance. As such, significant care is required throughout the boring, sampling, transport, sample preparation, and testing process in order to obtain accurate and unbiased measurements of consolidation properties. For soft to medium silts and clays, obtaining high quality samples generally requires using rotary wash boring or hollow-stem auger methods with a heavy drilling mud to reduce stress relief at the base of the borehole (e.g., Ladd and DeGroot, 2003). It also generally requires sampling with thin-walled samplers with low area ratios; at a minimum, nominal 3-inch diameter Shelby tubes should be used and various types of fixed piston samplers are even more desirable. Collected samples should be left in the sampling tubes during transport and storage, and should be kept upright as much as possible. Specimens for testing should be cut from the thin-walled tubes rather than extruded, and testing should generally be completed as promptly as possible. Ladd and Degroot (2003) and Santagata and Germaine (2002) provide additional recommendations for obtaining high quality test specimens. The influence of disturbance is often less significant for stiff soils, in which case some of these requirements can be relaxed; however, practices that produce substantial disturbance like using samplers with high area ratios should be avoided in all soils.

## 6.3 SELECTION OF SAMPLES FOR LABORATORY CONSOLIDATION TESTING

Selection of samples for consolidation testing should be performed deliberately since consolidations tests are relatively time consuming, costly, and important for effective design. Preconsolidation stress (or, alternatively, $OCR$) is perhaps the single most important property measured for sites containing predominantly fine-grained soils because $\sigma_p'$ significantly affects settlement calculations and evaluation of undrained shear strength. The number and location of samples for testing should therefore be selected to facilitate development of a profile of preconsolidation stress with depth as shown in Figure 6-3. Information on subsurface stratigraphy and basic index properties should also be considered with estimates of the in situ vertical effective stress, $\sigma_{vo}'$, to select undisturbed samples for consolidation testing. If the subsurface profile includes several discrete strata, sufficient numbers of samples should be selected within each stratum to capture the variation in consolidation properties for each material. The condition of test specimens should also be assessed during specimen preparation. Specimens that are obviously disturbed, or unrepresentative, should be abandoned and the test re-assigned to a higher quality or more representative sample. The magnitude of disturbance should also be assessed from consolidation test measurements, as described in Section 6.4, to inform interpretations for individual tests.

## 6.4 EFFECTS OF SAMPLING DISTURBANCE

Laboratory consolidation tests require high quality undisturbed soil samples in order to provide accurate measurements of consolidation properties. Even slightly disturbed samples can produce substantial errors in estimates of consolidation properties, primarily because sample disturbance tends to increase the recompression index, reduce the preconsolidation stress, and reduce the compression index. Disturbance is a particular concern in soft and very soft clays, but can be an issue in nearly all soils. As an example, Figure 6-4 shows consolidation test measurements from Bozozuk (1970) for specimens acquired using 5-inch diameter and 2-inch diameter thin-walled tubes in sensitive marine clay. The consolidation curves measured for specimens obtained using the 2-inch diameter tubes are more rounded, and $\sigma_p'$ values are less well-defined, as a result of the greater disturbance induced by the smaller sampling tubes. Lacasse et al. (1985) showed that even large-diameter thin-walled sampling tubes can produce sample disturbance and a reduction in preconsolidation stress in some cases. Landon et al. (2007) showed that drilling method may also influence sample disturbance. Figure 6-5 shows results from consolidation tests on Boston Blue Clay samples collected with a 3-inch diameter fixed piston sampler from borings advanced using drilling mud, with a 3-inch diameter floating piston sampler from borings advanced without the use of drilling mud, and using large diameter block samples. All of these results and many others illustrate the detrimental impact that sample disturbance has on interpretation of consolidation parameters and stress history, and the importance of obtaining high quality samples for consolidation testing.

While highly disturbed samples can sometimes be identified from visual inspection, it is often difficult to identify the degree of sample disturbance from observation alone. However, measurements of volumetric strain, $\varepsilon_{vol}$, during reconsolidation to the in situ vertical effective stress, $\sigma_{vo}'$, can be used to reasonably quantify the degree of sample disturbance. High quality samples show less volumetric strain when reloading to the in situ vertical effective stress than poorer quality samples (Andresen and Kolstad, 1979). Terzaghi et al. (1996) provided criteria for characterizing disturbance using a "specimen quality designation", $SQD$, established from the measured volumetric strain to return to the in situ stress as shown in Table 6-1. The highest quality samples are given an "A" rating while the poorest quality samples are given an "E" rating. Samples for consolidation testing of relatively soft clays should have at least a B rating, meaning that the volumetric strain required to reach the in situ vertical effective stress should be less than 2 percent. Lunne et al. (1997) also proposed an alternative measure for quantifying sample disturbance for soils with $OCR \leq 4$ based on values of $\Delta e/e_o$ required to reach the in situ effective stress, as summarized in Table 6-2.

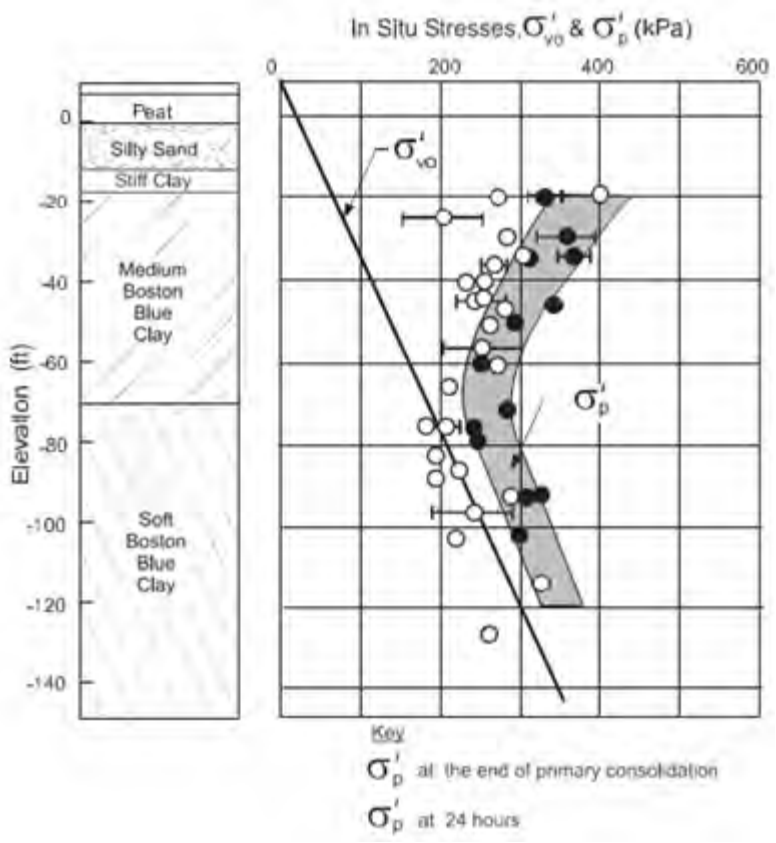


**Figure 6-3 Interpretation of preconsolidation stress from one-dimensional consolidation tests.**

**Table 6-1 Characterization of sample quality from volumetric strain to reach the in situ vertical effective stress (from Terzaghi, et al., 1996).**

| Volumetric Strain (%) | Specimen Quality Designation, $SQD$ |
|---|---|
| 1 | $A$ |
| 1 to 2 | $B$ |
| 2 to 4 | $C$ |
| 4 to 8 | $D$ |
| > 8 | $E$ |

**Table 6-2 Characterization of sample quality from $\Delta e/e_0$ to reach the in situ vertical effective stress (from Lunne, et al., 1997).**

| $\Delta e/e_0$ | | Rating |
|---|---|---|
| $OCR = 1$ *to* $2$ | $OCR = 2$ *to* $4$ | |
| < 0.04 | <0.03 | Very Good to Excellent |
| 0.04 to 0.07 | 0.03 to 0.05 | Good to Fair |
| 0.07 to 0.14 | 0.05 to 0.10 | Poor |
| >0.14 | >0.10 | Very Poor |

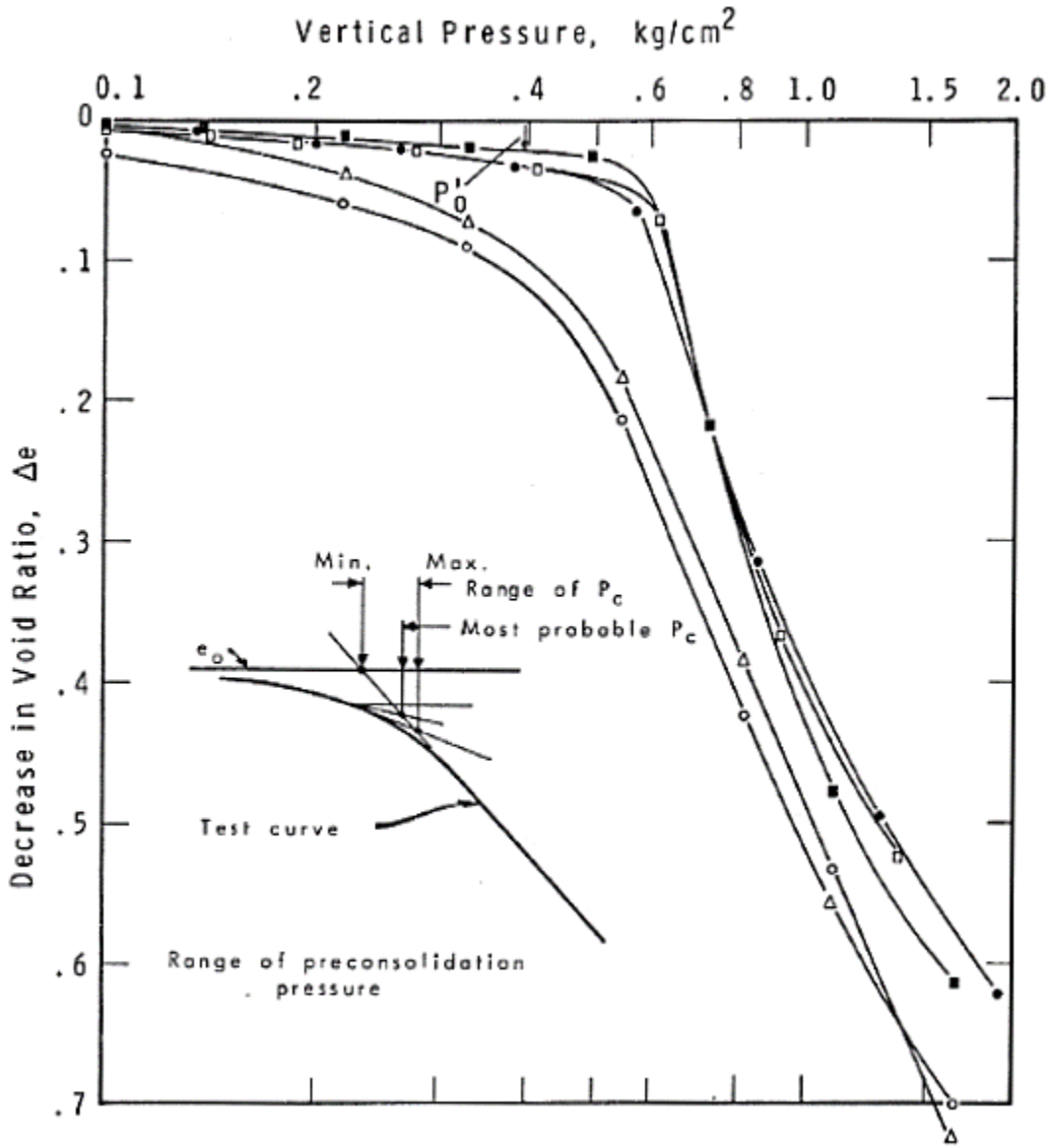


| Code | Number | Depth | Sampling Method | Area of Specimen | Probable $P_c$ |
|---|---|---|---|---|---|
| △ | 164-1-9 | 7.2ft (2.2 m) | 2" dia tube (5 mm) | 20 $cm^2$ | 0.44 tons/$ft^2$ ($kg/cm^2$) |
| ○ | 164-2-1 | 8.2ft (2.5 m) | 2" dia tube (5 mm) | 20 | 0.47 |
| ● | 164-25-3Z | 8.0ft (2.4 m) | 5" dia tube (12 mm) | 20 | 0.59 |
| □ | 164-25-3Y | 8.0ft (2.4 m) | 5" dia tube (12 mm) | 40 | 0.62 |
| ■ | 164-25-3X | 7.8ft (2.4 m) | 5" dia tube (12 mm) | 60 | 0.60 |

**Figure 6-4 Influence of sampling method on consolidation test results (Bozozuk, 1971).**

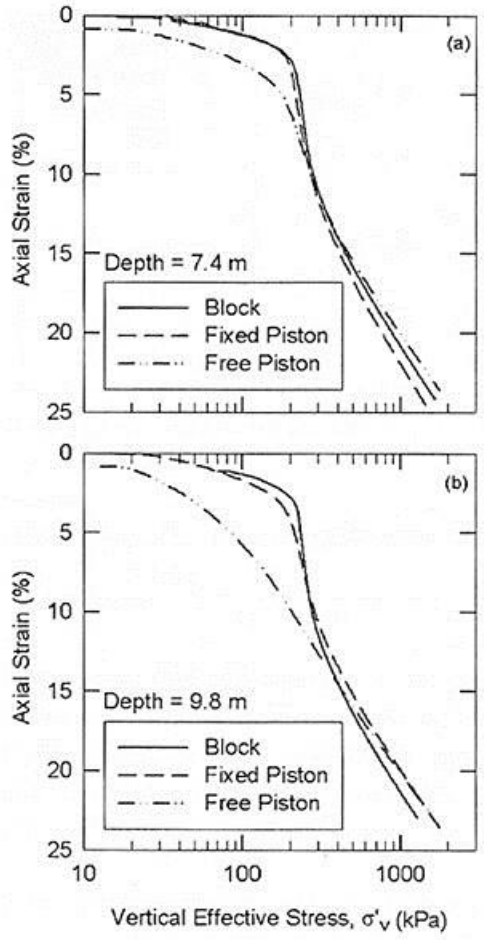


**Figure 6-5 Comparison of consolidation tests for specimens acquired from block samples, fixed piston samples for borings advanced using drilling mud, and free piston samples for borings advanced without drilling mud (from Landon, et al., 2007).**

There is a common misconception that there will be a sharp break in the consolidation curve for fine-grained soils, with a well-defined preconsolidation stress, if high quality samples are used. While this is usually true for soft clays, soils with high silt content or very stiff, non-structured soils may show a more gradual transition from recompression to virgin compression as illustrated in Figure 6-6. While such response is not indicative of disturbance (Boone, 2010), it nevertheless introduces greater uncertainty into establishing the preconsolidation stress than is present for measurements showing a more abrupt transition between recompression and virgin compression.

## 6.5 TYPES OF LABORATORY CONSOLIDATION TESTS

The incremental load (IL) consolidation test (ASTM D2435) is the most common method for measuring consolidation properties in the laboratory in routine practice. An alternative test that is gaining popularity

is the constant rate of strain (CRS) consolidation test (ASTM D4186). The CRS consolidation test applies loading continuously while measuring stress and pore water pressure, thereby reducing testing times from 1 to 2 weeks for conventional IL consolidation tests to a few days or less for CRS consolidation tests.

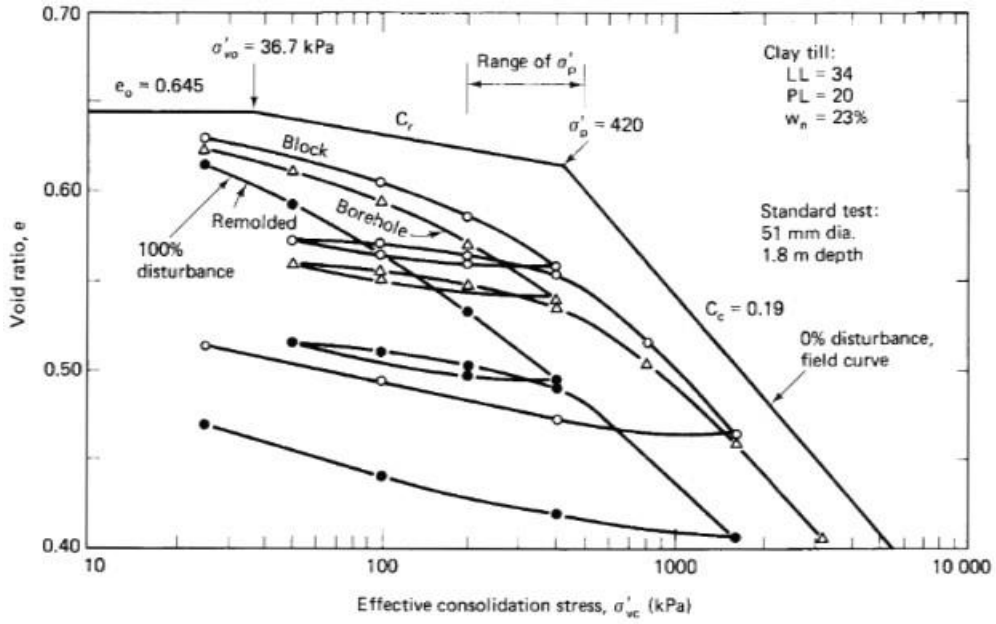


**Figure 6-6 Results from consolidation tests for samples of stiff glacial till of varying quality (from Holtz and Kovacs, 1981; after Soderman and Kim, 1970).**

### 6.5.1 Incremental Load Consolidation Test

The incremental load (IL) consolidation test standardized in ASTM D2435 is the most frequent test used in practice. In the IL test, loads are incrementally applied to a specimen placed within an open cell that laterally confines the specimen as shown in Figure 6-7. Loads are applied using dead weights and a mechanical lever arm, or using pneumatic or hydraulic actuators. The time-deformation response is measured for each load increment and measurements from a collection of load increments are combined to produce the overall consolidation curve, as shown in Figure 6-8. Each load increment in an IL test is maintained for a sufficient period for the end of primary consolidation to be complete (i.e. for complete dissipation of excess pore water pressures). In many cases, the load is held for 24 hours as a matter of convenience and the data are used to establish the time at the end of primary consolidation for each increment in order to plot the consolidation curve that represents the end of primary consolidation.

For all consolidation tests, it is important that specimens be loaded to stress levels much greater than the estimated preconsolidation stress, $\sigma_p'$, to facilitate accurate evaluation of $\sigma_p'$. The standard loading

schedule for IL tests consists of doubling the applied load for each successive increment, which gives a "load increment ratio" of 1. Smaller load increments are sometimes desirable to better define $\sigma_p'$. An unload-reload cycle is also often desirable after exceeding $\sigma_p'$ to better define the recompression behavior, which may be influenced by disturbance and can be difficult to establish from the initial recompression loading.

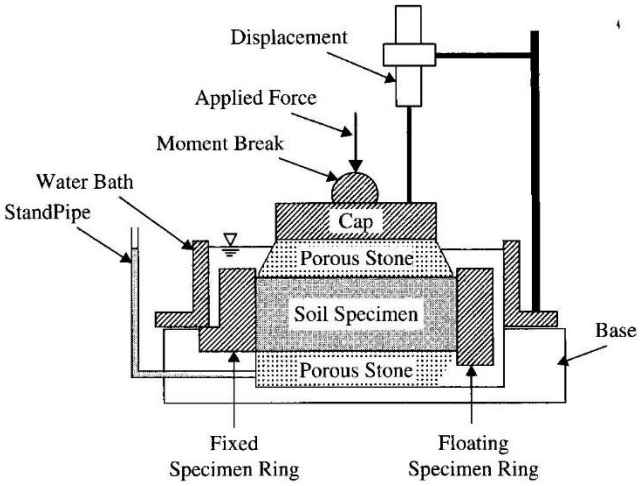


**Figure 6-7 Schematic of incremental load oedometer cell (from Germaine and Germaine, 2009).**

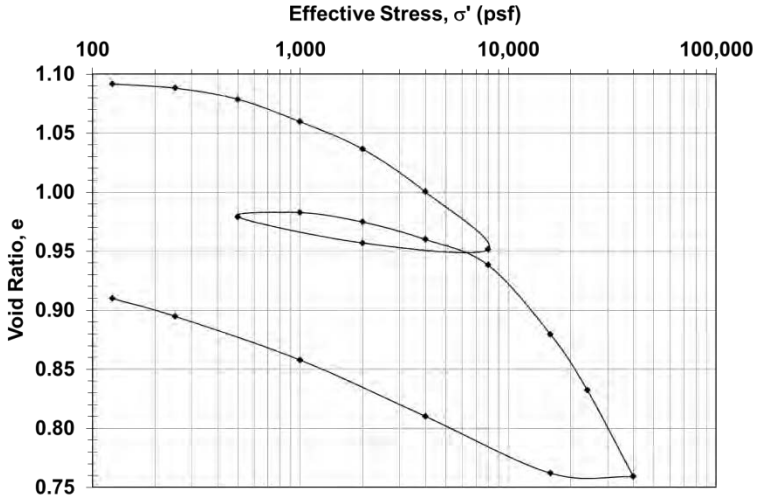


**Figure 6-8 Measured response from an incremental load consolidation test.**

In recent years, automated incremental load consolidation test devices have been developed to reduce the time required to measure the entire consolidation curve. With these devices, successive load increments are applied as soon as primary consolidation is complete rather than waiting for 24 hours before applying the next load increment. Such automation may substantially reduce testing times, although not as much as with CRS consolidation tests, while still maintaining traditional methods of interpretation.

### 6.5.2 Constant Rate of Strain Consolidation Test

An alternative to incremental load consolidation tests is the "constant rate of strain" (CRS) consolidation test described in ASTM D4186. The CRS test uses a sealed cell that restrains the specimen laterally and allows for measurement of pore water pressure that is generated during the test, as shown in Figure 6-9. Drainage is provided on one end of the specimen and the cell has provisions to apply back pressure to saturate the specimen. CRS tests are performed by placing the cell in a computer-controlled load frame that axially deforms the specimen at a constant rate while time, axial deformation, reaction force, chamber pressure, and pore water pressure are measured. One advantage of CRS tests is that they can often be completed in 24 to 48 hours as compared to several weeks for a traditional IL test, depending on the number of load increments and unload-reload cycles. CRS tests also produce a practically continuous measurement of the consolidation curve, as shown in Figure 6-10. The disadvantage of the test is that the equipment is relatively expensive and data analysis is slightly more complicated than for IL tests. Studies have shown that the consolidation response measured is CRS-type consolidation tests is generally consistent with that obtained from IL-type consolidation tests (e.g., Sheahan and Watters, 1997). One disadvantage of the CRS test is that it does not generally allow for evaluation of secondary compression characteristics of soil specimens.

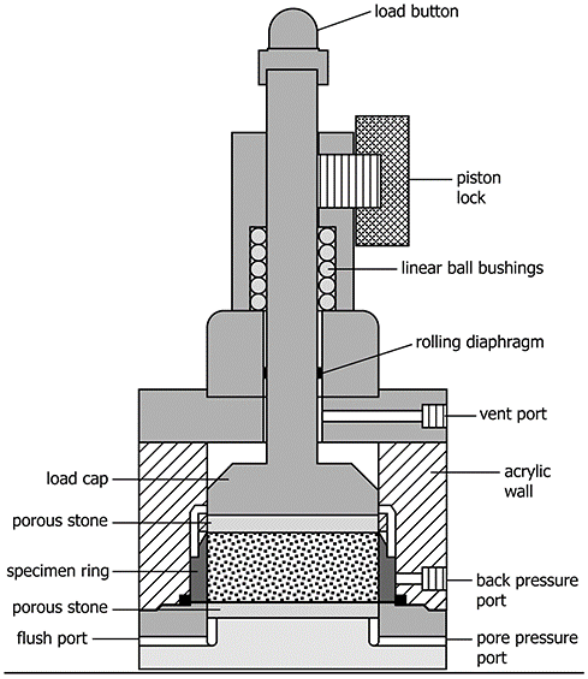


**Figure 6-9 Schematic of CRS oedometer cell (ASTM D4186, 2012).**

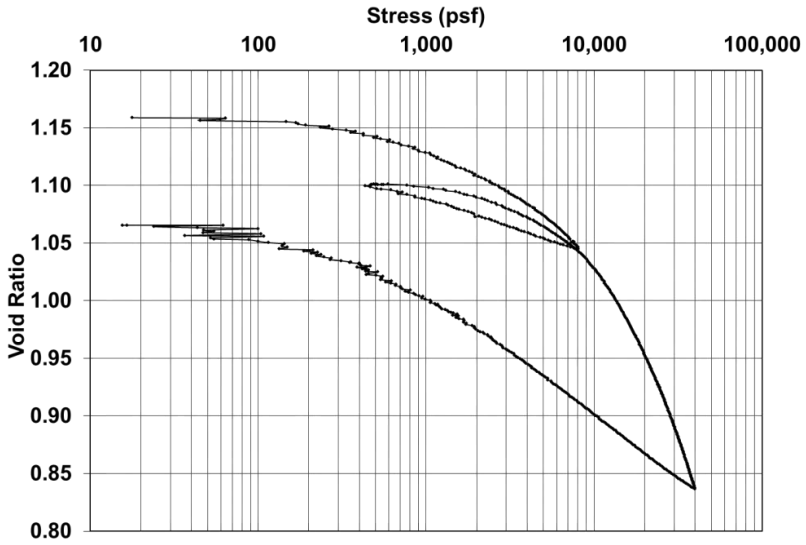


**Figure 6-10 Measured response from a CRS consolidation test.**

## 6.6 EVALUATION OF PRECONSOLIDATION STRESS FROM LABORATORY CONSOLIDATION TESTS

Preconsolidation stress is commonly interpreted from the measured response observed in one-dimensional consolidation tests. While estimates for $\sigma_p'$ can sometimes be established by inspection of the measured response, it is preferable that $\sigma_p'$ be established using one of several standard methods described in this section. Regardless of the quality of specimens and the specific interpretation procedure used, interpretations of $\sigma_p'$ are generally subject to considerable uncertainty that arises because judgment is required for interpretation and because interpretations are often made using log-scale graphs (Boone, 2010). Sample disturbance tends to increase this uncertainty and will often "lower" the overall $e - \log \sigma_v'$ curve relative to field conditions. Consequently, the value of $\sigma_p'$ is often underestimated from routine laboratory testing and interpretation.

### 6.6.1 Interpretation of Preconsolidation Stress Using Casagrande Method

Although several methods are available (Grozic, et al., 2003; Boone, 2010), preconsolidation stress is most commonly interpreted based on the measured $e - \log \sigma_v'$ relationship and the Casagrande (1936) graphical technique illustrated in Figure 6-11. In many clays and silts, this approach may be adequate for evaluating a reasonable value of $\sigma_p'$ for engineering purposes. The steps involved in the Casagrande method include:

1. Construct a line tangent to the steepest portion of the consolidation curve within the normally consolidated range of loading.
2. Locate the point of maximum curvature of the measured consolidation curve for stresses where the slope transitions from shallow to steep. Construct a horizontal line from this point of maximum curvature.
3. Construct a line tangent to the curve at the point of maximum curvature.
4. Construct a line that bisects the angle between the horizontal line constructed in Step 2 and the tangent line constructed in Step 3.
5. The stress value at the intersection between the bisector line (Step 4) and the first tangent line (Step 1) is taken to be the preconsolidation pressure.

Step 2 involves considerable judgment and should be performed carefully. In cases where the point of maximum curvature is unclear, several alternative interpretations of this point should be considered to establish a reasonable range of estimates for the preconsolidation stress.

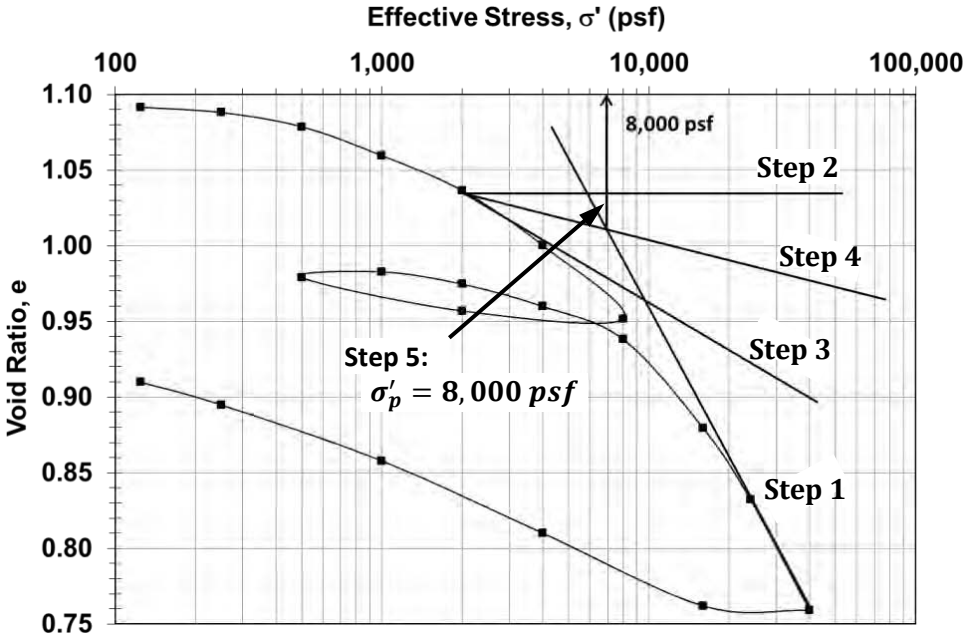


**Figure 6-11 Illustration of Casagrande method for interpreting preconsolidation stress.**

### 6.6.2 Interpretation of Preconsolidation Stress Using Strain Energy Method

Alternative graphical techniques can sometimes be utilized to better delineate the magnitude of $\sigma'_p$, particularly when the value for $\sigma'_p$ is not clearly indicated in the $e - \log \sigma'_p$ curve. One such method is the strain-energy method (Becker, et al., 1987). The strain-energy method involves plotting the cumulative

strain energy (i.e., the product of stress times strain) for each load increment in a laboratory consolidation test. The stress where a large incremental increase in strain energy is observed is taken to represent $\sigma_p'$ for the soil. The strain-energy method is outlined below:

1. Compute the increment of work, $\Delta W$, for each strain increment according to:

$$\Delta W = \left(\frac{\sigma_f' + \sigma_i'}{2}\right)(\varepsilon_f - \varepsilon_i) \tag{6.7}$$

   where $\sigma_i$ and $\sigma_f$ are stresses at the beginning and end of the loading increment, respectively, and $\varepsilon_i$ and $\varepsilon_f$ are strains (dimensionless) at the beginning and end of the increment, respectively.
2. Plot the cumulative strain energy versus the effective stress as shown in Figure 6-12. For plotting purposes, the stress value corresponding to the summation of work is taken to be the stress at the end of the loading increment. A noticeable change in slope should be evident at $\sigma_p'$.
3. The numeric values of $\sigma_p'$ should be established by constructing trend lines through the data at low stresses (slope 1) and high stresses (slope 2). The stress where these two trend lines intersect is taken to be the preconsolidation stress.

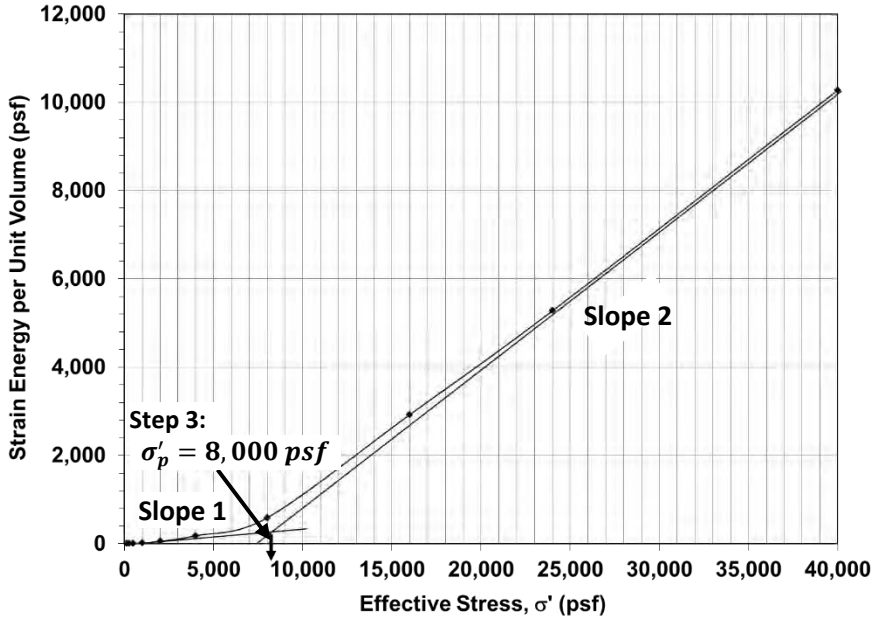


**Figure 6-12 Illustration of strain-energy method for interpreting preconsolidation stress.**

The strain energy method is somewhat subjective in that it involves interpretation of slopes for the respective portions of the curves, similar to what is done in the Casagrande method. However, the strain energy interpretation is conducted using an arithmetic scale, which does not compound slight differences

in interpretation, and has been found to produce more consistent results than the Casagrande method (Grozic, et al., 2003). The strain-energy method also tends to work better for consolidation curves that are more "rounded". Interpretations from either the Casagrande or strain-energy methods for determining preconsolidation pressure may be used to calculate the overconsolidation ratio, $OCR$, and to assign terminology based on the stress history of the soils as shown in Table 6-2.

**Table 6-3 Soil terminology applied to stress history.**

| $OCR$ | Terminology | Abbreviation |
|---|---|---|
| 1 | Normally Consolidated | NC |
| $1 < OCR < 2$ | Lightly Overconsolidated | LOC |
| $2 < OCR < 8$ | Moderately Overconsolidated | MOC |
| $OCR > 8$ | Heavily Overconsolidated | HOC |

### 6.6.3 Influence of Strain Rate and Temperature

Like many other characteristics of fine-grained soils, $\sigma_p'$ may be influenced by the strain rate and temperature used in the laboratory test procedure. Figure 6-13 and 6-14 respectively show how $\sigma_p'$ is influenced by strain rate and temperature. As a general rule, $\sigma_p'$ is observed to decrease by approximately 10 percent for every log-cycle reduction in strain rate while $\sigma_p'$ tends to increase by approximately 10 percent for every 12 degree drop in temperature (Laloui, et al., 2008). As a practical matter, these effects often partially offset each other since normal laboratory testing temperatures produce $\sigma_p'$ that are likely lower than in the field while normal laboratory testing strain rates produce $\sigma_p'$ that are likely greater than observed in the field. Given the uncertainty present in establishing appropriate values for $\sigma_p'$, effects of strain rate and temperature can often be neglected unless extreme strain rates or temperatures are encountered or anticipated.

## 6.7 EVALUATION OF COMPRESSION AND RECOMPRESSION INDICES FROM LABORATORY CONSOLIDATION TESTS

Values for the compression index, $C_c$, and recompression index, $C_r$, or related values for $C_{c\varepsilon}$ and $C_{r\varepsilon}$ or $\lambda$ and $\kappa$, respectively, define the slopes of the virgin compression and recompression portions of the consolidation curve as described in Section 6.1. Values for $C_c$ should be evaluated by drawing a best-fit line tangent to the measured $e - \log \sigma_v'$ response along the virgin compression portion of the curve. The modified compression index, $C_{c\varepsilon}$, should be similarly evaluated from a plot of $\varepsilon_v$ versus $\log \sigma_v'$, and values for $\lambda$ should be similarly determined from a graph of $\upsilon$ versus $\ln \sigma_v'$.

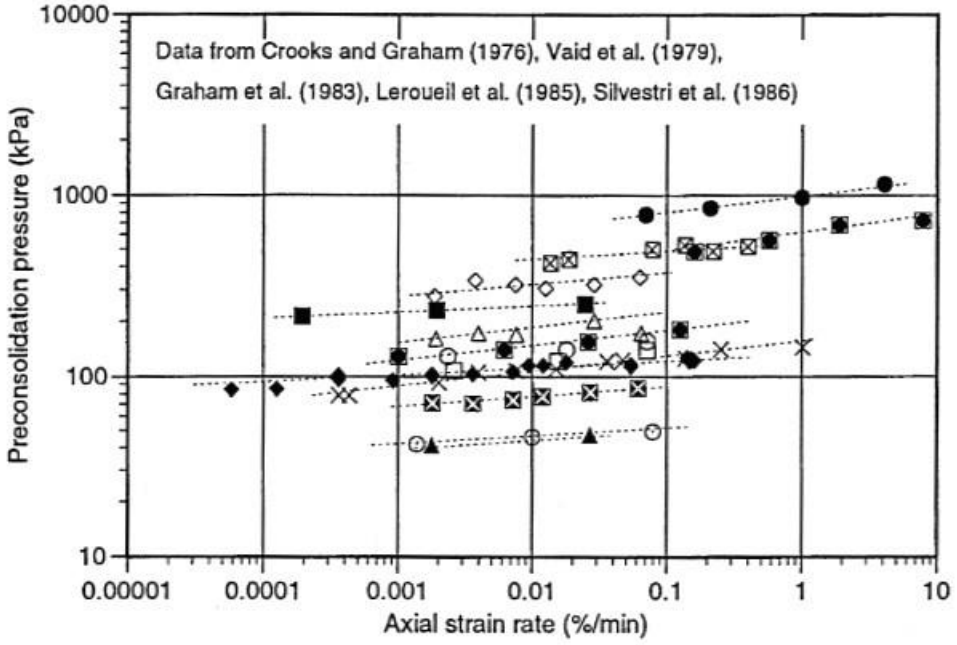


**Figure 6-13 Influence of strain rate on interpreted preconsolidation stress for several clays (Soga and Mitchell, 1996).**

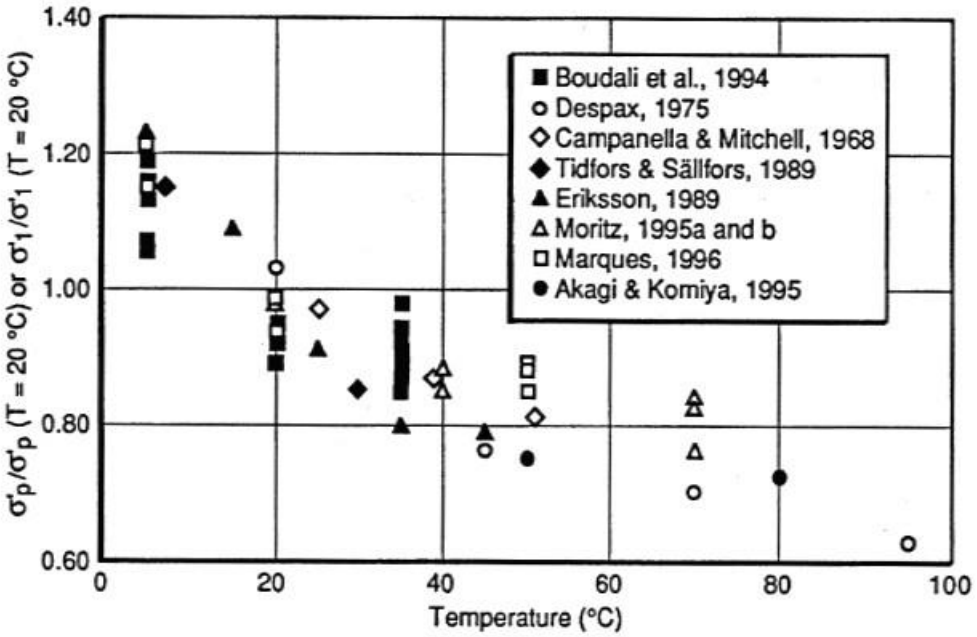


**Figure 6-14 Variation in preconsolidation stress with temperature for several clays (from Leroueil and Marques, 1996).**

Values for $C_r$ (or $C_{r\varepsilon}$ or $\kappa$) can be established by fitting a line tangent to the initial reloading portion of the appropriate consolidation curve. However, the initial portion of the measured consolidation curve is often unrepresentative of recompression in situ because of sample disturbance and other factors (Leonards,

1976). As such, values for $C_r$ (or $C_{r\varepsilon}$ or $\kappa$) are preferably evaluated from the slope of the rebound portion of the test or, even better, the slope observed during an unload-reload cycle.

As previously discussed, measured $C_c$ (or $C_{c\varepsilon}$) values from disturbed samples will usually be lower than those measured for higher quality samples. Reasonable estimates for $C_c$ will usually be obtained for samples with $SQD$ of $A$ or $B$ as defined in Table 6-1. Effects of sample disturbance can also be limited by loading specimens to stress levels that are substantially greater than $\sigma_p'$ and fitting the tangent line to the consolidation curve at high stress levels. In cases where such high stress levels cannot be achieved (e.g., for heavily overconsolidated samples), the slope used to establish $C_c$ should be appropriate for the stress range defined by the interpreted $\sigma_p'$ and the anticipated final effective stresses in the ground.

## 6.8 TANGENT MODULUS METHOD FOR INTERPRETING CONSOLIDATION TEST RESULTS

An alternative method for evaluating results from one-dimensional consolidation tests is the tangent modulus method (Janbu, 1967; Janbu, 1969). In this approach, consolidation measurements are plotted as strain, $\varepsilon_v$, versus effective vertical stress, $\sigma_v'$, on an arithmetic scale, as shown in Figure 6-15. The inverse of the slope of this curve is the tangent modulus, $M = d\sigma_v'/d\varepsilon$, which is a constrained modulus for the one-dimensional consolidation test. The tangent modulus determined from the slope of the measured strain versus effective stress response for a number of effective stress levels is then replotted versus the effective stress as shown in Figure 6-16.

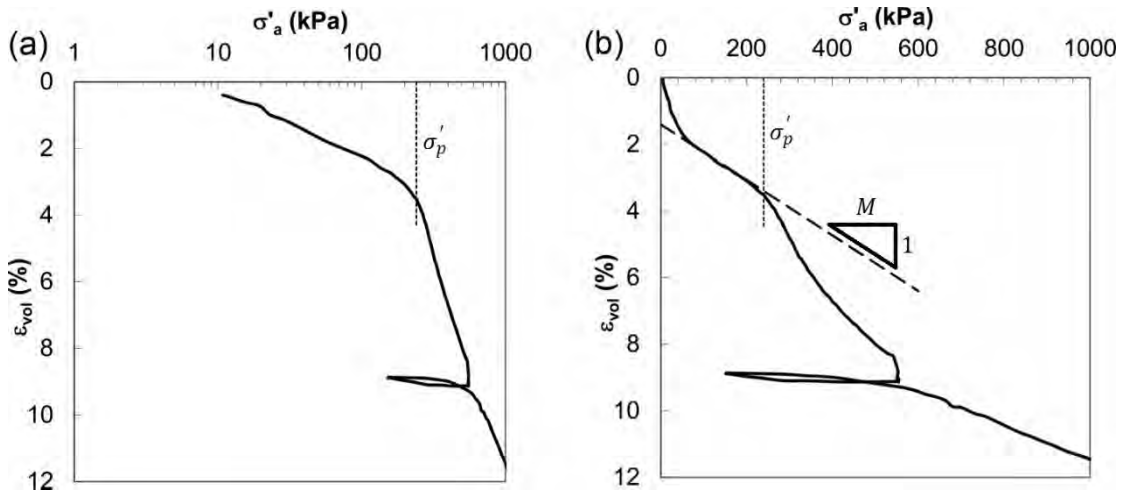


**Figure 6-15 Consolidation test measurements plotted as stress versus strain using: (a) logarithmic scale, and (b) arithmetic scale (adapted from Karlsrud and Hernandez-Martinez, 2013).**

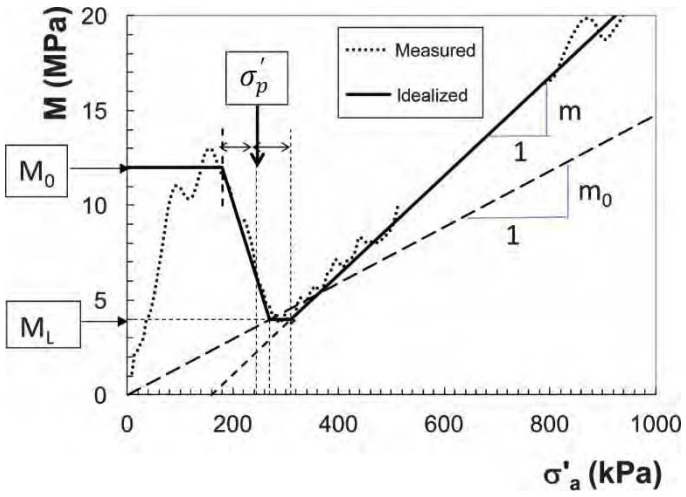


**Figure 6-16 Tangent modulus vs. effective stress showing estimate for preconsolidation stress (adapted from Karlsrud and Hernandez-Martinez, 2013).**

Janbu (1967) found that the tangent modulus, $M$, can be generally expressed using an exponential function of vertical effective stress as

$$M = m \cdot p_a \left(\frac{\sigma_v'}{p_a}\right)^{1-a} \tag{6.8}$$

where $m$ is a modulus number, $a$ is a stress exponent, and $p_a$ is atmospheric pressure (100 kPa = 14.7 psi) in the same units as stress. Equation 6.8 can be further simplified by fitting curves with the stress exponent $a$ equal to either 1, 0.5, or 0 to represent the initial elastic portion of the curve, the transition between elastic and plastic behavior, and the plastic portion of the curve, respectively. Thus, Equation 6.8 reduces to the following for different ranges of effective stresses:

$$M = m \cdot p_a = constant \qquad \text{(elastic behavior, } a = 1\text{)} \tag{6.9a}$$

$$M = m \cdot p_a \sqrt{\frac{\sigma_v'}{p_a}} \qquad \text{(elastic-plastic behavior, } a = 0.5\text{)} \tag{6.9b}$$

$$M = m \cdot p_a \left(\frac{\sigma_v'}{p_a}\right) \qquad \text{(plastic behavior, } a = 0\text{)} \tag{6.9c}$$

The tangent modulus approach is attractive since it uses units of strain that are familiar to engineers and there is no need to present test results in terms of void ratio.

The graph of tangent modulus versus effective stress can also be used to interpret $\sigma_p'$ as shown in Figure 6-16. Over the recompression range of stresses, the soil behaves elastically, with a practically constant

tangent modulus shown as $M_o$ in the figure. In the virgin compression range, the soil behaves plastically, with an initially low tangent modulus indicated as $M_L$ in the figure and increasing tangent modulus for increasing stresses. The preconsolidation stress separates the ranges of elastic and plastic behavior and is generally estimated to be the stress where there is a notable drop in the tangent modulus, or where the tangent modulus starts to increase linearly with stress as shown in Figure 6-16. In some cases, estimates of $\sigma_p'$ can also be established directly from the stress-strain response as shown in Figure 6-15.

## 6.9 ADJUSTMENT OF LABORATORY CONSOLIDATION TESTS TO OBTAIN FIELD CONSOLIDATION CURVE

Even with high quality sampling, and careful handling and trimming, the laboratory consolidation test is still a reloading test since the soil specimen has been removed from its in situ stress environment. This means that the actual in situ field consolidation curve will be somewhat different than what is measured in a laboratory consolidation test. Schmertmann (1955) suggested a relatively simple graphical method to correct laboratory consolidation curves to obtain more realistic field consolidation curves. The method adjusts for some disturbance from sampling, handling, and trimming that may not be obvious. The method is slightly different for normally consolidated soils and overconsolidated soils.

For normally consolidated soils, the procedure is illustrated in Figure 6-17 and includes the following steps:

1. Perform the Casagrande graphical construction to obtain the preconsolidation stress, $\sigma_p'$.
2. Calculate the initial void ratio, $e_o$. Draw a horizontal line from $e_o$, parallel to the effective stress axis, to the preconsolidation stress, $\sigma_p'$. This defines Point 1 in Figure 6-17.
3. Draw a horizontal line parallel to the effective stress axis at a void ratio of $e = 0.42 \cdot e_o$. Where this line intersects the extension of the measured virgin compression curve defines Point 2 in Figure 6-17.
4. Connect Points 1 and 2 with a straight line, $F$, to produce the estimated field virgin consolidation curve.

For overconsolidated soils, the procedure is illustrated in Figure 6-18 and includes the following steps:

1. Perform the Casagrande graphical construction to obtain the preconsolidation stress, $\sigma_p'$.
2. Calculate the initial void ratio, $e_o$. Draw a horizontal line from $e_o$, parallel to the effective stress axis, to the in situ vertical effective stress, $\sigma_{vo}'$. This defines Point 1 in Figure 6-18.

3. From Point 1, draw a line parallel to the measured unload-reload curve to the preconsolidation stress, $\sigma_p'$. This defines Point 2 in Figure 6-18.
4. Draw a horizontal line parallel to the effective stress axis at a void ratio of $e = 0.42 \cdot e_o$. Where this line intersects the extension of the laboratory virgin compression curve defines Point 3 in Figure 6-18.
5. Connect Points 1 and 2, and Points 2 and 3 by straight lines. The slope of the line connecting Points 1 and 2 is the estimated in situ recompression curve whereas the slope of the line connecting Points 2 and 3 represents the field virgin consolidation curve.

Note that the slope of the unload-reload cycle is used to establish the slope of the recompression range of loading ($C_r$) because the slope of the unload-reload curve is generally a better representation of recompression behavior for the soil than the initial recompression curve.

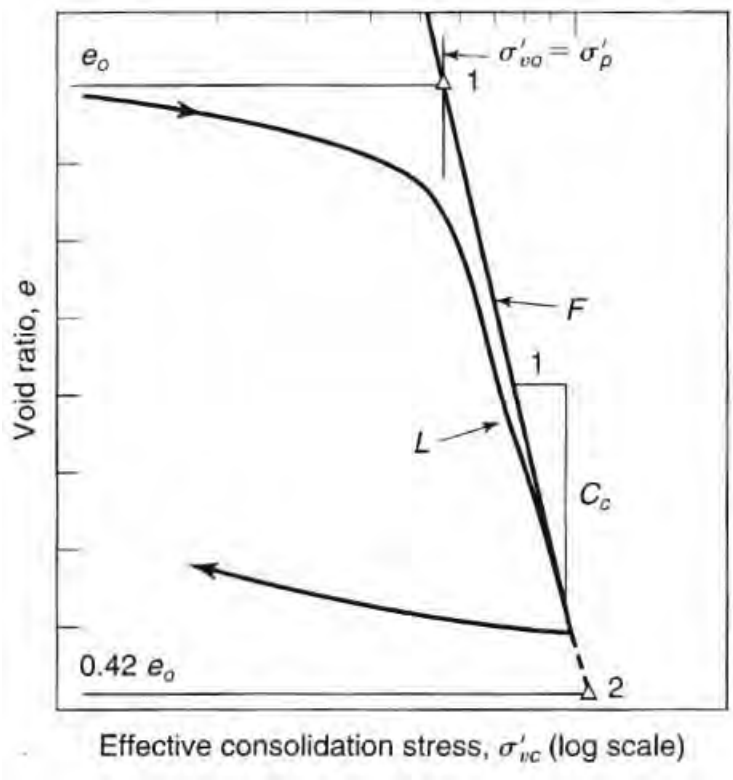


**Figure 6-17 Schmertmann (1955) method to obtain field consolidation curve for normally consolidated soils (from Holtz, et al., 2011).**

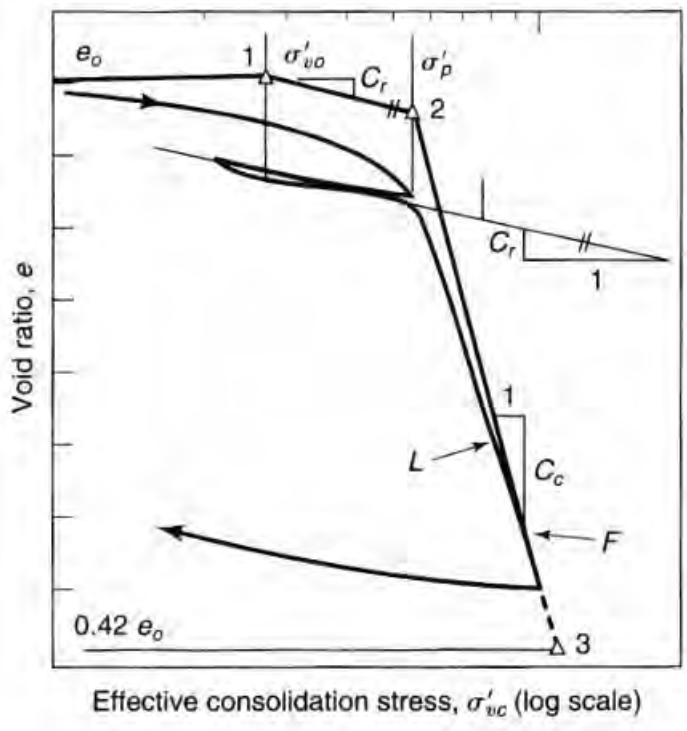


**Figure 6-18 Schmertmann (1955) method to obtain field consolidation curve for overconsolidated soils (from Holtz, et al., 2011).**

## 6.10 EVALUATION OF COEFFICIENT OF CONSOLIDATION FROM LABORATORY CONSOLIDATION TESTS

The time rate of settlement is typically represented in geotechnical practice via the coefficient of vertical consolidation, $c_v$, and the coefficient of horizontal consolidation, $c_h$. The parameter $c_v$ is appropriate for evaluating time rate of settlement for shallow foundations and large earth fills whereas $c_h$ is appropriate for estimating pore pressure dissipation around driven piles and designing prefabricated vertical drains (PVD). The coefficient of consolidation measured in laboratory one-dimensional consolidation tests is generally $c_v$ since the test enforces vertical drainage conditions. In some cases, $c_h$ can be measured in laboratory one-dimensional consolidation tests if test specimens are trimmed such that drainage in the test corresponds to horizontal drainage in situ. Unfortunately, such tests are rarely performed.

Historically, graphical procedures are used to evaluate $c_v$ from laboratory incremental load consolidation test measurements. The two most common procedures include: (1) Casagrande's logarithm of time method, and (2) Taylor's square root of time fitting method. Several additional methods listed in Table 6-4 have been proposed that appear to give equally valid results. Both Casagrande's method and Taylor's

method are described in AASHTO T216 and ASTM D2435 and are summarized here. Interested readers may consult the references given in Table 6-4 for details on other methods.

**Table 6-4 Alternative methods for determining the coefficient of consolidation, $c_v$.**

| Method | References |
|---|---|
| Casagrande's Log Time Method | Casagrande and Fadum (1940) |
| Taylor's Square Root of Time Method | Taylor (1948)<br>Robinson and Allam (1996)<br>Tewatia and Venkatachalam (1997)<br>Feng and Lee (2001) |
| Inflection Point Method | Cour (1971)<br>Messi et al. (1999) |
| Velocity Method | Parkin (1978, 1981)<br>Pandian et al. (1994)<br>McKinley and Sivakumar (2009) |
| Rectangular Hyperbola Method | Sridharan et al. (1987) |

### 6.10.1 Casagrande's Log Time Method

Casagrande's method uses a plot of deflection versus the logarithm of time, as shown in Figure 6-19. The method uses the time to complete 50 percent primary consolidation, $t_{50}$, to compute the coefficient of consolidation, $c_v$, according to:

$$c_v = \frac{T_{50} H_{dr}^2}{t_{50}} \tag{6.10}$$

where $T_{50}$ is the theoretical time factor to reach 50 percent consolidation (=0.197), $H_{dr}$ is the drainage height, and $t_{50}$ is the time required to achieve 50 percent primary consolidation. $H_{dr}$ is equal to one-half the average thickness of the test specimen during a given load increment for a double-drained specimen. The Casagrande method requires that a substantial portion of the consolidation curve be defined after 50 percent consolidation is complete to facilitate a good approximation of $t_{50}$. The method also requires a simple graphical procedure to obtain the initial, or zero reading since this cannot be plotted on a log scale.

### 6.10.2 Taylor's Square Root of Time Method

For Taylor's method, the deflection is plotted versus the square root of time as shown in Figure 6-20. The time for 90 percent primary consolidation, $t_{90}$, is obtained by plotting a line with a slope that is 1.15 times the slope of the initial straight line section. $t_{90}$ is taken to correspond to the point where this line intersects the time rate of consolidation curve. The coefficient of consolidation is then calculated according to:

$$c_v = \frac{T_{90} H_{dr}^2}{t_{90}} \tag{6.11}$$

where $T_{90}$ is the theoretical time factor for 90 percent consolidation, taken as 0.848. For the square root of time method, the test does not need to be carried out beyond $t_{90}$ to compute a value for $c_v$.

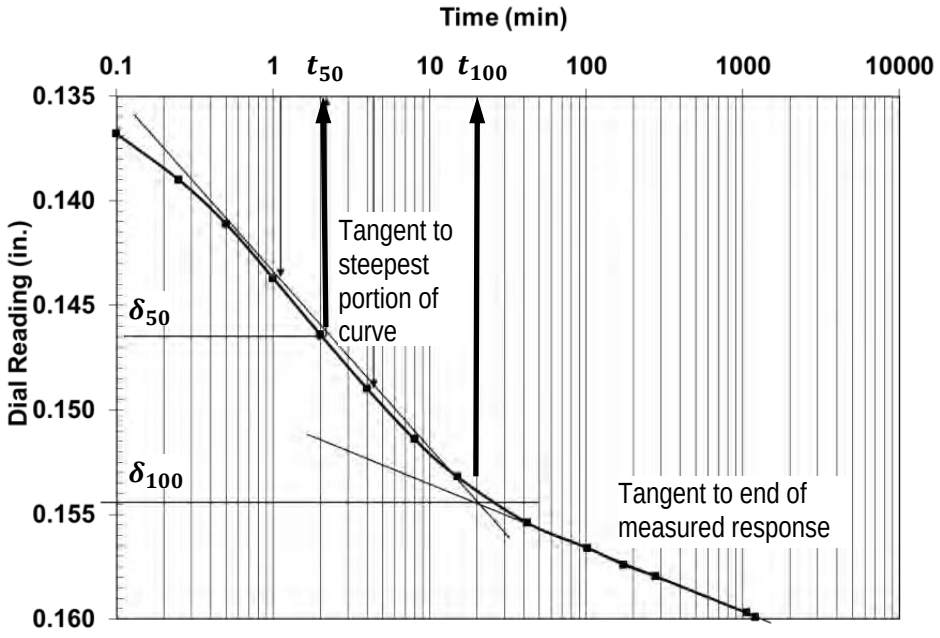


**Figure 6-19 Casagrande's log time method for determining the coefficient of consolidation.**

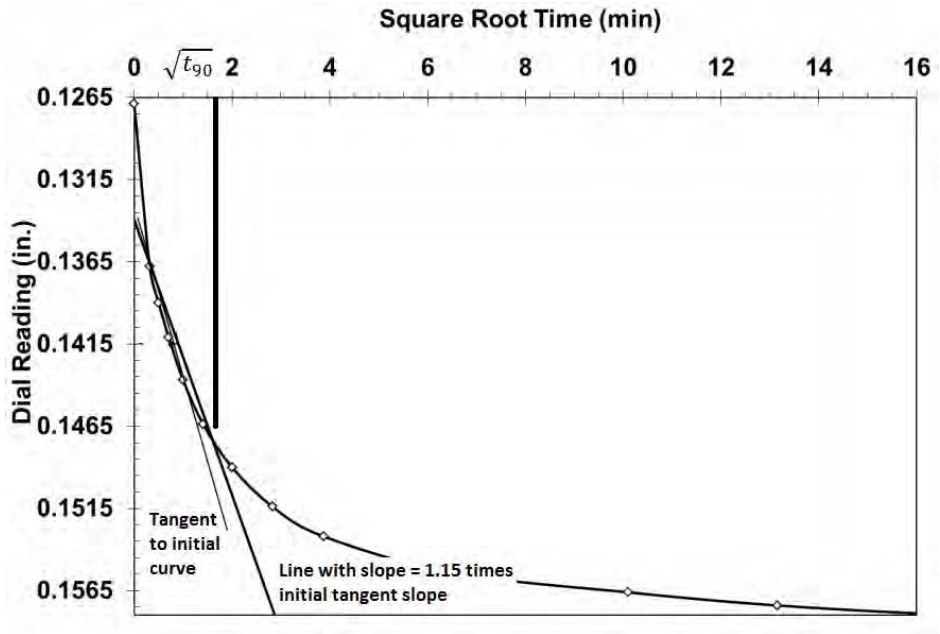


**Figure 6-20 Taylor's square root of time method for determining the coefficient of consolidation.**

Values for $c_v$ should be calculated for each load increment in a consolidation test and plotted as a function of $\log \sigma'_v$ as shown in Figure 6-21. Both graphical methods are approximate and will result in different

calculated values for $c_v$ for the same test measurements. Measurements for high quality specimens will typically exhibit a sharp reduction in calculated $c_v$ values near the preconsolidation stress. For load increments less than $\sigma_p'$, consolidation occurs relatively rapidly and $c_v$ values can be relatively high. Values for $c_v$ will be lowest for effective stresses that exceed $\sigma_p'$.

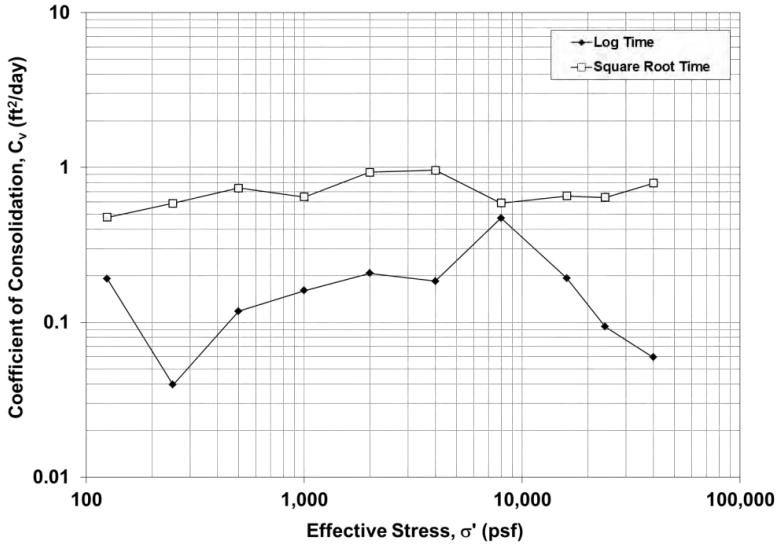


**Figure 6-21 Coefficients of consolidation determined using the log time and square root time methods for different applied effective stress.**

For some soils, such as those that undergo significant secondary compression, these graphical methods may be difficult to implement because the deformation versus time response may not "look" as expected. In such cases, it is often helpful to utilize multiple methods, potentially including alternative methods summarized in Table 6-4, to aid in establishing an appropriate value for $c_v$.

Significant scatter of calculated $c_v$ values in the overconsolidated range may result from the following: (1) consolidation occurs quite rapidly at these load levels making determination of the time to the end of primary consolidation difficult; and (2) in very stiff clays, fissures may exist at low stress levels, and may affect drainage rates. Some of the inherent variability associated with evaluation of $c_v$ can be reduced by focusing interpretation on values corresponding to a reload cycle and to values associated with virgin compression. Values from initial loading increments are often unreliable because of sample disturbance.

Value for $c_v$ based on laboratory consolidation results will often vary from actual values in the field. Time rate of settlement analyses based on consolidation test results often over predict the time actually required for primary consolidation to be completed in the field. This observation is largely attributed to the fact that most natural soil deposits have interbedded seams or layers of more permeable material that

are not represented in small test specimens. These seams reduce the drainage distance, which strongly influences consolidation rates. Disturbance of the tested samples likely also plays a role. All of these factors tend to make predictions of the time rate of settlement to be conservatively overestimated. In cases where settlement rates are important, the observational method should be adopted wherein the actual time rate of settlement is monitored in the early stages of field loading and used to refine predictions from laboratory tests.

## 6.11 EVALUATION OF COEFFICIENT OF SECONDARY COMPRESSION FROM LABORATORY CONSOLIDATION TESTS

For most geotechnical design analyses, settlement from secondary compression is relatively small compared to settlement from primary consolidation. However, secondary compression may be significant for some soils, especially organic soils. The magnitude of settlements from secondary compression are estimated using the coefficient of secondary compression, $C_\alpha$.

The coefficient of secondary compression, $C_\alpha$, is generally measured in common IL consolidation tests by extending the duration of loading increments to measure the time-deformation response after primary consolidation is complete. As shown in Figure 6-22, $C_\alpha$ is calculated from the measured time-void ratio response after primary consolidation is completed according to the following equation:

$$C_\alpha = \frac{\Delta e}{\Delta \log t} \tag{6.12}$$

where $\Delta e$ is the change in void ratio over an elapsed time equal to $t_2 - t_1$. The times $t_1$ and $t_2$ occur after the time to the end of primary consolidation, $t_{100}$ or $t_p$. Alternatively, the modified coefficient of secondary compression, $C_{\alpha\varepsilon}$, can be similarly evaluated using a plot of volumetric strain versus logarithm of time. For soils expected to demonstrate significant secondary settlements, it is important that load durations extend to times after primary consolidation is completed so that $C_\alpha$ can be reasonably observed. Depending on the rate of primary consolidation, loading increments may need to extend over a period of several days or even a week.

Values of $C_\alpha$ (or $C_{\alpha\varepsilon}$) vary with stress history, with the maximum values for $C_\alpha$ being observed for stresses that exceed $\sigma_p'$ (i.e., for loading in virgin compression). The anticipated final effective stress should therefore be considered when assessing values for $C_\alpha$ (or $C_{\alpha\varepsilon}$) for design. If anticipated effective stresses are less than approximately $0.8 \cdot \sigma_p'$, an average value of $C_\alpha$ determined from the overconsolidated range of stresses is appropriate. However, if anticipated effective stresses exceed $\sigma_p'$, $C_\alpha$

values should be conservatively established from measurements for stresses that are 1 to 2 times $\sigma_p'$. Laboratory-measured values of $C_\alpha$ from disturbed specimens are also generally less than values determined using high-quality specimens in the normally consolidated range. Measurements of the coefficient of secondary compression should therefore be made using high quality specimens when secondary compression is important for design.

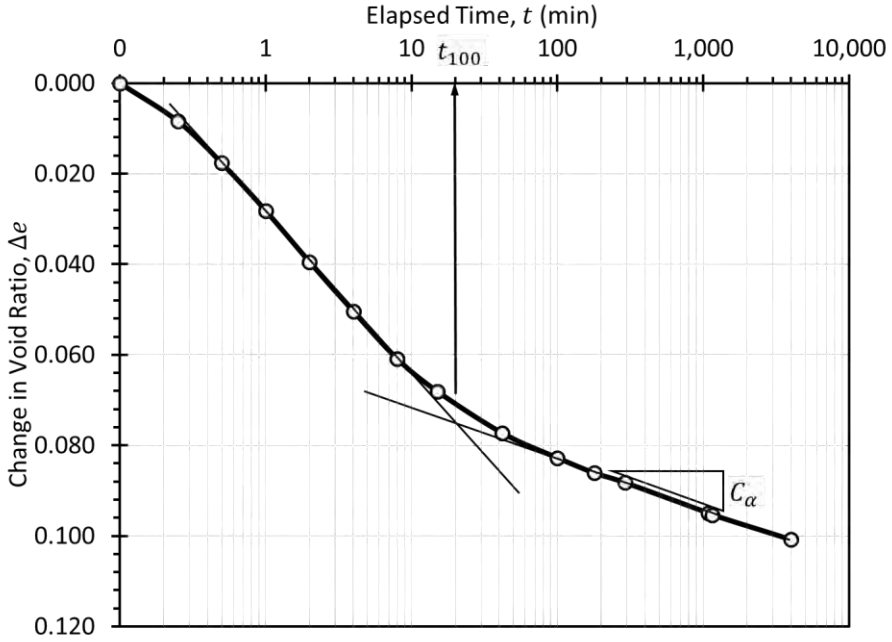


**Figure 6-22 Evaluation of $C_\alpha$ from time-deformation response for IL consolidation test increment.**

## 6.12 EVALUATION OF PRECONSOLIDATION STRESS FROM IN SITU TESTS

Several in situ tests may be used to provide estimates of $\sigma_p'$ (or $OCR$, which can be used to evaluate $\sigma_p'$) at specific points in the subsurface profile or as profiling tools to obtain a more continuous profile of $\sigma_p'$ with depth. Specifically, the cone penetrometer (CPT), piezocone (CPTU), flat dilatometer (DMT), pressuremeter (PMT), field vane shear device (FVT), and Standard Penetration (SPT) tests can be used to estimate $\sigma_p'$ or $OCR$. Use of these tests for developing estimates for $\sigma_p'$ in clayey soils is attractive since the tests are often conducted quickly and inexpensively and, thus, can be used to efficiently produce relatively large numbers of estimates. The near continuous measurements provided by several of these tests often also facilitate interpretation of potentially complex stress histories that can result from different mechanisms (e.g., erosion, reloading, aging, cementation, etc.). Table 6-5 summarizes the general applicability of in situ tests for evaluation of $\sigma_p'$ in different soil conditions.

**Table 6-5 Summary of in situ test methods for determining preconsolidation stress.**

| Test | Very Soft-Soft | Medium Stiff | Stiff | Very Stiff-Hard | Comments |
|---|---|---|---|---|---|
| CPT/CPTU | ✓ | ✓ | ✓ | - | Highest quality interpretation; theoretical and empirical data base |
| DMT | ✓ | ✓ | ✓ | - | High quality interpretation; empirical data base |
| FVT | ✓ | ✓ | - | - | High quality interpretation; theoretical and empirical data base |
| PMT | - | ✓ | ✓ | ✓ | Medium quality interpretation; empirical data base |
| SPT | - | ✓ | ✓ | ✓ | Low quality; rough estimate only; empirical data base |

While in situ tests have numerous advantages, the tests provide indirect measures of $\sigma_p'$ that must be transformed using empirically or theoretically derived functions to produce estimates of $\sigma_p'$. As discussed in Chapter 3, such transformations necessarily introduce uncertainty into estimates for $\sigma_p'$. As shown in the remainder of this section, the uncertainty introduced for broadly applicable transformations is substantial. However, this uncertainty can often be dramatically reduced by performing companion in situ tests and laboratory consolidation tests and using those measurements, combined with sound understanding of the local geologic setting, to develop "site specific" transformations. Development and use of site specific transformations is necessary for use of in situ tests when quantitative estimates for $\sigma_p'$ are important for design of specific features. General transformations, like those presented in the following subsections, are useful for establishing preliminary or approximate estimates for $\sigma_p'$, or for evaluating qualitative trends in $\sigma_p'$ with depth. General transformations may also be used for small projects when it is more cost effective to design for greater uncertainty than to reduce uncertainty through more extensive investigations.

### 6.12.1 CPT/CPTU

Empirical and analytical expressions for estimating $\sigma_p'$ from corrected CPT or CPTU tip resistance, $q_t$, and from excess pore water pressure measurements from CPTU tests have been suggested since the early 1980's. Since that time, measurements from many additional sites have been added and compiled, in some cases taking into account other soil behavioral parameters, such as rigidity index, $I_r$ $(= G/s_u)$. However, the basic expressions have changed very little. Figure 6-23 shows recent transformations between $\sigma_p'$ (denoted as $\sigma_y'$ in Figure 6-23) and the corrected net cone tip resistance $(q_t - \sigma_{vo})$, where $\sigma_{vo}$ is the in situ overburden stress, for a wide range of soil types (Mayne, 2014). The scatter in estimates

across all soil types for a given value of $q_t - \sigma_{vo}$ is quite large, spanning approximately an order of magnitude. The scatter is substantially reduced when considering a single soil type, although still relatively large (note the data are plotted using log scales). Site specific transformations will generally allow the transformation uncertainty to be notably reduced compared to that shown in the figure.

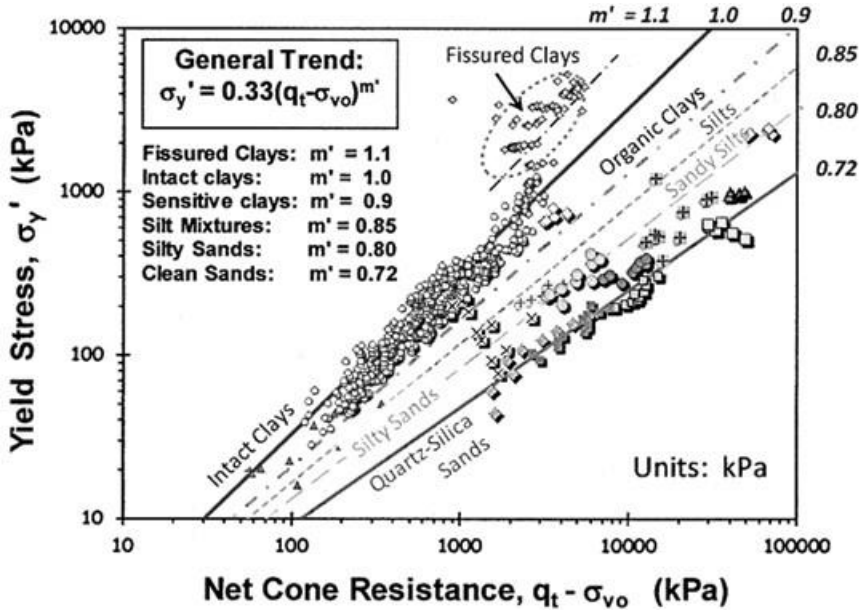


**Figure 6-23 Transformation from corrected net cone tip resistance to preconsolidation stress, or "yield stress" (from Mayne, 2014).**

Figure 6-24 shows similar transformations between $\sigma_p'$ and excess pore water pressures measured using Type 1 or Type 2 piezocones for clay soils (Mayne, 2007). In Figure 6-24, the excess pore water pressure is computed as the difference between the measured pore water pressure, $u_1$ or $u_2$ (for Type 1 and Type 2 piezocones, respectively), and the in situ pore water pressure, $u_o$. In the figure, both $\sigma_p'$ and excess pore water pressure are normalized with respect to atmospheric pressure, $p_a$, to make the transformation dimensionless. The uncertainty associated with the transformations in Figure 6-24 is somewhat greater than that shown for clays in Figure 6-23. It is also noteworthy that the transformations for fissured clays are substantially different from transformations for intact clays, and more variable.

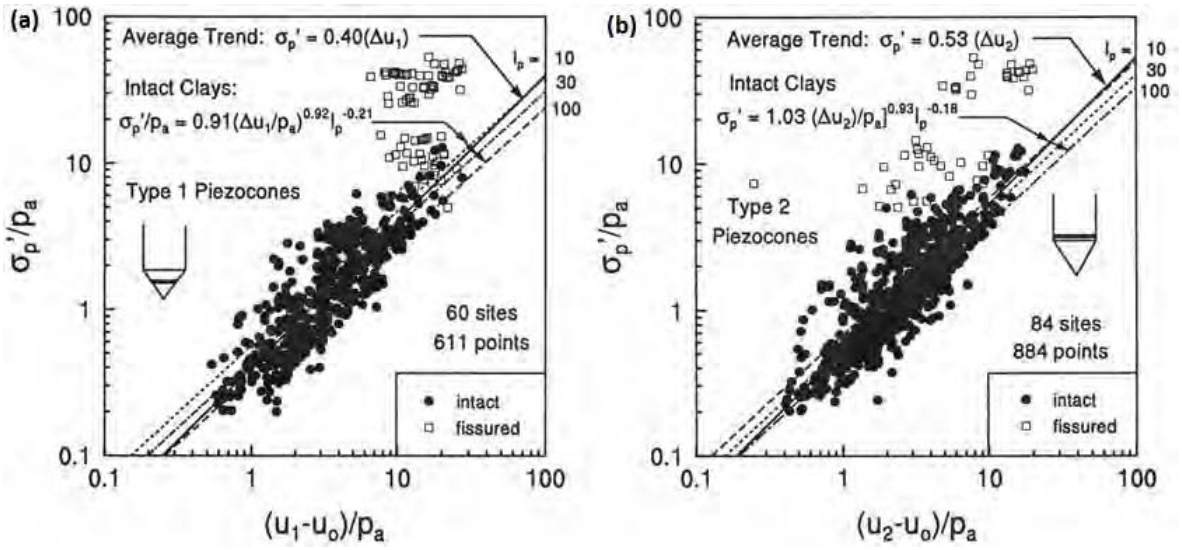


**Figure 6-24 Transformations from measured CPTU pore pressure to preconsolidation stress for clays: (a) Type 1 piezocones, and (b) Type 2 piezocones (from Mayne, 2007).**

### 6.12.2 DMT

The flat dilatometer test is now well established in geotechnical practice and standardized in ASTM D6635. DMT measurements have been shown to be correlated with $\sigma_p'$ determined from laboratory tests. Marchetti (1980) originally suggested a simple empirical expression to predict $OCR$ from the DMT horizontal stress index, $K_D$, as

$$OCR = (0.5 \cdot K_D)^{1.56} \tag{6.13}$$

$K_D$ is, in turn, related to the corrected lift-off pressure, $p_o$, and computed as

$$K_D = \frac{p_o - u_o}{\sigma_{vo}'} \tag{6.14}$$

where $u_o$ is the in situ pore water pressure and $\sigma_{vo}'$ is the in situ effective vertical stress at the testing depth. Alternative empirical transformations, often developed for specific local or regional geologic deposits, with similar form to Equation 6.13 are summarized in Table 6-6.

**Table 6-6 Summary of empirical transformations between preconsolidation stress and DMT $K_D$.**

| Equation | Soil Type | Reference |
|---|---|---|
| $OCR = (0.5 \cdot K_D)^{1.56}$ | misc. clays | Marchetti (1980) |
| $OCR = (0.372 \cdot K_D)^{1.40}$ | Florida clays | Davidson and Boghrat (1983) |
| $OCR = (0.24 \cdot K_D)^{1.32}$ | stiff clays in UK | Powell and Uglow (1988) |
| $OCR = (0.225 \cdot K_D)^{n}$ (n varies from 1.35 to 1.67) | Norwegian sensitive clays | Lacasse and Lunne (1988) |
| $OCR = 10(0.16K_D - 2.5)$ | Swedish clays | Larsson and Eskilson (1989) |
| $OCR = (0.5 \cdot K_D)^{0.84}$ | Singapore marine clay | Chang (1991) |
| $OCR = 0.34 \cdot K_D{}^{1.43}$ | Japan soft clay | Kamei and Iwasaki (1995) |
| $OCR = (0.3 \cdot K_D)^{1.36}$ | Leda clay | Tanaka and Bauer (1998) |

A more direct approach to estimating the stress history in clays is to relate the corrected DMT lift-off pressure, $p_o$, to $\sigma_p'$ as

$$\sigma_p' = \frac{p_o - u_o}{\alpha} \tag{6.15}$$

where $\alpha$ is an empirical factor. Based on consideration of a simple elastic-plastic model for expansion of a cylindrical cavity, the value of $\alpha$ in Equation 6.15 ranges between 0.8 and 2.5 for a typical range of rigidity index for clays. Mayne (1995) found that $\sigma_p'$ could be estimated as

$$\sigma_p' = \frac{p_o - u_o}{2} \tag{6.16}$$

based on empirical measurements for 24 intact natural clays, as shown in Figure 6-25. The variability of the measurements in Figure 6-25 is slightly greater than that shown for the CPT transformation for intact clays in Figure 6-23. As is true for CPT and CPTU measurements, use of DMT measurements for evaluating stress history is attractive since they can be used to obtain a large number of estimates and develop a near-continuous profile of $\sigma_p'$ estimates at close intervals (about 1 feet) in a single sounding.

### 6.12.3 Field Vane Shear Test (FVT)

Measurements of undrained shear strength from field vane shear tests (AASHTO T223 and ASTM D2573) are generally correlated with $\sigma_p'$ based on the relationship between normalized undrained shear strength and $OCR$ described in Chapter 7. Preconsolidation stress may thus be estimated as

$$\sigma_p' = \alpha_{FV} s_{u-FV} \tag{6.17}$$

where $s_{u-FV}$ is the undrained shear strength measured from field vane shear tests and $\alpha_{FV}$ is an empirical factor relating undrained shear strength to $\sigma'_p$. Figure 6-26 shows empirical measurements supporting this relation for a wide range of soils. The lines shown in Figure 6-26 correspond to predictions from Equation 6.17 for different values of the empirical factor, $\alpha_{FV}$. As shown in Figure 6-27, $\alpha_{FV}$ varies with the plasticity index of the soil.

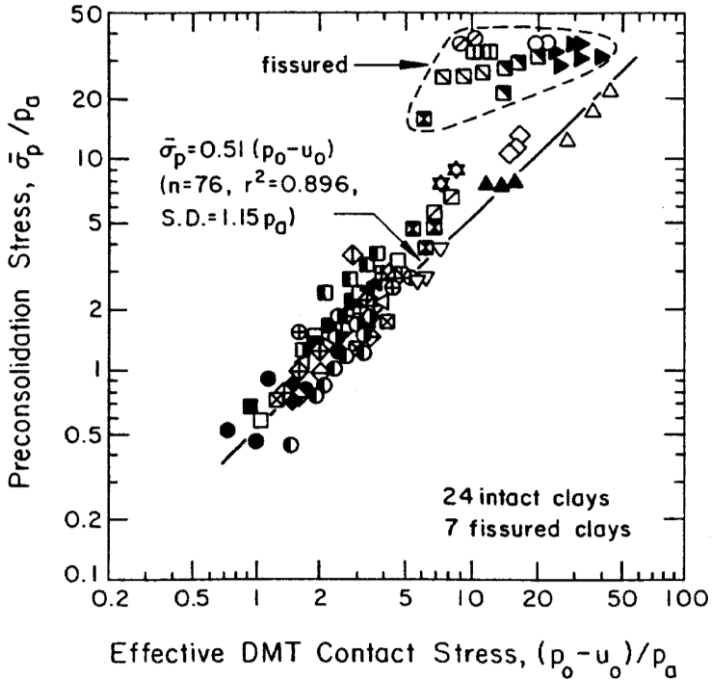


**Figure 6-25 Transformation from DMT $p_o$ to preconsolidation stress (from Mayne, 1995).**

### 6.12.4 Pressuremeter Test (PMT)

The pressuremeter test (ASTM D4719) may be used to provide estimates of $\sigma'_p$ at specific points but is not considered a profiling tool. As shown in Table 6-5, the pressuremeter is often best utilized in stiff to very stiff soils where alternative in situ tests cannot generally be used. Preconsolidation stress is most commonly estimated from direct correlation with the PMT limit pressure, $p_L$ as shown in Figure 6-28. Alternatively, as shown in Figure 6-29, $\sigma'_p$ may also be estimated as

$$\sigma'_p = 0.76\left(\frac{s_u}{p_a}\right)\ln I_r \qquad (6.18)$$

where $I_r = G/s_u$ is the soil rigidity index. The PMT creep pressure, $p_y$, is sometimes also used as a direct estimate of $\sigma'_p$.

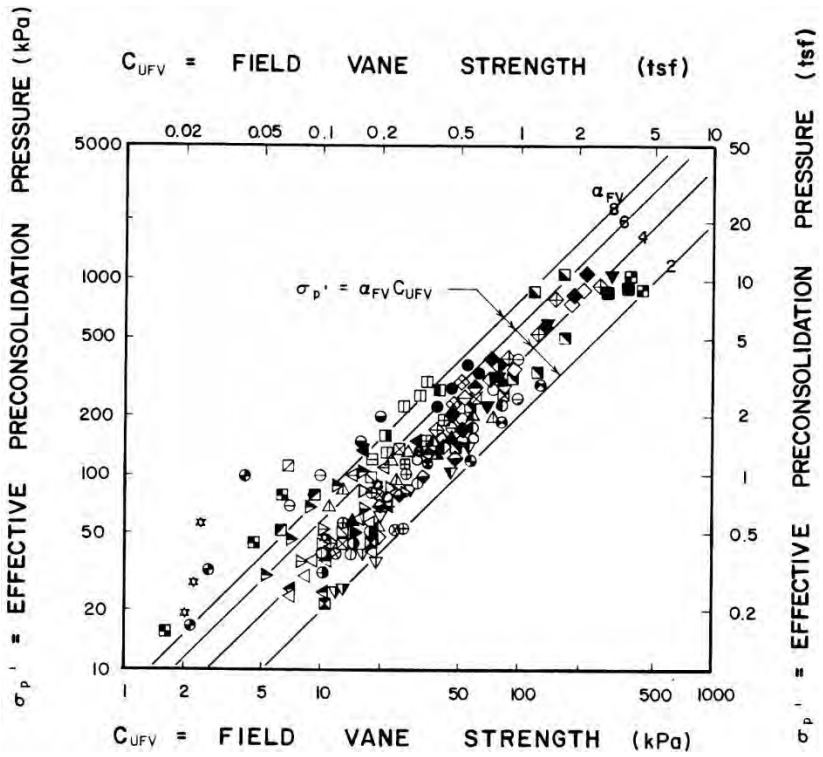


**Figure 6-26 Transformation from field vane shear strength to preconsolidation stress (from Mayne and Mitchell, 1988).**

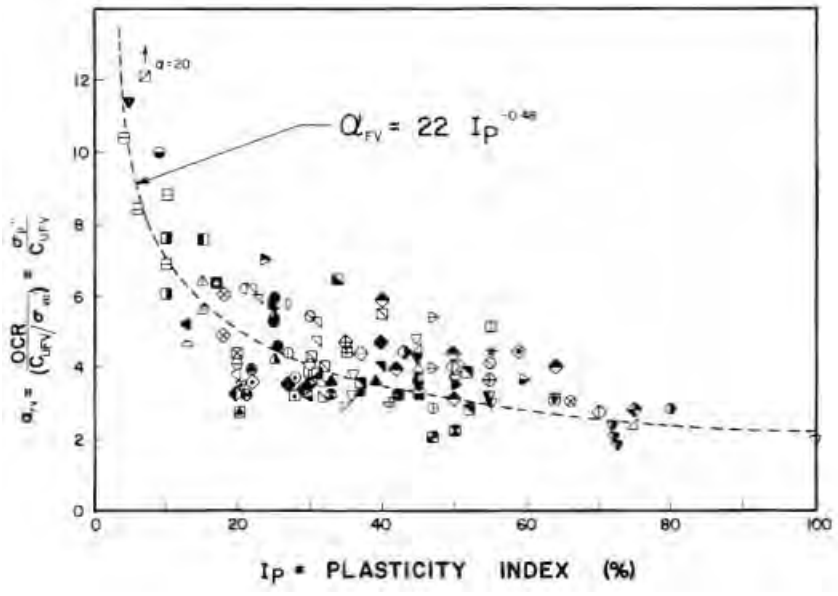


**Figure 6-27 Relationship between $\alpha_{FV}$ and plasticity index (from Mayne and Mitchell, 1988).**

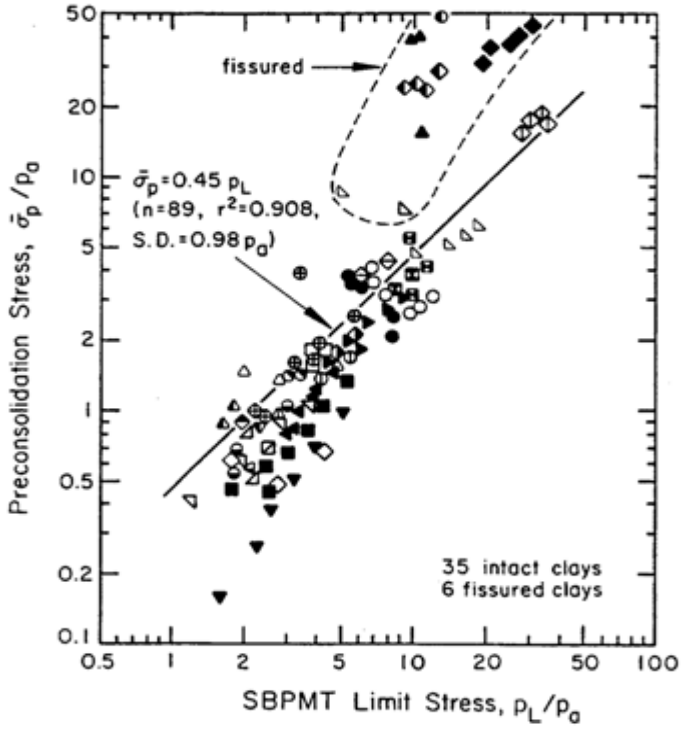


**Figure 6-28 Transformation from self-boring PMT $p_L$ to preconsolidation stress (from Kulhawy and Mayne, 1990).**

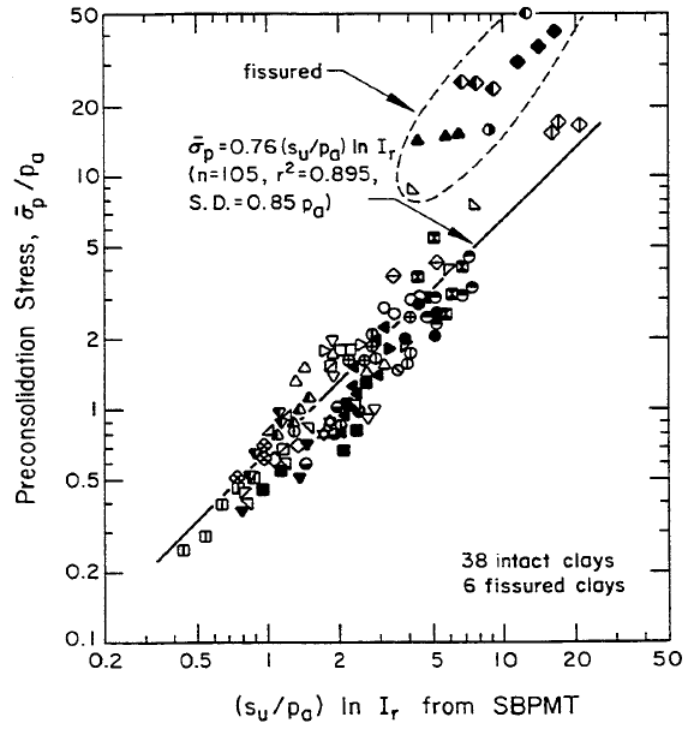


**Figure 6-29 Transformation from PMT undrained shear strength and rigidity index to preconsolidation stress (from Kulhawy and Mayne, 1990).**

### 6.12.5 Standard Penetration Test (SPT)

Standard Penetration test $N_{60}$-values can also be related to $\sigma_p'$, as shown in Figure 6-30. However, this relationship has the greatest scatter of all transformations presented for in situ tests, some of which is inevitably due to variations in both equipment and procedures that have been historically used for SPT measurements, and the quality of samples, test procedures, and interpretation of lab tests to obtain $\sigma_p'$. SPT measurements should not be used for quantitative estimation of $\sigma_p'$ for projects where $\sigma_p'$ is important for design. However, the transformation may be used to develop preliminary estimates for $\sigma_p'$ or to help interpret trends in $\sigma_p'$ across a site.

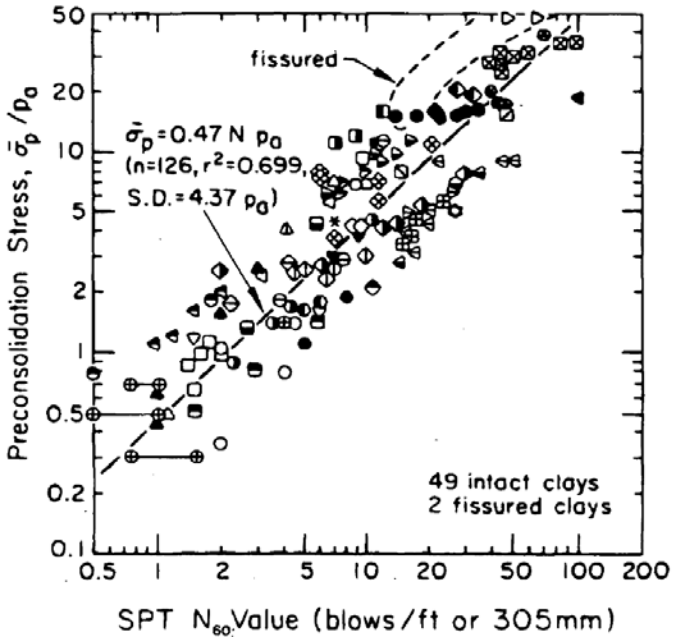


**Figure 6-30 Transformation from SPT $N_{60}$ to $\sigma_p'$ (from Mayne, 1995).**

## 6.13 EVALUATION OF COEFFICIENT OF LATERAL CONSOLIDATION FROM IN SITU TESTS

As described in Section 6.10, it is often difficult to measure the horizontal coefficient of consolidation, $c_h$, in laboratory consolidation tests. However, $c_h$ can often be effectively measured from pore pressure dissipation tests performed using piezocone or flat dilatometer devices. While conditions present for these tests do not strictly enforce purely horizontal dissipation of pore water pressure, values established from these tests are generally interpreted to represent horizontal coefficients of consolidation because dissipation is generally dominated by horizontal flow. Both tests are subject to potential "smearing" and remolding of the soil adjacent to the device, which may produce measurements that are less than those

actually present in situ. Nevertheless, dissipation tests represent one of the best means available for evaluating $c_h$.

### 6.13.1 CPTU Dissipation Tests

CPTU dissipation tests are probably the most common means for measuring the coefficient of lateral consolidation, $c_h$. In a CPTU dissipation test, cone advance is stopped at some desired testing depth and the pore pressure is monitored over time to determine the rate of pore pressure dissipation. The "monotonic" dissipation shown in Figure 6-31 is typical of soft, normally consolidated to lightly overconsolidated soils. For more heavily overconsolidated soils, the observed pore pressure may be "dilative", with pore pressures initially increasing with time during the test prior to decreasing to in situ pore pressure levels, especially for Type 2 piezocones. Numerous examples of CPTU dissipation tests have been reported in the literature for a variety of soils (e.g., Jones and Van Zyl, 1981; Tumay, et al., 1981; Battaglio, et al., 1981; Lacasse and Lunne, 1982; Tavenas, et al., 1982; Campanella, et al., 1983; Gupta and Davidson, 1986; Senneset, et al., 1988; Sills, et al., 1988; Kabir and Lutenegger, 1990; DeGroot and Lutenegger, 1994; Sully and Campanella, 1994; Burns and Mayne, 1995).

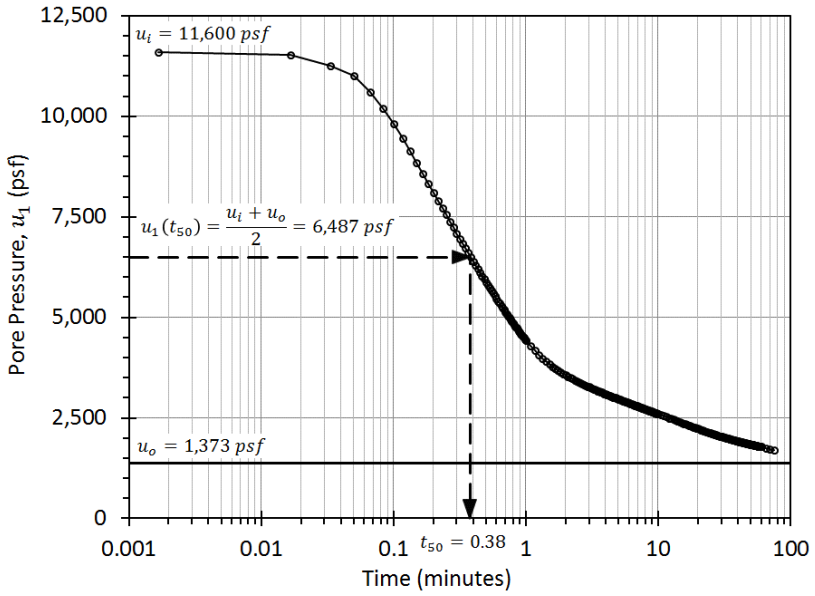


**Figure 6-31 Pore pressure dissipation measurements from CPTU in soft, clayey silt.**

The horizontal coefficient of consolidation is generally computed as

$$c_h = \frac{T^* a^2 \sqrt{I_r}}{t} \tag{6.19}$$

where $T^*$ is a modified time factor, $a$ is the cone radius, $I_r$ is the soil rigidity index, and $t$ is elapsed time to achieve a degree of dissipation that is consistent $T^*$. The value of $T^*$ is dependent on the type of piezocone, $I_r$, the pore pressure parameter, $A_f$, and the degree of pore pressure dissipation. Several analytical and numerical approaches have been used to develop appropriate values for $T^*$ (e.g., Torstensson, 1977; Baligh and Levadoux, 1986; Gupta and Davidson, 1986, Teh and Houlsby, 1991; Burns and Mayne, 1998). The most common means adopted for determining $T^*$ are based on the strain path method (Mayne, 2007), although some solutions are derived from cavity expansion and soil strength theories. Discussion of differences in theoretical time factors is given in Kabir and Lutenegger (1990) and Robertson et al. (1992).

The modified time factors developed by Teh and Houlsby (1991) and shown in Table 6-7 are commonly adopted for computing $c_h$ in relatively soft soils that produce pore pressure dissipation similar to that shown in Figure 6-31. $T^*$ values are provided for different degrees of consolidation; however, the accuracy of estimates for $c_h$ are much improved when dissipation tests are continued to achieve at least 50 percent dissipation. Alternative methods, such as the one described by Burns and Mayne (1998), are likely to be more appropriate for stiff, heavily overconsolidated soils that produce dilative pore pressure response.

**Table 6-7 Modified time factors, $T^*$, for analysis of CPTU dissipation tests (after Teh and Houlsby, 1991).**

| Normalized Excess Pore Pressure, $U_n$ | Degree of Consolidation, $1 - U_n$ (%) | $T^*$ for "Type 1" Piezocone with Element Located Mid- Face, $u_1$ | $T^*$ for "Type 2" Piezocone with Element Located Behind the Tip, $u_2$ |
|---|---|---|---|
| 0.8 | 20 | 0.014 | 0.038 |
| 0.7 | 30 | 0.032 | 0.078 |
| 0.6 | 40 | 0.063 | 0.142 |
| 0.5 | 50 | 0.118 | 0.245 |
| 0.4 | 60 | 0.226 | 0.439 |
| 0.3 | 70 | 0.463 | 0.804 |
| 0.2 | 80 | 1.04 | 1.60 |

The degree of pore pressure dissipation and the time to reach a given degree of dissipation are obtained from a normalized plot of excess pore water pressure, as shown in Figure 6-32. The normalized excess pore pressure, $U_n$, is computed as:

$$U_n = \frac{(u_t - u_o)}{(u_i - u_o)} \tag{6.20}$$

where $u_t$ is the measured pore water pressure at time, $t$, after stopping cone advance, $u_o$ is the in situ (initial) pore water pressure at the test depth, and $u_i$ is the pore water pressure at time zero. The degree of consolidation is the complement of $U_n$ as shown in Table 6-7. $U_n$ and the degree of consolidation (dissipation) should be computed using the initial excess pore pressure, $u_i$, not the maximum excess pore pressure measured during a dissipation test. Figure 6-32 shows the determination of $t_{50}$, the time required to achieve 50 percent dissipation of excess pore water pressure. Times for other degrees of consolidation are determined similarly. Reliable estimates of $u_o$ are needed to determine the normalized excess pore water pressure. Often, these are obtained from piezometer data or knowledge of groundwater conditions at the site. If dissipation tests are continued long enough to obtain an equilibrium value of the in situ pore water pressure at the test location, then that value may be used for $u_o$.

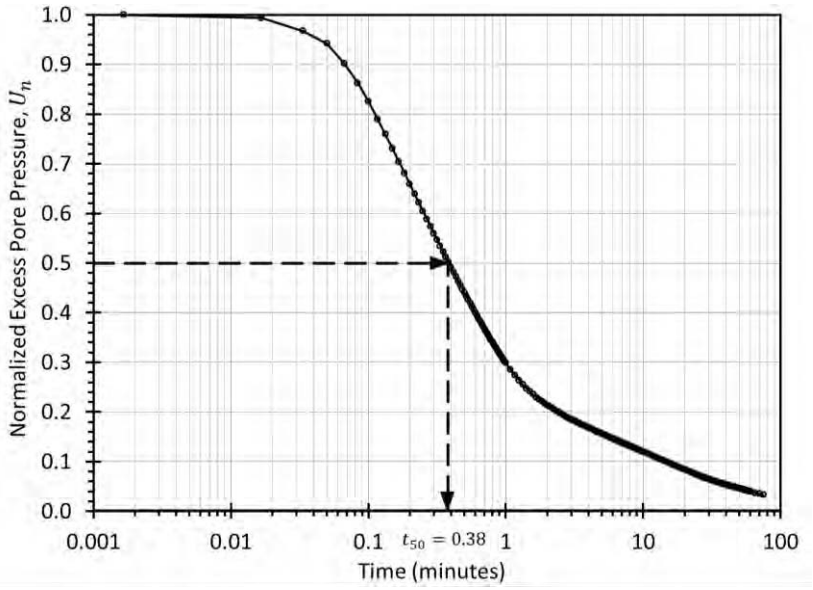


**Figure 6-32 Normalized pore pressure dissipation for measurements in Figure 6-31.**

The parameter $I_r$ can be measured using laboratory strength tests or using non-destructive seismic measurements (e.g., from seismic piezocone) coupled with means to measure or estimate undrained shear strength, $s_u$. Alternatively, $I_r$ can be estimated from Figure 6-33 based on $OCR$ and $PI$ for the soil.

As an alternative to determining $c_h$ using Equation 6.19, Robertson et al. (1992) developed a chart relating $c_h$ to $t_{50}$ for different values of $I_r$, as shown in Figure 6-34. This chart can only be used if dissipation tests are continued beyond 50 percent dissipation of excess pore water pressures.

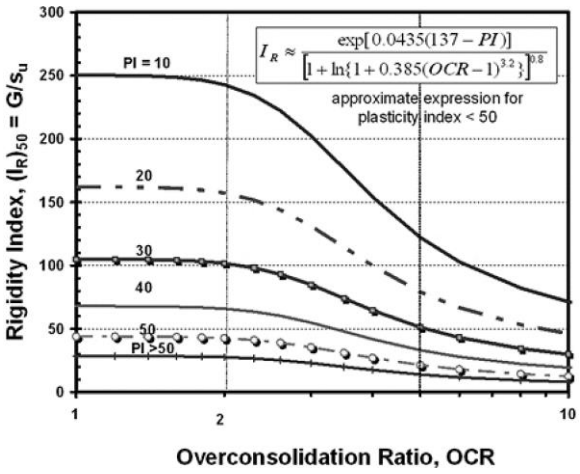


**Figure 6-33 Relation between rigidity index and *OCR* (from Mayne, 2007).**

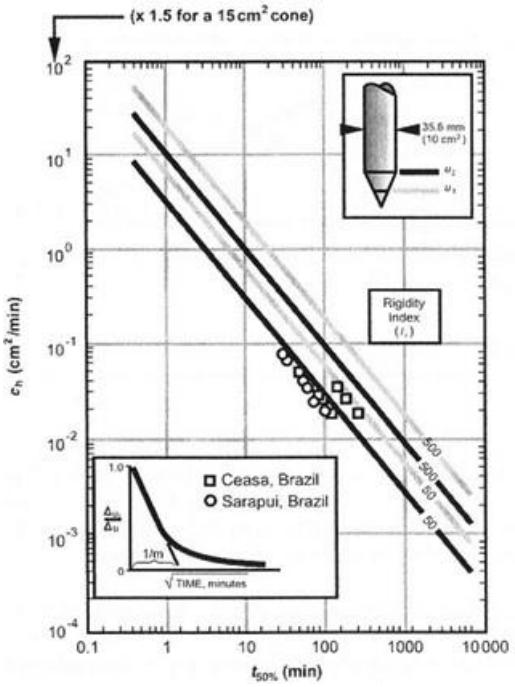


**Figure 6-34 Robertson et al. (1992) chart for determining $c_h$ from $t_{50}$ (from Schnaid, 2009).**

### 6.13.2 DMT Dissipation Tests

An estimate of $c_h$ may also be made using results from DMT dissipation tests. A procedure using only the "A-Reading" was presented by Marchetti and Totani (1989) and is referred to as the DMTA dissipation test. In this method, only the A-Reading is obtained from the test at selected time intervals following penetration to the test depth. As shown in Figure 6-35, a plot of A versus log time typically

shows a characteristic "S" shape. The point of contraflexure for this curve is defined as $T_{flex}$. The horizontal coefficient of consolidation, $c_h$, may be calculated from this value as

$$c_h = \frac{5 \text{ to } 10 \ cm^2}{T_{flex}} \tag{6.21}$$

The value of $c_h$ estimated from Equation 6.21 is appropriate for overconsolidated soils and should be appropriately adjusted (for example, using local experience) to give an estimate for normally consolidated conditions. Table 6-8 provides a qualitative rating of consolidation rate based on $T_{flex}$ suggested by Marchetti and Totani (1989).

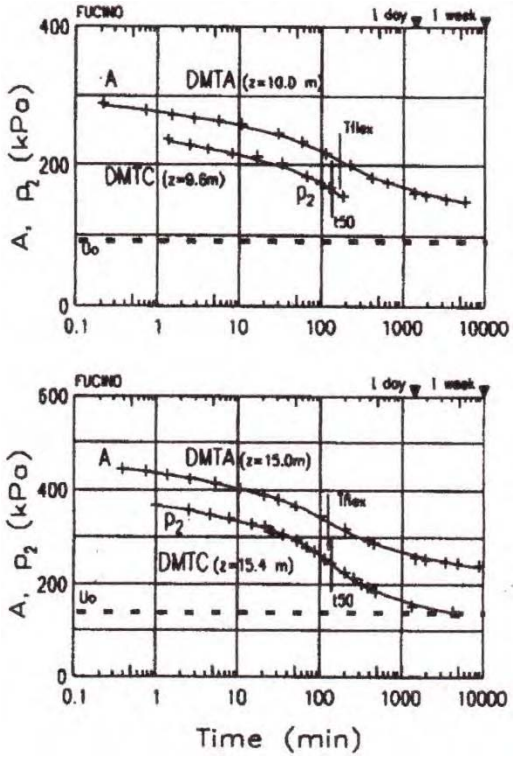


**Figure 6-35 Measurements from DMTA and DMTC dissipation tests in clay for two different depths.**

**Table 6-8 Rating of consolidation speed based on $T_{flex}$ (Marchetti and Totani, 1989).**

| $T_{flex}$ (min) | Rating |
|---|---|
| < 10 | Very fast |
| 10 to 30 | Fast |
| 30 to 80 | Medium |
| 80 to 200 | Slow |
| > 200 | Very slow |

An alternative procedure, referred to as a DMTC test or a "$C$-Reading" dissipation test, can also be used. Since the DMT recontact pressure, $P_2$, provides an indication of the excess pore water pressure generated, sequential measurements over time can be used to give an indication of the change or dissipation of pore water pressure following penetration of the blade. The DMTC test is conducted as follows:

1. Following penetration and release of the pushing thrust, a stopwatch is started to log the elapsed time after penetration. This then becomes time zero for the test.
2. The normal sequence of obtaining an $A$-, $B$-, and $C$-reading are first performed as a routine part of the test. The elapsed time to obtain the $C$-reading is noted.
3. At various time intervals, the sequence of obtaining the $A$-, $B$-, and $C$-reading is repeated, but only the $C$-reading and elapsed time are recorded.
4. A sufficient number of measurements are obtained over time until a minimum of 50 percent of the excess pore water pressure has dissipated (this may require a test to run for a few minutes to several hours, depending on the drainage characteristics).

The excess pore water pressure at any time can be obtained from:

$$u_F = P_2 - u_o \tag{6.22}$$

The initial excess pore water pressure is not actually measured in the test, because it takes about 1 minute after penetration to obtain the first $P_2$ reading. Schmertmann (1988) suggested that the initial excess pore pressure be established by plotting measured values of $P_2$ on a square-root-of-time plot and extrapolating the initial few data points back to $t = 0$ as a straight line. Typical results obtained from $C$-reading dissipation tests (corrected to $P_2$) are also shown in Figure 6-35, showing the characteristic shape of time-rate of consolidation tests.

The coefficient of consolidation is obtained in a manner similar to that described for the CPTU, according to Equation 6.19. For CPTU tests, $a$ is taken as the radius of the cone and $T$ is a function of the soil rigidity index, the pore pressure parameter at failure, $A_f$, and the cone type. For DMT, Robertson et al. (1988) proposed that an "equivalent radius" determined to have the same projected end area of the DMT blade (about 22mm) could be used with Equation 6.19 as an initial means of estimating $c_h$. Alternatively, Schmertmann (1988) suggested that an equivalent radius of 24 mm would produce approximately the same values for $c_h$ for both CPTU-dissipation and DMTC-dissipation tests in the same cohesive soil. While the "equivalent radius" technique may be used to provide an initial estimate of $c_h$, Kabir and Lutenegger (1990) back-calculated values for the equivalent radius to produce values of $c_h$ to match

measurements from horizontal flow oedometer tests. Back-calculated values of the equivalent radius ranged from 5 to 40 mm for different clays, which suggests that an alternative technique might be more appropriate.

There are several potential sources of error that may occur using this technique:

1. The apex angle of the DMT blade is only about 10 to 20 degrees in comparison to the 60 degree apex of most CPT cones. This means that the initial excess pore pressure distribution will be different.
2. The point of measurement of the pore water pressure in the DMT is about 7.6 blade thicknesses behind the base of the leading wedge and about 12.7 blade thicknesses behind the wedge tip. This is considerably different than where CPTU pore pressures are measured, which may affect the rate of pore pressure dissipation observed.
3. The geometry between the two instruments is different. In some soils (e.g., soft clays), this has little to no effect and the DMT blade approximates cylindrical cavity expansion, while in other soils the aspect ratio of the blade may have a significant influence on the results.

Another alternative is to treat the DMT as a cone with a radius equal to the half-thickness of the DMT blade (7.5 mm) and use the theoretical time factor for an 18 degree cone with pore water pressure measured 10 radii behind the tip. Gupta and Davidson (1986) reported a time factor, $T_{50} = 25$ for these conditions considering 50 percent consolidation. Thus, the coefficient of consolidation can be computed as

$$c_{hDMT} = \frac{(25)(7.5mm)^2}{t_{50}} = \frac{14.06mm^2}{t_{50}} \tag{6.23}$$

With this procedure, it is only necessary to evaluate the clock time necessary to reach 50 percent dissipation of the normalized excess pore water pressure.

## 6.14 ESTIMATION OF CONSOLIDATION PARAMETERS FROM INDEX PROPERTIES

For many projects, it is desirable to develop preliminary estimates of consolidation properties before detailed site investigation and testing is completed. Such estimates can be used to inform preliminary project decisions (e.g., preliminary selection of foundation type) and scoping of more thorough site characterization investigations. For projects with limited scope and importance, it may also sometimes be more cost effective to design conservatively using rough estimates for consolidation properties derived from index property measurements than to directly measure the properties using laboratory or in situ tests.

In both of these instances, indirect estimates of consolidation properties obtained from correlations with common soil index properties like those presented in this section may be useful. The relations presented in this section are also often useful as a "reasonableness" check for laboratory or in situ test measurements to evaluate whether the measurements fall within expected ranges for a given soil type.

There is a long history of developing empirical correlations between consolidation parameters and soil index properties like initial water content, initial void ratio, and Atterberg limits. All such correlations are indirect measurements that involve substantial variability and uncertainty, particularly when considered globally. The variability and uncertainty can be reduced somewhat when empirical relations are restricted to specific geologic settings or specific geographic regions, but will still be much greater than can be achieved using direct measurements (or better indirect measurements). Such correlations should therefore not be considered as equivalent substitutes for direct measurements and should not be relied upon for final design unless used with appropriate consideration for the uncertainty involved. The correlations presented here should also not be considered to be the "best", or preferred correlations. Rather, the correlations presented are provided as examples of correlations that have some global applicability. Many others developed from geographically restricted collections of measurements or for special soil types are not included, but may be appropriate when used for soil conditions that are consistent with their development.

### 6.14.1 Compression Index and Recompression Index

Numerous correlations relating soil index properties to $C_c$ and $C_r$ are available in the literature for silts and clays, such as that shown in Figure 6-36 relating $C_r$ and plasticity index, $PI$. There are no universal correlations that fit all fine-grained soils and different correlations may sometimes produce significantly different estimates. Table 6-9 through 6-16 provide some reported correlations between the compression index, $C_c$, and various index properties. Some of these correlations use a single parameter to estimate $C_c$ while others use multiple parameters.

**Table 6-9 Reported correlations between compression index, $C_c$, and liquid limit, $LL$.**

| Equation | Soil | Reference |
|---|---|---|
| $C_c = 0.007(LL - 10)$ | Remolded Clays | Skempton (1944) |
| $C_c = 0.009(LL - 10)$ | Undisturbed Clays | Skempton (1944) |
| $C_c = 0.009(LL - 10)$ | NC Clays | Terzaghi and Peck (1967) |
| $C_c = 0.011(LL - 12)$ | Offshore Marine Clays | Herrmann (1974) |
| $C_c = 0.006(LL - 9)$ | All Clays ($LL < 100$) | Azzouz et al. (1976) |
| $C_c = 0.0057(LL - 11)$ | Misc. Clays | Krizek et al. (1977) |
| $C_c = (LL - 13)/109$ | All Clays | Mayne (1980) |
| $C_c = 0.005 \cdot LL$ | Clay Till | Sauer et al. (1993) |

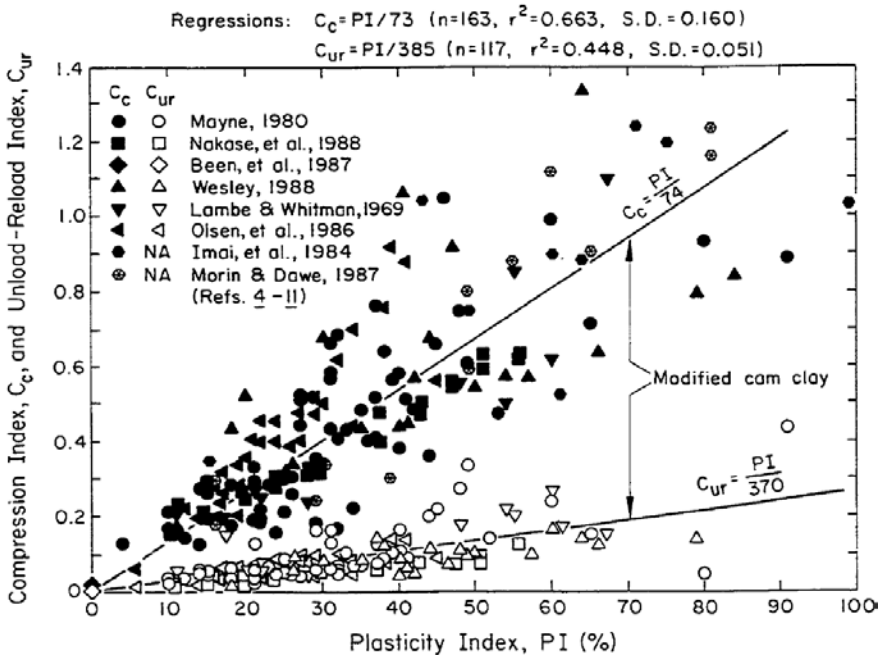


**Figure 6-36 Correlation between plasticity index and recompression and compression parameters (from Kulhawy and Mayne, 1990).**

**Table 6-10 Reported correlations between compression index, $C_c$, and natural water content, $\omega_n$.**

| Equation | Soil | Reference |
|---|---|---|
| $C_c = 0.01 \cdot w_n$ | Organic Soils, Peats and Clays | Moran et al. (1958) |
| $C_c = 0.01(w_n - 5)$ | All Clays | Azzouz et al. (1976) |
| $C_c = 0.0097(w_n - 7)$ | Misc. Clays | Krizek et al. (1977) |
| $C_c = 0.01 \cdot w_n$ | All Clays | Koppula (1981) |
| $C_c = 0.01(w_n - 7.55)$ | All Clays | Rendon-Herrero (1983) |

**Table 6-11 Reported correlations between compression index, $C_c$, and initial void ratio, $e_o$.**

| Equation | Soil | Reference |
|---|---|---|
| $C_c = 0.54(e_o - 0.35)$ | All Clays | Nishida (1956) |
| $C_c = 0.29(e_o - 0.27)$ | Inorganic, Cohesive Soil, Silty Clay, Clay | Hough (1957) |
| $C_c = 0.35(e_o - 0.50)$ | Organic, Fine-Grained Soil, Organic Clay | Hough (1957) |
| $C_c = 0.75(e_o - 0.55)$ | Residual Soils | Sowers (1963) |
| $C_c = 0.75(e_o - 0.50)$ | Residual Soils with Low Plasticity | Sowers (1970) |
| $C_c = 0.34(e_o - 0.3)$ | Offshore Marine Clays | Herrmann (1974) |
| $C_c = 0.40(e_o - 0.25)$ | All Clays | Azzouz et al. (1976) |
| $C_c = 0.3498(e_o - 0.168)$ | Misc. Clays | Krizek et al (1977) |
| $C_c = 0.2577 \cdot e_o + 0.0148$ | Glacial Till | Lutenegger et al. (1983) |
| $C_c = 0.39 \cdot e_o$ | All Clays | Nagaraj and Srinivasa Murthy (1986) |

**Table 6-12 Reported correlations between compression index, $C_c$, initial void ratio, $e_o$, and liquid limit, $LL$.**

| Equation | Soil | Reference |
|---|---|---|
| $C_c = 0.37(e_o + 0.003 \cdot LL - 0.34)$ | All Clays | Azzouz et al. (1976) |
| $C_c = 0.2745 \cdot e_o + 0.0019 \cdot LL - 0.0786$ | Misc. Clays | Krizek et al. (1977) |
| $C_c = 0.411 \cdot e_o + 0.00058 \cdot LL - 0.156$ | All Clays | Al-Khafaji and Andersland (1992) |

**Table 6-13 Reported correlations between compression index, $C_c$, natural water content, $\omega_n$, and liquid limit, $LL$.**

| Equation | Soil | Reference |
|---|---|---|
| $C_c = 0.009 \cdot w_n + 0.002 \cdot LL - 0.10$ | All Clays | Azzouz et al. (1976) |
| $C_c = 0.0071 \cdot w_n + 0.0024 \cdot LL - 0.0945$ | Misc. Clays | Krizek et al. (1977) |

**Table 6-14 Reported correlations between compression index, $C_c$, initial void ratio, $e_o$, and natural water content, $\omega_n$.**

| Equation | Soil | Reference |
|---|---|---|
| $C_c = 0.40(e_o + 0.001 \cdot w_n - 0.025)$ | All Clays | Azzouz et al. (1976) |
| $C_c = 0.3075 \cdot e_o + 0.0012 \cdot w_n - 0.0615$ | Misc. Clays | Krizek et al. (1977) |

**Table 6-15 Reported correlations between compression index, $C_c$, and plasticity index, $PI$.**

| Equation | Soil | Reference |
|---|---|---|
| $C_c = (PI + 26)/138$ | All Clays | Mayne (1980) |
| $C_c = PI/73$ | All Clays | Kulhawy and Mayne (1990) |

**Table 6-16 Reported correlations between compression index, $C_c$, initial void ratio, $e_o$, liquid limit, $LL$, and natural water content, $w_n$.**

| Equation | Soil | Reference |
|---|---|---|
| $C_c = 0.37(e_o + 0.003 \cdot LL + 0.004 \cdot w_n - 0.34)$ | All Clays | Azzouz et al. (1976) |
| $C_c = 0.1907 \cdot e_o + 0.0019 \cdot LL + 0.0024 \cdot w_n - 0.0844$ | Misc. Clays | Krizek et al. (1977) |

### 6.14.2 Coefficient of Consolidation

There is generally poor correlation between the coefficient of consolidation, $c_v$, and soil index properties. Estimates for $c_v$ derived from soil index properties are, therefore, not considered to be reliable. Figure 6-37 shows one general correlation between the liquid limit and $c_v$ that can be used to judge the reasonableness of computed $c_v$ values obtained from consolidation tests. However, values derived from Figure 6-37 should not be used for design.

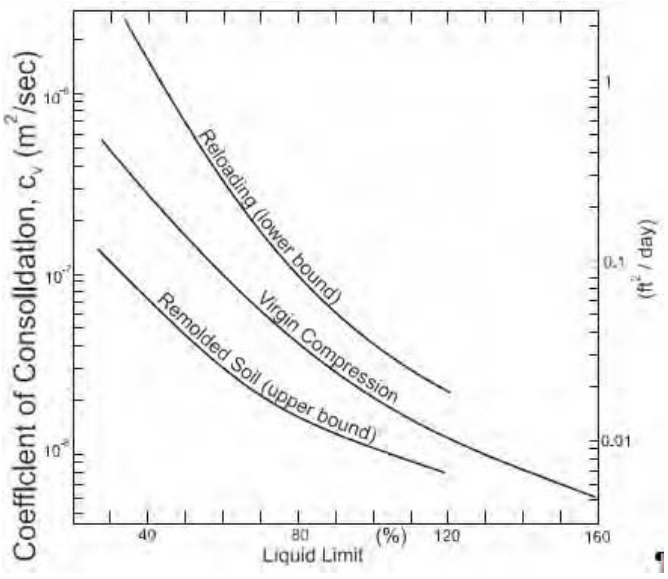


**Figure 6-37 Correlation of coefficient of consolidation to liquid limit (NAVFAC, 1986).**

### 6.14.3 Coefficient of Secondary Compression

For normally consolidated soils, the ratio of the coefficient of secondary compression to the compression index ($C_\alpha/C_c \approx C_{\alpha\varepsilon}/C_{c\varepsilon}$) is relatively constant for a given soil. A typical comparison between $C_\alpha$ and $C_c$ for two clays is shown in Figure 6-38. Values of $C_\alpha/C_c$ for several different inorganic clays and silts are provide in Table 6-17. Table 5-10 provides additional values of $C_\alpha/C_c$ for several organic soils. Often, the value of $C_\alpha/C_c$ for inorganic clays and silts is approximately 0.04±0.01. Values for organic clays and silts are often in the range 0.05±0.01 while values for peats are often approximately 0.06±0.01. These nominal values, or values provided in Table 6-17 and 5-10 may be used to estimate $C_\alpha$ when long duration load increments from consolidation tests are unavailable with the understanding that such estimates involve considerable uncertainty. These values may also be used to assess measured values from laboratory tests or for preliminary analyses. If the final effective stress in the ground is less than $\sigma_p'$, $C_\alpha$ should be estimated using $C_r$ instead of $C_c$.

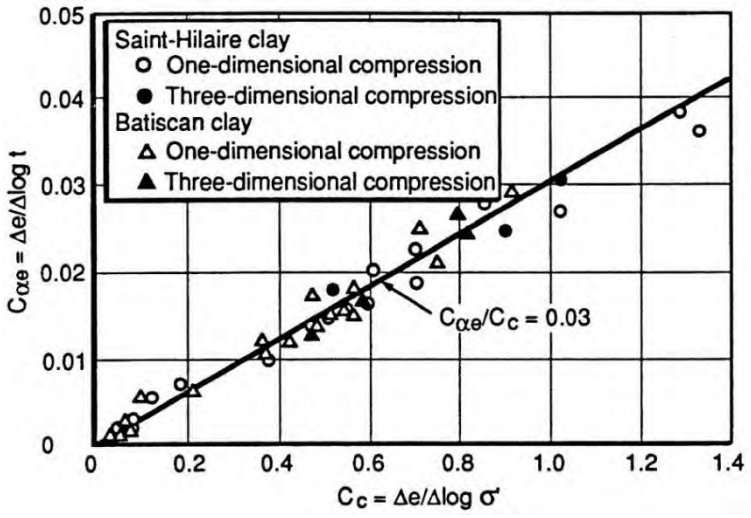


**Figure 6-38 Typical relationship between $C_{\alpha\varepsilon}$ and $C_c$ for two clays (from Mesri, et al., 1995).**

**Table 6-17 Values of $C_\alpha/C_c$ for several inorganic clays and silts (from Mesri and Godlewski, 1977).**

| Soil Type | $C_\alpha/C_c$ |
|---|---|
| Whangamarino clay | 0.03 to 0.04 |
| Leda clay | 0.025 to 0.06 |
| Soft blue clay | 0.026 |
| Portland sensitive clay | 0.025 to 0.055 |
| San Francisco Bay mud | 0.04 to 0.06 |
| New Liskeard varved clay | 0.03 to 0.06 |
| Silty clay | 0.032 |
| Near-shore clays and silts | 0.055 to 0.075 |
| Mexico City clay | 0.03 to 0.035 |
| Hudson River silt | 0.03 to 0.06 |

### 6.14.4 Stress History

Qualitatively, it is generally well known that the liquidity index, $LI$, provides an indirect indication of stress history. Soils with $LI \geq 1$ are typically normally consolidated while soils with $LI \leq 0$ are typically moderately to heavily overconsolidated. Several attempts have been made to directly correlate $LI$ to $OCR$ or $\sigma_p'$ for different soils. For soils with sensitivity between 1 and 10, Stas and Kulhawy (1984) suggested that $\sigma_p'$ is related to $LI$ as

$$\frac{\sigma_p'}{p_a} = 10^{(1.11-1.62\cdot LI)} \tag{6.24}$$

Figure 6-39 shows generalized relationships between liquidity index and preconsolidation stress, as related to sensitivity. The reliability of estimates from Figure 6-39 is unknown so values established from the figure should only be used for preliminary design or evaluation of laboratory or in situ measurements.

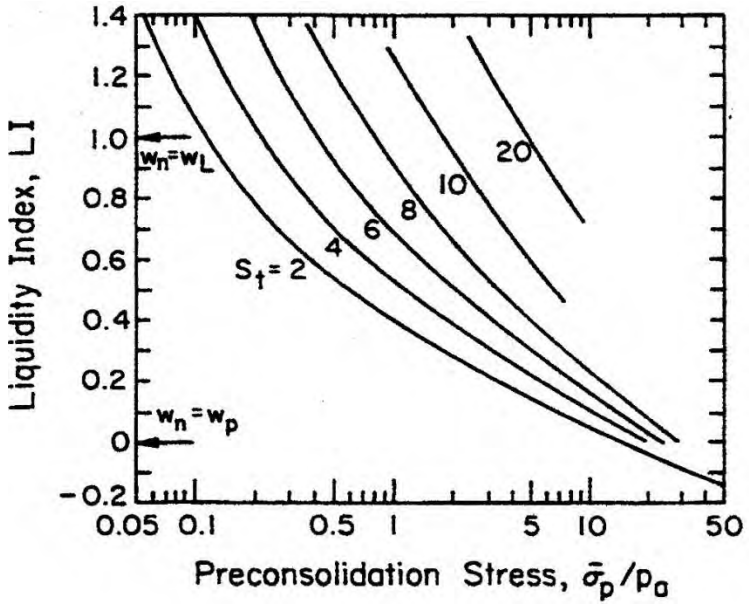


**Figure 6-39 Generalized relationship between preconsolidation stress and liquidity index (NAVFAC, 1986).**

# CHAPTER 7
# MEASUREMENT AND INTERPRETATION OF SHEAR STRENGTH PROPERTIES OF SOIL

Measurement and interpretation of shear strength properties of soils is a complex subject because the magnitude of the shear strength depends on many factors that extend beyond simple soil type. Shear strength, and shear strength properties may depend on the rate of loading, the loading "path", the magnitude of the effective confining stresses, the presence of secondary features (e.g., varves, fissures), and the degree of sample disturbance among many other factors. In this chapter, fundamental concepts related to soil shear strength are described to establish important background for measurement and interpretation of shear strength properties. Alternative methods for measuring soil shear strength or shear strength properties are discussed along with methods for interpreting individual measurements. This chapter focuses on shear strength, rather than on the stress-deformation-volume change response of soils, although some of the latter is included where pertinent to establishing appropriate values of soil strength properties for design. The content in this chapter focuses on interpreting measurements from individual tests; collective interpretation of multiple measurements for the purpose of establishing values for design parameters is addressed in Chapter 11.

## 7.1 USES FOR SHEAR STRENGTH PROPERTIES IN DESIGN AND CONSTRUCTION

Shear strength properties are perhaps the most commonly used and important of all geotechnical design parameters. Shear strength properties are primarily used to evaluate strength limit state criteria as part of geotechnical design, and it is common for such criteria to govern the eventual design. Some measure of shear strength is required for design of shallow and deep foundations, for design of man-made and natural earth slopes, and for design of earth retaining structures and tunnels. Shear strength properties are also required for evaluation of service limit states for some applications and can provide critical information for construction of specific features or elements. Selection of accurate and reliable values for shear strength parameters is therefore crucial for successful and cost effective geotechnical design and construction.

## 7.2 FUNDAMENTAL CONCEPTS OF SOIL SHEAR STRENGTH

Unlike many other soil properties, there is not a single unique value of shear strength for a specific soil (or rock) at a specific location in time and space. Instead, the value of shear strength depends on numerous factors that must be carefully considered to establish accurate and appropriate estimates for the shear strength of soil. In this section, fundamental concepts related to measurement and prediction of

shear strength are described to provide a basis for characterizing shear strength properties as part of geotechnical site characterization and design.

### 7.2.1 Shear Strength Envelopes

Soil is a fundamentally pressure dependent material in the sense that the shear strength, and the stress-strain response, depends on the magnitude of the effective confining stress. Because of this, soil strength is generally defined using the concept of a shear strength envelope as illustrated in Figure 7-1. The Mohr's circles shown in Figure 7-1 represent two states of stress in the soil: one being stable and one being at a state of failure. States of stress falling below the failure envelope are considered to be stable while states of stress that are tangent to the failure envelope are considered to be in a state of failure. States of stress passing above the envelope represent impossible states of stress.

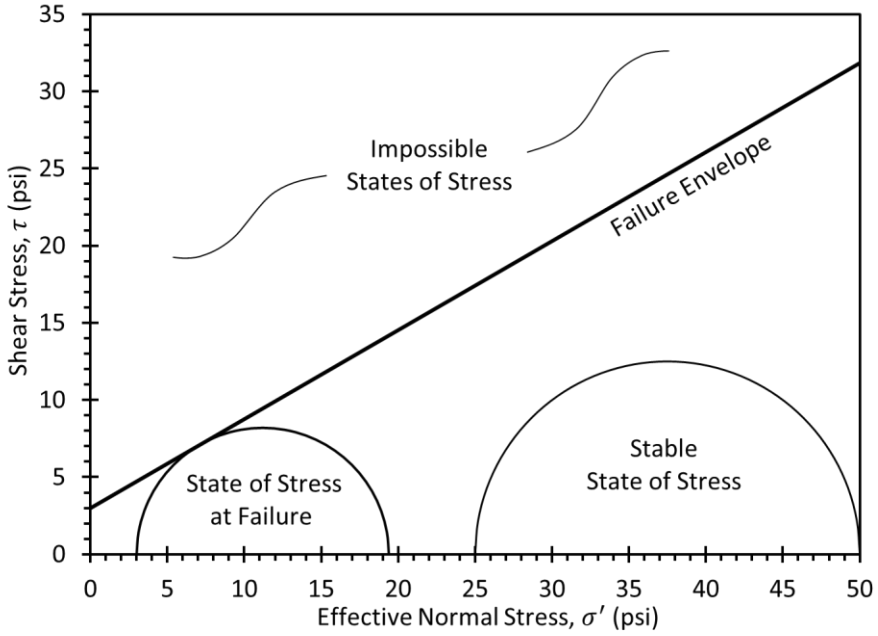


**Figure 7-1 Mohr-Coulomb diagram showing Mohr's circles representing failure and stable state of stress**

The primary approach used to characterize the shear strength envelope for a specific soil is to perform several tests at different confining stresses (or normal stresses). The state of stress at failure from each test is then plotted as illustrated in Figure 7-2 to establish the location of the failure envelope. If the shear strength envelope is linear, or can be practically approximated as linear, the shear strength can be expressed as

$$s = c' + \tan \phi' \tag{7.1}$$

where $s$ is the shear strength, $c'$ is the effective stress cohesion intercept, and $\phi'$ is the effective stress friction angle. Note that $s$ is used to denote shear strength, which should be distinguished from the shear stress, $\tau$, that can take on values that are less than the shear strength. The terms $c'$ and $\phi'$ are referred to as Mohr-Coulomb shear strength parameters, defined here in terms of the effective stress:

$$\sigma' = \sigma - u \tag{7.2}$$

where $\sigma'$ is effective stress, $\sigma$ is the total or applied stress, and $u$ is the pore water pressure. In some cases, the observed shear strength envelope may be curved. In cases where curve envelopes are observed, an alternative expression to Equation 7.1 can be considered to adequately represent the observed curvature or an approximate linear envelope can be fit to the observed measurements.

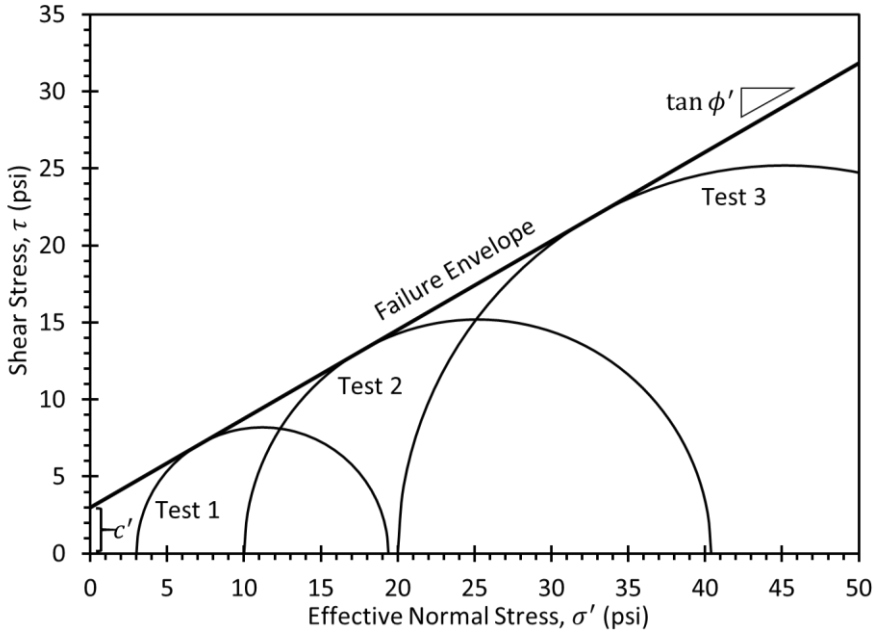


**Figure 7-2 Mohr-Coulomb diagram showing states of stress at failure for tests performed at different effective confining stress.**

While Mohr's circles and Mohr-Coulomb diagrams like those shown in Figure 7-1 and 7-2 have traditionally been used for plotting states of stress and establishing shear strength envelopes, it is often inconvenient to plot circles representing states of stress for such diagrams. Additionally, using Mohr's circles can make characterization of variability and uncertainty challenging. As such, it is often convenient to use alternative "modified" Mohr-Coulomb diagrams for establishing shear strength envelopes. In modified Mohr-Coulomb diagrams, states of stress are represented as a single point, rather than as a circle, which allows states of stress to be more easily plotted using commercial software.

One form of modified Mohr-Coulomb diagram is shown in Figure 7-3, with the two points shown corresponding to the states of stress for the two Mohr's circles in Figure 7-1. Using individual points to represent states of stress also allows "stress paths" to be plotted to illustrate and compare sequential states of stress. Finally, using individual points provides for more direct analysis of variability and uncertainty for the failure envelope. As illustrated in Figure 7-3, states of stress plotting below the failure envelope are again considered to be stable, states of stress on the failure envelope are at failure, and states of stress above the failure envelope represent impossible states of stress.

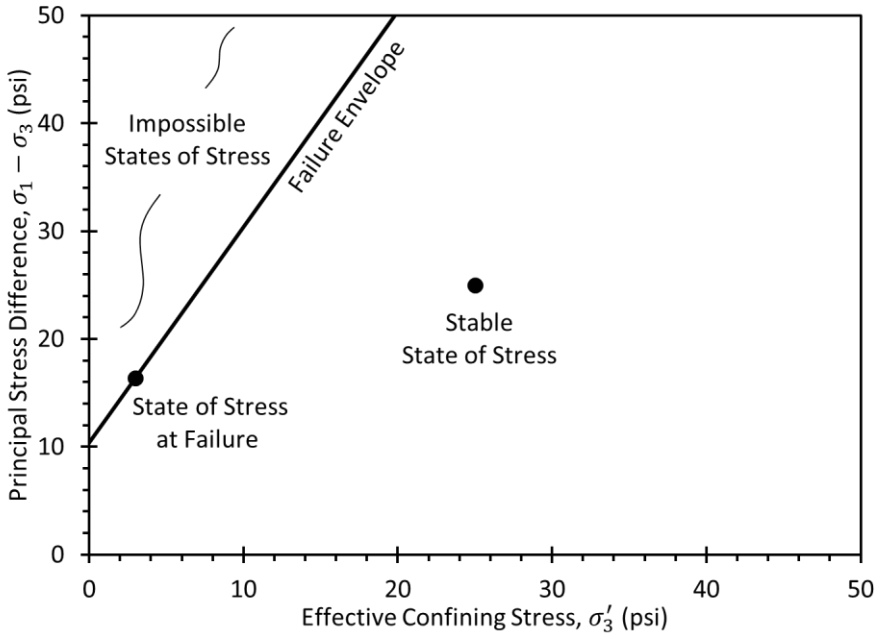


**Figure 7-3 Modified Mohr-Coulomb diagram showing state of stress at failure and stable state of stress.**

Several alternative modified Mohr-Coulomb diagrams can be used, each with advantages and disadvantages. Figure 7-4 shows a modified Mohr-Coulomb diagram that uses the principal stress difference, $(\sigma_1 - \sigma_3)$, and the effective confining stress, $\sigma_3'$, to represent states of stress, showing the same states of stress shown in Figure 7-2. Several additional common modified Mohr-Coulomb diagrams are summarized in Table 7-1. Because modified Mohr-Coulomb diagrams represent linear transformation of the traditional Mohr-Coulomb diagram, linear shear strength envelopes on a Mohr-Coulomb diagram will have corresponding linear envelopes in modified Mohr-Coulomb diagrams. However, the slope and intercept of shear strength envelopes in modified Mohr-Coulomb diagrams are not the Mohr-Coulomb shear strength parameters. The intercept and slope for modified Mohr-Coulomb diagrams are therefore generally denoted as $d$ and $\tan\psi$ as shown in Table 7-4. Fortunately, Mohr-Coulomb shear strength parameters can be directly calculated from values of $d$ and $\tan\psi$ established from modified Mohr-

Coulomb diagrams using the equations provided in Table 7-1. Because the equations provided are purely mathematical manipulations, no error is introduced by using modified Mohr-Coulomb diagrams to determine Mohr-Coulomb shear strength parameters.

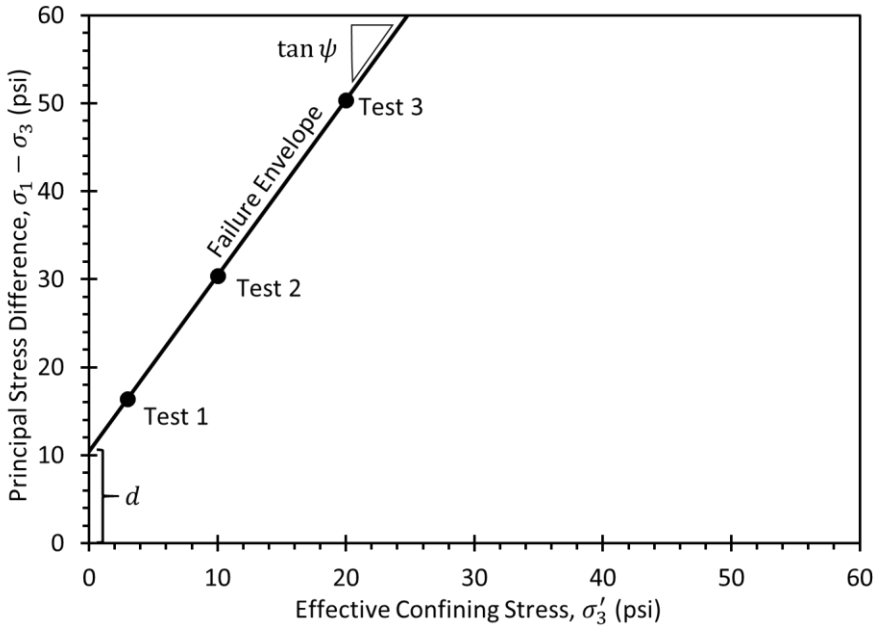


**Figure 7-4 Modified Mohr-Coulomb diagram showing same states of stress as shown in Figure 7-2.**

**Table 7-1 Common Modified Mohr-Coulomb diagrams.**

| Diagram | Abscissa | Ordinate | Mohr-Coulomb Cohesion Intercept | Mohr-Coulomb Friction Angle |
|---|---|---|---|---|
| $p$-$q$ diagram | $p = \frac{(\sigma_1 + \sigma_3)}{2}$ | $q = \frac{(\sigma_1 - \sigma_3)}{2}$ | $c = \frac{d}{\cos\phi}$ | $\phi = \sin^{-1}(\tan\psi)$ |
| $p$-$q$ diagram | $p = \frac{(\sigma_1 + 2\sigma_3)}{3}$ | $q = (\sigma_1 - \sigma_3)$ | $c = d\left(\frac{3 - \sin\phi}{6\cos\phi}\right)$ | $\phi = \sin^{-1}\left(\frac{3}{1 + \frac{6}{\tan\psi}}\right)$ |
| $(\sigma_1 - \sigma_3)$ vs. $\sigma_3'$ | $(\sigma_1 - \sigma_3)$ | $\sigma_3'$ | $c = d\left(\frac{1 - \sin\phi}{2\cos\phi}\right)$ | $\phi = \sin^{-1}\left(\frac{1}{1 + \frac{2}{\tan\psi}}\right)$ |
| $\sigma_1'$ vs. $\sigma_3'$ | $\sigma_1'$ | $\sigma_3'$ | $c = d\left(\frac{1 - \sin\phi}{2\cos\phi}\right)$ | $\phi = \sin^{-1}\left(\frac{\tan\psi - 1}{\tan\psi + 1}\right)$ |

Note: $d$ and $\tan\psi$ are the intercept and slope of the failure envelope from the respective diagram.
Equations apply to envelopes established in terms of total or effective stresses.

### 7.2.2 Defining Failure

Calculations described in the previous section are performed using knowledge of states of stress at failure. However, several criteria can be used to define failure. One common criterion for defining the so-called

"peak strength" is to define failure as the condition where the maximum shear stress is achieved. This criterion is referred to as the "peak principal stress difference" (PSD) criterion because it corresponds to the condition where the principal stress difference, $\sigma_1 - \sigma_3$, reaches the maximum value during a test. Alternatively, failure can be defined as the condition where the maximum principal effective stress ratio, $\sigma_1'/\sigma_3'$, is achieved. Figure 7-5 shows measured stress-strain responses from two consolidated-undrained triaxial compression tests on specimens of kaolinite to illustrate these two criteria. During drained tests, the two failure criteria are achieved simultaneously so there is no ambiguity about the state of stress at failure. However, in undrained tests like those shown in Figure 7-5, the two failure criteria may occur at substantially different points during a test, thus leading to two alternative states of stress at failure. Both states of stress have practical relevance, as described in more detail in Section 7.6.1. The peak principal stress difference criterion corresponds to the condition where the maximum load is applied during a test. Conversely, the peak principal effective stress ratio (PSR) criterion corresponds to the condition where the frictional resistance of the soil is fully mobilized (sometimes called "maximum obliquity").

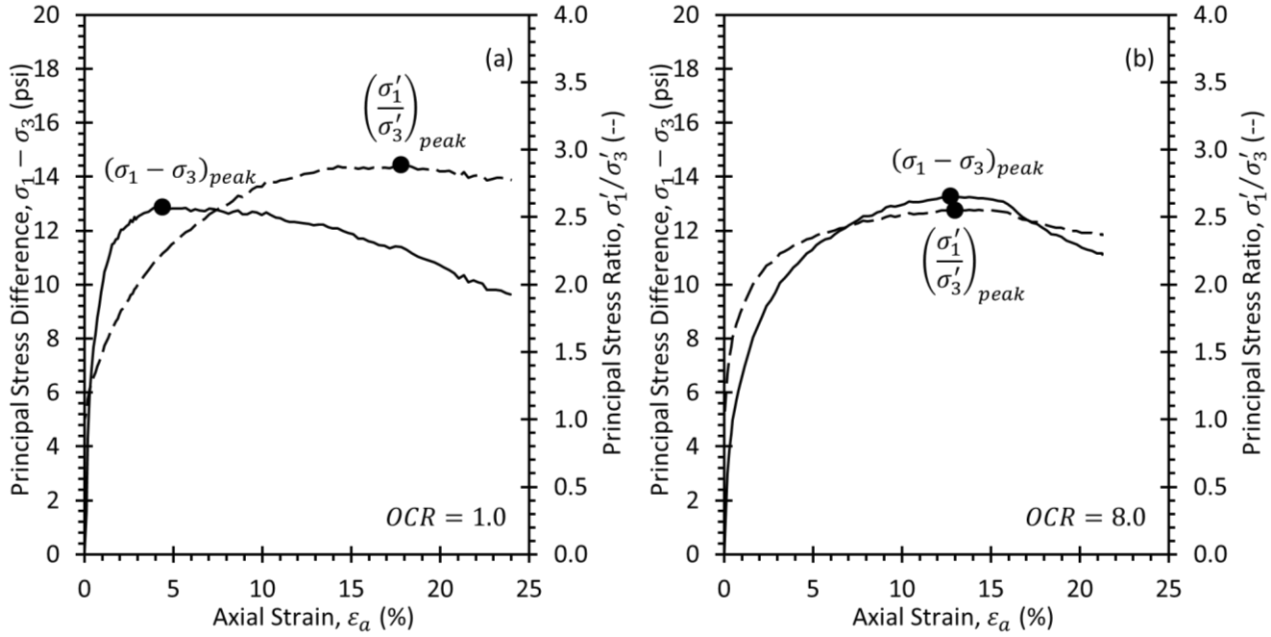


**Figure 7-5 Stress-strain response for kaolinite specimens showing two alternative failure criteria: (a) normally consolidated condition and (b) overconsolidated condition.**

Both the PSD and PSR failure criteria are considered to represent the "peak strength" of the soil. For some soils like heavily overconsolidated, stiff clays, the stress-strain response is such that the soil "softens" when sheared past the point where the peak strength is mobilized as shown in Figure 7-6. In such soils, it may be appropriate to consider the "residual strength" that represents the strength of the soil at very large displacements (e.g., if the soil has already been subjected to large displacements). As

described in more detail in Section 7.7, the residual shear strength cannot be reasonably measured in a triaxial test and must be measured using a direct shear or torsional ring shear device.

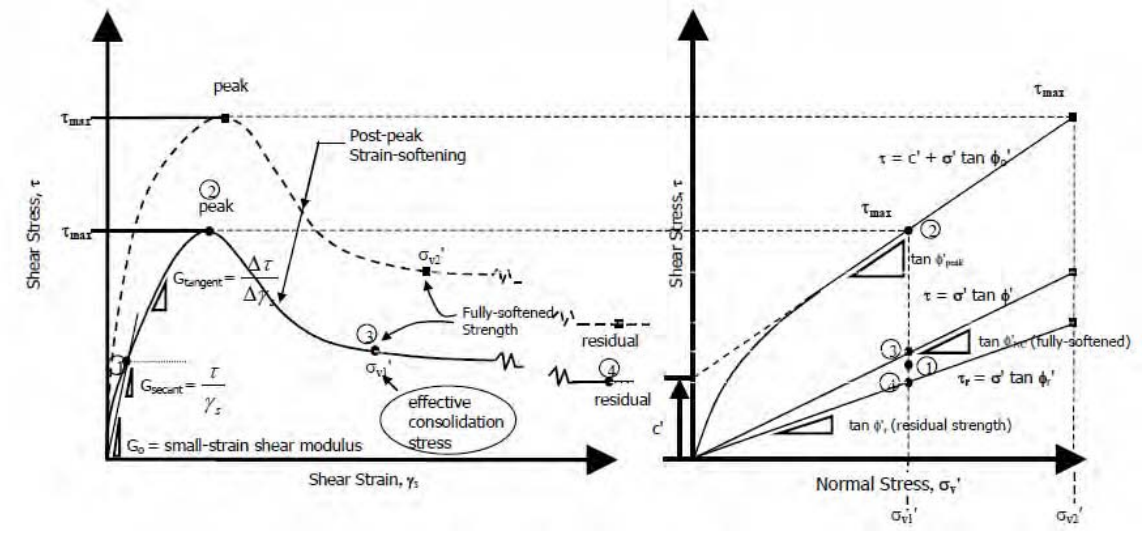


**Figure 7-6 Drained stress-strain behavior showing strain softening response typical of stiff, heavily overconsolidated clays.**

Finally, in some design conditions (e.g., design in stiff, fissured clays that have not been subjected to large displacements), it may be appropriate to use shear strength envelopes established to represent the "fully softened" shear strength. The fully softened condition generally corresponds to the strength that would exist if the soil were reconstituted to a normally consolidated condition at the same water content. The fully softened strength is seldom directly measured in practice. Instead, the fully softened shear strength envelope is often established from the measured peak strength friction angle, setting the cohesion intercept to zero. Alternatively, the fully softened strength envelope can be estimated as described in Section 7.7.

### 7.2.3 Measures of Shear Strength

Shear strength is generally understood to be the value of shear stress at failure. However, several values of shear stress can be adopted to represent shear strength. Figure 7-7 shows a Mohr's circle representing a state of stress at failure (for any of the failure criteria described in the previous section) showing two alternative definitions of shear strength. The more fundamental definition is that the shear strength corresponds to the magnitude of the shear stress on the failure plane at failure. This definition is denoted $\tau_{ff}$ and taken to be the value of shear stress at the point where Mohr's circle is tangent to the failure envelope, which corresponds the shear stress on the failure plane. The second definition corresponds to the maximum value of shear stress at the condition of failure, $\tau_{max}$, which represents the peak of the

Mohr's circle at failure. The latter definition is strictly incorrect because it doesn't represent the shear stress on the failure plane. It is sometimes adopted as a matter of convenience or necessity, but generally overestimates the true shear strength ($\tau_{ff}$) by 10 to 15 percent.

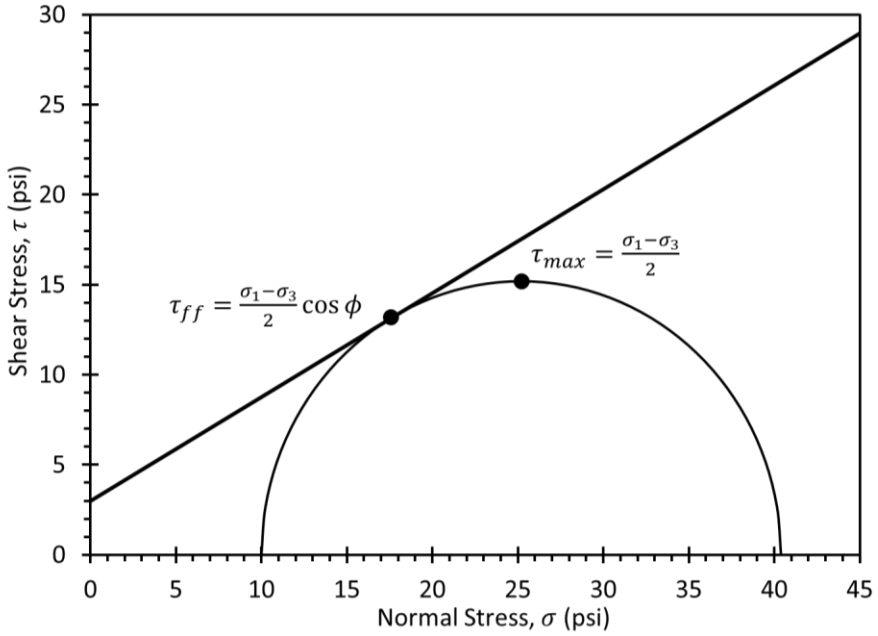


**Figure 7-7 Mohr's circle at failure showing alternative values of shear stress used to define shear strength.**

### 7.2.4 Drainage and Excess Pore Water Pressures

The strength and stress-strain response of soil depends significantly on the degree to which the soil is allowed to drain. When an element of soil is loaded under undrained conditions, without allowing water to enter or exit the element, "excess" pore pressure is generated that changes the pore water pressure in the element. The magnitude of the pore pressure can be expressed mathematically as

$$u = u_o + \Delta u \tag{7.3}$$

where $\Delta u$ is the excess pore pressure generated during undrained loading, $u_o$ is the initial pore pressure, and $u$ is the overall pore pressure. The magnitude of $u_o$ is generally controlled by hydraulic boundary conditions (e.g., from steady state seepage conditions) and potentially from prior increments of undrained loading. The magnitude of $\Delta u$ depends on characteristics of the applied load, on the degree of saturation, and the void ratio of the soil relative to the "critical" void ratio (which in turn depends on stress history). The excess pore pressure affects the magnitude of the effective stress (Equation 7.2) that, in turn, influences the soil strength and stress-strain response.

Excess pore pressures (positive or negative) generated during undrained loading will dissipate with time via the consolidation process described in Chapter 6. The rate of pore pressure dissipation is controlled by the hydraulic conductivity, $k$, or the related coefficient of consolidation, $c_v$, of the soil. Clean coarse-grained soils dissipate excess pore pressures very quickly while fine-grained soils often require substantial time for excess pore pressures to fully dissipate. The term "fully drained" is used to refer to conditions where all excess pore pressure has dissipated such that $\Delta u = 0$. Conversely, the term undrained is used to mean that no dissipation of excess pore pressure has occurred. Note that fully drained does not imply that there is no water in the soil, nor does it imply that the pore water pressure ($u$) is equal to zero. Rather, it simply implies that pore pressure is controlled exclusively by steady state seepage considerations (i.e., $u = u_o$).

A primary objective for geotechnical design is to ensure that a specific feature will perform acceptably throughout the intended life of the feature. Achieving this objective generally requires consideration of short-term conditions that are often considered undrained, long-term conditions that are considered fully drained, as well as intermediate term conditions that may be considered as partially drained. As a practical matter, however, undrained and fully drained conditions sufficiently bound performance; thus, partially drained conditions are infrequently considered unless notable loading is expected under partially drained conditions (e.g., staged loading of embankments on soft foundations). For geotechnical design at sites composed exclusively of soils that drain quickly, the short-term condition is often not explicitly considered because drainage is presumed to occur more quickly than load will be applied.

Fortunately, the shear strength of soil under both fully drained and undrained conditions is governed by the same effective stress strength envelope. Slight differences may be observed between effective stress strength envelopes established from drained and undrained laboratory tests; the observed differences are primarily attributed to differences in volume change between drained and undrained tests (Bjerrum and Simons, 1960; Bjerrum, et al., 1961). These slight differences generally have little practical significance for most geotechnical design. The same cannot be said about the magnitude of undrained and drained shear strengths, which are commonly quite different. This observation results from considerations of stress path and the methods used to establish undrained shear strengths, as described in more detail in the following sections.

### 7.2.5 Influence of Stress Path

As a general rule, the effective stress shear strength envelope, and the effective stress shear strength parameters used to represent the envelope, governs the shear strength of soil regardless of the method of

loading, drainage conditions, etc. This does not mean that the shear strength will be the same for all loading conditions, here distinguishing between the envelope and an actual value of shear strength derived from that envelope. The stress path taken strongly influences the magnitude of the actual shear strength because the stress path dictates where failure actually occurs along the envelope. The distinction between the shear strength and the shear strength envelope or shear strength parameters is illustrated in Figure 7-8. In the figure, stress paths for drained triaxial compression (TC), direct simple shear (DSS), and triaxial extension (TE) tests are shown for a specimen consolidated isotropically to an effective confining stress of 30 psi. As shown, the drained shear strength for identical specimens loaded along different stress paths will vary from 11.7 psi for loading in triaxial extension to 35.2 psi for loading in triaxial compression. The shear strength envelope for all three stress paths is identical; however, the shear strengths that result from the alternative stress paths is dramatically different.

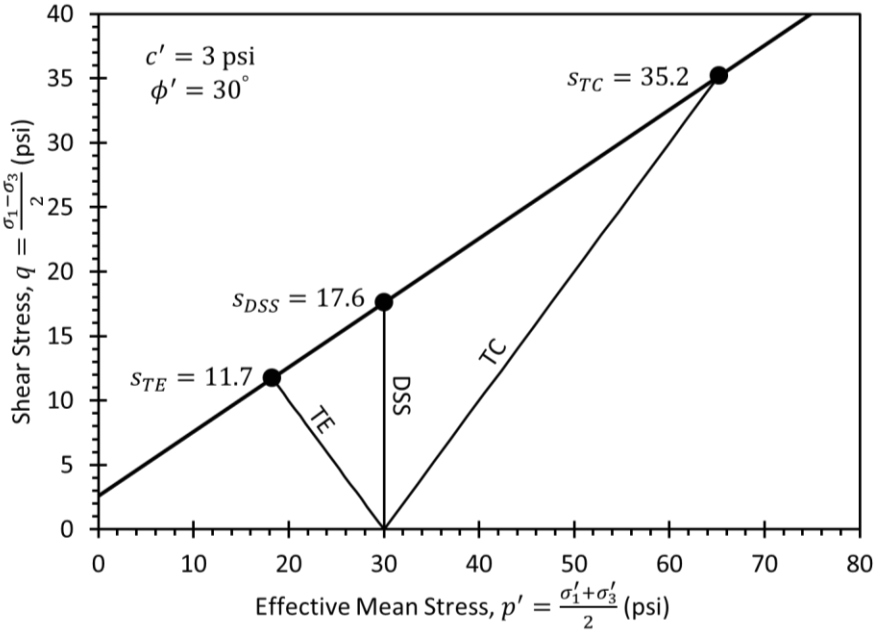


**Figure 7-8 Modified Mohr-Coulomb diagram showing drained stress paths and drained shear strengths for triaxial extension, direct simple shear, and triaxial compression tests.**

The same concept also applies for undrained loading, with added complication from the influence of excess pore pressures generated during undrained loading. Figure 7-9 shows two modified Mohr-Coulomb diagrams illustrating stress paths during undrained loading for normally consolidated and overconsolidated specimens. The drained stress paths from Figure 7-8 are also shown as dashed lines in Figure 7-9 for comparison. The undrained stress paths shown in Figure 7-9 depart from the drained stress paths as a result of excess pore pressures generated because loading is undrained. The pore pressures generated during undrained loading change along the stress path, and differ for the normally consolidated

condition shown in Figure 7-9a and the overconsolidated condition shown in Figure 7-9b. The excess pore pressures produce the effect of the stress path being shifted to the left or right of the corresponding paths for drained loading depending on whether the excess pore pressures are positive or negative.

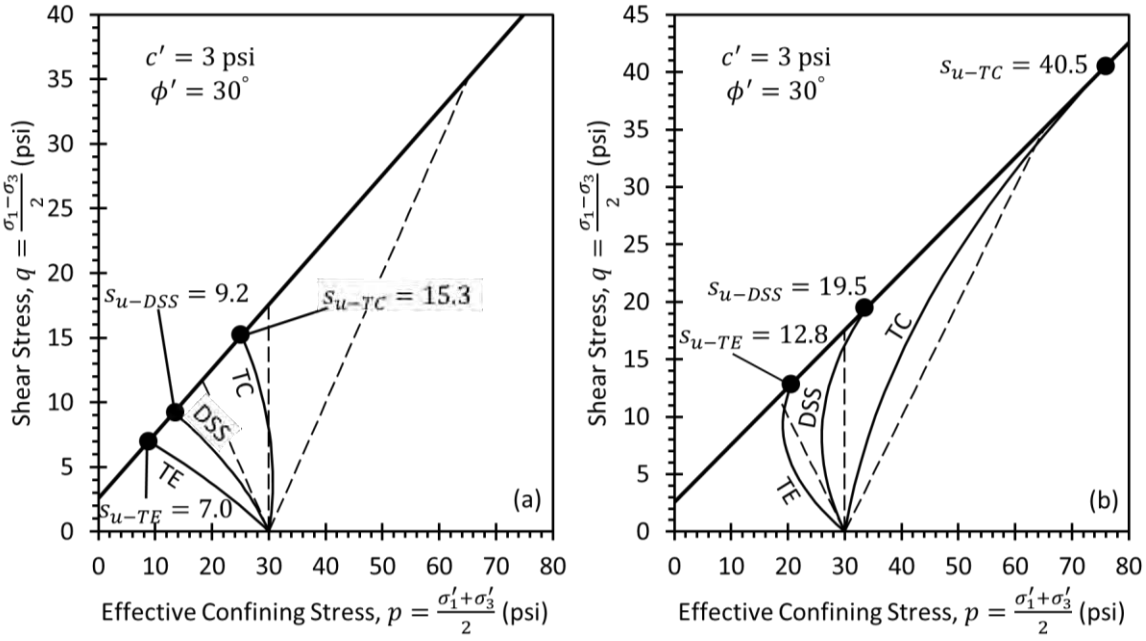


**Figure 7-9 Modified Mohr-Coulomb diagrams showing undrained stress paths and shear strengths for triaxial extension, direct simple shear, and triaxial compression tests: (a) normally consolidated condition and (b) overconsolidated condition.**

Excess pore pressures generated for soft, normally or near normally consolidated soils are generally positive and relatively large compared to more heavily overconsolidated soils. The excess pore pressures therefore cause the stress path to be shifted to the left of the drained stress path and to intersect the failure envelope to the left of where it would intersect if loading were drained as shown in Figure 7-9a. The positive pore pressures therefore produce the result that the undrained shear strength is less than the drained shear strength for similar applied loads (i.e., applied total stresses). For example, the drained shear strength for loading in triaxial compression ($s_{TC}$) in Figure 7-8 is 35.2 psi whereas the undrained shear strength for triaxial compression is 15.3 psi.

In contrast, excess pore water pressures generated for stiff, heavily overconsolidated soils are substantially less than those generated for normally consolidated soils and often become negative as the stress path approaches the failure envelope. This response is shown in Figure 7-9b, with the undrained stress paths initially being shifted to the left of the corresponding drained stress paths because of small positive excess pore pressures. As shear stresses are further increased and the stress path approaches the failure envelope, the undrained stress path approaches and eventually crosses to the right of the drained

stress paths due to excess pore pressures becoming negative. The net result of this response is that the undrained shear strength for heavily overconsolidated soils is generally greater than the corresponding drained shear strength, as shown in Figure 7-9b. Anisotropic consolidation, which effectively shifts the starting point for loading off the horizontal axis, also produces differences in stress paths and differences in undrained shear strength.

Figure 7-10 illustrates the practical relevance of stress path considerations for an embankment on soft foundation soils. Portions of the soil along the sliding surface shown are sheared in a manner consistent with triaxial compression, whereas other portions of the sliding surface are sheared in a manner consistent with direct simple shear or triaxial extension. Similar considerations apply to many other geotechnical design applications. Accurate evaluation of shear strength must therefore recognize differences in shear strengths obtained for each of these shearing modes. Fortunately, most methods of analyses adopted for evaluation of drained loading conditions accurately capture the influence of stress path and, thus, it is only necessary to prescribe the effective stress strength envelope for design analyses. However, the same cannot be said for commonly adopted analysis methods for undrained stability. It is therefore necessary to prescribe undrained shear strengths or shear strength parameters that accurately and practically account for differences in undrained shear strength due to different stress paths. In most cases, this is accomplished using undrained shear strength and total stress strength envelopes.

### 7.2.6 Undrained Shear Strength and Total Stress Strength Envelopes

The shear strength of soil is fundamentally governed by effective stress strength envelopes, regardless of whether loading is drained or undrained and regardless of the stress path taken to reach the failure envelope. However, use of effective stress strength envelopes for design requires that pore water pressures be predicted or estimated so that the magnitude of the effective stress can be used to establish the shear strength from equations like Equation 7.1. For problems involving consideration of fully drained conditions, pore water pressures can be predicted using steady state seepage analyses so effective stress analyses can be reasonably and practically used. However, when considering short-term conditions where the soil will be subjected to undrained (or partially drained) loading, the magnitude of pore pressures is more difficult to predict. As a result, analyses for short-term, undrained conditions are generally conducted in terms of total stresses using total stress strength envelopes or related soil strength parameters. Adopting total stress analyses for evaluating stability under undrained conditions simplifies conduct of the stability analyses. However, it complicates interpretation of shear strength because it becomes necessary to establish strengths or strength parameters that are consistent with the anticipated loading (which are still governed by the effective stress and the effective stress strength envelope).

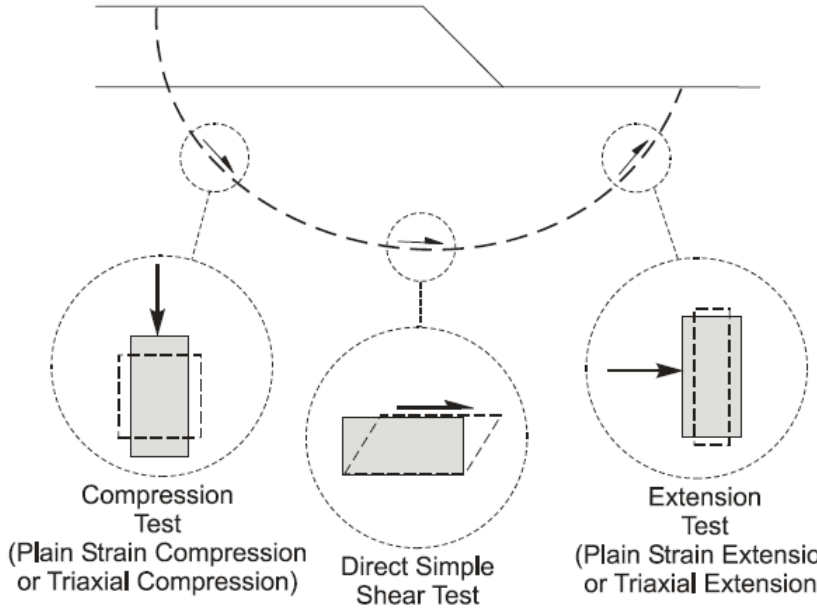


**Figure 7-10 Shearing modes along different portions of a potential sliding surface for an embankment on a soft foundation.**

In general, total stress strength envelopes are conceptually similar to effective stress strength envelopes except that the envelope is established by plotting measurements in terms of the total, or applied stresses instead of effective stresses. Figure 7-11 shows an example total stress strength envelope. All mathematical representations presented previously, including equations for Mohr-Coulomb and modified Mohr-Coulomb diagrams, are appropriately applied to consideration of total stresses by simple substitution of total stress, $\sigma$, in place of the effective stress, $\sigma'$.

As shown in Figure 7-11, if the total stress strength envelope can be approximated as being linear, the total stress shear strength can be expressed as

$$s_T = c + \tan\phi \tag{7.4}$$

where $s_T$ is the shear strength established in terms of total stress, $c$ is the total stress cohesion intercept, and $\phi$ is the total stress friction angle. Note that the total stress strength parameters, $c$ and $\phi$, should be distinguished from effective stress strength parameters, $c'$ and $\phi'$. While conceptually similar, they should not be used interchangeably because they represent completely different parameters that are appropriate for completely different loading conditions.

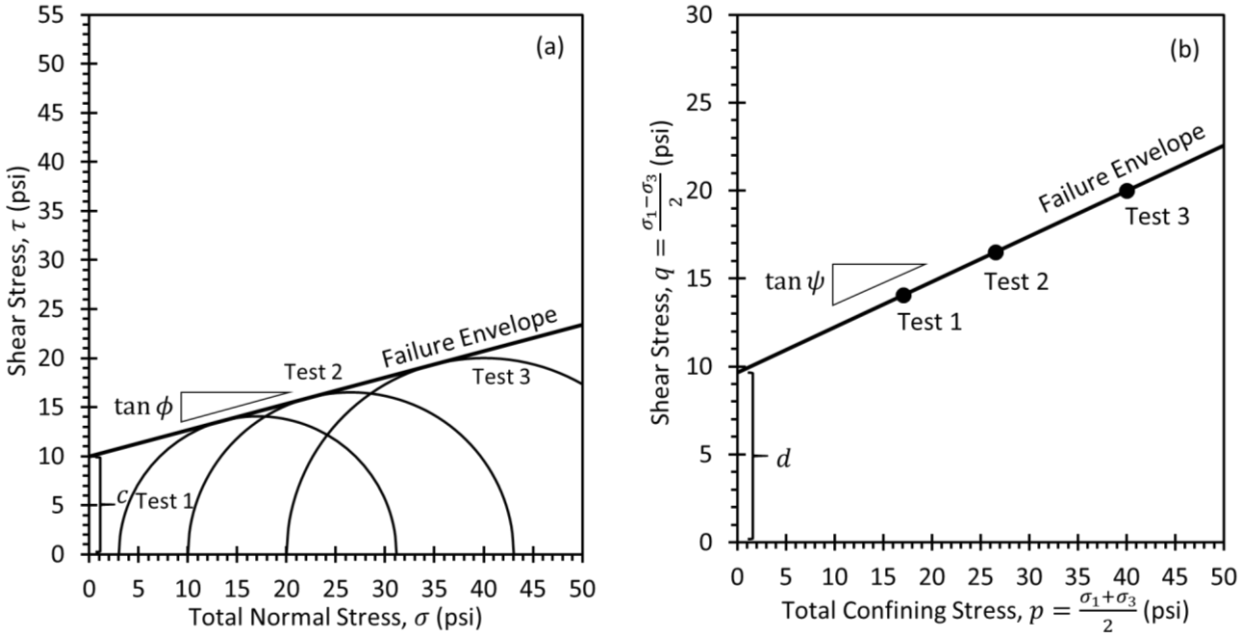


**Figure 7-11 Total stress strength envelopes for unsaturated soils: (a) Mohr-Coulomb diagram and (b) modified Mohr-Coulomb diagram.**

In the common, but special case where the soil is saturated and loading is undrained, application of total confining stress will not change the magnitude of the effective stress. This occurs because the excess pore pressure generated due to application of total confining stress without drainage will be equal to the total confining stress (i.e., $\Delta u = \Delta\sigma$). This, in turn, means that identical specimens subjected to different total confining stress will be subjected to identical effective stress. Since the effective stress controls failure, testing of identical saturated specimens at different total confining stresses produces the well-known $\phi = 0$ condition wherein the shear strength is observed to be independent of the total confining stress as shown in Figure 7-12. For this condition, the shear strength is commonly referred to as the undrained shear strength, $s_u$, and is equal in magnitude to the total stress cohesion intercept

$$s_u = c \tag{7.5}$$

Note that since total stress strengths are exclusively acquired from undrained tests, and exclusively used for analysis of undrained conditions, the shear strength given by Equation 7.4 is also technically an undrained shear strength and can be designated as $s_u$. However, use of the notation $s_u$ is commonly associated with $\phi = 0$ (i.e., saturated, undrained) conditions so the notation $s_T$ is adopted here to distinguish between these conditions.

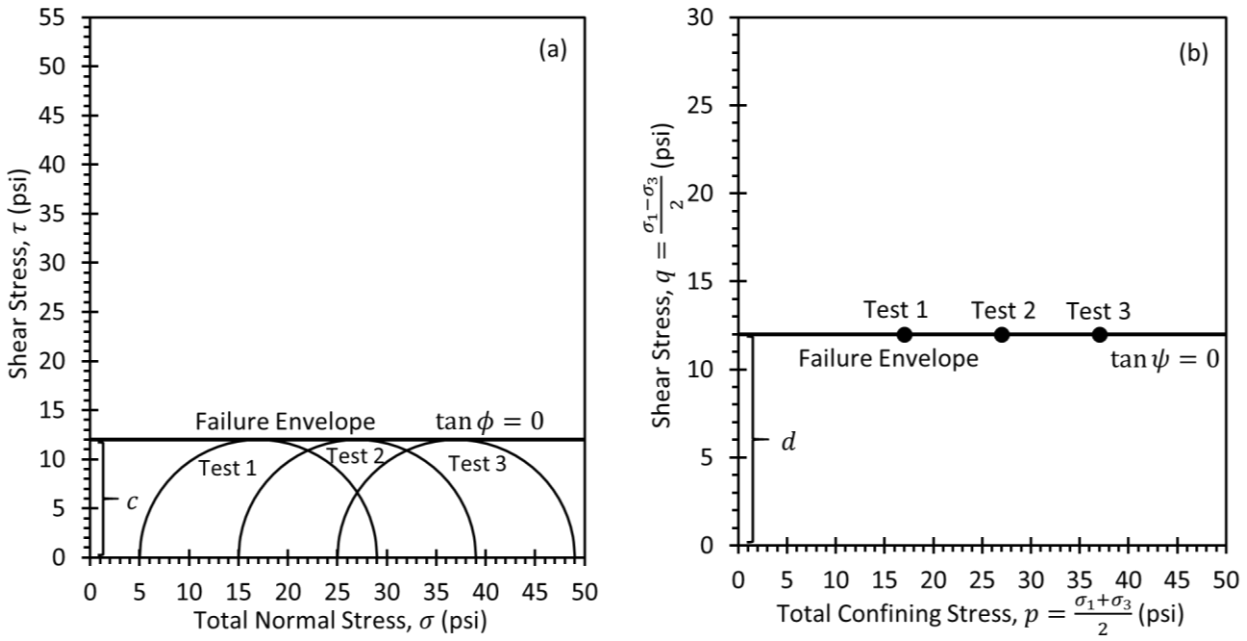


**Figure 7-12 Total stress strength envelopes for saturated soils ($\phi = 0$): (a) Mohr-Coulomb diagram and (b) modified Mohr-Coulomb diagram.**

It is important to recognize that the states of stress corresponding to failure in terms of total stresses (shown as Mohr's circles in Figure 7-11a and 7-12a, and as $p$-$q$ points in Figure 7-11b and 7-12b) are actually dictated by the magnitude of the effective stress, regardless of whether the effective stress is known. Thus, the diameter of the Mohr's circles, or the value of $q$ for points in the modified Mohr-Coulomb diagram, are controlled by the magnitude of the effective stresses and the effective stress strength envelope. Testing of specimens with different initial effective stress, prior to application of the total confining stress, will produce different total stress strength envelopes, different total stress strength parameters, and different values for undrained shear strength. Use of total stress analyses for evaluation of undrained conditions is therefore fundamentally predicated on the effective stress for specimens in the laboratory being the same as the effective stress for the soil in the field.

Although the total stress concept is simple, experience has shown that many factors influence the pore pressures that develop under undrained loading. As a result, determining undrained strengths by means of laboratory and in situ testing requires considerable attention to detail if reliable results are to be achieved. Shear strengths for total stress analyses must be measured using test specimens and loading conditions that closely duplicate conditions in the field. Alternatively, they can be measured using an appropriate in situ test as long as current in situ conditions are similar to those present during construction.

### 7.2.7 Normalized Soil Behavior

It has been recognized for many years that the strength and stress-strain response of many soils can be normalized with respect to the effective consolidation stress. As shown in Figure 7-13, the undrained stress-strain responses for four specimens of kaolinite consolidated to different effective stresses are notably different (Figure 7-13a). However, if these same measurements are normalized with respect to the consolidation stress, $\sigma'_{vc}$, for each test, the normalized responses are practically identical (Figure 7-13b) as long as all specimens have the same overconsolidation ratio, $OCR$. Most, but not all fine-grained soils with $OCR$ less than about 10 will exhibit normalized behavior similar to that shown in Figure 7-13. Highly structured soils may not exhibit normalized behavior because consolidation to different effective stress may alter the soil structure, thus changing the response in ways that are not proportional to the consolidation stress.

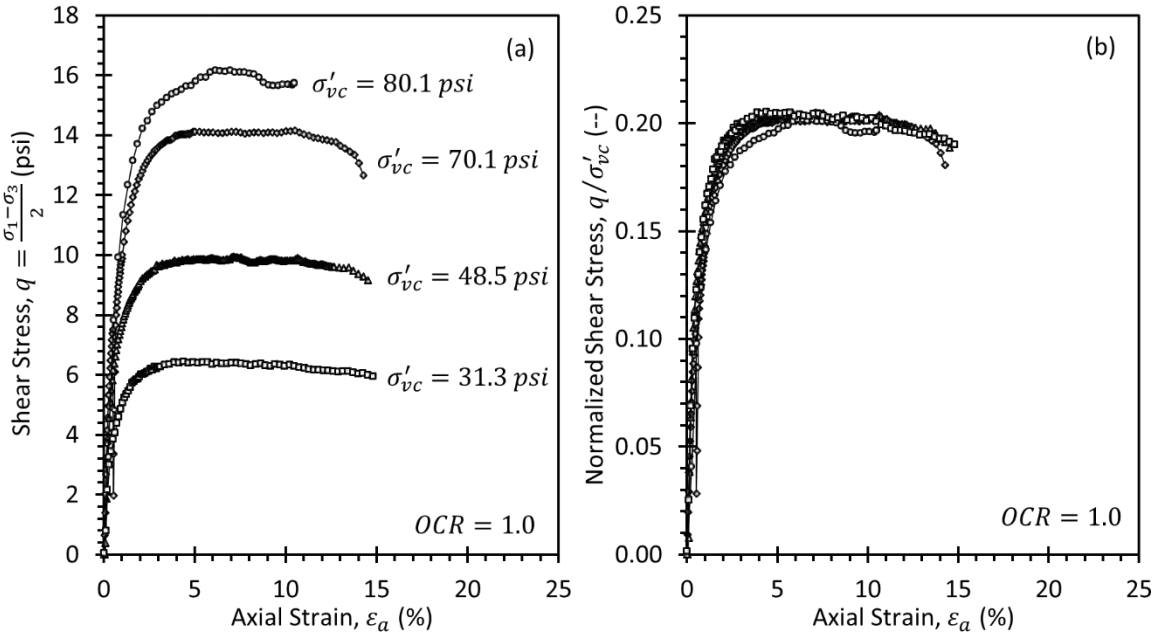


**Figure 7-13 Stress-strain response for normally consolidated kaolinite: (a) measured response, and (b) normalized response.**

Normalized soil behavior is particularly important for characterizing undrained shear strength because it means that $s_u$ is directly proportional to the consolidation stress for a given value of $OCR$. Thus, measured values of $s_u$ can be normalized by the effective consolidation stress ($\sigma'_{vc}$) to establish values for the normalized undrained shear strength ratio, $s_u/\sigma'_{vc}$ (often colloquially called the "c/p" ratio). Values of $s_u/\sigma'_{vc}$ can, in turn, be used to estimate the in situ $s_u$ based on knowledge of $\sigma'_{vo}$ in the field.

As shown in Figure 7-14, $s_u/\sigma'_{vc}$ is strongly dependent on $OCR$. The relationship between $s_u/\sigma'_{vc}$ and $OCR$ is generally expressed as

$$\frac{s_u}{\sigma'_{vc}} = S \cdot OCR^m \tag{7.6}$$

where $S$ and $m$ are fitting parameters. Fortunately, values for $S$ and $m$ generally fall within relatively small ranges, depending upon the method of loading (Jamiolkowski, et al. 1985; Koutsoftas and Ladd, 1985; Kulhawy and Mayne, 1990; Ladd, 1991; Ladd and DeGroot, 2003). As such, values for $S$ and $m$ can often be estimated with varying degrees of reliability as described in more detail in Section 7.4.8.

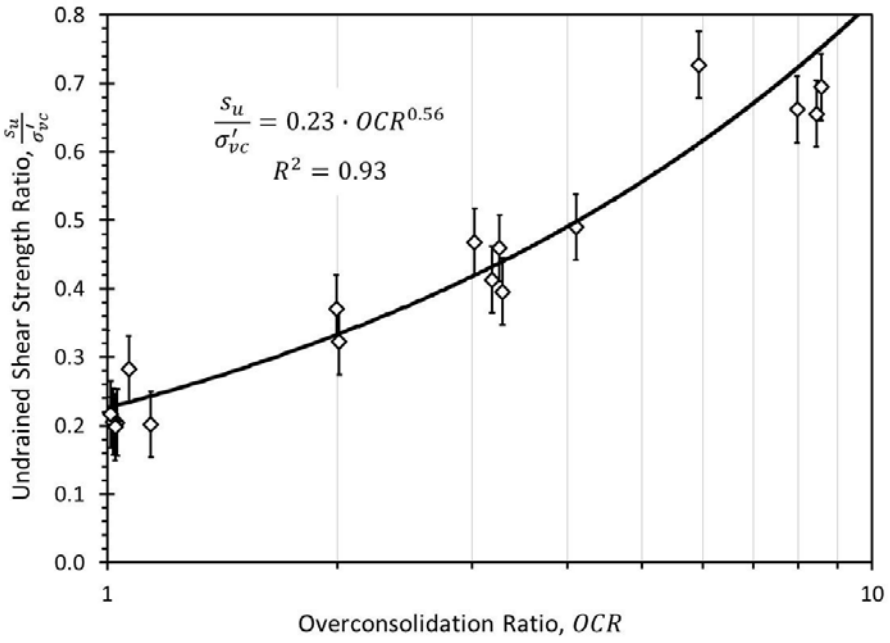


**Figure 7-14 Measured $s_u/\sigma'_{vc}$ for kaolinite specimens at different $OCR$.**

### 7.2.8 Influence of Anisotropy

A common assumption in many design and analysis methods is that the strength of soil can be considered isotropic. While this assumption is practically satisfied for many soils, it is not universally true for all soil and rock. Two forms of anisotropy are generally considered: inherent anisotropy and stress-induced anisotropy. Stress-induced anisotropy refers to differences in $s_u$ observed when loading a soil along different stress paths, as previously described in Section 7.2.5. Figure 7-15 shows measured values of $s_u/\sigma'_{vc}$ for tests of different normally consolidated clays in triaxial compression (TC), triaxial extension (TE), and direct simple shear (DSS), plotted as a function of the plasticity index, $PI$. From this figure, the magnitude of stress-induced anisotropy is greatest for fine-grained soils with low plasticity, which

suggests that the magnitude of stress-induced anisotropy also tends to increase with the magnitude of $\phi'$. Notably, stress-induced anisotropy occurs in all soils but does not affect the effective stress strength envelope. Rather, stress-induced anisotropy produces different $s_u$ (or total stress failure envelopes) for different stress paths while the effective stress strength envelope is entirely isotropic.

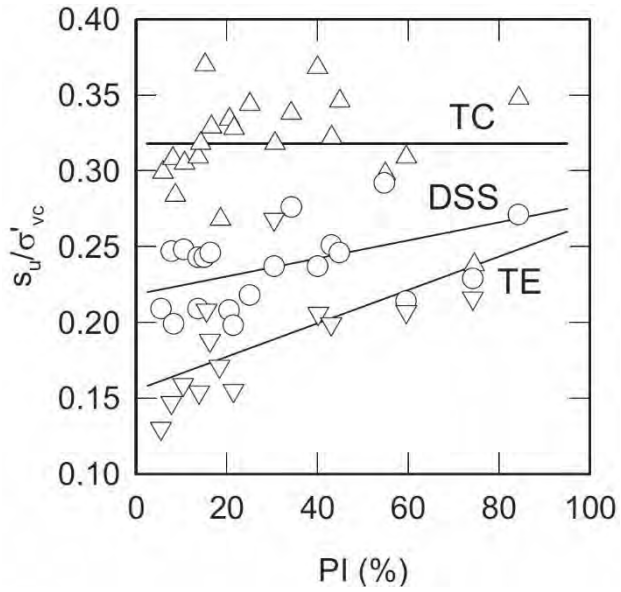


**Figure 7-15 Stress-induced anisotropy for undrained shear strength of normally consolidated clays (Ladd, 1991).**

Inherent anisotropy refers to anisotropy that arises from physical characteristics of soil or rock that produce different strengths, and strength envelopes, depending on the orientation of loading. Varved clays composed of thin, alternating layers of silt and clay are one relatively common soil type that exhibits inherent anisotropy. Heavily overconsolidated and fissured clays can also exhibit strong inherent anisotropy as shown in Figure 7-16. Inherent anisotropy produces differences in the effective stress strength envelope with the orientation of loading, which in turn also produces differences in undrained shear strength with loading direction.

### 7.2.9 Influence of Strain Rate

The rate at which load is applied, or more specifically the strain rate, has been found to have little effect on effective stress strength parameters for rates that are relevant for traditional construction. However, strain rate is widely recognized to influence the magnitude of the undrained shear strength. Figure 7-17 shows $s_u$ measurements made for a broad range in strain rate and various types of laboratory tests. The figure indicates that $s_u$ generally decreases by approximately 10 percent for each log-cycle decrease of strain rate. This is an issue of practical significance because $s_u$ is generally measured in the laboratory

over a matter of minutes to hours whereas typical construction generally occurs over a matter of weeks to months. As such, laboratory measured values of $s_u$ are likely to be 10 to 20 percent greater than is appropriate for typical loading rates in the field. While such a difference might be alarming to some, it is usually offset by compensating factors such as sample disturbance and partial drainage.

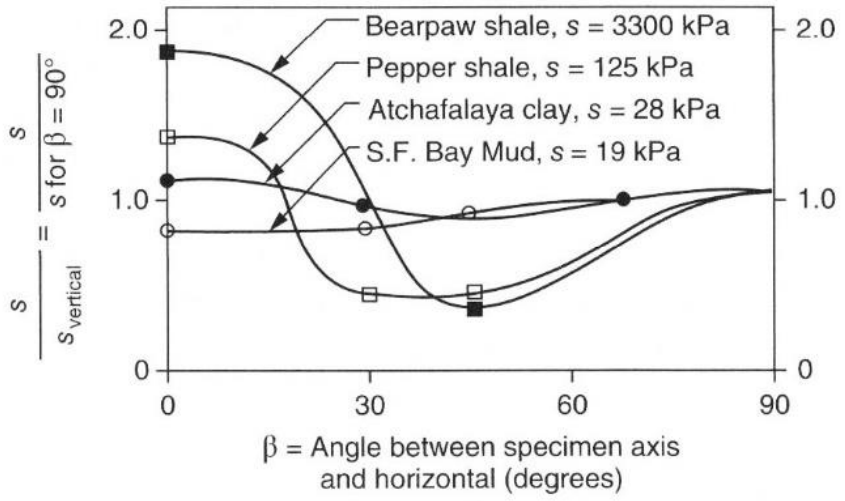


**Figure 7-16 Measured inherent anisotropy for several stiff clays and shales (Duncan, et al., 2014).**

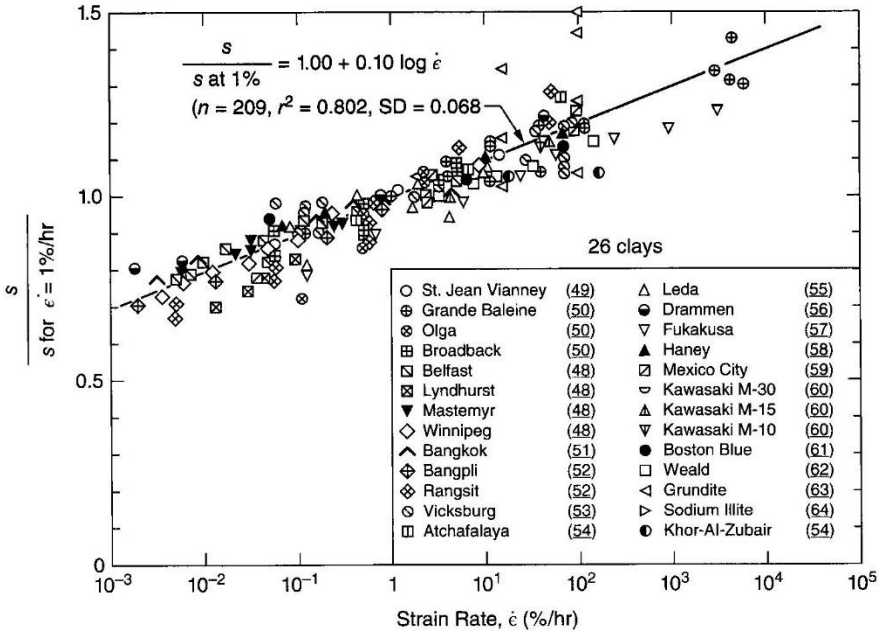


**Figure 7-17 Influence of strain rate on laboratory $s_u$ from different test methods (Kulhawy and Mayne, 1990).**

### 7.2.10 Influence of Cyclic Loading

Soils are often subjected to repeated or cyclic loading imposed due to earthquakes, wind, waves, and traffic. As a practical matter, the drained shear strength of soils is not significantly affected by cyclic loading, and drained shear strength may even improve as a result of densification. Under undrained loading conditions, however, many soils will fail at stresses that are substantially less than the "static" undrained shear strength when subjected to repeated load cycles. The observed loss of strength is predominantly attributed to generation of excess pore water pressures that reduce the effective stress and shear strength. In extreme cases, the excess pore pressures can become large enough to cause liquefaction as described in Chapter 5. Cyclic strength loss is generally most significant in saturated, sandy soils, but can also occur in fine-grained soils as shown in Figure 7-18. Strength loss will not generally occur for dense or unsaturated soils. As a practical matter for common transportation infrastructure, cyclic loading is predominantly a concern for seismic design, which is beyond the scope of this manual.

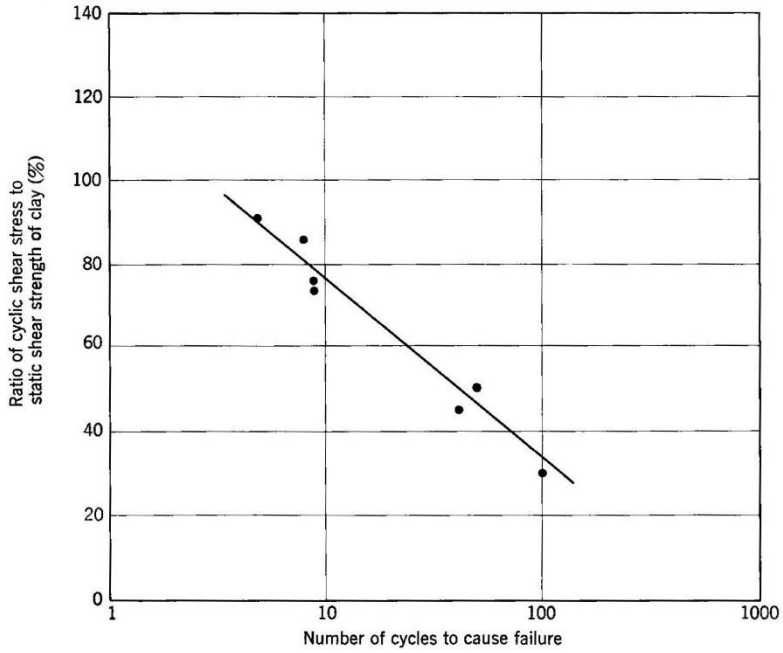


**Figure 7-18 Reduction of undrained shear strength for silty clay with number of loading cycles (Seed and Wilson, 1967)**

## 7.3 BORING AND SAMPLING REQUIREMENTS FOR LABORATORY STRENGTH TESTS

Laboratory measurement of shear strength and shear strength properties generally requires high quality specimens. In general, the quality of laboratory strength measurements can only be as good as the quality of the samples acquired for testing. This generally means using boring and sampling methods that are appropriate for obtaining samples with as little disturbance as possible. For soft to medium stiff, fine-

grained soils, rotary wash boring methods using heavy drilling mud are desirable to reduce stress relief at the base of the boring. Use of hydraulic or mechanical fixed piston samplers with thin-walled sampling tubes also helps to reduce disturbance. In stiffer fine-grained soils, use of traditional thin-walled tubes with diameters of 3 inches or greater are generally sufficient to acquire good quality samples. Disturbance can also be reduced by using 18- or 24-in long sampling tubes rather than longer tubes. Thin-walled tubes should be smoothly pushed rather than driven. In fine-grained soils that are too stiff for pushing thin-walled tubes, overcoring samplers such as the Pitcher or Denison samplers should be used. For all fine-grained soils, samples should be transported and stored in the sampling tubes and maintained in a vertical orientation for transportation and storage. Samples should also be sealed and protected from direct sunlight and extreme temperatures.

Acquiring undisturbed samples in clean coarse-grained soils is often extremely difficult and impractical. As a result, it is often necessary to utilize in situ testing to characterize the shear strength properties of such soils. In some cases, disturbed samples of clean coarse-grained soils can be acquired and "reconstituted" in the laboratory to void ratios similar to those encountered in the field. However, it is important to recognize that the process of acquiring and preparing reconstituted samples will necessarily destroy any inherent structure that is present in situ.

## 7.4 EVALUATION OF UNDRAINED SHEAR STRENGTH

Undrained shear strength can be evaluated using numerous types of laboratory and field tests, as described in the sections that follow. The specific choice of method is generally dictated by both the soil conditions present and the intended use. Because clean, coarse-grained soils are seldom loaded quickly enough for loading to be considered undrained, the content of this section is generally restricted to fine-grained soils. However, the content is also appropriate for coarse-grained soils that contain sufficient fines to behave like fine-grained soils (e.g., some clayey sands and silty sands).

### 7.4.1 Unconsolidated-Undrained Triaxial Tests

Unconsolidated-undrained (UU) triaxial tests (AASHTO T296 and ASTM D2850) are perhaps the most common type of test performed to measure the undrained shear strength of soils in practice. UU tests are most commonly performed as a triaxial compression test wherein the axial load in increased while the total confining stress is held constant, although alternative loading conditions can be imposed including triaxial extension. Figure 7-19 shows the measured stress-strain response from a UU triaxial compression test performed on a specimen of saturated kaolinite clay. As shown in the figure, $s_u$ is established as the maximum measured value of $(\sigma_1 - \sigma_3)/2$. It is not possible to establish the value of $\tau_{ff}$ (described in

Section 7.2.3) from results of UU tests because the magnitude of the effective stress friction angle ($\phi'$) is unknown. As such, it is usual practice to quantify $s_u$ as the maximum shear stress. While such practice slightly overestimates the value of $s_u$, experience has shown that this practice is usually compensated by other factors.

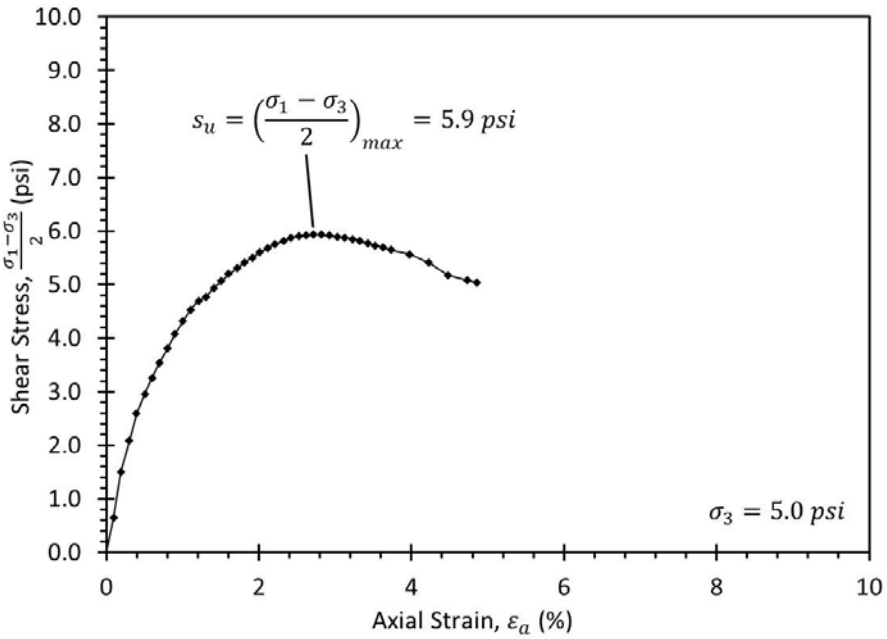


**Figure 7-19 Stress-strain response for UU triaxial compression test on saturated kaolinite.**

If the soil being tested is known to be saturated, results from UU triaxial tests should be interpreted based on the presumption that $\phi = 0$. As illustrated in Figure 7-20, it is common for results of replicate UU tests performed on identical specimens to produce different values of $s_u$ because of differences in sample disturbance or slight variations in specimen characteristics. If replicate tests are performed at different total confining stresses, as shown in Figure 7-21, it is sometimes possible for test measurements to indicate a trend that would suggest a non-zero value for the total stress friction angle, $\phi$. Such an interpretation would be incorrect since the observed trend is simply a result of variability in $s_u$ rather than a true reflection of increasing (or decreasing) $s_u$ with increasing confining stress. If the soil being tested is not saturated, measurements should not be interpreted assuming $\phi = 0$, but rather should be interpreted to establish the total stress shear strength envelope as described in Section 7.5.

Regardless of whether specimens are saturated or unsaturated, it is important to remember that the magnitude of $s_u$, or total stress strength parameters, are tied to the effective stresses in the specimens. Since the in situ effective stress is commonly depth dependent, measurements for specimens taken at

different depths should generally be considered separately and different values for $s_u$ or different total stress strength envelopes should be established for different depths.

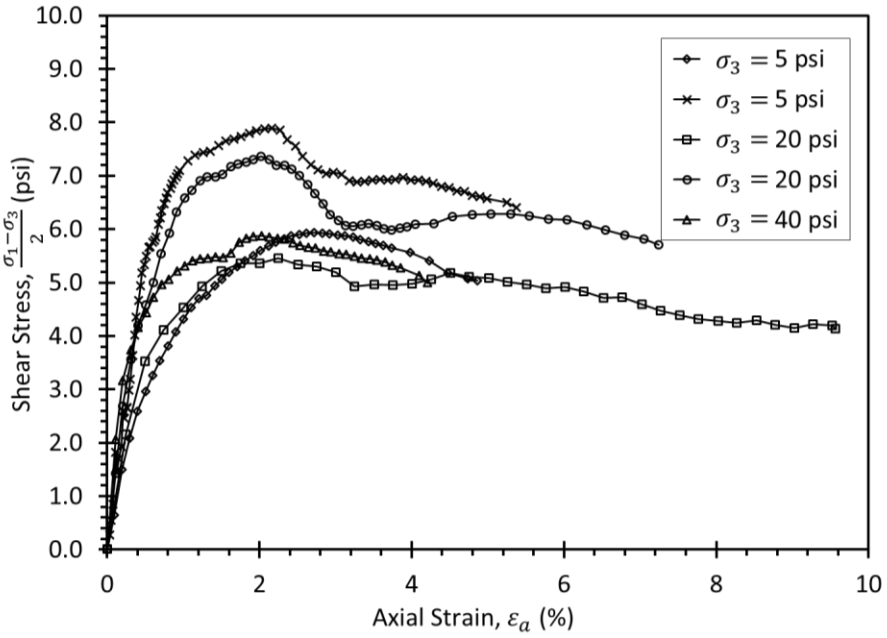


**Figure 7-20 Stress-strain response for UU triaxial compression tests on identical specimens of saturated kaolinite.**

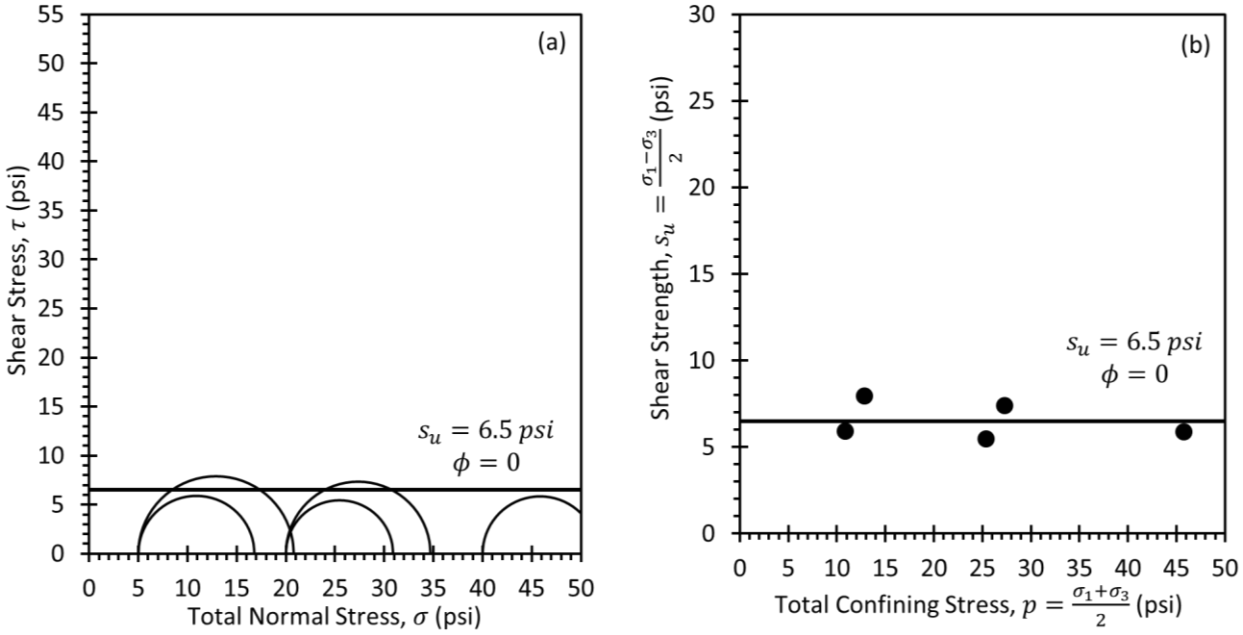


**Figure 7-21 Interpretation of failure envelope from tests on five identical specimens of saturated kaolinite: (a) Mohr-Coulomb diagram and (b) modified Mohr-Coulomb diagram.**

### 7.4.2 Unconfined Compression Tests

Unconfined compression (UC) tests (AASHTO T208 and ASTM D2166) are similar to UU triaxial compression tests in that specimens are not consolidated and loading is undrained. However, unconfined compression tests differ from UU tests in that they are performed with zero confining stress (i.e., $\sigma_3 = 0$) and no membrane. UC tests can be performed with simpler equipment because no confining stress is needed but cannot be performed on granular soils, extremely soft clays, or highly fissured soils that will not stand up without confinement. As shown in Figure 7-22, results from UC tests are generally interpreted in a manner similar to that for UU tests. However, by convention, the unconfined compressive strength, $q_u$, is reported, which represents the diameter of Mohr's circle rather than the radius of Mohr's circle at failure. Thus, $s_u$ must be computed as

$$s_u = \frac{q_u}{2} = \frac{P/A}{2} \tag{7.7}$$

where $P$ is the axial load at failure and $A$ is the cross-sectional area of the specimen.

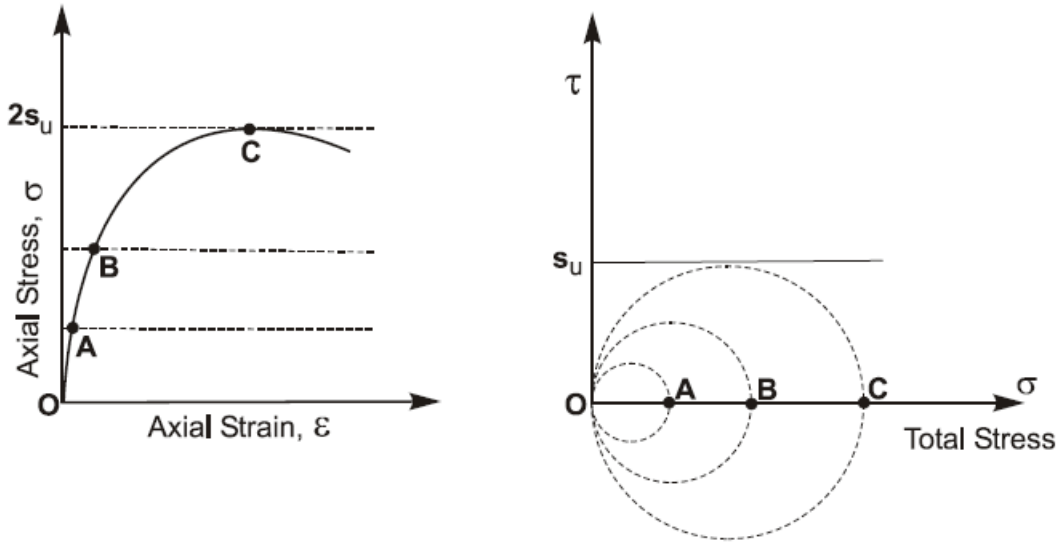


**Figure 7-22 Successive states of stress for unconfined compression test**

For saturated soils, UC tests should theoretically produce the same $s_u$ as UU compression tests because loading is undrained and $\phi = 0$. However, $s_u$ from UC tests are commonly observed to be substantially more variable and slightly lower than those from UU tests. In unsaturated soils, UC tests will consistently produce $s_u$ that is less than that determined from UU compression tests because shear strength increases with the total confining stress. As a result, UU compression tests are often preferable for establishing

more accurate and less variable values of $s_u$. Comparisons of $s_u$ determined from UU and UC tests are provided in Section 7.4.9.

### 7.4.3 Consolidated-Undrained Triaxial Tests

Consolidated-undrained (CU) triaxial tests (AASHTO T297 and ASTM D4767) can be used to measure undrained shear strength in both triaxial compression and triaxial extension. Unlike UU tests where the magnitude of effective stresses are generally unknown, specimens in CU triaxial tests are consolidated to some known effective stress in the laboratory prior to being sheared under undrained conditions to measure $s_u$. While CU triaxial tests are more time consuming than UU tests, CU tests have several notable advantages. The process of consolidating specimens prior to shearing tends to reduce effects of sample disturbance, which are largely attributed to changes in effective stress. Consolidation also allows the measured $s_u$ to be related to the magnitude of the effective consolidation stress, which has a strong, if not dominant, influence on the value of $s_u$ as described in Section 7.2.7. The reduced effect from disturbance, in turn, tends to reduce the variability of $s_u$ compared to what would be measured in UU tests, which improves the reliability for designs that rely on $s_u$. In addition, it is possible to measure pore water pressures during CU tests that allows for simultaneously determining both $s_u$ and effective stress strength parameters, $c'$ and $\phi'$. When pore pressures are measured in a CU test, the test is generally designated as a "CU-bar" ($\overline{CU}$) test to signify that pore water pressures are measured.

Values for $s_u$ are generally established from the peak of measured stress-strain curves similar to what is shown in Figure 7-19 for UU tests. Values for $s_u$ can also be established by plotting stress paths that demonstrate sequential states of stress during a test on modified Mohr-Coulomb diagrams as shown in Figure 7-23. CU triaxial tests cannot be used to establish total stress strength envelopes in the sense described in Sections 7.2.6 and 7.5 because specimens are consolidated prior to shearing under undrained conditions. Total stress analyses are fundamentally predicated on the assumption that the effective stress in the laboratory is identical to the effective stress in the field and the act of consolidating specimens eliminates this fundamental requirement. Appropriate total stress strength envelopes can therefore only be acquired using UU tests.

CU triaxial tests can be performed in several different variations. CU triaxial compression tests are standardized in AASHTO T297 and ASTM D4767 and are, by far, the most commonly performed CU test in practice. CU triaxial extension tests can also be performed with only slight modifications to conventional loading apparatus. Additionally, the consolidation phase of the test can be conducted using isotropic or anisotropic states of stress, with "$K_o$" consolidation being the most commonly adopted

method for anisotropic consolidation. Because of the different variants for the test, it is common to insert an "I", an "A", or a "$K_o$" within the test designation to indicate the method of consolidation and to append a "C" or an "E" to the end of the designation to indicate whether loading is in compression or extension. Thus, for example, the designation "CIUC" would be used to designate a CU triaxial compression test with isotropic consolidation. The designation "CAUE" or, preferably, "$CK_oUE$" would be used to designate a CU triaxial extension test with $K_o$ consolidation.

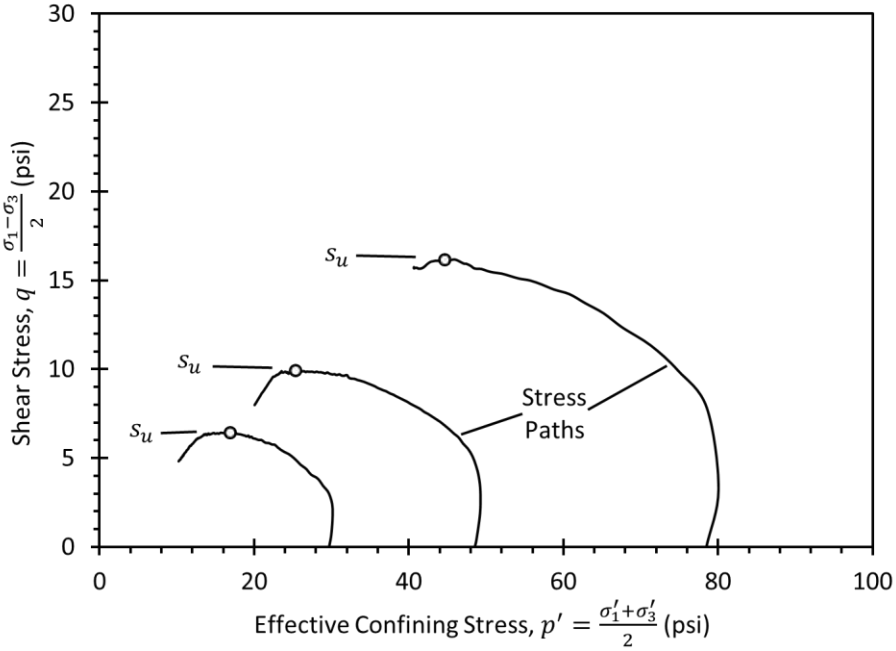


**Figure 7-23 Stress paths from $\overline{CU}$ triaxial compression tests.**

### 7.4.4 Direct Simple Shear Tests

Consolidated-undrained direct simple shear (DSS) tests can also be used to evaluate undrained shear strength. DSS tests are performed by consolidating specimens within some form of confining rings that impose 1-D consolidation conditions. Specimens are then sheared, usually under undrained conditions. DSS devices differ from the more common direct shear devices in that shearing is induced by "tilting" of specimens in simple shear, which produces more uniform states of stress than for the direct shear device. Direct shear devices also provide some ability to control drainage. DSS tests have the distinct advantage of using small, disc-shaped specimens, which allows specimens to be consolidated more quickly than common triaxial specimens. While DSS devices are less common than triaxial testing equipment, they have become much more common over the last decade.

Stress paths imposed in DSS tests often represent a better "average" stress path for many geotechnical applications, as illustrated in Figure 7-8 through 7-10 and Figure 7-15. Values of $s_u$ determined from DSS tests usually represent a slightly conservative average of $s_u$ from triaxial compression and triaxial extension tests and are often more representative of the average strength for many design applications.

Interpretation of DSS test measurements is performed similar to measurements from CU and UU triaxial tests except that the stress-strain curve is plotted as shear stress versus shear strain. Normalized undrained shear strength ratios are also computed using the effective vertical consolidation stress, $\sigma'_{vc}$. Figure 7-24 shows a comparison of $s_u/\sigma'_{vc}$ for a silty clay from CIUC and DSS tests.

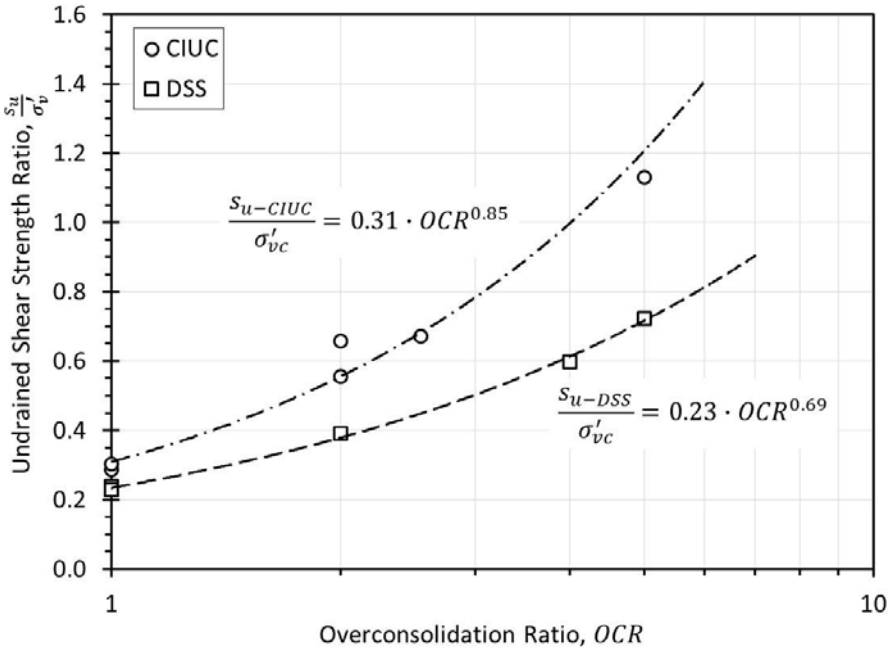


**Figure 7-24 Comparison of $s_u/\sigma'_{vc}$ relationship for CIUC and DSS tests for silty clay.**

### 7.4.5 Effects of Sample Disturbance

Sample disturbance can dramatically affect measurements of $s_u$ from UU or UC tests, particularly for soft, normally consolidated clays and silts. Sample disturbance is partly attributed to alteration of the physical structure of soils during sampling and test preparation. However, changes in effective stress during sampling and test preparation are generally the greater contributor to disturbance. With regard to $s_u$ measurements, sample disturbance will generally (Santagata and Germaine, 2002):

1. Reduce the magnitude of the measured $s_u$;
2. Increase the strain required to achieve the peak shear stress;

3. Reduce the soil stiffness; and
4. Potentially eliminate strain softening.

Each of these effects is illustrated in Figure 7-25, which shows measurements from UU triaxial compression tests performed for intact and laboratory prepared specimens subjected to different levels of disturbance. In the figure, the curve labeled "intact" represents the response for a specimen with little disturbance; curves labeled PSA, ISA±0.5, ISA±1.0, ISA±1.5, ISA±2.0, and ISA±5.0, respectively correspond to specimens with increasing disturbance (as represented by strains during sampling). Because disturbance varies from sample to sample, disturbance also tends to increase variability and uncertainty associated with measurements of $s_u$ from UU and UC tests compared to that present in situ, and that observed from CU type tests.

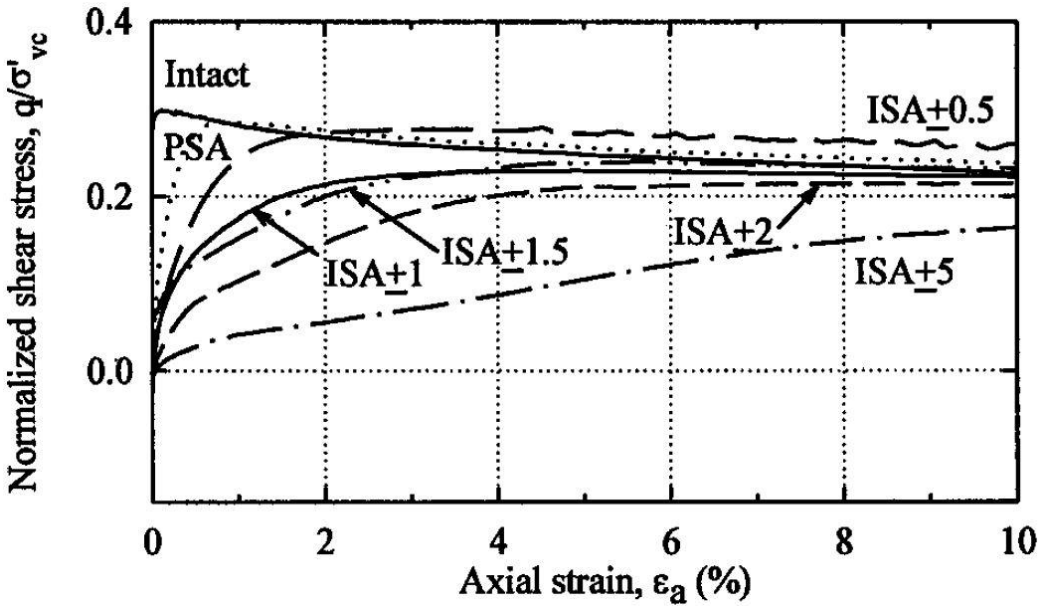


**Figure 7-25 Normalized stress-strain response for normally consolidated specimens with varying levels of disturbance (from Santagata and Germaine, 2002).**

The effects shown in Figure 7-25 are generally observed for normally consolidated to lightly overconsolidated clays and silts. In stiff, overconsolidated clays, disturbance often has less effect on measured values of $s_u$ from UU and UC tests, especially for stiff soils with low plasticity. In stiff clays with high plasticity (e.g., CH soils), disturbance may actually increase the effective stress and $s_u$ compared to what exists in situ (Vaughan, et al., 1993). Table 7-2 summarizes the potential influence of sample disturbance for $s_u$ measurements for different soil types.

**Table 7-2 Effect of sample disturbance on effective stress and $s_u$ for different soil types (after Vaughan, et al., 1993).**

| Soil Type | | Change in $\sigma'$ from Disturbance | | Change in $s_u$ |
|---|---|---|---|---|
| **Stiffness** | **Plasticity** | **From Axial Strain** | **From Side Shear** | |
| Soft Clay | Low plasticity | Very large decrease | Large decrease | Very large decrease |
| | High plasticity | Large increase | Large decrease | Large decrease |
| Stiff clay | Low plasticity | Large decrease | Large increase | Negligible |
| | High plasticity | Slight | Large increase | Large increase |

Disturbance tends have much less effect on $s_u$ measurements in consolidated-undrained tests (e.g., CU type triaxial and DSS tests) because sample disturbance is largely a product of changes in effective stress and the act of consolidating specimens to some known effective stress practically eliminates such stress changes. Consolidation in the laboratory does not necessarily return the soil to the in situ void ratio, nor does it correct for damage to soil structure so disturbance is not completely eliminated. As a practical matter, however, $s_u$ measurements in CU tests are far less sensitive to sample quality than measurements from UU or UC tests, and substantially less variable.

The sample quality measures presented in Chapter 6 can also be used to assess sample disturbance for specimens in CU strength tests based on volume changes that occur during consolidation back to in situ stress conditions. In general, $s_u$ should be derived from specimens with $SQD$ of $A$ or $B$ (Table 6-1), or rated as "very good to excellent" or "good to fair" (Table 6-2).

### 7.4.6 SHANSEP Procedure

In many soft to medium stiff clays and silts, effects of sample disturbance for $s_u$ can be practically eliminated using the SHANSEP procedure described by Ladd and Foott (1974). The SHANSEP procedure is a laboratory procedure for establishing values for $s_u$ using the normalized soil behavior concepts described in Section 7.2.7. Ladd and Foott (1974) showed that effects of disturbance can be largely eliminated by consolidating specimens to stresses sufficient to reach the virgin compression curve prior to measuring $s_u$. The laboratory consolidation procedure is illustrated in Figure 7-26, which shows the $e - \log \sigma_v'$ response to produce a specimen with a known value of $OCR$. Upon sampling, disturbance produces a reduction in the vertical effective stress from the in situ stress, $\sigma_{vo}'$, to some unknown value. From that point, reconsolidating the specimen back to the in situ preconsolidation stress, $\sigma_p'$, (point A in Figure 7-26) will produce a specimen that has a calculated $OCR$=1, but that is not truly normally consolidated because the specimen is not on the virgin compression curve due to sample disturbance. The SHANSEP procedure involves consolidating the specimen to a greater stress that is sufficient to reach the virgin compression curve so that the specimen has a new, known value of preconsolidation stress, $\sigma_p' =$

$\sigma'_{v-max}$, and an $OCR$ that is truly equal to 1.0. Subsequent rebound from that point to an effective stress, $\sigma'_{v-test}$, produces a specimen with the desired $OCR$. Measurement of $s_u$ following this consolidation procedure will produce a value of $s_u$ that is different from the in situ $s_u$, but a value of $s_u/\sigma'_{vc}$ that is appropriate for the specific $OCR$ applied to the specimen and practically free from effects of disturbance. The procedure is usually performed for several specimens consolidated to different values of $OCR$ to produce curves like those shown in Figure 7-24.

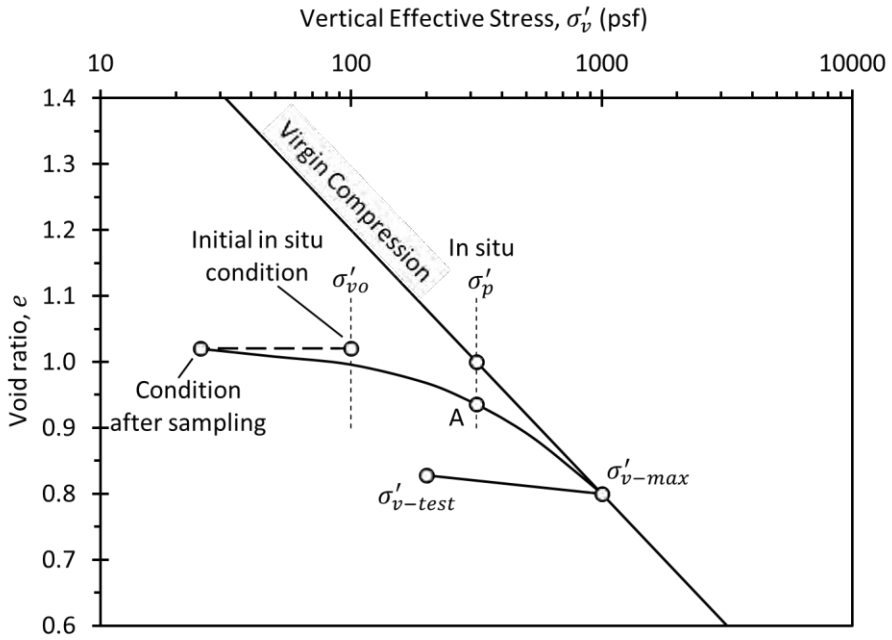


**Figure 7-26 Consolidation for SHANSEP method to achieve a known $OCR$ (adapted from Ladd and Foott, 1974).**

Once the relationship between $s_u/\sigma'_{vc}$ and $OCR$ is established, $s_u$ can be computed from Equation 7.6 as

$$s_u = (S \cdot OCR^m) \cdot \sigma'_v \tag{7.8}$$

where $\sigma'_v$ is the in situ vertical effective stress for a particular condition in the field. Sound application of Equation 7.8 requires reliable estimates of $\sigma'_p$, established as described in Chapter 6. Once appropriate values for $S$ and $m$ are established, Equation 7.8 can be used to estimate $s_u$ throughout the stratum as well as for evaluating $s_u$ for changing effective stresses (e.g., from changes in groundwater levels, or for staged construction).

The SHANSEP approach is not appropriate for all soils. The approach is generally impractical for stiff, heavily overconsolidated soils because most conventional laboratory equipment cannot achieve the high consolidation stress required to reliably reach the virgin compression curve. The SHANSEP approach is

also inappropriate for highly structured soils that may be altered by consolidation to high stresses. To identify such soils, Ladd and Foott (1974) recommend consolidating specimens to approximately 1.5, 2.5, and 4.0 times the estimated $\sigma_p'$ and plotting the measured values of $s_u/\sigma_{vc}'$ as shown in Figure 7-27. If values of $s_u/\sigma_{vc}'$ are similar for the two higher consolidation stresses as shown in Figure 7-27, the soil is considered to be "normalizable" and appropriate for SHANSEP use. However, if values of $s_u/\sigma_{vc}'$ at the higher consolidation stresses are different, the SHANSEP approach is not appropriate. In such cases, specimens should generally be reconsolidated to the in situ vertical stress, $\sigma_{vo}'$, prior to measuring $s_u$.

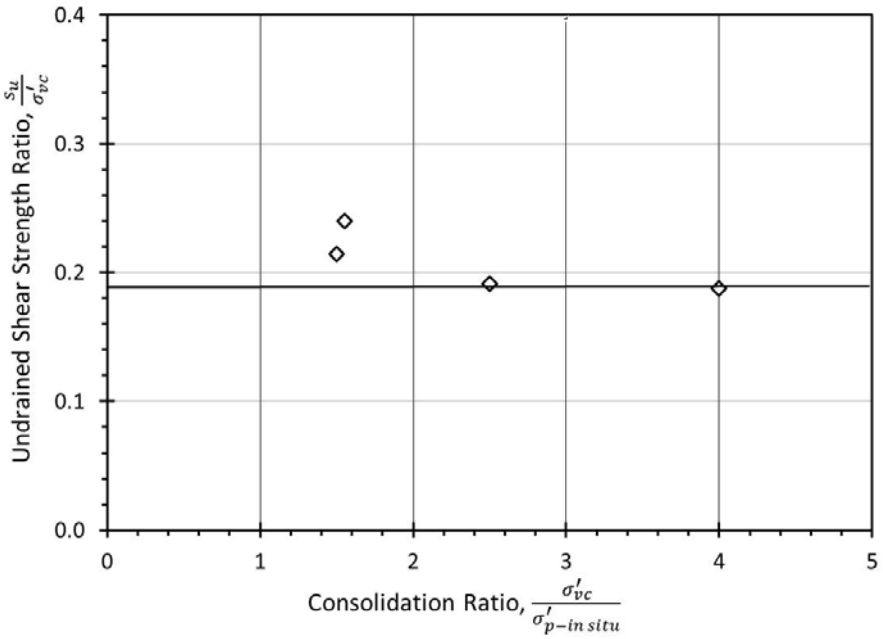


**Figure 7-27 Evaluation of whether soil is "normalizable".**

Importantly, Ladd and Foott (1974) also recognized that long-standing practice with use of $s_u$ for design relies on a somewhat fortuitous balance of compensating errors attributed to disturbance, strain rate, and anisotropy. As a result, use of $s_u$ derived from SHANSEP has the potential to produce unconservative values for $s_u$ if other factors are not simultaneously addressed. This is primarily accomplished by simultaneously accounting for anisotropy by using appropriate methods for measurement of $s_u$. For large projects that are predominantly controlled by the magnitude of $s_u$, such as construction of large fills over soft soils, measurements from triaxial compression, triaxial extension, and direct simple shear tests should be used to establish appropriate values for $s_u$. For less significant projects, $s_u$ should be determined from DSS tests or, alternatively, from the average of measurements from triaxial compression and triaxial extension tests. For smaller projects, values for $S$ and $m$ can often be reasonably estimated as described

in Section 7.4.8. It is generally inappropriate, and likely unconservative, to design using values of $s_u$ established from SHANSEP procedures considering triaxial compression tests alone.

### 7.4.7 Selection of Specimens for Measurement of Undrained Shear Strength

Selection of specimens is critically important for measurement of $s_u$ because of the dramatic effect of sample disturbance and because measurements are often linked with the depth (or really the effective stress) where the sample was obtained. High quality "undisturbed" specimens should be used for undrained shear strength testing to avoid introducing substantial bias into $s_u$ measurements. As a practical matter, samples of many clays should be acquired using 3-inch diameter thin-walled tube (a.k.a. "Shelby" tubes) samplers. In soft to medium clays, use of piston samplers will generally produce less disturbance. In stiff clays that are too stiff for using thin-walled tubes, overcoring samplers such as the Pitcher or Denison samplers are recommended.

When performing UU or UC tests, measurements are only representative of the depth (or effective stress) from which the sample was acquired. Thus, it is important to select specimens that are distributed throughout the range of depths for the stratum of interest. When performing CU triaxial or DSS tests, measurements can be applied to a much broader range of depths so selection of samples from throughout the stratum is less important as long as there are not significant physical changes in soil characteristics (in which case, the soils should be considered to be different strata). However, results from CU tests are dependent upon the overconsolidation ratio so it important than specimens be tested at different values of $OCR$ (but one can test samples from a similar depth at different $OCR$'s).

### 7.4.8 Estimation of Undrained Shear Strength from Indirect Measurements

Undrained shear strength can be estimated from several types of in situ tests that are considered to be indirect measurements. Common in situ tests for establishing $s_u$ include field vane shear tests (FVT), cone (CPT) or piezocone (CPTU) penetration tests, pressuremeter tests (PMT), dilatometer tests (DMT), and Standard Penetration tests (SPT). Additionally, estimates for $s_u$ can be indirectly established from measurements or estimates of $\sigma_p'$ combined with estimates of normalized undrained strength parameters, $S$ and $m$, and the in situ $\sigma_v'$.

Estimation of $s_u$ from these indirect measurements necessarily involves use of a transformation derived from empirical, analytical, or numerical methods. As described in previous chapters, these transformations introduce varying degrees of uncertainty that arises from variability and uncertainty in empirical measurements as illustrated for FVT measurements in Figure 7-28. Some uncertainty also

arises because $s_u$ varies substantially with stress history, loading conditions, and strain rate. As a result, it is relatively common to obtain different estimates for $s_u$ from different in situ test methods as shown in Figure 7-29. Fortunately, improved estimates for $s_u$ can often be established from "site specific" transformations developed using results from high-quality laboratory tests for the specific soil deposit and particular mode of loading that is of interest. Examples of application of site specific transformations are provided in Chapter 11 and Appendix 2.

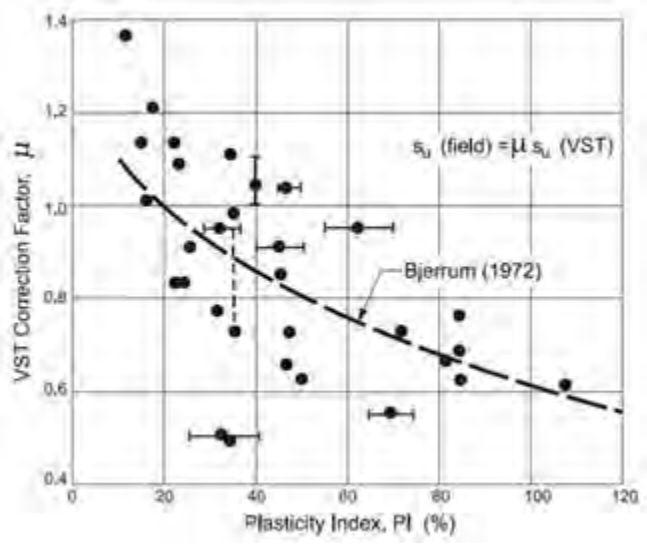


**Figure 7-28 Empirically derived correction for field vane shear test (FVT, or VST).**

***Field Vane Shear Test (FVT)***

The field vane shear test is useful for estimating $s_u$ in saturated, soft to medium stiff clays and high plasticity silts. The test is generally not practical in very stiff soils, and is inappropriate in highly permeable soils that drain rapidly. The test is standardized in ASTM D2573 and is generally performed by inserting a rectangular vane through the base of a borehole and measuring the torque required to rotate the vane. For vanes with a height-to-diameter ratio of 2, $s_u$ is generally computed as

$$s_u = \frac{6T_{max}}{7\pi D^3} \cdot \mu \qquad (7.9)$$

where $T_{max}$ is the maximum measured torque, $D$ is the diameter of the vane, and $\mu$ is an empirical correction factor. Alternative equations are used to determine $s_u$ for alternative vane geometries (Schnaid, 2009). A correction factor, $\mu$, should be determined from Figure 7-30 based on the anticipated loading time in the field and applied to Equation 7.9 when $s_u$ will be used for embankment design. The correction factor should not generally be applied when $s_u$ is used for other purposes.

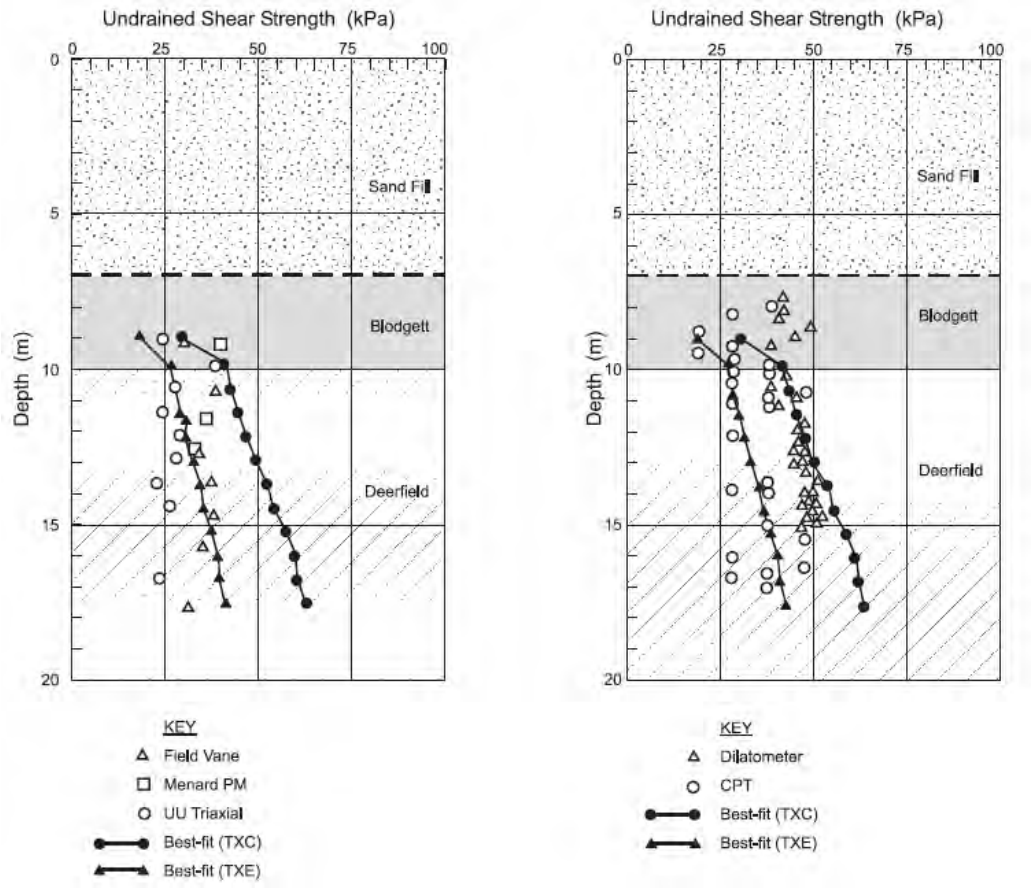


**Figure 7-29 Comparison of $s_u$ derived from different in situ test measurements using "general" transformations (after Finno and Chung, 1992).**

Field vane shear tests can also be used to evaluate sensitivity and anisotropy. Sensitivity is generally evaluated using the peak shear strength computed from Equation 7.9 combined with measurements of the remolded strength determined by repeating the test at the same location after rotating the vane through a minimum of five to ten revolutions. Sensitivity, $S_t$, is computed as

$$S_t = \frac{s_{u-FVT}}{s_{ur-FVT}} \tag{7.10}$$

where $s_{u-FVT}$ is the peak vane strength established from the maximum recorded torque, $T_{max}$, and $s_{ur-FVT}$ is the remolded vane strength determined from the recorded torque following remolding. Anisotropy can also be evaluated by performing tests using vanes with different aspect ratios as described in Schnaid (2009).

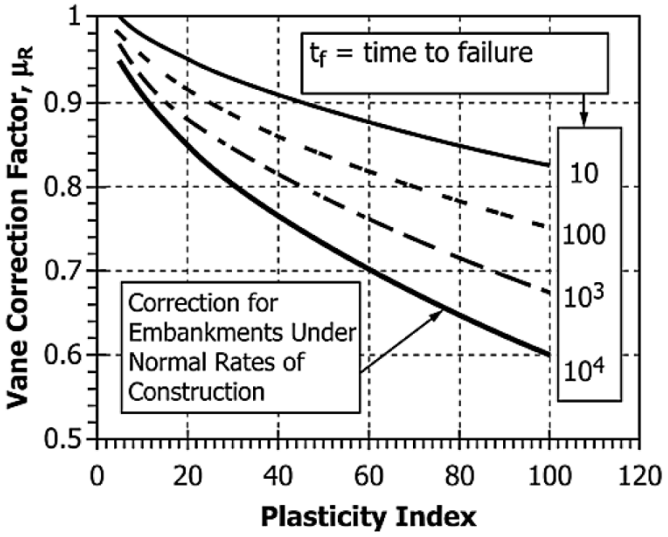


**Figure 7-30 Correction factor for FVT measurements from ASTM D2573 (after Chandler, 1988).**

***Pressuremeter Test (PMT)***

Based on cavity expansion theory, $s_u$ can be determined from the slope of PMT measurements plotted as cavity pressure, $p$, versus the natural logarithm of the volumetric strain, $\varepsilon_v = \Delta V/V$ (Windle and Wroth, 1977), as shown in Figure 7-31. Note that the linear slope shown in Figure 7-31 must correspond to the plastic portion of the pressuremeter response in order to determine an appropriate value for $s_u$, meaning that the cavity pressure must exceed $\sigma_p'$ by a substantial amount. Alternatively, $s_u$ can be calculated from the PMT "limit pressure", $p_L$, and "initial cavity pressure", $p_o \cong \sigma_{ho}$, as

$$s_u = \frac{(p_L - p_o)}{N_c} \tag{7.11}$$

where $N_c$ is a form of bearing capacity factor taken to be equal to 5.5 (Baguelin, et al., 1972). As described in Chapter 6, PMT tests can be performed in many soils, but are often best suited to measurements in medium to hard clays. PMT tests therefore serve as a good complement to other in situ tests that are often best used in softer soils.

***Cone Penetration Tests (CPT/CPTU)***

CPT and CPTU tip resistance measurements can be used to develop estimates for $s_u$ in many saturated clays and silts. For CPT tests, the uncorrected net cone tip resistance, $q_c - \sigma_{vo}$, is related to $s_u$ as

$$s_u = \frac{(q_c - \sigma_{vo})}{N_c} \tag{7.12}$$

where $q_c$ is the measured CPT tip resistance, $\sigma_{vo}$ is the total overburden stress at the test depth, and $N_c$ is a theoretical cone factor. $N_c$, can be established from classical bearing capacity theory, cavity expansion theory, the strain path method, or numerical analyses. $N_c$ is commonly taken to be between 7 and 10 based on classical bearing capacity theory. Alternative methods for computing $N_c$, many of which involve the rigidity index, $I_r = G/s_u$, and other parameters, are summarized in Schnaid (2009).

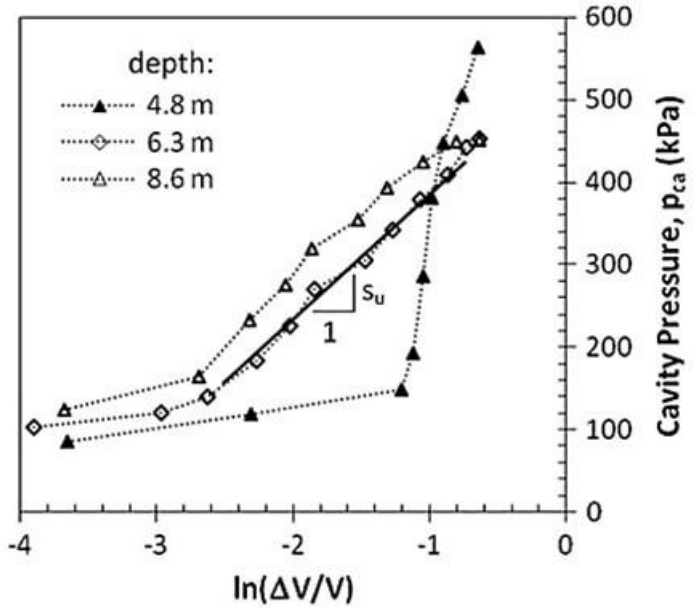


**Figure 7-31 Interpretation of $s_u$ from pressuremeter test (from Soleimanbeigi, 2013).**

Undrained shear strength can be similarly estimated from CPTU measurements as (Aas, et al., 1986):

$$s_u = \frac{(q_t - \sigma_{vo})}{N_{kt}} \tag{7.13}$$

where $q_t$ is the corrected CPTU tip resistance and $N_{kt}$ is an empirical cone factor. Values of $N_{kt}$ often range from 10 to 20 depending on the specific soil, the $OCR$, and the specific reference strength considered (DeGroot and Ladd, 2012). As a matter of routine practice, values of $N_{kt}$ around 15 are often used. However, values established from site specific transformations are far more reliable and are sometimes observed to be less than 10. Values for $N_{kt}$ should also be selected with consideration to the nature of loading; values of approximately 10 for triaxial compression, approximately 15 for DSS, and approximately 20 for triaxial extension are often appropriate.

Unfortunately, values of both $N_c$ and $N_{kt}$ are highly uncertain, which often leads to substantial challenges for establishing $s_u$ from CPT or CPTU measurements. An alternative approach is to estimate $s_u$ from

measured pore water pressures from CPTU tests (e.g., Tavenas, et al., 1982; Robertson and Campanella, 1983; Mayne and Bachus, 1989), wherein $s_u$ is calculated as

$$s_u = \frac{(u_2 - u_o)}{N_{\Delta u}} \tag{7.14}$$

where $u_2$ is the pore pressure measured using a Type 2 piezocone and $N_{\Delta u}$ is a pore pressure cone factor. Values of $N_{\Delta u}$ vary in the range of 2 to 20 (Mantaras, et al., 2015), although the range is generally smaller for more restrictive classes of soils.

Mantaras et al. (2015) also recently proposed a method for estimating $s_u$ from CPTU dissipation tests using Type 2 piezocones as

$$s_u = \frac{\Delta u_{max}}{4.2(\pm 0.2)\log(I_r)} \tag{7.15}$$

where $\Delta u_{max}$ is the maximum excess pore pressure measured at any time during a piezocone dissipation test and $I_r$ is the rigidity index. The method is reported to be particularly useful for soils with intermediate $OCR$ where the excess pore pressure tends to increase with time during dissipation tests.

***Dilatometer Test (DMT)***

Several approaches have been proposed for estimating $s_u$ from DMT tests. Based on empirical observations from laboratory UU and UC tests and FVT measurements shown in Figure 7-32, Marchetti (1980) found that $s_u$ could be estimated from the DMT horizontal stress index, $K_D$, as

$$s_u = 0.22\sigma'_{vo}\left(\frac{K_D}{2}\right)^{1.25} \tag{7.16}$$

where $\sigma'_{vo}$ is the in situ effective overburden stress at the test depth. Lacasse and Lunne (1988) subsequently adapted this expression to account for anisotropy and suggested that $s_u$ be computed as

$$s_u = d_s\sigma'_{vo}\left(\frac{K_D}{2}\right)^{1.25} \tag{7.17}$$

where $d_s$ is an empirical factor taken as 0.2 for triaxial compression, 0.14 for direct simple shear, and 0.19 for FVT. Based on cavity expansion theory, Schmertmann (1991) and Marchetti and Crapps (1981) recommend that $s_u$ be estimated as

$$s_u = \frac{p_o - u_o}{10} \tag{7.18}$$

where $p_o$ is the corrected DMT lift off pressure and $u_o$ is the in situ pore water pressure.

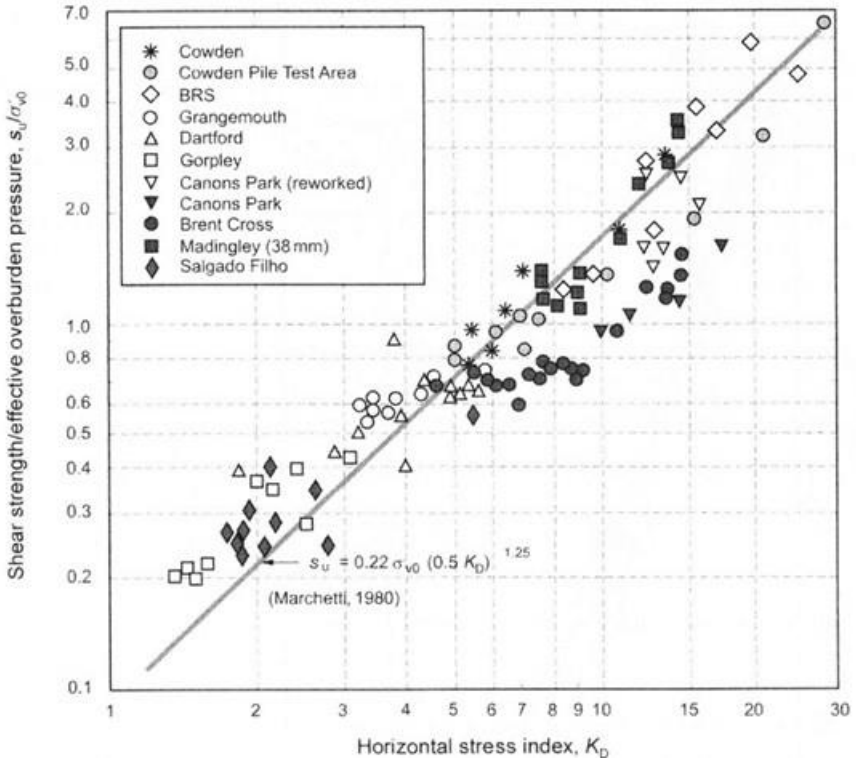


**Figure 7-32 Empirical measurements relating $s_u$ to DMT horizontal stress index, $K_D$ (from Schnaid, 2009)**

***Standard Penetration Test (SPT)***

SPT $N$-values are generally a poor predictor of undrained shear strength. Nevertheless, there are times when crude estimates of $s_u$ based on SPT measurements can be useful. Stroud (1974, 1989) recommended that $s_u$ be estimated as

$$s_u = f_1 N_{60} \frac{p_a}{100} \tag{7.19}$$

where $N_{60}$ is the SPT blow count corrected for hammer energy, $p_a$ is atmospheric pressure in the desired units, and $f_1$ is an empirical coefficient that is taken to be equal to 4.5 for $PI \gtrsim 30$ and equal to 5.5 for $PI \cong 15$. The relationship between $N_{60}$ and $s_u$ is subject to considerable scatter, but the values of $f_1$ proposed by Stroud generally represent somewhat lower bound values. Schnaid (2009) also describes a more rigorous relationship for estimating $s_u$ from SPT measurements, although it is unclear whether the additional rigor produces substantially improved estimates of $s_u$.

***Normalized Soil Strength Parameters***

For relatively soft clays and silts with $OCR$ less than approximately 10, reasonably reliable estimates for $s_u$ can be developed based on measurements of $\sigma'_p$ (or $OCR$), knowledge regarding the in situ vertical effective stress, $\sigma'_{vo}$, and estimates for normalized soil strength parameters, $S$ and $m$. Such estimates correspond to "level C" investigations for evaluating undrained stability problems (Ladd, 1991; Ladd and DeGroot, 2003), as described further in Section 7.4.9. The in situ distribution of $\sigma'_{vo}$ with depth is relatively straightforward to calculate based on measurements or estimates of unit weight and knowledge regarding groundwater conditions, both of which are necessary for effective design. The distribution of $\sigma'_p$ (or $OCR$) is more difficult to establish and requires devoted effort as described in Chapter 6. However, the distribution of $\sigma'_p$ is also required for settlement analyses, and thus is necessary regardless of whether it is used for estimating $s_u$. Values for the normalized soil strength parameters, $S$ and $m$, are not generally used for other purposes. However, values for $S$ and $m$ fortunately vary over relatively narrow ranges and can often be estimated with reasonable reliability.

Figure 7-33 shows the relationship between normalized undrained shear strength ($\tau_f/\sigma'_{vo} = s_u/\sigma'_{vo}$) and $OCR$ from DSS tests for six different clays. While the relationships vary for soils with different characteristics, the range of variation is relatively small. Values for the parameter $S$, which represents the value of $s_u/\sigma'_{vo}$ for $OCR = 1$, broadly vary from slightly less than 0.2 to less than 0.3. Values for the parameter $m$, which describes the growth in $s_u/\sigma'_{vo}$ with increasing $OCR$, broadly vary from about 0.6 to 1.0. Figure 7-15 provides additional guidance for estimating $S$ for triaxial compression, DSS, and triaxial extension, showing a general trend of decreasing values of $S$ with decreasing $PI$ for triaxial extension and DSS. Additionally, Ladd (1991) and Ladd and DeGroot (2003) provide recommendations for estimating values for $S$ and $m$ for different soil types, as summarized in Table 7-3 "Local" experience with different types of materials can also be used for estimating $S$ and $m$, often with substantial reductions in variability and uncertainty compared to that shown in Figure 7-33 and 7-15.

Given estimates for $S$ and $m$, along with interpretations of $\sigma'_p$ and $\sigma'_{vo}$ (e.g., Figure 6-3), the undrained shear strength at any specific depth can be computed from Equation 7.8. The accuracy and reliability of such estimates are often largely predicated on the accuracy and reliability of estimates for $\sigma'_p$.

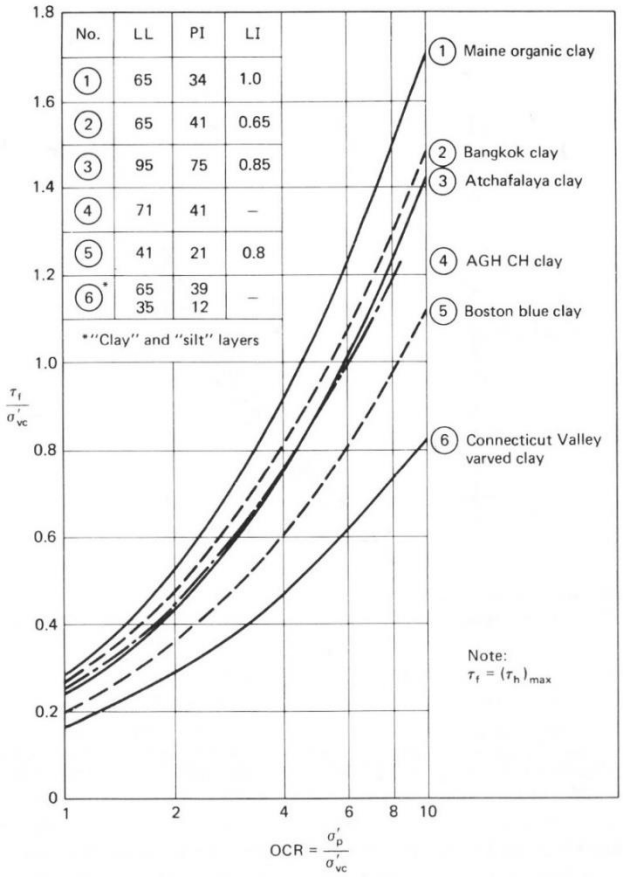


**Figure 7-33 Normalized undrained shear strength from DSS tests for several different clays (from Holtz and Kovacs, 1981, after Ladd, et al., 1977)**

**Table 7-3 Estimates for normalized undrained strength parameters, $S$ and $m$ (adapted from Ladd and DeGroot, 2003).**

| Soil Description | $S$ | $m^{\dagger}$ | Remarks |
|---|---|---|---|
| 1. Sensitive cemented marine clays ($PI < 30, LI > 1.5$) | $S = 0.20$ ($\sigma \approx 0.015$)[‡] | $m = 1.00$ | Champlain clays of Canada |
| 2. Homogeneous CL and CH sedimentary clays of low to moderate sensitivity ($20 \leq PI \leq 80$) | $S = 0.20 + 0.05\left(\frac{PI}{100}\right)$ or $S \approx 0.22$ | $m = 0.88\left(1 - \frac{C_s}{C_c}\right)$ ($\sigma \approx \pm 0.06$) or $m \approx 0.8$ | No shells or sand lenses/layers |
| 3. Northeastern US varved clays | $S = 0.16$ | $m = 0.75$ | Assumes DSS mode of failure |
| 4. Sedimentary deposits of silts and organic soils (Atterberg limits plot below A-line) or clays with shells | $S = 0.25$ ($\sigma \approx 0.05$) | $m = 0.88\left(1 - \frac{C_s}{C_c}\right)$ ($\sigma \approx \pm 0.06$) or $m \approx 0.8$ | Excludes peat |

[†] $m = 0.88(1 - C_s/C_c)$ based on $CK_oUDSS$ tests for 13 soils with max $OCR$ of 5 to 10
[‡] $\sigma$ denotes standard deviation

***Other Methods to Estimate $s_u$***

Estimates of $s_u$ can also be acquired from several laboratory or hand-held devices that include the fall cone, laboratory vane, Torvane, and the pocket penetrometer devices. When compared to more rigorous laboratory or field measurements, these tests tend to produce only approximate estimates for $s_u$ because they are small in scale, and thus potentially miss the influence of even moderate scale features within the soil. Additionally, each of the tests are indirect tests that introduce some uncertainty into interpretation. Despite these apparent limitations, however, each of the tests are generally simple and quick to perform, and can often provide useful information for site characterization. They are often particularly well-suited to qualitative assessment of variations of $s_u$ among different samples, or even within the same sample.

The undrained shear strength can be estimated from a fall cone test as

$$s_u = \frac{M_c K}{d^2} \tag{7.20}$$

where $s_u$ is in units of grams/mm$^2$, $M_c$ is the mass of the cone in grams, $K$ is a constant depending on the cone apex angle ($K = 0.8$ for a 30 degree cone and $K = 0.27$ for a 60 degree cone), and $d$ is the measured depth of penetration after 5 seconds in mm. As described in Chapter 4, the fall cone test is not currently standardized by AASHTO or ASTM, although a proposed standard is currently being balloted by ASTM. The fall cone test can often be effectively used to evaluate sensitivity of soils by conducting replicate tests on undisturbed and remolded specimens of a specific soil. The fall cone test can also be used as an alternative to the conventional liquid limit test, as described in Chapter 4. Tanaka, et al. (2012) presents comparisons of $s_u$ determined from the fall cone and other test methods.

The laboratory miniature vane shear test is standardized by ASTM D4648. The test is conceptually similar to the field vane test, but is smaller in scale and performed on laboratory specimens of intact or remolded specimens. $s_u$ is computed from the maximum measured torque, $T_{max}$, as

$$s_u = T_{max} \cdot \frac{1}{K} \tag{7.21}$$

where $K$ is a vane blade constant that depends on the dimensions of the vane blades. For a 0.5 inch by 1 inch blade, $K = 0.0002651$ ft$^3$. Like the field vane test, the laboratory vane can also be effectively used to evaluate soil sensitivity by performing tests on undisturbed and remolded samples. The laboratory vane can also be used to assess anisotropy by performing replicate tests with vanes having different aspect ratios.

Torvane and pocket penetrometer devices are both hand-held devices that are commonly used to assess relative shear strength on samples acquired in the field. The Torvane is conceptually similar to vane shear tests in that the device is inserted into a soil sample and the torque required to fail the soil is used to produce estimates of $s_u$. The pocket penetrometer is a penetration test wherein the force required to penetrate a blunt probe a specific distance into a soil sample is used to produce estimates of the unconfined compressive strength ($q_u = 2 \cdot s_u$). Both devices are calibrated to directly produce estimates of undrained strength. However, both are really indirect measurements. Because both devices are hand-held, the tests are generally conducted under less carefully controlled conditions and should be considered to produce only qualitative estimates of $s_u$.

### 7.4.9 Selection of Testing Method(s) for Undrained Shear Strength

Undrained shear strength is one of the most commonly required design parameters for geotechnical analysis and design. Unfortunately, $s_u$ is also one of the more difficult design parameters to reliably and accurately establish because it depends on the in situ state of effective stress, the applied stress path, sample quality, and strain rate or time to failure. In addition, the reliability of estimates for $s_u$ are dependent on the number of available measurements as described in Chapters 3 and 11. Thus, one has to balance requirements to acquire accurate and practically unbiased estimates of $s_u$ with the need to acquire sufficient numbers of measurements to produce appropriate reliability.

Figure 7-34 shows four interpretations of $s_u$ for a site established from: (1) the SHANSEP technique based on CIUC triaxial tests, (2) UU triaxial compression tests, (3) UC tests, and (4) Torvane (TV) measurements, respectively. Samples used for the CIUC and UU tests were acquired using high quality boring and sampling methods that included rotary wash boring with heavy drilling mud and fixed piston samplers. Conversely, the UC and TV measurements were performed on samples acquired using more common boring and sampling methods that included boring with hollow stem augers without drilling fluid, sampling with common 3-inch diameter thin-walled tubes, and extruding the samples in the field. Figure 7-35 shows a comparison of the relative $s_u$ interpreted from the different types of tests.

Figure 7-34 and 7-35 illustrate substantial differences in estimates of $s_u$ for the different sampling and testing methods. Both the CIUC and UU measurements produce interpretations that are practically similar, meaning they would likely produce similar designs. Conversely, measurements from the UC tests are substantially more variable and substantially biased compared to the CIUC and UU measurements. The combination of variability and bias not only results in overestimation of the in situ $s_u$ (considered to be that estimated using SHANSEP), but also produces a trend of $s_u$ with depth that is

substantially different than the true trend. The interpretation from Torvane measurements is even more biased and more variable. As illustrated in Figure 7-35b, some bias can be eliminated by correcting for strain rate effects and secondary compression, but such corrections do little to reduce variability.

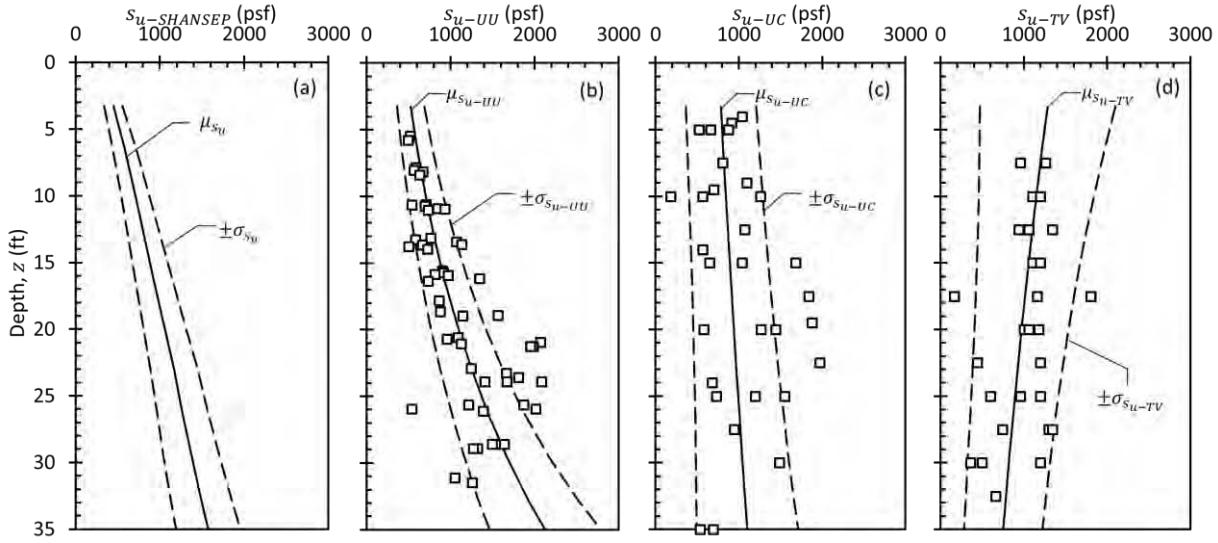


**Figure 7-34 Comparison of $s_u$ interpretations from: (a) SHANSEP using CIUC triaxial, (b) UU-triaxial compression, (c) unconfined compression, and (d) Torvane tests.**

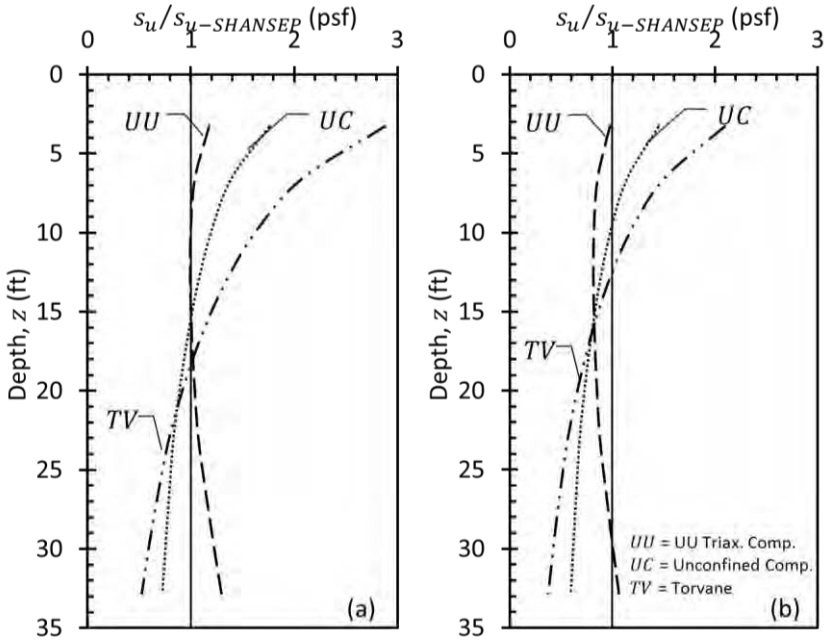


**Figure 7-35 Comparison of relative $s_u$ values determined from different testing methods: (a) uncorrected values and (b) values corrected for strain rate and secondary compression.**

Figure 7-34 and 7-35 strongly demonstrate the importance of selecting appropriate laboratory testing methods for design using $s_u$; Figure 7-29 demonstrates similar importance for in situ test methods.

Appropriate selection of testing methods often differs depending on the soils conditions that are present, and the intended use for $s_u$ as described in the following sections.

***Testing Methods for Global Stability of Embankments and Retaining Walls***

For sites composed of relatively soft, saturated soils with $OCR$ less than 5 to 10, Ladd (1991) and Ladd and DeGroot (2003) defined three levels of investigation for undrained stability analyses of embankments, as summarized in Table 7-4. Testing for "Level C" investigations includes high quality one-dimensional consolidation tests to establish accurate interpretations of $OCR$ along with estimated values of normalized undrained shear strength parameters, $S$ and $m$. Alternatively, in situ FVT measurements can be used to develop estimates for $s_u$ with depth, preferably in conjunction with one-dimensional consolidation tests to aid in interpretation of FVT measurements. Testing for "Level B" investigations also includes high quality one-dimensional consolidation tests, but with the addition of CU laboratory strength tests according to the SHANSEP approach to establish site specific values for $S$ and $m$. $S$ and $m$ values determined for Level B investigations should represent the average $s_u$ for different stress paths. Thus, laboratory strength tests should be performed using DSS tests or, alternatively, both triaxial compression and triaxial extension tests, and should be performed with $K_o$ consolidation (i.e., $CK_oU$ tests). Testing for "Level A" investigations includes high quality one-dimensional consolidation tests, and $CK_oU$ type laboratory strength tests performed according to the SHANSEP approach for triaxial compression, DSS, and triaxial extension. Unlike Level C and Level B investigations, which are intended to produce interpretations of the average $s_u$ with depth, Level A investigations are intended to produce values for $s_u$ as a function of both depth and loading orientation (i.e., stress path). All tests for embankments on relatively soft clays should be performed on high quality samples with as little disturbance as possible.

**Table 7-4 Estimates for normalized undrained strength parameters, $S$ and $m$ (adapted from Ladd and DeGroot, 2003).**

| Level of Investigation | Design Input Requirements | Recommended Strength Testing | Stress History |
|---|---|---|---|
| Level C | $s_{u-avg}$ vs. depth | Estimated $S$ and $m$ | Required |
| | | FVT | Desirable |
| Level B | $s_{u-avg}$ vs. depth | $CK_oU$ DSS Tests | Required |
| | | $CK_oU$ TC and TE Tests | Essential |
| Level A | $s_{u(\alpha)}$ vs. depth | $CK_oU$ TC, TE, and DSS Tests | Essential |

TC = triaxial compression; DSS = direct simple shear; TE = triaxial extension

Level C investigations are generally appropriate for design of routine embankments constructed in a single stage and are likely to be appropriate for the vast majority of highway embankment projects. However, Level C investigations will often greatly benefit from "local" estimates for $S$ and $m$ rather than more general estimates like those provided in Table 7-3. As such, site specific measurements for $S$ and $m$ should be considered for soils where such measurements have not previously been acquired. Level B investigations should be used for more significant embankments, or embankments that may require staged construction. Level A investigations are generally restricted to major projects with large embankments over soft soils that are likely to required staged construction or other measures to produce adequate short-term stability. Undrained shear strengths from UU and UC tests should also not be used for design of significant embankments on soft soils, except for preliminary evaluations.

In situ tests may also be helpful for design of embankments over soft soils. However, aside from field vane shear tests, which must be corrected according to Figure 7-30, $s_u$ should never be established exclusively from in situ test measurements for embankment design. In situ tests can be effectively used for determining stratigraphy and for helping to interpret spatial trends in $s_u$, particularly when used with site specific transformations.

SHANSEP procedures and strength estimates are generally neither appropriate nor practical for stiff, heavily overconsolidated soils. With the exception of pressuremeter tests, in situ tests are also usually impractical or inappropriate. Undrained shear strengths in stiff overconsolidated clays should therefore be measured using UU triaxial tests on high quality samples. In stiff fissured, or gravelly clays, that are difficult to sample, $s_u$ can often be best measured using the pressuremeter.

Shallow foundations are seldom, if ever, used to support bridges over soft soils. However, retaining walls are commonly constructed with shallow foundations. In such cases, $s_u$ should generally be evaluated according to the methods described for embankments since bearing capacity and slope stability represent similar failure mechanisms. Undrained shear strengths for evaluation of global stability of retaining walls should also be established using methods similar to those described for embankments.

***Testing Methods for Deep Foundations***

Estimates of $s_u$ for design of deep foundations should not generally be established using the methods described for global stability of embankments because most design methods for deep foundations are empirical methods. As such, $s_u$ should be established using methods that are consistent with the empirical methods. The vast majority of available methods for design of deep foundations in fine-grained soils are based on $s_u$ values determined from UU triaxial compression tests or UC tests, often for samples

acquired using 3-inch diameter Shelby tubes. Some design methods are also developed for use with specific in situ test measurements.

***Testing Methods for Design of Earth Retaining Structures***

Aside from considerations of bearing capacity and global stability, most methods for analysis of earth retaining structures rely on long-term, drained shear strengths so there is little need for evaluation of $s_u$. However, there are a few empirical design methods that require $s_u$ (e.g., methods for establishing apparent earth pressures for braced excavations). Since these methods are empirical, $s_u$ should be established from methods that are consistent with the empirical measurements used to develop the methods. As described for design of deep foundations, this commonly requires that $s_u$ be established from UU triaxial compression tests for specimens acquired using 3-inch diameter thin-walled tubes.

## 7.5 EVALUATION OF TOTAL STRESS STRENGTH PARAMETERS FOR UNSATURATED SOILS

In unsaturated soils, UU triaxial tests are the only viable option for measuring total stress strength parameters. If the soil being tested is not saturated, UU type shear strength measurements should not be interpreted as undrained shear strength considering that $\phi = 0$, but rather should be interpreted to establish the total stress shear strength envelope as illustrated in Figure 7-36. Unsaturated soils are also more likely to produce a curved total stress strength envelope. If the design analyses to be conducted can accommodate consideration of curved shear strength envelopes, the measurements can be interpreted as shown by the dashed line in Figure 7-36a. However, if design analyses cannot accommodate curved shear strength envelopes, an approximate linear envelope should be interpreted with due consideration given to the range of total confining stress over which the envelope will apply.

Effects of sample disturbance for unsaturated soils are qualitatively similar to those described in Section 7.4.5 for saturated soils. However, since unsaturated soils are often substantially stiffer and stronger than similar saturated soils, the magnitude of disturbance is likely to be less than would be observed if the soil were saturated.

Sample selection considerations for measurement of total stress strength parameters in unsaturated soils is also similar to considerations for saturated soils. As is true for UU tests in general, the measured total stress strength envelopes are fundamentally linked to the magnitude of the effective stress at the location where samples were acquired. Thus, the total stress strength envelopes determined from UU tests are fundamentally only appropriate for locations and times where similar effective stresses are present. As a

practical matter, this generally means that specimens used for measurement of a single total stress strength envelope for unsaturated soils should be acquired from consistent depths. Similarly, the total stress strength envelope established from those tests is fundamentally only appropriate for the depth where samples were acquired. Thus, it is often necessary to perform substantial numbers of UU tests so that total stress strength envelopes can be established over a range in applicable depths.

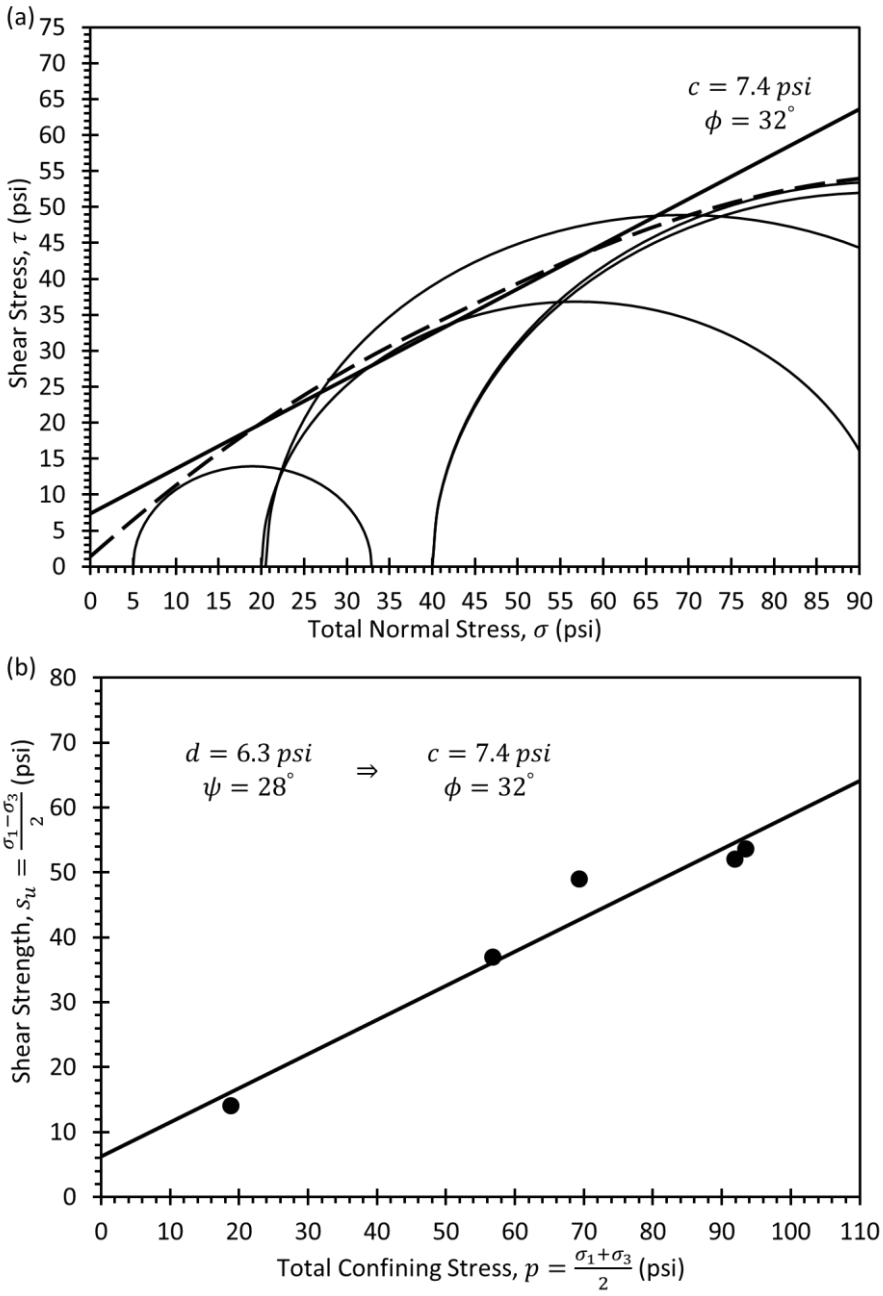


**Figure 7-36 Interpretation of total stress strength envelope from UU triaxial compression tests on unsaturated compacted clayey silt.**

## 7.6 EVALUATION OF EFFECTIVE STRESS STRENGTH PARAMETERS

Laboratory tests required for establishing effective stress strength envelopes or effective stress strength parameters are generally considered to be more complex and costly than tests commonly used to establish $s_u$ or total stress strength envelopes. However, it is also true that interpretation of measurements to establish effective stress strength envelopes is often much more straightforward than interpretation of $s_u$ because effective stress strength envelopes describe how soil shear strength varies with effective stress. Effective stress shear strength measurements are also substantially less variable than undrained strength measurements (e.g., Duncan, 2000), again because effective stress is the control variable. As a result, fewer tests are often required to establish effective stress strength envelopes with acceptable reliability than for $s_u$.

### 7.6.1 Consolidated-Undrained Triaxial Tests with Pore Pressure Measurements

The same consolidated-undrained triaxial tests described in Section 7.4.3 for determining undrained shear strength can be used for determining the effective stress strength envelope if pore pressure generated during undrained shearing of the specimens is measured. In such cases, the test is given the designation as a $\overline{CU}$ test to indicate that pore pressure is measured; otherwise, the test is identical to a CU test and the soil "feels" the same total and effective stresses throughout the test. Because effective stresses are known throughout the test, the measurements can be used to establish the effective stress strength envelope, which can be used for analyses of drained loading conditions. An advantage of $\overline{CU}$ tests is that they can generally be performed more quickly than consolidated-drained (CD) triaxial tests described in the following section. Additionally, since $s_u$ can be simultaneously determined, $\overline{CU}$ tests provide the ability to establish drained and undrained shear strength parameters with a single series of tests.

The effective stress strength envelope is generally best determined by plotting stress paths on a modified Mohr-Coulomb diagram as shown in Figure 7-37. Because specimens are sheared under undrained conditions, shear strength envelopes can be established using both the peak principal stress difference (PSD) and peak principal effective stress ratio (PSR) failure criteria described in Section 7.2.2. Figure 7-37 shows points representing the two respective criteria on each stress path, along with envelopes established to represent the two criteria. The two envelopes are practically similar for the measurements shown. However, differences between envelopes established for the two criteria may be greater for different soils, or for similar soils having different $OCR$. The shear strength envelope established using the PSR failure criterion is appropriate for evaluating stability for drained conditions whereas the envelope established using the PSD failure criterion is appropriate for use with effective stress analyses

performed to evaluate undrained conditions (which are more rare). It is also possible to interpret the effective stress strength envelope by plotting Mohr's circles that represent states of stress at failure using a conventional Mohr-Coulomb diagram.

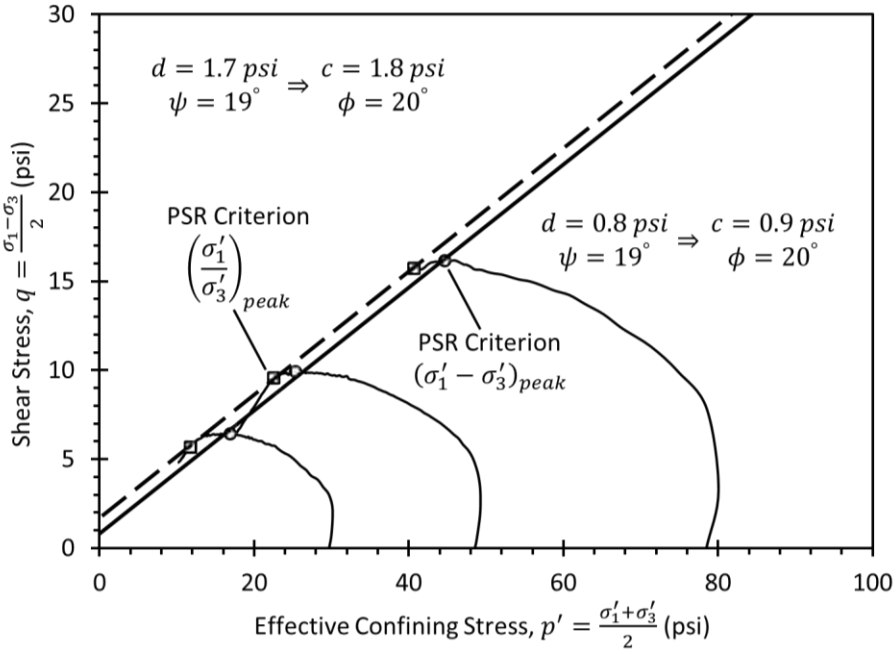


**Figure 7-37 Interpretation of $\overline{CU}$ triaxial compression tests to establish effective stress shear strength parameters.**

$\overline{CU}$ triaxial extension tests, or $\overline{CU}$ type direct simple shear tests can also be used to establish the effective stress strength envelope. However, effective stress envelopes established from different stress paths are practically similar so it is routine to perform the more common triaxial compression tests.

### 7.6.2 Consolidated-Drained Triaxial Tests

Consolidated-drained (CD) triaxial tests are similar to consolidated-undrained triaxial tests except that the shearing phase of the tests is performed slowly enough to prevent development of excess pore pressure. Since there is no excess pore pressure, the effective stress is known throughout the test and the measurements can be interpreted in terms of effective stresses. Because the shearing phase of the test must be performed more slowly, CD triaxial tests require longer testing times than CU tests. Furthermore, since the effective stress envelope determined from $\overline{CU}$ triaxial tests is often practically similar to the effective stress envelope determined from CD tests (only differing slightly because of corrections to account for volume change), there is often little motivation to perform CD tests unless the soil being tested drains quickly enough that differences in testing times are minimal (e.g., for clean

granular soils). Unlike what is observed for $\overline{CU}$ tests, the two alternative failure criteria (i.e., PSD and PSR) occur simultaneously during drained tests. Thus, there is no ambiguity about the state of stress at failure from tests that are fully drained.

### 7.6.3 Direct Shear Tests

Direct shear tests (AASHTO T236 and ASTM D3080) can be performed as an alternative to $\overline{CU}$ or CD triaxial tests to establish the effective stress strength envelope. Because direct shear testing equipment has no provisions for controlling drainage, tests must be performed as consolidated-drained tests where specimens are consolidated under one-dimensional conditions and then sheared slowly enough to prevent generation of excess pore pressures. However, because specimens are generally smaller than for triaxial testing, drainage occurs more quickly so direct shear tests can often be completed more quickly than triaxial tests for similar soils. The lack of drainage control makes use of direct shear tests for evaluation of undrained shear strength unreliable.

The effective stress shear strength envelope is interpreted by plotting the measured effective normal and shear stresses at failure on a conventional Mohr-Coulomb diagram as shown in Figure 7-38. If the "peak strength" envelope is desired, the maximum shear stress is selected and plotted on a Mohr-Coulomb diagram to establish the effective stress strength envelope. If the residual shear strength envelope is desired, the shear stress at large displacements is plotted as described in Section 7.7.

One potential issue with direct shear tests is that states of stress during the test are unknown and often non-uniform. Only the effective normal and shear stresses on the horizontal plane are measured so one cannot plot Mohr's circles for the condition at failure without making substantial assumptions and it is necessary to assume that the horizontal plane is the failure plane. While this assumption may not be universally satisfied for all tests, it generally has little practical consequence and it is common for effective stress strength envelopes from direct shear tests to be practically similar to those obtained from triaxial tests for isotropic soils (Taylor, 1939).

### 7.6.4 Effects of Sample Disturbance

Sample disturbance is substantially less significant for evaluating effective stress strength parameters than for measuring undrained shear strength. The difference is primarily a result of the fact that tests performed for establishing the effective stress strength envelope involve consolidation of specimens to known effective stresses. Disturbance can influence measured effective stress strength parameters if the unit weight (or related measures) is changed or if any soil structure (e.g., cementation) is altered during

sampling, transport, or test preparation. As such, high quality undisturbed specimens should be used for determining effective stress strength parameters, but effects of slight disturbance is usually much less significant than for measuring undrained shear strength (especially using UU or UC tests).

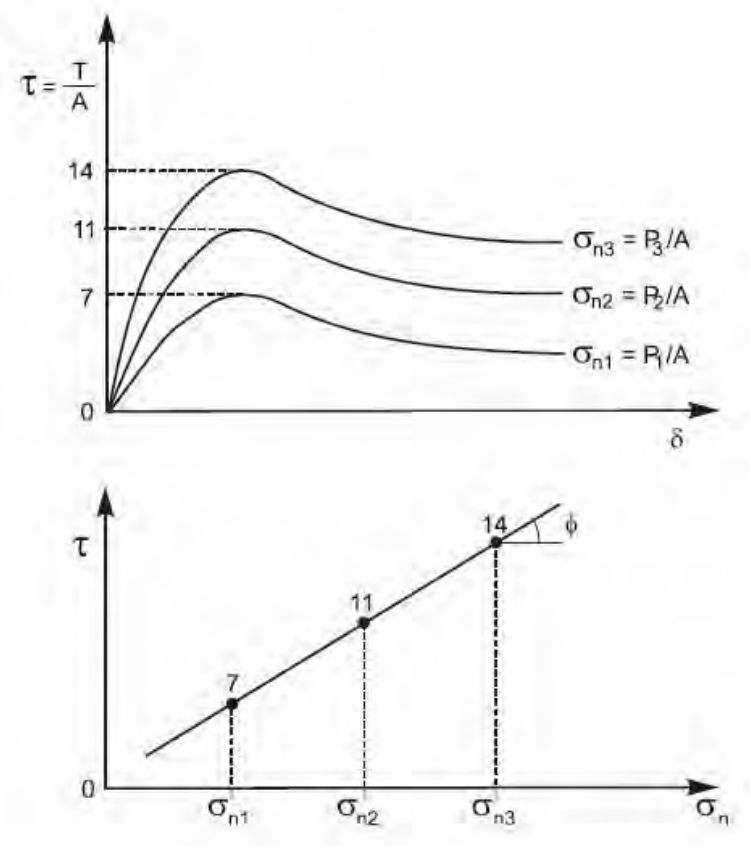


**Figure 7-38 Illustration of interpretation of direct shear test.**

### 7.6.5 Selection of Samples for Measurement of Effective Stress Strength Parameters

When selecting specimens for measurement of effective stress strength envelopes, it is not necessary to select specimens that are subjected to similar effective stress in the field as is required for measuring undrained shear strength or total stress strength parameters. As a result, it is only necessary to select specimens that are consistent in terms of composition and structure. Since a single effective stress strength envelope will generally be assigned for an entire stratum for design, it is preferable to use specimens collected from throughout the stratum so that the strength envelope represents the entire stratum rather than being a "point" measurement. Unlike $s_u$, the magnitude of effective stress strength parameters tend to be practically uniform with depth within a single stratum. It is also preferable to plot collections of individual measurements taken throughout a stratum for interpreting the strength envelope, rather than plotting two or three measurements taken from a single sampling tube for similar reasons.

### 7.6.6 Selection of Laboratory Testing Method

Selection of a laboratory testing method for determining effective stress strength envelopes is largely a matter of personal preference. As a practical matter, effective stress strength envelopes determined from $\overline{CU}$ and CD triaxial tests, and from direct shear tests are quite similar (Taylor, 1939; Bjerrum and Simons, 1960; Bjerrum et al, 1961) as long as the effective principal stress ratio (PSR) failure criterion is used to establish failure for the triaxial tests. Figure 7-39 shows a comparison of measurements from direct shear and $\overline{CU}$ triaxial compression tests for a clayey soil stratum along with effective stress strength envelopes interpreted from the respective measurements. Both types of measurements produce practically similar effective stress strength envelopes and strength parameters, as shown in the figure. The observed differences between the envelopes is likely due to differences in the volume change that occurs between the two types of tests since one test is drained and one test is undrained, and simple scatter among measurements.

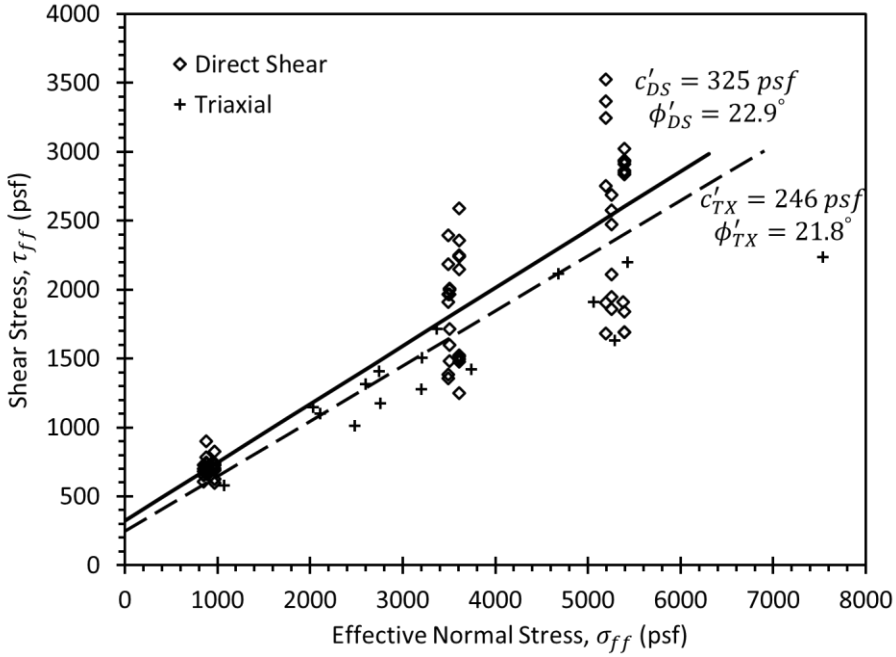


**Figure 7-39 Effective stress strength envelopes determined from direct shear and triaxial tests.**

While there is often little benefit for selecting triaxial tests over direct shear tests for many routine design situations, triaxial tests are strongly preferable if stiffness properties of the soil are also needed (e.g., for stress-deformation analyses). $\overline{CU}$ triaxial tests can also be used to establish both undrained shear strength parameters and effective stress strength parameters from the same tests if the testing program is carefully established. Thus, triaxial tests can provide additional information beyond just establishing the effective

stress strength envelope and are generally preferable when that additional information will provide benefits to a project.

### 7.6.7 Measurement of Effective Stress Strength Parameters Using Borehole Shear Test

While most in situ tests are indirect measurements that must be transformed to determine specific soil properties of interest, the borehole shear device produces a direct measurement of shear strength in a manner similar to laboratory direct shear tests. The borehole shear device is composed of two curved, serrated contact plates that are expanded against the walls of a borehole with a known force (Handy, 1986). After allowing time for consolidation to occur under the applied normal force, the device is pulled vertically while measuring the force required to displace the device, which is then converted to a shear stress. The maximum shear stress measured during the test is taken to be the shear strength, which can be plotted on a Mohr-Coulomb diagram to establish a shear strength envelope as shown in Figure 7-40. While some early test results were questioned regarding whether the tests were drained or undrained tests, studies by Lutenegger and Tierney (1986) and Demartinecourt and Bauer (1983) using borehole shear devices fitted with pore pressure transducers allowed procedures to be effectively established to produce reliable measurements of effective stress parameters. Borehole shear tests can be efficiently conducted in a broad range of geologic materials, including rock.

### 7.6.8 Estimation of Effective Stress Strength Parameters from Indirect Measurements

It is common practice to evaluate effective stress strength parameters for coarse-grained soils from in situ tests. In situ tests are particularly useful in clean coarse-grained soils that are notoriously difficult to sample using conventional methods. Clean coarse-grained soils also commonly have a negligible effective stress cohesion intercept so it is only necessary to evaluate the effective stress friction angle to appropriately represent the shear strength. In this section, commonly used methods are presented for establishing the effective stress friction angle from SPT, CPT, and DMT measurements. The transformations are often presented in the form of charts, but in some cases can be implemented into spreadsheet calculations to conveniently evaluate the effective stress friction angle as a function of depth.

Several different methods can be used to estimate values of the effective stress friction angle from uncorrected or corrected SPT $N$-values. Table 7-5 provides baseline relationships for evaluating the effective stress friction angle for coarse-grained soils from uncorrected $N$-values based on empirical measurements for relatively clean sands. Alternatively, the well-known empirical chart proposed by Schertmann (1975), shown in Figure 7-41, can be used to estimate $\phi'$. In this chart, $\phi'$ is related to corrected SPT blow counts to account for hammer efficiency, $N_{60}$. Results from this chart tend to be

somewhat conservative, especially for depths less than 6 ft. The transformation provided by Figure 7-41 can also be approximated as:

$$\tan\phi' = \left[\frac{N_{60}}{12.2+20.3\frac{\sigma'_{vo}}{p_a}}\right]^{0.34} \tag{7.22}$$

where $\sigma'_{vo}$ is the in situ vertical effective stress at the depth where $N$ is measured and $p_a$ is atmospheric pressure.

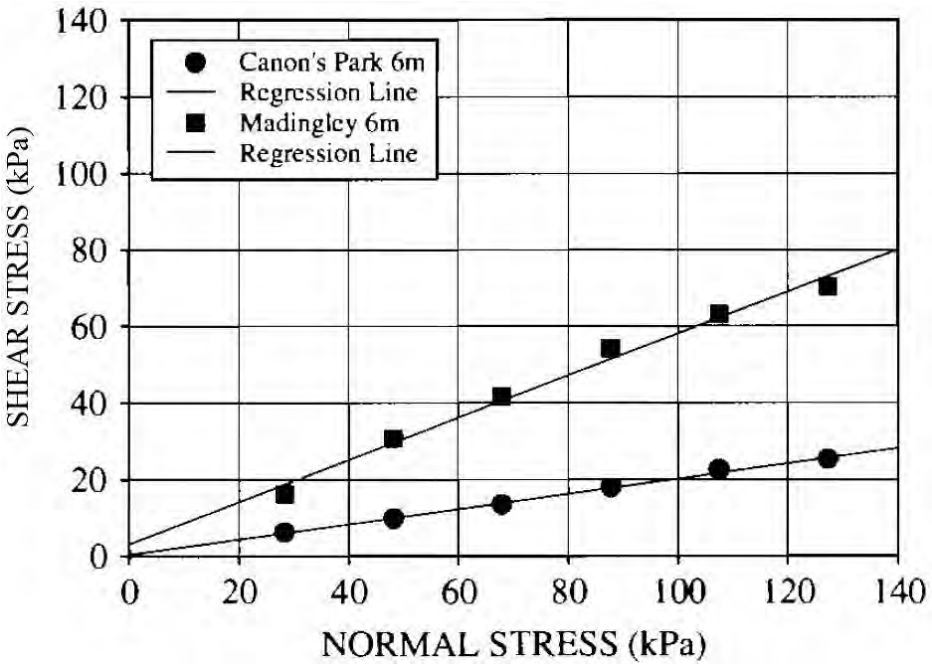


**Figure 7-40 Failure envelopes from borehole shear tests (from Lutenegger and Powell, 2008).**

**Table 7-5 Relationship among relative density, SPT $N$-value, and $\phi'$ for coarse-grained soils (after Meyerhof, 1956)**

| Condition | Relative Density (%) | SPT $N$-value (blows/ft) | Friction Angle, $\phi'$ (deg) |
|---|---|---|---|
| Very Loose | < 20 | <4 | <30 |
| Loose | 20-40 | 4-10 | 30-35 |
| Compact | 40-60 | 10-30 | 35-40 |
| Dense | 60-80 | 30-50 | 40-45 |
| Very Dense | >80 | >50 | >45 |

Note: $N = 15 + (N' - 15)/2$ for $N' > 15$ in saturated very fine or silty sand, where $N'$= measured blow count and $N$ = blow count corrected for dynamic pore pressure effects during the SPT.

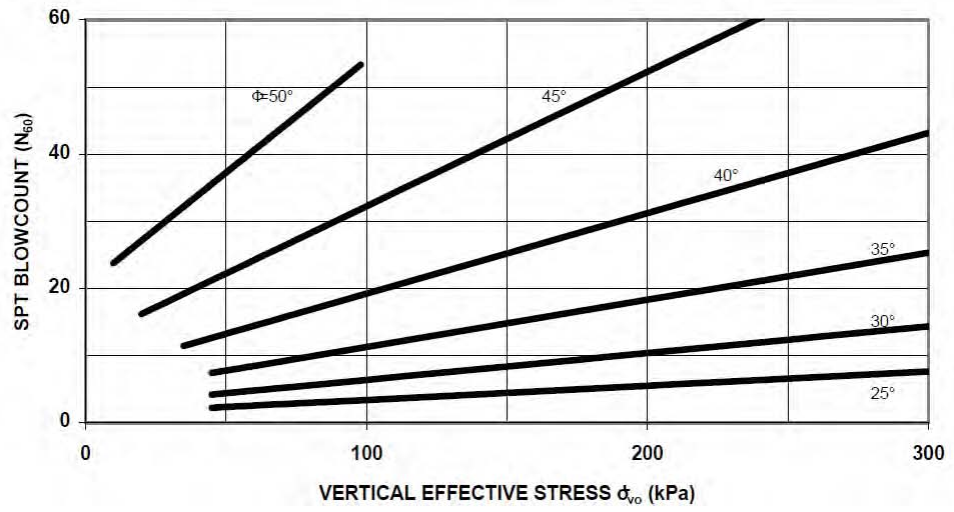


**Figure 7-41 Chart relating $\phi'$ to SPT $N_{60}$-value and $\sigma'_{vo}$ (after Schmertmann, 1975).**

Hatanaka and Uchida (1996) proposed an alternative transformation between $\phi'$ and corrected SPT blow count, $(N_1)_{60}$, based on direct measurements of $\phi'$ in triaxial cells using high-quality undisturbed samples of natural sands obtained by freezing the samples. The data used by Hatanaka and Uchida were obtained using an automatic trip hammer system with an efficiency of 78 percent. For an average state-of-practice hammer with 60 percent efficiency, the expression for peak $\phi'$ is:

$$\phi' = \sqrt{15.4(N_1)_{60}} + 20^{\circ} \tag{7.23}$$

It is important to recognize that these transformations were developed for relatively clean sands. Use of these correlations in, for example, micaceous sands is not recommended. The presence of mica in sand will tend to reduce the SPT blow count significantly below that which would be measured for the same sand without mica. However, the actual friction angle of clean sand and micaceous sand may not be significantly different when measured in laboratory triaxial tests. Laboratory triaxial tests should be performed on silty sand soils where more accurate values of $\phi'$ are required.

The transformations presented above, and SPT tests in general, should also not be used to estimate $\phi'$ for gravelly soils unless the transformations are used conservatively or can be confirmed or adapted based on local experience. Gravel particles are often larger than the inner diameter of the standard sampler used in the SPT test. As a result, measured $N$ values may be inappropriate high, which in turn can lead to overestimation of $\phi'$. In many design situations, $\phi'$ for gravelly soils can be conservatively estimated using empirical correlations like those presented in Section 7.6.9 without introducing substantial costs for design and construction. In cases where more precision is needed (e.g., for seismic design), it may be

necessary to use large penetration tests (LPT) or Becker penetration tests (BPT) with alternative transformations to evaluate $\phi'$.

The effective stress friction angle in coarse-grained soils can also be estimated from cone penetration tests (CPT) using transformations that are often derived from bearing capacity theory. The chart shown in Figure 7-42 by Robertson and Campanella (1983) is commonly used to estimate $\phi'$ from the corrected cone tip resistance, $q_t$, and $\sigma'_{vo}$. Alternatively, Mayne (2007) recommends using an alternative expression for predicting $\phi'$ from CPT measurements from Kulhawy and Mayne (1990):

$$\phi' = 17.6^{\circ} + 11.0^{\circ} \cdot \log(q_{t1}) \tag{7.24}$$

where $q_{t1} = (q_t/p_a)/\left(\sqrt{\sigma'_{vo}/p_a}\right)$.

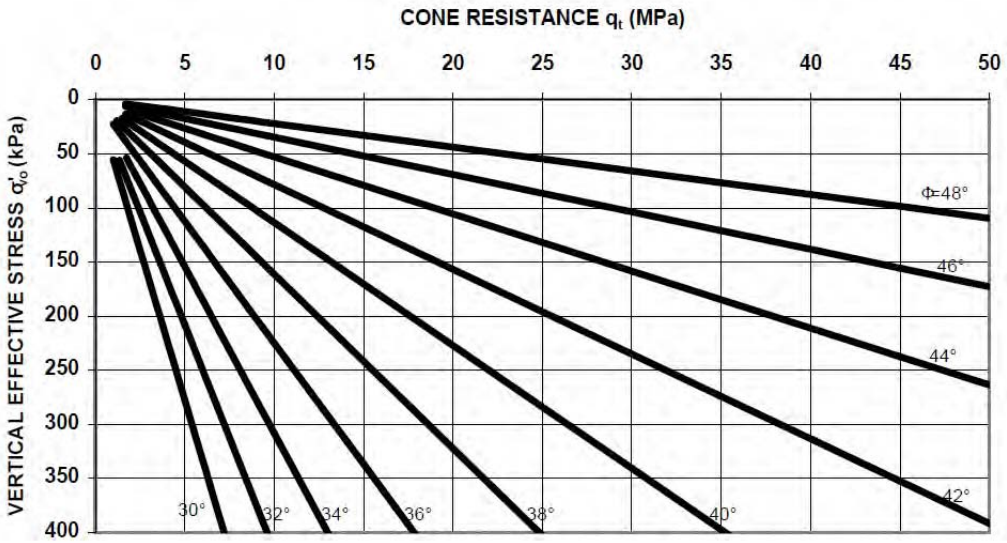


**Figure 7-42 Relation for $\phi'$ from CPT $q_t$ and $\sigma'_{vo}$ (after Robertson and Campanella, 1983).**

Finally, $\phi'$ can also be estimated from DMT measurements based on the DMT horizontal stress index, $K_D$, as (Marchetti, et al., 2001):

$$\phi' \approx 28^{\circ} + 14.6 \log K_D - 2.1(\log K_D)^2 \tag{7.25}$$

Values determined from Equation 7.25 are considered to be lower bound for $\phi'$, with actual values being 2 to 4 degrees greater than produced using the equation (Marchetti, et al., 2001; Schnaid, 2009).

### 7.6.9 Estimation of Effective Stress Strength Parameters from Empirical Correlations

The effective stress friction angle, $\phi'$, can also be estimated using so-called empirical correlations for many soils. Such correlations are really just transformations from one measurement to a different soil property. However, correlations involve substantial uncertainty because they are related to more general characteristics of the soil (e.g., soil type, or index properties) rather than measurements that more closely approximate the property of interest. Estimates from empirical correlations can be quite useful for preliminary design, for design in strata that have little influence on stability and performance, or even for final design if conservatively estimated and appropriately considered. In some materials, such as rockfill, there is seldom any practical alternative for establishing effective stress strength parameters.

Effective stress failure envelopes for many coarse-grained soils are often curved when considered over significant ranges of confining stress. Values of $\phi'$ are therefore generally reported as secant values computed assuming the effective stress cohesion intercept, $c'$, is equal to zero. Secant values of $\phi'$ are most commonly related to relative density, $D_r$, and some measure of effective confining stress. Figure 7-43 shows a recently proposed correlation for sands developed from measurements for 54 different sands, many of which are from offshore sites, but that include beach sands, river sands, and sands from onshore sites. While there is considerable scatter in the measurements, there are clear trends of increasing $\phi'$ with increasing relative density and decreasing effective confining stress (for this figure, defined as $\sigma_c' = (\sigma_1' + \sigma_2' + \sigma_3')/3$). Use of this figure requires that $\sigma_c'$ be estimated based on expected stresses for the specific application. If $\sigma_c'$ varies over a relatively large, a conservative value can be selected from the greatest estimated confining stress, or a strength envelope can be developed from values of $\phi'$ selected to represent smaller confining stress increments. Many alternative correlations for sands have also been proposed.

Figure 7-44 shows a chart developed by Duncan et al. (2014) based on measurements from Leps (1970) and Woodward-Clyde (1995) for gravels and rockfill materials. Relative densities for the measurements shown were unknown so the influence of $D_r$ is not characterized. However, based on analysis of alternative measurements from Marachi et al. (1969) and Becker et al. (1972) for sands, gravels, and rockfill materials, Duncan et al. propose that the secant friction angle be predicted as

$$\phi' = A + B \cdot D_r - (C + D \cdot D_r) \log\left(\frac{\sigma_N'}{p_a}\right) \tag{7.26}$$

where the parameters $A$, $B$, $C$, and $D$ are established from Table 7-6 based on grain size characteristics of the soils, and $\sigma_N'$ is the effective normal stress (computed as $\sigma_N' = (\cos^2 \phi')/(1 - \sin \phi')$).

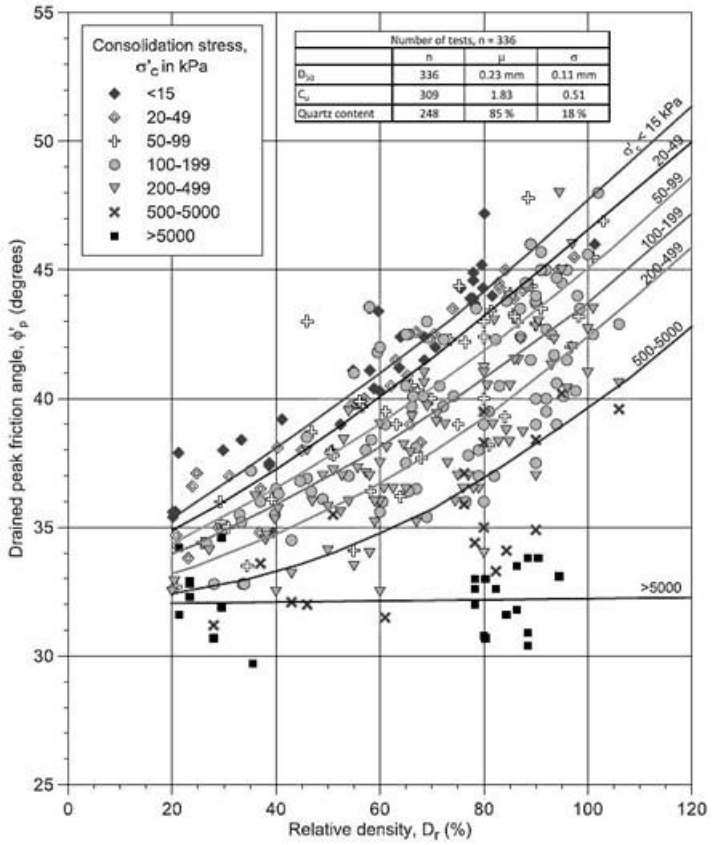


**Figure 7-43 Relation between $\phi'$, $D_r$, and $\sigma'_c$ for sands (from Andersen and Schjetne, 2013).**

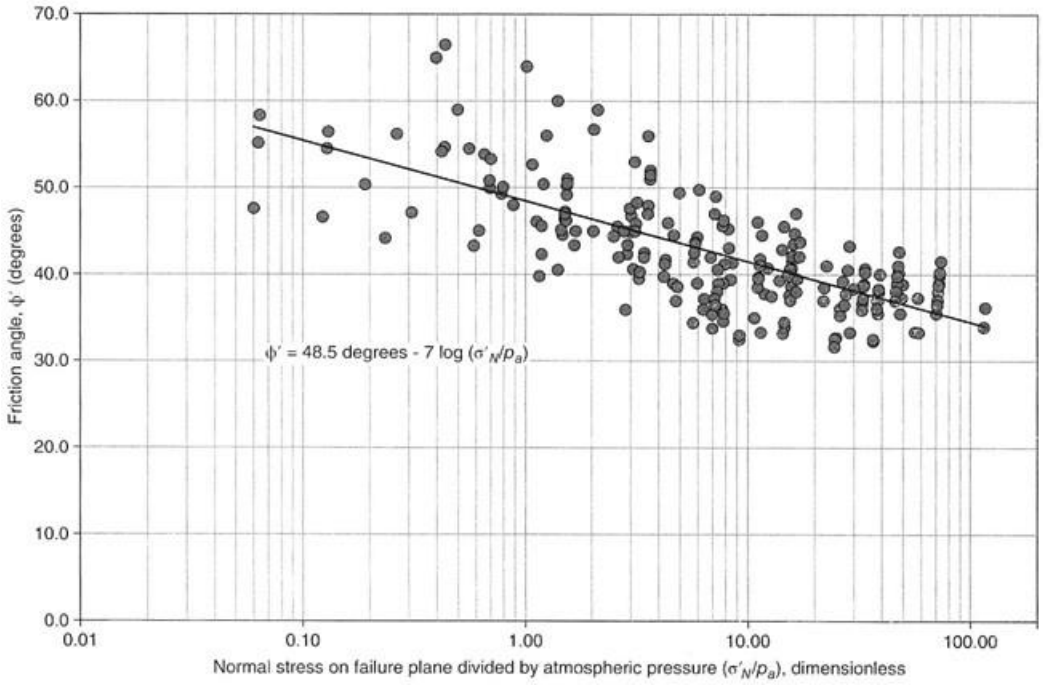


**Figure 7-44 Effective stress friction angles for rock fill and gravels (from Duncan, et al., 2014).**

**Table 7-6 Parameter values for use with Equation 7.26 (Duncan, et al., 2014).**

| Soil Characteristic | | Parameter Values in Degrees | | | | Std. Dev. |
|---|---|---|---|---|---|---|
| **Soil Type** | **Coeff. of Uniformity** | **A** | **B** | **C** | **D** | **(degrees)** |
| Gravel and cobbles | $C_u > 4$ | 44 | 10 | 7 | 2 | 3.1 |
| Sand | $C_u > 6$ | 39 | 10 | 3 | 2 | 3.2 |
| | $C_u < 6$ | 34 | 10 | 3 | 2 | 3.2 |

For fine-grained soils, $\phi'$ is generally considered to be related to the plasticity index. Figure 7-45 shows one such graphic for a broad range of $PI$ (note the change from arithmetic to logarithmic scales in the figure). The scatter shown in Figure 7-45 is considerable, indicating a range of approximately ±8 degrees. This variability and uncertainty can often be reduced through development and use of more local or regional correlations between $\phi'$ and $PI$. However, such improvements are seldom sufficient to replace actual testing for final design in fine-grained soils.

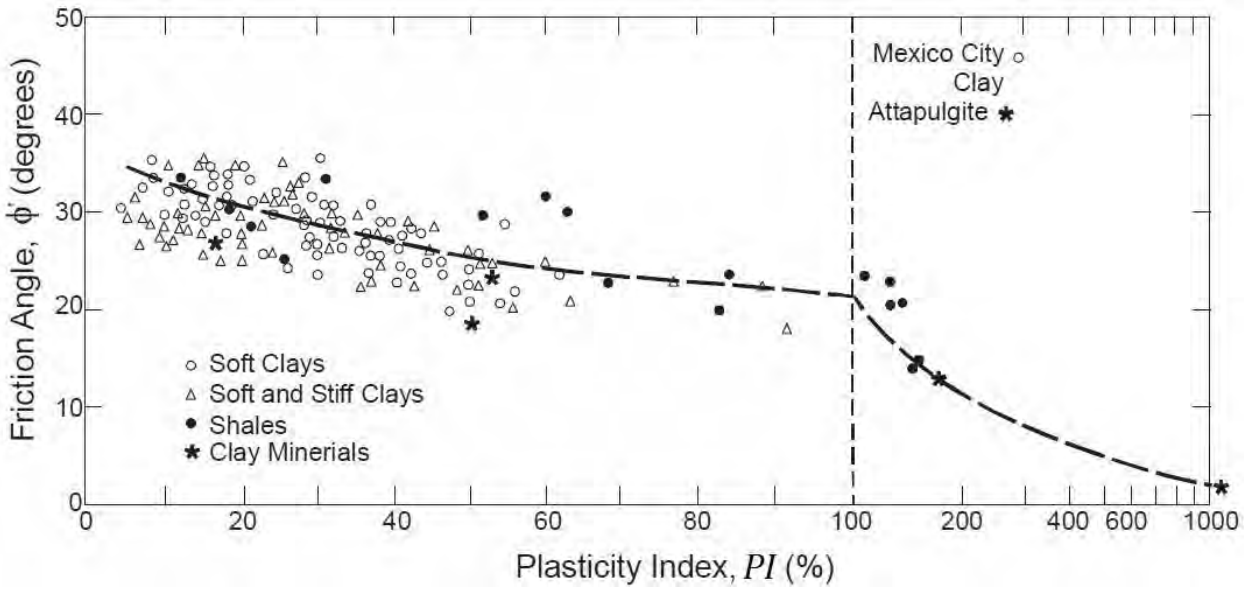


**Figure 7-45 Estimates of $\phi'$ based on plasticity index, $PI$ (adapted from Terzaghi, et al., 1996)**

## 7.7 EVALUATION OF RESIDUAL AND FULLY-SOFTENED SHEAR STRENGTH PARAMETERS

In some design situations and some soils, it is important to evaluate and consider shear strengths that are less than the peak shear strength that has been described throughout the remainder of this chapter. Such instances arise when encountering stiff fissured clays, compacted high plasticity clays, and clays that may have undergone substantial shear displacements (e.g., from a landslide). When previous sliding is known or suspected to have occurred, the residual shear strength is generally the appropriate strength to use for

design. The fully softened shear strength is often appropriate for design in stiff fissured clays and compacted high plasticity clays when prior sliding has not occurred (e.g., Wright, 2005; Wright, et al., 2007; Castellanos, et al., 2013; VandenBerge, et al., 2013; Gregory and Bumpas, 2013; Gamez and Stark, 2014). In this section, methods for measurement of residual shear strength are described along with methods for estimating the residual and fully softened friction angles for fine-grained soils.

### 7.7.1 Direct-Residual Shear Test

One means for measuring the residual shear strength is to repeatedly shear specimens back and forth in a direct shear device in what is often referred to as a direct-residual shear test. Figure 7-46 shows results from a direct-residual shear test on a heavily overconsolidated, stiff clay. As shown in the figure, as the specimen is repeatedly sheared, the sequential "peaks" in the shear stress-displacement curves reduce with increasing displacement until eventually approaching a condition where the maximum shear stress achieves a practically consistent value. This value is interpreted to be the residual shear strength of the soil. If several direct-residual shear tests are performed at different effective normal stresses, a residual shear strength envelope can be established as illustrated in Figure 7-47. Residual shear strength envelopes generally have negligible cohesion intercept, and friction angles that are often substantially less than values established for peak strengths. Since direct-residual shear tests are performed under fully drained conditions, the residual friction angle is an effective stress friction angle that is appropriate for analysis of long-term, fully drained conditions (if the soil has been subjected to considerable sliding).

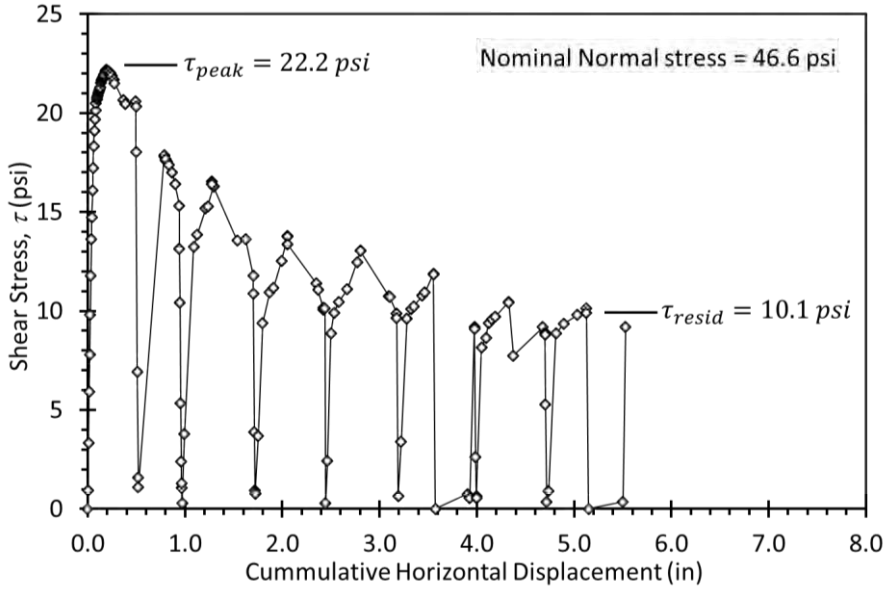


**Figure 7-46 Shear stress versus cumulative displacement from direct-residual shear test.**

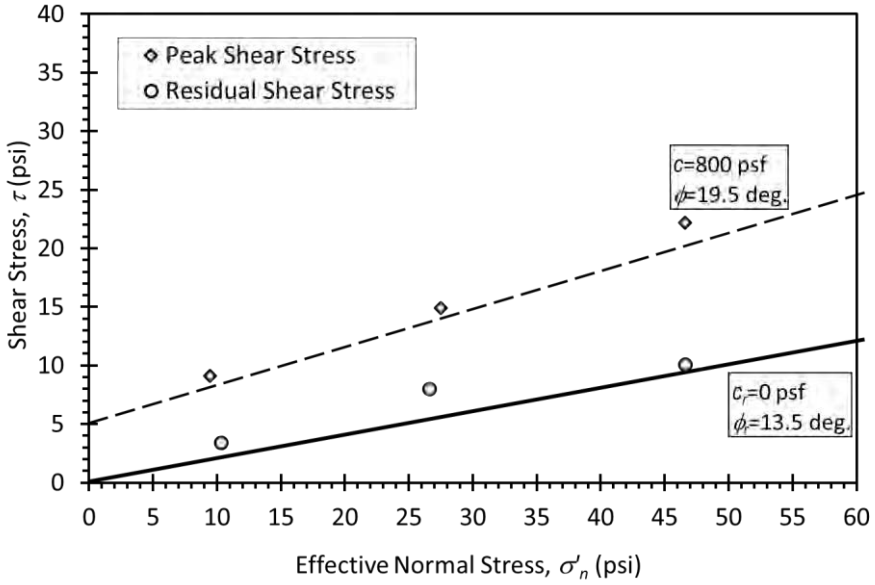


**Figure 7-47 Comparison of peak and residual strength envelopes from direct-residual shear test.**

### 7.7.2 Ring Shear Test

An alternative to the direct-residual shear test is the ring shear test (ASTM D6467). One issue that arises with direct-residual shear tests is that the shear direction must be repeatedly reversed, which can introduce practical issues associated with maintaining the soil specimen (i.e., some of the specimen is often "lost" with repeated shearing) that can influence the measured results. In addition, a large number of shearing cycles may be required to reach the residual condition and it can be difficult to achieve such displacements within a reasonable time frame. The ring shear test avoids such issues by providing for continuous shearing in the same direction for very large displacements. Since shearing is continued in the same direction, it is often much easier to reach and identify when the residual strength condition has been achieved. However, the equipment is relatively expensive and not readily available, and testing requires special sample preparation so ring shear tests are not commonly performed for most projects. Aside from the difference in loading mechanism, a ring shear test is interpreted like a direct-residual shear test.

### 7.7.3 Selection of Samples for Residual Shear Strength Measurement

No special requirements are imposed for soils selected for residual shear strength measurements. Selected specimens must obviously be of sufficient size for the intended tests and be representative of the stratum for which they represent. However, since both direct-residual shear and ring shear tests generally require significant testing times, careful selection is justified to ensure specimens are representative. Selection therefore often includes extensive index testing to verify that selected samples are

representative of the broader stratum. Since the residual strength condition represents a "destructured" condition that is largely dependent on the clay fraction and type of clay minerals present, sample quality and disturbance tend to have little effect on measured residual shear strengths.

### 7.7.4 Estimation of Residual and Fully Softened Shear Strength Parameters from Empirical Correlations

Because residual shear strength tests require substantial time to complete, it is often desirable to estimate values for residual strength from index property measurements. Fortunately, residual shear strength parameters are predominately governed by the mineralogy of the clay soil and the proportion of clay size particles in the soil, and thus are conducive to correlation (e.g., Stark and Eid, 1994; Stark, et al., 2005). Figure 7-48 shows one such correlation that relates the residual friction angle for clays to the liquid limit (*LL*) and the clay size fraction (*CF*). Because the residual friction angle is largely dependent on general soil characteristics, correlations like the one shown in Figure 7-48 tend to be substantially more reliable than many other correlations presented throughout this manual.

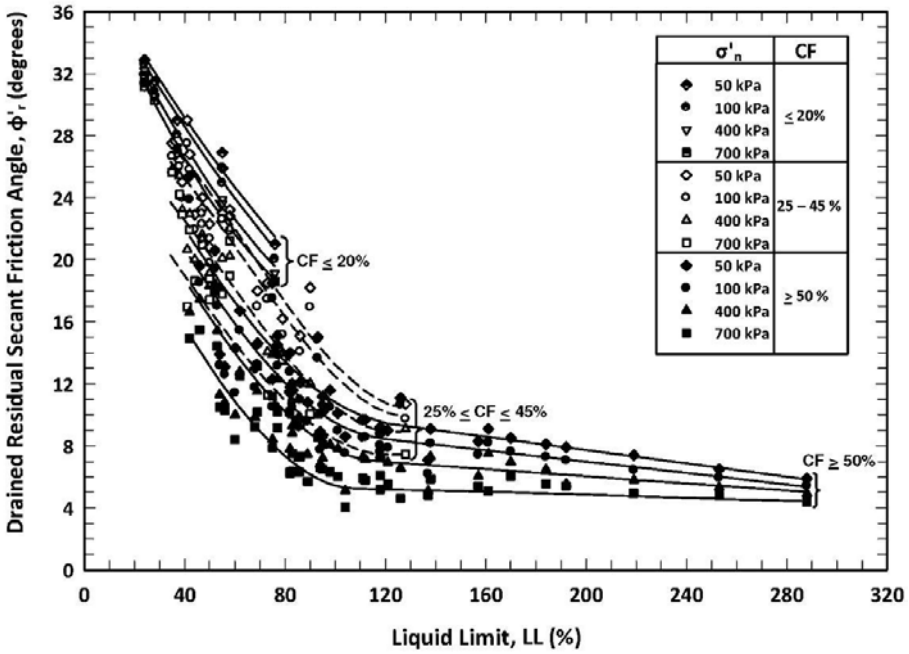


**Figure 7-48 Empirical estimates for drained residual friction angle from liquid limit and clay size fraction (from Stark and Hussain, 2013).**

Similar empirical correlations for estimating the fully softened friction angle for clayey soils have been developed as shown in Figure 7-49. As shown in the figure, these correlations are more sensitive to the magnitude of the effective normal stress and involve considerably more scatter. These results are likely

attributed to the fact that fully softened shear strength is more dependent on the structure of a particular soil than is the residual shear strength. Alternative correlations have also recently been proposed by Gamez and Stark (2014) and Castellanos et al. (2016). The secant friction angle generally decreases with increasing effective confining pressures, as shown in both Figure 7-48 and 7-49, because both the residual and fully softened failure envelopes are often curved.

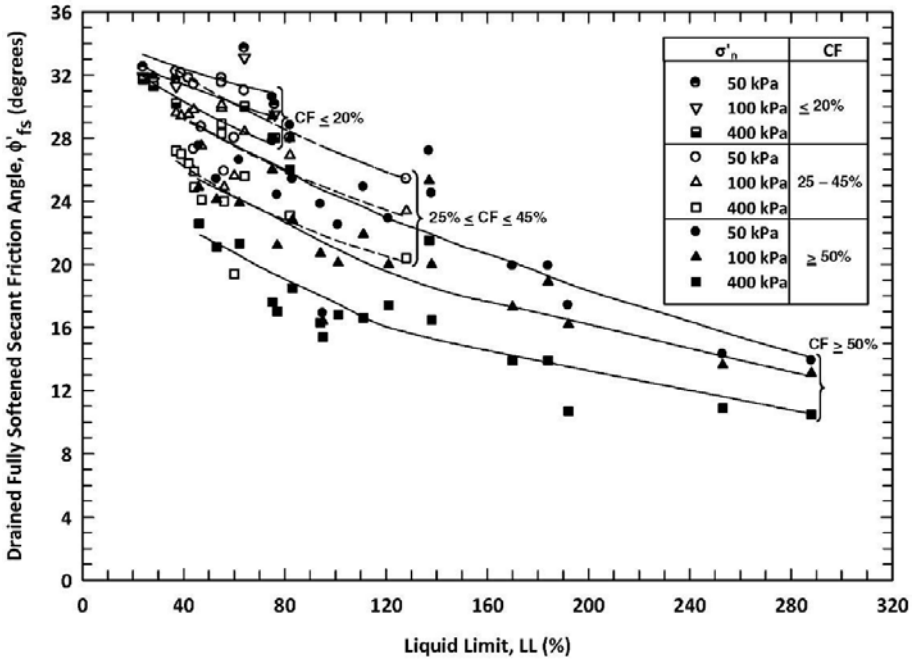


**Figure 7-49 Estimated drained, fully softened friction angle from *LL* and *CF* (from Stark and Hussain, 2013)**

Wright (2005) developed analytical expressions that can be used to predict the secant friction angle for both the residual and fully softened shear strength conditions based on empirical measurements from Stark and Eid (1994) and Stark et al. (2005). For the residual strength condition, Wright (2005) proposed the following expression for the secant residual friction angle:

$$\phi_{r-secant} = 52.5^{\circ} - 21.3^{\circ} \cdot \log_{10}(LL) - 3^{\circ} \cdot \log_{10}\left(\frac{\sigma_f'}{p_a}\right) \tag{7.27}$$

where $LL$ is the liquid limit, $\sigma_f'$ is the effective stress on the failure surface, and $p_a$ is atmospheric pressure in the same units as $\sigma_f'$. For the fully-softened strength condition, the secant friction angle can be similarly estimated as

$$\phi_{FS-secant} = 55.3^{\circ} - 16.7^{\circ} \cdot \log_{10}(LL) - 6^{\circ} \cdot \log_{10}\left(\frac{\sigma_f'}{p_a}\right) \tag{7.28}$$

Stark and Hussain (2013) provide alternative equations for predicting the secant friction angle for the residual and fully softened shear strength conditions.

## 7.8 EVALUATION OF SHEAR STRENGTH PARAMETERS FOR COMPACTED SOILS

The shear strength of compacted soils is fundamentally governed by the same principles that govern the strength of all soils. The concepts presented throughout this chapter therefore fundamentally apply to compacted soils as well. The primary additional challenge for characterizing compacted soils is that one cannot simply go out and sample the soil or perform in situ tests because the compacted soil does not exist prior to construction. Thus, it is necessary to collect samples from the anticipated borrow source and prepare specimens in the laboratory to reasonably mimic how the soil will be compacted during construction. Fortunately, it is possible to specify a practical range of compaction conditions that will be considered acceptable during construction and to confirm that those conditions are met through normal construction quality control and quality assurance practices.

Figure 7-50 shows a common graph of soil dry unit weight versus compaction moisture content that is used to represent compaction conditions. Measurements of the relationship between dry unit weight and compaction moisture content from Standard Proctor tests (AASHTO T99; ASTM D698) for soil from a selected borrow source are shown in the figure. An area designating acceptable compaction conditions during construction is also shown in the figure. Thus, one can anticipate that borrow soils from this source will be compacted to conditions that fall somewhere within the shaded region shown. The objective for characterization is therefore to establish appropriate values for shear strength parameters for the borrow soils if they are compacted somewhere within the region shown. As a general rule, both total and effective stress strength parameters must be established so that designers can consider both the undrained and drained strength of the soil for design.

Unfortunately, the strength of compacted soils under short-term, undrained conditions depends on the specific compaction conditions that are achieved during construction (e.g., Seed and Chan, 1959). Figure 7-50 shows two collections of points indicating samples that are compacted near to the bottom of the acceptable region, thus approximately corresponding to the minimum acceptable dry unit weight. One collection of points is designated as “dry” specimens because they are compacted dry of the optimum moisture content. The other is designated as “wet” because they are compacted wet of the optimum moisture content. Figure 7-51 shows shear strength measurements from UU triaxial compression tests for each of the specimens along with total stress envelopes established for specimens compacted wet and dry of the optimum moisture content, respectively. The total stress envelope determined for specimens

compacted wet of the optimum moisture content clearly reflects substantially lower shear strength than observed for specimens compacted at similar density but lower water content.

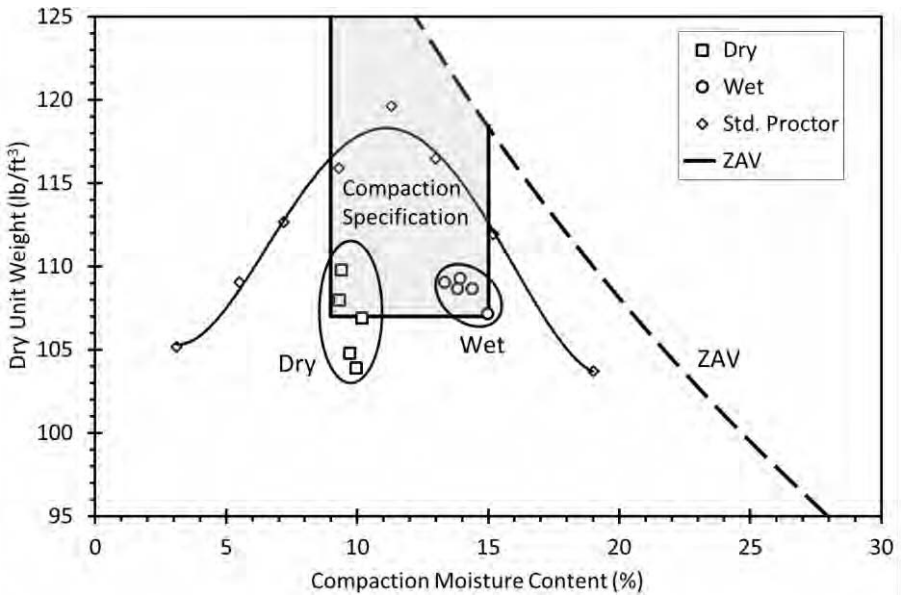


**Figure 7-50 Proctor curve for compacted silty clay showing region of compaction specification and compaction conditions for "wet" and "dry" specimens used for soil strength testing.**

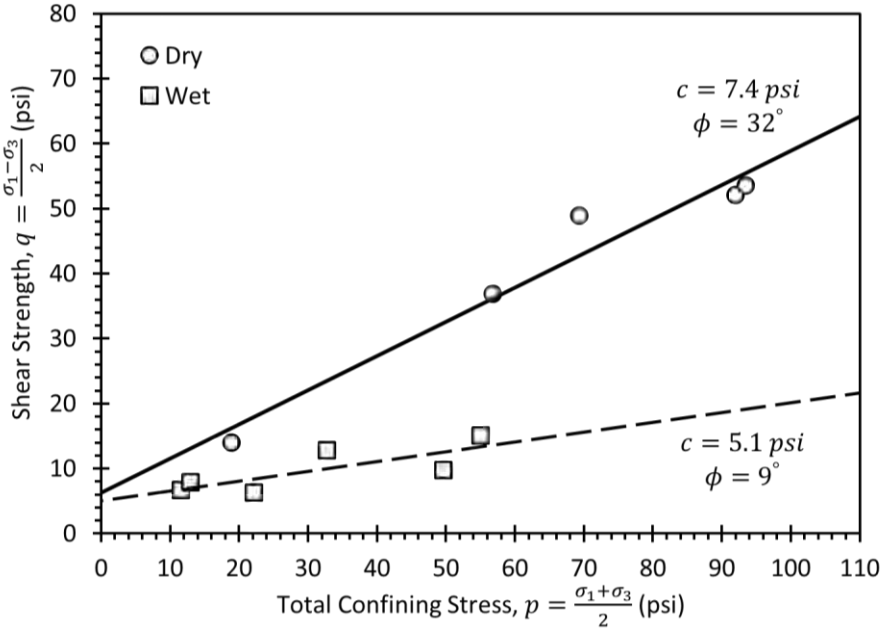


**Figure 7-51 Total stress shear strength envelopes determined from UU triaxial compression tests for silty clay specimens compacted "wet" and "dry".**

Figure 7-52 shows measurements of shear strength established for similarly prepared "wet" and "dry" specimens tested using $\overline{CU}$ triaxial compression tests and the associated effective stress strength envelope for the same soil. In contrast with what is shown in Figure 7-51 for total stress strength envelopes, effective stress envelopes determined for different compaction conditions are substantially more consistent, often producing virtually identical envelopes. Some dependence on the magnitude of the dry unit weight can be observed, but even these differences are small relative to differences observed in the total stress strength envelopes. Results shown in Figure 7-51 and 7-52 are typical of what is observed for compacted soils. As a general rule, it is therefore prudent to establish both total stress and effective stress strength envelopes based on measurements for specimens that are compacted near the bottom right boundary of the anticipated acceptable compaction region.

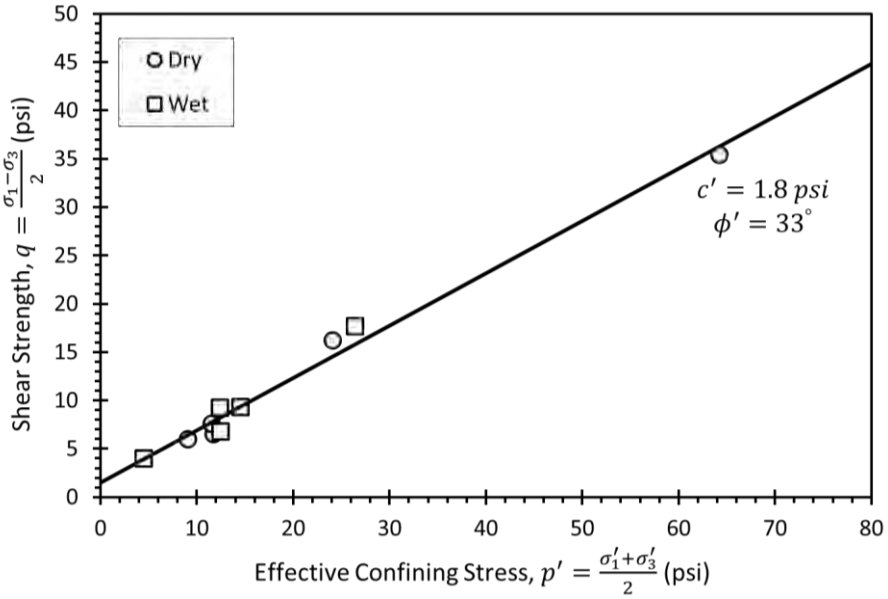


**Figure 7-52 Effective stress strength envelopes determined from $\overline{CU}$ type triaxial compression tests for specimens compacted "wet" and "dry" of standard Proctor optimum moisture content.**

There are many instances where preliminary estimates for effective stress strength parameters for compacted soils are needed for design of compacted embankments. Unfortunately, in situ tests are generally of no use because the compacted fills do not yet exist and measurements at the borrow source are unlikely to be representative of the as-compacted strength properties. However, preliminary estimates can be derived from the values provided in Table 7-7 based on USCS classifications, presuming that compactive effort in the field will be similar to that used to derive the properties shown. The data in Table 7-7 were derived from specimens compacted at the optimum moisture content and maximum dry unit weight for the U.S. Bureau of Reclamation (USBR) standard compaction method, which has similar compaction energy to AASHTO T99 and ASTM D698. Unfortunately, total stress strength

characteristics of compacted soils are strongly dependent on specific soil characteristics and compaction conditions so estimates from general soil properties are unreliable.

**Table 7-7 Estimated for effective stress strength parameters for compacted soils (adapted from U.S. Bureau of Reclamation, 1973).**

| USCS Classification | Maximum Dry Density† ($lb/ft^3$) | Optimum Water Content† (%) | Effective Stress Cohesion Intercept ($lb/ft^2$) | | Effective Stress Friction Angle, $\phi'$ (deg) |
|---|---|---|---|---|---|
| | | | As Compacted, $c'_o$ | Saturated, $c'_{sat}$ | |
| GW | $> 119$ | $< 13.3$ | -- | -- | $> 38$ |
| GP | $> 110$ | $< 12.4$ | -- | -- | $> 37$ |
| GM | $> 114$ | $< 14.5$ | -- | -- | $> 34$ |
| GC | $> 115$ | $< 14.7$ | -- | -- | $> 31$ |
| SW | $119 \pm 5$ | $13.3 \pm 2.5$ | $800 \pm 75$ | -- | $38 \pm 1$ |
| SP | $110 \pm 2$ | $12.4 \pm 1.0$ | $500 \pm 125$ | -- | $37 \pm 1$ |
| SM | $114 \pm 1$ | $14.5 \pm 0.4$ | $1000 \pm 125$ | $400 \pm 150$ | $34 \pm 1$ |
| SM-SC | $119 \pm 1$ | $12.8 \pm 0.5$ | $1000 \pm 450$ | $300 \pm 125$ | $33 \pm 4$ |
| SC | $115 \pm 1$ | $14.7 \pm 0.4$ | $1500 \pm 300$ | $200 \pm 125$ | $31 \pm 4$ |
| ML | $103 \pm 1$ | $19.2 \pm 0.7$ | $1400 \pm 200$ | $200 \pm ?$ | $32 \pm 2$ |
| CL-ML | $109 \pm 2$ | $16.8 \pm 0.7$ | $1300 \pm 350$ | $450 \pm ?$ | $32 \pm 3$ |
| CL | $108 \pm 1$ | $17.3 \pm 0.3$ | $1800 \pm 200$ | $300 \pm 50$ | $28 \pm 2$ |
| MH | $82 \pm 4$ | $36.3 \pm 3.2$ | $1500 \pm 600$ | $400 \pm 200$ | $25 \pm 3$ |
| CH | $94 \pm 2$ | $25.5 \pm 1.2$ | $2100 \pm 700$ | $200 \pm 125$ | $19 \pm 5$ |

† based on USBR standard compaction method
± values represent 90 percent confidence limits

THIS PAGE IS LEFT INTENTIONALLY BLANK

# CHAPTER 8
# MEASUREMENT AND INTERPRETATION OF STRESS-STRAIN AND STIFFNESS PROPERTIES

Geotechnical materials exhibit nonlinear stress-strain behavior that is influenced by many factors that include effective stress level, density, stress history, soil type, plasticity, gradation, age, strain rate, pore pressure generation, and soil structure. Ideally, geotechnical analyses would utilize a stress-strain model that accurately captures many of these factors. However, development and application of such a model is not practical for most routine geotechnical problems. For this reason, geotechnical deformation analysis procedures used for design typically require a simpler representation of soil or rock deformation behavior, often through use of a single "stiffness" property. Determining and selecting appropriate deformation properties can be challenging due to the many factors that affect soil modulus and the diverse applications that require modulus or stiffness values. Modulus or stiffness can be determined in a variety of ways, including: (1) laboratory measurements to directly measure the stress-strain response, (2) in situ and laboratory measurements of stress-wave velocity, (3) direct in situ measurement of soil deformations, and (4) indirect relationships with other soil properties or in situ measurements. This chapter describes the general stress-strain behavior of soil along with laboratory and field methods used for establishing deformation properties for geotechnical applications.

## 8.1 USES FOR STRESS-STRAIN AND STIFFNESS PROPERTIES

Table 8–1 summarizes many ways deformation properties are represented and used in geotechnical engineering. The most commonly used deformation properties are consolidation properties, which are covered separately in Chapter 6 because of their prevalence for geotechnical design. In many cases, deformation properties are expressed using familiar modulus values, such as shear modulus, $G$, Young's modulus, $E$, or constrained modulus, $M$. In other cases, modulus values are specific to a particular type of measurement, such as the pressuremeter modulus, $E_M$, or dilatometer modulus, $E_D$. Furthermore, some deformation properties represent the response of the soil using a simplified spring model, such as the coefficient of subgrade reaction and $p$-$y$ models for laterally loaded deep foundations.

As shown in Table 8–1, deformation properties are used for many applications that include both static and dynamic loading conditions. Prediction of foundation settlements under static loading is the most common application for deformation properties. Consolidation properties are used to predict settlement of fine-grained soils, as discussed in Chapter 6. Undrained elastic modulus values are also used for prediction of immediate settlements for shallow foundations on fine grained soils (e.g., Skempton and

Bjerrum, 1957). Many semi-empirical methods for predicting settlements of shallow foundations on coarse-grained soils (e.g., Schmertmann, 1970b; Schmertmann, et al., 1978) require a value for the secant elastic modulus, $E_s$, that is representative of the soil stiffness at intermediate strain levels. Furthermore, some methods for predicting foundation settlements are based on measurement-specific modulus values such as the pressuremeter modulus (e.g., Menard and Rousseau, 1962; Briaud, 1992) or dilatometer modulus (e.g., Schmertmann, 1986; Marchetti, et al., 2001). The coefficient of subgrade reaction (sometimes termed modulus of subgrade reaction) has also been used for estimating settlement of shallow foundations (e.g., NAVFAC, 1986) and to model soil-structure interaction of mat foundations or laterally loaded piles (e.g., Terzaghi, 1955; Honjo, et al., 2005). Soil stiffness models represented as *p-y* curves are also commonly used for analyzing laterally loaded piles (Reese and Welch, 1975).

**Table 8–1 Common deformation properties used for geotechnical applications.**

| Loading Condition | Deformation Property | Symbols | Applications | Sections |
|---|---|---|---|---|
| Static | Compression Indices | $C_c, C_r, C_\alpha$ | Consolidation settlements | 6.8 |
| | Tangent Constrained Modulus | $M$ | Consolidation settlements | 6.9 |
| | Equivalent or Secant Modulus | $E_s$ | Immediate foundation settlements; foundation settlement on coarse-grained soils | 8.8.1 |
| | Pressuremeter Modulus | $E_M$ | Foundation settlements; laterally loaded piles | 8.8.3 |
| | Dilatometer Modulus | $E_D$ | Foundation settlement | 8.8.4 |
| | Coefficient of Subgrade Reaction | $k$ | Soil structure interaction; Foundation settlement on coarse-grained soils; | 8.9 |
| | p-y Modulus | $E_{p-y}$ | Laterally loaded piles | 8.10 |
| | Small-strain elastic moduli | $G_{max}, E_{max}$ | Foundation settlement | 8.4, 8.5 |
| | Modulus reduction | $E/E_{max}$ | Foundation settlement | 8.8.2 |
| Dynamic | Small-strain shear modulus | $G_{max}$ | Dynamic response of foundations; earthquake site response analysis; soil structure interaction | 8.4, 8.5 |
| | Modulus reduction | $G/G_{max}$ | Earthquake site response | 8.6, 8.7 |
| | Shear wave velocity | $V_s$ | Site classification; liquefaction assessment | 8.4 |

Stress-strain and stiffness properties are also widely used for calculation of dynamic response for soils and foundations. For example, prediction of the vibratory response of foundations under dynamic loading requires the small-strain shear modulus of the soil (e.g., Gazetas, 1983). Calculation of site response under earthquake loading requires both small-strain shear modulus properties as well as modulus reduction curves describing the strain-dependent reduction in modulus. Code-based methods to

incorporate earthquake site effects also use small-strain soil properties to classify sites, as indicated by the average shear wave velocity in the top 100 ft. As described in Chapter 5, shear wave velocity measurements can also be used to assess liquefaction susceptibility for coarse-grained soils (e.g., Andrus and Stokoe, 2000).

## 8.2 GENERAL STRESS-STRAIN RESPONSE OF SOIL

The stress-strain response for soil under monotonic shear loading is highly nonlinear, as illustrated in Figure 8-1. The initial tangent modulus, denoted as $G_{max}$ or $G_o$, is the largest modulus value and is generally applicable to both static and dynamic loading (e.g., Lo Presti, et al., 1997). Secant modulus values decrease with increasing strain as shown in Figure 8-1b, and are denoted as $G_1$, $G_2$, $G_3$, etc. The nonlinearity is commonly represented by plotting secant modulus versus the logarithm of strain, as shown in Figure 8-2. The shear modulus is essentially constant below a certain level of strain, termed the elastic or linear threshold, $\gamma_t^e$. In this elastic region, soil can be modeled as a linear-elastic material with a shear modulus of $G_{max}$. The elastic threshold strain varies with soil type and other factors (e.g., effective confining stress), and is typically in the range of 0.001 to 0.01 percent (Stokoe, et al., 1999).

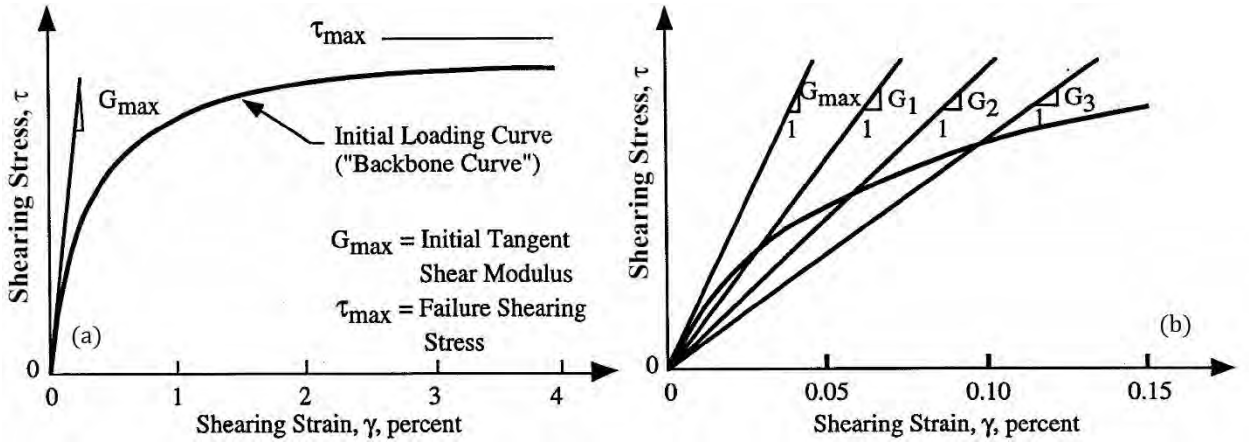


**Figure 8-1 Nonlinear stiffness of soil in shear: (a) general stress-strain response, and (b) secant shear modulus at different strain levels.**

The most reliable and economical method for determining small-strain modulus values is to measure the velocity of small-strain stress waves (e.g., compression, shear, or Rayleigh waves) propagated through the soil using methods described in Section 8.4. The velocity of shear waves, $V_s$, for example, is directly related to the shear modulus, $G$, and mass density, $\rho$, as

$$G = V_s^2 \cdot \rho \tag{8.1}$$

Likewise, constrained compression wave velocity, $V_p$, is related to constrained modulus, $M$, and unconstrained (i.e., longitudinal rod wave) compression wave velocity, $V_L$, is related to Young's modulus, $E$, as

$$M = V_p^2 \cdot \rho \tag{8.2}$$

$$E = V_L^2 \cdot \rho \tag{8.3}$$

Shear wave velocity measurements are commonly used in geotechnical engineering because they are largely unaffected by the presence of water in saturated soils and therefore provide information about the stiffness of the soil skeleton. The mass density in Equations 8.1 through 8.3 is determined as

$$\rho = \frac{\gamma_t}{g} \tag{8.4}$$

where $\gamma_t$ is the total unit weight of the soil and $g$ is the acceleration of gravity. For an isotropic material, Poisson's ratio, $\nu$, can also be determined from any two of the velocity values.

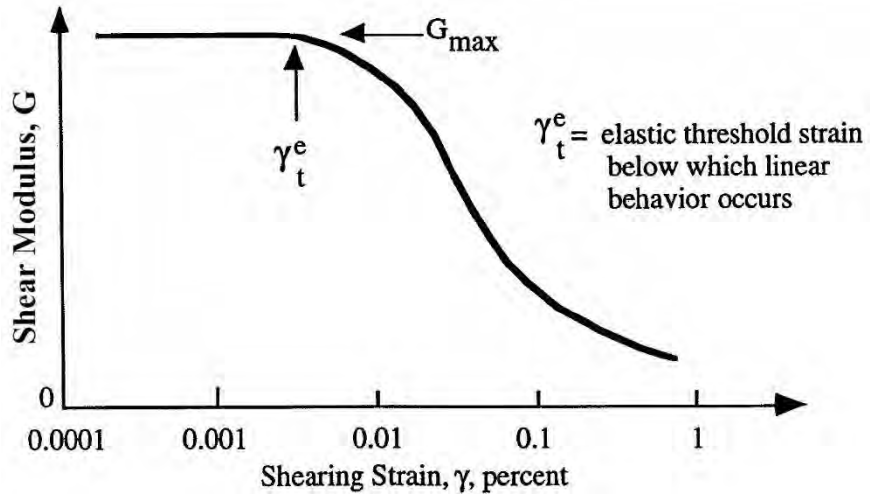


**Figure 8-2 Variation of shear modulus with shearing strain.**

For simplicity, soils are often assumed to be isotropic with respect to stiffness. In reality soils will usually exhibit some degree of stiffness anisotropy due to both inherent and stress-induced contributions. Inherent, or structural anisotropy is caused by the grain characteristics and deposition process. Typically a cross-anisotropic model can be used to represent inherent anisotropy, where the horizontal plane is a plane of isotropy and is typically stiffer than the vertical plane. Stress-induced anisotropy is caused by

the in-situ stress conditions where Young's modulus will depend on the stresses in the direction of loading, and shear modulus will depend on stress in the plane of distortion (Clayton, 2011).

One advantage of stress-wave measurements is that measurements can be performed in situ where waves are transmitted through truly undisturbed soil. However, evaluation of nonlinear properties at larger strains in the field is usually impractical with wave propagation methods due to the large input energy required to propagate waves at high strain levels. Therefore, nonlinear behavior of the soil (i.e., beyond the elastic threshold) is usually evaluated directly using laboratory methods or indirectly using empirical relationships. Nonlinear behavior is often represented by a modulus reduction curve showing normalized modulus values (i.e., $G/G_{max}$) plotted versus the logarithm of strain. Laboratory measured modulus values are usually smaller than values measured in the field due to sample disturbance, as illustrated in Figure 8-3. Therefore, modulus reduction curves measured in the lab should be corrected using small-strain modulus values measured in the field, as

$$G_{\gamma-field} = \left(\frac{G_{\gamma-lab}}{G_{max-lab}}\right) G_{max-field} \tag{8.5}$$

where $G_{\gamma-field}$ is the calculated in situ shear modulus for strain $\gamma$, $G_{\gamma-lab}$ is the laboratory measured shear modulus at strain $\gamma$, $G_{max-lab}$ is the laboratory measured small-strain shear modulus, and $G_{max-field}$ is the measured in situ small-strain shear modulus.

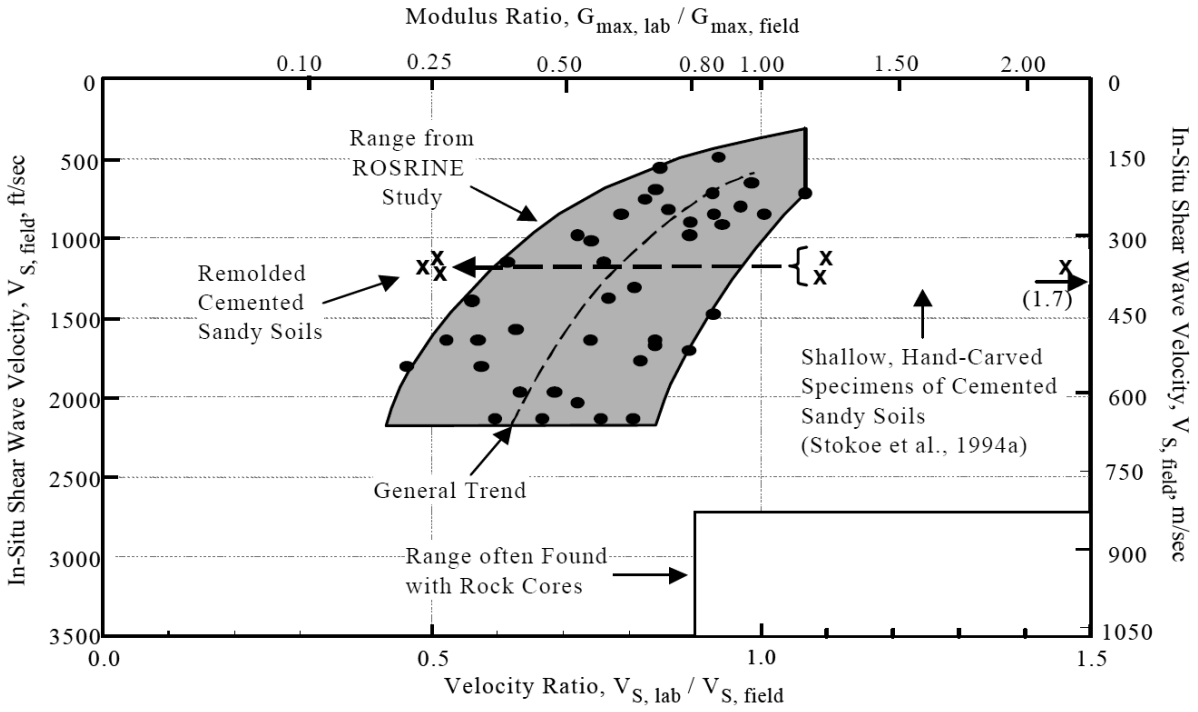


**Figure 8-3 Variation in small-strain modulus measured in the lab and field (Stokoe and Santamarina, 2000).**

Due to the time and expense associated with laboratory measurements, direct measurement of the full stress-strain response or modulus reduction curve is usually not warranted for most transportation projects. In these cases, modulus reduction curves can be estimated using indirect methods, as described in Section 8.8. For many static analysis methods, such as settlement predictions, a single representative soil modulus at intermediate working strain levels is often required. Methods to determine such values are described in Section 8.9.

## 8.3 BORING AND SAMPLING REQUIREMENTS FOR MEASUREMENT OF STRESS-STRAIN AND STIFFNESS PROPERTIES

As is true for consolidation and strength properties described in Chapters 6 and 7, laboratory stiffness and stress-strain measurements for most soils are sensitive to the degree of sample disturbance. As such, samples collected for evaluation of stress-strain and stiffness properties in the laboratory should be acquired using methods that limit disturbance. Recommended practices for acquiring high quality samples for stress-strain and stiffness properties are consistent with those described in Chapters 6 and 7 for consolidation and strength properties.

Borings made for in situ testing using seismic wave velocity measurements are an important part of such measurements and often have special requirements. Specifically, the orientation and position of borings is more critical than for general exploratory borings. Additionally, it is generally necessary to carefully grout casings within boreholes for intrusive seismic measurements, and to conduct borehole inclination surveys prior to making measurements so that the distance between boreholes, as a function of depth, can be accurately determined.

## 8.4 EVALUATION OF SMALL-STRAIN MODULUS FROM STRESS-WAVE VELOCITY MEASUREMENTS

The best practice for determining small-strain modulus is to directly measure the velocity of propagation of stress waves in the field and to transform these to the appropriate modulus values based on Equations 8.1 and 8.2. Wave sources used in common field methods excite strain levels that are well below the elastic threshold of the soil. Thus, stress-wave velocity measurements performed in the field provide measurements related to the small-strain stiffness of the soil (i.e., $G_{max}$ and $E_{max}$). Although such measurements are dynamic measurements, research has shown that small-strain modulus values determined from these measurements can be used for analyses involving static loading conditions (e.g., Jamiolkowski, et al., 1994; Lo Presti, et al., 1997).

Shear waves (also termed "s-waves" or "secondary waves") are stress waves with particle motion transverse to the direction of wave propagation and can be used to determine the shear modulus, $G$. Shear waves will not propagate through fluids, so shear wave velocities in saturated soils are largely unaffected by the presence of the water (apart from small changes in mass density). In contrast, compression waves (also termed "p-waves" or "primary waves") are waves with particle motion in the same direction as wave propagation and are related to the constrained modulus, $M$. Measurement of compression wave velocities in saturated soil will largely reflect the bulk modulus of water rather than the soil skeleton stiffness. For this reason, shear wave velocities should be used to establish soil stiffness properties at saturated soil sites but compression wave velocities can be used to help identify depths where the soil becomes saturated.

Field methods used to measure stress-wave velocities are generally classified as intrusive methods that require penetration into the soil, or non-intrusive methods that can be performed using instrumentation on the ground surface. Common intrusive and non-intrusive methods for stress-wave velocity measurements are described in the following sections.

### 8.4.1 Intrusive Field Methods for Stress-Wave Measurements

Intrusive methods are performed by either: (1) lowering sensors into one or more boreholes, or (2) pushing a probe into the ground with the capability to measure stress-wave arrivals. Commonly used intrusive methods include the crosshole seismic method, the downhole seismic method, seismic cone penetrometer (seismic CPT), seismic dilatometer (seismic DMT), and suspension logging, as shown in Figure 8-4. Recently, seismic SPT methods have also been developed and used for stress-wave measurements.

#### *Crosshole Seismic Method*

The crosshole method (ASTM D4428) uses a direct time-of-travel measurement of stress waves propagated between two or more boreholes as shown in Figure 8-4a. The source and receiver(s) are placed at the same depth and secured against the sides of separate boreholes. The source is normally a sliding hammer that can produce upward or downward impacts on an anvil that is locked against the side of the borehole. The vertical impacts produce shear waves with vertical particle motion (i.e., vertically polarized) and compression waves with horizontal particle motion. Horizontally and vertically oriented geophones in the receiver borehole(s) are used to record the arrival of the p- and s-waves, respectively. Seismic velocities are determined by dividing the distance between the boreholes at the depth of measurement by the measured travel times. Measurements are repeated at multiple depths to obtain profiles of shear wave velocity and compression wave velocity with depth.

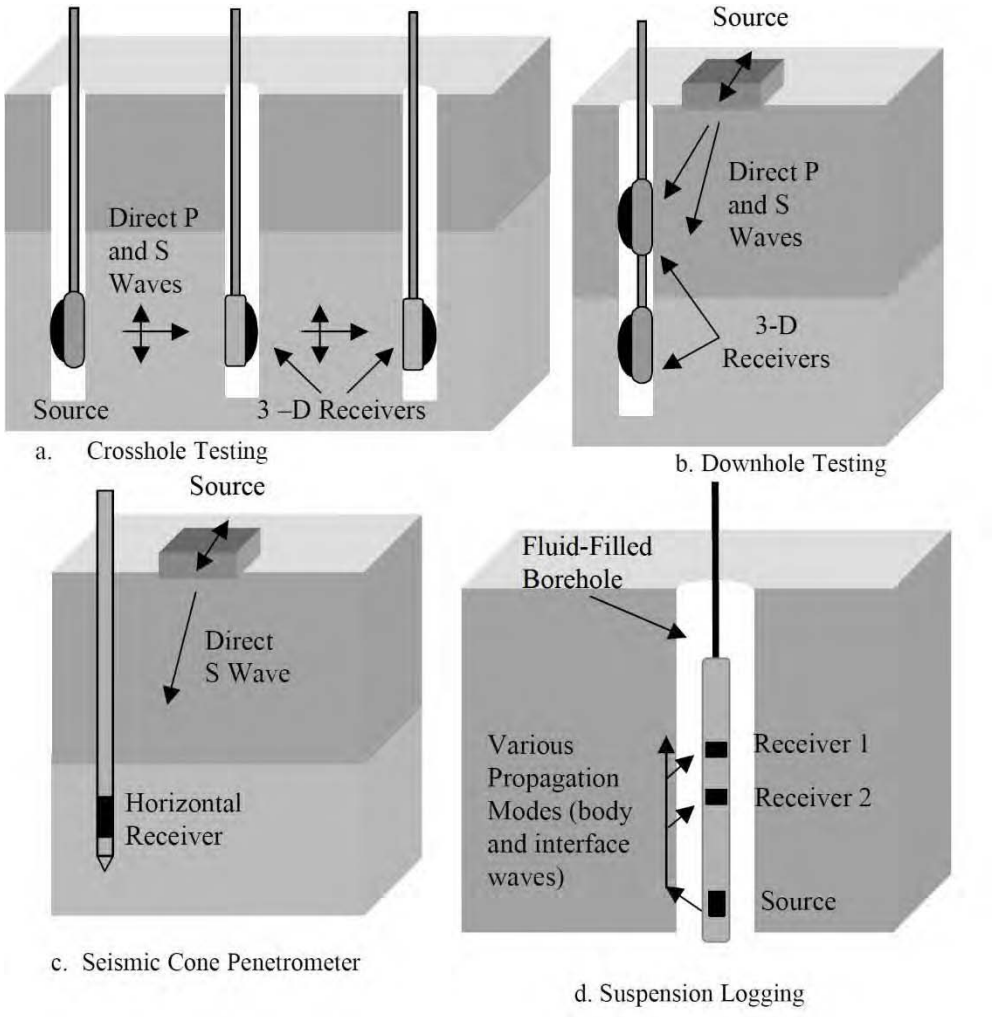


**Figure 8-4 Common intrusive methods to measure small-strain velocity: (a) crosshole, (b) downhole, (c) seismic CPT, and (d) suspension logging (Stokoe and Santamarina, 2000).**

Boreholes for crosshole seismic tests are typically spaced 10 to 15 feet apart to mitigate near-field effects and prevent refracted arrivals from deeper, higher velocity layers. Borehole inclination surveys must be performed to obtain accurate distances between boreholes with depth. Care must also be taken to properly grout the boreholes to maintain intimate contact between the casing and the surrounding soil. The primary advantages of the crosshole method are the reliability of the velocity values due to the short travel path and the generally good vertical resolution of the measurements. The primary disadvantage is the cost associated with installing inclinometer casing and measuring inclinations of multiple boreholes.

***Downhole Seismic Method***

The downhole seismic method (ASTM D7400) is also a direct-travel time method to measure compression and shear waves propagated from the ground surface to one or more receivers in a borehole.

An advantage of the downhole method compared to crosshole measurements is that only a single borehole is required. Horizontally polarized shear waves are excited using a horizontal impact on a surface source (typically a beam with a downward normal force applied), as shown in Figure 8-4b. Vertically propagating compression waves are excited using a vertical impact of a hammer source. Shear and compression waves are recorded with horizontally and vertically-oriented geophone receivers, respectively. Travel distances are usually calculated assuming a straight ray path between the source and receivers, although more advanced inversion methods can also be used. Wave arrival times at different depths are used to determine $V_s$ and $V_p$ profiles with depth.

One disadvantage of downhole measurements is that, unlike crosshole measurements, the distance travelled by the wave increases with depth. Wave arrival times may therefore be more difficult to identify at greater depths as higher frequency energy is attenuated. Also, the simple assumption of a straight ray path is tenuous when abrupt changes in the velocity of the material occur. Thus, there is greater uncertainty associated with velocities determined at great depths from downhole measurements compared to crosshole measurements.

***Seismic Cone Penetration Testing (SCPT)***

Downhole-type measurements can also be performed using cone penetration test (ASTM D5778) equipment as shown in Figure 8-4c. A common modification to the conventional CPT device, termed a seismic cone penetrometer (SCPT), is the addition of one or more sensors to record the arrival of stress waves (Campanella, et al., 1986). The measurement is performed much like the downhole measurement described in the previous section, except no borehole is required. The cone is advanced to the measurement depth by pushing the cone through the soil. After the velocity measurement is completed the cone is advanced to the next depth and the measurement is repeated.

***Seismic Dilatometer Testing (SDMT)***

The seismic dilatometer (SDMT) may represent the fastest growing in situ test being used in site characterization worldwide. The SDMT combines the standard DMT equipment with a seismic module attached behind the DMT blade for measuring shear wave velocity, $V_s$ (Martin and Mayne, 1997; Marchetti, et al., 2008; Amoroso, et al., 2013). The SDMT was initially used in the field in the late 1990's (Martin and Mayne, 1997; Martin and Mayne, 1998) but has recently gained popularity as a rapid method for measuring $V_s$ as a result of further development of the equipment. The seismic module is placed in a drill rod immediately behind the blade and is equipped with two receivers spaced 0.5 m apart. The test is performed similar to other downhole tests, except that $V_s$ is measured as a true interval velocity

as the ratio between the difference in distance between the source and the receivers and the delay of the wave arrival from the first to the second receiver. One significant advantage of the SDMT is that it can provide both small-strain modulus values from the wave velocity measurement, as well as deformation properties at larger strains, as described in Section 8.9.4.

***Seismic Standard Penetration Testing (S-SPT)***

A recent addition to conventional SPT measurements to allow for direct measurement of shear wave velocity has been presented by Kim et al. (2004) and Bang and Kim (2007). The seismic SPT (S-SPT) is an "uphole" test that uses receivers on the surface and a source at depth; essentially the reverse configuration of seismic CPT and seismic DMT measurements. Vertical driving of the SPT split-spoon sampler generates a shear wave that can be measured by the surface sensors. Bang & Kim (2007) used the standard SPT drop hammer (140 lbs.) while Pedrini and Giacheti (2013) suggest using a 2-kg sledge hammer to generate shear waves after the traditional SPT is completed. Comparisons of shear wave velocities from S-SPT and SCPT measurements at several sites have shown excellent agreement (e.g., Pedrini and Giacheti 2013; Rocha, et al. 2015.).

***Suspension PS Logging***

The suspension logger device (Kitsunezaki, 1980; Nigbor and Imai, 1994) includes a source and two receivers in a single device that is over 5 meters in length, as shown in Figure 8-4d. The tool is suspended in a fluid-filled borehole on a wireline and does not require contact with the walls of the borehole. The energy created by a solenoid source is coupled to the surrounding soil through the fluid in the borehole. The stress waves moving through the surrounding soil are also coupled through the fluid-filled borehole to two receivers located about 1 meter apart near the top of the device. The shear and compression wave velocities of the soil are determined from the measured wave arrivals. The method is best suited for deep investigations (several hundred feet) in uncased boreholes although plastic casing can also be used. The main limitations of the method are that a fluid-filled borehole is required and it cannot be performed in soft soil if a stiff casing is used.

### 8.4.2 Non-Intrusive Field Methods for Stress-wave Measurements

Non-intrusive methods are those that can be performed from the ground surface without the need for boreholes or penetration into the soil. Non-intrusive methods can be divided into those that use shear and compression waves, such as reflection and refraction surveys, and those that use surface waves.

***Reflection/Refraction Surveys***

Reflection and refraction surveys are based on recording arrivals of body wave energy that has interacted with subsurface layer boundaries. The surveys are performed with a seismic source (typically a sledge hammer for engineering applications) and a spread of geophones placed along the ground surface. Reflection surveys use the arrival of body wave energy that has reflected from subsurface layer boundaries. The magnitude of the reflected energy received at the surface is a function of the impedance contrast (mass density times velocity) at the layer boundary and the angle of incidence. Different data collection methods are used to optimize the measurements, as shown in Figure 8-5. Seismic reflection surveys have historically been used for imaging deep subsurface impedance boundaries using compression wave energy. Shear wave reflection surveys can be effectively used for shallow $V_s$ profiling (e.g., Williams, et al., 2005), but it is not a common practice.

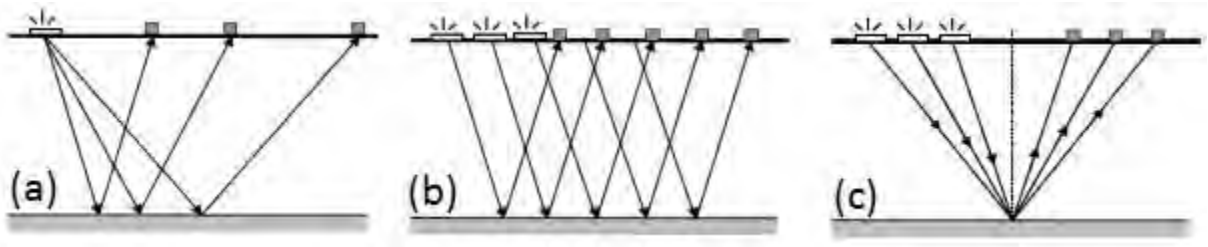


**Figure 8-5 Data collection methods for reflection surveys: (a) normal moveout (b) common offset and (c) common depth point (Stokoe and Santamarina, 2000).**

The refraction method is based on wave arrivals associated with propagation of critically refracted waves from interfaces of deeper, higher velocity material, as illustrated in Figure 8-6. The arrival times of refracted wave energy are plotted versus receiver location relative to the source. Changes in the slope of this plot indicate arrivals of refracted waves at interfaces below the subsurface. The inverse slope provides the layer velocity and the distance where changes in slope occur is used to determine the thickness of each layer. The main advantage of refraction surveys is the ability to non-intrusively determine layer velocities and thicknesses for layered profiles. The main limitations are that the method is only applicable for profiles where velocities increase with depth and processing and interpretation can be complicated at complex sites. Also, the refraction method generally requires a relatively large source spread to collect the data (approximately three times the desired profiling depth).

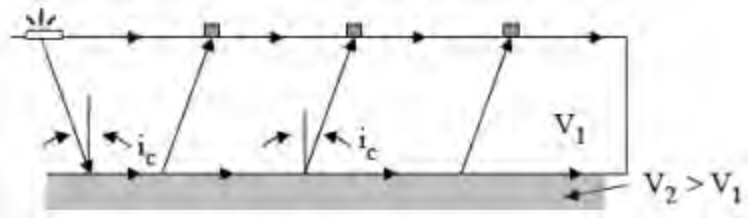


**Figure 8-6 General testing arrangement for refraction surveys showing arrival of critically refracted waves (Stokoe and Santamarina, 2000).**

***Surface Wave Methods***

Surface wave methods have become among the most common geophysical methods used in geotechnical practice for characterization of in situ shear wave velocity. Commonly used surface wave methods rely on the unique attributes of Rayleigh-type surface waves to infer subsurface shear wave velocity profiles. The Rayleigh wave is a cylindrically spreading wave that influences soil to a depth of about one wavelength, $\lambda$, below the ground surface. The Rayleigh wave velocity, $V_R$, is related to the wavelength and the excitation frequency, $f$, of the wave as

$$V_R = f \times \lambda_R \tag{8.6}$$

Decreasing the excitation frequency increases the wavelength and the depth of influence of the Rayleigh wave. Surface wave methods generally use a system like that shown in Figure 8-7 where an active source is used to excite surface wave energy and vertically oriented receivers record surface wave motions on the ground surface over a range of frequencies. The set-up shown in Figure 8-7 is for the SASW method. Multi-channel methods such as the MASW method will often utilize 24 to 48 receivers. The recorded motions are processed to develop an experimental "dispersion curve" that relates Rayleigh wave velocity to frequency (or wavelength), thereby producing velocities, $V_R$, for waves with different depths of influence. An inversion procedure is then used to establish the shear wave velocity profile ($V_s$ versus depth) that produces a theoretical dispersion curve that matches the measured dispersion curve. The final output from surface wave measurements is a shear wave velocity profile.

Both active and passive source surface wave methods have been developed and used to determine shear wave velocity profiles for geotechnical applications. Common active-source methods used in geotechnical practice include the SASW method (Stokoe, et al, 1994) and multi-channel methods, such as the MASW method (Park, et al., 1999). A more recent method, termed Refraction Microtremor or ReMi (Louie, 2001), uses a linear array and passive (or ambient) surface wave energy. The ReMi approach has more implicit assumptions than active source methods and may produce erroneous results in some cases

(Cox and Beekman, 2011; Zywicki, 2007). Passive methods that utilize two-dimensional receiver arrays are not subject to the same assumptions and are especially valuable for developing deep profiles (several hundred feet) that have been shown to compare well with active source methods (e.g., Rosenblad and Li, 2009).

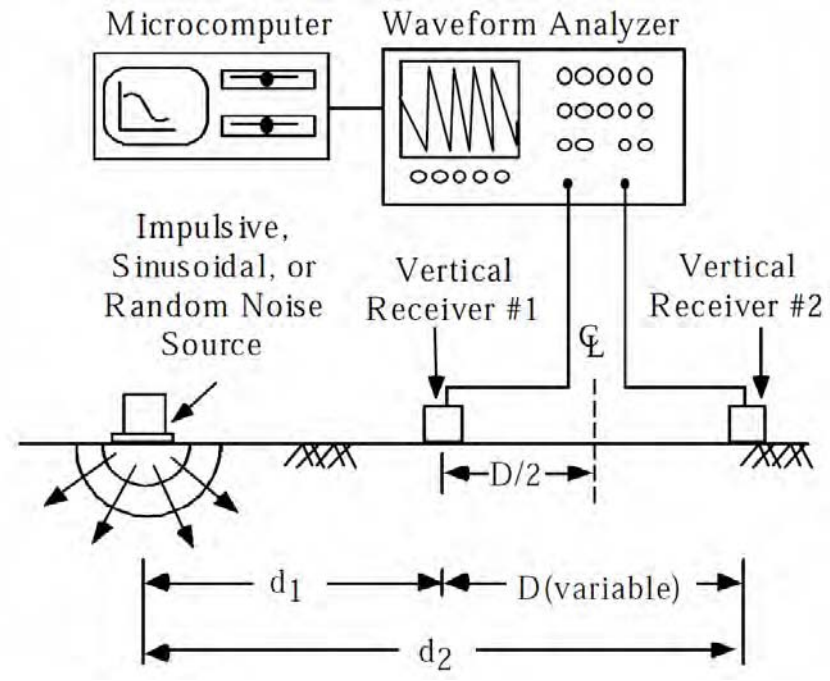


**Figure 8-7 Data collection arrangement for SASW Surface Wave Method (Stokoe and Santamarina, 2000).**

The main advantages of surface wave methods are simple implementation and relatively low cost. These methods can also provide reliable results for sites where stiffer materials overly softer materials that cannot be effectively captured with refraction surveys. However, studies have shown that some profile conditions can produce complex dispersion curves that are easily misinterpreted producing uncertainty for interpreted profiles (Cox, et al., 2014). Vertical resolution also decreases with depth for surface wave methods so deep, thin layers may not be detected.

## 8.5 LABORATORY MEASUREMENT OF SMALL-STRAIN MODULUS

Small strain modulus can also be measured in the laboratory using several methods described in this section. Unfortunately, laboratory and field measurements of small-strain modulus typically differ for several reasons and direct measurement of stress wave velocities in the field is the preferred approach. The primary reason for observed differences is sample disturbance present in specimens for laboratory testing, which generally produce lower laboratory values of small-strain modulus compared to field values. Effects due to differences in strain rate and frequency are relatively unimportant for determining

$G_{max}$, but a general trend of increasing stiffness with higher frequencies, especially for high plasticity soils has been shown by some researchers (e.g., Stokoe, et al., 1999). Last, whereas laboratory methods generally propagate waves over distances of a few inches, field measurements may propagate waves over tens or hundreds of feet. Therefore, it is understandable that velocities may differ if the soil is not truly homogeneous. Laboratory methods that can be used to measure small-strain modulus, including bender elements, resonance methods, and direct measurements from stress-strain curves, are briefly described in this section.

### 8.5.1 Bender Elements

Bender elements are small transducers that distort when electrical voltage is applied and generate electrical charge when distorted. They can be used to both excite and detect shear and compression waves propagated over short distances in soil samples. The size of bender elements can vary, but they are typically in the range of 8 to 15 mm in width and length. Bender elements are now commonly incorporated into many geotechnical laboratory methods, including triaxial cells, oedometers, and resonant column devices. Bender elements are formed from two piezoelectric ceramic elements glued to a metal shim. Bender elements are anchored to a support, such as the specimen end cap, with a portion extending into the soil. When voltage is applied to the bender element, one side elongates while the other shortens causing the element to bend. Shear and compression waves are produced from the bending of the element. The arrival of the waves is detected using another bender element secured on alternative support. Wave velocities are determined by dividing the distance between the source and receiver by the travel time of the wave. Detecting the arrival time can be complicated by the presence of near-field effects in the waveform (Lee and Santamarina, 2005). Typically, excitation frequencies are in the kHz range, which is much higher than used in field testing methods (generally in the tens to hundreds of Hz range, depending on the method).

### 8.5.2 Resonance Testing

Small-strain velocities can also be determined from resonance testing of soil specimens. Resonance testing involves measuring the resonant frequency of a soil specimen that has been excited using shear and compression waves. The resonant frequency is a function of the specimen dimensions, support conditions (including any added mass), and wave velocity in the soil. By exciting shear and/or compression wave energy and measuring the resonant frequency, the wave velocity can be determined if boundary conditions are known and accounted for. The resonant column device is an example of a device that can be used to measure wave velocities over a broad range of strain levels. The resonant column

device is commonly used to determine both small-strain modulus and modulus reduction curves at larger strains (up to about 0.1%). Simpler resonance testing devices can be used if only small strain measurements are required (e.g., Kalinski and Thummaluru, 2005).

### 8.5.3 Direct Measurement from Stress-Strain Curve

Small-strain modulus measurements determined from direct measurement of the soil stress-strain curve are not common. The primary reason for this is the difficulty involved in directly measuring strains at levels that are less than the elastic threshold (typically 0.01 to 0.001 percent). Deformation measurements from conventional laboratory testing equipment cannot accurately measure such small strains. Modifications to triaxial (e.g., Goto, et al., 1991) and direct simple shear equipment (Doroudian and Vucetic, 1995) have been made to enable small-strain measurements. Small-strain modulus can also be directly measured using the torsional shear device (e.g., Isenhower, et al., 1987).

### 8.5.4 Effects of Sample Disturbance

Measurements of soil modulus in the laboratory are affected by disturbance from sampling. Figure 8-8 show measurements of modulus reduction curves from Katayama et al. (1986) for a dense sand in both undisturbed and disturbed states. At small strains, the measured shear modulus for the disturbed specimens is less than half that measured for the undisturbed specimens. The difference in shear modulus diminishes with increasing strain and, at large strains, becomes practically negligible. The elastic threshold for the disturbed samples is also greater than that for the undisturbed specimens.

## 8.6 ESTIMATION OF SMALL-STRAIN MODULUS FROM INDIRECT METHODS

The most reliable means to determine $G_{max}$ is from $V_s$ values measured directly in the field using the methods described in Section 8.4. However, there are situations where it may be desirable to estimate approximate values of $G_{max}$ for preliminary assessments, for feasibility studies, or for comparison with actual measurements in similar soils. In these situations, several indirect relationships can be used to estimate $G_{max}$ from other soil properties or in situ test measurements. As is true for all indirect measurements, these relationships often involve significant uncertainty and should only be used to obtain approximate values.

### 8.6.1 Estimation of Small-Strain Shear Modulus from Soil Index Properties

In coarse-grained soils, laboratory studies have shown that the small strain shear modulus is primarily a function of void ratio, $e$, and effective confining stress, generally represented using the mean effective

stress, $\sigma'_m$. A common form of the relationship between $G_{max}$, $e$, and $\sigma'_m$, based on work by Hardin and Richart (1963), is

$$G_{max} = A \cdot F(e) \cdot {\sigma'_m}^n \tag{8.7}$$

where $A$ is a soil stiffness coefficient, $F(e)$ is a void ratio function, and $n$ is an exponent for $\sigma'_m$. Common forms of the function $F(e)$ include:

$$F(e) = \frac{1}{(0.3+0.7e^2)} \text{ (Hardin, 1978)} \tag{8.8}$$

$$F(e) = \frac{(2.97-e)^2}{(1+e)} \text{ for angular-grained soils (Hardin and Black, 1968)} \tag{8.9}$$

$$F(e) = \frac{(2.17-e)^2}{(1+e)} \text{ for round-grained soils (Hardin and Black, 1968)} \tag{8.10}$$

$$F(e) = e^{1.3} \text{ (Bellotti, et al., 1996)} \tag{8.11}$$

Values for $A$ and $n$ vary among different soils, as shown in Table 8–2. Because these relationships are empirical, they are strictly only appropriate for estimating $G_{max}$ for soils that are similar to those used to develop the respective relations. Site specific relations developed from site specific measurements are likely to substantially reduce the uncertainty associated with the general relations provided in Table 8–2

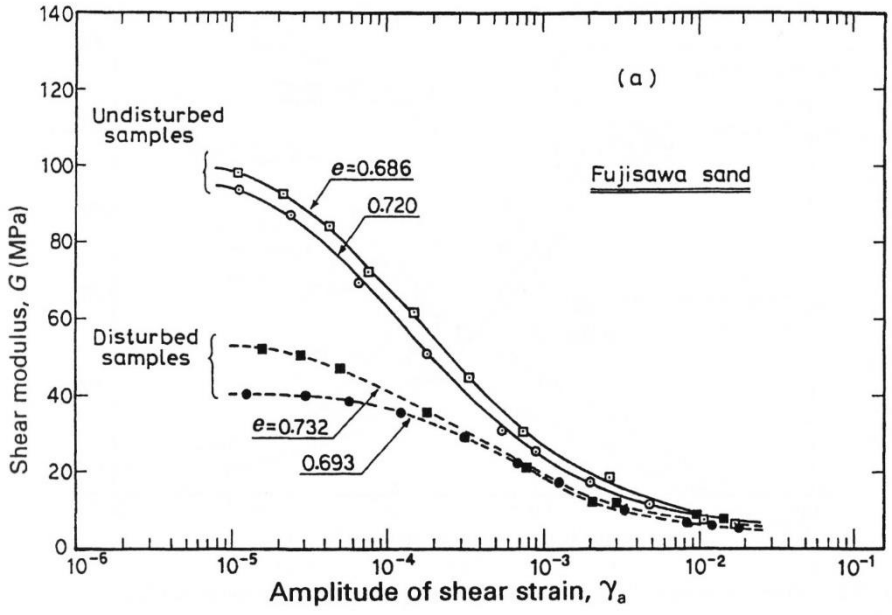


**Figure 8-8 Shear modulus for undisturbed and disturbed dense sand (from Ishihara, 1996).**

**Table 8–2 Values of $A$, $F(e)$, and $n$ for coarse-grained soils (modified from Kokusho, 1987).**

| Soil | Reference | $F(e)$ | $A$ | $n$ |
|---|---|---|---|---|
| Round Ottawa sand | Hardin and Richart (1963) | $F(e) = \frac{(2.17 - e)^2}{(1 + e)}$ | 7000 | 0.5 |
| Angular crushed quartz | Hardin and Richart (1963) | $F(e) = \frac{(2.97 - e)^2}{(1 + e)}$ | 3300 | 0.5 |
| Eleven clean sands | Iwasaki et al. (1978) | $F(e) = \frac{(2.17 - e)^2}{(1 + e)}$ | 9000 | 0.38 |
| Toyoura sand | Kokusho (1980) | $F(e) = \frac{(2.17 - e)^2}{(1 + e)}$ | 8400 | 0.5 |
| Three clean sands | Yu and Richart (1984) | $F(e) = \frac{(2.17 - e)^2}{(1 + e)}$ | 7000 | 0.5 |
| Ballast | Prange (1981) | $F(e) = \frac{(2.97 - e)^2}{(1 + e)}$ | 7230 | 0.38 |
| Crushed rock | Kokusho and Esashi (1981) | $F(e) = \frac{(2.17 - e)^2}{(1 + e)}$ | 13000 | 0.55 |
| Round gravel | Kokusho and Esashi (1981) | $F(e) = \frac{(2.17 - e)^2}{(1 + e)}$ | 8400 | 0.60 |
| Gravel | Tanaka et al. (1987) | $F(e) = \frac{(2.17 - e)^2}{(1 + e)}$ | 3080 | 0.60 |
| Round gravel | Goto et al. (1987) | $F(e) = \frac{(2.17 - e)^2}{(1 + e)}$ | 1200 | 0.885 |

Note: $G_{max} = A \cdot F(e) \cdot {\sigma'_m}^n$; $G_{max}$ and $\sigma'_m$ in kPa

Seed and Idriss (1970) proposed a similar but simpler equation for estimating $G_{max}$ for sand or gravel:

$$G_{max} = 1000 \cdot K_{2,max} \cdot \sqrt{\sigma'_m} \quad \text{(in psf)} \tag{8.12}$$

where $K_{2,max}$ is a soil modulus coefficient that is a function of $e$ (or relative density, $D_r$), and $\sigma'_m$ is mean effective stress in units of psf. Values of $K_{2,max}$ for sand estimated from plots in Seed and Idriss (1970) are shown in Table 8–3. Values of $K_{2,max}$ for gravels are typically in the range of 80 to 180.

**Table 8–3 $K_{2,max}$ values for sand (estimated from Seed and Idriss, 1970).**

| Relative Density, $D_r$ (%) | $K_{2,max}$ |
|---|---|
| 30 | 34 |
| 40 | 40 |
| 45 | 43 |
| 60 | 52 |
| 75 | 61 |
| 90 | 70 |

More recent relationships for coarse-grained soils have incorporated additional properties for estimating $G_{max}$. For example, Menq (2003) proposed a relationship that incorporates median grain size, $D_{50}$, and the coefficient of uniformity, $C_u$, to estimate $G_{max}$ for coarse-grained soils as

$$G_{max} = C_{G3} \cdot C_u^{b1} \cdot e^x \cdot \left(\frac{\sigma'_m}{p_a}\right)^{n_G} \tag{8.13}$$

where $C_{G3} = 1400\ ksf$, $b1 = -0.20$, $x = -1 - (D_{50}/20)^{0.75}$, and $n_G = 0.48 \cdot {C_u}^{0.09}$.

In fine-grained soils, $G_{max}$ is generally taken to be a function of $e$, $PI$, and $OCR$. Hardin (1978) proposed the following equation for estimating $G_{max}$ for fine-grained soils based on previous work by Rowe (1971), Janbu (1963), and Hardin and Black (1968):

$$G_{max} = A \cdot F(e) \cdot OCR^k \cdot {p_a}^{1-n} \cdot {\sigma'_m}^n \tag{8.14}$$

where $k$ is an exponent that is a function of $PI$ from Table 8–4 and all other terms are defined previously. Hardin (1978) found $A = 625$ and $n = 0.5$, and the void ratio function from Equation 8.8 for fine-grained soils. As with coarse-grained soils, the parameters $A$ and $n$ will vary for different fine-grained soils.

**Table 8–4 Values of $k$ as a function of $PI$ (Hardin, 1978).**

| $PI$ | $k$ |
|---|---|
| 0 | 0 |
| 20 | 0.18 |
| 40 | 0.30 |
| 60 | 0.41 |
| 80 | 0.48 |
| >100 | 0.50 |

### 8.6.2 Estimation of Small-Strain Shear Modulus from Indirect In situ Measurements

Due to the prevalence of in situ testing, there is often a desire to estimate $G_{max}$ or $V_s$ from in situ tests such as the standard penetration test (SPT), cone penetration test (CPT), and dilatometer test (DMT). It is important to note that these tests induce large strains so relationships among in situ test measurements are really just empirical transformations that involve considerable variability. As such, estimates of $G_{max}$ from these transformations should primarily be used for preliminary estimates.

#### *Estimates from SPT Measurements*

Estimates for $G_{max}$ from SPT $N$-values are usually established from empirical transformations between measured $V_s$ and SPT $N$-values using either assumed or measured unit weights. Numerous

transformations have been developed, most of which are related to SPT $N$-values corrected for hammer efficiency, $N_{60}$. These relationships are typically expressed as

$$V_s = a \cdot N^b \tag{8.15}$$

where $a$ and $b$ are empirical constants. Figure 8-9 shows a log-log plot of measurements from Ohta and Goto (1978) while measurements from Sykora and Stokoe (1983) are plotted using arithmetic scales in Figure 8-10 to illustrate typical scatter in these relationships. Wair et al. (2012) provides a detailed review of empirical relations between $V_s$ and SPT $N$-values. Table 8–5 summarizes relationships of the form of Equation 8.15. Other relationships incorporating specific soil types and ages, as well as relationships that include additional terms for depth or effective stress, are provided in Wair et al. (2012).

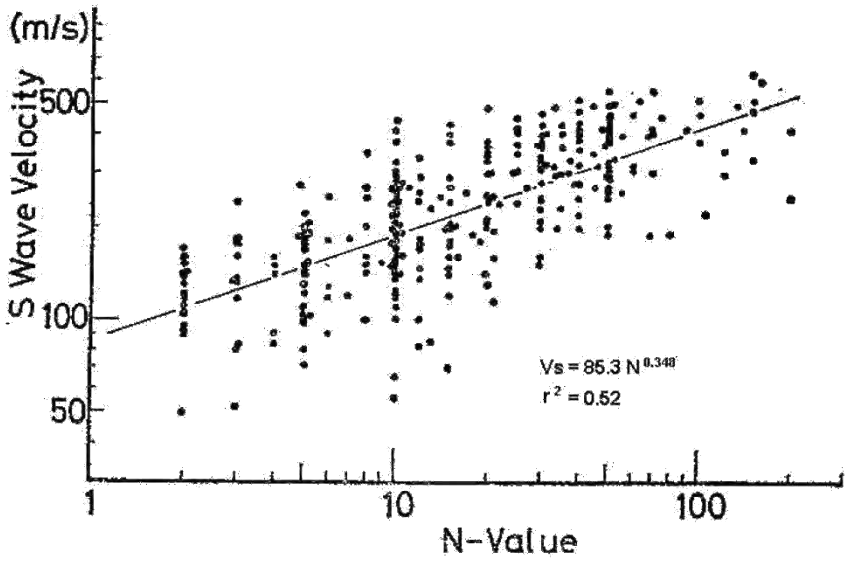


**Figure 8-9 Shear wave velocity versus *N*-value relationship from Ohta and Goto (1978).**

Published relationships between $G_{max}$ and $N_{60}$-values are less common and are typically developed from $V_s$ relationships. Two commonly used relationships for estimating $G_{max}$ for sands are presented in Table 8–6. The Imai-Tonouchi (1982) relationship is based on measured $V_s$ and unit weights while the Seed et al. (1986) relationship is based on $V_s$ values from Ohta and Goto (1978), shown in Figure 8-9, and assumed values of unit weight.

***Estimates from CPT Measurements***

$V_s$ can be directly measured using SCPT equipment as described in Section 8.4 and, where possible, $G_{max}$ should be determined from such measurements with Equation 8.1 using measured or assumed unit weights. For cases where only conventional CPT or CPTU measurements are available, transformations

relating $G_{max}$ and $V_s$ to measured CPT tip resistance and sleeve friction can be used to estimate values for $G_{max}$ and $V_s$. Table 8–7 and Table 8–8 provide several common empirical transformations for $G_{max}$ and $V_s$, respectively. Measurements used for developing the Mayne and Rix (1993) and Rix and Stokoe (1991) relationships are plotted in Figure 8-11.

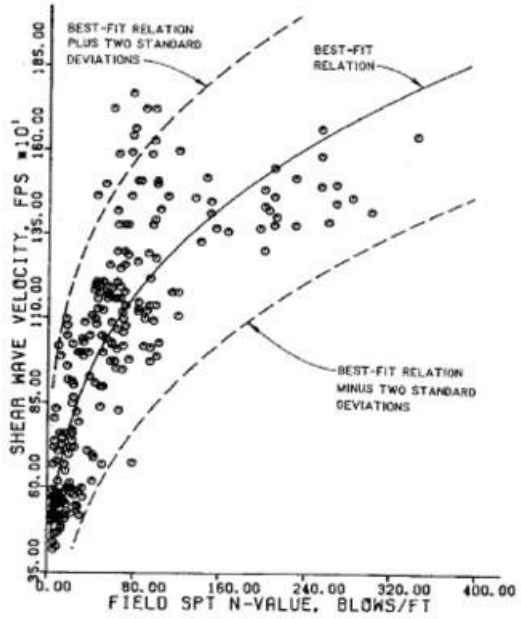


**Figure 8-10 Arithmetic plot of $V_s$ versus $N$-value (from Sykora and Stokoe, 1983).**

**Table 8–5 Transformations between $V_s$ and $N_{60}$ for all soil types (modified from Wair, et al., 2012).**

| Reference | $V_s$ Transformation (m/s) | $r^2$ | Notes |
|---|---|---|---|
| Ohba and Toriuma (1970) | $V_s = 82.5 \cdot {N_{60}}^{0.31}$ | -- | Alluvium |
| Ohsaki and Iwasaki (1973) | $V_s = 78.0 \cdot {N_{60}}^{0.39}$ | -- | Quaternary; Alluvium |
| Ohta and Goto (1978) | $V_s = 82.1 \cdot {N_{60}}^{0.35}$ | 0.52 | Holocene; Alluvium |
| Ohta and Goto (1978) | $V_s = 89.5 \cdot {N_{60}}^{0.27}$ | 0.61 | Pleistocene; Alluvium |
| Ohta and Goto (1978) | $V_s = 130.3 \cdot {N_{60}}^{0.27}$ | 0.61 | Holocene, Pleistocene, Tertiary; Alluvium, Fill |
| Imai and Tonouchi (1982) | $V_s = 93.7 \cdot {N_{60}}^{0.31}$ | 0.75 | Tertiary |
| Imai and Tonouchi (1982) | $V_s = 105.2 \cdot {N_{60}}^{0.32}$ | 0.51 | -- |
| Lin et al. (1984) | $V_s = 62.0 \cdot {N_{60}}^{0.50}$ | -- | -- |
| Sisman (1995) | $V_s = 31.0 \cdot {N_{60}}^{0.51}$ | -- | -- |
| Iyisan (1996) | $V_s = 48.6 \cdot {N_{60}}^{0.52}$ | -- | -- |
| Jafari et al. (1997) | $V_s = 20.0 \cdot {N_{60}}^{0.85}$ | -- | -- |
| Kiku et al. (2001) | $V_s = 66.1 \cdot {N_{60}}^{0.29}$ | -- | -- |
| Hasancebi and Ulusay (2007) | $V_s = 104.8 \cdot {N_{60}}^{0.26}$ | 0.53 | Quaternary; Alluvium |

**Table 8–6 Transformations between $G_{max}$ and SPT $N_{60}$-values.**

| Reference | Transformation | Soil | Notes |
|---|---|---|---|
| Imai and Tonouchi (1982) | $G_{max} = 325 \cdot {N_{60}}^{0.68}$ | Sand | $G_{max}$ in ksf |
| Seed et al. (1986) | $G_{max} = 20000 \cdot {(N_1)_{60}}^{0.333} \cdot \sqrt{\sigma'_m}$ | Sand | $G_{max}$ and $\sigma'_m$ in psf |

**Table 8–7 Transformations between $G_{max}$ and CPT tip resistance.**

| Reference | Transformation | Soil | Notes |
|---|---|---|---|
| Rix and Stokoe (1991) | $G_{max} = 1634 \cdot {q_c}^{0.25} \cdot {\sigma'_{vo}}^{0.375}$ | Quartz Sand | $G_{max}$, $q_c$, and $\sigma'_{vo}$ in kPa |
| Mayne and Rix (1993) | $G_{max} = 49.4 \cdot {q_t}^{0.695} \cdot e^{-1.130}$ | Clay | $G_{max}$ and $q_t$ in MPa |

**Table 8–8 Transformations between $V_s$ and CPT tip and sleeve resistance.**

| Reference | Relationship | Soil | Notes |
|---|---|---|---|
| Rix and Stokoe (1991) | $V_s = 277 \cdot {q_t}^{0.13} \cdot {\sigma'_{vo}}^{0.27}$ | Quartz Sand | $V_s$ in m/s; $q_t$ and $\sigma'_{vo}$ in MPa |
| Mayne and Rix (1995) | $V_s = 1.75 \cdot {q_t}^{0.627}$ | Soft to Stiff Clay | $V_s$ in m/s; $q_t$ in kPa |
| Mayne (2006) | $V_s = 118.8 \cdot \log f_s + 18.5$ | Saturated clay, silts and sands | $V_s$ in m/s; $f_s$ in kPa |

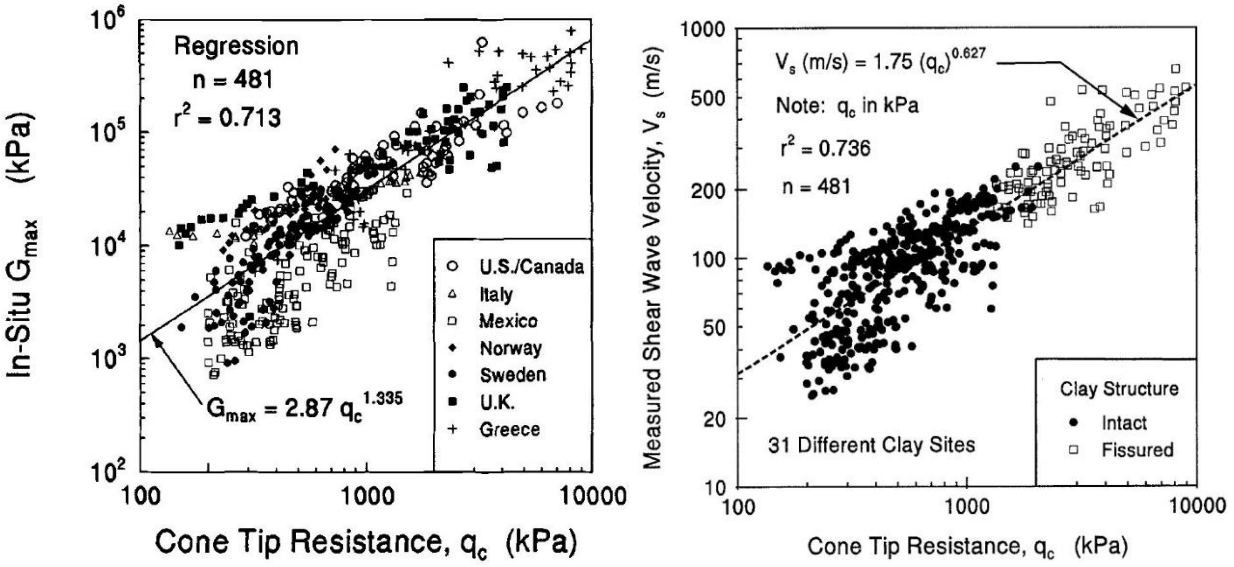


**Figure 8-11 Measurements used to develop transformations between cone tip resistance and: (a) $G_{max}$ (Mayne and Rix, 1993), and (b) $V_s$ (Mayne and Rix, 1995).**

***DMT Correlations***

The small-strain shear modulus can also be estimated from DMT measurements. Figure 8-12 shows the ratio of $G_{max}$ to the dilatometer modulus, $E_D$, plotted as a function of the DMT horizontal stress index, $K_D$, and the DMT material index, $I_D$. For sands, $G_{max}/E_D$ typically falls within a narrow range from about 1.5 to 3. Therefore, $G_{max}$ can be estimated for sands by multiplying $E_D$ by a constant as shown in Table 8–9. However, $G_{max}/E_D$ varies significantly with $I_D$ and $K_D$ for silts and clays so $G_{max}$ cannot be reliably estimated using a simple linear relationship. However, if $E_D$, $K_D$, and $I_D$ are known, values of

$G_{max}/E_D$ can be roughly approximated from Figure 8-12 (Marchetti, et al., 2008) and used to estimate $G_{max}$, recognizing that such estimates will be extremely approximate. Hryciw (1990) also developed a method to estimate $G_{max}$ using $K_o$ determined from DMT measurements with $\sigma'_{vo}$ and $\gamma_d$, with an average error of 23 percent between measured and predicted values of $G_{max}$.

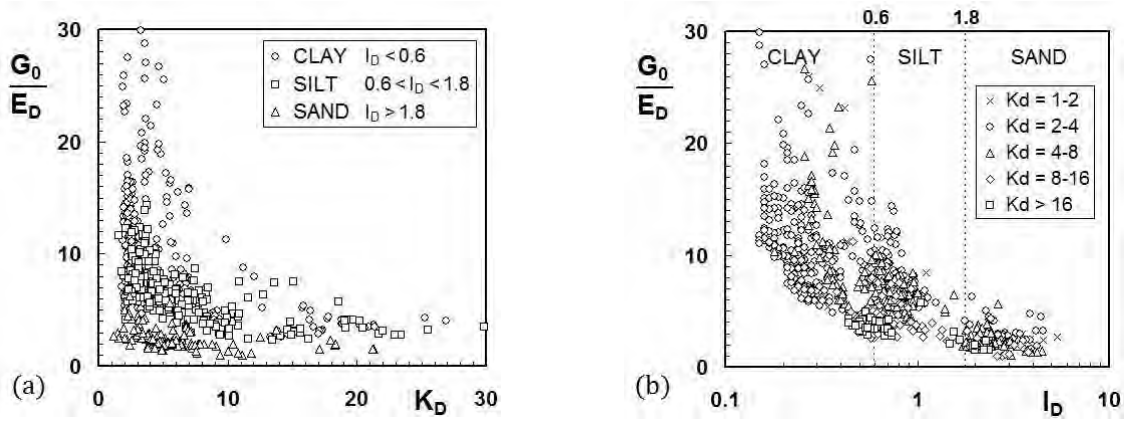


**Figure 8-12 Ratio of $G_{max}/E_D$ as a function of: (a) $K_D$, and (b) $I_D$ (Marchetti, et al., 2008).**

**Table 8–9 Transformations between $E_D$ and $G_{max}$ for sand.**

| Reference | Transformations | Soil | Notes |
|---|---|---|---|
| Baldi et al. (1986) | $\frac{G_{max}}{E_D} = 2.72 \pm 0.59$ | Sand | Calibration chamber tests |
| Bellotti et al. (1986) | $\frac{G_{max}}{E_D} = 2.2 \pm 0.7$ | Sand | Field tests |

## 8.7 EVALUATION OF MODULUS DEGRADATION CURVES FROM LABORATORY MEASUREMENTS

In earthquake engineering applications and some settlement analysis methods, soil nonlinearity is represented using modulus degradation curves (or modulus reduction curves) that describe soil stiffness over a broad range of strains, as shown in Figure 8-2. Modulus degradation curves are typically measured in the laboratory where larger strains can be imposed under controlled conditions. The resonant column test (ASTM D4015) is a widely used technique to evaluate modulus values over a broad range of strain levels. In the test, a soil sample is vibrated over a range of frequencies to identify the resonant frequency, which can be used to calculate $G$ based on known boundary conditions and specimen dimensions. By varying the torque applied to the sample, modulus values can be determined from strains less than the elastic threshold up to strains of about 0.1 percent. Testing frequencies in resonant column tests are a function of the size and stiffness of the samples, but generally are in the range of hundreds of Hz.

Modulus reduction curves can also be measured using torsional shear (TS) tests. In torsional shear tests, the shear stress-strain behavior is measured directly by applying a torque to the sample and measuring the angle of twist of the specimen using a proximity sensor. Torsional shear tests, therefore, do not operate at high frequencies like the resonant column test and do not apply as many cycles to the specimen. Resonant column and torsional shear measurements can be combined in a single device, termed a Resonant Column-Torsional Shear device (Isenhower, et al., 1987).

Modulus reduction curves cannot be measured over broad strain ranges using conventional triaxial equipment with external deformation sensors. Factors such as system compliance and bending errors do not allow for modulus values to be reliably determined at small strains. However, if the triaxial device is modified to allow for local measurement of deformation, Young's modulus values can be determined to strains as small as 0.0001 percent (e.g., Goto, et al., 1991). Likewise, direct simple shear tests are generally not used to measure modulus reduction curves, although small strain values can be determined if specialized equipment is used (e.g., Lanzo, et al., 1997).

## 8.8 ESTIMATION OF MODULUS DEGRADATION FROM EMPIRICAL RELATIONSHIPS

Laboratory measurements of modulus reduction curves are relatively expensive and uncommon for conventional transportation projects. Instead, modulus reduction curves are often estimated using indirect methods. Results from extensive laboratory studies have been used to develop empirical equations relating modulus reduction curves to soil index properties (e.g., Seed and Idriss, 1970). It has been found that the shape of the modulus reduction curve is a complex function of many variables, including $\sigma'_m$, $e$, $OCR$, $PI$, age, and strain rate. Relationships between soil plasticity and modulus reduction curves developed by Vucetic and Dobry (1991) are shown in Figure 8-13. Alternative equations have been presented by numerous investigators for different soil types and conditions. For example, Ishibashi and Zhang (1993) and Darendeli (2001) incorporated confining pressure in the modulus reduction relationships. Menq (2003) developed equations for sand and gravels based on grain size characteristics, such as $D_{50}$ and $C_u$. Modulus reduction curves are critical input for earthquake site response analysis. More detailed discussion of modulus reduction curves for earthquake engineering applications are provided in Geotechnical Engineering Circular No. 3 (Kavazanjian, et al., 2011).

As described in Section 8.9, methods have been developed that utilize modulus reduction curves along with small-strain modulus values to estimate modulus values at intermediate strain levels for calculation of foundation settlements (e.g., Lehane and Fahey, 2002; Lee and Salgado, 1999; Burns and Mayne, 1996). However, studies have shown that modulus reduction curves obtained from dynamic and cyclic

tests (such as resonant column tests) differ from curves determined using monotonic loading (e.g., Lo Presti, et al., 1997). Therefore, modulus reduction curves used for static settlement analyses described in Section 8.9 differ from the dynamic modulus reduction curves used in earthquake engineering applications.

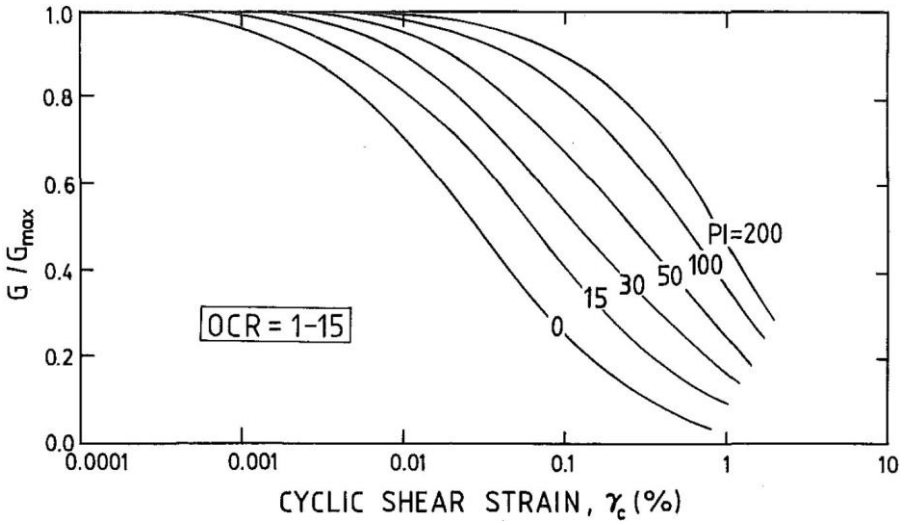


**Figure 8-13 Modulus reduction curves for fine-grained soils of different plasticity (Vucetic and Dobry, 1991).**

## 8.9 MODULUS VALUES AT INTERMEDIATE STRAIN LEVELS FOR SETTLEMENT ANALYSIS

Several methods for calculating settlement of shallow and deep foundations require input of a single modulus value that is representative of the strains imposed. This single modulus value is often termed as an elastic modulus, $E$, equivalent modulus, or secant modulus, $E_s$. The general equation for displacement at the center of an applied surface load is

$$s = \frac{qBI}{E_s} \cdot (1 - \nu^2) \tag{8.16}$$

where $q$ is the applied stress, $B$ is the width of the loaded area, $I$ is a settlement influence factor, $E_s$ is the equivalent elastic modulus, and $\nu$ is Poisson's ratio for the soil. In this equation, $E_s$ is a single representative value of the modulus that should be consistent with the strain levels imposed in the field. As illustrated in the idealized modulus reduction curve shown in Figure 8-14, strain levels for foundation settlements are usually orders of magnitude greater than strain levels for measurement of $G_{max}$.

Thus, reduced modulus values that are generally consistent with working strains induced in the field must be established. Modulus values can be measured using laboratory equipment, such as triaxial measurements, or using one of several alternative approaches described in this section.

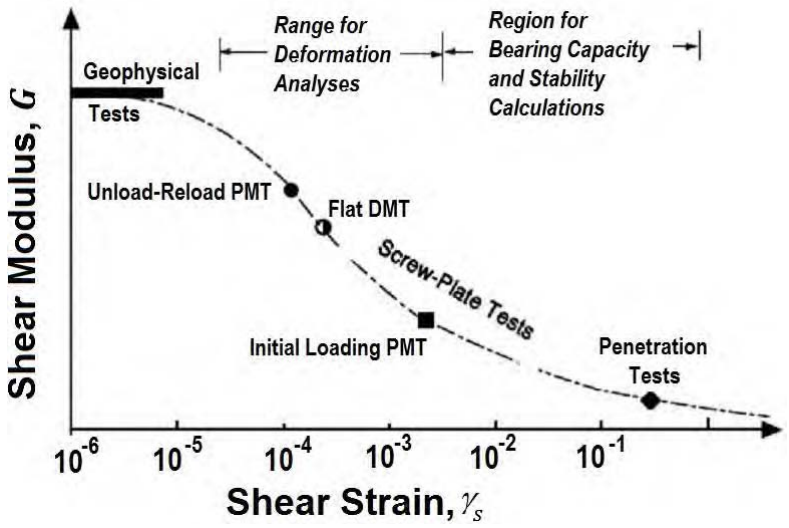


**Figure 8-14 Modulus variation with strain compared with strain range of common field tests.**

### 8.9.1 Simple Estimates for Equivalent Modulus

Preliminary estimates for an equivalent modulus can be made based on general soil characteristics or in situ test measurements, such as corrected SPT $N$-values or CPT tip resistance values. Table 8–10 summarizes typical values for $E_s$ and $\nu$ based on general soil descriptions (AASHTO, 2014). Table 8–11 presents transformations that can be used to estimate $E_s$ from stress-corrected SPT $N$-values, $(N_1)_{60}$ (AASHTO, 2014). Simple CPT transformations typically involve multiplying $q_c$ by an empirical constant. However, studies have shown that the $E_s/q_c$ ratio is influenced by many other factors (Jamiolkowski, et al., 1988). As described elsewhere in this chapter, the stiffness of soils depends on numerous factors in addition to simply soil type; thus, the relationships presented in these tables should only be considered as approximate estimates for $E_s$.

### 8.9.2 Equivalent Modulus Using Modulus Degradation

A better alternative to simple estimation is to use measured values of the small strain modulus and an estimated modulus reduction curve to establish an equivalent modulus value at working strain levels (Burns and Mayne, 1996). Using this approach, the equivalent elastic modulus can be calculated as

$$E_s = \left(\frac{E}{E_{max}}\right) E_{max} \tag{8.17}$$

where $E_{max}$ is the small-strain Young's modulus (also sometimes denoted as $E_o$). Using the relationship between Young's modulus and shear modulus, $E = 2G(1+\nu)$, and substituting Equation 8.1 for $G$, Equations 8.17 can be rewritten as

$$E_s = \left(\frac{E}{E_{max}}\right) 2\rho V_s^2 (1+\nu) \tag{8.18}$$

This equation indicates that an equivalent modulus, $E_s$, can be determined from measured values for $V_s$, the mass density, $\rho$, and an estimate for the modulus reduction ratio, $E/E_{max}$. Poisson's ratio ($\nu$) can generally be assumed to have a value of approximately 0.1 to 0.2 for drained loading of coarse-grained soils.

**Table 8–10 Typical values for $E_s$ and $\nu$ for different soil types (modified from AASHTO, 2014).**

| Soil Type | $E_s$ (ksi) | $\nu$ |
|---|---|---|
| Clay-Soft Sensitive | 0.347 to 2.08 | |
| Clay-Med Stiff to Stiff | 2.08 to 6.94 | 0.4 to 0.5 |
| Clay-Very Stiff | 6.94 to 13.89 | |
| Loess | 2.08 to 8.33 | 0.1 to 0.3 |
| Silt | 0.278 to 2.78 | 0.3 to 0.35 |
| Find Sand-Loose | 1.11 to 1.67 | |
| Fine Sand-Medium Dense | 1.67 to 2.78 | 0.25 |
| Fine Sand-Dense | 2.78 to 4.17 | |
| Sand-Loose | 1.39 to 4.17 | 0.2 to 0.36 |
| Sand-Medium Dense | 4.17 to 6.94 | |
| Sand-Dense | 6.94 to 11.11 | 0.3 to 0.4 |
| Gravel-Loose | 4.17 to 11.11 | 0.2 to 0.35 |
| Gravel Medium Dense | 11.11 to 13.89 | |
| Gravel -Dense | 13.89 to 27.78 | 0.3 to 0.4 |

**Table 8–11 Transformations between $E_s$ and SPT $(N_1)_{60}$ (modified from AASHTO, 2014).**

| Soil Type | $E_s$ (ksi) |
|---|---|
| Silts, sandy silts, slightly cohesive materials | $E_s = 0.056 \cdot (N_1)_{60}$ |
| Clean fine to medium sands and slightly silty sands | $E_s = 0.097 \cdot (N_1)_{60}$ |
| Coarse sands and sands with little gravel | $E_s = 0.139 \cdot (N_1)_{60}$ |
| Sandy gravels and gravels | $E_s = 0.167 \cdot (N_1)_{60}$ |

The modulus ratio can be estimated for foundations on intact and uncemented sands using Figure 8-15 and the anticipated factor of safety, $FOS$, for a particular foundation. The relation shown is a simple first-order approximation based on results from laboratory shear tests as well as back calculations from full-scale foundation load tests (Burns and Mayne, 1996; Kates, 1996). Use of Figure 8-15 for highly structured clays or cemented sands will generally produce conservative estimates of settlements from Equation 8.16.

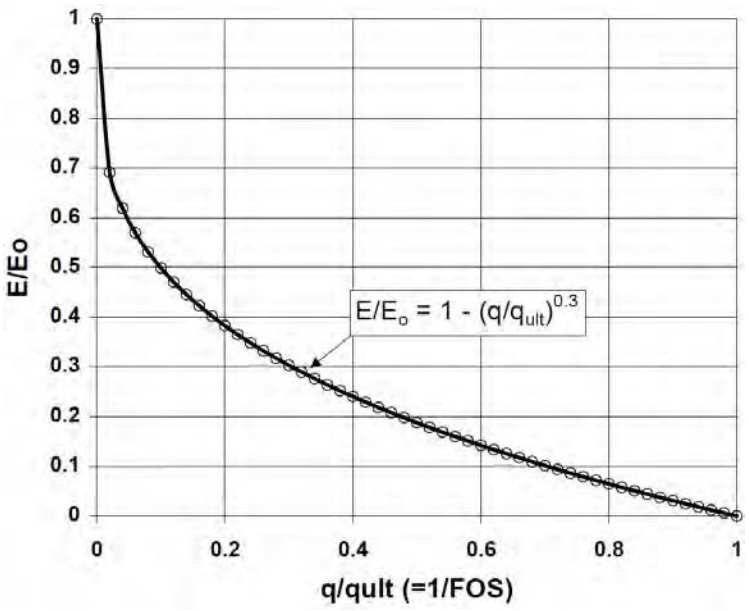


**Figure 8-15 Recommended modulus degradation ratio for intact clays and uncemented sands.**

### 8.9.3 Pressuremeter Modulus

Another alternative for estimation of $E_s$ is to use PMT or DMT measurements. As shown in Figure 8-14, field measurements from PMT and DMT devices produce modulus values at intermediate strains that are generally appropriate for estimation of foundation settlements. The modulus measured using the pressuremeter is termed the "pressuremeter modulus", usually denoted as $E_M$. $E_M$ is not the same as Young's modulus, $E$. However, $E_M$ provides valuable information about the stress-strain response of soils and is used directly in methods to predict settlements of shallow foundations (e.g., Menard and Rousseau, 1962; Briaud, 1992; Baguelin, et al, 1978) as well as deformations of laterally loaded piles (e.g., Briaud, 1997). Lutenegger and DeGroot (1995) provide a detailed review of pressuremeter-based settlement methods.

Typical measurements from a pressuremeter test using a pre-bored Menard type pressuremeter are shown in Figure 8-16. This test included a monotonic loading stage, a creep stage, and an unload-reload cycle. The pseudo-elastic modulus from pressuremeter tests can be calculated using one of two methods, depending upon whether the applied stress is plotted versus probe volume or versus probe radius. The equation to calculate the pressuremeter modulus from an applied stress versus probe volume curve is (ASTM D4719):

$$E_M = 2(1+\nu)(V_o + V_m)\frac{\Delta P}{\Delta V} \tag{8.19}$$

where $\nu$ is Poisson's ratio (usually taken as 0.33), $V_o$ is the initial volume of the probe, $V_m$ is the average volume of the probe over the stress range of interest, and $\Delta P/\Delta V$ is the slope of the linear portion of the stress versus probe volume curve. $\Delta P/\Delta V$ can be established from the initial loading, or from an unload-reload cycle. If the slope is determined from the unload-reload portion of the response, $E_M$ should be denoted as $E_{u-r}$. The equation to calculate the pressuremeter modulus from an applied stress versus probe radius curve is (ASTM D4719):

$$E_M = (1+\nu)\left(R_p + \Delta R_m\right)\frac{\Delta P}{\mathrm{d}\Delta \mathrm{R}} \tag{8.20}$$

where $R_p$ is the uninflated radius of the probe, $\Delta R_m$ is the increase in radius of the probe to where $E_M$ is measured, and $\Delta P/d\Delta R$ is the slope of the linear portion of the applied stress versus radius curve.

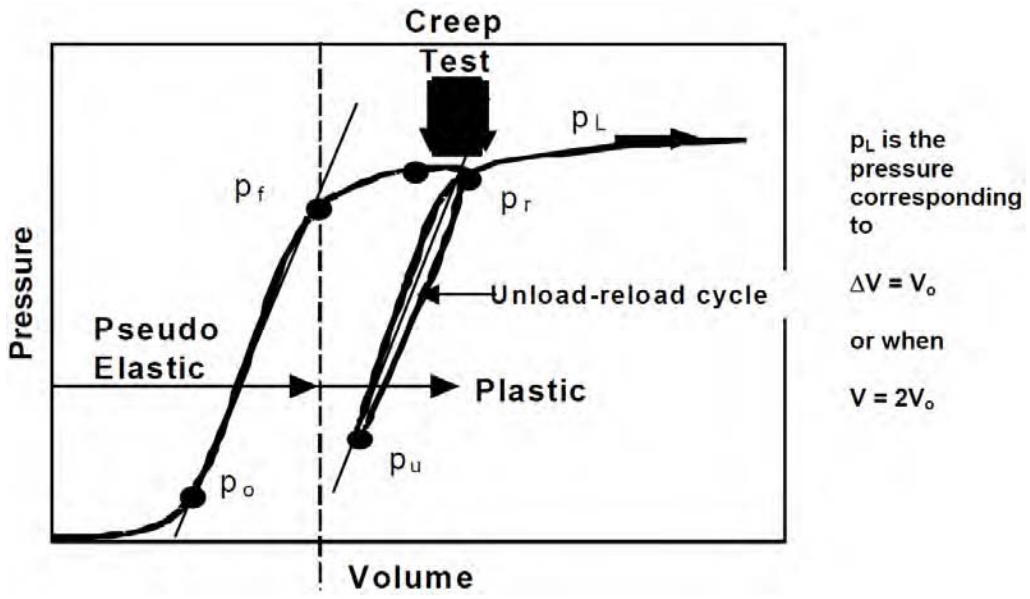


**Figure 8-16 Typical measurements from a pre-bored pressuremeter test.**

### 8.9.4 Dilatometer Modulus

The modulus measured using the DMT (ASTM D6635) is termed the dilatometer modulus, $E_D$, which also is not the same as Young's modulus, $E$. $E_D$ is calculated from elastic theory as

$$E_D = 34.7(p_1 - p_o) \tag{8.21}$$

where $p_1$ and $p_o$ are the corrected "expansion pressure" and "lift-off pressure", respectively. The dilatometer modulus is not directly used in settlement analyses. Instead, the constrained modulus, $M_{DMT}$, calculated as

$$M_{DMT} = R_M E_D \tag{8.22}$$

is used, where $R_M$ is a function of the DMT parameters, $I_D$ and $K_D$ (Marchetti, et al., 2001). Modulus values obtained from the DMT have been successfully used to predict settlements of shallow foundations (e.g., Marchetti, 1980; Schmertmann, 1986; Mayne and Frost, 1988; Marchetti, et al., 2001). Lutenegger and DeGroot (1995) provide a detailed review of dilatometer-based settlement methods.

## 8.10 OTHER SOIL STIFFNESS PROPERTIES

Several additional soil stiffness properties are commonly used in geotechnical engineering practice, including the coefficient of subgrade reaction and so-called $p$-$y$ curves that define the stiffness of soil or rock for laterally loaded deep foundations. Neither the coefficient of subgrade reaction nor $p$-$y$ curves represent unique or fundamental soil properties and neither is a true modulus. Rather, both are contrived concepts intended to enable practical analysis and design. Both approaches are based on simple models of soil "springs" that introduce several approximations. Nevertheless, both approaches have long proven to be effective and practical approaches for modeling soil stiffness for specific classes of problems.

### 8.10.1 Coefficient of Subgrade Reaction

The vertical coefficient of subgrade reaction, $k_s$ (also known as "modulus of subgrade reaction") is used in Winker-type analyses to determine stresses and strains in mat foundations and rigid pavements. The horizontal coefficient of subgrade reaction is sometimes used for design of laterally loaded piles (e.g., Terzaghi, 1955). The coefficient of subgrade reaction is a stiffness property developed from a simple, linear spring model of the subgrade that relates settlement or deformation ($\delta$) to applied bearing pressure ($q$) as

$$k_s = \frac{q}{\delta} \tag{8.23}$$

The coefficient of subgrade reaction is, thus, a spring constant with units of force per unit length, per unit area, which produces units of force per cubic length. Values for $k_s$ depend on the size of the loaded area, the shape of the loaded area, the level of pressure applied, and the location under the foundation. Values of $k_s$ are often derived from smaller scale deformation measurements, such as the plate load test (ASTM D1194) where the pressure-settlement response of a soil is measured using a small loaded plate. Table 8–12 provides typical values of $k_s$ for a 0.3-m by 0.3 m square loading. Values of $k_s$ obtained from small-scale tests must be adjusted to compensate for differences in the size, shape, and depth of the plate compared the actual foundation (e.g., Terzaghi, 1955). Alternatively, relationships have been developed

to relate $k_s$ values to modulus values (e.g., Vesic and Saxena, 1970; Scott, 1981) and local relationships between $k_s$ and SPT $N$-values have also been proposed (Moayed and Naeini, 2006; Moayed and Janbaz, 2011). Additional guidance regarding selection of appropriate coefficients of subgrade reaction is provided in Christopher, et al. (2006).

**Table 8–12 Typical subgrade reaction values for 0.3 m by 0.3 m square loading (Das, 2011).**

| Soil Type | | $k_{0.3}$ (MN/m$^3$) |
|---|---|---|
| Dry or Moist Sand | Loose | 8 to 25 |
| | Medium | 25 to 125 |
| | Dense | 125 to 375 |
| Saturated Sand | Loose | 10 to 15 |
| | Medium | 35 to 40 |
| | Dense | 130 to 150 |
| Clay | Stiff | 10 to 25 |
| | Very Stiff | 25 to 50 |
| | Hard | > 50 |

### 8.10.2 $p$-$y$ Curves

$p$-$y$ curves are similar in concept to the coefficient of subgrade reaction in that they define a conceptual spring stiffness, but are generally nonlinear and are used strictly for analysis of the response of laterally loaded deep foundations. The "$p$" in $p$-$y$ curves represents the soil reaction force to lateral deflection, "$y$", of a deep foundation. $p$ has units of force per unit of pile length and is generally taken to be a nonlinear function of the pile displacement, $y$, as shown in Figure 8-17. The soil reaction is related to the soil deflection at any point by $p$-$y$ curve. It is common to refer to a secant value of the soil stiffness as the "$p$-$y$ modulus", although the value is not really a modulus and should not be used as such.

The most reliable approach for establishing appropriate $p$-$y$ curves for design is to perform full-scale lateral load tests for the specific foundation being considered. However, such tests are generally reserved for relatively large projects where the lateral response of deep foundations is a controlling factor for design. More commonly, $p$-$y$ curves are selected from a family of general $p$-$y$ curves that have been developed to represent different types of soil or rock as summarized in Table 8–13. Alternative $p$-$y$ models have also been developed for local or regional applications in specific types of ground or for specific types of deep foundations. Additional information regarding $p$-$y$ curves and their use can be found in Reese et al. (2006) and Brown et al. (2010).

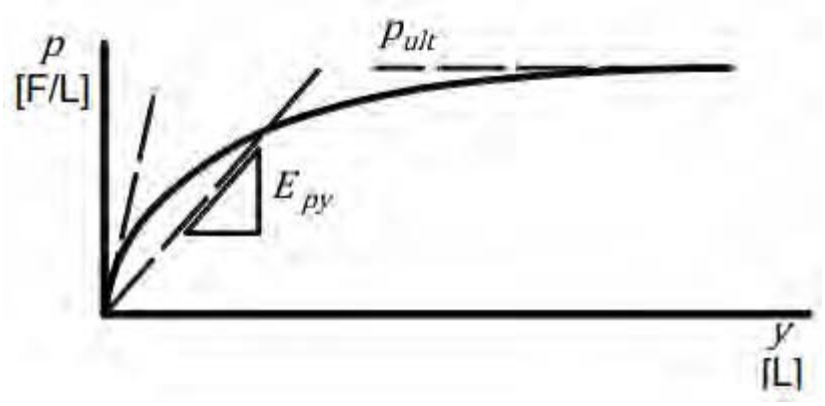


**Figure 8-17 Example $p$-$y$ curve (after Reese, et al., 2006).**

**Table 8–13 Common $p$-$y$ models for different soil or rock conditions (Pando, et al., 2006).**

| Soil Type | Reference |
|---|---|
| Soft clay w/ free water | Matlock (1970) |
| Stiff clay w/ free water | Reese, et al. (1975) |
| Stiff clay w/o free water | Welch and Reese (1972),<br>Reese and Welch (1975) |
| Sands | Reese, et al. (1974) |
| Sands | API (1993) |
| Soils with cohesion and friction | Evans and Duncan (1982) |
| Weak rock | Reese (1997) |
| Strong rock | Nyman (1980) |

THIS PAGE IS LEFT INTENTIONALLY BLANK

# CHAPTER 9
# MEASUREMENT AND INTERPRETATION OF ROCK PROPERTIES

"Rock" is generically considered to be an excellent material for many transportation applications because it often has substantial strength and stiffness. Many types of rock are quite desirable for supporting foundations for bridges and other structures, for constructing relatively steep cuts, for tunnels and other underground construction, and as sources of aggregate. However, not all rock formations are alike and some formations can be weak, degradable, soluble, or reactive. Even "desirable" rock can introduce challenges to effective design and construction. Accurate and reliable characterization of rock properties is thus critical for geotechnical design and construction. This chapter describes methods for effectively characterizing both intact rock properties and the properties of rock masses to improve design, construction, and long-term performance of transportation features constructed in, on, or with rock.

## 9.1 USES FOR ROCK PROPERTIES IN DESIGN AND CONSTRUCTION

Intact rock properties and the properties of rock masses are important for geotechnical design and construction. The strength and stiffness of rock significantly affect the design, construction, and performance of rock slopes, shallow foundations on rock, deep foundations founded on or in rock, rock fill embankments, and tunnels and other underground features constructed in rock. Rock characteristics and the depth to rock can strongly influence foundation selection for bridges and other structures (e.g., between shallow and deep foundations, or among different types of deep foundations). Foundation selection, in turn, can influence the reliability, constructability, and cost-effectiveness of the designed foundations. Rock characteristics may also affect design through secondary means. For example, the stiffness of rock strata can affect propagation of seismic waves, which in turn can influence earthquake ground motions. Rock characteristics also affect the suitability and economy of using different materials as aggregate and rock fill. Finally, the accuracy and reliability of rock properties established from site characterization directly influence the reliability and cost-effectiveness of designed features, which in turn affects costs and risks for design, construction, and performance.

Rock characteristics are also important for construction because of their relatively high strength and stiffness. Rock strength and stiffness significantly affect construction methods required for excavation of road cuts and foundations. For example, rock properties may dictate whether a specific formation can be excavated by "ripping" or whether drilling and blasting or other means will be required for removal. Hydraulic properties of rock also commonly affect construction, and may dictate both general and specific techniques for construction of transportation features (e.g., use of casing and/or slurry, need for

rock mass grouting, need for drainage, cofferdam construction methods, etc.). Some rock types also pose challenges for construction aside from increased strength and stiffness. For example, some types of rock can be highly abrasive, which poses challenges for construction tooling and often requires specialized tools, equipment, and techniques. Other types of rock can degrade rapidly, which can lead to stability issues during construction and in the long term. Finally, the presence and condition of rock may impose challenges for construction of certain types of elements, such as limitations on depths of driven piles, and potential damage for driven piles if rock characteristics are not effectively addressed. All of these observations and issues can directly affect both the cost and reliability of constructed features and, thus, broader project and agency budgets.

## 9.2 FUNDAMENTAL CONCEPTS IN ROCK BEHAVIOR

The mechanical behavior of "intact rock" is conceptually similar to the behavior of soils described in previous chapters. Intact rock is a pressure-dependent material that has strength and stiffness that depends on confining stress as illustrated in Figure 9-1. As such, many of the concepts described in previous chapters for soils also apply to intact rock. The primary difference between soil and intact rock is that rock generally has greater strength and stiffness, recognizing that there is a practical continuum of geologic materials with stiff soils being similar to soft rock. Intact rock will also often have considerable tensile strength, as illustrated in Figure 9-1 and discussed further in this chapter, in contrast with most soils that have minimal tensile strength.

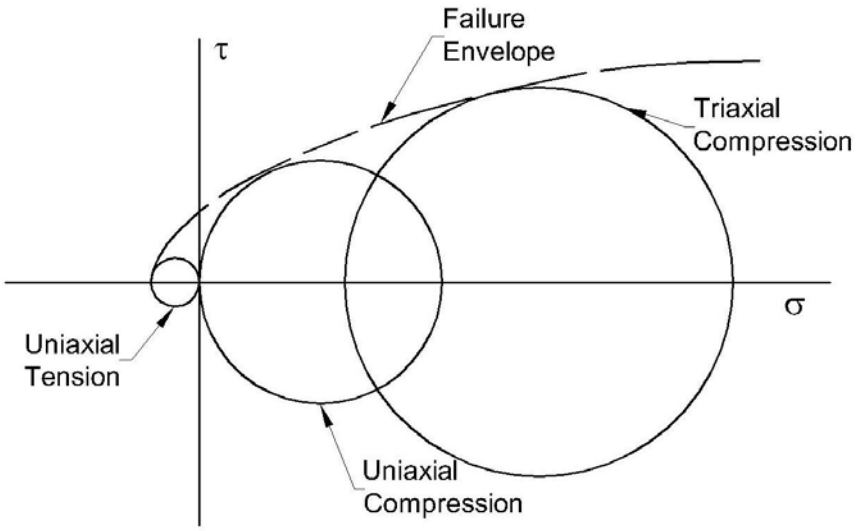


**Figure 9-1 Typical strength envelope for intact rock.**

Despite conceptual similarities between soil and intact rock, the mechanical behavior of "rock masses" can be quite different from the behavior of soil or intact rock because the behavior of rock masses is strongly affected by the presence and characteristics of "discontinuities". Several types of discontinuities are common, including cracks and fissures, fractures, joints, bedding planes, cleavage, foliations, and faults. These discontinuities lead to the result that a rock mass is often a "blocky" collection of intact rock pieces that may have substantially different mechanical behavior than the intact pieces themselves. Throughout this manual, and in this chapter specifically, the term "intact rock" is used to refer to intact pieces of rock that are largely devoid of significant discontinuities whereas the term "rock mass" is used to refer to a mass of rock that includes all discontinuities. The distinction between intact rock and rock masses is not always clear and is a matter of scale, since intact rock may include "micro" features such as micro-cracks and small fissures. Nevertheless, in most civil engineering applications, the rock mass is considered to include the collection of intact rock and discontinuities at "field scale" that is generally consistent with the scale of features being designed and constructed. For design and construction on, or in rock, it is the rock mass characteristics that govern performance, although properties of the intact rock within a given rock mass can and do affect the mechanical behavior of the rock mass. Intact rock properties often also influence construction means and methods. Properties of both intact rock and rock masses are addressed in this chapter.

Because the mechanical behavior of rock masses is difficult to rigorously model and/or measure, design and construction involving rock formations are often based on largely empirical methods that have been developed to consider important rock mass characteristics. The objective of site characterization for rock masses is therefore to provide required inputs to these empirical methods as illustrated in Figure 9-2. Inputs generally include intact rock characteristics, such as rock type, degree of weathering or alteration, and strength, as well as characteristics of discontinuities in the rock mass such as type, orientation, roughness, spacing, persistence, and aperture (opening thickness). Information about infilling material and seepage within discontinuities is also often required. The empirical methods, in turn, are used to develop more common mechanical properties (e.g., strength and stiffness) for the rock mass that are used for design. Many empirical methods rely on one of several alternative rock mass classification systems that are described subsequently in this chapter.

The strength and stiffness of intact rock depend on a number of different factors that include rock type, degree of weathering, and mineralogy. As shown in Table 9-1, the strength of intact rock can vary by several orders of magnitude across different types of rock, and sometimes even within a single rock type. However, because the properties of the intact rock do not completely reflect the properties of the rock mass, and because most methods for design in rock are highly empirical, the strength and stiffness of

intact rock are most commonly measured using relatively simple tests compared to those used to establish soil strength and stiffness. These observations do not diminish the importance of measuring properties for intact rock (because they can vary over a large range). However, the observations do provide important qualification to measurement of intact rock properties and suggest that use of relatively simple and consistent measurements is perhaps more important than performing more elaborate tests. Additional descriptions of alternative measures of strength are provided in subsequent sections of this chapter.

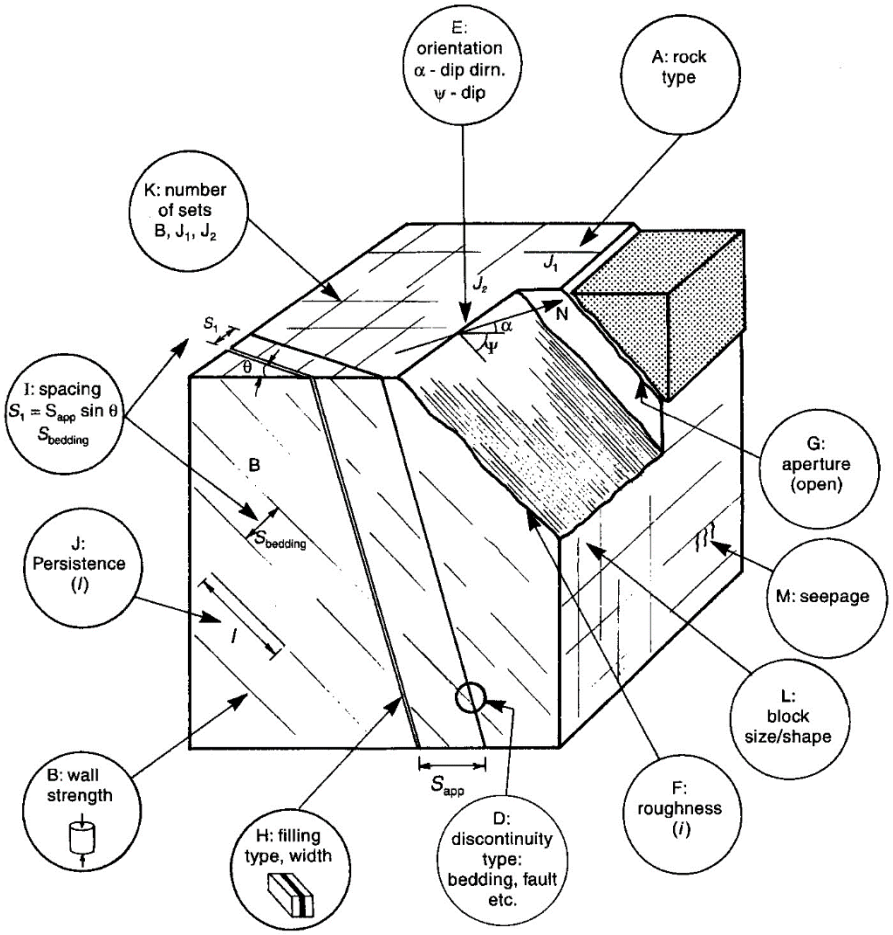


**Figure 9-2 Schematic illustration of rock mass showing relevant characteristics that affect mechanical behavior (Wyllie, 1999).**

Durability can be an important design issue for some rock types. As a general rule, the properties of nearly all rock types tend to degrade over time as a result of weathering processes or exposure. For many rock types, this degradation occurs very slowly; so slowly that the properties of the intact rock can be considered constant over time periods commonly considered for transportation features. However, degradation can occur much more quickly for other types of rock such that the potential degradation should be considered as part of design. For example, many shale formations are notorious for rapidly

degrading upon exposure to air and/or water. The strength and stiffness of such rock can degrade substantially over periods of minutes to days, which can lead to challenges with stability during construction. Such rapid degradation also poses challenges for effective characterization of rock properties. Other rock types degrade more slowly, but still quickly enough to have significance for design of transportation features. Characterization of the durability of susceptible rock types is therefore an important component of characterization. Common measurements for evaluation of durability are described in Chapter 4.

**Table 9-1 Representative strengths for different types of intact rock (after Goodman, 1989).**

| Intact Rock Material | $q_u$ (psi) | Ratio $q_u/q_t$ |
|---|---|---|
| Berea sandstone | 10,700 | 63.0 |
| Navajo sandstone | 31,030 | 26.3 |
| Tensleep sandstone | 10,500 | |
| Hackensack siltstone | 17,800 | 41.5 |
| Monticello Dam s.s. (greywacke) | 11,500 | |
| Solenhofen limestone | 35,500 | 61.3 |
| Bedford limestone | 7,400 | 32.3 |
| Tavernalle limestone | 14,200 | 25.0 |
| Oneota dolomite | 12,600 | 19.7 |
| Lockport dolomite | 13,100 | 29.8 |
| Flaming Gorge shale | 5,100 | 167.6 |
| Micaceous shale | 10,900 | 36.3 |
| Dworshak Dam gneiss (45º to foliation) | 23,500 | 23.5 |
| Quartz mica schist (⊥ schistocity) | 8,000 | 100.4 |
| Baraboo quartzite | 46,400 | 29.1 |
| Taconic marble | 8,990 | 53.0 |
| Cherokee marble | 9,700 | 37.4 |
| Nevada Test Site granite | 20,500 | 12.1 |
| Pikes Peak granite | 32,800 | 19.0 |
| Cedar City tonalite | 14,700 | 15.9 |
| Palisades diabase | 34,950 | 21.1 |
| Nevada Test Site basalt | 21,500 | 11.3 |
| John Day basalt | 51,500 | 24.5 |
| Nevada Test Site tuff | 1,650 | 10.0 |

As is true for soils, water can have a significant effect on the mechanical behavior of intact rock and rock masses, and thus the stability and performance of transportation features constructed in, or on rock. However, in the case of rock, the influence of water depends significantly on the type of rock and characteristics of the rock mass. For many rock types, common strength properties of the intact rock are similar whether they are wet or dry. Other rock types, such as shales that contain swelling clay minerals, may lose strength in the presence of water. The same is true of "infilling" materials within discontinuities. In such cases, it is necessary to assess whether the rock or infilling material is adversely

affected by the presence of water and, if so, to effectively characterize and address such behavior for design and construction. Regardless of the type of rock, the presence and pressure of water in discontinuities affects the strength and stiffness along the discontinuity, and therefore the behavior of the rock mass. In this context, the water pressure acting on the discontinuity reduces the effective normal stress along the discontinuity compared to the normal stress that would be present without water. This reduction in effective normal stress produces a corresponding reduction in the shear strength of the discontinuity, which in turn can mean the difference between acceptable and unacceptable performance if the water pressure is great enough. As such, accurate characterization of ground water conditions, and how those conditions may be affected by construction, is an important component of rock mass characterization.

## 9.3 BORING AND SAMPLING REQUIREMENTS FOR CHARACTERIZATION OF INTACT ROCK AND ROCK MASSES

Requirements for boring and sampling of intact rock and rock masses are substantially different than requirements for most soils. Since many types of rock can be hard, and potentially abrasive, specialized tooling is often required to produce reasonable production while still maintaining the condition of rock specimens (generally rock core). Samples are most commonly obtained using core barrels that "cut" samples rather than tubes that are commonly pushed in most soils. Use of "double-tube" core barrels is generally recommended for most rock to limit damage to the rock core and increase core recovery to better reflect actual conditions. "Triple-tube" core barrels may be appropriate in particularly challenging rock formations. Despite the apparent hardness of many rock formations, coring is generally straightforward in many competent rock formations. However, difficulties can arise with sampling in degradable or highly fractured rock masses.

Characterization of discontinuities in rock masses is often more difficult than characterization of intact rock core. Some degree of characterization can be derived from measurements made on rock core, such as core recovery ($CR$), rock quality designation ($RQD$), and fracture frequency ($FF$) that are described in Chapter 4. Additional information from careful observations during drilling (e.g., changes in drilling fluid color, gain/loss of drilling fluid, rod drops, drilling rates) can also facilitate characterization. Absolute orientation of discontinuities is often lost with most types of core barrels, although some core barrels include provisions that allow tracking of orientation using "oriented cores". In areas where vertical or near-vertical discontinuities are prevalent, and important, inclined borings may be required to characterize discontinuities. More recently, several types of downhole viewers have been developed that can dramatically improve characterization of discontinuities in boreholes and "measurement while

drilling" (MWD) techniques using instrumented drilling rigs also provide significant promise for characterization of intact rock and rock masses. It is also common to characterize rock masses using measurements on rock mass exposures that may be near to a site. Such exposures may be found in nearby quarries or roadway cuts, while others may be naturally occurring. Additional description of methods for characterizing discontinuities is provided subsequently in Section 9.5.

Following collection of rock core, the extracted core should be placed into dedicated rock core boxes that are often constructed of wood or heavy duty cardboard. Core recovery, $RQD$, and fracture frequency should be measured as soon after core extraction as possible because the core for some rock types, such as shales and mudstones, can quickly degrade. Many other rock types are more durable, however, so no special care is required other than careful handling to avoid breaking the core. For intermediate materials that represent the boundary between soil and rock, or for rock that is sensitive to moisture content changes, care is more critical. In such cases, rock core should be wrapped in plastic wrap and/or waxed following extraction to prevent changes in moisture content prior to testing. Additional guidance regarding effective practices for boring and sampling in rock can be found in Savidge et al. (2006), and in relevant standards that include ASTM D2113, ASTM D5079, and AASHTO T225.

## 9.4 MEASUREMENT AND INTERPRETATION OF INTACT ROCK PROPERTIES

Several different measures are commonly used to establish the strength and stiffness of intact rock. By far the most common measure of rock strength is the uniaxial compressive strength, $q_u$. Tensile strength and shear strength of intact rock are measured less frequently, primarily because they are infrequently required for geotechnical design in rock, but may be important for design of tunnels and rock slopes in rock masses that lack significant discontinuities. The shear strength of specific discontinuities is more frequently measured as it can significantly affect the stability and performance of rock slopes and tunnels. Several indirect measures such as the Brazilian "indirect" tensile strength, point load strength index, several hardness measurements, and seismic velocity may also be made and reported.

### 9.4.1 Uniaxial Compressive Strength

The uniaxial compression strength, $q_u$, is the most common measure of strength for intact rock. $q_u$ is measured in a uniaxial compression test (ASTM D7012), which is conceptually similar to the unconfined compression test for soil described in Section 7.4.2 and similar to uniaxial compression tests that are commonly performed on concrete cylinders. Tests are usually performed on selected pieces of rock core that are cut to form a specimen of appropriate dimensions. Uniaxial compressive strength can also be empirically estimated from indirect tests as described in more detail in Section 9.4.5.

An example result from a uniaxial compression test is shown in Figure 9-3. Interpretation of $q_u$ from uniaxial compression tests is usually straightforward, being established as

$$q_u = \frac{P_{max}}{A} \tag{9.1}$$

where $P_{max}$ is the applied axial load at failure and $A$ is the cross-sectional area of the specimen. For many rock types, failure occurs abruptly and is easily distinguished because of the brittle nature of the material. However, failure for other rock types can be less obvious. In such cases, $q_u$ should be calculated based on the maximum applied load. Measurement of displacement or strain is not required for uniaxial compression tests; however, such measurements are recommended to facilitate interpretation of rock behavior and to allow for measurement of intact rock modulus as described in Section 9.4.4.

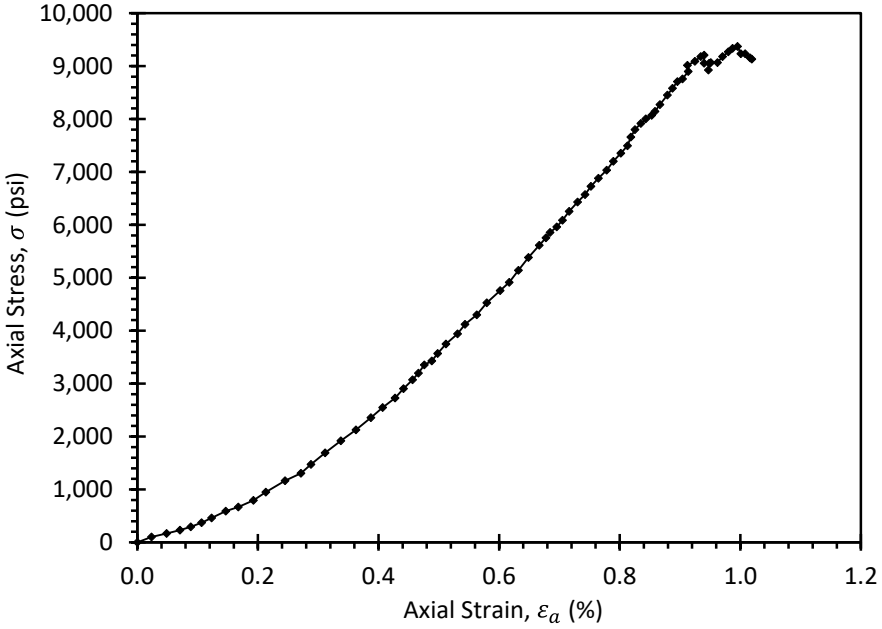


**Figure 9-3 Example result from uniaxial compression test.**

While $q_u$ is the most commonly used measure of strength for intact rock, it is important to recognize that $q_u$ represents the compressive strength of the intact rock under conditions with no confinement and may not reflect the actual strength of the rock under confined conditions that are present in situ (as illustrated in Figure 9-1). Nevertheless, $q_u$ is a common input parameter for many rock mass classification systems and empirical design and construction relations and, as such, can be considered a "reference" value for intact rock strength. Since it is most commonly used with empirical methods, it is important that the inputs are consistent with the development of the empirical methods even if those inputs do not

completely represent the true mechanical behavior in situ. This use is appropriate and consistent with the empiricism that has been adopted for design and construction in rock.

### 9.4.2 Shear Strength of Intact Rock

As illustrated in Figure 9-1, the shear strength of intact rock is a function of the confining stress imposed on the rock. While the shear strength of intact rock may affect the mechanical performance of rock masses, it is seldom directly measured because it is seldom required for design of transportation features in, or on those rock masses (since most design methods are empirical). In some cases, shear strength (or more commonly parameters describing shear strength) may be required for relatively soft rock formations that have the potential to affect stability and performance of transportation feature(s) such as rock slopes. In such cases, shear strength can be measured in triaxial (AASHTO T226, ASTM D7012) or direct shear tests (ASTM D5607) that are qualitatively similar to tests performed for soils described in Chapter 7. Because of the strength and stiffness of rock, tests for rock specimens often cannot be performed using conventional devices developed for soils but instead require specialized equipment that is appropriate for greater applied stresses. Both triaxial and direct shear tests can be used to establish the failure envelope for intact rock, similar to that shown in Figure 9-1.

Results from individual triaxial compression tests on rock are interpreted to obtain the "triaxial compressive strength", $q_{TX}$, computed as

$$q_{TX} = \left(\sigma_{1f} - \sigma_{3f}\right) = \frac{P_{max}}{A} \tag{9.2}$$

where $\sigma_{1f}$ and $\sigma_{3f}$ are respectively the major and minor principal stresses at failure, $P_{max}$ is the applied axial load at failure, and $A$ is the cross-sectional area of the specimen. More commonly, results from several triaxial compression tests performed at different confining pressures are combined to establish a failure envelope, such as the Mohr-Coulomb failure envelope illustrated in Figure 9-4.

The shear strength failure envelope can also be established using measurements from direct shear tests performed over a range of normal stresses. Figure 9-5 show typical results from such tests, including shear stress versus shear displacement measurements and a Mohr-Coulomb envelope derived from the test measurements. For these tests, the shear stress is computed as:

$$\tau = \frac{P_s}{A} \tag{9.3}$$

where $P_s$ is the applied shear load. The normal stress is computed as:

$$\sigma = \frac{P_n}{A} \tag{9.4}$$

where $P_n$ is the applied normal load. By convention, the nominal initial cross-sectional area of the specimen, $A$, is used for computing both the normal and shear stress for the direct shear test.

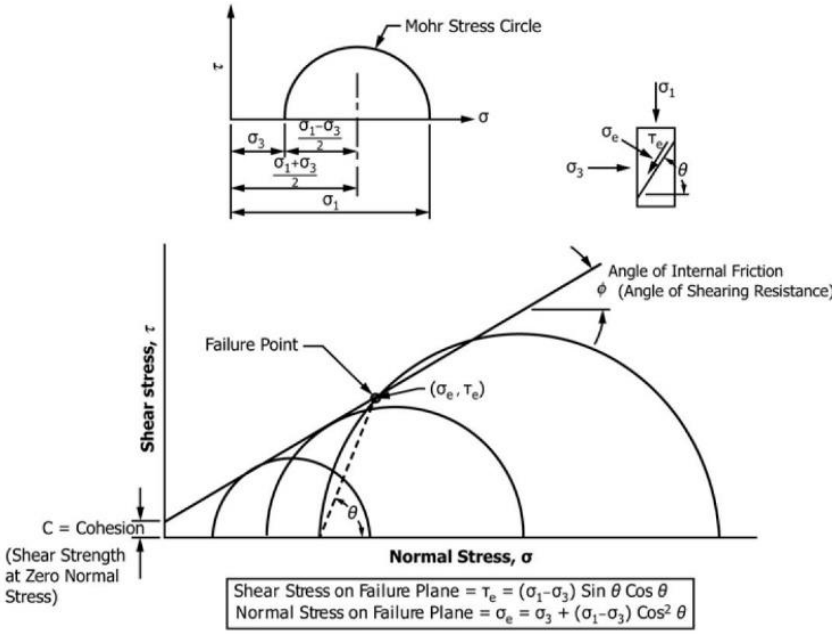


**Figure 9-4 Construction of Mohr-Coulomb failure envelope from measurements of triaxial tests on intact rock (from ASTM D7012, 2014).**

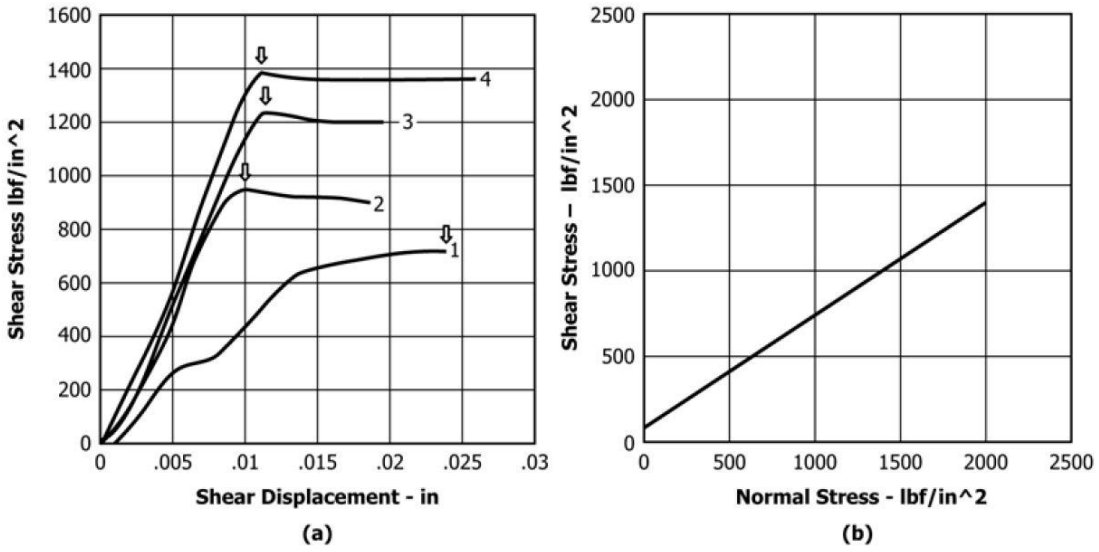


**Figure 9-5 Results from direct shear tests performed on intact rock (from ASTM D5607, 2008).**

For some rock types, the shear stress versus shear displacement response will indicate a "peak" shear stress at some displacement followed by a reduction or "strain softening" of shear stress with additional shear displacement. In such cases, two potential shear strength values can be established: one corresponding to the peak shear stress, $\tau_{peak}$, (the "peak shear strength") and one corresponding to the residual shear stress, $\tau_{resid}$, (the "residual shear strength") as described for soils in Section 7.7. Both the peak and residual strength failure envelopes can be appropriate for design in certain instances.

### 9.4.3 Tensile Strength of Intact Rock

The tensile strength, $q_t$, of intact rock is considerably less than $q_u$. The tensile strength, and its relation to compressive strength and the Mohr-Coulomb failure envelope is illustrated in Figure 9-1. Figure 9-6 shows comparison of tensile and compressive strengths (denoted as $UCS$ in the figure) for intact rock specimens from several different studies. A general relationship often exists between $q_t$ and $q_u$ for a specific rock type or formation. However, the proportionality between $q_t$ and $q_u$ varies substantially among different rock types as shown.

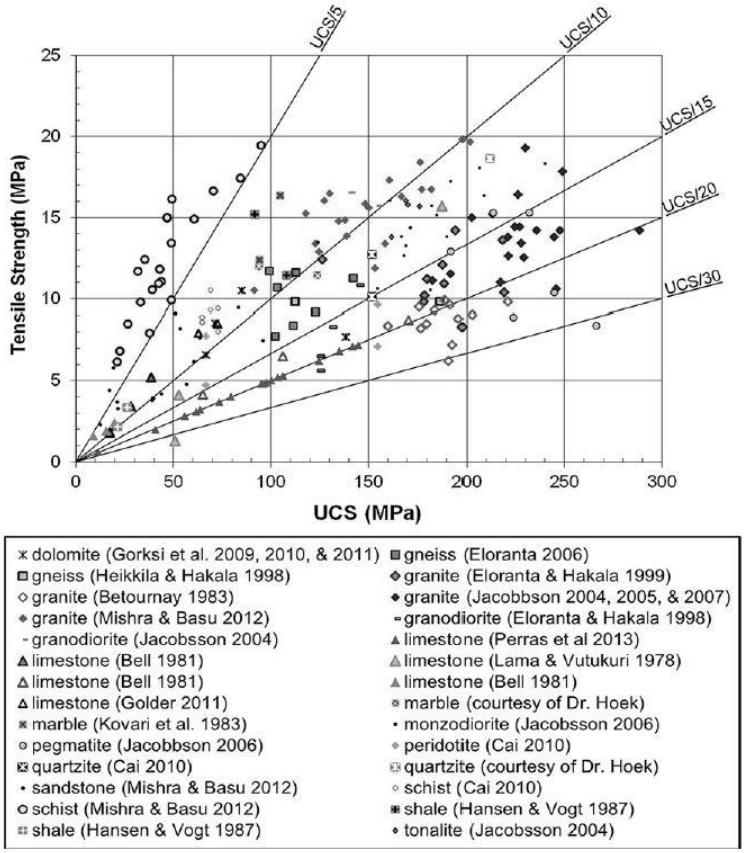


**Figure 9-6 Comparison of $q_t$ and $q_u$ for intact rock specimens (from Perras and Diederichs, 2014).**

The utility of tensile strength for many transportation applications is limited, although it can have significance for design of tunnels and other underground spaces. The direct means for measuring tensile strength is the "direct" tension test (ASTM D2936), which is performed in a manner similar to a uniaxial compression test except that the specimen is loaded in tension rather than compression. Displacements are not generally measured for direct tension tests. Thus, the tensile strength is simply computed as

$$q_t = \frac{P_{max}}{A} \tag{9.5}$$

where $P_{max}$ is the maximum applied (tensile) load and $A$ is the cross-sectional area of the specimen. Challenges associated with specimen preparation and applying a tensile load without inducing bending or torsional stresses make direct tension tests relatively difficult. As such, the so-called "split" (or "Brazilian split") tension test (ASTM D3967) is more commonly performed to indirectly measure tensile strength. Further description of the split tension test is provided in Section 9.4.5.

### 9.4.4 Intact Rock Modulus

Elastic constants representing the stiffness of intact rock can be determined from uniaxial compression tests described in Section 9.4.1 if provisions are made for measuring the axial and lateral strain during the tests. For such tests, the axial stress, $\sigma_a$, is determined as

$$\sigma_a = \frac{P}{A} \tag{9.6}$$

and axial strain, $\varepsilon_a$, is computed as

$$\varepsilon_a = \frac{\Delta L}{L} \tag{9.7}$$

where $\Delta L$ is the change in specimen height and $L$ is the initial undeformed specimen height. Figure 9-7 shows the axial stress versus axial strain response from a uniaxial compression test.

Young's modulus is derived from the slope of the measured axial stress versus axial strain curve. Several different values for Young's modulus can be established: tangent values established at stresses that are a fixed percentage of the compressive strength, an average modulus established over the linear portion of the stress-strain curve, or secant values established at stresses that are a fixed percentage of the compressive strength as illustrated in Figure 9-8. While different values of Young's modulus can be established, values of $E_{50}$ are most commonly reported, which corresponds to the slope of the line tangent to the stress-strain curve at a stress that is 50 percent of $q_u$, as shown in Figure 9-7.

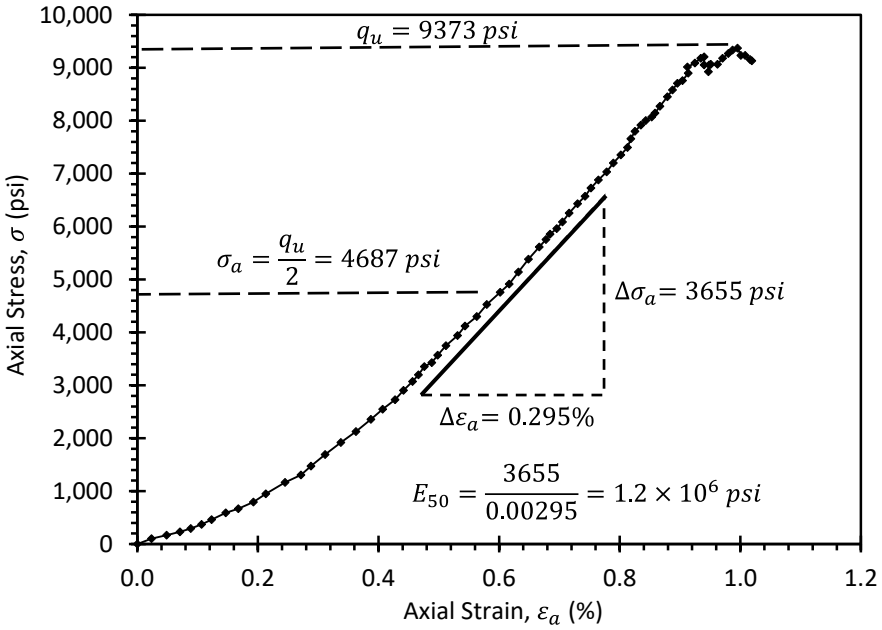


**Figure 9-7 Axial stress versus axial strain response from uniaxial compression test on intact rock.**

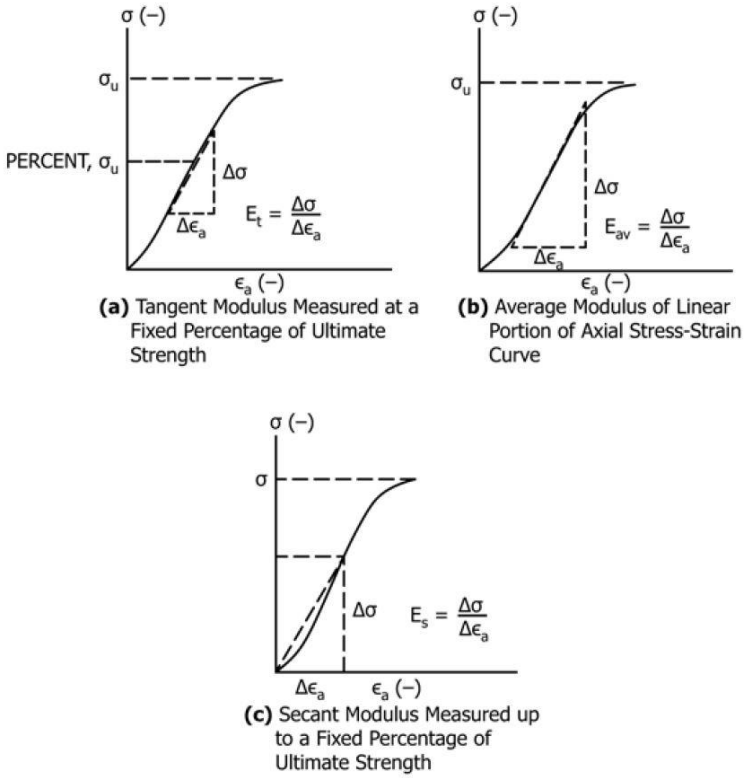


**Figure 9-8: Different methods for establishing Young's modulus from uniaxial compression tests (from ASTM D7012, 2014).**

In addition to Young's modulus, Poisson's ratio can also be established from uniaxial compression tests if lateral strain is measured during the test. Figure 9-9 shows conceptual results from such a test showing the axial stress plotted versus axial strain and lateral strain, where lateral strain is computed as

$$\varepsilon_l = \frac{\Delta D}{D} \tag{9.8}$$

$\Delta D$ is the change in specimen diameter, and $D$ is the initial diameter. From such results, Poisson's ratio can be calculated as

$$\upsilon = -\frac{slope\ of\ \sigma_a\ versus\ \varepsilon_a\ curve}{slope\ of\ \sigma_a\ versus\ \varepsilon_l\ curve} = -\frac{E}{slope\ of\ \sigma_a\ versus\ \varepsilon_l\ curve} \tag{9.9}$$

In calculating Poisson's ratio, the slope of the respective stress-strain curves should be established at some consistent percentage of the uniaxial compressive strength.

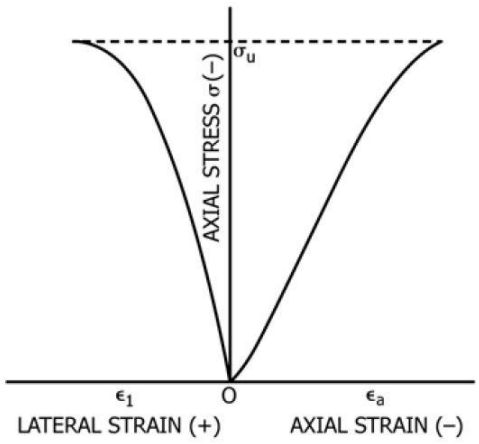


**Figure 9-9 Uniaxial compression test results showing $\sigma_a$ versus $\varepsilon_a$ and $\varepsilon_l$ to illustrate method for calculating Poisson's ratio (from ASTM D7012, 2014).**

Because of the loading conditions imposed during testing, Young's modulus ($E$) and Poisson's ratio ($\nu$) can be directly derived from test measurements; however, these constants can be converted to other elastic constants such as shear modulus ($G$) or bulk modulus ($K$) if the material can be considered to be isotropic. Given specific values of $E$ and $\nu$, one can compute corresponding values of $G$ and $K$ as:

$$G = \frac{E}{2(1+\nu)} \tag{9.10}$$

$$K = \frac{E}{3(1-2\nu)} \tag{9.11}$$

Analogous elastic constants can also be determined from triaxial tests on intact rock. However, such constants will not be $E$ and $\nu$ because of the confinement provided.

### 9.4.5 Evaluation of Intact Rock Properties from Indirect Measurements

Several indirect measurements are commonly used to establish properties of intact rock. The most common tests include the point load strength index test, several hardness tests, and the split tension test (a.k.a. Brazilian split tension test). Small-strain seismic tests are also commonly used to estimate intact rock modulus, either as part of other tests or using dedicated measurements. These tests can often be performed more quickly than the direct measurements described in the preceding sections, and for less cost. However, theoretical or empirical transformations are required to convert the indirect measurements to the property of interest. These indirect measurements are, thus, subject to additional variability and uncertainty that is not present with direct measurements as described in Chapter 3.

***Point Load Strength Index***

The point load strength index test (ASTM D5731) is performed using a compression testing device with special conical platens, as shown in Figure 9-10. The primary advantage of point load tests is that they can be rapidly performed in the laboratory or field to obtain an estimate for $q_u$. Point load tests can also be conducted on small sections of rock core, or even irregularly shaped lumps of intact rock, which is important when considering highly fractured rock that may not produce suitable sections of core for more reliable uniaxial compression tests.

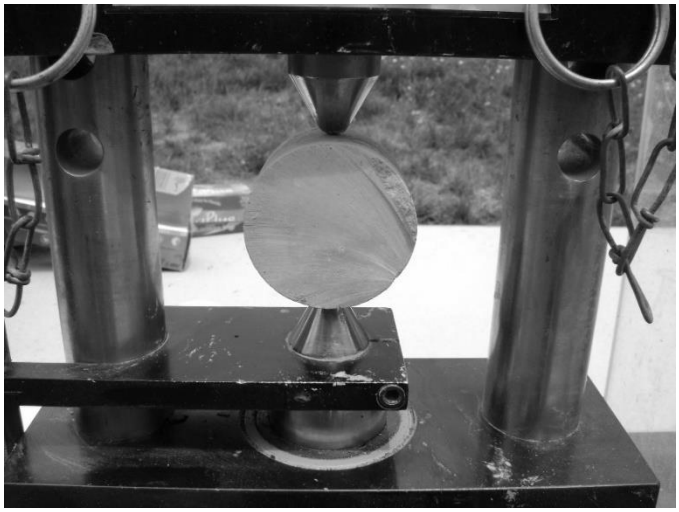

**Figure 9-10 Point load strength index test on segment of rock core.**

Point load strength index tests strictly produce measurements of the point load strength index, $I_s$. Measured values of $I_s$ should be corrected as described in ASTM D5731 to account for the size of the test specimen to produce corrected values that are generally denoted as $I_{s(50)}$, where the "50" denotes measurements for a standard 50-mm diameter core. $I_{s(50)}$ values can be transformed into estimates of $q_u$ using empirically derived expressions (e.g., Rusnak and Mark, 2000; Azimian, et al., 2014; Çobanoglu and Çelik, 2008; Kaya and Karaman, 2016) that are generally assumed to be linear with the form:

$$q_u = k \cdot I_{s(50)} + b \tag{9.12}$$

where $k$ and $b$ are empirically established coefficients. "Zero-intercept" relations with $b = 0$ are commonly adopted in the interest of simplicity, although use of non-zero intercepts may produce better statistical fits for some data sets. Table 9-2 summarizes some of the empirical transformations that have been proposed. Values for the coefficient $k$ generally range between about 15 and 30 for most rock formations, with greater $k$ values often being appropriate for strong rock and lesser $k$ values generally being appropriate for weaker rock.

Unfortunately, there is considerable uncertainty associated with empirical relations between $I_{s(50)}$ and $q_u$, and therefore considerable uncertainty in estimates of $q_u$ established from $I_{s(50)}$. The uncertainty is substantial when considering measurements taken from diverse rock types as illustrated in Figure 9-11. Some of the uncertainty introduced by the transformations can be reduced by considering relations developed for specific rock types or specific rock formations (Singh, et al., 2012; Kahraman and Gunaydin, 2009). Even greater reductions in uncertainty can be achieved using "local" or "site specific" transformations developed for more localized geographic areas.

***Portable Hardness Tests***

Several variations of hardness tests can be used to produce estimates for rock strength and stiffness, among other characteristics (e.g., Verwaal and Mulder, 1993; Buyuksagis and Goktan, 2007). The primary advantage of these tests is that the devices are simple and portable, and can be used to quickly produce non-destructive measurements for rock core, intact rock, or discontinuity walls. The devices are well-suited to evaluating the relative strength of different segments of rock core or exposed rock without going to the trouble of performing more destructive and time consuming tests. However, the tests are indirect measurements that introduce uncertainty into estimates of rock strength and stiffness.

By far the most common of these tests for evaluating properties of intact rock is the "Schmidt hammer" or "rebound hammer" test (ASTM D5873). The device consists of a spring-loaded "hammer" that is depressed on a segment of rock core as shown in Figure 9-12. The magnitude of rebound is measured and reported as a "rebound number", $R$.

**Table 9-2 Summary of relations proposed to transform $I_{s(50)}$ to $q_u$. (after Singh, et al., 2012)**

| Equation | Country | Rock Type(s) | Reference |
|---|---|---|---|
| $q_u = 23.7 \cdot I_{s(50)}$ | United Kingdom | Various | Broch & Franklin (1972) |
| $q_u = 23.9 \cdot I_{s(50)}$ | South Africa | Sandstones | Bieniawski (1975) |
| $q_u = 29 \cdot I_{s(50)}$ | United Kingdom | Sedimentary Rock | Hassani et al. (1980) |
| $q_u = 20 \cdot I_{s(50)}$ | Australia | Sedimentary Rock | Read et al. (1980) |
| $q_u = 20 \; to \; 25 \cdot I_{s(50)}$ | -- | -- | ISRM (1985) |
| $q_u = 26.5 \cdot I_{s(50)}$ | United Kingdom | Limestone | Hawkins & Olver (1986) |
| $q_u = 24.8 \cdot I_{s(50)}$ | United Kingdom | Sandstone | Hawkins & Olver (1986) |
| $q_u = 21.8 \cdot I_{s(50)} + 6210$ | United States | Sedimentary | O'Rourke (1989) |
| $q_u = 17.4 \cdot I_{s(50)}$ | United States | Sandstone | Vallejo et al. (1989) |
| $q_u = 12.6 \cdot I_{s(50)}$ | United States | Shale | Vallejo et al. (1989) |
| $q_u = 23.4 \cdot I_{s(50)}$ | India | Quartzite | Singh & Singh (1993) |
| $q_u = 14.7 \cdot I_{s(50)}$ | Canada | Siltstone | Das (1985b) |
| $q_u = 18 \cdot I_{s(50)}$ | Canada | Sandstone | Das (1985b) |
| $q_u = 12.6 \cdot I_{s(50)}$ | Canada | Shale | Das (1985b) |
| $q_u = 24 \cdot I_{s(50)}$ | Various | Sandstone/Limestone | Smith (1997) |
| $q_u = 12.6 \cdot I_{s(50)}$ | Various | Shale | Smith (1997) |
| $q_u = 21.8 \cdot I_{s(50)}$ | United States | Shale | Rusnak & Mark (2000) |
| $q_u = 20.2 \cdot I_{s(50)}$ | United States | Siltstone | Rusnak & Mark (2000) |
| $q_u = 20.6 \cdot I_{s(50)}$ | United States | Sandstone | Rusnak & Mark (2000) |
| $q_u = 21.9 \cdot I_{s(50)}$ | United States | Limestone | Rusnak & Mark (2000) |
| $q_u = 21.0 \cdot I_{s(50)}$ | United States | Shale | Osouli et al. (2014) |
| $q_u = 14.0 \cdot I_{s(50)}$ | United States | Black Shale | Osouli et al. (2014) |
| $q_u = 14.2 \cdot I_{s(50)}$ | United States | Sandy Shale | Osouli et al. (2014) |
| $q_u = 11.3 \cdot I_{s(50)}$ | United States | Claystone | Osouli et al. (2014) |
| $q_u = 20.2 \cdot I_{s(50)}$ | United States | Limestone | Osouli et al. (2014) |
| $q_u = 25 \cdot I_{s(50)}$ | United States | Shale Limestone | Osouli et al. (2014) |

The rebound number is commonly related to $q_u$ using either an exponential function of the form

$$q_u = a \cdot e^{bR} \tag{9.13}$$

or a power function of the form

$$q_u = a \cdot R^b \tag{9.14}$$

where $R$ is the measured rebound number and $a$ and $b$ are empirical coefficients (Aydin, 2009). Linear relations of the form shown in Figure 9-13 are also occasionally recommended. Similar forms of transformations are also used to transform $R$ to modulus of elasticity. Table 9-3 provides several

alternative transformations that have been proposed to transform $R$ to $q_u$, while Table 9-4 provides transformations between $R$ and $E$.

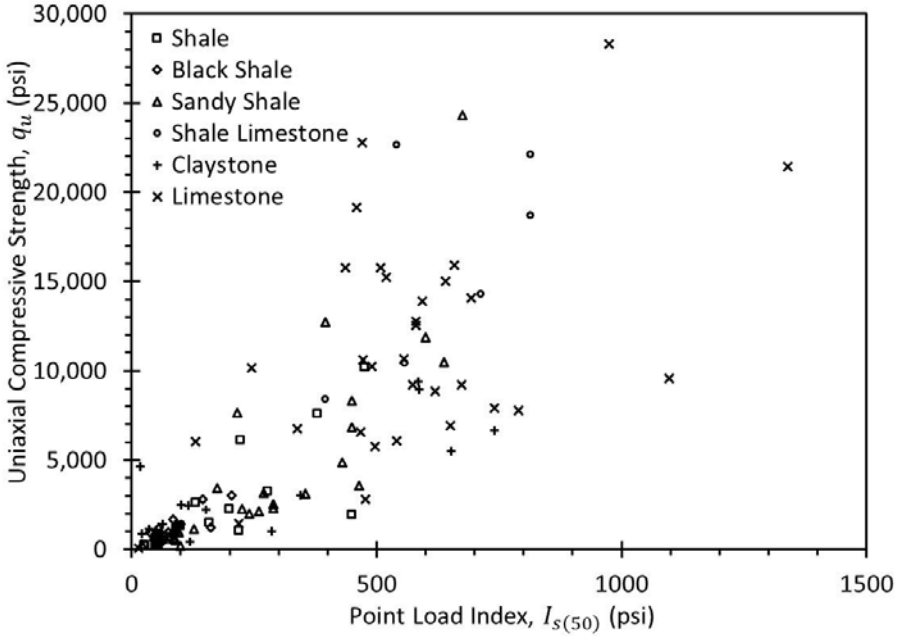


**Figure 9-11 Relationship between $I_{s(50)}$ and $q_u$ for several rock types (after Osouli, et al., 2014).**

**Figure 9-12 Apparatus for Schmidt hammer test (Photo courtesy Controls Group).**

Alternative hardness test devices that have been used for assessment of rock properties include the Equotip Hardness Tester and the DynaPocket Test that were both developed for evaluation of metal hardness. For both of these electronic devices, hardness values are determined from measurement of both the impact and rebound speeds of an impact body within the device, which are then correlated to rock

properties including $q_u$ (e.g., Verwaal and Mulder, 1993; Aoki and Matsukura, 2008). Both the Equotip and DynaPocket devices impart substantially less energy into the rock being tested than the Schmidt hammer.

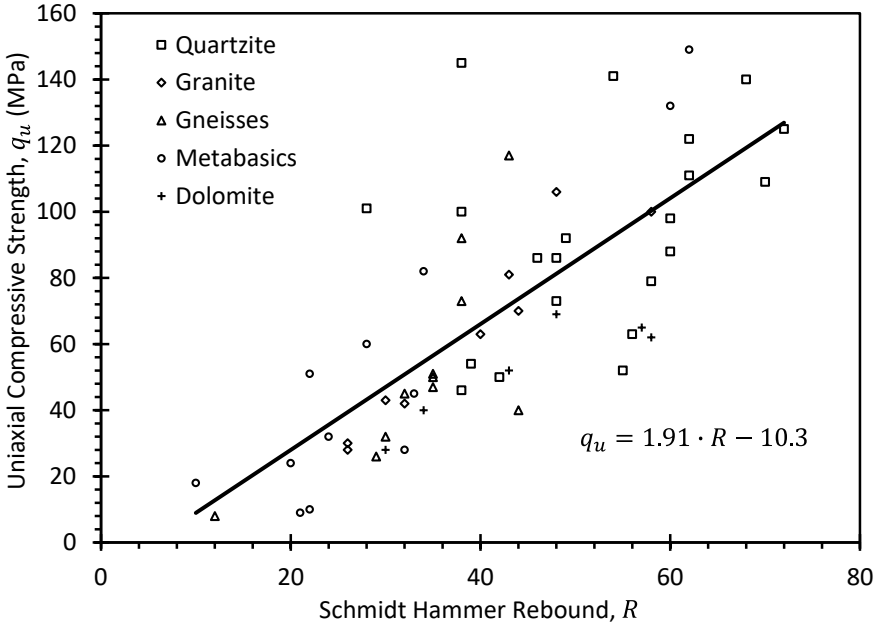


**Figure 9-13 Empirical transformation from Schmidt hammer rebound ($R$) to $q_u$ (adapted from Tandon and Gupta, 2015).**

**Table 9-3 Selected relations for transforming rebound hammer $R$ to $q_u$.**

| Transformation Equation | Units | Rock Type(s) | Reference |
|---|---|---|---|
| $q_u = 1246 \cdot R - 34890$ | psi | Various | Deere and Miller (1966) |
| $q_u = 6.9{\times}10^{(1.348\log(\gamma R)-1.325)}$ | MPa | Various | Aufmuth (1973) |
| $q_u = 2 \cdot R$ | MPa | Sedimentary | Singh et al. (1983) |
| $q_u = 4.84 \cdot R - 7.61$ | MPa | Anhydrite, siltstone, sandstone, limestone | O'Rourke (1989) |
| $q_u = 4.184 \cdot R - 65.792$ | MPa | Carbonate rock | Sachpazis (1990) |
| $q_u = 8.36 \cdot R - 416$ | MPa | Granite | Tugrul and Zarif (1999) |
| $q_u = 0.994 \cdot R - 0.383$ | MPa | | Haramy and DeMarco (1985) |
| $q_u = 2.208 \cdot e^{0.067R}$ | MPa | Chalk, limestone, sandstone, marble, granite, and syenite | Katz et al. (2000) |
| $q_u = e^{(0.059R+0.818)}$ | MPa | Gypsum | Yilmaz and Sedir (2002) |
| $q_u = 4{\times}10^{-6} \cdot R^{4.2917}$ | MPa | Limestone, marble, basalt, and sandstone | Yasar and Erdogan (2004a) |
| $q_u = 1.910 \cdot R - 10.30$ | MPa | Quartzite, Granite, Gneiss, Metabasics, and Dolomite | Tandon and Gupta (2015) |

**Table 9-4 Selected relations to transform rebound hammer $R$ to $E_{50}$.**

| Transformation Equation | Units | Rock Type(s) | Reference |
|---|---|---|---|
| $E_{50} = (0.259 \cdot R - 4.29) \times 10^6$ | psi | Various | Deere and Miller (1966) |
| $E_{50} = 0.00013 \cdot R^{3.09074}$ | MPa | Chalk, limestone, sandstone, marble, granite, and syenite | Katz et al. (2000) |
| $E_{50} = e^{(0.054R + 1.146)}$ | MPa | Gypsum | Yilmaz and Sendir (2002) |

***Seismic Velocity***

As described in Chapter 8, the modulus of intact rock can be evaluated from the measured propagation velocity of elastic waves. In the laboratory, velocity measurements can be performed on intact specimens using the pulse velocity method (ASTM D2845) or using a resonant column device, as discussed in Chapter 8. Velocity measurements can also be obtained in the field using several methods described in Chapter 8. The relationship between elastic wave velocity and modulus is a direct theoretical relationship based on the physics of wave propagation rather than an empirical relation like those used for many indirect measurements. Since seismic measurements are small-strain measurements, modulus values derived from wave velocities will generally be greater than large-strain values determined from laboratory tests described in Section 9.4.4. However, the correlation between modulus values determined from static and dynamic measurements is generally good as shown in Figure 9-14.

While seismic velocities can be measured in both the laboratory and the field, laboratory methods measure wave velocity through small intact specimens while field methods measure wave velocities through the larger rock mass that includes various types of discontinuities. For this reason, field measurements will often yield lower wave velocities than those measured on intact laboratory specimens. As discussed in Section 9.7, the difference between laboratory and field measurements of wave velocity can be used to infer information about rock mass quality.

Seismic wave velocities have also been used for estimating $q_u$. However, unlike the direct theoretical relationship between velocity and modulus, the relationship between $q_u$ and velocity is purely empirical and based on the observation that many of the same factors affecting strength also affect wave velocity. While reasonable relationships have been observed for specific rock formations or rock types (e.g., Yasar and Erdogan, 2004b; Oyler, et al., 2008), the relationship across many rock types and formation is generally quite poor as illustrated in Figure 9-15. Use of sonic velocities for estimating $q_u$ is therefore not recommended except as approximate estimates for preliminary design (Tandon and Gupta, 2015).

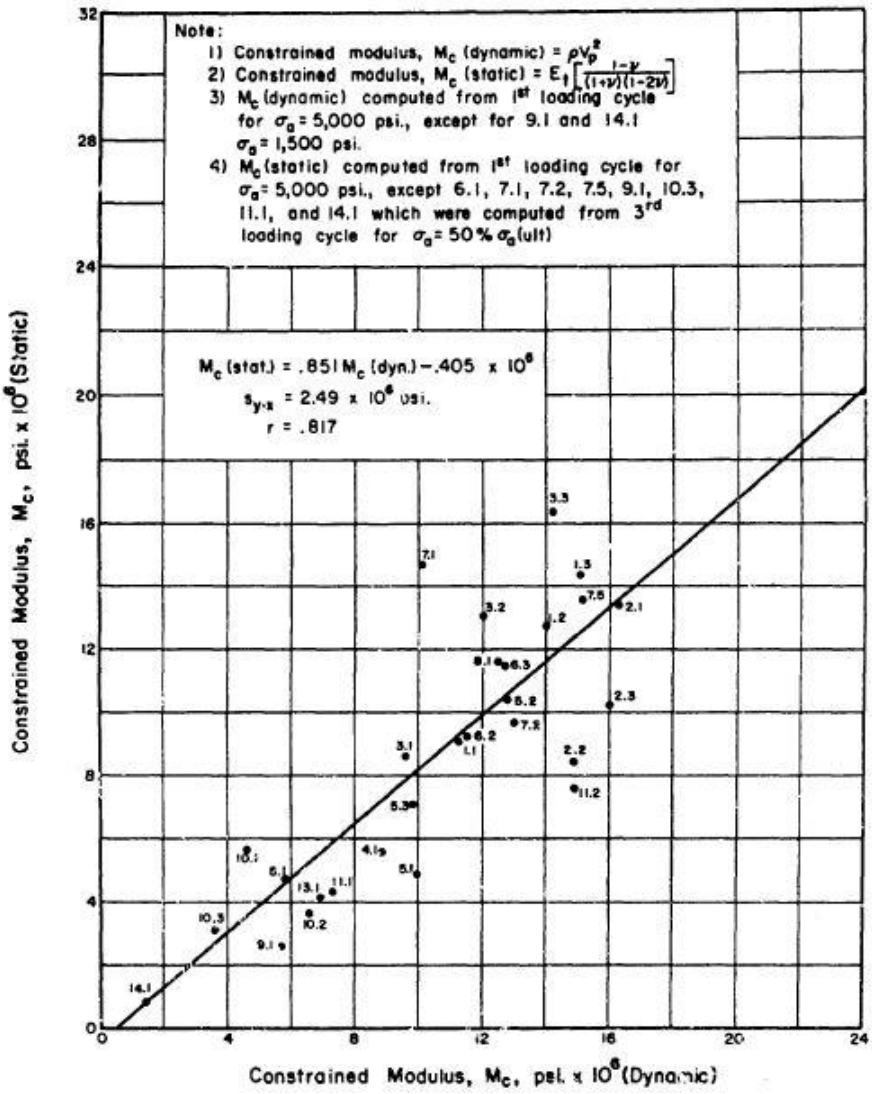


**Figure 9-14 Relationship between static and dynamics measurements of constrained modulus under uniaxial compressive stress up to 5000 psi (from Deere and Miller, 1966).**

### *Split Tension Test*

The split tension test (a.k.a. Brazilian split tension test) is an indirect means for measuring the tensile strength of intact rock, which can be difficult to measure directly. The test (ASTM D3967) is performed by applying an axial load across the diameter of a cylindrical specimen, as illustrated in Figure 9-16. The diametral load is incrementally increased until the specimen "splits" along the diameter between the end platens that apply load. The splitting tensile strength, $T_o$, is computed from elasticity theory as

$$T_o = \frac{2P}{\pi \cdot l \cdot D} \tag{9.15}$$

where $P$ is the maximum applied load, $l$ is the axial length of the specimen, and $D$ is the specimen diameter. Unlike most indirect measurements, which rely upon empirical measurements to transform indirect measurements to some other rock property, transformation of split tension test measurements to tensile strength relies on purely theoretical considerations.

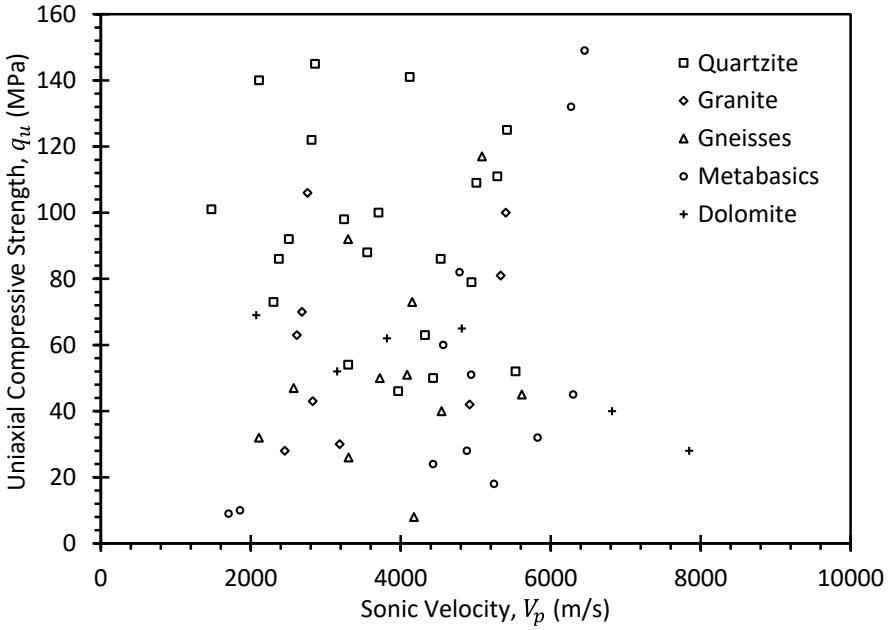


**Figure 9-15 Empirical measurements of sonic velocity ($V_p$) and $q_u$ (from Tandon and Gupta, 2015).**

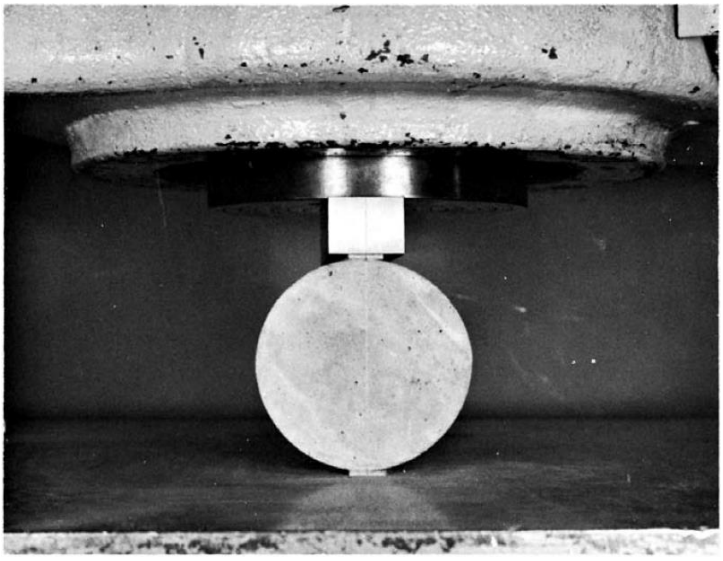

**Figure 9-16 Split tension test on a cylindrical concrete specimen (from ASTM C496, 2011)**

### 9.4.6 Selection of Specimens for Measurement of Intact Rock Properties

Selection of rock specimens is conceptually straightforward in that specimens are selected from segments of rock core that are of sufficient dimensions for testing. For uniaxial compression tests, standard test methods (e.g., ASTM D7012) require specimens that have a length that is at least twice the diameter of the rock core. Core sizes for direct mechanical tests described in this section should generally be at least NQ size (approximately 2 inch nominal diameter). Larger core (e.g., HQ size) is often more desirable and more likely to produce measurements that are representative of the in situ strength, especially in soft rock. Required specimen sizes for other tests can be found in relevant ASTM or AASHTO standards provided in Appendix 1.

Specimens should generally be selected to be representative of the range of core quality that is recovered (something that can be qualitatively assessed using hardness tests described in Section 9.4.5). Unfortunately, there is often some bias introduced through the specimen selection process since poorer sections of rock may not produce segments of core that are of sufficient size for testing. Furthermore, the poorest segments of rock may not survive coring and be recovered at all. As such, there is a tendency for measurements to be made on the higher quality rock present, which tends to produce estimates of rock strength that may be greater than is truly appropriate. Bias issues are particularly challenging in weak rock. Some bias is presumably reflected in the rock mass classification and characterization described subsequently in this chapter, which includes effects of discontinuities and discontinuity condition. Nevertheless, it is important to recognize this potential source of bias when interpreting properties of intact rock.

### 9.4.7 Special Considerations for Degradable Rock

As described previously, special care is often required when sampling and testing weak and/or degradable rock because such rock can be difficult to core without severely damaging the rock and because the core may degrade quickly when exposed to atmospheric conditions. Special care for such rock core may include wrapping with plastic wrap and/or waxing the core when extracted from the core barrel to reduce the potential for moisture content changes that can intensify degradation. Such core should also be tested as quickly as possible after removal from the ground to limit the amount of degradation that can occur. Since degradation can often occur over short periods of time, it is often desirable to perform tests in the field. Special drilling fluids may also be required in some cases. Additionally, it is often desirable to directly evaluate the degradability of rock specimens using durability tests described in Chapter 4.

Some agencies have adopted special in situ test measurements for degradable materials in an attempt to reduce challenges associated with estimating strength for weak and/or degradable rock from laboratory tests. The Texas Department of Transportation has adopted the so-called "Texas Cone Penetrometer" test in such materials for this purpose. Other agencies have utilized a modified form of the Standard Penetration Test to develop estimates for properties for degradable materials. All such tests are indirect measurements that generally rely upon empirical correlations to produce estimates of engineering properties. Unfortunately, such tests often introduce substantial uncertainty into estimates of uniaxial compressive strength (Loehr, et al., 2013a). However, there may be little choice in some conditions since acquiring and testing intact samples can be problematic and challenging.

## 9.5 CHARACTERIZATION OF DISCONTINUITIES IN ROCK

As described in Section 9.2, the performance of geotechnical features constructed in, or on rock is dictated by the behavior of the rock mass, which in turn is dictated by characteristics of intact rock described in Section 9.4 and characteristics of discontinuities that are described in this section. As illustrated in Figure 9-2, discontinuity features that affect rock mass performance include:

- the type of discontinuity;
- geometric characteristics such as spacing, orientation, aperture (width measured perpendicular to the discontinuity), and persistence (discontinuity length);
- the number of distinct "sets" of discontinuities; and
- the condition of discontinuities including the roughness, type, and quantity of "infilling" materials, and the presence of seepage within discontinuities.

These characteristics, or surrogate measurements that are indicative of these characteristics, are generally acquired through measurements made on rock core acquired from boring and sampling at a site and through mapping of exposed rock at, or near the site.

### 9.5.1 Representation of Discontinuity Orientation

Because discontinuities are inherently three-dimensional, it is generally necessary to characterize the orientation of discontinuities in three dimensions. While a number of alternatives exist for mathematically representing three-dimensional surfaces, the most common approach adopted for describing discontinuity orientation is to use "strike" and "dip" or "dip" and "dip direction". As illustrated in Figure 9-17, "strike" refers to the plan orientation of a horizontal line passing through the plane of the discontinuity, generally reported as a compass bearing direction (e.g., S60W to refer to a line

bearing 60 degrees west of south) or as an azimuth direction measured from north (e.g., 240 degrees). "Dip" refers to the inclination of the plane from the horizontal, measured in the dip direction. "Dip direction" refers to the plan orientation of the dip vector that is aligned with the direction of maximum plunge and is perpendicular to the strike direction. All potential orientations of a plane can be completely represented by establishing strike and dip, or the dip and dip direction, for the plane.

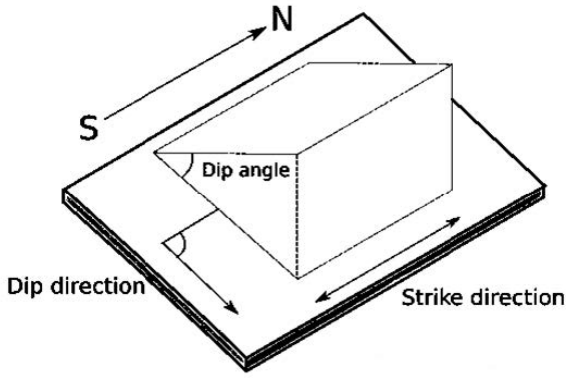


**Figure 9-17 Dip and Dip Direction for a planar feature**

Collective observation of the orientation of multiple discontinuities can be facilitated by plotting the discontinuities on a "stereo net". Different forms of stereo nets are available, each with different advantages and disadvantages (e.g., Wyllie and Mah, 1998; Wyllie, 1999). Figure 9-18 shows an example stereo net showing the orientation of discontinuities from a site in northern Minnesota. The symbols shown represent the measured orientation of 326 different discontinuities established using a borehole televiewer system described in Section 9.5.2. Inspection of the stereo net provides information that can help identify distinct sets of discontinuities as well as information regarding the variability of the discontinuity orientations. In the particular case shown, the stereo net indicates two distinct discontinuity sets: the first representing approximately horizontal discontinuities that are primarily associated with bedding planes, and the second representing predominantly vertical discontinuities induced by fracture of the intact rock.

### 9.5.2 Characterization of Discontinuities from Borehole and Rock Core Measurements

Some level of characterization of discontinuities in rock masses can be acquired through measurements made in boreholes or measurements made on rock core. However, borehole and rock core measurements can also be challenging because the coring process may introduce artificial ("drilling induced") fractures that are not representative of the in situ rock mass. Coring may also wash away infilling material, which makes characterization of the material difficult (although some indications of infilling can be gleaned

from careful observation of the drilling fluid). Despite these challenges, it is often possible to obtain measurements of apparent discontinuity spacing (measured in the direction of the borehole) from rock core and, in some cases, to acquire information about (and potentially small samples of) discontinuity infilling if it is not washed away during coring.

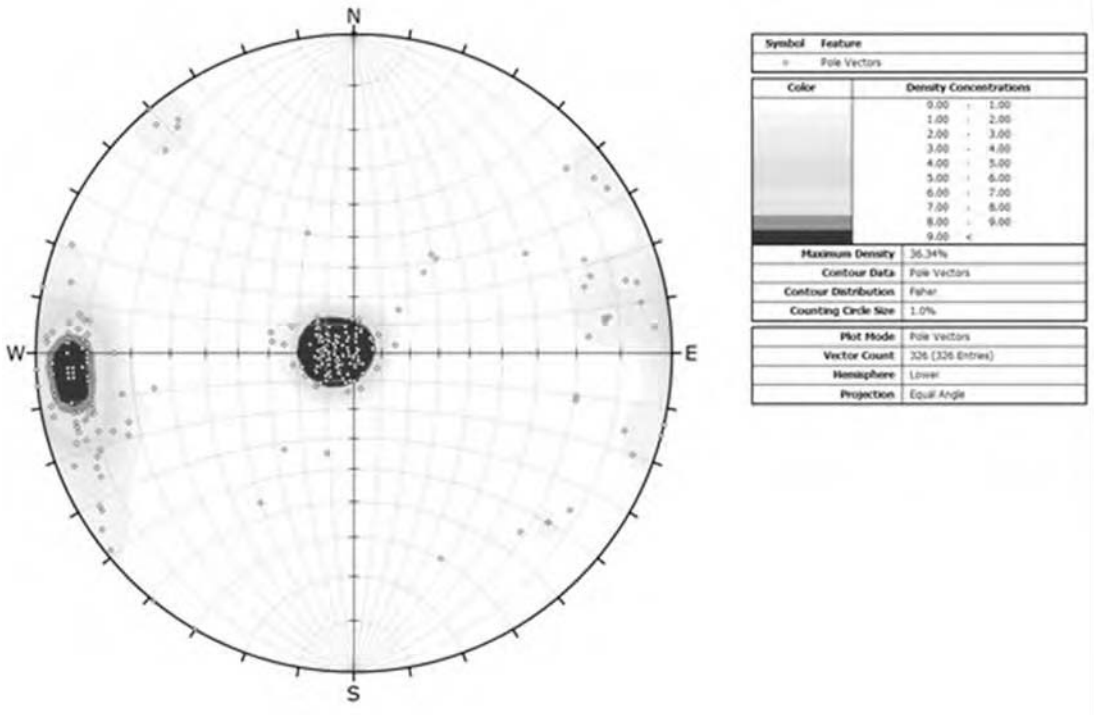


**Figure 9-18 Stereo net developed from acoustic televiewer measurements (courtesy of Dan Brown and Associates).**

It is generally more difficult to acquire measurements of discontinuity orientation from rock core because common coring methods do not maintain the orientation of the rock core. When orientation data is important, it is possible to perform "oriented coring" wherein downhole instrumentation can be used to establish the orientation of the borehole itself and some mechanical means can be used to "mark" the rock core so that the absolute orientation of the core, and discontinuities within the core can be maintained and measured. Such techniques are often challenging to implement in practice and potentially prone to error, but provide a means to acquire important information about discontinuity orientation when it cannot be acquired otherwise. Where possible, however, nearby outcrops of the same rock formations should be mapped as described in Section 9.5.3 to obtain a better assessment of rock mass characteristics.

Because of challenges associated with maintaining orientation during coring, it is more common to make surrogate measurements that are indicative of the general quality of the rock mass. The most common of such measurements are "core recovery" ($CR$), "rock quality designation" ($RQD$), and "fracture frequency"

($FF$) described in Chapter 4. While such measurements cannot be used to develop stereo nets like the one shown in Figure 9-18, they are common measures of rock mass quality that are frequently used for geotechnical design that is not sensitive to discontinuity orientation.

Fortunately, recent advances in development of several types of downhole viewers and associated data analysis software have largely resolved the long-standing challenge of determining discontinuity orientation from borehole measurements. Downhole viewers can be used to "map" the sides of the borehole following coring. Such surveys can be subsequently analyzed using largely automated methods to quickly and accurately produce measurements of discontinuities that are observed in the borehole walls. Figure 9-19 shows an example result from a downhole televiewer for a section of a borehole, complete with automatically generated information regarding the orientation and type of different discontinuities. The discontinuity orientations shown in Figure 9-19 are some of the orientations used to create the stereo net shown in Figure 9-18.

### 9.5.3 Characterization of Discontinuities from Mapping of Rock Exposures

Because of historical challenges associated with acquiring information about discontinuity orientation and condition from borehole and/or rock core measurements, it is common practice to use field "mapping" of discontinuities to support rock mass characterization. Field mapping is generally performed on exposed rock faces for the formations of interest located at or near the site of interest and generally includes making measurements of dip and dip direction for exposed discontinuities on the rock face. Additional characteristics of the discontinuities are also commonly measured including the aperture (width of discontinuity measured perpendicular to the discontinuity), spacing, infilling material, and any water flow. In some instances, samples of particularly important discontinuities, or infilling material may be taken for more refined characterization and/or laboratory testing. ISRM (1978) provides additional guidance on characterization of discontinuities.

Recent technological advancements are also influencing methods for characterizing discontinuities on exposed rock faces. Such advancements offer the promise for improving characterization of rock masses, for reducing the time required for field mapping, and therefore for improving the efficiency and accuracy of site characterization for rock masses. One example of such advancement is the potential to use remote sensing techniques to efficiently characterize discontinuities on exposed rock faces. Figure 9-20 shows an example of such efforts acquired using lidar measurements for an exposed rock cut. While such tools are currently not as well developed or as commonly used as the downhole tools described in Section 9.5.2, they do provide significant promise for future development and more widespread implementation.

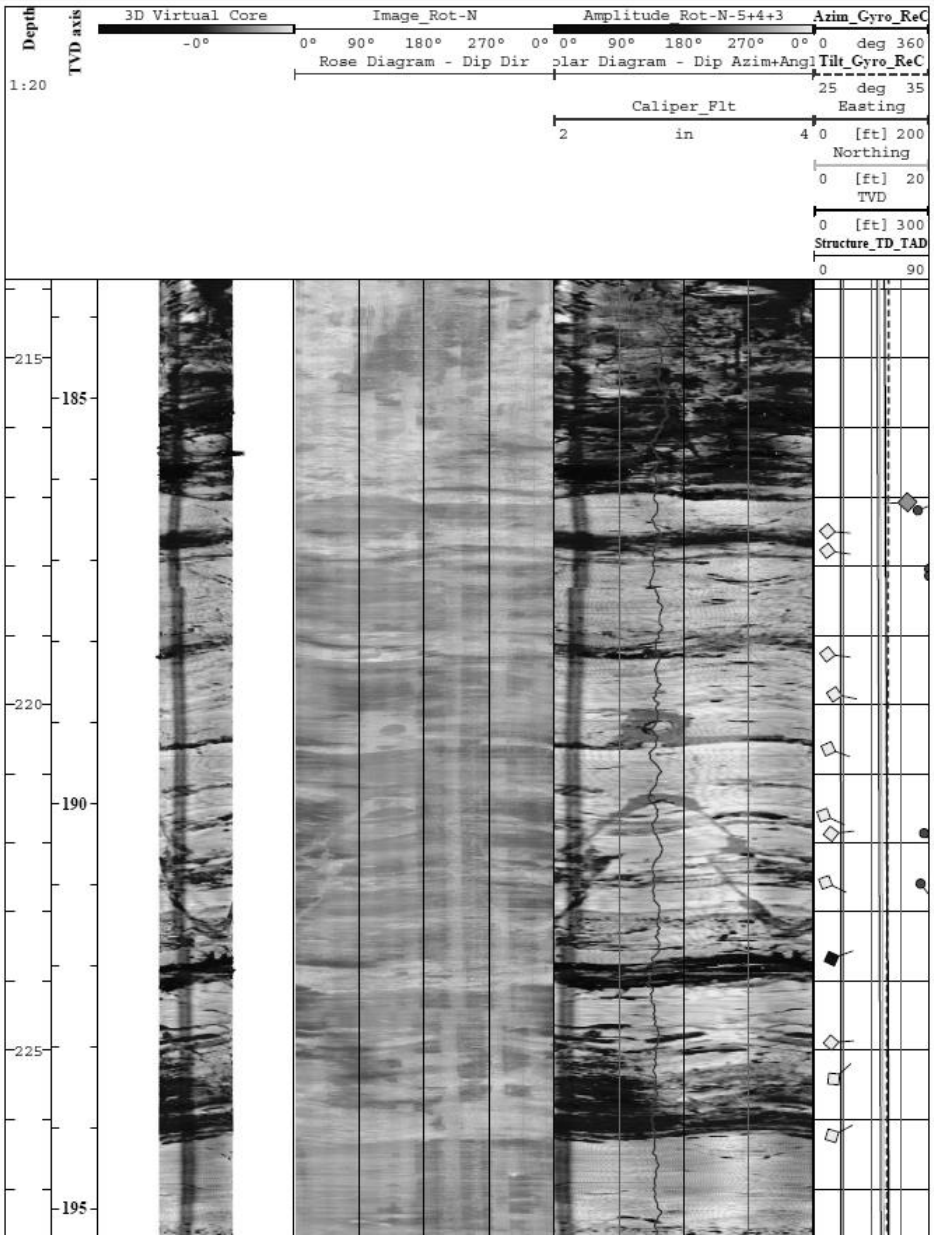


**Figure 9-19 Downhole televiewer measurements (courtesy of Dan Brown and Associates).**

Regardless of whether discontinuity orientation is derived using conventional mapping or using state of the art sensing techniques, consideration must be given to whether the observations are likely to be consistent with the conditions that exist in the ground at the specific site being considered (Marinos, et al., 2005). Rock mass conditions can change substantially over relatively short distances and elevations so measurements taken from "nearby" exposures should be interpreted with caution unless there is evidence to suggest that conditions are practically consistent. In addition, it is also possible for rock mass conditions at an exposure to differ from those beneath the ground, even if the exposure is located at the

specific site of interest, because of stress relief, weathering, or other forms of alteration. In most cases, such phenomena will produce less favorable indications of rock mass characteristics than is truly present underground and, thus, conservative indications of rock mass performance. While conservative bias is generally preferable to unconservative bias, excessively conservative indications of rock mass conditions may lead to costs for construction that are greater than is truly necessary. Fortunately, potential bias introduced because of unrepresentative conditions at rock exposures can generally be identified through combined consideration of both borehole measurements and exposures. Potential bias can sometimes also be identified using dedicated test pits or excavations since such exposures are less likely to be influenced by time dependent changes in the exposed rock. For design of excavated slopes in rock, however, data obtained from mapping rock outcrops may provide more reliable characterization of the long-term performance of proposed rock cuts.

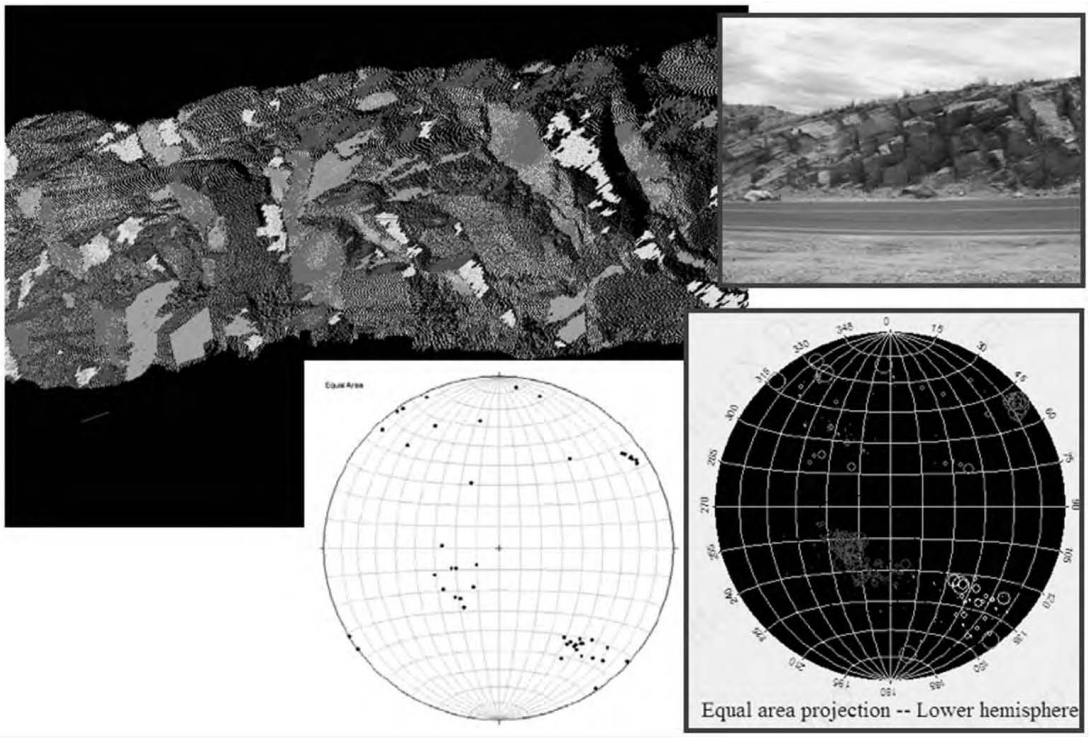


**Figure 9-20 Comparison of discontinuity orientation for exposed rock face from conventional mapping and automated lidar mapping (from Kemeny and Turner, 2008).**

### 9.5.4 Shear Strength of Rock Discontinuities

While geotechnical design in rock is often based on simple "kinematic" considerations or more general characterization of rock mass quality, there are instances where it is important to measure or estimate the shear strength of specific discontinuities. This is most commonly required for evaluation of rock slope stability, when joint orientation is unfavorable to stability. In most cases, the shear strength of

discontinuities is estimated from characteristics of the discontinuity. For rough, clean discontinuities without significant infilling, the shear strength can generally be expressed as (Wyllie, 1999):

$$s = c + \sigma' \tan(\phi + i) \tag{9.16}$$

where $s$ is shear strength, $c$ and $\phi$ are the Mohr-Coulomb shear strength parameters for the interface without asperities (i.e., representing the frictional resistance of a smooth interface), $\sigma'$ is the effective normal stress on the discontinuity, and $i$ represents the frictional resistance due to the roughness of the asperities. Based on measurements of artificial rough interfaces, Barton (1973) developed an empirical method for estimating the shear strength of discontinuities where shear strength is predicted as

$$s = \sigma' \tan\left(\phi + JRC \log_{10}\left(\frac{JCS}{\sigma'}\right)\right) \tag{9.17}$$

where $JRC$ is a joint roughness coefficient described in Section 9.5.5, $JCS$ is the compressive strength of the rock on the discontinuity surface, and $\sigma'$ is the effective normal stress on the discontinuity.

In cases where the strength of specific discontinuities is critical for design, the shear strength of specific discontinuities can be measured in the laboratory according to ASTM D5607 or in the field according to ASTM D4554. Laboratory tests are generally performed on sections of rock core that contain important discontinuities, which generally requires that specimens be cast within encapsulating material to hold the specimen in an appropriate orientation. Conversely, field tests generally require that some reaction is available so that appropriate normal stress can be applied. Both tests are relatively uncommon, and somewhat challenging to accurately conduct, but are available for instances where the frictional resistance of discontinuities is paramount for design and/or construction.

For discontinuities with infilling, the shear strength of the discontinuity may be controlled by the thickness and strength characteristics of the infilling material rather than the strength characteristics and roughness of the rock along the discontinuity. If such discontinuities are important for performance of a specific feature, the shear strength of the discontinuity should generally be measured or estimated conservatively. Wyllie (1999) provides additional considerations for estimating the shear strength of infilled discontinuities.

### 9.5.5 Surface Roughness

The frictional resistance of rock discontinuities is often dramatically influenced by the "roughness" of the discontinuity, with rougher discontinuities tending to have greater frictional resistance and greater dilation

than smooth discontinuities. In order to quantify the influence of roughness, Barton and Choubey (1977) proposed a series of ten different roughness profiles for discontinuities, shown in Figure 9-21, that serve as a reference scale for quantifying roughness and additionally assigned a series of Joint Roughness Coefficients ($JRC$) corresponding to each of the reference profiles. The value of $JRC$ can be used to estimate the shear strength of discontinuities using Equation 9.20. $JRC$ is also used as input for some rock mass classification systems as described in more detail in Section 9.6.

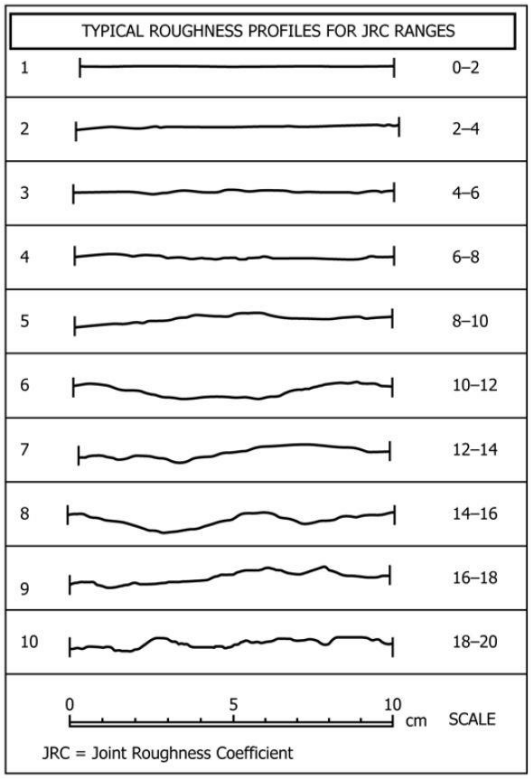


**Figure 9-21 Standard profiles for discontinuity roughness and the Joint Roughness Coefficient (after Barton and Choubey, 1977).**

The conventional means for measuring joint roughness is to use a carpenters profile gauge similar to that shown in Figure 9-22 to capture the roughness of a particular discontinuity and then to subsequently compare the trace of the discontinuity with the reference roughness classes shown in Figure 9-21. More recently, a number of investigators have proposed and evaluated use of several different electronic scanning methods (e.g., Hong, et al., 2006; Ficker and Martisek, 2015) to improve the precision and repeatability of roughness determinations. These scanning methods also permit capture of roughness in a three-dimensional sense, as compared to the simple two-dimensional characterization that is obtained using a profile gauge, and it is likely that such methods will eventually predominate determination of joint

roughness for rock mass classification. Wyllie (1999) describes several alternative means for measuring joint roughness for cases where roughness is critical for stability and performance.

**Figure 9-22 Profile gauge for measuring discontinuity roughness (courtesy of Controls Group).**

### 9.5.6 Discontinuity Infilling

In instances where rock discontinuities are filled with substantial amounts of infilling material, the performance of the discontinuity may be controlled more by characteristics of the infilling material than by characteristics of the intact rock that surrounds the infilling. In such cases, the characteristics of the infilling (especially the shear strength) may be measured by taking samples of the infilling material. Infilling material is often difficult to acquire from rock cores because the infilling is often washed away during coring. However, samples of infilling can often be acquired from exposed rock faces. In some cases, the quantity of infilling that can be acquired may restrict testing to simple index tests, whereas in other instances sufficient quantity and quality of infilling can be acquired for performing direct strength tests. In some cases, it may be appropriate to acquire samples of the discontinuity, with the infilling material, in which case direct shear tests can be performed on the entire discontinuity.

## 9.6 ROCK MASS CLASSIFICATION

For most transportation applications, geotechnical design and construction requires use of empirically established design and analysis procedures that rely on one of several rock mass classification systems. As such, rock mass classification system ratings often serve as an important and necessary input for design. In some cases, design is performed directly using ratings established from rock mass classifications, while in other cases design is performed using more fundamental engineering properties established from the classification system ratings. This section describes several rock mass classification systems that are commonly used for transportation applications. Subsequent sections of this chapter describe use of classification system ratings for establishing rock mass modulus and rock mass strength.

### 9.6.1 Alternative Rock Mass Classification Systems

Several systems for classification of rock masses have been developed (ASTM D5878). Two of the most widely used systems historically are the Rock Mass Rating ($RMR$) System (a.k.a. the Geomechanics Classification system) and the $Q$-system (a.k.a. the CSIR system after the Council for Scientific and Industrial Research that developed the system). Both systems were initially developed for application to design of tunnels. However, both systems have been adapted over time to address other applications. Design methods developed for other applications have also utilized these rating systems so that the ratings have become more generally applicable to design in rock. In addition, the same ratings have been used to address constructability issues such as borability, rippability, dredgability, and erodibility so that they also have many applications for construction. While both systems have proponents, the $RMR$ system is more broadly applicable for transportation applications and, as such, is generally preferred for most transportation applications.

More recently, the "Geological Strength Index", or $GSI$ system of rock mass classification was developed (Hoek, 1994; Hoek and Brown, 1997; Marinos and Hoek, 2000; Marinos and Hoek, 2001). The $GSI$ system is primarily intended for development of geotechnical design properties for rock masses, as opposed to being used directly for empirical design equations like the $RMR$ and $Q$ systems. However, because it is conceptually much simpler than previously developed systems and so broadly applicable for design, it has quickly become the recommended rock mass classification system for transportation applications.

Numerous other rock mass classification systems also exist (e.g., the Rock Structure Rating, or $RSR$ system, and the Unified Rock Classification System, $URCS$). However, such systems are generally developed for more restrictive applications and tend to be less widely adopted for U.S. transportation applications and, thus, are not presented here.

### 9.6.2 Rock Mass Rating ($RMR$) Classification System

The $RMR$ system primarily uses five basic parameters for classification of rock mass characteristics. A sixth parameter is sometimes used to help further assess issues of stability for specific problems. The $RMR$ system was originally intended for design of tunnels and mining applications, but has been extended to address design of excavated slopes and foundations in rock. The six parameters used to establish the $RMR$ value for specific sites include:

- Uniaxial compressive strength ($q_u$)

- Rock Quality Designation ($RQD$)
- Discontinuity spacing ($S$)
- Discontinuity condition
- Groundwater conditions
- Orientation of discontinuities

The rating is obtained by summing numeric values assigned for the first five components. Thus, $RMR$ is determined as

$$RMR = \sum_{i=1}^{5} R_i \tag{9.18}$$

where $R_i$ reflect the different components listed above and in Table 9-5. The sixth component, $R_6$, may be used to adjust the basic $RMR$ value depending on the specific type of feature (slope, foundation, tunnel) and the strike and dip of discontinuities relative to the orientation of the proposed feature. Values of $R_6$ range from 0 for the most favorable condition to as low as -60 for unfavorable discontinuity orientations for excavated slopes. Table 9-6 provides values for $R_6$ for tunnels, foundations, and slopes.

The $RMR$ system produces a value between 0 and 100, where 0 reflects very poor rock masses and 100 reflects excellent rock masses. The $RMR$ value is used to develop specific design parameters for specific design methods as described subsequently in this chapter. The $RMR$ system has been modified over the years as described in Bieniawski (1989), Hoek et al. (1995), and Wyllie (1999), among others.

### 9.6.3 Geological Strength Index ($GSI$) Classification System

The Geological Strength Index ($GSI$) system was more recently developed to provide a measure of rock mass quality for directly assessing the strength and stiffness of rock masses. The system is based on consideration of two fundamental characteristics that largely control the mechanical behavior of rock masses: the degree of interlocking of blocks of intact rock and the condition of discontinuity surfaces within the rock mass. Like the $RMR$ system, $GSI$ ratings range from 0 to 100. Greater ratings indicate higher quality rock masses with more tightly interconnected blocks, and tighter and rougher discontinuity surfaces; lesser ratings indicate poorer quality rock masses with more loosely interlocking blocks and/or poorer quality discontinuity surfaces. Experience with the GSI system since its initial development has demonstrated its general utility and effectiveness for a broad range of rock mass conditions. The $GSI$ system often seems more straightforward to apply for transportation applications and, thus, has increasingly been adopted since its initial development.

**Table 9-5 Rock Mass Rating ($RMR$) system of rock mass classification (from ASTM D5878, 2008).**

| PARAMETER | | | RANGES OF VALUES | | | | | | |
|---|---|---|---|---|---|---|---|---|---|
| 1 | Strength of intact rock material | Point-load strength index | >10 MPa | 4 -10 MPa | 2 - 4 MPa | 1 - 2 MPa | For this low range – uniaxial compressive test is preferred | | |
| | | Uniaxial compressive strength | >250 MPa | 100 - 250 MPa | 50 - 100 MPa | 25 - 50 MPa | 5-25 MPa | 1-5 MPa | <1 MPa |
| | Rating | | 15 | 12 | 7 | 4 | 2 | 1 | 0 |
| 2 | Drill core quality RQD | | 90% - 100% | 75% - 90% | 50% - 75% | 25% - 50% | < 25% | | |
| | Rating | | 20 | 17 | 13 | 8 | 3 | | |
| 3 | Spacing of discontinuities | | >2 m | 0,6 - 2 m | 200 - 600 mm | 60 - 200 mm | <60 mm | | |
| | Rating | | 20 | 15 | 10 | 8 | 5 | | |
| 4 | Condition of discontinuities | | Very rough surfaces. Not continuous No separation Unweathered wall rock. | Slightly rough surfaces. Separation < 1 mm Slightly weathered walls | Slightly rough surfaces. Separation < 1 mm Highly weathered walls | Slickensided surfaces OR Gouge < 5 mm thick OR Separation 1-5 mm. Continuous | Soft gouge > 5 mm thick OR Separation > 5 mm. Continous | | |
| | Rating | | 30 | 25 | 20 | 10 | 0 | | |
| 5 | Ground water | Inflow per 10 m tunnel length | None | <10 litres/min | 10-25 litres/min | 25 - 125 litres/min | >125 | | |
| | | Ratio joint water pressure / major principal stress | 0 | 0,0-0,1 | 0,1-0,2 | 0,2-0,5 | >0,5 | | |
| | | General conditions | Completely dry | Damp | Wet | Dripping | Flowing | | |
| | Rating | | 15 | 10 | 7 | 4 | 0 | | |

**Table 9-6 $RMR$ System parameter $R_6$ (from ASTM D5878, 2008).**

| Strike and dip orientations of joints | | Very favourable | Favourable | Fair | Unfavourable | Very unfavourable |
|---|---|---|---|---|---|---|
| Ratings | Tunnels | 0 | −2 | −5 | −10 | −12 |
| | Foundations | 0 | −2 | −7 | −15 | −25 |
| | Slopes | 0 | −5 | −25 | −50 | −60 |

Several methods are available for establishing appropriate values of $GSI$ for specific rock masses. The system was initially developed to be used based on qualitative descriptions of a rock mass, as illustrated in Figure 9-23. Use of the qualitative descriptions and diagrams for important characteristics of rock masses is generally straightforward to apply when observations of rock mass exposures are available and consistent with the precision with which rock masses can be practically classified. However, use of Figure 9-23 can be challenging when only borehole measurements are available.

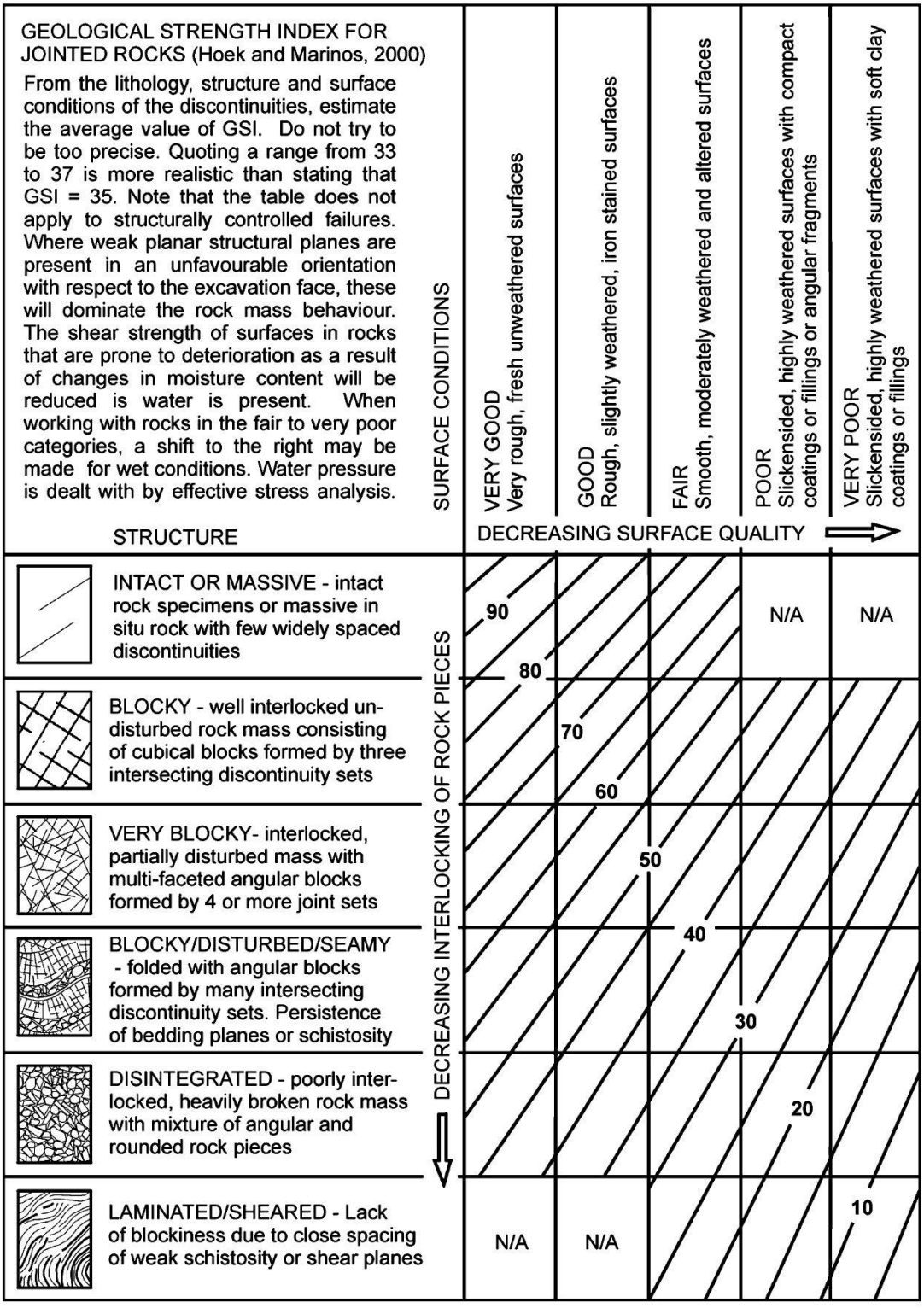


**Figure 9-23 Qualitative chart for estimation of geological strength index (GSI) in rock (from Marinos, et al., 2005).**

As an alternative to Figure 9-23, Hoek et al. (2013) proposed several alternative methods for establishing $GSI$ ratings based on quantitative measures of rock quality. The most practical of the quantitative means for establishing $GSI$ based on borehole measurements is to compute the rating as

$$GSI = 1.5 \cdot JCond_{89} + \frac{RQD}{2} \tag{9.19}$$

where $JCond_{89}$ is a joint condition rating established by Bieniawski (1989) and summarized in Table 9-7 based on criteria shown in Table 9-8. Alternatively, $GSI$ can be quantitatively established using a quantitative version of the $GSI$ chart shown in Figure 9-24 (Hoek, et al., 2013).

An alternative version of the $GSI$ chart, shown in Figure 9-25, was proposed by Marinos and Hoek (2001) for use with "heterogeneous" rock masses, such as those composed of alternating layers of harder and softer materials. This alternative chart is generally appropriate for use with rock masses that have been heavily altered, such as conditions consistent with the lower row of Figure 9-23 (Hoek, et al, 2013).

**Table 9-7 Definition of $JCond_{89}$ for estimating $GSI$ (Bieniawski, 1989; Hoek, et al., 2013)**

| Condition of Discontinuities | $JCond_{89}$ Rating |
|---|---|
| • Very rough surfaces<br>• Not continuous<br>• No separation<br>• Unweathered wall rock | 30 |
| • Slightly rough surfaces<br>• Separation < 1 mm<br>• Slightly weathered wall rock | 25 |
| • Slightly rough surfaces<br>• Separation < 1 mm<br>• Highly weathered wall rock | 20 |
| • Slickensided surfaces, or gouge < 5 mm thick, or Separation 1 – 5 mm<br>• Continuous discontinuity | 10 |
| • Soft gouge > 5 mm thick, or Separation > 5 mm<br>• Continuous discontinuity | 0 |

## 9.7 EVALUATION OF ROCK MASS MODULUS

Rock mass modulus can be an important input for geotechnical design in rock. As with most other design parameters considered in this manual, estimates for rock mass modulus can be obtained from several forms of direct measurements as well as through indirect means that are generally based on use of the rock mass ratings described in Section 9.6. In this section, several alternative means for measuring or estimating the modulus for rock masses are presented.

**Table 9-8 Guidelines for classifying discontinuity condition (Bieniawski, 1989; Hoek, et al., 2013)**

| Discontinuity Characteristic | Characteristic Value | Rating |
|---|---|---|
| Persistence (length) | < 1 m | 6 |
| | 1 to 3 m | 4 |
| | 3 to 10 m | 2 |
| | 10 to 20 m | 1 |
| | > 20 m | 0 |
| Separation (aperture) | None | 6 |
| | < 0.1 mm | 5 |
| | 0.1 to 1.0 mm | 4 |
| | 1 to 5 mm | 1 |
| | > 5 mm | 0 |
| Roughness | Very rough | 6 |
| | Rough | 5 |
| | Slightly Rough | 3 |
| | Smooth | 1 |
| | Slickensided | 0 |
| Infilling (gouge) | None | 6 |
| | Hard Infilling < 5 mm | 4 |
| | Hard infilling > 5 mm | 2 |
| | Soft infilling < 5 mm | 2 |
| | Soft Infilling > 5 mm | 0 |
| Weathering | Unweathered | 6 |
| | Slightly Weathered | 5 |
| | Moderately Weathered | 3 |
| | Highly Weathered | 1 |
| | Decomposed | 0 |

### 9.7.1 Evaluation of Rock Mass Modulus from in situ Test Measurements

Direct measurements of the rock mass modulus can be made using several different types of in situ test measurements. The most commonly used methods include the borehole dilatometer, borehole jack, plate load tests, and in situ seismic tests.

***Borehole Dilatometer***

The borehole dilatometer is similar to the pressuremeter used in soil in that a uniform radial pressure is exerted on the walls of a borehole using a flexible rubber sleeve. As the applied pressure is increased, the volumetric expansion of the borehole is measured by monitoring the inward flow of fluid or using electronic transducers that measure radial displacement inside the sleeve. Figure 9-26 shows typical borehole dilatometer measurements from a calibration chamber and in a rock mass.

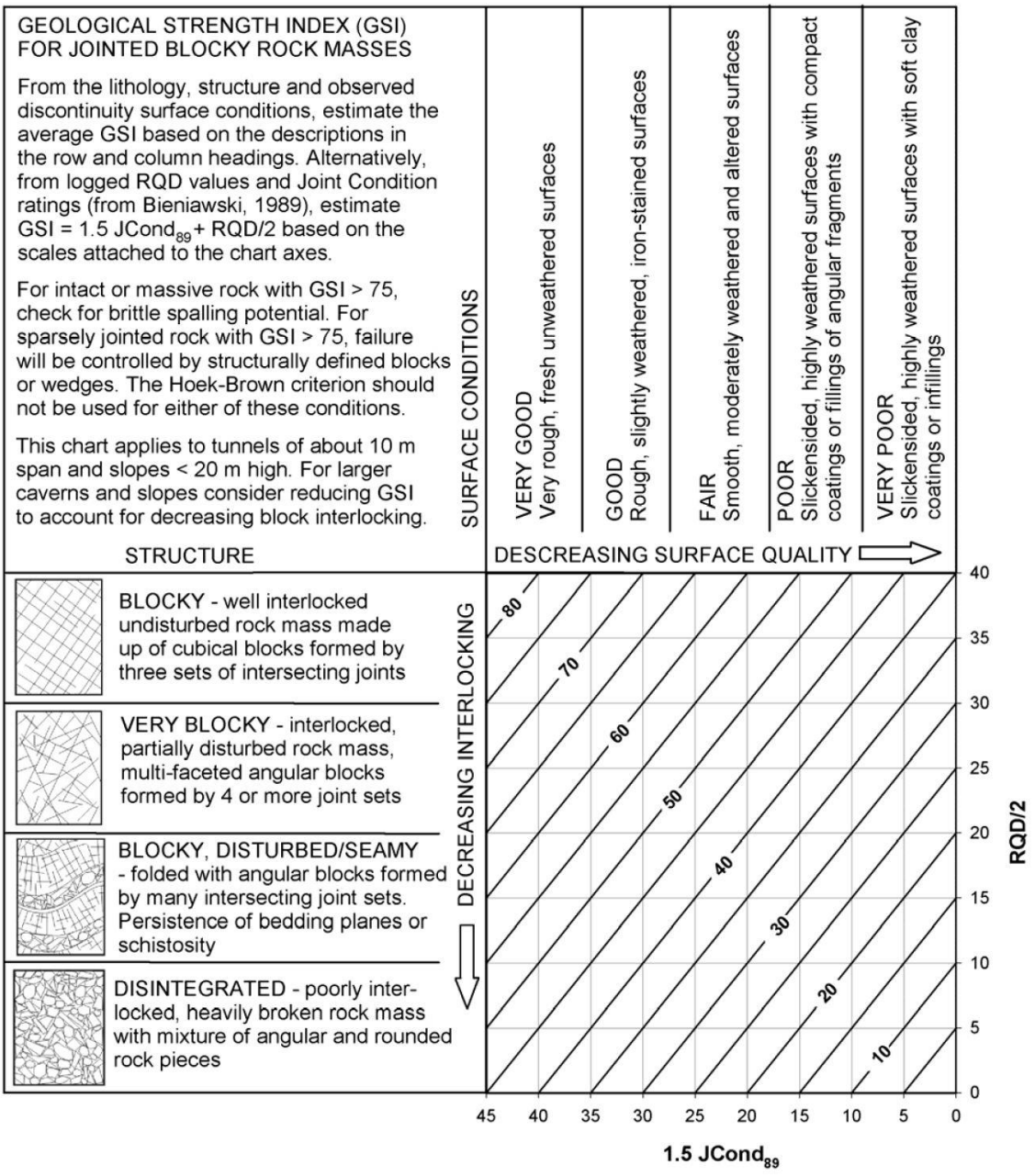


**Figure 9-24 Quantitative version of the geologic strength index (GSI) chart (from Hoek, et al., 2013).**

**Figure 9-25 Qualitative method for establishing GSI for heterogeneous rock masses (from Marinos, et al., 2005).**

From measurements like those shown in Figure 9-26, the shear modulus, $G_d$, and the modulus of elasticity, $E_d$, of the rock mass can be computed as (ISRM, 1987):

$$G_d = k_R \cdot \frac{\pi L d^2}{\rho} \tag{9.20}$$

and

$$E_d = 2(1 + \nu_R)G_d \tag{9.21}$$

where $L$ is the length of the cell membrane, $d$ is the diameter of the borehole, $\nu_R$ is Poisson's ratio of the rock, and $\rho$ is a pump constant defined as the fluid volume displaced per turn of the pump wheel. The term $k_R$ represents the stiffness of rock over the length of the membrane and is determine from:

$$k_R = \frac{k_s k_T}{(k_s - k_T)} \tag{9.22}$$

where $k_s$ is the stiffness of the hydraulic system and $k_T$ is the stiffness of overall system plus rock (ratio $D/C$ in Figure 9-26).

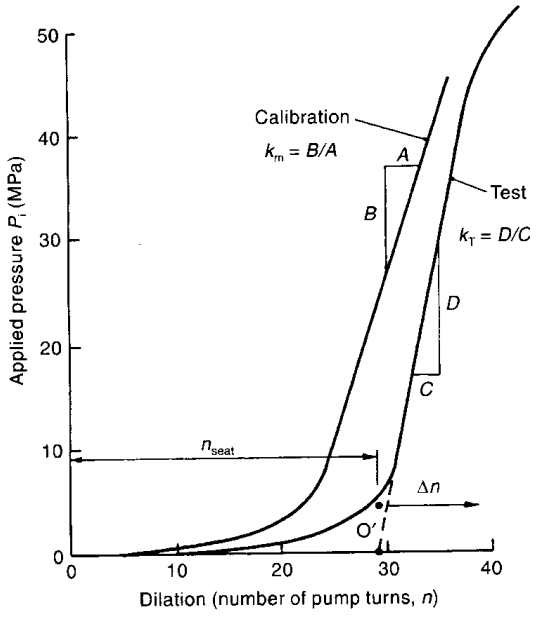


**Figure 9-26 Typical pressure-dilation graph for borehole dilatometer (after ISRM, 1987).**

Borehole dilatometer tests in rock masses are often more challenging than pressuremeter tests in soils because the stiffness of rock masses is generally much greater than soil and, therefore, is closer to the stiffness of the testing apparatus. As such, careful calibration is required to get meaningful measurements

of rock mass deformability. Wyllie (1999) provides additional details regarding required calibrations and challenges for borehole dilatometer tests.

***Borehole Jack***

The borehole jack (ASTM D4971) can be also used to evaluate rock mass modulus in a borehole and is often preferable to the dilatometer in stiff rock formations. The borehole jack is similar in concept to the dilatometer, but applies a directional pressure using steel loading platens rather than the flexible membrane used in the dilatometer. Deformations are measured with transducers built into the jack.

Figure 9-27 shows typical pressure-displacement measurements for a borehole jack test carried out in strong limestone. For the condition of full contact between the borehole jack and the borehole sidewall and for an assumed Poisson's ratio of 0.25, the calculated in situ rock mass modulus, $E_{calc}$, is given by

$$E_{calc} = \frac{1.24 \cdot JE \cdot \Delta Q_h}{\left(\frac{\Delta D}{D}\right)} \tag{9.23}$$

Where $JE$ is the jack efficiency ratio, $\Delta Q_h$ is the increment in hydraulic pressure, $\Delta D$ is the change in hole diameter resulting from application of $\Delta Q_h$, and $D$ is the initial hole diameter. Equation 9.26 varies depending on the assumed Poisson's ratio (see ASTM D4971). However, the effect of using different values for Poisson's ratio is relatively minor.

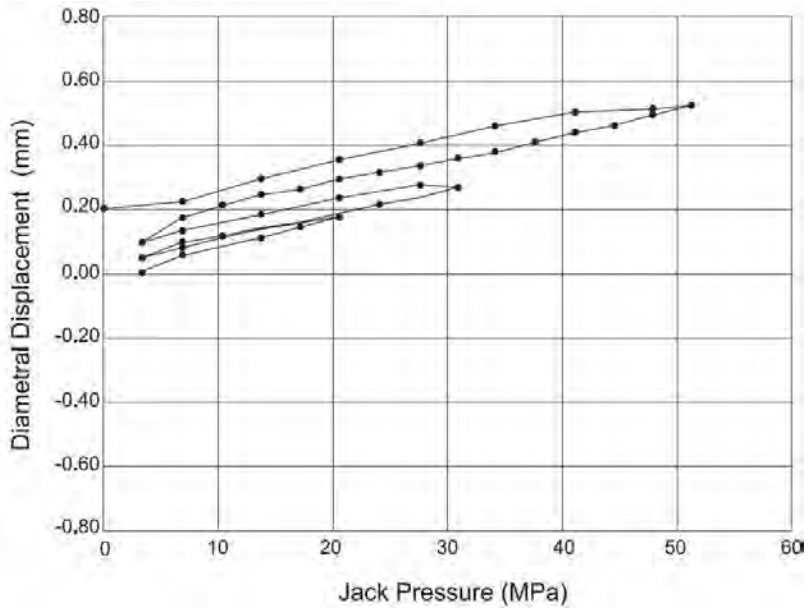


**Figure 9-27 Pressure-displacement plot for borehole jack.**

Calculated values of rock modulus from Equation 9.26 should generally be corrected using Figure 9-28 to account for variation in the ratio between the modulus of steel and the modulus of the intact rock. When the modulus of the steel is much greater than that of the intact rock, the correction factor is negligible because there is little deformation of the steel platens as the pressure is applied. However, when the intact rock modulus is substantially greater than the steel modulus, the modulus value calculated from the test is less than the "true" in situ rock mass modulus, $E_{true}$. In such cases, the rock mass modulus should be evaluated from Figure 9-28.

One issue with both borehole jack and borehole dilatometer measurements is that they both measure modulus in the horizontal direction whereas loading for most foundations is vertical. It is therefore important that consideration be given to possible anisotropy and the direction of anticipated loading.

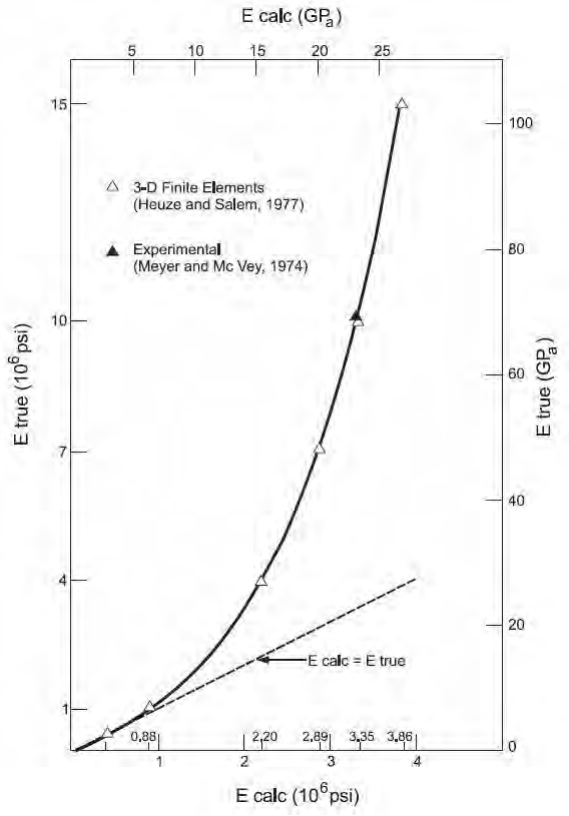


**Figure 9-28: Relationship between $E_{true}$ and $E_{calc}$ (after ASTM D4971).**

***Plate Load Tests***

The in situ modulus of rock masses can also be measured using plate load tests (ASTM D4394 and D4395). The fundamental premise of a plate load test is to apply load to the rock mass using a plate with known area and measure the deflection of the plate, and preferably the deformation of the rock mass

beneath the plate. Figure 9-29 shows a typical result from a plate load test. Because many rock masses are quite stiff, it can be difficult to develop sufficient reaction force to allow for loading to levels that are close to anticipated loading levels for the structure(s) being considered. To address this challenge, tests are often performed in small excavations or test adits so that jacks can react against the opposite site of the adit, although other forms of reaction can also be used (e.g., anchors and a reaction beam). Greater bearing pressures can also be achieved for a given load by using smaller bearing plates; however, it is important that the loaded area is large enough to engage the rock mass, including representative discontinuities, rather than intact rock within the rock mass.

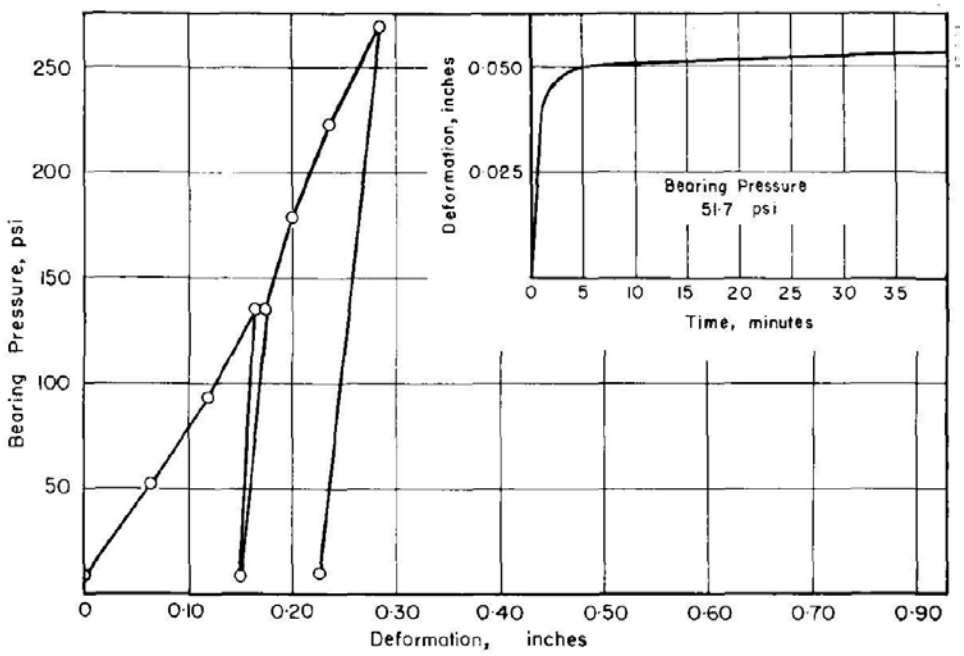


**Figure 9-29 Example plate load test result (from Coates and Gyenge, 1966).**

Calculations for the rock mass modulus from plate load tests vary depending on the specific devices used and measurements made. For a rigid, circular loading plate, the rock mass modulus can be calculated from deformations measured at the center of the plate as

$$E = \frac{(1-\nu^2)\cdot P}{2W_a \cdot R} \tag{9.24}$$

where $\nu$ is Poisson's ratio of the rock, $P$ is the total load on the plate, $W_a$ is the average deflection of the plate, and $R$ is the radius of the rigid plate. Alternative equations for different loading characteristics are described in ASTM D4394 and ASTM D4395.

***Seismic Velocity Measurements***

Rock mass modulus can also be determined from seismic velocities measured at the surface or in boreholes using methods described in Chapter 8. Laboratory methods, such as those described in Section 9.4.5, generally involve measurement of velocity through small intact specimens that correspond to the modulus of the intact rock. However, most field methods measure velocities through the larger rock mass, including the effect of discontinuities. For this reason, field methods will often yield much lower velocities than those measured for intact specimens in the lab.

Because laboratory measured velocities generally represent intact rock while field velocities generally represent the rock mass, the differences between laboratory and field-measured wave velocities can be used to infer information about rock quality such as $RQD$ and in situ modulus of deformation (e.g., Deere, et al., 1967; Coon and Merritt, 1970; Deere and Deere, 1989). For example, the relationship presented by Coon and Merritt (1970) between the "velocity index", $VI$, and $RQD$ is shown in Figure 9-30, where $VI$ is defined as the square of the ratio of in situ seismic velocities to laboratory sonic velocity. Low values of $VI$ correspond to a more fractured rock mass and hence lower $RQD$ values.

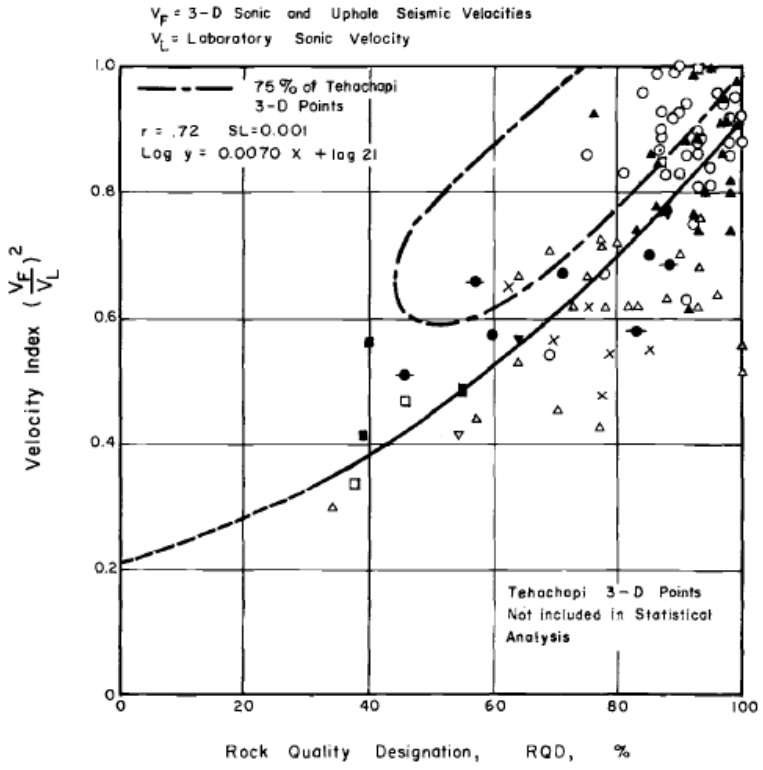


**Figure 9-30 Relationship between $RQD$ and Velocity Index (from Coon and Merritt, 1970).**

Seismic velocities measured in the field can also be used to provide guidance regarding equipment requirements for construction. Soft or highly fractured rock can generally be excavated using ripping equipment without the need for more elaborate excavation methods like blasting or cutting and in situ seismic velocities have been related to "rippability" to produce charts that can be used for construction planning. An example of a "rippablility" chart developed for a specific type of construction equipment is shown in Figure 9-31. Similar charts are available for other pieces of equipment. Seismic refraction measurements described in more detail in Chapter 8 are commonly effective for evaluation of constructability in this manner.

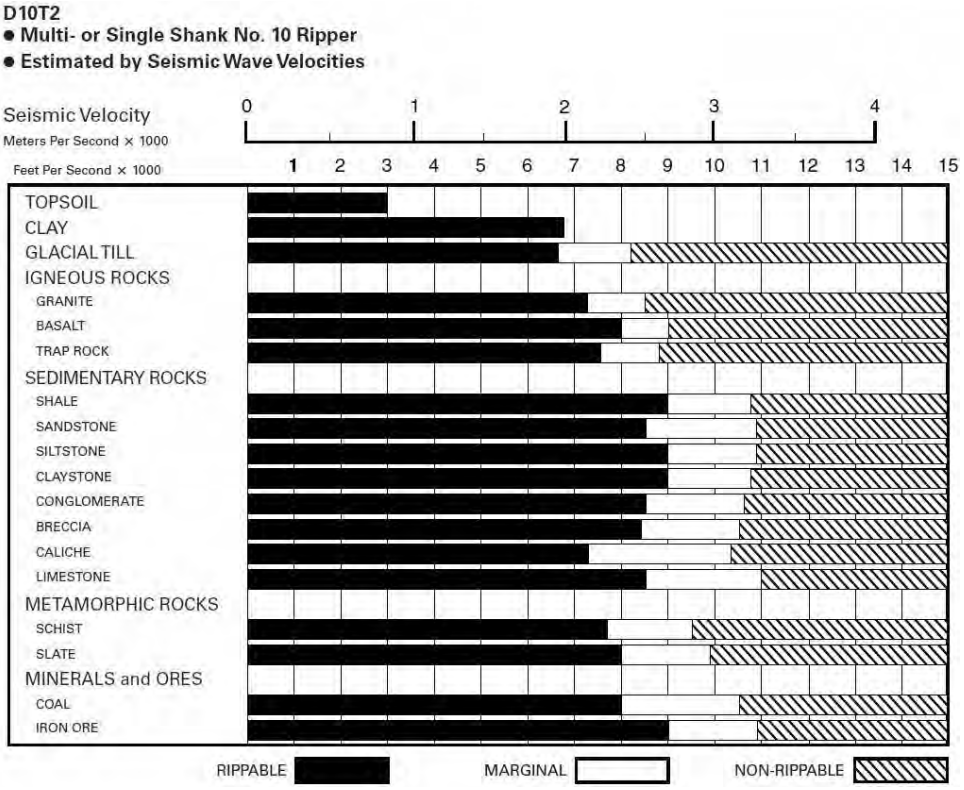


**Figure 9-31 Rippability chart for Caterpillar D10R ripper (Caterpillar, 2015).**

### 9.7.2 Estimation of Rock Mass Modulus from $RQD$

When in situ measurements of rock mass modulus are not available, it is possible to estimate rock mass modulus from information about rock mass quality. O'Neill et al. (1996) proposed an empirical method for evaluating the in situ rock mass modulus, $E_M$, based on measured values of $RQD$, measured or estimated values of the intact rock modulus, $E_R$, and a determination of whether discontinuities are open or closed. Table 9-9 shows recommended values of the ratio of $E_M$ to $E_R$ for different values of $RQD$. These values can be multiplied by measurements or estimates of the intact rock modulus to establish

estimates for the rock mass modulus. Values intermediate between the tabulated values may be obtained by linear interpolation.

**Table 9-9 Ratio of rock mass modulus to intact rock modulus (O'Neill, et al., 1996).**

| RQD (percent) | $E_M/E_R$ | |
|---|---|---|
| | Closed Joints | Open Joints |
| 100 | 1.00 | 0.60 |
| 70 | 0.70 | 0.10 |
| 50 | 0.15 | 0.10 |
| 20 | 0.05 | 0.05 |

### 9.7.3 Estimation of Rock Mass Modulus from Rock Mass Rating

Several empirical relations have been proposed to estimate values for rock mass modulus from values of $RMR$ established using the Rock Mass Rating system described in Section 9.6.2. Bieniawski (1978) recommended that the rock mass modulus, $E_M$, be estimated using the following linear relation

$$E_M = 2 \cdot RMR - 100 \quad \text{(in GPa)} \tag{9.25}$$

when $RMR$ is greater than 50. Serafim and Pereira (1983) subsequently considered a broader range of $RMR$ values and recommended that rock mass modulus be estimated as

$$E_M = 10^{\frac{(RMR-10)}{40}} \quad \text{(in GPa)} \tag{9.26}$$

Figure 9-32 shows the relations proposed by Bieniawski and by Serafim and Pereira along with empirical measurements. Both relations are practically consistent with empirical measurements for $RMR$ between approximately 55 and 85. The Bieniawski relation tends to predict values for $E_M$ that are lower than most observations for RMR less than 55, and to predict $E_M = 0$ for $RMR \leq 50$. Predicted values of $E_M$ from the Serafim and Pereira relation are more consistent with the observations shown for $RMR \leq 50$. In contrast, for $RMR$ greater than approximately 80 (i.e., "very good rock" according to the $RMR$ classification system), the Serafim and Pereira relation tends to over predict the empirical observations (especially when $RMR$ exceeds 90). Based on these observations, the Serafim and Pereira relation is generally preferable for rock masses with $RMR < 60$ while either relation is appropriate for $60 < RMR < 85$. For $RMR > 85$, considerable care should be adopted in applying either of the empirical relations since both relations predict values that exceed available empirical measurements. In such cases, designers might consider adopting an "upper bound" of the measured values of $E_M \approx 70$ GPa or, alternatively, assuming that the magnitude of the rock mass modulus, $E_M$, is equal to the magnitude of the

intact rock modulus, $E_R$. Alternative empirical relations proposed by others may also be considered (Hoek and Diederichs, 2006).

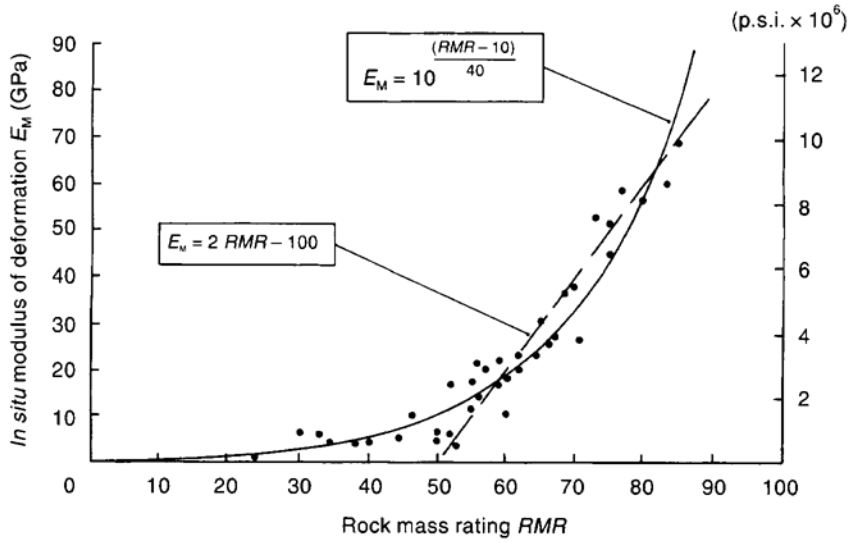


**Figure 9-32 Relation between $E_M$ and $RMR$ (after Bieniawski, 1978; Serafim and Pereira, 1983).**

### 9.7.4 Estimation of Rock Mass Modulus from Geological Strength Index

Hoek and Diederichs (2006) proposed an empirical method for estimating the value of rock mass modulus from $GSI$ based on empirical evaluation of a large collection of in situ test measurements. Two forms of equations were proposed: a "Simplified Hoek and Diederichs" relation and a more rigorous "Hoek and Diederichs" relation. The Simplified Hoek and Diederichs relation takes the form

$$E_M = 100{,}000\left(\frac{1-\frac{D}{2}}{1+e^{\left(\frac{75+25D-GSI}{11}\right)}}\right) \tag{9.27}$$

whereas the more rigorous Hoek and Diederichs relation has the following form

$$E_M = E_R\left(0.2+\frac{1-\frac{D}{2}}{1+e^{\left(\frac{60+15D-GSI}{11}\right)}}\right) \tag{9.28}$$

where $D$ is an empirical disturbance factor and $E_R$ is the modulus of the intact rock in the rock mass. The disturbance factor, $D$, is intended to account for disturbance imposed on the rock due to damage from blasting or stress relief. Values for $D$ range from 0 to 1, with $D = 0$ indicating no disturbance and $D = 1$ indicating substantial disturbance. Unfortunately, there is little direct guidance provided on selection of

appropriate values for $D$ for different applications. However, Hoek and Diederichs (2006) provide illustrative examples on selection of appropriate values for $D$.

The primary difference between the simplified and rigorous Hoek and Diederichs relations for rock mass modulus is that the rigorous relation requires an estimate of the value of the intact rock modulus whereas the simplified relation does not require such an estimate. Figure 9-33 and 9-34 respectively show comparisons of the two relations with the empirical data used to develop the relations for three different values of $D$. In general, the rigorous relation is significantly more reliable than the simplified relation and should be used when measurements of the intact rock modulus can be practically acquired.

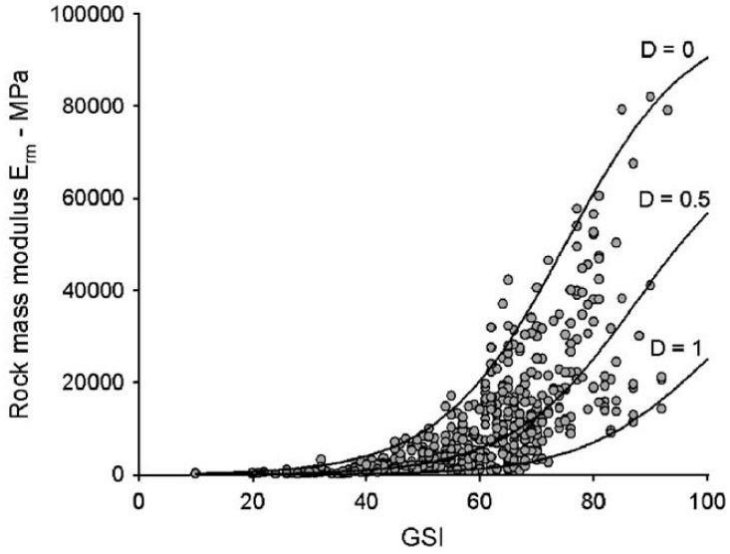


**Figure 9-33 Simplified Hoek and Diederichs (2006) relation for estimating $E_M$ from $GSI$.**

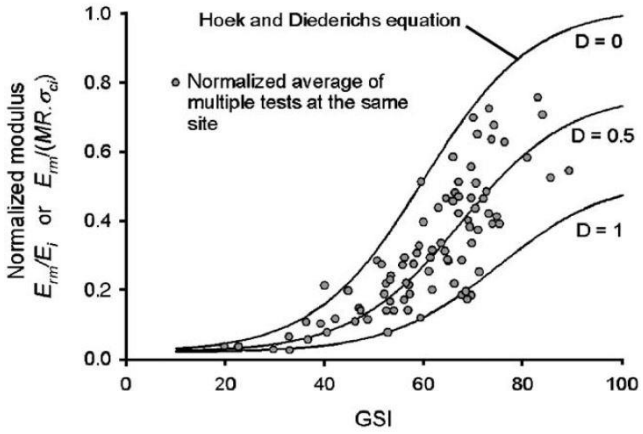


**Figure 9-34 Rigorous Hoek and Diederichs (2006) relation for estimating $E_M$ from $GSI$.**

While use of the $GSI$ system as a general rock mass classification system is fundamentally appropriate for rock masses with widely varying characteristics, the system was initially developed for establishing rational values for fundamental engineering properties for rock masses like rock mass modulus. When used for this purpose, it is important to consider the fundamental constraints and assumptions that were invoked in development of the equations. Foremost among these is that the rock mass is considered to be an isotropic collection of intact rock blocks. The implication of this assumption is that the behavior of the rock mass will not be controlled by one or two dominant discontinuities, but rather will be controlled by the collective response of a greater number of discontinuities. The decision about whether a specific rock mass can be considered to be isotropic is dependent on the scale of the feature being designed and the spacing of discontinuities in the rock mass. In general, the spacing of discontinuities should be less than approximately one-half of some characteristic dimension of the feature being designed for use of Equations 9.30 and 9.31 to be appropriate. Additional discussion of appropriate use of the $GSI$ system is provided in Marinos et al. (2005).

It should also be noted that discontinuity orientation will affect the rock mass modulus. For example, an unfavorably oriented, gouge-filled discontinuity with respect to settlement would be oriented in a direction at right angles to the loading direction resulting in closure of discontinuities and settlement. Conversely, an unfavorable orientation with respect to sliding for rock slope stability analyses would be in a direction parallel to the loading direction or inclined and dipping towards an open face.

## 9.8 EVALUATION OF SHEAR STRENGTH OF ROCK MASSES

When the performance of a rock mass for a particular application is control by distinct discontinuities, design must be performed with explicit consideration of the characteristics of individual discontinuities. In such cases, information regarding the shear strength of individual discontinuities as described in Section 9.5.4 is generally required for design. However, in many cases, the performance of the rock mass is governed by the collection of intact rock blocks that are formed by numerous discontinuities. In such cases, it is convenient and effective to model the rock mass using empirically established shear strength envelopes that reflect the response of the rock mass as described in this section. As described in Section 9.7.4, the decision about whether the rock mass can be modeled as an isotropic mass is scale dependent.

The most common model for representing the shear strength of fractured rock masses is the Hoek-Brown failure criterion. The model was originally published in 1980 (Hoek and Brown, 1980), and has since undergone several revisions (Hoek and Marinos, 2007) to produce the current version of the criterion published in 2002 (Hoek, et al., 2002). As illustrated in Figure 9-35, the Hoek-Brown failure criterion

represents shear strength as a curved envelope. The curved shear strength envelope reflects behavior where the blocks of rock are interlocked and the instantaneous friction angle is high at low confining (normal) stress levels whereas shearing of the intact rock is initiated at higher normal stress levels with the result that the friction angle is reduced. The instantaneous cohesion intercept progressively increases in proportion to the normal stress because of the greater confinement and interlocking of the rock mass.

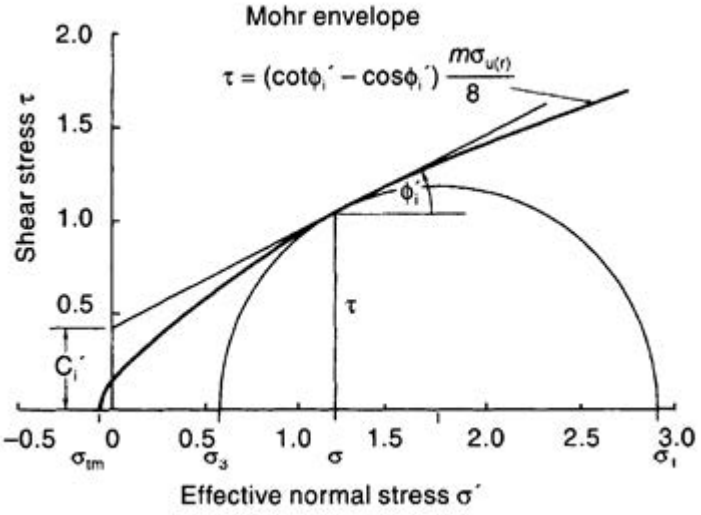


**Figure 9-35 Shear strength envelope defined by Hoek-Brown failure criterion (Hoek, 1983).**

The Hoek-Brown failure criterion is established in terms of the major and minor principal effective stresses, $\sigma_1'$ and $\sigma_3'$, as:

$$\sigma_1' = \sigma_3' + q_u \left( m_b \frac{\sigma_3'}{q_u} + s \right)^a \tag{9.29}$$

where $q_u$ is the uniaxial compressive strength of the intact rock, $m_b$ is a reduced value of a material constant $m_i$ that depends on rock type, and $s$ and $a$ are dimensionless constants that depend on the condition of the rock mass. The value for $m_b$ is computed as

$$m_b = m_i \cdot e^{\left(\frac{GSI-100}{28-14 \cdot D}\right)} \tag{9.30}$$

where the material constant $m_i$ is established from Table 9-10, $GSI$ is the geologic strength index, and $D$ is a disturbance factor, both described previously.

**Table 9-10 Values of material constant, $m_i$ (from Marinos and Hoek, 2001)**

| Rock type | Class | Group | Texture | | | |
|---|---|---|---|---|---|---|
| | | | Coarse | Medium | Fine | Very fine |
| SEDIMENTARY | Clastic | | Conglomerates (21 ± 3) Breccias (19 ± 5) | Sandstones 17 ± 4 | Siltstones 7 ± 2 Greywackes (18 ± 3) | Claystones 4 ± 2 Shales (6 ± 2) Marls (7 ± 2) |
| | Non-Clastic | Carbonates | Crystalline Limestone (12 ± 3) | Sparitic Limestones (10 ± 2) | Micritic Limestones (9 ± 2) | Dolomites (9 ± 3) |
| | | Evaporites | | Gypsum 8 ± 2 | Anhydrite 12 ± 2 | |
| | | Organic | | | | Chalk 7 ± 2 |
| METAMORPHIC | Non Foliated | | Marble 9 ± 3 | Hornfels (19 ± 4) Metasandstone (19 ± 3) | Quartzites 20 ± 3 | |
| | Slightly foliated | | Migmatite (29 ± 3) | Amphibolites 26 ± 6 | Gneiss 28 ± 5 | |
| | Foliated* | | | Schists 12 ± 3 | Phyllites (7 ± 3) | Slates 7 ± 4 |
| IGNEOUS | Plutonic | Light | Granite 32 ± 3 Diorite 25 ± 5 Granodiorite (29 ± 3) | | | |
| | | Dark | Gabbro 27 ± 3 Norite 20 ± 5 | Dolerite (16 ± 5) | | |
| | Hypabyssal | | Porphyries (20 ± 5) | | Diabase (15 ± 5) | Peridotite (25 ± 5) |
| | Volcanic | Lava | | Rhyolite (25 ± 5) Andesite 25 ± 5 | Dacite (25 ± 3) Basalt (25 ± 5) | |
| | | Pyroclastic | Agglomerate (19 ± 3) | Volcanic breccia (19 ± 5) | Tuff (13 ± 5) | |

NOTE: numbers in parentheses are estimates.

* Values for foliated metamorphic rock are for intact rock specimens tested normal to bedding or foliation. The value of $m_i$ will be significantly different if failure occurs along a weakness plane.

The dimensionless constants $s$ and $a$ are computed as

$$s = e^{\left(\frac{GSI-100}{9-3D}\right)} \tag{9.31}$$

$$a = \frac{1}{2} + \frac{1}{6}\left(e^{\left(\frac{-GSI}{15}\right)} - e^{\left(\frac{-20}{3}\right)}\right) \tag{9.32}$$

Equation 9.32 can be used directly for design with some commercial software. However, many common design methods are restricted to use of Mohr-Coulomb shear strength parameters, $c'$ and $\phi'$, that define a linear failure envelope. In such cases, Mohr-Coulomb strength parameters that approximate the Hoek-Brown criterion can be derived from Hoek-Brown parameters if an appropriate range in the minor principal effective stress is considered. For a range in minor principal effective stress extending from the tensile strength, $\sigma_t$, to a value of $\sigma'_{3-max}$, approximate Mohr-Coulomb shear strength parameters can be calculated as (Hoek, et al., 2002):

$$\phi' = \sin^{-1}\left[\frac{6am_b\left(s+m_b\frac{\sigma'_{3-max}}{q_u}\right)^{a-1}}{2(1+a)(2+a)+6am_b\left(s+m_b\frac{\sigma'_{3-max}}{q_u}\right)^{a-1}}\right] \tag{9.33}$$

$$c' = \frac{q_u\left[(1+2a)s+(1-a)m_b\frac{\sigma'_{3-max}}{q_u}\right]\left(s+m_b\frac{\sigma'_{3-max}}{q_u}\right)^{a-1}}{(1+a)(2+a)\sqrt{1+\frac{6am_b\left(s+m_b\frac{\sigma'_{3-max}}{q_u}\right)^{a-1}}{(1+a)(2+a)}}} \tag{9.34}$$

Figure 9-36 shows a comparison of the Hoek-Brown failure criterion with the approximate Mohr-Coulomb envelope. Hoek et al. (2002) provide guidance regarding estimation of $\sigma'_{3-max}$ for different geotechnical applications.

It should be noted that use of the $GSI$ system and the Hoek-Brown failure criterion may not be appropriate for extremely poor rock conditions (e.g., highly weathered and fractured rock). When such conditions are encountered, shear strength may be more reliably estimated considering the material to be a dense soil. Castelli et al. (2015) describe a case history involving extremely poor rock conditions and how appropriate shear strength properties can be established for such conditions.

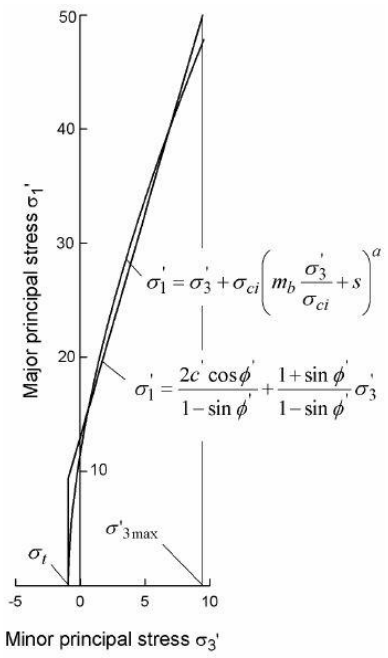


**Figure 9-36 Comparison of Hoek-Brown failure criterion with approximate Mohr-Coulomb envelope (from Hoek, et al., 2002)**

# CHAPTER 10
# MEASUREMENT AND INTERPRETATION OF GROUNDWATER CONDITIONS AND HYDRAULIC PROPERTIES OF SOIL AND ROCK

Groundwater conditions and groundwater flow through soil and rock are important aspects of transportation projects that can have dramatic, and often undesirable, impacts on construction and performance of transportation features (Boeckmann and Loehr, 2016). Groundwater conditions and flow may also greatly influence design. Accurate characterization of groundwater conditions and the hydraulic properties of soil and rock is therefore crucial to successful design, construction, and operation of many transportation facilities. This chapter addresses characterization of groundwater conditions from observations made during or after drilling of boreholes, from measurements made using monitoring wells or piezometers, and from in situ tests and geophysical measurements. Characterization of hydraulic conductivity for soil and rock using laboratory measurements, in situ field measurements, and correlations with other soil and rock properties is also described.

## 10.1 USES FOR HYDRAULIC PROPERTIES AND GROUNDWATER CONDITIONS FOR DESIGN AND CONSTRUCTION

Evaluation of groundwater conditions is an essential part of site characterization because groundwater conditions determine effective stresses that govern the performance of geotechnical features. Groundwater conditions are also needed to facilitate appropriate measurement and interpretation of geotechnical properties and design parameters. Finally, groundwater conditions may dramatically influence selection of appropriate means for below grade construction, and risks associated with such construction. The objectives of groundwater investigations for most transportation projects are to determine the location of groundwater, the magnitude of piezometric head in confined aquifers, and the direction and rate of groundwater flow. For projects where dewatering may be necessary, groundwater investigations must also characterize potential sources for groundwater flow (e.g., lakes/rivers, coasts, etc.), how stratigraphy affects groundwater flow, and the influence of pumping from wells. Some groundwater investigations may also include assessment of water quality and potential disposal or remediation options.

The nature of groundwater investigations is complex because of the interaction between geologic conditions at the site and the broader regional groundwater regime. It is important to understand that groundwater conditions are inevitably three-dimensional and time varying. The latter of these cannot be emphasized enough. The consequence of temporal variations in groundwater conditions is that

groundwater levels, and associated pore water pressures and groundwater flows, change with time because of changes in groundwater discharge and recharge. The most significant factors that drive changes in groundwater levels at most sites include seasonal variations in precipitation, withdrawal from local pumping, tidal fluctuations near shorelines, and fluctuations in stream/river levels.

Groundwater monitoring programs are usually developed to meet one or more of the following objectives:

1. Determine water levels and water pressures;
2. Determine water quality;
3. Characterize subsurface hydrogeology; and/or
4. Determine aquifer hydraulic characteristics.

To accurately interpret the hydrogeologic conditions at a site, and how those conditions vary over time, it is necessary to install monitoring equipment at the site so that water levels or water pressures can be measured over time. Most groundwater monitoring is conducted using either monitoring wells or piezometers that are installed in boreholes. It is generally necessary to install piezometers at a number of locations and at a number of depths, and to monitor conditions over some period of time. Ideally, piezometers should be located in each stratigraphic unit to allow the pore water pressure profile at a given location to be observed and to accurately determine the direction and rate of groundwater flow.

Hydraulic properties of soil and/or rock are generally used for analyses where predictions of groundwater flow and/or pore water pressure are necessary. For example, analyses might be performed to predict the quantity of flow into an excavation or to predict how construction of an embankment or roadway cut might change groundwater flow characteristics at a site. Such analyses can only be as accurate as the parameters used for the analyses, so accurate and reliable estimates for hydraulic properties are important in such cases. Hydraulic properties of soil and rock can be determined in several ways, including laboratory tests, in situ tests, and various forms of borehole flow tests as described in this chapter.

## 10.2 FUNDAMENTAL CONCEPTS OF SEEPAGE THROUGH SOIL AND ROCK

Groundwater flows from locations of higher hydraulic potential, or hydraulic "head", to locations of lower hydraulic head. Hydraulic head is generally composed of several components, as described by Bernoulli's equation:

$$h = h_e + h_p + h_v = h_e + \frac{u}{\gamma_w} + \frac{v^2}{2g} \qquad (10.1)$$

where $h$ is "total" hydraulic head, $h_e$ is elevation head measured relative to some selected datum, $h_p$ is "pressure" head, $h_v$ is "velocity" head, $u$ is pore water pressure, $\gamma_w$ is the unit weight of water, $v$ is velocity of flow, and $g$ is gravitational acceleration. The velocity of flow through most soil and rock is slow enough that the velocity head is small, and often neglected except for flow through clean gravel, clean coarse sand, and highly fractured rock with large, open discontinuities. Thus, the potential for flow through soil and rock is predominantly driven by elevation and pore water pressure.

### 10.2.1 Temporal Changes in Pore Water Pressures and Water Levels

Water levels and water pressures are known to change over time due to changes in hydraulic boundary conditions. The magnitude of fluctuations vary from site to site depending upon the regional groundwater regime, with some sites experiencing dramatic fluctuations over relatively short times and others experiencing relatively stable conditions. Figure 10-1 shows water levels (piezometric elevation) measured using standpipe piezometers over a period of 18 months at an alluvial site. At this site, water levels in shallow alluvial soils tend to fluctuate with the level of the nearby river whereas water levels for deeper rock strata are governed by artesian conditions from an unknown source. Total head profiles constructed from these measurements for several different dates are shown in Figure 10-2.

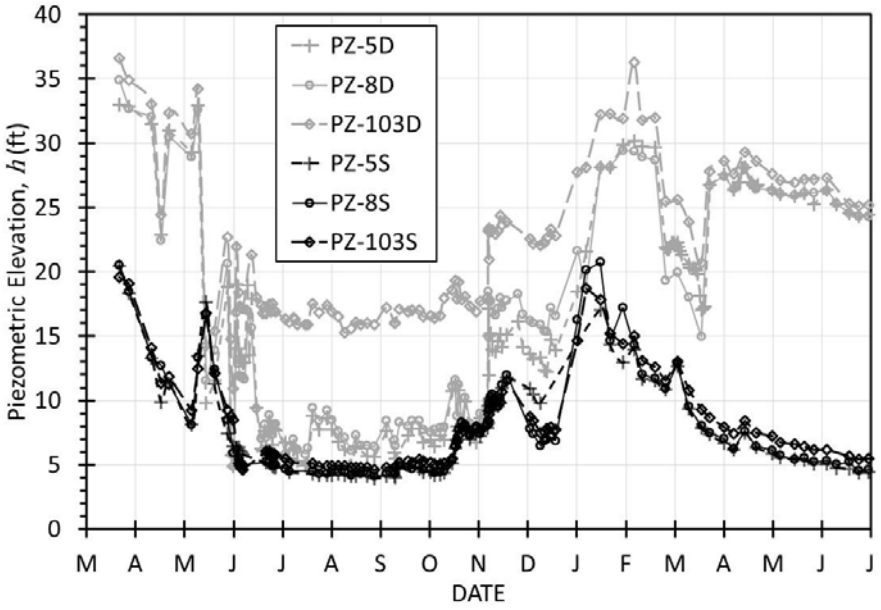


**Figure 10-1 Groundwater level fluctuations at an alluvial site.**

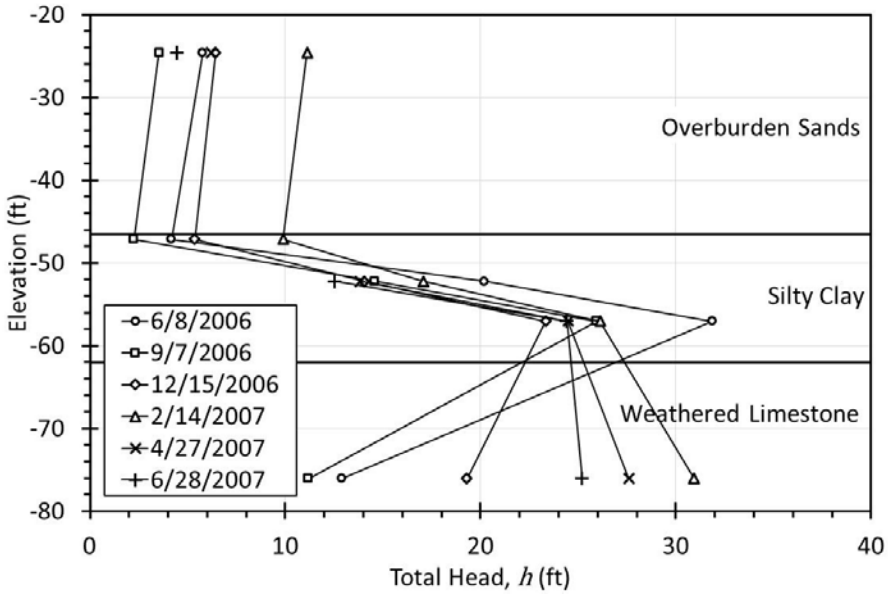


**Figure 10-2 Measured values of total head with depth from data in Figure 10-1.**

### 10.2.2 Water Flow and Hydraulic Conductivity

Flow of water through most soil or rock is governed by Darcy's Law, named after the French engineer Darcy who performed experiments on the flow characteristics of soil in the late 1700's. Considering the inclined cylindrical chamber filled with saturated soil shown Figure 10-3, the total head at any point within the soil may be obtained by inserting a simple standpipe and measuring the elevation of the top of the water column relative to a consistent, but arbitrary reference datum. Considering the two points shown in the figure separated by distance, $\ell$, the total head at the two points may be represented by $h_A$ and $h_B$, and the head loss between the two points is then given by $\Delta h = h_A - h_B$. The head loss between the two points arises from the fact that some energy is lost as the fluid flows through the soil.

Darcy performed laboratory experiments to evaluate the effect of changing $\Delta h$ and $\ell$ on the quantity of flow, or rate of discharge, $q$. He found that $q$ was directly proportional to $\Delta h$ for a given soil when $\ell$ was held constant, and inversely proportional to $\ell$ when $\Delta h$ was held constant. That is, if the cylinder of Figure 10-3 is rotated clockwise, causing $\Delta h$ to increase, the flow rate $q$ will increase. Similarly, if rotated counterclockwise, $\Delta h$ will decrease and $q$ will decrease. In fact, if held in a horizontal position such that $h_A = h_B$, then $\Delta h = 0$ and there will be no flow, and thus $q = 0$. On the other hand, if $h_A$ and $h_B$ are held constant, and the distance over which the flow takes place is decreased, the flow will increase. Similarly, if the flow path is increased while holding $\Delta h$ constant, the flow will decrease.

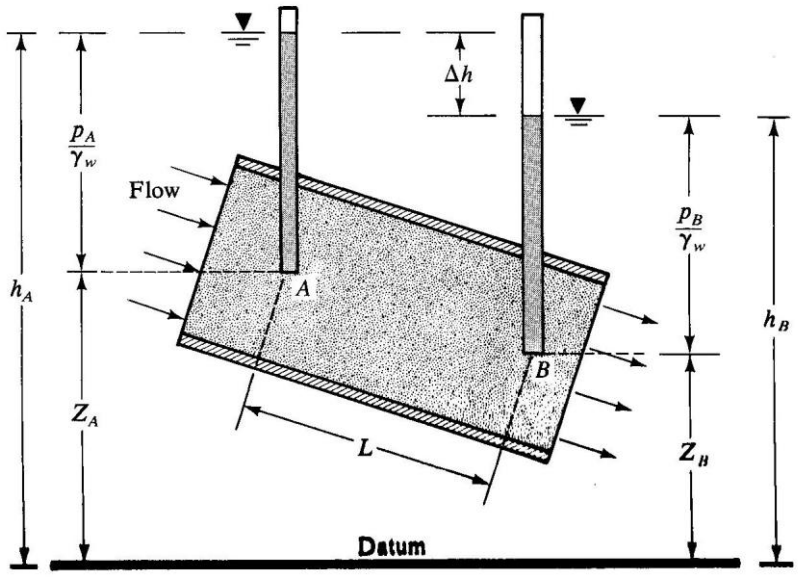


**Figure 10-3 Diagram illustrating Darcy's Law (from Das, 1985a).**

Darcy found that he could express his observations in the form of an empirical equation describing the flow rate, $q$, but also recognized that an additional term was required when he changed the nature of the porous medium:

$$q = k\frac{(h_A - h_B)}{\ell}A = kiA \tag{10.2}$$

where $k$ is a proportionality constant that depends on the nature of the porous medium, $A$ is the cross-sectional area of flow, and $i = (h_A - h_B)/\ell = \Delta h/\ell$ is hydraulic gradient. The units of flow rate, $q$, are volume of flow per unit time $[L^3/T]$. $k$ is usually referred to as the hydraulic conductivity and will generally be considered a soil property. In porous, open materials in which flow is almost unrestricted, $k$ will be high. In materials of low porosity that tend to restrict fluid flow, the value of $k$ will be low.

### 10.2.3 Fundamental Means for Measurement of Hydraulic Conductivity

Hydraulic conductivity can be directly measured in the laboratory or in the field. Details of specific laboratory and field tests are described in Sections 10.11 through 10.14. However, most tests fall into one of two main classes – constant head tests or falling head tests – and it is useful to describe fundamental differences between these two classes of tests at this point. Figure 10-4 shows schematics of the general setup of both constant head and falling head laboratory hydraulic conductivity tests.

In a constant head test, flow is initiated through a soil sample in a manner that keeps the total head difference between the inflow and outflow points constant as illustrated in Figure 10-4a. In practice,

constant level water baths or Mariotte devices are generally used to maintain constant water levels. Hydraulic conductivity is determined by measuring the volume of flow passing through the sample over some period of time. Since the length and area of the sample, and the difference in total head ($\Delta h$), are known, and the flow rate ($q$) is measured, the hydraulic conductivity is calculated as

$$k = \frac{q\ell}{\Delta h A} = \frac{Q\ell}{\Delta h A t} \tag{10.3}$$

where $Q$ is the total volume of flow and $t$ is the time over which the flow is measured.

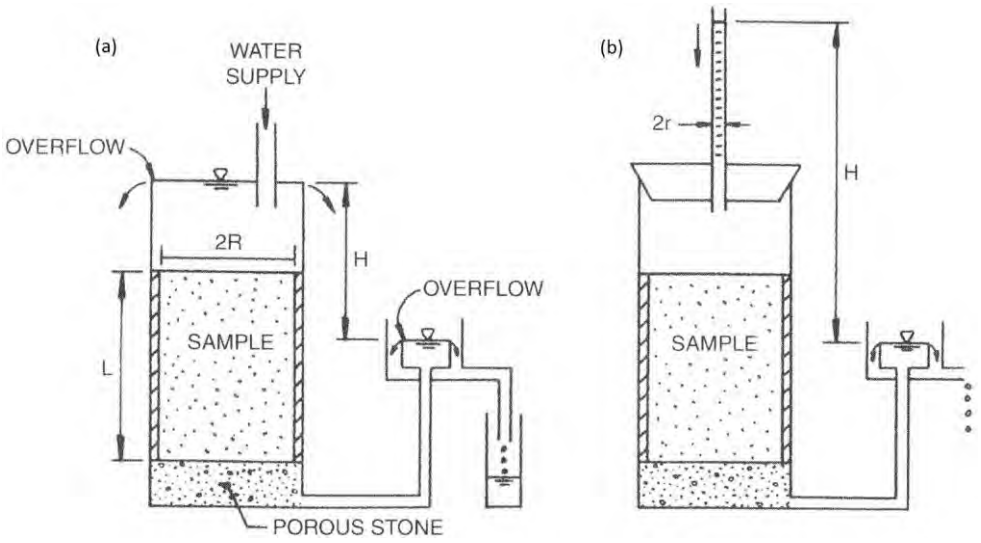


**Figure 10-4 Conceptual permeability tests: (a) constant head setup, and (b) falling head setup (from Sevee, 2006).**

In contrast, falling head tests are conducted by applying some initial head difference (gradient) across the specimen and observing the change in head difference that occurs as flow passes through the sample over some period of time. In a falling head test, the hydraulic conductivity is calculated as

$$k = \left[\frac{a\ell}{A\Delta t}\right] \ln\left(\frac{h_1}{h_2}\right) \tag{10.4}$$

where $a$ is the cross-sectional area of the inflow pipette or standpipe, $\ell$ is the specimen length in the direction of flow, $A$ is the cross-sectional area of the specimen measured perpendicular to the direction of flow, $h_1$ and $h_2$ are heads measured at two different times, and $\Delta t = (t_2 - t_1)$ is the elapsed time between measurements of head. Falling head tests are generally performed by taking a number of readings on the standpipe at various times and calculating $k$ for each pair of readings.

The primary advantage of constant head tests is that the test is conceptually simple and can be conducted using relatively simple and robust equipment. The primary disadvantage of the test is that it can take substantial time for a measurable quantity of flow to pass through many soil or rock specimens. Long testing times introduce problems associated with evaporation and temperature changes that can introduce errors into measurements of hydraulic conductivity. As such, constant head tests are generally only conducted on specimens with relatively high hydraulic conductivity (e.g., clean sands). Falling head tests can often be performed more quickly than constant head tests because it is not necessary to wait for a measurable quantity of flow to pass through the specimen; instead it is only necessary for a measurable change in head to occur, which can be controlled using pipettes of different diameter.

Similar concepts to the constant head and falling head tests are also adopted for many field tests. However, flow conditions are often more complex for field tests and it is necessary to use alternative expressions, or even numerical methods, to appropriately represent flow conditions that are two- or three-dimensional. In such cases, the fundamental approach of collecting measurements of flow and total head that allow $k$ to be calculated from an appropriate groundwater flow theory or model is still maintained. Equations for several specific field tests are provided in subsequent sections of this chapter.

## 10.3 BORING AND SAMPLING REQUIREMENTS

Boring and sampling requirements for observing groundwater conditions and determining hydraulic conductivity for soil and rock are largely consistent with requirements for other purposes, with a few special considerations. High quality, "undisturbed" samples are necessary for laboratory measurement of hydraulic conductivity for soil or intact rock. Careful sampling should be adopted to avoid "smearing" that may artificially limit flow and reduce measured hydraulic conductivities compared to what is truly appropriate in the field. If smearing is suspected, specimens for laboratory testing should be carefully trimmed. Larger sample sizes than are commonly required for strength and compressibility testing are also often desirable because hydraulic conductivity of some soil and intact rock can be dominated by small cracks and fissures that may not be present in smaller samples. This is especially true in fractured rock, which as a practical matter cannot be accurately replicated in laboratory tests, so field tests are commonly adopted in such formations.

Borehole testing is a suitable means to address challenges associated with obtaining representative samples for laboratory testing. However, care is still required to avoid artificially influencing the borehole measurements. Use of mineral slurries for borehole stability should generally be avoided in borings where hydraulic tests will be performed because such slurries form a "filter cake" that will often

influence field measurements. Instead, "clean" drilling methods (e.g., casing, hollow stem augers, using clean water as drilling fluid) should be adopted.

## 10.4 EVALUATION OF GROUNDWATER CONDITIONS FROM OBSERVATIONS DURING DRILLING

Important indications about groundwater conditions can be obtained from careful observations during and after drilling of boreholes. Useful observations during drilling generally include visible indications of changes in moisture content, changes in color of the drilling fluid or the soil, and sudden gains or losses of circulation fluid. Such observations should be documented in field boring logs and included in final boring logs. The depth of the borehole and the depth of any casing or hollow stem augers at the time observations are made should also be recorded. Observations of borehole fluid levels should also be recorded at the end of drilling (before drilling tooling is removed), after removal of drilling tools, after prolonged interruptions to drilling, and at one or more intervals after completion of a borehole (e.g., 24 hours, 48 hours).

While observations made during or after drilling provide indications of groundwater levels that may be helpful for interpretation of groundwater conditions, such observations may be heavily influenced by drilling procedures and other factors and are prone to misinterpretation. Borehole water levels following drilling will often change substantially with time as the water level in the borehole seeks to come to equilibrium with surrounding water levels. In silts and clays, such changes may require several hours, days, or even weeks depending on the hydraulic conductivity of the formation. In some fine-grained soils with low hydraulic conductivity, boreholes may even be "dry" shortly after drilling and show no groundwater level at all. In some cases, boreholes may collapse after the drill tooling is removed. In sands below the water table, the depth to the caved condition may be inferred as an approximate location of the groundwater level; however, in clayey soils such collapse may lead to erroneous indications of water levels. Finally, and most importantly, even if borehole water levels accurately represent conditions in the formation, such levels only represent an indication of groundwater levels at a single point in time and provide no indication of how significantly groundwater levels may change over time. Long-term observations are therefore needed to obtain an accurate indication of groundwater conditions. Such observations should be acquired using either monitoring wells or piezometers.

## 10.5 INVESTIGATION OF GROUNDWATER CONDITIONS USING MONITORING WELLS

Observations from monitoring wells are often used to determine groundwater levels at a site. As shown in Figure 10-5, a monitoring well is usually composed of an open pipe installed in a drilled hole that is

equipped with a screened section to allow water to enter the pipe and come to equilibrium with groundwater levels in the surrounding formation. The screened length may vary but commonly extends over most of the length of the borehole, or at least over the range of depths where the groundwater level is expected to fluctuate. Monitoring wells are effective for monitoring groundwater conditions at sites where groundwater conditions are largely hydrostatic (i.e., no flow) or where flow is unconfined and consistent throughout all strata. Monitoring wells are not useful for confined flow conditions where hydraulic head differs within different strata, and may produce erroneous indications of groundwater conditions when groundwater flow is complex. In such cases, piezometers should be installed within the different strata to allow groundwater conditions to be accurately observed. Monitoring wells are also commonly installed to allow for groundwater sampling, especially in situations where hydrocarbon contamination from gasoline or other light fluids is suspected since these fluids float on the water surface.

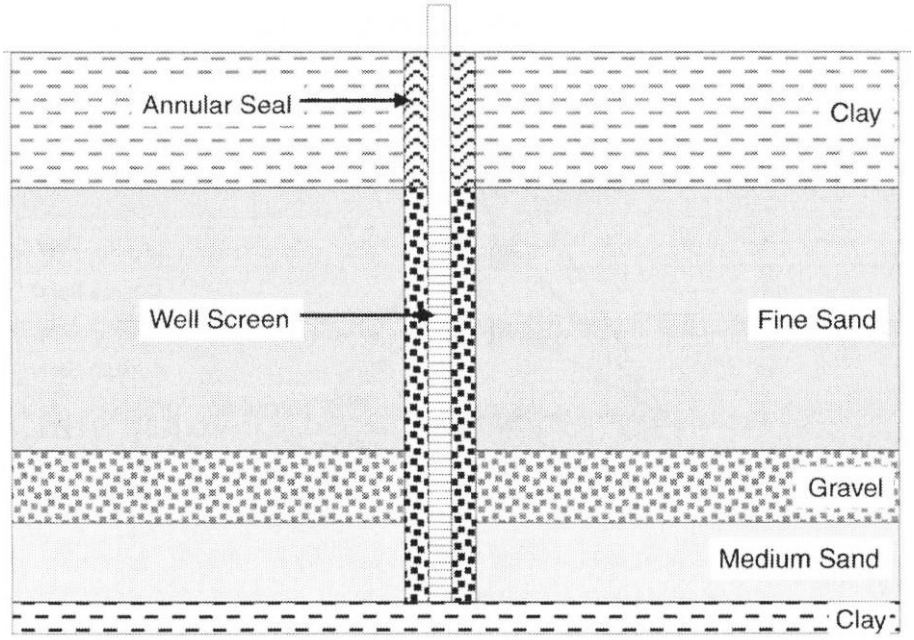


**Figure 10-5 Typical monitoring well (from Nielsen and Schalla, 2006).**

ASTM Standard Practice D5092 provides recommendations for design and installation of groundwater monitoring wells. Key features of monitoring wells that must be established from site and project specific information include the size of the well pipe and borehole, the size of the slots, and characteristics of the filter pack backfill. Monitoring wells may be constructed using PVC, HDPE, Teflon, fiberglass, or stainless steel pipe. Monitoring well pipe diameters typically vary from 1 to 8 inches depending on the conductivity of the formation and whether groundwater sampling is required. Larger diameter boreholes and pipes allow for insertion of various balers, pumps, or instrumentation, but take more time to respond

to changes in groundwater levels in some formations. Smaller diameter boreholes and pipes will generally respond more quickly.

The screened section of monitoring wells is surrounded with a clean, granular "filter pack" that serves to prevent particles from the formation from migrating into the well and potentially clogging the screen. The filter pack and screen slots must be selected to respectively filter the formation and the filter pack materials while still providing adequate conductivity to avoid substantial head loss through the filter pack and screen (which would mean that the well would not come to equilibrium with fluctuating groundwater levels in the surrounding formation). The size of slots in the well pipe should be selected to be compatible with the grain size of the filter pack material, which in turn must be appropriate for the grain size distribution of the surrounding formation. In most cases, a clean, washed silica sand is used as the filter pack. Table 10-1, taken from ASTM D5092, gives recommended filter pack characteristics for common screen slot sizes. A commercial filter fabric may also be placed around the screen and secured with plastic ties to prevent clogging from fines. An annular isolation seal is installed immediately above the filter pack to prevent surface water from entering around the well and inadvertently affecting groundwater level measurements.

**Table 10-1 Recommended filter characteristics for common screen slot sizes (ASTM D5092, 2010).**

| Slot No. | Size of Screen (mm) | Mesh Size Name | $D_1$ (mm) | $D_{10}$ (mm) | $D_{30}$ (mm) | $C_u$ | Roundness (Powers Scale) |
|---|---|---|---|---|---|---|---|
| 5 | 0.125 | 100 | 0.09-0.12 | 0.14-0.17 | 0.17-0.21 | 1.3-2.0 | 2-5 |
| 10 | 0.25 | 20-40 | 0.25-0.35 | 0.4-0.5 | 0.5-0.6 | 1.1-1.6 | 3-5 |
| 20 | 0.50 | 10-20 | 0.7-0.9 | 1.0-1.2 | 1.2-1.5 | 1.1-1.6 | 3-6 |
| 30 | 0.75 | 10-20 | 0.7-0.9 | 1.0-1.2 | 1.2-1.5 | 1.1-1.6 | 3-6 |
| 40 | 1.0 | 8-12 | 1.2-1.4 | 1.6-1.8 | 1.7-2.0 | 1.1-1.6 | 4-6 |
| 60 | 1.5 | 6-9 | 1.5-1.8 | 2.3-2.8 | 2.5-3.0 | 1.1-1.7 | 4-6 |
| 80 | 2.0 | 4-8 | 2.0-2.4 | 2.4-3.0 | 2.6-3.1 | 1.1-1.7 | 4-6 |

## 10.6 INVESTIGATION OF GROUNDWATER CONDITIONS USING PIEZOMETERS

Piezometers are generally the most reliable means for determining groundwater conditions at a site. In contrast to monitoring wells, piezometers are devices that are sealed within the ground to respond only to the hydraulic head near to the piezometer depth and not to hydraulic head at other elevations. Depending on the specific type of piezometer used, piezometers may or may not allow access for groundwater sampling. Piezometers are used to determine groundwater pressure (or pressure head) at a specific location. Measurements from several piezometers can be used to establish profiles of groundwater pressure (or head) with position or to determine hydraulic gradients and flow directions.

A number of different types of piezometers may be used, from simple open standpipe piezometers to more complex pneumatic, vibrating wire, and fiber-optic transducer piezometers. Table 10-2 summarizes advantages and limitations of several common types of piezometers. Only open standpipe piezometers allow access for groundwater samples to be taken, but these result in longer response time for measuring water pressures. Additional descriptions of the different types of piezometers are provided in the remainder of this section.

**Table 10-2 Instruments for measuring groundwater pressure (modified from Dunnicliff, 1993).**

| Instrument Type | Advantages | Limitations |
|---|---|---|
| Observation (Monitoring) Well | • Simple construction<br>• Easily installed by drillers<br>• Inexpensive | • Provides undesirable vertical connection between strata and can be misleading |
| Open Standpipe Piezometer | • Reliable<br>• Simple construction<br>• Inexpensive<br>• Successful performance record<br>• Can sample groundwater<br>• Can be used to measure *k* | • Potential for long time lag<br>• Filter section can plug from repeated inflow/outflow of water |
| Twin-Tube Hydraulic Piezometer | • Inaccessible components have no moving parts<br>• Reliable<br>• Successful performance record<br>• Piezometer cavity can be flushed<br>• Can be used to measure *k* | • Elaborate terminal connections needed<br>• Periodic flushing may be required<br>• Attention to many details required<br>• Tubing must be significantly above minimum piezometric elevation |
| Pneumatic Piezometer | • Short lag time<br>• Calibrated part of instrument accessible<br>• No freezing problems | • Attention to details required<br>• May deteriorate over time<br>• May need to be backflushed to dry out<br>• Generally requires manual reading |
| Vibrating Wire Piezometer | • Easy to read<br>• Short lag time<br>• Minimal lead wire effects<br>• Can measure negative water pressure<br>• No freezing problems | • Special manufacturing needed to minimize zero shift |
| Bonded Electrical Resistance Piezometer | • Easy to read<br>• Short lag time<br>• Can measure negative water pressure<br>• No freezing problems | • Low electrical output<br>• Lead wire effects<br>• Long-term stability uncertain<br>• Errors from moisture, temperature |
| Multipoint Piezometer | • Provides detailed pressure-depth measurements at a single location<br>• Simple installation | • Difficult to construct individual filter pack and isolation seal |
| Multipoint Push-In Piezometer | • Provides detailed pressure-depth measurements at a single location<br>• Simple installation | • Limited number of measurement points |

### 10.6.1 Standpipe Piezometers

Standpipe piezometers are similar to monitoring wells in that they consist of an open pipe that is generally placed within a drilled borehole with a screened section and an isolation seal as shown in Figure 10-6. However, standpipe piezometers differ from monitoring wells in that the screened section of a piezometer is much shorter than typically used for monitoring wells so that piezometers only respond to the hydraulic head at a discrete depth. Screen lengths (including the filter pack) for standpipe piezometers are often approximately 1 to 3 feet in length to isolate the groundwater response to as discrete a zone as possible. Standpipe piezometers are carefully sealed above and/or below the location of the screened section to prevent hydraulic "short circuiting" from formations at different depths and are usually grouted following installation.

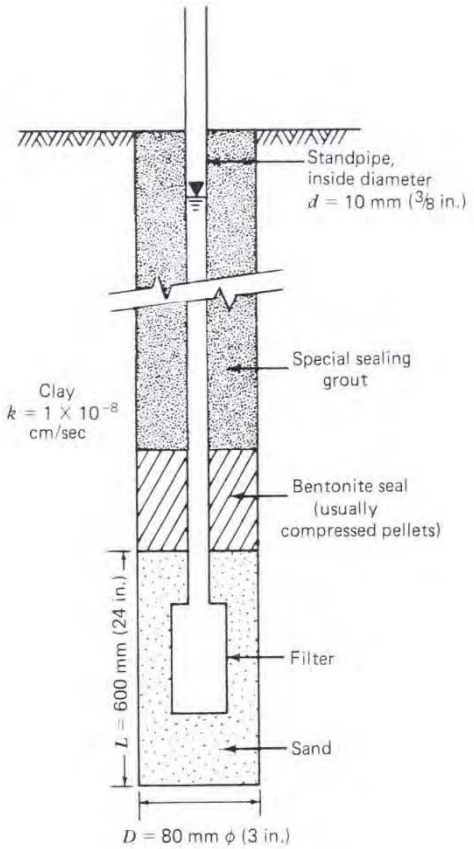


**Figure 10-6 Standpipe piezometer installed in a borehole (from Dunnicliff, 1993).**

Most standpipe piezometers are installed in drilled holes as shown in Figure 10-6. However, standpipe piezometers can also be constructed by pushing or driving pipe with a conical point at the tip. This type of installation has a number of advantages including:

1. Ease of installation;
2. No drill cuttings to dispose of;
3. Reduced time of installation;
4. Positive seal;
5. Known geometry;
6. Recoverable after use;
7. Reduced cost of installation; and
8. No isolation seal to construct.

Pushed/driven piezometers may also be subject to potential problems including the potential for clogging of the porous element during installation, smearing of the soil during installation, and installation difficulties in some soil deposits (e.g., deposits with dense soils, gravel, cobbles, and boulders, etc.). The size of most pushed/driven piezometers is also relatively small, typically less than about 1.5 inches in diameter. Parry (1971) describes the use of a driven standpipe piezometer designed with a sliding sleeve as shown in Figure 10-7. During installation, the sleeve is collapsed around the screened section to protect the screen from clogging. Once the desired depth is reached, the pipe is pulled back to expose the screen. This design is useful if a piezometer must be driven through fine-grained soil before reaching the desired depth.

The water level in a standpipe piezometer that has come to equilibrium with hydraulic conditions in the surrounding formation is a measure of total head if measured relative to some arbitrary datum, or a measure of pressure head if measured relative to the elevation of the piezometer screened section. ASTM D4750 describes a standard test method for determining liquid levels in boreholes, monitoring wells, or standpipe piezometers. It is also possible to install electronic instruments within standpipe piezometers to automatically measure and record the water level in the piezometer; however, in such cases it is important to account for changes in atmospheric pressure to avoid introducing error into the measurements.

Standpipe piezometers are subject to time lag effects that arise due to the time required for the piezometer to come to equilibrium with the surrounding formation when the hydraulic head in the formation changes. The duration of the time lag depends on the size of the screened section and filter pack, the diameter of the riser pipe, and the hydraulic conductivity of the formation. Penman (1960) suggests that the time lag for an open standpipe piezometer can be estimated as

$$t = 3.3 \times 10^{-6} \frac{\left[ d^2 \ln\left( \frac{L}{D} + \sqrt{1 + \left( \frac{L}{D} \right)^2} \right) \right]}{kL} \qquad (10.5)$$

where $t$ is the time for 90 percent response (days), $d$ is the inside diameter of the standpipe (cm), $L$ is the length of the sand pack or screen (cm), $D$ is the diameter of the sand pack or screen (cm), and $k$ is the hydraulic conductivity of the formation (cm/s). So, for example, if a PVC riser pipe with an inside diameter of 1.5 in is placed in a 3-inch diameter borehole in clay with hydraulic conductivity on the order of $1x10^{-6}$ cm/s and a sand pack with a length of 1 feet is used, it will take about 3 days to produce a reliable response. The time lag may be reduced substantially by using a larger diameter sand pack and a smaller diameter riser pipe. However, the diameter of the sand pack may be dictated by the size of available augers or drilling equipment and the minimum diameter of the riser pipe may be dictated by the need to obtain water samples, to insert automated instrumentation to measure water levels, or use an available bailer.

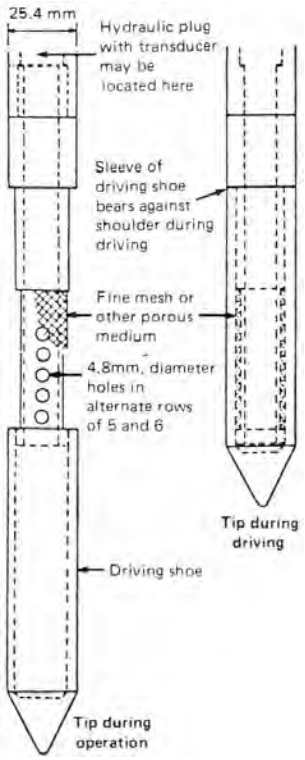


**Figure 10-7 Pushed/driven open standpipe piezometer (from Dunnicliff, 1993).**

Most other types of piezometers have substantially less time lag and are essentially considered "zero" volume displacement piezometers. Since a change in the groundwater pressure acts almost immediately on the response of the transducer, they give a better indication of rapid changes in water pressure. Of course, they cannot be used to obtain water samples or measure hydraulic conductivity.

### 10.6.2 Twin-tube Hydraulic Piezometers

A schematic of a twin-tube hydraulic piezometer is shown in Figure 10-8. Twin-tube hydraulic piezometers are closed piezometers that are filled with fluid and connected to dual pressure gages or transducers that are attached to each tube. The use of dual tubes and dual pressure gages provides for a check on saturation of the piezometers, wherein both gages will produce the same readings if the system is saturated but will produce different readings if the system becomes unsaturated. In instances where the system becomes unsaturated, it can be re-saturated by flushing fluid through the system. Measurements from twin-tube hydraulic piezometers can be collected and logged automatically using appropriate transducers at the end of each tube and a data acquisition system. Twin-tube hydraulic piezometers are relatively expensive compared to other alternative devices, but are quite effective for cases where long-term monitoring is needed (Dunnicliff, 1993).

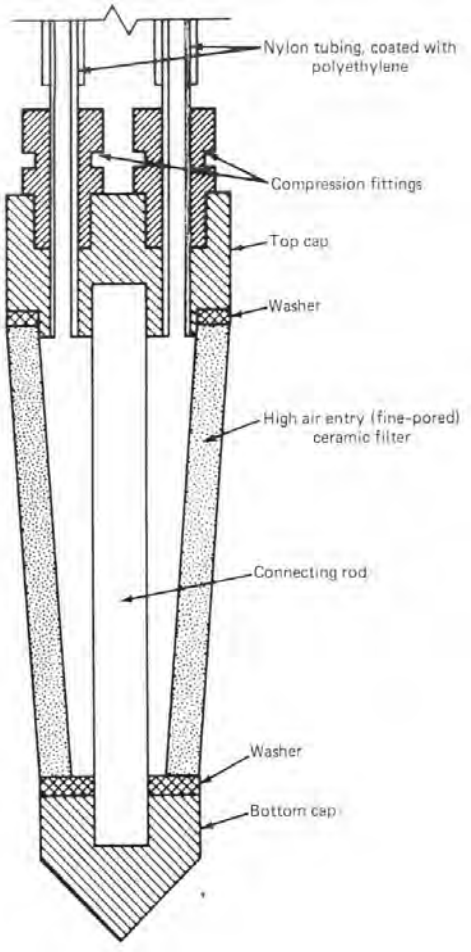


**Figure 10-8 Twin-tube hydraulic piezometer (from Dunnicliff, 1993).**

### 10.6.3 Pneumatic Piezometers

Pneumatic piezometers measure the in-place water pressure at a specific point using a simple twin tube diaphragm transducer as shown in Figure 10-9. A filter element, usually made of porous plastic, sintered stainless steel, or bronze, is attached to the front end of the transducer ahead of a flexible rubber diaphragm. In operation, water pressure acting on the outside of the diaphragm pushes the diaphragm against the body of the transducer to keep it in a closed position. To measure the water pressure, controlled flow gas pressure (usually nitrogen or dry air) is applied to the inlet tube while the outlet tube is left open to the atmosphere. When the applied gas pressure in the tube exceeds the water pressure on the outside of the diaphragm, the diaphragm lifts up allowing gas to pass to the outlet tube and back to the ground surface. Return gas flow in the outlet tube is identified by a flow meter or simple bubbling of gas if the end of the tube is held under water. The inlet tube is then closed off and gas inside the transducer bleeds off from the outlet tube at the ground surface. When the gas pressure on the inside of the diaphragm equals the water pressure on the outside of the diaphragm, the diaphragm closes on the transducer, gas flow stops, and the pressure is registered on the pressure gage of the console.

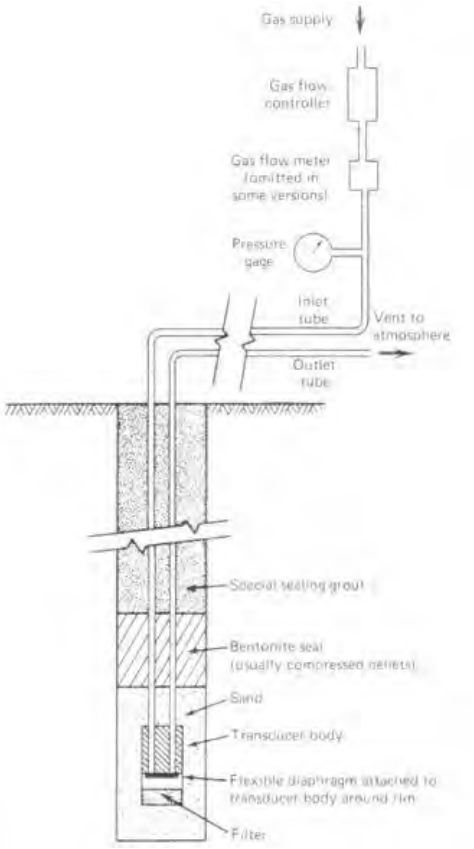


**Figure 10-9 Typical pneumatic piezometer (from Dunnicliff, 1993).**

Pneumatic transducers are available from a number of manufacturers and are generally inexpensive. They are typically installed in a borehole with a small sand pack zone so that the filter element is embedded in sand. The remainder of the hole is sealed with bentonite or grout and the twin tube leads are brought to the ground surface. An alternative is to push the piezometer from the bottom of the borehole. However, this is usually only possible in soft clay deposits when the piezometer is fitted with a conical tip. The primary advantage of pneumatic piezometers is that they are generally robust. However, they are not easily automated and thus have largely been supplanted by alternative piezometers.

### 10.6.4 Strain Gage Piezometers

Several widely used forms of piezometers rely on use of strain gages attached to a simple diaphragm to measure water pressure as illustrated in Figure 10-10 and 10-11. Each of these piezometers is composed of a cylindrical chamber about the size of a large pen with a diaphragm that is protected by a saturated porous element that transmits the pressure in the water to the face of the diaphragm. The diaphragm of the transducer is instrumented with one of several different types of strain gages, which are calibrated to produce measurements of water pressure that transmits a signal to a readout unit. The strain gages used can be electrical resistance type transducers (Figure 10-10) much like those used inside of a piezocone, vibrating wire transducers (Figure 10-11), or fiber-optic transducers. Electrical resistance piezometers have the advantages of requiring quite simple electronics and rapid sampling rates (i.e., quick measurement) but are sensitive to external sources of resistance (e.g., from cable length, water, etc.) and are subject to "zero drift", temperature effects, and electrical noise. Vibrating wire piezometers require specialized and slightly more expensive electronics, but are generally more stable, particularly when long-term monitoring is desired. Fiber-optic piezometers also require specialized readout electronics but come with the added advantage of being largely immune to electrical noise in addition to being quite stable. All strain gage piezometers transmit signals through a cable to some form of readout at the ground surface. Strain gage piezometers lend themselves to automated data acquisition and data logging, which often alleviates the need to repeatedly send personnel to a site to take readings.

### 10.6.5 Installation of Piezometer Elements

Twin-tube, pneumatic, and strain gage piezometers are often installed in a predrilled borehole or may be fitted with a conical point and pushed into the ground (Figure 10-12), either at the base of a borehole or from the ground surface. Twin-tube, pneumatic, and strain gage piezometers should generally not be driven into the ground.

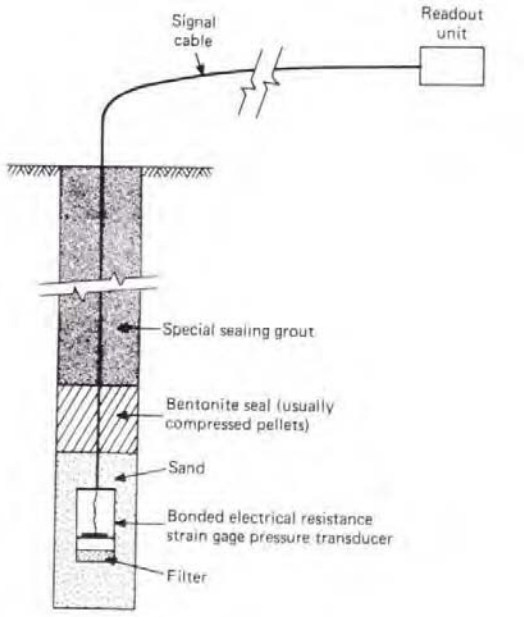


**Figure 10-10 Electrical resistance gage piezometer (from Dunnicliff, 1993).**

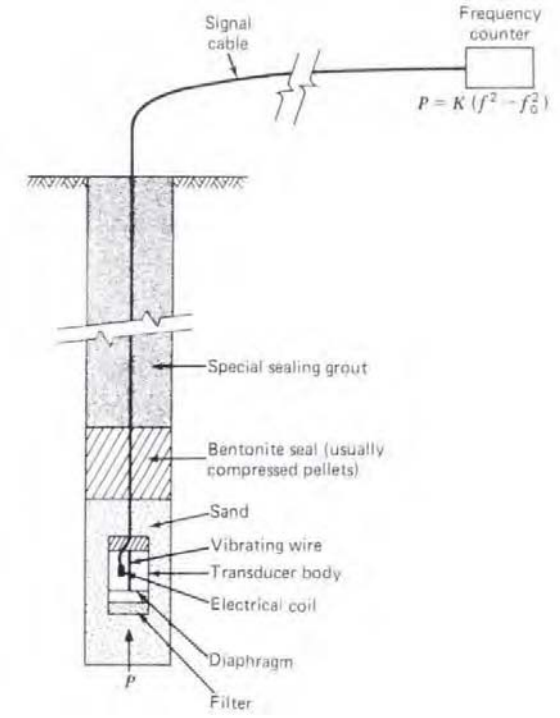


**Figure 10-11 Vibrating wire piezometer (from Dunnicliff, 1993).**

In many situations, it is desirable to install piezometers at different elevations within a formation at the same plan location. This may be accomplished by drilling individual boreholes adjacent to each other at the same location on the site and installing a single piezometer in each hole or by using nested

piezometers within a single borehole as shown in Figure 10-13. Multiple installations in a single borehole saves site space, drilling time, and expense but requires special care to ensure proper installation of each piezometer. Particular attention must be paid to the seals between piezometers to prevent hydraulic connectivity between the different piezometers. In general, a larger diameter borehole is required for nested piezometers and typically no more than three or four installations can be completed in one hole. Installing nested piezometers within a single borehole also introduces risks for obtaining erroneous measurements so it is generally preferable to install piezometers within separate, but closely spaced boreholes when possible.

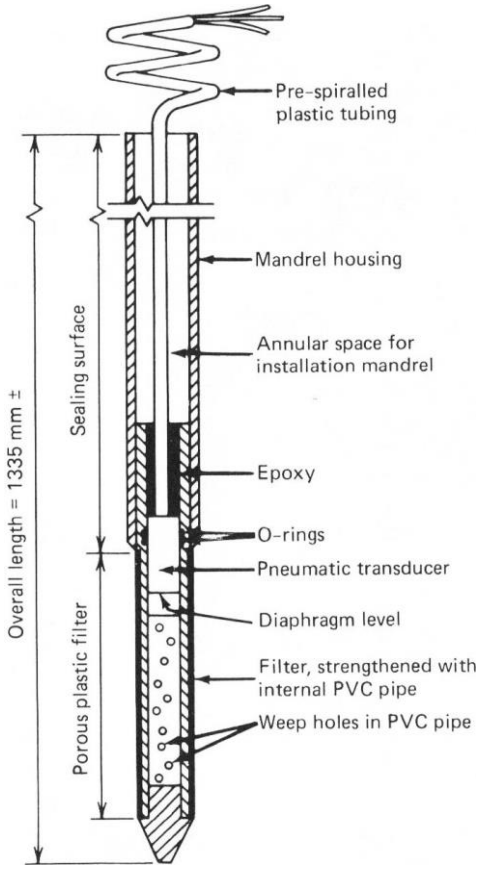


**Figure 10-12 Push-in pneumatic piezometer (from Dunnicliff, 1993).**

## 10.7 EVALUATION OF GROUNDWATER CONDITIONS USING IN SITU TEST MEASUREMENTS

In situ test measurements can also be effectively used to evaluate groundwater conditions. CPTU measurements, in particular, can be used to efficiently and effectively determine the magnitude of in situ pore water pressures through direct measurements. CPTU measurements are particularly efficient for determining pore water pressures and groundwater levels in clean coarse-grained soils, as illustrated in

Figure 10-14. In such soils, pore water pressure measurements are effectively a direct measurement of in situ pore pressure since the soils drain rapidly enough to prevent development of excess pore water pressures. Interpretation of groundwater levels is therefore straightforward as illustrated in Figure 10-14.

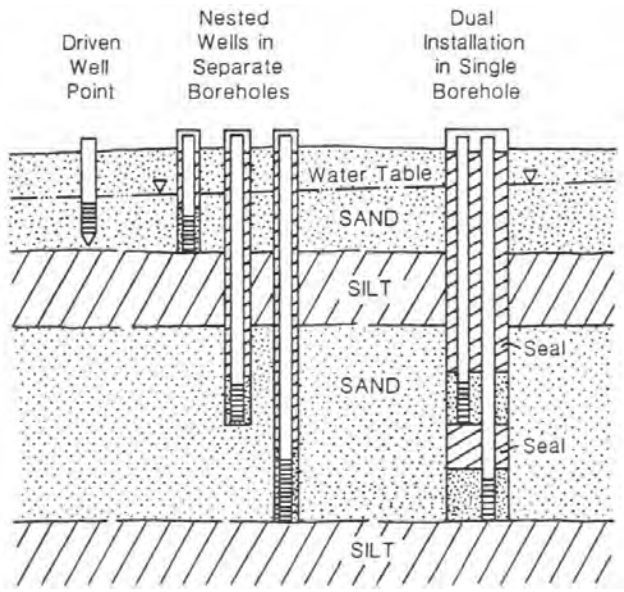


**Figure 10-13 Alternative methods for determining variation of pore water pressures with depth using piezometers (from Dalton, et al., 1991).**

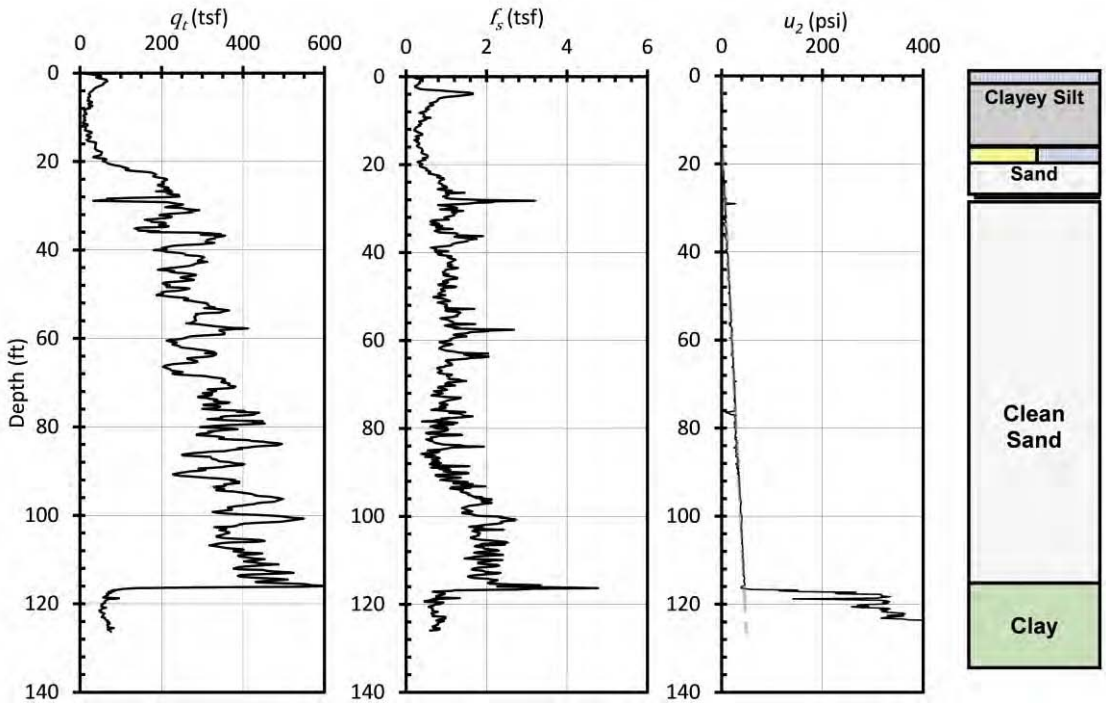


**Figure 10-14 Example CPTU measurements showing location of groundwater level in clean sand.**

Interpretation of groundwater conditions in fine-grained soils using CPTU measurements is more complex since excess pore water pressures will develop as the cone is pushed through fine-grained soils as shown in Figure 10-15. Measured pore water pressures in fine-grained soils therefore do not represent in situ pore water pressures but rather represent combined in situ and excess pore water pressures. Despite this complication, however, CPTU measurements can still be used to aid in interpretation of groundwater conditions. In cases where a fine-grained stratum contains numerous sand lenses, such as shown in Figure 10-15, it is often possible to use measurements within those lenses to interpret in situ pore water pressures and the groundwater level as shown in the figure. In cases, where such freely draining lenses are not present, in situ pore water pressures at select depths can still be measured by performing CPTU dissipation tests as described in Chapter 6. While such tests increase the time required for conducting CPTU soundings, they have the added advantage of producing estimates for the coefficient of consolidation or hydraulic conductivity, as described in more detail in Section 10.14.2.

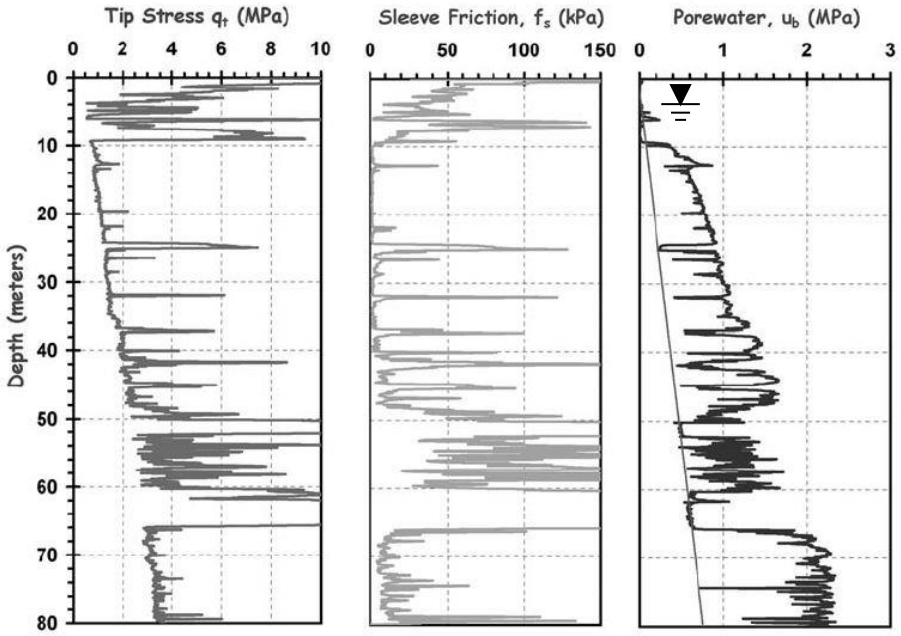


**Figure 10-15 Example CPTU measurements in clayey soil with sand lenses (from Mayne, 2007).**

Other in situ tests can also be used to infer information about groundwater conditions at a site, albeit in a more indirect way. As described in Chapter 6 and later in this chapter, DMT dissipation tests can be used to infer information about pore water pressures. Seismic CPT and DMT measurements can also be used to identify saturated soils as described in more detail in the following section.

## 10.8 EVALUATION OF GROUNDWATER CONDITIONS USING GEOPHYSICAL MEASUREMENTS

Several geophysical methods are available for evaluating groundwater conditions. These methods can be divided into those: (1) used to locate and map the groundwater surface, and (2) used to locate and map groundwater flow and seepage paths.

### 10.8.1 Location of Groundwater Surface

Geophysical methods used to detect groundwater work by detecting changes in the physical properties of the soil, primary electrical properties or seismic velocity, caused by the presence of water in the pores of the soil. In coarse-grained soils where the magnitude of capillary rise is small, the water table and the location of saturated soil are nearly coincident such that the water table can be fairly well defined by an abrupt change in physical properties. In fine-grained soils where capillary rise will cause a significant zone of saturated or nearly saturated soils well above the water table, the transition in physical properties will be gradual and may introduce challenges to precisely locating a clearly defined groundwater surface.

Resistivity soundings work by detecting differences in electrical resistivity of saturated and unsaturated soils. Resistivity measurements are performed by passing current into the ground using two outer electrodes inserted in the ground and measuring the voltage across two inner electrodes. Groundwater depth can be detected using resistivity soundings, whereby the electrode spacing is increased while keeping the center of the array fixed. The apparent resistivity is measured and plotted versus electrode spacing. Data from automated resistivity systems are interpreted using inversion methods to develop a model of subsurface resistivity. The separation of electrodes must be about three times the planned investigation depth, so resistivity surveys are best suited for shallow applications.

Time domain electromagnetic method (TDEM) is another means to detect resistivity changes with depth. A transmitter loop is used to induce secondary currents in the ground, as shown in Figure 10-16 (Wightman, et al., 2004). Higher amplitude secondary currents will be generated by more conductive (inverse of resistive) layers. The voltage measured versus time by a receiver coil placed within the transmitter loop can be related to resistivity. A sounding curve (Figure 10-16b) is made of delay time versus resistivity. Using the sounding curve, a model can be developed of layer resistivity and thickness. TDEM is better suited for deeper investigation (> 150 feet) than resistivity soundings (Wightman, et al., 2004). Also, unlike the resistivity method, no electrodes need to be inserted into the ground. Use of this method may not be possible if metal structures (fences, bridges) are present at the site.

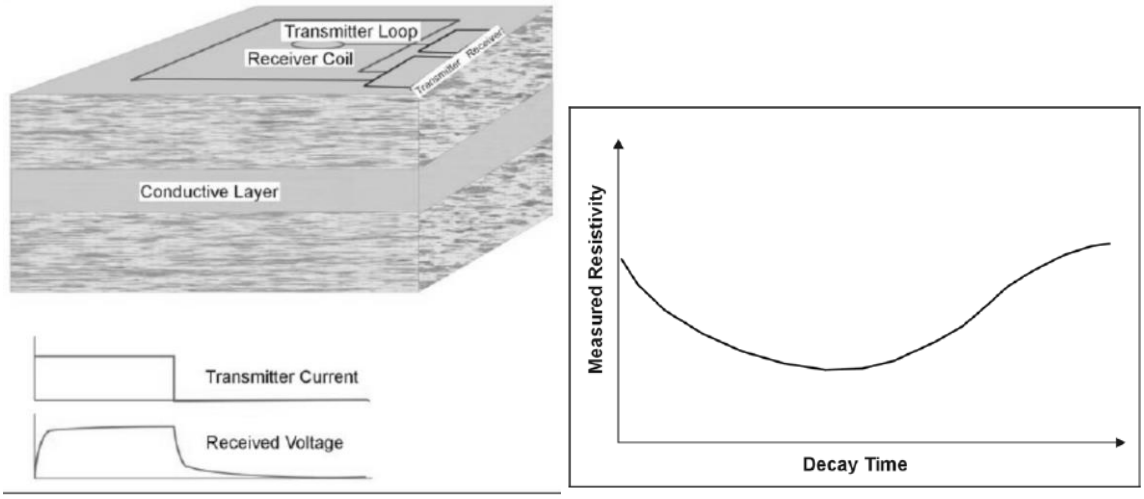


**Figure 10-16 Illustration of Time-domain Electromagnetic method (from Wightman, et al., 2004).**

Seismic refraction surveys are based on detecting the compression wave velocity contrast between unsaturated and saturated soils. Seismic compression waves excited at the surface critically refract off of the interface between unsaturated and saturated soils. The refracted arrival detected at the surface by a spread of geophones can be used to infer the depth of the interface and the velocity of the saturated soil. The method works best in coarse-grained soil where the transition between unsaturated and saturated soils is often quite abrupt. In fine-grained soils, the transition is less well defined and may be difficult to detect. The method is limited to depths of about 50 feet or less when using a simple sledge hammer source (Wightman, et al., 2004), but can work at greater depths with more significant seismic sources.

Ground penetrating radar (GPR) surveys are based on detecting the contrast in dielectric properties between unsaturated and saturated soils. GPR devices send an electromagnetic wave from a transmitting antenna into the ground that will reflect off interfaces with a contrast in dielectric properties. A receiving antenna is used to detect arrivals of reflected waves. The unit is pulled across the ground and the reflected arrivals are stored and displayed. The depth of penetration is a function of the soil type and the frequency of the antennae. A 100-MHz antenna can penetrate to depths of 50 to 65 feet under ideal conditions of dry granular soils (Wightman, et al., 2004). The presence of clay will greatly attenuate the signal and may limit the penetration depth to several feet.

### 10.8.2 Investigation of Groundwater Flow

The self-potential or spontaneous polarization (SP) method is a passive technique based on the measurement of electrical potentials between two points on the ground surface. Self-potentials are generated by a variety of sources, one of which is fluid flow. Figure 10-17 shows a schematic of SP

anomalies generated from flowing water. The anomaly may be positive or negative depending on the direction of flow. SP measurements are simple and inexpensive to perform. They can be performed using two electrodes with a constant spacing, or more commonly with one of the electrodes fixed as a permanent reference. Interpretation is performed by plotting measured voltage versus distance and looking for anomalies in the plot.

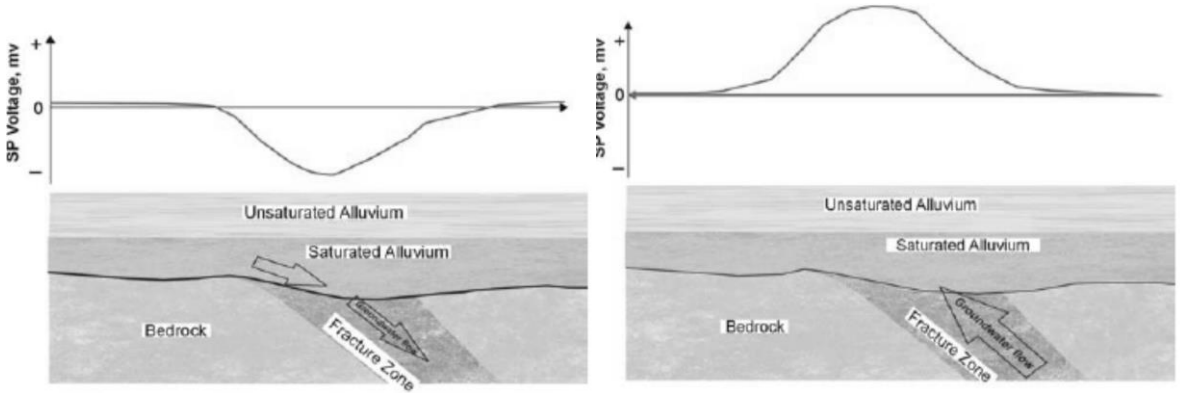


**Figure 10-17 Self-potential anomalies from flowing water (Wightman, et al., 2004).**

## 10.9 METHODS FOR EVALUATING HYDRAULIC CONDUCTIVITY OF SOIL AND ROCK

As described previously in this chapter, it is common practice to measure groundwater conditions at project sites to infer groundwater conditions that may be present over the life of a project. However, there are also inevitably times when current groundwater conditions may not accurately reflect conditions that may arise over the life of a project or when construction may alter local groundwater conditions. In such cases, it is necessary to predict groundwater conditions using seepage analyses of various forms, which require estimates for the hydraulic conductivity of the soil and/or rock that is present at a site. Estimates of hydraulic conductivity are also important when quantities of flow must be estimated, as is often required for construction. The remaining sections of this chapter address methods for measurement or estimation of hydraulic conductivity for soil and rock and the factors that influence hydraulic conductivity.

Several alternative approaches may be used to evaluate hydraulic conductivity for a given soil or rock formation as summarized in Table 10-3. These approaches range from simple estimates of hydraulic conductivity based on index properties to conducting laboratory or field flow tests to directly measure hydraulic conductivity. Additionally, several indirect in situ test measurements can also be used to develop estimates for hydraulic conductivity. Advantages and disadvantages of the alternative approaches are provided in Table 10-3.

**Table 10-3 Summary of methods for determining hydraulic conductivity.**

| Method | Example Tests | Comments |
|---|---|---|
| Estimation from Index Properties | • Atterberg limits<br>• Grain size distribution<br>• Weight-volume characteristics<br>• Fracture characteristics in rock<br>• General soil/rock type | • Crude, first order approximation based on a knowledge of soil/rock conditions.<br>• Usually based on grain-size distribution for coarse-grained soils, void ratio for fine-grained soils, and fracture characteristics for rock.<br>• Appropriate for preliminary evaluation or small projects without significant consequences. |
| Direct Laboratory Measurements | • Fixed-wall hydraulic conductivity tests<br>• Flexible-wall hydraulic conductivity test | • Require representative undisturbed or remolded specimens.<br>• Good control over boundary conditions and flow<br>• Can be difficult to obtain truly representative samples because of microscale problems. |
| Indirect Laboratory Measurements | • 1-D consolidation tests | • Same issues as direct laboratory measurements<br>• Additional complication of transformation errors<br>• Means for getting estimates from tests that produce measurements for other properties (e.g., consolidation tests). |
| Direct Field Measurements | • Borehole hydraulic conductivity tests<br>• Pumping tests<br>• Infiltrometer tests | • Borehole and pumping tests require quality boreholes<br>• Boundary conditions are difficult to control.<br>• More representative measurement of "field" hydraulic conductivity, including many macroscale effects.<br>• Better representation of in situ stress conditions.<br>• May be time consuming and costly in some formations. |
| Indirect Field Measurements | • Various direct push methods | • Often significantly faster than alternative direct measurements.<br>• Subject to transformation errors from empirical correlations.<br>• Remolding of soil during installation may be a problem in some soils. |

## 10.10 FACTORS AFFECTING HYDRAULIC CONDUCTIVITY FROM LABORATORY TESTS

Several factors influence measured values of hydraulic conductivity determined from laboratory tests. While it is often difficult to assess each of these factors independently, it is important to have some understanding of these factors so that test measurements can be properly interpreted. A number of the more important factors are briefly discussed in this section.

### 10.10.1 Size of Test Specimens

The size of test specimens may introduce a scale effect on the measured value of hydraulic conductivity. In general, larger specimens tend to produce greater values of $k$, primarily because larger specimens are

more likely to be representative of the parent formation. This is particularly true in formations that have macro structural features such as cracks and fissures, or lenses of dissimilar materials. The presence of macro structural features is taken to an extreme in fractured rock masses with open discontinuities where the predominant flow paths are through the discontinuities rather than through the intact rock. This phenomenon is often referred to as "secondary" hydraulic conductivity. Such response is analogous to what is observed for the mechanical behavior of rock, where the condition of discontinuities often control the mechanical response as described in Chapter 9. Because of this issue, the hydraulic conductivity of intact rock specimens is seldom a predominant concern for fractured rock masses.

### 10.10.2 Stress Level

The magnitude of stress applied to the soil and/or rock may influence measurements of hydraulic conductivity since higher stresses tend to produce more consolidation of specimens and a corresponding reduction in void ratio. Higher stresses can also close up micro-cracks and other structural features, which also tends to reduce hydraulic conductivity. Because of these issues, consideration should be given to replicating in situ stresses to the extent possible when measuring the hydraulic conductivity in the laboratory.

### 10.10.3 Sample Disturbance

Disturbance of soil and/or rock specimens can also influence measurements of hydraulic conductivity. "Smearing" of specimens during sampling can reduce the apparent hydraulic conductivity by impeding flow more than is truly appropriate for the intact soil or rock. Conversely, small cracks and fissures induced during sampling, transportation and handling, or stress relief can increase the measured hydraulic conductivity compared to what is truly appropriate in situ. Disturbance may also cause alteration of the natural fabric and structure of the soil, producing changes in hydraulic conductivity. Measurement of hydraulic conductivity thus requires that high quality, undisturbed samples be obtained for testing.

### 10.10.4 Hydraulic Gradient

While Darcy's equation is based on the presumption that hydraulic conductivity is independent of the hydraulic gradient, this is not strictly true for all materials and conditions. Typical field gradients for most natural geologic and hydrogeologic conditions vary from about 0.005 to 0.30. However, such gradients are too small for routine laboratory testing because the time required for flow is too long to be practical. As such, much larger gradients are often applied during laboratory testing. In some materials, such gradients can lead to differences between those measured in common tests and hydraulic

conductivities that are appropriate in the field. ASTM D5084 recommends maximum hydraulic gradients that range from 2 to 30 for soils with different hydraulic conductivity. However, the standard allows these limits to be exceeded if testing shows that greater hydraulic gradients do not affected the measured hydraulic conductivity for the specific soil being tested.

### 10.10.5 Permeant

The composition of the permeant liquid being passed through soil or rock can dramatically affect the hydraulic conductivity. Ideally, it is desirable to use the actual permeant liquid from the field for laboratory measurement of conductivity. However, this is not generally practical so a standard laboratory permeant prepared using a 0.005N to 0.01 N solution of $CaSO_4$ is generally used for routine laboratory testing.

### 10.10.6 Temperature

Temperature can also affect hydraulic conductivity because it influences the viscosity of water. Most laboratory tests are conducted at temperature that are greater than typical field temperatures below ground. It is routine to report the value of hydraulic conductivity at a standard temperature of 20 degrees C. This means that it is necessary to correct the measured value of $k$ according to:

$$k_{20} = k_{measured}\left(\frac{\mu_t}{\mu_{20}}\right) \tag{10.6}$$

where $\mu_t$ is the viscosity of water at the test temperature and $\mu_{20}$ is the viscosity of water at 20 degrees C.

### 10.10.7 Anisotropy of Hydraulic Conductivity

Many soils exhibit hydraulic conductivity anisotropy, having different flow characteristics in the horizontal direction as compared to the vertical direction. Natural hydraulic conductivity anisotropy has been reported for many clays and other fine-grained soils (e.g., Mitchell, 1956; Rowe, 1964; Kenney, 1976; Leroueil, et al., 1992). Macro-features, such as fissures, joints, or layering within a soil may produce differences in hydraulic conductivity in the horizontal and vertical directions. For example, the presence of varves in lacustrine deposits produces anisotropy with horizontal hydraulic conductivity being greater than vertical hydraulic conductivity. Induced anisotropy may also occur in compacted clays or clays subjected to consolidation if there is preferred orientation of the clay particles in the direction perpendicular to the compaction or applied vertical stress (e.g., Basak, 1972; Al-Tabbaa and Wood, 1987; Leroueil, et al., 1990; Dewhurst, et al., 1996). Horizontal or radial hydraulic conductivity may be

important for certain projects or problems as in the case of radial flow of groundwater to wells or wick drains. Horizontal hydraulic conductivity may also be important in analyzing slope stability problems.

To evaluate anisotropy, tests may be performed on specimens cut in the horizontal and vertical directions from block samples, as shown in Figure 10-18, or they may be trimmed from large diameter thin-walled tube samples. Alternatively, special permeameters or consolidometers have been fabricated to allow the determination of directional hydraulic conductivity on the same specimen, eliminating the potential influence of soil variability (e.g., Moore, 1979).

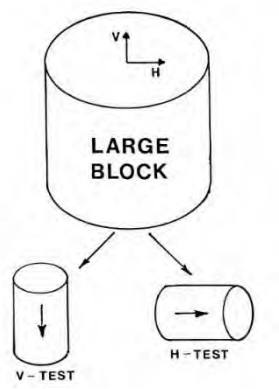


**Figure 10-18 Trimming oriented specimens to determine hydraulic conductivity anisotropy (from Chapuis and Gill, 1989).**

Chapuis and Gill (1989) summarized a number of reported cases of measured anisotropy of hydraulic conductivity for a wide range of soils including clays, silts, and sands, as well as some cases of sandstone. They suggested a relationship between the anisotropy ratio, $r_k = k_h/k_v$, and the "density index", $I_e$, defined as

$$I_e = \frac{(e_0 - e)}{(e_0 - e_1)} \tag{10.7}$$

where $e_0$ is the void ratio of the soil in its loosest state ($= e_{max}$ for sand and $e_{w=LL}$ for clay) and $e_1$ is the void ratio of the soil in its densest state ($= e_{min}$ for sand and $e$ at the maximum dry unit weight from a Modified Proctor for clay). For a soil in the densest state, $I_e = 1$; in the loosest state, $I_e = 0$. An example relationship for clay and sand is shown in Figure 10-19. Typical ranges of values for different soil types are provided in Table 10-4.

**Table 10-4 Reported hydraulic conductivity anisotropy.**

| Soil | $r_k = {k_h}/{k_v}$ | Reference |
|---|---|---|
| Varved Clay | 2 – 10 | Chan and Kenney (1973)<br>Wu et al. (1978) |
| Glacial Till | 0.9 – 2.2 | |
| Loess | 0.5 – 2.6 | |
| Marine Clay | 0.7 – 1.4 | Lumb and Holt (1968) |
| Boston Blue Clay | 0.7 – 4.0 | Olsen (1962)<br>Haley and Aldrich (1969) |

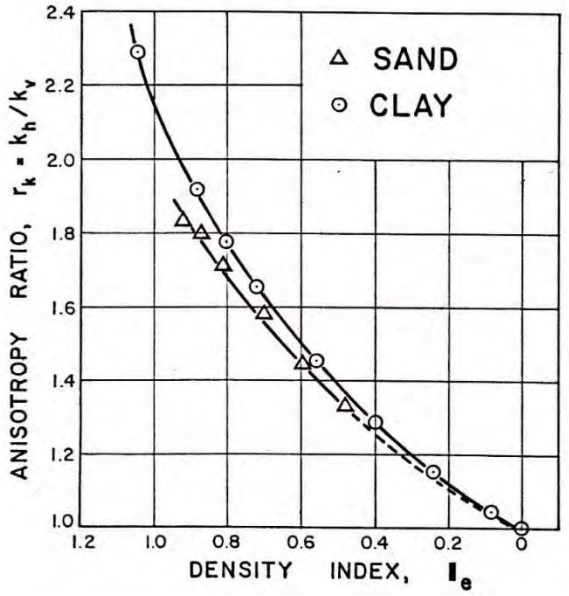


**Figure 10-19 Relationship between hydraulic conductivity anisotropy ratio and density index (from Chapuis and Gill, 1989).**

## 10.11 EVALUATION OF HYDRAULIC CONDUCTIVITY USING LABORATORY TESTS

Hydraulic conductivity can be directly measured in the laboratory using either rigid-wall permeameters or flexible-wall permeameters conducted as either constant head tests or falling head tests. Table 10-5 summarizes a number of common laboratory methods for measuring hydraulic conductivity. Additional descriptions of the alternative tests is provided in the following sections.

**Table 10-5 Summary of laboratory methods for determining hydraulic conductivity.**

| Method | Comments |
|---|---|
| Consolidation Test | Either indirect calculation of $k$ from coefficient of consolidation or direct measurement of $k$ from flow tests. |
| Shelby Tube Permeameter | Inexpensive setup for undisturbed field samples. |
| Compaction Mold Permeameter | Primarily used for compaction studies to relate $k$ to soil density. Very common for compacted clay landfill liners and covers. |
| Double-Ring Rigid Wall Permeameter | Used to evaluate the effects of sidewall leakage. |
| Rigid-Wall Permeameter for Granular Soils | Usually constant head tests performed on large diameter specimens |
| Controlled Vertical Stress Rigid-Wall Permeameter | Useful for evaluating influence of different vertical stress on hydraulic conductivity. |
| Oversized Rigid-Wall Permeameter | Oversized cell used to reduce sidewall leakage. Bentonite used to seal specimen. |
| Flexible-Wall Permeameter | Commonly used for undisturbed samples of fine-grained soils. Control on confining stresses. Can back pressure saturate and perform a check on saturation. |

### 10.11.1 One-dimensional Consolidation Tests

Conventional one-dimensional consolidation tests may be used to establish an indirect measure of hydraulic conductivity. As described in Chapter 6, the consolidation test is conventionally used to evaluate the stress history and compression characteristics of fine-grained soils and for evaluating the time rate of consolidation. As the one-dimensional consolidation test proceeds, test results may be used to indirectly calculate the hydraulic conductivity of the specimen based on one-dimensional consolidation theory. Use of such methods to determine hydraulic conductivity is considered an indirect measurement of $k$ since consolidation theory is necessary to transform the actual measurements (rate of compression) to an estimate of hydraulic conductivity.

From one-dimensional consolidation theory (e.g., Holtz and Kovacs, 1981), the hydraulic conductivity may be evaluated as

$$k = c_v \Delta_w m_v \tag{10.8}$$

where $c_v$ is the coefficient of consolidation, $\Delta_w$ is the density of water, and $m_v$ is the coefficient of compressibility. The value of $c_v$ is obtained by graphical means from the time versus deformation plot obtained for each load increment during the test, as described in Chapter 6. The coefficient of compressibility is equal to the slope of the strain versus effective stress curve for the load increment. Since the values of $c_v$ and $m_v$ may be evaluated for each load increment throughout the entire test, a value of $k$ may be calculated for each increment and plotted as a function of the average void ratio of the sample for each respective increment.

Hydraulic conductivity can also be directly measured in the oedometer cell during a one-dimensional consolidation tests with minor adaptations to the equipment to allow flow to be induced through the sample at the end of a load increment. Several different configurations of equipment may be used for determining hydraulic conductivity. Figure 10-20 shows a schematic of one configuration that has been used to directly measure $k$ in oedometer cells. Either constant or falling head arrangements may be used.

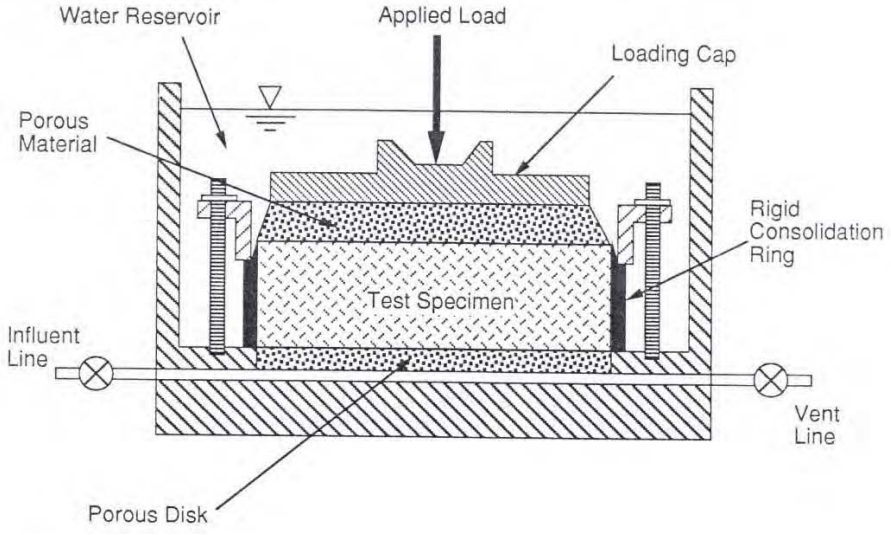


**Figure 10-20 One-dimensional consolidation cell used for direct measurement of hydraulic conductivity (from Daniel, 1994).**

The oedometer hydraulic conductivity test is useful if the relationship between hydraulic conductivity and void ratio or porosity is desired for a given soil, or if an estimate of $k$ is needed at a given vertical effective stress for one-dimensional loading conditions. However, the test may suffer from scale effects since a small sample (2.5 to 4.0-inch diameter and less than 1-inch thickness) is typically used.

### 10.11.2 Thin-Wall Shelby Tube Permeameters

An alternative to using the oedometer to measure hydraulic conductivity of undisturbed samples is to use the sampling tube as a rigid wall cell. A schematic of this test arrangement is shown in Figure 10-21. Typically, the sample tube will be a thin-walled Shelby tube that will be cut to a specified length to fit between two end caps. Porous stones are used at both ends and usually the ends of the sample must be trimmed to allow the stones to fit recessed into the ends of the tube. An O-ring or other type of seal is used on the end caps to prevent loss of water. This type of test arrangement is commonly used since the test equipment is inexpensive and the test procedure is simple. Different sizes of end caps are available to accommodate Shelby tubes ranging from 3 to 4 inches outside diameter. Generally, falling head tests are performed when conducting hydraulic conductivity tests in Shelby tubes.

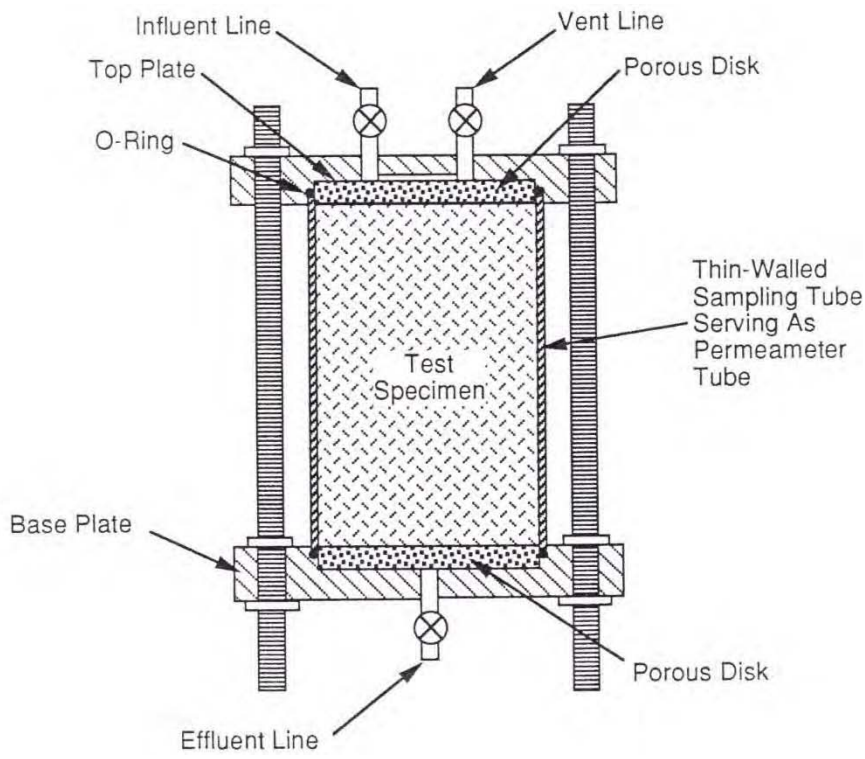


**Figure 10-21 Direct measurement of hydraulic conductivity in Shelby tube (from Daniel, 1994).**

### 10.11.3 Compaction Mold Permeameters

Laboratory evaluation of hydraulic conductivity for compacted soils is often performed using compaction mold permeameters in which the steel compaction mold used to compact specimens is used directly as the rigid wall container. Samples are compacted directly in the steel mold as a part of the compaction test and then, once the ends of the sample are trimmed, the soil and mold are transferred to a fixture to perform the hydraulic conductivity test. End caps are placed on either end of the steel mold and flow is initiated across the sample. A schematic of a typical compaction mold permeameter test is shown in Figure 10-22. Tests are commonly performed on either 4- or 6-inch diameter specimens, although larger and smaller specimens are sometimes used.

Compaction mold permeameters may be configured with a top cap that fits directly on top of compacted specimens or with a top cap with a small open space to allow the compacted specimen to swell. In this way, compacted specimens of fine-grained soils that initially begin as unsaturated, have the ability to expand when saturated. This more closely simulates what may occur in the field under certain situations, particularly with low vertical confining stress. The amount of expansion is dependent on the mineralogy and plasticity of the soil and the initial degree of saturation and initial void ratio.

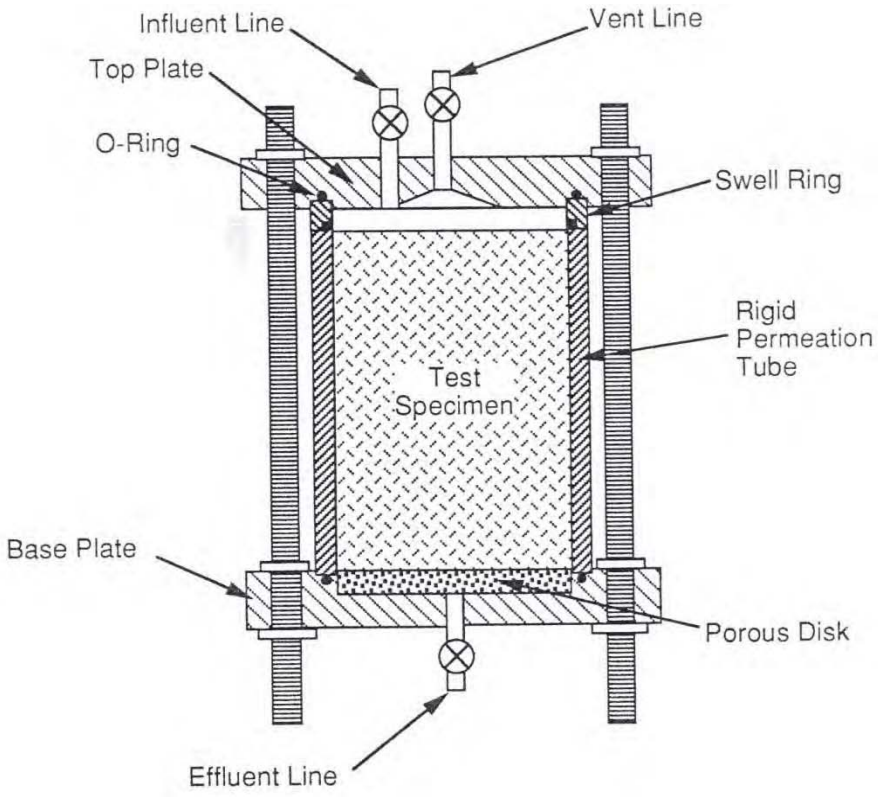


**Figure 10-22 Direct measurement of hydraulic conductivity in compaction mold (from Daniel, 1994).**

### 10.11.4 Double-Ring Compaction Mold Permeameters

To overcome the potential for sidewall leakage that may occur using rigid wall permeameters, it has been suggested that "double-ring" rigid wall permeameters be used. The equipment is similar to that used for a conventional compaction mold permeameter with the exception that an inner ring of smaller diameter is located on each end cap to separately measure flow passing through the inner and outer rings. Separate control of the inflow and outflow through the inner and outer rings allows for separate determination of hydraulic conductivity to be checked against the overall sample. Since the overall sample includes the rigid boundary effects of the outer wall, any difference in hydraulic conductivity may be attributed to sidewall leakage.

### 10.11.5 Oversized Rigid-Wall Permeameter

An alternative method of eliminating sidewall leakage is to use an oversized rigid-wall permeameter. The annulus between the sample and the wall of the permeameter is filled with a material having a very low hydraulic conductivity such as bentonite. The bentonite expands to seal the surfaces at the sample and the wall, thereby reducing the potential for sidewall leakage.

### 10.11.6 Variable Vertical Stress Rigid-Wall Permeameter

Typical rigid-wall permeameters are not designed to apply vertical stress to the sample, despite the fact that the soil in the field is often subject to vertical stress that may influence the measured value of hydraulic conductivity. A special arrangement of a rigid wall permeameter that allows a vertical stress to be applied to the top of the sample uses an internal floating piston positioned on top of the specimen. The piston is free to move so that when air pressure is applied to the top of the piston, the vertical stress on the specimen can be controlled. A modification to this arrangement is to have the floating piston rigidly connected to a plunger that extends out the end of the top cap. The entire cell can then be placed in a fixture that allows a constant load to be placed on the plunger, using hanging weights or air pressure to vary the vertical stress on the specimen.

The variable vertical stress rigid-wall cell may also be useful for evaluating the hydraulic conductivity of slurry materials, such as bentonite slurries or mixed soil-bentonite material that might be used in slurry or diaphragm walls. The use of different vertical stresses can simulate different depths in a slurry wall or can show the influence of consolidation and a reduction in void ratio on the hydraulic conductivity.

### 10.11.7 Flexible-Wall Permeameters

Flexible-wall permeameters are commonly used for measuring the hydraulic conductivity of natural or undisturbed soil samples although they may also be used for compacted soils. Flexible-wall tests are more commonly used for fine-grained soils than for granular soils. As the name implies, the specimen is encapsulated in a flexible membrane that allows a confining stress to be applied to seal the specimen and minimize the potential for sidewall leakage. A schematic of a typical flexible wall setup is shown in Figure 10-23. The test equipment and procedures are specified in ASTM D5084.

The flexible-wall test has several advantages over other types of permeameters. The flexible-wall test allows for application of confining pressure to simulate in situ stress conditions, and consolidation of specimens under different states of stress. Saturation of test specimens can also be evaluated by checking Skempton's "B" pore pressure parameter. Finally, since flexible rubber membranes are used to confine specimens, and such membranes conform to the sides of test specimens, there is little chance for sidewall leakage to affect test measurements.

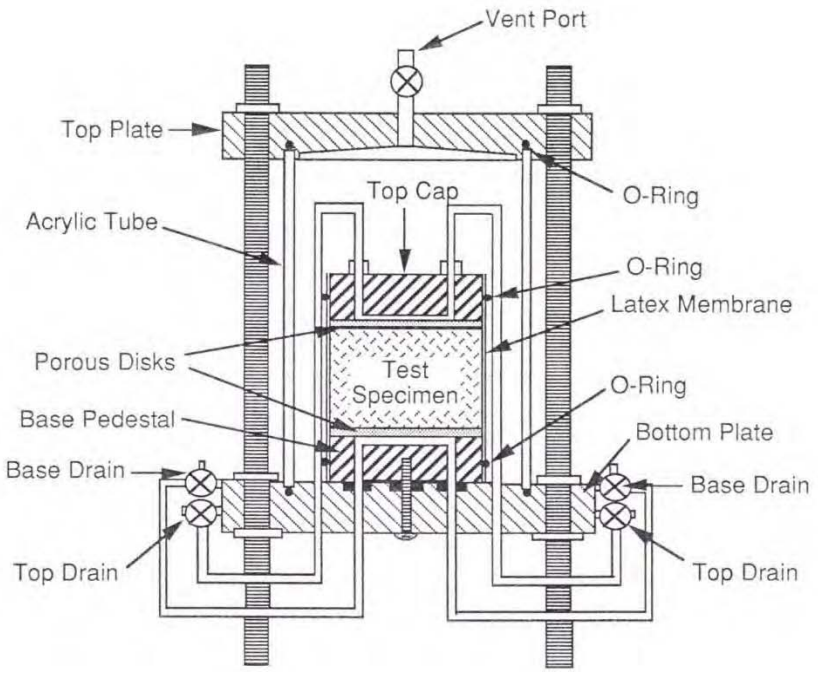


**Figure 10-23 Schematic of a flexible-wall permeameter (from Daniel, 1994).**

Selection of rigid-wall versus flexible-wall permeameters for an individual project depends largely on the requirements and scope of the project. Table 10-6 summarizes a number of advantages and disadvantages of both types of permeameters. Rigid-wall permeameters are perhaps more commonly used for tests involving compacted soils while flexible wall permeameters are perhaps more common for tests on undisturbed soils. The size of samples and available equipment, project budget, and time may all influence selection of the specific test equipment.

## 10.12 EVALUATION OF HYDRAULIC CONDUCTIVITY FROM BOREHOLE MEASUREMENTS

Groundwater flow at field scale is often controlled by macro-scale features such as cracks, fissures, and sand lenses, among others. Because of this, all laboratory tests are subject to potential bias because of small sample sizes. An attractive alternative to laboratory tests for evaluating hydraulic conductivity is to conduct field tests. Available field tests for measuring hydraulic conductivity are extremely varied and can range from the very simple to the very complex. Field methods may be generally categorized into one of four different classes of tests: (1) borehole methods; (2) direct push methods; (3) field pumping tests; and (4) infiltrometer methods. Test methods within each of these classes are described in the following sections.

Tests performed in open boreholes generally constitute the most common field methods for determining hydraulic conductivity of soils. The exception is compacted clays, which are generally tested using infiltrometer methods. Table 10-7 summarizes different aspects of common borehole methods.

**Table 10-6 Summary of advantages and disadvantages of rigid- and flexible-wall permeameters (modified from Daniel, 1994).**

| Type of Cell | Primary Advantages | Primary Disadvantages |
|---|---|---|
| Rigid-Wall Permeameter | 1. Simplicity of equipment and operation of test.<br>2. Low cost of equipment<br>3. Very large cells can be fabricated with relative ease.<br>4. Large size soil materials (including gravels) can be tested with relative ease.<br>5. Wide range of materials (including chemically resistant) can be used for the cell.<br>6. Unrestrained vertical swelling can be accommodated.<br>7. Zero vertical stress can be applied.<br>8. Variable vertical stress can be applied with special permeameter. | 1. Sidewall leakage is possible.<br>2. No control over horizontal stress.<br>3. If specimen shrinks, sidewall leakage will likely occur.<br>4. Cannot back pressure saturate.<br>5. Cannot confirm saturation with B-Parameter.<br>6. Longer testing time for low hydraulic conductivity materials. |
| Flexible-Wall Permeameter | 1. Can back pressure saturate.<br>2. Can confirm saturation with B-Parameter check.<br>3. Can control principal stresses.<br>4. Sidewall leakage is essentially eliminated even for specimens with rough walls.<br>5. Faster testing time for low hydraulic conductivity materials.<br>6. Can evaluate directional flow properties by orienting specimens. | 1. High cost of equipment.<br>2. Complexity of equipment and procedures.<br>3. Careful specimen handling and trimming required.<br>4. Problems with chemical compatibility of membrane and certain permeants.<br>5. Difficult to perform tests at low stress levels |

### 10.12.1 Auger Hole Method

The auger hole method (Spangler and Handy, 1973) is one of the simplest and easiest methods for rapid field evaluation of hydraulic conductivity. The method is best suited to give approximate values of $k$ in fine-grained soils that maintain an open borehole during drilling. In this method, a borehole of radius, $r$, is drilled to some depth, $d$, below the water table and the height of rise of water in the hole is observed over time. Most often, a number of observations are taken in order to give a measurement of $\Delta h$ and $\Delta t$. The hydraulic conductivity is determined from:

$$k = 0.617\left(\frac{r}{Sd}\right)\left(\frac{\Delta h}{\Delta t}\right) \tag{10.9}$$

where $r$ is the radius of the borehole, $d$ is the depth of the borehole below the water table, and $S$ is a factor that depends on dimensionless parameters $h/d$ and $r/d$ describing the borehole geometry, as shown in Figure 10-24. This method is only applicable when the length of the borehole is relatively large in comparison to the borehole radius (i.e., $d/r > 100$). In practice, the test should be performed a number of times by removing the water to help flush loose soil particle from the sides of the hole. Results from this method may be highly dependent on the quality of the hole and disturbance effects (e.g., smearing).

**Table 10-7 Borehole methods for determining in situ hydraulic conductivity.**

| Method | Comments |
|---|---|
| Auger Hole Method | Simple, inexpensive method based on observing rate of water inflow into an open borehole. Considered very approximate. |
| Open-End Method | Approximate method based on maintaining constant head of water in casing. Water flow is out the end of the casing. |
| Piezometer Slug Test | Falling head (inflow or outflow) in slotted screen piezometer. The most common test. |
| Packer Pumping Method | Pressurized packers seal a test zone in an open borehole. |
| Guelph Permeameter | Constant head tests performed in shallow boreholes. |
| Boutwell Permeameter | Simple two stage procedure produces measurements for both horizontal and vertical hydraulic conductivity. |
| Self-Boring Permeameter | Most complex equipment and procedure. Useful for profiling hydraulic conductivity in clays. |

### 10.12.2 Open End Pumping Tests

Another approximate field method for estimating hydraulic conductivity is the so-called open end pumping test. In this method, a casing is installed to some depth below the water table, as shown in Figure 10-25. The casing is cleaned out and clean water is added to the casing to maintain a constant water elevation (i.e., constant head). The volume of water, $Q$, added to maintain the constant head is measured and the hydraulic conductivity is determined as

$$k = \frac{Q}{5.5rH} \tag{10.10}$$

where $r$ is the radius of the casing and $H$ is the head of water above the water table. A convenient position for maintaining constant water flow is the top of the casing. One disadvantage to this method is that a small volume of soil is tested; however, tests can be performed as drilling proceeds so that values of $k$ can be determined at several depths in the same hole with the casing being advanced for each new test.

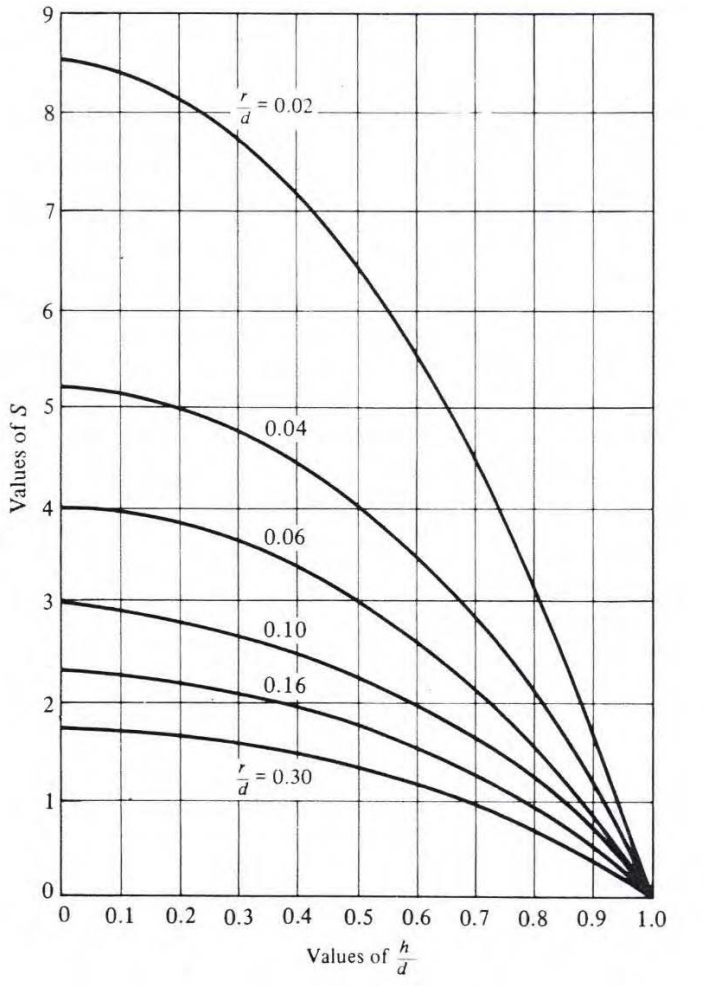


**Figure 10-24 Shape factor for auger hole seepage tests (from Spangler and Handy, 1973).**

### 10.12.3 Slug/Bail Tests in Standpipe Piezometers

One of the most common field methods used for determining hydraulic conductivity is to perform a so called "slug" or "bail" test in an open standpipe piezometer or monitoring well. In a slug test, the water level in a standpipe piezometer is artificially raised to increase the head in the piezometer above that for the surrounding formation. Raising the water level produces an outward gradient and flow as the fluid level in the piezometer seeks to reach equilibrium with the surrounding formation. The change in head is observed over time as this outflow occurs and can be interpreted to estimate the hydraulic conductivity.

Slug tests are commonly performed by lowering a weighted "slug" into the pipe to displace water and raise the water level by an amount proportional to the volume of the slug. The slug is left in place while the water level in the pipe is measured with time. It is then common practice to remove the slug, which lowers the water level below that of the surrounding formation, and monitor the recovery of the

piezometer over time. Several variations of slug tests can be performed, including a "bail" test, wherein a bailer or pump is used to remove water from the well, artificially lowering the water level. It is not generally necessary to wait for the well to completely return to equilibrium conditions; however, a general rule of thumb is to make sufficient observations to recover 80% of the original position.

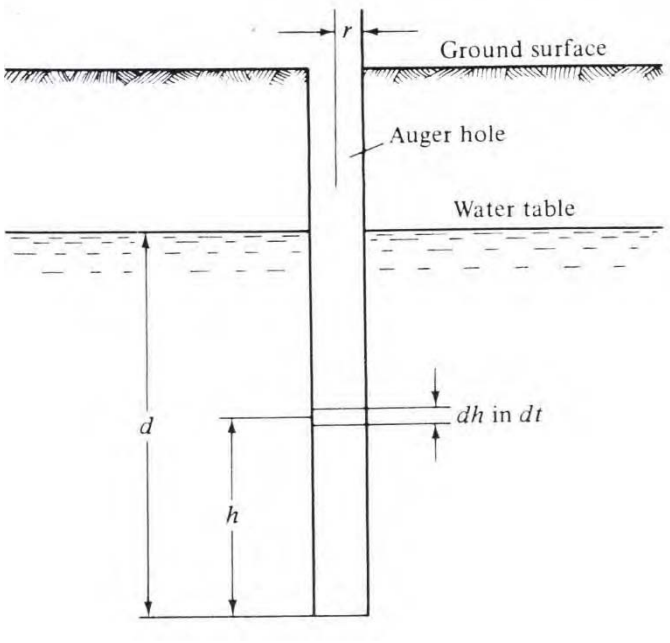


**Figure 10-25 Schematic diagram of open end pumping test (from Spangler and Handy, 1973).**

Interpretation of test results is essentially the same whether the water level is raised or lowered in the piezometer. Test results are usually plotted on a semi-log plot of log head versus time and typically show a straight line as illustrated in Figure 10-26. A common method used to reduce falling head slug or bail test results is to compute $k$ as

$$k = 2.3\frac{am}{F} \tag{10.11}$$

where $a$ is the cross sectional area of the standpipe, $m$ is the slope of the log head versus time curve, and $F$ is a geometric shape factor related to the length and diameter of the well (sand pack).

Chapuis (1989) considered two cases for evaluating the shape factor. For a well placed with sand pack open to the bottom of the hole, thereby allowing both horizontal and vertical flow, Chapuis (1989) suggested the following expression for the shape factor:

$$F = \frac{2\pi L}{\ln\left[\frac{L}{D}+\sqrt{1+\left(\frac{L}{D}\right)^2}\right]} \tag{10.12}$$

where $L$ is the length of the screened section and $D$ is the diameter of the hole. For the case were the base of the well is sealed off, say with a bentonite plug, flow is assumed to only take place in the horizontal direction and $F$ is taken as

$$F = \frac{2\pi L}{\ln\left[\frac{L}{D}+\sqrt{1+\left(\frac{L}{D}\right)^2}\right]} - 2.75D \tag{10.13}$$

Note that the head plotted in Figure 10-26 is the absolute value of the unrecovered head, determined as the water level in the well measured at time $t$ after the test is initiated minus the initial pre-test water level in the well. Equation 10.11 may be used for both slug and bail tests. If a bail test is performed, the reference datum for measuring the heads must be below the base of the well in order to keep the signs correct. Alternative methods for interpreting slug tests are also available (e.g., Hvorslev, 1951; Bouwer and Rice, 1976; Nguyen and Pinder, 1984).

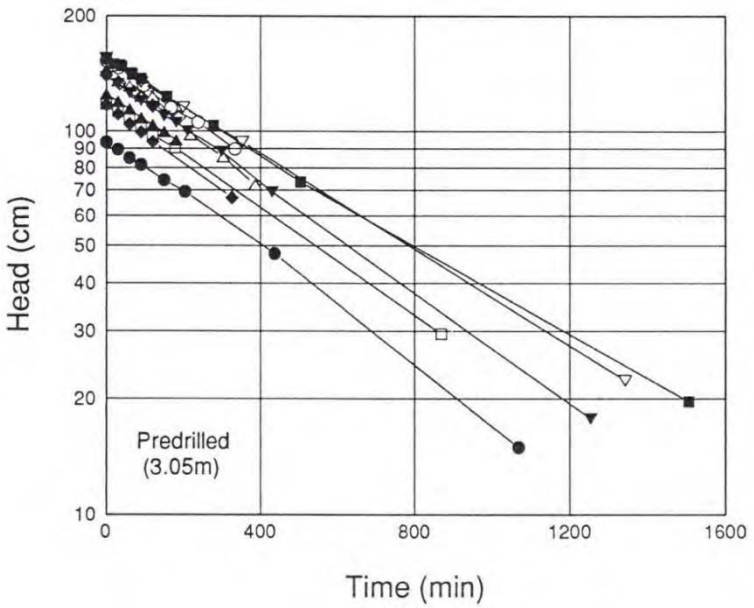


**Figure 10-26 Typical results from a slug test in clay (from Lutenegger and DeGroot, 1992).**

### 10.12.4 Packer Pumping Tests

Another common method for determining hydraulic conductivity in the field is to conduct tests in an open borehole using a packer system as shown in Figure 10-27. As indicated, one or two pneumatic packers are used to seal off a segment of the borehole. During the test, a constant fluid pressure is applied to the

segment of the borehole and the quantity of flow is measured over some time period to determine a flow rate, $q$. For cases where the length to diameter ratio, $L/d$, of the test zone is greater than about 5, the hydraulic conductivity is determined from

$$k = \frac{q}{2\pi LH} \ln \frac{L}{r} \tag{10.14}$$

The head, $H$, in Equation 10.14 is the equivalent head of fluid above the water table obtained by converting the pressure used into a pressure head with units of length.

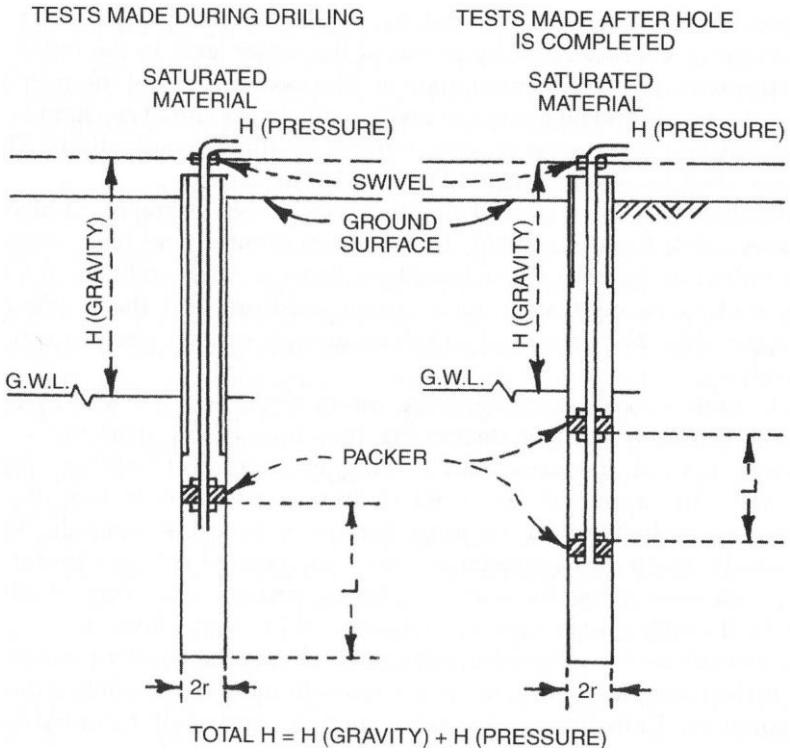


**Figure 10-27 Schematic of a borehole packer test (Sevee, 2006).**

Packer tests have the advantage that many tests can be conducted in the same borehole and are often used to evaluate the hydraulic conductivity of rock strata. In some cases, tests will be repeated at the same test depth using different values of $H$ to observe any changes in $k$ with $H$. For the most part, packer equipment is relatively simple and easy to use, but requires careful measurement of $q$.

### 10.12.5 Guelph Permeameter

The Guelph Permeameter (GP) uses a Mariotte siphon to conduct a constant head hydraulic conductivity test in a borehole as described by Reynolds and Elrick (1986). A schematic of the equipment is shown in Figure 10-28. The screen section is relatively small, on the order of 1.25 inches, and tests can be

performed in small diameter hand-augered holes. The annular space between the screen and the borehole is filled with clean silica sand.

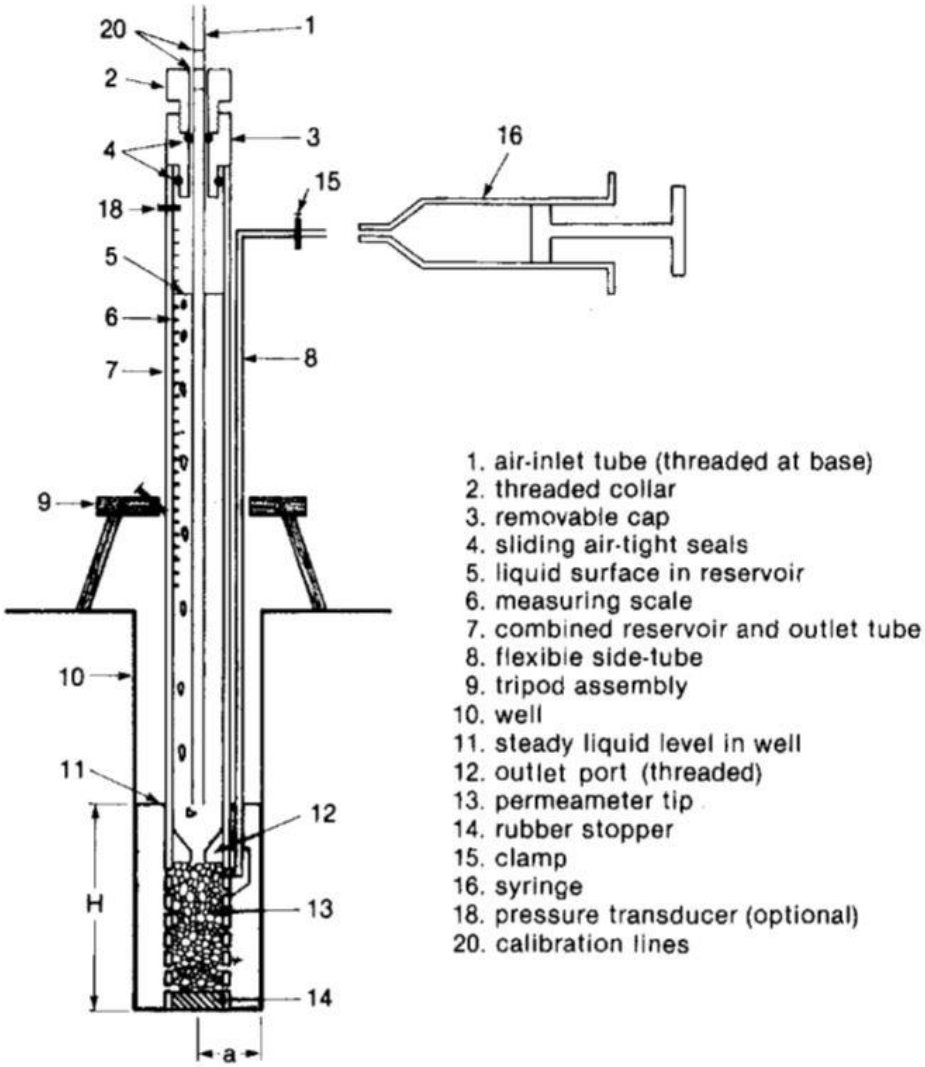


**Figure 10-28 Schematic of a Guelph permeameter (from Reynolds and Elrick, 1986).**

The rate of flow of water into the hole is monitored with a graduated supply reservoir. Several methods may be used to calculate the hydraulic conductivity; however, the simplest of these is:

$$k = \frac{Cq}{(2\pi H^2 + C\pi r^2)} \tag{10.15}$$

where $C$ is a dimensionless proportionality constant dependent on $H/r$, $q$ is the steady-state flow rate, $H$ is the steady depth of liquid in the borehole, and $r$ is the radius of the borehole. Values for the constant, $C$, are shown in Figure 10-29, as suggested by Reynolds and Elrick (1986).

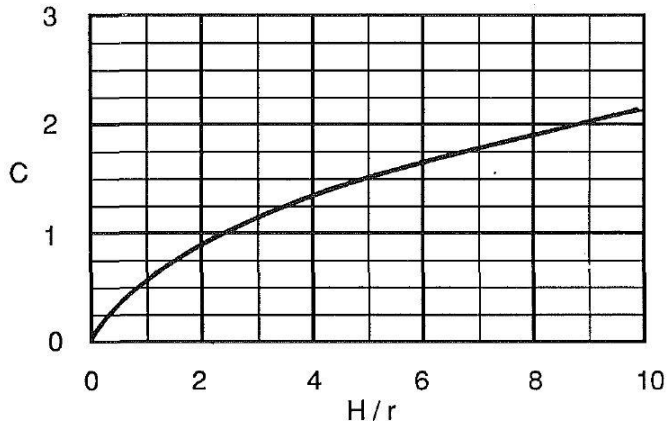


**Figure 10-29 Values of constant *C* for Guelph permeameter (from Daniel, 1989).**

### 10.12.6 Boutwell Two-Stage Permeameter

The Boutwell permeameter is a modification of an open-end permeability test that is performed by varying the geometry of the test zone so that both the vertical and horizontal hydraulic conductivity can be evaluated. In the first stage of the test (Stage I), a borehole is drilled and a casing is lowered into the hole. The annulus between the hole and the casing is filled with bentonite grout to create a seal as shown in Figure 10-30. A falling head test is then performed and the hydraulic conductivity is determined from:

$$k_1 = \left(\frac{Bd^2}{11D(t_2 - t_1)}\right) \ln\left(\frac{h_1}{h_2}\right) \tag{10.16}$$

Values of $k_1$ are plotted versus time and Stage I is considered to be complete when steady state (constant) conditions are reached.

Following completion of Stage I testing, the test hole is extended out the bottom of the casing by augering or pushing a thin-walled tube inside the casing. The length of this test section is typically kept small (approximately 1 to 1.5D), especially if tests are being performed on a compacted clay liner. A second (Stage II) falling head test is then conducted and the hydraulic conductivity is calculated as

$$k_2 = \left(\frac{A}{B}\right) \ln\left(\frac{h_1}{h_2}\right) \tag{10.17}$$

where

$$A = d^2 \ln\left(\frac{L}{D} + \sqrt{1 + \left(\frac{L}{D}\right)^2}\right) \tag{10.18}$$

$$B = 8D\left(\frac{L}{D}\right)(t_2 - t_1)\left[1 - 0.562e^{-1.57\left(\frac{L}{D}\right)}\right] \tag{10.19}$$

Stage II is continued until calculated values of $k_2$ are practically constant.

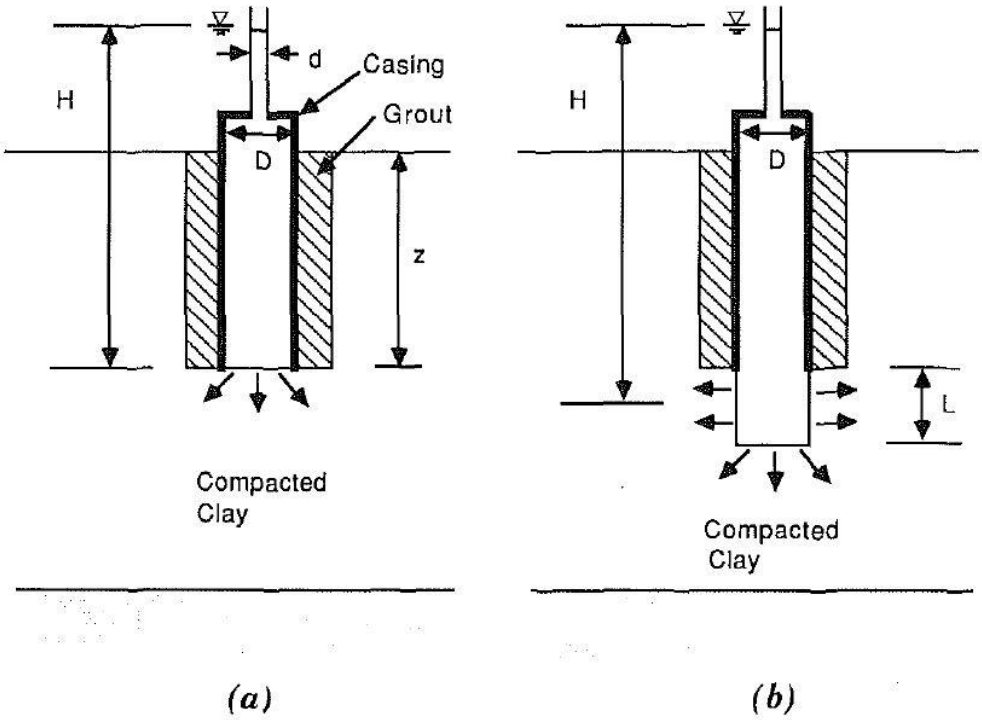


**Figure 10-30 Schematic of Boutwell permeameter: (a) Stage I and (b) Stage II (from Daniel, 1989).**

Values for the horizontal and vertical hydraulic conductivity, $k_h$ and $k_v$, are determined by plotting calculated values of the ratio $k_2/k_1$, computed as

$$\frac{k_2}{k_1} = m\left[\frac{ln\left(\frac{L}{D}+\sqrt{1+\left(\frac{L}{D}\right)^2}\right)}{ln\left(\frac{mL}{D}+\sqrt{1+\left(\frac{mL}{D}\right)^2}\right)}\right] \tag{10.20}$$

versus $m$ and $L/D$ to establish the appropriate value for $m$ that corresponds to the measured values for $k_2/k_1$. Values for horizontal and vertical hydraulic conductivity are then determined from:

$$k_h = mk_1 \tag{10.21}$$

$$k_v = \frac{k_1}{m} \tag{10.22}$$

The Boutwell permeameter is easy to use and has the advantage that the hydraulic conductivity in both the horizontal and vertical directions can be obtained.

### 10.12.7 Self-Boring (Reaming) Permeameter

Use of a self-boring permeameter for evaluating the hydraulic conductivity of clays has been described in some detail by Lafleur et al. (1987) and Tavenas et al. (1990). Initially, a 4-inch auger hole is drilled using either a continuous flight auger or a hand auger. As shown in Figure 10-31, the equipment consists of a self-boring fixture that is placed over the predrilled borehole. The self-boring component enlarges the diameter of the hole to a diameter of about 4.8 inches while advancing the test apparatus to the test depth. Soil cuttings from the tool fall to the bottom of the auger hole. Inflatable packers are used to isolate the test zone. The standard probe has a test length to diameter ratio ($L/D$) equal to 2; however, the ratio can be varied.

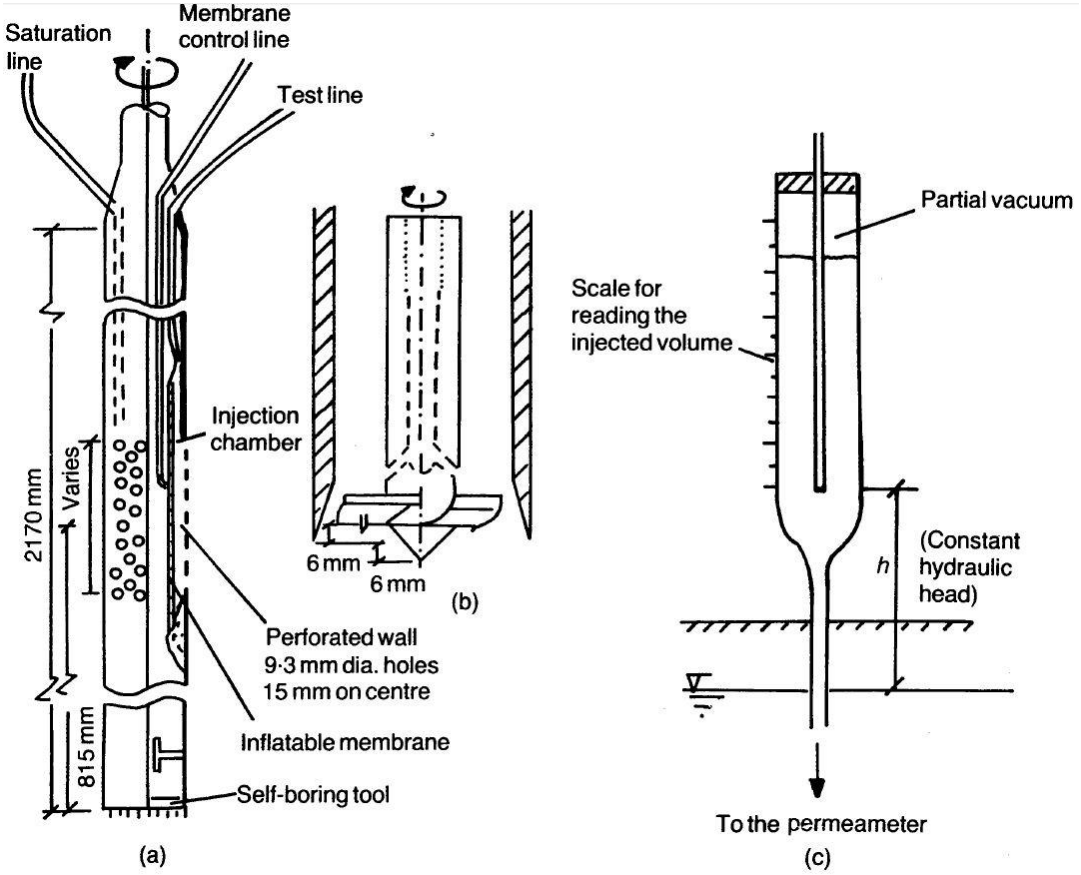


**Figure 10-31 Schematic of a self-boring permeameter (from Chandler, et al., 1990).**

The equipment is designed to overcome some of the shortcomings of other types of borehole tests. However, the equipment is highly specialized. Lafluer et al. (1987) indicate that the equipment was

designed to remove any smeared zone of clay left from augering, apply low heads, be completed in a reasonable time, and allow a continuous profile of hydraulic conductivity to be obtained. Tests may be performed as either falling head or constant head tests and are performed starting at the top of the hole.

### 10.12.8 Field Pumping Tests

Well pumping tests are often performed to determine the hydraulic conductivity of a formation at large scale, in addition to other groundwater flow characteristics that include transmissivity, storage or specific yield, long-term pumping rates, well efficiencies, and aquifer leakage. The content in this section is intended to address use of well pumping tests for interpreting hydraulic conductivity. Additional information regarding well pumping tests for other groundwater flow characteristics can be found in several excellent references on the topic (e.g., Driscoll, 1986; Powers, et al., 2007).

Field pumping tests are performed by pumping water from one well while observing the drawdown that occurs in adjacent observation wells. Field pump tests are considerably more expensive than other borehole tests because they require multiple boreholes and considerable time. However, such tests provide the most accurate means for determining hydraulic conductivity on a large scale, which can be useful for projects where dewatering is necessary for construction.

Interpretation of measurements from field pumping tests depends on whether the tests are performed in confined or unconfined aquifers. In an unconfined aquifer, the shape of the groundwater surface resembles that of an inverted hyperbolic cone, often referred to as the "cone of depression", during steady state pumping conditions. During pumping, the drawdown (drop in water level) at two observation wells located at different distances from the pumping well is measured. The observation wells are installed with sufficient length to extend below the maximum anticipated drawdown. The flow of water towards the well is considered to be radial and the soil is assumed to be homogeneous. The hydraulic conductivity may be obtained from

$$k = \frac{q \ln \frac{r_1}{r_2}}{\pi(h_1^2 - h_2^2)} \tag{10.23}$$

where $r_1$ is the distance from the pumping well to the far observation well, $r_2$ is the distance to the near observation well, $h_1$ is the head measured at the far well, and $h_2$ is the head measured at the near well. The reference datum is taken at some point below the base of the pumping well in order to maintain correct signs for the heads.

For pumping tests conducted in a confined aquifer (at the top and bottom), the observed drawdown in observation wells can be used to determine the hydraulic conductivity from

$$k = \frac{q \ln \frac{r_1}{r_2}}{2\pi B(h_1 - h_2)} \qquad (10.24)$$

where $B$ is the thickness of the aquifer. Equation 10.24 assumes that the pumping well penetrates the full thickness of the aquifer. Reduction of pumping test data using Equations 10.23 and 10.24 assume that the aquifer is homogeneous, the aquifer thickness is constant, the water table has no slope, laminar flow takes place, and the intake portion of the well penetrates the entire aquifer.

## 10.13 EVALUATION OF HYDRAULIC CONDUCTIVITY USING INFILTROMETER METHODS

Infiltrometers, as the name implies, are used to measure the rate of infiltration of water into the ground. Infiltrometer methods are often used for determining the hydraulic conductivity of compacted clays, such as those used for liners for landfills or lagoons, or final covers for landfills. They may also be used in test pits to measure the hydraulic conductivity of near-surface layers that are difficult to sample or otherwise determine $k$. Fractured and fissured deposits such as weathered clays, residual soils, and some glacial deposits are typical examples.

Several different types of infiltrometers have been used, especially for compacted clays as summarized in Table 10-8. Excellent reviews of these tests and typical test results have been presented by Daniel (1989), Sai and Anderson (1990), Fernuik and Haug (1990), and Trautwein and Boutwell (1994). Table 10-9 presents a summary of advantages and disadvantages for different infiltrometers.

**Table 10-8 Infiltrometer methods for determining hydraulic conductivity of compacted clay liners and covers.**

| Method | Comments |
|---|---|
| Open Single-Ring Infiltrometer | Simple single ring or box embedded in surface of soil. Infiltration rate is observed and measured. |
| Sealed Single-Ring Infiltrometer | Single ring is sealed to prevent evaporation losses. |
| Open Double-Ring Infiltrometer | Outer ring is used to maintain vertical flow of water in the inner ring. Simple equipment and easy to use. |
| Sealed Double-Ring Infiltrometer | Inner and outer ring are sealed to prevent evaporation losses. |
| Air-Entry Permeameter | Smaller diameter equipment than most ring infiltrometers. |
| Double-Ring Air-Entry Permeameter | Sealed system to maintain vertical flow as with double-ring infiltrometers. |

**Table 10-9 Advantages and disadvantages of different infiltrometers (modified from Daniel, 1989).**

| Infiltrometer | Advantages | Disadvantages |
|---|---|---|
| Open Single-Ring Infiltrometer | • Low equipment cost.<br>• Easy to install and use.<br>• Very large infiltrometers can be used.<br>• Hydraulic conductivity in the vertical direction is determined. | • Very low hydraulic conductivity is difficult to measure.<br>• Must account for evaporation.<br>• Lateral spreading of wetting front may occur.<br>• Long testing times required.<br>• Must estimate wetting front.<br>• Cannot be used on steep slopes. |
| Open Double-Ring Infiltrometer | • Low equipment cost.<br>• Minimal lateral spreading of wetting front.<br>• Hydraulic conductivity in the vertical direction is determined. | • Very low hydraulic conductivity is difficult to measure.<br>• Must account for evaporation.<br>• Long testing times required.<br>• Must estimate wetting front.<br>• Cannot be used on steep slopes. |
| Sealed Single-Ring Infiltrometer | • Low equipment cost.<br>• Hydraulic conductivity in the vertical direction is determined.<br>• Can measure low hydraulic conductivity. | • Relatively small volume of soil is tested.<br>• Long testing times required.<br>• Must estimate wetting front.<br>• Cannot be used on steep slopes. |
| Sealed Double-Ring Infiltrometer | • Moderate equipment cost.<br>• Minimal lateral spreading of wetting front.<br>• Hydraulic conductivity in the vertical direction is determined.<br>• Can measure low hydraulic conductivity. | • Long testing times required.<br>• Must estimate wetting front.<br>• Cannot be used on steep slopes. |
| Air-Entry Permeameter | • Moderate equipment cost.<br>• Relatively short testing time.<br>• Hydraulic conductivity in the vertical direction is determined.<br>• Can measure low hydraulic conductivity. | • Relatively small volume of soil is tested.<br>• Cannot be used on steep slopes.<br>• A number of important assumptions are needed. |

### 10.13.1 Open Single-Ring Infiltrometer

The simplest infiltrometer is the open single-ring infiltrometer (SRI) shown in Figure 10-32. The ring is embedded in a shallow trench in the soil surface that is sealed with a bentonite-based grout. The ring is typically constructed of either steel or fiberglass and is open at the top as the name implies. The ring is filled with water and the water level is monitored over time to determine the rate of infiltration.

While the wetting front flows downward inside the ring, flow is one-dimensional. However, once it passes the end of the ring, the flow spreads laterally. The infiltration rate is determined as

$$I = \frac{Q}{At} = \frac{q}{A} \tag{10.25}$$

where $I$ is the infiltration rate, $Q$ is the total quantity of flow, $A$ is the area of the ring, $t$ is the elapsed time, and $q$ is the flow rate. The hydraulic conductivity is then determined from:

$$k = \frac{I}{i} = \frac{I}{\frac{(H+L_f+P_f)}{L_f}} \tag{10.26}$$

where $i$ is the hydraulic gradient, $H$ is the depth of water in the ring, $L_f$ is the depth of the wetting front, and $P_f$ is the suction head at the wetting front. The value of $P_f$ can be determined from the hydraulic conductivities of the soil at different values of suction and at saturation, but is usually assumed to be zero. The depth of the wetting front, $L_f$, can be determined by installing tensiometers inside the ring at different depths below the surface or by soil water content measurements after the test is completed. In compacted soils, since the soil is initially unsaturated, plots of the infiltration rate and hydraulic conductivity will show a decrease with time.

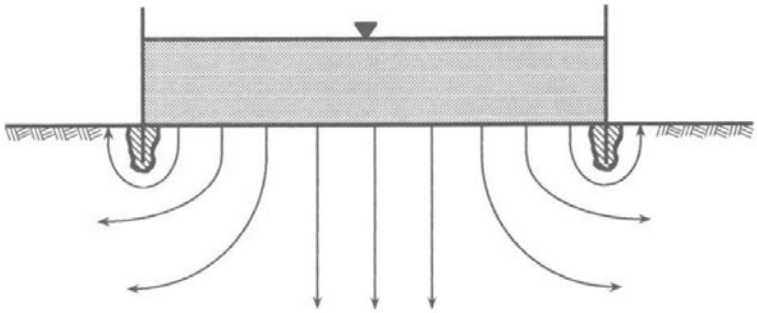

**Figure 10-32 Schematic of open single-ring infiltrometer (from Trautwein and Boutwell, 1994).**

The SRI is simple to perform and inexpensive to fabricate and can be of almost unlimited size. Measuring very low infiltration rates may be difficult and surface evaporation must be considered or controlled. This is usually done by placing a "dummy" ring on an impermeable base and measuring the evaporation loss.

### 10.13.2 Sealed Single-Ring Infiltrometer

In order to eliminate errors associated with evaporation from an open ring infiltrometer, a sealed single-ring infiltrometer (SSRI) may be used. The ring is installed in a narrow trench and sealed with bentonite grout as before. However, the top of the ring is covered and the water level is measured using an external standpipe or Mariotte system, as shown in Figure 10-33. Hydraulic conductivity is calculated using

Equation 10.26 (typically with the assumption that $P_f = 0$). A special design of a SSRI, called an air-entry permeameter, is described in a later section.

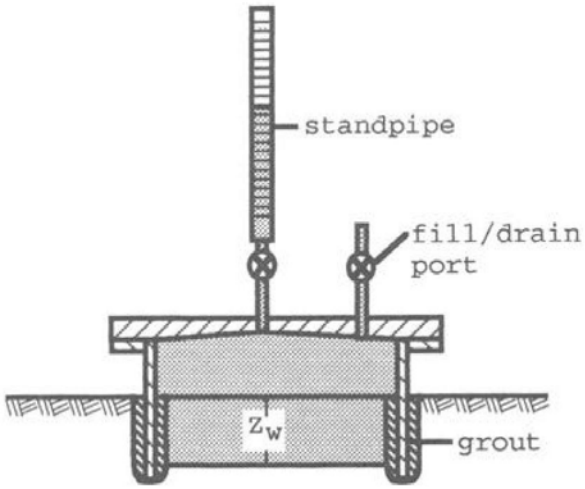


**Figure 10-33 Schematic of sealed single-ring infiltrometer (from Trautwein and Boutwell, 1994).**

### 10.13.3 Open Double-Ring Infiltrometer

In an open double-ring infiltrometer (DRI), two rings or boxes are installed at the surface of the soil just like with a SRI. The purpose of the outer ring is to maintain one-dimensional flow within the inner ring. Both rings are filled with water and the water level is usually maintained at a constant position. The infiltration rate from the inner ring is determined from Equation 10.25 and the hydraulic conductivity is calculated from Equation 10.26. The main advantage in using a DRI over a SRI is in maintaining one-dimensional flow of water that improves the accuracy of estimates for hydraulic conductivity because Equations 10.25 and 10.26 are based on assumed one-dimensional vertical flow.

### 10.13.4 Sealed Double-Ring Infiltrometer

The test equipment and test procedure for using a sealed double-ring infiltrometer (SDRI) are presented in ASTM D3385. Dual rings are embedded and sealed as before and a small flexible bag is attached to the inner ring, as shown in Figure 10-34. The entire test arrangement is covered and periodically, the bag is removed and weighed to determine the amount of flow that has occurred. Tensiometers are often installed to monitor the depth of the wetting front to improve the accuracy of the test. The infiltration rate is determined from Equation 10.25 and the hydraulic conductivity is obtained from Equation 10.26, usually assuming $P_f = 0$.

The SDRI avoids many of the shortfalls of other types of infiltrometers and permits testing of soils with very low infiltration rates. Testing can be performed over long periods, even weeks or months, with the equipment left essentially unattended.

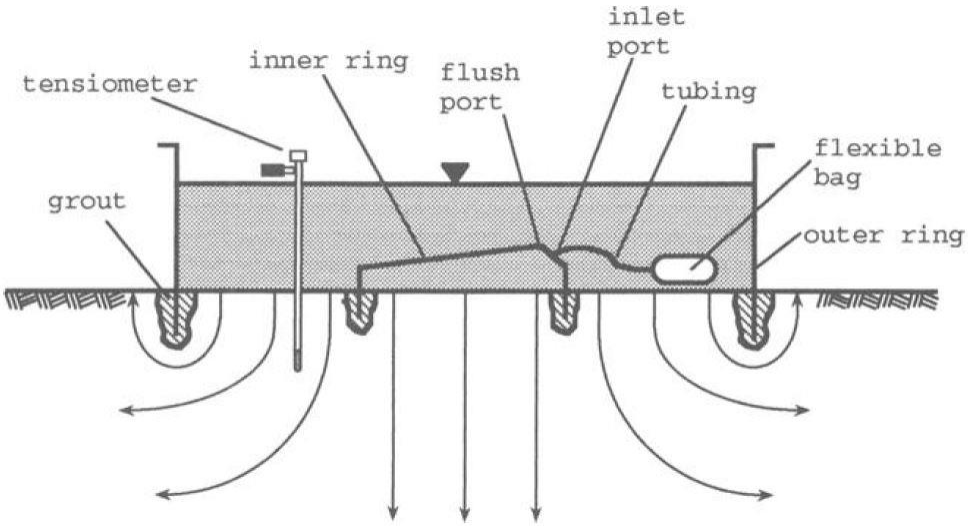


**Figure 10-34 Schematic of sealed double-ring infiltrometer (from Trautwein and Boutwell, 1994).**

### 10.13.5 Air Entry Permeameter

The air-entry permeameter (AEP) was developed and presented by Bouwer (Bouwer, 1966; Bouwer, 1978; Bouwer, 1986) as a simple and rapid method for measuring the hydraulic conductivity of soils in the absence of the water table. A schematic of the AEP is shown in Figure 10-35. The test consists of a steel ring about 24 inches in diameter that is embedded about 4 inches into the soil. A graduated fluid reservoir is attached to the top along with a vacuum gage. The test method measures the rate of infiltration from the changes in water volume from the reservoir over time. Sufficient time is allowed to let the wetting front advance about 4 to 6 inches and then the water supply is turned off. The pressure in the vacuum gage is then monitored and the maximum vacuum pressure is recorded as the air-entry pressure. In the Modified AEP, the depth to the wetting front is measured using tensiometers inside the ring or by taking water content samples after the test is complete.

The hydraulic conductivity is calculated from:

$$k = \frac{qW_f}{AHW_f(0.5P_a)} \tag{10.27}$$

where $k$ is the hydraulic conductivity (m/s), $W_f$ is the depth to the wetting front, $q$ is the water flow rate just before the supply valve is closed ($m^3$/sec.), $P_a$ is the air-entry pressure (m of water on pressure gage)

that is equal to $P_g \cdot G \cdot W_f$, $H$ is the height of the water level above the soil (m), $A$ is the area of the ring ($m^2$), and $G$ is the height of the vacuum gage above the soil surface (m).

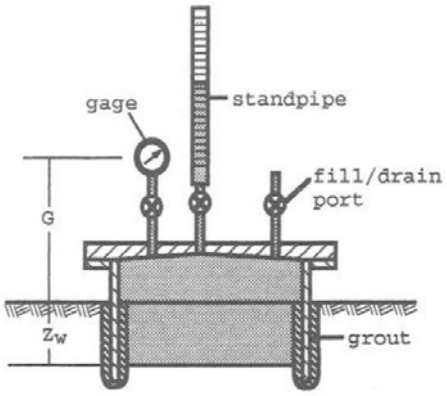


**Figure 10-35 Schematic of air entry permeameter (from Trautwein and Boutwell, 1994).**

Air-entry permeameters can rapidly measure hydraulic conductivity of soils with $k$ on the order of $1x10^{-7}$ cm/s and have been used for both natural and compacted soils (e.g., Nordquist, et al., 1986; Haile and Brown, 1988). However, the test only involves a relatively small volume of soil, which may not be representative. Trautwein and Boutwell (1994) suggested that some uncertainties arising from using an AEP can be addressed using a double-ring air-entry permeameter (DRAEP) as shown in Figure 10-36.

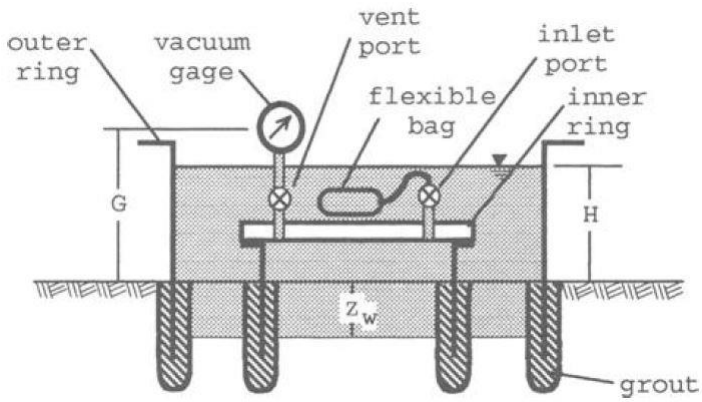


**Figure 10-36 Schematic of double-ring air entry permeameter (from Trautwein and Boutwell, 1994).**

## 10.14 EVALUATION OF HYDRAULIC CONDUCTIVITY USING IN SITU FIELD TESTS

Hydraulic conductivity can also be determined in many soil deposits using several forms of in situ field tests that are conducted without a borehole by pushing or driving a probe into the ground. These include a driven or pushed porous probe, the piezocone (CPTU), the flat dilatometer (DMT), and the BAT system as summarized in Table 10-10.

**Table 10-10 Direct push methods for determining in situ hydraulic conductivity.**

| Method | Comments |
|---|---|
| Pushed Probe | Porous element on pushed or driven standpipe piezometer. Falling head or constant head tests may be performed. |
| Piezocone | Excess pore water pressure dissipation tests in fine-grained soils. Very small filter element. |
| Dilatometer | Excess pore water pressure dissipation tests in fine-grained soils. |
| BAT Probe | Sealed pressure transducer attachment to standard BAT probe. |

### 10.14.1 Driven/Pushed Porous Probe

Hydraulic conductivity tests can be conducted using a simple probe equipped with a porous element that is pushed or driven into the ground. Push-in piezometers are often used in situations when it is advantageous to avoid drilling a borehole. Tests may be performed as either falling head or constant head tests. In a falling head test, the operation is similar to a slug test where the change in head is recorded over time. In this case, Equation 10.11 may be used to determine $k$. In a constant head test, a provision must be made to fill the probe with water and then connect the probe to a simple pressure control console and a graduated volume measure. The pressure to the column is maintained constant while the flow volume over some time period is recorded.

In some soils, there may be problems using driven or pushed piezometers for determining hydraulic conductivity. These problems include clogging of the filter element during installation, smearing or remolding of the soil adjacent to the filter element, and consolidation of the soil after installation. These effects appear to be most important in the case of soft clays and have been described in detail by Tavenas et al. (1986) and Lutenegger and DeGroot (1992).

### 10.14.2 Piezocone (CPTU) Dissipation Tests

Piezocone dissipation tests can also be used to indirectly measure hydraulic conductivity in situ using values for the coefficient of horizontal consolidation, $c_h$, determined as described in Chapter 6. The hydraulic conductivity can be estimated as

$$k_h = c_h \gamma_w m_v \tag{10.28}$$

where $k_h$ is the horizontal hydraulic conductivity (m/s), $\gamma_w$ is the unit weight of water (kN/m$^3$), and $m_v$ is the coefficient of volume change (m$^2$/kN). The value for $c_h$ can be established from dissipation test measurements as described in Section 6.13. The value of the coefficient of volume change, $m_v$, may be estimated using an empirical relationship between the constrained modulus, $M$, and cone tip resistance, $q_c$, as

$$m_v = \frac{1}{M} = \frac{1}{\alpha q_c} \tag{10.29}$$

where suggested values of $\alpha$ are given in Table 10-11.

**Table 10-11 Summary of $\alpha$ values for estimating constrained modulus from $q_c$.**

| Soil Type | Range of $q_c$ | $\alpha$ |
|---|---|---|
| Clay of low plasticity (CL) | $q_c$ < 7 bar<br>7 < $q_c$ <20 bar<br>$q_c$ > 20 bar | 3 < $\alpha$ < 8<br>2 < $\alpha$ < 5<br>1 < $\alpha$ < 2.5 |
| Silts of low plasticity (ML) | $q_c$ > 20 bar<br>$q_c$ < 20 bar | 1 < $\alpha$ < 6<br>1 < $\alpha$ < 3 |
| Highly plastic silts & clays (MH, CH) | $q_c$ < 20 bar | 2 < $\alpha$ < 6 |
| Organic silts (OL) | $q_c$ < 12 bar | 2 < $\alpha$ < 8 |
| Peat and organic clay (Pt OH) | $q_c$ < 7 bar:<br>50 < w < 100<br>100 < w < 200<br>W > 200 | 1.5 < $\alpha$ < 4<br>1 < $\alpha$ < 1.5<br>0.4 < $\alpha$ < 1 |

It should be noted that CPTU dissipation tests provide reasonable estimates of hydraulic conductivity in soils that produce a realistic dissipation curve, such as those shown in Figure 6-31. As a practical matter, this means that CPTU dissipation tests should predominantly be used in fine-grained soils with an upper limit of about $k$ = 1 x $10^{-4}$ cm/s, since the reliability of obtaining a $t_{50}$ value in granular soils is limited. Values of $t_{50}$ less than about 10 seconds may be subject to considerable errors.

Alternatively, the value of $k_h$ may be estimated using a simple empirical approach based on the measured value of $t_{50}$, provided that the cone characteristics (e.g., size, pore pressure element location, etc.) are consistent. Ventura (1983) suggested a simple expression relating hydraulic conductivity $k$ and $t_{50}$ as

$$k = \frac{(10^{-1})}{z t_{50}} \quad (\text{cm/s}) \tag{10.30}$$

where $z$ is the depth of the test in meters. Parez and Fauriel (1988) suggested an empirical chart for estimating $k_h$ based on $t_{50}$ measurements obtained with a porous element located behind the cone tip. A comparison between laboratory-measured values of $k_h$ and $t_{50}$ was presented by Robertson et al. (1992) and is shown in Figure 10-37.

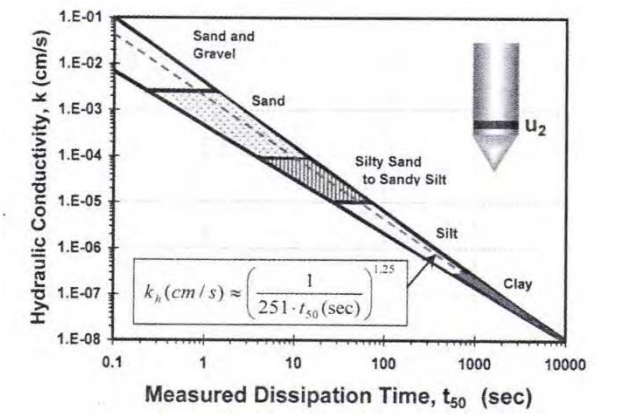


**Figure 10-37 Empirical relationship between $k_h$ and CPTU $t_{50}$ (from Mayne, 2007).**

### 10.14.3 Flat Dilatometer

Hydraulic conductivity can also be estimated from DMT measurements using time-pressure dissipation tests along with Equation 10.28. Values for $c_h$ are determined from the DMT dissipation test as described in Section 6.13. The value for $m_v = 1/M$ can be estimated from the dilatometer modulus, $E_D$, described in Chapter 8.

### 10.14.4 BAT Probe

The BAT water sampling system that is commonly used to obtain samples of groundwater at discrete depths using a hermetically sealed technique may also be used to evaluate hydraulic conductivity. The probe consists of a stainless steel body equipped with a sintered stainless steel porous element located behind a 60-degree conical point. In some respects, the probe resembles a piezocone except that no force or pore water pressures are measured. In operation, the probe is pushed or driven into the ground to some sampling depth. A septum at the top of the body seals the probe from the groundwater.

In order to estimate the hydraulic conductivity, the manufacturer of the BAT system offers an auxiliary kit consisting of a pressure transducer and readout, as shown in Figure 10-38. To perform a hydraulic conductivity test, an evacuated and sealed glass sampling vial is attached to the pressure transducer and lowered down to the probe through a series of extension rods that extend to the ground surface. A double-ended hypodermic needle is used to connect the stem of the probe to the sampling vial and the change in gas pressure inside the vial is measured over time using the pressure transducer.

According to Boyle's law, the change in gas pressure inside the sample vial can be translated to a change in volume. The hydraulic conductivity can then be computed as

$$k = \left(\frac{P_o V_o}{F}\right)\left(\frac{1}{\left(P_t^2 P_3\right)\left(\frac{P_t}{t}\right)}\right) \tag{10.31}$$

where $P_o$ is the initial gas pressure in the sample vial, $V_o$ is the initial volume of gas in the sample vial, $P_t$ is the average measured pressure between $t_1$ and $t$, $P_3$ is the net pressure applied to chamber, $P_t/t$ is the rate of change of pressure, and $F$ is a shape factor.

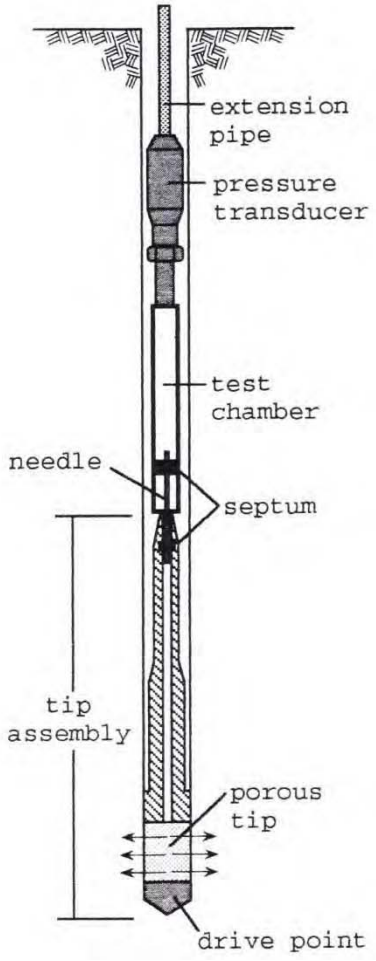


**Figure 10-38 BAT system for determining hydraulic conductivity (from Trautwein and Boutwell, 1994).**

## 10.15 ESTIMATION OF HYDRAULIC CONDUCTIVITY FROM CORRELATIONS

In many cases, it is desirable to make approximate estimates of $k$ for preliminary design purposes. A number of approaches can be taken and used with engineering judgement to choose appropriate values for design. Instead of simply guessing a value for $k$, it is more desirable to make initial estimates of $k$ based on other more easily measured soil properties.

### 10.15.1 Estimating Hydraulic Conductivity for Granular Soils

Several empirical and semi-empirical equations have been proposed to relate the hydraulic conductivity of coarse-grained soils to different soil properties. In general, the grain size characteristics (e.g., mean grain size, grain-size distribution curve, uniformity coefficient, etc.) and density (or void ratio, porosity, etc.) are the two most important factors that influence the hydraulic conductivity of granular soils. This is illustrated in Figure 10-39, which shows values of hydraulic conductivity for granular soils as a function of grain-size characteristics and density.

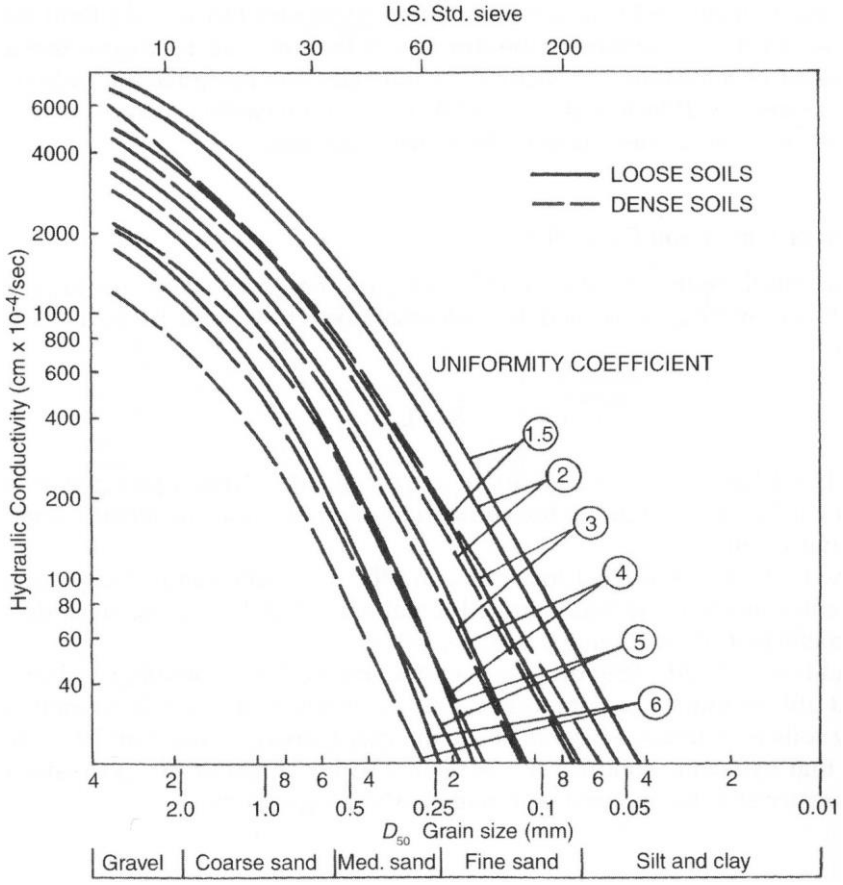


**Figure 10-39 Hydraulic conductivity for sands as a function of porosity (from Sevee, 2006).**

Based on observations of the flow of water through clean, loose sand, Hazen (1911) proposed that hydraulic conductivity could be estimated from:

$$k = C \cdot D_{10}^2 \qquad (10.32)$$

where $k$ is the hydraulic conductivity in cm/s, $C$ is a constant, and $D_{10}$ is the "effective" grain size (in this case, the grain size having 10 percent finer) in units of cm. The value of the constant, $C$, in Equation 10.32 typically varies from about 90 to 120 and a value of 100 is often assumed.

Shepherd (1989) suggested that a general expression relating hydraulic conductivity to grain size could be expressed as

$$k = cd^2 \tag{10.33}$$

where $c$ is a constant and $d$ is particle diameter. The coefficient, $c$, is intended to represent all factors intrinsic to the material that affect hydraulic conductivity, other than grain size. Shepherd (1989) presented a statistical evaluation of 19 sets of published data from laboratory hydraulic conductivity tests and suggested a simple power function for the constant c of the form:

$$c = ax^b \tag{10.34}$$

The regression coefficients $a$ and $b$ in Equation 10.34 were determined by Shepherd using least squares linear regression with $x$ taken as the mean grain size, $D_{50}$. While the coefficient $a$ showed a variation ranging from about 1000 to 200,000 for $k$ in gallons/day/ft$^2$, the coefficient $b$ only ranged from about 1.1 to 2.0.

Because hydraulic conductivity is also dependent on density, Carrier (2003) recommended using the Kozeny-Carman equation for estimating hydraulic conductivity for sands, which accounts for both grain-size characteristics and density. The Kozeny-Carman equation can be expressed as

$$k = 1.99 \times 10^4 \cdot D_{eff}^2 \cdot \frac{1}{SF^2} \cdot \left(\frac{e^3}{1+e}\right) \tag{10.35}$$

where $k$ is hydraulic conductivity in cm/s, $D_{eff}$ is the effective grain-size in cm, and $e$ is void ratio. $SF$ is a dimensionless shape factor to account for the angularity of soil particles that can be taken as 6.6 for rounded particles, 7.5 for particles with medium angularity, and 8.4 for angular particles (Loudon, 1952). $D_{eff}$ is established from grain-size distributions measured from sieve analyses as

$$D_{eff} = \frac{100\%}{\Sigma\left(\frac{f_i}{D_{\ell-i}^{0.404} \cdot D_{s-i}^{0.595}}\right)} \tag{10.36}$$

where $f_i$ is the fraction of particles between two sieve sizes, $D_{\ell-i}$ is the opening size for the sieve with the larger opening size, and $D_{s-i}$ is the opening size for the sieve with the smaller opening size. The

summation in Equation 10.36 is taken for all sieve sizes used to determine the grain-size distribution. The Kozeny-Carman formula is not appropriate for clayey soils, or for gravelly soils where flow may not be laminar, but it is generally appropriate for silts, sands, and gravelly sands. Equation 10.35 is strictly applicable for temperatures of 20 degrees C; alternative forms of the equation can be developed for other temperatures as described by Carrier (2003).

### 10.15.2 Estimating Hydraulic Conductivity for Fine-Grained Soils

In fine-grained soils, the most important factor affecting the hydraulic conductivity is the porosity or void ratio. This is primarily because of the fact that there is a relatively small range in individual particle sizes, with most of the particles being smaller than 0.074 mm (No. 200 sieve). This means that particle arrangement or packing, which is best described by the total porosity or void ratio, is important. In fact, since the flow of water actually takes place through the pore space, the pore-size distribution will in large part control the hydraulic conductivity; however, this is difficult to quantify for routine investigations.

A number of laboratory investigations have demonstrated that, for a given clay, there is a fairly unique relationship between hydraulic conductivity and void ratio. Test results show that a plot of log $k$ versus void ratio is nearly linear, as illustrated in Figure 10-40. Unfortunately, different clays show different relationships between $e$ and $k$. At a fixed void ratio, the range in $k$ for a number of different soft clays may vary by more than 2 orders of magnitude as shown in Figure 10-41. However, as the void ratio approaches very small values, on the order of 0.2 to 0.3 that are indicative of very dense materials approaching rock, the curves tend to converge.

Mesri et al. (1994) proposed an empirical expression for hydraulic conductivity of clays that accounts for differences in pore size and shape arising from differences in clay content and mineralogy and suggested:

$$k = 6.5 \times 10^{-11} \left[ \frac{\frac{e}{CF}}{A_c + 1} \right]^4 \qquad (10.37)$$

where $k$ is the hydraulic conductivity (m/s), $e$ is void ratio, $CF$ is the clay size fraction (percent < 0.002 mm), and $A_c = PI/CF$ is the clay "activity".

The rate of change in hydraulic conductivity with a change in void ratio is sometimes referred to as the "change of permeability index", denoted as $C_k$, where $C_k = \Delta e / \Delta \log k$. Tavenas et al. (1983) suggested that an empirical relationship for soft clays existed between $C_k$ and the in situ void ratio as

$$C_k = 0.5(e) \qquad (10.38)$$

For a given change in void ratio, large values of $C_k$ imply small changes in $k$ whereas small values of $C_k$ correspond to large changes in $k$. For soft clays, typical values of $C_k$ range from about 0.4 to 1.6.

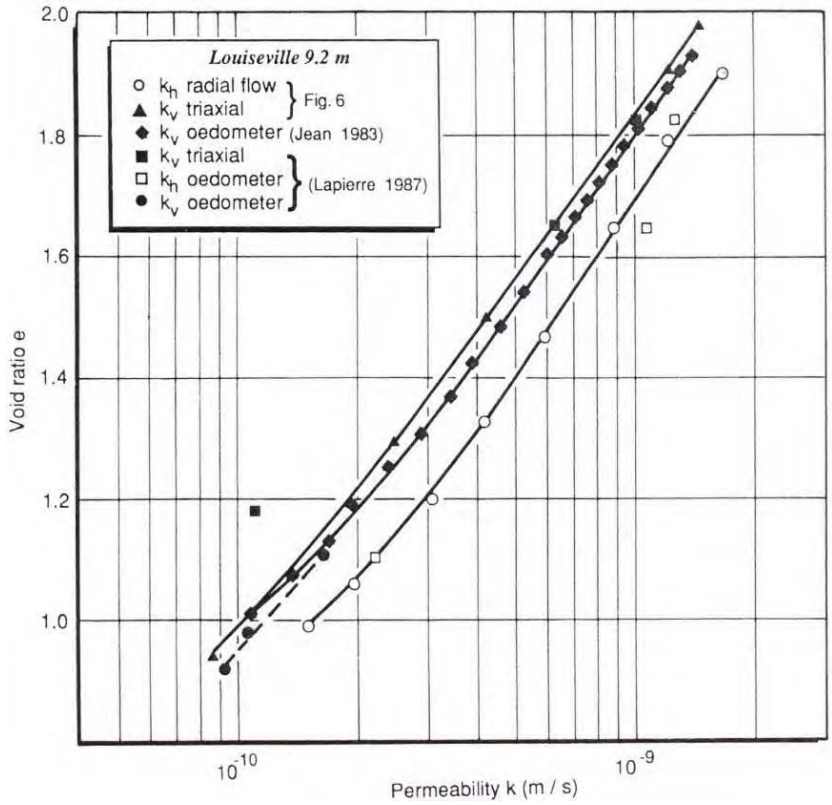


**Figure 10-40 Hydraulic conductivity of a clay as a function of void ratio (Leroueil, et al., 1990).**

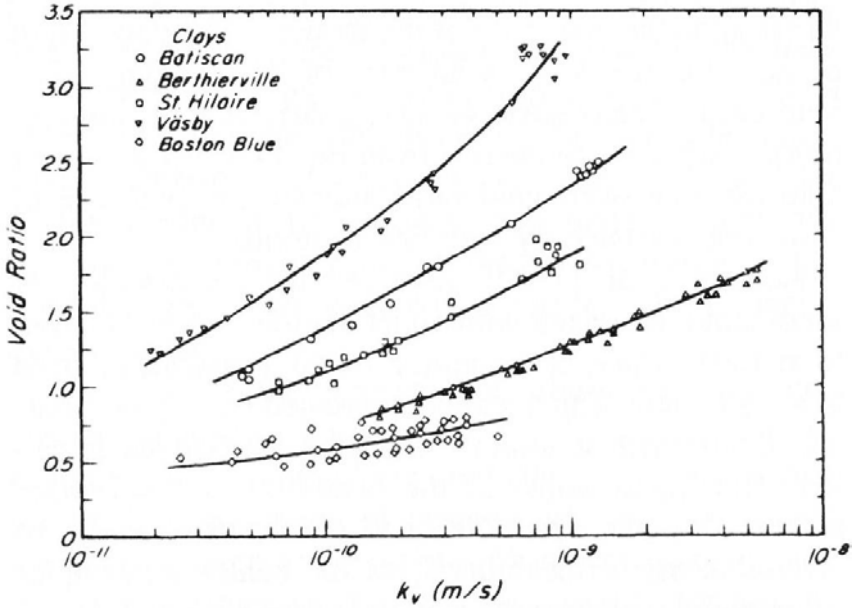


**Figure 10-41 Relationship between $k$ and $e$ for five different clays (from Terzaghi, et al., 1996).**

# CHAPTER 11
# DEVELOPMENT OF DESIGN MODELS AND SELECTION OF DESIGN PARAMETERS

Site characterization activities for engineering design generally culminate with development of appropriate site models for design and selection of required design parameter values for all strata within those models. As described in Chapter 1, the term "property" is used in this manual to refer to a specific characteristic of soil or rock, something that can generally be directly measured in a test, whereas the term "parameter" is used to represent a specific term or input variable in some model or design and analysis method. Previous chapters have described how specific soil and rock properties should be interpreted from individual field or laboratory measurements. The content of this chapter focuses on establishing appropriate design parameters based on collective interpretation and synthesis of available soil or rock property measurements. In this chapter, activities and considerations required for synthesizing available measurements to develop rational site models for geotechnical design are described, including estimates for required engineering design parameters.

## 11.1 OBJECTIVES FOR INTERPRETATION OF DESIGN PARAMETERS

The fundamental objective for interpretation of design parameters is to establish an appropriate, rational, and defensible site "model" that can be used for analysis and design of specific transportation features. Here, the term model is used to refer to a conceptual representation of actual site conditions. Site models are inherently three-dimensional because sites are three-dimensional, although it is common to simplify and characterize the three-dimensional conditions using one or more two-dimensional "design cross-sections" similar to that shown in Figure 11-1. For many design problems, design models may be further simplified into what are effectively one-dimensional models, or "design profiles", that represent conditions at a specific site location, as illustrated in Figure 11-2. Throughout this chapter, site models developed for design are collectively referred to as "design models", which may include design cross-sections, design profiles, or even complete three-dimensional models of a site. Design models are generally not complete and thorough representations of actual site conditions, but instead are practical interpretations of site conditions subject to varying degrees of simplification and approximation for the purpose of design.

In addition to providing a practical representation of interpreted site stratigraphy, design models also include values for specific design parameters, potentially including interpretations of how specific parameter values vary spatially with depth, elevation, or lateral position within the model domain. Individual design models are generally developed to represent a specific time or time period (e.g., short-

term, long-term, etc.), although several versions of models may be developed to represent conditions at different times or stages of construction. Values for design parameters are generally established to represent some volume of soil or rock that can practically be considered to be consistent for design purposes. Design models should also include characterization of the variability and uncertainty associated with the design parameters so that designers can effectively address the uncertainty present for specific parameters.

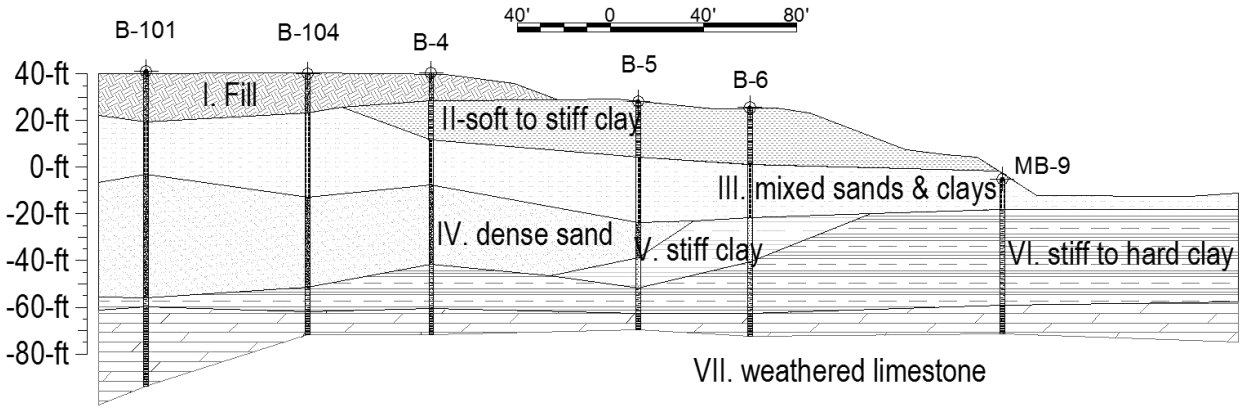


**Figure 11-1 Design cross-section illustrating conceptual stratigraphy adopted for design.**

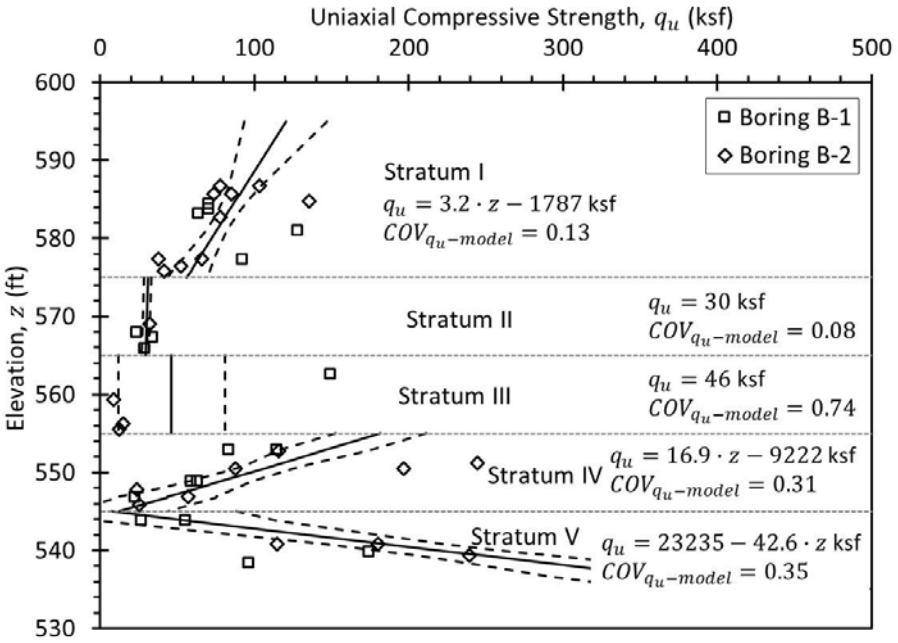


**Figure 11-2 Design profile showing constant or linearly varying $q_u$ for individual strata.**

One challenge for developing appropriate design models is that the process is inherently non-unique. It is common, and perfectly acceptable, for different individuals to rationally choose to represent the same

collection of measurements somewhat differently, and for both representations to appropriately reflect conditions at a site. Such differences are inherent to site characterization with limited data. These statements should not be taken to imply that any arbitrary representation will be appropriate but rather that there is simply no single "correct" interpretation. The appropriateness of a specific interpretation should be judged based on the following criteria:

1. Is the model consistent with available measurements from the site, with due consideration for potential bias in the measurements and potential changes in soil/rock properties?
2. Is the model consistent with the geologic setting at the site location?
3. Is the model practical and appropriate for the intended use?
4. Is this model compatible with the design and analysis methods that will be adopted for design?
5. Is the model consistent with previous experience and observed performance in the site vicinity (if available)?

Alternative design models satisfying these criteria will generally produce practically consistent results for design as long as sufficient numbers of measurements are used, as described in Chapter 3. For example, Figure 11-3 shows two different design models developed to represent the same collection of compressibility index, $C_c$, measurements. While the two models are slightly different, both can be considered rational and appropriate for the conditions encountered and consistent with available measurements, and both are practically quite similar. Additional illustrations of alternative interpretations for the same collections of measurements are provided in Appendix 2.

Judgment regarding comparison of alternative design models can be quantitatively informed by computing the variability of available measurements about the interpreted design parameter values as described in more detail in Section 11.5. In general, interpretations of design parameter values with lesser variability can be considered as superior interpretations. For example, computed values for the coefficients of variation of the measurements, $COV_{C_c-meas}$, shown in Figure 11-3 suggest that the interpretation in Figure 11-3a is quantitatively better than the interpretation in Figure 11-3b. Both interpretations are certainly reasonable and appropriate for design, but the interpretation considering two layers with constant properties is slightly more reliable than the interpretation considering linearly increasing values of $C_c$ with depth. Such quantitative comparisons should be combined with sound judgment and should not be taken to the extreme (which might lead to interpretations with many thin layers, all having a single measurement), but they do provide an objective means to compare alternative interpretations. Methods for calculating variability and uncertainty for various forms of design models are provided in Section 11.5 and Appendix 3.

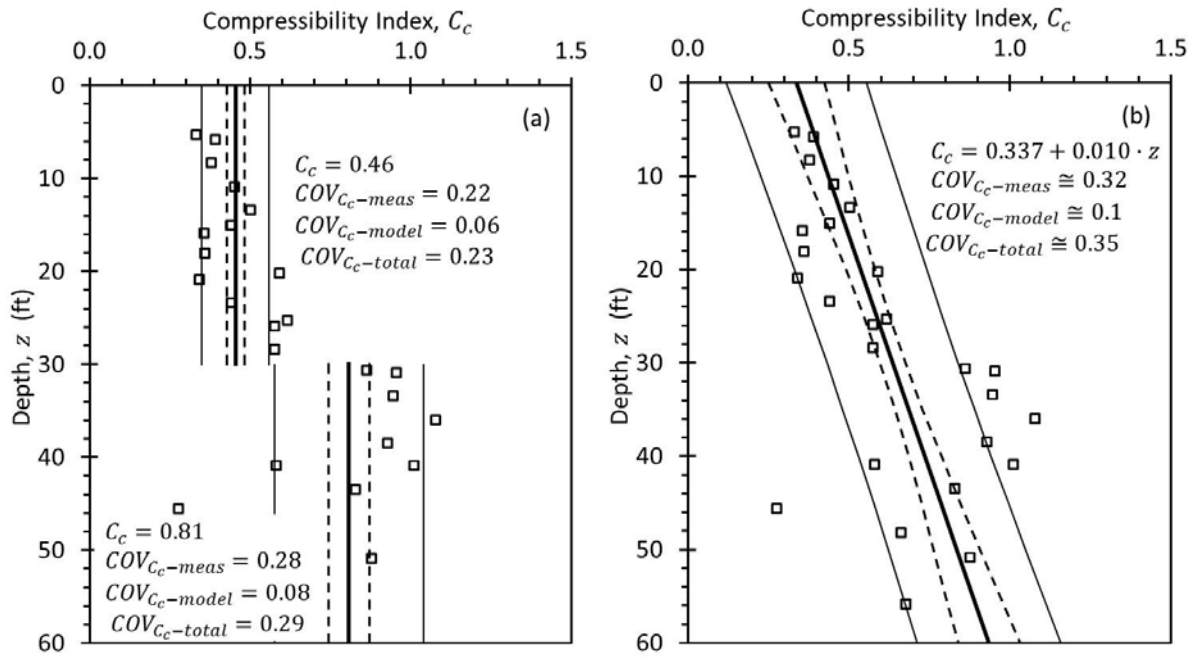


**Figure 11-3 Alternative interpretations of $C_c$ measurements.**

It is also important to recognize that it is commonly appropriate and acceptable to develop different interpretations of the same site for different applications or design conditions. A common example of this is encountered when considering short-term and long-term stability of embankments founded on soft soils. The undrained shear strength that is appropriate for short-term stability evaluations is often observed to vary substantially with depth and might require representation using several different strata (or "sub-strata") or using a model with some linear variation within the strata. Conversely, the effective stress strength parameters for the same clay will often be practically uniform over the entire stratum. In the end, different interpretations developed for different applications or design conditions at the same site should be fundamentally consistent and compatible, but they do not have to be identical.

## 11.2 PROCESS FOR INTERPRETATION OF DESIGN PARAMETERS

No single procedure will always lead to development of rational and reliable design models. Development of effective design models requires significant judgment and effort, combined with sound knowledge of soil and rock mechanics, thorough understanding of the intended use for the interpretations, and knowledge of the geologic setting and character of the site. The process generally involves developing trial interpretations with progressive revisions that should be guided by judgment, experience, and knowledge of the mechanical behavior of soil and rock, geology, and geomorphology. Common steps generally include:

1. Developing one or more preliminary cross-sections or profiles characterizing the general stratigraphy at the site, often based on qualitative descriptions of soil/rock type from field exploration logs or soil behavior type designations from cone penetration test (CPT), piezocone (CPTU), or dilatometer (DMT) soundings combined with results of index property tests and knowledge of the geologic setting.
2. Establishing preliminary "design domains" over which conditions can practically be considered to be consistent, and developing additional cross-sections or profiles to represent each distinct design domain.
3. Collecting field and laboratory measurements for relevant design parameters within each design domain and plotting the measurements versus depth or elevation for each domain.
4. Reviewing graphs of measurements versus depth or elevation, and evaluating whether measurements of the relevant design parameter are consistent with the stratigraphy developed for the preliminary cross-section or profile.
5. Establishing preliminary interpretations for design values for each specific design parameter based on available measurements.
6. Repeating these steps and progressively refining the design model until the model is practical, consistent with available measurements, and compatible with the intended use.

Additional discussion of Steps 1 and 2 is provided in Section 11.3. Additional discussion of Steps 3 through 6 is provided in Sections 11.4 through 11.7. While the process described here is presented as being sequential, it is important to emphasize that the process is iterative and should involve progressive development, evaluation, and refinement of the model(s) to arrive at interpretations that are consistent with observations from the site and appropriate for the intended use.

An important final step in the process of developing design models is to establish appropriate methods for verifying, and potentially modifying design models during construction. Common verification methods range from relatively simple requirements for verifying the presence of specific materials or bearing conditions during construction, to more formal measurements like proof rolling, compaction quality assurance tests, or pilot borings for deep foundations. For more substantial projects, or cases with complex ground conditions where it is difficult to develop reliable design parameters, verification may rely on various forms of instrumentation (e.g., piezometers, inclinometers, strain gages) to assess performance during construction using the "observational method" described in Section 11.7.

A similar process is usually adopted for design-build projects. However, final design models are only developed after the design-build contract is awarded and the design-build team completes final site

investigations. Design-build teams will generally develop one or more tentative design models for design prior to bidding. After contract award, additional investigations should be completed to confirm or modify these tentative design models.

## 11.3 INTERPRETATION OF SUBSURFACE STRATIGRAPHY

Interpretation of stratigraphy is an important component of site characterization and geotechnical design. Failure to identify and characterize important stratigraphic features can lead to problems during construction, problems with long-term performance, and, in some cases, collapse or failure of geotechnical features (e.g., Hendron and Patton, 1985). However, it is also important to recognize that it is impractical (if not impossible) to accurately and precisely model all stratigraphic features at a site for design and that some level of simplification and approximation is necessary. Thus, the challenge for site characterization is to accurately identify and model all *important* stratigraphic units within the constraints of practicality and the design and analysis methods that will be used.

Design cross-sections or profiles for a single design domain are generally assumed to be composed of one or more individual strata. Within an individual stratum, the value of a design parameter can fundamentally be represented with varying degrees of complexity. However, as a practical matter, the design parameter of interest is generally assumed to have values that are constant throughout the stratum, or vary linearly with depth or elevation as illustrated in Figure 11-2 and 11-3. All design profiles can be reasonably represented in this way.

There are numerous ways to interpret stratigraphy. Stratigraphy can be interpreted from careful observation of field boring and sampling activities, from in situ test measurements, from geophysical measurements, from measurements of index properties, and from measurements of design properties. Interpretations of stratigraphy for design are often developed progressively using several of these sources of information. Initial interpretations of stratigraphy are often derived from observations drawn from field boring logs or in situ test measurements, combined with knowledge of the geologic setting for the site. These initial interpretations are then reviewed and compared with measurements from laboratory index property tests and engineering property tests in order to evaluate whether the initial interpretation is consistent with available measurements that are relevant for the particular application of interest. Initial interpretations are then refined based on consideration of available measurements for design properties and the intended use of the interpretations. Such a process is often performed progressively as additional measurements are acquired and additional uses are considered.

In establishing preliminary cross-sections or profiles, it is common to observe that field exploration logs and in situ test soundings indicate substantially more "material boundaries" than can practically be considered, or more "layers" than are truly consequential for design. This condition arises frequently because field interpretations are generally based on visual and textural characteristics that may have little influence on values for design parameters, but may be important for other uses. Different "layers" from these sources can often be combined without substantially impacting design. For example, a thick clay stratum with several sand lenses may rationally be represented as a single clay layer for many design purposes. However, the presence of even a thin permeable sand layer within the clay could have a major impact for construction of an excavation support system or tunnel. Such decisions should therefore be made using sound judgment and understanding of the intended use for the design models. While simplicity is advantageous for design models, it should not be accomplished at the cost of ignoring potentially important stratigraphic features that could impact design or construction.

Geophysical measurements and in situ tests can be particularly helpful in establishing interpretations of stratigraphy, depending on the character of the stratigraphy at a site. Geophysical measurements are often useful for characterizing the depth to stratigraphic interfaces between strongly dissimilar materials (e.g., depth to bedrock), for helping to interpolate between sparsely located borings, and for identifying anomalies that warrant further investigation. However, many geophysical measurements involve some "averaging" of the geophysical response over some tested volume and, therefore, may not be appropriate for characterizing localized features. Conventional sampling and testing also has some precision related to identifying localized features because continuous sampling is seldom performed. As such, both types of measurements have the potential to miss thin, localized, or discontinuous strata. Continuous profiling techniques like CPT, CPTU, and DMT measurements are well suited to identification of abrupt or subtle changes in stratigraphy when the strata can be practically penetrated.

Selection of appropriate design domains is also a matter of considerable judgement. For sites with straightforward stratigraphy and consistent properties, a single design domain encompassing the entire site may be appropriate. Conversely, for sites with highly variable stratigraphy and/or properties, numerous design domains may be appropriate, with each domain representing conditions appropriate for only a small portion of the site. Considering design for a significant bridge for example, a single design profile may appropriately be used for design of all bridge foundations if properties are relatively uniform. Conversely, individual design domains for each foundation may be appropriate for complex or highly variable sites, with each domain having different stratigraphy and design parameter values. As is true of interpretation in general, selection of appropriate design domains is necessarily a non-unique exercise. Nevertheless, it is important that the significance of different domain choices be deliberately considered

because “lumping” an entire site into a single domain as a matter of convenience can have dramatic consequences for design and construction when such a choice is not supported by available evidence (e.g., Graham, et al, 2013).

## 11.4 INTERPRETATION OF DESIGN PARAMETERS FROM AVAILABLE MEASUREMENTS

Establishing appropriate values for design parameters based on available measurements is critically important for geotechnical design. Selecting values that exceed those that actually exist at the site will lead to increased risk from unacceptable performance while selecting values that are substantially less than actually exist will lead to costs for construction that are greater than required. Selection of appropriate values for design parameters therefore warrants deliberate effort and careful attention.

As described in more detail throughout the remainder of this section, values for design parameters should be established by separately plotting available measurements for each identified stratum and design domain. When collectively plotting measurements, it is advantageous to plot measurements from different borings or field test locations using different symbols to help distinguish among measurements from different locations as illustrated in Figure 11-4. For similar reasons, it is advantageous to plot measurements for a single design parameter from different types of tests (e.g., measurements of $s_u$ from UU triaxial tests, unconfined compression tests, and field vane shear tests) using different symbols to help identify potential biases among different types of measurements. Graphs should also generally be plotted as discrete symbols, without connecting lines, because connecting lines may suggest relationships that are neither reasonable nor adequately justified by available measurements. These simple practices can dramatically improve one’s ability to identify discrepancies in preliminary interpretations and improve the quality of interpretations overall. In many cases, observations from review of collective plots may motivate or dictate refinement or revision of preliminary design cross-sections or design profiles. Measurements from different borings may also motivate or dictate revision or refinement of selected design domains if the measurements indicate substantial differences for different locations (recalling that design domains should be selected to represent a consistent portion of a site).

As described throughout this manual, values for design parameters can be established using some combination of direct or indirect measurements acquired as part of site characterization activities. In addition, it is relatively common to have some quantity of historical measurements that can also be used to help develop interpretations for relevant design parameters. While there are similarities among

interpretation of direct, indirect, and historical measurements, there are also special considerations that must be considered for each as described in the following sections.

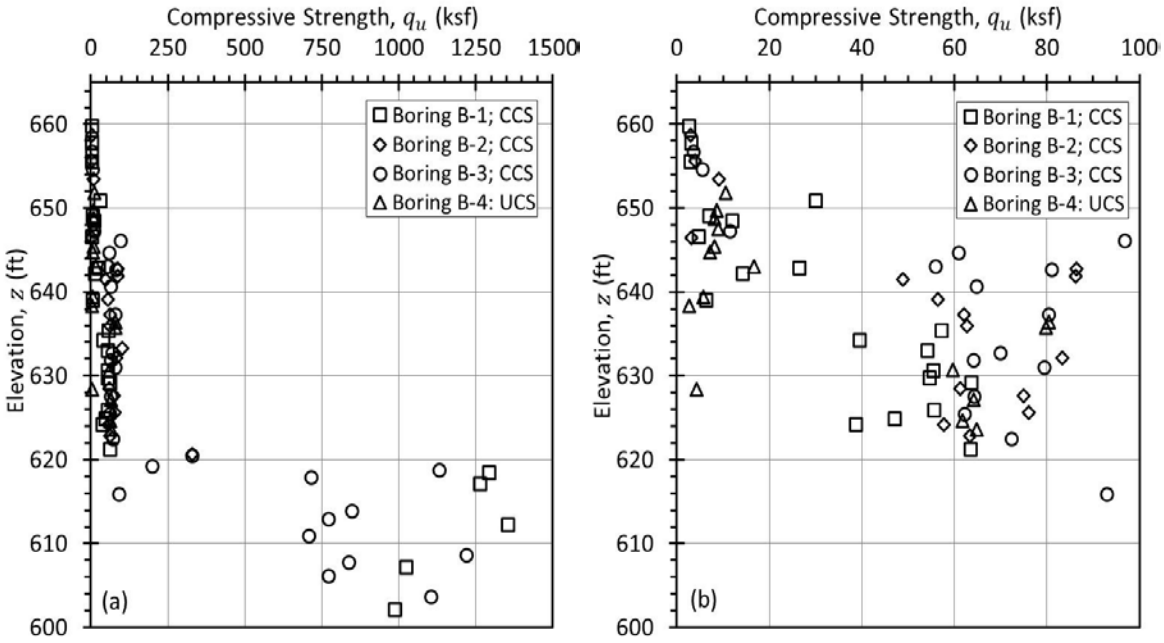


**Figure 11-4 Direct measurements of $q_u$ from uniaxial ($UCS$) and confined compression tests ($CCS$) from four borings plotted using different symbols: (a) full scale and (b) expanded scale.**

### 11.4.1 Selection of Design Parameters from Direct Measurements

Direct measurements are often the most straightforward means to establish values for design parameters because no transformation is required to establish estimates for design parameters. Several approaches can be adopted for establishing values for design parameters from direct measurements, each with advantages and disadvantages.

Traditionally, values for design parameters have been established from inspection of available measurements, preferably plotted in graphs similar to those shown in Figure 11-4. Based on inspection of such graphs, a designer traditionally selects some representation of the parameter value that the designer considers to practically represent the design parameter based on available measurements. The selected representation is commonly established considering the quality and quantity of the measurements, the criticality of the feature being designed, and perhaps the importance of the particular design parameter for the design analyses. The selected representations commonly follow the general trend of the available measurements, but are often slightly less than the mean value of the measurements to account for variability and uncertainty in the measurements. In cases with few measurements, highly variable

measurements, measurements of questionable quality, or for critical features, designers might select values that are substantially less than the "mean" trend of the measurements to compensate for these factors. Conversely, in cases with large numbers of high quality measurements and little variability, designers will commonly select parameter values that are closer to the mean value.

This traditional approach has generally produced designs that perform acceptably. However, the approach is highly subjective and introduces potential for different designers to produce substantially different interpretations depending on how an individual judges and weights considerations of measurement quantity, quality, and variability. More conservative interpretations will produce more conservative designs that are likely to perform acceptably, but that may cost more to construct than is truly required. Conversely, less conservative interpretations will produce designs that can be constructed more cost effectively, but have greater likelihood of performance problems. The traditional approach is also inconsistent with load and resistance factor design (LRFD) methods, which predominate design practice for transportation features in the U.S. and generally rely on estimates of the mean value for design parameters.

A more objective and more formal alternative to the traditional approach is to use regression analyses for available measurements to inform interpretations of specific design parameters within individual strata. For strata where a design parameter can be considered constant, the arithmetic mean of the available measurements, computed as

$$\bar{y}_d = \frac{\sum_{i=1}^{n_d} y_i}{n_d} \tag{11.1}$$

often serves as the "regression", where $y_i$ are direct measurements of a particular design parameter, $n_d$ is the number of available direct measurements, and $\bar{y}_d$ is the mean value. Note that the subscript $d$ is used here to indicate that the mean value is derived from direct measurements. For strata where a soil or rock property varies continuously throughout the stratum, several different regression methods can be used. The most common method is least squares regression, and specifically the Ordinary Least Squares (OLS) method, which is readily implemented in commercial spreadsheet software. When considering a stratum with properties that vary linearly throughout a stratum, the regression produces an expression of the form

$$\bar{y}_d(z) = \beta_0 + \beta_1 z \tag{11.2}$$

where $\beta_0$ and $\beta_1$ are regression coefficients that, respectively, represent the intercept and slope of the regression function, $z$ is the regression parameter (often depth or elevation), and $\bar{y}_d$ represents the mean value of the design parameter at a given value of $z$.

Regardless of the specific regression method selected, use of regression techniques has the distinct advantage of providing greater consistency among interpretations developed by different individuals, thus avoiding the potential inconsistency of the traditional approach. Regression analyses also produce interpretations that represent the "mean" trend of the available measurements, which is appropriate for use with AASHTO LRFD methods. However, thoughtless application of regression analyses for interpretation of available measurements also has significant disadvantages. OLS regression techniques are notoriously sensitive to extreme measurements or "outliers", which can produce interpretations that poorly represent available measurements, and actual site conditions. The outlier problem is exacerbated when few measurements are available. Even more importantly, application of regression techniques can tend to limit careful thought and consideration that is commonly applied when following the traditional approach. Application of regression methods without careful consideration of soil and rock mechanics, geology, and geomorphology can lead to design models that are poor representations of actual conditions and the true behavior of the soil and/or rock.

Because both the traditional approach and regression have limitations for developing appropriate interpretations of design parameter values, a combined or hybrid approach that utilizes regression analyses to inform and support application of sound judgment is recommended for interpretation when sufficient numbers of measurements are available within an individual stratum. In this approach, regression analyses are performed to establish an estimate for the design parameter, but this estimate is then carefully considered, and perhaps revised, based on observation of the available measurements, knowledge of how the soil or rock was formed, knowledge of fundamental soil and rock mechanics, knowledge of how the design parameter will actually be used for design, and knowledge of potential implications for inappropriately selecting values for the design parameter. Figure 11-5 shows the measurements from Figure 11-4 plotted along with an interpretation of $q_u$ for the shale and limestone present. In this instance, the interpreted values of $q_u$ for each stratum are taken to be the mean values of measurements within each stratum.

The specific number of measurement needed for regression analyses depends on the quality and consistency of the measurements and is generally ill defined. However, rather than seeking to acquire some minimum number of measurements needed to establish a suitable regression, designers should instead seek to acquire sufficient measurements to produce acceptable model uncertainty, where model

uncertainty is represented by $COV_{model}$ described in Section 11.5. As described in Chapter 3, designs performed using parameters established from mean values with $COV_{model} \leq 0.3$ are likely to have reliability that practically equals or exceeds the target reliability for design according to the AASHTO LRFD Bridge Design Specifications. In cases where the number of measurements for a particular stratum is insufficient to produce $COV_{model} \leq 0.3$ and the design parameter for that stratum is important for design, additional measurements should be acquired if possible. If acquiring additional measurements is not practical, or if the cost of acquiring additional measurements exceeds the benefits that may be derived from having additional measurements, conservative values of the design parameter should be selected based on the measurements that are available.

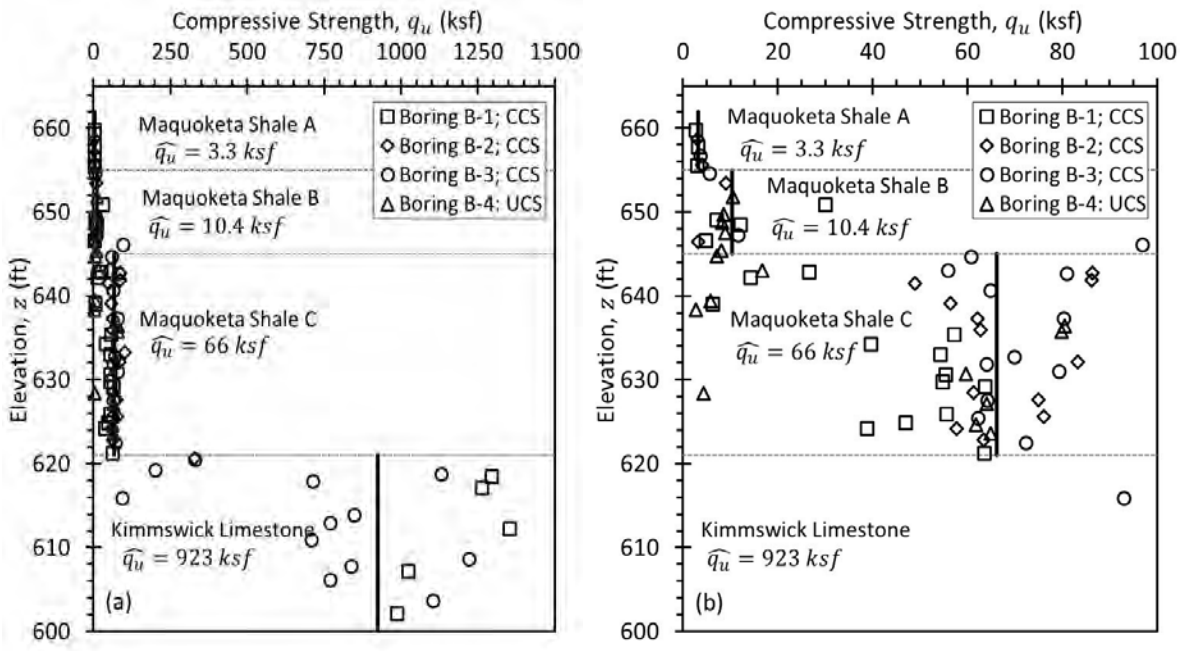


**Figure 11-5 Interpretation of stratigraphy and $q_u$ from direct measurements: (a) full scale and (b) expanded scale.**

Another important consideration when establishing values for design parameters is the specific design methods that will be employed for design. Design practice for most of the U.S. transportation industry has predominantly adopted load and resistance factor design (LRFD) methods for geotechnical design. The vast majority of these methods adopt load and resistance factors that have been calibrated considering that design parameters used for the methods represent mean values. Thus, it is important that interpreted design parameters practically represent mean values when using these methods since the combined effect of the load and resistance factors theoretically accounts for some nominal level of uncertainty in the design parameters, in addition to other sources of uncertainty. Use of design parameter values that are less than mean values with such design methods will produce designs with greater reliability than would

be achieved using mean values, but also generally greater costs, which violates the intent and spirit of LRFD. The requirement to use mean values for design parameters does not diminish the importance of applying sound judgment when selecting design parameter values, especially when available measurements may be subject to bias from various sources (e.g., sample disturbance, only testing intact rock, biased testing methods) or when the model uncertainty is greater than 0.3.

If alternative design methods that have not been calibrated for use with mean values of design parameters are to be used, it is important that values for design parameters be selected to be consistent with those methods. For example, design methods from Eurocode standards utilize so-call "characteristic values" of design parameters in conjunction with partial factors (analogous to load and resistance factors in LRFD). In U.S. design practice, some methods prescribed by the U.S. Army Corps of Engineers have historically been developed to adopt a so-called "2/3 rule" wherein values for design parameters should be interpreted such that 2/3 of the available measurements fall above the design value and 1/3 of available measurements fall below that value. The main point to these issues is that values for design parameters should be established in the spirit of the design methods that will be used.

While established values for design parameters should generally reflect measurements of associated soil or rock properties that have been made at the site, there are also instances where judgment should be invoked to produce values for design parameters that may rationally differ from available measurements because of known bias in the measurements (e.g., Ladd and Foott, 1974). An example of such a case arises in staged construction, where undrained shear strength measurements made during site investigations may not accurately reflect the actual $s_u$ during staged construction because consolidation of the soil will change $s_u$. Such judgments should be made carefully, with full consideration of fundamental concepts of soil and/or rock mechanics.

Alternatively, it is sometimes rational to select design parameters that are consistent with extreme measurements (e.g., lower bound) of soil or rock properties, if such values tend to control design. As an example, when designing deep foundations for axial loading, the axial capacity of the foundation is often strongly influenced by the average shear strength over the length of the foundation rather than by lesser values of shear strength measured at individual locations (because the total side resistance is the integral of unit side resistance along the foundation). In contrast, design of earth slopes may be strongly influenced by lower-bound measurements of shear strength, if such strengths represent a persistent weak seam across a site since a sliding surface may form that closely follows the "weak seam". Such considerations again support the recommendation that considerable judgment is required when developing "design models", requiring sound knowledge of how design parameters will actually be used.

Additional discussion of extreme measurements, and how they should be considered for design is provided in Section 11.6.

### 11.4.2 Estimation of Design Parameters from Indirect Measurements

As described in Chapter 3, indirect measurements require that some transformation be applied to the actual measurements to produce an estimate for the soil or rock property of interest. Interpretation of design parameters from indirect measurements should therefore include all of the considerations described for interpreting direct measurements, with the additional consideration of the transformation.

Given an appropriate transformation function, two general approaches can be adopted for establishing values for design parameters from indirect measurements:

1. Transforming individual indirect measurements to produce an estimated "measurement" for each indirect measurement, then collectively interpreting the estimated measurements.
2. Interpreting the actual indirect measurements to produce some interpretation (i.e., "model") of the actual measurements, then transforming the model values to produce an estimate for the design parameter.

In the first approach, each indirect measurement is transformed to produce a transformed "measurement" of the design property of interest as

$$y_{s-i} = f(x_i) \tag{11.3}$$

where $y_{s-i}$ is a transformed measure for the design property of interest derived from indirect or "surrogate" measurements, $f$ is a function representing the transformation, and $x_i$ is an individual indirect measurement in the stratum of interest. Using this approach, an estimate for the design parameter of interest is established in a manner similar to that described in the previous section for direct measurements, but instead using transformed measurements. In contrast, using the second approach, the estimate for the design parameter of interest is established from an interpretation of the indirect measurements, $\hat{x}$, as

$$\hat{y}_s = f(\hat{x}) \tag{11.4}$$

where $\hat{y}_s$ is the estimate for the design parameter derived from indirect measurements, $f$ is a function representing the transformation, and $\hat{x}$ is the interpreted value of the indirect measurement in the stratum

of interest. For strata where the indirect measurement can be practically represented as uniform, the value for $\hat{x}$ can be computed as the mean value of the indirect measurements:

$$\hat{x} = \bar{x} = \frac{\sum_{i=1}^{n_x} x_i}{n_x} \tag{11.5}$$

where $\bar{x}$ is the mean of the indirect measurements, $x_i$ represents the individual indirect measurements, and $n_x$ is the number of indirect measurements. In strata where the indirect measurements can be represented as linearly varying, regression analyses can be performed directly on the indirect measurements as described for direct measurements in Section 11.4.1.

Each of these approaches have advantages and disadvantages, with neither approach being clearly superior and both approaches producing similar, if not identical interpretations. The first approach has the advantage of allowing one to interpret in terms of design property values, which allows the interpreter to more easily consider the magnitude of the values in the context of design. Conversely, the second approach allows one to more explicitly consider the variability of the indirect measurements and the uncertainty introduced by the transformation as described in more detail in Section 11.5.

Figure 11-6 illustrates application of the alternative approaches for point load strength index, $I_s$, measurements taken from three borings at a site composed of shale overlying competent limestone. Since the transformation for point load strength index is linear, i.e., $q_u = k \cdot I_s$, both approaches produce identical interpretations in this case. Additional description of these issues is provided in Section 11.5.

So-called empirical correlations that relate estimates for soil or rock properties to measurements of soil/rock index properties are fundamentally just indirect measurements. As such, the methods described in this section should be applied to estimates derived from empirical correlations, with due consideration of the uncertainty present in the transformations. Some common transformations, including many that have been presented in previous chapters, may produce estimates for design parameters that dramatically exceed actual properties. As such, considerable caution is warranted when applying general transformations and users are strongly encouraged to quantify and consider the uncertainty in estimates of design parameters established from indirect methods as described subsequently in this chapter. In many cases, site-specific transformations can be developed and used to produce substantially more reliable estimates for design parameters, as illustrated subsequently in this chapter.

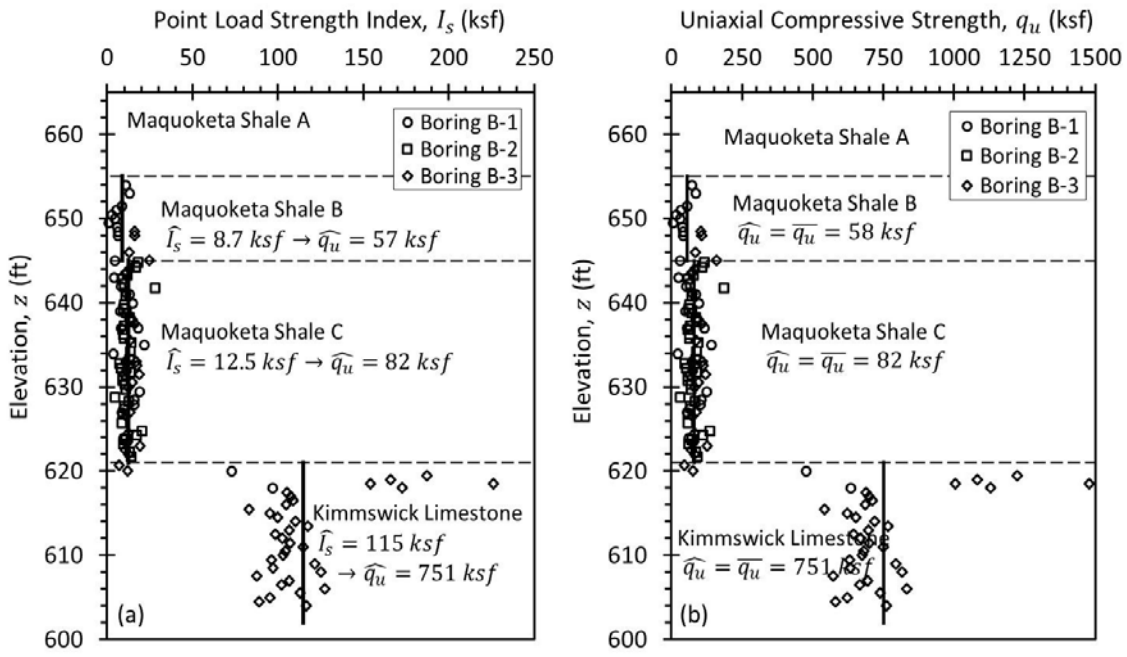


**Figure 11-6 Alternative approaches for interpreting indirect measurements: (a) interpretation of $I_s$ prior to transformation and (b) transformation of $I_s$ prior to interpretation.**

### 11.4.3 Use of Historical Data for Establishing Design Parameters

In some cases, historical measurements collected from previous investigations at a site may be available. Historical measurements can be useful for interpretation because they provide additional measurements beyond what is collected for the current project, which can help to reduce uncertainty for relevant design parameters. Historical measurements may also be used to provide information regarding whether soil or rock properties may have changed over time.

As a general rule, historical measurements can often be treated like recent measurements. However, it is important to consider whether the measurements are representative of current conditions and whether the equipment and procedures used to acquire the measurement may have changed over time. For example, standard penetration tests (SPT) were historically performed using hammers that are dramatically different than those in current use today. Older SPT hammers were often substantially less efficient than those in current use and it was uncommon for hammer energy to be measured or documented in historical practice. As such, SPT $N$-values acquired several decades ago are often substantially and systematically greater than SPT $N$-values that are acquired today because modern hammers are more efficient than historical hammers. These differences are not a result of changes in site conditions, but rather are a result of changes in equipment and practice over time. Many current design procedures often require interpretation of $N_{60}$ values that are corrected for hammer efficiency. Historical SPT measurements are

therefore not appropriate for supplementing current measurements of $N_{60}$ values because hammer efficiency was often not recorded. While it may be possible to estimate hammer efficiency based on the type of hammer used (if that information was recorded), such estimates introduce substantial uncertainty into the historical measurements, which makes them less reliable than current measurements. Similar arguments can be made regarding potential changes in soil or rock conditions for a specific site, for example due to changes in effective stress as a result of excavation. Thus, historical measurements introduce a degree of uncertainty into values of specific properties or measurements and this uncertainty should be considered when selecting values for design parameters.

A common and logical approach to using historical measurements is to perform sufficient numbers of measurements during current investigations to allow historical measurements to be evaluated. As an example of such an approach, Figure 11-7 shows a comparison of SPT $N$-value measurements collected for a site over a period of 21 years using different SPT equipment. While similar trends are observed with depth, there is a clear tendency for the measurements made in 1978 to produce lower $N$-values than measurements made in 1999 in this particular case. Measurements from 1978 should therefore be used with caution when deriving estimates for design parameters.

## 11.5 CALCULATION OF VARIABILITY AND UNCERTAINTY FOR DESIGN PARAMETERS

Selection of nominal values for geotechnical design parameters is usually the primary objective of interpretation for site characterization since the selected values have a direct and observable influence on the resulting geotechnical design(s). For example, selecting lesser values for soil or rock strength will generally lead to requiring greater foundation sizes, or perhaps progressing to more costly foundation types altogether, as a direct result of applying the selected parameter values. However, it is also important to recognize that the uncertainty associated with selected design parameters has a direct influence on the reliability of designs produced using those parameters. While many designers recognize this relation, the unfortunate reality is that such considerations are generally subjective and often underappreciated. As demonstrated in Chapter 3, the degree to which target reliabilities are achieved in design is closely tied to the variability of a given site and to the quantity and quality of measurements that are available for interpretation of geotechnical design parameters. Judicious and appropriate interpretation of design parameters therefore requires that the uncertainty of estimates for design parameters be quantified to reduce the likelihood for producing under-reliable designs. Explicit and quantitative evaluation of uncertainty in geotechnical design parameters also provides means to assess the relative uncertainty among different sites and different site investigations so that scoping for future

investigations can be improved. Methods for quantifying variability and uncertainty are described in this section.

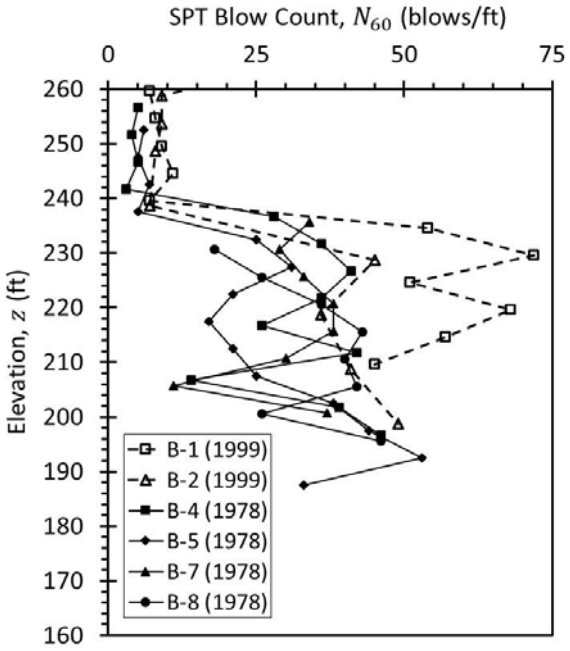


**Figure 11-7 Comparison of SPT *N*-values measured at similar location in 1978 and 1999.**

### 11.5.1 Calculation of Variability and Uncertainty for Direct Measurements

Direct measurements are subject to variability and uncertainty introduced due to natural variability in the samples acquired for testing and due to variability and uncertainty in the measurement techniques. As such, the variability and uncertainty in design parameters established from direct measurements is controlled by these same sources. As described in Chapter 3, the term "variability" is used in this manual to represent the consistency of actual properties, or measurements of a property, within a particular site or stratum whereas "uncertainty" is used to represent the level of knowledge about a specific property. In this section, specific quantitative measures for representing both variability and uncertainty are presented.

Several quantitative statistical measures can be used to represent variability and/or uncertainty including the mean squared error ($MSE$), the variance ($Var$ or $\sigma^2$), the standard deviation ($\sigma$), and the coefficient of variation ($COV$). For strata that are considered to have a constant value of a property (i.e., a "uniform" stratum), the mean squared error of a collection of independent, direct measurements of an arbitrary property, $y$, is defined as:

$$MSE_d = \frac{\sum_{i=1}^{n_d}(y_i - \hat{y}_d)^2}{n_d - 1} \tag{11.6}$$

where $y_i$ is the $i^{\text{th}}$ measurement of $y$, $\hat{y}_d$ is the estimated value of $y$, and $n_d$ is the number of direct measurements. Note that the subscript "$d$" is used here to indicate that the estimate is derived from direct measurements and the "hat" accent "$\hat{}$" is used to indicate an estimated value of the parameter $y$. $MSE_d$ is a measure of the scatter of measured values (specifically the second moment of the error) about the estimated value of a property that incorporates both variability and bias of the measurements for the property. If the estimate for the property is unbiased, meaning that the estimate is taken to be equal to the mean (i.e., $\hat{y}_d = \bar{y}_d$), the variance, $Var$, is equal to $MSE_d$, i.e.,

$$Var(y) = \sigma^2_{d-meas}(y) = MSE_d = \frac{\sum_{i=1}^{n_d}(y_i - \hat{y}_d)^2}{n_d - 1} \tag{11.7}$$

where $\sigma_{d-meas}$ is the standard deviation of the measurements and the subscript $d$ again indicates that the unbiased estimate is derived from direct measurements. Thus, the standard deviation is simply the square root of the variance

$$\sigma_{d-meas} = \sqrt{Var(y)} = \sqrt{MSE_d} = \sqrt{\frac{\sum_{i=1}^{n_d}(y_i - \hat{y}_d)^2}{n_d - 1}} \tag{11.8}$$

The standard deviation, $\sigma_{d-meas}$, describes the variability of the *measurements* about the estimated value of the parameter and is perhaps the most familiar measure of variability.

Several alternative measures of variability and uncertainty are likely less familiar to many readers, but often more relevant for geotechnical site characterization. Specifically, the variance of the estimated value of the parameter, which represents the level of confidence in the estimated value given the available measurements, can be computed as

$$\sigma^2_{d-model} = \frac{MSE_d}{n_d} = \frac{1}{n_d} \cdot \frac{\sum_{i=1}^{n_d}(y_i - \hat{y}_d)^2}{n_d - 1} \tag{11.9}$$

where

$$\sigma_{d-model} = \sqrt{\frac{MSE_d}{n_d}} = \sqrt{\frac{1}{n_d} \cdot \frac{\sum_{i=1}^{n_d}(y_i - \hat{y}_d)^2}{n_d - 1}} \tag{11.10}$$

will be referred to as the "model" standard deviation. The model variance and model standard deviation represent the uncertainty in the estimated value of the parameter $y$. Finally, the combined variability and uncertainty of an estimate for a specific parameter is represented by combined consideration of the

variability of the measurements about the estimate (i.e., the standard deviation of the measurements, $\sigma_{d-meas}$) and the uncertainty of the model (i.e., the model standard deviation, $\sigma_{d-model}$) to compute the "total" variance, $\sigma_{d-total}^2$, as

$$\sigma_{d-total}^2 = \sigma_{d-meas}^2 + \sigma_{d-model}^2 = \left(\frac{\sum_{i=1}^{n_d}(y_i - \hat{y}_d)^2}{n_d - 1}\right)\left(1 + \frac{1}{n_d}\right) \tag{11.11}$$

where

$$\sigma_{d-total} = \sqrt{\sigma_{d-meas}^2 + \sigma_{d-model}^2} = \sqrt{\left(\frac{\sum_{i=1}^{n_d}(y_i - \hat{y}_d)^2}{n_d - 1}\right)\left(1 + \frac{1}{n_d}\right)} \tag{11.12}$$

is the total standard deviation computed as the square root of the sum of the squares of the measurement variability and the model uncertainty.

Figure 11-8 shows the model interpretations from Figure 11-5 with indications of the three alternative measures of variability and uncertainty: the measurement variability (represented using $\sigma_{d-meas}$), the model uncertainty (represented using $\sigma_{d-model}$), and the total variability and uncertainty (represented using $\sigma_{d-total}$). The total standard deviation is the greatest of the three alternative measures and is appropriate for use when predicting a new instance of a measurement using the established model for the parameter value. For example, if one had ten specific measurements, and wanted to estimate the value that might be measured for an eleventh measurement, the total standard deviation appropriately represents the combined variability and uncertainty since the value of the new measurement depends on both the variability of available measurements and the uncertainty in the estimated or "model" value. In contrast, the model standard deviation is the smallest of the three alternative measures and is generally appropriate when one is interested in the uncertainty of an estimate for the parameter. When considering design parameters, the model standard deviation is generally the relevant measure because it reflects the level of confidence in the estimated value of the design parameter. The fact that additional measurements may be scattered due to variability of the specimens and the measurements is not important in such cases. Thus, the model standard deviation is generally the measure that should be adopted for most design analyses.

Figure 11-9 shows similar interpretations derived from a smaller set of measurements taken from a single boring. In this case, fewer measurements are considered, so confidence in the estimated values for $q_u$ decreases and this is reflected in the magnitude of $\sigma_{d-model}$. In contrast, the standard deviation of the measurements, $\sigma_{d-meas}$, and the total standard deviation, $\sigma_{d-total}$, both may increase slightly, decrease slightly, or remain practically unchanged, as the number of measurements considered changes. Table 11–

1 summarizes the quantitative measures of variability and uncertainty for the interpretations shown in Figure 11-8 and 11-9.

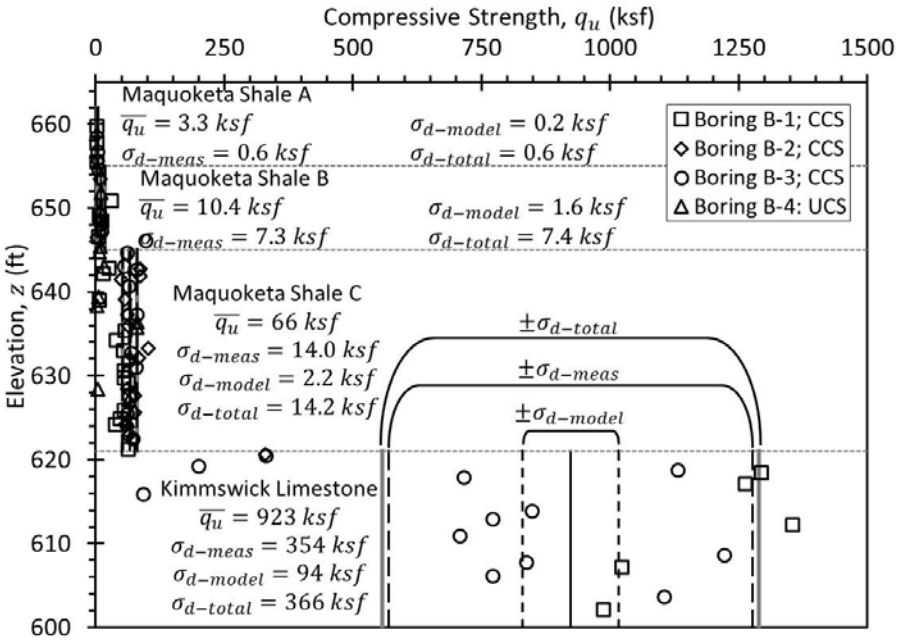


**Figure 11-8 Measured values of $q_u$ showing three measures of variability and uncertainty.**

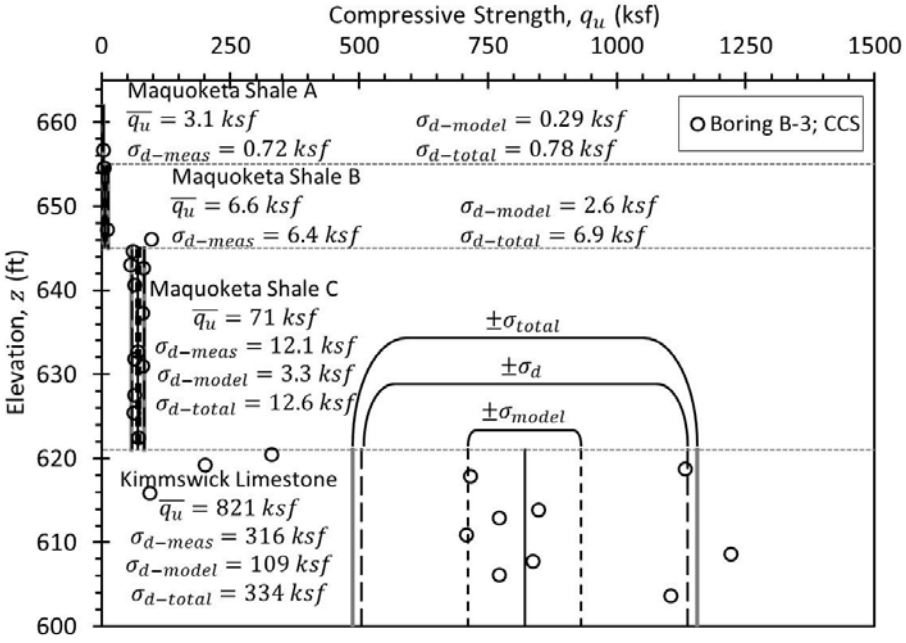


**Figure 11-9 Measured values of $q_u$ showing variability and uncertainty for fewer measurements.**

**Table 11–1 Measures of variability and uncertainty for $q_u$ from Figures 11-8 and 11-9.**

| Stratum | Estimated Value, $\mu_{q_u}$ | | Measurement Variability, $\sigma_{q_u-meas}$ | | Model Uncertainty, $\sigma_{q_u-model}$ | | Total Variability & Uncertainty, $\sigma_{q_u-total}$ | |
|---|---|---|---|---|---|---|---|---|
| | 4 boring | 1 boring | 4 boring | 1 boring | 4 boring | 1 boring | 4 boring | 1 boring |
| Maquoketa Shale A | 3.3 | 3.1 | 0.55 | 0.72 | 0.20 | 0.29 | 0.59 | 0.78 |
| Maquoketa Shale B | 10.4 | 6.6 | 7.3 | 6.4 | 1.6 | 2.6 | 7.4 | 6.9 |
| Maquoketa Shale C | 66.2 | 71.0 | 14.0 | 12.1 | 2.2 | 3.3 | 14.2 | 12.6 |
| Kimmswick Limestone | 923 | 821 | 354 | 316 | 94 | 109 | 366 | 334 |

One characteristic of the standard deviation (any of the three standard deviations noted) is that the magnitude is dependent on the magnitude of the estimated value. While this characteristic is sometimes useful and informative, it makes comparison of variability and uncertainty for parameters from different strata and different sites difficult. When comparing variability and/or uncertainty for different strata or different sites, it is often helpful to represent variability and uncertainty in dimensionless form using the coefficient of variation, which is simply the standard deviation normalized by the mean value. Thus, three alternative coefficients of variation can be computed to represent the variability of the measurements, $COV_{d-meas}$, the model uncertainty, $COV_{d-model}$, and the total variability and uncertainty, $COV_{d-total}$, respectively:

$$COV_{d-meas} = \frac{\sigma_{d-meas}}{\bar{y}_d} = \frac{\sqrt{\frac{\sum_{i=1}^{n_d}(y_i-\bar{y}_d)^2}{n_d-1}}}{\bar{y}_d} \tag{11.13}$$

$$COV_{d-model} = \frac{\sigma_{d-model}}{\bar{y}_d} = \frac{\sqrt{\frac{1}{n_d}\cdot\frac{\sum_{i=1}^{n_d}(y_i-\bar{y}_d)^2}{n_d-1}}}{\bar{y}_d} \tag{11.14}$$

$$COV_{d-total} = \frac{\sigma_{d-total}}{\bar{y}_d} = \frac{\sqrt{\sigma_{d-meas}^2+\sigma_{d-model}^2}}{\bar{y}_d} \tag{11.15}$$

Coefficients of variation are commonly reported as decimal values or percentage values. Table 11–2 summarizes coefficients of variation associated with the standard deviations shown in Table 11–1.

**Table 11–2 Coefficients of variation for direct measurements of $q_u$ from Figures 11-8 and 11-9.**

| Stratum | Estimated Value, $\mu_{q_u}$ | | Measurement Variability, $COV_{q_u-meas}$ | | Model Uncertainty, $COV_{q_u-model}$ | | Total Variability & Uncertainty, $COV_{q_u-total}$ | |
|---|---|---|---|---|---|---|---|---|
| | 4 boring | 1 boring | 4 boring | 1 boring | 4 boring | 1 boring | 4 boring | 1 boring |
| Maquoketa Shale A | 3.3 | 3.1 | 0.17 | 0.23 | 0.06 | 0.09 | 0.18 | 0.25 |
| Maquoketa Shale B | 10.4 | 6.6 | 0.70 | 0.97 | 0.15 | 0.39 | 0.72 | 1.05 |
| Maquoketa Shale C | 66.2 | 71.0 | 0.21 | 0.17 | 0.03 | 0.05 | 0.22 | 0.18 |
| Kimmswick Limestone | 923 | 821 | 0.38 | 0.38 | 0.10 | 0.13 | 0.40 | 0.41 |

Inspection of Table 11–2 shows that values for the model uncertainty, $COV_{q_u-model}$, are substantially less than the model uncertainty threshold of 0.3 when measurements from all four borings are used to estimate values for $q_u$. This observation, in turn, indicates that designs based on the estimated values for $q_u$ are likely to achieve the target probability of failure. When measurements from a single boring are used to estimate values for $q_u$, however, the model uncertainty determined for the Maquoketa Shale B stratum does not satisfy the model uncertainty threshold. This result arises both because the variability of measurements in the stratum is substantially greater than for other strata, as shown by the magnitudes of $COV_{q_u-meas}$, and because only three measurements from this stratum are available to estimate a value for $q_u$. When such cases arise, one must consider whether the stratum is important for design and decide whether it is preferable to collect additional measurements, or use a conservative estimate of $q_u$ for the stratum. If the characterization is being performed for a bridge that is likely to be placed on deep foundations founded on or in the limestone stratum, the capacity and performance of such foundations are unlikely to be significantly affected by the strength of Maquoketa Stratum B. In such a case, selecting a conservative estimate for $q_u$, say 4 or 5 ksf, is probably more appropriate than collecting additional measurements. However, if the characterization is being performed for a lightly loaded structure that may be placed on relatively shallow spread footings, or for an earth retaining structure, collecting additional measurements may be more appropriate. The appropriate decisions for such cases fall back to the fundamental value proposition described in Chapter 1. If estimated costs for collecting additional measurements are likely to exceed any cost savings that may be achieved, conservative estimates should be used for the design parameter in the stratum. Conversely, if cost savings from using a less conservative estimate for $q_u$ are likely to exceed costs for collecting additional measurements, the additional measurements should be collected.

Similar concepts to those presented thus far in this section also apply when a property is considered to vary linearly within a stratum, but alternative computations are required to compute values for $\sigma_{d-model}$, $\sigma_{d-meas}$, and $\sigma_{d-total}$ (or $COV_{d-meas}$, $COV_{d-model}$, and $COV_{d-total}$) as described in Appendix 3. Figure 11-10 shows the three respective measures of variability and uncertainty determined using methods described in Appendix 3 for a collection of undrained shear strength, $s_u$, measurements that increase with depth. As shown in the figure, values for both $\sigma_{d-model}$ and $\sigma_{d-total}$ vary with depth for strata deemed to have linearly varying parameter values. Within such strata, $\sigma_{d-model}$ and $\sigma_{d-total}$ will tend to be smaller at depths where more measurements are available and larger at depths where fewer measurements are available because the uncertainty is greater where fewer measurements are available. When measurements are evenly distributed throughout the stratum, $\sigma_{d-model}$ and $\sigma_{d-total}$ will tend to be least near the middle of the stratum and greatest near the upper and lower boundaries of the stratum because the estimate is better constrained "in the middle" of the data. The value of $COV_{d-meas}$ will be constant throughout the stratum unless weighted least squares regression is performed.

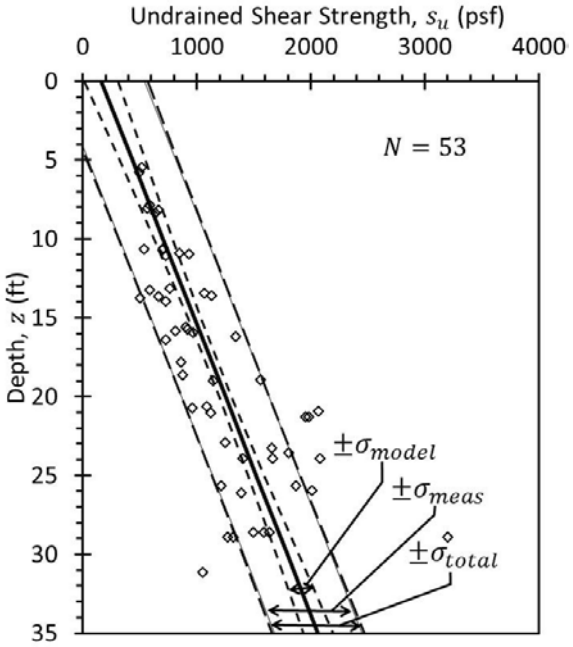


**Figure 11-10 Interpretation of $s_u$ assuming linear variation depth.**

Figure 11-11 shows an alternative interpretation of the measurements in Figure 11-10, in which the regression was established considering the natural logarithm of the measurements. As shown, this approach produces a slightly non-linear trend of $s_u$ with depth. This approach also considers variability and uncertainty to be lognormally distributed, and thus avoids producing interpretations that imply negative values of $s_u$. Comparison of Figure 11-10 and 11-11 reveals that both interpretations are

practically consistent with available measurements and either could be selected for design. Equations for calculation of variability and uncertainty under the assumption of lognormal measurements are provided in Appendix 3, along with descriptions of several alternative variants of regression.

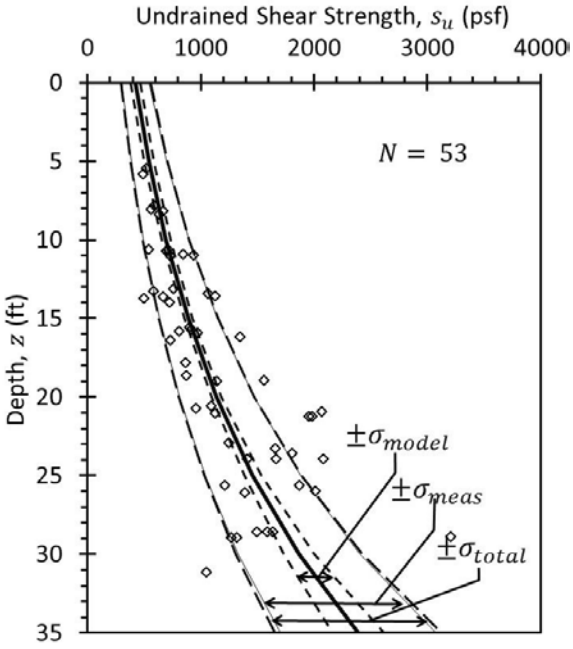


**Figure 11-11 Interpretation of $s_u$ presuming measurements are lognormally distributed.**

### 11.5.2 Calculation of Variability and Uncertainty for Indirect Measurements

Indirect measurements are also subject to variability and uncertainty due to variability in the indirect measurements and variability in the soil or rock being tested. However, the variability and uncertainty in design parameters established from indirect measurements is also influenced by variability and uncertainty in the relation used to transform the indirect measurements to a design parameter value. Thus, indirect measurements involve an additional source of uncertainty that is not present with direct measurements. Some indirect measurements correlate very closely with some design parameters, in which case the variability and uncertainty in such design parameters may be similar to, or even less than those established from direct measurements. In other cases, indirect measurements can be relatively poor predictors for design parameters, in which case the variability and uncertainty in design parameters established from indirect measurements may be substantially greater than those established from direct measurements.

In order to compute the variability and uncertainty for a design parameter established from indirect measurements, it is first necessary to compute the variability and uncertainty of the indirect measurements

themselves. This is done similarly to computation of variability and uncertainty from direct measurements (Equations 11.8, 11.10, and 11.12) so that

$$\sigma_{x-meas} = \sqrt{Var(x)} = \sqrt{MSE_x} = \sqrt{\frac{\sum_{i=1}^{n_x}(x_i - \hat{x})^2}{n_x - 1}} \tag{11.16}$$

$$\sigma_{x-model} = \sqrt{\frac{MSE_x}{n_x}} = \sqrt{\frac{1}{n_x} \cdot \frac{\sum_{i=1}^{n_x}(x_i - \hat{x})^2}{n_x - 1}} \tag{11.17}$$

$$\sigma_{x-total} = \sqrt{\sigma_{x-meas}^2 + \sigma_{x-model}^2} = \sqrt{\left(\frac{\sum_{i=1}^{n_x}(x_i - \hat{x})^2}{n_x - 1}\right)\left(1 + \frac{1}{n_x}\right)} \tag{11.18}$$

where $\sigma_{x-meas}$ is the standard deviation of the indirect measurements, $\sigma_{x-model}$ is the model standard deviation representing uncertainty in the estimated value of the indirect measurements, and $\sigma_{x-total}$ is the total standard deviation representing the combined variability and uncertainty of the indirect measurements. In Equations 11.16 through 11.18, the variable $x_i$ represents the individual indirect measurements and the subscript $x$ is used to indicate that the measures of variability and uncertainty are for indirect measurements. Thus, $n_x$ represents the number of indirect measurements, $MSE_x$ is the mean squared error for the indirect measurements, and $\hat{x}$ represents the estimated value of the indirect measurement in the stratum of interest.

For many types of indirect measurements, the indirect measurements can be transformed to the design parameter of interest using linear transformations of the form

$$\hat{y}_s = \beta_0 + \beta_1 \hat{x} \tag{11.19}$$

where $\hat{y}_s$ is the estimated value of the design parameter established from indirect measurements, $\hat{x}$ is the estimated value of the indirect measurements in a particular stratum, and $\beta_0$ and $\beta_1$ are regression coefficients for the transformation from indirect measurements to the parameter of interest. For such transformations, the variability and uncertainty in the design parameter established exclusively from the indirect measurements can be computed as

$$\sigma_{s-meas} = \sqrt{MSE_r\left[1 + \frac{1}{m} + \frac{(\hat{x} - \bar{x}_r)^2 + \sigma_{x-meas}^2}{s_{xx}}\right] + \beta_1^2 \sigma_{x-meas}^2} \tag{11.20}$$

$$\sigma_{s-model} = \sqrt{MSE_r\left[1 + \frac{1}{m} + \frac{(\hat{x} - \bar{x}_r)^2 + \sigma_{x-model}^2}{s_{xx}}\right] + \beta_1^2 \sigma_{x-model}^2} \tag{11.21}$$

$$\sigma_{s-total} = \sqrt{MSE_r \left[1 + \frac{1}{m} + \frac{(\hat{x} - \bar{x}_r)^2 + \sigma_{x-total}^2}{s_{xx}}\right] + \beta_1^2 \sigma_{x-total}^2} \quad (11.22)$$

where $\sigma_{s-meas}$ is the standard deviation of the transformed measurements, $\sigma_{s-model}$ is the model standard deviation representing the uncertainty of the estimated or "model" value $\hat{y}_s$, and $\sigma_{s-total}$ is the total standard deviation representing the combined variability and uncertainty of the design parameter $y_s$. The terms $\hat{x}$, $\sigma_{x-meas}$, $\sigma_{x-model}$, and $\sigma_{x-total}$ are all derived from analysis of the indirect measurements from a particular site/stratum: $\hat{x}$ is the estimated (usually mean) value of the indirect measurements in the stratum of interest and $\sigma_{x-meas}$, $\sigma_{x-model}$, and $\sigma_{x-total}$ respectively represent the standard deviation of the indirect measurements, the model standard deviation for the estimated value $\hat{x}$, and the total standard deviation for the indirect measurements. The remaining terms in Equations 11.20 through 11.22 are measures derived from the transformation. $MSE_r$ is the mean squared error of the regression used to establish the transformation, $\bar{x}_r$ is the mean value of the indirect measurements used to establish the regression, $\beta_1$ is the slope of the regression equation, $m$ is the number of measurements used to establish the regression, and $s_{xx}$ is a quantity related to the variance of the indirect measurements used to establish the transformation. $s_{xx}$ is computed as

$$s_{xx} = \sum_{i=1}^{m} (x_{r-i} - \bar{x}_r)^2 \quad (11.23)$$

where $x_{r-i}$ represents the individual indirect measurements in the regression data set. While Equations 11.20 through 11.22 involve a number of different terms, it is important to note that many of these terms are associated with the transformation equation ($MSE_r$, $\bar{x}_r$, $\beta_1$, $m$, and $s_{xx}$). Once these values are established, it is only necessary to compute values for $\hat{x}$ and the appropriate standard deviation ($\sigma_{x-meas}$, $\sigma_{x-model}$, or $\sigma_{x-total}$) from the available indirect measurements to apply Equations 11.20 through 11.22.

The measurements shown in Figure 11-5 and 11-6 can be used to illustrate use of Equations 11.20 through 11.22 on a "site specific" basis. Figure 11-12 shows paired measurements of the point load strength index ($I_s$) and uniaxial compressive strength ($q_u$) taken from the same three boreholes along with a transformation equation established using OLS regression for the regression data set shown. Required quantities from the regression needed to use Equations 11.20 through 11.22 are also shown in Figure 11-12. Figure 11-13 shows estimated values for $I_s$ in each stratum along with the variability and uncertainty in the indirect measurements calculated from Equations 11.16 through 11.18.

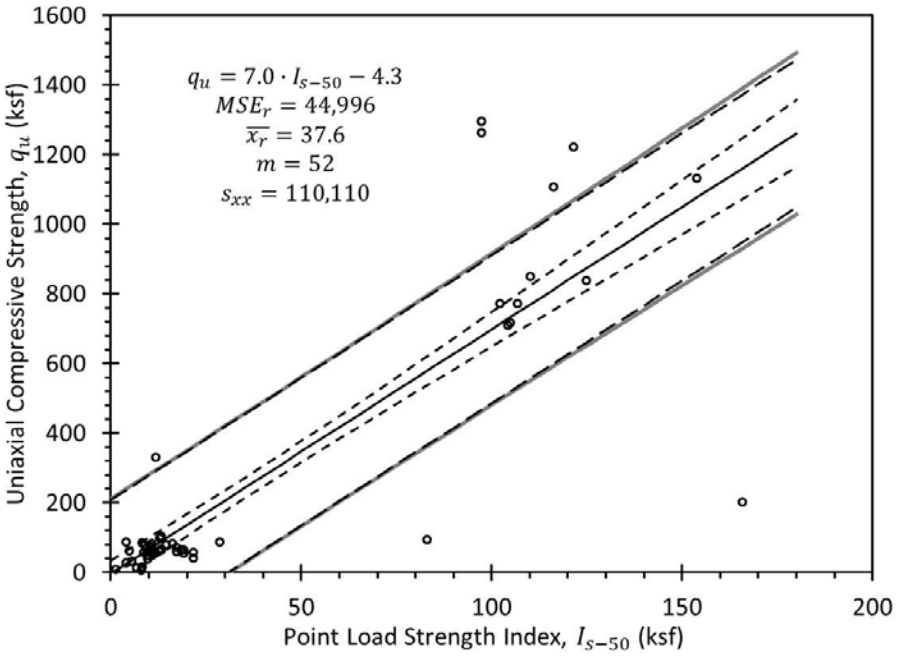


**Figure 11-12 Empirical transformation from $I_s$ to $q_u$ using site-specific measurements from Figures 11-5 and 11-6.**

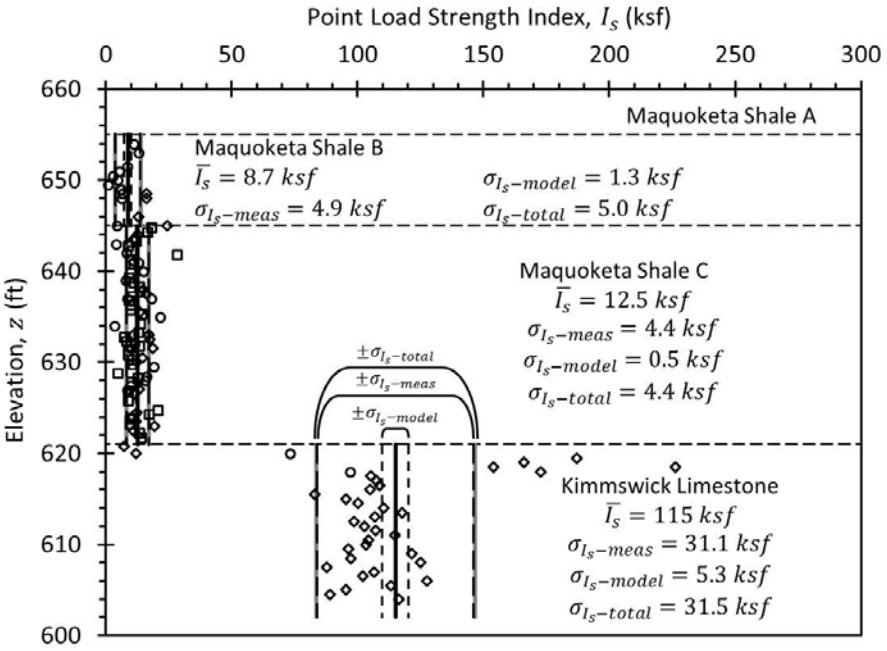


**Figure 11-13 Interpretation of $I_s$ measurements and associated measures of variability and uncertainty.**

Table 11–3 shows calculated values for the variability and uncertainty in the indirect measurements along with corresponding values of variability and uncertainty for the design parameter, $q_u$, established from

Equations 11.20 through 11.22 using the values provided in the table and Figure 11-12. The variability and uncertainty for the design parameters are also shown graphically in Figure 11-14. Comparison of values in Table 11–3 and Figure 11-14 with values shown in Table 11–1 and Figure 11-8 indicate that model uncertainty for estimates of $q_u$ is substantially greater when $q_u$ is determined from indirect point load strength index measurements than when established using direct confined and uniaxial compression test measurements. This observation is a direct result of variability and uncertainty in the transformation function shown in Figure 11-12. It is noteworthy that estimated values for $q_u$ determined from indirect measurements are substantially greater than estimated values for $q_u$ from direct measurements, which suggests that the greater uncertainty is appropriate.

**Table 11–3 Calculation of variability and uncertainty in $q_u$ from $I_s$.**

| Stratum | Indirect Measurements, $I_s$ (ksf) | | | | | Design Parameter, $q_u$ (ksf) | | |
|---|---|---|---|---|---|---|---|---|
| | $n_x$ | $\hat{x}$ | $\sigma_{x-meas}$ | $\sigma_{x-model}$ | $\sigma_{x-total}$ | $\sigma_{s-meas}$ | $\sigma_{s-model}$ | $\sigma_{s-total}$ |
| Maquoketa Shale B | 13 | 8.7 | 4.9 | 1.3 | 5.0 | 218 | 215 | 306 |
| Maquoketa Shale C | 77 | 12.5 | 4.4 | 0.5 | 4.4 | 217 | 215 | 305 |
| Kimmswick Limestone | 35 | 115 | 31.1 | 5.3 | 31.5 | 311 | 223 | 382 |

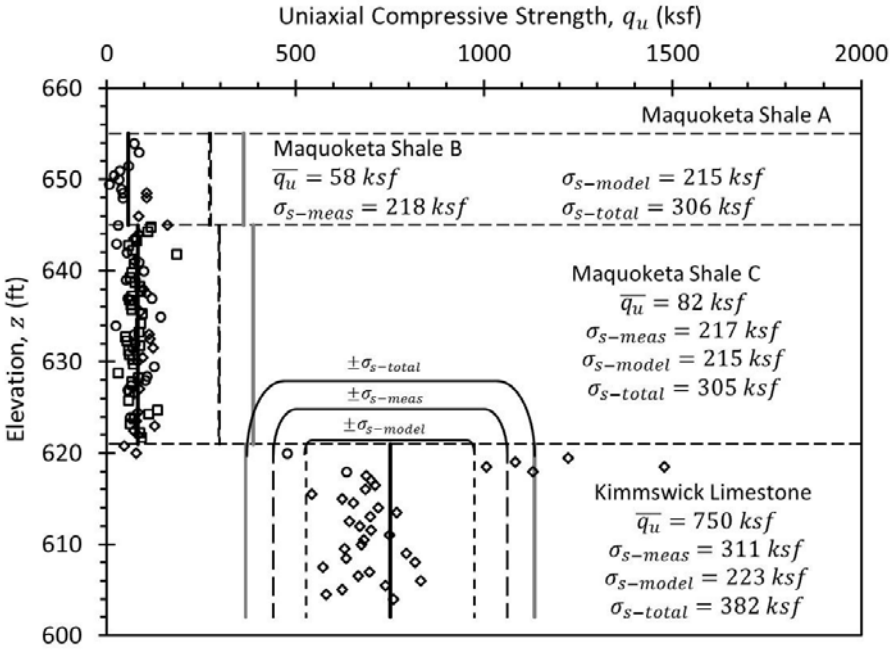


**Figure 11-14 Measures of variability and uncertainty for $q_u$ when established from $I_s$ measurements.**

### 11.5.3 Calculation of Variability & Uncertainty for Combined Direct & Indirect Measurements

When both direct and indirect measurements are available for a particular design parameter, it is possible to derive estimates for the design parameter value, and variability and uncertainty for the design

parameter, from combined consideration of the direct and indirect measurements. This can be done using weighted averages of estimates derived from the direct and indirect measurements, respectively. The mean value for the design parameter, $\bar{y}$, can be estimated as

$$\bar{y} = \frac{\frac{\bar{y}_d}{\sigma_d^2} + \frac{\bar{y}_s}{\sigma_s^2}}{\frac{1}{\sigma_d^2} + \frac{1}{\sigma_s^2}} = \frac{\bar{y}_d \cdot \sigma_s^2 + \bar{y}_s \cdot \sigma_d^2}{\sigma_d^2 + \sigma_s^2} \tag{11.24}$$

where $\bar{y}_d$ and $\bar{y}_s$ are mean values for the design parameter determined from the available direct and indirect measurements, respectively, and $\sigma_d$ and $\sigma_s$ are the standard deviations determined from the direct and indirect measurements, respectively. Equation 11.24 can be applied using any of the three measures of variability and uncertainty (i.e., $\sigma_{meas}$, $\sigma_{model}$, or $\sigma_{total}$), but it is most commonly appropriate to use the model uncertainty. Estimates for the standard deviation can similarly be determined as

$$\sigma_y = \frac{\sigma_d^2 \cdot \sigma_s^2}{\sigma_d^2 + \sigma_s^2} \tag{11.25}$$

where $\sigma_y$ can correspond to the model uncertainty ($\sigma_{model}$) or the total variability and uncertainty ($\sigma_{total}$) depending on the values of $\sigma_d$ and $\sigma_s$ used.

Table 11–4 and Figure 11-15 show results of calculations performed using Equations 11.24 and 11.25, along with $\sigma_{model}$ and $\sigma_{total}$ values reported in Table 11–1 for direct measurements and Table 11–3 for indirect measurements. Values for $\sigma_{meas}$ are not reported because they are not generally meaningful when considering estimates for design parameters. In this particular case, estimates determined for $\hat{q}_u$, $\sigma_{model}$, and $\sigma_{total}$ from the combined direct and indirect measurements are practically identical to those determined from the direct measurements alone for the Maquoketa Shale strata. This is largely a result of the fact that relatively large numbers of direct measurements are available and the fact that the transformation from $I_s$ to $q_u$ involves substantial uncertainty, particularly for low values of $I_s$. However, for the Kimmswick Limestone stratum, the estimate for $\hat{q}_u$ from combined direct and indirect measurements is observed to fall between those determined from direct or indirect measurements alone, but is closer to that determined from the direct measurements. Even more importantly, both $\sigma_{model}$ and $\sigma_{total}$ determined from combined direct and indirect measurements are less than corresponding values determined using the direct or indirect measurements alone. Such a result derives from consideration of the greater number of collective measurements when both direct and indirect measurements are used.

The magnitude of the improved reliability that results from consideration of combined direct and indirect measurements depends on a number of different factors. These factors include the absolute and relative

number of direct and indirect measurements, the uncertainty in the transformation function for the indirect measurements, and the general variability of the specific stratum. In cases like the example presented where relatively large numbers of direct measurements are available, consideration of additional indirect measurements may produce little improvement in estimates for the design parameter of interest or the uncertainty in the estimate for that design parameter. Conversely, in cases where relatively few direct measurements are available, combined consideration of direct and indirect measurements can produce substantial improvements in estimates for the design parameter of interest and the uncertainty in the design parameter over what could be established considering the direct measurements alone.

**Table 11–4 Summary of variability and uncertainty in $q_u$ from direct measurements, indirect measurements, and combined direct and indirect measurements.**

| Type of Measurement | Parameter | Stratum | | | |
|---|---|---|---|---|---|
| | | Maquoketa Shale A | Maquoketa Shale B | Maquoketa Shale C | Kimmswick Limestone |
| Direct | $n_d$ | 6 | 20 | 41 | 13 |
| | $\hat{q}_u$ | 3.3 | 10.4 | 66.2 | 923 |
| | $\sigma_{d-model}$ | 0.2 | 1.6 | 2.2 | 94 |
| | $\sigma_{d-total}$ | 0.6 | 7.4 | 14.2 | 366 |
| Indirect | $n_s$ | 0 | 13 | 77 | 35 |
| | $\hat{q}_u$ | -- | 57 | 82 | 751 |
| | $\sigma_{s-model}$ | -- | 215 | 215 | 223 |
| | $\sigma_{s-total}$ | -- | 306 | 305 | 382 |
| Combined | $\hat{q}_u$ | 3.3 | 10.4 | 66.2 | 897 |
| | $\sigma_{c-model}$ | 0.2 | 1.6 | 2.2 | 87 |
| | $\sigma_{c-total}$ | 0.6 | 7.4 | 14.2 | 265 |

Several different approaches can be used to reduce model uncertainty when necessary or desirable. As described previously, the most straightforward means to reduce model uncertainty in estimates for design parameters is to collect additional measurements. In general, additional direct measurements will have greater impact on a "per test" basis, but additional indirect measurements will also reduce uncertainty depending on the reliability of the transformation. Alternatively, it is possible to reduce uncertainty in estimates for design parameters by improving transformations for indirect measurements if indirect measurements are being used. Transformation relations can be improved on a broad scale by performing dedicated research to improve the reliability of transformation relations, either by developing new relations that better "fit" to existing data or by collecting additional measurements for improving the transformation. However, it is commonly more effective to develop "site specific" transformations for individual projects if both direct and indirect measurements are collected. Finally, one can also revisit initial interpretations for stratigraphy and initial selections for design domains and consider subdividing

design domains or strata, which may reduce model uncertainty within individual strata or design domains. However, such considerations should not be taken to an extreme.

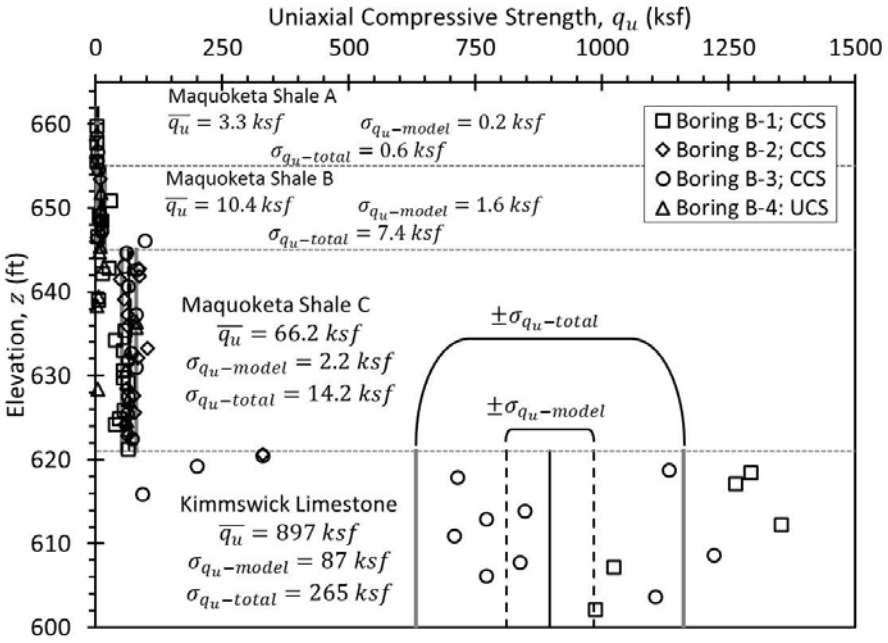


**Figure 11-15 Interpretation of $q_u$ established from combined direct and indirect measurements.**

## 11.6 IDENTIFYING OUTLIERS AND RESOLVING INCONSISTENCIES

One of the more difficult aspects of interpreting test measurements is distinguishing whether extreme measurements, or "outliers", are representative of actual conditions, or whether the outliers are a result of sampling or testing errors. Decisions about whether a specific measurement should be disregarded in developing estimates for design parameter values should be made with careful judgment and consideration, at least including the considerations raised in this section.

As described in Chapter 3, it is important to recognize that available measurements for some design property are simply statistical "samples" from a larger population of measurements that could be obtained in the absence of constraints of time and money. Thus, available measurements should be considered as estimates of a property taken from some distribution of values that actually represents in situ conditions rather than a deterministic measurement of actual conditions.

As a general rule, all valid available measurements should be considered when interpreting values for design parameters. However, measurements that are truly believed to be erroneous should be disregarded. Such conditions can arise from a number of sources including equipment malfunctions,

testing or recording errors, extreme sample disturbance, unrepresentative samples, and sample preparation problems, among others. Judgment regarding whether a specific measurement is truly erroneous should primarily be derived from consideration of results from the individual test. For example, one can observe the stress-strain response, stress paths, and pore pressure response for triaxial tests to gather information regarding test validity. Truly erroneous tests will generally have noticeable issues. Some judgment can also be derived from comparison of results with other measurements, or from comparison of results with "typical" or historical measurements. However, such comparisons have the potential to bias interpretations to support what one believes should exist, rather than evaluating what actually exists. Does the atypical result simply represent an extreme result that is truly reflective of actual conditions, or is it erroneous? That is a difficult question to answer in many cases. In the absence of clear and convincing evidence that a measurement is truly erroneous, the measurement should be included in evaluations of design parameters. Consideration can also be given to "weighting" questionable measurements, such that they do not overly influence interpretations, instead of completely disregarding them.

It is generally easier, and more rational to discard measurements that are substantially unconservative (e.g., greater strength, lesser compressibility, lesser hydraulic conductivity, etc.) compared to other measurements since ignoring such measurements may avoid unconservatism. Disregard of conservative measurements (e.g., lower strength, greater compressibility, etc.) should be done with thoughtful consideration and care since disregarding an accurate measurement in such cases can potentially lead to unconservative design or catastrophic results. Conservative measurements that are truly erroneous should absolutely be disregarded. However, designers should be hesitant to disregard measurements in order to support some presumed interpretation of conditions.

It is also important to recognize that disregarding measurements as "outliers" can have a substantial, and potentially unconservative impact on estimates of variability and uncertainty for a design parameter. When considering variability and uncertainty, even disregarding measurements that are substantially advantageous will tend to produce estimates of variability and uncertainty that are lower than what is actually appropriate, which is unconservative.

## 11.7 USE OF OBSERVATIONAL METHOD

Once appropriate values for design parameters have been established, it is possible to complete the design and proceed to construction. However, there is one final step that can be performed on some projects to validate estimates for design and potentially improve the accuracy of selected values. The process

generally involves: (1) using established values for design parameters to predict the anticipated response in the field; (2) systematically monitoring field performance and comparing it to the anticipated response; and (3) "back calculating" apparent values for design parameters of interest that would produce the observed response. This process of prediction, monitoring, and reassessment is known as the observational method (Peck, 1969) and is often particularly effective for projects involving complex ground conditions that are difficult to reliably characterize using conventional site characterization methods (e.g., Castelli, et al., 2015). Common applications of the observational method involve use of piezometers and settlement plates to monitor the rate of pore pressure dissipation and settlement for embankment fills, or use of inclinometers and strain gages to monitor lateral displacements and support system loads for deep excavations. Use of the observational method to "calibrate" design models and design parameters can improve the accuracy of estimates for settlement of foundations or fills, or the lateral loads on an excavation support system. The improved estimates can, in turn, be used to improve decision making about staged construction or to improve design for other features at the site. The observational method also produces advantages prior to actual observation and monitoring since designers can develop designs with the knowledge and comfort of knowing that performance will be monitored during construction so that design changes can be made if necessary.

## 11.8 INTERPRETATION OF IN SITU STRESS STATE FOR DESIGN

In situ stress state is most commonly used for calculation of settlement for embankments and shallow foundations, but may also be important for determining undrained shear strength (e.g., using SHANSEP or similar techniques), for design of earth retaining structures, for evaluation of liquefaction potential, for design of tunnels and other underground structures, and for numerical modeling applications. Characterizing the in situ stress state routinely requires estimation of the total vertical stress, pore water pressure, vertical effective stress, and preconsolidation stress. For some applications, estimation of horizontal total and/or effective stress is also required.

### 11.8.1 Total Vertical Stress

The total vertical stress, $\sigma_{vo}$, in the ground is seldom directly measured because of difficulties associated with measuring in situ stress. However, it is routinely and reliably calculated based on measured values of unit weight for the soil or rock present at a site. Total vertical stress at a given depth, $z$, is strictly the integral of unit weight from the ground surface to depth $z$:

$$\sigma_{vo} = \int_{z=0}^{z} \gamma \cdot dz \tag{11.26}$$

where $\gamma$ is the total unit weight of the soil or rock above depth $z$. $\sigma_{vo}$ is more commonly calculated using summation to approximate the integral as

$$\sigma_{vo} = \sum_{i=1}^{n} \gamma_i \cdot \Delta z_i \qquad (11.27)$$

where $i$ represents a layer or sublayer above depth $z$, and $\gamma_i$ and $\Delta z_i$ respectively represent the unit weight and thickness of the individual layers or sublayers.

Figure 11-16 shows a typical profile of the calculated total vertical stress. The magnitude of the total vertical stress increases continuously with increasing depth (i.e., there are no discrete "jumps" in total vertical stress). In a profile with constant unit weight, the rate of increase of total vertical stress with depth is proportional to the unit weight of the soil or rock within a particular stratum; changes in the slope of the line representing total vertical stress with depth will occur with changes in total unit weight. Such changes in total unit weight can occur within an individual stratum, but most commonly occur at changes in stratigraphy, and near the location of the water table.

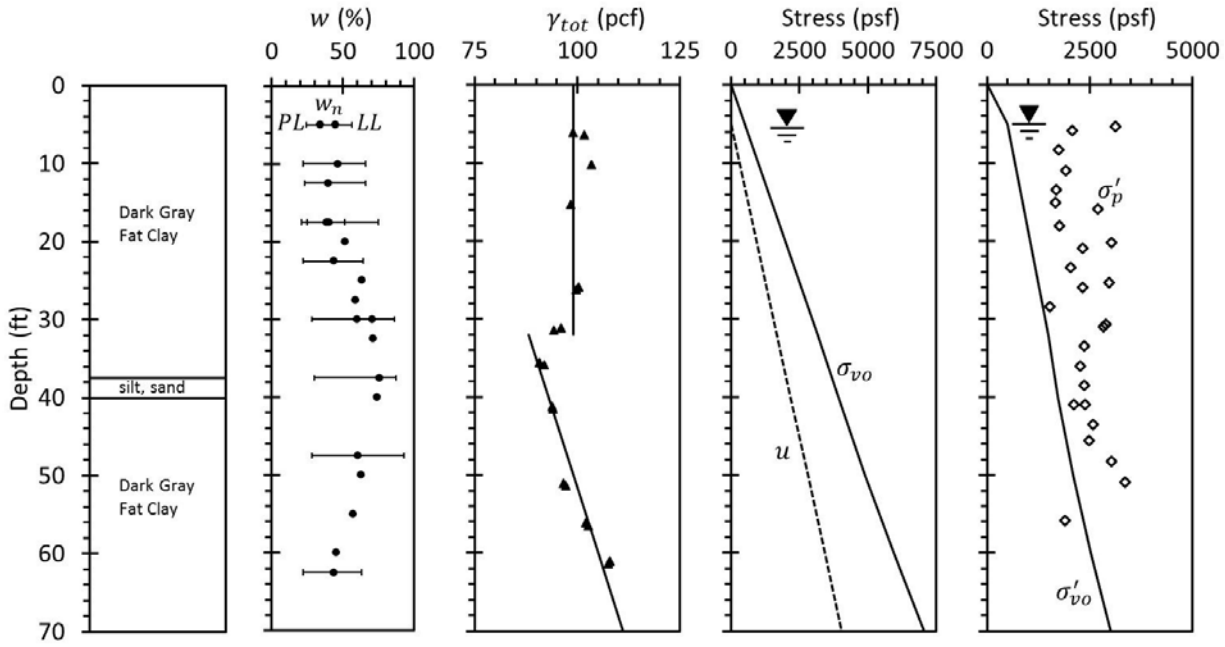


**Figure 11-16 Generalized profile, moisture content, total unit weight, and in situ stress profile.**

### 11.8.2 Pore Water Pressure

The magnitude of pore water pressures is commonly estimated from measurements of groundwater levels made during subsurface investigations. If hydrostatic groundwater conditions are presumed, the pore water pressure, $u$, at a given depth below the groundwater table is calculated as

$$u\,(z) = \gamma_w \cdot z_w \qquad (11.28)$$

where $\gamma_w$ is the unit weight of water (= 62.4 pcf for fresh water) and $z_w$ is the depth below the water table. While such calculations are straightforward and relatively common, it is crucial to recognize that these calculations are based on the presumption of hydrostatic (i.e., no flow) groundwater conditions. Use of Equation 11.28 for conditions that are not hydrostatic will introduce errors in the estimated pore water pressures, which will propagate to errors in the vertical effective stress, and subsequently to errors in soil strength and perhaps stability in subsequent design calculations. Designers should therefore be deliberate in evaluating whether groundwater conditions can be reasonably considered as hydrostatic.

In cases where groundwater conditions cannot reasonably be considered hydrostatic, pore water pressures can be measured using piezometers of various types as described in Chapter 10 or using CPTU soundings. Pore water pressures can also be predicted using steady state seepage analyses, which are readily performed using commercially available computer software.

It is also possible for groundwater conditions in select strata to be hydrostatic while conditions in other strata are not. In such cases, it is perfectly acceptable to compute pore water pressures in strata with hydrostatic conditions using Equation 11.28, while using measurements or seepage analyses to establish pore water pressures for strata that are not hydrostatic.

Pore water pressures are commonly transient, with rising and falling groundwater table elevations, or changes in flow being quite common for most sites. As such, it is critical for designers to carefully consider how groundwater conditions may change over time, and how such changes may influence soil or rock properties, design, and construction. Potential ranges for groundwater conditions can be derived from monitoring of piezometers over time, from borings or piezocone soundings conducted at different times, or using a variety of groundwater modeling techniques. It is also important to consider potential changes in groundwater conditions that may be induced by construction of specific transportation features. Some of such changes may be temporary conditions (e.g., from dewatering during construction) while others may be more permanent (e.g., from excavation of cut slopes that introduces a drainage boundary).

In many cases, “design pore water pressures” may not reflect actual measurements made during subsurface investigations. This is entirely appropriate and representative of the fact that design is generally performed to account for the worst-case pore water pressures that will be experienced over the design life of the transportation feature.

### 11.8.3 Vertical Effective Stress

The vertical effective stress, $\sigma'_{vo}$, is a quantity that cannot be directly measured, but instead must be calculated from the magnitude of the total vertical stress and pore water pressure. Given values for $\sigma_{vo}$ and $u$ at a given depth, the magnitude of $\sigma'_{vo}$ at that same depth is calculated as

$$\sigma'_{vo} = \sigma_{vo} - u \tag{11.29}$$

Figure 11-16 also shows the computed magnitude of the vertical effective stress for the example shown in the figure. Equation 11.29 is valid, regardless of whether pore water pressures are derived from hydrostatic groundwater conditions, or more complex seepage patterns.

### 11.8.4 Preconsolidation Stress and Overconsolidation Ratio ($OCR$)

Preconsolidation stress, $\sigma'_p$, is most commonly measured and interpreted for saturated clayey and silty soils because the behavior of such soils are often influenced by stress history. Preconsolidation stress is not commonly measured for coarse-grained soils or rock, because stress history has less influence on those materials for engineering design of transportation features; however, $\sigma'_p$ is sometimes measured in coarse-grained soils when estimates of the at-rest earth pressure coefficient are needed, which generally require estimation of $OCR$ as described in Section 11.8.5.

The magnitude of $\sigma'_p$ is most commonly estimated from results of one-dimensional consolidation tests on high quality undisturbed specimens, or from alternative indirect measurements as described in Chapter 6. The magnitude of $\sigma'_p$ for a given design domain is therefore commonly estimated from collective interpretation of measurements as described in previous sections of this chapter. The magnitude of $\sigma'_p$ is also often characterized using the overconsolidation ratio, $OCR$, as defined in Equation 6.5.

The variation of $\sigma'_p$, or $OCR$, with depth for a given site is generally dictated by the geologic history of the site and can range from relatively simple and predictable trends to trends that are quite complex depending upon how the soils were formed and past use of the site. Despite these complications, there are "typical" distributions for $\sigma'_p$ and $OCR$ that should be considered as a first approximation and confirmed by actual measurements at the site. Figure 11-17 shows typical distributions of $\sigma'_p$ and $OCR$ for two common conditions. Figure 11-17a shows $\sigma'_p$ for a typical "soft clay" site. Such sites often include a "dessicated crust" near the ground surface where the soil has been overconsolidated by desiccation. The magnitude of $OCR$ generally decreases with depth below the ground surface and often reaches the condition of becoming normally consolidation at greater depth. Such sites tend to produce a "u-shaped"

trend for $\sigma_p'$ with depth, with relatively high preconsolidation stresses in the desiccated crust, lower preconsolidation stress below the desiccated crust, and increasing preconsolidation stress at greater depths. This condition produces greater $OCR$ at shallow depths, which decrease with depth and often approach a value of 1.0 (indicating normal consolidation) at greater depths. In contrast, "stiff clay" sites will often tend to exhibit more uniform values of $\sigma_p'$ as a function of depth, as shown in Figure 11-17b. Intermediate conditions between typical observations for "soft clay" and "stiff clay" sites are also common, as are cases with mixtures of soft and stiff clay responses.

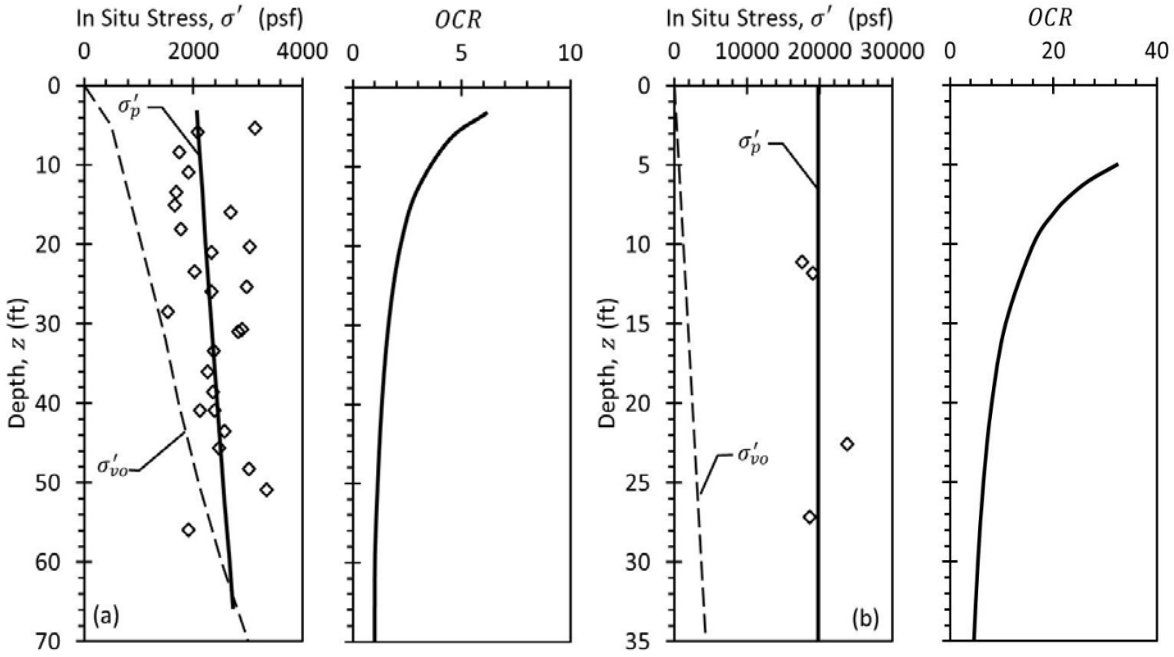


**Figure 11-17 Typical profiles of $\sigma_p'$ and OCR for: (a) soft clay site, (b) stiff clay site.**

As described in Chapter 6, precise measurement of $\sigma_p'$ is challenging because the measurements are strongly affected by the quality of the test specimens (e.g., sample disturbance), by specific details of tests (e.g., load increments used), as well as the method(s) used for interpretation of individual test results. As such, measured values of $\sigma_p'$ are commonly more scattered and variable than many other geotechnical properties (e.g., Duncan, 2000). Considerable judgment is therefore required for interpretation of $\sigma_p'$. It is often useful to hypothesize some general anticipated behavior (e.g., those shown in Figure 11-17) and evaluate whether available measurements support the hypothesis rather than simply fitting some trend through available measurements without consideration for whether that trend is consistent with the actual site characteristics. This is particularly true for cases where $\sigma_p'$ is interpreted from relatively few measurements.

### 11.8.5 Horizontal Stresses

Unlike the vertical stress parameters described in previous subsections, in situ horizontal stresses are not commonly required or evaluated for routine design. Nevertheless, in situ horizontal stresses may be required or desirable for design of underground structures or for numerical analyses of transportation features. The most common means for representing horizontal stress in soil and rock is to use an "earth pressure coefficient", $K$, to represent the magnitude of horizontal stresses in a normalized manner. Generically, $K$ is defined as

$$K = \frac{\sigma_h'}{\sigma_v'} \tag{11.30}$$

where $\sigma_h'$ is the horizontal effective stress and $\sigma_v'$ is the vertical effective stress at a specific location. When considering the in situ stress state, a special value of $K$, referred to as the coefficient of lateral earth pressure *at rest* and denoted, $K_o$, is used to represent the in situ horizontal stresses.

Measurement of the in situ horizontal stress is challenging, but can be accomplished using several different in situ tests that include flat plate dilatometer tests (DMT), pressuremeter tests (PMT), as well as several other indirect means including CPT and geophysical tests. If such measurements are available, the in situ horizontal stress can be interpreted following procedures described previously in this chapter to establish the magnitude of the horizontal total or effective stress with depth as shown in Figure 11-18. Alternatively, and perhaps more commonly, the magnitude of $K_o$ can be estimated from one of several established empirical correlations (e.g., Kulhawy and Mayne, 1990). Perhaps the most commonly used of these empirical correlations is:

$$K_o = (1 - \sin\phi')OCR^{\sin\phi'} \tag{11.31}$$

where $\phi'$ is the effective stress friction angle for the soil. As is true for $\sigma_p'$, and perhaps more so, measurements and estimates for in situ horizontal stresses, or $K_o$, are notoriously variable and subject to multiple sources of potential error as illustrated in Figure 11-19. As such, considerable judgment should be applied when interpreting and using these parameters.

$K_o$ is largely dependent on stress history and the "frictional strength" of the soil. However, the in situ horizontal stress can also be affected by regional tectonic stresses and can vary with time (Mitchell and Soga, 2005). In such conditions, common correlations may not produce reasonable estimates for in situ horizontal stress, in which case designers must rely on measurements of horizontal stresses despite the challenges involved.

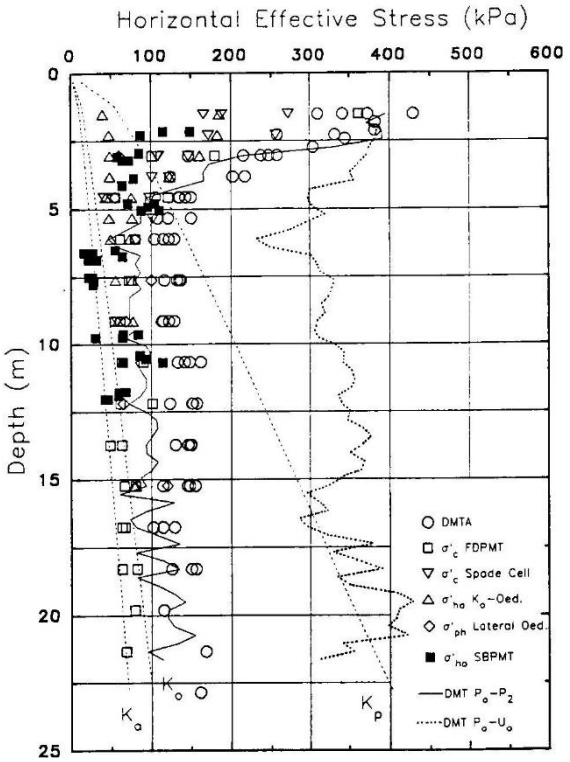


**Figure 11-18 In situ horizontal stress from laboratory and in situ tests (from Benoit and Lutenegger, 1992).**

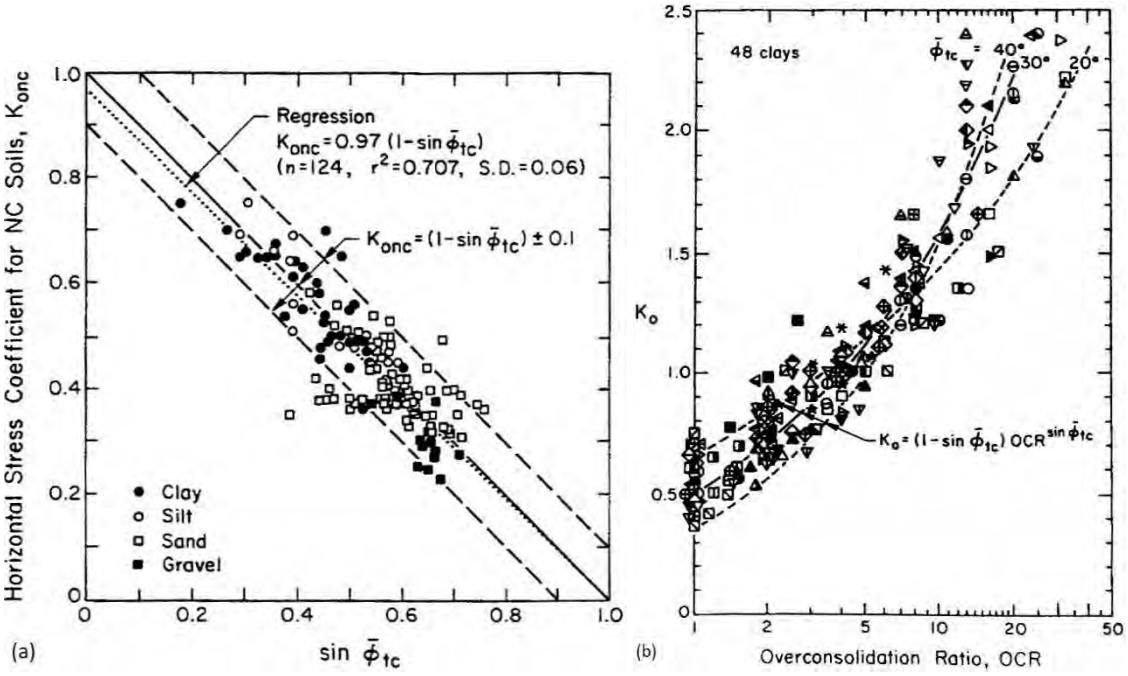


**Figure 11-19 Measured values of $K_o$: (a) as function of $\phi'$ for normally consolidated soils, and (b) as function of $OCR$ (from Kulhawy and Mayne, 1990).**

## 11.9 INTERPRETATION OF UNDRAINED SHEAR STRENGTH FOR DESIGN

Undrained shear strength, $s_u$, or the related unconfined compressive strength, $q_u$, is one of the most commonly used parameters for geotechnical design. Undrained shear strength is used for design of shallow and deep foundations, for evaluation of short-term stability for excavated slopes and embankments on soft foundations, and for design of excavation support systems in soils that can be considered undrained during construction. Since $s_u$ represents the strength of a soil subjected to loading under undrained conditions, $s_u$ values are seldom required for design in soils that can be considered "freely draining" such as clean coarse-grained soils and perhaps even some silts. However, it is important to recognize that even relatively small percentages of clay or silt within a soil that is predominately coarse-grained can lead to the soil behaving more like a fine-grained soil. As such, estimates for $s_u$ are commonly required for clays, many silts, as well as sandy clays and silts, and silty or clayey sands.

Interpretation of $s_u$ measurements is often conceptually straightforward in the sense that one can take a collection of measurements and interpret them as described in Sections 11.4 through 11.6. However, appropriate interpretation of $s_u$ is actually more complicated than many other geotechnical parameters because $s_u$ depends significantly on a number of factors that include:

1. The in situ effective stress in the ground,
2. The stress history of the deposit,
3. The method of loading (e.g., compression, extension, simple shear, etc.), and
4. The rate of loading

In addition, for some test methods, the measured $s_u$ may be strongly influenced by the degree of disturbance introduced during sampling and test preparation so measurements are sensitive to the quality of sampling and testing. The net result of these facts is that all measurements of $s_u$ are not equivalent. Interpreting accurate and reliable estimates for $s_u$ is therefore a substantial challenge that requires deliberate consideration of these factors and knowledge about the intended use.

Because $s_u$ for soils can be significantly influenced by disturbance and other factors, it is often useful to hypothesize what $s_u$ should be considering qualitative or quantitative knowledge of the stress history of the site and how it was formed. Measurements of $s_u$ can then be compared to the hypothesized strengths and considered with other site characteristics and test measurements to sequentially develop a holistic interpretation that is consistent with all available information. As a practical matter, this can largely be done considering the stress history of the site. Figure 11-20 shows "typical" profiles of $s_u$ for sites composed of normally consolidated or slightly overconsolidated clays that are often generally

characterized as "soft clays" and sites composed of more heavily overconsolidated clays that can be considered "stiff clays". Soft clay sites will often have $s_u$ that increases with depth because of increases in effective stress. Many such sites may have greater $s_u$ nearer to the ground surface that results from desiccation of soils above the water table and, thus, greater preconsolidation stress. In contrast, stiff clays are prone to having more uniform $s_u$ within a given stratum. While it is obvious that sites can fall anywhere within a broad spectrum of characteristics, many silty and clayey strata will have profiles of $s_u$ that qualitatively fall within the bounds represented in Figure 11-20. The process of starting with some hypothesized interpretation, which is subsequently revised based on actual measurements, should not be construed as assuming the magnitude of $s_u$; rather, the process is more one of facilitating interpretation of $s_u$ to arrive at a more accurate and rational interpretation.

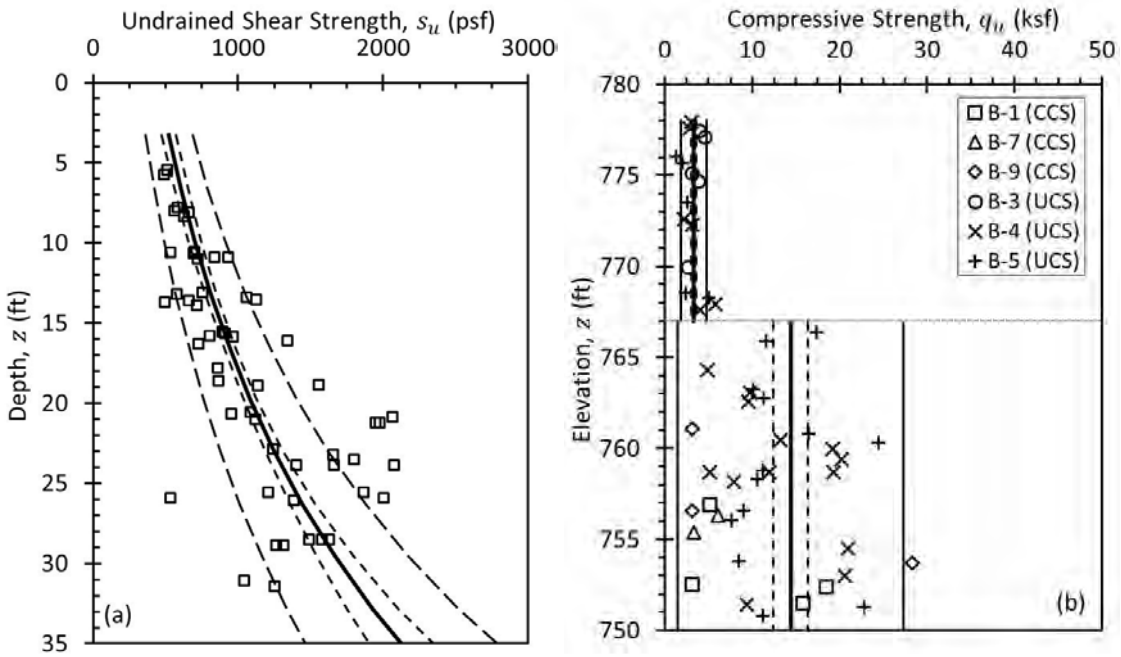


**Figure 11-20 Undrained strength measurements from: (a) soft clay site and (b) stiff clay site.**

As described in Chapter 7, the challenge of interpreting $s_u$ is compounded because it can be measured using a relatively large number of different laboratory tests, as well as several types of in situ tests. Because methods for interpreting $s_u$ from different types of tests varies, recommendations for interpretation are provided separately in the following sections.

### 11.9.1 Interpretation of $s_u$ from UU Triaxial Tests and Unconfined Compression Tests

The most direct and perhaps most common means for determining $s_u$ in practice is using unconsolidated-undrained (UU) triaxial compression tests, commonly performed at total confining stresses that

approximate the in situ stress level. UU triaxial extension tests are much less commonly performed, but can also be used to evaluate $s_u$, although it should be recognized that $s_u$ in triaxial compression will be significantly greater than $s_u$ in triaxial extension. Because $s_u$ is theoretically independent of the total confining stress for saturated soils, $s_u$ can also be measured using unconfined compression (UC) tests, although results of such tests are often observed to be more variable than UU triaxial tests as demonstrated in Chapter 7. Results of all three tests can only be interpreted in terms of total stresses because effective stresses are neither controlled nor measured in any of the tests.

One of the greatest challenges with interpretation of both UU and UC tests is that the measurements are often sensitive to disturbance, which introduces an often unknown and variable bias into the measurements. Such bias is often conservative in that disturbance generally produces $s_u$ that are less than what exists in the field but may, in part, be compensated by other factors such as strain rate and stress path effects (Ladd, 1991) as described in Chapter 7. The net effect of these compensating factors is often unknown except to say that it "generally works" if performed using traditional levels of investigations. Effects of disturbance and other compensating factors generally tend to be more pronounced and significant for soft to medium clays and less significant for stiff clays.

It is also important to recognize that $s_u$ measurements from UU triaxial tests and unconfined compression tests represent $s_u$ at a specific point in space and time, as well as a specific method of loading (e.g., compression, extension, simple shear, etc.), as described in more detail in Chapter 7. This characteristic generally makes interpretation of $s_u$ relatively straightforward. However, it limits the potential uses for such measurements to be representative of the effective stress conditions that exist in the field at the time of sampling (or more precisely, to the effective stress conditions that exist in test specimens at the time of testing) and the stress path applied during the test. Changes in effective stress between the time of sampling/testing and the time of construction cannot be accounted for with UU and UC measurements. The assumption inherent with application of such measurements is therefore that in situ stress conditions at the time of sampling and/or testing are practically similar to those that will be present at the time of construction.

### 11.9.2 Interpretation of $s_u$ from Consolidated-Undrained Tests

Undrained shear strength can also be established from consolidated-undrained type triaxial compression or extension tests, or from consolidated-undrained direct simple shear tests. In all such tests, specimens are consolidated to a known state of effective stress in the laboratory and then sheared to failure under undrained conditions. As such, it is possible to establish a relationship between $s_u$ and the effective

consolidation stress, and to subsequently use that information to establish the magnitude of $s_u$. The so-called "$c/p$ ratio", or more precisely the $s_u/\sigma'_{vc}$ ratio, represents the ratio of $s_u$ to the effective stress at consolidation. As described in Chapter 7 and shown in Figures 7-14, 7-24, and 7-33, the magnitude of $s_u/\sigma'_{vc}$ is predominately dependent on $OCR$ and the method of loading and is often expressed in terms of coefficients $S$ and $m$ from Equation 7.6. Given an appropriate relationship between $s_u/\sigma'_{vc}$ and $OCR$, $s_u$ can be estimated from knowledge of $\sigma'_{vo}$ and $OCR$ in the field, and knowledge of the anticipated method of loading.

As described in Section 11.8, $\sigma'_{vo}$ is generally computed from knowledge of the in situ total unit weight and estimates or measurements of the in situ pore water pressure. The magnitude of $OCR$ is determined from estimates of $\sigma'_p$, usually derived from results of one-dimensional consolidation tests. Figure 11-21 shows a profile of $s_u$ derived from interpreted values for $\sigma'_p$ shown in the figure and values for $S = 0.25$ and $m = 0.77$ determined from CUIC tests as shown in Figure 11-22. Estimates of variability and uncertainty shown in Figure 11-21 for $s_u$ were established using equations provided in Section 11.5.2, considering $\sigma'_p$ to be an indirect measurement for $s_u$ and the $s_u/\sigma'_{vc}$ versus $OCR$ relation to be the transformation.

Estimation of $s_u$ from knowledge of $s_u/\sigma'_c$ and $OCR$ has several distinct advantages. Since the approach directly addresses and utilizes the fundamental relationship among $s_u$, effective consolidation stress, and overconsolidation ratio, it provides greater flexibility for use since $s_u$ can be estimated for a range of effective stress conditions. For example, $s_u$ can be estimated for current conditions, conditions during staged construction, or conditions under other changes to effective stress. Furthermore, the approach is less sensitive to effects of sample disturbance since the process of consolidating specimens to a known effective stress significantly reduces effects of disturbance. This is particularly true if the SHANSEP procedure described in Chapter 7 is used during testing, which can dramatically reduce effects of sample disturbance for many soft soils if conducted appropriately.

Because specimens are consolidated in the laboratory to some desired effective stress, the specimens effectively become representative of conditions in the field where the same effective stresses are present (presuming similar $OCR$ and soil fabric). As such, it is possible to utilize test results performed for specimens from one depth to establish $s_u$ at other depths as long as the effective stress and $OCR$ are appropriate and as long as the soil composition is similar to that tested. However, it is also true that $s_u$ measurements for a specific specimen will not be representative of the actual $s_u$ at the location where the specimen was acquired in the field if the effective consolidation stress in the laboratory is not consistent

with what exists in the field. Thus, results from CU tests should not be considered as "point" tests that are representative of a specific location.

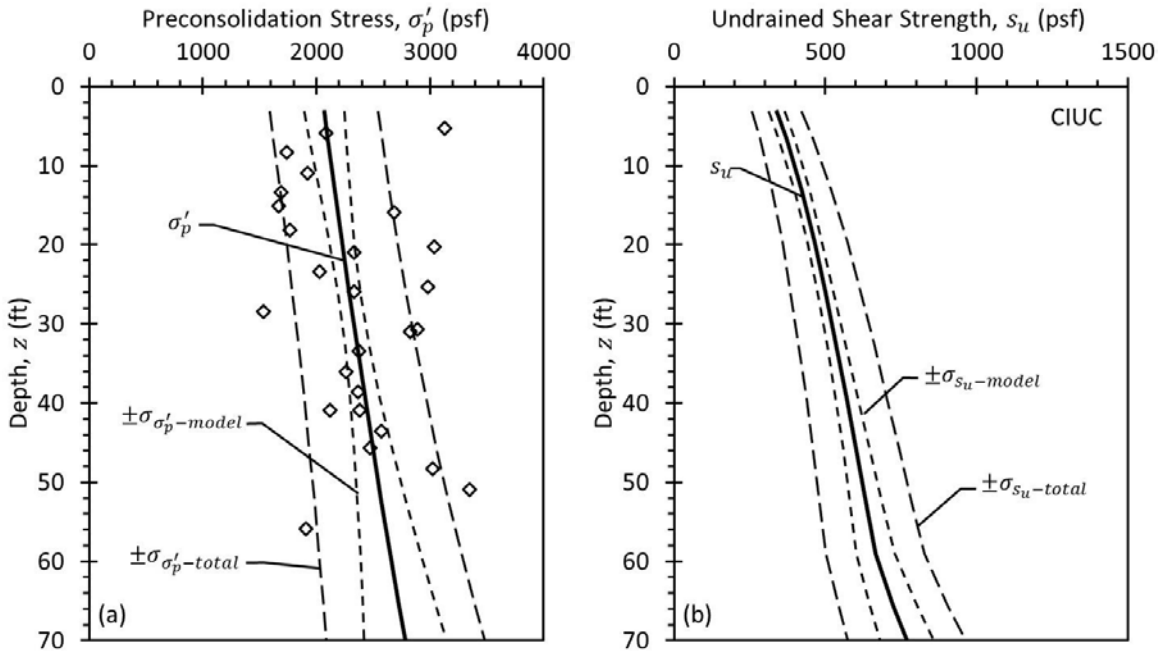


**Figure 11-21 Interpretation of $s_u$ from CIUC tests: (a) $\sigma_p'$, and (b) $s_u$.**

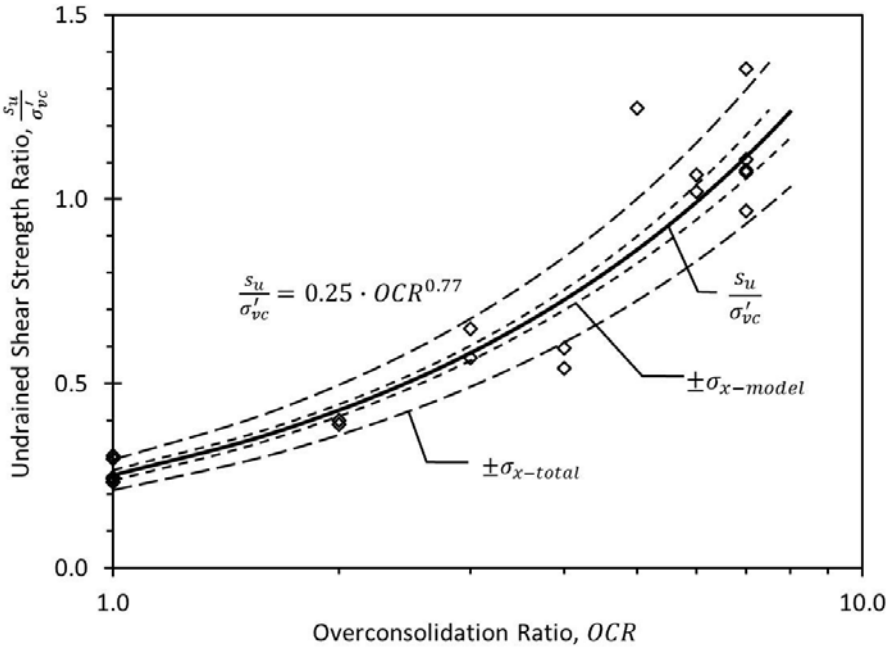


**Figure 11-22 $s_u/\sigma_{vc}'$ versus $OCR$ relation used to establish $s_u$ shown in Figure 11-21.**

The primary disadvantage of estimating $s_u$ from $s_u/\sigma'_c$ and $OCR$ is that more elaborate testing is required than for determining $s_u$ from UU tests. Nevertheless, it is commonly true that $s_u$ determined from consolidated-undrained type tests are substantially more accurate than $s_u$ determined from UU and/or UC tests as long as accurate estimates of $OCR$ are used. It is also generally true that, despite requiring more elaborate tests, $s_u$ can be more reliably and accurately determined using fewer overall tests in many cases so that differences in costs between using UU and/or UC tests and using CU tests are often much less than suggest by comparison of costs for individual tests.

### 11.9.3 Interpretation of Undrained Shear Strength from Indirect Laboratory and Field Tests

A variety of indirect laboratory and field tests can also be used to estimate $s_u$ for fine-grained soils. As described in Chapter 7, $s_u$ can be estimated from in situ field tests that include CPT, CPTU, FVT, DMT, PMT, and SPT measurements. Undrained shear strength can also be estimated using pocket penetrometer tests, Torvane tests, fall cone tests, and laboratory vane tests. Since all of these tests are considered to be indirect tests, interpretation of collections of the indirect measurements should generally be accomplished following the procedures described in Sections 11.4.2 and 11.5.2.

## 11.10 INTERPRETATION OF TOTAL STRESS STRENGTH PARAMETERS FOR DESIGN IN UNSATURATED SOILS

A fundamental assumption when using $s_u$ measurements as described in the previous section is that the soil is saturated, or nearly saturated such that the common "$\phi = 0$" condition is appropriate wherein $s_u$ is independent of total confining stress. This assumption is practically satisfied for many soil deposits, but is not universally satisfied. One quite common feature involving unsaturated soils is compacted embankments and fills. In cases, where undrained shear strengths are required for compacted embankments or other unsaturated soils, undrained shear strengths should be represented using total stress strength parameters, $c$ and $\phi$. Unlike $s_u$, which can be established from a large number of different tests, the total stress strength envelope can only be established using UU triaxial tests.

Like $s_u$, the total stress strength envelope is dependent on the effective stress in the ground or in specimens at the time of testing. As such, interpretation of measurements should be restricted to measurements made on specimens with practically similar effective stress. In many cases, this means that measurements considered collectively for interpretation should be acquired from approximately the same depth. It is inappropriate to combine measurements made for substantially different depths into a single total stress failure envelope. For compacted specimens prepared to evaluate total stress strength

parameters for compacted fills, this generally means that measurements considered collectively should be compacted with similar compactive effort at similar compaction moisture contents.

It is not unusual to observe curved failure envelopes for unsaturated soils. For some common methods of analysis (e.g., limit equilibrium slope stability analysis), it is possible to model curved envelopes using a piecewise linear approximation of the envelope. However, many other design and analysis methods are predicated on use of a linear Mohr-Coulomb failure envelope that can be represented by a cohesion intercept (either $c$ or $c'$) and angle of internal friction (either $\phi$ or $\phi'$). In such cases, it is necessary to approximate the observed curve failure envelope using a linear approximation. When developing such an approximation, it is important that the linear envelope be fit to available measurements for confining stresses that are appropriate for the problem being evaluated. As illustrated in Figure 11-23, fitting of a linear envelope over an inappropriate range of confining stresses will generally lead to overestimation of measured strengths and potentially unconservative analyses.

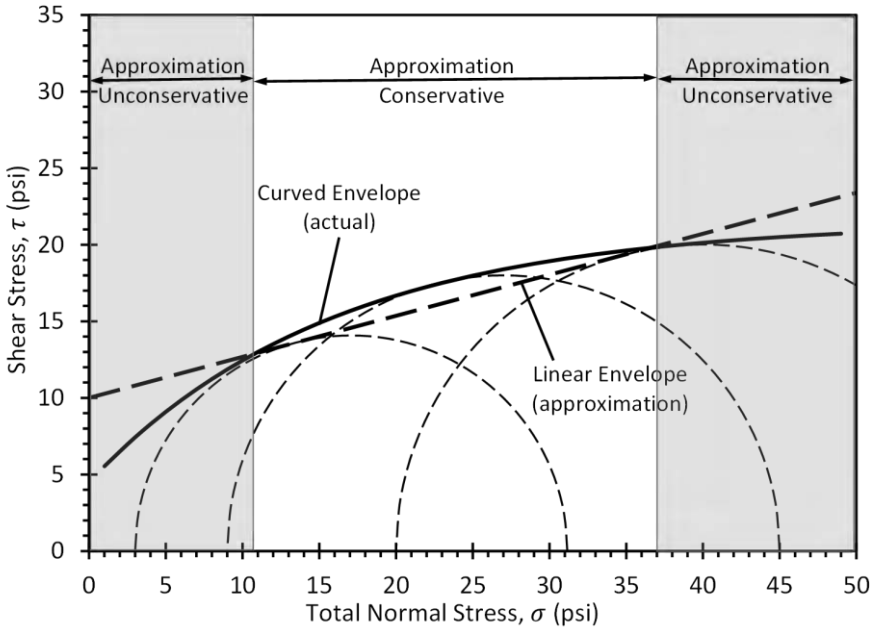


**Figure 11-23 Mohr-Coulomb diagram showing linear approximation of curved failure envelope.**

## 11.11 INTERPRETATION OF EFFECTIVE STRESS STRENGTH PARAMETERS FOR DESIGN

As described in Chapter 7, the effective stress failure envelope truly represents the fundamental strength envelope for soil since it describes how strength varies with the magnitude of the effective stress acting on the soil. Effective stress strength parameters, $c'$ and $\phi'$, are required for geotechnical design in

practically all soil types. Effective stress strength parameters are utilized for evaluation of stability under long-term, fully drained conditions and, thus, are often referred to as "drained" shear strength parameters. However, the effective stress failure envelope is strictly applicable for both drained and undrained loading conditions (and, in fact, partially drained conditions) if appropriate consideration is given to development of excess pore water pressures generated during undrained loading. The effective stress failure envelope, or effective stress strength parameters that describe the envelope, can be determined using several laboratory tests as well as a number of in situ field tests as described in the following sections.

### 11.11.1 Interpretation of Effective Stress Strength Parameters from Laboratory Tests

In the laboratory, the effective stress strength envelope, or effective stress strength parameters, are most commonly established using consolidated-drained type triaxial tests, consolidated-undrained type triaxial tests with pore water pressure measurements, or consolidated-drained type direct shear tests. While slight differences can be observed among effective stress failure envelopes determined from different tests (e.g., due to differences volume change or stress state among the different tests), measured failure envelopes from different tests are often similar as a practical matter. It is also common to observe less variability and uncertainty in effective stress strength envelopes than is commonly seen for $s_u$ and total stress strength envelopes (both of which depend on the magnitude of the effective stress, among other factors) because the effective stress strength envelope describes how soil strength varies with effective stress. While effective stress strength envelopes do depend on the specific soil being tested, and specifically the density and/or stress history of the soil, they are much less sensitive to these parameters than $s_u$ and total stress strength parameters. As such, it is often a relatively simple matter to establish effective stress strength parameters, despite the fact that the tests are slightly more complex than those used for $s_u$ and total stress strength parameters.

Interpretation of effective stress strength envelopes is generally a straightforward issue of collectively plotting results from individual tests performed within a soil stratum and interpreting the results to establish an appropriate failure envelope as illustrated in Figure 11-24. Since the effective stress failure envelope describes how soil strength varies with the magnitude of the effective confining stress, it is perfectly acceptable, and in fact desirable, to combine measurements made for similar soils taken from different depths and different borings to establish appropriate values for effective stress strength parameters. This is far preferable to establishing a collection of different values of effective stress strength parameters considered to be "point" values, and then combining them by averaging or otherwise interpreting values for effective stress strength parameters. The former generally produces a better representation of the effective stress strength envelope for a stratum within an established design domain,

and provides a sound basis upon which to quantify uncertainty in the established envelope. A similar approach should also be used for interpretation of measurements from direct shear tests.

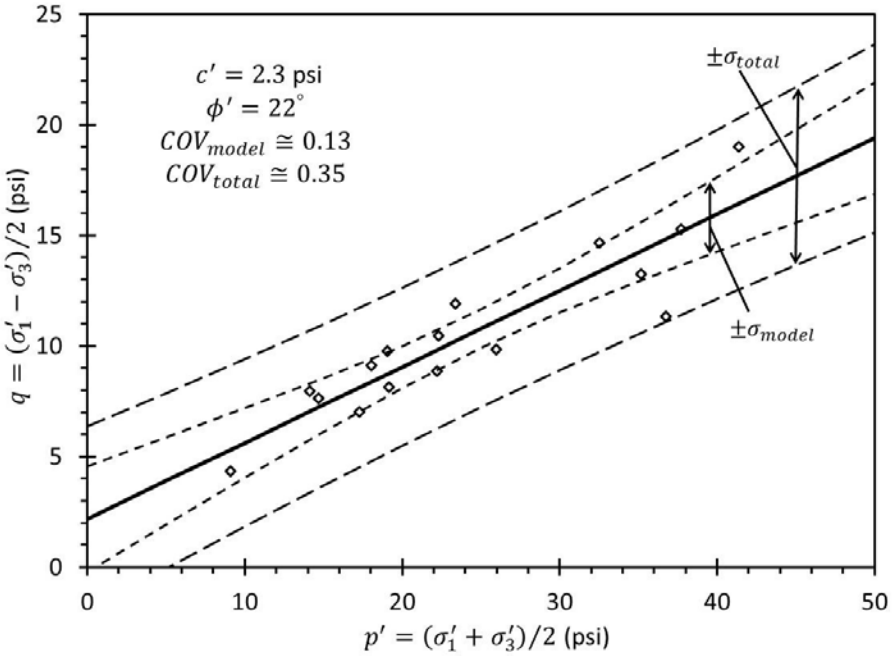


**Figure 11-24 Effective stress failure envelope from CU type triaxial compression tests.**

Since effective stress strength envelopes are often presumed to be linear, the variability and uncertainty associated with the envelopes can be determined according to methods described for linear relations in Section 11.5 and Appendix 3. In this case, however, the regression parameter will be some measure of the effective confining stress rather than depth or elevation as illustrated in Figure 11-24. As is true for regression for other linear relations, the magnitude of the model uncertainty, $COV_{d-model}$, will generally vary with the magnitude of the effective confining stress, generally being least near the average of the effective confining stresses applied for the tests and greatest at very small and very large values of confining stress. When comparing computed values for $COV_{d-model}$ with the model uncertainty threshold of 0.3, an average value of $COV_{d-model}$ taken over an appropriate range of confining stresses for the problem being considered should be used.

In some cases, measured values of shear strength for establishing effective stress strength envelopes will tend to be more variable at higher confining stresses and less variable at lower confining stresses as shown for the direct shear test measurements in Figure 11-25. In such cases, conventional ordinary least squares regression may produce estimates for variability and uncertainty that are inconsistent with the available measurements. In such cases, so-called "weighted" least squares regression techniques may produce estimates that more closely approximate the observed variability.

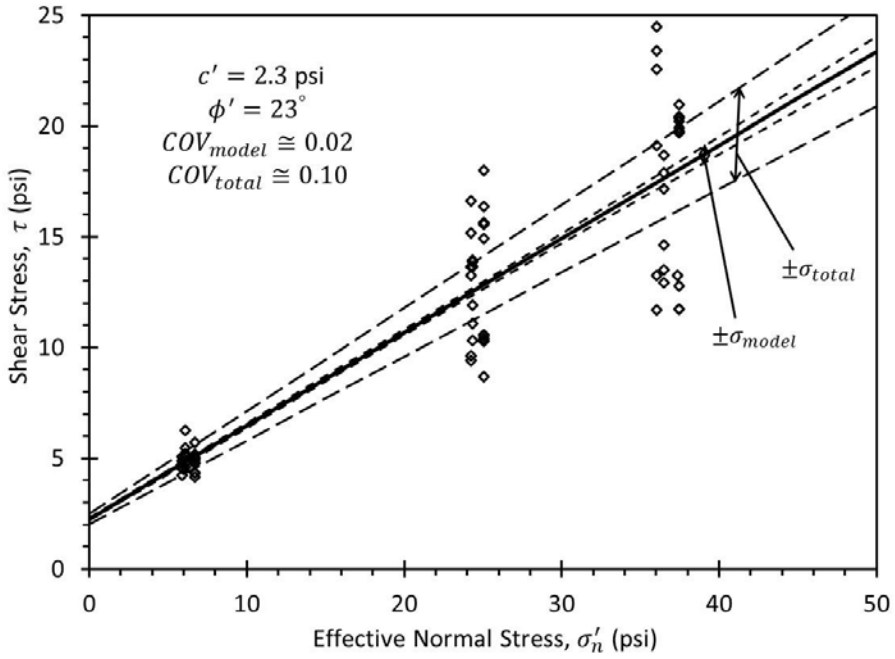


**Figure 11-25 Effective stress failure envelope interpreted using weighted least squares regression.**

### 11.11.2 Interpretation of Effective Stress Friction Angle from In Situ Tests

As described in Chapter 7, the magnitude of the effective stress friction angle can also be estimated indirectly from in situ test measurements and empirical correlations. In situ tests are particularly important for investigation of clean coarse-grained soils that are difficult to sample using commonly available sampling methods. In such soils, effective stress strength parameters can often be more reliably established using in situ test methods than laboratory measurements. Effective stress strength parameters are commonly estimated from CPT, SPT, and DMT tests, and can be measured directly using borehole shear tests as described in Chapter 7. Approximate values for effective stress strength parameters can also be estimated from correlations with Atterberg limits and other index properties. Regardless of the specific indirect measurements used to estimate effective stress strength parameters, the process for interpretation is basically the same, and consistent with that described for indirect measurements in Sections 11.4 and 11.5.

## 11.12 INTERPRETATION OF CONSOLIDATION PARAMETERS FOR DESIGN

Interpretation of consolidation parameters for design is generally performed following procedures that have been described in this chapter for other design parameters. Figure 11-26 shows an example interpretation of measurements of consolidation properties from laboratory one-dimensional consolidation tests performed on high quality fixed-piston samples for a soft clay site.

### 11.12.1 Compressibility Parameters

Compression and recompression indices should be interpreted based on a rational assessment of available measurements with the objective of assigning a value to each behaviorally different stratum. As a general rule, such parameters should generally be established from laboratory one-dimensional consolidation tests performed on high quality samples, although it may be acceptable to use estimates derived from in situ tests in cases where settlement is not expected to control design.

### 11.12.2 Coefficient of Consolidation

The coefficient of consolidation, $c_v$, can be interpreted in a similar manner to the compressibility indices. However, one needs to consider the expected magnitude of loading when interpreting $c_v$ because the magnitude of $c_v$ depends on the load level. A rational approach to interpreting $c_v$ values for design is to first assess whether design loads are sufficiently high to reach stress levels that exceed $\sigma_p'$. If anticipated stress levels are less than about 80 percent of $\sigma_p'$, one should plot average values of $c_v$ for stress levels below $0.8 \cdot \sigma_p'$ and interpret those values as shown in Figure 11-26. Conversely, if the anticipated loading will reach stress levels that exceed $\sigma_p'$, one should consider average $c_v$values for stresses that range from $\sigma_p'$ to the anticipated final vertical effective stress in the ground.

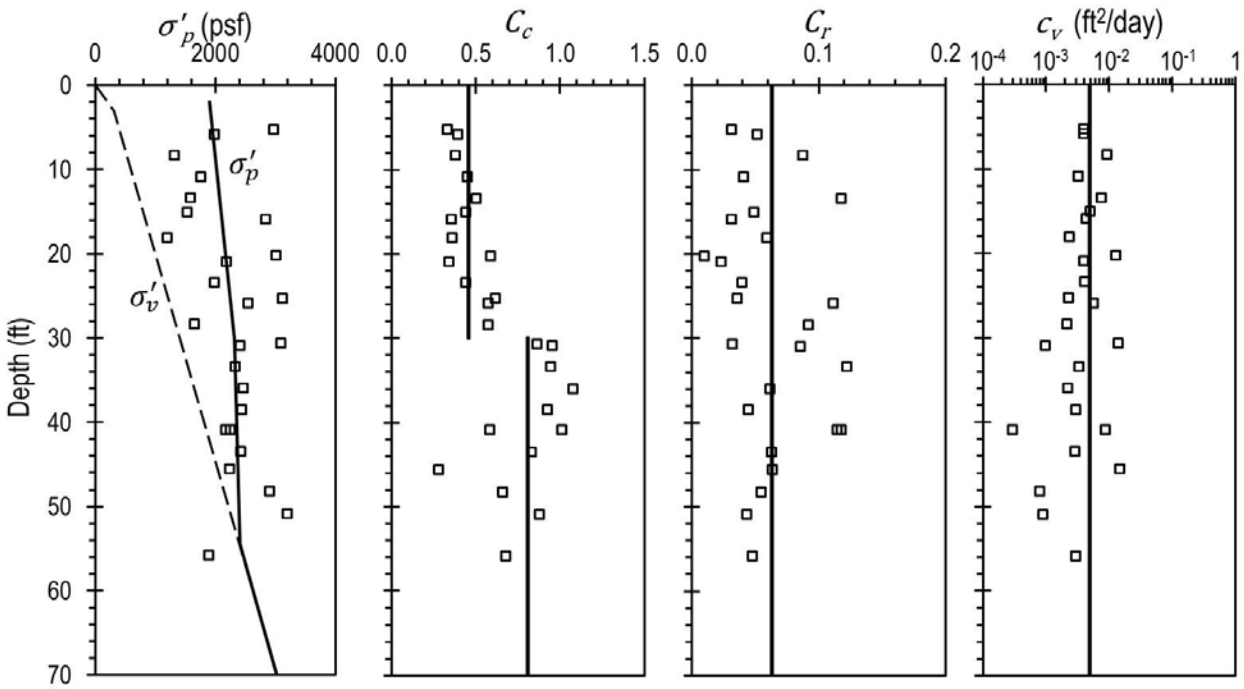


**Figure 11-26 Interpretation of consolidation parameters (modified after Ding, et al., 2014).**

Observations of time rates of settlement during construction often reveal that actual rates of settlement exceed predicted rates developed based on values of $c_v$ established from laboratory consolidation tests. This result is predominantly attributed to the presence of thin lenses of soil with greater coefficients of consolidation (or hydraulic conductivity) that act to reduce the "drainage distance", which has a significant effect on time rates of consolidation. This phenomenon is unfortunately difficult to confidently evaluate during design. Improved indications can sometimes be observed from CPTU or DMT dissipation tests to measure the horizontal coefficient of consolidation ($c_h$). However, for significant projects where time rates of settlement are important for design and performance, the observational method described in Section 11.7 should generally be implemented and used to develop improved estimates for time rates of settlement.

### 11.12.3 Coefficient of Secondary Compression

Values of $C_\alpha$, or $C_{\alpha\varepsilon}$, can also be interpreted using the methods described in this chapter. Like $c_v$, however, values for $C_\alpha$ vary with stress history in that maximum values for $C_\alpha$ are generally observed for stress levels greater than $\sigma_p'$ (i.e., at stresses corresponding to virgin compression). Therefore, to assess values for $C_\alpha$ for design analyses, the final effective stress in the ground after primary consolidation is completed should be evaluated. If the final effective stress is less than approximately $0.8 \cdot \sigma_p'$, an average value of $C_\alpha$ (or $C_{\alpha\varepsilon}$) evaluated in the overconsolidated range should be used for design. Conversely, if final effective stresses in the ground exceed $\sigma_p'$, it is conservative to select $C_\alpha$ values corresponding to stresses in the range of 1 to 2 times $\sigma_p'$. It is important to note that laboratory-measured values of $C_\alpha$ from disturbed samples often produce values that are less than is truly appropriate in the field when loading in the normally consolidated range. Effects of sample disturbance therefore need to be carefully assessed, especially for soils that may undergo significant secondary compression such as organic clays and peats.

## 11.13 EVALUATION OF GROUNDWATER CONDITIONS FOR DESIGN

A final, but critical and challenging aspect of interpretation for site characterization is interpretation of groundwater conditions for design. If groundwater conditions can be reasonably considered as hydrostatic for all relevant strata, interpretation of groundwater conditions can rely on establishing an appropriate elevation (or depth) for the groundwater table. However, if groundwater conditions are more complex, such as when encountering significant groundwater flow, artesian conditions, or in soils that are partially consolidated, interpretation may include specification of the magnitude of pore water pressures throughout a model domain. The latter is obviously more complex than the former; however, neither

represent the most significant challenge associated with interpretation of groundwater conditions for design.

The most significant challenge associated with interpretation of groundwater conditions for design arises because design should be performed considering the "worst case" groundwater conditions that may rationally arise during construction or operation. Such conditions are unlikely to be present during site characterization. Thus, interpretation of groundwater conditions for design can seldom be simply measured like most other important design parameters. Rather, the worst-case design conditions must be inferred using considerable judgment, knowledge of the groundwater regime at the site location, and perhaps other information regarding boundary conditions for groundwater flow. Acquisition of field measurements can often dramatically improve such interpretation, and reduce the uncertainty associated with the extreme groundwater conditions that may be encountered. However, it is important to recognize that extreme conditions are unlikely to be observed during site characterization.

THIS PAGE IS LEFT INTENTIONALLY BLANK

# CHAPTER 12
# IDENTIFICATION AND CHARACTERIZATION OF GEOTECHNICAL HAZARDS

Geotechnical hazards are conditions that have the potential to negatively impact the design, construction and long-term performance of transportation facilities. Failure to identify geotechnical hazards early in project development will often result in design changes during construction or poor performance following construction, both of which lead to costs that are inevitably greater than would be incurred if hazards had been identified earlier. Identification and characterization of geotechnical hazards are therefore important components of geotechnical site characterization programs. Identification of geotechnical hazards requires understanding of the potential susceptibility of a site to a given hazard and the means to observe or detect evidence of the hazardous condition. In this chapter, six geotechnical hazards are discussed: karst; seismic hazards; underground mines; groundwater hazards; landslides and rockfalls; and landfill or geo-environmental hazards. Each section provides an overview of the geotechnical hazard, potential negative consequences of the hazard, and a discussion of methods and techniques that can be used to identify and characterize the respective hazard.

## 12.1 OBJECTIVES FOR IDENTIFICATION AND CHARACTERIZATION OF GEOTECHNICAL HAZARDS

Failure to identify and properly characterize geotechnical hazards can have dramatic financial and human consequences for transportation agencies. Geotechnical hazards introduce risk to design, construction, and preservation of many transportation projects. Identification of geotechnical hazards is therefore one of the foremost objectives of site characterization because it allows agencies to identify risks to transportation projects or facilities. Once geotechnical hazards are identified and judged to present risks, it is then necessary to more thoroughly characterize the hazard so that risks can be quantified and mitigated. It is generally desirable to identify and characterize geotechnical hazards early in the project development process because doing so often allows risks to be mitigated more cost effectively.

## 12.2 KARST HAZARDS

The term “karst” refers to landscapes with surface and underground features formed by dissolution of soluble rock. Karst features are most commonly associated with carbonate rocks, such as limestone and dolomite, but may also form in evaporites such as gypsum or salt rock. As weakly acidic groundwater moves through fractures in carbonate rock, the water slowly dissolves the surrounding rock and enlarges underground openings. Over time, these openings may grow to considerable size resulting in the

formation of a network of interconnected underground caves and caverns. A common surface expression of karst is the presence of sinkholes. Sinkholes may form gradually as exposed bedrock is slowly dissolved (solution sinkholes) or as soil gradually moves into subsurface cavities (subsidence sinkholes). Alternatively, sinkholes may form suddenly if a cavern grows to a size such that the weight of the overlying soil and rock can no longer be supported and the overlying ground collapses into the underground opening (collapse sinkholes), as shown Figure 12-1a. While growth of subsurface voids is generally a slow process, changes in stress conditions, due to lowering of groundwater levels for example, will often initiate sudden collapse. Movement of water along fractures and joints can also create highly irregular, or "pinnacled" bedrock features like shown in Figure 12-1b. Karst environments may also have extensive underground drainage systems with surface features such as disappearing streams (where surface water flows into underground conduits) and springs. An illustration of a mature karst environment is presented in Figure 12-2.

**Figure 12-1 Surface expressions of karst: (a) sinkhole in Tennessee and (b) pinnacled bedrock.**

A map of karst areas and potential karst areas in the contiguous United States is presented in Figure 12-3 (Weary and Doctor, 2014). As can be seen in this figure, karst occurs in nearly every state, but is especially prevalent in certain states such as Florida, Kentucky, Tennessee, Texas, and Missouri.

### 12.2.1 Implications of Karst Hazard for Transportation Projects

From a geotechnical perspective, karst is considered a hazard because it can negatively impact: (1) support conditions for structures, and (2) flow of water and/or contaminants. Karst environments produce highly variable and unpredictable subsurface conditions that can negatively impact transportation facilities if not properly identified and characterized. The most obvious implication of karst is the

potential to adversely affect foundation support, with impacts ranging from excessive settlements to total collapse. In cases like the one shown in Figure 12-1a, collapse sinkholes may develop without warning, resulting in total loss of support. Gradual settlement and loss of support may be observed over subsidence sinkholes. Support conditions for foundations can also be highly variable due to local features such as infilled sinkholes, solution cavities, and clay seams. It is important that site characterization programs identify and characterize subsurface karst features so hazards can be avoided or mitigated.

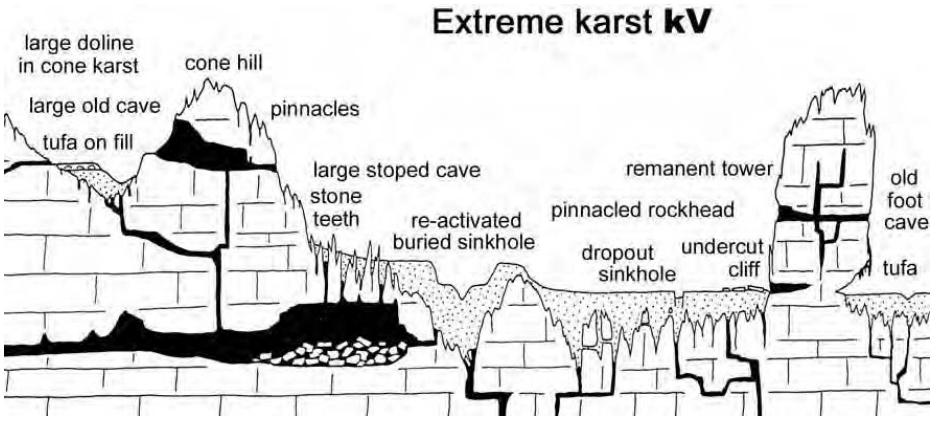


**Figure 12-2 Features of extreme karst landscape (Waltham and Fookes, 2003).**

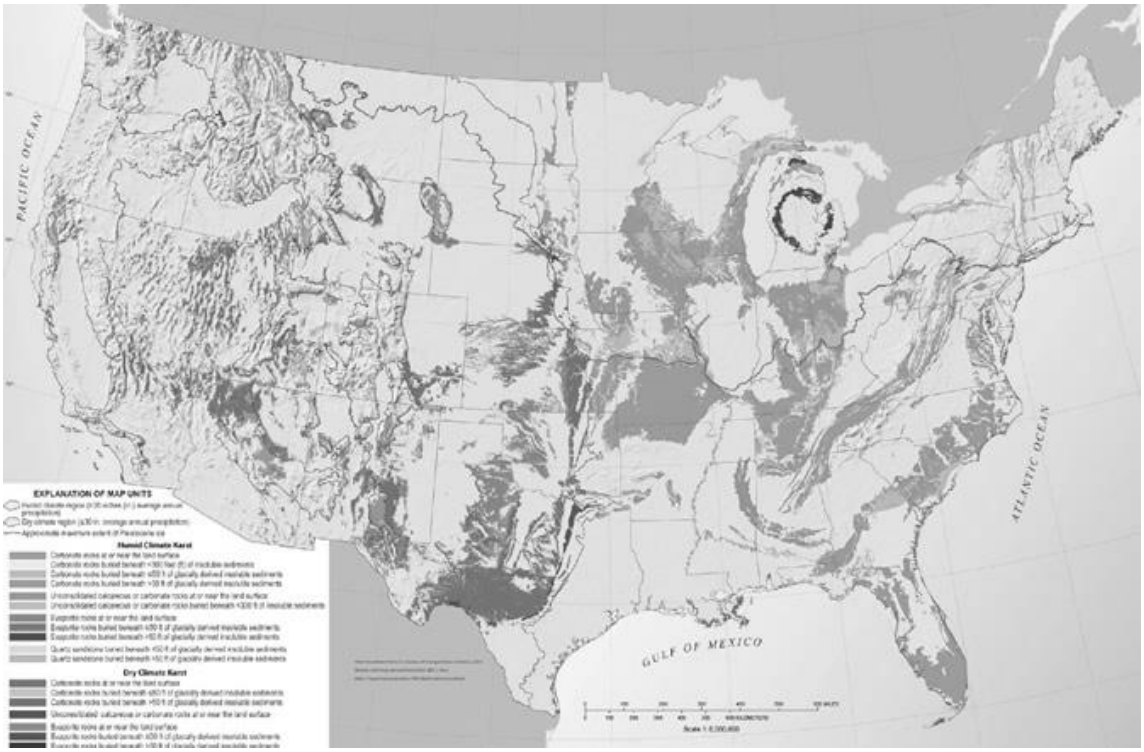


**Figure 12-3 Map of karst and potential karst areas in soluble rocks in the contiguous United States (Weary and Doctor, 2014)**

Karst environments can also impact the construction and integrity of deep foundations. As noted above, karst environments may produce highly irregular bedrock features where the depth to intact rock can fluctuate by tens of feet over short distances. Between bedrock pinnacles, collapsed rock blocks may be interspersed with infilled material, clay seams, and residual soil making identification of competent bedrock more difficult. Improper identification of bedrock conditions may result in insufficient support for deep foundations, or erroneous construction quantities that can dramatically impact construction budgets and schedules. The presence of voids or soil-filled seams beneath deep foundations also threatens the integrity of the foundation. Some common support condition problems encountered with drilled shafts constructed in karstic regions are illustrated in Figure 12-4 (Brown, 1990). Insufficient site characterization may result in design changes and increased costs after construction begins. Karst conditions also have implications on the constructability of foundation elements. Features such as artesian conditions, infilled soil seams and cavities, rock blocks, sudden groundwater flow into shafts, and large concrete overpours can negatively impact construction of deep foundation elements.

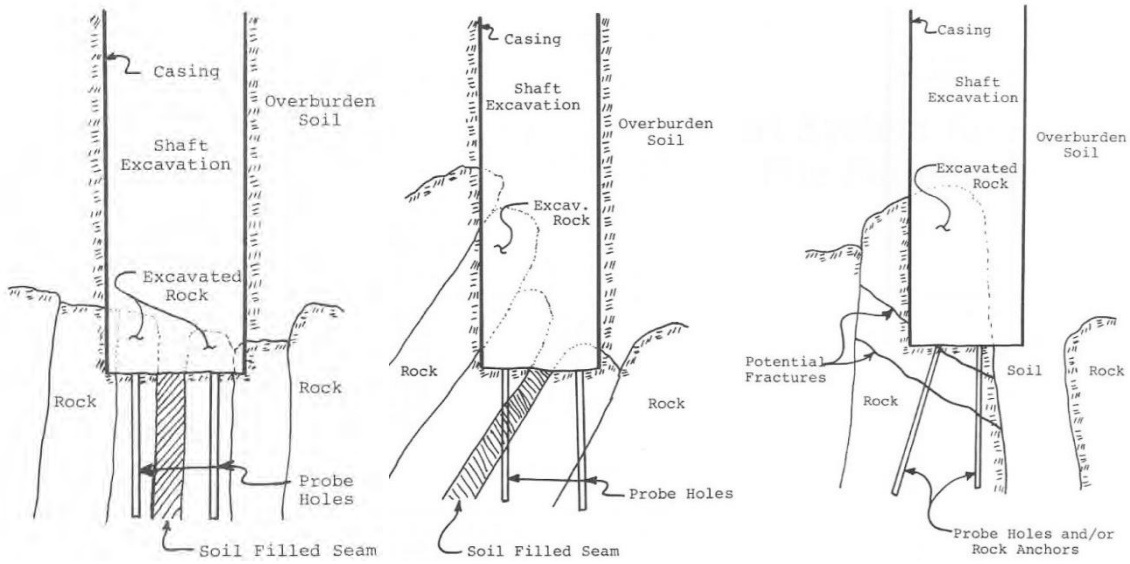


**Figure 12-4 Commonly encountered problems in pinnacled limestone (Brown, 1990)**

In addition to impacts on structural support, karst environments produce unique groundwater and surface water conditions that can affect construction and performance. Unlike soil and intact rock, the subsurface flow of water in karst is not primarily governed by the permeability of the rock, but instead by the interconnected network of underground fissures and caves. As noted above, the potential for groundwater flow into drilled shafts from these conduits presents complications for construction. In addition, contaminants can be rapidly transported over large distances in karst environments, so environmental impacts to groundwater are a particular concern in karst environments. Natural springs and artesian

conditions also occur in karst environments and may directly impact surface facilities and affect subsurface stress conditions. Furthermore, large surface depressions caused by sinkholes may be subject to flooding in rain events if drainage from the sinkhole is blocked.

### 12.2.2 Identification and Characterization of Karst Hazards

Important elements of site characterization in karst environments include:

(1) Desk study to determine site susceptibility and evidence of karst;
(2) Identification and characterization of surface karst features; and
(3) Identification and characterization of subsurface karst features.

Each of these three elements are described in the following sections.

***Desk Study***

The objective of the desk study is to determine if a site is susceptible to karst conditions. Geologic setting is the main factor governing susceptibility to karst conditions. Karst is mainly associated with carbonate rocks like limestone and dolomite and evaporite rocks like gypsum and salt rock. In addition, the term pseudo-karst is sometimes used to describe karst-like features that form in ways other than rock solutioning. Examples of pseudo-karst include voids produced by lava flows, piping of sediments in arid environments, and melting of permafrost (Weary and Doctor, 2014). Geologic maps produced by state geologic surveys or the U.S. Geological Survey (USGS) are good sources of information on the potential for karst formation. In addition, USGS recently published a digital map and database of karst in the United States (Weary and Doctor, 2014) that were developed to delineate regions in the U.S. having karst or the potential for karst. Maps of areas with the potential for pseudo-karst are also included. Some state geologic surveys also publish maps of known caves or karst features. Topographic maps and aerial photographs can be good preliminary sources of information, as they may show large-scale surface depressions indicative of karst. However, smaller karst features are often obscured by vegetation in aerial photographs, and topographic maps may not provide sufficient resolution to identify small surface depressions. Small features may be evident in high-resolution airborne lidar imagery that is available from some state geological surveys. "Bare-earth" lidar imagery that effectively removes vegetation from lidar images will often produce a detailed image of surface topography that can aid in identification of karst features. A comparison of the same scene from aerial photography and lidar imagery is shown in Figure 12-5, illustrating the advantages of lidar imagery for detecting small surface features. The desk study should also include a search for articles documenting sinkhole formations as well as published

studies of geophysical or subsurface exploration performed in the area. Lastly, geotechnical reports from nearby projects can be a great resource if available.

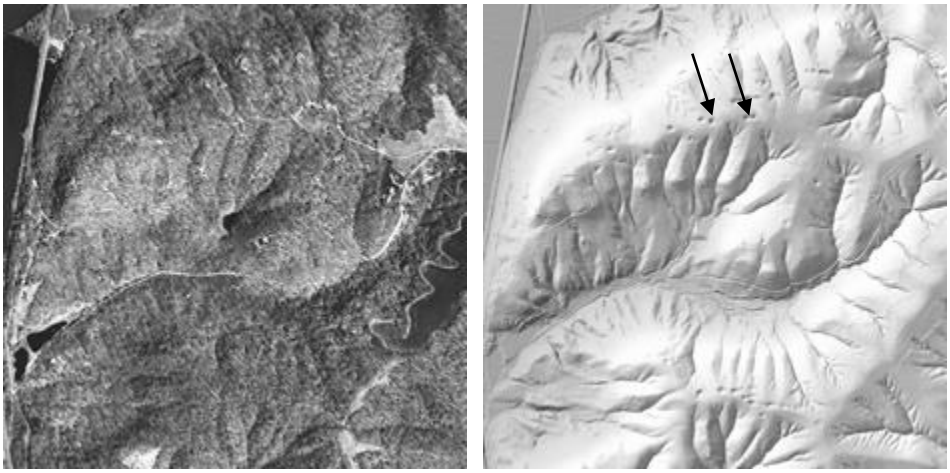

**Figure 12-5 Comparison of aerial photograph and lidar imagery showing detection of small surface depressions (black arrows) using lidar imagery (Illinois State Geological Survey, 2016)**

***Identification and Characterization of Surface Karst Features***

A site visit should be made to identify and document surface expressions of karst features. These features may include surface depressions caused by sinkholes, collapse features, exposed pinnacled bedrock, disappearing streams, and springs. The presence of such features is indicative of a karst environment and suggests that the subsurface is likely to contain karst features. Exposed rock cuts should also be visually inspected to identify the presence and frequency of dissolution features and fractures and to assess the quality of the rock. As noted above, remote sensing technology can be a valuable tool for identifying surface expressions of karst. Several studies have documented the effectiveness of airborne lidar for detecting sinkholes in karst environments (e.g., Zhu, et al., 2014). Another remote sensing technology called satellite-based interferometric synthetic aperture radar (InSAR) has also been used to measure and track ground subsidence over evaporite karst features (Conway and Cook, 2013) and identify developing sinkholes (Bruckno, et al., 2013).

***Identification and Characterization of Subsurface Karst Features***

Due to the highly variable nature of karst, identifying and characterizing subsurface karst features is challenging. However, the consequences of not detecting these features can be severe. The primary tool for investigating subsurface conditions is exploratory drilling. Drilling is quite effective for identifying karst features at specific locations of interest. Drilling programs should be more extensive in karst conditions due to the complex three-dimensional variability at the site, often involving relatively large

numbers of borings at relatively close spacing. For example, at least one boring should be located at each deep foundation location in karst environments to assure that karst features are not present at that location. For large shafts, pile groups, and footings, multiple boreholes may be necessary to avoid conditions such as those shown in Figure 12-4. In karst landscapes, exploratory drilling should extend to depths well beyond the expected depth of the foundation. Figure 12-6 shows the elastic stress distribution beneath a circular loaded area on an elastic material. The decrease in stress is a function of the diameter of the loaded area. The stress drops to 10% of the loaded value at a depth of approximately two diameters below the base of the loaded area. Investigations should extend well beyond this depth to confirm the presence of competent material.

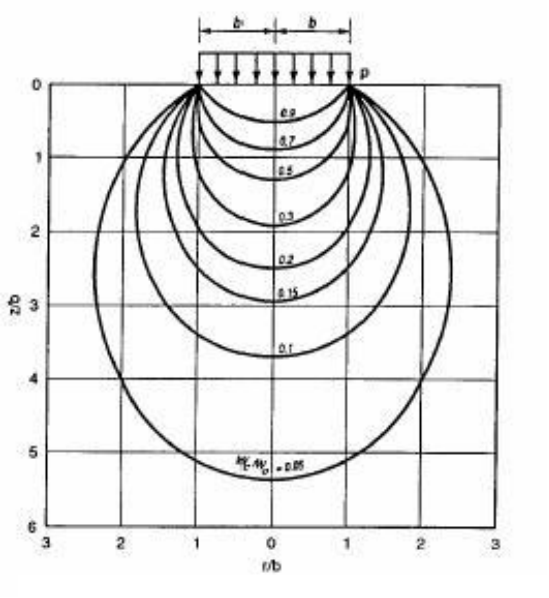


**Figure 12-6 Stress distribution beneath a square foundation**

Subsurface drilling provides excellent information at specific locations of interest, but is less effective for characterizing karst features over large areas because conditions can vary significantly over short distances in karst environments. It is often not practical or effective to use boreholes to characterize lateral variability at karst sites. In such cases, geophysical investigations may be used to supplement information obtained from drilling programs and to help target anomalous areas for further investigation. Common geophysical methods used in karst environments include electromagnetic conductivity, ground penetration radar, resistivity, seismic, and gravity surveys. Two subsurface conditions of particular interest in karst environments include: (1) the presence of sinkholes or voids below the subsurface, and (2) the depth to bedrock. Table 12-1 and 12-2 summarize the applicability of different geophysical methods for identifying voids and locating the depth to bedrock, where A indicates preferred methods and B indicates alternative methods as suggested by ASTM (ASTM D6429, 2011).

The usefulness and value of geophysical methods for any application will always be controlled by site conditions and the objectives of the geophysical investigation. The ability to detect voids of a given size decreases with depth for all of the listed methods. Detecting the interface between soil and competent bedrock also becomes more difficult when the rock is highly weathered or when the bedrock surface is highly irregular, both of which are common in karst environments. It is therefore strongly advisable to consult with a geophysicist to determine the most appropriate techniques for specific sites. Each of the methods is briefly discussed below. More detailed discussion of geophysical methods for karst applications can be found in Wightman et al. (2004).

**Table 12-1 Applicability of geophysical methods for identifying voids and sinkholes (ASTM D6429, 2011)**

| Method | Applicability Rating* |
|---|---|
| Ground Penetrating Radar | A |
| Gravity | A |
| Seismic Reflection/Refraction | B |
| Resistivity | B |
| Frequency Domain Electromagnetics | B |
| Time Domain Electromagnetics | B |

* Note: A – preferred methods; B-alternative method

**Table 12-2 Applicability of geophysical methods for identifying depth to bedrock (ASTM D6429, 2011)**

| Method | Applicability Rating* |
|---|---|
| Ground Penetrating Radar | A |
| Seismic Reflection/Refraction | A |
| Gravity | B |
| DC Resistivity | B |
| Frequency Domain Electromagnetics | B |
| Time Domain Electromagnetics | B |

* Note: A – preferred methods; B-alternative method

*Ground Penetrating Radar*: Ground penetrating radar (GPR) is based on detecting the reflection of electromagnetic waves from interfaces between materials with different dielectric constants, as illustrated in Figure 12-7. The system consists of a recorder, a transmitting antenna, and receiving antennae that are pulled along the ground surface. GPR provides excellent lateral and vertical resolution and can be a very effective method for detecting subsurface voids as well as the soil/bedrock interface. The primary limitation is high signal attenuation in conductive, clayey soils, which greatly limits the penetration depth below the surface. In sand and rock, the depth of penetration can be 50 feet or more, while in clay the penetration may be less than a few feet (ASTM D6429, 2011).

*Gravity:* Gravity methods are based on detecting changes in the earth's gravitation field caused by variations in soil and rock density below the surface. Microgravity surveys detect small changes in

gravity using closely spaced (5 to 50 feet) measurements (ASTM D6429, 2011). If a void is present below the surface, a decrease in the gravity field will be detected as illustrated in Figure 12-8. The magnitude of the change is a function of the size and depth of the void. Generally, it is difficult to detect voids with dimensions smaller than the depth to the top of the void. Data collection is performed using non-contacting instrumentation and requires accurate elevation measurements.

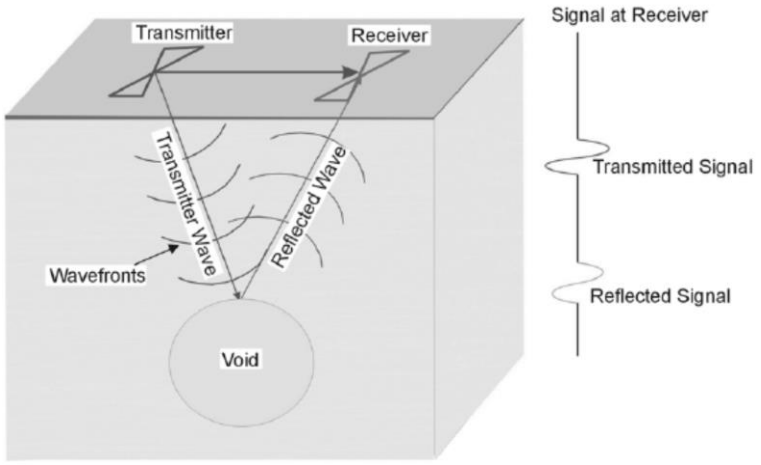


**Figure 12-7 GPR for detecting subsurface voids (Wightman, et al., 2004).**

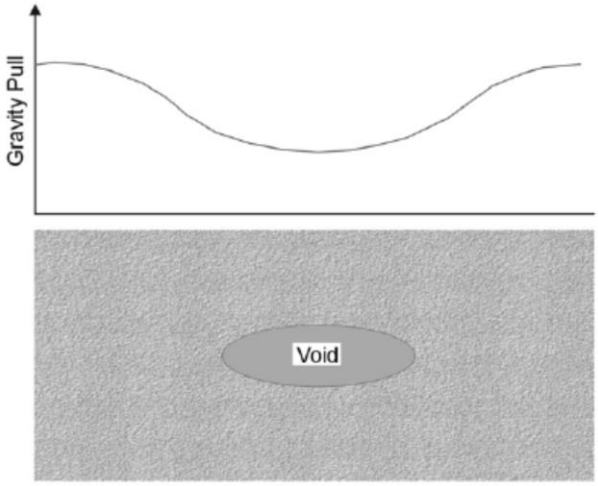


**Figure 12-8 Idealized gravity measurements over a subsurface void (Wightman, et al., 2004).**

*Seismic Reflection*: Seismic reflection detects the arrival of waves reflected from subsurface features with different material properties (wave velocity and/or density). The method is commonly used to map the depth of bedrock and can also be used for detecting subsurface voids. The basic concept behind seismic reflection for detecting voids is illustrated in Figure 12-9. Seismic reflection can also be used to determine shear wave velocity profiles as described in Chapter 8. The distance between the source and

farthest receiver should be about 1 to 2 times the desired depth of investigation and lateral resolution is a function of receiver spacing – typically 1 to 10 feet (ASTM D6429, 2011). Seismic reflection data collection is relatively labor intensive and processing of the data can be time consuming.

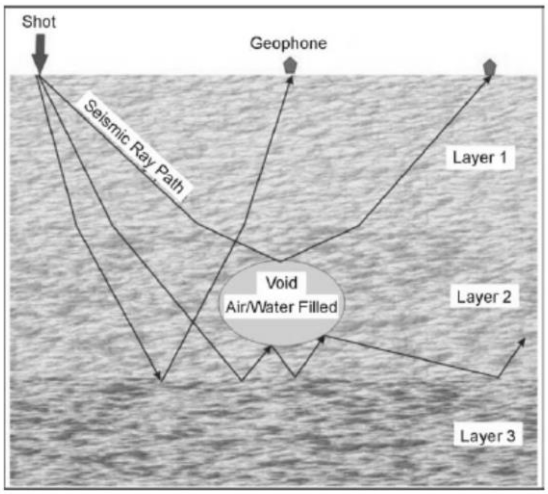


**Figure 12-9 Seismic reflection measurements for detecting subsurface voids (Wightman, et al., 2004).**

*Surface Refraction*: Seismic refraction is based on detecting the arrival of seismic waves that are critically refracted at the interface between a lower velocity layer and an underlying higher velocity layer as shown in Figure 12-10. The method is primarily used for detecting the depth, thickness, and velocity of subsurface layers, including the depth to bedrock, as described in Chapter 8. However, seismic refraction can also be used to detect fractures in the bedrock by examining the amplitude of the refracted signal, which may be indicative of underlying voids (Wightman, et al., 2004). The primary limitation of the refraction method is that it is not effective when lower velocity material underlies higher velocity material. Therefore, it cannot be used to directly detect a void in rock. The depth of investigation is also on the order of one third the length of the receiver spread.

*Resistivity:* Resistivity is based on detecting changes in electrical properties (i.e., resistivity) of the subsurface soil and rock. Direct current is introduced into the ground using two electrodes and the resulting voltage is measured using two additional electrodes. Deeper penetration is achieved by increasing the spacing between the electrodes. Using multiple electrode configurations, a 2-D map of subsurface resistivity can be developed. Subsurface features such as air-filled voids, clay-filled voids, and bedrock depth can often be detected by changes in resistivity values as shown in Figure 12-11. The main limitation is that a long array is required for deep penetration (array length about three times the depth of penetration). Smaller voids are more difficult to detect when they are at greater depths.

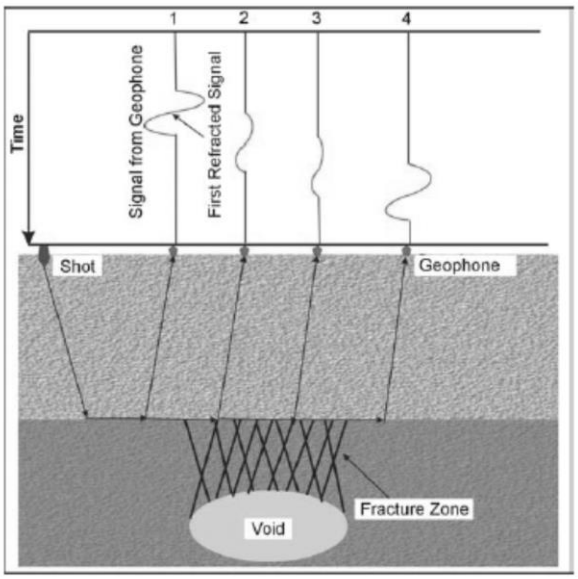


**Figure 12-10 Seismic refraction measurements for detecting subsurface voids (Wightman, et al., 2004).**

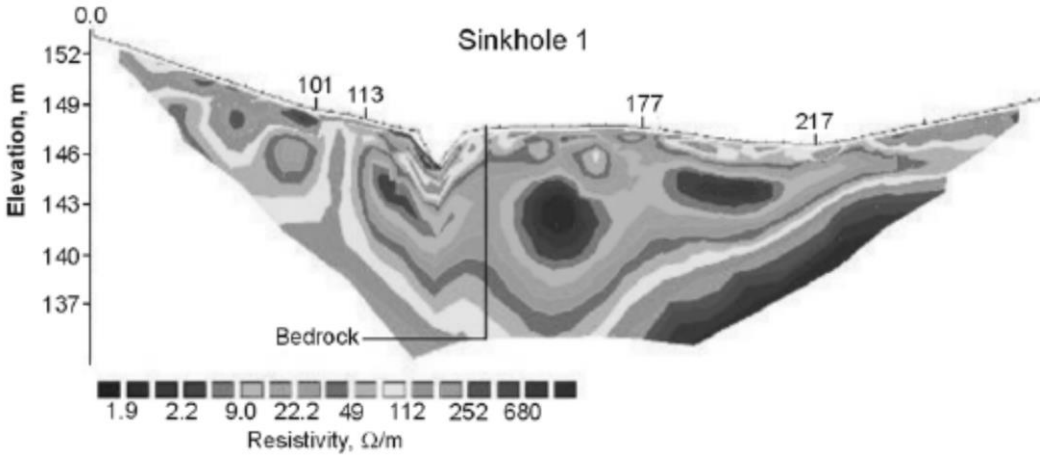


**Figure 12-11 Example resistivity image showing low values indicative of voids or highly fractured rocks (Wightman, et al., 2004)**

*Frequency Domain Electromagnetics:* Frequency-domain electromagnetics (also called terrain conductivity) measures the electrical conductivity of the subsurface using secondary fields generated from induced electromagnetic currents. The depth of penetration is typically in the range of 2 to 200 feet (ASTM D6429, 2011). The measurements are non-contacting and the instruments can be carried by hand or in a vehicle. The results are presented as a map of conductivity values that can be used to identify the location of subsurface features with different electrical properties (i.e., soil/rock, voids, pore fluids).

*Time Domain Electromagnetics:* Time domain electromagnetics measures the electrical resistivity of the subsurface using induced pulse currents in the ground (ASTM D6429, 2011). A square loop is laid on the ground and a receiver coil is placed inside of the square loop as shown in Figure 12-12. A pulse of electrical current is applied to the square loop and the resulting decaying voltage measured by the receiving coil due to secondary currents in the ground can be used to infer subsurface electrical properties. The method is often used as a sounding method to determine the vertical distribution of resistivity in the ground. Unlike the resistivity method, no electrodes need to be placed in the ground. One of the limitations is that data recording can be adversely affected by power lines and metal structures.

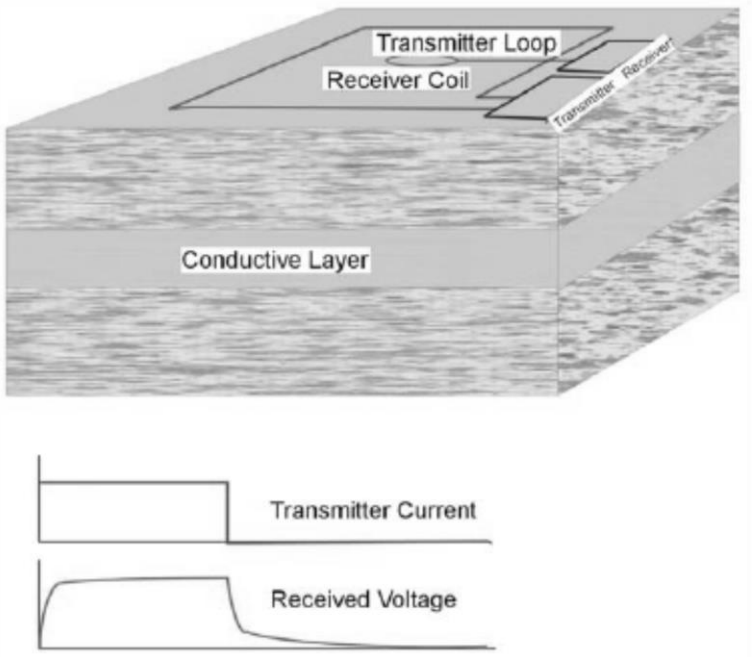


**Figure 12-12 Time-domain electromagnetic measurements (Wightman, et al., 2004)**

*Surface Wave Methods*: Seismic surface wave methods described in Chapter 8 have also been applied to void detection. Surface wave methods are based on the frequency-dependent penetration of Rayleigh-type surface waves into the subsurface. By measuring the surface wave velocity at different frequencies, a dispersion curve showing changes in velocity with frequency can be used to develop a profile of shear wave velocity versus depth. When performed along a traverse, a pseudo-2-D profile can be developed. Surface wave velocities and amplitudes may be altered by subsurface voids and fracture zones as illustrated in Figure 12-13, and thus can be used to help identify and/or characterize underground voids.

*Crosshole Seismic Tomography*: Crosshole seismic tomography is an intrusive geophysical method that can be used for high-resolution imaging of the subsurface between boreholes. As shown in Figure 12-14, waves are propagated between boreholes using many different combinations of source and receiver pairs.

An inversion procedure is then used to produce an image of the velocity and attenuation characteristics of the material between the boreholes. Using this approach, the size and shape of the anomaly can be imaged.

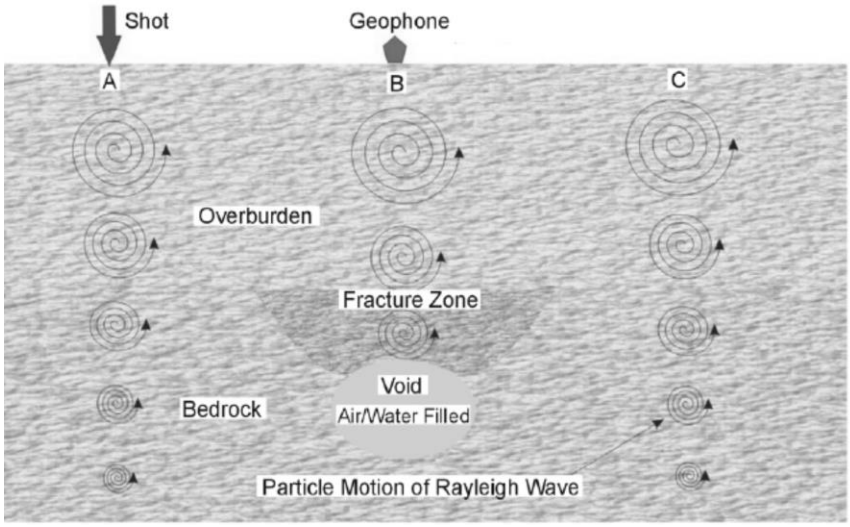


**Figure 12-13 Changes in surface wave motions due to subsurface voids (Wightman, et al., 2004)**

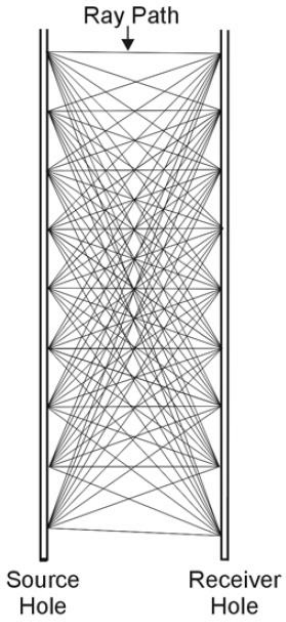


**Figure 12-14 Subsurface cross-hole seismic tomography method (Wightman, et al., 2004)**

## 12.3 UNDERGROUND MINE HAZARDS

Man-made underground openings from mining activities are another type of geotechnical hazard. Mining operations for coal, minerals, and metals produce underground openings from excavation of material and

construction of access and ventilation shafts. Many of these subsurface excavations are undocumented and their locations largely forgotten. Support for these openings may fail, impacting transportation facilities located above and near such mines. Abandoned mine hazards are particularly abundant and problematic in historical coal mining states, although non-coal mines also pose hazards. The U.S. Department of Labor's Mine Safety and Health Administration (MSHA) estimates that there are approximately 300,000 abandoned mines in the Appalachian region alone (MSHA, 2016). These abandoned mines are often located near highly populated areas and have the potential to impact major transportation facilities.

### 12.3.1 Implications of Underground Mine Hazards for Transportation Projects

Underground mine hazards have the potential to impact transportation facilities in a manner similar to those described for karstic voids. Potential impacts include settlement of bridges and structures located over mines, loss of foundation support above mine openings, creation of roadway sinkholes and/or settlement features, and surface water drainage issues. Figure 12-15 shows examples of surface manifestations of subsurface mines along interstates I-470 and I-70, respectively, in Ohio.

**Figure 12-15 Surface effects from subsurface mines in Ohio: (a) I-470 and (b) I-70 (Lefchik, et al., 2003).**

### 12.3.2 Identification and Characterization of Underground Mine Hazards

Common elements of site characterization programs intended to identify and characterize underground mine hazards are similar to those described for karst investigations, namely:

(1) Desk study to identify past mining activity;
(2) Identification and characterization of surface features indicative of subsurface mines; and
(3) Identification and characterization of subsurface mine openings.

***Desk Study***

Desk studies are generally performed to determine if subsurface mining activity has been performed in the region of interest. Published maps of abandoned mines serve as the primary source of information for this stage of investigation. Many states have abandoned mine land programs that can often provide useful information for identification and characterization of underground mine hazards. Published studies of geophysical or subsurface explorations performed in the area and geotechnical reports from nearby projects may also provide valuable information if available. The Office of Surface Mining Reclamation and Enforcement (OSMRE) also maintains a national mine map repository for all types of mining for the entire country (https://mmr.osmre.gov/). Several states maintain publically available digital mine maps; the MSHA website also provides links to several sources (http://www.msha.gov/minemapping/minemapping.asp). It is important to understand that these maps may only provide approximate locations of known mines and show only a portion of existing abandoned mines. For example, the Ohio Department of Natural Resources has maps for 4,000 abandoned mines but estimates there are about 2,000 addition mines in Ohio for which no detailed maps are available (Ruegsegger, 1999).

***Identification and Characterization of Surface Features***

Surface features that may indicate the potential presence of subsurface mines include: (1) evidence of past mining activities and/or (2) surface deformation features. Evidence of past mining activities include features such as mine openings, mine structures, waste piles, railroad spurs, and orange-colored water seeps or springs (Ruegsegger, 1999). Surface deformation features, such as cracks or dips in the roadway; damaged or displaced drainage structures; movements of bridges, poles, culverts, and guardrails; unusual vegetation; drag patches; water impoundments (Figure 12-16); and other topographic anomalies, may also indicate the potential presence of underground mines (Ruegsegger, 1999). Remote sensing technology such as lidar and aerial photography may be useful for identifying small mine-related surface features over large spatial regions. Other remote sensing technologies such as InSAR and photogrammetry may be useful for detecting and monitoring active surface movements if the size of the feature and magnitude of movement is sufficiently large.

***Identification and Characterization of Subsurface Mine Hazards***

Techniques for subsurface identification and characterization of underground mines are essentially the same as those described in Section 12.2.2 for karst. Figure 12-17 shows an example of the use of GPR to check for voids beneath the pavement of I-77 during work to repair a mine.

**Figure 12-16 Surface water collected in subsidence feature in Missouri (Lefchik, et al., 2003).**

**Figure 12-17 Use of GPR to check for voids beneath a pavement during work to repair a mine (Lefchik, et al., 2003).**

## 12.4 SEISMIC HAZARDS

Seismic hazard refers to the potential for earthquake events to produce adverse effects on transportation facilities. Seismic hazard assessment is a function of several factors, including: (1) proximity to sources of seismic energy, (2) characteristics of the seismic sources (magnitude potential, recurrence intervals, depth, fault type, etc.), (3) attenuation of seismic waves along the source-to-site path, and (4) local soil and rock conditions. The seismic hazard level for a given location is typically expressed quantitatively in terms of a ground motion parameter (e.g., peak ground acceleration, response spectrum values) with some probability of exceedance in a given time frame. The USGS produces maps of ground motion parameters with some probability of exceedance ($PE$). Maps produced by USGS for AASHTO are based on a 7 percent $PE$ in 75 years for rock sites. An example map of seismic design coefficients with 7 percent $PE$ in 75 years is shown in Figure 12-18. As can be seen in this map, much of the Western United States, as well as portions of the Central and Eastern United States, are high seismic hazard regions. Site characterization in seismic regions is often more extensive than site characterization in non-seismic regions because additional soil parameters must be measured. Soil parameters from these additional

measurements may be used, for example, to incorporate effects of local soil and rock conditions in seismic hazard analyses or to assess the susceptibility of a site to liquefaction or excessive settlements. Specific geotechnical seismic hazards are described in the following section, along with additional site characterization methods for investigations performed in seismic regions.

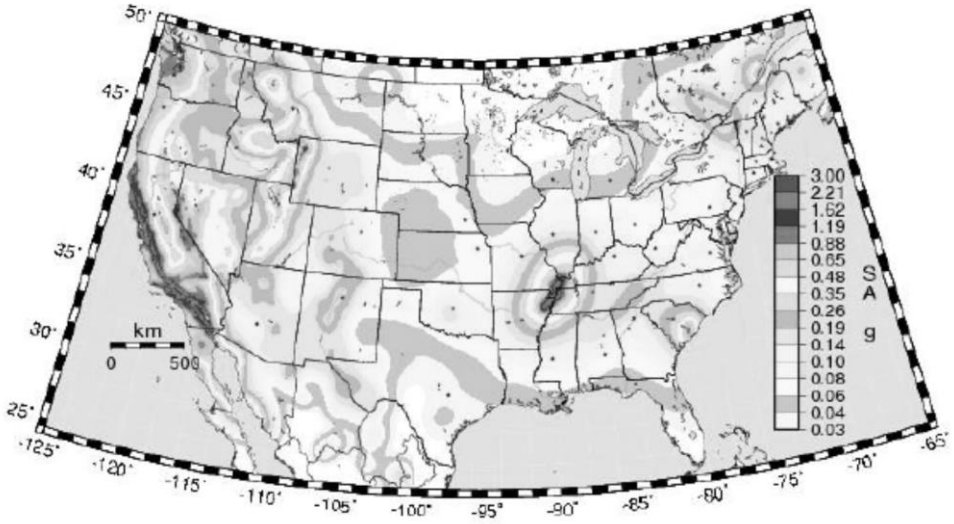


**Figure 12-18 USGS 2008 seismic hazard map for seismic design coefficient at one second period for 7 percent *PE* in 75 years and competent (B/C boundary) soil (Marsh, et al., 2014).**

### 12.4.1 Implications of Seismic Hazards for Transportation Projects

Earthquake motions affect transportation facilities by increasing the imposed load and, in some cases, decreasing soil resistance. Seismic design of geotechnical features requires an understanding of how loading and resistance will change under anticipated earthquake motions. Earthquake-induced ground motions produce inertial forces in earth slopes and embankments that can lead to instability or unacceptable deformations. Slope failures due to seismic events are a major geotechnical hazard caused by increased loading. An example of a slope failure caused by earthquake loading is shown in Figure 12-19. The ground motions (and associated inertial forces) are affected by the properties of the near-surface soil and rock.

Earthquake ground motions can also influence the resistance properties of the soil. As described in Chapter 5, soil liquefaction is a major geotechnical hazard caused by generation of positive pore water pressures in loose, saturated, cohesionless soils that results in substantial loss of soil strength. The consequences of soil liquefaction include foundation bearing capacity reduction, flow liquefaction slides, lateral spreading, ground settlement, and increased lateral pressures on retaining walls. Figure 12-20 shows a photograph illustrating the impact of soil liquefaction. Site characterization in seismic regions

must include measurements of soil properties to assess liquefaction susceptibility, as well as residual strength properties of liquefied soils.

**Figure 12-19 Route 17 landslide from Loma Prieta earthquake (from Kavazanjian, et al., 2011).**

**Figure 12-20 Disrupted fill and pavement due to liquefaction in Rio Estrella, Costa Rica during 1991 earthquake (Kavazanjian, et al., 2011).**

Ground settlement of dry or partially saturated cohesionless soils is another major geotechnical hazard from earthquake ground shaking. The tendency of loose cohesionless soils to contract under dynamic loading results in a denser configuration of soil particles and an associated settlement of the ground surface. Seed and Silver (1972) report settlements of 4 to 6 inches for a building supported by shallow foundations on a 40-ft deep sand deposit. Site characterization of these deposits must include measurement of relevant properties to estimate the magnitude of earthquake-induced ground settlement.

Finally, surface fault rupture is a major geotechnical hazard resulting from ground displacements that occur when movement of a fault extends to the surface. Fault ruptures can produce abrupt movements from several inches to tens of feet and can be catastrophic to structures spanning the fault. Figure 12-21 shows a photograph illustrating the effect of fault ruptures on a structure.

**Figure 12-21 Collapse of overpass on highway in Kocaeli, Turkey earthquake (from Erdik, 2001).**

### 12.4.2 Identification and Characterization of Geotechnical Seismic Hazards

Seismic hazard assessment often requires information commonly collected for non-seismic site characterization including stratigraphy, groundwater levels, bedrock depth, soil and rock mass classification, unit weight, relative density, and in situ test measurements. However, additional soil and rock parameters that may not be part of conventional geotechnical site characterization programs are also required for geotechnical seismic hazard assessment as described in the following paragraphs. Detailed description of the methods used to assess seismic hazards is beyond the scope of this document but can be found in Kavazanjian et al. (2011).

*Seismic Slope Instability:* Current practice for analyzing seismic slope stability is to use either: (1) limit equilibrium analyses with a pseudo-static representation of seismic force, or (2) a displacement-based analysis such as the Newmark sliding block method. The limit equilibrium approach is a simplified approach that uses a seismic coefficient to represent the inertial force caused by the earthquake. The seismic coefficient is typically assumed to be a function of the site-adjusted Peak Horizontal Ground Acceleration, $PGA$, which can be calculated from a seismic hazard analysis multiplied by an appropriate site factor, $F_{pga}$. The site factor is a function of the Site Class, which can be calculated from the average shear wave velocity, $\bar{V}_s$, in the top 100 feet. Table 12-3 shows the relationship between $\bar{V}_s$ and site classification. The $PGA$ from USGS mapped values is for Site Class B conditions and must be adjusted using the values shown in Table 12-4. Therefore, the $V_s$ profile in the top 100 feet should be measured as part of site characterization programs where seismic hazard must be assessed. Methods to measure $V_s$ profiles are described in Chapter 8. Relevant soil strength parameters must also be obtained for implementation into slope stability analyses. In most cases, total stress strength parameters appropriate for undrained conditions should be used for seismic stability models, rather than drained or effective stress parameters. Details of pseudo-static analysis procedures are provided in Kavazanjian et al. (2011).

**Table 12-3 Site class definitions (AASHTO, 2012).**

| Site Class | Soil Type and Profile |
|---|---|
| A | Hard rock with measured shear wave velocity, $\bar{v}_s > 5{,}000$ ft/s |
| B | Rock with $2{,}500 < \bar{v}_s < 5{,}000$ ft/s |
| C | Very dense soil and soil rock with $1{,}200 < \bar{v}_s < 2{,}500$ ft/s, or with either $\bar{N} > 50$ blows/ft, or $\bar{s}_u > 2.0$ ksf |
| D | Stiff soil with $600 < \bar{v}_s < 1{,}200$ ft/s, or with either $15 < \bar{N} < 50$ blows/ft, or $1.0 < \bar{s}_u < 2.0$ ksf |
| E | Soil profile with $\bar{v}_s < 600$ ft/s or with either $\bar{N} < 15$ blows/ft or $\bar{s}_u < 1.0$ ksf, or any profile with more than 10 ft of soft clay defined as soil with $PI > 20$, $w > 40$ percent and $\bar{s}_u < 0.5$ ksf |
| F | Soils requiring site-specific evaluations, such as:<br>• Peats or highly organic clays ($H > 10$ ft of peat or highly organic clay where $H$ is thickness of soil)<br>• Very high plasticity clays ($H > 25$ ft with $PI > 75$)<br>• Very thick soft/medium stiff clays ($H > 120$ ft) |

Exceptions: Where the soil properties are not known in sufficient detail to determine the site class, a site investigation shall be undertaken sufficient to determine the site class. Site classes E and F should not be assumed unless the authority having jurisdiction determines that site classes E or F could be present at the site or in the event that site classes E or F are established by geotechnical data.

**Table 12-4 Values for site factor ($F_{pga}$) at zero period on acceleration spectrum (AASHTO, 2012).**

| Site Class | $PGA < 0.10^1$ | $PGA = 0.20$ | $PGA = 0.30$ | $PGA = 0.40$ | $PGA > 0.50$ |
|---|---|---|---|---|---|
| A | 0.8 | 0.8 | 0.8 | 0.8 | 0.8 |
| B | 1.0 | 1.0 | 1.0 | 1.0 | 1.0 |
| C | 1.2 | 1.2 | 1.1 | 1.0 | 1.0 |
| D | 1.6 | 1.4 | 1.2 | 1.1 | 1.0 |
| E | 2.5 | 1.7 | 1.2 | 0.9 | 0.9 |
| F[2] | * | * | * | * | * |

Notes:
[1] Use straight-line interpolation for intermediate values of PGA.
[2] Site-specific geotechnical investigation and dynamic site response analysis should be performed for all sites in Site Class F.

Displacement-based seismic stability analysis involves calculation of cumulative seismic deformations of a potential failure mass. In the Newmark method, the failure mass is assumed to be rigid, while more advanced methods assume a deformable body. Kavazanjian et al. (2011) provides a recommended methodology for displacement-based seismic stability assessment. In this methodology, evaluation of site classification is required to obtain peak ground acceleration site factors ($F_{pga}$) as well as long-period (1 second) spectral acceleration site factors, $F_v$. Evaluation of the $V_s$ profile to a depth of 100 feet is therefore again required for the analysis.

Analyses of rock slopes follow the same principles used for soil slopes and embankments with the additional challenge of evaluating rock mass strength parameters. Evaluation of rock mass properties is described in Chapter 9.

*Liquefaction:* Soil liquefaction is the phenomenon where cohesionless soils experience a substantial reduction in strength due to generation of positive excess pore pressures and the associated reduction in effective stress. The susceptibility of a site to liquefaction is a function of both the level of seismic loading and the properties of the soil. Buckle et al. (2006) provide recommendations on how to evaluate the need to perform evaluation of liquefaction. This assessment is based first on the seismic hazard level, which depends on the value of site class-adjusted long-period and short-period spectral acceleration values. Determination of site class should be based on measurements of $V_s$ values in the top 100 feet as described previously. The specific seismic hazard level criteria are described in Kavazanjian et al. (2011). For sites where the hazard is high enough to justify a liquefaction analysis, additional screening criteria based on soil characteristics are used to evaluate the need for an analysis. Relative susceptibility ratings are based on the geologic age and depositional environment. Sites with very low susceptibility (based on Table 12-5) do not require a liquefaction analysis. Further screening criteria for soils below the water table are based on clay content, liquid limit, natural water content, and liquidity index for clayey

soils, as well as corrected SPT blow counts, $(N_1)_{60}$, or cone penetration resistance. Detailed susceptibility criteria are provided in Kavazanjian et al. (2011). Site characterization programs in areas of seismic hazard should therefore include collection of measurements to assess the need to perform a liquefaction analysis. If evidence exists that prior liquefaction has occurred at a site, further evaluation of liquefaction potential must be performed regardless of what the screening criteria indicate. Therefore, a review of the earthquake history of the area and any published post-earthquake reconnaissance reports should be performed as part of the site characterization program desk study.

**Table 12-5 Liquefaction susceptibility of sedimentary deposits during strong ground motion (Youd and Perkins, 1978).**

| Type of Deposit | General Distribution of Cohesionless Sediments in Deposits | Likelihood that Cohesionless Sediments, When Saturated, Will be Susceptible to Liquefaction (by Age of Deposit) | | | |
|---|---|---|---|---|---|
| | | <500 yr Modern | Holocene >11 ka | Pleistocene 11 ka - 2 Ma | Pre-Pleistocene >2 Ma |
| **(a) Continental Deposits** | | | | | |
| River channel | Locally variable | Very high | High | Low | Very low |
| Floodplain | Locally variable | High | Moderate | Low | Very low |
| Alluvial fan and plain | Widespread | Moderate | Low | Low | Very low |
| Marine terraces and plains | Widespread | — | Low | Very low | Very low |
| Delta and fan-delta | Widespread | High | Moderate | Low | Very low |
| Lacustrine and playa | Variable | High | Moderate | Low | Very low |
| Colluvium | Variable | High | Moderate | Low | Very low |
| Talus | Widespread | Low | Low | Very low | Very low |
| Dunes | Widespread | High | Moderate | Low | Very low |
| Loess | Variable | High | High | High | Unknown |
| Glacial till | Variable | Low | Low | Very low | Very low |
| Tuff | Rare | Low | Low | Very low | Very low |
| Tephra | Widespread | High | High | ? | ? |
| Residual soils | Rare | Low | Low | Very low | Very low |
| Sebka | Locally variable | High | Moderate | Low | Very low |
| **(b) Coastal Zone** | | | | | |
| Delta | Widespread | Very high | High | Low | Very low |
| Estuarine | Locally variable | High | Moderate | Low | Very low |
| Beach | | | | | |
| High wave-energy | Widespread | Moderate | Low | Very low | Very low |
| Low wave-energy | Widespread | High | Moderate | Low | Very low |
| Lagoonal | Locally variable | High | Moderate | Low | Very low |
| Fore shore | Locally variable | High | Moderate | Low | Very low |
| **(c) Artificial** | | | | | |
| Uncompacted fill | Variable | Very high | — | — | — |
| Compacted fill | Variable | Low | — | — | — |

For sites that do not meet the screening criteria (i.e., soils that may be susceptible to liquefaction), a more detailed evaluation is required. The more detailed approach involves collection of in situ test measurements to quantitatively evaluate liquefaction potential as described in Chapter 5. Site characterization programs for detailed seismic evaluation should include means to: (1) establish the

spatial limits of liquefiable soil deposits, (2) establish the location of the groundwater level, (3) determine the maximum anticipated depth of liquefaction, and (4) collect relevant in situ test measurements to evaluate liquefaction susceptibility. The spatial extent of liquefiable deposits should be determined by performing an investigation at the location of interest (e.g., bridge pier location) as well as a sufficient number of additional locations moving away from the location of interest. The investigation should also establish the depth of groundwater. If groundwater levels are thought to fluctuate significantly, piezometers should be installed and monitored for sufficient time to characterize seasonal fluctuations in the depth of the groundwater table. Field explorations should also establish the maximum depth and thickness of potentially liquefiable soil. In thick liquefiable soil deposits, the investigation depth should extend to at least 80 feet below the ground surface or lowest proposed finished grade, whichever is deeper (Kavazanjian et al., 2011). For deep foundations, the investigation should extend at least 20 feet below the tip of the foundations or at least 80 feet below the ground surface or lowest proposed finished grade, whichever is deeper (Kavazanjian, et al., 2011).

In addition to assessing liquefaction potential, it is often necessary to evaluate the post-liquefaction residual undrained shear strength. Two approaches commonly used in practice are based on SPT blow counts (Idriss and Boulanger, 2007) or CPT tip resistance (Olson and Johnson, 2008).

*Soil Settlement:* Earthquake ground motions may also induce substantial settlements in dry or partially saturated cohesionless soils. A widely used design method developed by Tokimatsu and Seed (1987) requires parameters determined from in situ test measurements collected as part of site characterization. These parameters include $(N_1)_{60}$ from SPT measurements, total vertical stress, and small-strain shear modulus, $G_{max}$. Specific procedures are described in Kavazanjian et al. (2011).

*Surface Fault Rupture:* Displacements from an active fault rupture that extends to the ground surface can range from a few inches to tens of feet. These movements can be devastating to structures located at or near the rupture. It is important, therefore, to identify these hazards. It can be assumed that a significant hazard does not exist if: (1) there is no evidence of a fault trace traversing the site, or (2) it can be determined that an existing fault trace is not from an active fault. In the central and eastern United States, few active faults extend to the surface so fault rupture hazard is low. In the western United States, however, hazard screening is important and should include: (1) review of geologic maps and consultation with geologists, and (2) site reconnaissance and review of aerial photographs or other remote sensing data (e.g., lidar) for evidence of surface fault features. Faults that have been covered by soils or structures may be identified using geophysical techniques, such as seismic refraction surveys. The USGS also provides interactive maps of faults that are believed to be sources of magnitude 6 and greater earthquakes during

the past 1,600,000 years (USGS, 2006). Trenching operations may also be performed to precisely locate and characterize faults. Discontinuities in material type determined from subsurface borings may also provide evidence of faulting.

## 12.5 GROUNDWATER HAZARDS

Groundwater impacts transportation projects in a variety of ways. Hydrostatic and flowing water influence effective stress conditions and the associated engineering properties (e.g., strength, stiffness) of soil and rock. Seepage forces may also contribute to slope instability or produce quick conditions if upward hydraulic gradients are sufficiently high. Characterization of groundwater conditions is also important for constructability of excavations, where contractors need to determine expected or potential flow rates into excavations, select appropriate dewatering methods, and evaluate stability of excavations. Inadequate characterization or failure to account for groundwater conditions can often lead to poor performance or failure. Detailed discussion of groundwater investigations and methods to determine hydraulic conductivity is provided in Chapter 10. This section focuses on two groundwater hazards that may be encountered: artesian conditions and high groundwater flows.

Artesian conditions exist where a relatively permeable soil or rock formation (aquifer) is confined by a less permeable formation and is hydraulically connected to a source with piezometric potential (i.e., head) that is greater than the elevation of the ground surface as shown in Figure 12-22. Alternatively, the term *artesian* is sometimes used to indicate the condition where the piezometric elevation is at or above the ground surface and the term *sub-artesian* is used to indicate cases where the piezometric elevation is greater than exists for the overlying formation but is lower than the ground surface. In this discussion, the term artesian is used to indicate the condition where a confined aquifer has a piezometric elevation that is greater than the elevation of the ground surface.

High flow rates in subsurface strata can also be a geotechnical hazard. As described in more detail in Chapter 10, subsurface groundwater flow is driven by changes in total head. The flow rate is a function of the hydraulic gradient and the hydraulic conductivity of the soil. High subsurface flow rates can develop in materials with high hydraulic conductivity (e.g., open gravels, fractured rock, and subsurface voids) and sufficient hydraulic gradient.

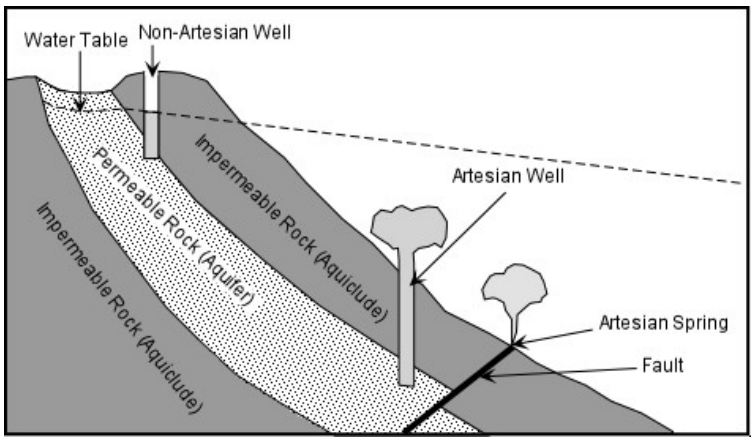


**Figure 12-22 Settings that produce artesian conditions (Earth Science Australia, 2017).**

### 12.5.1 Implications of Groundwater Hazards for Transportation Projects

Artesian conditions have the potential to impact the design, construction, and operation of transportation features if not properly identified, characterized, and addressed. Identifying and characterizing artesian conditions is especially important for evaluating the stability of excavations. If not properly considered, artesian conditions can result in heave or blow out of excavations. Artesian conditions must also be considered for design and execution of dewatering operations. Design of dewatering systems will be different for gravity flow versus artesian groundwater conditions. Drilled shaft construction is also impacted by artesian conditions, which can lead to caving of shaft excavations and inconsistent placement of concrete. In some cases, shaft casing may be maintained at an elevation well above the ground surface or heavy drilling mud may be used to produce enough static head to counteract artesian pressures. Casing is sometimes also left permanently in place through the confined aquifer. Upward flow of water in a site characterization boring can also influence measurements obtained from in situ tests. For example, Standard penetration tests (SPT) performed in soils that have been disturbed from upward flowing water will commonly yield much lower measured $N$-values than are truly representative of the formation.

High subsurface flow conditions also have similar effects for drilled shaft construction and other excavations. Caving of shaft walls and difficulty placing concrete may occur if not properly controlled or mitigated. Furthermore, high flow rate conditions may also lead to piping and erosion in some soils if not properly controlled.

### 12.5.2 Identification and Characterization of Groundwater Hazards

Artesian conditions are typically identified using exploratory borings, piezometers, or piezocone (CPTU) measurements. Borings that penetrate the confining layer over an artesian aquifer will often experience a

rapid inflow of water. It is important that these observations are noted on boring logs so that further characterization of the condition can be performed. Characterization of artesian conditions also requires measuring water pressures within the artesian formation, preferably over some period of time, as described in Chapter 10. Upward flow of soil and water in the borehole can make placement of piezometer seals difficult. In cases where the pressure head is not too great, stability can often be maintained by extending the height of the casing above the ground surface to provide a static head of water to counter the artesian pressure. Push-in piezometers may also be a preferred option in these cases.

Identification of high subsurface flow conditions is also typically achieved using exploratory borings. Borings that intersect high-flow strata will likewise experience a rapid inflow of water into the boring, which will often cause borehole stability problems. As described in Chapter 10, use of geophysical methods like the self-potential (or spontaneous polarization) method can be used to detect anomalies generated from the presence of subsurface flowing water. Characterization of high flow strata often requires measurements of hydraulic conductivity as well as multiple spatial measurements of pressure to determine subsurface hydraulic gradients. Characterization may also require that sites be monitored over time since flows can fluctuate over time and are likely to be much greater during and soon after heavy precipitation. High flow conditions are common in karst environments, where flow is not dominated by the micro-scale hydraulic conductivity of the rock, but by the macro-scale interconnected network of voids, fractures, and conduits within the rock mass. Identifying and characterizing high flow conditions in karst environments can therefore be quite challenging. If detailed knowledge of subsurface flow paths is required, specialized techniques such as dye tracing can be performed to characterize subsurface flow.

## 12.6 LANDSLIDE AND ROCKFALL HAZARDS

Landslide and rockfall hazards refer to gravity-driven movements of earthen material that have the potential to adversely impact transportation facilities. Landslides may occur in natural or constructed slopes and embankments. Slopes may be initially stable but become unstable due to changes in the loading and/or resistance of the soil or rock. Landslides may be triggered by a variety of events that include earthquakes, blasting, cut and fill operations, erosion, scour, gradual changes in pore water pressure, build-up of pore water pressure due to poor drainage, and excessive precipitation. Landslide movements may be in the form of rotational movements, translational slides, or earthflows. Landslide movements can be localized, such as small surface slumps, or massive in extent, covering several square miles. The rate of landslide movements can also vary greatly. Some movements may be almost imperceptibly slow, while others may accelerate rapidly and catastrophically over a span of a few seconds. Landslide movements may proceed at a near continuously rate or occur episodically.

Rockfall refers to episodic events of falling rock fragments from steep natural or constructed slopes over time. Rockfall events occur when rock detaches from the slope and moves rapidly down slope. Several modes of rock slope failures may contribute to rockfall events including planar sliding, wedge sliding, toppling, and circular sliding as illustrated in Figure 12-23. Rockfalls may also occur because of rock block fall-out. Rockfall events are typically caused by gradual weathering and erosion of rock or surrounding materials that provide support for rock blocks. For example, rockfall may be caused by: differential weathering of layered rock strata; erosion of the soil matrix supporting cobbles and boulders (i.e., boulder fall); or loosening of rock blocks (i.e., raveling) caused by degradation processes such as freeze-thaw, weathering of cemented materials, and jacking action of tree roots (Turner and Schuster, 2012). Changes in water pressure in rock discontinuities caused by fluctuating groundwater conditions may also influence the stability of rock blocks. Excavation of rock slopes for construction of transportation facilities may also destabilize rock slopes, particularly if poor blasting or excavation techniques are used that cause unnecessary damage to the rock. Vibrations from seismic events or blasting may also trigger rockfall events.

### 12.6.1 Implications of Landslide and Rockfall Hazards for Transportation Projects

Landslides and rockfalls can dramatically affect transportation facilities. Transportation facilities constructed on or near unstable slopes may sustain extensive damage or be made inoperable for long periods of time due to earth movements. The massive slope failure in Idaho along a highway, shown in Figure 12-24, is an extreme example of damage that can occur from a major landslide. Rockfall events also threaten transportation facilities and the travelling public. The aftermath of a large rockfall event in Glenwood Canyon, Colorado in 2010 is shown in Figure 12-25. This event closed Interstate 70 for over three days and required substantial repairs to the roadway. Even small earth movements or rockfall events that move into the roadway pose a hazard to the travelling public.

### 12.6.2 Identification and Characterization of Landslide and Rockfall Hazards

Site characterization programs for evaluating landslide and rockfall hazards should include methods to identify the existence of the hazard, followed by measurements to characterize the hazard. Recommended elements for site characterization programs to assess landslide and rockfall hazards are provided in the following paragraphs.

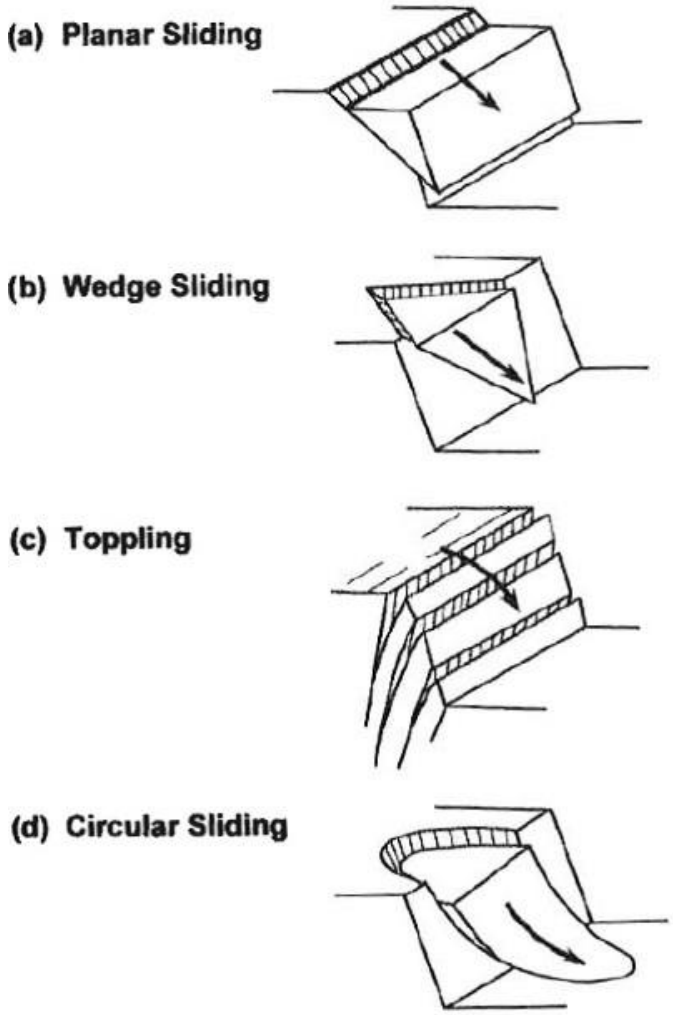


**Figure 12-23 Modes of rock slope failure leading to rockfall events (Turner and Schuster, 2012).**

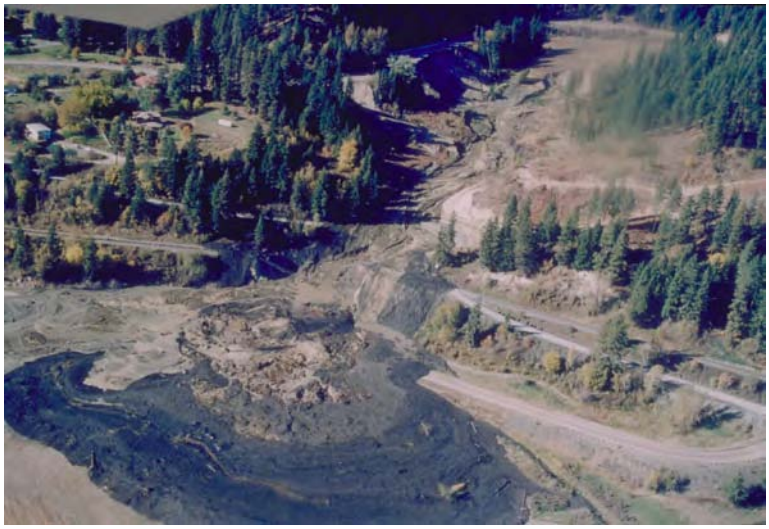

**Figure 12-24 Landslide event affecting highway (Courtesy of USGS/Photo by D. Krammer).**

**Figure 12-25 Rockfall event in Glenwood Canyon, CO affecting I-70 in 2010 (CDOT, 2017).**

*Landslides:* Landslide hazards are often identified from evidence of prior movements at a site. Identification of landslide hazards should begin with a desk study of geotechnical reports, papers, or articles documenting instability near the location of interest. Many states also have landslide hazard maps that should be carefully reviewed. Visual observations at the site should be performed to identify and document evidence of instability. Telling features of prior or ongoing slope movements include scarps, tension cracks, hummocky terrain, curved or tilted tree trunks, deformed pavement, and tilting of embedded structures. Evidence of distress to existing structures may also indicate active slope movements. To assess large spatial-scale regions, remote sensing imagery from aerial photography and airborne lidar can be useful for identifying surface features that may be indicative of active or prior movements. These methods can also be useful for delineating the spatial extent of movements.

If prior or active movements are identified at the site, characterization of the landslide hazard should include the following elements:

- Determination of the slope geometry;
- Measurement of the magnitude and rate of active movements;
- Measurement of the spatial extent of active movement;
- Determination of the depth of active movements and slide surface;
- Characterization of groundwater conditions and temporal changes in groundwater conditions;
- Determination of the subsurface stratigraphy; and
- Determination of relevant soil and rock design parameters.

Slope geometry information can be derived from topographic maps, remote sensing data, or optical surveys. Site characterization should often include installation of instrumentation to characterize the magnitude and rate of slope movements and identify the depth to sliding surfaces. Remote sensing measurements such as differential lidar, photogrammetry, and InSAR can also be used to monitor the magnitude and rate of active movements. Collectively, these measurements provide the information needed to characterize the spatial extent, depth, and rate of movement for hazardous slopes.

Since groundwater conditions often trigger slope instability, it is important that groundwater conditions are well understood, both spatially and with time. A comprehensive program of groundwater monitoring should therefore be part of site characterization programs for landslide prone areas. Measurements should be performed using the methods described in Chapter 10 to characterize groundwater levels, flow conditions, pore water pressures, and temporal changes in groundwater conditions. Measurements should be made within, around, and below the zone of movement.

Exploratory borings should be completed to characterize the soil and rock stratigraphy. It is critically important that stratigraphy is accurately established so it can be modeled effectively in slope stability analyses. Slope failures may occur along thin layers of weak soil/rock, so continuous sampling should be performed and careful attention should be given to identifying thin, weak layers. Observations of features indicative of movement such as slickensides in clay should be identified and noted in boring logs. Failure may also occur along preexisting discontinuities in rock. Rock coring operations should therefore identify the depth and orientation of discontinuities as described in Chapter 9. Evidence of prior movement, such as clay gouge or striations in rock discontinuities should also be noted in boring logs.

Finally, slope stability analyses require information on the unit weight, pore water pressures, and shear strength parameters for the soil or rock at a site. The relevant soil strength parameters will depend on the drainage conditions in the soil and whether short-term or long-term stability is being considered as described in Chapter 7.

*Rockfall:* As with landslides, rockfall hazards can often be identified from evidence of prior rockfall events. A literature review of landslide hazard maps, reports, papers or newspaper articles documenting rockfall events is a good starting point. Agency records of accidents and maintenance resulting from rockfall events may also be a useful source of information. Visual assessment of the site will often provide evidence of recent rockfall events. Deposits of rock blocks, boulders, and talus at the base of a slope as well as fresh detachment surfaces on the rock face are obvious signs of past events. Potentially

hazardous conditions can also be identified based on general observations of the geologic conditions and patterns of discontinuities. Conditions that are well suited for rockfall events include:

- steep slopes,
- rock with an extensive system of interconnected discontinuities,
- rock blocks or boulders surrounded by weak or erodible material,
- groundwater in joints or cracks, and
- lack of obstructions (i.e., trees) to inhibit downward movement.

Steep slopes require less erosion of supporting material to initiate movement and produce high-energy rockfall events. Rockfall events are possible in alternating strata of competent and erodible rocks, where erosion of weaker material removes support for more competent rock. Likewise, conditions where large boulders are surrounded by an erodible matrix are susceptible to rockfall events. Raveling failures may also occur, resulting from slow weathering and loosening of rock blocks due to factors such as jacking from ice or tree roots, and deterioration of cemented materials (Turner and Schuster, 2012).

Characterization of rockfall hazards requires collection of specific information about site conditions. Rock mass descriptions should include the type of rock and discontinuity characteristics that include orientation (dip and dip direction), discontinuity spacing, persistence, surface roughness, aperture, filling material, seepage, and number of discontinuity sets. Rock coring may also be performed to collect samples for strength testing, document groundwater conditions, record information on rock discontinuities, and collect rock cores for measuring rock mass characterization parameters such as $RQD$, $CR$, and discontinuity spacing. Detailed description of each of these elements is provided in Chapters 4 and 9. As is done for landslides, rock slope movements may also be characterized using various forms of instrumentation, surveying, and remote sensing technologies.

## 12.7 LANDFILL AND GEOENVIRONMENTAL HAZARDS

Landfill hazards refer to conditions where a heterogeneous mixture of soil, construction debris, organic material, building rubble, or other refuse has been used as fill material and been placed in an uncontrolled manner. Such fills often have undesirable engineering properties that may pose hazards to transportation features constructed near, on, or in the uncontrolled fill. It is therefore important that the presence of these deleterious materials be identified and the spatial extent and engineering characteristics be characterized as part of the site characterization program.

Geoenvironmental hazards refer to conditions where contaminants have been released into the environment. Sources of these contaminants may include waste piles, waste fills without engineered liners, leaking underground or above ground storage tanks, leaking surface impoundments, or contamination from agricultural sources. In some cases, the source of contaminants may be obvious, but in other cases prior use of the land is long forgotten and geoenvironmental hazards go unrecognized. It is important that site characterization programs identify and characterize geoenvironmental hazards so that effective mitigation can be accomplished.

### 12.7.1 Implications of Landfill and Geoenvironmental Hazards for Transportation Projects

The primary consequence of unidentified landfill material is poor engineering performance of constructed facilities. Fill material that is essentially dumped instead of being placed and compacted in a controlled manner will usually have poor strength and stiffness characteristics and be susceptible to excessive settlement and stability problems. The engineering properties of these materials are often highly variable, which can lead to damaging differential settlements. Decomposition of organic materials, collapse of large objects, and potential voids may lead to large settlements over time. Uncontrolled fills may also be susceptible to piping or "running" of smaller particles through larger openings when water flows through the fill. For these reasons, uncontrolled fills are undesirable for engineering purposes and should generally be avoided or remediated. Because mitigation measures are generally costly, it is critically important that the extent of these materials be properly characterized. If not identified and spatially characterized, landfill material can lead to construction delays, increased costs, and poor structural performance.

There are also severe implications associated with contaminated sites. First, the contamination may be a threat to human health. Contaminated soil and water can impact site characterization personnel, construction workers, and the public if not properly identified. Second, contaminated sites may impact construction materials placed at the site through chemical reactions. For example, concrete or steel piles placed at the site may be more susceptible to deterioration or corrosion. Third, if the hazard is not properly identified, the cost associated with construction delays and site remediation may be considerable.

### 12.7.2 Identification and Characterization of Landfill and Geoenvironmental Hazards

Identification of landfill materials should begin with a desk study involving a review of documents showing the prior use of the site, newspaper articles documenting activities at the site, and geotechnical reports from other investigations performed in the area. Review of historical maps and aerial imagery may provide evidence of prior activity that could indicate placement of uncontrolled fills. Field

reconnaissance visits may provide surface evidence of construction debris or other fill materials. Subsurface drilling operations will often provide the most direct approach to characterizing the extent and depth of landfill material and drilling operations should be developed primarily to determine the depth and lateral extent of the fill material. In cases where it is clear that the uncontrolled fill will be remediated in some way, it is often not necessary to characterize the engineering properties of the fill. Drilling operations may be complicated by the presence of large obstructions (e.g., construction debris) that may require special drilling techniques. If contaminated fill material is suspected, appropriate health and safety precautions should be followed before and during drilling. Geophysical methods may also be helpful for identifying the lateral extent of the landfill material. Seismic methods, such as surface wave methods or refraction, are often suitable for delineating landfill material based on observed wave velocities of loose fill materials. Landfill materials can also potentially be differentiated from natural materials based on differing electrical properties. Therefore, in many cases resistivity or ground penetrating radar can be effectively used. This is especially true for fill material containing metals constituents.

Identification of contaminated sites should also begin with a desk study. Field visits may provide visual evidence of contamination such as observations of dead vegetation, containment ponds, tanks or other evidence of industrial activity. Identification and characterization of contamination generally requires special drilling and sampling procedures with appropriate health and safety precautions. The extent of these precautions will depend on the type of contamination encountered, but may include hazardous material suits, face masks, respirators, and monitoring of air quality. Drilling and sampling procedures should be designed to minimize further transport of contaminants. For example, casing of boreholes and careful borehole sealing may be required to prevent vertical migration of contaminants. In situ tests that do not produce drilling spoils are also often quite appealing. Samplers and equipment used at contaminated sites must be cleaned and decontaminated using appropriate procedures, as described in ASTM D5088.

Characterization of contamination should generally include defining the lateral extent of the contaminated region and sampling the soil or water to test for the type and concentration of contamination present. Electrical and electromagnetic geophysical methods can be useful for characterization of the lateral extent of contaminated soil and contaminant plumes if the electrical properties are sufficiently different from the groundwater.

THIS PAGE IS LEFT INTENTIONALLY BLANK

# CHAPTER 13
# DOCUMENTATION, REPORTING, AND COMMUNICATION FOR SITE CHARACTERIZATION

Documentation, reporting, and communication are critical aspects of all site characterization programs. Regardless of how well a site characterization program is executed, it is of little use if the results, findings, conclusions, and recommendations are not effectively communicated to others involved with design, construction, and operation of the specific infrastructure being considered. Additionally, documentation of efforts and measurements is critical because it is quite common for the project development cycle to last many years, and sometimes decades. Without adequate documentation, critical and expensive observations and measurements can be effectively lost. This chapter addresses important aspects of documentation, reporting, and communication for site characterization. The chapter includes discussion of the primary objectives for various reports and documents produced from site characterization and guidance for presentation of information within these documents.

## 13.1 OBJECTIVES FOR DOCUMENTATION AND REPORTING OF SITE CHARACTERIZATION

The objective for documentation and reporting for site characterization is to capture and record the knowledge gained from the investigations. Additionally, the developed reports serve as the primary vehicle for communicating results from site characterization investigations to those responsible for design and construction, which facilitates effective decision making. Finally, documentation and reporting serve to archive results of site characterization for future use in design and construction, as well as for advancing site characterization practices through research and development.

Several different forms of geotechnical reports were described in Chapter 2. In this chapter, guidance for developing specific content for those reports is provided.

## 13.2 DOCUMENTATION AND REPORTING OF LABORATORY AND FIELD TEST MEASUREMENTS

As described in Chapter 2, laboratory and field test measurements are generally documented in reports referred to as geotechnical data reports. Geotechnical data reports are often composed of a relatively brief narrative to provide context for the investigations described, document the scope of investigations performed, and describe the procedures used to conduct investigations. The narrative is then followed by collections of documents that include field investigation logs, laboratory and field test reports, summary

tables of measured soil and rock properties, and other factual observations. The Table of Contents for a geotechnical data report should commonly include the following items:

1. Introduction
2. Scope of Work
3. Site Description
4. Site Conditions, Geologic Setting, & Topographic Information
5. Scope and Procedures for Field Investigations
   - 5.1. Borings
   - 5.2. In Situ Test Soundings
   - 5.3. Geophysical Investigations
   - 5.4. Exploration Pits
   - 5.5. Groundwater Investigations
6. Scope and Procedures for Laboratory Testing
   - 6.1. Index Property Testing
   - 6.2. Testing for Design Properties
7. Results from Laboratory and Field Investigations

   Appendix A – Field Investigation Plan

   Appendix B – Boring Logs

   Appendix C – In Situ Test Soundings

   Appendix D – Geophysical Measurements

   Appendix E – Exploration Pit Logs

   Appendix F – Groundwater Observations and Test Results

   Appendix G – Laboratory Test Results

   Appendix H – Historical Information

Initial sections of geotechnical data reports summarize background information about the project and the purpose(s) for the site characterization investigations. These sections should include information on planned structures or features that are to be constructed as well as design, construction, and performance requirements for the project. These sections should also include a description of general site conditions, the general geologic setting, and any peculiarities of the site that may affect the project.

Subsequent sections of the narrative should document the scope of investigations performed and specific procedures used to perform the work. These sections should identify the investigation methods used; the number, location, and depths of borings, exploration pits, and in situ test soundings; the types and

frequency of samples obtained; the dates when field investigations were performed; the subcontractor(s) used to perform the work; the types and number of laboratory tests performed; the testing standards used; and any variations from conventional procedures. Differences between the planned scope of investigations and the scope of investigations actually performed should also be addressed in this section of the narrative.

The final component of geotechnical data reports is to present results from the completed investigations. Much of this information is commonly presented in a series of appendices, although a brief narrative summarizing information provided in the appendices should be included in the narrative portion of the report. Appendices should include a collection of tables summarizing results from different types of laboratory tests, reports from individual tests, and final logs for all borings, exploration pits, and in situ test soundings. Appendices may also document piezometer or well installations, water level readings, rock core photographs, and geologic mapping data sheets, and may include copies of information collected from previous investigations at the project site (e.g., boring logs, test data, etc.). Geotechnical data reports do not typically include interpretations of subsurface conditions but may include select graphs of collective measurements.

## 13.3 DOCUMENTATION AND REPORTING FOR DESIGN PARAMETERS

Geotechnical design reports should generally provide interpretations of subsurface conditions at a project site, documentation of procedures for and findings from geotechnical analyses, and recommendations for design and construction. Geotechnical design reports should also include much of the same information provided in geotechnical data reports as described in Section 13.2, although sometimes geotechnical data reports are incorporated by reference. The table of contents for geotechnical design reports should generally include at least the following items:

1. Introduction
    1.1. Project Description
    1.2. Scope of Work
2. General Site Conditions
    2.1. Topography
    2.2. Geologic Setting (including Seismicity)
    2.3. Geotechnical Hazards
3. Summary of Field and Laboratory Investigations
4. Interpretation of Design Parameters

4.1. Stratigraphy
4.2. Design Parameters for Soil
4.3. Design Parameters for Rock
4.4. Groundwater Conditions

5. Recommendations for Design
6. Recommendations for Construction
7. Recommendations for Inspection, Instrumentation, and Monitoring

Appendix A – Site Plan with Boring Locations
Appendix B – Interpreted Design Cross-sections
Appendix C – Geotechnical Data Report

In some instances, geotechnical data and design reports are prepared as a single combined document. In such cases, the "Summary of Field and Laboratory Investigations" section in this table of contents is generally replaced by the content of items 5, 6, and 7 from the table of contents provided for geotechnical data reports. Additionally, the content of the appendices described for geotechnical data reports are generally included in a combined report.

Since the scope, site conditions, and design and construction requirements for each project are unique, the specific contents of geotechnical design reports must be tailored for individual projects. Early sections of geotechnical design reports should include general descriptions of the project and site, any special or unique project requirements, the general geologic setting, and the scope of investigations and analyses performed. Much of this content is often similar to what should be included in geotechnical data reports.

Geotechnical design reports should document site conditions based on collective interpretation of all information acquired as part of site characterization investigations. These sections should identify all soil and rock units of engineering significance and will often include interpretation of the depths and extent of each unit, usually presented in the form of one or more design cross-sections or design profiles. Interpreted values for all relevant design parameters should be clearly and succinctly documented for each unit, along with descriptions of how the parameter values were established and indications or quantitative measures of the uncertainty in the parameter values. The geotechnical design report should also specifically address groundwater conditions for both design and construction. In many cases, this should include description of groundwater conditions at the time of field investigations as well as recommendations about how such conditions may change with time. Finally, geotechnical design reports should specifically address geotechnical hazards that may be present at a site. The report should document the source of the hazard and address the potential likelihood of the hazard impacting

construction or long-term performance of the planned transportation features. Recommendations for mitigating hazards that impose substantial risks to construction and/or long-term performance should also be provided.

Geotechnical design reports should then present recommendations developed from geotechnical design. Since different projects have different requirements, the specific content for each of these sections should be developed according the project being considered. However, it is common for these sections to have subsections that address analyses and recommendations for foundations, for excavated or fill slopes, for retaining walls, for roadway, for ground improvement, etc.

Similarly, recommendations for construction of specific features should be included in geotechnical design reports. Such content will often include special requirements for select geotechnical features (e.g., dewatering requirements, staged construction, fill placement and compaction, etc.), and may include recommendations for inspection, instrumentation, load testing, and monitoring of specific features.

Appendices for geotechnical design reports should also generally include much of the same factual information provided in geotechnical data reports such as site plans, boring locations, boring logs, and test results, unless the design report refers to a separate data report for this information. Appendices for geotechnical design reports should also include additional content to document or illustrate interpretations of site conditions that are described in the report. Such content will often include interpreted drawings of stratigraphy for relevant design domains, and tables documenting interpreted values for design parameters.

## 13.4 GEOTECHNICAL BASELINE REPORTS

As described in Chapter 2, geotechnical baseline reports (GBR) are a special type of geotechnical report that establishes a contractually binding interpretation of specific ground conditions for a specific project. As such, the content and requirements for GBR are different from the more traditional geotechnical data reports and geotechnical design reports. While GBR are used to establish an interpretation of ground conditions for contractual purposes, it is not necessary or even desirable for GBR to include supporting information used to develop the contractual interpretation. Rather, GBR should concisely and clearly define the established interpretation along with means that will be used to assess any deviations encountered during construction. GBR will also usually include contractual content like differing site conditions clauses and dispute resolution provisions. Since GBR are contractual documents, qualifying language such as “may” and “should” must be avoided.

Notably, GBR are not intended to, and should not, "baseline" all soil and rock conditions and parameters. Rather, GBR should only baseline specific parameters that are judged to have the greatest influence on project cost and schedule. For example, baselined parameters may include the location and extent of specific important strata (e.g. weak strata, highly permeable strata, etc.), the shear strength of specific units, and groundwater levels. Baselined parameters should not include properties that do not directly impact construction, and should not include computed design values like side or tip resistance for deep foundations. All baselined parameters must be measurable, and GBR should clearly document how all baselined parameters are to be measured and the criteria to be used to establish whether conditions encountered during construction represent a deviation from the established baseline. GBR should also document requirements for construction inspection by both the contractor and owner. Finally, GBR will often include factual geotechnical data reports, but should not include much of the interpretive content that is often included in geotechnical design reports.

## 13.5 GENERAL FORMS OF DOCUMENTATION FOR SITE CHARACTERIZATION

Geotechnical reports commonly include graphical and tabular documentation of site characterization activities in addition to the narrative provided in the body of the reports. The following sections provide descriptions and recommendations for such documentation.

### 13.5.1 Site Plans

A site location plan should be provided in all geotechnical data and design reports for reference on a regional or local scale as illustrated in Figure 13-1. Locations for all borings and field tests should be shown clearly on a scaled plan map of the specific site being investigated. Plans should preferably show topography with well-delineated elevation contours and a properly established benchmark. The direction of (magnetic or true) north should be shown along with indications of important structures, roadways, utilities, and other items that might impact design or construction. Recent advances in global positioning systems (GPS) and geographic information systems (GIS) have dramatically improved the efficiency and accuracy for acquiring and documenting location information. If multiple types of exploratory methods are used (e.g., borings, CPT soundings, test pits, etc.), separate symbols should be used for each method and a clear legend should be included to clearly distinguish among the different types of soundings. A horizontal scale should also be presented.

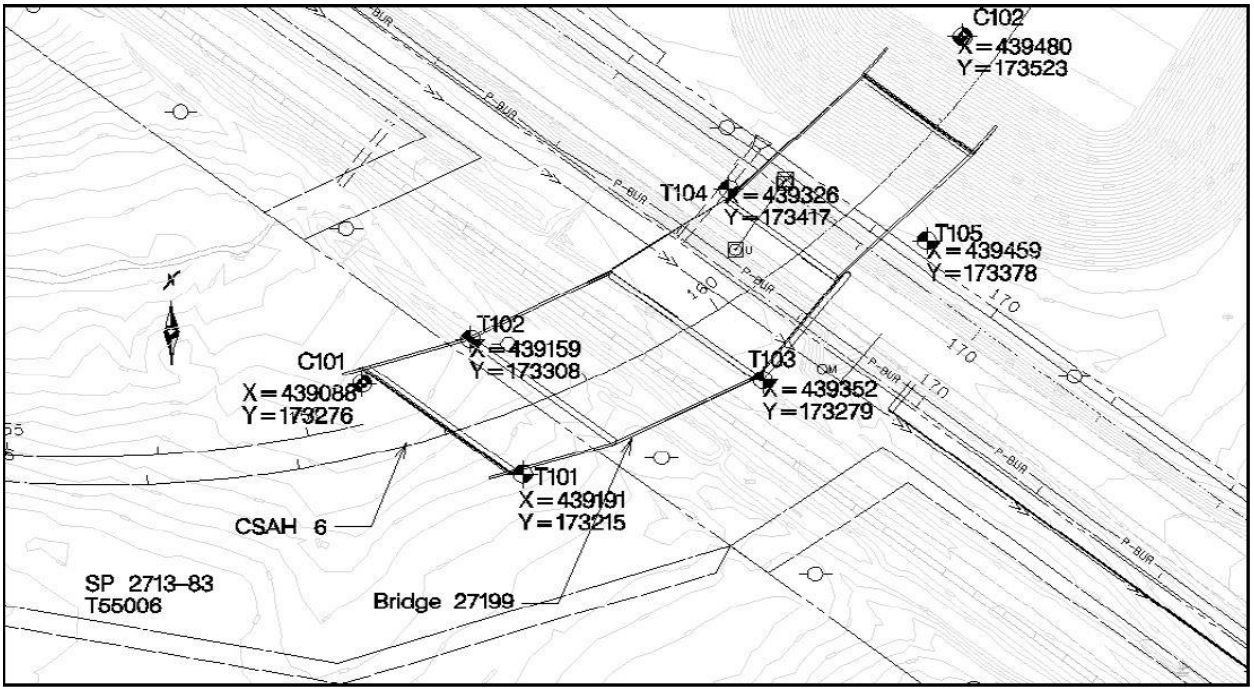


**Figure 13-1 Site plan showing locations of borings and in situ test soundings (MnDOT, 2013).**

### 13.5.2 Final Field Investigation Logs

Final field investigation logs, including logs of borings, in situ test soundings, test pits, groundwater monitoring wells, and piezometers, should be prepared and provided in geotechnical data reports, and geotechnical design reports when a separate geotechnical data report is not prepared. Example final boring logs are shown in Figures 13-2 and 13-3. An example log for an in situ test sounding is provided in Figure 13-4. Many commercial software programs are available for preparation of field investigation logs, which dramatically improve the accuracy, efficiency, and even the effectiveness of final logs. Computer-aided drafting tools let users create custom log formats, which can include graphic logs, monitoring well details, and data plots. Custom designed legends explaining graphic symbols and containing additional notes can be added to logs for greater clarity. These can include a library of soil types, sampler symbols, and well symbols, as well as other nomenclature used for final logs.

In addition to providing graphical and/or numerical representations of observations and measurements made during investigations, field investigation logs should include basic logistical information. Such information should include the specific location of the field investigation, date(s), ground elevation, personnel conducting the investigation, and identification of the specific equipment and methods used. Methods used to seal and close borings should also be included as well as any groundwater observations.

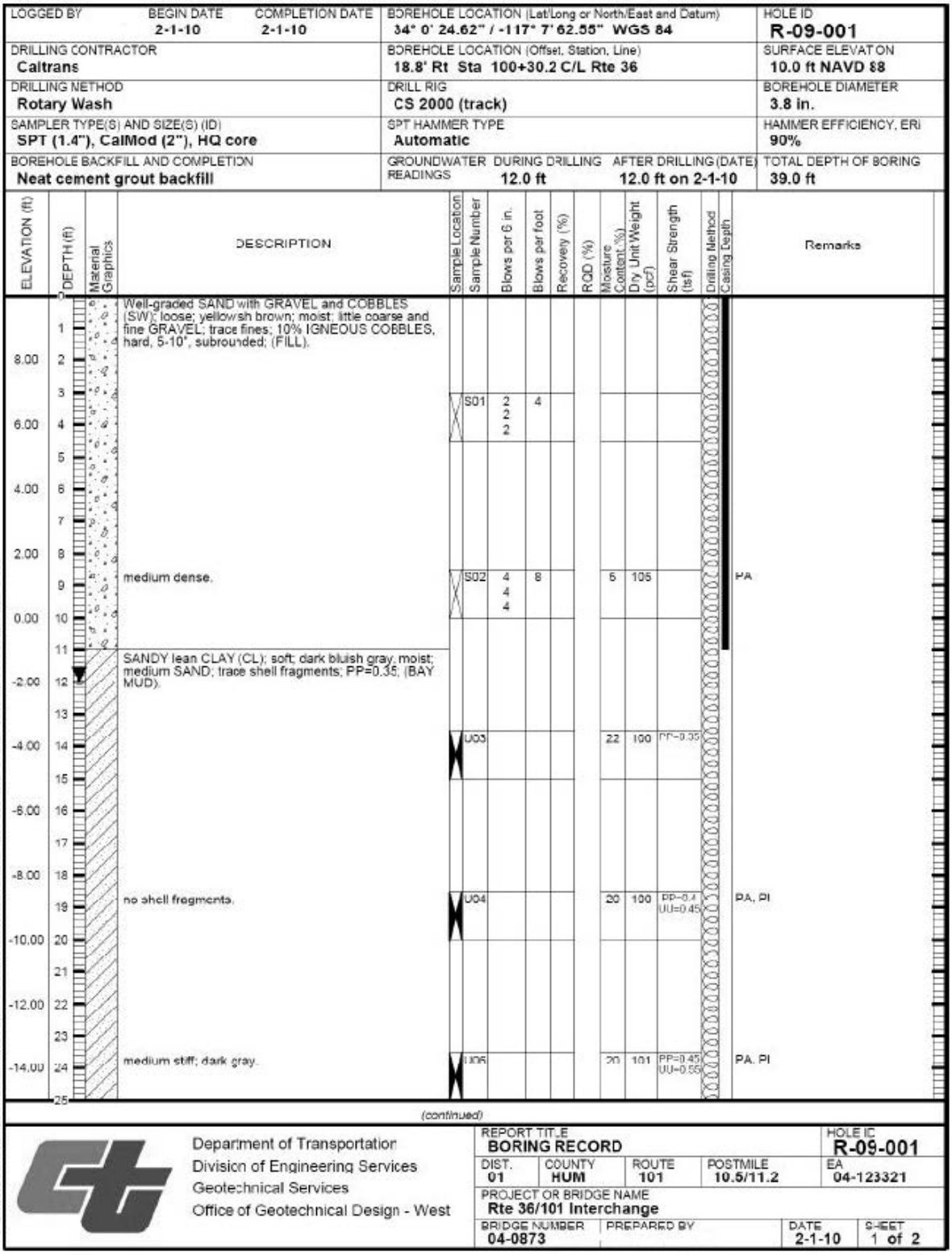


**Figure 13-2 Example boring log from California Department of Transportation (Caltrans, 2010).**

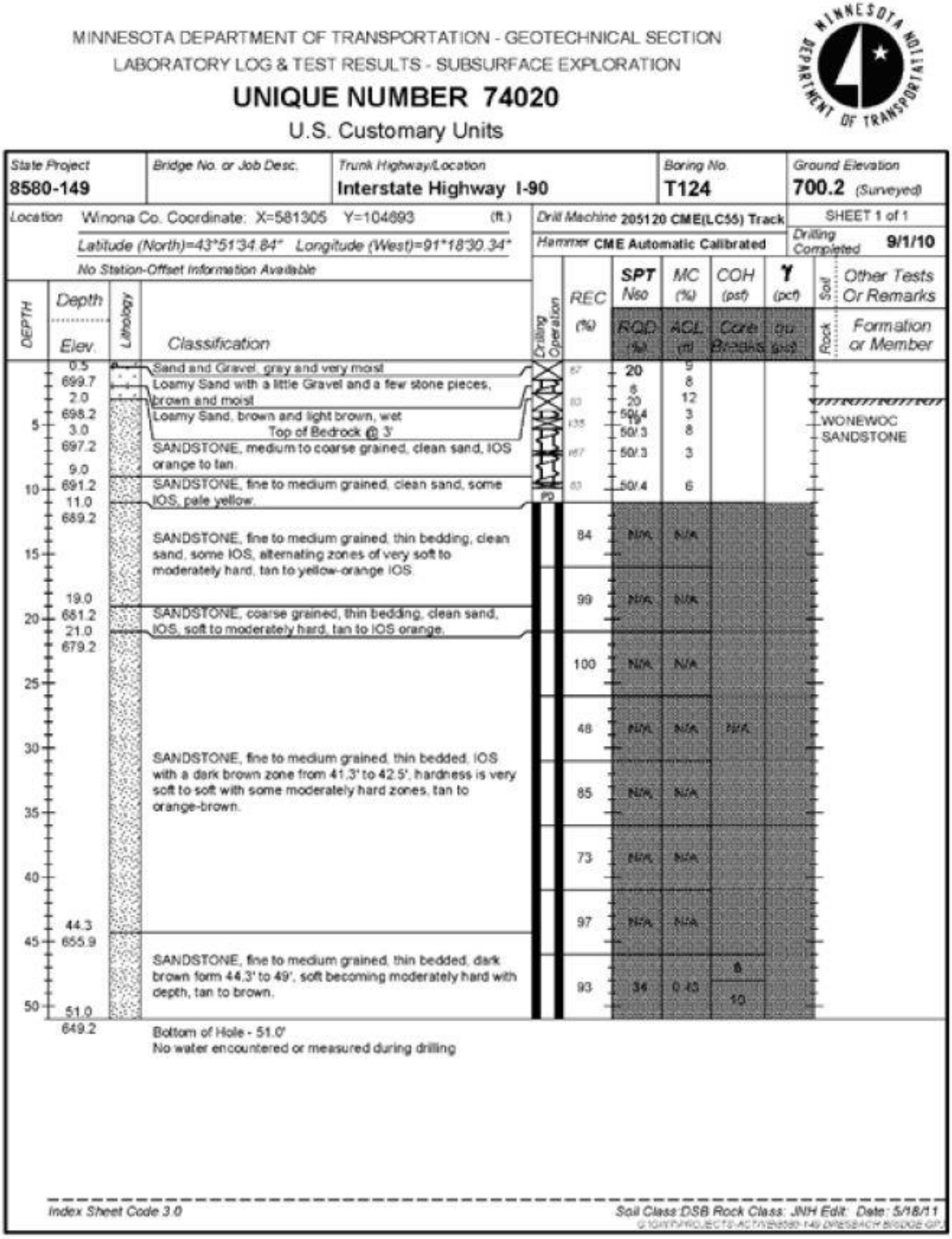


**Figure 13-3 Example boring log from Minnesota Department of Transportation (MnDOT, 2013).**

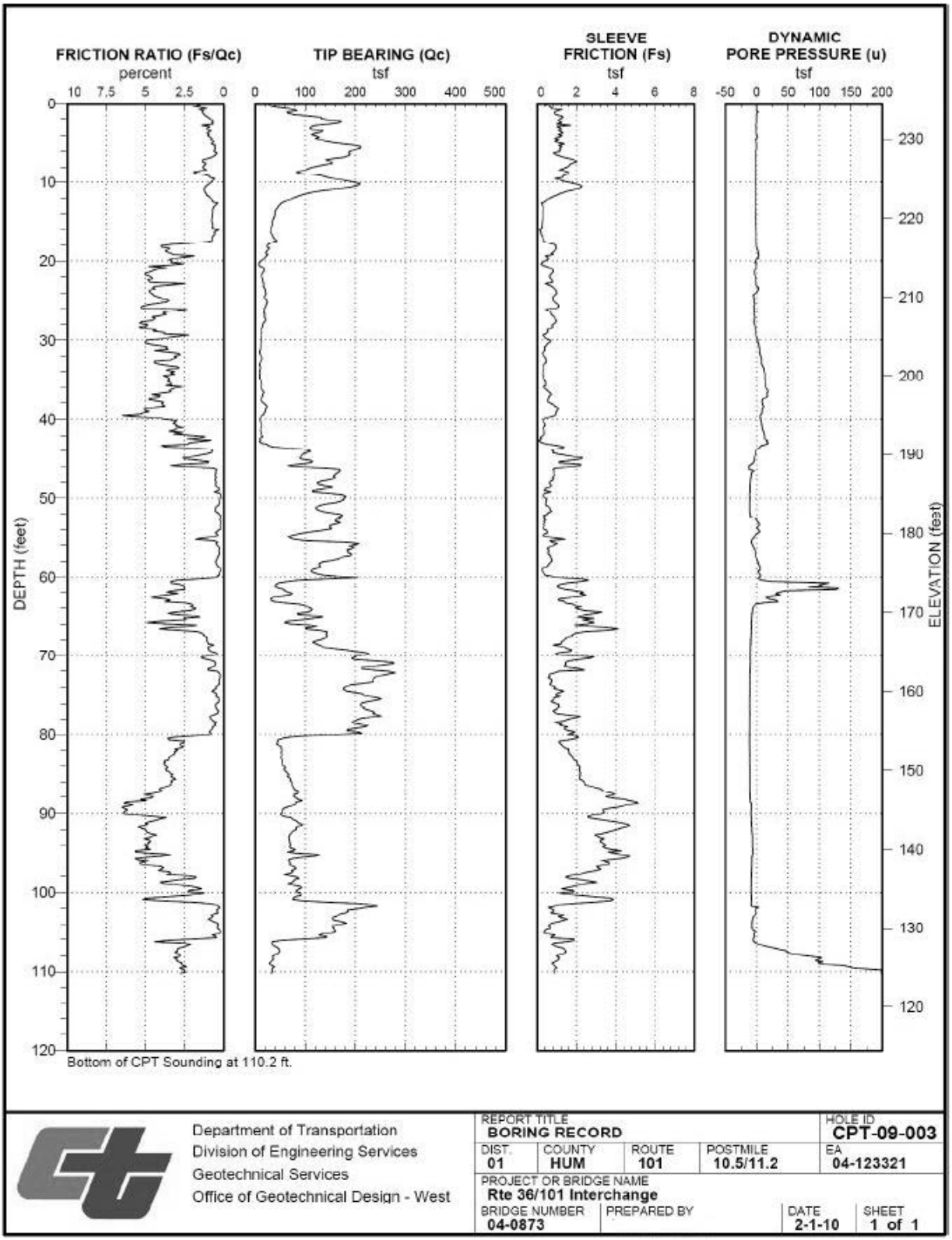


**Figure 13-4 Example CPTU log from California Department of Transportation (Caltrans, 2010).**

### 13.5.3 Laboratory Test Reports

Geotechnical data reports, and some geotechnical design reports, should include appendices that contain reports from individual laboratory tests as well as summary tables documenting collected measurements from different types of laboratory tests. Figure 13-5 shows an example laboratory test report for a $UU$ triaxial compression tests. Figures 13-6 through 13-8 show example summary tables for one-dimensional consolidation tests, $UU$ triaxial tests, and $\bar{C}U$ triaxial tests, respectively.

Reports for individual laboratory tests should not only present results of the primary measurements, but should also document additional measurements that facilitate collective interpretation of the test results when combined with other measurements from the site. Additional measurements shown in Figure 13-5 include index properties like water content, dry unit weight, degree of saturation, Atterberg limits, and specific gravity. The report also includes important testing parameters such as specimen dimensions, loading rate, and applied loads at failure. The report includes information about the location where the specimen was obtained such as the boring number, sample number, and sample depth. Finally, the report provides a graphic to illustrate the test results and documents the nomenclature used for the report.

The summary tables shown in Figures 13-6 through 13-8 also show similar information, but tabulated in a way to provide for direct comparison of measurements from different tests. Summary tables are often drawn directly from spreadsheet software, which provides convenient means to generate graphics to facilitate collective interpretation of measurements within individual strata and for development of graphics to demonstrate how values for design parameters were established as described in Section 13.5.4.

### 13.5.4 Design Profiles and Design Cross-sections

Geotechnical reports are normally accompanied by presentation of interpreted design profiles or design cross-sections developed from field and laboratory test measurements. Design profiles, similar to that illustrated in Figure 13-9, are prepared to represent conditions for a localized area (e.g., at the location of a bridge pier) or for areas with practically uniform stratigraphy and properties. Design cross-sections are often developed to represent conditions along the length of a roadway or bridge to illustrate the variability in subsurface conditions along the project alignment. A limited number of transverse cross-sections may also be developed for key locations such as at major bridge foundations, cut slopes, or high embankments. Figure 13-10 shows an example design cross-section.

## Unconsolidated-Undrained Type Triaxial Compression Test Report

### Project Information

Project: Big Embankment Project
Client:
Report Date: March 2, 2016

| Sample Data | |
|---|---|
| Boring: | T-3 |
| Sample: | T3-2 |
| Sample Depth: | 25.0-27.5 ft |
| Sampling Method: | Hydraulic (Osterberg) Piston Sampler |
| Sample Type: | 3-in dia. Shelby Tube |
| Sampling Date: | 2/10/2016 |
| Test Date: | 2/15/2016 |
| Liquid Limit | 31 |
| Plastic Limit | 22 |
| Plasticity Index: | 9 |
| Specific Gravity: | 2.71 |
| USCS Classification: | CL |
| Remarks: | Small gravel particles and root holes were detected in specimen during trimming |

| Specimen Data | |
|---|---|
| Depth (ft): | 26.4 |
| Diameter (in): | 1.57 |
| Height (in): | 2.93 |
| Pre-test $\omega$ (%): | 28.1 |
| Pre-test $\gamma_d$(pcf) | 87.1 |
| Pre-test $e$: | 0.94 |
| Pre-test $S_r$: | 0.81 |
| Shear Rate (in/min): | 0.029 |
| Post-test $\omega$ (%): | 27.9 |
| Post-test $\gamma_d$(pcf) | -- |
| Post-test $e$: | 0.94 |
| Post-test $S_r$: | 0.81 |
| $\sigma_{cell}$ (psi): | 23.2 |
| $(\sigma_1 - \sigma_3)_{peak}$ (psi): | 22.9 |
| $(\sigma_1 - \sigma_3)_{ult}$ (psi): | 15.8 |

### Shear Stress-Strain response

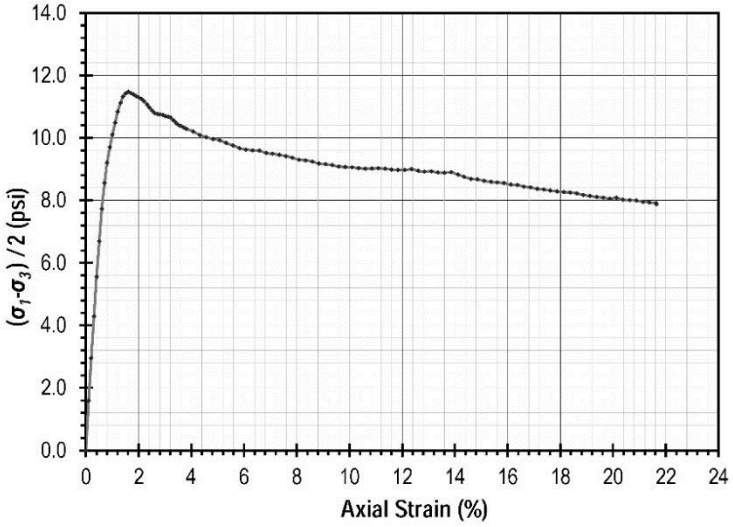


### Nomenclature

$\omega$ = moisture content
$\gamma_d$ = dry unit weight
$e$ = void ratio
$S_r$ = degree of saturation
$\sigma_{cell}$ = cell pressure
$(\sigma_1 - \sigma_3)_{peak}$ = peak principal stress difference
$(\sigma_1 - \sigma_3)_{ult}$ =ultimate principal stress difference

University of Missouri
Soil Characterization Laboratory

**Figure 13-5 Example laboratory test report for *UU* triaxial compression tests**

| | Parameter | Units | Specimen | | | | | | | | |
|---|---|---|---|---|---|---|---|---|---|---|---|
| Sample | Boring | -- | B-1 | B-1 | B-1 | B-1 | B-2 | B-2 | B-2 | B-2 | B-2 |
| | Tube | -- | O-1 | ST-5 | O-9 | O-13 | O-1 | O-3 | O-5 | O-11 | O-13 |
| | Depth | ft | 6.67 | 18.42 | 28.72 | 42.26 | 5.95 | 10.91 | 15.66 | 30.83 | 35.87 |
| | *LL* | -- | 34 | 48 | 27 | 35 | 41 | 32 | 41 | 31 | 43 |
| | *PL* | -- | 21 | 21 | 19 | 24 | 19 | 18 | 19 | 21 | 22 |
| | $G_s$ | -- | 2.7 | 2.74 | 2.71 | 2.72 | | | | | |
| pre-test | $h_{init}$ | in | 1.000 | 0.945 | 1.000 | 0.932 | 1.000 | 1.000 | 1.000 | 1.000 | 1.000 |
| | $d$ | in | 2.50 | 2.50 | 2.50 | 2.50 | 2.50 | 2.50 | 2.50 | 2.50 | 2.50 |
| | $W_{init}$ | g | 150.29 | 152.77 | 149.29 | 142.76 | 148.54 | 154.83 | 145.61 | 146.01 | 160.09 |
| | $\omega_{init}$ | % | 26.30 | 23.51 | 27.25 | 28.97 | 25.22 | 27.84 | 33.51 | 30.68 | 25.13 |
| | $\gamma_{init}$ | pcf | 116.64 | 125.41 | 115.86 | 118.88 | 115.28 | 120.16 | 113.01 | 113.32 | 124.24 |
| | $S_{r\text{-}init}$ | -- | 86.05 | 96.17 | 79.89 | 94.39 | 81.58 | 94.37 | 93.94 | 87.82 | 91.60 |
| | $e_o$ | -- | 0.8252 | 0.6601 | 0.9899 | 0.8286 | 0.8376 | 0.7992 | 0.9366 | 0.9424 | 0.6914 |
| post test | $h_{final}$ | in | - | - | - | - | - | - | - | - | - |
| | $W_{final}$ | g | 141.71 | 152.82 | 144.83 | 138.28 | 144.68 | 149.91 | 140.86 | 138.59 | 159.44 |
| | $\omega_{final}$ | % | 21.89 | 23.85 | 23.67 | 25.88 | 22.41 | 24.19 | 25.60 | 23.95 | 24.17 |
| | $e_f$ | -- | 0.5217 | 0.4367 | 0.5260 | 0.6199 | 0.5720 | 0.5750 | 0.1900 | 0.6474 | 0.5864 |
| interpretted values | $e_o$ | -- | 0.8250 | 0.6601 | 0.9899 | 0.8286 | 0.8376 | 0.7992 | 0.9366 | 0.9424 | 0.6914 |
| | $e_f$ | -- | 0.5220 | 0.4367 | 0.5260 | 0.6199 | 0.5720 | 0.5750 | 0.1900 | 0.6474 | 0.5864 |
| | $c_c$ | -- | 0.1675 | 0.1912 | 0.3107 | 0.2376 | 0.2215 | 0.2211 | 0.3167 | 0.267 | 0.2082 |
| | $c_r$ | -- | 0.0311 | 0.0549 | 0.0249 | 0.0443 | 0.0447 | 0.0194 | 0.0236 | 0.0154 | 0.0212 |
| | $\sigma'_{p}$ | psf | 384 | 2733 | 2813 | 3750 | 1777 | 3364 | 2825 | 2875 | 5500 |
| | $e_{\sigma'p}$ | -- | 0.7387 | 0.5394 | 0.7067 | 0.7362 | 0.7038 | 0.6809 | 0.3808 | 0.8404 | 0.6021 |
| | $\sigma'_{p\text{-}tangent}$ | psf | 384 | 2313 | 2803 | 3180 | 1070 | 3000 | 2500 | 2000 | 4778 |
| | $e_{\sigma'p\text{-}tangent}$ | -- | 0.7387 | 0.5470 | 0.7067 | 0.7448 | 0.7327 | 0.6853 | 0.3846 | 0.8750 | 0.6106 |
| | $\sigma'_{p\text{-}Casagrande}$ | psf | 316 | 2000 | 2813 | 3000 | 1138 | 3167 | 2825 | 2353 | 5500 |
| | $e_{\sigma'p\text{-}Casagrande}$ | -- | 0.7453 | 0.5530 | 0.7067 | 0.7500 | 0.7327 | 0.6838 | 0.3808 | 0.8615 | 0.6021 |
| | $\sigma'_{p\text{-}strain\ energy}$ | psf | - | 2733 | 2785 | 3750 | 1777 | 3364 | 2688 | 2875 | 5000 |
| | $e_{\sigma'p\text{-}strain\ energy}$ | -- | - | 0.5394 | 0.7067 | 0.7362 | 0.7038 | 0.6809 | 0.3769 | 0.8404 | 0.6074 |
| | $c_v$ | ft²/day | 1.2670 | 0.0261 | 0.0446 | 0.0305 | 0.0415 | 0.0526 | 0.0146 | 0.0334 | 0.0350 |

**Figure 13-6 Example summary table for one-dimensional consolidation tests.**

| | Parameter | Units | Specimen | | | | | | | | | | |
|---|---|---|---|---|---|---|---|---|---|---|---|---|---|
| Sample | Boring # | | K-B1 | K-B1 | K-B1 | K-B1 | K-B1 | K-B1 | K-B1 | K-B1 | K-B1 | K-B1 | K-B1 |
| | Depth | ft | 105.50 | 115.60 | 120.20 | 126.70 | 129.90 | 131.40 | 132.20 | 139.00 | 141.10 | 132.20 | 147.00 |
| | coring date | | 9/29/2009 | 9/30/2009 | 9/30/2009 | 9/30/2009 | 10/5/2009 | 10/5/2009 | 10/5/2009 | 10/5/2009 | 10/5/2009 | 10/5/2009 | 10/5/2009 |
| | test date | | 9/29/2009 | 9/30/2009 | 9/30/2009 | 9/30/2009 | 10/5/2009 | 10/5/2009 | 10/5/2009 | 10/5/2009 | 10/5/2009 | 10/5/2009 | 10/5/2009 |
| | location | -- | KCICON | KCICON | KCICON | KCICON | KCICON | KCICON | KCICON | KCICON | KCICON | KCICON | KCICON |
| Initial Condition | $h_{init}$ | in | 3.33 | 3.96 | 3.92 | 4.11 | 4.02 | 3.66 | 3.78 | 3.76 | 3.84 | 3.36 | 3.67 |
| | $d_{init}$ | in | 1.63 | 1.92 | 1.83 | 1.95 | 1.85 | 1.86 | 1.86 | 1.85 | 1.85 | 1.86 | 1.87 |
| | $W_{sample}$ | lb | 0.5830 | 0.9095 | 0.9135 | 0.9175 | 0.9355 | 0.8635 | 0.8950 | 0.8745 | 0.9075 | 0.7905 | 0.8755 |
| | $\gamma_t$ | pcf | 144.3 | 136.9 | 153.1 | 129.1 | 150.2 | 150.5 | 151.1 | 149.9 | 151.7 | 150.7 | 150.7 |
| Shearing | *strain rate* | %/min | 1.00 | 1.00 | 1.00 | 1.00 | 1.00 | 1.00 | 1.00 | 1.00 | 1.00 | 1.00 | 1.00 |
| | $\sigma_{cell}$ | psi | 79.10 | 86.70 | 90.20 | 95.03 | 97.43 | 98.55 | 99.15 | 104.25 | 105.83 | 0.00 | 0.00 |
| Interpretted Q | $(\sigma_1 - \sigma_3)_{max}$ | psf | 43876.0 | 7148.0 | 162312.0 | 18476.8 | 120892.0 | 137686.0 | 137934.0 | 131460.0 | 145014.0 | 160902.0 | 110650.0 |
| | $\varepsilon_{psd}$ | % | 5.26 | 11.52 | 3.30 | 14.98 | 2.91 | 3.04 | 2.92 | 2.71 | 3.14 | 3.04 | 2.61 |
| | $s_u$ | psf | 21938 | 3574 | 81156 | 9238 | 60446 | 68843 | 68967 | 65730 | 72507 | - | - |
| | $qu$ | psf | - | - | - | - | - | - | - | - | - | 160902 | 110650 |

**Figure 13-7 Example summary table for UU triaxial compression tests.**

| | Parameter | Units | Specimen | | | | | | | | |
|---|---|---|---|---|---|---|---|---|---|---|---|
| | | | B1-T13a | B1-T09 | B2-T03a | B2-T05 | B2-T07a | B2-T07b | B2-T09c | B2-T11a | B2-T11c |
| Sample | Boring | -- | B-1 | B-1 | B-2 | B-2 | B-2 | B-2 | B-2 | B-2 | B-2 |
| | Tube | -- | T13 | T09 | T-03 | T05 | T-07 | T-07 | T-09 | T-11 | T-11 |
| | Depth | ft | 40.8 | 28.1 | 10.7 | 15.4 | 21.7 | 20.2 | 26.1 | 30.5 | 31.83 |
| | LL | | 35 | 27 | 32 | 41 | 37 | 37 | 39 | 31 | 31 |
| | PL | | 24 | 19 | 18 | 19 | 18 | 18 | 21 | 21 | 21 |
| | $G_s$ | | 0.72 | 2.71 | 2.65 | 2.65 | 2.65 | 2.65 | 2.65 | 2.65 | 2.65 |
| | Lab | -- | MU | MU | MU | MU | MU | MU | MU | MU | MU |
| Target | $\sigma'_{3\text{-max}}$ | psi | 75 | 75 | 60 | 75 | 75 | 75 | 65 | 37.5 | 40.0 |
| | $\sigma'_{3\text{-shear}}$ | psi | 75 | 75 | 60 | 25 | 21.4 | 10 | 14.4 | 5 | 20.0 |
| | OCR | -- | 1.0 | 1.0 | 1.0 | 3.0 | 3.5 | 7.5 | 4.5 | 7.5 | 2.0 |
| | $d$ | in | 1.50 | 1.50 | 1.50 | 1.50 | 1.50 | 1.50 | 1.50 | 1.50 | 1.50 |
| Initial Conditions | $\omega_{init}$ | % | 28.57 | 28.42 | 27.93 | 29.52 | 25.68 | 26.11 | 26.97 | 29.56 | 27.79 |
| | $h_{init}$ | in | 3.32 | 2.90 | 3.12 | 2.92 | 2.96 | 3.10 | 3.02 | 3.25 | 3.02 |
| | $d_{init}$ | in | 1.52 | 1.50 | 1.58 | 1.50 | 1.54 | 1.49 | 1.53 | 1.51 | 1.56 |
| | $W_{sample}$ | g | 190.40 | 150.98 | 189.60 | 158.28 | 170.69 | 167.14 | 175.22 | 170.18 | 164.17 |
| | $e_{init}$ | -- | -0.52 | 0.94 | 0.80 | 0.83 | 0.77 | 0.77 | 0.75 | 0.93 | 0.94 |
| | $S_r$ | -- | -0.40 | 0.82 | 0.93 | 0.95 | 0.89 | 0.90 | 0.96 | 0.84 | 0.78 |
| | $B_{init}$ | -- | 0.63 | 0.60 | 0.61 | | | 0.66 | 0.74 | 0.87 | 0.70 |
| After Saturation | $\sigma_{cell}$ | psi | 50.0 | 50.0 | 50.0 | 35.0 | 35.0 | 35.0 | 35.0 | 55.0 | 60.0 |
| | $\sigma_{back}$ | psi | 40.0 | 40.0 | 40.0 | 25.0 | 25.0 | 25.0 | 25.0 | 50.0 | 55.0 |
| | $\sigma'_{cell}$ | psi | 10.0 | 10.0 | 10.0 | 10.0 | 10.0 | 10.0 | 10.0 | 5.0 | 5.0 |
| | $B_{sat}$ | -- | 0.73 | 0.71 | 0.76 | 0.77 | 0.84 | 0.76 | 0.75 | 0.92 | 0.92 |
| | $e_{sat}$ | -- | 0.18 | 0.69 | 0.69 | 0.90 | 0.66 | 0.70 | 0.65 | 0.75 | 0.76 |
| Virgin Consolidation | $\sigma_{cell}$ | psi | 100.0 | 115.0 | 100.0 | 100.0 | 100.0 | 100.0 | 90.0 | 90.0 | 95.0 |
| | $\sigma_{back}$ | psi | 25.0 | 40.0 | 40.0 | 25.0 | 25.0 | 25.0 | 25.0 | 52.5 | 55.0 |
| | $\sigma'_{cell}$ | psi | 75.0 | 75.0 | 60.0 | 75.0 | 75.0 | 75.0 | 65.0 | 37.5 | 40.0 |
| | $\Delta V$ | cc | 6.00 | 4.16 | 5.33 | 7.90 | 5.79 | 5.00 | 3.86 | 4.96 | 6.24 |
| | $e_{vc}$ | -- | 0.15 | 0.60 | 0.59 | 0.73 | 0.55 | 0.60 | 0.58 | 0.66 | 0.64 |
| | $t_{100}$ | min | 100.0 | 18.3 | 90.0 | 70.0 | 60.0 | 90.0 | 17.8 | 22.5 | 18.0 |
| | $B_{vc}$ | -- | 0.73 | 0.71 | 0.76 | | 0.28 | 0.12 | 0.68 | 0.77 | 0.76 |
| Rebound Consolidation | $\sigma_{cell}$ | psi | 100.0 | 115.0 | 100.0 | 100.0 | 100.0 | 100.0 | 90.0 | 90.0 | 95.0 |
| | $\sigma_{back}$ | psi | 25.0 | 40.0 | 40.0 | 75.0 | 78.6 | 90.0 | 75.6 | 85.0 | 75.0 |
| | $\sigma'_{cell}$ | psi | 75.0 | 75.0 | 60.0 | 25.0 | 21.4 | 10.0 | 14.4 | 5.0 | 20.0 |
| | $\Delta V$ | cc | -2.00 | 0.00 | 0.00 | -1.18 | -1.12 | -2.17 | -1.17 | -1.18 | -0.38 |
| | $e_{final}$ | -- | 0.16 | 0.60 | 0.59 | 0.75 | 0.57 | 0.65 | 0.60 | 0.68 | 0.65 |
| | $t_{100}$ | min | | | | 80.0 | 32.0 | 65.0 | 11.0 | 18.0 | 1.8 |
| | $h_{consol}$ | in | 3.09 | 2.74 | 3.09 | 2.92 | 2.87 | 2.98 | 2.82 | 3.09 | 2.89 |
| | $B_{shear}$ | -- | | | | 0.90 | 0.75 | 0.73 | 0.88 | 0.93 | 0.85 |
| Shearing | $d\varepsilon/dt$ | in/min | 0.0019 | 0.0007 | 0.0008 | 0.0019 | 0.0019 | 0.0013 | 0.0019 | 0.0037 | 0.0040 |
| | $\omega_{final}$ | % | 22.34 | 22.23 | 22.45 | 28.40 | 21.58 | 24.37 | 22.56 | 25.63 | 24.41 |
| | $h_{final}$ | in | | | | 2.00 | 2.11 | 2.48 | 2.28 | 2.30 | 2.07 |
| Interpretted Quantities | $\omega_{final}$ | % | 22.34 | 22.23 | 22.45 | 28.40 | 21.58 | 24.372 | 22.5632 | 25.63 | 24.41 |
| | $e_{final}$ | -- | 0.16 | 0.60 | 0.59 | 0.75 | 0.57 | 0.65 | 0.60 | 0.68 | 0.65 |
| | $e_{vc}$ | -- | 0.15 | 0.60 | 0.59 | 0.73 | 0.55 | 0.60 | 0.58 | 0.66 | 0.64 |
| | $(\sigma_1 - \sigma_3)_{max}$ | psi | 56.9 | 43.0 | 41.4 | 26.2 | 37.4 | 31.6 | 42.3 | 17.5 | 18.1 |
| | $\sigma'_{3\text{-psd}}$ | psi | 28.6 | 43.1 | 19.9 | 16.8 | 19.3 | 15.4 | 19.6 | 7.7 | 10.8 |
| | $\varepsilon_{psd}$ | % | 15.6 | 2.6 | 12.9 | 13.8 | 18.7 | 16.4 | 20.3 | 16.6 | 2.0 |
| | $(\sigma'_1/\sigma'_3)_{max}$ | -- | 3.15 | 2.62 | 3.15 | 2.6 | 3.07 | 4.14 | 3.39 | 3.38 | 3.50 |
| | $(\sigma_1 - \sigma_3)_{psr}$ | -- | 55.9 | 37.8 | 40.1 | 26.2 | 35.1 | 22.6 | 35.5 | 16.4 | 17.4 |
| | $\sigma'_{3\text{-psr}}$ | psi | 26.0 | 23.4 | 18.7 | 16.8 | 16.9 | 7.2 | 14.8 | 6.9 | 6.9 |
| | $\varepsilon_{psr}$ | % | 12.6 | 13.4 | 5.9 | 13.8 | 8.2 | 1.3 | 4.3 | 6.4 | 11.8 |
| | $(\sigma_1 - \sigma_3)_{ult}$ | psi | 50.1 | 35.0 | 38.1 | 24.9 | 36.8 | 31.5 | 40.5 | 16.7 | 14.9 |
| | $(\sigma'_1/\sigma'_3)_{ult}$ | -- | 2.68 | 2.39 | 2.86 | 2.4 | 2.82 | 3.01 | 3.01 | 3.15 | 3.27 |
| | $\sigma'_{3\text{-ult}}$ | psi | 29.8 | 25.1 | 20.5 | 17.7 | 20.2 | 15.7 | 20.2 | 7.8 | 6.6 |
| | $p'_{ult}$ | psi | 54.8 | 42.6 | 39.6 | 30.1 | 38.6 | 31.4 | 40.4 | 16.1 | 14.0 |
| | $q_{ult}$ | psi | 25.1 | 17.5 | 19.1 | 12.4 | 18.4 | 15.7 | 20.3 | 8.3 | 7.5 |
| | $\varepsilon_{ult}$ | % | 33.9 | 25.8 | 26.4 | 28.9 | 26.4 | 17.7 | 27.5 | 26.9 | 27.3 |

**Figure 13-8 Example summary table for $\overline{CU}$ triaxial compression tests performed following SHANSEP procedure.**

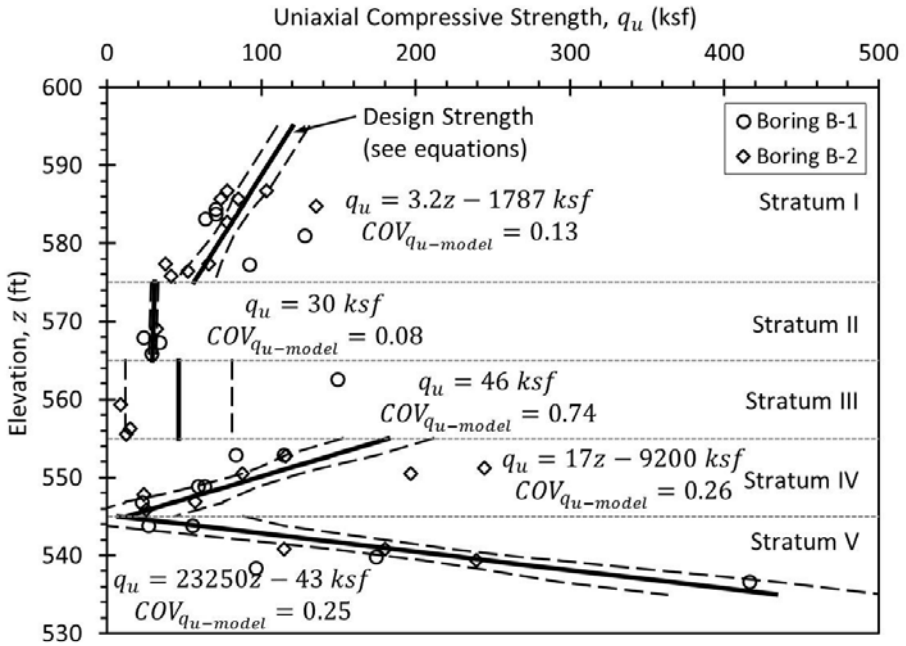


**Figure 13-9 Design profile showing measurements with interpretation for each stratum.**

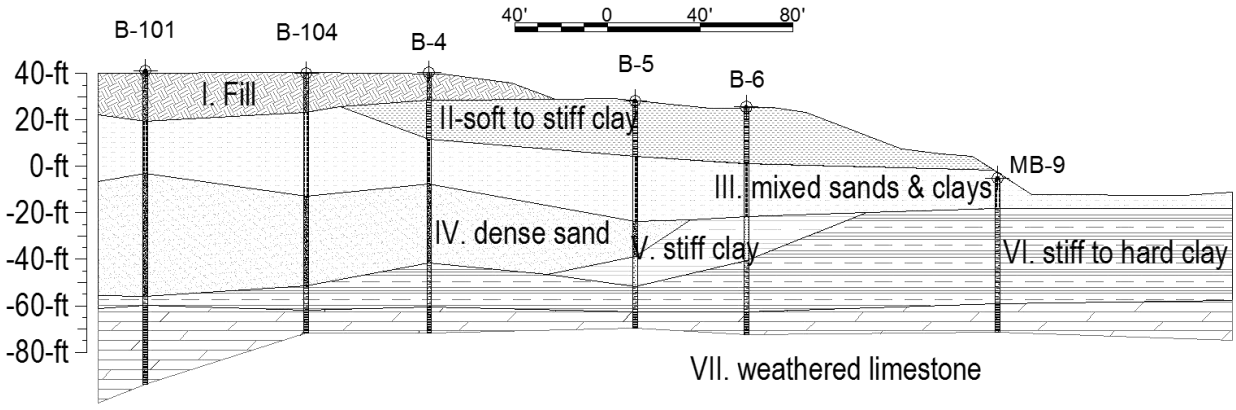


**Figure 13-10 Design cross-section showing interpretation of stratigraphy.**

Design profiles should be presented to show available measurements along with interpretations of stratigraphic boundaries as illustrated in Figure 13-9. Interpretations for design parameters should also be clearly shown, preferably with numerical values for the parameters and quantification of the uncertainty associated with the parameter values (e.g., the model uncertainty, $\sigma_{model}$). Separate profiles should be presented for each relevant design parameter. In cases where the magnitude of parameter values for different strata cover a large range, duplicate graphics should generally be presented to clearly show the measurements and interpretations at different scales so that the interpretations are clearly understood.

Design cross-sections should be presented at a scale appropriate to the depth and length of the cross-section. Because the length and depth dimensions are often quite different, it is common to plot design cross-sections using an exaggerated vertical scale [e.g., 1(V):10(H) or 1(V):20(H)]. Design cross-sections should clearly present interpretations of important stratigraphic units. Representations of borings falling near to the cross-section should also be shown to illustrate locations where stratigraphy is relatively well-defined and locations where stratigraphy is being interpreted. In cases where stratigraphy at a specific location is quite uncertain, it is common to draw stratigraphic interfaces using dashed lines and/or to indicate great uncertainty using question marks.

### 13.5.5 Observations from Field Instrumentation

Geotechnical data and design reports should also include documentation of observations made from field instrumentation, if available. Common observations for many projects will include observations about groundwater conditions from monitoring wells or piezometers and observations of deformations from slope inclinometers or settlement plates/settlement devices. Figure 13-11 shows an example of measurements made from a collection of piezometers to document fluctuations in pore water pressures over time. When the site is near a stream or other waterway where water levels may fluctuate, it is also informative to include observations of the water level in the waterway within the plot to compare with measured groundwater levels as shown in Figure 13-11.

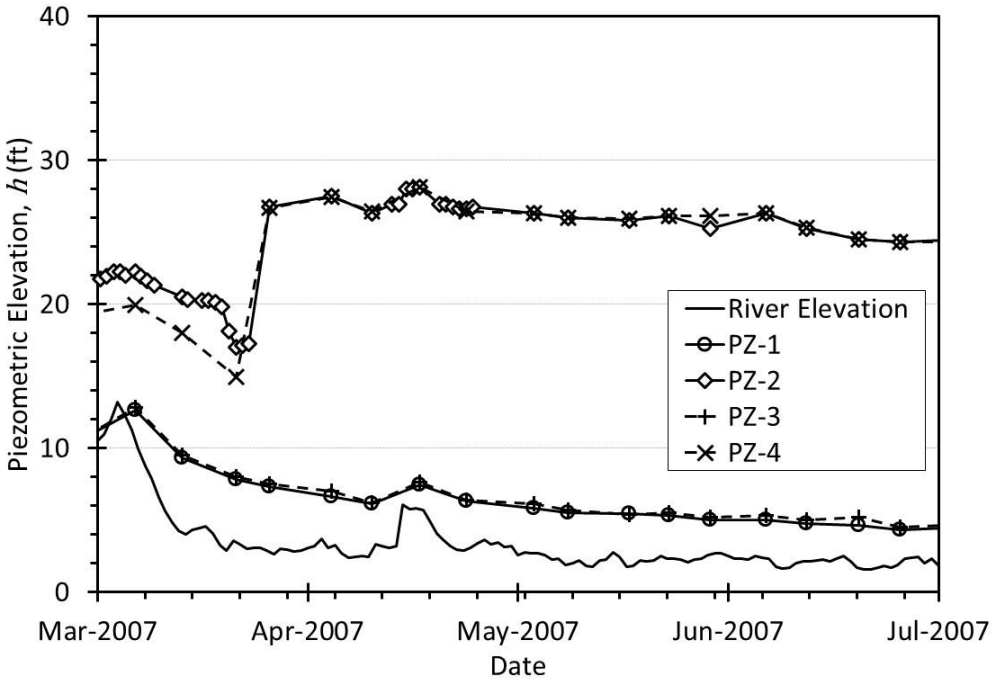


**Figure 13-11 Observations from piezometers and nearby waterway.**

## 13.6 GEOTECHNICAL DATA MANAGEMENT SYSTEMS

Geotechnical data management systems have become an important component of geotechnical site characterization, design, and construction. As a result, incorporation of laboratory and field measurements from site characterization into geotechnical data management systems has become an important part of reporting for site characterization. At present, most transportation agencies utilize proprietary geotechnical management systems. Some states have developed "in-house" systems while others use commercial systems or some combination of the two. Some systems are relatively mature data management systems, while others are largely based on access to scanned documents.

Geotechnical data management generally refers to a data architecture and data transfer standard that synchronizes how geotechnical subsurface and construction data are controlled, accessed, and disseminated among various users, computer programs, and devices that require geotechnical data. Implementation of standards is intended to improve communication and efficient use of geotechnical data among agency/owners, engineers, and contractors. Examples of computer programs and devices intended to comply with geotechnical data management standards include not just programs for subsurface reporting (i.e., investigation log creation) but also field and laboratory data acquisition equipment and geotechnical analysis software. Geotechnical data management standards are intended to apply to all types of geotechnical data, including measurements from exploratory drilling and sampling, in situ testing, geophysics, and laboratory testing, as well as various data collected during construction. A prominent component of geotechnical data management standards is the inclusion of location data with all geotechnical information.

In the U.S., geotechnical data management efforts are ongoing and have focused on developing the Data Interchange for Geotechnical and Geoenvironmental Specialists (DIGGS) standard. Technically, DIGGS is an extensible markup language (XML) data exchange format. Practically, computer programs that comply with the data transfer standard can readily share location-based geotechnical information in a usable format. For example, if the DIGGS standard is used, a CPT sounding originating from a specialty contractor using one subsurface data program could be read by an agency using a different subsurface data program with ease, and without loss of information. The transfer would include numeric data and would not suffer from confusion regarding units of measure. The current version, DIGGS 2.0b, was released in May 2016 and is currently at the stage of being implemented by software vendors. DIGGS is intended to be an international standard. It is anticipated that the new DIGGS standard will be adopted by the Association of Geotechnical and Geoenvironmental Specialists (AGS) in the United Kingdom, replacing the current AGS standard.

THIS PAGE IS LEFT INTENTIONALLY BLANK

# CHAPTER 14
# REFERENCES


Aas, G., S. Lacasse, T. Lunne, and K. Hoeg (1986), "Use of In Situ Tests for Foundation Design on Clay," *Use of In Situ Tests in Geotechnical Engineering*, S.P. Clemence, Ed., ASCE, GSP 6, pp. 1-30.

AASHTO (2014), *AASHTO LRFD Bridge Design Specifications*, Seventh Edition, American Association of State Highway and Transportation Officials.

ACI (2008), *Building Code Requirements for Structural Concrete (ACI318-08) and Commentary*, American Concrete Institute, 465 pp.

Al-Khafaji, A.W.N., and O.B. Andersland (1992), "Equations for Compression Index Approximation," *Journal of Geotechnical Engineering*, ASCE, Vol. 118, No. 1, pp. 148-153. DOI: 10.1061/(ASCE)0733-9410(1992)118:1(148)

Al-Tabbaa, A., and D.M. Wood (1987), "Some measurements of the permeability of kaolin" *Geotechnique*, Institution of Civil Engineers, Vol. 37, No. 4, pp. 499-514. DOI: 10.1680/geot.1987.37.4.499

Altmeyer, W.T. (1955), "Discussion of Engineering Properties of Expansive Clays," *Proceedings of the American Society of Civil Engineers*, ASCE, Vol. 87 (658), pp. 17-19.

Alwail, T.A., C.L. Ho, and R.J. Fragaszy (1994), "Collapse mechanism of compacted clayey and silty sands," *Vertical and Horizontal Deformations of Foundations and Embankments*, Proceedings of Settlement '94, A.T. Yeung and G.Y Felio, Eds, ASCE, GSP 40, Vol. 2, pp. 1435-1446.

Amoroso, S., P. Monaco, F. Totani, G. Totani, and D. Marchetti (2013), "Site characterization by Seismic Dilatometer (SDMT) in the area of L'Aquila following the April 6, 2009 earthquake," *Geotechnical and Geophysical Site Characterization 4*, Proceedings of the 4th International Conference, Taylor and Francis Group, London, pp. 481-488.

Anderson, S.A. (2013), "Remote Sensing Applications for Landslides, Slopes and Embankments," *Proceedings of Geo-Congress 2013: Stability and Performance of Slopes and Embankments III*, ASCE, pp. 2211-2230. DOI: 10.1061/9780784412787.221

Anderson, D.M., and A.R. Tice (1972), "Predicting Unfrozen Water Contents in Frozen Soils from Surface Area Measurements," *Highway Research Record*, Highway Research Board, No. 393, pp. 12-18.

Andersen, K.H, and K. Schjetne (2013), "Database of Friction Angles of Sand and Consolidation Characteristics of Sand, Silt, and Clay," *Journal of Geotechnical and Geoenvironmental Engineering*, ASCE, Vol. 139, No. 7, pp. 1140-1155. DOI: 10.1061/(ASCE)GT.1943-5606.0000839.

Andresen, A., and P. Kolstad (1979), "The NGI 54-mm Samplers for Undisturbed Sampling of Clays and Representative Sampling of Coarser Materials," *Proceedings of the International Symposium on Soil Sampling*, Singapore, Japanese Society of Soil Mechanics and Foundation Engineering, pp. 13-21.

Andrus, R.D., and K.H. Stokoe, II (2000), "Liquefaction Resistance of Soils from Shear-Wave Velocity," *Journal of Geotechnical and Geoenvironmental Engineering*, ASCE, Vol. 126, No. 11, pp. 1015-1025. DOI: 10.1061/(ASCE)1090-0241(2000)126:11(1015)

Aoki, H., and Y. Matsukura (2008), "Estimating the unconfined compressive strength of intact rocks from Equotip hardness," *Bulletin of Engineering Geology and the Environment*, Springer-Verlag, Vol. 67, No. 1, pp. 23-29. DOI: 10.1007/s10064-007-0116-z

API (1993), *Recommended Practice for Planning, Designing and Constructing Fixed Offshore Platforms: Working Stress Design*, 20th Edition, American Petroleum Institute, Washington, DC, 191 pp.

Arango, I. (1997), "Historical and Continued Role of the Standard Penetration Test Method in Geotechnical Earthquake Engineering," *3rd Seismic Short Course on Evaluation and Mitigation of Earthquake Induced Liquefaction Hazards*, San Francisco, California.

ASCE (2007), *Geotechnical Baseline Reports for Construction: Suggested Guidelines*, American Society of Civil Engineers, Technical Committee on Geotechnical Reports of the Underground Technology Research Council, Reston, Va., 72 pp.

ASTM C496 (2011), *Standard Test Method for Splitting Tensile Strength of Cylindrical Concrete Specimens*, ASTM International. DOI: 10.1520/C0496_C0496M-11

ASTM D2487 (2011), *Standard Practice for Classification of Soils for Engineering Purposes (Unified Soil Classification System)*, ASTM International. DOI: 10.1520/D2487-11

ASTM D2573 (2015), *Standard Test Method for Field Vane Shear Test in Saturated Fine-Grained Soils*, ASTM International. DOI: 10.1520/D2573_D2573M-15

ASTM D3282 (2015), *Practice for Classification of Soils and Soil-Aggregate Mixtures for Highway Construction Purposes*, ASTM International. DOI: 10.1520/D3282-15

ASTM D4186 (2012), *Standard Test Method for One-Dimensional Consolidation Properties of Saturated Cohesive Soils Using Controlled-Strain Load*, ASTM International, DOI: 10.1520/D4186_D4186M-12E01

ASTM D4647 (2013), *Standard Test Methods for Identification and Classification of Dispersive Clay Soils by the Pinhole Test*, ASTM International. DOI: 10.1520/D4647_D4647M-13

ASTM D4971 (2016), *Standard Test Method for Determining In Situ Modulus of Deformation of Rock Using Diametrically Loaded 76-mm (3-in) Borehole Jack*, ASTM International. DOI: 10.1520/D4971-16

ASTM D5092 (2010), *Standard Practice for Design and Installation of Groundwater Monitoring Wells*, ASTM International. DOI: 10.1520/D5092-04R10E01

ASTM D5607 (2008), *Standard Test Method for Performing Laboratory Direct Shear Strength Tests of Rock Specimens Under Constant Normal Force*, ASTM International. DOI: 10.1520/D5607-08.

ASTM D5878 (2008), *Standard Guides for Using Rock-Mass Classification Systems for Engineering Purposes*, ASTM International. DOI: 10.1520/D5878-08

ASTM D6429 (2011), *Standard Guide for Selecting Surface Geophysical Methods*, ASTM International. DOI: 10.1520/D6429-99R11E01

ASTM D7012 (2014), *Standard Test Methods for Compressive Strength and Elastic Moduli of Intact Rock Core Specimens under Varying States of Stress and Temperatures*, ASTM International. DOI: 10.1520/D7012-14.

Aufmuth, R.E. (1973), "A systematic determination of engineering criteria for rocks," *Bulletin of the Association of Engineering Geologists*, Vol. 11, pp. 235-245.

Aydin, A. (2009), "ISRM Suggested method for determination of the Schmidt hammer rebound hardness: Revised version," *International Journal of Rock Mechanics and Mining Sciences*, Elsevier, Vol. 46, No. 3, pp. 627-634. DOI: 10.1016/j.ijrmms.2008.01.020

Azadi, M.R.E., and S.R. Monfared (2012), "Fall Cone Test Parameters and Their Effects on the Liquid and Plastic Limits of Homogeneous and Non-Homogeneous Soil Samples," *Electronic Journal of Geotechnical Engineering*, Vol. 17, pp. 1615-1646. http://www.ejge.com/2012/Ppr12.132alr.pdf

Azimian, A., R. Ajalloeian, and L. Fatehi (2014), "An Empirical Correlation of Uniaxial Compressive Strength with P-Wave Velocity and Point Load Strength Index on Marly Rocks Using Statistical Method," *Geotechnical and Geological Engineering*, Vol. 32, No. 1, pp. 205-214. DOI: 10.1007/s10706-013-9703-x

Azzouz, A.S., R.J. Krizek, and R.B. Corotis (1976), "Regression analysis of soil compressibility," *Soils and Foundations*, Japanese Society for Soil Mechanics and Foundation Engineering, Vol. 16, No. 2, pp. 19-29. DOI: 10.3208/sandf1972.16.2_19

Baecher, G.B. (1982), "Statistical methods in site characterization," *Proceedings of the Engineering Foundation Conference on Updating Subsurface Exploration and Testing for Engineering Purposes*, Santa Barbara, pp. 463-492.

Baecher, G.B. (1983), "Simplified geotechnical data analysis," In *Reliability Theory and Its Application in Structural and Soil Mechanics*, Springer, pp. 257-277.

Baecher, G.B., and J.T. Christian (2003), *Reliability and Statistics in Geotechnical Engineering*, John Wiley and Sons, 605 pp.

Baguelin, F., J.F. Jezequel, E. Le Mee, and A. Le Mehaute (1972), "Expansion of cylindrical probes in cohesive soils, *Journal of the Soil Mechanics and Foundations Division*, ASCE, Vol. 98, No. SM11, pp. 1129-1142.

Baguelin, F., J.F. Jezequel, and D.H. Shields (1978), *The Pressuremeter and Foundation Engineering*, Trans Tech Publications, 617 pp.

Baldi, G., R. Bellotti, V. Ghionna, M. Jamiolkowski, S. Marchetti, and E. Pasqualini (1986), "Flat Dilatometer Tests in Calibration Chambers," *Use of In Situ Tests in Geotechnical Engineering*, S.P. Clemence, Editor, ASCE, GSP No. 6., pp. 431-446.

Baligh, M.M., and J-N Levadoux (1986), "Consolidation after Undrained Piezocone Penetration. II: Interpretation," *Journal of Geotechnical Engineering*, ASCE, Vol. 112, No. 7, pp. 727-745. DOI: 10.1061/(ASCE)0733-9410(1986)112:7(727)

Bang, E-S, and D-S Kim (2007), "Evaluation of shear wave velocity profile using SPT based uphole method," *Soil Dynamics and Earthquake Engineering*, Elsevier, Vol. 27, No, 8, pp. 741-758. DOI: 10.1016/j.soildyn.2006.12.004

Barden, L., A. McGown, and K. Collins (1973), "The collapse mechanism in partly saturated soil," *Engineering Geology*, Elsevier, Vol. 7, No. 1, pp. 49-60. DOI: 10.1016/0013-7952(73)90006-9

Barton, N. (1973), "Review of a new shear-strength criterion for rock joints," *Engineering Geology*, Elsevier, Vol. 7, No. 4, pp. 287-332. DOI: 10.1016/0013-7952(73)90013-6

Barton, N., and V. Choubey (1977), "The Shear Strength of Rock Joints in Theory and Practice," *Rock Mechanics*, Springer-Verlag, Vol. 10, No. 1-2, pp. 1-54.

Basak, P. (1972), "Soil Structure and Its Effects on Hydraulic Conductivity," *Soil Science*, Williams and Wilkins, Vol. 114, No. 6, pp. 417-422.

Battaglio, M., M. Jamiolkowski, R. Lancellotta, and R. Maniscalco (1981), "Piezometer Probe Test in Cohesive Deposits," *Proceedings of the ASCE National Convention*, St. Louis, Missouri, ASCE, pp. 264-302.

Becker, E., C.K. Chan, and H.B. Seed (1972), *Strength and Deformation Characteristics of Rockfill Materials in Plane Strain and Triaxial Compression Tests*, Department of Civil Engineering, University of California, Berkeley, Report No. TE-72-3.

Becker, D.B., J.H.A. Crooks, K. Been, and M.G. Jefferies (1987), "Work as a criterion for determining in situ and yield stresses in clays," *Canadian Geotechnical Journal*, National Research Council of Canada, Vol. 24, No. 4, pp. 549-564. DOI: 10.1139/t87-070

Begemann, H.K.S.P. (1965), "The Friction Jacket Cone as an Aid in Determining the Soil Profile," *Proceedings of the 6th International Conference on Soil Mechanics and Foundation Engineering*, Butterworth and Company, Vol. 1, pp. 17-20.

Bell, F.G., and R.R. Maud (1994), "Dispersive soils: a review from a South African perspective," *Quarterly Journal of Engineering Geology and Hydrology*, Geological Society of London, Vol. 27, No. 3, pp. 195-210. DOI: 10.1144/GSL.QJEGH.1994.027.P3.02

Bellotti, R., V. Ghionna, M. Jamiolkowski, R. Lancellotta, and G. Manfredini, (1986), "Deformation Characteristics of Cohesionless Soils from In Situ Tests," *Use of In Situ Tests in Geotechnical Engineering*, S.P. Clemence, Editor, ASCE, GSP No. 6, pp. 47-73.

Bellotti, R., M. Jamiolkowski, D.C.F. Lo Presti, and D.A. O'Neill (1996), "Anisotropy of Small Strain Stiffness in Ticino sand," *Geotechnique*, Institution of Civil Engineers, Vol. 46, No. 1, pp.115-132. DOI: 10.1680/geot.1996.46.1.115

Benoit, J. and A.J. Lutenegger (1992), "Determining lateral stress in soft clays," *Predictive Soil Mechanics*, Proceedings of the Wroth Memorial Symposium, G.T. Houlsby and A.N. Schofield, Editors, Oxford, U.K., Thomas Telford, pp. 135-155.

Bieniawski, Z.T. (1975), "The point-load test in geotechnical practice," *Engineering Geology*, Vol. 9, No. 1, pp. 1-11.

Bieniawski, Z.T. (1978), "Determining rock mass deformability – experiences from case histories," *International Journal of Rock Mechanics and Mining Sciences & Geomechanics Abstracts*, Elsevier, Vol. 15, No. 5, pp. 237-247.

Bieniawski, Z.T. (1989), *Engineering Rock Mass Classifications*, John Wiley and Sons, 251 pp.

Bjerrum, L., and N.E. Simons (1960), "Comparison of Shear Strength Characteristics of Normally Consolidated Clays," *Proceedings of the ASCE Research Conference on Shear Strength of Cohesive Soils*, ASCE, pp. 711-726.

Bjerrum, L., S. Kringstad, and O. Kummeneje (1961), "The Shear Strength of a Fine Sand," *Proceedings of the 5th International Conference on Soil Mechanics and Foundation Engineering*, Paris, Vol. 1, pp. 29-38.

Boeckmann, A.Z., and J.E. Loehr (2016), *The Influence of Geotechnical Investigation and Subsurface Conditions on Claims, Change Orders, and Cost Overruns*, NCHRP Synthesis of Highway Practice, Transportation Research Board, 102 pp.

Boone, S.J., and A.J. Lutenegger (1997), "Carbonates and cementation of glacially derived cohesive soils in New York State and southern Ontario," *Canadian Geotechnical Journal*, NRC Research Press, Vol. 34, No. 4, pp. 534-550. DOI: 10.1139/t97-017

Boone, S.J. (2010), "A critical reappraisal of 'preconsolidation pressure' interpretations using the oedometer test," *Canadian Geotechnical Journal*, NRC Research Press, Vol. 47, No. 3, pp. 281-296. DOI: 10.1139/T09-093

Boulanger, R.W., and I.M. Idriss (2006), "Liquefaction Susceptibility Criteria for Silts and Clays," *Journal of Geotechnical and Geoenvironmental Engineering*, ASCE, Vol. 132, No. 11, pp. 1413-1426. DOI: 10.1061/(ASCE)1090-0241(2006)132:11(1413)

Bouwer, H. (1966), "Rapid field measurement of air entry value and hydraulic conductivity of soil as significant parameters in flow system analysis," *Water Resources Research*, American Geophysical Union, Vol. 2, No. 4, pp. 729-738. DOI: 10.1029/WR002i004p00729

Bouwer, H., and R.C. Rice (1976), "A Slug Test for Determining Hydraulic Conductivity of Unconfined Aquifers With Completely or Partially Penetrating Wells," *Water Resources Research*, American Geophysical Union, Vol. 12, No. 3, pp. 423-428. DOI: 10.1029/WR012i003p00423

Bouwer, H. (1978), *Groundwater Hydrology*, McGraw-Hill, 480 pp.

Bouwer, H. (1986), "Intake Rate: Cylinder Infiltrometer," *Methods of Soil Analysis. Part 1. Physical and Mineralogical Methods*, Agronomy Monograph No. 9, American Society of Agronomy, Madison, Wisconsin, pp. 825-844.

Bozozuk, M. (1971), "Effect of Sampling, Size, and Storage on Test Results for Marine Clay," *Sampling of Soil and Rock*, American Society for Testing and Materials, ASTM STP 483, pp. 121-131. DOI: 10.1520/STP26663S

Bray, J.D., and R.B. Sancio (2006), "Assessment of the Liquefaction Susceptibility of Fine-Grained Soils," *Journal of Geotechnical and Geoenvironmental Engineering*, ASCE, Vol. 132, No. 9, pp. 1165-1177. DOI: 10.1061/(ASCE)1090-0241(2006)132:9(1165)

Briaud, J.L. (1992), *The Pressuremeter*, A.A. Balkema, 336 pp.

Briaud, J.L. (1997), "SALLOP: Simple Approach for Lateral Loads on Piles," *Journal of Geotechnical and Geoenvironmental Engineering*, ASCE, Vol 123, No. 10, pp. 958–964. DOI: 10.1061/(ASCE)1090-0241(1997)123:10(958)

Briaud, J-L, X. Zhang, and S. Moon (2003), "Shrink Test – Water Content Method for Shrink and Swell Predictions," *Journal of Geotechnical and Geoenvironmental Engineering*, ASCE, Vol. 129, No. 7, pp. 590-600. DOI: 10.1061/(ASCE)1090-0241(2003)129:7(590)

Briaud, J-L (2013), *Geotechnical Engineering: Unsaturated and Saturated Soils*, John Wiley and Sons, 1024 pp.

Broch, E., and J.A. Franklin (1972), "The point-load strength test," *International Journal of Rock Mechanics and Mining Sciences & Geomechanics Abstracts*, Vol. 9, No. 6, pp. 669-676. DOI: 10.1016/0148-9062(72)90030-7

Brown, D.A. (1990), "Construction and Design of Drilled Shafts in Hard Pinnacled Limestones," *Transportation Research Record*, Transportation Research Board, National Research Council, Washington, D.C., Vol. 1277, pp. 148–152.

Brown, D.A., J.P. Turner, and R.J. Castelli (2010), *Drilled Shafts: Construction Procedures and LRFD Design Methods*, Geotechnical Engineering Circular No. 10, National Highway Institute, Federal Highway Administration, Report FHWA NHI-10-016, 970 pp.

Brown, R.J.E. (1970), *Permafrost in Canada: Its Influence on Northern Development*, University of Toronto Press, 242 pp.

Bruckno, B., A. Vaccari, E. Hoppe, W. Niemann, and E. Campbell (2013), "Validation of Interferometric Synthetic Aperture Radar as a Tool for Identification of Geohazards and At-Risk Transportation Infrastructure," *Proceedings of the 64th Highway Geology Symposium (HGS)*, North Conway, New Hampshire, Highway Geology Symposium.

Bryson, L.S., I.C. Gomez-Gutierrez, and T.C. Hopkins (2012), "Development of a new durability index for compacted shale," *Engineering Geology*, Vol. 139-140, pp. 66-75. DOI: 10.1016/j.enggeo.2012.04.011

Buckle, I., I. Friedland, J. Mander, G. Martin, R. Nutt, and M. Power (2006), *Seismic Retrofitting Manual for Highway Structures: Part I – Bridges*, Federal Highway Administration, FHWA-HRT-06-032, 656 pp.

Budhu, M. (1985), "The Effect of Clay Content on Liquid Limit from a Fall Cone and the British Cup Device," *Geotechnical Testing Journal*, American Society for Testing and Materials, Vol. 8, No. 2, Paper GTJ10515J, pp. 91-95. DOI: 10.1520/GTJ10515J

Burns, S.E., and P.W. Mayne (1995), "Coefficient of Consolidation from Piezocone Dissipation Tests in Over-consolidated Clays," *Proceedings of Cone Penetration Testing (CPT'95)*, Swedish Geotechnical Society, Vol. 2, pp. 137-142.

Burns, S.E., and P.W. Mayne (1996), "Small-and High-Strain Measurements of In Situ Soil Properties Using the Seismic Cone Penetrometer," *Transportation Research Record: Journal of the Transportation Research Board*, Vol. 1548, pp.81-88. DOI: 10.3141/1548-12

Burns, S.E., and P.W. Mayne (1998), "Monotonic and dilatory pore-pressure decay during piezocone tests in clay," *Canadian Geotechnical Journal*, National Research Council of Canada, Vol. 35, No. 6, pp. 1063-1073. DOI: 10.1139/t98-062

Buyuksagis, I.S., and R.M. Goktan (2007), "The effect of Schmidt hammer type on uniaxial compressive strength prediction of rock," *International Journal of Rock Mechanics and Mining Sciences*, Elsevier, Vol. 44, No. 2, pp. 299-307. DOI: 10.1016/j.ijrmms.2006.07.008

Caltrans (2010), *Soil and Rock Logging, Classification, and Presentation Manual*, 2010 Edition, State of California Department of Transportation, Division of Engineering Services, Geotechnical Services, 82 pp.

Campanella, R.G., P.K. Robertson, and D.J. Gillespie (1983), "Cone penetration testing in deltaic soils," *Canadian Geotechnical Journal*, National Research Council of Canada, Vol. 20, No. 1, pp. 23-35. DOI: 10.1139/t83-003

Campanella, R.G., P.K. Robertson, and D. Gillespie (1986), "Seismic cone penetration test," *Use of In Situ Tests in Geotechnical Engineering*, S.P. Clemence, Ed., ASCE, GSP 6, pp. 116-130.

Campanella, R.G., and P.K. Robertson (1988), "Current status of the piezocone test," *Penetration Testing 1988*, Proceedings of the 1st International Symposium on Penetration Testing, A.A. Balkema, Vol. 1, pp. 93-116.

Carrier, W.D., III (2003), "Goodbye, Hazen; Hello, Kozeny-Carman," *Journal of Geotechnical and Geoenvironmental Engineering*, ASCE, Vol. 129, No. 11, pp. 1054-1056. DOI: 10.1061/(ASCE)1090-0241(2003)129:11(1054)

Carter, D.L., M.D. Heilman, and C.L. Gonzalez (1965), "Ethylene Glycol Monoethyl Ether for Determining Surface Area of Silicate Minerals," *Soil Science*, The Williams and Wilkins Company, Vol. 100, No. 5, pp. 356-360.

Casagrande, A. (1936), "The Determination of the Preconsolidation Load and Its Practical Significance," *Proceedings of the First International Conference on Soil Mechanics and Foundation Engineering*, Cambridge, Massachusetts, Harvard Printing Office, Vol. 3, pp. 60-64.

Casagrande, A., and R.E. Fadum (1940), *Notes on Soil Testing for Engineering Purposes*, Harvard Soil Mechanics Series, No. 8, Cambridge, Massachusetts.

Castellanos, B., T.L. Brandon, I. Stephens, and L. Walshire (2013), "Measurement of Fully Softened Shear Strength," *Proceedings of Geo-Congress 2013: Stability and Performance of Slopes and Embankments III*, ASCE, pp. 234-244. DOI: 10.1061/9780784412787.024

Castellanos, B.A., T.L. Brandon, and D.R. VandenBerge (2016), "Correlations for Fully Softened Shear Strength Parameters," *Geotechnical Testing Journal*, ASTM International, Vol. 39, No. 4, pp. 568-581. DOI: 10.1520/GTJ20150184

Castelli, R.J., D.P. Richards, and G.T. Clark (2015), "Design and Construction of a Deep Excavation in Extremely Poor Rock Mass," *Proceedings of the 49th U.S. Rock Mechanics/Geomechanics Symposium*, San Francisco, American Rock Mechanics Association, Paper ARMA 15-396.

Caterpillar (2015), *Caterpillar Performance Handbook*, Caterpillar, Peoria, Illinois, Edition 45.

CDOT (2017), Glenwood Canyon, Colorado Department of Transportation. Web: https://www.codot.gov/programs/geotech/rockfall/gleenwood-canyon.html Accessed February 14, 2017.

Cerato, A.B., and A.J. Lutenegger (2002), "Determination of Surface Area of Fine-Grained Soils by the Ethylene Glycol Monoethyl Ether (EGME) Method," *Geotechnical Testing Journal, ASTM International*, Vol. 25, No. 3, pp. 1-7. DOI: 10.1520/GTJ11087J

Cerato, A.B., and A.J. Lutenegger (2006), "Shrinkage of Clays," *Unsaturated Soils 2006*, Proceedings of the 4th International Conference on Unsaturated Soils, ASCE, GSP 147, pp. 1097-1108. DOI: 10.1061/40802(189)89

Chabrillat, S., A.F.H. Goetz, L. Krosley, and H.W. Olsen (2002), "Use of hyperspectral images in the identification and mapping of expansive clay soils and the role of spatial resolution," *Remote Sensing of Environment*, Vol. 82, No. 2-3, Elsevier, pp. 431-445. DOI: 10.1016/S0034-4257(02)00060-3

Chan, H.T., and T.C. Kenney (1973), "Laboratory Investigation of Permeability Ratio of New Liskeard Varved Soil," *Canadian Geotechnical Journal*, National Research Council of Canada, Vol. 10, No. 3, pp. 453-472. DOI: 10.1139/t73-038

Chandler, R.J. (1988), "The In-Situ Measurement of the Undrained Shear Strength of Clays Using the Field Vane," *Vane Shear Testing in Soils: Field and Laboratory Studies*, American Society for Testing and Materials, A.F. Richards, Ed., ASTM STP 1014, pp. 13-44. DOI: 10.1520/STP10319S

Chandler, R.J., S. Leroueil, and N.A. Trenter (1990), "Measurements of the permeability of London Clay using a self-boring permeameter," *Geotechnique*, ICE Publishing, Vol. 40, No. 1, pp. 113-124. DOI: 10.1680/geot.1990.40.1.113

Chang, M.F. (1991), "Interpretation of overconsolidation ratio from in situ tests in recent clay deposits in Singapore and Malaysia," *Canadian Geotechnical Journal*, National Research Council of Canada, Vol. 28, No. 2, pp. 210-225. DOI: 10.1139/t91-028

Chapuis, R.P. (1989), "Shape Factors for Permeability Tests in Boreholes and Piezometers," *Groundwater*, National Ground Water Association, Vol. 27, No. 5, pp. 647-654. DOI: 10.1111/j.1745-6584.1989.tb00478.x

Chapuis, R.P., and D.E. Gill (1989), "Hydraulic anisotropy of homogeneous soils and rocks: influence of the densification process," *Bulletin of the International Association of Engineering Geology*, Springer-Verlag, Vol. 39, No. 1, pp. 75-86. DOI: 10.1007/BF02592538

Christian, J.T. (2004), "Geotechnical engineering reliability: How well do we know what we are doing?" *Journal of Geotechnical and Geoenvironmental Engineering*, ASCE, Vol. 130, No. 10, pp. 1556-1571. DOI: 10.1061/(ASCE)1090-0241(2004)130:10(985)

Christopher, B.R., C. Schwartz, and R. Boudreau (2006), *Geotechnical Aspects of Pavements*, National Highway Institute, Federal Highway Administration, Report FHWA NHI-05-037, 888 pp.

Churchman, G.J., and C.M. Burke (1991), "Properties of sub soils in relation to various measures of surface area and water content," *Journal of Soil Science*, Blackwell Publishing Ltd., Vol. 42, No. 3, pp. 463-478. DOI: 10.1111/j.1365-2389.1991.tb00423.x

Clayton, C.R.I. (2001), "Managing geotechnical risk: time for a change?," *Proceedings of the Institution of Civil Engineers – Geotechnical Engineering*, ICE Publishing, Vol. 149, No. 1, pp. 3-11. DOI: 10.1680/geng.2001.149.1.3

Clayton, C.R.I. (2011), "Stiffness at small strain: research and practice," *Geotechnique*, ICE Publishing, Vol 61, No. 1, pp. 5-37. DOI: 10.1680/geot.2011.61.1.5

Clemence, S.P., and A.O. Finbarr (1981), "Design Considerations for Collapsible Soils," *Journal of the Geotechnical Engineering Division*, ASCE, Vol. 107, No. 3, pp. 305-317.

Clough, G.W., N.S. Rad, R.C. Bachus, and N. Sitar (1981), "Cemented Sands Under Static Loading," *Journal of the Geotechnical Engineering Division*, ASCE, Vol. 107, No. 6, pp. 799-817.

Coates, D.F., and M. Gyenge (1966), "Plate-Load Testing on Rock for Deformation and Strength Properties," *Testing Techniques for Rock Mechanics*, ASTM STP 402, ASTM International, pp. 19-35. DOI: 10.1520/STP45134S

Çobanoglu, I., and S.B. Çelik (2008), "Estimation of uniaxial compressive strength from point load strength, Schmidt hardness and P-wave velocity," *Bulletin of Engineering Geology and the Environment*, Springer-Verlag, Vol. 67, No. 4, pp. 491-498. DOI: 10.1007/s10064-008-0158-x

Coduto, D.P. (2001), *Foundation Design: Principles and Practices*, 2nd Edition, Prentice-Hall, 883 pp.

Conway, B.D., and J.P. Cook (2013), "Monitoring Evaporite Karst Activity and Land Subsidence in the Holbrook Basin, Arizona using Interferometric Synthetic Aperture Radar (InSAR)," *Sinkholes and the Engineering and Environmental Impacts of Karst*, Proceedings of the Thirteenth Multidisciplinary Conference, National Cave and Karst Research Institute, Carlsbad, New Mexico, pp. 187-194.

Coon, R.F., and A.H. Merritt (1970), "Predicting In Situ Modulus of Deformation Using Rock Quality Indexes," *Determination of the In Situ Modulus of Deformation of Rock*, American Society for Testing and Materials, ASTM STP 477, pp. 154-173. DOI: 10.1520/STP29146S

Cour, F.R. (1971), "Inflection Point Method for Computing $c_v$," *Journal of the Soil Mechanics and Foundations Division*, ASCE, Vol. 97, No. 5, pp. 827-831.

Cox, B.R., and A.N. Beekman (2011), "Intramethod Variability in ReMi Dispersion Measurements and $V_s$ Estimates at Shallow Bedrock Sites," *Journal of Geotechnical and Geoenvironmental Engineering*, ASCE, Vol. 137, No. 4, pp. 354-362. DOI: 10.1061/(ASCE)GT.1943-5606.0000436

Cox, B.R., C.M. Wood, and D.P. Teague (2014), "Synthesis of the UTexas1 Surface Wave Dataset Blind-Analysis Study: Inter-Analyst Dispersion and Shear Wave Velocity Uncertainty," *Geo-Congress*

*2014 Technical Papers: Geo-Characterization and Modeling for Sustainability*, ASCE, GSP 234, pp. 850-859. DOI: 10.1061/9780784413272.083

Dakshanamurthy, V., and V. Raman (1973), "A simple method of identifying an expansive soil," *Soils and Foundations*, Japanese Society of Soil Mechanics and Foundation Engineering, Vol. 13, No. 1, pp. 97-104. DOI: 10.3208/sandf1972.13.97

Dalton, M.G., B.E. Huntsman, and K. Bradbury (1991), "Acquisition and Interpretation of Water-Level Data," *Practical Handbook of Ground-Water Monitoring*, Lewis Publishers, D.M. Nielsen, Ed., pp. 367-395.

Daniel, D.E. (1989), "In Situ Hydraulic Conductivity Tests for Compacted Clay," *Journal of Geotechnical Engineering*, ASCE, Vol. 115, No. 9, pp. 1205-1226. DOI: 10.1061/(ASCE)0733-9410(1989)115:9(1205)

Daniel, D.E. (1994), "State-of-the-Art: Laboratory Hydraulic Conductivity Tests for Saturated Soils," *Hydraulic Conductivity and Waste Contaminant Transport in Soil*, American Society for Testing and Materials, D.E. Daniel and S.J. Trautwein, Editors, ASTM STP 1142, pp. 30-78. DOI: 10.1520/STP23884S

Darendeli, M.B. (2001), *Development of a New Family of Normalized Modulus Reduction and Material Damping Curves*, Ph.D. Dissertation, Department of Civil Engineering, The University of Texas, Austin, Texas, 362 pp.

Das, B.M. (1985a), *Principles of Geotechnical Engineering*, PWS Publishers, Boston, 571 pp.

Das, B.M. (1985b), "Evaluation of the Point Load Strength for Soft Rock Classification," *Proceedings of the Fourth International Conference on Ground Control in Mining*, Morgantown, West Virginia, pp. 220-226.

Das, B.M. (2011), *Principles of Foundation Engineering*, Cengage Learning, 7th Edition, 794 pp.

Dascal, O., G. Pouliot, and J. Hurtubise (1977), "Erodibility Tests on a Sensitive, Cemented Marine Clay (Champlain Clay)," *Dispersive Clays, Related Piping, and Erosion in Geotechnical Projects*, J.L. Sherard and R.S. Decker, Eds., American Society for Testing and Materials, ASTM STP 623, pp. 74-93. DOI: 10.1520/STP26981S

Dasog, G.S., D.F. Acton, A.R. Mermut, E De Jong (1988), "Shrink-Swell Potential and Cracking in Clay Soils of Saskatchewan," *Canadian Journal of Soil Science*, NRC Research Press, Vol. 68, No. 2, pp. 251-260. DOI: 10.4141/cjss88-025

Davidson, J.L., and A. Boghrat (1983), "Flat Dilatometer Testing in Florida, U.S.A.," *Proceedings of the International Conference on Soil and Rock Investigation by In Situ Testing*, Paris, France, Vol. II, pp. 251-255.

Decker, R.S., and L.P. Dunnigan (1977), "Development and Use of the Soil Conservation Service Dispersion Test," *Dispersive Clays, Related Piping, and Erosion in Geotechnical Projects*, J.L. Sherard and R.S. Decker, Eds., American Society for Testing and Materials, ASTM STP 623, pp. 94-109. DOI: 10.1520/STP26982S

Decker, J.B., K.M. Rollins, and J.C. Ellsworth (2008), "Corrosion Rate Evaluation and Prediction for Piles Based on Long-Term Field Performance," *Journal of Geotechnical and Geoenvironmental Engineering*, ASCE, Vol. 134, No. 3, pp. 341-351. DOI: 10.1061/(ASCE)1090-0241(2008)134:3(341)

Deere, D.U., and R.P. Miller (1966), *Engineering classification and index properties of rock*, Air Force Weapons Laboratory, New Mexico, Technical Report No. AFWL-TR-65-116, 300 pp.

Deere, D.U., A.J. Hendron, F.D. Patton, and E.J. Cording (1967), "Design of surface and near surface construction in rock," *Proceedings of the 8th U.S. Symposium on Rock Mechanics – Failure and Breakage of Rock*, American Institute of Mining, Metallurgical and Petroleum Engineers, Inc., pp. 237-302.

Deere, D.U., and D.W. Deere (1988), "The Rock Quality Designation (RQD) Index in Practice," *Rock Classification Systems for Engineering Purposes*, Louis Kirkaldie, Ed., American Society for Testing and Materials, ASTM STP 984, pp. 91-101.

Deere, D.U., and D.W. Deere (1989), *Rock quality designation (RQD) after 20 years*. U.S. Army Corps of Engineers Contract Report GL-89-1, Waterways Experiment Station, 100 pp. DOI: 10.1520/STP48465S

DeGroot, D.J., and A.J. Lutenegger (1994), "A Comparison Between Field and Laboratory Measurements of Hydraulic Conductivity in a Varved Clay," *Hydraulic Conductivity and Waste Contaminant Transport in Soil*, American Society for Testing and Materials, ASTM STP 1142, pp. 300-317. DOI: 10.1520/STP23894S

DeGroot, D.J., and C.C. Ladd (2012), "Site Characterization for Cohesive Soil Deposits Using Combined In Situ and Laboratory Testing," *Geotechnical Engineering State of the Art and Practice*, ASCE, pp. 565-607. DOI: 10.1061/9780784412138.0022

Demartinecourt, J.P., and G.E. Bauer (1983), "The Modified Borehole Shear Device," *Geotechnical Testing Journal*, American Society for Testing and Materials, Vol. 6, No. 1, pp. 24-29. DOI: 10.1520/GTJ10820J

Denisov, N.J. (1951), *The Engineering Properties of Loess and Loess Loams*, Gosstroiizdat, Moscow, USSR.

Dewhurst, D.N., K.M. Brown, M.B. Clennell, and G.K. Westbrook (1996), "A comparison of the fabric and permeability anisotropy of consolidated and sheared silty clay," *Engineering Geology*, Elsevier, Vol. 42, No. 4, pp. 253-267. DOI: 10.1016/0013-7952(95)00089-5

Dickenson, S.E., and M.W. Baillie (1999), *Predicting Scour in Weak Rock of the Oregon Coast Range*, Oregon Department of Transportation, SPR 382, 101 pp.

Ding, D., W.J. Likos, and J.E. Loehr (2014), "Variability and Uncertainty in Consolidation and Settlement Parameters from Different Sampling and Testing Methods," *From Soil Behavior Fundamentals to Innovations in Geotechnical Engineering*, Symposium Honoring Roy E. Olson, ASCE, GSP 233, pp. 338-351. DOI: 10.1061/9780784413265.027

Douglas, B.J., and R.S. Olsen (1981), "Soil Classification Using Electric Cone Penetrometer," *Proceedings of the Symposium on Cone Penetration Testing and Experience*, G.M. Norris and R.D. Holtz, Eds., ASCE, pp. 209-227.

Douglas, B.J. (1984), *The Electric Cone Penetrometer Test: A User's Guide to Contracting for Services, Quality Assurance, Data Analysis*, The Earth Technology Corporation, Long Beach, California.

Doroudian, M., and M. Vucetic (1995), "A Direct Simple Shear Device for Measuring Small-Strain Behavior," *Geotechnical Testing Journal*, ASTM International, Vol. 18, No. 1. pp 69-85. DOI: 10.1520/GTJ10123J

Dos Santos, M.P.P., and E. DeCastro (1965), "Soil Erosion in Roads," *Proceedings of the 6th International Conference on Soil Mechanics and Foundation Engineering*, Butterworth and Company Ltd., Vol. 1, pp. 116-118.

Dreimanis, A. (1968), "Quantitative Gasometric Determination of Calcite and Dolomite by Using Chittick Apparatus," *Journal of Sedimentary Petrology*, Society for Sedimentary Geology, Vol. 32, No. 3, pp. 520-529. DOI: 10.1306/74D70D08-2B21-11D7-8648000102C1865D

Driscoll, F.G. (1986), *Groundwater and Wells*, 2nd Edition, Johnson Division, Signal Environmental Systems, 1089 pp.

Dudley, J.H. (1970), "Review of Collapsing Soils," *Journal of the Soil Mechanics and Foundations Division*, ASCE, Vol. 96, No. 3, pp. 925-947.

Duncan, J.M. (2000), "Factors of Safety and Reliability in Geotechnical Engineering," *Journal of Geotechnical and Geoenvironmental Engineering*, ASCE, Vol. 126, No. 4, pp. 307-316. DOI: 10.1061/(ASCE)1090-0241(2000)126:4(307)

Duncan, J.M., S.G. Wright, and T.L. Brandon (2014), *Soil Strength and Slope Stability*, 2nd Edition, John Wiley and Sons, 317 pp.

Dunnicliff, J. (1993), *Geotechnical Instrumentation for Monitoring Field Performance*, John Wiley and Sons, 577 pp.

Earth Science Australia (2017), *Aquifers*, Earth Science Australia. Web: http://earthsci.org/education/teacher/basicgeol/groundwa/groundwa.html#Aquifers Accessed January 28, 2017.

Elias, V., K.L. Fishman, B.R. Christopher, and R.R. Berg (2009), *Corrosion/Degradation of Soil Reinforcements for Mechanically Stabilized Earth Walls and Reinforced Soil Slopes*, National Highway Institute, Federal Highway Administration, Report FHWA-NHI-09-087, 142 pp.

EPRI (2012), *Transmission Structure Foundation Design Guide*, Electrical Power Research Institute, Report 1024138, 378 pp.

Erdik, M. (2001), "Report on 1999 Kocaeli and Duzce (Turkey) Earthquakes," *Structural Control for Civil and Infrastructure Engineering: Proceedings of the 3rd International Workshop on Structural Control*, Paris, France, F. Casciati and G. Magonette, Eds., World Scientific, pp. 149-186.

Evans, L.T., and J.M. Duncan (1982), *Simplified Analysis of Laterally Loaded Piles*, University of California, Berkeley, California, Report No. UCB/GT/82-04, 245 pp.

Farrar, D.M., and J.D. Coleman (1967), "The Correlation of Surface Area with other Properties of Nineteen British Clay Soils," *Journal of Soil Science*, Blackwell Publishing Ltd., Vol. 18, No. 1, pp. 118-124. DOI: 10.1111/j.1365-2389.1967.tb01493.x

Feda, J. (1964), "Colloidal Activity, Shrinking and Swelling of Some Clays," *Proceedings of the Soil Mechanics Seminar*, Loda, pp. 531-546.

Feng, T-W, and Y-J Lee (2001), "Coefficient of consolidation from the linear segment of the $t^{1/2}$ curve," *Canadian Geotechnical Journal*, National Research Council of Canada, Vol. 38, No. 4, pp. 901-909. DOI: 10.1139/t01-008

Fernuik, N., and M. Haug (1990), "Evaluation of In Situ Permeability Testing Methods," *Journal of Geotechnical Engineering*, ASCE, Vol. 116, No. 2, pp. 297-311. DOI: 10.1061/(ASCE)0733-9410(1990)116:2(297)

Ficker, T., and D. Martisek (2015), "Alternative Method for Assessing the Roughness Coefficients of Rock Joints," *Journal of Computing in Civil Engineering*, ASCE, Vol. 30, No. 4. DOI: 10.1061/(ASCE)CP.1943-5487.0000540

Finno, R.J., and C-K Chung (1992), "Stress-Strain-Strength Responses of Compressible Chicago Glacial Clays," *Journal of Geotechnical Engineering*, ASCE, Vol. 118, No. 10, pp. 1607-1625. DOI: 10.1061/(ASCE)0733-9410(1992)118:10(1607)

Franklin, J.A. (1981), "A Shale Rating System and Tentative Applications to Shale Performance," *Transportation Research Record*, Transportation Research Board, No. 790, pp. 2-12.

Fredlund, D.G., H. Rahardjo, and M.D. Fredlund (2012), *Unsaturated Soil Mechanics in Engineering Practice*, John Wiley and Sons, 926 pp. DOI: 10.1002/9781118280492

Gamez, J.A., and T.D. Stark (2014), "Fully Softened Shear Strength at Low Stresses for Levee and Embankment Design," *Journal of Geotechnical and Geoenvironmental Engineering*, ASCE, Vol. 140, No. 9, pp. 1-6. DOI: 10.1061/(ASCE)GT.1943-5606.0001151

Gazetas, G. (1983), "Analysis of machine foundation vibrations: state of the art," *International Journal of Soil Dynamics and Earthquake Engineering*, CML Publications, Vol. 2, No. 1, pp.2-42.

Geological Society of London (1977), "The Description of Rock Masses for Engineering Purposes," *Quarterly Journal of Engineering Geology*, Geological Society of London, Vol. 10, No. 4, pp. 355-388. DOI: 10.1144/GSL.QJEG.1977.010.04.01

Gerber, F.A., and H.J. Von Maltitz Harmse (1987), "Proposed Procedure for Identification of Dispersive Soils by Chemical Testing," *The Civil Engineer in South Africa*, Vol. 29, No. 10, pp. 397-399.

Germaine, J.T., and A.V. Germaine (2009), *Geotechnical Laboratory Measurements for Engineers*, John Wiley and Sons, 351 pp.

Gharahbagh, E.A., J. Rostami, and A.M. Palomino (2011), "New soil abrasion testing method for soft ground tunneling applications," *Tunnelling and Underground Space Technology*, Elsevier, Vol. 26, No. 5, pp. 604-613. DOI: 10.1016/j.tust.2011.04.003

Giacheti, et al. (2012)…Chapter 8, Section 8.4.1…

Gibbs, H.J. (1961), *Properties Which Divide Loose and Dense Uncemented Soil*, U.S. Bureau of Reclamation, Report No. EM-608.

Gibbs, H.J., and J.P. Bara (1962), "Predicting Surface Subsidence from Basic Soil Tests," *Field Testing of Soils*, P. Brown and W. Shockly, Eds., American Society for Testing and Materials, ASTM STP 322, pp. 231-247. DOI: 10.1520/STP47043S

Gibbs, H.J., and J.P. Bara (1967), "Stability Problems of Collapsing Soil," *Journal of the Soil Mechanics and Foundations Division*, ASCE, Vol. 93, No. 4, pp. 577-594.

Goodman, R.E. (1989), *Introduction to Rock Mechanics*, Second Edition, John Wiley and Sons, New York, 562 pp.

Goto, S., Y. Shamoto, and K. Tamaoki (1987), "Dynamic properties of undisturbed gravel sample by the in situ frozen," *Proceedings of the 8th Asian Regional Conference on Soil Mechanics and Foundation Engineering*, Kyoto, Vol. 1, pp. 233-236.

Goto, S., F. Tatsuoka, S. Shibuya, Y. Kim, and T. Sato (1991), "A simple gauge for local small strain measurements in the laboratory," *Soil and Foundations*, Japanese Society of Soil Mechanics and Foundation Engineering, Vol. 31, No. 1, pp. 169-180. DOI: 10.3208/sandf1972.31.169

Gould, R.A., P.R. Bedell, and J.G. Muckle (2002), "Construction over organic soils in an urban environment: four case histories," *Canadian Geotechnical Journal*, National Research Council of Canada, Vol. 39, No. 2, pp. 345-356. DOI: 10.1139/t01-090

Graham, D.S., S.D. Dapp, D.A. Brown, and R.T. McGillivray (2013), "Selmon Expressway, Tampa: Case History of Drilled Shaft Design for Extreme Variability", *Proceedings of the 38th Annual Conference on Deep Foundations*, Phoenix, Arizona, Deep Foundations Institute, pp. 317-328.

Gregory, G.H., and K.K. Bumpas (2013), "Post-peak Fully-Softened Strength and Curved Strength Envelope in Shallow Slope Failure Analysis," *Proceedings of Geo-Congress 2013: Stability and Performance of Slopes and Embankments III*, ASCE, pp. 255-268. DOI: 10.1061/9780784412787.026

Ground Board (1991), *Inadequate site investigation*, Institution of Civil Engineers, Thomas Telford, 26 pp.

Grozic, J.L.H., T. Lunne, and S. Pande (2003), "An oedometer test study on the preconsolidation stress of glaciomarine clays," *Canadian Geotechnical Journal*, NRC Canada, Vol. 40, No. 5, pp. 857-872. DOI: 10.1139/T03-043

Gui, M.W., K. Soga, M.D. Bolton, and J.P. Hamelin (2002), "Instrumented Borehole Drilling for Subsurface Investigation," *Journal of Geotechnical and Geoenvironmental Engineering*, ASCE, Vol. 128, No. 4, pp. 283-291. DOI: 10.1061/(ASCE)1090-0241(2002)128:4(283)

Guo, T., and S. Prakash (1999), "Liquefacation of Silts and Silt-Clay Mixtures," *Journal of Geotechnical and Geoenvironmental Engineering*, ASCE, Vol. 125, No. 8, pp. 706-710. DOI: 10.1061/(ASCE)1090-0241(1999)125:8(706)

Gupta, R.C., and J.L. Davidson (1986), "Piezoprobe Determined Coefficient of Consolidation," *Soils and Foundations*, Japanese Society of Soil Mechanics and Foundation Engineering, Vol. 26, No. 3, pp. 12-22. DOI: 10.3208/sandf1972.26.3_12

Haile, J.P., and B.S. Brown (1988), "Design and Construction of Clay Liners for Gold Tailings Facilities and Heap Leach Pads," *Proceedings of the 2nd International Conference on Gold Mining*, Vancouver, British Columbia, Society of Mining Engineering.

Haley and Aldrich (1969), *Report No. 1 – Engineering Properties of Foundation Soils at Long Creek-Fore River Areas and Back Cove*, Report to Maine State Highway Commission.

Handy, R.L. (1986), "Borehole Shear Test and Slope Stability," *Use of In Situ Tests in Geotechnical Engineering*, S.P. Clemence, Ed., ASCE, GSP 6, pp. 161-175.

Handy, R.L., and M.G. Spangler (2007), *Geotechnical Engineering: Soil and Foundation Principles and Practice*, 5th Edition, McGraw-Hill Education, 904 pp.

Haramy, K.Y., and M.J. DeMarco (1985), "Use of Schmidt hammer for rock and coal testing," *Proceedings of the 26th U.S. Symposium on Rock Mechanics*, Balkema, pp. 549-555.

Hardin, B.O., and F.E. Richart, Jr. (1963), "Elastic wave velocities in granular soils," *Journal of the Soil Mechanics and Foundations Division*, ASCE, Vol. 89, No. SM1, pp. 33-65.

Hardin, B.O., and W.L. Black (1968), "Vibration modulus of normally consolidated clay," *Journal of the Soil Mechanics and Foundations Division*, ASCE, Vol. 94, No. SM2, pp. 353–369.

Hardin, B.O. (1978), "The nature of stress-strain behavior for soils," *Earthquake Engineering and Soil Dynamics, Proceedings of the ASCE Geotechnical Engineering Division Specialty Conference*, ASCE, Vol. 1, pp. 3-90.

Harris, J.P., S. Sebesta, and T. Scullion (2004), "Hydrated Lime Stabilization of Sulfate-Bearing Vertisols in Texas," *Transportation Research Record: Journal of the Transportation Research Board*, Transportation Research Board, National Research Council, No. 1868, pp. 31-39. DOI: 10.3141/1868-04

Hasancebi, N., and R. Ulusay (2007), "Empirical correlations between shear wave velocity and penetration resistance for ground shaking assessments," *Bulletin of Engineering Geology and the Environment*, Springer-Verlag, Vol. 66, No. 2, pp. 203-213. DOI: 10.1007/s10064-006-0063-0

Hassani, F.P., M.J. Scoble, and B.N. Whittacker (1980), "Application of the point load index test to strength determination of rock and proposals for a new size correction chart," *Rock Mechanics: A State of the Art – Proceedings of the 21st U.S. Symposium on Rock Mechanics*, University of Missouri-Rolla, Rolla, Missouri, pp. 543-553.

Hatanaka, M., and A. Uchida (1996), "Empirical Correlation Between Penetration Resistance and Internal Friction Angle of Sandy Soils," *Soils and Foundations*, Japanese Geotechnical Society, Vol. 36, No. 4, pp. 1-9. DOI: 10.3208/sandf.36.4_1

Hawkins, A.B., and J.A.G. Olver (1986), "Point Load Tests: Correlation Factors and Contractual Use. An example from the Corallian at Weymouth," *Site Investigation Practice: Assessing BS 5930*, Geological Society of London, pp. 269-271.

Hazen, A. (1911), "Discussion of 'Dams on sand foundations' by A.C. Koenig," *Transactions of the American Society of Civil Engineers*, Vol. 73, pp. 199-203.

Heidema, P.B. (1957), "The Bar-Shrinkage Test and the Practical Importance of Bar-Linear Shrinkage as an Identifier of Soils," *Proceedings of the 4th International Conference on Soil Mechanics and Foundation Engineering*, Butterworths, Vol. 1, pp. 44-48.

Hendron, A.J., and F.D. Patton (1985), *The Vaiont Slide, A Geotechnical Analysis Based on New Geologic Observations of the Failure Surface*, Department of the Army, U.S. Army Corps of Engineers, Washington, D.C., Technical Report GL-85-5.

Herrmann, H.G., and P.J. Valent (1974), *Interim Design Guidelines for Seafloor Footing Foundations*, Naval Civil Engineering Lab Technical Report.

Hoek, E., and E.T. Brown (1980), "Empirical strength criterion for rock masses," *Journal of the Geotechnical Engineering Division*, ASCE, Vol. 106, No. GT9, pp. 1013-1035.

Hoek, E. (1983), "Strength of jointed rock masses," *Geotechnique*, Vol. 33, No. 3, pp. 187-223.

Hoek, E. (1994), "Strength of Rock and Rock Masses," *ISRM News Journal*, Vol. 2, No. 2, pp. 4-16.

Hoek, E., P.K. Kaiser, and W.F. Bawden (1995), *Support of Underground Excavations in Hard Rock*, A.A. Balkema, 215 pp.

Hoek, E., and E.T. Brown (1997), "Practical estimates of rock mass strength," *International Journal of Rock Mechanics and Mining Sciences*, Elsevier, Vol. 34, No. 8, pp. 1165-1186. DOI: 10.1016/S1365-1609(97)80069-X

Hoek, E., and A. Palmeiri (1998), "Geotechnical risks on large civil engineering projects," *Proceedings of the 8th IAEG Congress*, International Association for Engineering Geology and the Environment.

Hoek, E., C. Carranza-Torres, and B. Corkum (2002), "Hoek-Brown Failure Criterion – 2002 Edition," *Proceedings of NARMS-TAC Conference*, Toronto, Vol. 1, pp. 267-273.

Hoek, E., and M.S. Diederichs (2006), "Empirical estimation of rock mass modulus," *International Journal of Rock Mechanics and Mining Sciences*, Elsevier, Vol. 43, No. 2, pp. 203-215. DOI: 10.1016/j.ijrmms.2005.06.005

Hoek, E., and P. Marinos (2007), "A brief history of the development of the Hoek-Brown failure criterion," *Soils and Rocks*, Brazilian Association for Soil Mechanics and Geotechnical Engineering, Vol. 30, No. 2.

Hoek, E., T.G. Carter, and M.S. Diederichs (2013), "Quantification of the Geological Strength Index Chart," *Proceedings of 47th U.S. Rock Mechanics/Geomechanics Symposium*, San Francisco, American Rock Mechanics Association, Paper 13-672.

Holtz, R.D., and W.D. Kovacs (1981), *An Introduction to Geotechnical Engineering*, Prentice-Hall, 733 pp.

Holtz, R.D., W.D. Kovacs, and T.C. Sheahan (2011), *An Introduction to Geotechnical Engineering*, 2nd Edition, Pearson, 853 pp.

Holtz, W.G., and H.J. Gibbs (1956), "Engineering properties of expansive clays," *Transactions of the American Society of Civil Engineers*, ASCE, Vol. 121, No. 1, pp. 641-663.

Hong, E-S, I-M Lee, and J-S Lee (2006), "Measurement of Rock Joint Roughness by 3D Scanner," *Geotechnical Testing Journal*, ASTM International, Vol. 29, No. 6, pp. 1-8. DOI: 10.1520/GTJ100169

Honjo, Y., Y. Zaika, and G. Pokharel (2005), "Estimation of Subgrade Reaction Coefficient for Horizontally Loaded Piles by Statistical Analyses," *Soils and Foundations*, Japanese Geotechnical Society, Vol. 45, No. 3, pp. 51-70. DOI: 10.3208/sandf.45.3_51

Hough, B.K. (1957), *Basic Soils Engineering*, The Ronald Press Company, 513 pp.

Hryciw, R.D. (1990), "Small-Strain-Shear Modulus of Soil by Dilatometer," *Journal of Geotechnical Engineering*, ASCE, Vol. 116, No. 11, pp.1700-1716. DOI: 10.1061/(ASCE)0733-9410(1990)116:11(1700)

Huang, P-T, M. Patel, M.C. Santagata, and A. Bobet (2009), *Classification of Organic Soils*, Report to Indiana Department of Transportation, Report FHWA/IN/JTRP-2008/2, 180 pp.

Hunter, D. (1988), "Lime-Induced Heave in Sulfate-Bearing Clay Soils," *Journal of Geotechnical Engineering*, ASCE, Vol. 114, No. 2, pp. 150-167. DOI: 10.1061/(ASCE)0733-9410(1988)114:2(150)

Hvorslev, M.J. (1949), *Subsurface Exploration and Sampling of Soils for Civil Engineering Purposes*, U.S. Army Engineer Waterways Experiment Station, Vicksburg, MS, 521 pp.

Hvorslev, M.J. (1951), *Time Lag and Soil Permeability in Ground-Water Observations*, Bulletin Non. 36, Waterways Experiment Station, U.S. Army Corps of Engineers, Vicksburg, Mississippi, 50 pp.

Idriss, I.M., and R.W. Boulanger (2007), "SPT- and CPT-based Relationships for the Residual Shear Strength of Liquefied Soils," *Earthquake Geotechnical Engineering*, Proceedings of the 4th International Conference on Earthquake Geotechnical Engineering, K.D. Pitilakis, Ed., Springer, pp. 1-22. DOI: 10.1007/978-1-4020-5893-6_1

Illinois State Geological Survey (2016), "LiDAR Imagery Identifies Karst Features," Web. Accessed November 28, 2016. https://www.isgs.illinois.edu/lidar-imagery-karst-features

Imai, T., and K. Tonouchi (1982), "Correlation of N-value with S-wave velocity and shear modulus," *Proceedings of the 2nd European Symposium on Penetration Testing*, Amsterdam, Vol. 1, pp. 67-72.

Isenhower, W.M., K.H. Stokoe, II, and J.C. Allen (1987), "Instrumentation for Torsional Shear/Resonant Column Measurements Under Anisotropic Stresses," *Geotechnical Testing Journal*, American Society for Testing and Materials, Vol. 10, No. 4, pp. 183-191. DOI: 10.1520/GTJ10544J

Ishibashi, I., and X. Zhang (1993), "Unified Dynamic Shear Moduli and Damping Ratios of Sand and Clay," *Soils and Foundations*, Japanese Society of Soil Mechanics and Foundation Engineering, Vol.33, No.1, pp.182-191. DOI: 10.3208/sandf1972.33.182

Ishihara, K. (1996), *Soil Behaviour in Earthquake Geotechnics*, Oxford University Press, 350 pp.

ISRM (1978), "Suggested Methods for the Quantitative Description of Discontinuities in Rock Masses," *International Journal of Rock Mechanics and Mining Sciences & Geomechanics Abstracts*, Permagon Press, Vol. 15, No. 6, pp. 319-368. DOI: 10.1016/0148-9062(78)91472-9

ISRM (1985), "Suggested Method for Determining Point Load Strength," *International Journal of Rock Mechanics and Mining Sciences & Geomechanics Abstracts*, Vol. 22, No. 2, Permagon Press, pp. 51-60. DOI: 10.1016/0148-9062(85)92327-7

ISRM (1987), "Suggested Methods for Deformability Determination Using a Flexible Dilatometer," *International Journal of Rock Mechanics and Mining Sciences & Geomechanics Abstracts*, Permagon Press, Vol. 24, No. 2, pp. 123-134. DOI: 10.1016/0148-9062(87)91931-0

Iwasaki, T., F. Tatsuoka, K.I. Tokida, and S. Yasuda (1978), "A practical method for assessing soil liquefaction potential based on case studies at various sites in Japan," *Proceedings of the 2nd International Conference on Microzonation*, Washington, D.C., National Science Foundation, pp. 885-896.

Iyisan, R. (1996), "Correlations between shear wave velocity and in situ penetration test results (in Turkish)," *Teknik Dergi*, Chamber of Civil Engineers of Turkey, Vol. 7, No. 2, pp. 1187-1199.

Jafari, M.K., A. Asghari, and I. Rahmani (1997), "Empirical correlation between shear wave velocity ($V_s$) and SPT N value for South of Tehran soils," *Proceedings of 4th International Conference on Civil Engineering*, Tehran, Iran.

Jamiolkowski, M., C.C. Ladd, J.T. Germaine, and R. Lancellotta (1985), "New developments in field and laboratory testing of soils," *Proceedings of the 11th International Conference on Soil Mechanics and Foundation Engineering*, San Francisco, A.A. Balkema, Vol. 1, pp. 57-154.

Jamiolkowski, M., V.N. Ghionna, R. Lancellotta, and E. Pasqualini (1988), "New Correlations of Penetration Tests for Design Practice," *Penetration Testing 1988*, Proceedings of the 1st International Symposium on Penetration Testing, A.A. Balkema, Vol. 1, pp. 263-296.

Jamiolkowski, M., R. Lancellotta, and D.C.F. Lo Presti (1994), "Remarks on the Stiffness at Small Strains of Six Italian Clays," *Proceedings of International Symposium on Pre-Failure Deformation Characteristics of Geomaterials*, Sapporo, Japan, A.A. Balkema, pp. 817-836.

Janbu, N. (1963), "Soil compressibility as determined by oedometer and triaxial tests," *Proceedings of the European Conference on Soil Mechanics and Foundation Engineering*, Wiesbaden, Germany, Vol. 1, pp. 19-25.

Janbu, N. (1967), *Settlement Calculations Based on the Tangent Modulus Concept*, Institutt for Geoteknikk og Fundamenteringslaere, Meddelelse 2, Norge Tekniske Hogskole, Trondheim, Norway, 57 pp.

Janbu, N. (1969), "The Resistance Concept Applied to Deformation of Soils," *Proceedings of the 7th International Conference on Soil Mechanics and Foundation Engineering*, A.A. Balkema, Vol. 1, pp. 191-196.

Jefferies, M., and K. Been (2006), *Soil Liquefaction: A Critical State Approach*, Taylor and Francis, London, 480 pp.

Jones, G.A., and E.A. Rust (1982), "Piezometer Penetration Testing CUPT," *Proceedings of the 2nd European Symposium on Penetration Testing*, Amsterdam, CRC Press, Vol. 2, pp. 607-613.

Jones, G.A., and D.J.A. Van Zyl (1981), "The Piezometer Probe – A Useful Tool," *Proceedings of the 10th International Conference on Soil Mechanics and Foundation Engineering*, A.A. Balkema, Vol. 2, pp. 489-496.

Jotisankasa, A., M. Coop, and A. Ridley (2007), "The Development of a Suction Control System for a Triaxial Apparatus," *Geotechnical Testing Journal*, ASTM International, Vol. 30, No. 1, pp. 1-7. DOI: 10.1520/GTJ100026

Kabir, M.G., and A.J. Lutenegger (1990), "In Situ Estimation of Coefficient of Consolidation in Clays," *Canadian Geotechnical Journal*, National Research Council of Canada, Vol. 27, No. 1, pp. 58-67. DOI: 10.1139/t90-006

Kahraman, S., and O. Gunaydin (2009), "The effect of rock classes on the relation between uniaxial compressive strength and point load index," *Bulletin of Engineering Geology and the Environment*, Spring-Verlag, Vol. 68, No. 3, pp. 345-353. DOI: 10.1007/s10064-009-0195-0

Kalinski, M.E., and M.S.R Thummaluru (2005), "A new free-free resonant column device for measurement of $G_{max}$ and $D_{min}$ at higher confining stresses," *Geotechnical Testing Journal*, ASTM International, Vol. 28, No. 2, pp. 180-187. DOI: 10.1520/GTJ12187

Kamei, T., and K. Iwasaki (1995), "Evaluation of Undrained Shear Strength of Cohesive Soils Using a Flat Dilatometer," *Soils and Foundations*, Japanese Society of Soil Mechanics and Foundation Engineering, Vol. 35, No. 2, pp. 111-116. DOI: 10.3208/sandf1972.35.2_111

Karlsrud, K., and F.G. Hernandez-Martinez (2013), "Strength and deformation properties of Norwegian clays from laboratory tests on high-quality block samples," *Canadian Geotechnical Journal*, NRC Research Press, Vol. 50, No. 12, pp. 1273-1293. DOI: 10.1139/cgj-2013-0298

Kassif, G., and E.N. Henkin (1967), "Engineering and Physico-Chemical Properties Affecting Piping Failure of Loess Dams in the Negev," *Proceedings of the 3rd Asian Regional Conference on Soil Mechanics and Foundation Engineering*, Jerusalem Academic Press, Vol. 1, pp. 13-16.

Katayama, I., F. Fukui, M. Satoh, Y. Makihara, and K. Tokimatsu (1986), "Comparison of dynamic soil properties between undisturbed and disturbed dense sand samples," *Proceedings of 21st Annual Conference of the Japanese Society for Soil Mechanics and Foundation Engineering*, pp. 583-584.

Kates, G.L. (1996), *Development and Implementation of a Seismic Flat Dilatometer Test for Small and High- Strain Soil Properties*, M.S. Thesis, School of Civil and Environmental Engineering, Georgia Institute of Technology, Atlanta, Georgia, 173 pp.

Katz, O., Z. Reches, and J-C Roegiers (2000), "Evaluation of mechanical rock properties using a Schmidt Hammer," *International Journal of Rock Mechanics and Mining Sciences*, Elsevier, Vol. 37, No. 4, pp. 723-728. DOI: 10.1016/S1365-1609(00)00004-6

Kavazanjian, E., Jr., J.J. Wang, G.R. Martin, A. Shamsabadi, I. Lam, S.E. Dickenson, and C.J. Hung (2011), *LRFD Seismic Analysis and Design of Transportation Geotechnical Features and Structural Foundations*, National Highway Institute, Federal Highway Administration, Geotechnical Engineering Circular No. 3, Report FHWA-NHI-11-032, 592 pp.

Kaya, A., and K. Karaman (2016), "Utilizing the strength conversion factor in the estimation of uniaxial compressive strength from the point load index," *Bulletin of Engineering Geology and the Environment*, Springer-Verlag, Vol. 75, No. 1, pp. 341-357. DOI: 10.1007/s10064-015-0721-1

Keaton, J.R., S.K. Mishra, and P.E. Clopper (2012), *Scour at Bridge Foundations on Rock*, National Cooperative Highway Research Program, Report 717, Transportation Research Board, 174 pp. http://onlinepubs.trb.org/onlinepubs/nchrp/nchrp_rpt_717.pdf

Keaveny, J.M., and J.K. Mitchell (1986), "Strength of Fine-Grained Soils Using the Piezocone," *Use of In Situ Tests in Geotechnical Engineering*, S.P. Clemence, Ed., ASCE, GSP 6, pp. 668-699.

Kemeny, J., and K. Turner (2008), *Ground-Based LiDAR Rock Slope Mapping and Assessment*, Federal Highway Administration, Central Federal Lands Highway Division, Publication FHWA-CFL/TD-08-006, 114 pp.

Kenney, T.C. (1976), "Formation and Geotechnical Characteristics of Glacial-Lake Varved Clays," *Laurits Bjerrum Memorial Volume – Contributions to Soil Mechanics*, Norwegian Geotechnical Institute, pp. 15-40.

Kiku, H., N. Yoshida, S. Yasuda, T. Irisawa, H. Nakazawa, Y. Shimizu, A. Ansal, and A. Erkan (2001), "In situ penetration tests and soil profiling in Adapazari, Turkey," *Proceedings of ICSMGE/TC4 Satellite Conference on Lessons Learned from Recent Strong Earthquakes*, pp. 259-265.

Kim, D-S, E-S Bang, and W-S Seo (2004), "Evaluation of Shear Wave Velocity Profile Using SPT-Uphole Method," *Proceedings of the 2nd International Site Characterization Conference*, ISC-2, Porto, Portugal, Vol. 1, pp. 339-344.

Kitsunezaki, C. (1980), "A new method for shear-wave logging," *Geophysics*, Society for Exploration Geophysicists, Vol. 45, No. 10, pp. 1489-1506. DOI: 10.1190/1.1441044

Knight, K. (1963), "The Origin and Occurrence of Collapsing Soils," *Proceedings of the 3rd Regional Conference for Africa on Soil Mechanics and Foundation Engineering*, Vol. 1, pp. 127-130.

Kokusho, T. (1980), "Cyclic Triaxial Test of Dynamic Soil Properties for Wide Strain Range," *Soils and Foundations*, Japanese Society of Soil Mechanics and Foundation Engineering, Vol. 20, No. 2, pp. 45-60. DOI: 10.3208/sandf1972.20.2_45

Kokusho, T., and Y. Esashi (1981), "Cyclic triaxial test on sands and coarse materials," *Proceedings of the 10th International Conference on Soil Mechanics and Foundation Engineering*, Stockholm, Vol. 1, pp. 673-679.

Kokusho, T. (1987), "In situ dynamic soil properties and their evaluation," *Proceedings of the 8th Asian Regional Conference on Soil Mechanics and Foundation Engineering*, Kyoto, Vol. 2, pp.215-435.

Koppula, S.D. (1981), "Statistical Estimation of Compression Index," *Geotechnical Testing Journal*, American Society for Testing and Materials, Vol. 4, No. 2, pp. 68-73. DOI: 10.1520/GTJ10768J

Koutsoftas, D.C., and C.C. Ladd (1985), "Design Strengths for an Offshore Clay," *Journal of Geotechnical Engineering*, ASCE, Vol. 111, No. 3, pp. 337-355. DOI: 10.1061/(ASCE)0733-9410(1985)111:3(337)

Kramer, S.L. (1996), *Geotechnical Earthquake Engineering*, Prentice-Hall, 653 pp.

Krizek, R.J., R.B. Corotis, and H.H. El-Moursi (1977), "Probabilistic analysis of predicted and measured settlements," *Canadian Geotechnical Journal*, National Research Council of Canada, Vol. 14, No. 1, pp. 17-33. DOI: 10.1139/t77-002

Kulhawy, F.H., and P.W. Mayne (1990), *Manual on Estimating Soil Properties for Foundation Design*, Electrical Power Research Institute, Report EL-6800, 273 pp.

Kuzukami, H., E. Ozaki, and M. Nakaya (1971), "Relationship Between Specific Surface and Liquid Limit," *Transactions of the Japanese Society of Irrigation, Drainage and Reclamation Engineering*, Vol. 37, pp. 61-67. DOI: 10.11408/jsidre1965.1971.37_61

Lacasse, S., and T. Lunne (1982), "Penetration tests in two Norwegian clays," *Proceedings of the Second European Symposium on Penetration Testing*, Amsterdam, A.A. Balkema, Vol. 2, pp. 661-669.

Lacasse, S., T. Berre, and G. Lefebvre (1985), "Block Sampling of Sensitive Clays," *Proceedings of the 11th International Conference on Soil Mechanics and Foundation Engineering*, San Francisco, A.A. Balkema, pp. 887-892.

Lacasse, S., and T. Lunne (1988), "Calibration of Dilatometer Correlations," *Penetration Testing 1988*, Proceedings of the 1st International Symposium on Penetration Testing, A.A. Balkema, Vol. 1, pp. 539-548.

Ladd, C.C., and R. Foott (1974), "New Design Procedure for Stability of Soft Clays," *Journal of the Geotechnical Engineering Division*, ASCE, Vol. 100, No. GT7, pp. 763-786.

Ladd, C.C., R. Foott, K. Ishihara, F. Schlosser, and H.G. Poulos (1977), "Stress-Deformation and Strength Characteristics: State-of-the-Art Report," *Proceedings of the 9th International Conference on Soil Mechanics and Foundation Engineering*, Tokyo, Japanese Society for Soil Mechanics and Foundation Engineering, Vol. 2, pp. 421-494.

Ladd, C.C. (1991), "Stability Evaluation During Staged Construction," *Journal of Geotechnical Engineering*, ASCE, Vol. 117, No. 4, pp. 540-615.

Ladd, C.C., and D.J. DeGroot (2003), "Recommended Practice for Soft Ground Characterization," *Proceedings of Soil and Rock America 2003*, 12th Panamerican Conference on Soil Mechanics and Geotechnical Engineering and 39th U.S. Rock Mechanics Symposium, Verlag Gluckauf GMBH, Vol. 1, pp. 3-57.

Lafleur, J., F. Giroux, and M. Huot (1987), "Field permeability of the weathered Champlain clay crust," *Canadian Geotechnical Journal*, National Research Council of Canada, Vol. 24, No. 4, pp. 581-589. DOI: 10.1139/t87-072

Laloui, L., S. Leroueil, and S. Chalindar (2008), "Modelling the combined effect of strain rate and temperature on one-dimensional compression of soils," *Canadian Geotechnical Journal*, NRC Canada, Vol. 45, No. 12, pp. 1765-1777. DOI: 10.1139/T08-093

Landon, M.M., D.J. DeGroot, and T.C. Sheahan (2007), "Nondestructive Sample Quality Assessment of a Soft Clay Using Shear Wave Velocity," *Journal of Geotechnical and Geoenvironmental Engineering*, ASCE, Vol. 133, No. 4, pp. 424-432. DOI: 10.1061/(ASCE)1090-0241(2007)133:4(424)

Landva, A.O., E.O. Korpijaakko, and P.E. Pheeney (1983), "Geotechnical Classification of Peats and Organic Soils," *Testing of Peats and Organic Soils*, P.M. Jarrett, Ed., American Society for Testing and Materials, ASTM STP 820, pp. 37-51. DOI: 10.1520/STP37333S

Lanzo, G., M. Vucetic, and M. Doroudian (1997), "Reduction of Shear Modulus at Small Strains in Simple Shear," *Journal of Geotechnical and Geoenvironmental Engineering*, ASCE, Vol. 123, No. 11, pp. 1035-1042. DOI: 10.1061/(ASCE)1090-0241(1997)123:11(1035)

Larsson, R., and S. Eskilson (1989), "Dilatometerforsok I Lera (DMT Investigations in Clay)," Swedish Geotechnical Institute, Publication No. 243. (in Swedish)

Lawton, E.C., R.J. Fragaszy, and J.H. Hardcastle (1989), "Collapse of Compacted Clayey Sand," *Journal of Geotechnical Engineering*, ASCE, Vol. 115, No. 9, pp. 1252-1267. DOI: 10.1061/(ASCE)0733-9410(1989)115:9(1252)

Lawton, E.C., R.J. Fragaszy, and M.D. Hetherington (1992), "Review of Wetting-Induced Collapse in Compacted Soil," *Journal of Geotechnical Engineering*, ASCE, Vol. 118, No. 9, pp. 1376-1394. DOI: 10.1061/(ASCE)0733-9410(1992)118:9(1376)

Lee, J.H., and R. Salgado (1999), "Determination of Pile Base Resistance in Sands," *Journal of Geotechnical and Geoenvironmental Engineering*, ASCE, Vol. 125, No. 8, pp. 673-683. DOI: 10.1061/(ASCE)1090-0241(1999)125:8(673)

Lee, J.S., and J.C. Santamarina (2005), "Bender elements: performance and signal interpretation," *Journal of Geotechnical and Geoenvironmental Engineering*, ASCE, Vol. 131, No. 9, 1063-1070. DOI: 10.1061/(ASCE)1090-0241(2005)131:9(1063)

Lefchik, T.E., L.R. Ruegsegger, and R.W. Henthorne (2003), "Avoiding Voids," *Public Roads*, Vol. 66, No. 3, Web. Accessed April 9, 2016. http://www.fhwa.dot.gov/publications/publicroads/03may/01.cfm

Lehane, B., and M. Fahey (2002), "A simplified nonlinear settlement prediction model for foundations on sand," *Canadian Geotechnical Journal*, NRC Canada, Vol 39, No. 2, pp. 293-303. DOI: 10.1139/t01-091

Leonards, G.A. (1976), "Estimating Consolidation Settlements of Shallow Foundations on Overconsolidated Clays," *Estimation of Consolidation Settlements: Manual of Practice*, TRB Special Report 163, Transportation Research Board, pp. 13-16.

Leps, T.M. (1970), "Review of the shearing strength of rockfill," *Journal of the Soil Mechanics and Foundations Division*, ASCE, Vol. 96, No. SM4, pp. 1159-1170.

Leroueil, S., M. Kabbaj, F. Tavenas, and R. Bouchard (1985), "Stress-strain-strain rate relation for the compressibility of sensitive natural clays, *Geotechnique*, Vol. 35, No. 2, pp. 159-180. DOI: 10.1680/geot.1985.35.2.159

Leroueil, S., G. Bouclin, F. Tavenas, L. Bergeron, and P. La Rochelle (1990), "Permeability anisotropy of natural clays as a function of strain," *Canadian Geotechnical Journal*, National Research Council of Canada, Vol. 27, No. 5, pp. 568-579. DOI: 10.1139/t90-072

Leroueil, S., P. Leart, D.W. Hight, and J.J.M. Powell (1992), "Hydraulic conductivity of a recent estuarine silty clay at Bothkennar," *Geotechnique*, Institution of Civil Engineers, Vol. 42, No. 2, pp. 275-288. DOI: 10.1680/geot.1992.42.2.275

Leroueil, S., and M.E.S. Marques (1996), "Importance of strain rate and temperature effects in geotechnical engineering," *Measuring and Modeling Time Dependent Soil Behavior*, T.C. Sheahan and V.N. Kaliakin, Eds., ASCE, GSP 61, pp. 1-60.

Liao, S.S.C., and R.V. Whitman (1986), "Overburden Correction Factors for SPT in Sand," *Journal of Geotechnical Engineering*, ASCE, Vol. 112, No. 3, pp. 373-377. DOI: 10.1061/(ASCE)0733-9410(1986)112:3(373)

Likos, W.J., K. Akunuri, and J.E. Loehr (2005), "Performance of PHPA Polymer Slurries for Applications in Missouri Shales," *Advances in Deep Foundations*, Proceedings of GeoFrontiers 2005, ASCE, GSP 132, pp. 1-12. DOI: 10.1061/40778(157)7

Lim, Y.Y., and G.A. Miller (2004), "Wetting-Induced Compression of Compacted Oklahoma Soils," *Journal of Geotechnical and Geoenvironmental Engineering*, ASCE, Vol. 130, No. 10, pp. 1014-1023. DOI: 10.1061/(ASCE)1090-0241(2004)130:10(1014)

Lin, J.S., J.G. Deng, and Y.A. Su (1984), *Application of Finite Element Method in the Analysis of Deep Excavation*, Research Report of Taiwan Construction Technology Research.

Little, D.N., and S. Nair (2009), *Recommended Practice for Stabilization of Sulfate Rich Subgrade Soils*, NCHRP Web-Only Document 145, Final Task Report for NCHRP Project 20-07, 54 pp. http://onlinepubs.trb.org/onlinepubs/nchrp/nchrp_w145.pdf

Lo Presti, D.C.F., M. Jamiolkowski, O. Pallara, A. Cavallaro, and S. Pedroni (1997), "Shear modulus and damping of soils," *Geotechnique*, Institution of Civil Engineers, Vol. 47, No. 3, pp. 603-617. DOI: 10.1680/geot.1997.47.3.603

Locat, J., G. Lefebvre, and G. Ballivy (1984), "Mineralogy, Chemistry, and Physical Property Interrelationships of Some Sensitive Clays from Eastern Canada," *Canadian Geotechnical Journal*, Vol. 21, No. 3, pp. 530-540. DOI: 10.1139/t84-055

Loehr, J.E., J.J. Bowders, L. Ge, W.J. Likos, R. Luna, N. Maerz, B.L. Rosenblad, and R.W. Stephenson (2011a), *Engineering Policy Guidelines for Design of Drilled Shafts*, Missouri Department of Transportation, Report cmr12003, 75 pp.

Loehr, J.E., J.J. Bowders, L. Ge, W.J. Likos, R. Luna, N. Maerz, B.L. Rosenblad, and R.W. Stephenson (2011b), *Engineering Policy Guidelines for Design of Earth Slopes*, Missouri Department of Transportation, Report cmr12004, 19 pp.

Loehr, J.E., J.J. Bowders, L. Ge, W.J. Likos, R. Luna, N. Maerz, B.L. Rosenblad, and R.W. Stephenson (2011c), *Engineering Policy Guidelines for Design of Spread Footings*, Missouri Department of Transportation, Report cmr12005, 42 pp.

Loehr, J.E., A.Z. Boeckmann, P.L. Speckman, and D. Ding (2013a), *Procedures for Establishing Geotechnical Design Parameters from Two Data Sources*, Missouri Department of Transportation, Report cmr 14-002, 22 pp.

Loehr, J.E., J.J. Bowders, B.L. Rosenblad, R. Luna, N. Maerz, R.W. Stephenson, W.J. Likos and L. Ge (2013b), "Implementation of LRFD Methods to Quantify Value of Site Characterization Activities," *Proceedings of the 18th International Conference on Soil Mechanics and Geotechnical Engineering*, Paris, France, Vol. 3, pp. 1831-1834. http://www.issmge.org/en/resources/publications/18th-icsmge

Loehr, J.E., D. Ding, and W.J. Likos (2015), "Effect of Number of Soil Strength Measurements on Reliability of Spread Footing Designs," *Transportation Research Record: Journal of the Transportation Research Board*, No. 2511, Transportation Research Board, pp. 37-44. DOI: 10.3141/2511-05

Loudon, A.G. (1952), "The computation of permeability from simple soil tests," *Geotechnique*, Institution of Civil Engineers, Vol. 3, No. 4, pp. 165-183. DOI: 10.1680/geot.1952.3.4.165

Louie, J.N. (2001), "Faster, better: shear-wave velocity to 100 meters depth from refraction microtremor arrays," *Bulletin of the Seismological Society of America*, Vol. 91, No. 2, pp. 347-364. DOI: 10.1785/0120000098

Low, P.F. (1980), "The Swelling of Clay: II. Montmorillonite," *Soil Science Society of America Journal*, Vol. 44, No. 4, pp. 667-676. DOI: 10.2136/sssaj1980.03615995004400040001x

Lu, N., and W.J. Likos (2004), *Unsaturated Soil Mechanics*, John Wiley and Sons, 584 pp.

Lumb, P., and J.K. Holt (1968), "The Undrained Shear Strength of a Soft Marine Clay from Hong Kong," *Geotechnique*, Institution of Civil Engineers, Vol. 18, No. 1, pp. 25-36. DOI: 10.1680/geot.1968.18.1.25

Lunne, T., T. Berre, and S. Strandvik (1997), "Sample Disturbance Effects in Soft Low Plasticity Norwegian Clays," *Proceedings of the Conference on Recent Developments in Soil and Pavement Mechanics*, Rio de Janeiro, Brazil, M. Almeida, Ed., A.A. Balkema, pp. 81-102.

Lutenegger, A.J., N.C. Wollenhaupt, and R.L. Handy (1979), "Laboratory simulation of shale expansion by induced gypsum growth," *Canadian Geotechnical Journal*, National Research Council of Canada, Vol. 16, No. 2, pp. 405-409. DOI: 10.1139/t79-040

Lutenegger, A.J., T. Kemmis, and G.R. Hallberg (1983), "Origin and Properties of Glacial Till and Diamictons," *Geological Environment and Soil Properties*, ASCE, pp. 310-331.

Lutenegger, A.J., and K.F. Tierney (1986), "Pore Pressure Effects In Borehole Shear Testing," *Use of In Situ Tests in Geotechnical Engineering*, S.P. Clemence, Ed., ASCE, pp. 752-764.

Lutenegger, A.J., and R.T. Saber (1988), "Determination of Collapse Potential of Soils," *Geotechnical Testing Journal*, ASTM, Vol. 11, No. 3, pp. 173-178. DOI: 10.1520/GTJ10003J

Lutenegger, A.J., and G.R. Hallberg (1988), "Stability of Loess," *Engineering Geology*, Elsevier, Vol. 25, No. 2-4, pp. 247-261. DOI: 10.1016/0013-7952(88)90030-0

Lutenegger, A.J., and D.J. DeGroot (1992), "Measurement of Hydraulic Conductivity in Clay Using Push-In Piezometers," *Current Practices in Ground Water and Vadose Zone Investigations*, American Society for Testing and Materials, D.M. Nielson and M.N. Sara, Eds., ASTM STP 1118, pp. 362-374. DOI: 10.1520/STP19140S

Lutenegger, A.J., and D.J. DeGroot (1995), *Settlement of Shallow Foundations on Granular Soils*, University of Massachusetts Transportation Center, 222 pp.

Lutenegger, A.J. (2008), "Schmertmann's Swell Sensitivity – Revisited," *From Research to Practice in Geotechnical Engineering*, Symposium Honoring Dr. John H. Schmertmann, ASCE, pp. 193-205. DOI: 10.1061/40962(325)1

Lutenegger, A.J., and J.J.M. Powell (2008), "Borehole shear tests in stiff London and Gault Clay," *Geotechnical and Geophysical Site Characterization*, Taylor and Francis, pp. 719-723.

Lutenegger, A.J. (2012), "Collapse 'Sensitivity' of Midcontinent and Lower Mississippi Valley Loess," *GeoCongress 2012: State of the Art and Practice in Geotechnical Engineering*, ASCE, pp. 880-889. DOI: 10.1061/9780784412121.091

Maerz, N.H., K.A. Magner, W.J. Likos, J.E. Loehr, D. Ding, and A. Miller (2010), "Evaluating Properties of Weak Shales in Western Missouri," *Proceedings of 44th U.S. Rock Mechanics Symposium and 5th U.S.-Canada Rock Mechanics Symposium*, American Rock Mechanics Association, Paper 10-290.

Mantaras, F.M., E. Odebrecht, and F. Schnaid (2015), "Using piezocone dissipation test to estimate the undrained shear strength in cohesive soil," *Canadian Geotechnical Journal*, National Research Council of Canada, Vol. 52, No. 3, pp. 318-325. DOI: 10.1139/cgj-2014-0176

Marachi, N.D., C.K. Chan, H.B. Seed, and J.M. Duncan (1969), *Strength and Deformation Characteristics of Rockfill Materials*, Office of Research Services, University of California, Berkeley, Report No. TE 69-5.

Marchetti, S. (1975), "A New In Situ Test for the Measurement of Horizontal Soil Deformability," *In Situ Measurement of Soil Properties*, Proceedings of a Specialty Conference, Raleigh, North Carolina, ASCE, Vol. 2, pp. 255-259.

Marchetti, S. (1980), "In Situ Tests by Flat Dilatometer," *Journal of the Geotechnical Engineering Division*, ASCE, Vol. 106, No. GT3, pp. 299-321.

Marchetti, S., and D. Crapps (1981), *DMT Operating Manual*, GPE, Inc.

Marchetti, S., and G. Totani (1989), "$c_h$ evaluations from DMTA dissipation curves," *Proceedings of the 12th International Conference on Soil Mechanics and Foundation Engineering*, Rio de Janeiro, Vol. 1, pp. 281-286.

Marchetti, S., P. Monaco, G. Totani, and M. Calabrese (2001), *The Flat Dilatometer Test in Soil Investigations*, Report of the ISSMGE Technical Committee 16 on Ground Property Characterisation from In-situ Testing, International Society for Soil Mechanics and Geotechnical Engineering (ISSMGE), 41 pp.

Marchetti, S., P. Monaco, G. Totani, and D. Marchetti (2008), "In situ tests by seismic dilatometer (SDMT)," *From Research to Practice in Geotechnical Engineering*, ASCE, GSP No. 180, pp. 292-311. DOI: 10.1061/40962(325)7

Marinos, P., and E. Hoek (2000), "GSI: A Geologically Friendly Tool for Rock Mass Strength Estimation," *Proceedings of GeoEng2000*, Melbourne, Australia, Australian Geomechanics Society, pp. 1422-1442.

Marinos, P., and E. Hoek (2001), "Estimating the geotechnical properties of heterogeneous rock masses such as flysch," *Bulletin of Engineering Geology and the Environment*, Springer-Verlag, Vol. 60, No. 2, pp. 85-92. DOI: 10.1007/s100640000090

Marinos, V., P. Marinos, and E. Hoek (2005), "The geological strength index: applications and limitations," *Bulletin of Engineering Geology and the Environment*, Springer-Verlag, Vol. 64, No. 1, pp. 55-65. DOI: 10.1007/s10064-004-0270-5

Marsh, M.L., I.G. Buckle, and E. Kavazanjian (2014), *LRFD Seismic Analysis and Design of Bridges,* National Highway Institute Course No. 130093 and 130093A Reference Manual, Federal Highway Administration, FHWA-NHI-15-004, 608 pp.

Martin, G.K., and P.W. Mayne (1997), "Seismic Flat Dilatometer Tests in Connecticut Valley Varved Clay," *Geotechnical Testing Journal*, American Society for Testing and Materials, Vol. 20, No. 3, pp. 357-361. DOI: 10.1520/GTJ19970011

Martin, G.K., and P.W. Mayne (1998), "Seismic Flat Dilatometer Tests in Piedmont Residual Soils," *Geotechnical Site Characterization*, A.A. Balkema, Vol. 2, pp. 837-843.

Matlock, H. (1970), "Correlations for Design of Laterally Loaded Piles in Soft Clay," *Proceedings of the Offshore Technology Conference*, Houston, Texas, pp. 557-594.

Matteo, L.D. (2012), "Liquid limit of low- to medium-plasticity soils: comparison between Casagrande cup and cone penetrometer test," *Bulletin of Engineering Geology and the Environment*, Springer-Verlag, Vol. 71, No. 1, pp. 79-85. DOI: 10.1007/s10064-011-0412-5

Mayne, P.W. (1980), "Cam-Clay Predictions of Undrained Strength," *Journal of the Geotechnical Engineering Division*, ASCE, Vol. 106, No. GT11, pp. 1219-1242.

Mayne, P.W., and D.D. Frost (1988), "Dilatometer Experience in Washington D.C.," *Transportation Research Record*, Transportation Research Board, No. 1169, pp. 16-23.

Mayne, P.W., and J.K. Mitchell (1988), "Profiling of overconsolidation ratio in clays by field vane," *Canadian Geotechnical Journal*, National Research Council of Canada, Vol. 25, No. 1, pp. 150-157. DOI: 10.1139/t88-015

Mayne, P.W., and R.C. Bachus (1989), "Penetration Porewater Pressures in Clay by CPTU, DMT, and SBP," *Proceedings of the 12th International Conference on Soil Mechanics and Foundation Engineering*, Vol. 1, pp. 291-294.

Mayne, P.W., and G.J. Rix (1993), "$G_{max}$-$q_c$ Relationships for Clays," *Geotechnical Testing Journal*, American Society for Testing and Materials, Vol. 16, No. 1, pp. 54-60. DOI: 10.1520/GTJ10267J

Mayne, P.W. (1995), "Profiling Yield Stresses in Clays by In Situ Tests," *Transportation Research Record*, Transportation Research Board, No. 1479, pp. 43-50. http://onlinepubs.trb.org/Onlinepubs/trr/1995/1479/1479-006.pdf

Mayne, P.W., and G.J. Rix (1995), "Correlations Between Shear Wave Velocity and Cone Tip Resistance in Natural Clays," *Soils and Foundations*, Vol. 35, No. 2, pp. 107-110. DOI: 10.3208/sandf1972.35.2_107

Mayne, P.W. (2006), "In-situ Test Calibrations for Evaluating Soil Parameters," *Characterization and Engineering Properties of Natural Soils*, Proceedings of the Second International Workshop on Characterization and Engineering Properties of Natural Soils, Taylor & Francis, Vol. 3, pp. 1602-1652.

Mayne, P.W. (2007), *Cone Penetration Testing – A Synthesis of Highway Practice*, NCHRP Synthesis 368, Transportation Research Board, Washington, DC, 117 pp.

Mayne, P.W., M.R. Coop, S.M. Springman, A-B Huang, and J.G. Zornberg (2009), "Geomaterial behavior and testing," *Proceedings of the 17th International Conference on Soil Mechanics and Geotechnical Engineering*, Millpress/IOS Press, State-of-the-Art Paper SOA-1, Vol. 4, pp. 2777-2872.

Mayne, P.W. (2014), "Generalized CPT Method for Evaluating Yield Stress in Soils," *Geo-Congress 2014 Technical Papers: Geo-Characterization and Modeling for Sustainability*, ASCE, GSP 234, pp. 1336-1346. DOI: 10.1061/9780784413272.130

McKinley, J.D., and V. Sivakumar (2009), "Coefficient of consolidation by plotting velocity against displacement," *Geotechnique*, Institution of Civil Engineers, Vol. 59, No. 6, pp. 553-557. DOI: 10.1680/geot.7.00130

Menard, L., and J. Rousseau (1962), "L'evaluation des tassements. Tendances nouvelles," *Sols Soils No. 1*, Paris, pp. 13-20.

Menq, F-Y (2003), *Dynamic Properties of Sandy and Gravelly Soils*, Ph.D. dissertation, Department of Civil Engineering, The University of Texas, Austin, Texas, 364 pp.

Mesri, G., and P.M. Godlewski (1977), "Time- and Stress-Compressibility Interrelationship," *Journal of the Geotechnical Engineering Division*, ASCE, Vol. 103, No. 5, pp. 417-430.

Mesri, G., and A. Castro (1987), "$C_\alpha/C_c$ Concept and $K_o$ During Secondary Compression," *Journal of Geotechnical Engineering*, ASCE, Vol. 113, No. 3, pp. 230-247. DOI: 10.1061/(ASCE)0733-9410(1987)113:3(230)

Mesri, G., T.W. Feng, S. Ali, and T.M. Hayat (1994), "Permeability Characteristics of Soft Clays," *Proceedings of the 13th International Conference on Soil Mechanics and Geotechnical Engineering*, A.A. Balkema, Vol. 2, pp. 187-192.

Mesri, G., M. Shahien, and T.W. Feng (1995), "Compressibility parameters during primary consolidation," *Compression and Consolidation of Clayey Soils, Proceedings of the IS-Hiroshima '95 International Symposium*, A.A. Balkema, Vol. 2, pp. 1021-1037.

Mesri, G., T.D. Stark, M.A. Ajlouni, and C.S. Chen (1997), "Secondary Compression of Peat with or without Surcharging," *Journal of Geotechnical and Geoenvironmental Engineering*, Vol. 123, No. 5, pp. 411-421. DOI: 10.1061/(ASCE)1090-0241(1997)123:5(411)

Mesri, G., T.W. Feng, and M. Shahien (1999), "Coefficient of Consolidation by Inflection Point Method," *Journal of Geotechnical and Geoenvironmental Engineering*, ASCE, Vol. 125, No. 8, pp. 716-718. DOI: 10.1061/(ASCE)1090-0241(1999)125:8(716)

Meyerhof, G.G. (1951), "The Ultimate Bearing Capacity of Foundations," *Geotechnique*, Institution of Civil Engineers, Vol. 2, No. 4, pp. 301-332. DOI: 10.1680/geot.1951.2.4.301

Meyerhof, G.G. (1956), "Penetration Tests and Bearing Capacity of Cohesionless Soils," *Journal of the Soil Mechanics and Foundations Division*, ASCE, Vol. 82, No. 1, pp. 1-19.

Mitchell, J.K. (1956), "The fabric of natural clays and its relation to engineering properties," *Proceedings of the Thirty-Fifth Annual Meeting of the Highway Research Board*, Highway Research Board, Vol. 35, pp. 693-713.

Mitchell, J.K., and K. Soga (2005), *Fundamentals of Soil Behavior*, Third Edition, John Wiley & Sons, 577 pp.

Mitchell, J.K. (2009), "Geotechnical Surprises-Or Are They?" The 2004 H. Bolton Seed Lecture, *Journal of Geotechnical and Geoenvironmental Engineering*, ASCE, Vol. 135, No. 8, pp. 998-1010. DOI: 10.1061/(ASCE)GT.1943-5606.0000040

MnDOT (2013), *2013 Geotechnical Engineering Manual*, Geotechnical Engineering Section, Minnesota Department of Transportation, 159 pp.

Moayed, R.Z., and S.A. Naeini (2006), "Evaluation of modulus of subgrade reaction ($K_s$) in gravely soils based on standard penetration test (SPT)," *Physical Modelling in Geotechnics*, Proceedings of The Sixth International Conference, Hong Kong, Vol. 2, pp. 801-804.

Moayed, R.Z., and M. Janbaz (2011), "Subgrade reaction modulus of Tehran alluvium," *Proceedings of the Institution of Civil Engineers-Geotechnical Engineering*, Vol. 164, No. 4, pp. 283-288. DOI: 10.1680/geng.9.00076

Mock, R.G., and S.L. Pawlak (1983), "Alluvial fan hazards at Glenwood Springs," *Special Publication on Geological Environment and Soil Properties*, R.N. Yong, Editor, ASCE, pp. 221-233.

MoDOT (2015), *Engineering Policy Guide*, Missouri Department of Transportation, Web. Accessed November 12, 2015. http://epg.modot.org

Moore, P.J. (1979), "Determination of Permeability Anisotropy in a Two-Way Permeameter," *Geotechnical Testing Journal*, American Society for Testing and Materials, Vol. 2, No. 3, pp. 167-169. DOI: 10.1520/GTJ10450J

Morgenstern, N.R., and B.I. Balasubramanian (1980), "Effects of Pore Fluid on the Swelling of Clay-Shale," *Proceedings of the 4th International Conference on Expansive Soils*, Vol. 1, pp. 190-205.

Morin, P., and C.R. Dawe (1986), "Geotechnical Properties of Two Deep Sea Marine Soils from Labrador Sea Area," *Proceedings of the 3rd Canadian Conference on Marine Geotechnical Engineering*, Vol. 1, pp. 117-134.

Moran, Proctor, Mueser, and Rutledge (1958), *Study of Deep Soil Stabilization by Vertical Sand Drains*, Contract No. NOY-88812, Bureau of Yards and Docks, Department of the Navy, 440 pp.

MSHA (2016), *Digitized Mine Maps*, Mine Safety and Health Administration, U.S. Department of Labor, Web. Accessed April 9, 2016. http://www.msha.gov/minemapping/minemapping.asp

Mulder, V.L., S. de Bruin, M.E. Schaepman, and T.R. Mayr (2011), "The use of remote sensing in soil and terrain mapping – A review," *Geoderma*, Vol. 162, No. 1-2, Elsevier, pp. 1-19. DOI: 10.1016/j.geoderma.2010.12.018

Murff, J.D. (1987), "Pile Capacity in Calcareous Sands: State of the Art," *Journal of Geotechnical Engineering*, ASCE, Vol. 113, No. 5, pp. 490-507. DOI: 10.1061/(ASCE)0733-9410(1987)113:5(490)

Muromachi, T. (1981), "Cone penetration testing in Japan," *Proceedings of the Symposium on Cone Penetration Testing and Experience*, G.M. Norris and R.D. Holtz, Eds., ASCE, pp. 49-75.

Nagaraj, T.S., and B.R. Srinivasa Murthy (1986), "A critical reappraisal of compression index equation," *Geotechnique*, Institution of Civil Engineers, Vol. 36, No. 1, pp. 27-32. DOI: 10.1680/geot.1986.36.1.27

NAVFAC (1986), *Soil Mechanics: Design Manual 7.01*, Naval Facilities Engineering Command, 348 pp.

Nguyen, V., and G.F. Pinder (1984), "Direct Calculation of Aquifer Parameters in Slug Test Analysis," *Groundwater Hydraulics*, J.S. Rosenshein and G.D. Bennett, Eds., American Geophysical Union, pp. 222-239. DOI: 10.1029/WM009p0222

Nielsen, D.M., and R. Schalla (2006), "Design and Installation of Ground-water Monitoring Wells," *Practical Handbook of Environmental Site Characterization and Ground-Water Monitoring*, Taylor & Francis, D.M. Nielsen, Ed., 2nd Edition, pp. 639-805.

Nigbor, R. L., and T. Imai (1994), "The Suspension P-S Velocity Logging Method," *Geophysical Characterization of Sites*, International Science, New York, R. Woods, Ed., pp. 57-61.

Nishida, Y. (1956), "A Brief Note on Compression Index of Soil," *Journal of the Soil Mechanics and Foundations Division*, ASCE, Vol. 82, No. 3, pp. 1-14.

Nixon, J.F. (1991), "Discrete Ice Lens Theory for Frost Heave in Soils," *Canadian Geotechnical Journal*, National Research Council of Canada, Vol. 28, No. 6, pp. 23-32. DOI: 10.1139/t91-102

Nordquist, J.E., G.S. Mason, Jr., and G.L. Olson (1986), "Clay Liner Hydraulic Conductivity: Comparison of Field and Laboratory Tests," *Environmental Engineering: Proceedings of a Specialty Conference*, Cincinnati, Ohio, ASCE, pp. 401-406.

NRCS (2012), *Chapter 4: Engineering Classification of Rock Materials*, National Engineering Handbook, Part 631, Natural Resources Conservation Service, U.S. Department of Agriculture, 210-VI-NEH, Amend. 55, 53 pp.

NRCS (2016), *Web Soil Survey*, National Resources Conservation Service, U.S. Department of Agriculture, Web. Accessed August 6, 2016. http://websoilsurvey.sc.egov.usda.gov/App/WebSoilSurvey.aspx

Nyman, K.J. (1980), *Field Load Tests of Interpreted Drilled Shafts in Coral Limestone*, M.S. Thesis, The University of Texas, Austin, Texas, 181 pp.

Ohba, S., and I. Toriuma (1970), "Research on Vibrational Characteristics of Soil Deposits in Osaka, Part 2, on Velocities of Wave Propagation and Predominant Periods of Soil Deposits," *Abstracts of Technical Meeting of Architectural Institute of Japan*.

Ohsaki, Y., and R. Iwasaki (1973), "On Dynamic Shear Moduli and Poisson's Ratios of Soil Deposits," *Soil and Foundations*, Japanese Society of Soil Mechanics and Foundation Engineering, Vol. 13, No. 4, pp. 61-73. DOI: 10.3208/sandf1972.13.4_61

Ohta, Y., and N. Goto (1978), "Empirical Shear Wave Velocity Equations in Terms of Characteristic Soil Indexes," *Earthquake Engineering and Structural Dynamics*, Vol. 6, No. 2, pp. 167-187. DOI: 10.1002/eqe.4290060205

Ohtsubo, M., M. Takayama, and K. Egashira (1983), "Relationships of Consistency Limits and Activity to Some Physical and Chemical Properties of Ariake Marine Clays," *Soils and Foundations*, Japanese Society of Soil Mechanics and Foundation Engineering, Vol. 23, No. 1, pp. 38-46. DOI: 10.3208/sandf1972.23.38

Olive, W.W., A.F Chleborad, C.W. Frahme, J. Shlocker, R.R. Schneider, and R.L. Schuster (1989), *Swelling Clays Map of the Conterminous United States*, U.S. Geological Survey, Map I-1940, Web. Accessed December 2, 2016. https://pubs.er.usgs.gov/publication/i1940

Olsen, H.W. (1962), "Hydraulic Flow Through Saturated Clays," *Clays and Clay Minerals*, Proceedings of the Ninth National Conference on Clays and Clay Minerals, Permagon Press Ltd., Vol. 9, pp. 131-161.

Olsen, H.W., T.L. Rice, P.W. Mayne, and R.D. Singh (1986), "Piston Core Properties and Disturbance Effects," *Journal of Geotechnical Engineering*, ASCE, Vol. 112, No. 6, pp. 608-625. DOI: 10.1061/(ASCE)0733-9410(1986)112:6(608)

Olson, S.M., and C.I. Johnson (2008), "Analyzing Liquefaction-Induced Lateral Spreads using Strength Ratios," *Journal of Geotechnical and Geoenvironmental Engineering*, ASCE, Vol. 134, No. 8, pp. 1035-1049. DOI: 10.1061/(ASCE)1090-0241(2008)134:8(1035)

O'Neill, M.W., F.C. Townsend, K.M. Hassan, A. Buller, and P.S. Chan (1996), *Load Transfer for Drilled Shafts in Intermediate Geomaterials*, Report FHWA-RD-95-171, Federal Highway Administration, 184 pp.

O'Rourke, J.E. (1989), "Rock index properties for geoengineering in underground development," *Mining Engineering*, Vol. 41, No. 2, pp. 106-110.

Osouli, A., B. Moradi Bajestani, I. Shafii, and K.S. Singh (2014), "Conversion of Point Load Test Results to Conventional Strength Tests for Shale, Claystone and Limestone Rocks," *Proceedings of the 48th US Rock Mechanics/Geomechanics Symposium*, Minneapolis, Minnesota, American Rock Mechanics Association, paper ARMA 14-7424.

Oyler, D.C., C. Mark, and G.M. Molinda (2008), "Correlation of Sonic Travel Time to the Uniaxial Compressive Strength of U.S. Coal Measure Rocks," *Proceedings of the 27th International Conference on Ground Control in Mining*, Morgantown, West Virginia, pp. 338-346.

Ozer, M. (2009), "Comparison of liquid limit values determined using the hard and soft base Casagrande apparatus and the cone penetrometer," *Bulletin of Engineering Geology and the Environment*, Springer-Verlag, Vol. 68, No. 3, pp. 289-296. DOI: 10.1007/s10064-009-0191-4

Pandian, N.S., A. Sridharan, and K.S. Kumar (1994), "Improved Velocity Method for the Determination of Coefficient of Consolidation," *Geotechnical Testing Journal*, American Society for Testing and Materials, Vol. 17, No. 1, pp. 113-118. DOI: 10.1520/GTJ10079J

Pando, M.A., C.D. Ealy, G.M. Filz, J.J. Lesko, and E.J. Hoppe (2006), *A Laboratory and Field Study of Composite Piles for Bridge Substructures*, Federal Highway Administration, Report FHWA-HRT-04-043, 384 pp.

Parez, L., and R. Faureil (1988), "Le Piézocone. Améliorations Apportées á la Reconnaissance de Sols," *Revue Française de Géotech*, Vol. 44, pp. 13-27.

Park, C.B., R.D. Miller, and J. Xia (1999), "Multichannel analysis of surface waves," *Geophysics*, Society of Exploration Geophysicists, Vol. 64, No. 3, pp. 800-808. DOI: 10.1190/1.1444590

Parkin, A.K. (1978), "Coefficient of Consolidation by Velocity Method," *Geotechnique*, Institution of Civil Engineers, Vol. 28, No. 4, pp. 472-474. DOI: 10.1680/geot.1978.28.4.472

Parkin, A.K. (1981), "Consolidation Analysis by Velocity Method," *Proceedings of the 10th International Conference on Soil Mechanics and Foundation Engineering*, Stockholm, Vol. 1, pp. 723-726.

Parry, R.H.G. (1971), "A Simple Driven Piezometer," *Geotechnique*, Institution of Civil Engineers, Vol. 21, No. 2, pp. 163-167. DOI: 10.1680/geot.1971.21.2.163

Peck, R.B. (1967), "Bearing Capacity and Settlement: Certainties and Uncertainties," *Proceedings of a Symposium on Bearing Capacity and Settlement of Foundations*, A.S Vesic, Editor, Department of Civil Engineering, Duke University, pp. 3-7.

Peck, R.B. (1969), "Advantages and Limitations of the Observational Method in Applied Soil Mechanics," *Geotechnique*, Vol. 19, No. 2, pp. 171-187. DOI: 10.1680/geot.1969.19.2.171

Peck, R.B., W.E. Hanson, and T.H. Thornburn (1974), *Foundation Engineering*, John Wiley and Sons, 2nd Edition, 514 pp.

Pedrini, R.A.A., and H.L. Giacheti (2013), "The Seismic SPT to Determine the Maximum Shear Modulus," *Geotechnical and Geophysical Site Characterization 4*, CRC Press, Vol. 1, pp. 337-342.

Penman, A.D.M. (1960), "A Study of the Response Time of Various Types of Piezometers," *Proceedings of the Conference on Pore Pressure and Suction in Soils*, Butterworths, London, pp. 53-58.

Penner, E., W.J. Eden, and P.E. Gattan-Bellow (1972), "Expansion of Pyritic Shales," *Canadian Building Digest*, CBD-152, National Research Council of Canada.

Perras, M.A., and M.S. Diederichs (2014), "A Review of the Tensile Strength of Rock: Concepts and Testing," *Geotechnical and Geological Engineering*, Springer International Publishing, Vol. 32, No. 2, pp. 525-546. DOI: 10.1007/s10706-014-9732-0

Petley, D. (2010), "The mechanism of the Highway 3 landslide in Taiwan," The Landslide Blog, American Geophysical Union. Web: http://blogs.agu.org/landslideblog/2010/04/26/the-mechanism-of-the-highway-3-landslide-in-taiwan/ Accessed February 14, 2017.

Petry, T.M., and D.N. Little (1992), "Update on Sulfate-Induced Heave in Treated Clays: Problematic Sulfate Levels," *Transportation Research Record*, Transportation Research Board, No. 1362, pp. 51-55. http://onlinepubs.trb.org/Onlinepubs/trr/1992/1362/1362-007.pdf

Phoon, K-K, F.H. Kulhawy, and M.D. Grigoriu (1995), *Reliability-Based Design of Foundations for Transmission Line Structures*, Report TR-105000, Electrical Power Research Institute, 380 pp.

Phoon, K-K, F.H. Kulhawy, and M.D. Grigoriu (2000), "Reliability-based design for transmission line structure foundations," *Computers and Geotechnics*, Elsevier, Vol. 26, No. 3-4, pp. 169-185. DOI: 10.1016/S0266-352X(99)00037-3

Powell, J.J.M., and I.M. Uglow (1988), "The Interpretation of Marchetti Dilatometer Test in UK Clays," *ICE Proceedings of the Conference on Penetration Testing in the U.K.*, Institution of Civil Engineers, Paper No. 34, pp. 269-273.

Powers, J.P., A.B. Corwin, P.C. Schmall, and W.E. Kaeck (2007), *Construction Dewatering and Groundwater Control*, 3rd Edition, John Wiley and Sons, 638 pp. DOI: 10.1002/9780470168103

Prange, B. (1981), "Resonant Column Testing of Railroad Ballast," *Proceedings of the 10th International Conference on Soil Mechanics and Foundation Engineering*, Stockholm, Vol. 1, pp. 273-278.

Puppala, A.J., E. Wattanasanticharoen, N. Intharasombat, and L.R. Hoyos (2003), "Studies to Understand Soil Composition and Environmental Variables Effects on Sulfate Heave Problems," *Soil and Rock America 2003*, Proceedings of the 12th Panamerican Conference on Soil Mechanics and Geotechnical Engineering and the 39th U.S. Rock Mechanics Symposium, Verlag Glückauf GmbH, Vol. 1, pp. 833-839.

Quigley, R.M., J.E. Zajic, E. McKyes, and R.N. Yong (1973), "Oxidation and Heave of Black Shale," *Journal of the Soil Mechanics and Foundations Division*, ASCE, Vol. 99, No. 5, pp. 417-421.

Raman, V. (1967), "Identifications of expansive soils from the plasticity index and the shrinkage index data," *The Indian Engineer*, Vol. 11, No. 1, pp. 17-22.

Read, J.R.L., P.N. Thornten, and W.M. Regan (1980), "A rational approach to the point load test," *Proceedings of the 3rd Australia-New Zealand Conference on Geomechanics*, Wellington, New Zealand, New Zealand Institution of Engineers, Vol. 2, pp. 35-39.

Reese, L.C., W.R. Cox, and F.D. Koop (1974), "Analysis of Laterally Loaded Piles in Sand," *Proceedings of the VI Annual Offshore Technology Conference*, Houston, Texas, II(OTC 2080), pp. 473-485.

Reese, L.C., and R.C. Welch (1975), "Lateral Loading of Deep Foundations in Stiff Clay," *Journal of Geotechnical Engineering, ASCE*, Vol. 101, No. 7, pp. 633-649.

Reese, L.C., W.R. Cox, and F.D. Koop (1975), "Field testing and analysis of laterally loaded piles in stiff clay," *Proceedings of the VII Annual Offshore Technology Conference*, Houston, Texas, II(OTC 2312), pp. 672-690.

Reese, L.C. (1997), "Analysis of Laterally Loaded Piles in Weak Rock," *Journal of Geotechnical and Geoenvironmental Engineering*, ASCE, Vol. 123, No. 11, pp. 1010-1017. DOI: 10.1061/(ASCE)1090-0241(1997)123:11(1010)

Reese, L.C., W.M. Isenhower, and S.T. Wang (2006), *Analysis and Design of Shallow and Deep Foundations*, John Wiley and Sons, 574 pp.

Rendon-Herrero, O. (1983), "Closure to 'Universal Compression Index Equation' by O. Rendon-Herrero (1980)," *Journal of Geotechnical Engineering*, Vol. 109, No. 5, pp. 755-761. DOI: 10.1061/(ASCE)0733-9410(1983)109:5(755)

Reynolds, W.D. and D.E. Elrick (1986), "A Method for Simultaneous In Situ Measurement in the Vadose Zone of Field Saturated Hydraulic Conductivity, Sorptivity and the Conductivity-Pressure Head Relationship. *Groundwater Monitoring and Remediation*, Wiley, Vol. 6, No. 1, pp. 84-95.

Rieke, R.D., T.S. Vinson, and D.W. Mageau (1983), "The Role of Specific Surface Area and Related Index Properties in the Frost Heave Susceptibility of Soils," *Proceedings of the 4th International Permafrost Conference*, Fairbanks, Alaska, pp. 1066–1071.

Rix, G.J., and K.H. Stokoe, II (1991), "Correlation of initial tangent modulus and cone penetration resistance," *Proceedings of the First International Symposium on Calibration Chamber Testing*, Potsdam, New York, Elsevier, pp. 351-362.

Roberge, P.R. (2000), *Handbook of corrosion engineering*, McGraw-Hill, 1140 pp.

Robertson, P.K., and R.G. Campanella (1983), "Interpretation of cone penetration tests. Part II: Clay," *Canadian Geotechnical Journal*, National Research Council of Canada, Vol. 20, No. 4, pp. 734-745. DOI: 10.1139/t83-079

Robertson, P.K., R.G. Campanella, D. Gillespie, and J. Greig (1986), "Use of Piezometer Cone data," *Use of In Situ Tests in Geotechnical Engineering*, S.P. Clemence, Ed., ASCE, GSP 6, pp. 1263-1280.

Robertson, P.K., R.G. Campanella, D.G. Gillespie, and T. By (1988), "Excess Pore Pressure and the Flat Dilatometer Test," *Penetration Testing 1988*, Proceedings of the 1st International Symposium on Penetration Testing, A.A. Balkema, Vol. 1, pp. 567-576.

Robertson, P.K. (1990), "Soil classification using the cone penetration test," *Canadian Geotechnical Journal*, National Research Council of Canada, Vol. 27, No. 1, pp. 151-158. DOI: 10.1139/t90-014

Robertson, P.K., J.P. Sully, D.J. Woeller, T. Lunne, J.J.M. Powell, and D.G. Gillespie (1992), "Estimating coefficient of consolidation from piezocone tests," *Canadian Geotechnical Journal*, National Research Council of Canada, Vol. 29, No. 4, pp. 539-550. DOI: 10.1139/t92-061

Robertson, P.K., and C.E. (Fear) Wride (1998), "Evaluating cycle liquefaction potential using the cone penetration test," *Canadian Geotechnical Journal*, NRC Canada, Vol. 35, No. 3, pp. 442-459. DOI: 10.1139/t98-017

Robertson, P.K. (2009), "CPT-DMT Correlations," *Journal of Geotechnical and Geoenvironmental Engineering*, ASCE, Vol. 135, No. 11, pp. 1762-1771. DOI: 10.1061/(ASCE)GT.1943-5606.0000119

Robertson, P.K. (2010), "Soil behavior type from the CPT: an update," *Proceedings of the 2nd International Symposium on Cone Penetration Testing*, Huntington Beach, California, Paper 2-56.

Robertson, P.K., and K.L. Cabal (2015), *Guide to Cone Penetration Testing for Geotechnical Engineering*, Gregg Drilling & Testing, Inc., 6th Edition, 133 pp.

Robinson, R.G., and M.M. Allam (1996), "Determination of Coefficient of Consolidation from Early Stage of Log t Plot," *Geotechnical Testing Journal*, American Society for Testing and Materials, Vol. 19, No. 3, pp. 316-320. DOI: 10.1520/GTJ10358J

Rocha, B.P., R.A.A. Pedrini, and H.L. Giacheti (2015), "$G_o$/N ratio in Tropical Soils from Brazil," *Electronic Journal of Geotechnical Engineering*, Vol. 20, pp. 1915-1933. http://www.ejge.com/2015/Ppr2015.0262ma.pdf

Rogers, C.D.F., T.A. Dijkstra, and I.J. Smalley (1994), "Hydroconsolidation and subsidence of loess: Studies from China, Russia, North America and Europe: In memory of Jan Sajgalik," *Engineering Geology*, Elsevier, Vol. 37, No. 2, pp. 83-113. DOI: 10.1016/0013-7952(94)90045-0

Rogers, C.D.F. (1995), "Types and Distribution of Collapsible Soils," *Genesis and Properties of Collapsible Soils*, Kluwer Academic Publishers, NATO Science Series C, Vol. 468, pp. 1-17.

Rosenblad, B.L., and J. Li (2009), "Comparative study of refraction microtremor (ReMi) and active source methods for developing low-frequency surface wave dispersion curves," *Journal of Environmental & Engineering Geophysics*, Vol. 14, No. 3, pp. 101-113. DOI: 10.2113/JEEG14.3.101

Rosenblad, B.L., F. Gomez, J.E. Loehr, J. Legarsky, W. Jenkins, and B. Held (2013), "Ground-based Interferometric Radar for Monitoring Slopes and Embankments," *Proceedings of Geo-Congress 2013: Stability and Performance of Slopes and Embankments III*, ASCE, pp. 323-332. DOI: 10.1061/9780784412787.032

Ross, G.J. (1978) "Relationships of Specific Surface Area and Clay Content to Shrink-Swell Potential of Soils Having Different Clay Mineralogic Compositions," *Canadian Journal of Soil Science*, Vol. 58, No. 2, pp. 159–166. DOI: 10.4141/cjss78-020

Rowe, P.W. (1964), "The Calculation of the Consolidation Rates of Laminated, Varved or Layered Clays, with Particular Reference to Sand Drains," *Geotechnique*, Institution of Civil Engineers, Vol. 14, No. 4, pp. 321-340. DOI: 10.1680/geot.1964.14.4.321

Rowe, P.W. (1971), "Theoretical meaning and observed values of deformation parameters for soil," *Stress-Strain Behaviour of Soils: Proceedings of the Roscoe Memorial Symposium*, Cambridge University, The Whitefriars Press, Ltd., pp. 143-194.

Ruegsegger, L.R. (1999), *Manual for Abandoned Underground Mine Inventory and Risk Assessment*, Federal Highway Administration, Report FHWA-IF-99-007, 166 pp.

Rusnak, J. and C. Mark (2000), "Using the point load test to determine the uniaxial compressive strength of coal measure rock," *Proceedings of the 19th International Conference on Ground Control in Mining*, S.S. Peng and C. Mark, editors, West Virginia University, Morgantown, West Virginia, pp. 362-371.

Sachpazis, C.I. (1990), "Correlating Schmidt hardness with compressive strength and Young's modulus of carbonate rocks," *Bulletin of the International Association of Engineering Geology*, Springer-Verlag, Vol. 42, No. 1, pp. 75-83. DOI: 10.1007/BF02592622

Sai, J.O., and D.C. Anderson (1990), "Field Hydraulic Conductivity Tests for Compacted Soil Liners," *Geotechnical Testing Journal*, American Society for Testing and Materials, Vol. 13, No. 3, pp. 215-225. DOI: 10.1520/GTJ10160J

Santagata, M.C., and J.T. Germaine (2002), "Sampling Disturbance Effects in Normally Consolidated Clays," *Journal of Geotechnical and Geoenvironmental Engineering*, ASCE, Vol. 128, No. 12, pp. 997-1006. DOI: 10.1061/(ASCE)1090-0241(2002)128:12(997)

Santi, P.M. (1998), "Improving the Jar Slake, Slake Index, and Slake Durability Tests for Shales," *Environmental & Engineering Geoscience*, Association of Engineering Geologists, Vol. IV, No. 3, pp. 385-396. DOI: 10.2113/gseegeosci.IV.3.385

Santi, P.M. (2006), "Field Methods for Characterizing Weak Rock for Engineering," *Environmental and Engineering Geoscience*, Association of Engineering Geologists, Vol. XII, No. 1, pp. 1-11. DOI: 10.2113/12.1.1

Sauer, E.K., A.K. Egeland, and E.A. Christiansen (1993), "Compression characteristics and index properties of tills and intertill clays in southern Saskatchewan, Canada," *Canadian Geotechnical Journal*, National Research Council of Canada, Vol. 30, No. 2, pp. 257-275. DOI: 10.1139/t93-022

Savidge, J., K. Bennett, A. Lutenegger, and C-J Hung (2006), *Subsurface Investigation Qualification: Participant Workbook*," Participant workbook for NHI Course 132079, National Highway Institute, Federal Highway Administration, Publication FHWA-NHI-05-035, 838 pp.

Schmertmann, J.H. (1955), "The Undisturbed Consolidation Behavior of Clay," *Transactions of the American Society of Civil Engineers*, ASCE, Vol. 120, pp. 1201-1233.

Schmertmann, J.H. (1969), "Swell Sensitivity," *Geotechnique*, Vol. 19, No. 4, pp. 530-533. DOI: 10.1680/geot.1969.19.4.530

Schmertmann, J.H. (1970a), "Suggested Method for Deep Static-Cone Penetration Test," *Special Procedures for Testing Soil and Rock for Engineering Purposes: Fifth Edition*, American Society for Testing and Materials, ASTM STP 479, pp. 71-77. DOI: 10.1520/STP38475S

Schmertmann, J.H. (1970b), "Static cone to compute static settlement over sand," *Journal of the Soil Mechanics and Foundations Division*, ASCE, Vol. 96, No. 3, pp. 1011-1043.

Schmertmann, J.H. (1975), "Measurement of In-Situ Shear Strength," *In Situ Measurement of Soil Properties*, Proceedings of a Specialty Conference, Raleigh, North Carolina, ASCE, Vol. 2, pp. 57-138.

Schmertmann, J.H., J.P. Hartmann, and P.R. Brown (1978), "Improved strain influence factor diagrams," *Journal of the Geotechnical Engineering Division*, ASCE, Vol. 104, No. 8, pp. 1131-1135.

Schmertmann, J. H. (1986), "Dilatometer to compute foundation settlement," *Use of In Situ Tests in Geotechnical Engineering*, S.P. Clemence, Ed., ASCE, GSP 6, pp. 303-321.

Schmertmann, J.H. (1988), *Guidelines for Using CPT, CPTU and Marchetti DMT for Geotechnical Design*, FHWA Office of Research and Special Studies, Report FHWA-PA-87-022-84-24, 183 pp.

Schmertmann, J.H. (1991), "Undrained Strength of Weak Clays," *DMT Digest No. 12*, Section 12E, pp. 6-7.

Schnaid, F. (2009), *In Situ Testing in Geomechanics – The Main Tests*, Taylor and Francis, London, 327 pp.

Schneider, J.A., and R.E.S. Moss (2011), "Linking cyclic stress and cyclic strain based methods for assessment of cyclic liquefaction triggering in sands," *Geotechnical Letters*, ICE Publishing, Vol. 1, No. 2, pp. 31-36. DOI: 10.1680/geolett.11.00021

Scott, R.F. (1981), *Foundation Analysis*, Prentice Hall, Englewood Cliffs, New Jersey, 545 pp.

Seed, H.B., and C.K. Chan (1959), "Structure and Strength Characteristics of Compacted Clays," *Journal of the Soil Mechanics and Foundations Division*, ASCE, Vol. 85, No. SM5, pp. 87-128.

Seed, H.B., R.J. Woodward, and R. Lundgren (1962), "Prediction of Swelling Potential for Compacted Clays," *Journal of the Soil Mechanics and Foundations Division*, ASCE, Vol. 88, No. 3, pp. 53-87.

Seed, H.B., and S.D. Wilson (1967), "The Turnagain Heights Landslide, Anchorage, Alaska," *Journal of the Soil Mechanics and Foundations Division*, ASCE, Vol. 93, No. SM4, pp. 325-353.

Seed, H. B., and I.M. Idriss (1970), *Soil Moduli and Damping Factors for Dynamic Response Analyses*, Earthquake Engineering Research Center, University of California, Berkeley, Report EERC 70-10.

Seed, H.B., and M.L. Silver (1972), "Settlement of Dry Sands During Earthquakes," *Journal of the Soil Mechanics and Foundations Division*, ASCE, Vol. 98, No. SM4, pp. 381-397.

Seed, H.B., R.T. Wong, I.M. Idriss, and K. Tokimatsu (1986), "Moduli and Damping Factors for Dynamic Analyses of Cohesionless Soils," *Journal of Geotechnical Engineering*, Vol. 112, No. 11, pp. 1016-1032. DOI: 10.1061/(ASCE)0733-9410(1986)112:11(1016)

Senneset, K., and N. Janbu (1985), "Shear Strength Parameters Obtained from Static Cone Penetration Tests," *Strength Testing of Marine Sediments: Laboratory and In-Situ Measurements*, American Society for Testing and Materials, ASTM STP 883, pp. 41-54. DOI: 10.1520/STP36328S

Senneset, K., R. Sandven, T. Lunne, T. By, and T. Amundesen (1988), "Piezocone Testing in Silty Soil," *Penetration Testing 1988*, Proceedings of the 1st International Symposium on Penetration Testing, A.A. Balkema, Vol. 2, pp. 955-966.

Serafim, J.L., and J.P. Periera (1983), "Consideration of the geomechanics classification of Bieniawski," *Proceedings of the International Symposium on Engineering Geology and Underground Construction*, Lisbon, Portugal, pp. 1133-1144.

Sevee, J. (2006), "Methods and Procedures for Defining Aquifer Parameters," *Practical Handbook of Environmental Site Characterization and Ground-Water Monitoring*, Taylor & Francis, D.M. Nielsen, Ed., 2nd Edition, pp. 913-958.

Sheahan, T.C., and P.J. Watters (1997), "Experimental Verification of CRS Consolidation Theory," *Journal of Geotechnical and Geoenvironmental Engineering*, ASCE, Vol. 123, No. 5, pp. 430-437. DOI: 10.1061/(ASCE)1090-0241(1997)123:5(430)

Shepherd, R.G. (1989), "Correlations of Permeability and Grain Size," *Groundwater*, National Ground Water Association, Vol. 27, No. 5, pp. 633-638. DOI: 10.1111/j.1745-6584.1989.tb00476.x

Sherard, J.L., E.F. Steele, R.S. Decker, and L.P. Dunnigan (1976a), "Pinhole Test for Identifying Dispersive Soils," *Journal of the Geotechnical Engineering Division*, ASCE, Vol. 102, No. 1, pp. 69-85.

Sherard, J.L., R.S. Decker, and L.P. Dunnigan (1976b), "Identification and Nature of Dispersive Soils," *Journal of the Geotechnical Engineering Division*, ASCE, Vol. 102, No. 4, pp. 287-301.

Sills, G.C., M.S.S. Almeida, and F.A.B. Danziger (1988), "Coefficient of consolidation from piezocone dissipation tests in a very soft clay," *Penetration Testing 1988*, Proceedings of the 1st International Symposium on Penetration Testing, A.A. Balkema, Vol. 2, pp. 967-974.

Singh, R.N., F.P. Hassani, P.A.S. Elkington (1983), "The application of strength and deformation index testing to the stability assessment of coal measures excavations," *Proceedings of the 24th U.S. Symposium on Rock Mechanics*, Balkema, Rotterdam, pp. 599-609.

Singh, T.N., A. Kainthola, and A. Venkatesh (2012), "Correlation between Point Load Index and Uniaxial Compressive Strength for Different Rock Types," *Rock Mechanics and Rock Engineering*, Spring-Verlag, Vol. 45, No. 2, pp. 259-264. DOI: 10.1007/s00603-011-0192-z

Singh, V.K., and D.P. Singh (1993), "Correlation between point load index and compressive strength for quartzite rocks," *Geotechnical and Geological Engineering*, Kluwer Academic Publishers, Vol. 11, No. 4, pp. 269-272. DOI: 10.1007/BF00466369

Sisman, H. (1995), *An Investigation on Relationships between Shear Wave Velocity, and SPT and Pressuremeter Test Results*, Master of Science Thesis, Ankara University, Turkey.

Skempton, A.W. (1944), "Notes on the Compressibility of Clays," *Quarterly Journal of the Geological Society*, The Geological Society, London, Vol. 100, pp. 119-135. DOI: 10.1144/GSL.JGS.1944.100.01-04.08

Skempton, A.W., and R.D. Northey (1952), "The Sensitivity of Clays," *Geotechnique*, Institution of Civil Engineers, Vol. 3, No. 1, pp. 30-53. DOI: 10.1680/geot.1952.3.1.30

Skempton, A.W. (1953), "The colloidal 'activity' of clays," *Proceedings of the 3rd International Conference on Soil Mechanics and Foundation Engineering*, Zurich, Vol. 1, pp. 57-61.

Skempton, A.W., and L. Bjerrum (1957), "A contribution to the settlement analysis of foundations on clay," *Geotechnique*, Institution of Civil Engineers, Vol. *7*, No. 4, pp. 168-178. DOI: 10.1680/geot.1957.7.4.168

Smith, C. W., A. Hadas, J. Dan, and H. Koyumdjisky (1985), "Shrinkage and Atterberg Limits in Relation to Other Properties of Principle Soil Types in Israel," *Geoderma*, Elsevier, Vol. 35, No. 1, pp. 47–65. DOI: 10.1016/0016-7061(85)90055-2

Smith, H.J. (1997), "The point load test for weak rock in dredging applications," *International Journal of Rock Mechanics and Mining Sciences*, Elsevier, Vol. 34, No. 3-4, Paper No. 295, pp. 295.e1-295.e13. DOI: 10.1016/S1365-1609(97)00063-4

Soderman, L.G., and Y.D. Kim (1970), "Effect of Groundwater Levels on Stress History of the St. Clair Clay Till Deposit," *Canadian Geotechnical Journal*, National Research Council of Canada, Vol. 7, No. 2, pp. 173-187. DOI: 10.1139/t70-022

Soga, K., and J.K. Mitchell (1996), "Rate-dependent deformation of structured natural clays," *Measuring and Modeling Time Dependent Soil Behavior*, T.G. Sheahan and V.N. Kaliakin, Editors, ASCE, GSP 61, pp. 243-257.

Soleimanbeigi, A. (2013), "Undrained Shear Strength of Normally Consolidated and Overconsolidated Clays from Pressuremeter Tests: A Case Study," *Geotechnical and Geological Engineering*, Springer, Vol. 31, No. 5, pp. 1511-1524. DOI: 10.1007/s10706-013-9675-x

Sowers, G.F. (1963), "Engineering Properties of Residual Soils Derived from Igneous and Metamorphic Rocks," *Proceedings of the Second Pan American Conference on Soil Mechanics and Foundation Engineering*.

Sowers, G.B., and G.F. Sowers (1970), *Introductory Soil Mechanics and Foundations*, 3rd Edition, The MacMillan Publishing, 556 pp.

Spangler, M.G., and R.L. Handy (1973), *Soil Engineering*, Third Edition, Intext Press, Inc., 748 pp.

Sridharan, A., N.S. Murthy, and K. Prakash (1987), "Rectangular hyperbola method of consolidation analysis," *Geotechnique*, Institution of Civil Engineers, Vol. 37, No. 3, pp. 355-368. DOI: 10.1680/geot.1987.37.3.355

Stark, T.D., and H.T. Eid (1994), "Drained Residual Strength of Cohesive Soils," *Journal of Geotechnical Engineering*, ASCE, Vol. 120, No. 5, pp. 856-871. DOI: 10.1061/(ASCE)0733-9410(1994)120:5(856)

Stark, T.D., H. Choi, and S. McCone (2005), "Drained Shear Strength Parameters for Analysis of Landslides," *Journal of Geotechnical and Geoenvironmental Engineering*, ASCE, Vol. 131, No. 5, pp. 575-588. DOI: 10.1061/(ASCE)1090-0241(2005)131:5(575)

Stark, T.D., and M. Hussain (2013), "Empirical Correlations: Drained Shear Strength for Slope Stability Analyses," *Journal of Geotechnical and Geoenvironmental Engineering*, ASCE, Vol. 139, No. 6, pp. 853-862. DOI: 10.1061/(ASCE)GT.1943-5606.0000824

Stas, C.V., and F.H. Kulhawy (1984), *Critical Evaluation of Design Methods for Foundations Under Axial Uplift and Compression Loading*, Electrical Power Research Institute, Report EL-3771, 198 pp.

Stokoe, K.H., S.G. Wright, J.A. Bay, and J.M. Roesset (1994), "Characterization of Geotechnical Sites by SASW Method," *Geophysical Characterization of Sites*, in Proceedings of the 13th International Conference on Soil Mechanics and Foundation Engineering, A.A. Balkema, pp. 15-25.

Stokoe, K.H., M.B. Darendeli, R.D. Andrus, and L.T. Brown (1999), "Dynamic Soil Properties: Laboratory, Field and Correlation Studies," *Proceedings of the Second International Conference on Earthquake Geotechnical Engineering*, Lisbon, Portugal, Vol. 3, pp. 811-845.

Stokoe, K.H., II, and J.C. Santamarina (2000), "Seismic-Wave-Based Testing in Geotechnical Engineering," *Proceedings of GeoEng 2000: International Conference on Geotechnical and Geological Engineering*, Melbourne, Australia, Technomic Publishing, pp. 1490-1536.

Strohm, W.E., G.H. Bragg, and T.W. Ziegler (1978), *Design and Construction of Compacted Shale Embankments: Volume 5 – Technical Guidelines*, Federal Highway Administration, Report FHWA-RD-78-141, 154 pp.

Stroud, M.A. (1974), "The standard penetration test in insensitive clays and soft rocks," *Proceedings of the 2nd European Symposium on Penetration Testing, ESOPT-II*, A.A. Balkema, Vol. 2, pp. 367-375.

Stroud, M.A. (1989), "The standard penetration test – its application and interpretation," *Penetration Testing in the UK, Proceedings of the Geotechnology Conference*, Institution of Civil Engineers, pp. 89-95.

Sully, J.P., and R.G. Campanella (1994), "Evaluation of Field CPTU Dissipation Data in Overconsolidated Fine-Grained Soils," *Proceedings of the 13th International Conference on Soil Mechanics and Foundation Engineering*, New Delhi, India, Oxford and IBH Publishing, Vol. 1, pp. 201-205.

Suzuki, Y., K. Tokimatsu, Y. Taya, and Y. Kubota (1995), "Correlation between CPT Data and Dynamic Properties of In Situ Frozen Samples," *Proceedings of the 3rd International Conference on Recent Advances in Geotechnical Earthquake Engineering and Soil Dynamics*, St. Louis, Missouri, University of Missouri-Rolla, pp. 249-252. http://scholarsmine.mst.edu/icrageesd/03icrageesd/session03/13

Sykora, D.E., and K.H. Stokoe, II (1983), *Correlations of In Situ Measurements in Sands of Shear Wave Velocity, Soil Characteristics and Site Conditions*, Civil Engineering Department, University of Texas at Austin, Report GR83-33, 484 pp.

Talluri, N., A.J. Puppala, B.C.S. Chittoori, A.H. Gaily, and P. Harris (2013), "Stabilization of High Sulfate Soils by Extended Mellowing," *Transportation Research Record: Journal of the*

*Transportation Research Board*, Transportation Research Board of the National Academies, No. 2363, pp. 96-104. DOI: 10.3141/2363-11

Tanaka, Y., K. Kudo, Y. Yoshida, and M. Ikemi (1987), *A Study on the Mechanical Properties of Sandy Gravel-Dynamic Properties of Reconstituted Sample*, Central Research Institute of Electric Power Industry. Report U87019.

Tanaka, A., and G.E. Bauer (1998), "Dilatometer Tests in a Leda Clay Crust," *Proceedings of the 1st International Conference on Site Characterization*, Atlanta, Georgia, A.A. Balkema, pp. 877-882.

Tanaka, H., H. Hirabayashi, T. Matsuoka, and H. Kaneko (2012), "Use of fall cone test as measurement of shear strength for soft clay materials," *Soil and Foundations*, Elsevier, Vol. 52, No. 4, pp. 590-599. DOI: 10.1016/j.sandf.2012.07.002

Tandon, R.S., and V. Gupta (2015), "Estimation of strength characteristics of different Himalayan rocks from Schmidt hammer rebound, point load index, and compressional wave velocity," *Bulletin of Engineering Geology and the Environment*, Springer-Verlag, Vol. 74, No. 2, pp. 521-533. DOI: 10.1007/s10064-014-0629-1

Tavenas, F., S. Leroueil, and M. Roy (1982), "The piezocone test in clays: Use and limitations," *Penetration Testing: Proceedings of the 2nd European Symposium on Penetration Testing, ESOPT II*, A.A. Balkema, Vol. 2, pp. 889-894.

Tavenas, F., P. Jean, P. Leblond, and S. Leroueil (1983), "The permeability of natural soft clays. Part II: Permeability Characteristics," *Canadian Geotechnical Journal*, Natural Research Council of Canada, Vol. 20, No. 4, pp. 645-660. DOI: 10.1139/t83-073

Tavenas, F., M. Tremblay, G. Larouche, and S. Leroueil (1986), "In Situ Measurement of Permeability in Soft Clays," *Use of In Situ Tests in Geotechnical Engineering*, S.P. Clemence, Ed., ASCE, GSP 6, pp. 1034-1048.

Tavenas, F., M. Diene, and S. Leroueil (1990), "Analysis of the in situ constant-head permeability test in clays," *Canadian Geotechnical Journal*, National Research Council of Canada, Vol. 27, No. 3, pp. 305-314. DOI: 10.1139/t90-041

Taylor, D.W. (1939), "A Comparison of Results of Direct Shear and Cylindrical Compression Tests," *Proceedings of Symposium on Shear Testing of Soils*, ASTM, Vol. 39, pp. 1058-1070.

Taylor, D.W. (1948), *Fundamentals of Soil Mechanics*, John Wiley and Sons, 700 pp.

Teh, C.I., and G.T. Houlsby (1991), "An analytical study of the cone penetration test in clay," *Geotechnique*, Institution of Civil Engineers, Vol. 41, No. 1, pp. 17-34. DOI: 10.1680/geot.1991.41.1.17

Terzaghi, K. (1955), "Evaluation of Coefficients of Subgrade Reaction," *Geotechnique*, Institution of Civil Engineers, Vol. 5, No. 4, pp. 297-326. DOI: 10.1680/geot.1955.5.4.297

Terzaghi, K., and R.B. Peck (1967), *Soil Mechanics in Engineering Practice*, 2nd Edition, John Wiley and Sons, 729 pp.

Terzaghi, K., R. Peck, and G. Mesri (1996), *Soil Mechanics in Engineering Practice*, 3rd Edition, Wiley-Interscience, 592 pp.

Tewatia, S.K., and K. Venkatachalam (1997), "Improved $\sqrt{t}$ Method to Evaluate Consolidation Test Results," *Geotechnical Testing Journal*, American Society for Testing and Materials, Vol. 20, No. 1, pp. 121-125. DOI: 10.1520/GTJ11426J

Tokimatsu, K., and H.B. Seed (1987), "Evaluation of Settlements in Sands Due to Earthquake Shaking," *Journal of Geotechnical Engineering*, ASCE, Vol. 113, No. 8, pp. 861-878. DOI: 10.1061/(ASCE)0733-9410(1987)113:8(861)

Torstensson, B.A. (1977), "The Pore Pressure Probe," *Norsk Jord-Og Fjellteknisk Forbund*, Oslo, Paper No. 34, pp. 34.1-34.15.

Trautwein, S.J., and G.P. Boutwell (1994), "In-Situ Hydraulic Conductivity Tests for Compacted Soil Liners and Caps," *Hydraulic Conductivity and Waste Contaminant Transport in Soil*, D.E. Daniel and S.J. Trautwein, Editors, ASTM STP 1142, pp. 184-223. DOI: 10.1520/STP23889S

Tugrul, A., and I.H. Zarif (1999), "Correlation of mineralogical and textural characteristics with engineering properties of selected granitic rocks from Turkey," *Engineering Geology*, Elsevier, Vol. 51, No. 4, pp. 303-317. DOI: 10.1016/S0013-7952(98)00071-4

Tumay, M.T., R.L. Boggess, and Y. Acar (1981), "Subsurface Investigations with Piezocone Penetrometer," *Proceedings of the ASCE National Convention*, St. Louis, Missouri, ASCE, pp. 264-301.

Tumay, M.T., and Y. Hatipkarasulu (2011), "Impact of Using Measured v. Corrected Tip Resistance Values in PCPT-based Soil Characterization and Modeling," *Geo-Frontiers 2011: Advances in Geotechnical Engineering*, ASCE, GSP 11, pp. 2544-2553. DOI: 10.1061/41165(397)260

Turner, A.K., and R.L. Schuster (2012), *Rockfall: Characterization and Control*, Transportation Research Board, 658 pp.

U.S. Bureau of Reclamation (1973), *Design of Small Dams*, A Water Resources Technical Publication, U.S. Department of the Interior, 2nd Edition, Government Printing Office, 816 pp.

USGS (2006), *Quaternary Fault and Fold Database of the United States*, U.S. Geological Survey, Web. Accessed June 3, 2016. http//earthquakes.usgs.gov/regional/qfaults/

Vallejo, L.E., R.A. Welsh, and M.K. Robinson (1989), "Correlation Between Unconfined Compressive and Point Load Strengths for Appalachian Rocks," *Proceedings of the 30th U.S. Symposium on Rock Mechanics*, American Rock Mechanics Association, ARMA-89-0461, pp. 461-468.

Van Der Merwe, D.H. (1964), "The prediction of heave from the plasticity index and percentage clay fraction of soils," *Civil Engineer in South Africa*, Vol. 6, No. 6, pp. 103-106.

VandenBerge, D.R., J.M. Duncan, and T.L. Brandon (2013), "Fully Softened Strength of Natural and Compacted Clays for Slope Stability," *Proceedings of Geo-Congress 2013: Stability and Performance of Slopes and Embankments III*, ASCE, pp. 221-233. DOI: 10.1061/9780784412787.023

Vaughan, P.R., R.J. Chandler, J.P. Apted, W.M. McGuire, and S.S. Sandroni (1993), "Sampling disturbance – with particular reference to its effect on stiff clays," *Predictive Soil Mechanics: Proceedings of the Wroth Memorial Symposium*, G.T. Houlsby and A.N. Schofield, Eds., Thomas Telford, pp. 685-708.

Ventura, P. (1983), "Piezometer Cone Penetration Tests in Marine Subsoil Profiles," *Proceedings of the Symposium on In Situ Testing of Soil and Rock*, Vol. 2, pp. 425-430.

Verwaal, W., and A. Mulder (1993), "Estimating Rock Strength with the Equotip Hardness Tester, *International Journal of Rock Mechanics and Mining Sciences & Geomechanics Abstracts*, Permagon Press, Vol. 30, No. 6, pp. 659-662. DOI: 10.1016/0148-9062(93)91226-9

Vesic, A.S., and S.K. Saxena (1970), *Analysis of Structural Behavior of AASHO Road Test Rigid Pavements*, Transportation Research Board, NCHRP Report No. 97, 37 pp.

Vesic, A.S. (1977), *Design of Pile Foundations: Synthesis of Highway Practice 42*, Transportation Research Board, National Research Council, 68 pp.

Vucetic, M., and R. Dobry (1991), "Effect of Soil Plasticity on Cyclic Response," *Journal of Geotechnical Engineering*, ASCE, Vol. 117, No. 1, pp. 89-107. DOI: 10.1061/(ASCE)0733-9410(1991)117:1(89)

Wair, B.R., J.T. DeJong, and T. Shantz (2012), *Guidelines for Estimation of Shear Wave Velocity Profiles*, Pacific Earthquake Engineering Research Center, PEER Report 2012/08, 68 pp.

Walkinshaw, J.L., and P.M. Santi (1996), "Shales and Other Degradable Materials," *Landslides: Investigation and Mitigation*, Transportation Research Board, Special Report 247, Chapter 21, pp. 555-576.

Waltham, A.C., and P.G. Fookes (2003), "Engineering classification of karst ground conditions," *Quarterly Journal of Engineering Geology and Hydrogeology*, Geological Society of London, Vol. 36, No. 2, pp. 101-118.

Warkentin, B.P. (1972), "Use of the Liquid Limit in Characterizing Clay Soils," *Canadian Journal of Soil Science*, Vol. 52, No. 3, pp. 457–464. DOI: 10.4141/cjss72-057

Weary, D.J., and D.H. Doctor (2014), *Karst in the United States: A Digital Map Compilation and Database*, U.S. Department of the Interior, U.S. Geological Survey, Open-File Report 2014-1156, 23 pp. DOI: 10.3133/ofr20141156

Welch, R.C., and L.C. Reese (1972), *Laterally Load Behavior of Drilled Shafts*, Center for Highway Research, The University of Texas, Austin, Texas, Research Report 89-10, 215 pp.

Wightman, W.E., F. Jalinoos, P. Sirles, and K. Hanna (2004), *Application of Geophysical Methods to Highway Related Problems*, Federal Highway Administration, Central Federal Lands Highway Division, FHWA-IF-04-021, 742 pp.

Williams, R.A., W.J. Stephenson, J.K. Odum, and D.M. Worley (2005), "P- and S-wave Seismic Reflection and Refraction Measurements at CCOC," *Blind Comparisons of Shear-Wave Velocities at Closely Spaced Sites in San Jose, California*, M.W. Asten and D.M. Boore, Eds., USGS Open-File Report 2005-1169, 17 pp.

Windle, D., and C.P. Wroth (1977), "The use of a self-boring pressuremeter to determine the undrained properties of clays," *Ground Engineering*, EMAP Construction Ltd., Vol. 10, No. 6, pp. 37-46.

Wood, D.M. (1990), *Soil Behavior and Critical State Soil Mechanics*, Cambridge University Press, 462 pp.

Woodward-Clyde Consultants (1995), *Working documents regarding friction angles of rockfill materials.*

Wright, S.G. (2005), *Evaluation of Soil Shear Strengths for Slope and Retaining Wall Stability Analyses with Emphasis on High Plasticity Clays*, Center for Transportation Research, Report No. FHWA/TX-06/5-1874-01-01, 100 pp.

Wright, S.G., J.G. Zornberg, and J.E. Aguettant (2007), *The Fully Softened Shear Strength of High Plasticity Clays*, Center for Transportation Research, Report No. FHWA/TX-07/0-5202-3, 132 pp.

Wu, T.H., N.Y. Chang, and E.M. Ali (1978), "Consolidation and strength properties of a clay," *Journal of Geotechnical Engineering*, ASCE, Vol. 104, No. GT7, pp. 889-905.

Wyllie, D.C., and C.W. Mah (1998), *Rock Slopes Reference Manual*, National Highway Institute, Federal Highway Administration, Publication FHWI-HI-99-007, 393 pp.

Wyllie, D.C. (1999), *Foundations on Rock*, E&FN Spon, Second Edition, 401 pp.

Yasar, E., and Y. Erdogan (2004a), "Estimation of rock physicomechanical properties using hardness methods," *Engineering Geology*, Elsevier, Vol. 71, No. 3-4, pp. 281-288. DOI: 10.1016/S0013-7952(03)00141-8

Yasar, E., and Y. Erdogan (2004b), "Correlating sound velocity with the density, compressive strength, and Young's modulus of carbonate rocks," *International Journal of Rock Mechanics and Mining Sciences*, Elsevier, Vol. 41, No. 5, pp. 871-875. DOI: 10.1016/j.ijrmms.2004.01.012

Yilmaz, I., and H. Sedir (2002), "Correlation of Schmidt hardness with unconfined compressive strength and Young's modulus in gypsum from Sivas (Turkey)," *Engineering Geology*, Elsevier, Vol. 66, No. 3-4, pp. 211-219. DOI: 10.1016/S0013-7952(02)00041-8

Youd, T.L., and D.M. Perkins (1978), "Mapping Liquefaction-Induced Ground Failure Potential," *Journal of the Geotechnical Engineering Division*, Vol. 104, No. 4, pp. 433-446.

Youd, T.L., I.M. Idriss, R.D. Andrus, I. Arango, G. Castro, J.T. Christian, R. Dobry, W.D. Liam Finn, L.F. Harder, Jr., M.E. Hynes, K. Ishihara, J.P. Koester, S.S.C. Liao, W.F. Marcuson, III, G.R. Martin, J.K. Mitchell, Y. Moriwaki, M.S. Power, P.K. Robertson, R.B. Seed, and K.H. Stokoe, II (2001), "Liquefaction Resistance of Soils: Summary Report from the 1996 NCEER and 1998 NCEER/NSF Workshops on Evaluation of Liquefaction Resistance of Soils," *Journal of Geotechnical and Geoenvironmental Engineering*, ASCE, Vol. 127, No. 10, pp. 817-833. DOI: 10.1061/(ASCE)1090-0241(2001)127:10(817)

Yu, P., and F.E. Richart, Jr (1984), "Stress Ratio Effects on Shear Modulus of Dry Sands," *Journal of Geotechnical Engineering*, ASCE, Vol. 110, No. 3, pp. 331-345. DOI: 10.1061/(ASCE)0733-9410(1984)110:3(331)

Zervogiannis, C.S., and N.A. Kalteziotis (1988), "Experiences and relationships from penetration testing in Greece," *Penetration Testing 1988*, Proceedings of the 1st International Symposium on Penetration Testing, A.A. Balkema, Vol. 2, pp. 1063-1071.

Zhu, J., T.P. Taylor, J.C. Currens, and M.M. Crawford (2014), "Improved karst sinkhole mapping in Kentucky using LIDAR techniques: a pilot study in Floyds Fork Watershed," *Journal of Cave and Karst Studies*, National Speleological Society, Vol. 76, No. 3, pp. 207-216. DOI: 10.4311/2013ES0135

Zywicki, D.J. (2007), "The Impact of Seismic Wavefield and Source Properties on ReMi Estimates," *Innovative Applications of Geophysics in Civil Engineering*, Proceedings of Geo-Denver 2007, ASCE, GSP 164, pp. 1-10. DOI: 10.1061/40908(227)5

## APPENDIX 1

## ASTM/AASHTO STANDARDS REFERENCED

### CHAPTER 4

| Standard Topic | ASTM | AASHTO |
|---|---|---|
| Test method for particle-size analysis of soils | D422[1] | T88 |
| Test methods for specific gravity of soil solids by water pycnometer | D854 | T100 |
| Test method for density and unit weight of soil in place by sand-cone method | D1556 | T191 |
| Test method for density and unit weight of soil in place by the rubber balloon method | D2167 | - |
| Test methods for determining laboratory water (moisture) content of soil and rock | D2216 | T265 |
| Standard practice for classifying soils (Unified Soil Classification System) | D2487 | M145 |
| Standard practice for description and identification of soils using visual-manual procedure | D2488 | - |
| Test method for density of soil in place by the drive-cylinder method | D2937 | - |
| Test methods for moisture, ash, and organic matter of peat and other organic soils | D2974 | T267 |
| Test method for water content of soil and rock in place by nuclear methods (shallow depth) | D3017 | T310 |
| Standard specification for classification of soils and soil-aggregate mixtures for highway construction purposes | D3282 | M145 |
| Test methods for liquid limit, plastic limit and plasticity index of soils | D4318 | T89/ T90 |
| Test method for rapid determination of carbonate content of soils | D4373 | - |
| Test method for determination of water (moisture) content of soil by microwave oven heating | D4643 | - |
| Test method for slake durability for shales and similar weak rocks | D4644 | - |
| Test method for shrinkage factors of soils by the wax method | D4943 | - |
| Test method for field determination of water (moisture) content of soil by the calcium carbide gas pressure tester | D4944 | T217 |
| Test method for determination of water content of soil by direct heating | D4959 | - |
| Test method for density of soil and rock in-place at depths below surface by nuclear methods | D5195 | - |
| Test method for specific gravity of soil solids by gas pycnometer | D5550 | T100 |
| Test method for electronic friction cone and piezocone penetration testing of soils | D5778 | - |
| Test method for determination of rock hardness by rebound hammer method | D5873 | - |
| Test method for logging in situ moisture content and density of soil and rock by nuclear method in horizontal, slanted, and vertical access tubes | D6031 | - |
| Test method for determining rock quality designation (RQD) of rock core | D6032 | - |
| Test methods for particle-size distribution (gradation) of soils using sieve analysis | D6913 | T88 |
| Test methods for in-place density and water content of soil and soil-aggregate by nuclear methods (shallow depth) | D6938 | T310 |
| Test method for measuring the exchange complex and cation exchange capacity of inorganic fine-grained soils | D7503 | - |
| Test method for aggregate resistance to abrasion and impact in the Los Angeles Machine | C131/ C535 | T96 |

[1] ASTM D422 was officially withdrawn in January of 2016. Sieve analyses are now covered under ASTM D6913, but there is no current ASTM standard for hydrometer analyses.

**CHAPTER 5**

| Standard Topic | ASTM | AASHTO |
|---|---|---|
| Test method for determining water-soluble sulfate ion content in soil | C1580 | T290 |
| Test method for determining shrinkage factors of soils by the Mercury method | D427[2] | T92 |
| Test methods for determining organic content of peat and other organic soils | D2974 | T267 |
| Test method for dispersive characteristics of clay soil by double hydrometer | D4221 | - |
| Test method for Anions in water by suppressed ion chromatography | D4327 | - |
| Test methods for one-dimensional swell or collapse of cohesive soils | D4546 | T258 |
| Test method for identification and classification of dispersive clay soils by the pinhole test | D4647 | - |
| Test method for determining shrinkage factors of soils by the wax method | D4943 | - |
| Test method for determination of collapse potential of soils | D5333 | - |
| Test method for determining water-soluble chloride ion content in soil | - | T291 |
| Test method for measuring $pH$ of soil for use in corrosion testing | G51 | T289 |
| Test method for field measurement of soil resistivity using the Wenner four-electrode method | G57 | - |
| Test method for measurement of soil resistivity using the two-electrode soil box method | G187 | T288 |

**CHAPTER 6**

| Standard Topic | ASTM | AASHTO |
|---|---|---|
| Test method for conducting standard penetration test | D1586 | T206 |
| Test method for one dimensional consolidation properties of soil by incremental loading procedure | D2435 | T216 |
| Test method for conducting field vane shear test in cohesive soil | D2573 | T223 |
| Test method for performing the mechanical cone penetration test in soils | D3441 | - |
| Test method for one dimensional consolidation properties of soil by controlled-strain loading | D4186 | - |
| Test method for prebored pressuremeter testing in soils | D4719[3] | - |
| Test method for performing electronic friction cone and piezocone penetration testing of soils | D5778 | - |
| Test method for performing flat plate dilatometer test | D6635 | - |

**CHAPTER 7**

| Standard Topic | ASTM | AASHTO |
|---|---|---|
| Test methods for laboratory compaction characteristics of soil using standard effort | D698 | T99 |
| Test method for unconfined compressive strength of cohesive soil | D2166 | T208 |
| Test method for conducting field vane shear test in cohesive soil | D2573 | T223 |
| Test method for unconsolidated undrained compressive strength of soils in triaxial compression | D2850 | T296 |
| Test method for direct shear testing of soils for consolidated drained strength | D3080 | T236 |
| Test method for laboratory miniature vane test for saturated fine-grained clayey soils | D4648 | - |

[2] ASTM D427 was officially withdrawn in March of 2008.

[3] ASTM D4719 was officially withdrawn in January of 2016.

| Standard Topic | ASTM | AASHTO |
|---|---|---|
| Test method for consolidated undrained triaxial compressive strength of soils | D4767 | T297 |
| Test method for torsional ring shear tests to determine drained residual shear strength of cohesive soils | D6467 | - |

**CHAPTER 8**

| Standard Topic | ASTM | AASHTO |
|---|---|---|
| Test method for plate load tests of soils | D1194 | T222; T235 |
| Test method for determining modulus and damping of soils by resonant column | D4015 | - |
| Test method for performing crosshole seismic testing | D4428 | - |
| Test methods for prebored pressuremeter testing in soils | D4719[4] | - |
| Guide for using seismic refraction for subsurface investigation | D5777 | - |
| Test method for electronic friction cone and piezocone testing of soils | D5778 | - |
| Test method for performing the flat plate dilatometer | D6635 | - |
| Test method for performing downhole seismic testing downhole | D7400 | - |

**CHAPTER 9**

| Standard Topic | ASTM | AASHTO |
|---|---|---|
| Practice for rock core drilling and sampling of rock for site exploration | D2113 | T225 |
| Test method for undrained triaxial compressive strength of rock cores | D2664[5] | T226 |
| Test method for determining pulse velocity and elastic constants of rock | D2845 | - |
| Test method for determining direct tensile strength of rock cores | D2936 | - |
| Test method for splitting tensile strength of intact rock core specimens | D3967 | - |
| Test method for determining in situ modulus of deformation of rock mass using rigid plate loading method | D4394 | - |
| Test method for determining in situ modulus of deformation of rock mass using flexible plate loading method | D4395 | - |
| Test method for in situ determination of direct shear strength of rock discontinuities | D4554 | - |
| Test method for determining in situ modulus of rock using diametrically loaded 76-mm (3-in) borehole jack | D4971 | - |
| Practice for preserving and transporting rock core samples | D5079 | - |
| Test method for performing direct shear tests on rock cores under constant normal force | D5607 | - |
| Test method for determination of the point load strength index of rock and application to rock strength classifications | D5731 | - |
| Test method for determination of rock hardness by rebound hammer method | D5873 | - |
| Guides for using rock-mass classification systems for engineering purposes | D5878 | - |
| Test method for determining compressive strength and modulus of rock cores under varying states of stress and temperatures | D7012 | - |

[4] ASTM D4719 was officially withdrawn in January of 2016.

[5] ASTM D2664 was officially withdrawn in 2005 and replaced with ASTM D7012.

**CHAPTER 10**

| Standard Topic | ASTM | AASHTO |
|---|---|---|
| Test method for determining permeability of granular soils using constant head procedure | D2434[6] | T215 |
| Test method for infiltration rate of soils in field using double-ring infiltrometer | D3385 | - |
| Test method for conducting field slug tests to determine hydraulic properties of aquifers | D4044 | - |
| Test method for conducting field well pumping tests to determine hydraulic properties of aquifers | D4050 | - |
| Test method for determining subsurface liquid levels in a borehole or monitoring well or open piezometer | D4750 | - |
| Test method for determining hydraulic conductivity of soils using flexible wall permeameter | D5084 | - |
| Practice for design and installation of ground water monitoring wells | D5092 | - |
| Practice for monitoring well protection | D5787 | - |
| Guide for installation of direct push groundwater monitoring wells | D6724 | - |

**CHAPTER 12**

| Standard Topic | ASTM | AASHTO |
|---|---|---|
| Practice for decontamination of field equipment used at waste sites | D5088 | |
| Guide for selecting surface geophysical methods | D6429 | |

[6] ASTM D2434 was officially withdrawn in January 2015.

# APPENDIX 2
# EXAMPLES

This Appendix presents examples of developing design models for three sites following the procedures recommended in this manual. In particular, the examples follow procedures outlined in Chapter 11, though lessons from other chapters are used as well.

## A2.1 EXAMPLE 1: BRIDGE SITE WITH SAND OVER SHALE AND LIMESTONE

A river bridge is proposed at a site with alluvial sands over shale and limestone. Geotechnical analyses to support bridge design will primarily involve calculations of deep foundation capacity for drilled shafts and driven piles. In this example, SPT measurements are characterized for design of driven piles and rock is characterized for drilled shaft design and construction.

A boring location plan for the bridge is shown in Figure A2-1. This example focuses on the south end bent, where driven piles are planned to support the bridge abutment, and on the pylon bent, where drilled shafts are anticipated. Site characterization information was collected from three main sources: historic information from investigations performed just west of the new structure from the 55-year-old bridge being replaced; "pre-bid" information collected during the project planning phase; and investigations completed following contract award by the selected design-build team. Available logs for historic borings show only stratigraphy with brief material descriptions and SPT blow counts. For both pre-bid and project borings on land, hollow stem augers were used in soils above the groundwater table and mud rotary drilling was used below the groundwater table. Pre-bid and project borings in the river were drilled from a barge using mud rotary methods. Sampling of the alluvial overburden soils was performed using a split-spoon sampler with SPT testing at 5-ft intervals. Coring in rock for both land and river borings was completed in 5-ft runs using a NX double-tube core barrel.

### A2.1.1 Characterization for South End Bent

At the south end bent, subsurface information was derived from four project borings and one pre-bid boring, as well as from SPT records for three historical borings. A design model characterizing stratigraphy and SPT $N$-values was developed for design of driven piles.

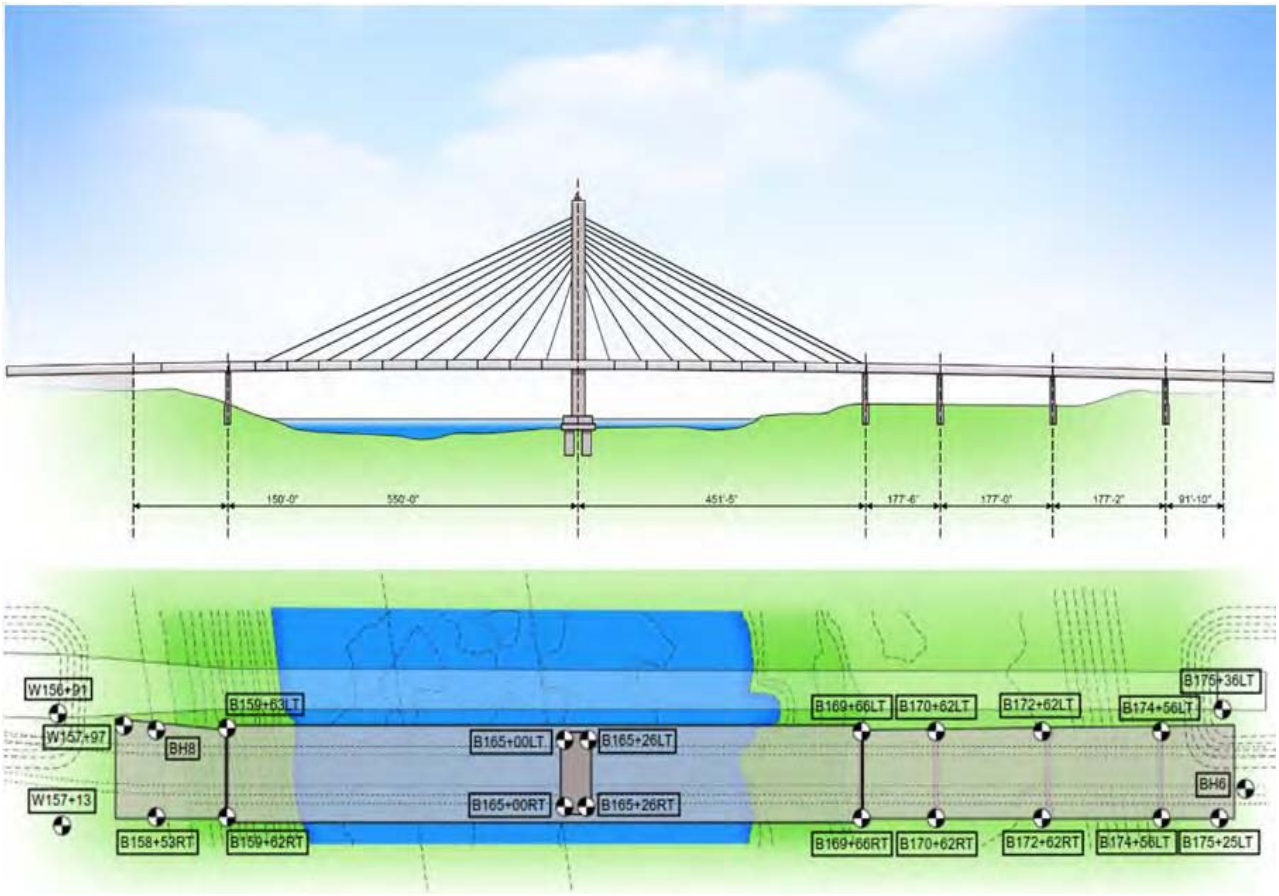


**Figure A2-1 Boring location plan.**

Stratigraphy at the south end bent was evaluated graphically by plotting representations from individual borings together along a cross-section of the end bent. The resulting "stick log" profile is shown in Figure A2-2. All boring logs indicate alluvial soils extending from the ground surface, at approximate elevation 755 feet, to rock at approximately elevation 645 feet. The alluvial soils are predominately sand, but the sand is interbedded with layers of fine-grained soil between elevation 735 feet and 717 feet. Groundwater was observed between elevation 722 and 724 feet in all project and pre-bid borings.

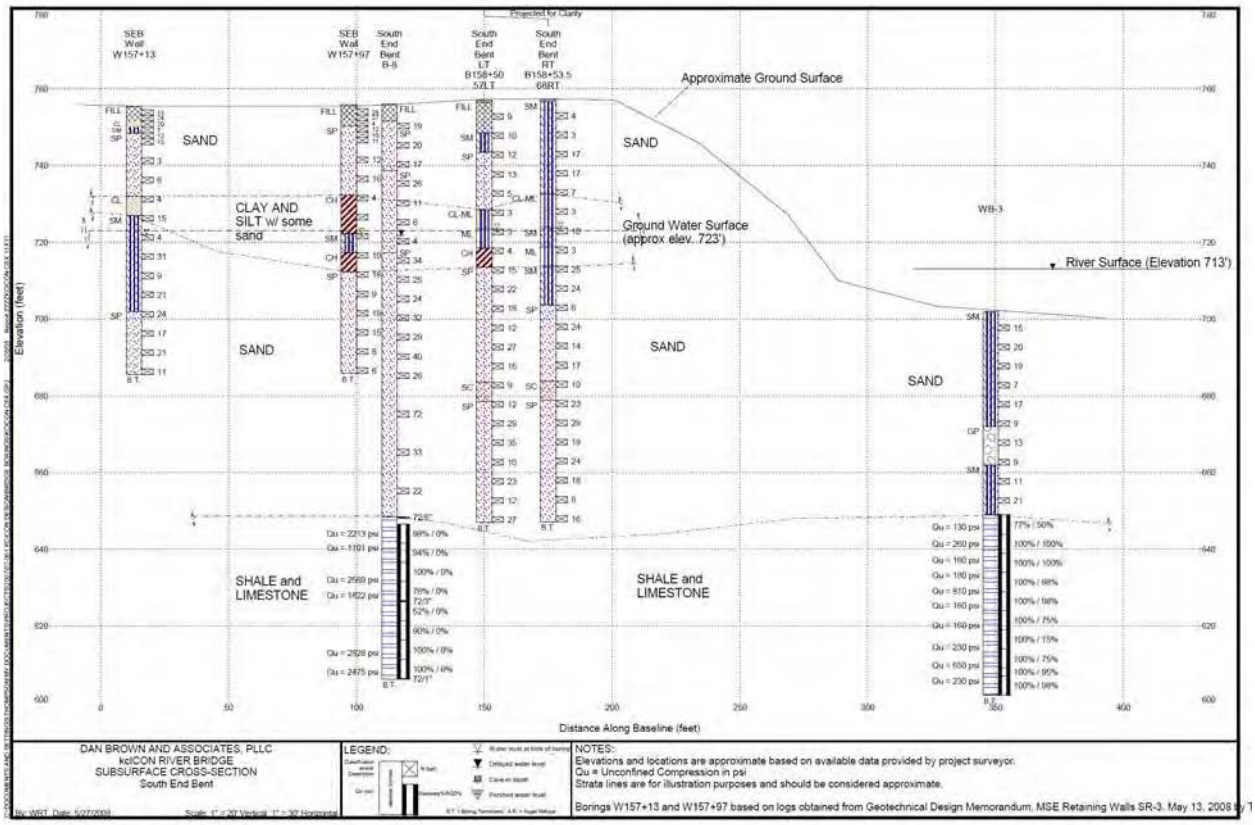


**Figure A2-2 Interpreted stratigraphy showing boring logs (courtesy Dan Brown and Associates).**

SPT measurements from each of the borings are plotted together versus elevation in Figure A2-3 to assess the interpreted stratigraphy and to begin characterizing soil strength for design of driven piles. Measurements shown in the figure suggest conditions can be represented using three layers: "Layer 1" extends from the ground surface to approximately elevation 735 feet, "Layer 2"extends from elevation 735 feet to about elevation 717 feet, and "Layer 3" extends below elevation 717 feet to the contact with rock. SPT $N_{60}$-values in Layer 1 range from about 3 to 30 and are approximately centered around $N_{60} = 15$. $N_{60}$-values in Layer 2 are less, ranging from 3 to 16. SPT $N_{60}$-values in Layer 3 are greatest but also most variable, with $N_{60}$-values between 6 and 40 except for one value around 70. These three layers are consistent with the stratigraphy presented in Figure A2-2, with Layer 1 and Layer 3 representing sand layers and Layer 2 representing fine-grained soils.

Unlike measurements from the project and pre-bid borings, the historic SPT measurements plotted in Figure A2-3a are not corrected for hammer efficiency (i.e., the historic SPT measurements are plotted as $N$, not $N_{60}$) since hammer type and efficiency are unknown. As shown in Figure A2-3a, the uncorrected historic measurements appear to be biased toward greater values than recent measurements for each layer. If the historic data are corrected for a hammer efficiency of 45 percent (typical of a donut hammer), as

shown in Figure A2-3b, the historic $N_{60}$ are more consistent with the project and pre-bid boring measurements. However, this interpretation is entirely speculative since the actual hammer efficiency was not recorded, so the historic measurements are neglected for developing the design model presented below. In addition to potentially affecting nominal interpreted $N_{60}$ values, including the historic data in the interpretation would inappropriately and unconservatively reduce the interpreted model uncertainty. Measurements for each layer are provided in Table A2–1.

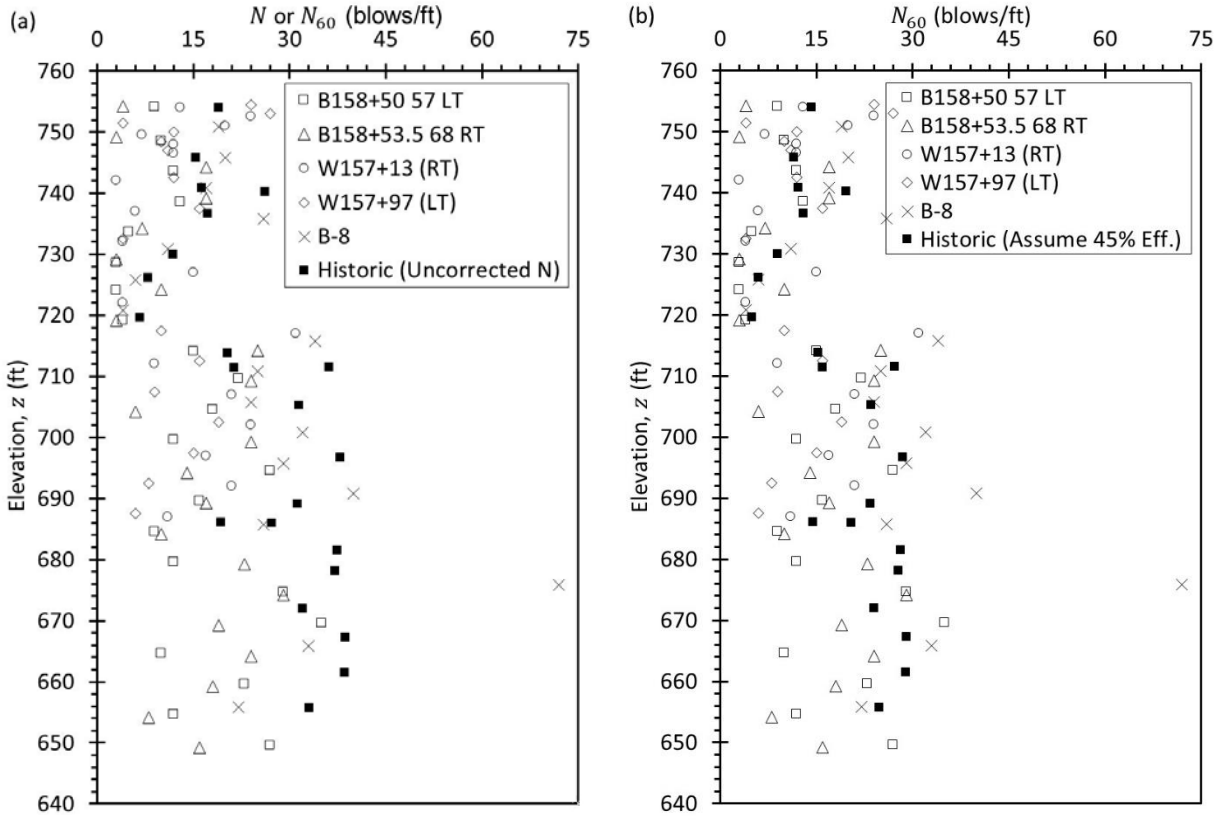


**Figure A2-3 SPT measurements from borings at south end bent with: (a) uncorrected historic measurements and (b) corrected historic measurements assuming hammer efficiency of 45 percent.**

**Table A2–1 $N_{60}$ measurements within each layer at south end bent.**

| Layer Designation | Elevation Range (ft) | SPT $N_{60}$ Measurements (bpf) |
|---|---|---|
| Layer 1 | 755-735 | 24, 4, 9, 13, 27, 24, 4, 20, 19, 12, 7, 3, 10, 10, 12, 11, 12, 20, 17, 12, 12, 3, 17, 17, 13, 16, 6, 26 |
| Layer 2 | 735-717 | 7, 5, 4, 4, 11, 3, 3, 15, 6, 10, 3, 4, 4, 3, 4, 10 |
| Layer 3 | 717-649 | 31, 34, 25, 15, 16, 9, 25, 22, 24, 9, 21, 24, 18, 6, 19, 24, 32, 12, 24, 15, 17, 29, 27, 14, 8, 21, 40, 16, 17, 6, 11, 26, 9, 10, 12, 23, 72, 29, 29, 35, 19, 33, 10, 24, 23, 18, 22, 12, 8, 27, 16 |

A design profile was created to represent $N_{60}$ for the south end bent using mean $N_{60}$-values as shown in Figure A2-4. In this case, it is reasonable to use mean values for estimates since the variation in $N_{60}$ within each layer appears random rather than increasing or decreasing with depth. Similarly, no consistent differences are observed in different borings that might suggest separating the measurements into distinct design domains.

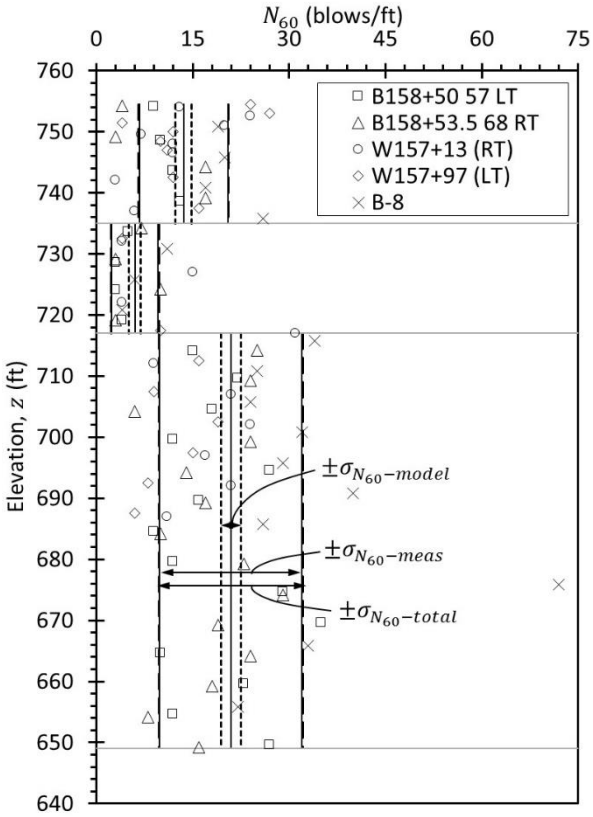


**Figure A2-4 Design profile for $N_{60}$ at south end bent showing variability and uncertainty.**

Standard deviations and coefficients of variation representing variability and uncertainty as described in Chapter 11 were calculated for each layer and are provided in Table A2–2 and shown in Figure A2-4. Calculations were performed according to equations presented in Chapter 11 for direct measurements. While SPT $N_{60}$-values are often considered to be indirect measurements for many design parameters, in this case pile design will be directly determined from the $N_{60}$-values. Thus, the measured $N_{60}$-values should be considered to be direct measurements. Example calculations are provided below for Layer 2.

$$\bar{y} = \frac{\sum_{i=1}^{n} y_i}{n} = \frac{7+5+4+4+11+3+3+15+6+10+3+4+4+3+4+10}{16} = 6.0 \text{ bpf} \quad \text{(A2.1)}$$

$$MSE_y = \frac{\sum_{i=1}^{n} (y_i - \bar{y})^2}{n-1} = \frac{(7-6)^2+(5-6)^2+(4-6)^2+(4-6)^2+\cdots+(10-6)^2}{16} = 13.1 \text{ bpf}^2 \quad \text{(A2.2)}$$

$$\sigma_{meas} = \sqrt{MSE} = \sqrt{13.1\ \text{bpf}^2} = 3.6\ \text{bpf} \quad \text{(A2.3)}$$

$$\sigma_{model} = \sqrt{\frac{MSE}{n}} = \sqrt{\frac{13.1\ \text{bpf}^2}{16}} = 0.90\ \text{bpf} \quad \text{(A2.4)}$$

$$\sigma_{total} = \sqrt{\sigma_{meas}^2 + \sigma_{model}^2} = \sqrt{13.1 + 0.82} = 3.7\ \text{bpf} \quad \text{(A2.5)}$$

$$COV_{N_{60}-meas} = \frac{\sigma_{N_{60}-meas}}{\bar{y}} = \frac{3.6}{6.0} = 0.60 \quad \text{(A2.6)}$$

$$COV_{N_{60}-model} = \frac{\sigma_{N_{60}-model}}{\bar{y}} = \frac{0.90}{6.0} = 0.15 \quad \text{(A2.7)}$$

$$COV_{N_{60}-total} = \frac{\sigma_{N_{60}-total}}{\bar{y}} = \frac{3.7}{6.0} = 0.62 \quad \text{(A2.8)}$$

**Table A2–2 Summary of design model characteristics for SPT $N_{60}$-values at south end bent.**

| Layer | Model Value (bpf) $\widehat{N_{60}} = \overline{N_{60}}$ | Standard Deviation (bpf) | | | Coefficient of Variation | | |
|---|---|---|---|---|---|---|---|
| | | $\sigma_{meas}$ | $\sigma_{model}$ | $\sigma_{total}$ | $COV_{meas}$ | $COV_{model}$ | $COV_{total}$ |
| Layer 1 | 14 | 6.9 | 1.3 | 7.0 | 0.51 | 0.10 | 0.52 |
| Layer 2 | 6 | 3.6 | 0.9 | 3.7 | 0.60 | 0.15 | 0.62 |
| Layer 3 | 21 | 11.1 | 1.6 | 11.2 | 0.53 | 0.07 | 0.53 |

The model shown in Figure A2-4 is a simple, reasonable, and useful characterization of $N_{60}$ shown in Figure A2-3. Additionally, the model is consistent with the stratigraphy interpreted from the boring logs. The standard deviation bounds are also useful representations of the variation of the SPT data. The relatively narrow bounds shown for $\sigma_{model}$ indicate that there is relatively little uncertainty regarding the mean value within each layer. The model uncertainty represented by $COV_{model}$ range from 0.07 to 0.15, which are well below the model uncertainty threshold recommended in Chapter 11. If another boring were to be completed with SPT measurements at the south end bent, it is unlikely that the mean $N_{60}$ values would change significantly from the model shown in Figure A2-4 because values for $COV_{model}$ are relatively small. However, it would nevertheless be difficult to predict the individual SPT measurements in the new boring because such estimates are controlled by $COV_{total}$, which are relatively large.

Two alternative models for $N_{60}$ at the south end bent are shown in Figure A2-5. The first model shown in Figure A2-5a models $N_{60}$ using a single value, 16 bpf, corresponding to the average of all data, irrespective of depth. The second alternative model, shown in Figure A2-5b, is a linear regression model with $N_{60} = 107 - 0.13 \cdot z$, where $z$ is elevation. Calculated values for $\sigma_{meas}$, $\sigma_{model}$, and $\sigma_{total}$ for the two alternative models are provided in Table A2–3, along with calculated values for $COV_{meas}$, $COV_{model}$,

and $COV_{total}$. Although both alternative models appear at first glance to be reasonable approximations of the available measurements, closer examination reveals both models are inappropriate, primarily because they greatly overpredict $N_{60}$ in the fine-grained layer from Elevation 735 feet to 717 feet. Comparison of the calculated variability of measurements, $\sigma_{meas}$, relative to the respective estimates for the three models also suggests that the three-layer model is a more appropriate model; values for $\sigma_{meas}$ for the two alternative models are substantially greater than values determined for the three layer model, which indicates that the three layer model is a better representation of the available measurements. Numerical comparisons of $\sigma_{model}$ should not be used exclusively to establish the appropriateness of interpreted design models; however, such comparisons can often facilitate comparison of alternative models as illustrated in this example. Numerical comparisons of $\sigma_{model}$ should not be used for evaluation of alternative interpretations of the same measurements because values of $\sigma_{model}$ are strongly influenced by the number of measurements for a particular stratum.

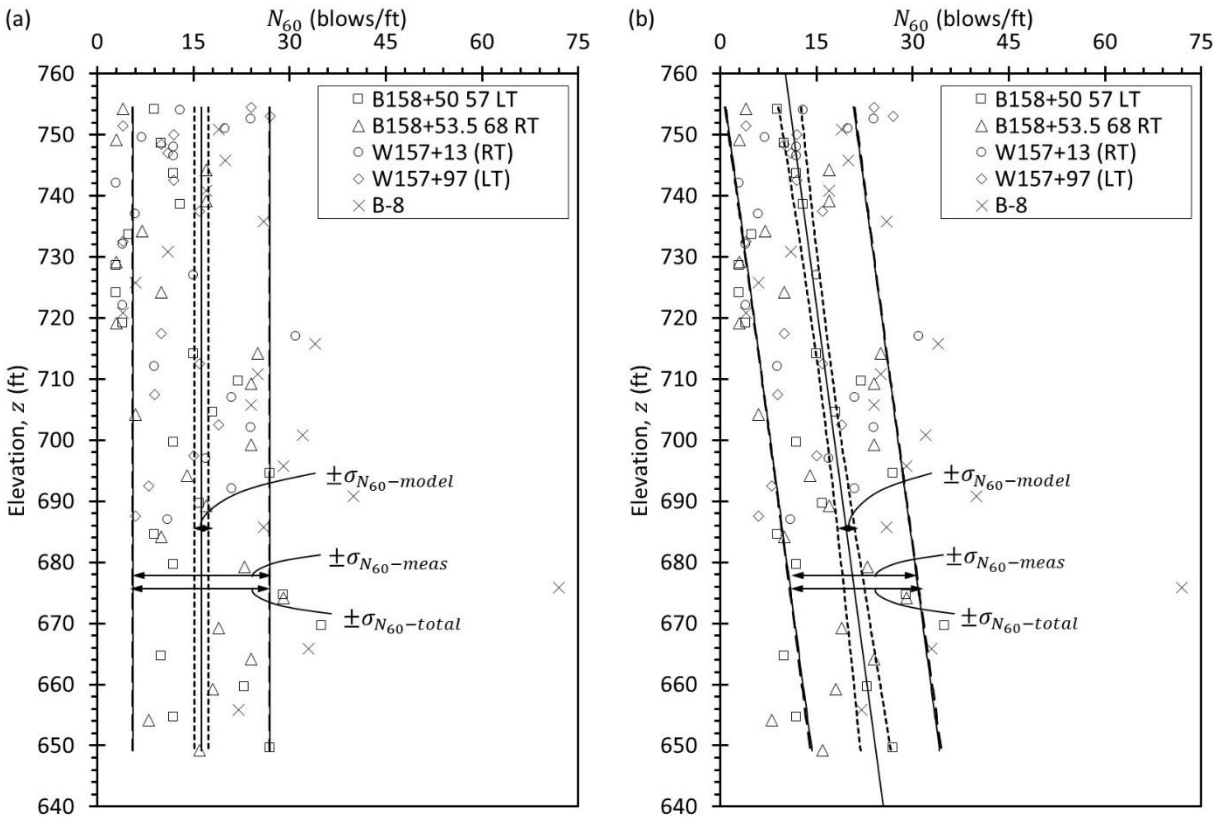


**Figure A2-5 Alternative design profiles for $N_{60}$ at the south end bent: (a) single layer with uniform $N_{60}$, and (b) single layer with $N_{60}$ increasing linearly with depth.**

**Table A2–3 Summary of alternative design model characteristics for SPT $N_{60}$-values.**

| Model | Model Value (bpf) $\widehat{N_{60}} = \overline{N_{60}}$ | Standard Deviation (bpf) | | | Coefficient of Variation | | |
|---|---|---|---|---|---|---|---|
| | | $\sigma_{meas}$ | $\sigma_{model}$ | $\sigma_{total}$ | $COV_{meas}$ | $COV_{model}$ | $COV_{total}$ |
| Alt. 1 | 16.3 | 10.6 | 1.1 | 10.7 | 0.65 | 0.07 | 0.66 |
| Alt. 2 | $107 - 0.13 \cdot z$ | 9.9 | 1.40 | 10.1 | 0.65 | 0.09 | 0.65 |

### A2.1.2 Pylon

The pylon is the main tower of the cable-stayed bridge and is located in the river. Subsurface information at the pylon is derived from five project borings drilled from a barge, all of which encountered approximately 55 feet of sand over shale and limestone bedrock. The foundation for the pylon will consist of a group of large-diameter drilled shafts socketed into bedrock to support large axial and lateral loads. The design model for the pylon includes characterization of stratigraphy, SPT measurements in the sand, and the rock mass below the sand.

Stratigraphy at the pylon was evaluated by creating a stick log plot from the five borings at the pylon as shown in Figure A2-6. The observed stratigraphy is rather consistent among the five borings, with material descriptions that vary little from one boring to the next in addition to material contacts that are practically horizontal. Sand with gravel is present from the mudline (elevation 702 feet) to approximately elevation 647 feet. The sand is loose to medium dense and poorly graded. As noted in each boring log, cobbles and boulders are present in the sand, an observation of consequence for shaft construction. Below the sand is bedrock, which is predominantly shale. From elevation 647 feet to approximately elevation 593 feet the shale is described as slightly weathered, with occasional limestone laminations as well as 1-in. coal seams. Most core runs in the shale had full recovery, and $RQD$ values were generally greater than 70 percent. Below elevation 593 feet, the shale is highly weathered, with $RQD$ values as low as 28 percent, although the minimum core recovery was 88 percent. The highly weathered shale layer is approximately 6 feet thick and overlies a limestone stratum from elevation 587 feet to approximately elevation 575 feet. Core runs in the limestone mostly had full recovery, and significant hydrocarbon staining was observed in the limestone cores. Below the limestone, shale was encountered. The deeper shale was hard with limestone laminations. All core runs in the deep shale had full recovery and $RQD$ greater than 80 percent. The deepest boring terminated in the shale at elevation 560 feet.

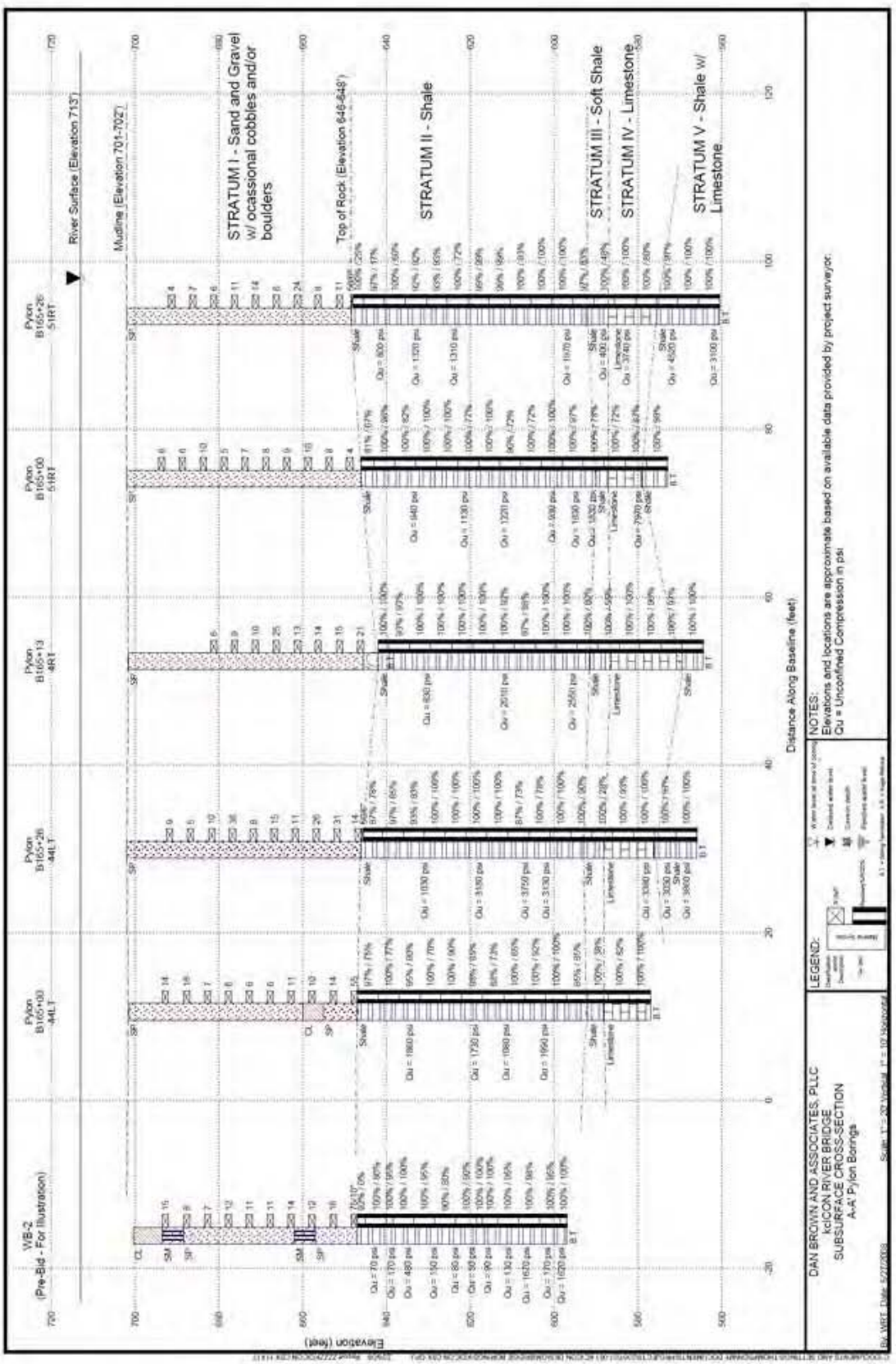


**Figure A2-6 Stratigraphy at pylon. (courtesy Dan Brown and Associates)**

The sand at the pylon is characterized using $N_{60}$ measurements, similar to the approach adopted at the south end bent. Figure A2-7 shows values of $N_{60}$ from the pylon borings plotted versus elevation. $N_{60}$ values do not vary considerably with depth, but there is a slight increase below elevation 670 feet, which corresponds to where a greater proportion of gravel was noted in several boring logs. For the developed design profile, $N_{60}$ is modeled using two layers, separated at elevation 670 feet, with uniform properties within each layer as shown in Figure A2-8. Table A2–4 provides the $N_{60}$ measurements within each layer. Model values for $N_{60}$ within each layer were again established using the mean of the measured $N_{60}$ values as summarized in Table A2–5. Variability and uncertainty measures are also provided in Table A2–5.

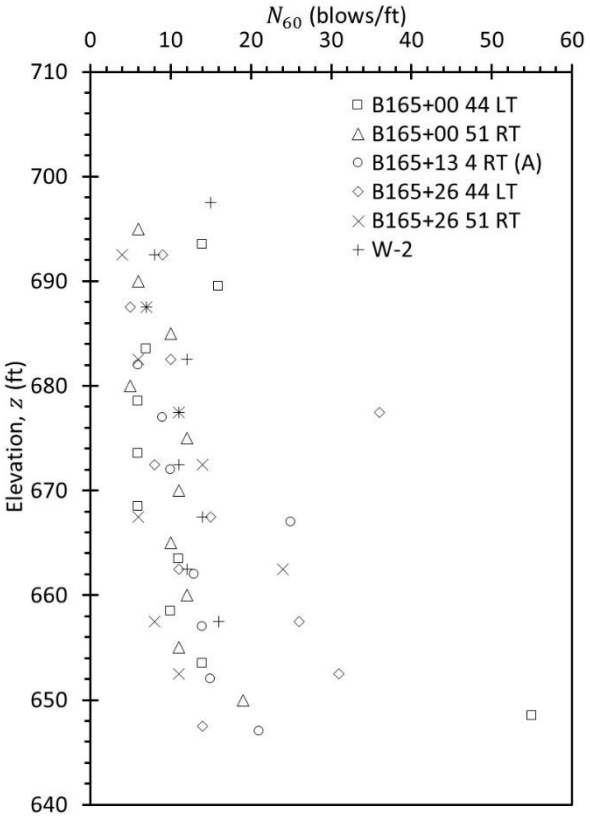


**Figure A2-7 $N_{60}$ measurements from pylon borings.**

**Table A2–4 $N_{60}$ measurements within each layer at pylon.**

| Layer Designation | Elevation Range (ft) | SPT $N_{60}$ Measurements (bpf) |
|---|---|---|
| Layer 1 | 702-670 | 15, 6, 14, 9, 4, 8, 6, 16, 5, 7, 7, 10, 7, 10, 6, 12, 6, 5, 6, 36, 11, 11, 9, 12, 6, 8, 14, 11, 10, 11, 6 |
| Layer 2 | 670-648 | 15, 6, 14, 25, 10, 11, 11, 24, 12, 13, 12, 10, 26, 8, 16, 14, 11, 14, 31,11, 15, 19, ***55***, 14, 21 |

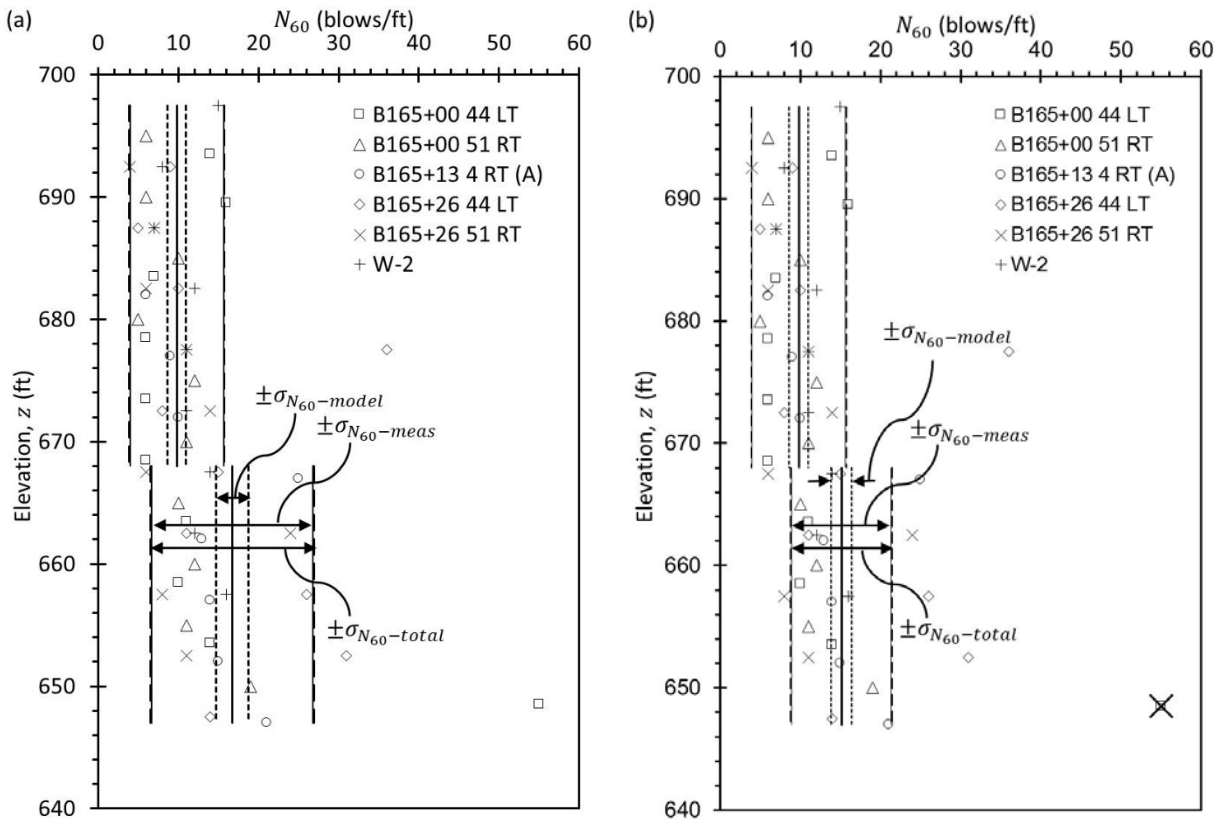


**Figure A2-8 Design profiles of $N_{60}$ for sand at the pylon: (a) all measurements, and (b) excluding $N_{60} = 55$ bpf at El. 648.5 feet.**

**Table A2–5 Summary of design model characteristics for SPT $N_{60}$-values at pylon.**

| Layer | Model Value (bpf) $\widehat{N_{60}} = \overline{N_{60}}$ | Standard Deviation (bpf) | | | Coefficient of Variation | | |
|---|---|---|---|---|---|---|---|
| | | $\sigma_{meas}$ | $\sigma_{model}$ | $\sigma_{total}$ | $COV_{meas}$ | $COV_{model}$ | $COV_{total}$ |
| Layer 1 | 10 | 5.8 | 1.2 | 5.9 | 0.59 | 0.12 | 0.60 |
| Layer 2 | 17 | 10.0 | 2.0 | 10.2 | 0.60 | 0.12 | 0.61 |
| | *15* | *6.2* | *1.3* | *6.3* | *0.41* | *0.08* | *0.42* |

As shown in Figure A2-7, the $N_{60}$-value from boring B165+00 44 LT at elevation 648.5 feet is substantially greater than any other measured and is potentially an outlier. Excluding measurements as outliers should always be approached with caution and should generally be saved for situations where there is some rational explanation for why the measurement is inconsistent with others. In this case, the measured $N_{60} = 55$ bpf was measured immediately above the shale layer where the measurement could have been influenced by penetration into the shale. Values for $N_{60}$ for Layer 2 were therefore interpreted considering the measurement to be accurate, and considering the measurement to be erroneous as shown in Figure A2-8 and Table A2–5. In this case, excluding the potential outlier reduces the mean slightly, from 17 bpf to 15 bpf, and reduces the variability considerably, with $COV_{model}$ decreasing from 0.12 to

0.08 and $COV_{total}$ decreasing from 0.61 to 0.42. It is also significant that the calculated measures of variability more accurately represent the observed scatter in the measurements when the outlier is neglected as shown in Figure A2-8b. Given that the measurement is substantially different from others, that there is a plausible and practical explanation for the observed outlier, and that calculated measures of variability more appropriately represent observations when the outlier is neglected, the interpretation neglecting the outlier (Figure A2-8b) is judged to be more appropriate for design in this case. Note that this interpretation is also more conservative for design in this case.

Plots of material descriptions, $RQD$, and $q_u$ versus depth from the five borings were prepared to characterize the rock strata at the pylon. Material descriptions, select core photographs, and $RQD$ are plotted versus elevation in Figure A2-9, and $q_u$ is plotted versus elevation in Figure A2-10.

The information provided in Figure A2-9 and A2-10 can be used to estimate the rock mass rating ($RMR$) and geologic strength index ($GSI$) for each rock stratum. Estimates for each $RMR$ component were developed using Tables 9-5 and 9-6 and are provided in Table A2–6 for each stratum. The first component, $R_1$, is based on $q_u$; values of $R_1$ were selected based on the $q_u$ model described subsequently. All rock strata at the pylon have relatively low $q_u$ values, thus producing relatively low ratings. The second component, $R_2$, is based on $RQD$; values of $R_2$ were selected using the data plotted in Figure A2-9c. The stepwise function for $R_2$ makes assigning precise values of $RQD$ unnecessary. The third component, $R_3$, is based on joint spacing, which was estimated from the distance between joints in the core samples. The fourth component, $R_4$, was evaluated from descriptions of weathering provided in field boring logs. Because joint water pressure was not measured, the fifth $RMR$ component is assumed to be 10 to facilitate comparisons with $GSI$. The resulting $RMR$ values are consistent with descriptions provided in field boring logs and with observations from the recovered core.

$GSI$ values were determined by comparing core photographs and descriptions with those provided in Figure 9-23. Figure A2-11 shows the chart with shaded areas indicating the ranges judged for rock strata at the pylon, which are also provided in Table A2–7. Ranges are used rather than specific values in keeping with an important instruction on the graphic: “Do not try to be too precise.” Structure for each strata was determined primarily by comparing the images shown on the graphic with core photographs. Surface quality was discerned from core photographs and descriptions from boring logs.

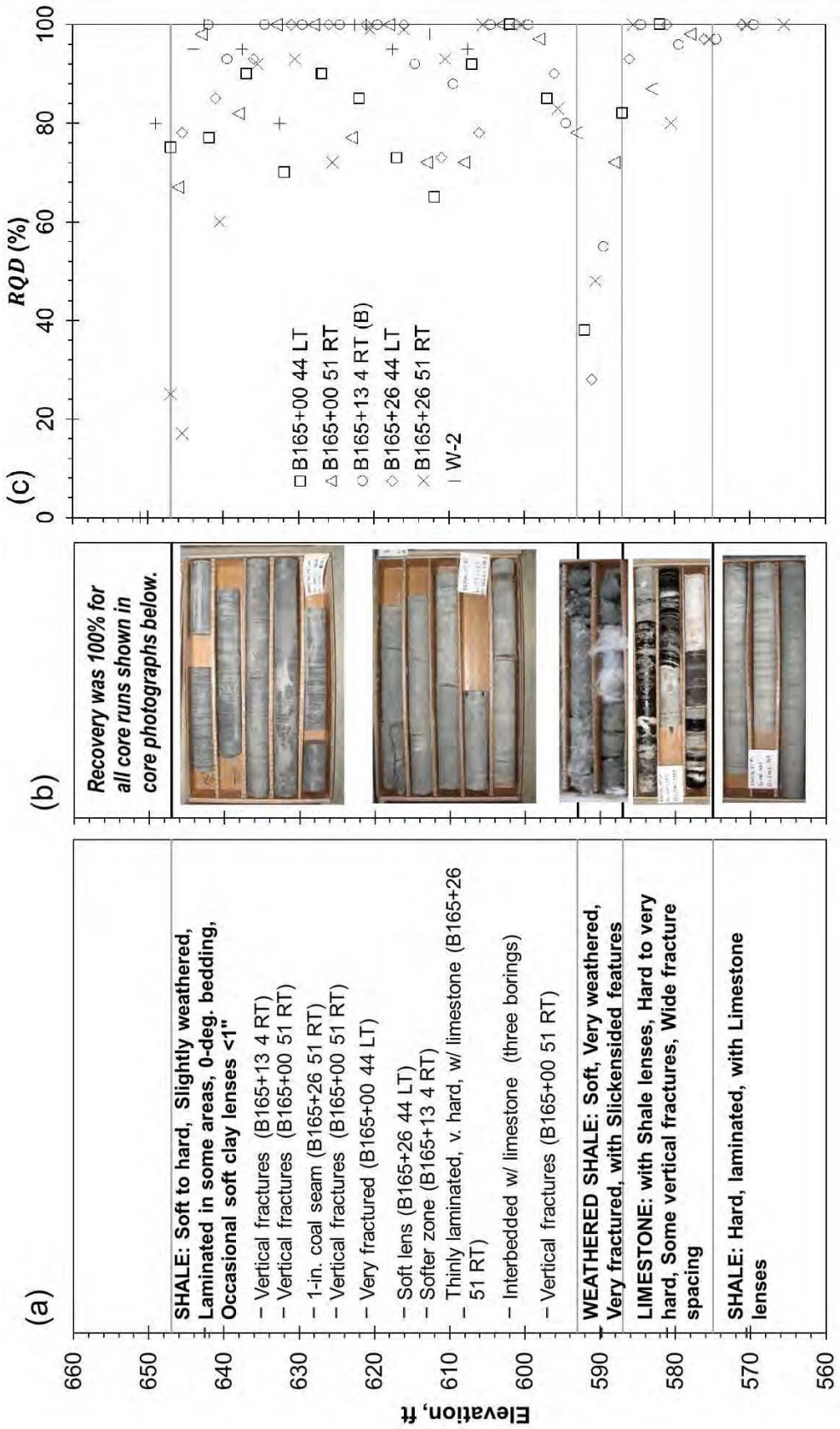


**Figure A2-9 Information used to characterize rock strata: (a) material descriptions, (b) representative core photographs, and (c) *RQD*.**

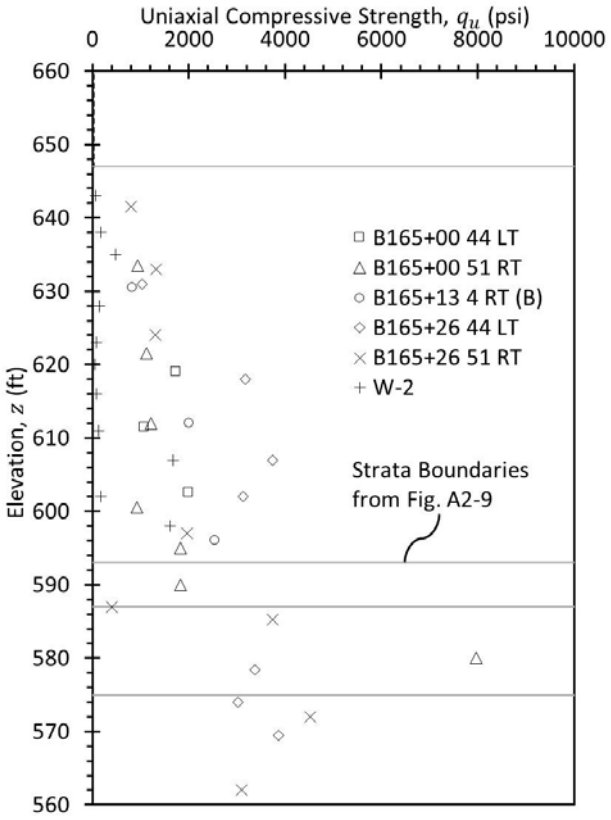


**Figure A2-10 Measured $q_u$ versus elevation.**

**Table A2–6 Rock mass rating, *RMR*, for rock strata at the pylon.**

| Layer | Elevation Range (ft) | $R_1$ | $R_2$ | $R_3$ | $R_4$ | $R_5$ (Assumed) | *RMR* |
|---|---|---|---|---|---|---|---|
| Shale | 647-593 | 2 | 17 | 10 | 20 | 10 | 59 |
| Weathered Shale | 593-587 | 1 | 8 | 5 | 10 | 10 | 24 |
| Limestone | 587-575 | 4 | 17 | 15 | 30 | 10 | 66 |
| Shale | 575-560 | 4 | 20 | 15 | 25 | 10 | 64 |

**Table A2–7 Summary of rock mass parameters for rock strata at pylon.**

| Layer | Elevation Range (ft) | *RMR* | *GSI* | $m_i$ | $m$ | $s$ | $a$ |
|---|---|---|---|---|---|---|---|
| Shale | 647-593 | 59 | 45-70 | 4-8 | 0.6-2.7 | 0.002-0.04 | 0.51-0.50 |
| Weathered Shale | 593-587 | 24 | 8-25 | 4-8 | 0.1-0.6 | 0 | 0.60-0.53 |
| Limestone | 587-575 | 66 | 60-80 | 7-11 | 1.7-5.4 | 0.01-0.1 | 0.50-0.50 |
| Shale | 575-560 | 64 | 60-80 | 4-8 | 1.0-3.9 | 0.01-0.1 | 0.50-0.50 |

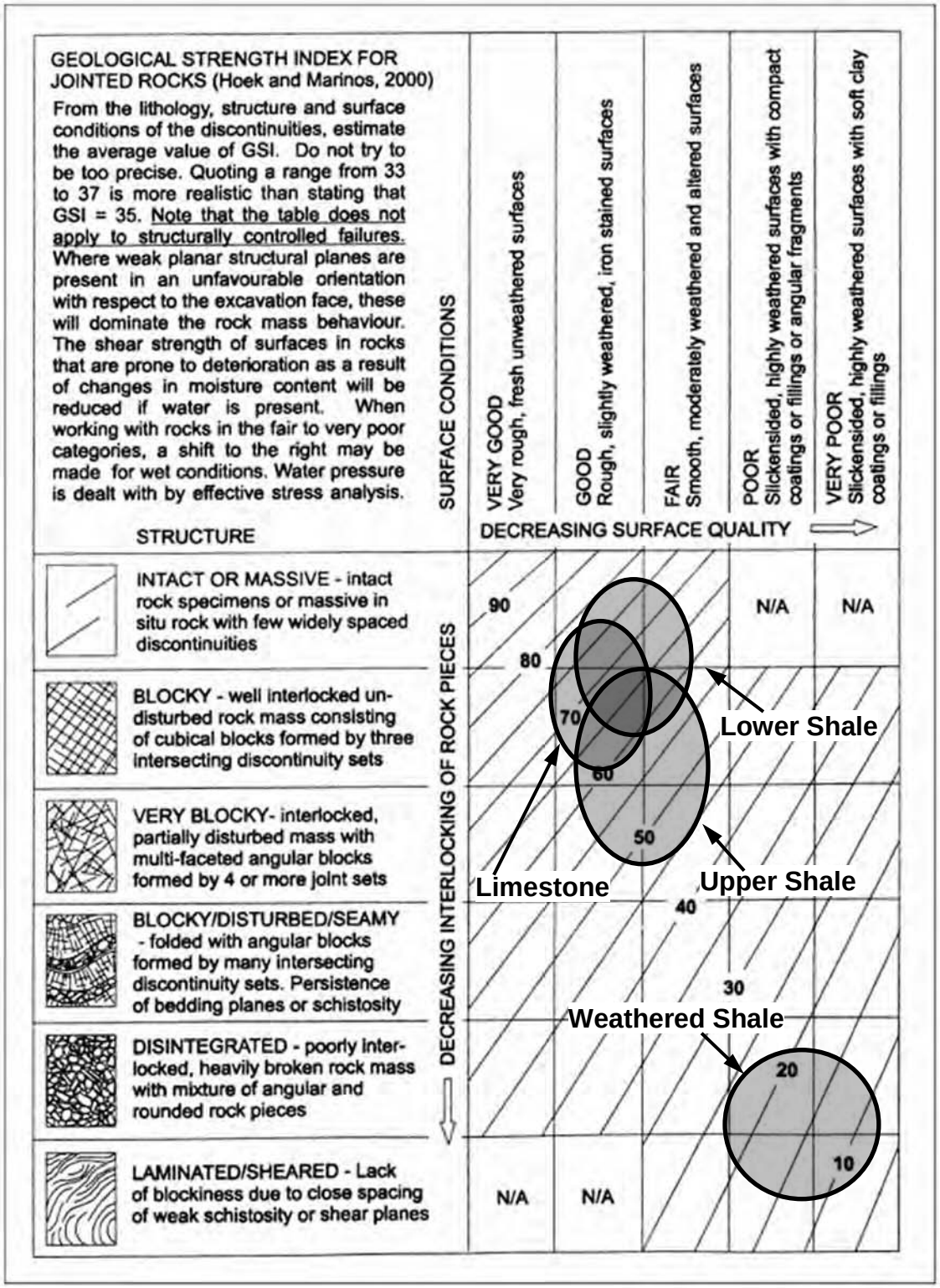


**Figure A2-11 Estimates for *GSI* in rock strata (adapted from Marinos and Hoek, 2000).**

Hoek and Brown (1997) strength parameters were determined from the established $GSI$ values and rock type. Values for the pylon rock strata are shown in Table A2–7. The parameter $m_i$ is based on rock type and was determined from Table 9-10. For shale, $m_i$ is $6 \pm 2$, and for limestone (micritic), $m_i$ is $9 \pm 2$. Parameters $m_b$, $s$, and $a$ were established from Equations 9.33, 9.34, and 9.35, respectively. Calculations for lower bound estimates for the upper shale layer are included below as an example. Values for the parameters $m_b$, $s$, and $a$ are listed as ranges since the inputs, $GSI$ and $m_i$, were specified as ranges. Ranges shown for $m_b$ and $s$ are rather large, with upper bounds for $m_b$ typically about 5 times the lower bound, and upper bounds of $s$ about 10 to 20 times the lower bound. Ranges for $a$ are much smaller.

$$m = m_i \cdot e^{\left(\frac{GSI-100}{28}\right)} = 4 \cdot e^{\left(\frac{45-100}{28}\right)} = 0.56 \tag{A2.9}$$

$$s = e^{\left(\frac{GSI-100}{9-3D}\right)} = e^{\left(\frac{45-100}{9}\right)} = 0.002 \tag{A2.10}$$

$$a = \frac{1}{2} + \frac{1}{6}\left(e^{\left(\frac{-GSI}{15}\right)} - e^{\left(\frac{-20}{3}\right)}\right) = \frac{1}{2} + \frac{1}{6}\left(e^{\left(\frac{-45}{15}\right)} - e^{\left(\frac{-20}{3}\right)}\right) = 0.51 \tag{A2.11}$$

A design model for $q_u$ was created for the rock strata at the pylon to accompany the Hoek-Brown parameters for characterization of rock strength. The $q_u$ model is shown in Figure A2-12. In the upper shale, a linear regression model was fit to the data with $q_u = 21{,}534 - 32.2 \cdot z$ (psi). The regression line fits the data well and the model uncertainty, $\sigma_{model} \cong 0.15$, is less than the model uncertainty threshold of 0.3. An alternative model for the upper shale that assigns one average value above elevation 620 feet and another average value below would likely be appropriate as well. In the weathered shale, only two $q_u$ tests were performed since the degree of weathering makes $q_u$ testing difficult. Considering the limited number of tests, it is prudent to use the lower of the two measurements, 400 psi, as the design value $q_u$. Average values were used for $q_u$ in the limestone and lower shale layers. The number of tests in these layers was limited, which results in $\sigma_{model} = 0.30$ for the limestone model and $\sigma_{model} = 0.10$ for the lower shale. Since the model uncertainty for the limestone just meets the model uncertainty threshold of 0.30, additional sampling and testing should be considered if design analyses indicate that drilled shafts must extend into the limestone. Alternatively, a conservative estimate for $q_u$ in the limestone could be used instead of conducting additional tests.

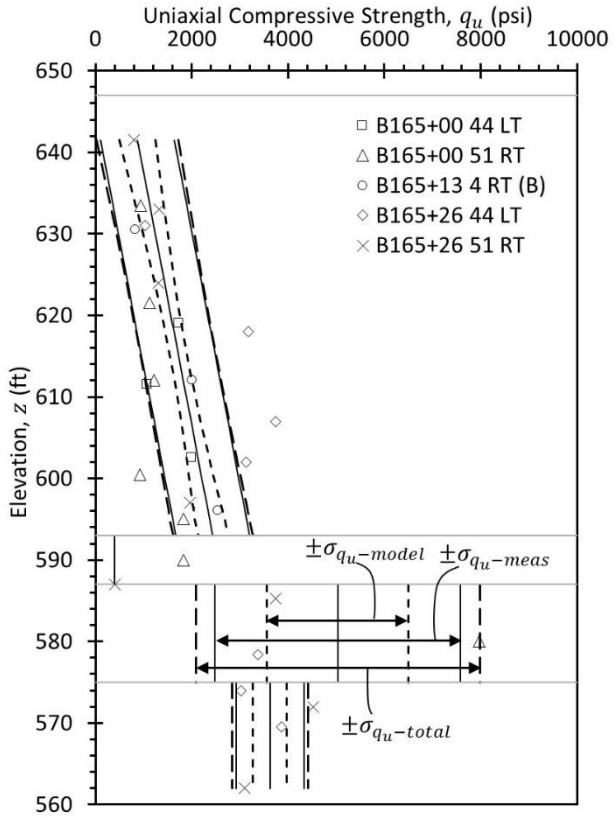


**Figure A2-12 Design profile of $q_u$ for rock strata at pylon.**

## A2.2 EXAMPLE 2: HIGHWAY ATOP LEVEE ON SILT OVER SAND

A regional levee district and state transportation agency are partnering to raise a levee along a small tributary to the Mississippi River and the highway that runs atop it. A thick sand aquifer exists along the extent of the levee raise that is overlain by a blanket of fine-grained soil that varies in thickness and characteristics along the length of the levee. The levee fill is primarily fine-grained. Settlement, slope stability, and underseepage concerns are the primary focus for design of the levee/highway raise.

### A2.2.1 Planning for Geotechnical Site Investigation and Characterization

Historical information for the site includes the cross-section shown in Figure A2-13, which was originally developed for a post-flood reconnaissance of the levee in 1993. The cross-section is drawn at the location of a piezometer near the protected side toe of the levee that recorded piezometric levels in the aquifer throughout the flood. Piezometer data and river levels were included in the reconnaissance report and are presented later in this example. Although the historical cross-section reflects only one specific location within the project extent, it is believed to be generally representative of subsurface conditions along most

of the levee project and is therefore a useful basis for planning geotechnical investigations. The historical cross-section shows a poorly graded sand aquifer extending to a depth of 100 feet below the protected ground surface. The sand is overlain by a 15-ft thick blanket of fine-grained soils. The top 10 feet of the blanket is silty lean clay. The bottom 5 feet of the blanket is sandy silt that grades into the aquifer sand. The levee itself is silty clay fill, presumably dredged from the river side of the levee.

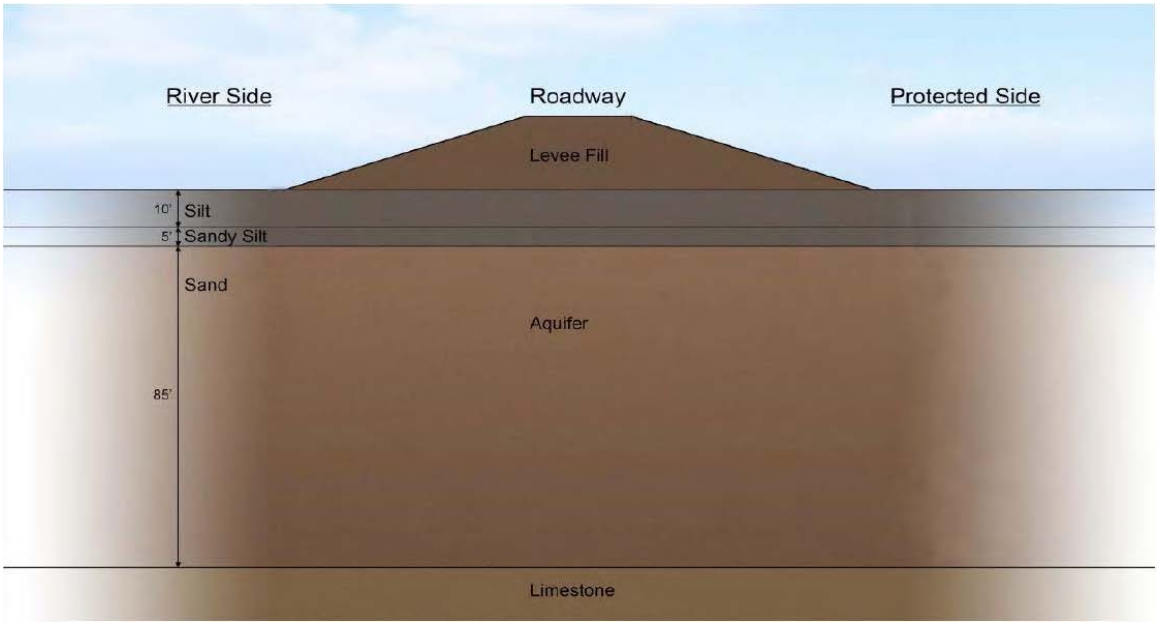


**Figure A2-13 Stratigraphic cross-section for project.**

The proposed levee/highway raise is superimposed on the reconnaissance cross-section in Figure A2-13. Considering the raise, potential flood levels, and subsurface materials, critical geotechnical analyses are settlement of the levee and roadway; stability of the levee under short-term, end-of-construction conditions; stability of the levee under long-term, flood conditions; and underseepage during flood conditions, including the potential for heave of the protected side blanket. Geotechnical information required for each analysis is shown in Table A2–8. Stratigraphy is not listed in the table, but is important for any geotechnical analysis and for seepage analyses in particular (e.g., blanket thickness substantially influences seepage factors of safety).

**Table A2–8 Critical analyses for the levee/highway raise and corresponding required information.**

| Geotechnical Analysis | Required Information | | | | |
|---|---|---|---|---|---|
| | **Levee Fill** | **Silt Layer, Upper 10 ft** | **Silt Layer, Lower 5 ft** | **Sand Aquifer** | **Ground-water** |
| Settlement | $\gamma_T$ | $C_c$, $C_r$, $c_v$, $c_h$ | Likely negligible. Could predict using layer stiffness, $E_s$, established from CPT data | | Piezometric conditions under range of typical river levels |
| Short-term Slope Stability | $\gamma_T$, $s_u$ | $\gamma_T$, $s_u$ | $\gamma_T$, $s_u$, $c'$, $\phi'$ | $\gamma_T$, $c'$, $\phi'$ | Piezometric conditions under range of typical river levels |
| Long-term Slope Stability | $\gamma_T$, $c'$, $\phi'$ | $\gamma_T$, $c'$, $\phi'$ | $\gamma_T$, $c'$, $\phi'$ | | Piezometric response to elevated river levels |
| Underseepage | Not critical | $\gamma_T$ | $\gamma_T$ | $k_v$, $k_h$ | |

Interpretation of stratigraphy, particularly related to the silt stratum, is important for the analyses in Table A2–8. Historical information indicates the upper 10 feet of the silt stratum is silty clay (ML-CL) and the bottom 5 feet is sandy silt (ML). The silty clay is expected to have engineering characteristics typically associated with clay materials, primarily compressibility and shear strength that is governed by undrained loading conditions. In contrast, the engineering behavior of the sandy silt is difficult to predict, but is possibly more similar to the aquifer sand than to the silty clay: non-plastic (i.e., the plastic limit cannot be determined), relatively permeable (although less so than the aquifer), and with shear strength governed by drained loading conditions. Because the difference in expected behavior within the silt stratum strongly influences the analyses listed in Table A2–8, characterization of the silt stratum and especially the boundary between the plastic and non-plastic silt is critical. Additional discussion regarding characterization of the silt layer is presented later in this example.

Fourteen borings and twelve CPT soundings were completed along the length of the project as shown in Figure A2–14. Borings were drilled with hollow stem augers until encountering groundwater, at which point mud rotary drilling methods were used. Most borings were located near the protected side toe of the levee, but two borings were drilled from the highway through the crest of the levee. The two crest borings extended to rock, more than 100 feet below the levee crest, whereas most other borings were terminated in the aquifer sand at depths between 35 and 50 feet. CPT soundings were conducted on the river side of the levee and extended to depths around 35 feet. Table A2–9 summarizes the means developed to address the information requirements listed in Table A2–8.

### A2.2.2 Stratigraphy

The borings support the generalized stratigraphy indicated in the historical report. Figure A2–15 shows new subsurface information on the historical cross-section first presented in Figure A2-13. The new subsurface information presented on the cross-section, a stick log of boring B-5, and a depiction of CPT Soil Behavior Type (Robertson, 1990) with depth for CPT-5, is from the explorations closest to the section in the historical report. As shown in Figure A2–15, the new information confirms a blanket primarily composed of silt with some clay overlying a deep sand aquifer.

**Table A2–9 Design parameters required for project analyses and how they were determined.**

| Required Information | Stratum | Geotechnical Site Characterization Plan |
|---|---|---|
| Stratigraphy | All | Every 300 ft: boring at crest, boring at protected side toe, CPT at river side toe |
| Groundwater Condition | All | Continued monitoring of piezometers, particularly during periods of high water. Potentially add new piezometers at critical locations. |
| $\gamma_T$ | Levee Fill | Determined from Shelby tube samples |
| $s_u$ | | UU triaxial tests on Shelby tube specimens<br>Parameter only necessary for end-of-construction stability; reasonable to assume unsaturated fill. |
| $c'$, $\phi'$ | | $\overline{CU}$ triaxial tests on Shelby tube specimens |
| $\gamma_T$ | Silty Clay | Determined from Shelby tube samples<br>Parameter of particular importance for underseepage analyses. |
| $s_u$ | | UU triaxial tests on Shelby tube specimens<br>*and/or*<br>Determined from alternative interpretation of the $\overline{CU}$ triaxial tests required for effective stress strength parameters. |
| $c'$, $\phi'$ | | $\overline{CU}$ triaxial tests on Shelby tube specimens |
| $C_c$, $C_r$ | | Consolidation tests on Shelby tube specimens |
| $c_v$ | | |
| $\gamma_T$ | Sandy Silt | Determined from Shelby tube samples |
| $s_u$ | | Depends on plasticity of material. If material appears to be plastic during drilling, take Shelby tube samples and perform UU triaxial tests. If material is nonplastic, $s_u$ does not apply and split spoon samples are adequate. |
| $c'$, $\phi'$ | | $\overline{CU}$ triaxial tests on Shelby tube specimens |
| $\gamma_T$ | Sand | Determined from Shelby tube samples |
| $\phi'$ | | Interpreted from transformation of in situ test data (SPT, CPT) |
| $k_v$, $k_h$ | | Hydraulic conductivity estimated from calibration of seepage models using historic piezometric and river level data. It is reasonable to apply the same calibrated hydraulic conductivity values to all project sections where the sand gradation is similar to that at the calibrated section(s). For sections where the sand gradation is significantly different, the calibrated estimates of conductivity should be adjusted.<br>Depending on the seepage remediation measures indicated by preliminary analysis, a pump test may be justified but is not recommended initially due to expense. |

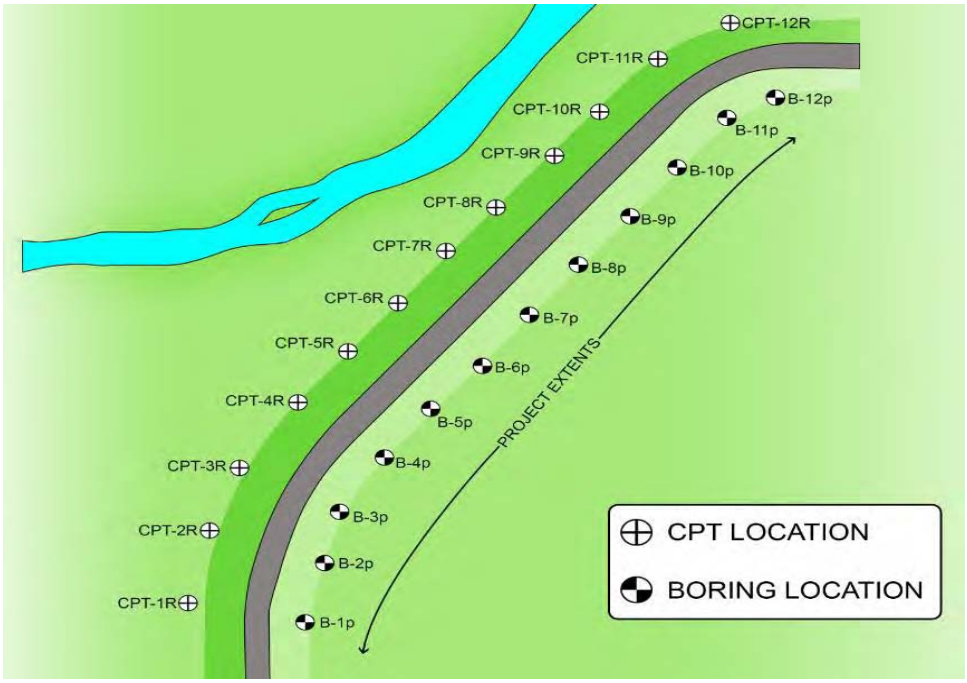


**Figure A2-14 Boring location plan.**

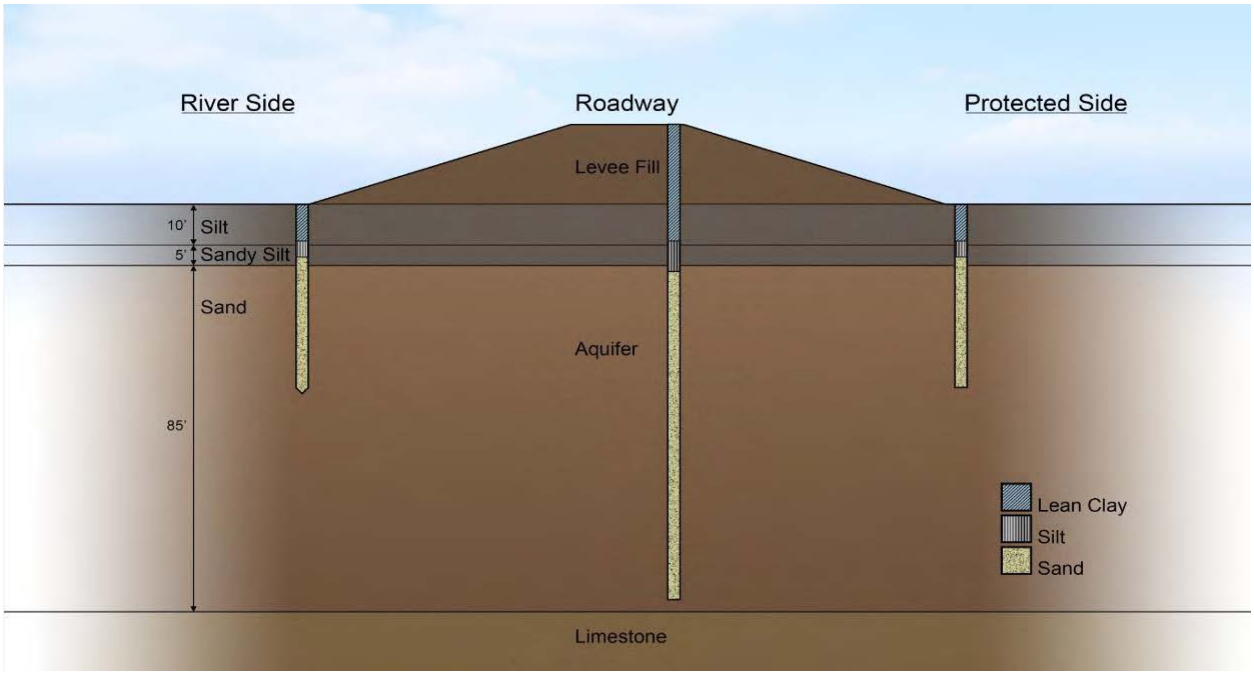


**Figure A2-15 Historical cross-section with information collected from field investigations.**

Table A2–10 presents a summary of the subsurface investigation results for each of the twelve investigation cross-sections. The table is useful for dividing the project into distinct design domains with similar stratigraphy. Considering the blanket materials and thickness values listed in Table A2–10, one

reasonable approach is to divide the sections into three domains, or "regions", with Region 1 including Sections 1 through 4, Region 2 including Sections 5 through 8, and Region 3 including Sections 9 through 12. For this example, each region is coincidentally the same length, but the establishment of design domains should be governed by site conditions, not length.

The practice of assigning design domains with similar subsurface profiles is useful not only for site characterization but also for design and analysis. Information like that presented in Table A2–10 can be used to identify critical sections, i.e., sections where analyses will indicate problems are most likely (lowest factor of safety, highest probability of failure, etc.). For example, considering the regions established using Table A2–10, Sections 1, 6, and 11 are likely critical for seepage analysis based on the thickness of the blanket. However, Sections 3, 8, and 10 are likely critical for settlement and slope stability analyses because of the predominance of clay at those sections.

**Table A2–10 Summary of information related to stratigraphy for Example 2.**

| Section | Blanket Thickness, ft | | Blanket Material | | Elevation of Top of Aquifer, ft | | Loose Sand?[1] | |
|---|---|---|---|---|---|---|---|---|
| | Boring | CPT | Boring (USCS) | CPT (SBT[2]) | Boring | CPT | Boring | CPT |
| 1 | 5 | 7 | Lean Clay | Clay | 428 | 426 | Yes | |
| 2 | 8 | 12 | Lean Clay | Clay over Clayey Silt | 425 | 421 | Yes | Yes |
| 3 | 12 | 9 | Lean Clay | Clay over Clayey Silt | 426 | 429 | | |
| 4 | 9 | 5 | Lean Clay | Silty Clay | 428 | 432 | | |
| 5 | 13 | 18 | Silty Clay over Sandy Silt | Clayey Silt over Sandy Silt | 428 | 423 | | Yes |
| 6 | 13 | 12 | Silty Clay over Sandy Silt | Clayey Silt over Sandy Silt | 422 | 420 | Yes | |
| 7 | 15 | 17 | Silty Clay | Clayey Silt | 417 | 415 | | Yes |
| 8 | 20 | 17 | Silty Clay over Sandy Silt | Sandy Silt | 415 | 415 | | |
| 9 | 7 | 6 | Sandy Silt | Silty Sand | 426 | 427 | | |
| 10 | 14 | 10 | Silty Clay over Sandy Silt | Sandy Silt | 426 | 425 | Yes | |
| 11 | 7 | 5 | Lean Clay over Sandy Silt | Silty Sand | 433 | 433 | Yes | |
| 12 | 12 | 5 | Clay over Sandy Silt | Silty Sand | 426 | 433 | | |

[1]Loose sand in aquifer detected by SPT $N_{60}$ values less than 10 bpf or CPT $q_t$ values less than 20 tsf.
[2]CPT Soil Behavior Type per Robertson, 1990

In addition to the practical exercise of establishing subsurface design domains and identifying likely critical sections, Table A2–10 includes noteworthy information about the stratigraphy of the site and the exploration methods. The stratigraphy from the historical report generally applies to the entire length of

the project, but with considerable variation among the cross-sections. Observed values of the thickness of the fine-grained blanket range from 5 to 20 feet. Observations of blanket thickness from the borings generally agree with values from CPT soundings, although values at Sections 2, 4, 5, and 12 were different by 4 feet or more. Differences in blanket thickness are to be expected since the explorations were completed on different sides of the levee. Material descriptions of the blanket indicate considerable variation in the blanket consistency, with explorations in Region 1 encountering strictly lean clay, explorations in Region 2 encountering some mixtures of clay and silt, and explorations in Region 3 encountering sandy silt or silty sand. For Region 3, it is difficult to discern the bottom of the blanket from the top of the aquifer, a statement that reflects the difficulties of characterizing the site. Blanket material descriptions from borings and CPT soundings at a given cross section are generally similar but not perfectly consistent. Some of the difference is likely a result of the explorations being on different sides of the levee, but some is also likely a result of difficulties classifying similar materials (e.g., silty clay versus clayey silt, sandy silt versus silty sand, etc.). Such difficulties can be compounded when comparing information from different types of explorations (in this case, borings versus CPT).

Aquifer characteristics are also summarized in Table A2–10. The elevations at which the top of the aquifer was encountered are consistent with the blanket thickness values since elevation changes along the length of the project are small. Elevations at which loose sand was encountered, based on SPT or CPT tests, are also included in Table A2–10. Based on descriptions in the boring logs, the loose zones generally represent areas where the sand is silty. At one cross-section (Section 2), the silty zones appear to be continuous underneath the levee but otherwise the silt zones are likely discrete pockets. Characterization of the sand strength is discussed further in the aquifer section below.

### A2.2.3 Groundwater Conditions

Groundwater conditions are critical for geotechnical analysis of the levee/highway raise. Groundwater conditions govern seepage, which in turn influences slope stability and settlement. Groundwater conditions at the site were evaluated using observations from borings, piezometer readings, and field reconnaissance during a high-water event. Groundwater conditions are dominated by the water elevation in the river.

The subsurface exploration was completed during a period of relatively low river levels when groundwater levels in the aquifer were comfortably below the bottom of the blanket. Groundwater levels were inferred from borings installed at the protected side toe based on the depth at which caving occurred with hollow stem augers and mud rotary drilling methods were initiated. These inferred groundwater

elevations are listed in Table A2–11. Piezometers were installed at three of the protected side toe locations during subsurface investigations with the top of each 5-ft long well screen installed approximately 20 feet below the top of the aquifer. Observed groundwater levels from the piezometers are also shown in Table A2–11. The inferred values from drilling are similar to those observed in the corresponding piezometers, with two borings indicating groundwater elevations above those from the piezometer and one boring indicating an elevation below that from the piezometer. The agreement is reasonable. In general, detecting relatively shallow groundwater elevations in sands during drilling with hollow stem augers is relatively reliable although imprecise. Note that the inferred groundwater elevations from borings in Table A2–11 are from the time of drilling, which is a reasonable approach for sands. For detecting groundwater elevations in fine-grained materials, subsequent observations of the groundwater depth should be made to allow time for seepage through the fine-grained material.

**Table A2–11 Groundwater elevations inferred from borings and observed in piezometers.**

| Section | Groundwater Elevation, ft | | |
|---|---|---|---|
| | Boring | Piezometer | Difference |
| 1 | 423.4 | | |
| 2 | 424.4 | 423.1 | +1.3 |
| 3 | 421.1 | | |
| 4 | 422.2 | | |
| 5 | 425.2 | | |
| 6 | 421.0 | 421.3 | −0.3 |
| 7 | 420.1 | | |
| 8 | 422.2 | | |
| 9 | 421.6 | | |
| 10 | 421.9 | 420.0 | +1.9 |
| 11 | 422.4 | | |
| 12 | 424.1 | | |

Several months after the subsurface exploration was completed, river levels rose to near-flood levels in response to upstream snowmelt and precipitation. The river level near the center of the project site and piezometric elevations from the three piezometers are plotted versus time during the high-water event in Figure A2-16. The piezometric elevations are considerably higher than those observed during drilling; the piezometric elevation at the protected side toe of Section 6 was more than 20 feet higher during the high water event than during the subsurface investigation. The increase in piezometric elevation reflects two vastly different groundwater conditions: during the subsurface exploration, the groundwater was several feet below the fine-grained blanket; during the high-water event, the piezometric head in the aquifer is actually above the ground surface. The high-water groundwater conditions in the aquifer result in significant pressures on the bottom of the blanket, which produced sand boils documented in a field

reconnaissance effort as shown in Figure A2-17. Data from the reconnaissance and from the piezometers are valuable information that can be used to predict future groundwater conditions. Additional discussion regarding interpretation of piezometric data is included in the aquifer section below.

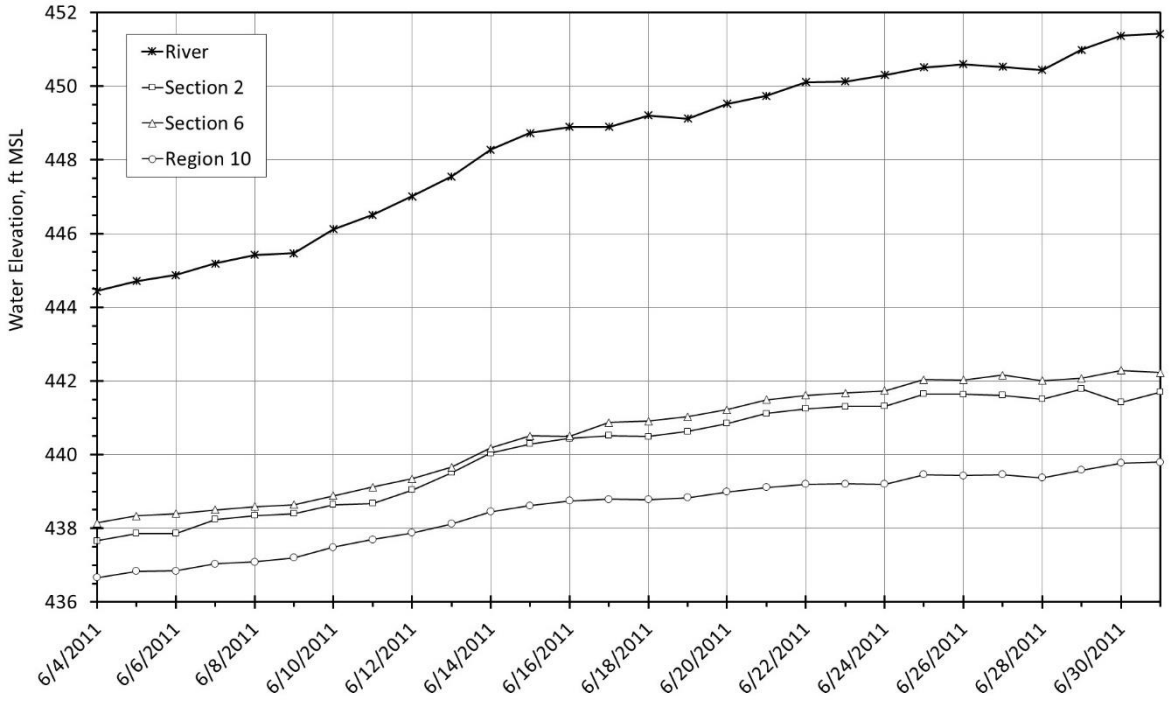


**Figure A2-16 River and piezometric elevations during high-water event.**

**Figure A2-17 Sand boil documented during field reconnaissance during high water event.**

### A2.2.4 Silt

As discussed in the stratigraphy section and presented in Table A2–10, the consistency of the fine-grained blanket is highly variable along the length of the project. In Region 1, characterization of the blanket is relatively straightforward since it is primarily composed of lean clay. For Regions 2 and 3, the blanket composition is less straightforward, generally consisting of silty clay over sandy silt as indicated in the historic information. The engineering behavior of silt is variable and dependent on composition, with more plastic silts typically behaving similar to clays and more non-plastic silts often behaving like sands. Grain-size distributions and Atterberg limits were therefore used to characterize whether silts will behave more like clay or sand. The strength and time rate of consolidation of the clayey silt were then characterized using laboratory and in situ test measurements.

Atterberg limits and coarse-grained fraction (i.e., the percent coarser than the No. 200 sieve) measurements from borings in Region 2 are plotted in Figure A2-18. The results are consistent with descriptions in Table A2-10 and confirm the characterization from the historic report: 10 feet of silty clay over sandy silt. Atterberg limits for the top 10 feet of the blanket consistently classify as silty clay, in the CL-ML region of the USCS plasticity chart. In the upper 10 feet, the sand fraction is generally between 20 and 30 percent, earning the soil the USCS description "with sand." At depths below 10 feet, the material is mostly non-plastic meaning Atterberg limit tests cannot be completed. Below 10 feet, the sand fraction is generally between 30 and 50 percent, classifying the soil as sandy silt. The soil is classified as silt because more than 50 percent of the material passes the No. 200 sieve.

The strength of the silty clay layer is critical for stability analyses. Drained shear strength of the silty clay layer is likely critical for long-term conditions considering elevated river levels for long-duration floods and corresponding piezometric pressures. Drained shear strength parameters for the silty clay layer are evaluated here using results of $CIUC$ triaxial tests. Results from three $CIUC$ tests performed for a sample from boring B-8 at 13-ft depth are shown in Figure A2-19. The shape of the stress paths indicates the sample is normally consolidated or lightly overconsolidated, which is reasonable considering the site. A linear regression line through points corresponding to failure according to the peak principal effective stress ratio ($PSR = \sigma_1'/\sigma_3'$) suggest the envelope can be represented using $\phi' = 27°$ and $c' = 1.5$ psi.

Results from eighteen $CIUC$ triaxial tests performed for specimens of silty clay from throughout the three design domains are plotted in Figure A2-20. The measurements shown support use of a consistent failure envelope and collective interpretation of effective stress strength parameters for all design domains. The linear regression through the points shown suggests that the envelope can be represented using $\phi' = 28°$

and $c' = 1.3$ psi. Bounds showing the model uncertainty for the failure envelope, $\pm\sigma_{q-model}$, are also shown in the figure. As is generally true when using regression for a linear relationship, values for $\sigma_{q-model}$ and $COV_{q-model}$ vary with the magnitude of $p'$. If considering a range of $p'$ between 5 and 30 psi, the average $COV_{q-model} \cong 0.07$, which satisfies the model uncertainty threshold of 0.3.

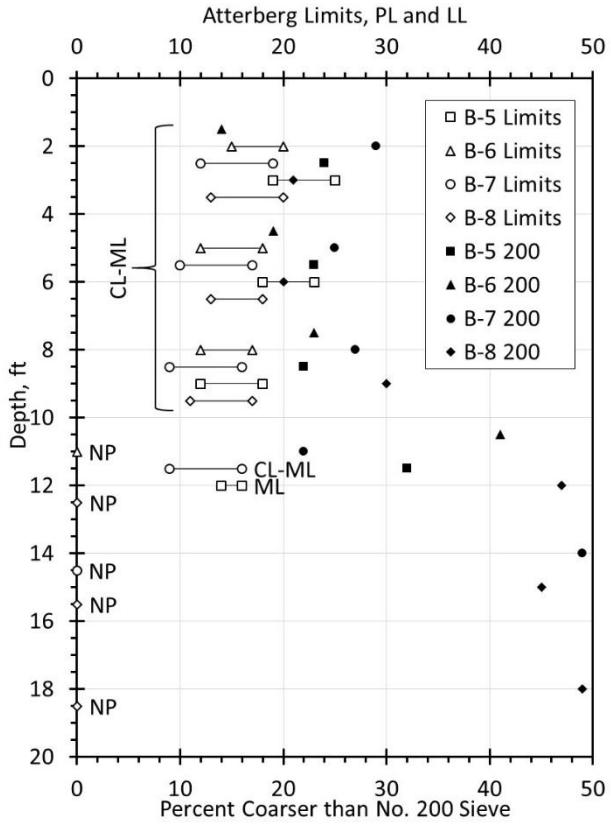


**Figure A2-18 Index properties from Region 2 borings.**

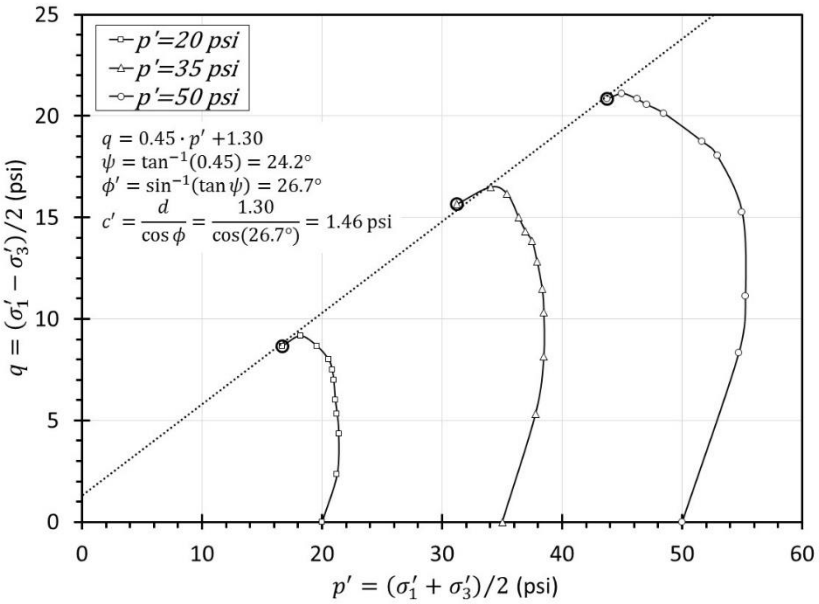


**Figure A2-19 $p - q$ diagram for $CIUC$ tests for specimens from B-8 at 13-ft depth.**

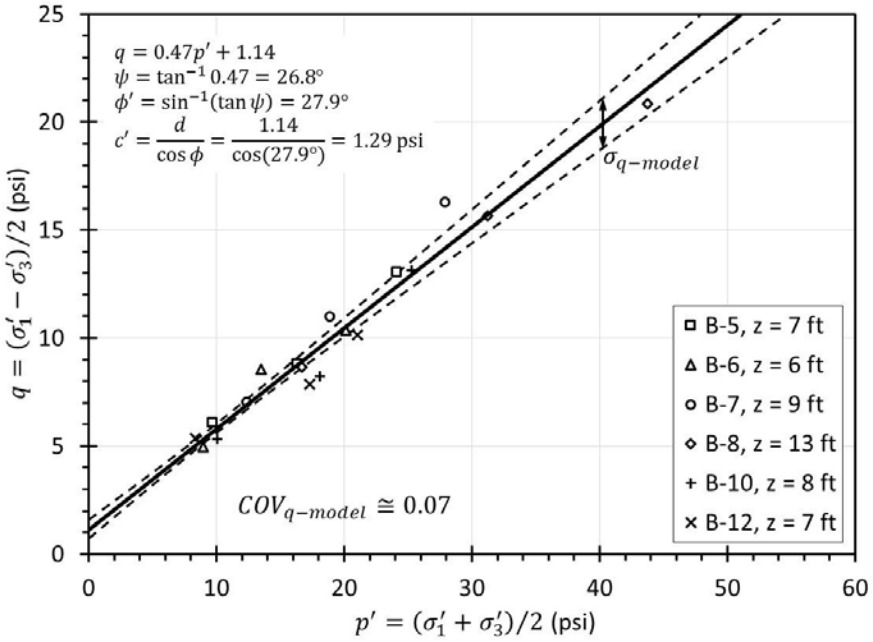


**Figure A2-20 $p - q$ diagram showing results from all $CIUC$ for silty clay.**

### A2.2.5 Sand Aquifer

The sand aquifer is critical to the geotechnical performance of the levee/highway system because it governs underseepage, which in turn governs long-term stability. The strength of the sand is also an important parameter for stability. Characterization of the hydraulic conductivity and strength of the sand aquifer are therefore the primary objectives for this section.

Characterization of hydraulic conductivity is closely tied to analysis of groundwater conditions for the project site, which was presented in a previous section. In particular, the plot of river elevation and piezometric elevations with time from Figure A2-16 provides valuable information that can be used to estimate the field hydraulic conductivity of the aquifer. The piezometric elevation indicated by each piezometer tracks closely with the river elevation, showing changes that correlate closely with changes in the river elevation. Figure A2-21 shows the piezometric elevation from Section 6 plotted versus the corresponding river level using the same data presented in Figure A2-16. The data are linear, indicating that for each 1-ft increase in river elevation, the piezometric head at the location of the piezometer in Section 6 is expected to increase 0.6 feet. This information can be used directly in underseepage analyses (because the piezometers are located at the critical location of the protected side toe), and can also be used to estimate the hydraulic conductivity of the aquifer based on back-calculations using seepage models.

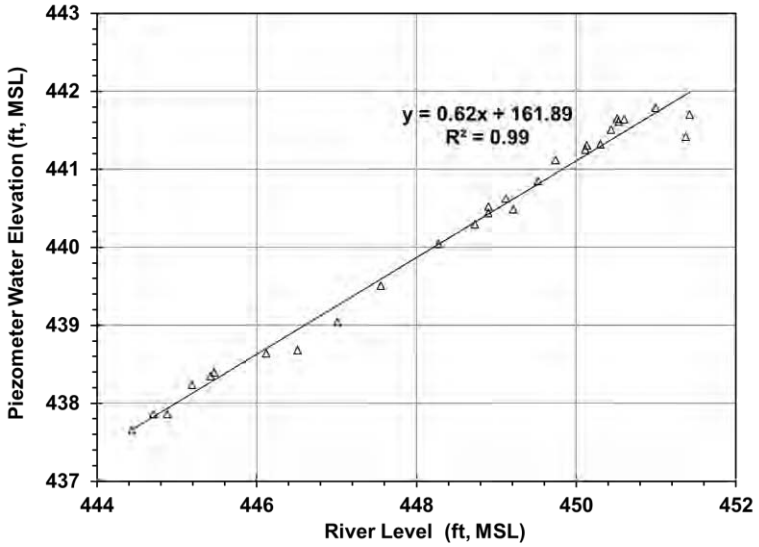


**Figure A2-21 Piezometric elevation from piezometer at Section 6 versus water elevation in river based on data presented in Figure A2-16.**

Since all three piezometers show similar responses to changes in river level (Figure A2-16), it is reasonable to expect the hydraulic conductivity of the aquifer does not vary significantly along the length of the project. Another method for assessing potential variation is to consider the variability of the gradation of the sand. Figure A2-22 shows grain-size distributions from sieve analysis measurements completed for samples of the aquifer sand. Some of the variability among the curves is considerable, particularly among larger particle sizes. However, for the small particle sizes that tend to dominate hydraulic conductivity, the gradations are rather consistent, with all samples having less than 10 percent passing the No. 200 sieve.

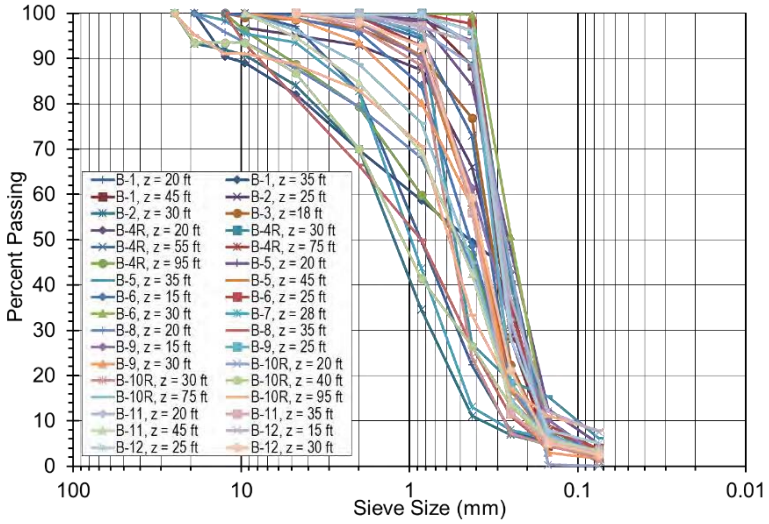


**Figure A2-22 Grain-size distribution curves for the aquifer sand.**

Since the sand is generally clean sand, it was not practical to acquire undisturbed specimens for direct measurements of shear strength parameters. Instead, estimates for the effective stress friction angle $\phi'$ were established indirectly from SPT and CPT measurements. Figure A2-23 shows measured values for $N_{60}$ and $(N_1)_{60}$ from the available borings. The measurements have considerable scatter but suggest a slight trend for decreasing $N$-values with depth between elevation 430 and elevation 415, increasing $N$-values with depth between elevation 415 and elevation 395, and widely scattered $N$-values below elevation 395. Most of the variability appears to be random, although there are a few borings that tend to have lower $N$-values than average (B-1, B-6) and a few that tend to have somewhat higher $N$-values (B-4, B-8). However, borings with $N$-values that vary from the average appear to vary randomly rather than systematically so it is reasonable to consider the measurements collectively. It is also notable that the overburden correction for $N$-values reduces the variability.

Transformations presented in Chapter 7 by Schmertmann (1975) and by Hatanaka and Uchida (1996) were both utilized to estimate $\phi'$ from the measured $N$-values as shown in Figure A2-24. Estimates for $\phi'$ are similarly variable to the measured $N$-values, even without considering the uncertainty introduced by the transformations. The Hatanaka and Uchida transformation produces slightly less variability, most likely because the transformation is based on $(N_1)_{60}$ rather than $N_{60}$. Unfortunately, the uncertainty associated with both the Schmertmann (1975) and Hatanaka and Uchida (1996) transformations has not been quantified so it is not possible to quantify the uncertainty associated with interpreted estimates for $\phi'$.

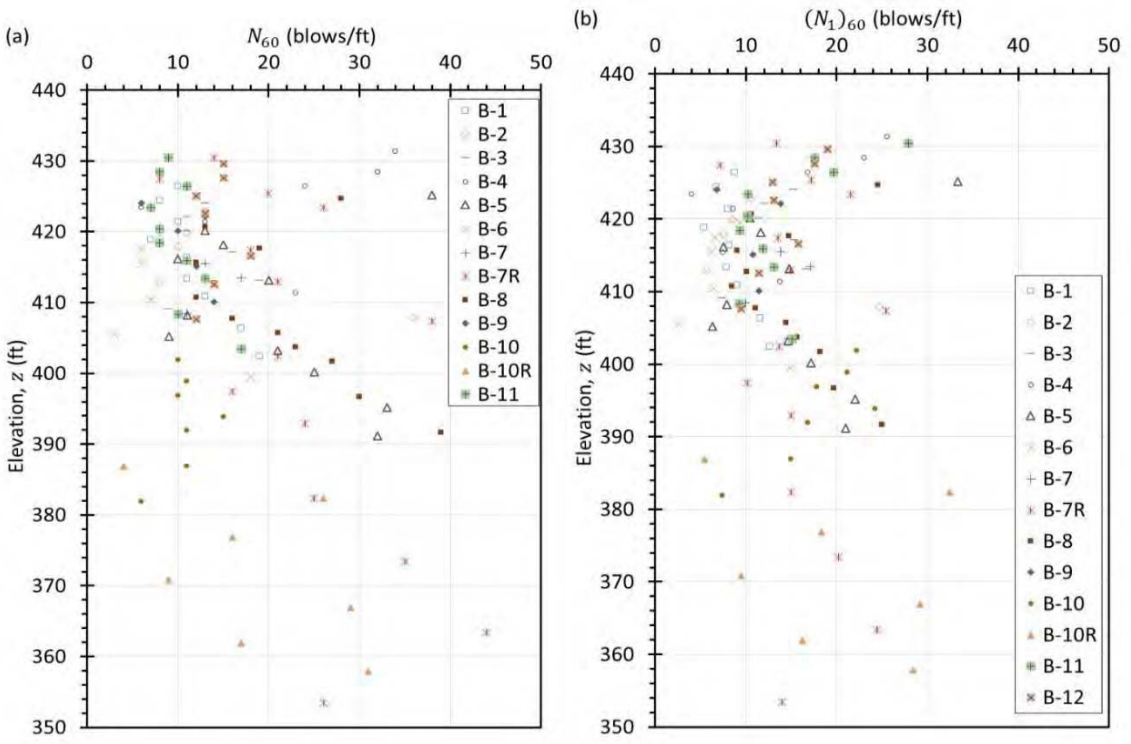


**Figure A2-23 SPT measurements versus elevation: (a) $N_{60}$-values, and (b) $(N_1)_{60}$-values.**

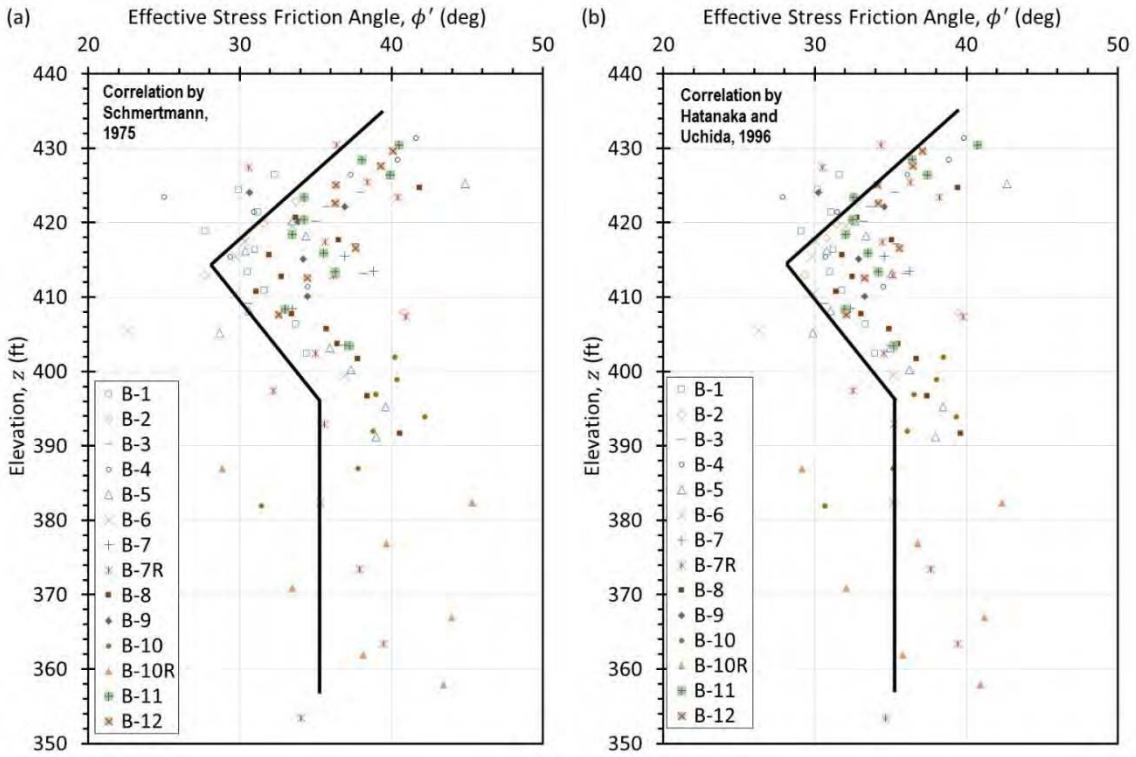


**Figure A2-24 Predictions of $\phi'$ from *N*-values: (a) Schmertmann (1975) transformation, and (b) Hatanaka and Uchida (1996) transformation.**

The considerable variability makes interpretation of an obvious trend difficult. It is therefore prudent to select conservative estimates for $\phi'$ based on the transformed measurements to qualitatively account for the transformation uncertainty that is not reflected in Figure A2-24. The solid lines shown in Figure A2-24 represent one reasonable interpretation for a design model; alternative models could also certainly be justified.

Figure A2-25 shows the corrected cone tip resistance, $q_t$, measured for all twelve CPT soundings plotted versus elevation. The cone tip resistance for each sounding generally increases with depth, but fluctuates significantly in what appears to be a random manner. The range of $q_t$-values for a given depth is relatively wide, but as was true for the measured SPT $N$-values, there does not appear to be locations where $q_t$ is systematically less than or greater than other locations. Measurements from CPT-5 and CPT-7 do indicate lower $q_t$ for a range of depths between elevation 415 feet and elevation 425 feet. Thus, it is rational to consider the CPT measurements collectively, but to also consider the potential for separately considering several of the individual soundings.

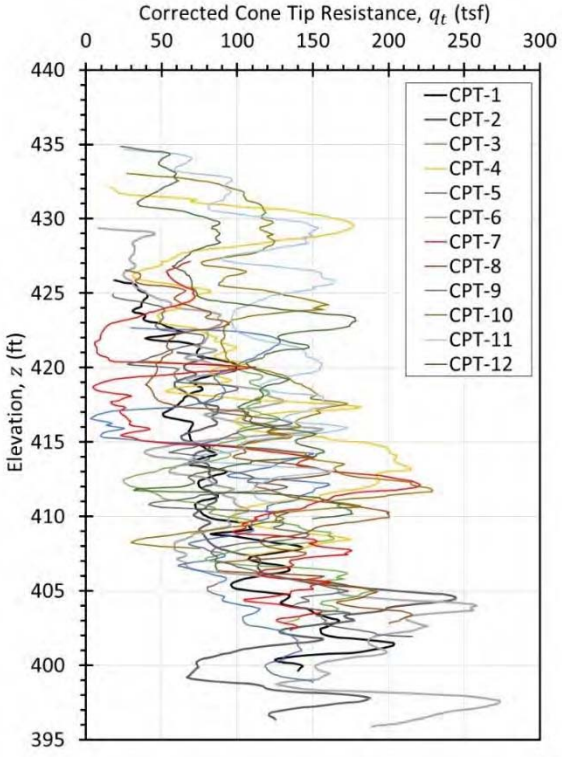


**Figure A2-25 Corrected cone tip resistance in the aquifer sand.**

Figure A2-26 shows estimates for $\phi'$ derived from the measured $q_t$-values using transformations by Robertson and Campanella (1983) and by Kulhawy and Mayne (1990). Both transformations produce similar estimates for $\phi'$, with both indicating that $\phi'$ is nearly constant with depth, generally varying

between 38 and 42 degrees. For both transformations, estimates of $\phi'$ are less variable than measured values for $q_t$, because the transformation equations involve the logarithm function. Estimates for $\phi'$ from from CPT-5 and CPT-7 are notably lower than other measurements between elevation 415 and 425. This observation is generally consistent with the measured SPT $N$-values, which also showed lower measurements for those depths. As such, some consideration should be given to separating these soundings from the remaining soundings, and considering the locations as separate design domains. Thus, one might use the solid black lines in Figure A2-26 as the design model for most locations, but use models represented by the dashed lines for locations that may have looser sands between elevations 415 and 425. Unfortunately, the uncertainty associated with the transformations by Robertson and Campanella (1983) and by Kulhawy and Mayne (1990) have also not been quantified, so no estimates for model uncertainty can be established at this time. As such, the interpretations shown were conservatively selected to subjectively account for the additional transformation uncertainty that is not reflected in the values plotted in Figure A2-26.

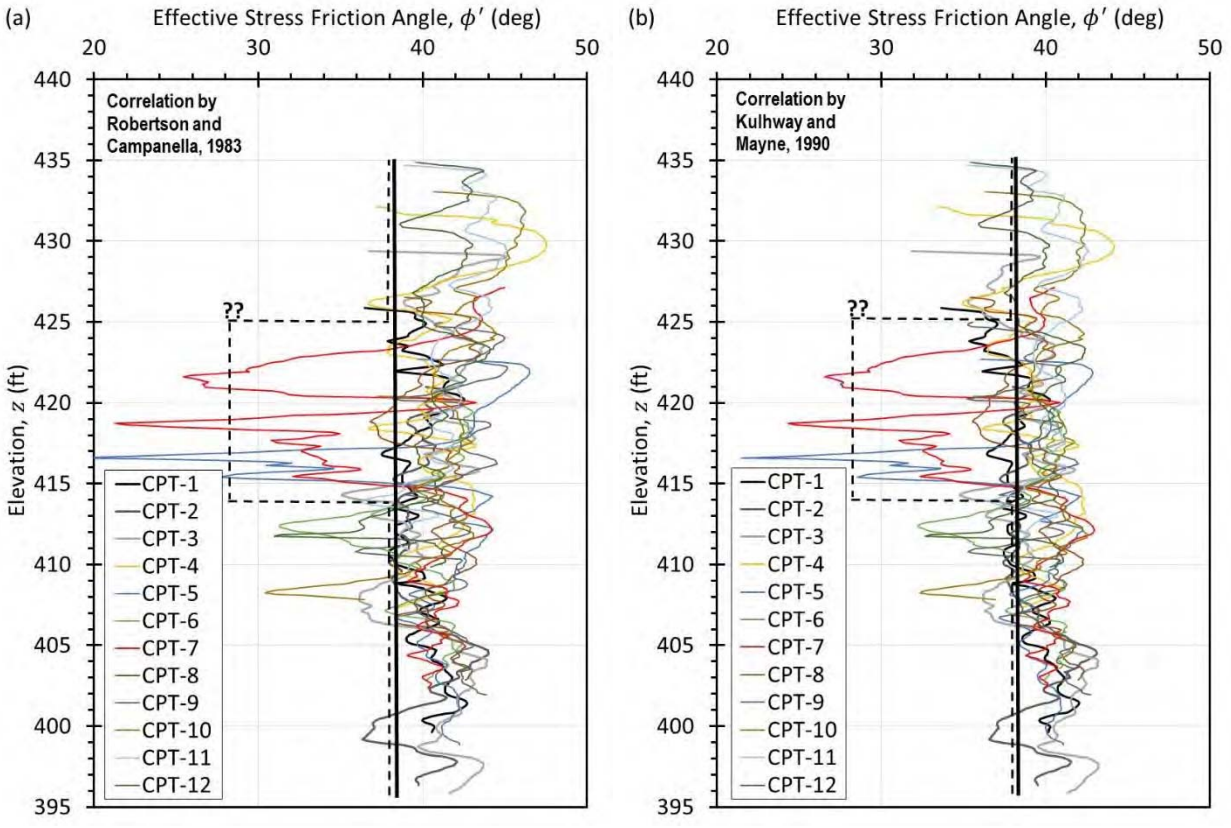


**Figure A2-26 Predictions of $\phi'$ from CPT measurements: (a) Robertson and Campanella (1983) transformation and (b) Kulhawy and Mayne (1990) transformation.**

## A2.3 EXAMPLE 3: EMBANKMENT ON SOFT CLAY – CONSOLIDATION SETTLEMENT AND STABILITY

A raised interchange is proposed at an alluvial site located within the floodplain near the confluence of the Mississippi and Missouri rivers in eastern Missouri. To support the raised interchange, embankments are to be constructed over approximately 25 feet of soft, highly plastic clay overlying silt and alluvial sands. Geotechnical analyses of the embankments will primarily consider embankment stability and settlement. These analyses require characterization of the strength and compressibility of the soft clay, which are the focus of this example. Subsurface investigations completed at the site included three rotary wash borings and three CPT soundings. Locations for the borings and CPT soundings are shown in Figure A2-27. All borings and CPT soundings indicate approximately 25 to 30 feet of highly plastic clay over 5 to 10 feet of silt over sand.

**Figure A2-27 Boring locations for soft clay site (Google® Earth™, 2017).**

### A2.3.1 In Situ Stress State in Soft Clay

In situ effective stress conditions and stress history govern undrained shear strength and settlement for soft clay sites like the one being considered. Interpretation of the in situ stress state is therefore critical. The total vertical stress was calculated based on measurements of total unit weight, $\gamma$, which are plotted in Figure A2-28. Design values of $\gamma$ were selected by observing a shift in the measurements wherein values for samples above a depth of 15 feet were notably less than values for samples below 15 feet. Accordingly, the measurements were averaged to assign design values of $\gamma = 104$ pcf from the ground surface to a depth of 15 feet, and $\gamma = 111$ pcf below a depth of 15 feet. Pore water pressures were

calculated assuming hydrostatic conditions with a groundwater table at a depth of 23 feet based on observations during drilling as shown by the dashed line in Figure A2-28b. The in situ vertical effective stress, $\sigma'_{vo}$, was calculated from $\sigma'_{vo} = \sigma_{vo} - u$. The calculated effective stresses are identical to the total vertical stress for depths above the groundwater table (23 feet), at which point the slope changes as a result of increasing pore water pressure with depth.

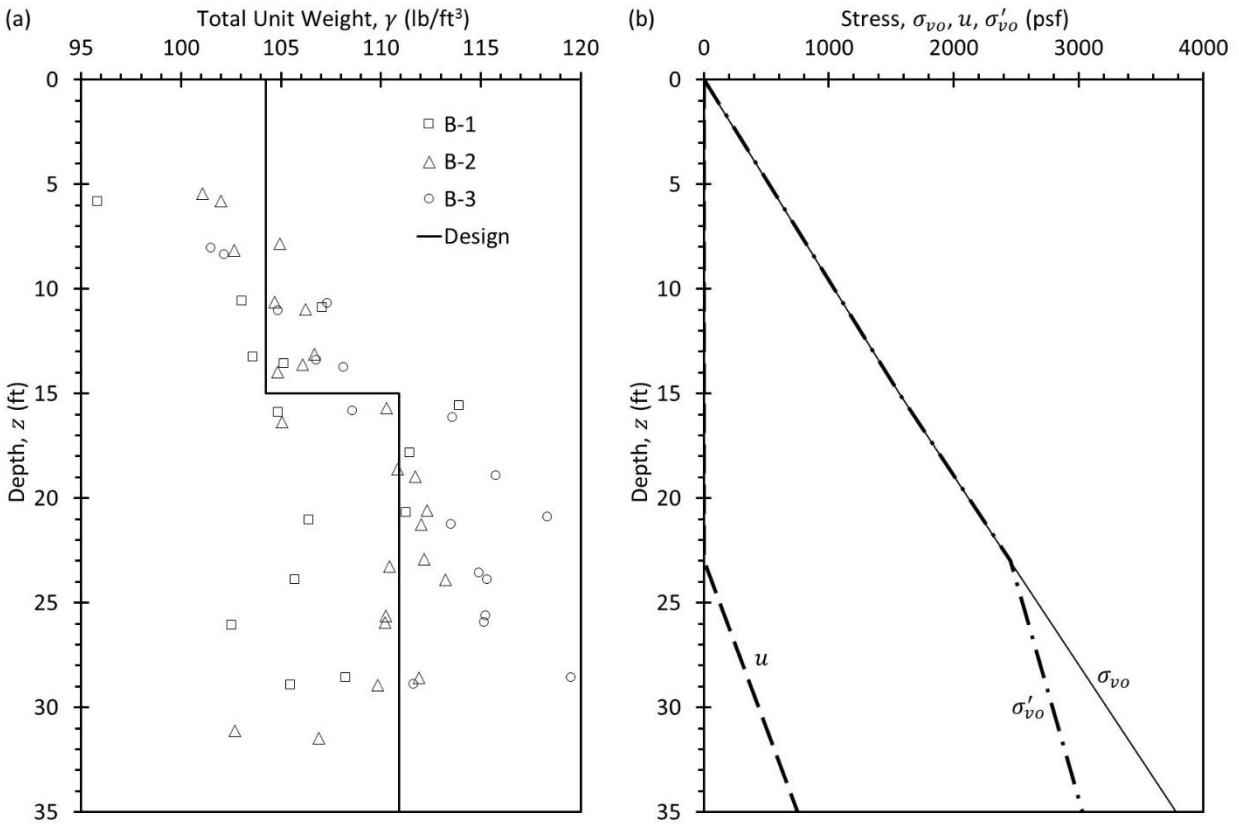


**Figure A2-28 In situ stress state: (a) $\gamma$, and (b) $\sigma_{vo}$, $u$, and $\sigma'_{vo}$ for the soft clay site.**

The magnitude of the preconsolidation stress ($\sigma'_p$) and corresponding values of overconsolidation ratio ($OCR$) were interpreted from thirty CRS consolidation test measurements. Figure A2-29 shows interpretation of $\sigma'_p$ using the strain energy method for the specimen from boring B-3 at a depth of 16 feet. Interpreted values of $\sigma'_p$ for all tests are shown in Figure A2-30. Values of $\sigma'_p$ are generally consistent with those often observed for soft, fine-grained soils with modest overconsolidation near the ground surface and decreasing $OCR$ to near 1.0 with depth. The collective interpretation shown by the solid lines in Figure A2-30 was established by fitting a regression line to measured values of $\sigma'_p$, but selectively ignoring some measurements using judgment to produce an interpretation that was judged to appropriately represent conditions at the site. The model uncertainty bounds shown for the estimated $\sigma'_p$ are less than 0.10, largely because a large number of measurements are available.

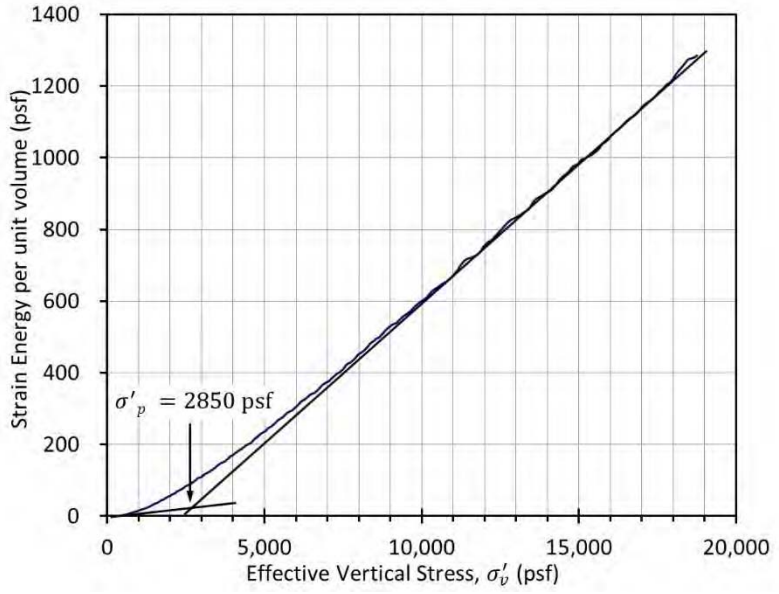


**Figure A2-29 Determination of $\sigma'_p$ for test in Figure A2-31 using strain energy method.**

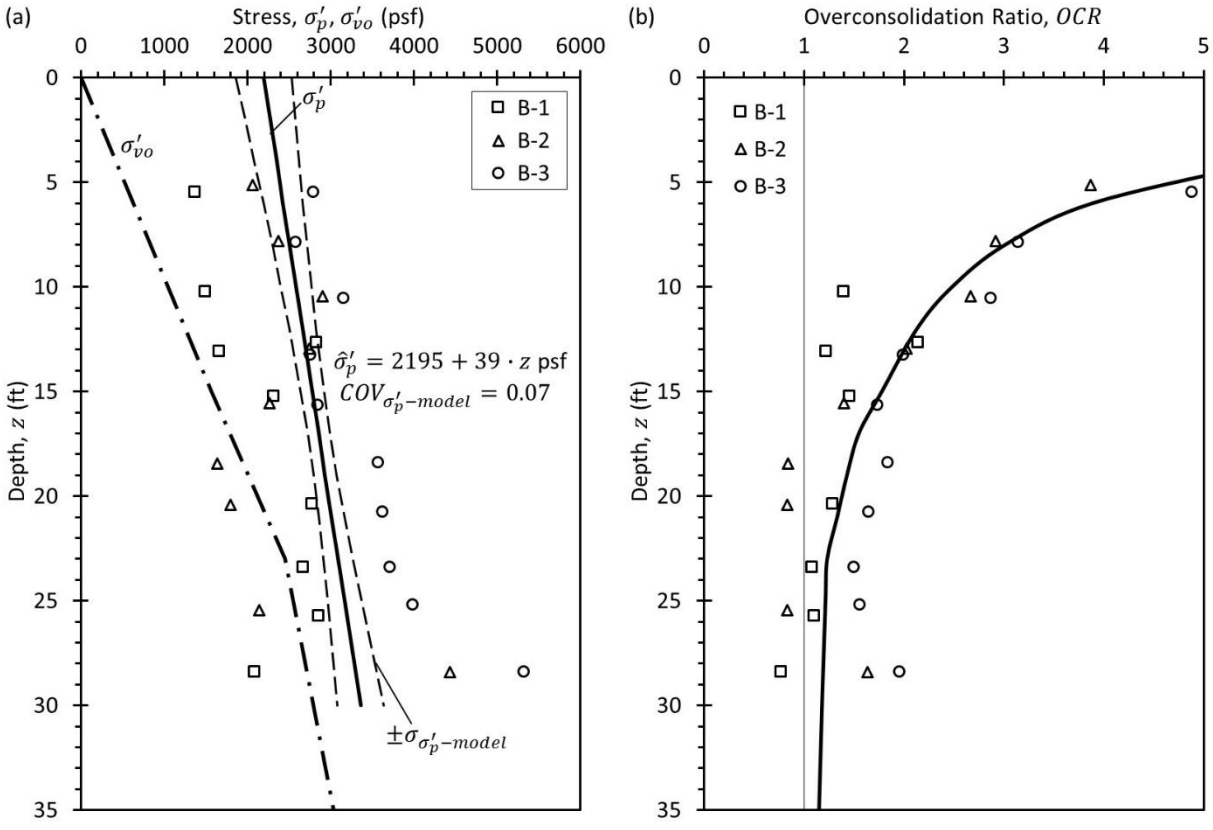


**Figure A2-30 Stress history for soft clay site: (a) $\sigma'_{vo}$ and $\sigma'_p$, and (b) $OCR$.**

The interpreted $OCR$ shown in Figure A2-30b was computed directly from the interpreted trend for $\sigma_p'$ shown in Figure A2-30a, not from regression of the $OCR$ values plotted for specific tests that are also shown in the figure for comparison. This approach is preferable to performing regression for computed values of $OCR$ for individual tests, primarily because it is easier to apply judgment for interpretation of $\sigma_p'$. Additionally, the variation of $\sigma_p'$ with depth is often closer to linear than is $OCR$ so the regression is simpler. It is not appropriate to separately interpret $\sigma_p'$ and $OCR$ using independent regression analyses because doing so will produce estimates for interpreted $\sigma_p'$ and $OCR$ that are inconsistent and incompatible.

### A2.3.2 Compressibility Parameters for Soft Clay

Measurements from the CRS consolidation tests were also used to interpret values for compressibility parameters, $C_{c\varepsilon}$ and $C_{r\varepsilon}$. Figure A2-31 show interpretations for these properties from measurements for the specimen from boring B-3 at a depth of 16 feet. The interpreted value for $C_{c\varepsilon}$ was determined to be $C_{c\varepsilon} = 0.18$ based on the steepest portion of the consolidation curve while the interpreted value of $C_{r\varepsilon}$ was determined to be $C_{r\varepsilon} = 0.05$ based on the slope from the unload-reload cycle.

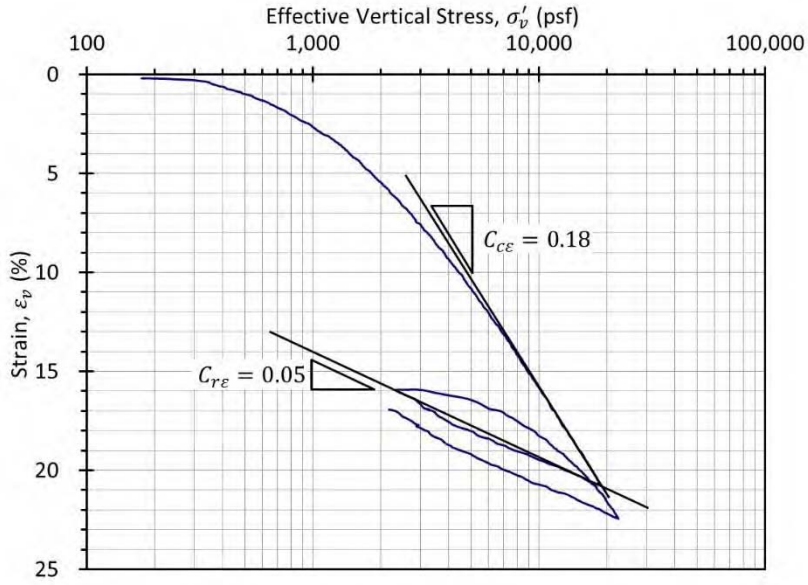


**Figure A2-31 CRS consolidation measurements for specimen from boring B-3 at 16-feet depth.**

Interpretations of $C_{c\varepsilon}$ and $C_{r\varepsilon}$were similarly determined for the remaining tests and are plotted versus depth in Figure A2-32. For both sets of data, results from all three borings are reasonably similar, so it is appropriate to proceed with one design domain for compressibility values. Additionally, there is no apparent trend with depth, so it is also appropriate to assign one value of $C_{c\varepsilon}$ and one value of $C_{r\varepsilon}$ to the

entire clay layer. The estimated values shown in Figure A2-32, $C_{r\varepsilon} = 0.05$ and $C_{c\varepsilon} = 0.17$, are mean values for all tests. Computed values for $COV_{model}$ for both parameters are both quite small, and well below the model uncertainty threshold of 0.30.

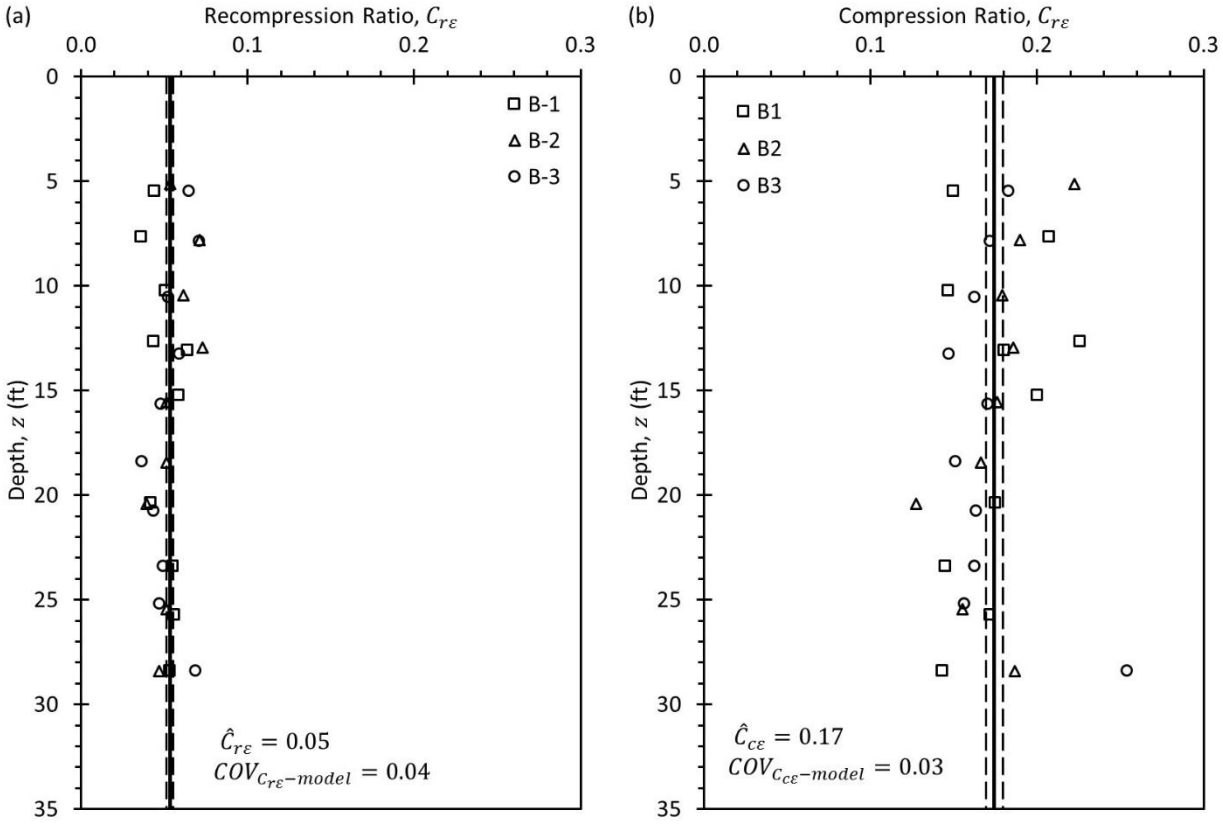


**Figure A2-32 Design profiles for compressibility parameters: (a) $C_r$, and (b) $C_c$.**

### A2.3.3 Undrained Shear Strength of Soft Clay

As described in Chapters 7 and 11, interpretation of $s_u$ is a nontrivial exercise that should include consideration of in situ effective stresses, the stress history of the deposit, the method of loading, and the degree of sample disturbance, among other considerations. The site conditions (floodplain) and interpreted in situ stress state and stress history are consistent with sites characterized as "soft clay" sites. $s_u$ is therefore hypothesized to be relatively low near the ground surface and to increase with depth as is typical of such sites. For this example, $s_u$ is estimated directly from UU triaxial compression tests and indirectly from CIUC triaxial tests conducted following SHANSEP procedures and from CPT measurements. Specimens for UU and CIUC tests were trimmed from 3-in. diameter fixed piston samples acquired from the rotary wash borings, so disturbance is considered limited.

***Undrained Shear Strength from UU Triaxial Compression Tests***

Fifty-five UU triaxial compression tests were performed on specimens acquired from the three borings. The measurements are plotted graphically in Figure A2-33 and listed in Table A2–12.

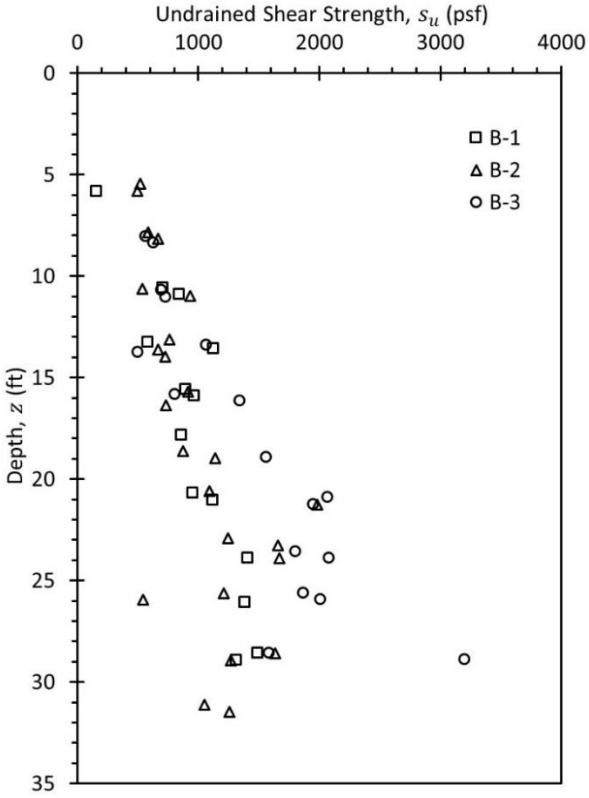


**Figure A2-33 Measurements of $s_u$ from UU triaxial compression tests.**

**Table A2–12 Measurements from UU triaxial compression tests at soft clay site.**

| | Depth, ft | $s_u$, psf |
|---|---|---|
| B-1 | 5.8 | 160 |
| B-1 | 10.9 | 844 |
| B-1 | 10.6 | 706 |
| B-1 | 13.6 | 1128 |
| B-1 | 13.3 | 585 |
| B-1 | 15.9 | 970 |
| B-1 | 15.6 | 900 |
| B-1 | 17.8 | 863 |
| B-1 | 21.0 | 1124 |
| B-1 | 20.7 | 959 |
| B-1 | 23.9 | 1407 |
| B-1 | 26.1 | 1387 |
| B-1 | 28.9 | 1316 |
| B-1 | 28.6 | 1492 |

| | Depth, ft | $s_u$, psf |
|---|---|---|
| B-2 | 5.8 | 493 |
| B-2 | 5.5 | 519 |
| B-2 | 8.2 | 667 |
| B-2 | 7.8 | 587 |
| B-2 | 11.0 | 935 |
| B-2 | 10.6 | 540 |
| B-2 | 14.0 | 724 |
| B-2 | 13.6 | 666 |
| B-2 | 13.1 | 762 |
| B-2 | 16.4 | 730 |
| B-2 | 15.7 | 915 |
| B-2 | 19.0 | 1141 |
| B-2 | 18.6 | 873 |
| B-2 | 20.6 | 1090 |

| | Depth, ft | $s_u$, psf |
|---|---|---|
| B-2 | 21.3 | 1980 |
| B-2 | 23.3 | 1660 |
| B-2 | 22.9 | 1247 |
| B-2 | 23.9 | 1667 |
| B-2 | 26.0 | 540 |
| B-2 | 25.6 | 1212 |
| B-2 | 28.9 | 1271 |
| B-2 | 28.6 | 1634 |
| B-2 | 31.5 | 1258 |
| B-2 | 31.1 | 1048 |
| B-3 | 8.4 | 634 |
| B-3 | 8.1 | 564 |
| B-3 | 11.0 | 729 |
| B-3 | 10.7 | 696 |

| | Depth, ft | $s_u$, psf |
|---|---|---|
| B-3 | 13.8 | 500 |
| B-3 | 13.4 | 1066 |
| B-3 | 16.2 | 1343 |
| B-3 | 15.8 | 811 |
| B-3 | 18.9 | 1561 |
| B-3 | 21.3 | 1951 |
| B-3 | 20.9 | 2069 |
| B-3 | 23.9 | 2082 |
| B-3 | 23.6 | 1803 |
| B-3 | 26.0 | 2009 |
| B-3 | 25.6 | 1869 |
| B-3 | 28.9 | 3204 |
| B-3 | 28.6 | 1586 |

As hypothesized for the soft clay site, $s_u$ shown in Figure A2-33 increases with depth in an approximately linear manner. It is therefore appropriate to model $s_u$ as

$$\hat{s}_u(z) = \beta_0 + \beta_1 \cdot z \tag{A2.12}$$

where $\beta_0$ and $\beta_1$ are regression coefficients that, respectively, represent the intercept and slope of the regression function, $z$ is depth, and $\hat{s}_u$ represents the estimated value of $s_u$ at a given value of $z$. Using ordinary least squares (OLS) regression implemented with the MS Excel™ "LINEST" function, the slope of the best-fit regression line is determined to be 53 psf/ft and the intercept is 160 psf so that

$$\hat{s}_u(z) = 160 + 53 \cdot z \tag{A2.13}$$

where $z$ is in feet and $s_u$ is in psf. The resulting line is plotted with the measurements in Figure A2-34. The regression model is a reasonable approximation of the data.

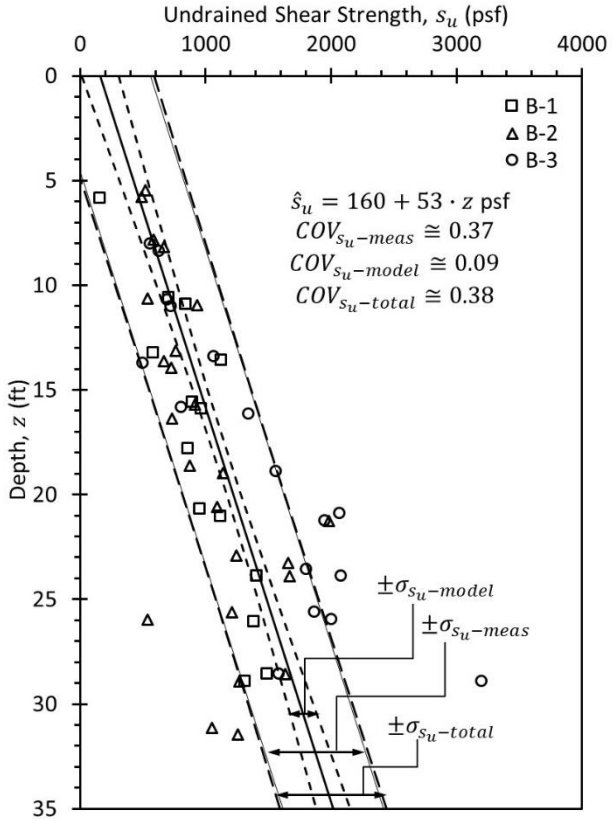


**Figure A2-34 Design profile with linear interpretation of $s_u$ from UU measurements.**

The variability of the $s_u$ model is computed using equations provided in Appendix 3. First, the mean squared error of the regression is computed as

$$MSE_{s_u} = \frac{\sum_{i=1}^{n_d}(y_i - \hat{y}_d)^2}{n_d - 2} = \frac{\sum_{i=1}^{55}(y_i - \hat{y}_d)^2}{55-2} = \frac{8{,}583{,}138}{53} = 161{,}946 \text{ psf}^2 \quad \text{(A2.14)}$$

where $y_i$ is the $i^{\text{th}}$ measurement of $s_u$, $\hat{y}_d$ is the estimated value of $s_u$ at the same value of depth $z$, and $n_d$ is the number of direct measurements (i.e., the number of UU tests). The standard deviation of the measurements, $\sigma_{s_u-meas}$, is simply the square root of $MSE_{s_u}$:

$$\sigma_{s_u-meas} = \sqrt{MSE_{s_u}} = \sqrt{161{,}946} = 402 \text{ psf} \quad \text{(A2.15)}$$

The model standard deviation, $\sigma_{s_u-model}$, is computed as

$$\sigma_{s_u-model}(z) = \sqrt{MSE_{s_u}\left(\frac{1}{n_d} + \frac{(z-\bar{z})^2}{\sum_{i=1}^{n_d}(z_i-\bar{z})^2}\right)} = \sqrt{161{,}946\left(\frac{1}{55} + \frac{(z-18.4)^2}{\sum_{i=1}^{55}(z_i-18.4)^2}\right)} =$$

$$\sqrt{161{,}946\left(\frac{1}{55} + \frac{(z-18.4)^2}{2914}\right)} = \sqrt{2944 + 55.6 \cdot (z-18.4)^2} \quad \text{(A2.16)}$$

where $z_i$ represents the depth for each individual measurement, $\bar{z}$ is the average depth of all available measurements, and $z$ is an arbitrary depth where the model uncertainty is being calculated. The total standard deviation, $\sigma_{s_u-total}$, is computed as

$$\sigma_{s_u-total}(z) = \sqrt{\sigma_{s_u-meas}^2 + \sigma_{s_u-model}^2} = \sqrt{MSE_{s_u}\left(1 + \frac{1}{n_d} + \frac{(z-\bar{z})^2}{\sum_{i=1}^{n_d}(z_i-\bar{z})^2}\right)} =$$

$$\sqrt{161{,}946\left(1 + \frac{1}{55} + \frac{(z-18.4)^2}{2914}\right)} = \sqrt{164{,}890 + 55.6 \cdot (z-18.4)^2} \quad \text{(A2.17)}$$

Figure A2-34 shows bounds represent the model plus or minus these measures of variability and uncertainty.

The standard deviation of the measurements represents the variability of the measurements about the linear regression model. As shown in Figure A2-34, $\sigma_{s_u-meas}$ is constant with depth. In contrast, $\sigma_{s_u-model}$ represents the uncertainty of established model. $\sigma_{s_u-model}$ varies with depth, with minimum calculated at a depth of 18.4 feet, which is the average depth of all UU measurements. Finally, $\sigma_{s_u-total}$ represents the combined variability of the measurements and uncertainty of the model. As described in Chapter 11, $\sigma_{s_u-model}$ is usually the appropriate measure to use for design because it reflects the level of confidence in the established design parameter given the available measurements. $\sigma_{s_u-total}$ is appropriate if one was interested in the value for a new measurement, in this case characterizing the

anticipated value for a new measurement of $s_u$. $\sigma_{s_u-meas}$ is not generally useful for design, but it can be useful for comparing the "goodness" of alternative interpretations of a collection of measurements.

***Undrained Shear Strength from CIUC Triaxial Tests***

Fifteen CIUC triaxial tests with pore pressure measurements were performed on specimens from the soft clay layer for depths ranging from 5 to 30 feet. Each specimen was saturated and consolidated to a known state of effective stress and known $OCR$ following the SHANSEP procedures described in Chapter 7. The measured $s_u$ for each specimen was established from the shear stress-strain response observed in each test and plotted as the undrained shear strength ratio, $s_u/\sigma'_{vc}$, versus $OCR$ for the respective specimens, as shown in Figure A2-35. Regression analysis for these measurements indicates the relationship can be represented as

$$\frac{s_u}{\sigma'_{vc}} = 0.34 \cdot OCR^{0.70} \qquad \text{(A2.18)}$$

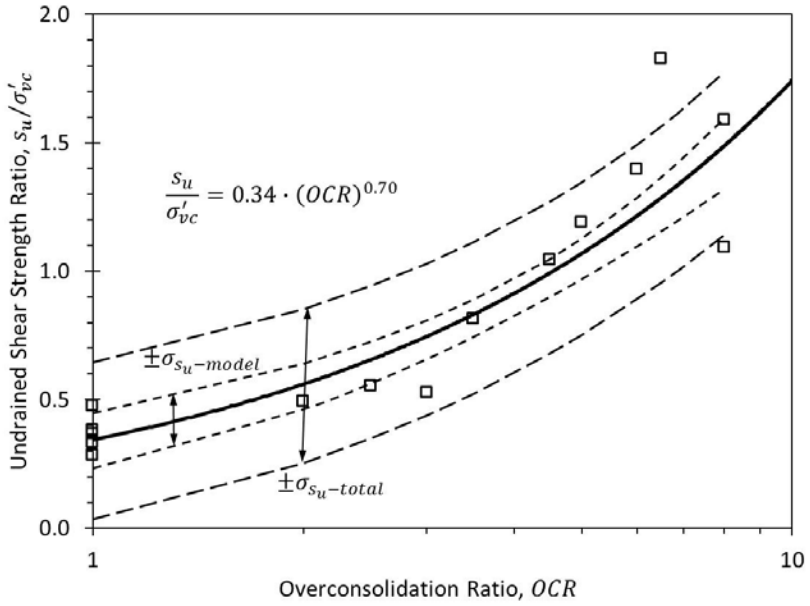


**Figure A2-35 Relationship between $s_u/\sigma'_{vc}$ and $OCR$ for the soft clay site from 15 $\overline{CU}$ tests.**

The $s_u/\sigma'_{vc}$ versus $OCR$ relationship can be used with the in situ effective stresses and stress history information presented in a previous section to predict $s_u$ as a function of depth. Rearranging the relationship shown in Equation A2.18, and substituting $\sigma'_{vo}$ for $\sigma'_{vc}$ leads to

$$s_u = 0.34 \cdot OCR^{0.70} \cdot \sigma'_{vo} \qquad \text{(A2.19)}$$

Figure A2-36 shows the estimated $s_u$ from Equation A2.19, along with uncertainty bounds representing the model uncertainty.

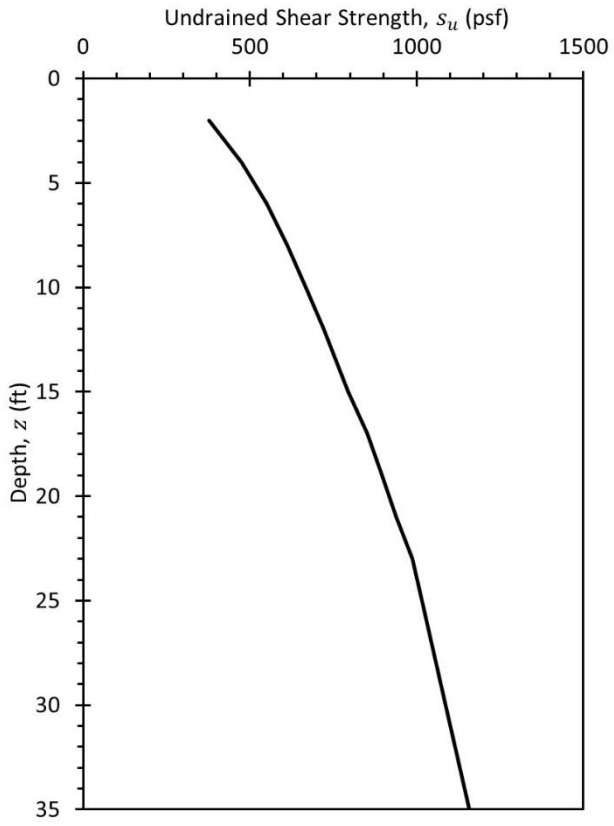


**Figure A2-36 Interpreted model of $s_u$ from $s_u/\sigma'_{vc}$ versus $OCR$ for CIUC loading.**

***Undrained Shear Strength from CPT Measurements***

Indirect measurements of $s_u$ were also calculated from the CPT measurements shown in Figure A2-37. The corrected cone tip resistance is transformed to $s_u$ according to Equation 7.13:

$$s_u = \frac{(q_t - \sigma_{vo})}{N_{kt}} \qquad \text{(A2.20)}$$

where $N_{kt}$ ranges from 10 to 20. Results of the transformation with $N_{kt} = 10$ and $N_{kt} = 20$ are shown in Figure A2-38. Included on the plots are the linear regression model developed from UU triaxial compression measurements. The results generally support the hypothesized strength model for the soft clay site, indicating $s_u$ that increase approximately linearly with depth. Near the surface, the transformed $s_u$ values are highly variable, with some low values consistent with transformed strengths at greater depths but many substantially higher values likely resulting from desiccation near the ground surface. The transformed $s_u$ values are also highly variable below a depth of 25 feet, in the silty transition zone.

The transformed $s_u$ values based on $N_{kt} = 20$ are similar to $s_u$ values from UU tests, whereas the values based on $N_{kt} = 10$ are significantly greater than $s_u$ from UU tests. Accordingly, subsequent analyses are based on the values determined with $N_{kt} = 20$. The variability of $N_{kt}$ is a significant challenge for interpreting $s_u$ from CPT measurements. Comparison with other $s_u$ measurements improves the CPT transformation, particularly if a site-specific value of $N_{kt}$ can be determined.

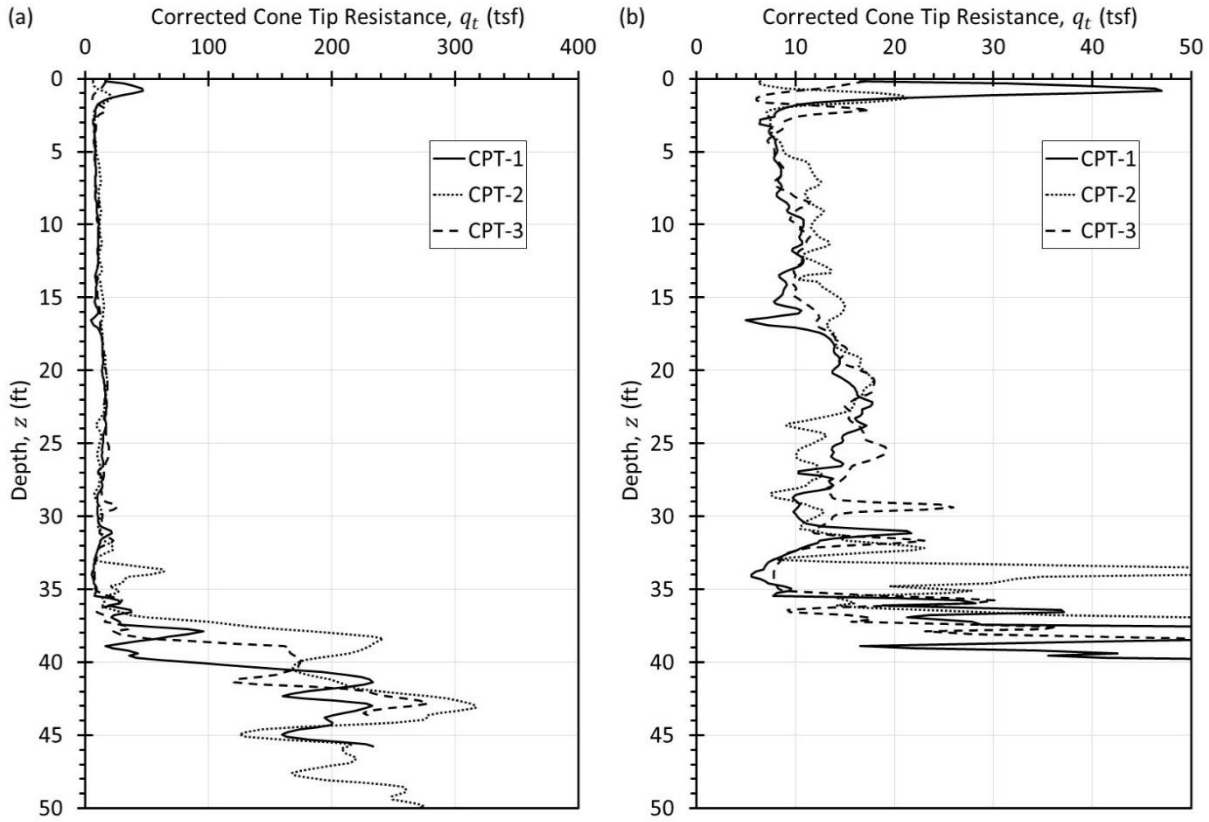


**Figure A2-37 CPT measurements from soft clay site: (a) full scale and (b) reduced horizontal scale to show variability in clay.**

A linear regression model was created using the transformed CPT measurements with $N_{kt} = 20$. The model was terminated at a depth of 25 feet to limit application of the transformation to the soft clay layer and not the silty transition zone. Two regression models are shown in Figure A2-39. The first, shown in Figure A2-39a, includes all data above a depth of 25 feet. In the second model, shown in Figure A2-39b, transformed strength values greater than 1000 psf were excluded from the regression analysis. The resulting model is

$$\bar{s}_u(z) = 658 + 33z \tag{A2.21}$$

where $z$ is in feet and $s_u$ is in psf. Comparison of Figure A2-39a and A2-39b reveals that ignoring the extreme values near the ground surface improves the model, since the second model has a slope that is more consistent with the increase in the transformed $s_u$ with depth.

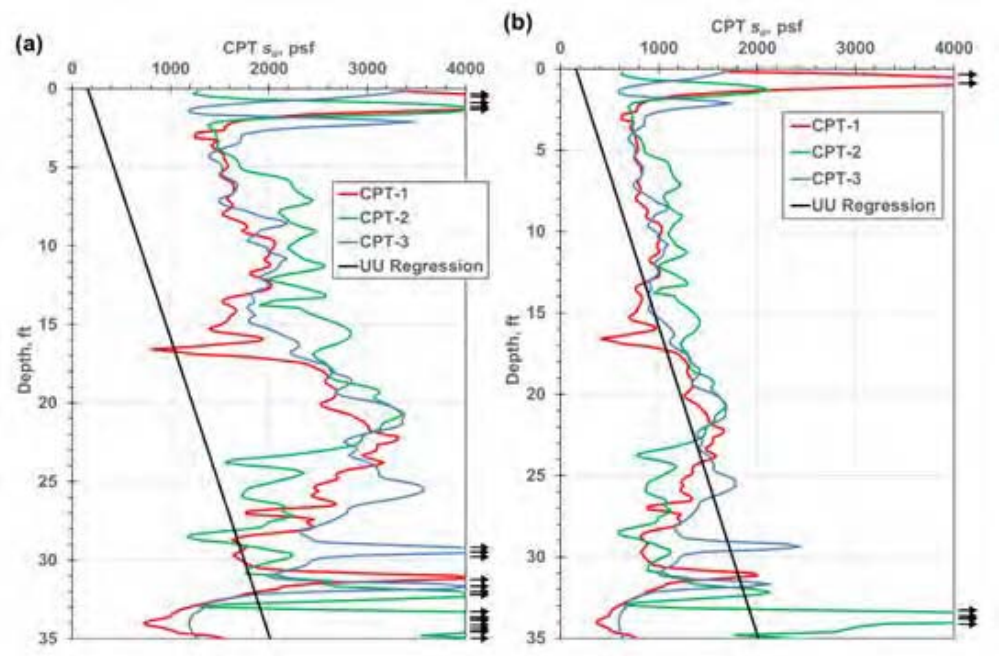


**Figure A2-38 Indirect estimates of $s_u$ from CPT measurements: (a) using $N_{kt} = 10$ and (b) using $N_{kt} = 20$.**

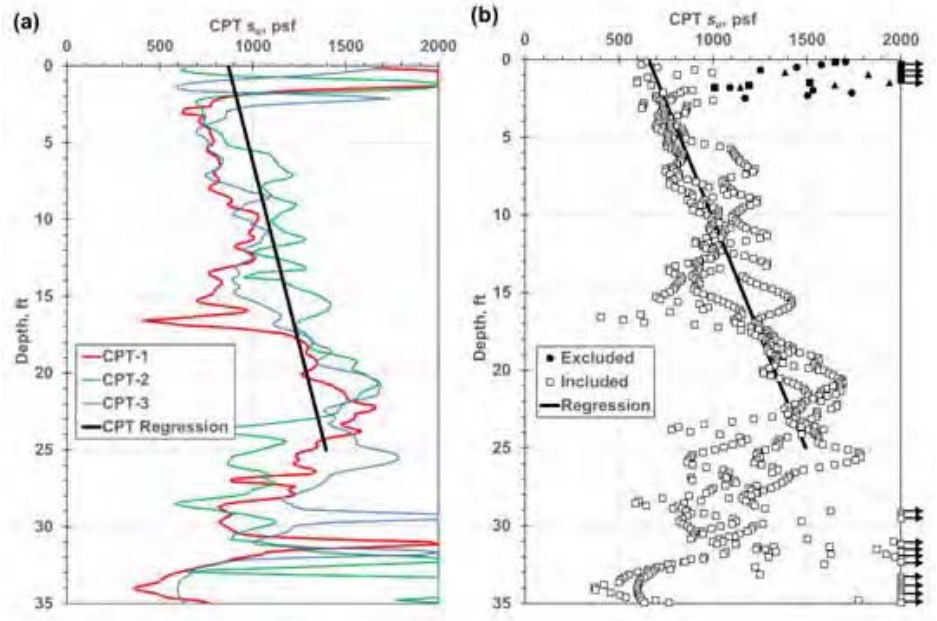


**Figure A2-39 Design profile for $s_u$ determined from CPT measurements: (a)including all data above a depth of 25 feet and (b) excluding "outliers" (solid point markers) indicating undrained strength greater than 2000 psf near the surface.**

***Comparison of Undrained Strength Models***

Results presented in this example demonstrate differences between the various method to measure and model $s_u$. The $s_u$ models developed from UU tests, *CIUC* tests, and CPT tests are plotted together in Figure A2-40. The UU, and CPT models were all developed using linear regression techniques, whereas the *CIUC* tests were interpreted using the undrained strength ratio associated with SHANSEP. In Figure A2-40b, the models have been normalized by the SHANSEP model values, which is likely the best representation of the actual $s_u$ as discussed in Chapter 7. Each of the models indicate $s_u$ values that increase with depth below a depth of 3 feet, consistent with the original hypothesis for the site. However, there are noteworthy differences between the models. The UU and SHANSEP models are similar, with the UU model predicting $s_u$ about 1.4 times greater than SHANSEP model above a depth of 23 feet, the location of the groundwater table during exploration. Below 23 feet, the difference between the two model is greater, with the SHANSEP model increasing less with depth as a result of effective stress increases being less below the water table. The CPT model is substantially greater than the SHANSEP model, with the greatest differences near the ground surface.

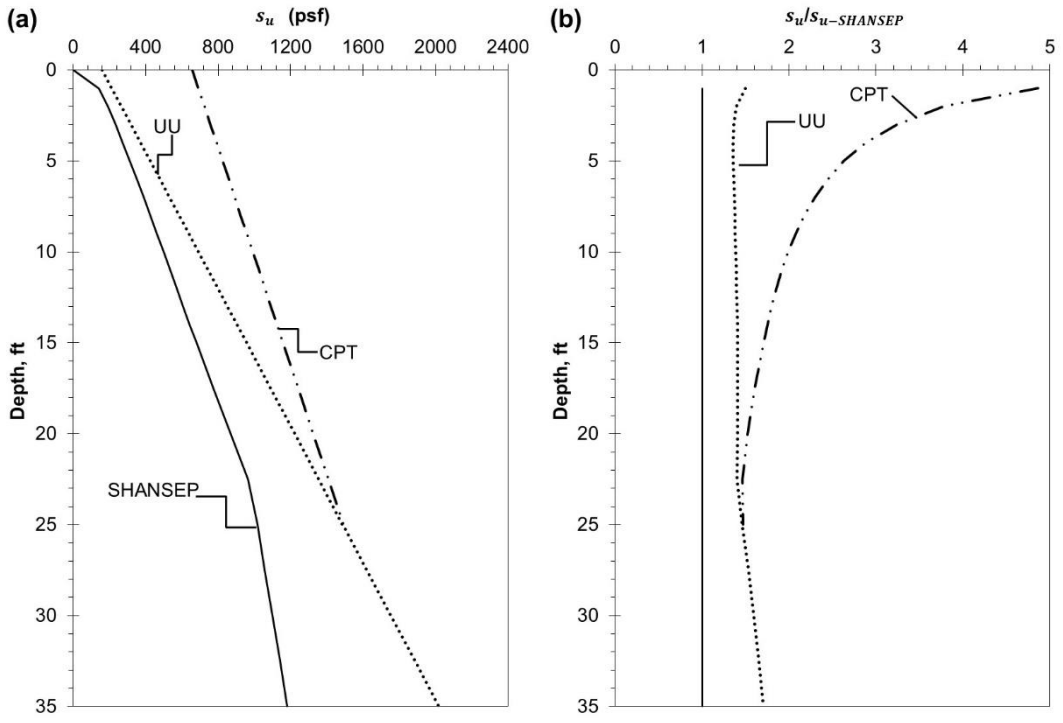


**Figure A2-40 Interpretations of $s_u$ from direct and indirect measurements: (a) model values, and (b) model values normalized by SHANSEP values.**

***Effect of Stress Path***

The discussion of $s_u$ for this example has focused on measurements pertaining to triaxial compression. It is important to also consider $s_u$ from other stress paths, notably direct simple shear and triaxial extension. As discussed in Chapter 7, different portions of the sliding surface are best represented by different loading applications, but the shear strength on average is best represented by the direct simple shear test. Therefore, the results shown in Figure A2-40 should be reduced if they are to be applied to slope stability analyses. Ideally, direct simple shear tests should be performed to develop the design shear strength profile or to confirm the modified profile developed from compression-type shear strength tests.

THIS PAGE IS LEFT INTENTIONALLY BLANK

# APPENDIX 3
# STATISTICS OF GEOTECHNICAL SITE CHARACTERIZATION

This Appendix provides equations pertaining to specific types of datasets commonly encountered in geotechnical site characterization. The information presented in this appendix follows from and builds upon the concepts presented in Chapters 3 and 11, and follows the same notation. The types of datasets covered are presented from simplest to most complex:

- Uniform layer with only direct measurements (normal data)
- Uniform layer with only indirect measurements
- Uniform layer with combined direct and indirect measurements
- Parameters that vary with depth
- Lognormal parameters

## A3.1 UNIFORM LAYER WITH DIRECT MEASUREMENTS ONLY

For strata where a soil or rock property can be considered constant, the design value can be interpreted from the arithmetic mean of the available measurements:

$$\bar{y}_d = \frac{\sum_{i=1}^{n_d} y_i}{n_d} \tag{A3.1}$$

where $y_i$ are direct measurements of a particular design parameter, $n_d$ is the number of available direct measurements, and $\bar{y}_d$ is the mean value. Note that the subscript $d$ is used here to indicate that the mean value is derived from direct measurements.

Several different quantitative statistical measures can be used to represent variability and/or uncertainty including the mean squared error ($MSE$), the variance ($Var$ or $\sigma^2$), the standard deviation ($\sigma$), and the coefficient of variation ($COV$). For strata that are considered to have a constant value of a property, the mean squared error of a collection of independent, direct measurements is defined as:

$$MSE_d = \frac{\sum_{i=1}^{n_d} (y_i - \hat{y}_d)^2}{n_d - 1} = \frac{\sum_{i=1}^{n_d} (y_i - \bar{y}_d)^2}{n_d - 1} \tag{A3.2}$$

where $y_i$ is the $i^{\text{th}}$ measurement of $y$, $\hat{y}_d$ is the estimated value of $y$, and $n_d$ is the number of direct measurements. Note that the subscript "$d$" is used here to indicate that the estimate is derived from direct measurements and the "hat" accent "$\widehat{\ }$" is used to indicate an estimated value of the parameter $y$. For

uniform strata, the estimated value of the parameter is taken to be equal to the mean (i.e. $\hat{y}_d = \bar{y}_d$) and the variance is equal to $MSE_d$, i.e.

$$Var(y) = \sigma^2_{d-meas}(y) = MSE_d = \frac{\sum_{i=1}^{n_d}(y_i - \hat{y}_d)^2}{n_d - 1} \tag{A3.3}$$

where $\sigma_{d-meas}$ is the standard deviation of the measurements and the subscript $d$ again indicates that the unbiased estimate is derived from direct measurements. Thus, the standard deviation is simply the square root of the variance

$$\sigma_{d-meas} = \sqrt{Var(y)} = \sqrt{MSE_d} = \sqrt{\frac{\sum_{i=1}^{n_d}(y_i - \hat{y}_d)^2}{n_d - 1}} \tag{A3.4}$$

The standard deviation, $\sigma^2_{d-meas}$, is perhaps the most familiar measure of variability to readers of this circular, and it describes the variability of the *measurements* about the estimated value of the parameter.

Several alternative measures of variability and uncertainty are likely less familiar to many readers, but often more relevant for geotechnical site characterization. Specifically, the variance of the estimated value of the parameter, which represents the level of confidence in the estimated value of the parameter given the available measurements, can be computed as

$$\sigma^2_{d-model} = \frac{MSE_d}{n_d} = \frac{1}{n_d} \cdot \frac{\sum_{i=1}^{n_d}(y_i - \hat{y}_d)^2}{n_d - 1} \tag{A3.5}$$

where

$$\sigma_{d-model} = \sqrt{\frac{MSE_d}{n_d}} = \sqrt{\frac{1}{n_d} \cdot \frac{\sum_{i=1}^{n_d}(y_i - \hat{y}_d)^2}{n_d - 1}} \tag{A3.6}$$

will be referred to as the "model" standard deviation. The model variance and model standard deviation represent the uncertainty in the estimated value of the parameter $y$. Finally, the combined variability and uncertainty of an estimate for a specific parameter is represented by combined consideration of the variability of the measurements about the estimate (i.e. the standard deviation of the measurements, $\sigma_{d-meas}$) and the uncertainty of the model (i.e. the model standard deviation, $\sigma_{d-model}$) to compute the "total" variance, $\sigma^2_{d-total}$, as

$$\sigma^2_{d-total} = \sigma^2_{d-meas} + \sigma^2_{d-model} = \left(\frac{\sum_{i=1}^{n_d}(y_i - \hat{y}_d)^2}{n_d - 1}\right)\left(1 + \frac{1}{n_d}\right) \tag{A3.7}$$

where

$$\sigma_{d-total} = \sqrt{\sigma_{d-meas}^2 + \sigma_{d-model}^2} = \sqrt{\left(\frac{\sum_{i=1}^{n_d}(y_i - \hat{y}_d)^2}{n_d - 1}\right)\left(1 + \frac{1}{n_d}\right)} \quad \text{(A3.8)}$$

is the total standard deviation computed as the square root of the sum of the squares of the measurement variability and the model uncertainty.

It is often helpful to represent variability and/or uncertainty in dimensionless form using the coefficient of variation, which is simply the standard deviation normalized by the mean value. Thus, three alternative coefficients of variation can be computed to represent the variability of the measurements ($COV_{d-meas}$), the model uncertainty ($COV_{d-model}$), and the total variability and uncertainty ($COV_{d-total}$), respectively:

$$COV_{d-meas} = \frac{\sigma_{d-meas}}{\bar{y}_d} = \frac{\sqrt{\frac{\sum_{i=1}^{n_d}(y_i - \hat{y}_d)^2}{n_d - 1}}}{\bar{y}_d} \quad \text{(A3.9)}$$

$$COV_{d-model} = \frac{\sigma_{d-model}}{\bar{y}_d} = \frac{\sqrt{\frac{1}{n_d}\frac{\sum_{i=1}^{n_d}(y_i - \hat{y}_d)^2}{n_d - 1}}}{\bar{y}_d} \quad \text{(A3.10)}$$

$$COV_{d-total} = \frac{\sigma_{d-total}}{\bar{y}_d} = \frac{\sqrt{\sigma_{d-meas}^2 + \sigma_{d-model}^2}}{\bar{y}_d} \quad \text{(A3.11)}$$

Coefficients of variation are commonly reported as decimal values or percentage values.

## A3.2 UNIFORM LAYER WITH INDIRECT MEASUREMENTS ONLY

Indirect measurements are measurements that require some transformation be applied to the actual measurements to produce an estimate for the design property of interest. Given an appropriate transformation function, two general approaches can be adopted for establishing values for design parameters from indirect measurements:

1. Transforming the individual indirect measurements to produce an estimated measurement for each individual indirect measurement, then collectively interpreting the estimated measurements.
2. Interpreting the actual indirect measurements to produce some interpretation (i.e. "model") of the actual measurements, then transforming the model values to produce an estimate for the design parameter.

In the first approach, each indirect measurement is transformed to produce a transformed "measurement" of the design property of interest as

$$y_{s-i} = f(x_i) \tag{A3.12}$$

where $y_{s-i}$ is a transformed measure for the design property of interest derived from indirect or "surrogate" measurements, $f$ is a function representing the transformation, and $x_i$ is an individual indirect measurement in the stratum of interest. Using this approach, an estimate for the design parameter of interest is established in a manner similar to that described in the previous section for direct measurements. In contrast, using the second approach, the estimate for the design parameter of interest is established from an interpreted estimate for the indirect measurement, $\hat{x}$, as

$$\hat{y}_s = f(\hat{x}) \tag{A3.13}$$

where $\hat{y}_s$ is the estimate for the design parameter derived from indirect or "surrogate" measurements, $f$ is a function representing the transformation, and $\hat{x}$ is the estimated value of the indirect measurement in the stratum of interest. For strata where the indirect measurement can be practically represented as uniform, the value for $\hat{x}$ can be computed as the mean value of the indirect measurements

$$\hat{x} = \bar{x} = \frac{\sum_{i=1}^{n_x} x_i}{n_x} \tag{A3.14}$$

where $\bar{x}$ is the mean of the indirect measurements, $x_i$ represents the individual indirect measurements, and $n_x$ is the number of indirect measurements.

In order to compute the variability and uncertainty of a design parameter established from indirect measurements, it is first necessary to compute the variability and uncertainty of the indirect measurements themselves. This is done similarly to computation of variability and uncertainty from direct measurements (Equations A3.4, A3.6, and A3.8) so that

$$\sigma_{x-meas} = \sqrt{Var(x)} = \sqrt{MSE_x} = \sqrt{\frac{\sum_{i=1}^{n_x}(x_i-\hat{x})^2}{n_x-1}} \tag{A3.15}$$

$$\sigma_{x-model} = \sqrt{\frac{MSE_x}{n_x}} = \sqrt{\frac{1}{n_x} \cdot \frac{\sum_{i=1}^{n_x}(x_i-\hat{x})^2}{n_x-1}} \tag{A3.16}$$

$$\sigma_{x-total} = \sqrt{\sigma_{x-meas}^2 + \sigma_{x-model}^2} = \sqrt{\left(\frac{\sum_{i=1}^{n_x}(x_i-\hat{x})^2}{n_x-1}\right)\left(1+\frac{1}{n_x}\right)} \tag{A3.17}$$

where $\sigma_{x-meas}$ is the standard deviation of the indirect measurements, $\sigma_{x-model}$ is the model standard deviation representing the uncertainty in the estimated value of the indirect measurements, and $\sigma_{x-total}$ is the total standard deviation representing the combined variability and uncertainty of the indirect measurements. In Equations A3.15-A3.17, the variable $x_i$ represents the individual indirect measurements and the subscript $x$ is used to indicate that the measures of variability and uncertainty are for indirect measurements. Thus, $n_x$ represents the number of indirect measurements, $MSE_x$ is the mean squared error for the indirect measurements, and $\hat{x}$ represents the estimated value of the indirect measurement in the stratum of interest.

For many types of indirect measurements, the indirect measurements can be transformed to the design parameter of interest using linear transformations of the form

$$\hat{y}_s = \beta_0 + \beta_1 \hat{x} \tag{A3.18}$$

where $\hat{y}_s$ is the estimated value of the design parameter established from indirect measurements, $\hat{x}$ is the estimated value of the indirect measurements in a particular stratum, and $\beta_0$ and $\beta_1$ are regression coefficients for the transformation from indirect measurements to the parameter of interest. For such transformations, the variability and uncertainty in the design parameter established exclusively from the indirect measurements can be computed as

$$\sigma_{s-meas} = \sqrt{MSE_r\left[1 + \frac{1}{m} + \frac{(\hat{x}-\bar{x}_r)^2+\sigma^2_{x-meas}}{s_{xx}}\right] + \beta_1^2\sigma^2_{x-meas}} \tag{A3.19}$$

$$\sigma_{s-model} = \sqrt{MSE_r\left[1 + \frac{1}{m} + \frac{(\hat{x}-\bar{x}_r)^2+\sigma^2_{x-model}}{s_{xx}}\right] + \beta_1^2\sigma^2_{x-model}} \tag{A3.20}$$

$$\sigma_{s-total} = \sqrt{MSE_r\left[1 + \frac{1}{m} + \frac{(\hat{x}-\bar{x}_r)^2+\sigma^2_{x-total}}{s_{xx}}\right] + \beta_1^2\sigma^2_{x-total}} \tag{A3.21}$$

where $\sigma_{s-meas}$ is the standard deviation of the transformed measurements, $\sigma_{s-model}$ is the model standard deviation representing the uncertainty of the estimated or "model" value $\hat{y}_s$, and $\sigma_{s-total}$ is the total standard deviation representing the combined variability and uncertainty of the design parameter $y_s$. The terms $\hat{x}$, $\sigma_{x-meas}$, $\sigma_{x-model}$, and $\sigma_{x-total}$ are all derived from analysis of the indirect measurements: $\hat{x}$ is the estimated (usually mean) value of the indirect measurements in the stratum of interest and $\sigma_{x-meas}$, $\sigma_{x-model}$, and $\sigma_{x-total}$ respectively represent the standard deviation of the indirect measurements (Equation A3.15), the model standard deviation for the estimated value $\hat{x}$ (Equation

A3.16), and the total standard deviation for the indirect measurement (Equation A3.17). The remaining terms in Equations A3.19-A3.21 are measures derived from the transformation. $MSE_r$ is the mean squared error of the regression used to establish the transformation, $\bar{x}_r$ is the mean value of the indirect measurements used to establish the regression, $\beta_1$ is the slope of the regression equation, $m$ is the number of measurements used to establish the regression, and $s_{xx}$ is a quantity related to the variance of the indirect measurements used to establish the transformation. $MSE_r$ is fundamentally similar to the $MSE_d$ term discussed in Section A3.5 regarding parameters that vary linearly with depth and can therefore be calculated according to Equation A3.28. $s_{xx}$ is computed as

$$s_{xx} = \sum_{i=1}^{m}(x_{r-i} - \bar{x}_r)^2 \qquad \text{(A3.22)}$$

where $x_{r-i}$ represents the individual indirect measurements in the regression data set. While Equations A3.19-A3.21 involve a number of different terms, it is important to note that many of these terms are associated with the transformation equation ($MSE_r$, $\bar{x}_r$, $\beta_1$, $m$, and $s_{xx}$). Once these values are established, it is only necessary to compute values for $\hat{x}$ and the appropriate standard deviation ($\sigma_{x-meas}$, $\sigma_{x-model}$, or $\sigma_{x-total}$) from the available indirect measurements to apply Equations A3.19-A3.21.

### A3.3 UNIFORM LAYER WITH COMBINED DIRECT AND INDIRECT MEASUREMENTS

When both direct and indirect measurements for a particular design parameter are available, it is possible to derive estimates for the design parameter value and variability and uncertainty for the design parameter from combined consideration of the direct and indirect measurements. This can be done using weighted averages of the estimates derived from the direct and indirect measurements, respectively. The mean value for the design parameter, $\bar{y}$, can be estimated as

$$\bar{y} = \frac{\frac{\bar{y}_d}{\sigma_d^2} + \frac{\bar{y}_s}{\sigma_s^2}}{\frac{1}{\sigma_d^2} + \frac{1}{\sigma_s^2}} = \frac{\bar{y}_d \cdot \sigma_s^2 + \bar{y}_s \cdot \sigma_d^2}{\sigma_d^2 + \sigma_s^2} \qquad \text{(A3.23)}$$

where $\bar{y}_d$ and $\bar{y}_s$ are mean values for the design parameter determined from the available direct and indirect measurements, respectively, and $\sigma_d$ and $\sigma_s$ are the standard deviations determined from the direct and indirect measurements, respectively. Equation A3.23 can be applied using any of the three measures of variability and uncertainty (i.e. $\sigma_{meas}$, $\sigma_{model}$, or $\sigma_{total}$), but it is most commonly appropriate to use the model uncertainty. Estimates for the standard deviation can similarly be determined as

$$\sigma_y = \frac{\sigma_d^2 \cdot \sigma_s^2}{\sigma_d^2 + \sigma_s^2} \qquad \text{(A3.24)}$$

where $\sigma_y$ can correspond to the model uncertainty ($\sigma_{model}$) or the total variability and uncertainty ($\sigma_{total}$) depending on the values of $\sigma_d$ and $\sigma_s$ used in Equation A3.24.

## A3.4 PARAMETERS THAT VARY WITH DEPTH

When considering a stratum with properties that vary linearly throughout the stratum, the regression produces an expression of the form

$$\bar{y}_d(z) = \beta_0 + \beta_1 z \tag{A3.25}$$

where $\beta_0$ and $\beta_1$ are regression coefficients that, respectively, represent the intercept and slope of the regression function, $z$ is the regression parameter (usually depth or elevation), and $\bar{y}_d$ represents the mean value of the design parameter at a given value of $z$. Regression coefficients can be calculated for ordinary least squares (OLS) regression as

$$\beta_1 = \frac{\sum_{i=1}^{n_d}(y_i - \bar{y}_d)(z_i - \bar{z})}{\sum_{i=1}^{n_d}(z_i - \bar{z})^2} \tag{A3.26}$$

$$\beta_0 = \bar{y} - \beta_1 \bar{z} \tag{A3.27}$$

where $y_i$ is the $i^{\text{th}}$ measurement of $y$, $\bar{y}_d$ is the mean measurement value of $y$, $z_i$ is the depth corresponding to the $i^{\text{th}}$ measurement of $y$, $\bar{z}$ is the mean depth of all measured values of $y$, and $n_d$ is the number of direct measurements. The OLS regression coefficients are also readily calculated using functions built into data analysis and spreadsheet computer programs. For OLS regression, the mean squared error is computed as

$$MSE_d = \frac{\sum_{i=1}^{n_d}(y_i - \hat{y}_d)^2}{n_d - 2} \tag{A3.28}$$

where $y_i$ is the $i^{\text{th}}$ measurement of $y$, $\hat{y}_d$ is the estimated value of $y$ at the same value of $z$, and $n_d$ is the number of direct measurements. Note that the 2 in the denominator accounts for the additional degree of freedom associated with the linear function. Respective values of the alternative standard deviations are computed as

$$\sigma_{d-meas} = \sqrt{MSE_d} = \sqrt{\frac{\sum_{i=1}^{n_d}(y_i - \hat{y}_d)^2}{n_d - 2}} \tag{A3.29}$$

$$\sigma_{d-model}(z) = \sqrt{MSE_d\left(\frac{1}{n_d} + \frac{(z-\bar{z})^2}{\sum_{i=1}^{n_d}(z_i-\bar{z})^2}\right)} \quad \text{(A3.30)}$$

$$\sigma_{d-total}(z) = \sqrt{\sigma_{d-meas}^2 + \sigma_{d-model}^2} = \sqrt{MSE_d\left(1 + \frac{1}{n_d} + \frac{(z-\bar{z})^2}{\sum_{i=1}^{n_d}(z_i-\bar{z})^2}\right)} \quad \text{(A3.31)}$$

where $z_i$ are depths (or elevations) of available direct measurements and $\bar{z}$ is the average depth of all available measurements. Corresponding coefficients of variation can be computed by dividing these values by the computed mean value at the same depth (from the regression coefficients $\beta_0$ and $\beta_1$ using Equation A3.25). The value for $MSE_d$ is commonly provided, or can be calculated from output provided using commonly available data analysis software.

## A3.5 LOGNORMAL PARAMETERS

It is frequently useful to assume measurements of geotechnical parameters are lognormally distributed rather than normally distributed. The primary advantage of the lognormal distribution is that it is strictly non-negative, as are many geotechnical parameters. If measurements of a parameter are lognormally distributed, the natural logarithms of the measurements are normally distributed. The simplest method for calculating lognormally distributed parameters is first to find the natural logarithm of each measurement and calculate a mean and standard deviation for the log-transformed dataset, similar to calculations for uniform, direct measurements:

$$\mu_{ln-d} = \frac{\sum_{i=1}^{n_d} \ln y_i}{n_d} \quad \text{(A3.32)}$$

$$s_{ln-d-meas} = \sqrt{\frac{\sum_{i=1}^{n_d}(\ln y_i - \bar{y}_{ln-d})^2}{n_d - 1}} \quad \text{(A3.33)}$$

where $y_i$ are direct measurements of a particular design parameter, $n_d$ is the number of available direct measurements, $\mu_{ln-d}$ is the mean of the log-transformed data, and $s_{ln-d-meas}$ is the standard deviation of the log-transformed measurements. The mean and standard deviation of the log-transformed dataset can then be used to calculate a mean, $\bar{y}_{ln-d}$, and standard deviation of measurements, $\sigma_{ln-d-meas}$, for the lognormal parameter:

$$\bar{y}_{ln-d} = e^{\mu_{ln-d} + \frac{1}{2}s_{ln-d-meas}^2} \quad \text{(A3.34)}$$

$$\sigma_{ln-d-meas} = \sqrt{(e^{s_{ln-d-meas}} - 1)(\bar{y}_{ln-d})^2} \quad \text{(A3.35)}$$

A similar approach can be used for model and total standard deviation values from lognormal parameters.

THIS PAGE IS LEFT INTENTIONALLY BLANK